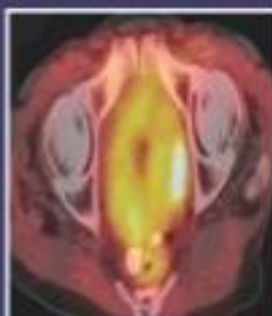
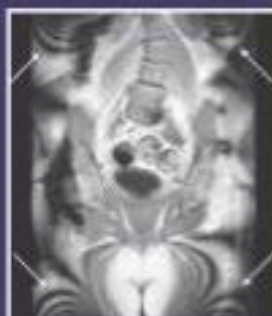


AIIMS-MAMC-PGI IMAGING SERIES



# DIAGNOSTIC RADIOLOGY

## Recent Advances and Applied Physics in Imaging

*Editors*

**Arun Kumar Gupta**  
**Veena Chowdhury**  
**Niranjan Khandelwal**

*Associate Editors*

**Sanjay Sharma**  
**Ashu Seith Bhalla**  
**Smriti Hari**

**2nd Edition**

**JAYPEE**

# **DIAGNOSTIC RADIOLOGY**

## **Recent Advances and Applied Physics in Imaging**



AIIMS-MAMC-PGI Imaging Series

# DIAGNOSTIC RADIOLOGY

## Recent Advances and Applied Physics in Imaging

Second Edition

### Editors

**Arun Kumar Gupta** MD MNAMS FAMS

Professor and Head  
Department of Radio-diagnosis  
All India Institute of Medical Sciences  
(AIIMS), New Delhi, India

**Veena Chowdhury** MD

Director Professor and Head  
Department of Radio-diagnosis  
Maulana Azad Medical College  
(MAMC), New Delhi, India

**Niranjan Khandelwal** MD Dip NBE FICR

Professor and Head  
Department of Radio-diagnosis  
Postgraduate Institute of Medical Education  
and Research (PGIMER), Chandigarh, India

### Associate Editors

**Sanjay Sharma** MD DNB FRCR

Additional Professor  
Department of Radio-diagnosis  
All India Institute of Medical Sciences  
(AIIMS), New Delhi, India

**Ashu Seith Bhalla** MD MNAMS

Additional Professor  
Department of Radio-diagnosis  
All India Institute of Medical Sciences  
(AIIMS), New Delhi, India

**Smriti Hari** MD

Associate Professor  
Department of Radio-diagnosis  
All India Institute of Medical Sciences  
(AIIMS), New Delhi, India



**JAYPEE BROTHERS MEDICAL PUBLISHERS (P) LTD**

New Delhi • London • Philadelphia • Panama



**Jaypee Brothers Medical Publishers (P) Ltd.**

#### **Headquarters**

Jaypee Brothers Medical Publishers (P) Ltd.  
4838/24, Ansari Road, Daryaganj  
New Delhi 110 002, India  
Phone: +91-11-43574357  
Fax: +91-11-43574314  
**Email:** [jaypee@jaypeebrothers.com](mailto:jaypee@jaypeebrothers.com)

#### **Overseas Offices**

J.P. Medical Ltd.  
83, Victoria Street, London  
SW1H 0HW (UK)  
Phone: +44-2031708910  
Fax: +02-03-0086180  
**Email:** [info@jpmedpub.com](mailto:info@jpmedpub.com)

Jaypee-Highlights Medical Publishers Inc.  
City of Knowledge, Bld. 237, Clayton  
Panama City, Panama  
Phone: + 507-301-0496  
Fax: + 507-301-0499  
**Email:** [cservice@jphmedical.com](mailto:cservice@jphmedical.com)

Jaypee Brothers Medical Publishers Ltd  
The Bourse  
111, South Independence Mall East  
Suite 835, Philadelphia, PA 19106, USA  
Phone: + 267-519-9789  
**Email:** [joe.rusko@jaypeebrothers.com](mailto:joe.rusko@jaypeebrothers.com)

Jaypee Brothers Medical Publishers (P) Ltd.  
17/1-B Babar Road, Block-B, Shaymali  
Mohammadpur, Dhaka-1207  
Bangladesh  
Mobile: +08801912003485  
**Email:** [jaypeedhaka@gmail.com](mailto:jaypeedhaka@gmail.com)

Jaypee Brothers Medical Publishers (P) Ltd.  
Shorakhute, Kathmandu  
Nepal  
Phone: +00977-9841528578  
**Email:** [jaypee.nepal@gmail.com](mailto:jaypee.nepal@gmail.com)

Website: [www.jaypeebrothers.com](http://www.jaypeebrothers.com)  
Website: [www.jayeedigital.com](http://www.jayeedigital.com)

© 2013, Jaypee Brothers Medical Publishers

All rights reserved. No part of this book may be reproduced in any form or by any means without the prior permission of the publisher.

**Inquiries for bulk sales may be solicited at:** [jaypee@jaypeebrothers.com](mailto:jaypee@jaypeebrothers.com)

This book has been published in good faith that the contents provided by the contributors contained herein are original, and is intended for educational purposes only. While every effort is made to ensure accuracy of information, the publisher and the editors specifically disclaim any damage, liability, or loss incurred, directly or indirectly, from the use or application of any of the contents of this work. If not specifically stated, all figures and tables are courtesy of the editors. Where appropriate, the readers should consult with a specialist or contact the manufacturer of the drug or device.

***Diagnostic Radiology: Recent Advances and Applied Physics in Imaging***

*First Edition:* 2000

*Second Edition:* 2013

ISBN: 978-93-5090-497-8

*Printed at*

# Contributors

## Ajay Gulati MD

Assistant Professor  
Department of Radio-diagnosis  
PGIMER, Chandigarh, India

## Ajay Kumar MD

Assistant Professor  
Department of Radio-diagnosis  
PGIMER, Chandigarh, India

## Akshay Kumar Saxena MD Dip NBE

Additional Professor  
Department of Radio-diagnosis  
PGIMER, Chandigarh, India

## Alpana Manchanda MD

Professor  
Department of Radio-diagnosis  
MAMC, New Delhi, India

## Anil Chauhan MBBS Board Certified in

Radiology, USA  
Fellow, Body imaging, Department of Radiology  
University of Texas MD Anderson Cancer center, Houston, USA

## Anil K Pandey PhD

Assistant Professor (Medical Physics)  
Department of Nuclear Medicine  
AIIMS, New Delhi, India

## Anindita Sinha MD

Assistant Professor  
Department of Radio-diagnosis  
PGIMER, Chandigarh, India

## Anish Bhattacharya DNB DRM MNAMS

Additional Professor  
Department of Nuclear medicine  
PGIMER, Chandigarh, India

## Anjali Prakash DMRD DNB MNAMS

Professor  
Department of Radio-diagnosis  
MAMC, New Delhi, India

## Anju Garg MD

Director Professor  
Department of Radio-diagnosis  
MAMC, New Delhi, India

## Anupam Lal MD

Associate Professor  
Department of Radio-diagnosis  
PGIMER, Chandigarh, India

## Arun Deep Arora MD

Senior Research Associate  
Department of Radio-diagnosis  
AIIMS, New Delhi, India

## Arun Kumar Gupta MD MNAMS FAMS

Professor and Head  
Department of Radio-diagnosis  
AIIMS, New Delhi, India

## Ashu Seith Bhalla MD MNAMS

Additional Professor  
Department of Radio-diagnosis  
AIIMS, New Delhi, India

## Atin Kumar MD DNB MNAMS

Associate Professor  
Department of Radio-diagnosis  
(Trauma Centre Division)  
AIIMS, New Delhi, India

## BR Mittal MD DRM DNB FICNM FAMS

Professor and Head  
Department of Nuclear Medicine  
PGIMER, Chandigarh, India

## Chandan Jyoti Das MD DNB MNAMS

Assistant Professor  
Department of Radio-diagnosis  
AIIMS, New Delhi, India

## Chandrashekha SH MD DNB MNAMS

Assistant Professor  
Department of Radio-diagnosis  
(BRAIRCH Division)  
AIIMS, New Delhi, India

## Deep Narayan Srivastava MD MNAMS

FAMS  
Professor  
Department of Radio-diagnosis  
AIIMS, New Delhi, India

## Devasenathipathy Kandasamy MD DNB

FRCR  
Assistant Professor  
Department of Radio-diagnosis  
(BRAIRCH Division)  
AIIMS, New Delhi, India

## Gaurav Pradhan DMRD DNB

Professor  
Department of Radio-diagnosis  
MAMC, New Delhi, India

## Jyoti Kumar MD DNB MNAMS

Associate Professor  
Department of Radio-diagnosis  
MAMC, New Delhi, India

## Kushaljit Singh Sodhi MD MNAMS FICR

Associate Professor  
Department of Radio-diagnosis  
PGIMER, Chandigarh, India

## Madhusudhan KS MD FRCR

Assistant Professor  
Department of Radio-diagnosis  
AIIMS, New Delhi, India

## Mandeep Kang MD

Additional Professor  
Department of Radio-diagnosis  
PGIMER, Chandigarh, India

## Manisha Jana MD DNB FRCR

Assistant Professor  
Department of Radio-diagnosis  
(BRAIRCH Division)  
AIIMS, New Delhi, India

## Manphool Singhal MD DNB MNAMS

Assistant Professor  
Department of Radio-diagnosis  
PGIMER, Chandigarh, India

## Manavjit Singh Sandhu MD FICR

Professor  
Department of Radio-diagnosis  
PGIMER, Chandigarh, India

## Mukesh Kumar Yadav MD

Assistant Professor  
Department of Radio-diagnosis  
PGIMER, Chandigarh, India

## Naveen Kalra MD

Additional Professor  
Department of Radio-diagnosis  
PGIMER, Chandigarh, India

## Niranjan Khandelwal MD Dip NBE FICR

Professor and Head  
Department of Radio-diagnosis  
PGIMER, Chandigarh, India

## Pratik Kumar PhD Dip RP

Additional Professor  
Medical Physics Unit (BRAIRCH)  
AIIMS, New Delhi, India

**Rajat Jain** MD

Senior Resident  
Department of Radio-diagnosis  
MAMC  
New Delhi, India

**Raju Sharma** MD

Professor  
Department of Radio-diagnosis  
AIIMS  
New Delhi, India

**Rakesh Kumar** MD PhD

Additional Professor  
Department of Nuclear Medicine  
AIIMS  
New Delhi, India

**Rashmi Dixit** MD

Professor  
Department of Radio-diagnosis  
MAMC  
New Delhi, India

**Sameer Vyas** MD

Assistant Professor  
Department of Radio-diagnosis  
PGIMER  
Chandigarh, India

**Sanjay Sharma** MD DNB FRCR

Additional Professor  
Department of Radio-diagnosis (RPC Division)  
AIIMS, New Delhi, India

**Sapna Singh** MD DNB MNAMS

Associate Professor  
Department of Radio-diagnosis  
MAMC, New Delhi, India

**SC Bansal** MA MSc (Med Tech) PhD

Lecturer  
Department of Radio-diagnosis  
PGIMER, Chandigarh, India

**Shashi Bala Paul**

Senior Scientist  
Department of Radio-diagnosis  
AIIMS, New Delhi, India

**Shivanand Gamanagatti** MD MNAMS

Associate Professor  
Department of Radio-diagnosis  
(Trauma Centre Division)  
AIIMS, New Delhi, India

**Smriti Hari** MD

Associate Professor  
Department of Radio-diagnosis  
AIIMS, New Delhi, India

**Surabhi Vyas** MD

Assistant Professor  
Department of Radio-diagnosis  
AIIMS, New Delhi, India

**Thulkar S** MD

Additional Professor  
Department of Radio-diagnosis (BRAIRCH)  
AIIMS, New Delhi, India

**Tulika Singh** MD

Assistant Professor  
Department of Radio-diagnosis  
PGIMER  
Chandigarh, India

**Veena Chowdhury** MD

Director Professor and Head  
Department of Radio-diagnosis  
MAMC, New Delhi, India

**Veenu Singla** MD

Assistant Professor  
Department of Radio-diagnosis  
PGIMER, Chandigarh, India

**Vivek Gupta** MD DM (Neuroradiology)

Associate Professor  
Department of Radio-diagnosis  
PGIMER, Chandigarh, India

# Preface to the Second Edition

The First Edition of diagnostic radiology volume on *Advances in Imaging Technology* was published in the year 2000. During the second series, technical advances were dealt with under different organ systems, and no separate volume was compiled. The explosion of imaging technology in the last decade and the imperative need for the radiologist to stay abreast with these, motivate us to release a new volume on topic. The ever-evolving field of radiology makes continuing education in technical advances almost a compulsion rather than an option for those in the field. As a commitment to our readers and as part of our constant endeavor to improve as students ourselves, we publish the new edition titled *Recent Advances and Applied Physics in Imaging*.

Recent years have witnessed an astounding revolution in the field of imaging technology. At the heart of this revolution are major strides taken by the industry in all modalities including radiography, ultrasonography, digital subtraction angiography, computed tomography and magnetic resonance imaging. The imaging has moved from anatomic to functional, from static to real-time and from 2 dimensional to 3 or even 4 dimensional. All these major advancements in the information provided are expected at a faster rate and with lesser radiation dose. It is truly a tribute to science that several of these goals have actually been achieved. As radiologists, we have been privileged to be the chosen few to deliver these stunning images to the medical community. With this, however, comes greater responsibility. Our ability to create and interpret these amazing pictures requires us to comprehend the physics that goes into creating them. Also, the onus of minimizing the cost of imaging, selection of the optimal modality and minimizing radiation exposure finally rests on us.

This book has hence been planned as a volume attempting to summarize and deliver the advances in imaging technology relevant to the radiologist in a manageable capsule. We hope that it will serve as your friend and companion in understanding and negotiating the labyrinth of Imaging Physics. Compared to the First Edition published in 2000, the book has understandably been majorly restructured. We have attempted to cover all major aspects of technological advances relevant to a practicing radiologist, while keeping the book compact. It is our earnest hope that our readers will find this text informative and that it will aid in their learning process and daily practice.

We wish to thank all the contributors from the institutions, i.e. All India Institute of Medical Sciences, New Delhi, Maulana Azad Medical College, New Delhi and Postgraduate Institute of Medical Education and Research, Chandigarh, India, for their efforts in compiling this edition. We would also like to express our sincere appreciation to Shri Jitendar P Vij (Group Chairman), Mr Ankit Vij (Managing Director), Mr Tarun Duneja (Director-Publishing), Mrs Samina Khan (PA to Director-Publishing), Mr KK Raman (Production Manager), Mr Sunil Kumar Dogra (Production Executive), Mr Neelambar Pant (Production Coordinator), Mr Subrata Adhikary (Commissioning Editor), Dr Mohd Naved (Senior Proofreader), Mr Girish Pandey (Typesetter), Mr Dinesh Joshi (Graphic Designer) and other staff of M/s Jaypee Brothers Medical Publishers (P) Ltd, New Delhi, India, for their professionalism and dedication towards publication of this edition.

**Arun Kumar Gupta  
Veena Chowdhury  
Niranjan Khandelwal**



# Preface to the First Edition

Diagnostic imaging has undergone an astonishingly rapid transformation over the last two decades. The constant expansion of imaging techniques and their potential is based on scientific and technical advances including improvement in computer hardware and software technology. The fusion of computer technology to diagnostics imaging was indeed a turning point in the history of diagnostics imaging. This, in fact, has brought medical imaging to the forefront of various clinical disciplines.

The amazing speed at which the field of radiology is mushrooming today would have surely astounded Roentgen, the "Father" of radiology. While physicians, a century ago, struggled with the notion of looking inside the living body without the cutting it open. At present, the physicians find it almost impossible to practice medicine without the help of sophisticated diagnostics imaging.

Cross-sectional imaging modalities have revolutionized the concept of imaging. Ultrasonography has advanced into wider areas of applications with increasing contrast use of color Doppler and Power Doppler techniques. The introduction of ultrasound contrast media and tissue harmonic imaging has further opened up new vistas in clinical applications of ultrasonography.

Since its introduction in 1971, computed tomography (CT) technology has come a long way. Modern scanners, capable of subsecond scanning, are ideal for the scanning chest and abdomen in a single breath-hold. Additional improvement includes more detectors to increase resolution and finer collimation allowing a reduction in slice thickness to minimize partial volume averaging. Introduction of spiral scanners has widened the scope of imaging by making 3D CT and 3D CT angiography possible.

Magnetic resonance imaging (MRI) was introduced into clinical medicine in 1981 and within a short time, it has assumed a role of unparalleled importance in diagnostic medicine. It is probably the most important imaging advancement since the introduction of X-rays in 1895. The resolution of 3D MR and 3D MR angiography has also advanced to the stage, where the replacement of conventional invasive angiography is now in sight. However, MR spectroscopy has failed to fill its early promise and still await routine clinical acceptance.

The role of the radiology is fast changing from that of a diagnostician usually supporting clinical diagnosis to that of a more active colleague tackling various clinical problems and performing a wide gamut of interventional procedures. The interventional radiologist of today is indeed going to be surgeon of the new millennium.

Functional neuroimaging with PET and SPET is emerging from the research stages and when more freely available, may have a major influence on clinical practice.

Teleradiology, which allows long distance transmission of images by extensive networking, has expanded the scope of diagnostic imaging well beyond our expectation.

The student of radiology needs constant guidance through this bewildering plethora of new information on imaging technology. A comprehensive understanding of technological advances in imaging and their clinical applications are necessary for practicing radiologists to be able to make an optimal choice of investigation in helping the referring physician to reach at a diagnosis.

Keeping this in mind, the faculty of radio-diagnosis at the All India Institute of Medical Sciences, Maulana Azad Medical College, New Delhi and Postgraduate Institute of Medical Education and Research, Chandigarh, India, present this seventh book in the series of Diagnostic Radiology, devoted to Advances in Imaging Technology, thus concluding the series of AIIMS, MAMC, PGI Imaging Courses.

This book comprises of 16 chapters, covering the recent advances in ultrasonography, computed tomography, magnetic resonance imaging, nuclear medicine, digital radiography and interventional radiology. In addition, a full chapter has been devoted to the role of Internet in Radiology. Also, this book includes 7 more chapters on the subjects, which could not be covered in earlier volumes.

We hope, the reader shall find this book informative and valuable for better use of imaging technology.

We wish to take this opportunity to thank our faculty colleagues from AIIMS, MAMC and PGIMER for their active support and cooperation. We also express our sincere thanks to Shri Jitendar P Vij (Group Chairman) and other staff of M/s Jaypee Brothers Medical Publishers (P) Ltd., New Delhi, India, for timely publication of all previous books including the present one.

**Manorama Berry**  
**Veena Chowdhury**  
**Sudha Suri**  
**Sima Mukhopadhyay**

# Contents

## SECTION 1 ADVANCES IN ULTRASOUND IMAGING

<b>Chapter 1</b>	Ultrasound Instrumentation: Practical Applications <i>Kushaljit Singh Sodhi, Akshay Kumar Saxena, Mukesh Kumar Yadav</i>	3
	• Machine Controls 3 • Frequency of Transducers 3 • Types of Transducers 5	
	• Extended Field of View 9 • Clinical Applications of Fusion Imaging 12	
<b>Chapter 2</b>	Image Optimization in Ultrasound <i>Rashmi Dixit</i>	17
	• Gray Scale Imaging 18 • Artifacts in B Mode Imaging 20 • Spectral and Color Doppler Examination 26 • Special Imaging Modes 32 • Compound Imaging 33	
<b>Chapter 3</b>	Ultrasound Elastography: Principles and Application <i>Veenu Singla, Tulika Singh, Anindita Sinha</i>	37
	• Basic Physics 37 • Depiction of Elastograms 38 • Different Elastography Techniques 38 • Elastography Applications 41 • Other Applications 50	

## SECTION 2 ADVANCES IN COMPUTED TOMOGRAPHY

<b>Chapter 4</b>	CT Hardware: An Update <i>Ashu Seith Bhalla, Arun Deep Arora</i>	57
	• Basic Workflow of CT Scanner 57 • Determinants of an Optimal Image 58	
	• Advances in Hardware 59 • Special Computed Tomography 62	
<b>Chapter 5</b>	Dual Energy CT <i>Arun Kumar Gupta, Manisha Jana</i>	66
	• Historical Perspective 66 • Principle 66 • Dual Energy Ratio 67	
	• Applications of DECT 72 • Dose Considerations 81	
<b>Chapter 6</b>	CT Perfusion Imaging <i>Veena Chowdhury</i>	86
	• Perfusion CT Technique Basic Principle 86 • Perfusion CT Protocols 87 • CT Perfusion in Acute Ischemic Stroke 88 • CT Perfusion in Oncology 92 • Hepatic CT Perfusion 92	
	• CT Perfusion in Pancreatic Neoplasms 95 • CT Perfusion in Colorectal Carcinoma 97	
	• CT Perfusion in Prostate Cancer 100 • CT Perfusion in Lymphoma 108 • CT Perfusion in Brain Tumors 108 • CT Perfusion in Head and Neck Tumors 109 • CT Perfusion in Lung Cancer 109 • Other Applications 115 • Radiation Issues 115	

## SECTION 3 ADVANCES IN MAGNETIC RESONANCE IMAGING

<b>Chapter 7</b>	MR Instrumentation: An Update <i>Anjali Prakash</i>	123
<ul style="list-style-type: none"> <li>• The Magnet 123 • Prepolarized MRI 125 • Magnet Geometry 127 • 3 Tesla and Higher Magnet Strengths 129 • Multichannel RF Coils and Parallel Imaging 134 • Advanced MR Applications and Hardware 135</li> </ul>		
<b>Chapter 8</b>	Image Optimization in MRI <i>Jyoti Kumar</i>	138
<ul style="list-style-type: none"> <li>• Signal-to-noise Ratio 138 • Contrast to Noise Ratio 141 • Spatial Resolution 142</li> <li>• Scan Time 142 • Artifacts 144</li> </ul>		
<b>Chapter 9</b>	Diffusion Weighted MRI <i>Devasenathipathy Kandasamy, Raju Sharma</i>	157
<ul style="list-style-type: none"> <li>• Basic Principle 157 • B Value 158 • ADC and Exponential Image 159 • DWI Sequences and Optimization 159 • Artifacts and Pitfalls 160 • Advanced DW Techniques 161 • Diffusion Kurtosis Imaging 161 • Clinical Applications of DWI 162</li> </ul>		
<b>Chapter 10</b>	Functional MR: Perfusion and Dynamic Contrast-enhanced MRI <i>Niranjan Khandelwal, Sameer Vyas</i>	171
<ul style="list-style-type: none"> <li>• Perfusion Magnetic Resonance Imaging 171 • Dynamic Contrast-enhanced MRI 178</li> </ul>		
<b>Chapter 11</b>	MR Angiography <i>Ajay Kumar, Sameer Vyas, Naveen Kalra</i>	183
<ul style="list-style-type: none"> <li>• History and Introduction 183 • Flow Phenomena 183 • Time-of-Flight Angiography: Techniques 185 • Phase Contrast Angiography 187 • Contrast-enhanced MR Angiography 189</li> </ul>		
<b>Chapter 12</b>	MRI Pulse Sequences: An Evolution <i>Vivek Gupta, Niranjan Khandelwal</i>	195
<ul style="list-style-type: none"> <li>• Basic Terminologies 195 • Sequences Types 195</li> </ul>		

## SECTION 4 ADVANCES IN RADIOGRAPHY AND INTERVENTIONAL RADIOLOGY

<b>Chapter 13</b>	Digital Radiography: An Update <i>Alpana Manchanda</i>	205
<ul style="list-style-type: none"> <li>• Limitations of Film Screen Radiography 205 • Advantages of Digital Radiography 205</li> <li>• Evolution of Digital Radiography 206 • The Physics Behind Digital Radiography 206</li> <li>• Principle of Digital Radiography 206 • Digital Radiography Systems 206 • Types of Scintillators 210 • Image Processing 212 • Aspects of Image Quality 212</li> </ul>		
<b>Chapter 14</b>	Digital Mammography <i>Smriti Hari, Chandrashekha SH, Surabhi Vyas</i>	217
<ul style="list-style-type: none"> <li>• Digital Mammography 217 • Basic Physics of Digital Mammography 217</li> <li>• Applications of Digital Mammography 221</li> </ul>		

## Contents

<b>Chapter 15</b>	Fluoroscopy and Digital Subtraction Angiography <i>Deep Narayan Srivastava, Madhusudhan KS</i>	226
	• Overview 226 • Fluoroscopy 226 • Digital Subtraction Angiography 234	
<b>Chapter 16</b>	Tools in Interventional Radiology <i>Atin Kumar, Chandan Jyoti Das</i>	245
	• Puncture Needles 245 • Dilators 246 • Sheaths 247 • Catheters 247 • Guidewire 250	
	• FNAC and Biopsy Needle 251 • Stent 252 • Embolising Agents 254	

**SECTION 5 UPDATE IN CONTRAST MEDIA**

<b>Chapter 17</b>	MR Contrast Media <i>Anju Garg</i>	259
	• Basic Principles of MR Contrast Agents 259 • Classification of MR Contrast Agents 260	
	• Gadolinium Based Contrast Agents 260 • Manganese Based Contrast Agents 267	
	• Iron Oxide Based Contrast Agents 267 • Oral Contrast Agents 268	
<b>Chapter 18</b>	Ultrasound Contrast Agents <i>Shashi Bala Paul, Manisha Jana</i>	271
	• Evolution of UCAs 271 • Technique of CEUS 273 • Safety of UCAs 273	
	• Diagnostic Applications of UCAs 273	
<b>Chapter 19</b>	Iodinated Contrast Media: An Update <i>Chandrashekhar SH, Thulkar S</i>	289
	• History of Development of ICM 289 • Basic chemistry of ICM 290	
	• ICM Pharmacokinetics 292 • Future of ICM 295	
<b>Chapter 20</b>	Contrast Reactions and Its Management <i>Gaurav Pradhan, Rajat Jain</i>	297
	• Types of Adverse Reaction 297	

**SECTION 6 MISCELLANEOUS**

<b>Chapter 21</b>	Picture Archiving and Communication System and Radiology Information System <i>Shivanand Gamanagatti, Devasenathipathy Kandasamy, Arun Kumar Gupta</i>	309
	• Picture Archiving and Communication System 309 • Radiology Information System 317	
<b>Chapter 22</b>	Evidence Based Radiology <i>Sanjay Sharma, Manisha Jana</i>	319
	• Background 319	
<b>Chapter 23</b>	Radiation Hazards and Radiation Units <i>Pratik Kumar, Anil K Pandey</i>	329
	• Radiation Hazards 329 • Damage to DNA by the Radiation 330 • The Effect of Radiation 330	

<b>Chapter 24</b>	Radiation Protection	338
	<i>Sapna Singh</i>	
	• Historical Perspective 338 • Radiation Units 339 • Specific Quantities and Their Associated Units 339 • Biological Impact 339 • Interaction of Radiation with Matter 340 • Biological Effect of Radiation 342 • Classification of Radiation Injury 342 • Deterministic Effects as Documented from Radiation Accidents 343 • The Regulatory Bodies 343 • Protection Against Radiation Hazard 345 • Cardinal Principle of Radiation Protection 346 • Safety of Radiographic Imaging During Pregnancy 350 • Recommended Dose Limits to Pregnant Women 351 • Radiation Detection and Measurement 351 • Personnel Dosimetry 352	
	• Computed Tomography (Radiation Exposure and Dose Modulations) 353 • Typical Dose Measurements 354 • Using Automated Exposure Control 356 • Modifying the Acquisition Parameters 356 • Iterative Reconstruction 356	
<b>Chapter 25</b>	Planning a Modern Imaging Department	359
	<i>SC Bansal, Niranjan Khandelwal, Ajay Gulati</i>	
	• Planning and Organization 359 • Location 360 • Layout 360 • Equipment 360	
	• Mammography 363 • Computed Tomography 364 • Ultrasound 365 • Picture Archiving and Communication Systems 368 • Safety Standards and Quality Assurance 369 • Teleradiology 370	
<b>Chapter 26</b>	Recent Advances in PET/CT and PET/MR	373
	<i>Rakesh Kumar, Anil Chauhan</i>	
	• PET/CT 373 • PET/MR 381	
<b>Chapter 27</b>	Common Drugs Used in an Imaging Department	392
	<i>Anupam Lal, Vivek Gupta, Manphool Singhal</i>	
	• Drugs for Patient Preparation 392 • Drugs used for Optimizing Imaging Evaluation 393	
	• Drugs Affecting Coagulation 395 • Sclerosants and Embolic Agents 398 • Gelatin Foam 398 • Polyvinyl Alcohol 398 • Tris-Acryl Gelatin Microspheres 399 • N-Butyl-2 Cyanoacrylate 399 • Ethylene Vinyl Alcohol Copolymer 400 • Absolute Alcohol 400	
	• Sodium Tetradecyl Sulfate 400	
<b>Chapter 28</b>	Molecular Imaging	402
	<i>Anish Bhattacharya, BR Mittal</i>	
	• Molecular Imaging Probes in Nuclear Medicine 402 • Clinical Applications of Nuclear Molecular Imaging 403 • Central Nervous System Disorders 404	
	• Cardiovascular Disorders 405 • Infectious and Inflammatory Processes 406	
<b>Chapter 29</b>	Ethical and Legal Issues in Radiology	409
	<i>Mandeep Kang, Manavjit Singh Sandhu</i>	
	• Ethical Issues 409 • Doctor-Patient Relationship 409 • Radiation Issues 410	
	• Legal Issues 411 • Laws/Legal Acts Applicable to Medicine 412	
	• Teleradiology: Who is Responsible? 415	
<b>Index</b>		417

## Section

# 1

# Advances in Ultrasound Imaging

**Chapter 1** • Ultrasound Instrumentation: Practical Applications

*Kushaljit Singh Sodhi, Akshay Kumar Saxena, Mukesh Kumar Yadav*

**Chapter 2** • Image Optimization in Ultrasound

*Rashmi Dixit*

**Chapter 3** • Ultrasound Elastography: Principles and Application

*Veenu Singla, Tulika Singh, Anindita Sinha*



## Chapter

# 1

# Ultrasound Instrumentation: Practical Applications

*Kushaljit Singh Sodhi, Akshay Kumar Saxena, Mukesh Kumar Yadav*

## INTRODUCTION

Ultrasonography in the last few decades has undergone massive transformation and today occupies a crucial role in practice of most of the domains of medicine. Advances in ultrasound technology include enhanced spatial, vascular and contrast resolution, besides encompassing various therapeutic options. New transducers and emerging imaging paradigms allow real time acquisition of large field of views and even three dimensional volumetric data. In sonography, transducer, is the central component, which is responsible for both, generation of ultrasound beam and detection of returning echoes.<sup>1</sup> It is the changes in the generation of echo signals, its reception, analysis and display that helps to differentiate one scanner from another.<sup>1</sup> Its safety, portability, low cost, and real time application makes it one of the most widely used imaging modalities. This section provides a brief overview of practical aspects of ultrasound instrumentation.

## MACHINE CONTROLS

In this section we shall briefly talk about some of the most frequently used functions of the ultrasound machine (**Figs 1A and B**). It is of course recommended that all sonologists learn the different capabilities of their own equipment to optimize image quality and diagnosis.

- **Keyboard:** Various capabilities as provided by manufacturer
- **Transducer select:** To chose one of the many transducer probes attached to the transducer ports on the ultrasound machine

## FREQUENCY OF TRANSDUCERS

Transducer frequency can vary from 2.0 to 16.0 MHz and its selection is primarily based upon patient's body habitus and the region to be scanned.<sup>2</sup>

### *High Frequency Transducer*

- Frequency range of 7.0 to 14.0 MHz
- Linear transducer mostly, sector transducer more suited for children
- Provides increased resolution of images, however, with reduced penetration
- Linear probes best for evaluation of superficial structure like, thyroid, scrotum, etc.

### *Medium Frequency Transducer*

- Frequency range of 3.0 to 5.0 MHz
- Curvilinear or sector transducers
- Most commonly used probe for adult abdominal imaging.

### *Low Frequency Transducer*

- Frequency of 2.0 MHz
- Transducer is sector type
- Provides increased depth of penetration but also results in loss of resolution
- More suited for ultrasound studies of obese patients<sup>2</sup>



**Figs 1A and B** Modern ultrasound scanning unit with LCD screen

- **Overall gain control:** This is used to amplify all received signals equally.
- **Time gain compensation:** This is used to balance for attenuation of the ultrasound beam in the scanned tissue.<sup>2</sup> With time gain compensation, a depth-dependent gain is applied to the echoes; with echoes that originate deeper in tissue (which are attenuated to a larger degree) have much larger gain factors than those echoes which originate close to the transducer.<sup>2,3</sup> Simply put, echo signals from deep structures are amplified more than signals from shallow structures. This process thus results in producing equally reflective structures to be displayed in B-mode image with the same brightness, regardless of their age. Time gain compensation is controlled in most machines using a set of 6 to 10 gain knobs, each adjusting the receiver gain at a different depth.
- **Near and far gains:** These controls are used to equalize the differences in echoes received from various depths as they are displayed on the screen. When compensating for sound attenuation, the near to far gain controls (usually slide pods) should be gradually increased.<sup>2,3</sup>
- **Compression:** This is used to vary the amplitude range (dynamic range) of echoes displayed as shades of gray on the image. Most of the ultrasound machines apply logarithmic compression to the echo signals emerging from the receiver; amount of compression is under operator control.<sup>2</sup>
- **Depth:** This control is used to adjust the size of the image so that organs and adjacent structures or regions of interest are equally well visualized.
- **Focal point(s):** A control that has one or more toggle buttons. This allows the operator to choose the level at which the ultrasound beam is focused to increase the resolution at a specific point or points. This control

should be set at the most posterior aspect of the organ or structure being imaged.<sup>2,3</sup>

- **Postprocessing:** This can be used to change the appearance of echo signals, already stored in memory, on the image. Various postprocessing applications are available; each emphasizes different portions of the echo amplitudes stored in the image memory.
- Failure to properly adjust the gain control and/or poor placement of focal point during scanning may result in suboptimal image quality and misdiagnosis.

## TYPES OF TRANSDUCERS

Ultrasound scanners automatically scan ultrasound beam using transducers consisting of array of many narrow piezoelectric elements.<sup>3</sup> Array may be made up of as many as 128 to 196 elements.<sup>4</sup>

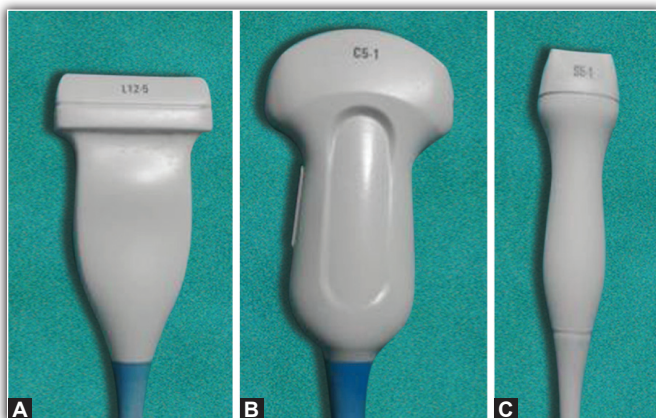
Ultrasound transducers convert mechanical energy into electrical energy and produce images that can be displayed subsequently in variety of formats. These can be of following types (Figs 2A to C).

### Linear Array Transducer

Linear array transducers are optimal for superficially placed structures, such as vessels, neck, testes. In this, final image is displayed as a rectangle. In a linear array, each time only a group of elements work together to transmit or receive.<sup>2,5</sup> The ultrasound beam is perpendicular to the transducer surface, centered over element subset and scans a rectangular area. Size of the field of view is equal in both the far field (area of penetration farthest away from transducer) and near field (area of penetration closest to transducer).<sup>2</sup>

### Curvilinear Array Transducer

These are commonly used for routine abdominal and pelvic imaging. In curvilinear array transducer, array of elements instead of a straight line (linear array) are arranged across a



**Figs 2A to C** Photograph showing various types of transducers: linear (A), curvilinear (B) and sector (C) array transducer

convex arc.<sup>2,5</sup> This fan like arrangement of elements results in a sector shaped imaging field. Compared to linear array, curved array provides a wider image at large depths (field of view is wide in far field than near field) from a narrow scanning window.

### Phased Array Transducer

In contrast to linear and curved arrays, all the elements work together in phased array (all elements are used for each beam line).<sup>5</sup> Phase array steer the beam by applying different delay on each element, and it requires small acoustic window. Its main advantage is in providing a very broad imaged field at larger depths that too with a narrow transducer footprint. It is widely used in cardiac scanning as the transducer fits easily between the ribs (rib gap is a small acoustic window).

### Doppler

The Doppler effect was first proposed by Christian Doppler, an Austrian physicist, in 1843.<sup>6</sup> According to this effect, if there is relative motion between an object and an observer (receiver), the frequency of sound wave perceived by the observer (receiver) is different from that emitted/reflected by the object.<sup>5,6</sup>

In diagnostic radiology, Doppler effect is utilized to detect blood flow in peripheral vessels (e.g. lower limb) as well as those supplying different organs (renal artery, portal vein, etc.). The information provided by a Doppler examination includes presence or absence of blood flow, direction of blood flow, type of blood flow (arterial high resistance/venous, presence and quantification of arterial stenosis etc.).<sup>2</sup> The difference in emitted frequency and received frequency is called the Doppler shift and is given by the equation:<sup>6</sup>

$$\Delta v = 2 v S \cos \theta / V$$

where  $\Delta v$  = frequency change (Doppler shift)

$v$  = frequency of original beam

$S$  = velocity of blood

$V$  = velocity of sound (1540 m/sec)

$\theta$  = angle between the direction of blood flow and sound beam

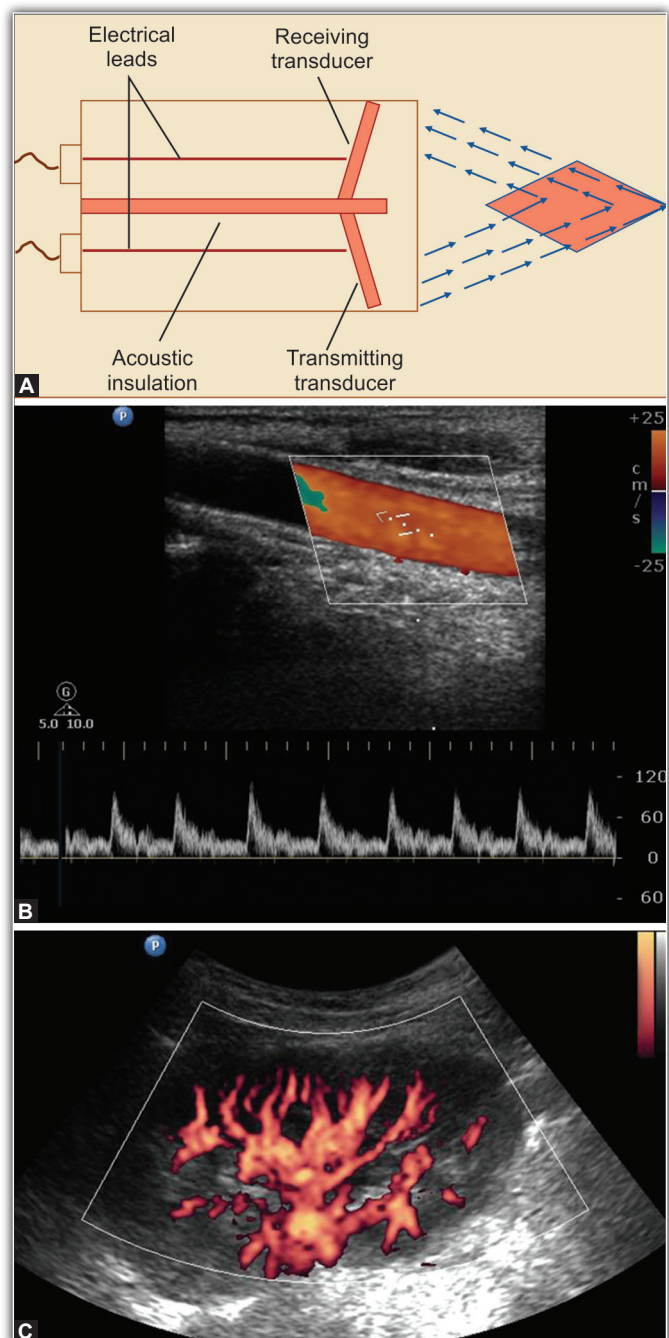
In clinical practice, three different Doppler techniques are utilized. Continuous wave Doppler is used for evaluation of peripheral vessels and the fetal heart. It provides information regarding the blood flow but lacks information regarding the depth from which the Doppler signal is coming from. Pulsed Doppler provides information regarding the presence, direction and depth from which the Doppler signal is coming from. Power Doppler is useful for the evaluation of slow flow.

The basic transducer for continuous wave Doppler contains an oscillator, two piezoelectric crystals and a demodulator (Fig. 3A).<sup>6</sup> One of these crystals acts as the transmitter while the other acts as the receiver. Both of these crystals work continuously. The two crystals are inclined at

an angle to each other. The purpose of inclining the crystals is to cause overlap between the beam regions of the transmitter and receiver which in turn increases the sensitivity for detecting the returning signal (beam). The oscillator provides electrical voltage at the resonant frequency of the transducer which is converted into the transmitted ultrasound beam by the transmitter. The beam, after reflection, is received by the receiver piezoelectric crystal. The frequency of received beam is different from the transmitted frequency because of Doppler shift. The received signal is amplified and fed into the demodulator which also receives signal from the oscillator. The comparison of signals from the oscillator and received beam provides Doppler shift signal. The demodulator can also detect whether the received beam has frequency higher or lower than the transmitted frequency which provides information regarding the flow of blood towards or away from the transducer. It is important to note that apart from the moving blood, the moving vessel wall also generates Doppler shift. However, it has low frequency. The machines are equipped with circuits which filter off such low level frequencies and ensure that the signal from moving vessel wall does not hamper the evaluation of blood flow.<sup>8-11</sup>

The problem with continuous wave Doppler is that all the moving objects within the sonographic beam contribute to frequency shift. Thus, the observer cannot ascertain the depth from which the signal originates. This problem can be overcome by the use of pulsed Doppler. In this technique, very short bursts of the sound wave are repetitively emitted by the transducer. However, a new pulse is not emitted till such time the returning signal from the previous pulse is detected by the transducer. The receiver is designed to be turned on for a short period on at a specific moment. The time at which receiver is turned on (or gated on) provides the information regarding the depth at which the signal originated. The duration for which the receiver (or the gate) is turned on determines the axial length of the beam over which the signal is received. A combination of real time imaging and pulsed Doppler is known as Duplex Doppler.

Although pulsed Doppler and duplex scanners provide information regarding the depth from which Doppler signal originates, it is limited to a very small region of the image. As a result, the sonologist needs to sample large number of areas to evaluate the entire vessel. This limitation is overcome in the color flow Doppler imaging. Recall that in pulsed (and duplex) Doppler, the depth from which Doppler signal is recorded is determined by the time lag (after emission of sound beam) after which the gate is opened to receive the signal.<sup>9,10</sup> Use of multiple gates, which open after different time lags, allows detection of depths of multiple Doppler signals. A modification of this principle is utilized in color flow imaging where in electronically steered (phased array) transducers are used to detect signals at different depths of a real time image. Thus, the signal can be detected from the vessels as well as surrounding tissues. The Doppler signal is



**Figs 3A to C** Components of a typical Doppler ultrasound transducer (A), Color Doppler scan of common carotid artery (B) and Power Doppler image showing normal Doppler signals in kidney (C)

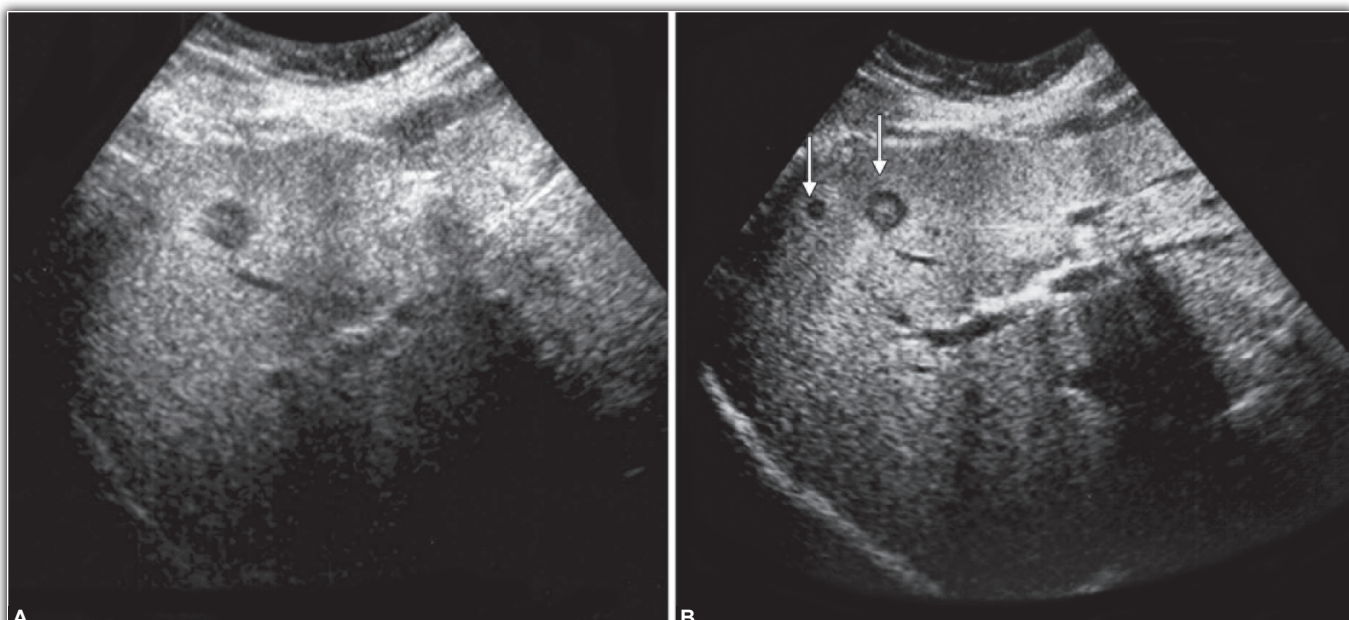
assigned color proportionate to the strength of the Doppler signal. The superimposition of such colored information on the gray scale image generates the color flow image.

Pulsed Doppler does not provide information regarding the intensity (or power) of the Doppler signal. This

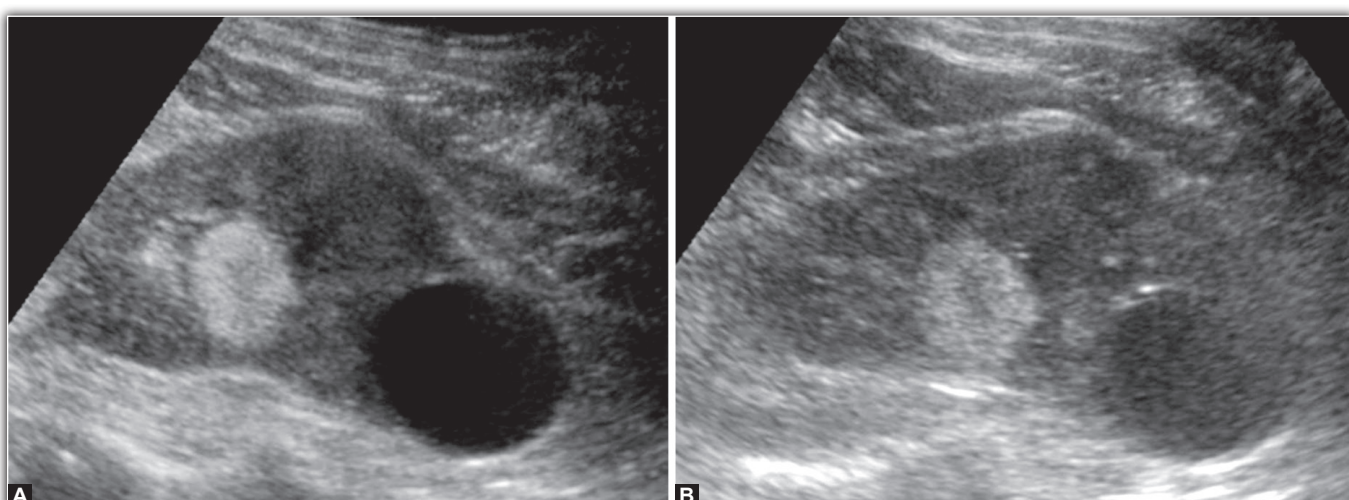
information can be obtained in the power Doppler mode which displays the power (or intensity) of the Doppler signal, as it changes with time in every region within the chosen area. Higher intensity Doppler signals are imparted lighter hue of color. However, there is no information available regarding the velocity. The power Doppler has superior flow sensitivity as compared to conventional color Doppler and is used to evaluate the presence and characteristics of the flow in blood vessels that are poorly imaged with conventional color Doppler (**Figs 3B and C**).<sup>7,11</sup>

### Tissue Harmonic Imaging

Tissue harmonic imaging (THI) is a grayscale ultrasound mode that provides images of higher quality than conventional sonography by using information from harmonics (which are generated by nonlinear wave propagation of ultrasound in tissue).<sup>12-15</sup> Harmonics are produced by tissue vibration and are usually integral multiples of the transmitted frequency. In conventional grayscale sonography, the same frequency spectrum that is transmitted into the patient is subsequently



**Figs 4A and B** Comparison of conventional gray scale imaging (A) with tissue harmonic imaging (B) THI clearly demonstrates target lesions (indeterminate on conventional) in a metastatic liver disease. Also note that additional lesions are also detected at THI



**Figs 5A and B** Tissue harmonic imaging (A) demonstrates much better delineation of both cystic and solid lesions in this patient of Renal angiomyolipomas, when compared to conventional grayscale imaging (B)

received to produce the sonographic image. In THI, however, higher harmonic frequencies (multiples) generated by the propagation of the ultrasound beam through tissues are used to produce the image. Currently, only the second harmonic, or twice the fundamental frequency, is used for imaging. Tissue harmonic imaging has a huge potential for improving image quality because it gives improved lateral resolution, reduced side lobe artifacts and improved signal to noise ratio.<sup>12,16</sup>

The higher harmonic can also be used but extremely wide bandwidth transducers would be required.<sup>14</sup> In THI, it is the reduced width of the ultrasound beam that improves lateral resolution (more harmonics are produced at the center of a pulse than at the periphery). Increased lateral resolution improves the ability to resolve small anatomic structures and detail. Harmonic imaging is especially useful in obese patients because of reduction in deleterious effects of body wall. Intensity of harmonic waves generated depends on the non-linearity coefficient of the tissue insonated. Body tissues with a higher amount of fat have the highest non-linearity coefficients, which increase the intensity of harmonic waves generated, thus improving lesion visibility in obese patients, whose body walls typically contain an elevated proportion of fat.<sup>12,16,17</sup>

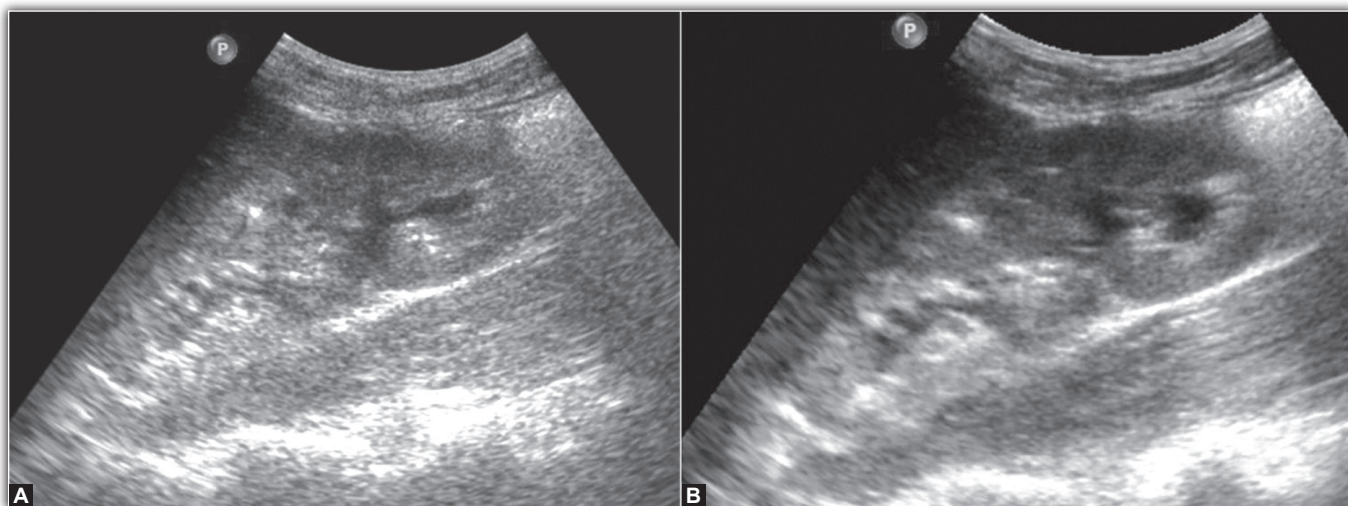
Side lobe artifacts result when the ultrasound beam hits an interface and is reflected back to the transducer, producing artifactual echoes. Reduction in side lobe artifacts improves the signal-to-noise ratio, resulting in an image in which tissues appear brighter and cavities appear darker. Harmonics are generated deep in relation to the body wall and because they are produced in tissues, they pass through the body wall only once, leading to decreased artifacts from the body wall.<sup>18-20</sup>

Although better demonstration of cystic structures by THI has been emphasized, authors have now observed that tissue harmonic imaging provides additional information in both solid and cystic lesions<sup>12,18</sup> (**Figs 4 and 5**). Harmonic imaging increases diagnostic confidence in differentiating cystic from solid hepatic lesions, improves detection of gallbladder and biliary calculi, improves pancreatic definition and allows distinction of simple from complex renal cysts.

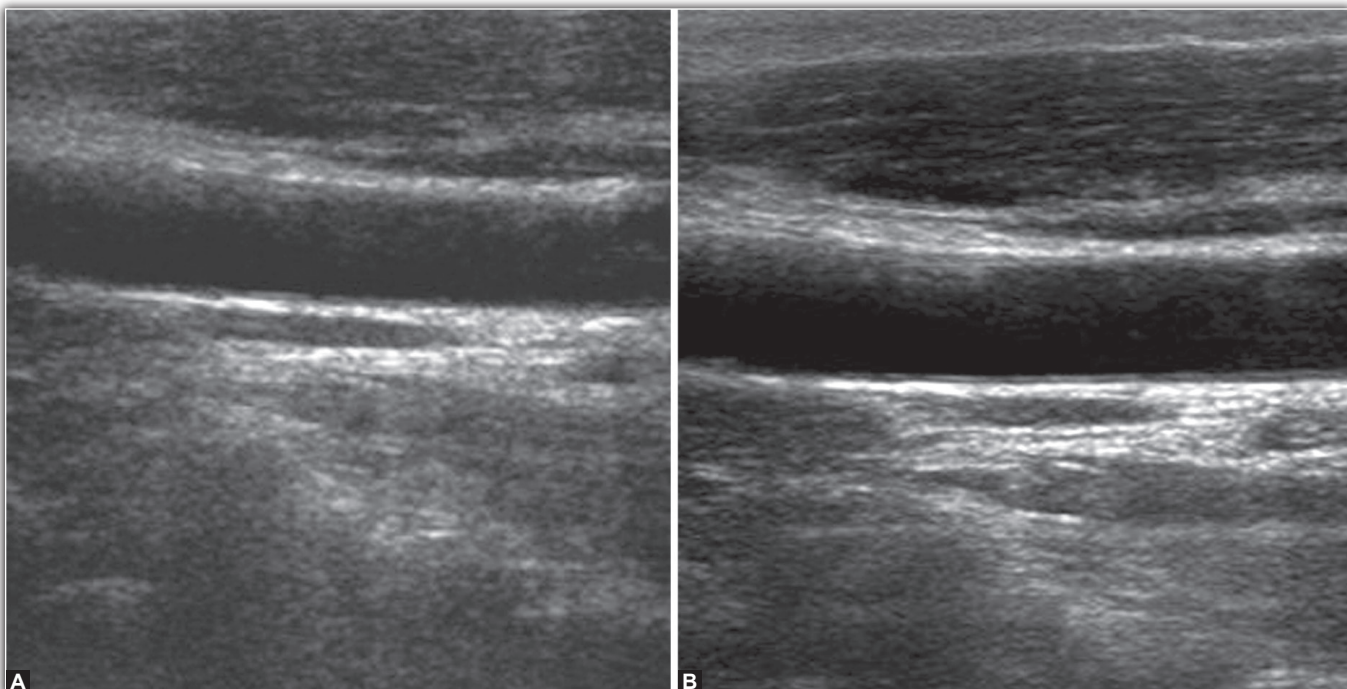
Another harmonic technique, known as 1.5 harmonic imaging has also been described.<sup>21</sup> This detects and visualizes signals that are a factor of 1.5 times higher than the fundamental center frequency of the transducer and are intermediate between the fundamental and the second harmonic frequency spectrum.<sup>21,22</sup> Obvious advantage is that this frequency range is nearly free of tissue echoes and only contains microbubbles echoes. Hence, it is featured with contrast improvement between tissue and microbubbles of 20dB or more compared to the second harmonic technique.

### Spatial Compound Imaging

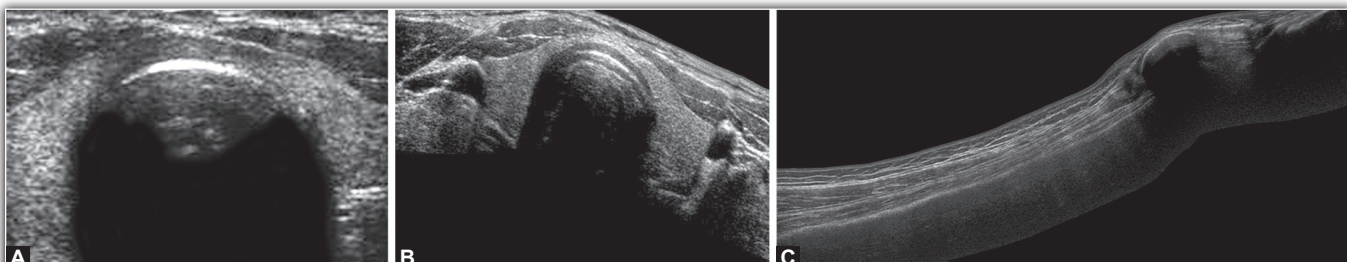
Spatial compound imaging is a speckle reducing ultrasound technique, which uses electronic steering of ultrasound beams from a transducer array to obtain overlapping scans of a target object from different angles (same tissue is imaged many times by using parallel beams directed along different directions).<sup>3,23</sup> Resulting echoes from these multiple acquisitions are then averaged to produce a single compound image of improved quality due to reduction in image speckle. When compared to conventional B-mode imaging, in compound imaging, more time is required for acquisition of data (as here multiple ultrasound beams are used to evaluate same tissue) and frame rate is also reduced. Spatial compound imaging demonstrates reduced level of speckle,



**Figs 6A and B** Spatial compound imaging in a patient with nephrocalcinosis. Note medullary hyperechogenicity is not well appreciated on conventional grayscale mode (A), but is clearly demonstrated on compound imaging (B)



**Figs 7A and B** Spatial compound imaging in carotid vessels helps clear depiction of intima-media thickness for accurate measurements. (A) refers to conventional grayscale while (B) refers to compound imaging



**Figs 8A to C** Extended field of view. Routine grayscale mode (A) is able to demonstrate only limited part of thyroid in a single image, while extended field of view mode (B) clearly demonstrates the composite image showing both lobes of thyroid, isthmus besides cervical vessels in a single image. Extended field of view (C) demonstrates quadriceps tendon, patella and patellar tendon in a single image

noise, refraction, reduced shadowing and enhancement artifacts and improved contrast and margin definition<sup>3,23,24</sup> (**Figs 6 and 7**).

Application of spatial compound imaging has been described in imaging of breast, peripheral vessels, and musculoskeletal system. It can also be combined with other ultrasound applications, e.g. harmonic imaging.

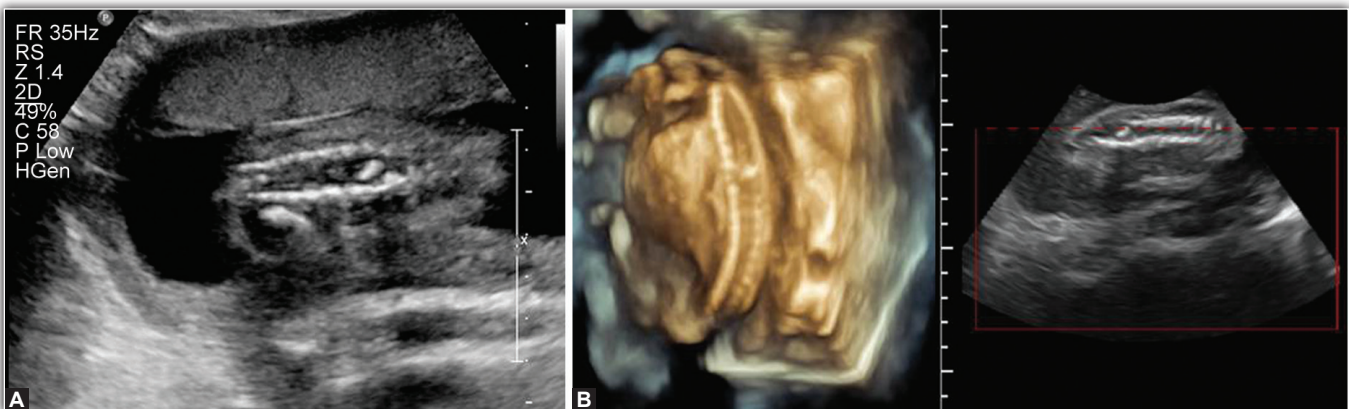
### EXTENDED FIELD OF VIEW

This technique available in most of the new scanners allows sonologists to visualize large anatomic regions in a single image. It can be performed on superficial structures with a linear array transducer or abdominal structures using a curvilinear probe, although most of its applications are in

superficial structures.<sup>3,23</sup> Extended field of view imaging, also called panoramic imaging in some machines allows easy measurements of large lesions/structures and exact delineation of anatomical relationships in a single image (**Figs 8A to C**). Transducer is initially moved laterally across the anatomic area of interest and multiple images are acquired from many transducer positions.<sup>3</sup> Images are registered with respect to each other. This registered data is subsequently combined to form one complete large field of view image.

### Elastography

Imaging of tissue stiffness or elasticity is one of the rapidly evolving ultrasound based application. It is based on the fact that stiffness of tissue tends to alter with disease and can be



**Figs 9A and B** (A) Transabdominal sonographic coronal 2D image showing bony spur in a case of diastematomyelia, (B) is corresponding 3D image showing the bony spur

imaged by measuring the tissue's distortion (strain) under an applied stress (compression from ultrasound transducer).<sup>23</sup> Images produced may be in grayscale, color or both. Although most of its initial application has been carried out in the breast, it is now increasingly being evaluated in diagnosis of complex cysts, liver cirrhosis, characterization of thyroid nodules and metastatic lymph nodes.<sup>25</sup>

More details on elastography are provided in next chapter in this book.

### 3D and 4D Ultrasound

3D ultrasonography or volume sonography is the imaging technology which involves acquiring a large number of data sets of 2D images from patient. After acquisition, this volumetric data can be qualitatively and quantitatively assessed with the use of many analysis tools such as surface and volume rendering, multiplanar imaging and volume calculation techniques, etc. Hence similar to other cross sectional imaging like CT and MRI, the volumetric data of this 3D ultrasound can also be 'post-processed'. Because of volume imaging it is possible to display information in any orientation and any of the planes. If the 3D ultrasound is acquired and displayed over time, it is termed as 4D ultrasound, live 3D ultrasound or real time 3D ultrasound.<sup>26</sup>

Currently there are two commonly used techniques to acquire 3D volumetric data - free hand technique and automated technique. In the free hand technique the examiner requires to manually move the probe within the region of interest. In the automated technique dedicated 3D probes (also called volume probes) have to be used. In this method probe is held stationary and on activation the transducer elements within the probes automatically sweep through the 'volume box' which has been selected by the operator. The resultant images are digitally stored and can be 'processed' later in various display modes for analysis.<sup>27</sup>

It is perceived that the potential of 3D and 4D ultrasound has not been fully utilized till now. It is still being used as

problem solving tool although it can be incorporated in routine day to day practice. There are numerous areas in which the use of 3D and 4D can be very useful (**Figs 9A and B**). Few of these are as follows:<sup>26</sup>

### Gynecology

1. For assessment of congenital anomalies of uterus<sup>28,29</sup>
2. For evaluation of endometrial and uterine cavity (can also be done with saline infusion sonohysterography)
3. For preprocedure localization of fibroids for planning myomectomy
4. For evaluation of possible cornual ectopic pregnancies
5. For exact delineation of intrauterine device location and type
6. For imaging of adnexal lesions for better differentiation of ovarian lesions from tubal or uterine lesions
7. Three dimensional guidance for interventional procedures
8. Evaluation and follow-up of patients of polycystic ovaries and tubal occlusion for infertility work-up.

### Obstetrics

1. For evaluation of facial anomalies like cleft palate and cleft lip
2. Evaluation of nasal bone, ears and cranial sutures
3. Detection of central nervous system anomalies like corpus callosum agenesis and Dandy-Walker cyst
4. For evaluation of ribs and intrathoracic masses
5. For evaluation of spine, e.g. vertebral abnormalities, neural tube defect,<sup>30,31</sup> diastematomyelia (**Fig. 9**), etc.
6. For evaluation of extremities like club feet and skeletal dysplasia, etc.
7. For evaluation of heart, placenta and umbilical cord
8. For evaluation of multiple gestations for mapping of vasculature for twin transfusion syndrome
9. Telemedicine and education

10. Storing volumetric data for subsequent interpretation and review
11. For quality control by way of central monitoring, e.g. procedures done at different peripheral sites and in multicenter research studies
12. Teaching postprocessing techniques and standardized views to residents.

Studies have suggested that the mothers who are viewing the 3D images of the babies feel enhanced bonding with their fetus.<sup>32</sup>

With the use of 4D ultrasound many facial expressions such as yawning, tongue protrusion, mouth opening, eye opening and blinking, etc. can also be studied in greater details.<sup>33-35</sup> 4D ultrasound has also been used in the evaluation of fetal heart.<sup>36-38</sup>

Three dimensional images are very useful for demonstrating the abnormality to the referring physician as these images are better comprehended by those who are not tuned to understand grayscale format of 2D images. Similarly storage of 'volume' data allows us to reprocess the data in future for subsequent interpretation or reviews. These volume data can be sent to remote workstations for telemedicine and teaching purposes. It has also been shown in a few studies that acquisition of 3D data needs less time which can potentially increase patient through put and increase efficiency of the imaging department.<sup>39</sup>

#### *Limitations*

As 3D ultrasound information is dependent on reformation of acquired 2D ultrasound data, it is expected that the problems

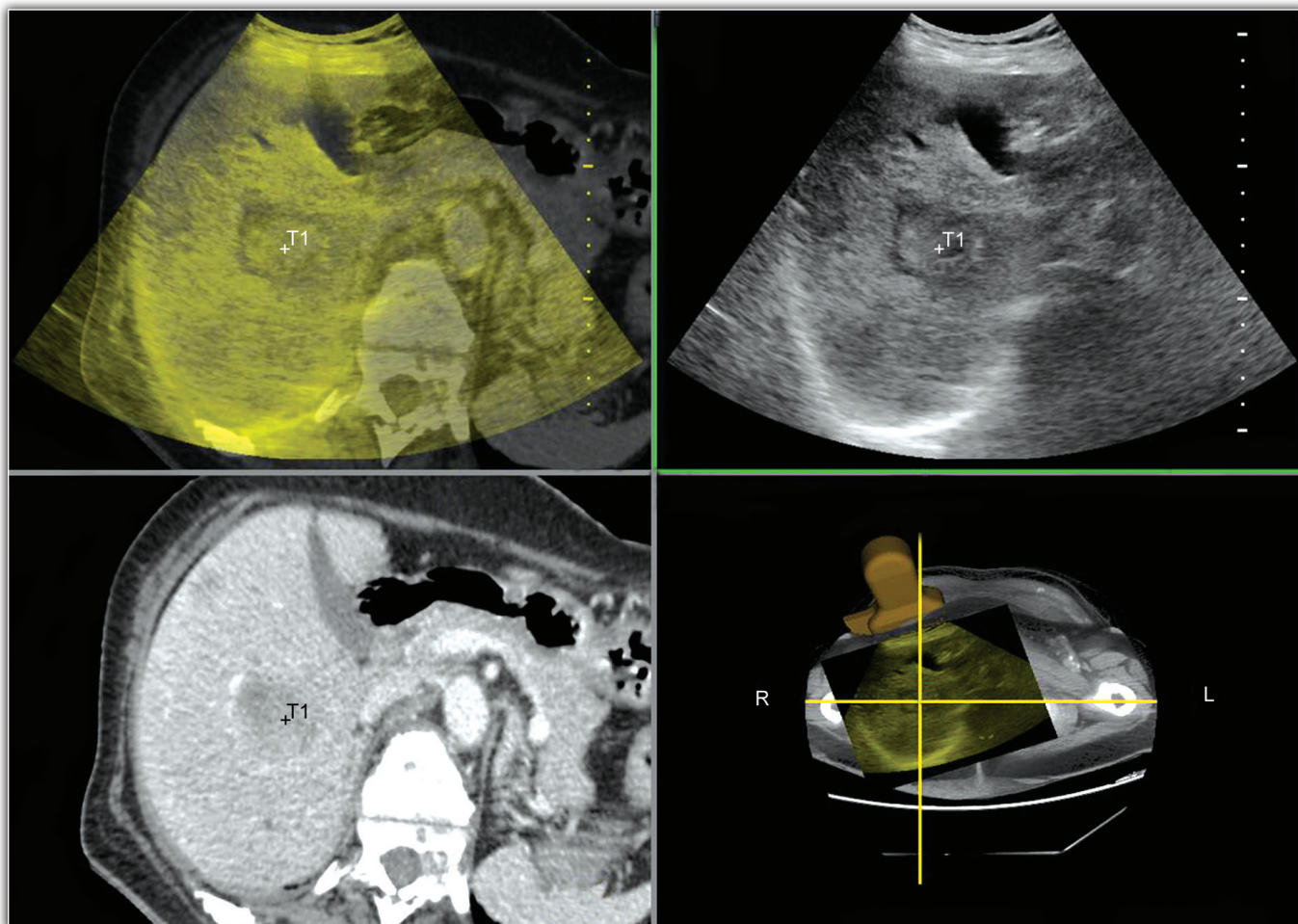


**Fig. 10** Figure shows application of fusion imaging on a patient with well visualized lesion on both CT as well as on USG. Four split images seen on the screen. Image in lower left corner is a previously acquired CT images feeded in ultrasound machine. On moving the ultrasound transducer, there will be automatic reformation of these feeded images corresponding to the axis of ultrasound transducer so that the same imaging plane is matched to the ultrasound image. Right upper corner is current sonographic image. Image in left upper corner is an overlay image showing good matching of the lesions from sonographic and CT images. Right lower image shows the 3D view which is being displayed during the fusion work flow

which affect the 2D ultrasound like motion, unfavorable body habitus, shadowing artifacts and suboptimal scanning techniques also result in poor quality 3D images.<sup>27</sup>

### Fusion Imaging

Fusion imaging or hybrid imaging means combination of two imaging techniques. This can be in the form of fusion of two anatomical techniques like ultrasound with MRI or CT; or it can be fusion of anatomical technique (ultrasound, CT or MRI) with molecular imaging technique like SPECT or PET (**Fig. 10**). One example of fusion imaging is real time virtual sonography (RVS).

To obtain virtual fusion images, an initial step is to transfer the previously acquired CT or MRI data to the ultrasound machine.<sup>40</sup> A point like magnetic positioning sensor unit is attached to the ultrasound probe to detect any change in position of probe during investigation. The transmitter of this sensor unit is placed onto the surface of patient. During examination ultrasound screen is seen as split images with virtual reconstructed CT/MR image on one side and currently acquired USG image on other side of the screen. An attempt is made to match these two images with each other. This is usually done by freezing the CT or MR section with some clearly visible anatomic landmark (e.g. portal vein bifurcation, superior most margin of kidney or the lesion itself, etc.) and identifying the same landmark by freehand USG.<sup>41</sup> Then these two images are matched. The real time USG image can also be superimposed on the virtual reconstructed CT image with adjustable difference in the grayness (**Fig. 10**).

### CLINICAL APPLICATIONS OF FUSION IMAGING

It has been observed that there are few lesions/tumors in liver which are iso-echoic and hence not well appreciable on gray-scale ultrasound. Similarly there are subgroups of patients who have been treated with either TACE or RFA and now there is recurrence in the vicinity of the primary tumor site. These lesions are also poorly localized on grayscale USG. Hence detection by USG or further biopsy/ treatment by the local ablative therapies were difficult for such lesions. These lesions are usually clearly visible on contrast enhanced CT/ MR. However interventional treatment is usually easier to perform with USG guidance which also avoids radiation to the operator. The RVS combines the advantages of both imaging techniques.<sup>42</sup> In one way this technique provides real time visualization of the needles in pre-procedural CT scan images. The feasibility of RVS module has been proven in many studies.<sup>43-45</sup> The RVS module has been shown to be compatible with B mode, color Doppler mode as well as with harmonic imaging mode.<sup>46</sup> However the data on accuracy and efficacy of this technique are still emerging.<sup>47</sup>

### Limitations

Real time virtual sonography (RVS) cannot be used in those patients in whom CT/MRI are contraindicated (e.g. contrast allergy, renal failure, metallic implants, etc). Another limitation is that sometimes the best synchronization is not achievable hence limiting the utility.<sup>46</sup> It definitely prolongs the examination time and it is more expensive as it adds the cost of CT/MRI also.

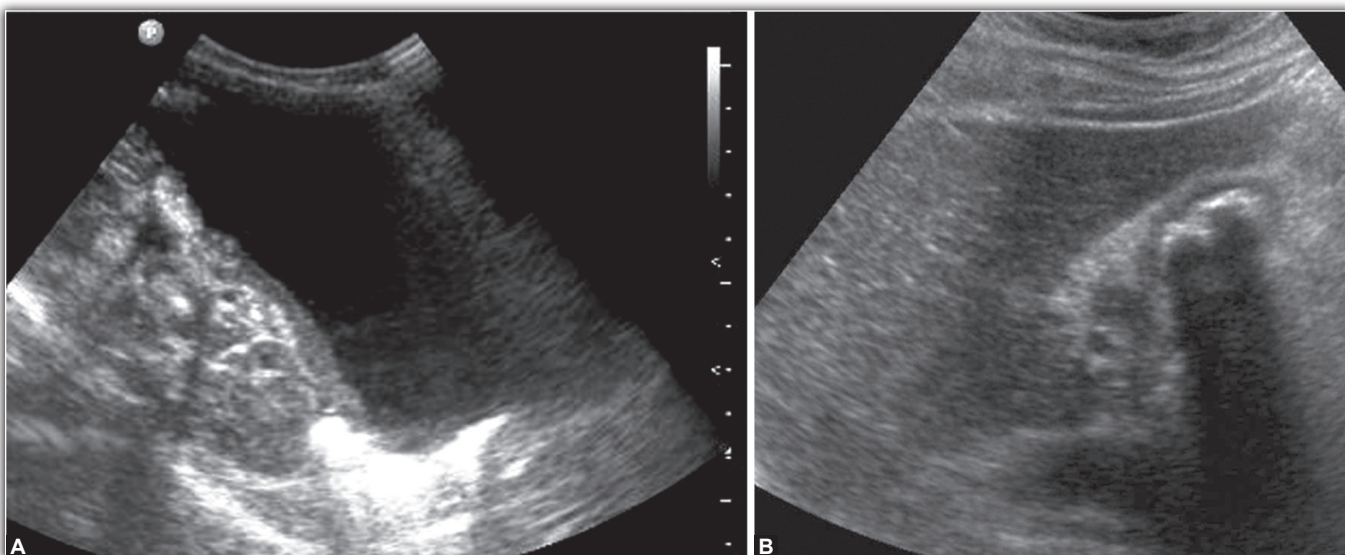
### Therapeutic Applications of Ultrasound

- Ultrasound guided aspirations, drainages and biopsies form the backbone of any interventional radiology unit. With the help of ultrasound, one can easily track the needle path and perform any such interventional procedure easily. Not only it is noninvasive, radiation free, portable modality, it also offers a real time navigation facility to the interventionists.
- **High intensity focused ultrasound (HIFU):** High intensity focused ultrasound is rapidly emerging as a noninvasive method for tumor ablation. In this, high intensity ultrasonic waves are focused at a focal lesion with high accuracy, resulting in an lethal elevation of temperature at the desired target site, with resultant damage of the tumoral cells.<sup>48</sup> Simply put, transducers help to thermally ablate tumors without introducing needles or wires into the tumor.<sup>49</sup> High intensity energy is absorbed and converted into heat at the focal lesion. This heat raises the temperature causing coagulative necrosis at the site.<sup>50</sup>

It is guided by real time ultrasound imaging and can be run by one of several transducers with focal lengths varying from 90 to 160 mm. Although choice of transducer would depend upon depth of the target lesion, the most commonly used transducer is the one with a focal length of 135 mm and operating frequency of 0.8 MHz.<sup>48,49</sup> Presently, HIFU is used for ablation of both benign and malignant tumors. It's most common applications worldwide are in the treatment of uterine fibroids, liver tumors and prostate cancer. Apart from these, it has also been used in the ablation of breast, bone, pancreas and soft tissue tumors.

### Ultrasound Based Molecular Imaging and Oncotherapy

Ultrasound molecular imaging, which is based on the use of molecularly targeted contrast agents, combines the advantages of contrast enhanced ultrasound with the ability to characterize neoplastic processes at a molecular level.<sup>51</sup> Ultrasound molecular imaging has enormous potential applications, which can range from early cancer detection and tumor characterization to monitoring treatment response and guiding cancer therapies.<sup>51,52</sup> There is also potential role for ultrasound contrast agents in improved delivery of



**Figs 11A and B** Ultrasound image artifact shadowing (A) and enhancement (B) in two different patients. (A) Demonstrates shadowing with gallbladder calculi and (B) demonstrates enhancement from a large abdominal cystic lesion

chemotherapeutic drugs and gene therapies across existing biological barriers. Most of the preclinical studies have used contrast micro bubbles, which are emulsions (gas-liquid) of several micrometer in size, confined to intravascular space. Much smaller newer nanoparticles are currently being investigated for future application.

### Ultrasound Image Artifacts

Image artifacts on ultrasound are commonly seen in day to day clinical ultrasound practice. Some artifacts are generated by the physical limitations of the modality while some arise secondary to improper scanning technique. Artifacts can interfere with image interpretation. Ultrasound artifacts can be understood with a basic appreciation of the physical properties of the ultrasound beam, the propagation of sound in matter, and the assumptions of image processing.<sup>53</sup> US artifacts often arise secondary to errors inherent to the ultrasound beam characteristics, the presence of multiple echo paths, velocity errors, and attenuation errors. The beam width, side lobe, reverberation, comet tail, ring-down, mirror image, speed displacement, refraction, attenuation, shadowing, and increased through-transmission artifacts are encountered routinely in clinical practice.<sup>53</sup> The ability to recognize and correct potentially correctable ultrasound artifacts is important for patient care and image quality improvement.

*Ultrasound artifacts can be grouped under:*

1. **Resolution related artifacts includes:** Speckle in conventional ultrasound imaging results from the use of phase-sensitive transducer and occurs when structure

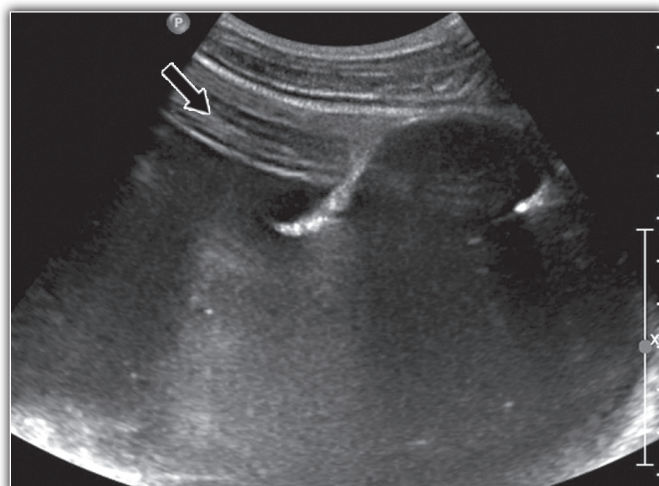


**Fig. 12** Reverberation artifact (arrow) at anterior part of grossly hydronephrotic kidney

in the object is on a scale too small to be resolved by the imaging system.<sup>54</sup> It is an interference phenomenon—small scatterers cause constructive and destructive phase interference at the receiving array. Speckle is an undesirable property as it can mask small but perhaps diagnostically significant image features.<sup>55</sup>

Speckle pattern does not change with time, so repeat imaging if obtained through same plane with same transducer position and orientation, will show same speckle pattern. However, if we change the transducer orientation and position, the speckle pattern shall also change.

2. **Attenuation related artifacts include** attenuation, shadowing and enhancement attenuation: It occurs due to lack of transmission of sound through a mass lesion. It points to solid internal consistency of the lesion.<sup>2</sup>

When an ultrasound beam encounters a focal object that attenuates the sound to a greater or lesser extent than in the surrounding tissue, the strength of the beam distal to this given structure will be either weaker or stronger than in the adjoining field. Thus, when the ultrasound beam encounters a strongly attenuating or highly reflective structure, the amplitude of the beam distal to this structure is diminished. The echoes returning from structures beyond the highly attenuating structure will also be diminished. In clinical practice, this is seen as a dark band known as a “shadow” deep to a highly attenuating structure (calculi). (**Fig. 11A**)

Similarly, when the ultrasound beam traverses a focal weakly attenuating structure within the imaging field, the amplitude of the beam beyond this structure is greater than the beam amplitude at the same depth in the rest of the field and thus echoes returning from structures deep to the focal weak attenuator will be of higher amplitude and will be falsely displayed as increased in echogenicity or “enhancement”, typically seen posterior to a cystic lesion (low attenuation lesion)<sup>53-55</sup> (**Fig. 11B**)

3. **Propagation related (artifacts associated with multiple echoes) (Fig. 12)**<sup>56</sup> includes Reverberation, Comet tail, Ring down, Sidelobe and Mirror image artifacts.

**Reverberation:** In the presence of two parallel highly reflective surfaces, the echoes generated from a primary ultrasound beam may be repeatedly reflected back and forth before returning to the transducer for detection. When this occurs, multiple echoes are recorded and displayed. At imaging, this is seen as multiple equidistantly spaced linear reflections and is referred to as reverberation artifact.<sup>53,56</sup> Typically, it occurs when sound beam travels with minimal or no attenuation through a cystic (fluid) structure. These become weak as sound travels into the tissue deeper and can mimic solid component in a cystic structure (urinary bladder). This artifact can be resolved by simply changing the scanning angle.

Comet tail artifact is a form of reverberation. In this artifact, the two reflective interfaces and thus sequential echoes are closely spaced. On the display, the sequential echoes may be so close together that individual signals are not perceivable. It appears as a dense, tapering echoes distal to a structure which reflects strongly.<sup>2</sup> Classic examples include metallic objects which may produce such artifacts.

**Mirror image artifacts:** are generated when the primary beam encounters a highly reflective interface. The reflected echoes then encounter the “back side” of a structure and are reflected back toward the reflective

interface before being reflected to the transducer for detection.<sup>53</sup> The display shows a duplicated structure equidistant from but deep to the strongly reflective interface. In clinical imaging, this duplicated structure is commonly identified at the level of the diaphragm, with the pleural-air interface acting as the strong reflector.

4. **Ultrasound beam characteristics related artifacts**

**Beam width artifact:** A highly reflective object located within the widened beam beyond transducer's margin may generate detectable echoes. Ultrasound display presumes echoes to be originating from within narrow imaging plane and displays them as such.<sup>53</sup> Its clinical application can be manifested as when anechoic structure (urinary bladder) shows peripheral echoes. This can be corrected and removed during scanning by adjusting the focal zone to the level of interest and by placing transducer at the center of the object. Side lobes are multiple beams of low amplitude ultrasound energy that project radially from the main beam axis and artifacts seen mainly with linear array transducers.<sup>53</sup> Similar to beam width artifact, this phenomenon is most likely to be recognized as extraneous echoes present within an expected anechoic structure such as the bladder.<sup>57</sup>

## REFERENCES

- Rizzatto G. Ultrasound transducers. Eur J Radiol. 1998;27(Suppl 2):S188-95.
- Cynthia Silkowski. Ultrasound Nomenclature, Image Orientation and Basic Instrumentation. In: Emergency Medicine Sonography. By Dunstan Abraham, Cynthia Silkowski, and Charles Odwin. Jones and Bartlett Publishers 2010. pp. 1-24.
- Hangiandreou NJ. Radiographics AAPM/RSNA physics tutorial for residents. Topics in US: B-mode US: basic concepts and new technology. 2003;23(4):1019-33.
- Thomenius KE. Instrumentation for B-mode imaging. In: Goldman LW, Fowlkes JB (Eds). Categorical course in diagnostic radiology physics: CT and US cross-sectional imaging. Oak Brook, Ill; Radiological society of North America, 2000. pp. 9-20.
- Zagzebski JA. Physics and Instrumentation in Doppler and B-mode ultrasonography. In Introduction to Vascular Ultrasonography by Zwiebel & Pellerito. 5<sup>th</sup> Edn. Elsevier Saunders. Philadelphia. Chapter 2. 2005. pp. 19-60.
- Curry ST, Dowdye JE, Murry RC. Ultrasound. In Christensen's Physics of Diagnostic Radiology. 4th Edn. Lea & Febiger. 1990. pp. 323-70.
- Martinoli C, Derchi LE, Rizzatto G, Solbiati L. Power Doppler sonography: general principles, clinical applications, and future prospects. Eur Radiol. 1998;8:1224-35.
- Kremkau F. Diagnostic ultrasound principles, Instrumentation and Exercises, 5th Edn. Orlando FL, Grune & Startton, 1993.
- Taylor KJW, Wells PNT, Burns PN. Clinical applications of doppler ultrasound. New York, Raven Press, 1995.
- Evans D. Doppler ultrasound physics instrumentation and clinical applications. New York, John Wiley and Sons. 1989.
- Rubin JM, Bude RO, Carson PL, et al. Power Doppler US: A potentially useful alternative to mean frequency-based color doppler US. Radiology. 1994;190:853-6.

12. Sodhi KS, Sidhu R, Gulati M, Saxena A, Suri S, Chawla Y. Role of tissue harmonic imaging in focal hepatic lesions: comparison with conventional sonography. *J Gastroenterol Hepatol.* 2005;20(10):1488-93.
13. Shapiro RS, Wagreich J, Parsons RB, Pasik AS, Yeh HC, Lao R. Tissue harmonic imaging sonography: evaluation of image quality compared with conventional sonography. *AJR.* 1998;171:1203-6.
14. Yucel C, Ozdemir H, Asik E, Oner Y, Isik S. Benefits of tissue harmonic imaging in the evaluation of abdominal and pelvic lesions. *Abdom Imaging.* 2003;28:103-9.
15. Ward B, Baker AC, Humphrey VF. Nonlinear propagation applied to the improvement of resolution in diagnostic medical ultrasound. *J Acoust Soc Am.* 1997;101:143-54.
16. Rosenthal SJ, Jones PH, Wetzel LH. Phase inversion tissue harmonic sonographic imaging: a clinical utility study. *AJR* 2001;176:1393-8.
17. Choudhry S, Gorman B, Charboneau JW, et al. Comparison of tissue harmonic imaging with conventional US in abdominal disease. *Radiographics.* 2000;20:1127-35.
18. Hann LE, Bach AM, Cramer LD, Siegel D, Yoo HH, Gaxia R. Hepatic sonography: comparison of tissue harmonic and standard sonography techniques. *AJR* 1999; 173: 201-6.
19. Desser TS, Jeffrey RB. Tissue harmonic imaging techniques: physical principles and clinical applications. *Semin. Ultrasound CT MR.* 2001;22:1-10.
20. Lencioni R, Cioni D, Bartolozzi C. Tissue harmonic and contrast specific imaging: back to gray scale in ultrasound. *Eur. Radiol.* 2002;12:151-65.
21. Kollmann C. New sonographic techniques for harmonic imaging--underlying physical principles. *Eur J Radiol.* 2007;64(2):164-72. Epub 2007 Sep 17. Review.
22. Kawagishi T. Technical description of 1.5 harmonic imaging, an effective technique for contrast-enhanced ultrasound diagnosis. Medical review 2003-Cardiology special Issue. Cardiac imaging & Networking. Toshiba Medical systems.
23. Harvey CJ, Pilcher JM, Eckersley RJ, Blomley MJK, Cosgrove DO. Advances in Ultrasound. *Clin Radiol.* 2002;57:157-77.
24. Jespersen SK, Wilhjelm JE, Sillesen H. Multiangle compound imaging. *Ultrason Imaging.* 1998;20:81-102.
25. Garra BS. Elastography Current status, future prospects and making it work for you. *Ultrasound Quarterly.* 2011;27:177-86.
26. Benacerraf BR, Benson CB, Abuhamad AZ, et al. Three- and 4-dimensional ultrasound in obstetrics and gynecology: proceedings of the American Institute of Ultrasound in Medicine Consensus Conference. *J Ultrasound Med.* 2005;24(12):1587-97.
27. Bega G, Lev-Toaff AS, O'Kane P, et al. Three-dimensional Ultrasonography in Gynecology Technical Aspects and Clinical Applications. *J Ultrasound Med.* 2003;22(11):1249-69.
28. Raga F, Bonilla-Musoles F, Blanes J, et al. Congenital mullerian anomalies: diagnostic accuracy of three-dimensional ultrasound. *Fertil Steril.* 1996;65(3):523-8.
29. Wu MH, Hsu CC, Huang KE. Detection of congenital mullerian duct anomalies using three-dimensional ultrasound. *J Clin Ultrasound.* 1997;25(9):487-92.
30. Dyson RL, Pretorius DH, Budorick NE, et al. Three dimensional ultrasound in the evaluation of fetal anomalies. *Ultrasound Obstet Gynecol.* 2000;16(4):321-8.
31. Lee W, Chaiworapongsa T, Romero R et al. A diagnostic approach for the evaluation of spina bifida by three-dimensional ultrasonography. *J Ultrasound Med.* 2002;21(6):619-26.
32. Ji E, Pretorius D, Newton R, et al. Effects of ultrasound on maternal-fetal bonding: a comparison of two- and three-dimensional imaging. *Ultrasound Obstet Gynecol.* 2005; 25(5):473-7.
33. Kurjak A, Azumendi G, Vecek N, et al. Fetal hand movements and facial expression in normal pregnancy studied by four-dimensional sonography. *J Perinat Med.* 2003;31(6):496-508.
34. Kurjak A, Stanojevic M, Andonotopo W, et al. Behavioral pattern continuity from prenatal to postnatal life: a study by four-dimensional (4D) ultrasonography. *J Perinat Med.* 2004;32(4):346-53.
35. Kurjak A, Stanojevic M, Azumendi G, et al. The potential of four-dimensional (4D) Ultrasonography in the assessment of fetal awareness. *J Perinat Med.* 2005;33(1):46-53.
36. DeVore GR, Falkensammer P, Sklansky MS, et al. Spatio-temporal image correlation (STIC): new technology for evaluation of the fetal heart. *Ultrasound Obstet Gynecol.* 2003;22(4):380-7.
37. Viñals F, Poblete P, Giuliano A. Spatio-temporal image correlation (STIC): a new tool for the prenatal screening of congenital heart defects. *Ultrasound Obstet Gynecol.* 2003;22(4):388-94.
38. Gonçalves LF, Lee W, Chaiworapongsa T, et al. Four dimensional ultrasonography of the fetal heart with spatiotemporal image correlation. *Am J Obstet Gynecol.* 2003;189(6):1792-802.
39. Benacerraf BR, Shipp TD, Bromley B. How sonographic tomography will change the face of obstetric sonography: a pilot study. *J Ultrasound Med.* 2005;24(3):371-8.
40. Real-time Virtual Sonography Unit. Instruction Manual. Hitachi Medical Corporation. 2004-2006.
41. Sandulescu L, Saftoiu A, Dumitrescu D, Ciurea T. The role of real-time contrast-enhanced and real-time virtual sonography in the assessment of malignant liver lesions. *J Gastrointest Liver Dis.* 2009;18(1):103-8.
42. Sandulescu L, Dumitrescu D, Rogoveanu I, Saftoiu A. Hybrid ultrasound imaging techniques (fusion imaging). *World J Gastroenterol.* 2011;17(1):49-52.
43. Minami Y, Kudo M, Chung H, et al. Percutaneous radiofrequency ablation of sonographically unidentifiable liver tumors. Feasibility and usefulness of a novel guiding technique with an integrated system of computed tomography and sonographic images. *Oncology.* 2007;72(Suppl 1):11-6.
44. Minami Y, Chung H, Kudo M, et al. Radiofrequency ablation of hepatocellular carcinoma: value of virtual CT sonography with magnetic navigation. *AJR Am J Roentgenol.* 2008;190(6): W335-W341.
45. Kitada T, Murakami T, Kuzushita N, et al. Effectiveness of real-time virtual sonography guided radiofrequency ablation treatment for patients with hepatocellular carcinomas. *Hepatol Res.* 2008;38(6):565-71.
46. Sandulescu L, Saftoiu A, Dumitrescu D, Ciurea T. Real-time contrast-enhanced and real-time virtual sonography in the assessment of benign liver lesions. *J Gastrointest Liver Dis* 2008;17(4):475-8.
47. Krücker J, Xu S, Venkatesan A, et al. Clinical Utility of Real-time Fusion Guidance for Biopsy and Ablation. *J Vasc Interv Radiol.* 2011;22(4):515-24.
48. Shehata IA. Treatment with high intensity focused ultrasound: secrets revealed. *Eur J Radiol.* 2012;81(3):534-41.
49. Wu F, Wang ZB, Chen WZ, Zhu H, Bai J, Zou JZ, et al. Extracorporeal high intensity focused ultrasound ablation in

- the treatment of patients with large hepatocellular carcinoma. Ann Surg Oncol. 2004;11(12):1061-9.
- 50. Dubinsky TJ, Cuevas C, Dighé MK, Kolokythas O, Hwang JH. High-intensity focused ultrasound: current potential and oncologic applications. AJR Am J Roentgenol. 2008;190(1):191-9.
  - 51. Kaneko OF, Willmann JK. Ultrasound for molecular imaging and therapy in cancer. Quant Imaging Med Surg. 2012;2(2):87-97.
  - 52. Kircher MF, Willmann JK. Molecular body imaging: MR imaging, CT, and US. Part II. Applications. Radiology. 2012;264(2):349-68.
  - 53. Feldman MK, Katyal S, Blackwood MS. US artifacts. Radiographics. 2009;29(4):1179-89.
  - 54. Burckhardt CB. Speckle in ultrasound B-Mode scans, IEEE Trans. Sonics Ultrasonics, SU-25, 1- 6;(1978).
  - 55. Chen Y, Broschat SL, Flynn PJ. Phase Insensitive Homomorphic Image Processing for Speckle Reduction Ultrasonic Imaging 1996;18:122-39.
  - 56. Bushberg JT, Seibert JA, Leidholdt EM, Boone JM. The essential physics of medical imaging. 2nd Edn. Philadelphia, Pa: Lippincott Williams & Wilkins, 2002.pp. 469-553.
  - 57. Laing FC, Kurtz AB. The importance of ultrasonic side-lobe artifacts. Radiology. 1982;145(3):763-8.

## Chapter

# 2

# Image Optimization in Ultrasound

Rashmi Dixit

Ultrasound imaging with its inherent flexibility, low cost and real time physiologic measurement capability with no known bioeffects, at intensities used in medical imaging, plays a vital role in diagnostics.

Image formation in ultrasound depends on the physical properties of ultrasound pulse formation, transmission and interaction with tissues. Acoustic energy undergoes essentially three different types of interactions in the tissues—reflection (specular and diffuse), refraction, and attenuation.

Diagnostic applications of ultrasound are based on detection and display of acoustic energy reflected from interfaces within the body. The amplitude of the reflected energy is used to generate ultrasound images while frequency shifts in backscattered ultrasound provide information relating to moving targets such as blood. Real time, Gray Scale, B-mode display, in which variations in display intensity or brightness are used to show signals of differing amplitude, is the mainstay of ultrasound imaging. Real time ultrasound produces an impression of motion by generating a series of 2D images several times per second or frames per second.

The quality of an ultrasound image<sup>1-3</sup> depends on its spatial resolution, temporal resolution, contrast resolution and freedom from certain artifacts. Spatial resolution has three components axial, lateral and elevational or azimuthal resolution. Axial resolution is the resolution along the axis of the ultrasound beam. It is also called longitudinal or depth resolution and depends on spatial pulse length, which is the product of wavelength and number of pulses, being equal to half the spatial pulse length. As frequency increases the pulse length decreases permitting resolution of smaller details. Hence, axial resolution improves with increasing

frequency (which reduces wavelength). Axial resolution at a frequency of 3.5 MHz is 0.5 to 1.0 mm. It does not change significantly with depth. Lateral resolution refers to the ability to distinguish two structures lying side by side. The width of the main beam defines the lateral resolution of the ultrasound image because objects can be resolved separately only if the beam is narrower than the distance between them. Hence in modern systems transducers are focused to reduce beam width. Focal zone is the area where the beam is 3 to 4 wavelengths wide and the area where lateral resolution is highest, deteriorating rapidly beyond it. Lateral resolution with frequency of 3.5 MHz is approximately 2 mm. Focusing in the elevation plane is also possible with current technology.

Temporal resolution refers to the ability to locate the position of a particular moving structure in time. This increases as the frame rate increases. Contrast resolution is the ability to show very subtle difference in echo strength. Contrast resolution improves when a system can recognize and store a wide range of echo amplitudes.

New technical developments and remarkable improvement in image quality have marked several new applications for diagnostic ultrasound. The rise of state of the art, expensive equipment has greatly eased the sonologist's job. Nonetheless, it does not by itself guarantee, high quality ultrasound images. Variables, many of which are under direct user control must be managed to guarantee the production of quality studies. An accurate ultrasound diagnosis relies heavily on the experience and skill of the examiner and requires adjustment of the equipment settings from patient to patient and organ to organ. Hence, the image optimization is an essential prerequisite for diagnostic ultrasound imaging.

## GRAY SCALE IMAGING

### Basic Guidelines<sup>2-5</sup>

Patient should be positioned in such a way that the area of interest can be easily accessed and the patient is comfortable during the examination. Changing the patient position to better elucidate pathology is also important, e.g. an extended neck for thyroid examination, left lateral decubitus position for gallbladder calculi, etc.

A good acoustic window improves scanning accuracy and image quality. Solid organs like the liver or spleen or fluid filled structures, which do not attenuate the sound beam, e.g. full bladder or fluid filled stomach provide a good acoustic window to see deeper structures. Use of adequate amount of coupling gel is essential as air has high acoustic impedance.

### Factory Presets

The more complicated machine settings are saved as presets. Presets provide a useful starting point, however, these are settings which are optimized for patients of average body habitus and further optimization of the image by manual adjustments is invariably required in order to increase diagnostic confidence and avoid artifacts. A single touch image optimization is also available on some systems however this only resets the parameters to the chosen preset.

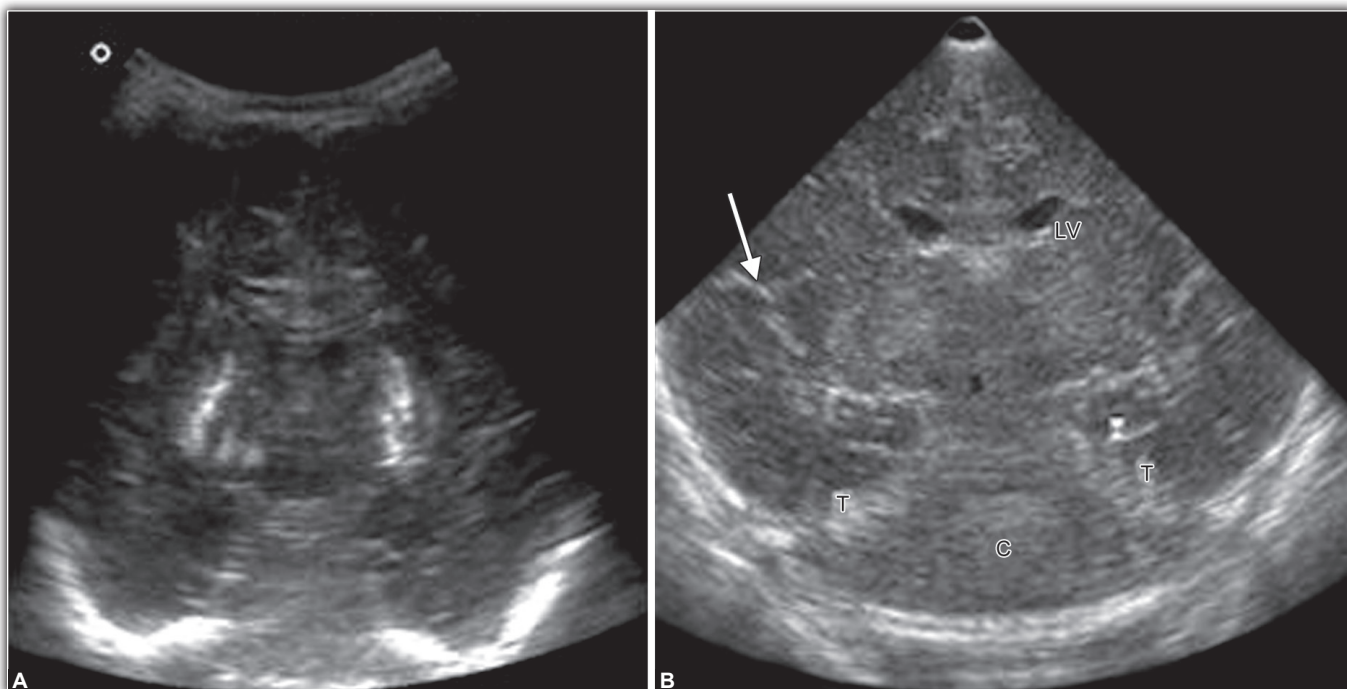
### Transducer Selection

Choosing the appropriate transducer both in terms of frequency as well as footprint is extremely important for a good examination. Higher frequencies provide a better resolution but are attenuated much more as attenuation is proportional to the fourth power of frequency. A trade off thus has to be made between the need for penetration and resolution.

While performing superficial scans as for the thyroid, musculoskeletal system or testicular examination a linear transducer with a high frequency (7-10 mHz or even 15-17 MHz) is suitable but for deeper structures a lower frequency such as 2.5 to 3 MHz is used. Currently many multifrequency and broad band width transducers are available. For intercostal scanning or scanning the neonatal brain transducers with a smaller footprint which fit into the small acoustic window are appropriate (**Figs 1A and B**). Sector transducers are thus useful to evaluate deeper structures through a small acoustic window, e.g. echocardiography. In sector scanning, however, resolution becomes poorer with increasing depth as the same echo lines are spread out over a wider area deeper in the tissue.

### Overall Gain

Overall gain amplifies all the returning echoes/signals uniformly. An excessively high gain can result in a washed out image and can obscure many details.



**Figs 1A and B** Cranial sonogram performed with a curvilinear array abdominal probe (A) shows shadowing obscuring the cerebral convexities on both sides due to mismatch between the large transducer footprint and acoustic window. The second scan (B) performed with a small footprint transducer shows good visualization of cerebral convexitities. Arrow – sylvian fissure T-tentorium C-cerebellum

### Time Gain Compensation

Time gain compensation (TGC) is also referred to as distance gain compensation (DGC) or spatial time compensation (STC). Signals that arrive later, i.e. from greater depths are amplified more than earlier signals to compensate for the attenuating effect of tissues. TGC controls permit the user to selectively amplify the signals from deeper structures or suppress signals from superficial tissues so that a smooth gray scale picture can be obtained (**Figs 2A and B**). Although most newer machines provide for some automatic TGC, manual adjustment by the user is one of the most important factors that may have a profound effect on image quality.

### Depth Setting

This parameter selects the depth of the imaging field. If too much depth is selected the image will be small and the area of interest difficult to visualize, measurements may also be inaccurate. On the other hand if the depth setting is too shallow the complete region or organ is not visualized and pathology at a deeper levels may be completely missed (**Figs 3A and B**). Practically depth can be adjusted by starting at a higher depth, subsequently depths should be decreased so that the area of interest is at about three-fourths the depth of the screen. A small area should be available behind the area of interest to observe useful artifacts.

### Focal Zone Setting

To improve resolution diagnostic transducers are focused electronically. As already discussed, the resolution of ultrasound is best in the focal zone. The focal zone should

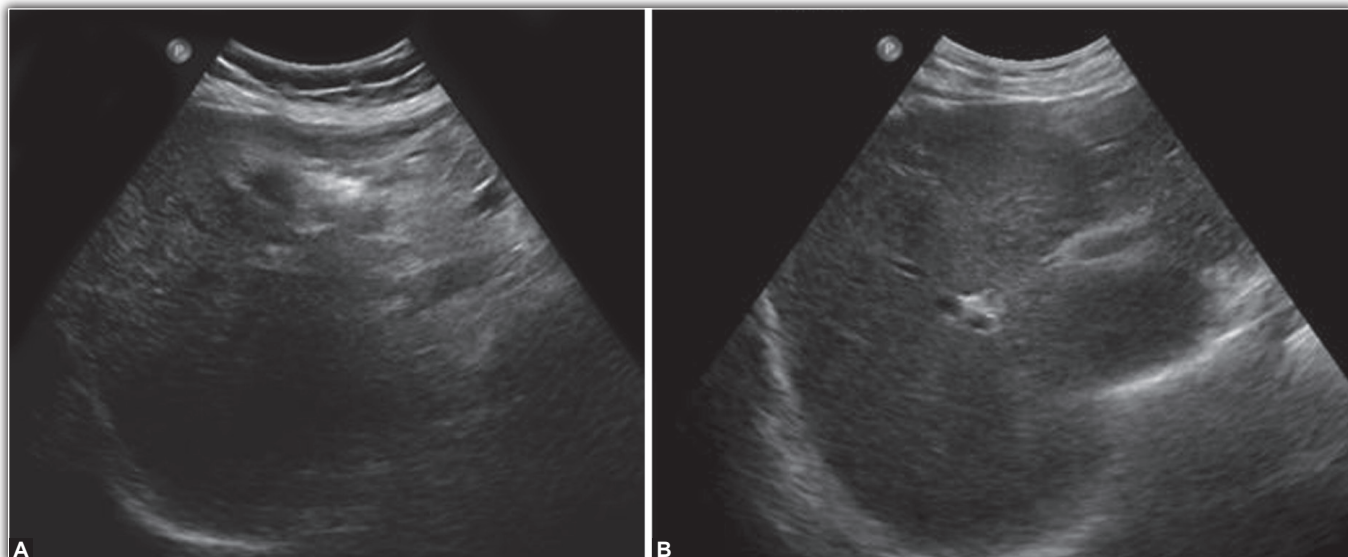
thus be set over the area of interest. A significant difference in image resolution depending on the focal zone setting is the hallmark of a well-focused beam (**Figs 4A and B**). Modern scanners allow the use of multiple focal zones however this may result in decreased frame rate and hence decreased temporal resolution.

### Zoom

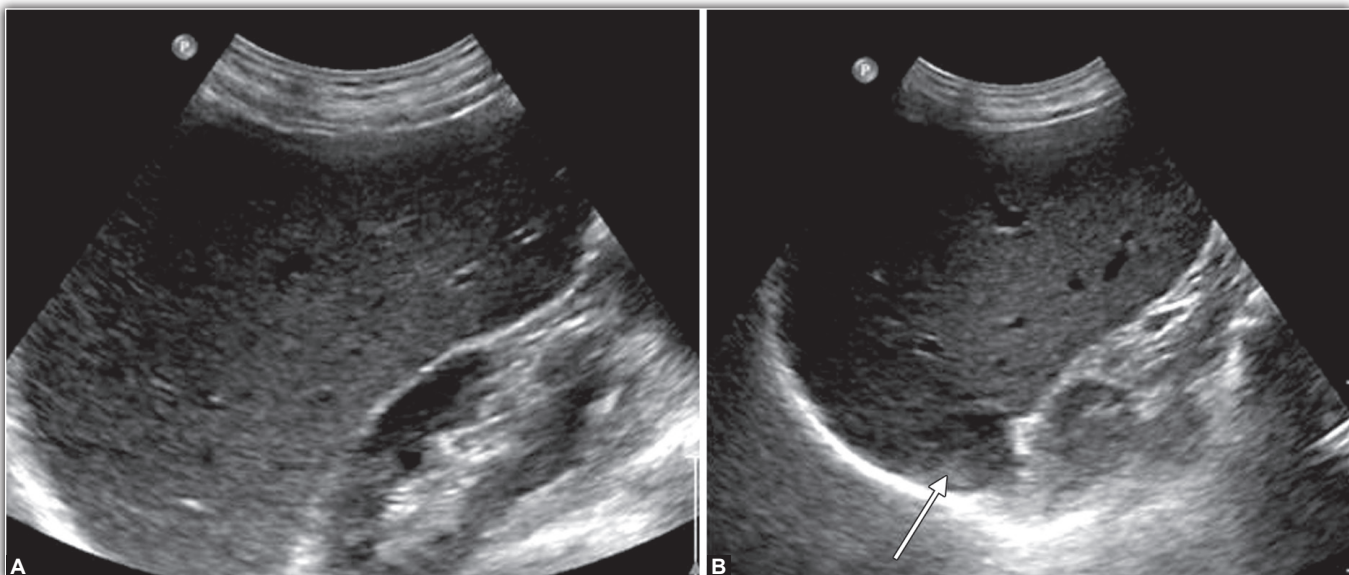
Zoom is used to magnify the area of interest. There are two types of zoom available. Read zoom is used to enlarge a frozen image whereas write zoom is used to enlarge the display magnification, when scanning is taking place.

In read zoom gray level values are read only from a small part of the computer memory and the pixels are enlarged while displaying, something like a magnifying glass. If the magnification factor is too large image matrix becomes obvious and renders the image to grainy.

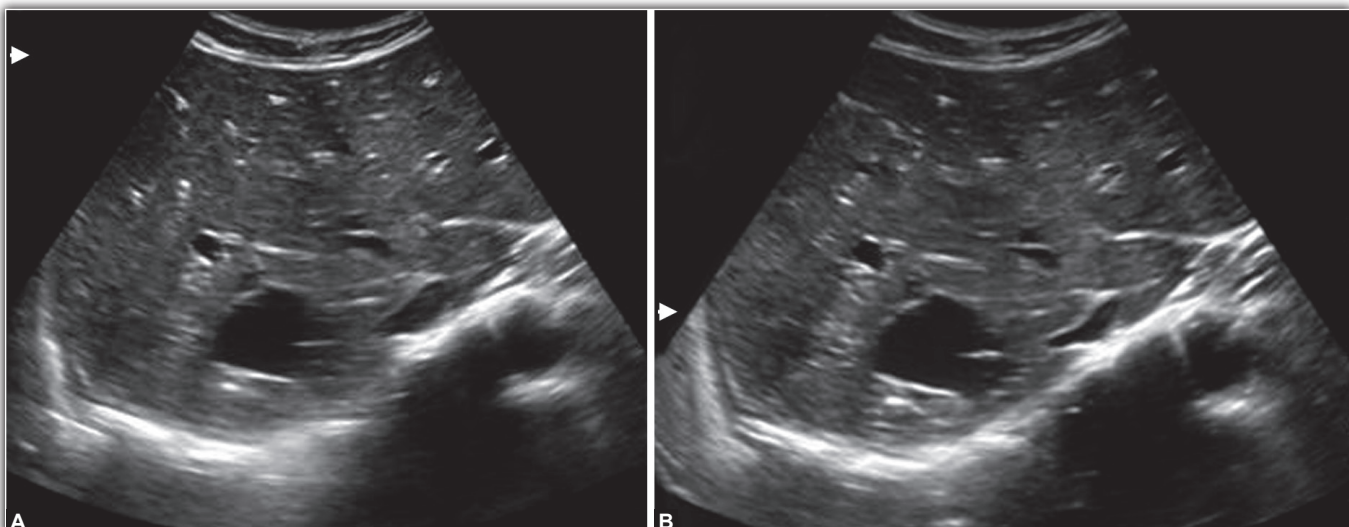
In write zoom use is made of the fact that the echo samples are received fast enough for several samples to occur in each pixel. In this situation, the image scale can be enlarged to a point where only one sample occurs in each pixel. Each pixel, whose size remains unchanged, displays less tissue. Thus, there is magnification without loss of definition. If the scale is increased further there is a larger space between scan lines so that further interpolation and smoothening may be required to maintain an acceptable image. More real scan lines can be introduced using sophisticated signal processing so that definition is improved. One such option is referred to as high density (HD) zoom. This magnifies the region of interest while increasing line density by redistributing and reformatting all scan lines for the defined region of interest.



**Figs 2A and B** Improper TGC setting resulting in a dark band over the deep aspect of the liver (A). With the correct TGC setting the whole liver shows a uniform echopattern (B)



**Figs 3A and B** Improper depth setting in (A) results in non-visualization of posterior most portion of liver with consequently missed metastatic focus, which is easily appreciated (arrow) with proper depth setting in (B)



**Figs 4A and B** Effect of focal zone: In (A) the focal zone (denoted by the small arrowhead) is placed anteriorly resulting in a blurred appearance of the posteriorly placed hepatic cyst and diaphragm. These become more sharply defined with proper focal zone positioning over the area of interest (B)

Hence one should always try to use the write zoom. Zoom is extremely useful for accurate measurement of small structures as the CBD.

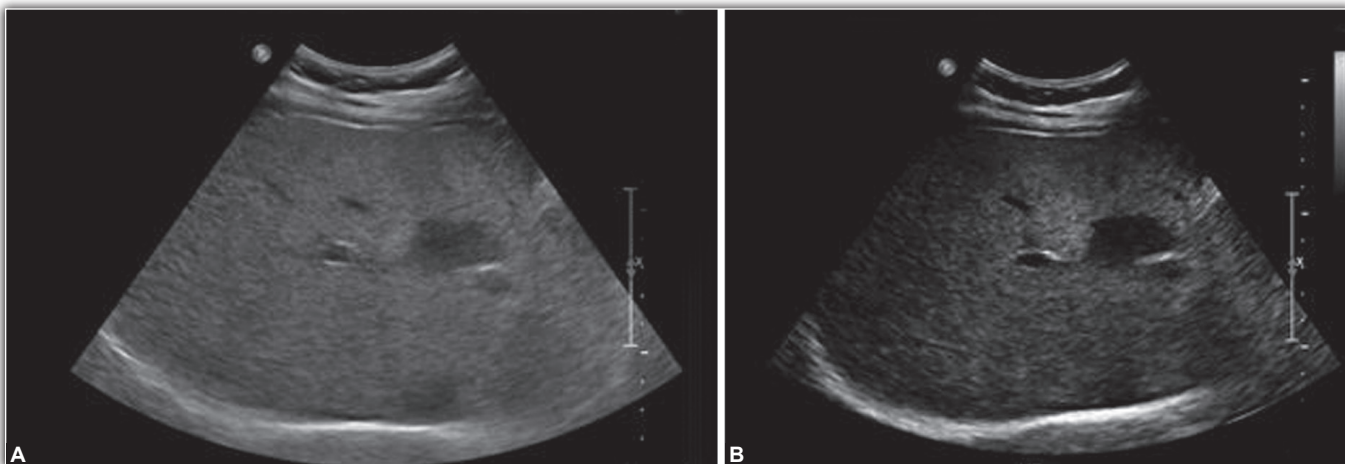
### Dynamic Range

Dynamic range is the ratio of the highest to the lowest amplitudes that can be displayed, expressed in decibels. Dynamic range adjustment changes the contrast. The widest dynamic

range that permits best differentiation of subtle differences in echo intensity is preferred for the most applications. The narrower ranges increase the conspicuity of larger echo differences (**Figs 5A and B**).

### ARTIFACTS IN B MODE IMAGING<sup>3,5-7</sup>

Artifact is a term used to describe any unwanted information generated in the process of image formation. Most artifacts



**Figs 5A and B** Images of the liver displayed at dynamic ranges of 70 and 36 dB are shown. The wide dynamic range (A) permits appreciation of subtle differences in echointensity between the diffusely fatty liver and a focal area of sparing. The narrow range (B) increases the conspicuity of larger echo differences with the area of focal sparing appearing darker and the diaphragm brighter than the wide dynamic range image

interfere with image interpretation while some artifacts which contain diagnostic information are referred to as friendly artifacts.

A number of artifacts may occur during scanning. Understanding how and why a particular artifact occurs is imperative to eliminate it and avoid errors in diagnosis.

The ultrasound equipment relies on physical assumptions to assign location and intensity of each received echo. The assumptions are:

- The echo detected arose from within the main US beam
- It has returned to the transducer after a single reflection
- The depth on an object is related only to the time taken by an ultrasound pulse to return as an echo to the transducer.
- Sound travels at a constant speed and in a straight line in human tissue
- The acoustic energy in an ultrasound field is uniformly attenuated.

While examining patients using ultrasound these assumptions are often not maintained resulting in artifacts.

### Beam Width Artifact

The real ultrasound beam is not of a uniformly narrow, laser-like configuration which would be optimal for image resolution. A typical ultrasound focused ultrasound beam exits the transducer at the same width as transducer and progressively narrows to a focus after which it spreads rapidly in the far field, where it may widen beyond the actual width of the transducer. A highly reflective object located within the widened beam beyond the edges of the transducer may generate detectable echoes. The system assumes that these echoes arose from within the imaging plane and displays them accordingly (Fig. 6). The more intense the reflection the further off axis its echoes will be received.

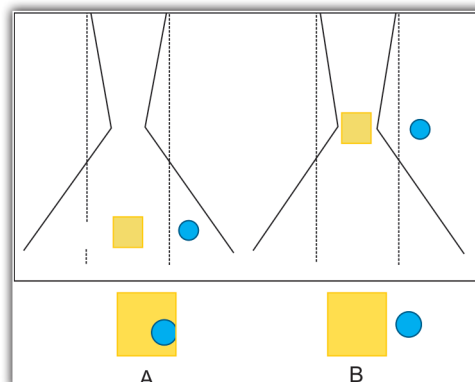


**Fig. 6** Mechanism of beam width artifact. Dotted lines represent the imaging plane. Echoes from the circle are assumed to arise from within the imaging plane in A and displayed within the square. This is rectified with proper focal zone setting in B

During clinical scanning the artifact is recognized when a structure which should be anechoic has peripheral echoes. It is generally most obvious when a bony or gaseous structure lies adjacent to a fluid space (Fig. 7).

This also means that a strong reflector will continue to give detectable echoes further from the central axis than a weak reflector. Hence, the resolution is better for weak reflectors than strong reflectors which tend to blur laterally and are therefore seen as cigar shaped smears or streaks so that the width is exaggerated. It also results a general tendency to fill in small echo free regions, such as ducts producing slightly reduced measurements.

This can be rectified and image quality improved by adjusting the focal zone to the area of interest and placing the transducer over the center of the object of interest.

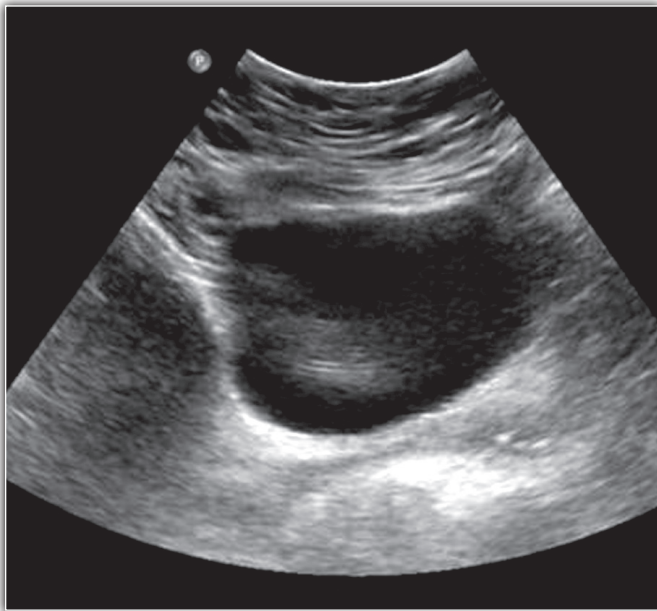


**Fig. 7** Beam width artifact: strong echoes arising from a gas filled bowel loop in the pelvis smear across the bladder

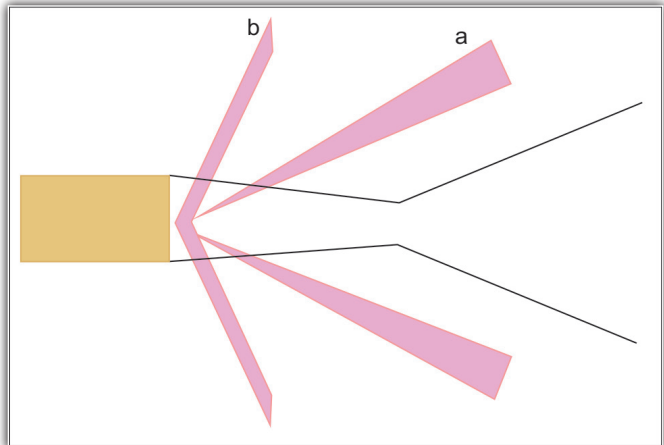


**Fig. 9** Off axis beams: side lobes (a) and grating lobes (b)

The beam width may be wider than a fluid collection. Some of the sound energy may hit structures outside the plane of intersection and may be projected into it to simulate a layer of sludge causing a simple fluid collection to appear complicated (**Fig. 8**). Since the reflector which has caused the artifact is not visualized in the image it is more difficult to recognize them than the same artifact occurring in the scanned plane. However with the latest 2 D and X-matrix transducers it is possible to focus the beam in the elevation plane as well providing a uniformly focused ultrasound beam.

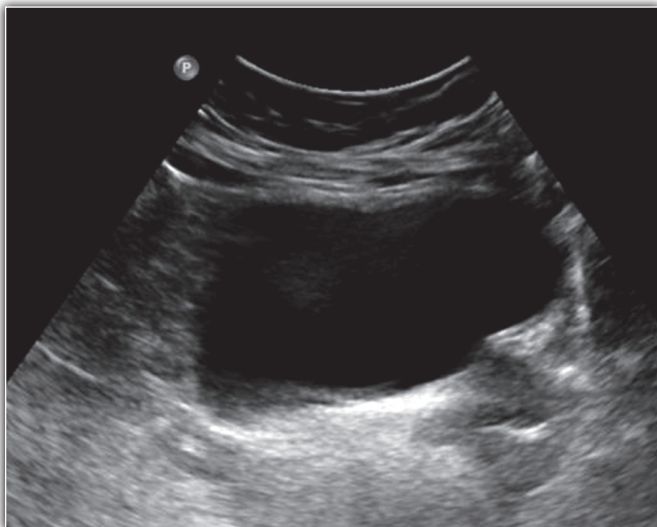


**Fig. 8** Low level echoes are seen in the bladder not from debris but due to slice thickness artifact arising from gas present in the bowel in the adjacent planes

### Slice Thickness Artifact

Beam width artifacts also occur in the orthogonal plane, i.e. in the slice thickness or elevation plane. With circular transducers either simple disc or annular array types the beam is symmetrical in all planes but for linear and phased array transducers the beam wider in the orthogonal plane resulting in information from adjacent planes being depicted in the image.

### Side Lobe and Grating Lobe Artifacts

These are low energy beams directed at angles away from the central line due to vibration of the edges of the transducer called side lobes and grating lobes. The latter occur only in array transducers (**Fig. 9**).

Strong reflectors present in the path of these low energy off axis beams may generate echoes detectable by the transducer. These are displayed as having originated from within the main beam usually within an anechoic structure. They often have a convex shape and are also referred to as **Chinese hat artifacts**.

### Artifacts Associated with Multiple Echoes

#### Reverberation Bands

A very important assumption in pulse echo ultrasound imaging is that an echo returns to the transducer after a single reflection and that the depth is related to the time taken for the echo to return. If two highly reflective surfaces lie parallel to each other, the echoes generated may be reflected back and forth before they reach the transducer. The first echo returning after a single reflection is displayed in its proper position. The later echoes returning after multiple reflections are presumed to be arising deeper to the original structure (due to the delay) and are displayed as equally spaced linear

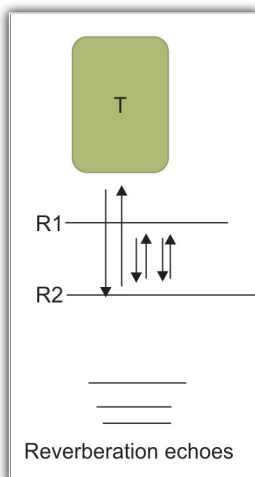


**Fig. 10** Mechanism of reverberation artifact: T transducer, R<sub>1</sub>, R<sub>2</sub> reflecting surfaces

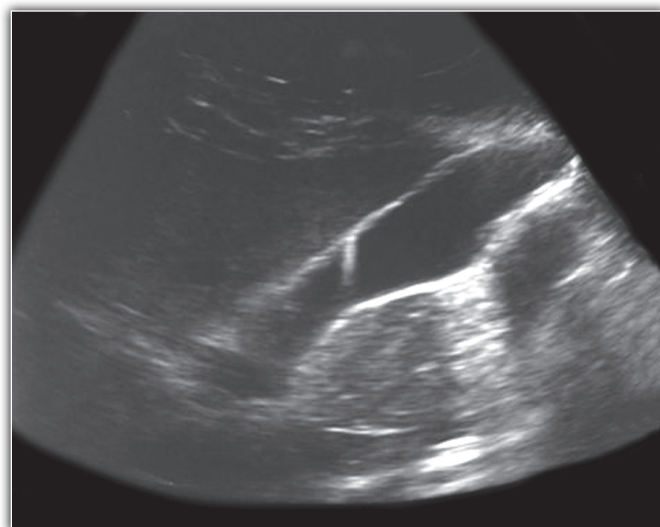


**Fig. 12** Adenomyosis of the anterior wall of gallbladder producing a typical comet tail artifact



**Fig. 11** Multiple equally spaced lines are seen within the gallbladder due to multiple reflections originating in the anterior abdominal wall

reflections in a striped pattern called **reverberation artifact** (**Figs 10 and 11**). The deeper echoes are weaker than the superficial ones due to loss of sound energy due to attenuation by intervening tissues and incomplete reflection so that the bands become narrower and less intense with depth.

Since the distance between the reverberation bands depends on the distance between the reflectors if the reflectors are very closely spaced the sequential echoes may be so close that individual bands cannot be seen. The resulting artifact is triangular with a tapered shape resembling a comet with its bright tail hence referred to as a **comet tail artifact**. This artifact is commonly seen deep to calcifications, surgical clips, IUD and in adenomyosis of gallbladder. It is presumed that many small fluid spaces like the Aschoff-Rokitansky sinuses in the wall of the gallbladder

in this condition cause repeated reflections from the walls of the fluid space producing reverberation or the comet tail artifact. The artifact is diagnostic of adenomyosis (**Fig. 12**).

Another artifact the **ring down** artifact was previously thought to be a variant of comet tail artifact because of the similar appearance of the two, however, this has a separate mechanism. The ultrasound energy is believed to cause vibrations within fluid trapped between air bubbles. These vibrations create a continuous sound wave that is transmitted back to the receiver. This is displayed as a line or series of parallel bands extending posterior to a gas collection.

#### Mirror Image Artifact

This artifact is also generated by a repeat echo. It is sometimes also referred to as a multipath artifact. The ultrasound beam encounters a highly reflective surface. The reflected echoes then encounter another reflective structure on their way back and are reflected back towards the reflective interface before being reflected to the transducer, where they are detected. The display shows a duplicated structure equidistant but deep to the strongly reflective interface. This artifact is commonly seen at the diaphragm with the air-pleural interface acting as a strong reflector. It is recognized as hepatic parenchyma seen in the expected position of the lung (**Fig. 13**).

At this level it does not cause any diagnostic problem, in fact may be useful, e.g. increased through transmission behind a peripheral cyst may be seen in the mirror image which would otherwise be obscured by the hyperechoic reflection of air in the lung.

In some situations, this artifact can be confusing for example in the pelvis a repeat echo of the bladder or structures just behind it may appear as a deeper line apparently marking back of an echo poor mass. This in reality is a mirror

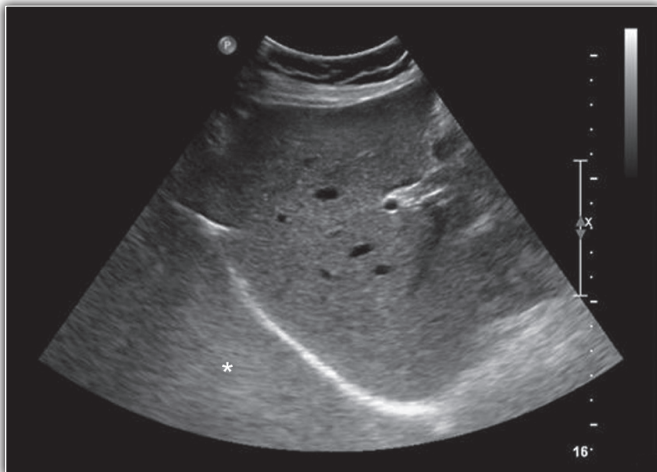


**Fig. 13** Mirror reflection of the liver is seen above the diaphragm in this patient (asterix)

**Table 1** Velocity of ultrasound in biologically important materials<sup>3</sup>

Tissue type	Velocity (m/s)
Air	330
Fat	1450
Water	1480
Brain	1565
Muscle	1580
Liver	1600
Lens of eye	1650
Soft tissue average	1540

image of the bladder. The clues that help to distinguish this pseudomass from the true mass are: the typical position, the back wall of the mass often lies behind the sacrum and hence is anatomically not possible, and the poorly discerned or weak superior and inferior walls compared to strong anterior and posterior walls.

### Artifacts Associated with Velocity Errors

An important assumption in ultrasound imaging is that the velocity of US in soft tissues is constant (1540 m/s). This is not absolutely true in clinical sonography, fat for example conducts sound about 15 percent slower than most other soft tissues (**Table 1**).

When sound travels through a tissue with a velocity significantly lower than the assumed constant of 1540 m/sec the returning echo takes longer to return to the transducer. Scanners use the amount of delay to calculate the depth of the echo (0.13 µs delay corresponding to ~1 cm depth on final image). The processor assumes that the delay is due to the

increased distance traveled by the echo. The echoes are thus displayed deeper on the image than they actually are. This is called **speed displacement artifact** or **propagation velocity artifact**. This geometric distortion does not affect the lateral dimension of the image as this is determined by the scanning action of the transducer rather than by the speed of sound. In clinical practice, this artifact is most commonly seen when an area of focal fat is encountered, e.g. areas of focal fat in the subdiaphragmatic region of the liver can result in a discontinuous appearance of the diaphragm because of fallacious posterior displacement of diaphragmatic segments behind the fatty change.

In most cases, velocity errors are too small to be clinically significant and may in fact provide diagnostic clues to the presence of fat within lesions. However, in ophthalmic measurement where great precision is required the distortion caused by the significantly higher velocity in the lens can be important. The speed of sound in the lens of the eye is 1620 m/s (vs 1540 of average soft tissues) so regions of the retina imaged through the lens appear closer than the parts imaged through the sclera producing a shelf-like anterior distortion called **Baum's bumps** after sonologist who first described them.

### Refractory Errors

Changes in velocity also produces refractory errors. When a nonperpendicular incident ultrasound beam encounters an interface between two materials with different speeds of sound, it changes direction. The degree of this change and the direction is dependent both on the angle of incidence and the difference in velocity between the two media. The scanner working on the assumption that the US beam travels in a straight line misplaces the echoes to the side of their true location. This situation may become important clinically during transabdominal pelvic scans due to refraction occurring deep to the junction of rectus abdominis muscle and midline fat. This can cause lateral stretching of pelvic structures and obstetric measurements made under these conditions may be erroneous. In more extreme cases, it may cause apparent duplication of structures. Repositioning the transducer eliminates this artifact.

### Attenuation Errors

As an ultrasound beam travels through the tissues its energy gets attenuated due to combined effect of absorption, scattering and reflection. The greater distance the ultrasound beam travels through the body the more the attenuation for a beam of similar energy. To compensate for this attenuation, ultrasound processing incorporates a compensatory amplification of echoes that take longer to return i.e. arising in the deeper tissues. Attenuation also varies with different tissues depending on the attenuation coefficient which expresses the loss of ultrasound intensity per distance travelled (**Table 2**).

**Table 2** Attenuation coefficients for selected tissues<sup>6</sup>

Material	Attenuation coefficient (dB/cm)
Water	0.0002
Soft tissue	0.3–0.8
Fat	0.5–1.8
Bone	13–26
Air	40

### Acoustic Shadowing

When the ultrasound beam encounters a tissue that attenuates sound to a greater extent than the majority of the tissue in the beam shadowing occurs. This is because the gain compensation is only set to an average value hence an inadequate correction will be applied to this region. Both it and tissues deeper to it are depicted as less reflective than they actually are. This is visible as a dark band called an acoustic or distal shadow (**Fig. 14**). Shadowing can also be caused by an extremely efficient reflector such as gas bubble or calcification where 99 and 80 percent of the incident sound beam respectively is reflected back. This is because very little of the sound energy penetrates to insonate deeper tissues and in addition any echoes from them would probably not cross the reflective layer on the return journey since they would be re-reflected distally.

### Edge Shadowing

Shadowing is also sometime seen deep to the edges of strongly curved surfaces, such as cyst walls, fetal skull and vessels. Fine dark lines can be seen extending distal to such edges and become even more striking in the case of a cyst due to the increased through transmission behind the cyst itself.

Two explanations have been offered for this: refraction of the ultrasound beam as it strikes a curved surface and **increased attenuation** at the edges because the ultrasound beam passing through the edge travels a larger distance through the cyst wall than that passing through the diameter of the cyst. Since, the cyst wall is presumed to be more attenuating than the surrounding tissues, the beam is attenuated more resulting in shadowing. Although acoustic shadows have diagnostic significance and are useful for diagnosis of calcification or calculi, edge shadows do not have this diagnostic significance (**Figs 15A and B**). Edge shadows commonly occur in situations where shadowing erroneously suggests calcification, e.g. vessel walls in renal sinus or malignancy, Coopers ligaments in the breast. It is important to recognize them as artifactual and dismiss them.

### Increased Through Transmission or Distal Bright Up'

Attenuation errors also occur if a tissue attenuates less than its surrounding tissues (e.g. a full bladder or a simple cyst). In this situation the echoes from it and the tissues posterior to

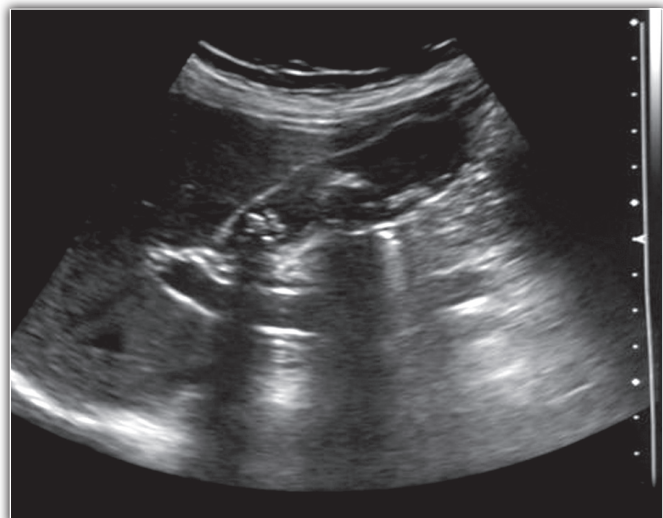


**Fig. 14** Acoustic shadows: Seen as dark bands posterior to multiple gallbladder calculi

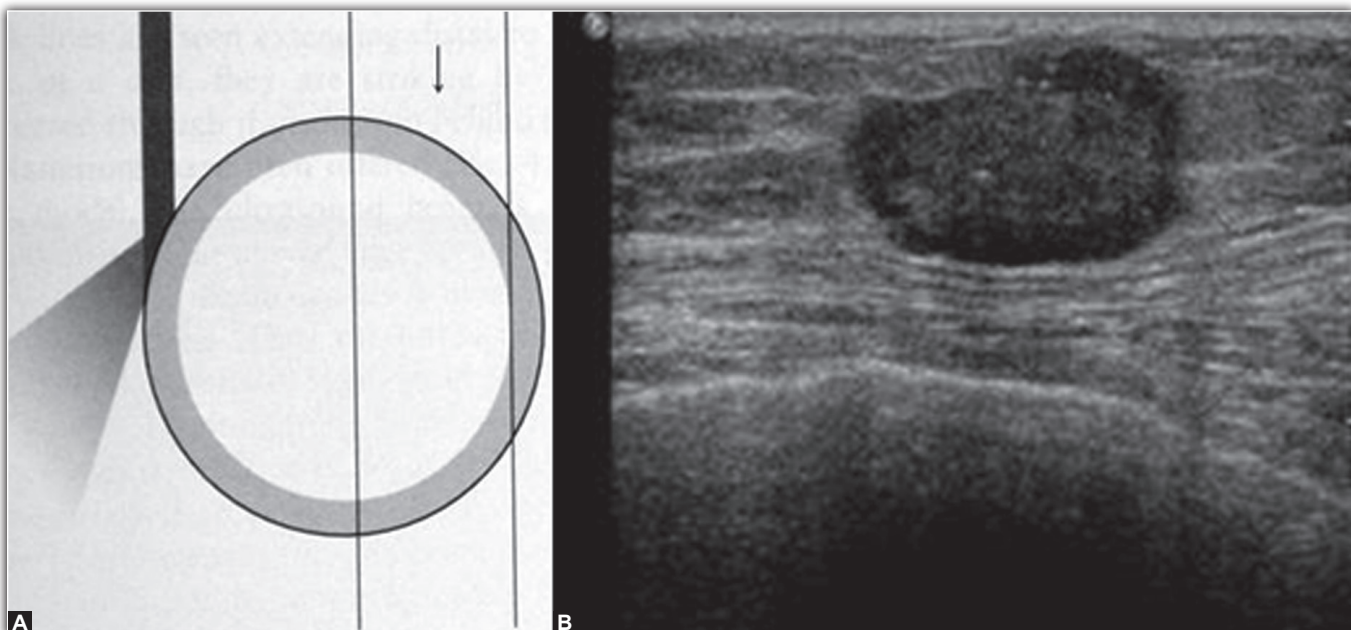
it are overcorrected appearing as a bright band often termed 'distal enhancement' but in view of the enhancing effect of ultrasound contrast agents it is better termed increased through transmission or distal bright up (**Fig. 16**).

### Noise

All imaging systems are prone to two types of noise random and structured. Electrical components produce random low level voltages which, when amplified, are seen as fluctuating moving grey spots on the image producing a snow storm appearance.

There are various other sources of 'noise' within ultrasound images. Perhaps the most important is **speckle**. Speckle is an important source of image degradation and loss of contrast in ultrasound image. Small tissue reflectors approximately the size of wavelength of sound cause scattering of sound waves which are sent out almost uniformly in all directions. Constructive and destructive interference of these acoustic fields result in speckle. Most biologic tissues appear in US images as though they are filled with tiny scattering structures. Most of the visible signal in US images results from speckle interactions. The interference pattern also gives ultrasound images a characteristic grainy appearance reducing contrast and making identification of subtle features and abnormal tissue patterns more difficult.

Another problem is **clutter**, which arises from electrical interference or beamforming artifacts, reverberations, and other acoustic phenomena. Clutter consists of spurious echoes which can often be seen within structures of low echogenicity, such as a cysts, or within amniotic fluid, and which may be confused with 'real' targets as already discussed. Finally, another potential source of noise, especially in deep-lying regions, is thermal noise arising in the electronics of the



**Figs 15A and B** Refractive and attenuation model to explain mechanism of edge shadowing (A). Subtle edge shadowing seen along the edges of fibroadenoma breast (B)

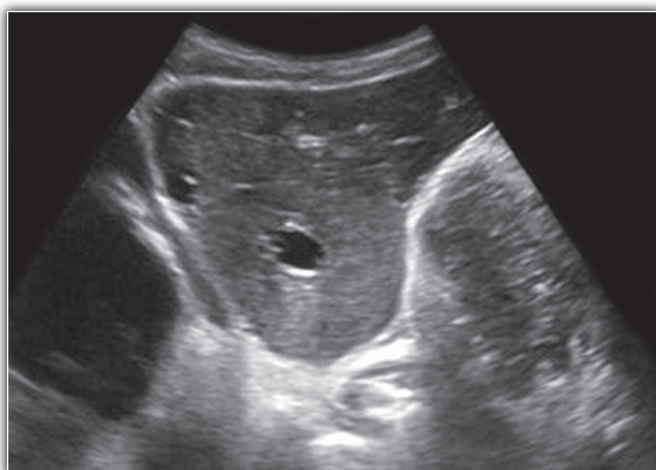


**Fig. 16** A bright band is seen posterior to this hepatic cyst—increased through transmission or distal bright-up

transducer or beamformer. All these sources of noise affect the ability of the radiologist to recognize tissue anomalies by interfering with the pattern recognition process in the observer's brain. Various Techniques such as temporal smoothening (i.e. frame averaging or persistence) are used to reduce noise. The real information is reinforced while noise cancels out. In addition a number of special imaging modes are available on high end scanners to deal with these problems which are discussed later.

## SPECTRAL AND COLOR DOPPLER EXAMINATION

### Basic Guidelines<sup>7</sup>

**Gray Scale settings** should always be optimized before color Doppler flow mapping is applied. Fine details such as small plaques or intimal thickening may be washed over by color if the gray scale image is not evaluated first.

Of the various technical parameters that can be controlled the choice of the correct transducer or the correct transducer frequency is the most important like grey scale imaging. A trial of different transducer frequencies till the best compromise between penetration and signal strength is reached is usually required.

Knowledge of anatomic variants is very important while scanning for vascular especially venous disease, for example failure to recognize duplication of common femoral vein can result in missing the diagnosis of deep venous thrombosis.

It is important to scan the entire length of vessel from its origin to termination when possible. If the ostium of a vessel is not evaluated, lesions at the ostia may be missed, e.g. atherosclerotic plaque commonly involve the origin of carotid and vertebral arteries. In such a situation, the elevated velocities may render evaluation of more distal stenotic lesions by velocity criteria alone difficult. Each vessel must also be examined in two planes, i.e. longitudinal and transverse to avoid missing partially occlusive eccentric thrombi, which may not be centered in the imaging plane in a longitudinal scan alone.

While scanning peripheral vessels it is important not to mistake a collateral that runs parallel and close to the occluded vessels for the main vessel. Identification of the vein that accompanies the artery and familiarity with the normal orientation of the vessels can help in distinguishing a parallel collateral from the main vessel as the collateral usually runs quite separate from the vein. Use of a lower frequency transducer with a wide field of view which enables visualization of both the patent segments of the native vessel and the collateral is also useful. Another useful technique is to follow the vessel from its origin to be certain of its source.

### Optimizing Color Doppler and Spectral Doppler Settings<sup>7-11</sup>

#### *Color Box or Color Doppler Sampling Window*

The color box is a user adjustable area within the ultrasound image in which all color Doppler information is displayed. The angle of incidence of the color box can be changed by angling the color box to the 'right' or 'left' so called 'steering' or by angling the transducer. As the size width and depth of color box increases frame rate decreases, image resolution and quality are affected. Thus, the box should be as small and superficial as possible while still providing the necessary information. This will maximize the frame rate. The frame rate refers to the rate at which complete images are produced. Frame rate affects the temporal resolution. With Gray Scale imaging alone the frame rate can exceed 50 fps but the time required to produce color images is much longer. The frame rate in color imaging is dependent on several factors. The wider the color box more the scan lines required and longer it will take to acquire data to produce the image. Increasing the depth (or height) of the box alone will not produce any major change in the frame rate, increasing the imaging depth however will require a lower PRF (due to more time for the echo to travel to and fro) hence decreasing the frame rate.

#### *Doppler or Color Gain*

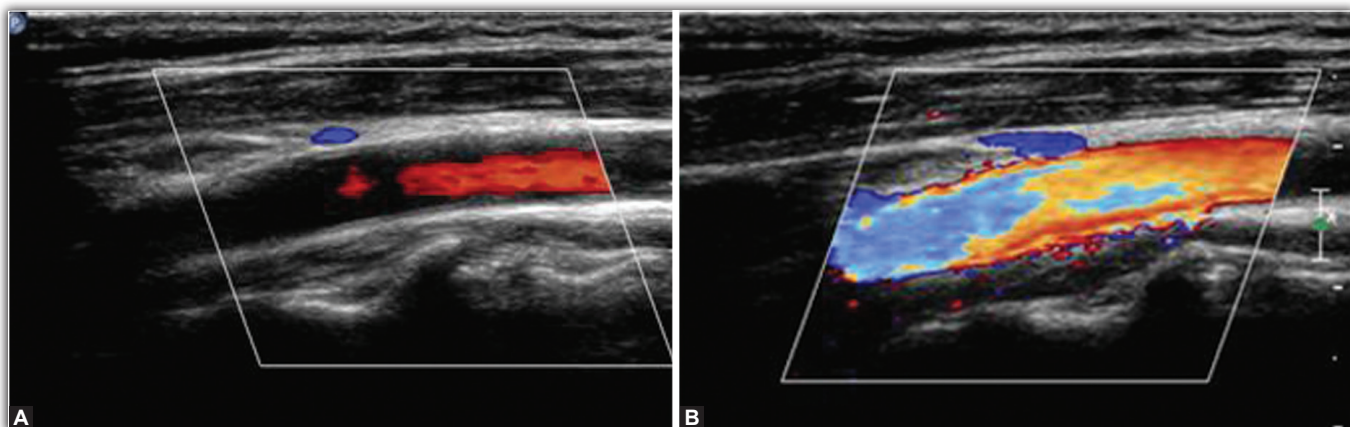
Gain refers to amplification of sampled information for purposes of improving the depiction of acquired data. It controls the amplitude of color display in color or power mode and the spectral display in pulsed Doppler mode. If flow is present and the gain is set too low it is possible that no flow will be depicted on the monitor, however, an excessively high gain setting produces noise obscuring true Doppler signal and filling in the spectral waveform resulting in falsely increased flow with little meaningful quantitative flow data.

For spectral Doppler the gain should be adjusted so that the tracing should be continuous and easy to visualize without any low level noise band above and below baseline.

For color imaging the color gain should be set as high as possible without displaying random color speckles. This is set by turning it up until noise (i.e. scattered isolated color pixels overwriting gray scale pixels) is encountered and then backing off until the noise just clears. The color should just reach the intimal surface of the vessel. A high color gain setting may cause bleeding of color or blooming into the wall or even outside the vessel lumen. This impairs visualization of plaques and partial thrombi (**Figs 17A and B**).

#### *Velocity Scale*

This is one of the most important parameters under user control during a Doppler examination. It determines the range of velocities that are depicted with either the color or spectral component. It is not synonymous with pulse repetition frequency (PRF) but PRF is related to the velocity scale setting so that increasing the velocity scale increases the PRF and vice versa. If the velocity setting is too low for the velocities being examined, the high velocity signals will not be displayed accurately and aliasing results. Aliasing is an incorrect and paradoxical display of the colors or spectral Doppler velocity. This is related to the fact Doppler and



**Figs 17A and B** Color Doppler images of the carotid with very low color gain showing incomplete color fill in the carotid (A). Excessively high color gain resulting in bleeding of color into the wall of the carotid and some noise in the surrounding tissues (B)

color flow utilize pulsed beams which are transmitted and received by the transducer. The number of such pulses sent determines the pulse repetition frequency. If the Doppler shift is higher than PRF/2 or the Nyquist limit then the display wraps around the scale and appears to change direction. For spectral Doppler the velocity peak is cut-off at the top of the scale and written from the lowest portion of the scale back toward the top. On the color Doppler image aliasing is seen as color change from red to yellow to light blue to dark blue. Color aliasing projects the color of reversed flow within central areas of higher laminar velocity. With aliasing no black stripe is seen from the low velocity filter between the reversed colors unlike flow reversal (**Figs 18A to D**). Higher velocities require a higher PRF for accurate sampling.

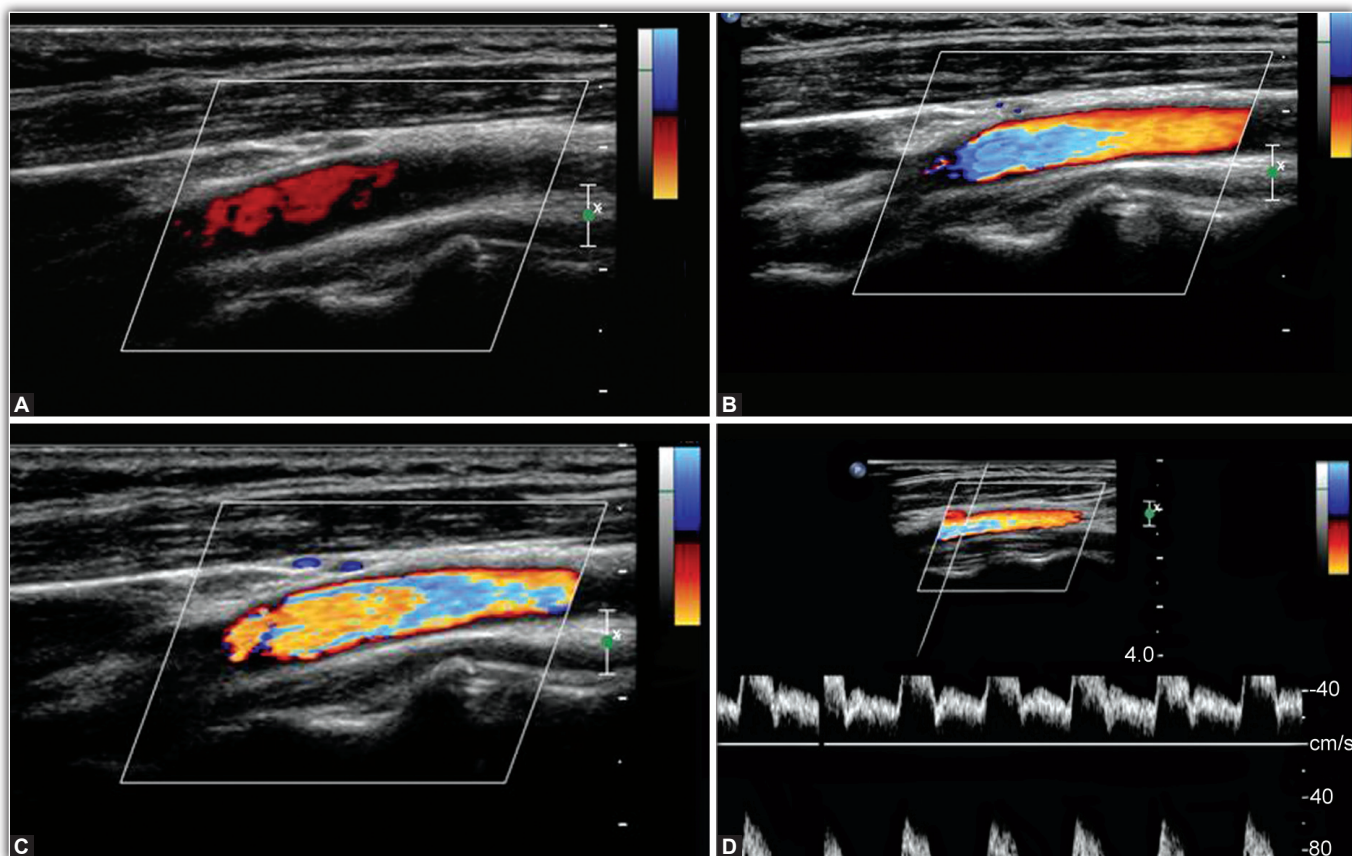
Aliasing is one of the most important artifacts in Doppler and can be advantageously used to demonstrate high or low flow turbulence. It can be useful to quickly identify the higher velocity region within the vessel and readily place the sample volume for velocity measurement. However, if the color velocity scale is set much lower than the mean velocity of blood flow, aliasing occurs throughout the vessel lumen making it difficult to identify the high velocity turbulent jet

associated with a significant stenosis. Tortuosity of a vessel can cause erroneously produce the appearance of aliasing.

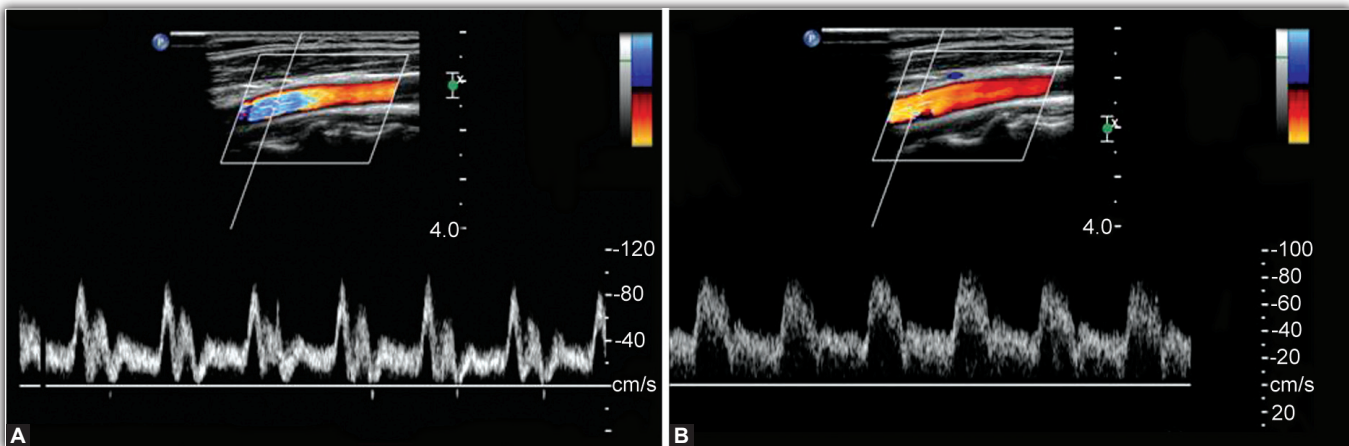
The options available to reduce spectral aliasing are increasing the Doppler angle with resultant decrease Doppler shift, increasing velocity scale, changing the baseline setting or using a lower ultrasound frequency. Aliasing is not seen in power Doppler because it has no directional or velocity component.

#### *Gate Size or Sample Volume Box*

It is the user defined area from where the spectral Doppler information is obtained depicted as a pair of cross hairs within the 2D image. Although on the image it looks like a flat box, sample volume has a third dimension in and out of the plane of the image which may be up to a centimeter at times. Hence, signals may be displayed from unwanted areas of vessels or even unwanted vessels. Normally, the gate should cover approximately two-thirds of the vessel lumen (**Figs 19A and B**). If the sample volume encompasses the entire vessel slower velocities from the vessel margins are included resulting in spectral broadening. However, if the gate is too small the Doppler signal may be missed. In



**Figs 18A to D** At high PRF settings of 12000 Hz only minimal flow is seen in the carotid artery (A). When the velocity scale is lowered to 4000 Hz complete wall-to-wall color fill is seen with an area of aliasing seen where the artery dips away from the transducer (B). A very low PRF results in aliasing throughout the vessel (C) Aliasing in spectral Doppler with the top of the peak being cut off and written at the bottom (D)



**Figs 19A and B** A properly positioned sample volume in the center of the vessel covering almost 2/3rd of vessel lumen results in a spectral trace with a clear window (A). An excessively large sample volume covering the entire vessel lumen results in inclusion of lower flow from the edges with consequent spectral widening (B)

addition, if the vessel is mobile as well the Doppler signal may be discontinuous with loss of diastolic signal in each cycle.

Increasing the Doppler gate is helpful when searching for trickle flow or trying to obtain a Doppler signal from behind a calcified plaque.

#### Sample Volume or Gate Position

The optimal position of a sample volume in a normal vessel is in the midposition parallel to the wall whereas in a diseased vessel there is some controversy whether the cursor should be angled parallel to the flow or parallel to the vessel wall. Whichever method is used the same technique must be used every time to allow reproducibility and standardization. If the sample volume is placed eccentrically too close to the vessel wall it will be degraded by signal from vessel wall motion and will also show artificial spectral broadening.

#### Angle Correction

In vascular applications optimal imaging of the vessel wall is obtained when the transducer is perpendicular to the vessel wall. However, this selection is not suitable for Doppler examination. In diagnostic Doppler imaging the Doppler equation is used to calculate the blood flow velocity, i.e.

$$\Delta f = (2f v/c) \cos \theta$$

where

$\Delta f$  = Change in frequency

$f$  = Original transmitted frequency

$v$  = Velocity of blood flow

$c$  = Speed of sound in tissue

$\theta$  = Angle of insonation.

Thus, the angle  $\theta$  which is the angle between the direction of Doppler pulses and the direction of blood flow affects the frequency shift. At a Doppler angle of  $0^\circ$  the maximum Doppler shift is achieved as cosine of  $0^\circ$  equals 1, conversely no Doppler shift will be recorded if the angle is

$90^\circ$  because cosine of  $90^\circ$  is 0. Ideally a small Doppler angle, i.e. less than  $60^\circ$  should be used approximately between  $45^\circ$  and  $60^\circ$  because within this range a linear relationship exists between Doppler shifts and velocity. The cosine of Doppler angle changes rapidly for angles more than  $60^\circ$  hence a small change in the angle is associated with a large change in the value of  $\cos \theta$ . Hence a small error in estimation of Doppler angle will result in a large change in the estimated velocity producing unreliable results.

#### Color Write Priority

Color write priority is a setting closely related to color gain.

This selects a gray scale value above which all color information is suppressed. While larger vessels require a low setting of color write priority, in small vessels that do not have resolvable anechoic lumen on gray scale color information can be suppressed by inappropriate color write priority. In such a situation color is not seen in the image even when the system has detected it. This is of particular importance in areas like the testis where the intratesticular vessels are small and Doppler is an important means of diagnosing torsion.

#### Baseline

The baseline is depicted on both the color bar and spectral waveform. It divides the color bar into positive and negative Doppler shifts. Baseline can be adjusted to emphasize certain aspects of flow, although the overall range of depicted velocities does not change, the depicted flow that is emphasized changes. Adjustment of baseline is one method to prevent aliasing.

#### Wall Filters

Wall filters selectively filter out all information below a defined frequency threshold. It eliminates the typically low

frequency-high intensity noise that may arise from vessel wall motion. There are usually preset by the manufacturer as high, medium or low which can be applied separately to spectral, color and power imaging. The aim is to eliminate low frequency noise but if it is set too high it can result in the loss of signal from slow flow. In some arteries diastolic flow may be eliminated resulting in errors in calculation of Doppler indices, hence it should be kept as low as possible (typically in the range of 50-100 Hz). Filters can be applied separately to the color Doppler image or spectral Doppler depending on which scanning mode is active. On the color bar the filter setting is indicated by a black band on both sides of the baseline. Increase in filter settings show up as widening of the black band. On spectral waveform a high wall filter wall results in loss of depicted spectral information immediately above baseline. Reducing the wall filter setting results in filling of spectral data towards the baseline.

### *Inversion of Flow*

It is possible to electronically invert the direction of flow as depicted on both color flow and spectral waveform. This can result in red-blue color inversion on the color Doppler image and inversion of spectral waveform with spectral Doppler. Hence flow direction in a vessel should never be presumed but carefully determined after comparing with the color bar. Misinterpretation of flow direction may erroneously suggest a malfunctioning TIPS or result in a missed flow reversal in an artery.

### *Directional Ambiguity*

Directional ambiguity or indeterminate flow direction refers to a spectral Doppler tracing in which the waveform is displayed with nearly equal amplitude above and below the baseline in a mirror image pattern. Directional ambiguity can result when the interrogating beam intercepts the vessel at 90° (or close to 90°). If a Doppler signal is detected it is seen as a tracing both above and below the baseline. At higher gain settings directional ambiguity is worse. This can be corrected by changing the angle of interrogation.

This should be distinguished from true bidirectional flow. In this case blood actually flows in two directions such as in the neck of a pseudo-aneurysm. The clue here is that flow here is first in one direction and then in the other in the same cardiac cycle. It is never simultaneously symmetric above and below the baseline. Bidirectional flow can also be seen in the setting of high resistance organ flow such a torsion, venous thrombosis etc. and is seen as diastolic reversal.

### *Slow Flow*

If one is unable to visualize color flow in a vessel despite optimization of all Doppler parameters, the flow may be too slow for the color flow image to visualize. In such a situation use of power Doppler or spectral Doppler which are more sensitive to slow flow may help to detect flow. The

power Doppler technique uses the intensity or power of the Doppler signal rather than the frequency shift. Strength of a Doppler signal that exceeds a particular threshold level is displayed, hence it is less angle dependent. It is also more sensitive as more extensive dynamic range can be used than with standard color Doppler imaging because noise that would overwhelm the color Doppler image can be assigned a uniform background color. The spectral wave form makes use of 256 pulse cycles per scan line and contains qualitative and quantitative diagnostic information for interpretation. The color map on the other hand contains only about 8 pulse cycles per scan line thereby providing considerably less information than spectral Doppler. Also the color Doppler images display the mean frequency shift rather than the peak frequency shift.

Appropriate settings of the above mentioned Doppler parameters eliminate or greatly reduce Doppler artifacts related to machine settings. There are certain other artifacts such as those due to anatomical factors or those unrelated to blood flow which one must be aware of to avoid misinterpreting the artifact as true flow.<sup>7-12</sup>

### *Anatomically Related Artifacts*

#### *Mirror image artifacts*

As already discussed in the section on gray scale imaging, reflection of ultrasound by an interface between zones of high and low acoustic impedance produces an image of an object on both sides although it is located only on one side. A similar artifact can occur with color Doppler imaging most often in the supraclavicular region where mirror images of the subclavian artery or vein are caused by reflection from the pleura/lung causing apparent duplication of the vessel with the phantom vessel being projected deeper in the image. Carotid and brachial arteries may also show mirror images. Changing the scanning angle will cause the mirror artifact to disappear.

### *Artifacts Unrelated to Blood Flow*

#### *Pseudo flow*

Pseudo flow artifact is related to motion of fluid rather than blood flow within a vessel. The signal will appear as long as fluid motion continues. Pseudo flow may be caused by motion of ascites, amniotic fluid and urine from the ureteric orifice. It can mimic real blood flow on color or power Doppler. Spectral analysis reveals the presence of a Doppler signal but that which is atypical for a normal vessel. Some pseudo flow artifacts such as those seen at ureteral orifice are useful to identify the ureteric orifice and can be useful to exclude complete obstruction.

#### *Twinkling Artifact*

This occurs behind a strongly reflecting granular interfaces such as urinary tract stones or parenchymal calcification.

Although primarily seen posterior to urinary calculi and parenchymal calcification it can also be seen behind any irregular highly reflective surface, biliary calculi, gallbladder adenomyosis and cholelithiasis. Twinkling artifact is believed to be caused by a narrow band of intrinsic machine noise called phase (or clock) jitter. On a flat surface, system noise generates a narrow band of Doppler shift as a result of tiny clock errors. This is generally excluded by wall filters and not displayed. Rough surfaces increase the delays in measuring the signal and amplify the errors which increases the spectral bandwidth of this noise above the level of wall filter.

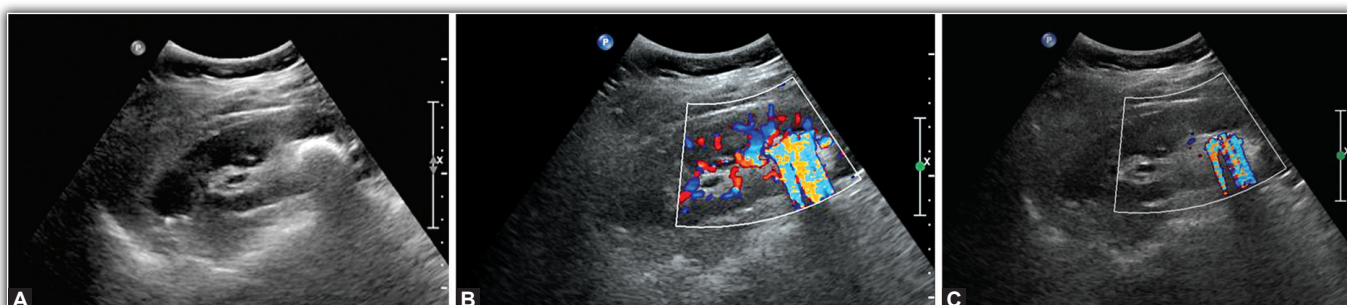
It is seen as rapidly fluctuating mixture of Doppler signals, i.e. red and blue pixels which imitate turbulent flow. On spectral Doppler analysis the tracing is absolutely flat suggestive of noise. The artifact is dependent on the color write priority and Gray Scale gain. As the color write priority decreases the twinkling artifact decreases. The key to the identification of twinkling artifact is that color is produced behind the calcification and concomitant Doppler spectral trace shows noise thus a calcified carotid plaque with twinkling can be differentiated from a potentially ulcerated

plaque with flow in ulcer cavities. Also increasing the velocity scale eliminates flow signal but not twinkling (**Figs 20A to C**).

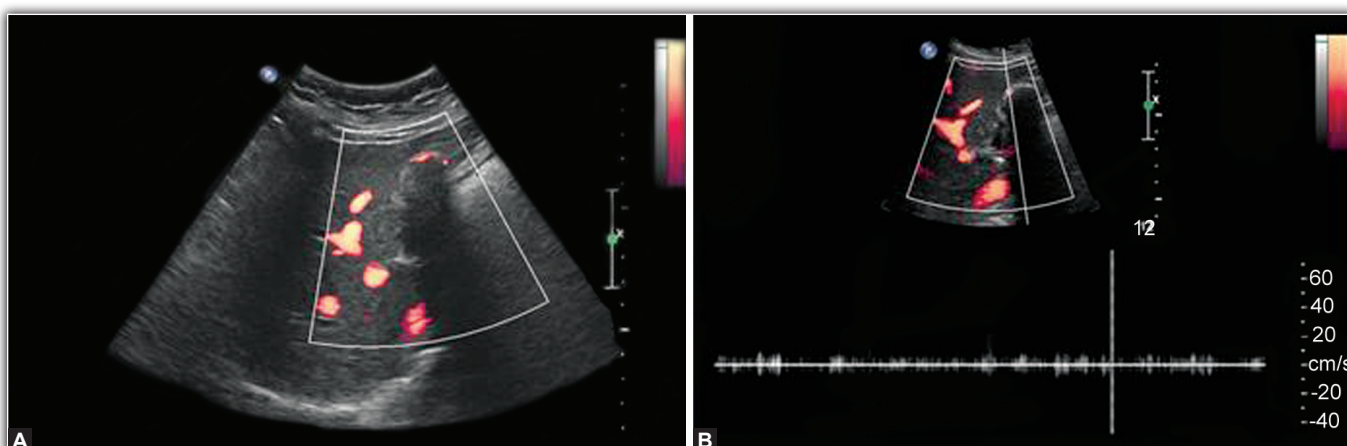
It is important to recognize this signal as artifactual in the gallbladder because it may simulate high velocity blood flow within a gallbladder mass suggesting the diagnosis of gallbladder carcinoma. On the other hand, the presence of twinkling artifact can be very useful for diagnosis of small stones that do not generate a strong echo. However, twinkling is not invariable. Authors suggest that calcium oxalate dihydrate and calcium phosphate calculi always produce twinkling artifact while calcium oxalate monohydrate and urate stones may lack a twinkling artifact.

#### *Edge artifact*

This is related to strong specular reflectors and is seen as steady color along the rim of calcified structures such as gallstones or cortical bone. It is more commonly seen with power Doppler than color Doppler. The spectral Doppler tracing is characteristic being a straight line pattern equal above and below the baseline representing noise not true flow (**Figs 21A and B**).



**Figs 20A to C** The Gray Scale image shows a large renal calculus with distal acoustic shadowing (A). On application of color a mosaic of color is seen behind the calculus due to the twinkling artifact. Note the presence of flow in the intrarenal vessels as well (B). On increasing the velocity scale the intrarenal flow disappears but the twinkling artifact persists (C)



**Figs 21A and B** Edge artifact: Power Doppler image showing steady color along the rim of a gallbladder calculus (A). The spectral trace is characteristic of noise being a straight line pattern above and below the base line (B)

### Flash artifact

Flash artifact is a sudden burst of random color that fills the frame obscuring the gray scale image. It can be caused by tissue motion or transducer motion. It is most commonly seen in hypoechoic areas such as cysts or fluids collection and in the left lobe of liver (due to cardiac pulsation). Power Doppler is more susceptible to flash artifact than color flow Doppler because of the longer time required to build the image as more frames are averaged to create a power Doppler image than with standard color Doppler.

Flash artifact occurs due to a system setting that suppresses color pixels which would otherwise overwrite gray scale echoes or the color write priority. In the absence of gray scale echoes, color pixels take priority so that flow is seen in nearly stationary fluid. The artifact is transitory coinciding with transducer or patient motion such as respiration or cardiac pulsation and hence can be easily interpreted. In fact the flash artifact may at times be used to denote fluid nature of solid appearing material.

### Perivascular or Color Bruit Artifact

This is a tissue motion artifact in which movement is generated within an organ rather than involving an entire organ or image. It is seen as a color mosaic in soft tissue (rather than a single homogeneous color) adjacent to vessels with turbulent flow and is thought to be caused by actual vascular tissue vibration. These artifacts are more common with low PRF as a result of increased sensitivity of the system but may also be caused by low wall filter setting.

This artifact is the imaging equivalent of an auditory bruit or palpable thrill. It varies with the cardiac cycle being most prominent in systole and least in diastole. It is commonly seen in association with anastomotic sites, stenotic arteries or arteriovenous fistulae and can be useful to detect their presence.

## SPECIAL IMAGING MODES<sup>1-3,10,13-16</sup>

The modern imaging systems incorporate a number of special imaging modes involving advances in beamforming, ultrasound signal acquisition, and postprocessing to deal with inherent artifacts in ultrasound and improve image quality.

### Tissue Harmonic Imaging

Difference in propagation velocity of ultrasound between tissues such as fat and other soft tissues, near the transducer results in phase aberrations that distort the ultrasound field producing noise and clutter. In addition, the focusing of the ultrasound beam depends on phase coherence of the sound waves at the focal zone and at the transducer surface during receive focusing. If the intervening tissue has heterogeneous velocities defocusing will occur because the waves no longer coincide precisely, degrading lateral resolution. Tissue

harmonic imaging provides a means to reduce the effects of phase aberrations. The term harmonic refers to frequencies that are integral multiples of true frequency of the transmitted pulse which is called the fundamental frequency or first harmonic. The second harmonic has a frequency twice the fundamental.

Harmonics are generated due to the non-linear propagation of sound waves in the tissues. The wave velocity is higher for high pressure waves, i.e. compression than low pressure component, i.e. rarefaction. This causes increasing distortion of the ultrasound pulse as it travels through the tissue changing the wave pattern from a perfect sinusoidal shape to a sharper saw tooth shape. This generates waves of higher frequencies which are multiple of the fundamental frequency (2nd, 3rd, 4th, etc.) which are referred to as harmonics (Fig. 22). The intensity decreases as the order of the harmonics increases. In addition, the higher frequency harmonics are also attenuated more. Hence current harmonic imaging is mostly performed using the second harmonic component (Work is in progress in order to utilize higher order harmonics or the so called superharmonic imaging and frequencies lower than the transmitted frequency or subharmonic imaging for use with ultrasound contrast media) The final image is formed by the harmonic frequency bandwidth in the received signal after eliminating the transmitted frequency by frequency filtering, pulse inversion/phase cancellation or coded harmonics.

The generation of harmonics requires interaction of transmitted pulse with the propagating tissues hence harmonic generation is not important near the transducer or skin surface and becomes important only some distance away from the transducer. Harmonic images therefore show good rejection of artifacts and clutter arising from the body wall and also reduce the defocusing effect of the body wall. Artifacts are also reduced in harmonic imaging as the amplitude of the harmonic waves is relatively small reducing detection of echoes from multiple scatters. In addition artifacts produced by the fundamental frequency and side lobes do not have sufficient energy to generate harmonic frequencies and are therefore filtered out during image formation. Penetration can be improved by using a low fundamental transmitted pulse and imaging at the higher harmonic frequency.

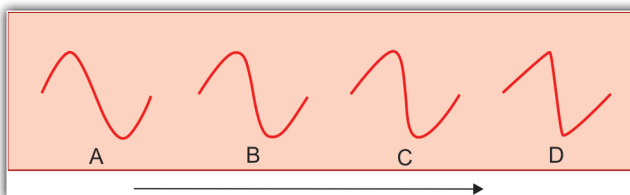
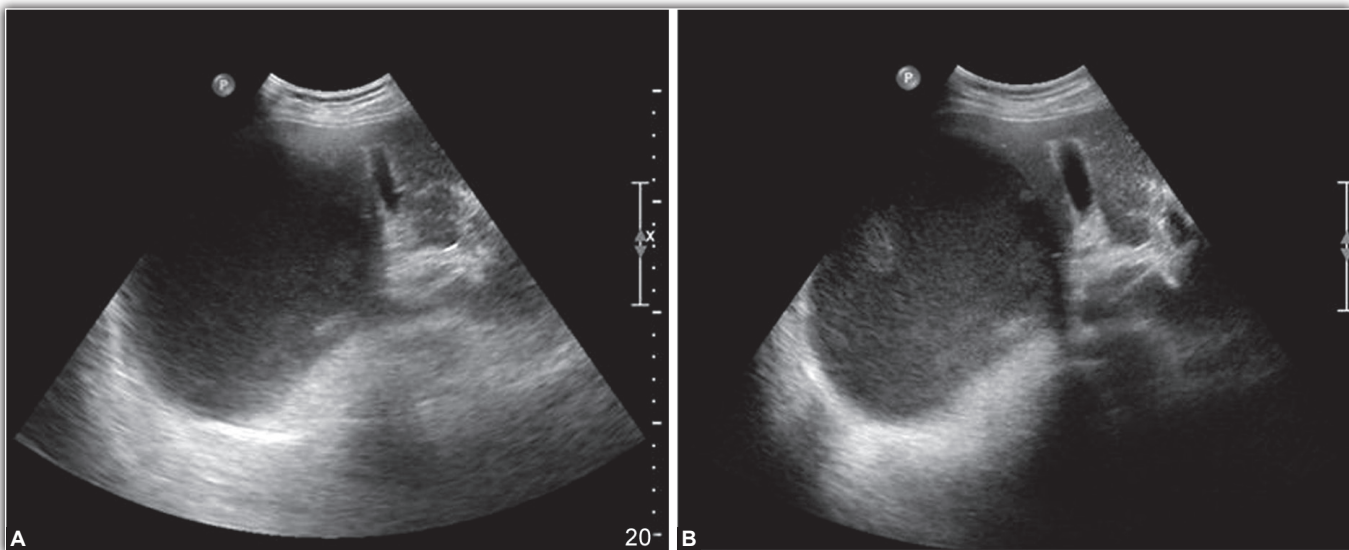


**Fig. 22** Generation of harmonics: As the path length through the tissue increases the sinusoidal waveform (A). Changes to a more saw tooth pattern with higher frequency due to the compression wave traveling faster than the rarefaction wave (D)



**Figs 23A and B** A transverse scan of the liver in a relatively obese patient with a large right lobe abscess. Although the abscess is visualized in the image without harmonics (A), the margins of the abscess, its internal echopattern and the diaphragm are much better appreciated in the harmonic imaging mode (B)

Other advantages include improved axial resolution due to shorter wavelength and better lateral resolution due to improved focusing with higher frequencies. Also because harmonics originate in regions of the ultrasound pulse with the greatest pressure amplitude, i.e. near the pulse center (as the amplitude at the periphery is too weak to generate harmonics) it results in a narrower beam producing images with superior lateral and elevational resolution. Harmonic images thus show less haze, noise, clutter and better cyst clearance (**Figs 23A and B**).

The technique is most useful in patients with thick complicated body wall structure or the so-called difficult patients for mid field imaging. At greater depths harmonic signals begin to decrease substantially relative to fundamental signal due to increased attenuation.

### ■ COMPOUND IMAGING

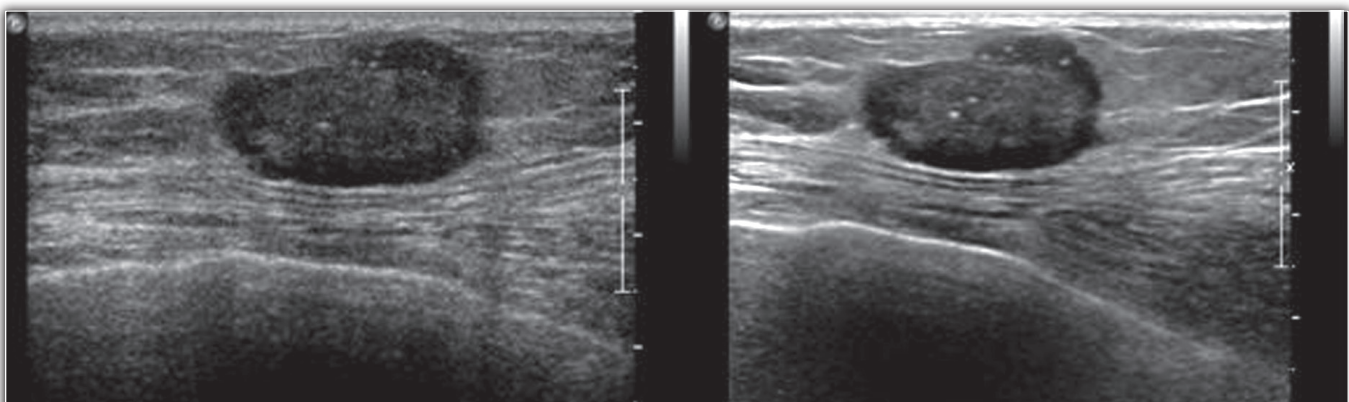
Compound imaging is the ability to acquire multiple frames from different-frequencies, i.e. **frequency compound imaging** or from different angles, i.e. **spatial compound imaging**. Frequency compounding is the combination of multiple images detected from different frequency bands into a single image. This reduces noise and speckle as the appearance of speckle varies with frequency. This is possible with the use of broad band width transducers.

### Spatial Compound Imaging

In spatial compound imaging electronic steering of ultrasound beams from an array transducer is used to image the same tissue multiple times by using parallel beams oriented in different directions. Data from many such beam

lines is acquired and averaged together into a single image. The appearance of speckle varies according to the beam line direction, averaging echoes from different directions tends to average and smooth speckle making the images look less grainy. Since speckle noise is random it cancels out during compounding while signal is reinforced.

Spatial compounding is also useful to image specular reflectors. Relatively large smooth surfaces reflect sound like a mirror with angle of incidence being equal to angle of reflection. Such specular reflectors include diaphragm, wall of urinary bladder, endometrial stripe, etc. Since the ultrasound beam is not dispersed like scatters, the signals are much stronger but are highly directional. Display of specular interfaces is therefore highly dependent on angle of insonation and specular reflectors return echoes to the transducer only if the sound beam is perpendicular to the interface. As the surface is titled away from 90° the signal intensity falls rapidly (as the sound beam is reflected away from the transducer). This results in poor margin definition and less distinct boundaries for cysts and other masses in conventional imaging where each scan line used to generate the image. It is of particular importance in sonography of the **musculoskeletal system** because of the anisotropic nature of muscles and tendons. The fibrillar pattern of a tendon is best appreciated when the ultrasound beam is perpendicular to the tendon and appears relatively echo-poor at oblique angles simulating tears or tendinosis. In spatial compound imaging since the image is generated from more than one angle of insonation the chances that at least one of these is perpendicular to the specular reflector is greater, reducing anisotropic effects improving tissue plane definition and display of curved structures.



**Figs 24A and B** Fibroadenoma of the breast imaged without (A) and with spatial compound imaging (B). The margins of the lesion, internal architecture and calcifications are better visualized. Note the reduced edge shadows

Spatial compound images show reduced levels of speckle, noise, clutter and refractive shadows and improve contrast and margin definition. Enhancement and shadowing artifacts may be reduced which may be an advantage or potential drawback depending on the clinical situation (**Figs 24A and B**).

Another drawback is that because multiple US beams are used to image one tissue region instead of just one beam as in conventional B-mode imaging more time is required for data acquisition and processing so the compound frame rate is reduced compared to conventional B-mode imaging depending on the processing capabilities of the imaging system.

Spatial compounding can also be achieved by using a single transmit pulse and varying the crystals that receive. This typically maintains higher frame rates as less transmit pulses are used.

### Coded Pulse Excitation

Higher frequency US pulses produce images with better spatial resolution, however, increased attenuation with increasing frequency limits evaluation of deep structures with high frequencies. Coded pulse excitation is a means of overcoming this limitation providing good penetration at higher frequencies necessary for high spatial resolution. This technique uses longer ultrasound pulses instead of the routinely used short ultrasound pulses. These longer pulses carry greater ultrasound energy, which increases the energy of echoes that return from the deeper tissues allowing use of higher frequencies. The coded pulses are produced with a very characteristic shape and the returning echoes also have a similar shape, which makes their identification from background noise easier (**Fig. 25**). The returning echoes are then processed using a pulse compression technique in which the location of the long characteristic pulse shapes are identified. These pulse shape locations may be determined

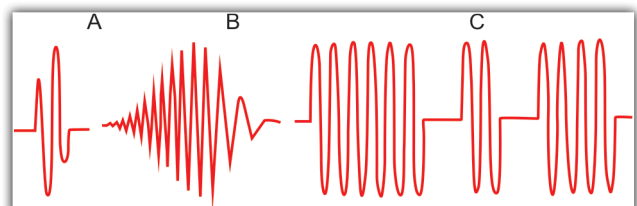


**Fig. 25** (A) Normal pulse (B) a chirp pulse and (C) a coded pulse

with a tight spatial tolerance and correspond to the location of structures from where they are reflected. Hence, the location of reflectors is identified with good spatial resolution. This produces an image with good echo signal and good spatial resolution at greater depths.

### Adaptive Image Processing

An adaptive image processing algorithm is one that able to recognize the difference between real targets and artifacts, and to modify its processing accordingly. Multiresolution adaptive image processing algorithms to smooth speckle and enhance structural edges are now available (e.g. XRES Philips).

It involves an analysis phase (in which artifacts and targets are identified) and an enhancement phase (in which artifacts are suppressed and targets enhanced). The analysis phase takes into account multiple characteristics of the target, such as local statistical properties, textural and structural properties. The textural and structural information in particular is vital for identifying the strength and orientation of interfaces and thus allowing directional filtering of these targets in the enhancement phase. For example, smoothing is applied along an interface to improve continuity, while edge enhancement is applied in the perpendicular direction. In regions identified by the analysis phase as being homogeneous, smoothing is applied equally in all directions.

### Photopic Ultrasound Imaging

This technique can be used to optimize image contrast. Grey levels are converted to monochromatic color value, allowing very subtle structural differences to be appreciated.

### Extended Field of View Imaging

Early static B-mode scanners had a large field of view (FOV) which was lost with the introduction of real time scanning. Extended FOV imaging restores the capability of visualizing large anatomic regions in a single image.

The transducer is translated across the region of interest, during which multiple images are acquired from multiple transducer positions. Image features in regions of overlap between successive images are used to determine the exact position of the multiple images relative to each other by the scanner. The images are thus registered with respect to each other accounting for both translation and in plane rotation of the transducer. The registered image data is processed in a large image buffer and combined to form the large FOV image. It is a useful image presentation format

### B-Mode Flow Imaging

B-mode flow imaging is a new method for flow imaging available in ultrasound. This technique shows blood flow with Gray Scale or B-mode imaging and is not a Doppler method. For B flow imaging digitally encoded wide band pulses are transmitted and reflected from moving blood cells. The returning echoes are decoded and filtered to increase sensitivity of moving scatterers and distinguish blood from tissue. Both the surrounding stationary tissue and flowing blood are shown in shades of gray.

As this is not a Doppler technique no velocity or frequency information is provided. It is a purely visual nonquantitative method. The major advantage is that it allows precise definition of the boundary between flowing blood and vessel wall. There is no problem of blooming or over amplification of flow signals as this is a non-Doppler technique. The technique does not degrade the spatial or temporal resolution of the Gray Scale image unlike color Doppler and is more accurate in showing the extent of plaque and surface irregularity of the plaque as compared to color Doppler or Gray Scale imaging alone in superficial vessels.

The technique is, however, most useful in superficial vessels as it relies on amplification of very weak echoes from red blood cells.

### 3D-4D Ultrasound

Although 3D/4D technology has been available in ultrasound for years it is mainly used in cardiology, obstetrics and gynecology. Uses in other areas are being gradually explored.

Among the primary approaches used for 3D data acquisition are the free hand scanning, mechanical devices integrated into the transducer and matrix array technology.

The 4D refers to real time acquisition of 3D data set. Volume data is generally displayed using three primary methods, multiplanar images (3 slices orthogonal to each other) and rendered images that show entire structures throughout volume.

The 3D/4D ultrasound, provides the ability to acquire the entire volume at one time so that there is no risk of missing out details which were not included in the original scan. Organ volumes, especially of irregularly shaped organs may be more accurately measured using volume data, 3D data results in more reproducible measurements can thereby assist in monitoring therapy and allow better definition of fetal facial features , uterine congenital anomalies, etc.

### CONCLUSION

With increasing technological advances, applications of ultrasound and Doppler have grown tremendously both for detection of pathology and physiology. Gaining maximum benefit from this complex technology requires a combination of skills, including knowledge of physical principles that empower ultrasound with its unique diagnostic unique capabilities. With this information the radiologist can gather maximum information from each examination while avoiding pitfalls and errors in diagnosis that may result from omission of information or misinterpretation of artifacts. Careful attention to technical parameters, appropriate use of special imaging features and diligence of examination technique will avoid day-to-day scanning pitfalls and result in studies with improved diagnostic accuracy.

### REFERENCES

1. Hangiandreou NJ. B-mode US: basic concepts and new technology. Radiographics. 2003;23(4):1019-33. Review.
2. Merrit Christopher RB. Physics of ultrasound in Diagnostic ultrasound vol 1, 3rd edn. Rheumack Wilson SR Charboneau JW (Eds). Elsevier. 2005.pp.3-34.
3. Cosgrove D. Artefacts in B mode imaging in Abdominal and general ultrasound vol 1, 2nd edn. Meire H , Cosgrove D, Dewbury K, Farrant P (Eds). Churchill livingstone. 2001.pp. 47-65.
4. Rubens DJ, Bhatt S, Nedelka S, Cullinan J. Doppler artifacts and pitfalls. Radiol Clin North Am. 2006;44(6):805-35.
5. Farina Robrerto Saparano Amelia. Errors in ultrasonography in Errors in Radiology. Luigia Romano Antonio Pinto (Eds). Springer Verlag. 2012.pp.76-85.
6. Feldman MK, Katyal S, Blackwood MS. US artifacts. Radiographics. 2009;29(4):1179-89.
7. Acampara Ciro, Fabia Pinto, Magistris Giuseppe De Errors in color Doppler ultrasonography in Errors in Radiology. Springer Verlag. 2012.pp.86-103.
8. Tahmasebpour HR, Buckley AR, Cooperberg PL, Fix CH. Sonographic examination of the carotid arteries. Radiographics. 2005;25(6):1561-75.
9. Kruskal JB, Newman PA, Sammons LG, Kane RA. Optimizing Doppler and color flow US: application to hepatic sonography. Radiographics. 2004;24(3):657-75.

10. Zagzebski James A. Physics in Doppler and B-mode ultrasound in Introduction to vascular sonography, 6 Edn. Pellirito, Polak (Eds) Elsevier. 2012.pp.20-51.
11. Campbell SC, Cullinan JA, Rubens DJ. Slow flow or no flow? Color and power Doppler US pitfalls in the abdomen and pelvis. Radiographics. 2004;24(2):497-506.
12. Rahmouni A, Bargoin R, Herment A, Bargoin N, Vasile N. Color Doppler twinkling artifact in hyperechoic regions Radiology. 1996;199(1):269-71.
13. Choudhry S, Gorman B, Charboneau JW, Tradup DJ, Beck RJ, Kofler JM, Groth DS. Comparison of tissue harmonic imaging with conventional US in abdominal disease. Radiographics. 2000;20(4):1127-35.
14. Rosenthal SJ, Jones PH, Wetzel LH. Phase inversion tissue harmonic sonographic imaging: a clinical utility study. AJR Am J Roentgenol. 2001;176(6):1393-8.
15. Desser TS, Jeffrey RB. Tissue harmonic imaging techniques: physical principles and clinical applications. Semin Ultrasound CT MR. 2001;22(1):1-10.
16. Lin DC, Nazarian LN, O'Kane PL, McShane JM, Parker L, Merritt CR. Advantages of real-time spatial compound sonography of the musculoskeletal system versus conventional sonography. AJR Am J Roentgenol. 2002;179(6):1629-31.

## Chapter

# 3

# Ultrasound Elastography: Principles and Application

*Veenu Singla, Tulika Singh, Anindita Sinha*

## INTRODUCTION

Elastography is a noninvasive technique of imaging stiffness or elasticity of tissues by measuring movement or deformation of tissue in response to a small applied pressure. It is a method of "virtual palpation" of tissue or lesions, which has the potential to overcome the subjectivity associated with clinical palpation. It can also provide objective and quantitative measures of tissue stiffness.

## BASIC PHYSICS

Some common terminology like stress, strain, shear, elasticity, viscoelasticity and Hooke's law and Young's modulus are often used and a basic understanding of these is required to understand elastography.

### Stress

Stress is defined as force per unit area. Unit of stress is Pascal or pounds per square inch (psi). (Pascal = Newton/m<sup>2</sup>).

Stress can be due to compression, which acts perpendicular to a surface and causes shortening of an object.

Shear stress acts parallel to a surface and causes deformation.

In elastography, stress can be applied exogenously-by transducer compression, vibrators or acoustic radiation force. Endogenous motion of vessels, cardiac or respiratory motion can also be utilized. Although endogenous sources overcome the shortcomings of exogenous source like attenuation (e.g. due to obesity or ascites), endogenous stress is difficult to quantify.<sup>1</sup>

### Strain

When subjected to stress an object tends to undergo deformation of its original size and shape; the amount of deformation is known as strain. Longitudinal strain, like compression causes change in length of an object. Shear strain causes changes in angles of an object.

Strain is unitless, expressed as change in length per unit length of the object. So, hard objects have lower strain values than softer objects. When compression is applied, lesions nearer the applied force undergo more displacement than objects lying in a deeper plane. This is similar to clinical difficulty in palpating deep seated lesions and is one of the factors which may influence efficacy of elastography.

### Elasticity

The property of materials to return back to its original form after stress is removed is known as elasticity. Elastic materials strain immediately when stressed and also return quickly back to their original position.

### Viscosity

Viscosity is the measure of resistance of a fluid when it undergoes shear stress or tensile (compression or stretching) stress.

### Viscoelasticity

This is the property of materials to exhibit both viscous and elastic properties. In viscoelastic material like soft tissue, there is a time delay between application of force and displacement. When stress is applied, the strain increases rapidly as free

fluid in soft tissues is exuded. Then, the relationship of stress over strain becomes linear for small changes.

### Poroelasticity

A material in which a solid matrix is permeated by an interconnecting network of fluid filled pores.

Tissue may be viscoelastic, poroelastic, anisotropic (e.g. muscle fibers or nerve fibers oriented in a particular direction) or contractile or a combination of these and disease conditions may modify their character.

Elastography techniques which can estimate visco-poroelasticity give a more accurate estimate of tissue conditions than techniques where simple stress, strain or Young's modulus is measured, as here tissue is assumed to be a homogeneous and isotropic material.

Hooke's Law states that stress is proportional to the strain within an object's elastic limit. Young's Modulus (E) is the ratio of stress over strain and has the same unit as stress. Young's Modulus measures the tissue's resistance to compression.

Hooke's law holds true for homogeneous isotropic solids.

Softer tissues like fat undergo more deformation (strain) when stress (e.g. compression during palpation) is applied. Harder tissues like muscle and fibrous tissue resist strain and thus have a higher Young's modulus.<sup>2-4</sup>

**Poisson's Ratio:** When exposed to stress, tissue may contract in one dimension (like width) while its length increases.

Poisson's ratio = lateral contraction per unit breadth/longitudinal extension per unit length.<sup>5</sup>

Poisson's ratio for normal soft tissue is 0.5.

**Shear modulus:** Shear modulus or modulus of rigidity (G) is a ratio between shear stress and shear strain.

Elasticity imaging can be based on imaging either strain, stress or Young's Modulus, shear modulus or shear wave velocity imaging.

### DEPICTION OF ELASTOGRAMS

Elastograms are generally viewed simultaneously with a sonogram to identify area of abnormality. This can be done with either Gray Scale depiction or a semi-transparent color overlay of the elastogram over the sonogram.

On Gray Scale elastograms, stiffer lesions are darker and appear to increase in size when compared to sonograms. On color overlay images, blue and green depicts stiff areas and red to yellow denotes soft areas.

### DIFFERENT ELASTOGRAPHY TECHNIQUES

Elastographic techniques vary depending upon:

1. The method used for tissue excitement (either mechanical or ultrasonic force)
2. By the response of tissue to compression, i.e. static or quasistatic, where a single compression is applied or

dynamic system in which response to rapid compression or vibration is measured.

### Compression Elastography

Compression elastography is calculating a strain profile in a direction perpendicular to the tissue surface in response to an externally applied force. This technique is most widely used in different ultrasound systems to evaluate the elastic properties of the tissues by analyzing the radiofrequency pulses generated by a structure in response to external compression.<sup>6</sup> Compression causes deformation of the tissue that varies as a function of the elastic coefficient. This principle is expressed by Young's modulus of elasticity.<sup>7</sup> RF waveform before and after compression are windowed and the signals in the same segment are compared to calculate the displacement. Around 97 percent of transmitted ultrasound waves are absorbed, only 3 percent of energy is scattered. Scattering occurs at the tissue boundaries, especially collagenous and fat surfaces.

Tracking of displacement of this scatter in real time is the objective of strain imaging.<sup>8</sup> A simple approach to extract elasticity information from soft tissue involves acquiring maps of the tissues before and after the compression (**Fig. 1**). Radiofrequency echo signals are typically the "map of tissue" used and tiny motion induces a change in the phase of radiofrequency echoes that can be tracked.<sup>9</sup> The amount of shift in the signal equals the amount of tissue displacement at the point in the image frame. This rate of change values are known as strain. Specialized software is used to calculate the relative difference in the tissue movement from one frame to another and then to estimate the tissue deformation.<sup>10</sup>

Three methods have been introduced for measuring tissue strain at elastography are the spatial correlation method, phase shift tracking method and combined autocorrelation method. The spatial correlation method is 2D pattern matching algorithm to search for the position

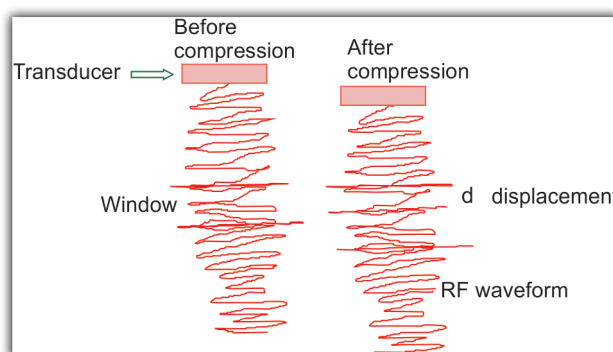


**Fig. 1** The windowed segment of scattered RF waveform is cross-correlated with the waveform obtained pre- and post-compression. The amount of shift between the matching segments is equal to tissue displacement (d).

that maximizes the cross correlation between ROIs selected from two images. The phase shift tracking method is based on autocorrelation method and can be used to rapidly and precisely to determine longitudinal tissue motion because of phase domain processing. This method fails when used for large displacement and it poorly compensates for lateral movement known as lateral slip.<sup>11</sup>

To overcome this problem a method known as combined autocorrelation method is employed, which enables rapid and accurate detection of longitudinal displacement by using phase domain processing without aliasing.<sup>12</sup> Clinical implementation typically involves freehand scanning, which requires real time implementation for instant feedback to the user to control the direction of deformation.<sup>13</sup> Hard or stiff materials tend to move as a whole with all points displacing with the same amount on compression, which results in zero or small rate of change of displacement called as zero or no strain. Softer tissue shows larger change in rate of displacement versus depth giving large strain values. The deformation measurement is mapped on elastogram on which stiffer areas are depicted as dark and more elastic area are lighter. This actually allows the differentiation of the lesion, which otherwise isoechoic on Gray Scale ultrasound image.<sup>10</sup> Free hand scanning is usually induced at a rate resulting in nearly completely elastic deformation making interpretation much easier than it otherwise. The most common clinical application is breast imaging. But any organ which can be clinically palpated has been scanned for elastography including breast, prostate, thyroid muscle and lymph node.

### *Limitations*

The amount of tissue displacement and the rate of change in displacement vary with the amount of compression applied. Hence, the tissue strain is dependent on the amount of the compression applied and it does not quantify the intrinsic elastic property of the given tissue. This makes it operator dependent. It is a qualitative imaging of relative stiffness so the actual strain value cannot be compared with the next imaging.<sup>6</sup> However, it can be used as semi-quantitative elastography with evaluation of strain ratio, which is the ratio of strain between the lesion and adjoining normal tissue. Because it shows only changes in strain from one area to other in the same image, hence it is suitable for the detection and evaluation of the small focal lesion and not sensitive to the diffuse disease process that produces same stiffness all over in one image.

### **Acoustic Radiation Force Impulse**

#### *Principle and Technique*

Acoustic radiation force impulse (ARFI) imaging is a technique where short duration acoustic forces known as pushing pulses are used to cause tissue displacements.

No external or physiological (pulsation or respiration) compression is needed. The cessation of force causes tissue to return to its original position. Pushing pulses can be applied by the ultrasound transducer array (frequency of 2-7 MHz) to a volume of  $2 \text{ mm}^3$  for 1 ms per pulse resulting in a displacement of 10 to 20 μm. Pushing frequency is in the lower end of the transducer bandwidth, and the transmit voltage is at the upper end of the system capability. The pushing pulses are similar to those for Power Doppler imaging; however, they are much longer in duration (200 cycles vs. 10 cycles).

### *Measurement*

Ultrasound pulses track these displacements by locating change in the peak along multiple tracking lines. The excitation can be performed in a sequential fashion by translating the tracking line along the tissue to assess the response. Parallel acquisition of push pulses and tracking displacements can also be done. Peak displacement, time taken to reach peak displacement and recovery time are utilized to characterize tissue response.

Tissue recoil also generates shear waves, which propagate away from the focal point of excitation. The speed of the shear waves is proportional to the tissue stiffness. Shear modulus can be calculated from the shear wave velocity (**Fig. 2**). Mapping shear wave velocity (cm/sec or m/sec) at multiple lateral points from the region of excitation can generate quantitative measurements of tissue stiffness.

### *Quantitative versus Qualitative*

In lesion identification and monitoring ablation procedures, higher spatial resolution qualitative images are required. Quantitative analysis is required for diffuse stiffening associated with advanced liver fibrosis, differentiation of malignant and benign lesions based upon their absolute

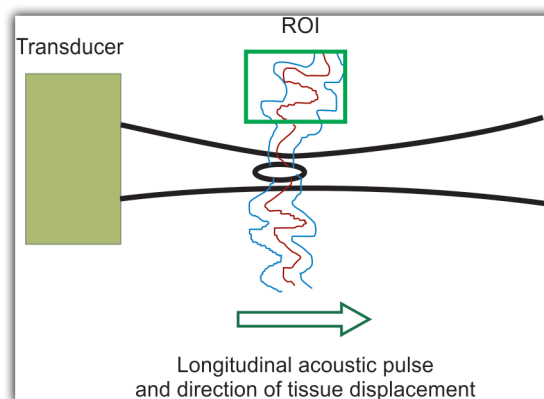


**Fig. 2** Schematic diagram for shear wave sonography. Longitudinal acoustic pulse transmission causes tissue displacement. Shear waves propagate away perpendicular to transmitted pulse. Separate tracking pulses in the region of interest (ROI) track these shear waves. The stiffer the tissue, faster the shear wave velocity

stiffness, and monitoring of disease progression and response to therapy.

### **Advantages**

The ARFI images are found to be more homogeneous and have better contrast than surface displacement (compression) elastography. Deeper tissue, not accessible by superficial external compression elastography can be evaluated.

### **Disadvantages**

Physiological (respiration, pulsation) and transducer motion can degrade image quality as 1 to 3 ms is required per tracking line pair. Lower ultrasound frequencies and motion compensation techniques like premonitory physiological motion and subtracting this expected motion have been applied to overcome these limitations.<sup>5,14</sup>

Tissues at a depth of more than 10 cm cannot be accurately assessed due to attenuation of the radiation force at greater depths.

### **Safety**

Peak temperature increase for one pushing pulse from a single excitation is largest near the focal point. The typical temperature rise associated with an individual excitation ranges from 0.02 to 0.2°C, varying primarily as a function of transmit frequency and pulse duration. The duration of pushing pulses and the frame rate are limited to keep within the standard diagnostic limits of mechanical and thermal index.<sup>15</sup>

## **Shear Wave Imaging**

### **Principle and Technique**

Shear waves are induced remotely within tissue when an impulsive acoustic radiation force of a focused ultrasound beam produced by the transducer interacts with tissue.

Shear waves propagate perpendicular to the axial displacement caused by the ultrasound pulse and attenuate about 10000 times more rapidly than compression waves.<sup>5</sup> The high attenuation of shear waves enables mechanical oscillations to be induced within a very limited area of tissue. Deformations by the focused ultrasound radiation are generally very small (at submicron level). Sophisticated signal processing is required to detect such motion differences. A shear wave is created and tracked at lateral, spatially offset positions from the radiation force excitation by a parallel tracking method (**Fig. 2**).<sup>5,9</sup>

### **Measurement**

Velocity of shear waves (in  $\text{cms}^{-1}$ ) can be measured and used to evaluate tissue stiffness by calculating the elastic Young's

modulus according to the formula:  $E=3V^2(E\text{-Young's modulus in kPa, } V\text{-shear wave velocity in } \text{cms}^{-1})$ .

### **Qualitative versus Quantitative**

This technique results in both qualitative color coded elastogram and also quantitative maps either of elasticity (in kPa) or of shear wave velocity (in  $\text{cms}^{-1}$ ).

### **Advantages**

Lack of tissue compression makes it a more objective measurement, the direct assessment of elasticity and the quantitative measurements are provided.

### **Disadvantages**

Assessment of superficial structures may be difficult, as a certain depth of ultrasound penetration is needed for shear waves to be produced.

### **Advances in Shear Wave Imaging**

1. **Spatially modulated ultrasound radiation force (SMURF):** In this technique, a linear array transducer is used to acquire a reference scan at a specified position. Two pushing pulses are then transmitted and focused at the same depth laterally from the original position. This is followed by a series of scan lines, from which the induced shear wave peaks are estimated. This allows fast and accurate estimation of shear modulus with improved resolution.<sup>16</sup>
2. **Supersonic shear wave imaging:** In supersonic shear wave imaging, the focus of the radiation force from one location is changed to different depths (typically five) along the beam axis. Shear waves are created at multiple locations and these interfere constructively to create a conical shear wave front like a Mach cone of an aircraft traveling at supersonic speed.

Imaging the shear wave propagation requires an ultrafast scanner capable of 5000 frames per second. This is achieved by elimination of focusing of the pulses used for motion detection. One plane wave or a set of plane waves is transmitted with different angular direction to track the shear wave. B-mode data is also acquired in real time at about 50 frames per second.

**Measurement:** Shear wave propagation is measured and wave speeds are assessed to give viscoelastic moduli.<sup>17</sup>

3. **Axial shear strain imaging:** Malignant lesions tend to be more tightly bound to surrounding tissue than benign lesions. Axial shear strain images how tightly the lesion is fixed to the surrounding tissue. Loosely bound lesions have a thin band of color at the boundary whereas malignant lesions have a much thicker band. This simple depiction is much easier to interpret than elastography images.<sup>18</sup>

## Harmonic Motion Imaging

### Technique

Low frequency ultrasound (10-300 Hz) produces oscillations in tissue, which is measured at the center of vibration. Two separate focused ultrasound transducers are used. One transducer has a very large aperture, which is used to generate the radiation force. A small phased array transducer placed through a hole in the larger transducer detects motion.

### Applications

The same transducer, which generates the radiation force, can be utilized for creating thermal lesions. This allows real time and simultaneous generation and monitoring of high intensity focused ultrasound (HIFU) therapy. Tissue stiffening signifying successful ablation can be monitored and the treatment procedure can be performed in a time-efficient manner. Real time monitoring of RF ablation of arrhythmogenic foci in the heart may help spare the surrounding healthy myocardium from ablation.<sup>19</sup>

## Shear Dispersion Ultrasound Vibrometry

### Technique

This involves creating a shear wave by an external actuator or by acoustic radiation force. Multiple pushing pulses or excitation pulses are transmitted at a particular frequency and motion stimulated at harmonic frequencies is detected by ultrasound.

### Measurement

Shear wave speed dispersion is measured from the data generated at several frequencies. Dispersion of shear wave gives a measurement of the viscoelastic properties of tissue.

## Mechanical Imaging

Stress patterns of internal structures of tissue are measured by compressing the tissue by an ultrasound probe. Pressure sensors mounted on the contact surface of the probe detects the temporal and spatial changes in stress pattern, thus providing information about the different elastic properties (viscosity and porosity).

### Measurement

Surface stress data is recorded, allowing 2D and 3D reconstruction of tissues on the basis of elasticity. Nonlinear elasticity imaging which is most sensitive to cancerous changes can be evaluated by mechanical imaging.<sup>20</sup>

### Applications

Detection of cancer and differentiating benign from malignant lesions.

## ELASTOGRAPHY APPLICATIONS

### Breast

As the breast cancer tissue is harder than the adjoining normal breast parenchyma, because of its desmoplastic reaction, the evaluation of breast masses to differentiate benign lesion from malignant was one of the initial application of the ultrasound elastography.<sup>21</sup> Initially elastograms were done by using a computer controlled device, which needed precise control of amount of compression which is typically very small (0.1–0.5 mm). It was slow and very few elastogram could be taken. It also needs post processing. Over a period of time, hand held compression with the ultrasound transducer was substituted with more recently developed real time processing.<sup>22</sup>

The evaluation of hardness has the same principle of conventional clinical examination, i.e., palpation of any breast lump. Initial clinical work in this field appeared in 1997 and showed that cancer generally appeared stiffer (darker) than benign lesion and surrounding normal breast tissue.<sup>23</sup> Cancerous lesions almost invariably appeared larger on elastography. Other authors demonstrate the use of color maps to depict the tissue stiffness.<sup>24</sup> A proposed scoring system for the lesions on color maps is based upon elastographic properties of the tissue.

### Elastosonographic Score (Fig. 3)

**Score 1:** Presence of even strain in the lesion (green)

**Score 2:** Prevalence of green with few, if any blue spots with inconstant locations.

**Score 3:** Prevalently green but with central blue area.

**Score 4:** Almost completely blue, with few green points, most of all in periphery.

**Score 5:** Completely blue, also with a peripheral glow around the nodule.

For elastography score when cut-off point is taken between 3 to 4 for the malignant lesion it showed 86.5 percent sensitivity, 89.8 percent specificity and 88.3 percent accuracy in one study.<sup>24</sup> This gives information is about local strain estimated at a given location in tissues, but it depends on surrounding mechanical properties and it is not quantitative (**Figs 4 to 7**).<sup>25</sup>

Recently, the methods of semi-quantitative assessment of the breast lesions with strain ratio between the nodule and the

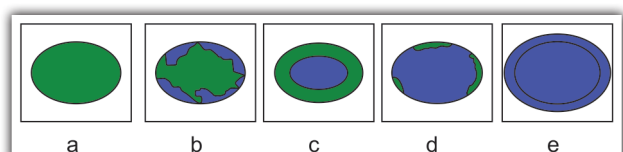


**Fig. 3** Colored diagrams representing the general appearance of elasticity score breast nodule in Tsukuba scoring of 1(a), 2(b), 3(c), 4(d) and 5(e)

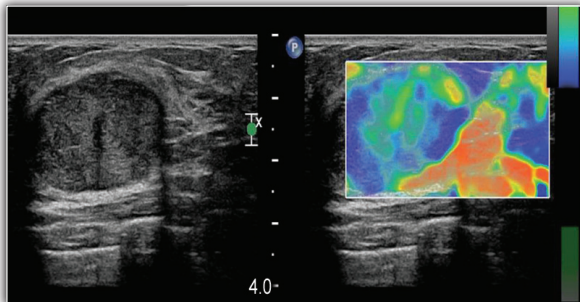


**Fig. 4** Elastography image of fibroadenoma showing elastographic score 2 with few small blue areas of no strain in the periphery. B-mode image shows well-defined ovoid hypoechoic nodule with posterior acoustic enhancement

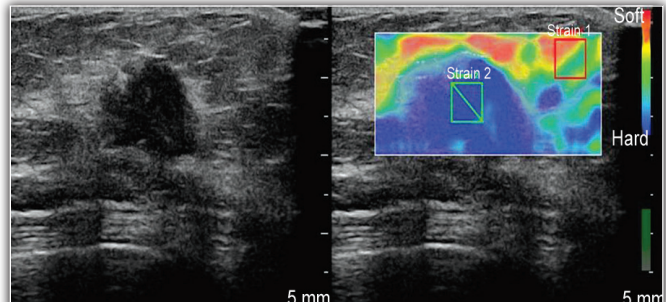


**Fig. 7** Elastographic image of IDC breast shows elastographic score 5 with blue area of no strain in the lesion and in the peripheral echogenic halo

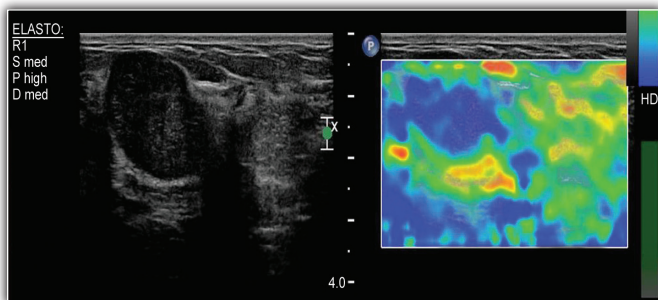


**Fig. 5** Elastographic image of another fibroadenoma showing elastographic score 3 with more central blue areas of no strain

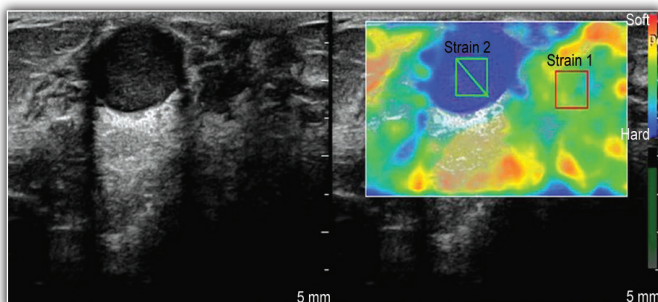


**Fig. 6** Electrographic image IDC breast shows elastographic score 4 with complete lesion appearing blue with no strain. The picture also shows the strain ratio 4.4 between the lesion and the adjoining normal breast

adjoining normal breast tissue is used for the differentiation of benign versus malignant nodule have been developed.<sup>26</sup> With freehand compression, the influence of probe movement has certain limitation as the elasticity map obtained is highly dependent on the organ's compressibility limits under pressure and on the extent of tissue compression applied. This makes it operator dependent. To overcome this problem, the quantitative methods are developed with assessment of the shear module, which is overall tissue stiffness like shear wave

elastography and supersonic shear imaging. It combines two concepts. Instead of using mechanical external compression, the system itself remotely induces mechanical vibration by using acoustic radiation force created by a focused ultrasound beam. The displacement induced at the focus generates a shear wave that conveys information linked to the local viscoelastic properties of the tissue, thus enabling a quantitative approach to elasticity values.<sup>27</sup>

The interpretation and measurement of elasticity is done in terms of the Young's modulus (in kilo Pascal, kPa). It is reported that mean elasticity values are significantly higher in malignant masses ( $153.3 \text{ kPa} \pm 58.1$ ) than in benign masses ( $46.1 \text{ kPa} \pm 42.9$ ) (Fig. 8).<sup>28</sup>

### Elastographic Appearances of the Breast Masses

#### Simple cyst versus complex cyst

Simple cyst is the most common type of breast lesion. It usually appears on conventional ultrasound as anechoic round or oval well-defined lesion with posterior acoustic enhancement, with imperceptible posterior wall. On elastography, it gives a target or bulls-eye appearance, with central bright area surrounded by a dark concentric rim.<sup>29</sup> Complex cyst with debris because of its internal contents can appear as a solid lesion on B-mode conventional ultrasound, and can be subjected to biopsy. Ultrasound elastography can help in revealing the cystic nature of the lesion with the typical target appearance.

**Fibroadenoma:** Represent most common type of solid breast lesion. Ultrasound typically shows fibroadenoma as well-circumscribed hypoechoic masses, which are wider than tall with long axis parallel to the chest wall. Sometimes, fibroadenoma can present as atypical shape like taller than wide.

In such cases, sonoelastography can help elucidate the benign nature of the lesion. Usually, it appears smaller than B-mode images in contrast to the malignant lesion, which show larger size on elastography because of its desmoplastic reaction in surrounding tissue. In one study as many as 73 percent of fibro-adenoma could be differentiated from

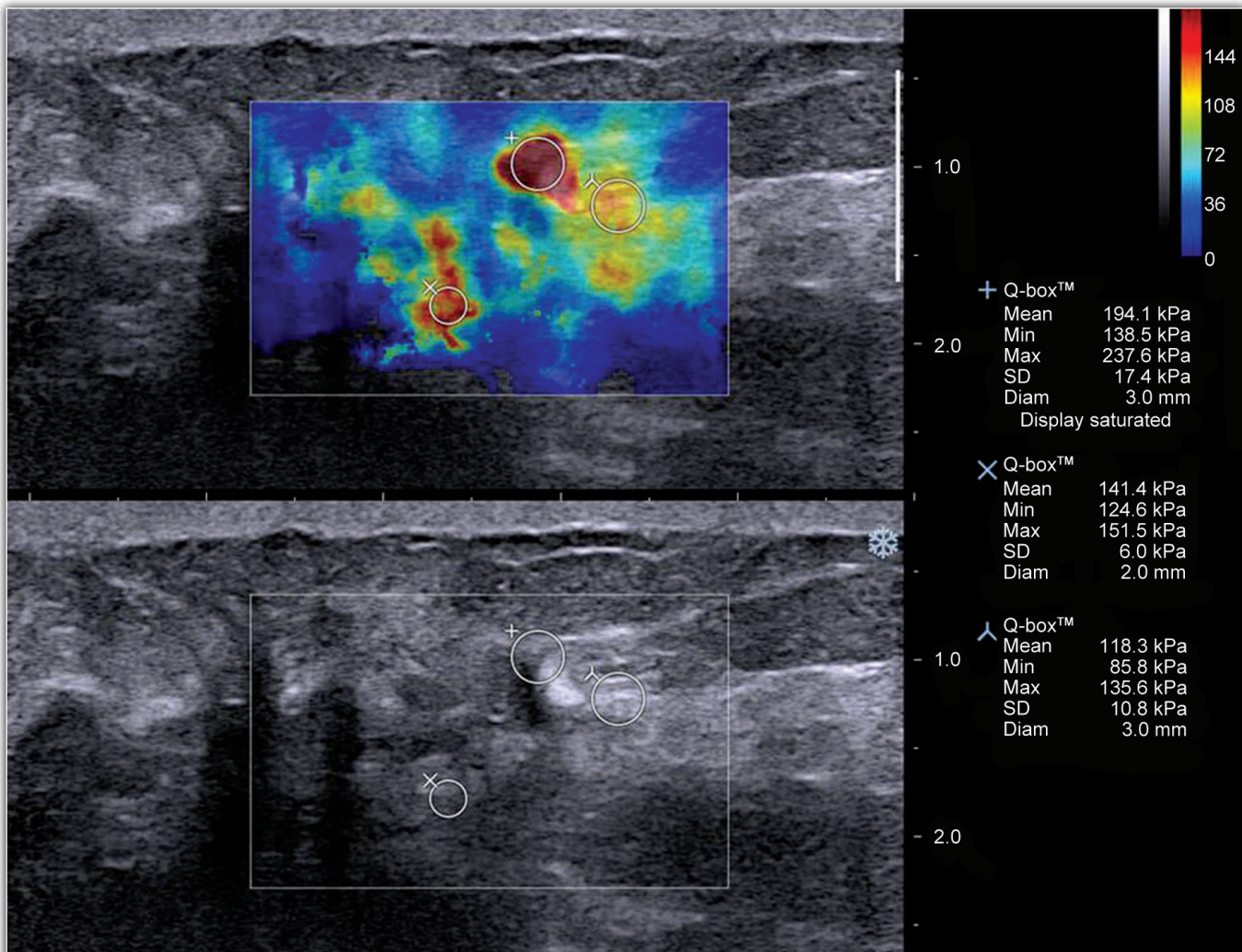


**Fig. 8** Shear wave elastography image of malignant breast lesion showing red color in hard tissue with values above 130 kpa

malignant on the basis of elastographic size and brightness criteria. Other methods to differentiate are quantitative and semi-quantities like calculating the strain ratio or assessment of overall stiffness as discussed earlier. Fibroadenoma larger than 2 cm and with calcification can give false positive for malignancy on elastography.<sup>30</sup>

**Invasive ductal carcinomas:** It is the most common invasive tumor of the breast. On B-mode ultrasound it appears as a hypoechoic spiculated or micro lobulated mass, which is taller than wide with angular margins and a hyperechoic halo. On sonoelastography invasive ductal carcinoma typically appears darker than normal tissue or benign lesion and it is slightly larger on the elastogram as compare to the B-mode ultrasound images.

Overall ultrasound elastography is reported to have a sensitivity of greater than 95 percent and specificity of about 85 percent for differentiation between benign and malignant

lesion using different qualitative and quantitative methods.<sup>31</sup> False negative elastogram can be seen in few well-defined benign looking masses, masses with tumor necrosis with acoustic enhancement can mimic cysts.

## Liver

### *Diffuse Liver Diseases: Fibrosis, Cirrhosis, Acute Hepatitis, Nonalcoholic Fatty Liver Disease*

In diffuse liver diseases, imaging modalities like B-mode ultrasound, CT and MRI have limited role in diagnosing liver fibrosis and early cirrhosis.

On ultrasound hyperechoic nodular liver may be present both liver fibrosis as well as fatty liver. A normal CT or MRI cannot rule out cirrhosis. Liver biopsy has been the reference method for diagnosing liver inflammation and fibrosis. However, it is an invasive procedure with accompanying risk

and even life threatening complications and also prone to sampling errors as only a small volume of the liver is sampled. Interobserver variability is also high.

Elastography (by ultrasound or magnetic resonance) is a noninvasive modality for assessment of fibrosis and degree of fibrosis. It is painless, reproducible and repeatable and easy to perform, allowing monitoring of disease. Although MRI elastography is sensitive for evaluation of fibrosis, it has limited availability; is time consuming and costly and not suitable for screening patients for presence or degree of fibrosis.

### *Factors Influencing Liver Stiffness*

1. Chronic liver parenchymal pathology may cause changes in liver stiffness by inducing fibrotic changes.

On liver biopsy, fibrosis can be divided into four stages<sup>32</sup>

*Stage 0 (normal):* No fibrosis around portal triads

*Stage 1 (portal fibrosis):* Fibrosis surrounds the portal triads, but is limited to these areas

*Stage 2 (periportal fibrosis):* Fibers begin to extend into the periportal space, but do not connect with other portal triads

*Stage 3 (septal fibrosis):* Fibrous connective tissue links neighboring portal triads and begins to extend to the central veins. Shape of lobule is distorted

*Stage 4 (cirrhosis):* Most portal triads are connected by fibrous tissue. Some portal triads and central veins are also connected.

2. Necro-inflammatory activity in the setting of acute hepatitis which causes hepatocyte swelling, edema and inflammatory infiltration also may increase liver stiffness. Patients with acute hepatitis (viral, autoimmune and drug-induced) may have a discrepancy between the liver stiffness measurement (LSM) and the fibrosis grade by biopsy.

Liver stiffness may be in the cirrhotic range (above 12.5 kPa) whereas fibrosis staging by biopsy is not more than stage 2. Similar increase in stiffness measurement is found in patients with chronic viral hepatitis who have acute exacerbations associated with rise in alanine amino transferase.<sup>33</sup>

3. Congestive cardiac failure and extra hepatic cholestasis or congestive heart failure. Light meals also alter elastography values.<sup>34-36</sup>

### *Ultrasound Elastography*

#### *Techniques for liver stiffness measurement*

Transient elastography-Fibroscan™ apparatus (Echosens, Paris, France)—is a non-imaging modality which has been widely used for liver stiffness measurement (**Figs 9A and B**).

It uses a single cycle of low amplitude low frequency (50 Hz) vibration to induce a shear wave. The velocity of the shear wave is faster in dense fibrotic tissue.

Transient elastography probe has a 5 MHz ultrasound transducer probe mounted on the axis of a piston, which acts as a vibrator. The tip of the probe is placed in the intercostal space with the patient lying supine with abducted arms. Under control time motion (TM) and A-mode, the operator chooses a liver portion within the right liver lobe at least 6 cm thick, free of large vascular structures and gallbladder. Stiffness is measured on a cylinder of hepatic tissue of 1 cm diameter and 2 to 4 cm length. The median value of 10 successful acquisitions, expressed in kilopascal (kPa), is taken as the liver stiffness. Measurements of 10 successful acquisitions with a success rate of at least 60 percent, and with Inter Quartile Range (IQR- median of the middle 50 percent of the values) <30 percent of the median value are generally considered valid.

Values range from 2.5 to 75 kPa, with normal values around 5.5 kPa. Wide range of liver stiffness values are observed in patients with cirrhosis (13–75 kPa).<sup>37</sup> Transient elastography has excellent accuracy in diagnosing cirrhosis and significant degrees of fibrosis.

#### *Comparison Between ARFI, Real Time Elastography and Transient Elastography for Liver Stiffness Measurement (Table 1)*

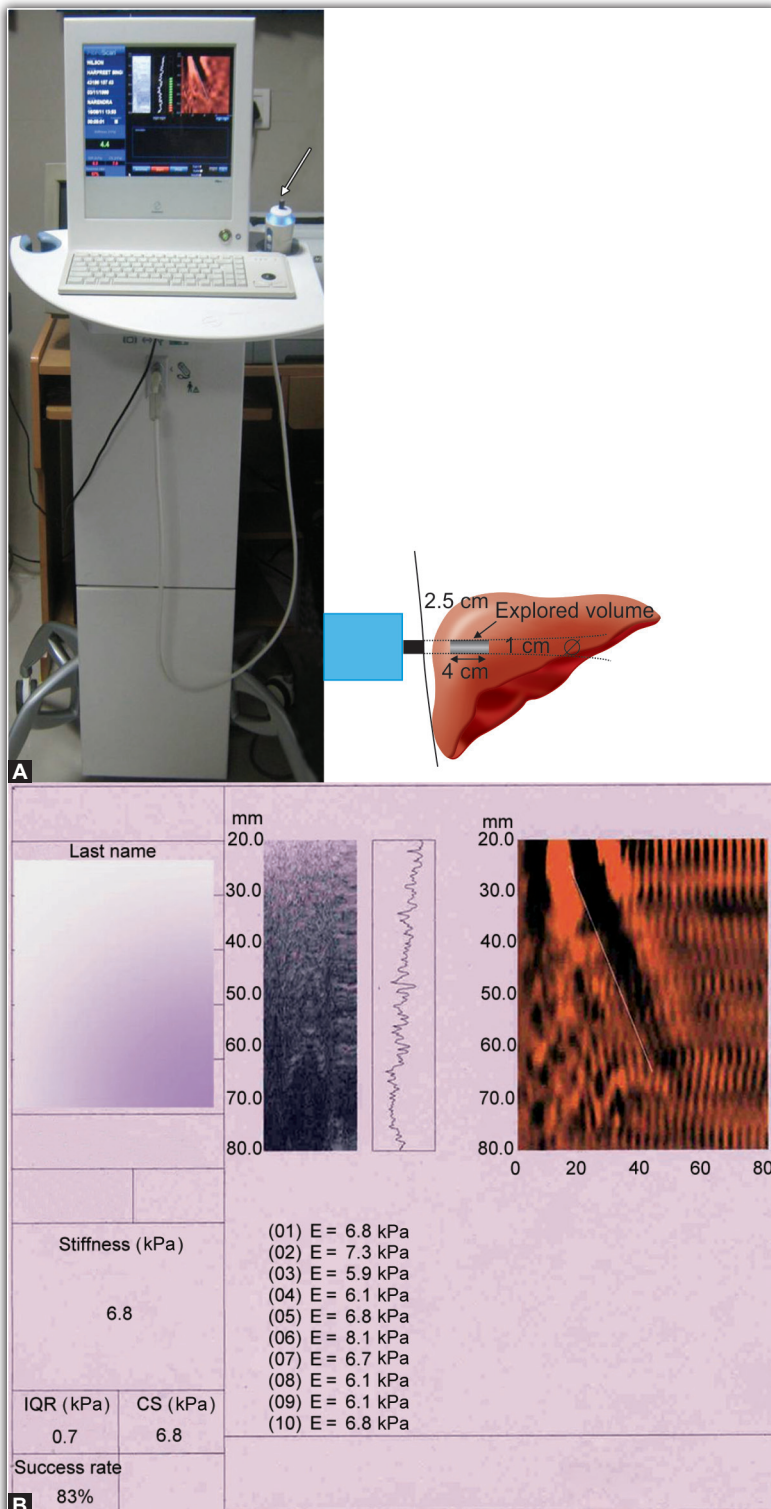
ARFI also has equal reliability in diagnosing liver fibrosis. ARFI is more sensitive for lesser degrees of fibrosis. Acute exacerbations of chronic liver disease have less influence on the liver stiffness by ARFI.<sup>38,39</sup>

Values for the liver stiffness measured with a transient elastography cannot be directly compared with ARFI or real time (shear wave) elastography since in the former a low frequency low amplitude pulse is given. This will lead to lower values when compared with real time elastography.

The liver stiffness values with a transient elastography have a wide range (2.5–75 kPa), whereas ARFI values are in a very narrow range (0.5–4.4 m/s). This might make it difficult to differentiate normal from abnormal values with ARFI in a clinical setting, although values in healthy donors range between 0.85 and 1.25 m/sec.<sup>37,40</sup>

#### *Post-treatment assessment*

Elastography is also used for measuring liver stiffness changes in responders and relapsers undergoing antiviral treatment with interferon and ribavirin. Liver stiffness measurements show significant decrease in patients of viral hepatitis undergoing treatment with interferon and ribavirin. Relapse after treatment also leads to increase in stiffness.<sup>41</sup>



**Figs 9A and B** Image of the Fibroscan device (Echosens, Paris) for transient elastography. (A) The probe has a piston (arrow), which is placed in the right intercostal space. A single low frequency vibration is generated and shear wave elasticity in a cylinder of 1cm × 4cm of hepatic tissue is measured (inset). Measurements of 10 successful acquisitions in a normal liver (B) with a success rate of at least 60%, and with InterQuartile Range(IQR- median of the middle 50% of the values)<30% of the median are taken. (Courtesy: Dr Ajay Duseja, Associate Professor, Department of Hepatology, PGIMER, Chandigarh)

**Table 1** Comparison of different elastography techniques for liver diseases

	Fibroscan (Transient elastography)	ARFI	Shear wave elastography
Imaging	Not possible	Yes	Yes
Assessment of focal lesions	Possible for large ( $>5$ cm) and superficial lesions. Requires prior localization with B-mode imaging. No real time image guidance	Yes	Yes Different areas within focal lesion can also be measured
Maximum depth of tissue for assessment	2.5 cm to 6.5 cm from skin	10 cm from skin	8 cm from skin
Maximum region of interest	1 cm $\times$ 5 cm	0.6 $\times$ 0.5 cm – 0.6 $\times$ 10 mm	Variable
Technique	Static – no images generated	Static images	Real time 2D evaluation
Obesity	Difficult (better with XL probe)	Less difficult	Less difficult
Ascites	Difficult to impossible	Difficult assessment	Difficult assessment
Quantification	Yes	Possible	Yes
Range of values	Large	Small	Large

Abbreviation: ARFI: Acoustic radiation force imaging

#### Assessment of portal hypertension/varices

Hepatic venous pressure gradient (HVPG) is the reference standard for measuring portal venous pressure (values  $> 6$  mm Hg). However, it is an invasive procedure. Patients with cirrhosis and gastroesophageal varices have an HVPG of at least 10 to 12 mm Hg. Variceal hemorrhage, ascites or encephalopathy may develop when HVPG increases over a threshold value of 10 to 12 mm Hg.

Splenic elasticity has a close linear relationship with HVPG and can help predict the presence of esophageal varices in patients with chronic liver disease.

Values of splenic stiffness above 8.7 kPa correlates with HVPG above 6 mm Hg and values above 17.6 to 23 kPa correlate with severe portal hypertension (HVPG  $> 12$  mm Hg). Splenic stiffness measurements show better and linear correlation with degree of portal hypertension than liver stiffness measurements. Combination of the liver stiffness with spleen diameter and platelet count however better correlates with degree of portal hypertension.<sup>42</sup>

#### Assessment of TIPSS

Splenic stiffness also decreases significantly with a functional TIPSS, whereas liver stiffness measurements do not show significant changes.<sup>43</sup>

#### Assessment of liver transplant

Repeated liver stiffness measurements (LSM) following transplant can discriminate between slow and rapid fibroses (fibrosis stage F2-F4 at 1 year). Liver transplant recipients with hepatitis C virus infection undergo rapid fibrosis within the first year. Serial measurements of elastography within the

first year shows much higher LSM than non-HCV infected recipients; (9.9, 9.5, 12.1 kPa vs 6.9, 7.5, 6.6 kPa).<sup>44</sup>

#### Assessment of nonalcoholic fatty liver disease

Nonalcoholic fatty liver disease (NAFLD) is a range of liver disorders with hepatic steatosis without alcohol consumption, viral, or drug-related etiologies. Histologically, it can be a simple accumulation of triglyceride droplets in hepatocytes or may progress to cellular injury and inflammation with resultant fibrosis and even cirrhosis and HCC.

Fibrosis and cirrhosis due to NAFLD can be detected by transient elastography or other routine elastographic techniques. A newer technique of Controlled Attenuation Parameter (CAP) gives an estimate of the attenuation of ultrasound at 3.5 MHz and is expressed in decibel per meters (dB/m). CAP is evaluated using the same radiofrequency data and in the same region of interest that is used for transient elastography and is a non-imaging based modality which shows promise in assessing the degree of steatosis noninvasively.<sup>45</sup>

#### Advantages

Elastography is a noninvasive, painless and repeatable procedure.

- It can evaluate a much larger liver volume than liver biopsy.
- It can be used for initial assessment, monitoring as well as diagnosis of complications (portal hypertension, esophageal varices).
- It can help in biopsy planning from stiffest regions to reduce sampling error.
- Tumor ablation monitoring is also possible real time with this procedure.

### Limitations

Parenchymal thickness of <4 cm under the probe, presence of ascites, severe obesity, and the absence of an intercostal space sufficiently wide for probe limit the usage of elastography. Male sex, body mass index >30, metabolic syndrome and acute viral hepatitis are all known to cause increased liver stiffness.<sup>46</sup>

### Focal Liver Lesions

#### ARFI

Malignant and benign liver lesions appeared stiffer compared with the surrounding liver parenchyma on ARFI in a study by Shuang-Ming T et al. There were statistical differences between malignant and benign liver lesions. The median value of malignant and benign liver lesions were 3.14 m/sec (average value  $3.16 \pm 0.80$  m/sec, range 1.17-4.45 m/sec) and 1.35 m/sec (average value  $1.47 \pm 0.53$  m/sec, range 0.74-3.26 m/sec).

A cut-off value of 2.22 m/sec resulted in sensitivity, specificity, and accuracy for malignancy of 89.7 percent, 95.0 percent, and 92.2 percent, respectively.<sup>47</sup>

#### Compression ultrasonography

Onur MR et al evaluated benign and malignant focal hepatic lesions, such as hemangiomas, focal nodular hyperplasia (FNH), nodular regenerative hyperplasia, adenomas, hepatocellular carcinomas, metastases, and cholangiocarcinomas. The strain ratio of liver parenchyma was compared with that of the focal lesion to give the strain index value. Mean strain index values of malignant liver lesions were significantly higher than that of benign lesions [The mean strain index value of malignant liver lesions  $\pm$  SD ( $2.82 \pm 1.82$ ) was significantly higher than that of benign liver lesions ( $1.45 \pm 1.28$ )]. Stiffness of hemangiomas vary depending on the amount of fibrotic septa dividing the vascular spaces. Strain index as well as mean values of hemangiomas on ARFI (1.5-2.3 m/sec) are significantly low.<sup>48,49</sup>

#### Shear wave

Shear wave values (in kPa), can distinguish between FNH and adenoma. The FNH have a radial pattern of elasticity whereas adenomas and hemangiomas are homogeneous. Scars from radiofrequency ablation or healed abscesses have the highest stiffness values among benign lesions.

A significant difference was also found between HCCs and cholangiocarcinoma elasticity. Cholangiocarcinomas were the stiffest among malignant lesions ( $56.9 \pm 25.6$  kPa)

The HCC stiffness depends on the underlying liver, with lesions in cirrhotic livers appearing softer than lesions in normal or mildly cirrhotic livers. Metastasis stiffness also is highly variable and depends on the primary source. Carcinoid metastases are stiffer than colorectal metastases.<sup>50</sup>

### Prostate

Prostate gland was one of the earliest organs for which elastography was proposed. Endorectal ultrasound continues to be most commonly used imaging modality for assessing the prostate. On B-mode ultrasound most carcinoma prostate show varying echogenicity mostly being hypoechoic to few isoechoic or hyperechoic also. So the overall sensitivity is approximately 50 percent.<sup>51</sup>

Real time endorectal elastography shows the sensitivity 68 percent with accuracy of about 76 percent.<sup>52</sup> Prostate cancers have a higher elastic modulus than that of surrounding normal prostate tissue.<sup>53</sup>

Eventually, the prostate cancer appears dark on elastogram more in the peripheral lesion. Sometimes, the malignant lesions which are very small or invisible on B-mode ultrasound images are prominent on elastogram as dark area of low strain (**Fig. 10**).

Elastographic imaging of the prostate gland can be performed with manual compression strain imaging (two-dimensional) or with external vibration with Doppler imaging, which permits two and three-dimensional imaging. Vibration elastography generates tissue displacement through the use of an independent external vibration source. Relative displacement is measured by using a variant of Doppler imaging that depicts differential motion of tissue types. This technique provides good correlation for tissues that have a large difference in stiffness.<sup>54</sup> Another role is for sonoelastographic guided prostate biopsies which increase the detection rate about three times than the routine endorectal ultrasound guided biopsies.<sup>55</sup>

Benign prostatic hyperplasia appears as heterogeneous hypoechoic area on endorectal B-mode ultrasound. Area with benign hyperplasia also show higher stiffness than that of normal prostate tissue but less than that of carcinoma prostate. However, it is difficult on differentiate between two and sometime it can give a false positive findings for the cancer prostate.<sup>54</sup> In a recent study, the ARFI was implemented to

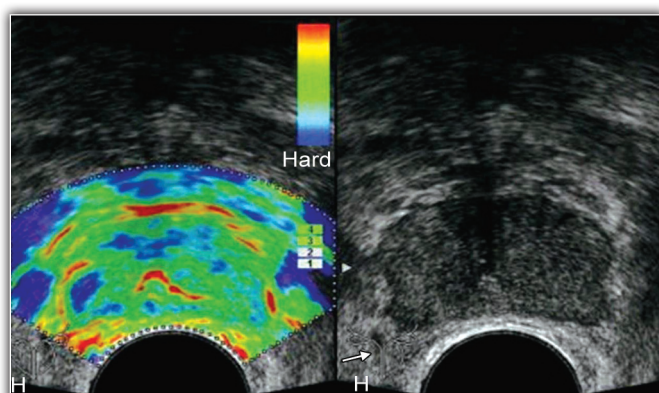


**Fig. 10** Elastography image is showing hard nodule in the prostate in the right peripheral zone in blue color. Same nodule appeared hyper-echoic on B-mode ultrasound image

image excised human prostate.<sup>55</sup> The ARFI imaging is an elasticity imaging technique, which uses remotely generated, focused acoustic beam to excite tissue and generate the images of tissue displacement response.<sup>56</sup>

Various prostatic zonal structures and pathologies were demonstrated on ARFI imaging. The ARFI images are produced by evaluation of displacement within the ROE from multiple excitation and formation of an image from all location. The central zone (CZ), Ca prostate and atrophy show smaller displacement than the normal tissue in transitional zone (TZ) and peripheral zone (PZ). The stiffness ratio of Ca prostate to normal tissue calculated to be 2.2 with their shear moduli for Ca prostate, CZ and atrophy are from 8 to 10 kPa and for PZ and TZ/BPH are 4 to 5 kPa respectively.<sup>55</sup>

More recently ARFI imaging is used for human prostate *in vivo*. Carcinoma prostate appears as bilaterally asymmetric stiff structures; benign prostatic hyperplasia (BPH) appears heterogeneous with a nodular texture, and the boundary of the transitional zone (TZ) forms a stiff rim separating the TZ from the peripheral zone (PZ). Compared with the matched B-mode images, ARFI images, in general, portray prostate structures with higher contrast. The ARFI imaging holds promise for guidance of targeted prostate needle biopsies and therapy.<sup>57</sup>

## Lymph Nodes

Elastography is also useful in differentiating reactive and metastatic axillary lymph nodes in carcinoma breast. As axillary lymph nodes status is the most important prognostic factor in carcinoma breast. The B-mode USG criteria for metastasis have based on the size, shape, hilum and the cortical thickening of lymph nodes.<sup>58,59</sup> For elastography axillary lymph nodes also given on elasticity scoring system on the basis of color coding.

**Score 1:** Absent or very small blue area.

**Score 2:** Small, scattered blue area, total blue area <45 percent

**Score 3:** Large blue area, total blue area >45 percent

**Score 4:** Blue area with or without a green rim.

Reported elasticity score of metastatic axillary lymph nodes is  $(3.1 \pm 0.7)$  is significantly higher than the score for reactive lymph nodes  $(2.2 \pm 0.7; p < 0.001)$ ,<sup>60</sup> when the cut-off was taken between 2 and 3 the sensitivity and specificity was approximately 80 percent.

Similar kind of scoring done for cervical lymph nodes by Deng ke Teng et al in which they found most benign lymph nodes shows elasticity score 1 or 2 and most of malignant node shows elasticity score 3 or 4 with sensitivity and specificity of 88.4 percent and 35.1 percent respectively. They also calculated the strain ratio which showed strain ratio cut-off for malignant  $>1.78$  and for benign  $<1.78$  with sensitivity and specificity of 98.1 percent and 64.9 percent respectively.<sup>61</sup>

## Thyroid

Another area of potential usefulness is the evaluation of thyroid nodule because the ultrasound and nuclear medicine criteria for differentiating between benign versus malignant nodules are not reliable. A number of articles have shown the potential utility of nodular stiffness for characterizing it as malignant.<sup>62,63</sup> Similar to the breast and other nodular lesion, the malignant thyroid nodule is stiffer than the benign thyroid nodules. Mainly semi quantitative methods with compression elastography using strain index is utilized. It is calculated by dividing nodule strain value by the strain of adjacent normal thyroid tissue. Good quality elastography of thyroid is challenging because of the shape of neck with sloping contour, which can cause lateral movement of thyroid and the pulsation from the adjoining carotid artery. Even with these technical difficulties as more and more results are reported, it can be used to help in deciding which nodule to be biopsied when there are many nodules are present.<sup>64</sup> For the diffuse diseases of the thyroid quantitative or semi-quantitative elastography is used. One study with shear wave velocity analysis shows increase stiffness in case of Hashimoto's thyroiditis.<sup>65</sup>

## Gynecology

### Cervical Elastography

#### Labor assessment

Cervical consistency and dilatation of internal os is assessed by palpation before induction of labor by prostaglandin or oxytocin. Cervical length measurement is done by ultrasound. Ripening of the internal os, which is not routinely evaluated during pregnancy by vaginal examination, can be assessed by transvaginal elastography. A soft internal os and harder external parts of the cervix are predictors of a favorable reaction to oxytocin during induction of labor. This can also help in deciding whether prostaglandins are required. Failed induction rates were higher in patients with increased stiffness of the internal os in a study by M Swiatkowska-Freund.<sup>66</sup>

#### Role

Elastography may play a role in predicting delivery, and in detecting patients with a high risk of preterm delivery.

### Cervical Cancer

Transvaginal elastography has been evaluated for the diagnosis of cervical lesions. Malignant lesions are stiffer (blue on color coded maps), whereas benign lesions are of intermediate stiffness (green).

Significant differences in strain ratios have been noted between benign (polyp/fibroid/erosion/inflammation) and malignant lesions (Strain ratio was obtained by dividing the mean strain within the lesion by the mean strain from the parametrial tissue).

A cut-off value of strain ratio of 4.53 or higher has been suggested for confident diagnosis of malignancy. Elastography helps in the detection of endophytic cancers, which are more common in elderly women and are difficult to diagnose clinically or colposcopically. Depth of invasion of stroma can also be accurately assessed by elastography, helping in staging.<sup>67</sup> However, elastography is not helpful in the diagnosis of cervical intraepithelial neoplasia.<sup>68</sup>

#### Pitfalls

Transvaginal elastography of the cervix lacks a proper reference tissue where comparison studies are possible. Infiltration of parametrial tissue by tumor would give rise to errors in strain ratio measurement as parametrial tissue is taken as reference.

Normal cervix itself has heterogeneous elasticity. Moreover the portion of the cervix nearest the transducer tip is prone to compression and even the mildest movement or pressure may result in erroneous impression of softening.<sup>69</sup>

#### Fibroids

Fibroids are often dense and the posterior acoustic shadowing poses difficulty in correct assessment of size and extent on ultrasound. Fibroids appear harder and have well demarcated borders on elastography. Color coded images in elastography can help in better delineation of fibroids and also in characterizing changes associated with treatments like embolization.<sup>70</sup>

#### Fibroids vs Adenomyosis

In adenomyosis and adenomyomas, which is often difficult to diagnose on B-mode ultrasound, elastographic color maps show a typical pattern of a soft lesion (green) with a central core which is even less stiff (red). This pattern persists in both diffuse as well as focal varieties, though the margins are irregular in diffuse and well demarcated in the focal variety. Fibroids in comparison are stiffer and are depicted in blue on color maps.<sup>71</sup>

#### Endometrial Pathologies

Color coded elastographic images and elasticity indices (where stiffer tissues are given lower scores) have shown that normal or atrophic endometrium has significantly lower scores than endometrial hyperplasia, cancer or polyps.<sup>72</sup>

#### Musculoskeletal

Compression ultrasonography has been the most commonly used technique for musculoskeletal applications. Strain of the region of interest is compared with the remaining tissue (usually fat) within the elastogram. The semi-quantitative measurement method includes the ratio of the relative strains between the area of interest and a reference area. The ARFI and shear wave elasticity imaging are being increasingly used for musculoskeletal applications.

#### Appearance of Normal Tendons

##### Compression elastography

In healthy volunteers, the normal Achilles tendons were found to have two distinct elastography patterns. They were either homogeneously hard structures or in the majority they had considerable inhomogeneity with soft areas (longitudinal bands or spots), which did not correspond to any changes in B-mode or Doppler ultrasound.<sup>73</sup>

##### Shear wave

Shear wave elastography has also been used to measure mean elasticity values of muscles. For the gastrocnemius and masseter muscles, supraspinatus tendon, and Achilles tendon in both the longitudinal and transverse planes, shear wave elastographic values ranged from  $11.1 \pm 4.1$  kPa (range, 2–28 kPa),  $10.4 \pm 3.7$  kPa (range, 2–23 kPa),  $31.2 \pm 13$  kPa (range, 6–90 kPa),  $74.4 \pm 45.7$  kPa (range, 6–242 kPa), and  $51.5 \pm 25.1$  kPa (range, 10–111 kPa). The mean elasticity values for the muscles and tendons in the longitudinal plane were greater in men than in women, but the Achilles tendon in the transverse plane did not exhibit a significant difference between sexes. There was no significant correlation between age and elasticity for the muscles.<sup>74</sup>

##### Tendinopathy

Symptomatic tendons were found in compression elastography to contain marked softening in 57 percent, mild softening in 11 percent and no soft areas (hard structures) in 32 percent of cases.<sup>75</sup> The alterations in asymptomatic tendons were seen in the tendon mid-portion and were not always found to correspond to alterations in conventional ultrasound. Mild softening was not correlated with conventional ultrasound abnormalities, whereas marked softening was found mainly in cases with ultrasound evidence of disease. This could signify either a false positive finding or the increased sensitivity of elastography in early diagnosis.

Another study has found increasing stiffness in diseased tendons, probably reflecting the stage of the disease, with fibrosis being the predominant component.<sup>76</sup> Increased stiffness of extensor tendon has been noted in lateral epicondylitis, with elastography being more sensitive than conventional ultrasound.<sup>77</sup>

##### Normal muscle

Elastographic appearance of normal muscle needs further detailed investigation. Relaxed muscle gives an inhomogeneous appearance of intermediate or increased stiffness (green/yellow or blue color, respectively) with scattered softer and harder areas especially at the periphery near boundaries.<sup>73</sup>

##### Exercise

Elastography has also shown increase in muscle hardness (changes in strain ratio) immediately after exercise which lasted from 30 minutes to 4 days.<sup>78,79</sup>

### *Rheumatological disorders*

**Soft tissue nodules:** Elastography helps in differentiation of rheumatoid nodules and tophi; rheumatoid nodules were significantly less elastic than tophi and suggesting a possible role of this method for the investigation of soft tissue nodules.<sup>80</sup>

**Synovitis:** Inflammatory synovitis due to rheumatoid arthritis was shown to be of intermediate stiffness, infectious synovitis (due to tuberculosis) was softer, whereas fatty villous proliferations (lipoma abrorescens) and pigmented villonodular synovitis were predominantly soft, as opposed to synovial sarcoma, which was hard.<sup>81</sup>

**Skin:** Elasticity of skin over the forearm in scleroderma patients have been evaluated with compression elastography leading to predominant blue areas (hard) as compared to green (intermediate) stiffness in controls.<sup>82</sup>

### *Soft tissue masses*

Data on the elastographic appearance of soft tissue masses with histological confirmation is limited. One study revealed lipoma and low flow vascular malformations and thyroglossal cysts to be soft due to fat/liquid content. Neurogenic tumors and dermoid/sebaceous cysts were stiffer. Stiffness of abscesses varied from soft to intermediate, probably due to varying liquid and solid components.

Considerable overlap in elastography measurement was present. Elastography may be beneficial in cases of equivocal B-mode findings and for guiding aspiration or biopsy in abscesses or mixed solid/cystic lesions.<sup>83</sup>

### *Myofascial pain*

Elastography has also been utilized in identifying active trigger points in myofascial pain, which is a major cause of non-articular pain with motor and sensory symptoms. Measurements have shown increased hardness in trigger points as compared to normal areas. This helps in objective classification instead of the subjective clinical assessment of nodular hard areas in involved muscles.<sup>84</sup>

### *Inflammatory/Dystrophic Conditions*

In inflammatory myositis, increased stiffness due to fibrosis and decrease in fatty infiltration has been documented using compression strain imaging. Elastography has shown correlation with serum markers in inflammatory myopathies and could help in disease monitoring.<sup>85</sup> Elastography may also be more sensitive in detecting dystrophic changes in muscle stiffness earlier than ultrasound and MRI.<sup>86</sup> In spasticity due to cerebral palsy, elastography has helped to establish site of botulinum toxin injection.<sup>87</sup>

**Hyaline cartilage:** Evaluation of elasticity of hyaline cartilage may help in evaluation prior to arthroscopy and in monitoring treatment.<sup>88</sup>

### *Standardization*

Standardization is required, especially in musculoskeletal imaging. Differences in applied transducer pressure and ROI size can affect the elastic modulus even on shear wave imaging significantly. The larger the ROIs size, the higher the chance to include the muscle fascia, dense collagen fiber, bone. This leads to increase in the maximum value of elastic modulus, although mean values over large areas may remain the same. Increase in acquisition times may also lead to slippage of transducer from intended position.

Elastography on muscle and tendon should be performed with the lightest transducer pressure and a shorter acquisition time.<sup>89</sup> For the Achilles tendon, the suggested standard size for longitudinal scans is a depth of three times the tendon and about three-quarters of the screen, and for transverse scans the para-Tenon should be included.<sup>90</sup>

### *Role in musculoskeletal imaging*

Elastography may be utilized for early diagnosis, staging and monitoring inflammatory, degenerative, myopathic or dystrophic conditions. It may also have a role in guiding interventions. However clinical utility and validity of ultrasound elastography in musculoskeletal applications is still to be established by further studies involving larger number of patients.

## OTHER APPLICATIONS

### **Renal Transplant Assessment**

Supersonic shear wave imaging, transient elastography and strain imaging have been utilized to diagnose chronic allograft injury. It can be used to monitor allograft stiffness, so that patients with serial increase can be subjected to a biopsy before renal function deteriorates, instead of all patients undergoing routine protocol biopsies. It can also monitor effect of treatment. However, subclinical rejection, infection or recurrence of underlying disease cannot be detected.<sup>91</sup>

### **Cardiovascular Applications**

The two major areas of cardiovascular applications are strain imaging of the myocardium and of atherosomatous plaque and the arterial wall.<sup>92</sup> Myocardial evaluation focuses on evaluation of localized areas of ischemia, infarction, and scarring. Arterial elasticity evaluation has focused on detection of vulnerable plaque and estimation of arterial wall compliance, as vulnerable plaques are known to be much softer than stable plaques. Elasticity estimation in these organs makes use of the normal movement of myocardium and vessel walls during the cardiac cycle rather than externally applied vibrations or pressure. Early work focused on intravascular ultrasound imaging of plaque,<sup>93</sup> but that method is invasive, and much current work is focused on external methods of plaque stiffness imaging.

## Venous Thrombosis

The use of elasticity imaging for evaluation of venous thrombosis has also been reported.<sup>94</sup> This application is important because new thrombi are at a higher risk for embolization than are older more fibrotic thrombi. Because the stiffness of a thrombus increases with increasing age,<sup>95</sup> elasticity imaging may offer a way of gauging the age of thrombi, which can be difficult using Gray Scale sonography alone.

## Skin and Soft Tissue

Elastography can visualize components of skin and soft tissue abscesses, including the abscess cavity and surrounding induration. A percentage of patients who fail therapy will progress to more invasive infections, either by local spread such as deeper tissue infection or via systemic spread such as bacteremia. While B-mode sonography can help differentiate the contents of an abscess cavity from the surrounding tissue, sonoelastography by measuring tissue stiffness can visualize the indurated tissue surrounding the abscess cavity. Asymmetry of the inflammatory changes surrounding abscess cavities has been reported to be associated with a higher rate of failure after standard therapy.<sup>96</sup> Also the size of the tissue indurations may predict progression to bacteremia or the time to resolution.<sup>97</sup>

## Endoscopic Ultrasonography

**Endoscopic ultrasonography** (EUS) is one of the most recent advances in gastrointestinal endoscopy. The EUS with real time tissue elastography can be more useful than EUS with only a B-mode imaging ability. Real-time EUS elastography can be performed with the conventional EUS probes without any need for additional equipment that induces vibration or pressure. Elastographic imaging of the normal pancreas is characterized by a uniform, homogeneous green color distribution (representing intermediate stiffness) throughout the organ. A green-predominant pattern, either homogeneous or heterogeneous, excludes malignancy with a high accuracy. On the contrary, a blue-predominant pattern, either homogeneous or heterogeneous, favors the diagnosis of malignant tumor. On quantitative analysis, a healthy pancreas shows a mean elasticity value of 0.55 percent. A strain ratio higher than 15.41 or a mass elasticity value below 0.03 percent is 100 percent specific for malignancy.<sup>98</sup>

### *Limitations of EUS Elastography*

The main pitfall of EUS elastography is the inability to control tissue compression by the EUS transducer. Use of EUS elastography is also hampered by the induction of motion artifacts due to respiratory or heart movements, which cannot be adequately eliminated or quantified. The presence of

nearby structures with very low or high density and stiffness, such as the heart, major vessels or spine are also difficult to be excluded from the ROI analyzed. Selection of the ROI has to carefully include surrounding soft tissues only, since the methodology of elastography assumes computations relative to the average strain inside the ROI. An intrinsic limitation of qualitative elastography is the subjective interpretation of the elastographic pattern that may be associated with significant intra-and interobserver variability.

### *Pitfalls*

Large lesions can be under assessed, with portions of the lesion lying out of the field of view. Moreover, painful lesions may be under represented because of the increased discomfort related to elastography. Performing ultrasound elastography can be technically challenging in organs like the salivary glands in terms of achieving only longitudinal transducer compression, i.e. avoiding lateral or out-of beam movements, and achieving the correct amount of compression. In this respect, even slight non-axial transducer movements detrimentally affect elastogram quality, observed as background noise, due to mistracking artifacts.

## CONCLUSION

In conclusion, elastography has emerged as a useful adjunct tool for ultrasound diagnosis. Elastograms are images of tissue stiffness and may be in color, Gray Scale, or a combination of the two. In a typical elastogram, low strain areas denoting a stiff or hard material are given darker gray values, whereas high strain areas denoting very soft tissues are given lighter gray values. The rapidly advancing field of tissue elasticity imaging and estimation has already produced several applications. The goal in breast elastography is not necessarily to diagnose cancers but to confidently classify questionable lesions on the sonogram as definitely benign. This will help reduce the number of biopsies of a benign lesion.

Recent advances in elastography include quantification using strain ratios, acoustic radiation force impulse imaging, and shear wave velocity estimation. These are useful not only for characterizing focal masses but also for diagnosing diffuse organ diseases, such as liver cirrhosis. Beyond breast mass evaluation, elastography is showing the greatest potential in the liver. Other promising applications include prostate cancer detection, atheromatous plaque and arterial wall evaluation, venous thrombus evaluation, graft rejection, and monitoring of tumor ablation therapy. Other modalities may be used for elasticity imaging, the most powerful being magnetic resonance elastography. Ultrasound, being less expensive and easier to use, will likely become the most widely used modality for clinical elasticity estimation and imaging.

**REFERENCES**

1. Mark L Palmeri, Kathryn R Nightingale. What challenges must be overcome before ultrasound elasticity imaging is ready for the clinic? *Imaging Med.* 2011;3:433-44.
2. Duck F. *Physical Properties of Tissue, A Comprehensive Reference Book.* NY; Academic Press;1990.
3. Sarvazyan A, Skovaroda AR, Emelianov SY, et al. Biophysical bases of elasticity imaging. *Acoust Imaging.* 1995;21:223-40.
4. Sarvazyan, A. *Handbook of Elastic Properties of Solids, Liquids and Gases.* Elastic properties of soft tissue. 2001,pp.107-27.
5. Peter NT Wells, Hai-Dong Liang. Medical ultrasound: imaging of soft tissue strain and elasticity. *J. R. Soc. Interface* published online 16 June 2011 doi: 10.1098/rsif.2011.0054.
6. Garra BS. Imaging and estimation of tissue elasticity by ultrasound. *Ultrasound Q.* 2007;23:255-68.
7. Fehrenbach J. Influence of Poisson's ratio on elastographic direct and inverse problems. *Phys Med Biol.* 2007;52:707-16.
8. Insana MF, Pellet-Barakat C, Sridhar M, Lindfors KK. Viscoelastic imaging of breast tumor microenvironment with ultrasound. *J Mammary Gland Biol Neoplasia.* 2004;9:393-404.
9. Sarvazyan A, Timothy J Hall, Matthew W Urban, Mostafa Fatemi, Salavat R, et al. An overview of elastography-An emerging branch of medical imaging. *Curr Med Imaging Rev.* 2011;7:255-82.
10. Daniel T Ginat, Stamatia V Destounis, et al. US Elastography of breast and prostate lesion. *Radiographics.* 2009;29:2007-16.
11. Itoh A, Ueno E, Tohno E, Kamma H, Takahashi H, Shiina T et al. Breast disease: clinical application of US elastography for diagnosis. *Radiology.* 2006;239(2):341-50.
12. Shiina T, Dooley MM, Bamber JC. Strain imaging using combined RF and envelope autocorrelation processing. In: Proceedings of the IEEE Ultrasonics Symposium. Savoy, Ill: Institute of Electrical and Electronics Engineers Ultrasonics, Ferroelectrics, and Frequency Control Digital Archive. 1996;2:1331-6.
13. Zhang M, Nigwekar P, Castaneda B, Hoyt K, Joseph JV, Agnese AD, Messing EM, Strang JG, Rubens DJ, Parker KJ. Quantitative characterization of viscoelastic properties of human prostate correlated with histology. *Ultrasound Med Biol.* 2008;34:1033-42. [PubMed: 18258350]
14. Kathy Nightingale. Acoustic Radiation Force Impulse (ARFI) Imaging: a Review. *Curr Med Imaging Rev.* 2011;7(4):328-39. doi:10.2174/157340511.
15. EE Drakonaki, GM Allen, DJ. Ultrasound elastography for musculoskeletal applications. *Wilson. British Journal of Radiology.* 2012;85:1435-45.
16. McAleavey SA, Menon M, Orszulak J. Shear-modulus estimation by application of spatially-modulated impulsive acoustic radiation force. *Ultrason. Imaging.* 2007;29:87-104.
17. Bercoff J, Tanter M, Fink M. Supersonic shear imaging: a new technique for soft tissue elasticity mapping. *IEEE Trans Ultrason Ferro electr Freq Control.* 2004;51:396-409.
18. Thitai-Kumar A, Garra BS, Ophir J. Visualization of bonding at an inclusion boundary using axial-strain elastography: a feasibility study. *Phys Med Biol.* 2007;52(9):2615.
19. Maleke C, Konofagou EE. In vivo feasibility of real-time monitoring of focused ultrasound surgery (FUS) using harmonic motion imaging (HMI). *IEEE Trans Biomed Eng.* 2010;57:7-11.
20. Krouskop TA, Wheeler TM, Kallel F, Garra BS, Hall T. Elastic moduli of breast and prostate tissues under compression. *Ultrason Imaging.* 1998;20:260-74.
21. Cespedes I, Ophir J, Ponnekanti H, et al. Elastography: elasticity imaging using ultrasound with application to muscle and breast in vivo. *Ultrasound Imaging.* 1993;15:73-88.
22. Hall TJ, Zhu Y, Spalding CS. In vivo real-time freehand palpation imaging. *Ultrasound Med Biol.* 2003;29:427-35.
23. Garra BS, Cespedes EI, Ophir J, Spratt SR, Zuurbier RA, Magnant CM, Pennanen MF. Elastography of breast lesions: initial clinical results. *Radiology.* 1997;202:79-86.
24. Itoh A, Ueno E, Tohno E, Kamma H, Takahashi H, Shiina T et al. Breast disease: clinical application of US elastography for diagnosis. *Radiology.* 2006;239(2):341-50.
25. Burnside ES, Hall TJ, Sommer AM, et al. Differentiating benign from malignant solid breast masses with US strain imaging. *Radiology.* 2007;245(2):401-10.
26. Zhi H, Xiao X-Y, Yang H-Y, Wen Y-L, Ou B, Luo B-M, Liang B-I. Semi quantitating stiffness of breast solid lesions in ultrasonic elastography. *Academic Radiology.* 2008;15:1347-53.
27. Tanter M, Bercoff J, Athanasiou A, et al. Quantitative assessment of breast lesion viscoelasticity: initial clinical results using supersonic shear imaging. *Ultrasound Med Biol.* 2008;34(9):1373-86.
28. Chang JM, et al. Clinical Applications of Shear Wave Elastography (SWE) in the diagnosis of benign and malignant breast diseases *Breast Cancer Res Treat.* 2011;29(1):89-97.
29. Booi RC, Carson PL, O'Donnell M, Richards MS, Rubin JM. Diagnosing cysts with correlation coefficient images from 2-dimensional freehand elastography. *J Ultrasound Med.* 2007;26(9):1201-7.
30. Giuseppetti GM, Martegani A, Di Cioccio B, Baldassarre S. Elastosonography in the diagnosis of the nodular breast lesions: preliminary report. *Radiol Med.* 2005;110(1-2):69-76.
31. Barr RG. Initial results of breast real-time elasticity imaging to characterize lesions [abstr]. In: Radiological Society of North America Scientific Assembly and Annual Meeting Program. Oak Brook: Radiological Society of North America;2006,p.644.
32. Emily Carey, William D Carey. Noninvasive tests for liver disease, fibrosis, and cirrhosis: Is liver biopsy obsolete? *Cleaveland Clinic J Med.* 2010;77:519-27.
33. Abdurrahman Sagir, Andreas Erhardt, Marcus Schmitt, Dieter Ha Üssinger. Transient Elastography Is Unreliable for Detection of Cirrhosis in Patients with Acute Liver Damage. *Hepatology.* 2008;47:592-5.
34. Millonig G, Reimann FM, Friedrich S, Fonouni H, Mehrabi A, Buchler MW, et al. Extrahepatic cholestasis increases liver stiffness (FibroScan) irrespective of fibrosis. *Hepatology.* 2008;48:1718-23.
35. Millonig G, Friedrich S, Adolf S, Fonouni H, Golriz M, Mehrabi A, et al. Liver stiffness is directly influenced by central venous pressure. *J Hepatol.* 2010;52:206-10.
36. Berzigotti A, de Gottardi A, Delgado MG, Seijo S, Abraldes JG, Garcia-Pagan JC, et al. Liver stiffness increases after a meal in patients with cirrhosis but its change does not correlate with the changes in HVPG (abstract). *Hepatology.* 2010;52:1074A.
37. Laurent Castera Non-invasive assessment of liver fibrosis in chronic hepatitis C. *Hepatol Int.* 2011;5:625-34.

38. Sporea I, Bota S, Peck-Radosavljevic M, Sirli R, Tanaka H, Iijima H, et al. Acoustic Radiation Force Impulse Elastography for fibrosis evaluation in patients with chronic hepatitis C: An international multicenter study. *Eur J Radiol.* 2012;81(12):4112-8. doi: 10.1016/j.ejrad.2012.08.018. Epub 2012 Sep 20.
39. Rizzo L, Calvaruso V, Cacopardo B, Alessi N, Attanasio M, Petta S, et al. Comparison of transient elastography and acoustic radiation force impulse for non-invasive staging of liver fibrosis in patients with chronic hepatitis C. *Am J Gastroenterol.* 2011 Dec;106(12):2112-20. doi: 10.1038/ajg.2011.341. Epub 2011 Oct 4.
40. Son CY, Kim SU, Han WK, Choi GH, Park H, Yang SC, Choi JS, Park JY, Kim do Y, Ahn SH, Chon CY, Han KH. Normal liver elasticity values using acoustic radiation force impulse imaging: a prospective study in healthy living liver and kidney donors. *J Gastroenterol Hepatol.* 2012;27(1):130-6. doi: 10.1111/j.1440-1746.2011.06814.x.
41. Martinez SM, Foucher J, Combis JM, Métivier S, Brunetto M, Capron D, Bourlière M, Bronowicki JP, Dao T, Maynard-Muet M, Lucidarme D, Merrouche W, Forns X, de Lédinghen V. Longitudinal liver stiffness assessment in patients with chronic hepatitis C undergoing antiviral therapy *PLoS One.* 2012;7(10):e47715. doi: 10.1371/journal.pone.0047715. Epub 2012 Oct 17.
42. Laurent Castera, Massimo Pinzani, Jaime Bosch. Noninvasive evaluation of portal hypertension using transient elastography. *J Hep.* 2012;56 j:696-703.
43. Gao J, Ran HT, Ye XP, Zheng YY, Zhang DZ, Wang ZG. The stiffness of the liver and spleen on ARFI Imaging pre and post TIPS placement: a preliminary observation. *Clin Imaging.* 2012; 36(2):135-41.
44. Carrión JA, Torres F, Crespo G, Miquel R, García-Valdecasas JC, Navasa M, Forns X. Liver stiffness identifies two different patterns of fibrosis progression in patients with hepatitis C virus recurrence after liver transplantation. *Hepatology.* 2010;51(1):23-34. doi: 10.1002/hep.23240.
45. Sasso M, Beaugrand M, de Ledinghen V, Douvin C, Marcellin P, Poupon R, Sandrin L, Miette V. Controlled attenuation parameter (CAP): a novel VCTE™ guided ultrasonic attenuation measurement for the evaluation of hepatic steatosis: preliminary study and validation in a cohort of patients with chronic liver disease from various causes. *Ultrasound Med Biol.* 2010;36(11):1825-35. doi: 10.1016/j.ultrasmedbio.2010.07.005. Epub 2010 Sep 27.
46. Roulot D, Czernichow S, Le Clésiau H, Costes JL, Vergnaud AC, Beau-grand M. Liver stiffness values in apparently healthy subjects: influence of gender and metabolic syndrome. *J Hepatol.* 2008;48:606-13.
47. Shuang-Ming T, Ping Z, Ying Q, Li-Rong C, Ping Z, Rui-Zhen L. Usefulness of acoustic radiation force impulse imaging in the differential diagnosis of benign and malignant liver lesions. *Acad Radiol.* 2011;18(7):810-5. Epub 2011 Mar 21.
48. Onur MR, Poyraz AK, Ucak EE, Bozgeyik Z, Özercan IH, Ogur E. Semi quantitative strain elastography of liver masses. *J Ultrasound Med.* 2012;31(7):1061-7.
49. Gallotti A, D'Onofrio M, Romanini L, Cantisani V, PozziMucelli R. Acoustic radiation force impulse (ARFI) ultrasound imaging of solid focal liver lesions. *Eur J Radiol.* 2012;81:451-5.
50. Aymeric Guibal, Camille Boullaran, Matthew Bruce, Mélanie Vallin, Frank Pilleul, Thomas Walter, Jean Yves Scoazec, Nawele Boublay, Jérôme Dumortier, Thibaut Lefort. Evaluation of shear wave elastography for the characterisation of focal liver lesions on ultrasound. *Eur Radiol.* DOI 10.1007/s00330-012-2692-y.
51. Kamoi K, Okihara K, Ochiai A, et al. The utility of trans rectal real-time elastography in the diagnosis of prostate cancer. *Ultrasound Med Biol.* 2008;34(7):1025-32.
52. Akin O, Hricak H. Imaging of prostate cancer. *Radiol Clin North Am.* 2007;45(1):207-22.
53. Zhang M, Nigwekar P, Castaneda B, et al. Quantitative characterization of viscoelastic properties of human prostate correlated with histology. *Ultrasound Med Biol.* 2008;34(7):1033-42.
54. Daniel T, Ginat, Stamatia V Destounis, et al. US Elastography of breast and prostate lesion. *Radiographics.* 2009;29:2007-16.
55. Zhai, et al. Characterizing the stiffness of Human Prostates using Acoustic Radiation Force, Ultrasound Imaging. 2010;32(4):201-13.
56. Nightingale K, Palmeri M, Nightingale R, et al. On the feasibility of remote palpation using acoustic radiation force. *JASA.* 2001; 110:625-34.
57. Zhai, et al. Acoustic radiation force impulse imaging of Human Prostate: Initial in vivo demonstrations. *Ultrasound Med Biol.* 2012;38(1):50-61.
58. Choi YJ, Ko EY, Han BK, Shin JH, Kang SS, Hahn SY. High-resolution ultrasonographic features of axillary lymph node metastasis in patients with breast cancer. *Breast.* 2009;18:119-122.
59. Bedi DG, Krishnamurthy R, Krishnamurthy S, et al. Cortical morphologic features of axillary lymph nodes as a predictor of metastasis in breast cancer: in vitro sonographic study. *AJR Am J Roentgenol.* 2008;191:646-52.
60. Jae Jeong Choi, et al. Role Sonographic Elastography in the Differential Diagnosis of Axillary Lymph Nodes in Breast Cancer. *J Ultrasound Med.* 2011;30:429-36.
61. Deng Ke Teng, et al. Value of US Elastography in Assessment of Enlarged Cervical Lymph Nodes. *Asian Pacific J Cancer Prev,* 13, 2081-85
62. Hong Y, Liu X, Li Z, et al. Real-time ultrasound elastography in the differential diagnosis of benign and malignant thyroid nodules. *J Ultrasound Med [serial online].* 2009;28(7):861Y867.
63. Lyshchik A, Higashi T, Asato R, Tanaka S, Ito J, Mai JJ, Pellot-Barakat C, Insana MF, Brill AB, Saga T, Hiraoka M, Togashi K. Thyroid gland tumor diagnosis at US elastography. *Radiology.* 2005;237:202-11.
64. Dighe M, Kim J, Luo S, Kim Y. Utility of the ultrasound elastographic systolic thyroid stiffness index in reducing fine-needle aspirations. *J Ultrasound Med.* 2010;29:565-74.
65. Bahn MM, Brennan MD, Bahn RS, Dean DS, Kugel JL, Ehman RL. Development and application of magnetic resonance elastography of the normal and pathological thyroid gland in vivo. *J Magn Reson Imaging.* 2009;30:1151-4.
66. M Swiatkowska-Freund, K Preis. Elastography of the uterine cervix: implications for success of induction of labor. *Ultrasound Obstet Gynecol.* 2011;38:52-6.
67. Sun LT, Ning CP, Liu YJ, Wang ZZ, Wang LD, Kong XC, Tian JW. Is transvaginal elastography useful in pre-operative diagnosis of cervical cancer? *Eur J Radiol.* 2012 Aug;81(8):e888-92. doi: 10.1016/j.ejrad.2012.04.025. Epub 2012 Jun 18.
68. Thomas A, Kümmel S, Gemeinhardt O, Fischer T. Real-time sonoelastography of the cervix: tissue elasticity of the normal and abnormal cervix. *Acad Radiol.* 2007;14(2):193-200.

69. FS Molina, LF Gómez, J Florido, MC Padilla, KH Nicolaides. Quantification of cervical elastography: a reproducibility study. *Ultrasound in Obstetrics & Gynecology*. 2012;39(6):685-9.
70. O Ami, F Lamazou, M Mabille, jM Levaillant, X Deffieux, R Frydmanand D. Musset. Real-time transvaginal elastosonography of uterine fibroids. *Ultrasound Obstet Gynecol*. 2009;34:486-8.
71. Marco Tessarolo, Luca Bonino, Marco Camanni, Francesco Deltetto. Elastosonography: a possible new tool for diagnosis of adenomyosis? *EurRadiol* (2011) 21:1546–1552 DOI 10.1007/s00330-011-2064-z.
72. Preis Krzysztof, Zielinska Katarzyna, Swiatkowska-Freund Małgorzata, WydraDariusz, Kobierski Juliusz. The role of elastography in the differential diagnosis of endometrial pathologies- preliminary report. *GInekol Pol*. 2011;82:494-7.
73. EE Drakonaki, GM Allen, DJ Wilson. Elastography for musculoskeletal applications. *BJR*. 2012;85:1435-45.
74. Kemal Arda, NazanCiledag, ElifAktas, Bilgin Kadri Aribas, KenanKöse. Quantitative Assessment of Normal Soft-Tissue Elasticity Using Shear-Wave Ultrasound Elastography. *AJR*. 2011;197:532-6.
75. De Zordo T, Chem R, Smekal V, Feuchtnner G, Reindl M, Fink C, et al. Real-time sonoelastography: findings in patients with symptomatic Achilles tendons and comparison to healthy volunteers. *Ultraschall Med*. 2010;31:394-400.
76. De Sconfienza LM, Silvestri E, Cimmino MA. Sonoelastography in the evaluation of painful Achilles tendon in amateur athletes. *ClinExpRheumatol*. 2010;28:373-8.
77. De Zordo T, Lill SR, Fink C, Feuchtnner GM, Jaschke W, Bellmann-Weiler R, et al. Real-time sonoelastography of lateral epicondylitis: comparison of findings between patients and healthy volunteers. *Am J Roentgenol*. 2009;193:180-5.
78. Niitsu M, Michizaki A, Endo A, Takei H, Yanagisawa O. Muscle hardness measurement by using ultrasound elastography: a feasibility study. *Acta Radiol*. 2011;52(1):99-105.
79. Yanagisawa O, Niitsu M, Kurihara T, Fukubayashi T. Evaluation of human muscle hardness after dynamic exercise with ultrasound real-time tissue elastography: a feasibility study. *Clin Radiol*. 2011;66(9):815-9.
80. Sconfienza LM, Silvestri E, Bartolini B, Garlaschi G, Cimmino MA. Sonoelastography may help in the differential diagnosis between rheumatoid nodules and tophi. *Clin Exp Rheumatol* 2010;28:144-5. Epub 2011 May 6. 80.
81. Lalitha P, Reddy MCh, Reddy KJ. Musculoskeletal applications of elastography: a pictorial essay of our initial experience. *Korean J Radiol*. 2011;12:365-75.
82. J Iagnocco A, Kaloudi O, Perella C, Bandinelli F, Riccieri V, Vasile M, Porta F, Valesini G, Matucci-Cerinic M. Ultrasound elastography assessment of skin involvement in systemic sclerosis: lights and shadows. *Rheumatol*. 2010;37(8):1688-91. doi: 10.3899/jrheum.090974. Epub 2010 Jun 15.
83. Bhatia KS, Rasalkar DD, Lee YP, Wong KT, King AD, Yuen YH, et al. Real-time qualitative ultrasound elastography of miscellaneous non-nodal neck masses: applications and limitations. *Ultrasound Med Biol*. 2010;36:1644-52.
84. Jeffrey J Ballyns, Jay P Shah, Jennifer Hammond, Tadesse Gebreab, Lynn H. Gerber, Siddhartha Sikdar. Objective Sonographic Measures for Characterizing Myofascial Trigger Points Associated With Cervical Pain *Ultrasound Med*. 2011; 30(10):1331-40.
85. Botar-Jid C, Damian L, Dudea SM, Vasilescu D, Rednic S, Badea R. The contribution of ultrasonography and sonoelastography in assessment of myositis. *Med Ultrason*. 2010;12:120-6.
86. Drakonaki EE, Allen GM. Magnetic resonance imaging, ultrasound and real-time ultrasound elastography of the thigh muscles in congenital muscle dystrophy. *Skeletal Radiol*. 2010; 39:391-6.
87. Vasilescu D, Dudea S, Botar-Jid C, Sfrangeu S, Cosma D. Sonoelastography contribution in cerebral palsy spasticity treatment assessment, preliminary report: a systematic review of the literature apropos of seven patients. *Med Ultrason*. 2010;12:306-10.
88. Zheng YP Mak, AFT Qin, L Ding CX. Ultrasound elastography of articular cartilage: a preliminary study. 20th Annual International Conference of the IEEE Engineering in Medicine and Biology Society; 1998. pp.1940-2.
89. Kot BCW, Zhang ZJ, Lee AWC, Leung VYF, Fu SN. (2012) Elastic Modulus of Muscle and Tendon with Shear Wave Ultrasound Elastography: Variations with Different Technical Settings. *PLoS ONE* 7(8): e44348. doi:10.1371/journal.pone.0044348.
90. Klausner AS, Faschingbauer R, Jaschke WR. Is sonoelastography of value in assessing tendons? *Semin Musculoskeletal Radiol*. 2010;14:323-33.
91. Robert Arndt, Sven Schmidt, ChristophLoddenkemper, Maria Grünbaum, Walter Zidek, Markus van der Giet, Timm H Westhoff. Noninvasive evaluation of renal allograft fibrosis by transient elastography – a pilot study. *Transplant International*. 2010;23:871-7.
92. Brian Stephen Garra. Imaging and Estimation of Tissue Elasticity by Ultrasound *Ultrasound Quarterly*, 2007;23(4).
93. de Korte CL, Cespedes EI, van der Steen AFW, et al. Intravascular ultrasound elastography: assessment and imaging of elastic properties of diseased arteries and vulnerable plaque. *Eur J Ultrasound*. 1998;7:219-24.
94. Rubin JM, Xie H, Kim K, et al. Sonographic elasticity imaging of acute and chronic deep venous thrombosis in humans. *J Ultrasound Med*. 2006;25:1179-86.
95. Geier B, Barbera L, Muth-Werthmann D, et al. Ultrasound elastography for the age determination of venous thrombi. Evaluation in an animal model of venous thrombosis. *Thromb Haemost*. 2005;93:368-74.
96. Gaspari R, Blehar D, Briones J, Dayno M. Sono elastographic characteristics of abscess in duration associated with therapy failure. *J Ultrasound Med*. 2012;31(9):1405-11.
97. Gaspari R, Blehar D, Mendoza M, Montoya A, Moon C, Polan D. Use of ultrasound elastography for skin and subcutaneous abscesses. *J Ultrasound Med*. 2009;28(7):855-60.
98. Lee TH, Cha S, Cho YD. EUS Elastography: Advances in Diagnostic EUS of the Pancreas. *Korean J Radiol*. 2012; 13(S1):S12-S16.

## Section

# 2

# Advances in Computed Tomography

**Chapter 4** • CT Hardware: An Update  
*Ashu Seith Bhalla, Arun Deep Arora*

**Chapter 5** • Dual Energy CT  
*Arun Kumar Gupta, Manisha Jana*

**Chapter 6** • CT Perfusion Imaging  
*Veena Chowdhury*



## Chapter

# 4

# CT Hardware: An Update

Ashu Seith Bhalla, Arun Deep Arora

Since the first clinical use of computed tomography (CT) in 1972, its technology has made notable advances. The first CT scanner which was built by British engineer Hounsfield had a rotation time of about 300 seconds with a maximum image matrix of  $80 \times 80$  pixels. It has been a long journey to the present day 256 to 320-slice scanners with rotation times of 0.33 seconds and an image matrix of  $512 \times 512$  pixels. Several vendors today offer 256-slice spiral CT scanners and even 320 slice is now available. But the ever evolving technology has more in store: scanners with new detector materials for higher sensitivity, dual-source CT, dual-energy detectors, and flat-panel detectors are further milestones of CT development.<sup>1</sup> The subject will be discussed under the following headings:

- Basic workflow of a CT scanner
- Determinants of an optimal image
- Advances in hardware
- Special CT: Cone Beam CT (CBCT)/Volume CT, Navigation Systems.

### BASIC WORKFLOW OF CT SCANNER

The CT scanner is made up of three primary systems; including the gantry, the computer, and the operating console. Each of these is composed of various subcomponents. The gantry assembly is the largest of these systems. It is made up of all the equipment related to the patient positioning, including patient support, the positioning couch, mechanical supports, and the scanner housing. It also contains the heart of the CT scanner, the X-ray tube, as well as detectors arranged around the patient (Fig. 1). Earlier versions of CT employed a pencil-like X-ray

beam (with single detector) and the tube-detector movement was both linear and rotary, termed as the “rotate-translate” motion. In an attempt to shorten the scan time, a fan shaped beam with multiple detectors was adopted. The approach then shifted to “rotate-rotate” where multiple detectors are aligned as an arc and both detector arc and X-ray tube rotate around the patient. The quantum leap took place with the next level where the detectors formed a complete ring around the patient and only the X-ray tube rotates inside the detector ring, described as “rotate-fixed” motion.<sup>2</sup>

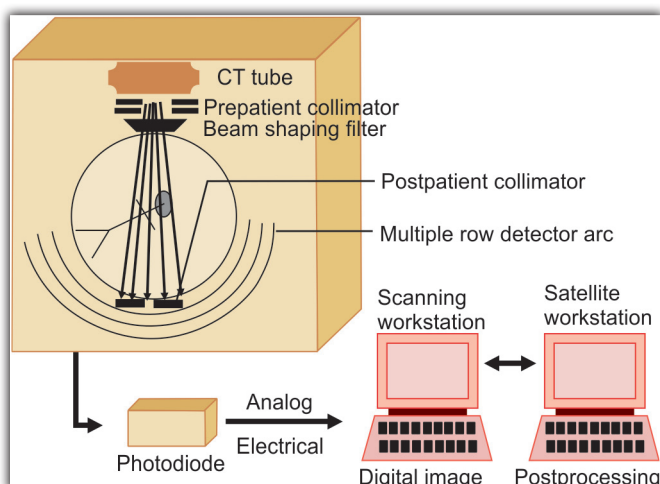
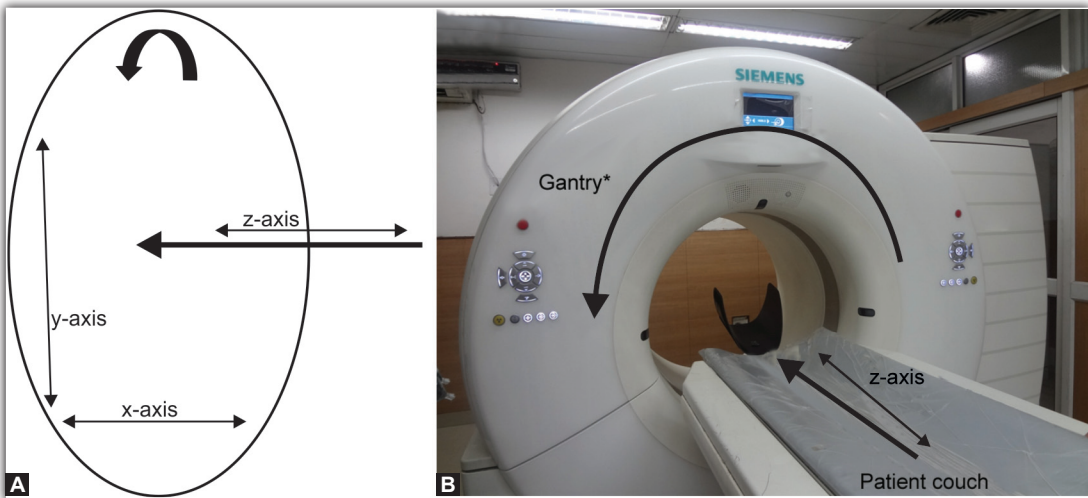


**Fig. 1** Schematic diagram showing the basic components and workflow of a CT scanner



**Figs 2A and B** (A) Diagram showing the orientation of x, y and z-axis.(B) Photograph of a CT scanner. The gantry\* houses the CT tube and the detector rows

## ■ DETERMINANTS OF AN OPTIMAL IMAGE

Determinants of an optimal image in CT as in any image acquisition system are:

1. Spatial resolution
2. Contrast resolution
3. Temporal resolution.

### Spatial Resolution

The key factors determining the spatial resolution are the detector size in the z-axis direction, reconstruction algorithms, and patient motion. Spatial resolution is specified in the axial as well as z-axis plane. Scan plane is also called x-y plane and z-axis plane is also called out of plane (**Figs 2A and B**). The axial or x-y plane spatial resolution is dependent on the pixel size, which is a ratio of scan field of view (SFOV) and image reconstruction matrix. On the other hand, the number of rows in MDCT scanner and the detector size determines the out of plane (z-axis) resolution. The detector row width defines the minimum thickness of the reconstructed CT image and is influenced by the z-axis dimension of the individual detector element. For example, a detector row width of 0.6 mm allows a slice thickness of 0.6 mm. To achieve improved through-plane spatial resolution, some systems use an X-ray focal spot that alternates between two z-positions (i.e. z-flying focal spot) to acquire two overlapping slices for each detector row. This feature has been reported to improve z-plane spatial resolution to 0.4 mm<sup>3</sup>.

Cone beam CT uses a high-resolution two-dimensional detector and allows isotropic data acquisition and reconstruction leading to higher spatial resolution. These systems however offer poor contrast resolution as shall be discussed subsequently in the chapter.

### Temporal Resolution

The temporal resolution is determined by the gantry rotation time, acquisition mode, type of image reconstruction, and pitch. Gantry rotation time is the amount of time required to complete one full rotation (360°) of the X-ray tube and detector around the patient. The recent advances in technology have considerably decreased the gantry rotation time to as low as 330 to 370 msec. The lesser the gantry rotation time, the greater the temporal resolution achieved. Acquisition mode becomes especially important in cardiac CT where the dataset need be acquired at a very rapid speed to overcome the cardiac motion. It may be done through prospective ECG triggering wherein the data is acquired for only part of the complete gantry rotation, at a desired distance from the R-R peak in the cardiac cycle. This partial scanning reduces the radiation dose to the patient and achieves a temporal resolution in the range of 200 to 250 msec. The other mode of retrospective ECG gating in which data is acquired throughout the cardiac cycle and segmented reconstruction done from different cardiac cycles to increase temporal resolution to 80 to 250 msec. Multiple segment reconstruction, though increases the temporal resolution, but runs the risk of misregistration artifacts as the reconstruction data is selected from different heartbeat cycles. The pitch is defined as the ratio of table increment per gantry rotation to the total X-ray beam width. The pitch factor plays a major role in improving both the temporal and spatial resolution but at the same time has a dramatic effect on the overall radiation dose delivered during a spiral CT examination. Because radiation dose is inversely proportional to the pitch, the low pitch protocols substantially increase radiation dose to patients.<sup>3</sup>

Another approach to increase the temporal resolution is to increase the number of X-ray sources (tubes) generating

the X-rays. For a single-source scanner, the time required to collect all data needed for reconstruction of images (i.e. the acquisition time) is approximately one-half the gantry rotation time. The fastest single-source scanner currently available spins at 270 milliseconds per rotation, for a nominal acquisition time and temporal resolution of 135 milliseconds. For a dual-source scanner, the acquisition time is approximately one-fourth the gantry rotation time, because the two X-ray source/detector systems collect data in half the time needed for a single X-ray source/detector array. The fastest dual-source scanner currently available spins at 280 milliseconds per rotation, for a nominal acquisition time of 70 milliseconds.<sup>3</sup>

### Contrast Resolution

Contrast resolution is the ability of a CT scanner to differentiate small attenuation differences on the CT image. It is important to remember that the linear attenuation coefficient is an absorption measurement and it is dependent on thickness of a material, density of a material, atomic number and photon energy. A change in kVp results in alteration of linear attenuation coefficient of the structure, even if the same structure is being imaged. Contrast resolution is limited by noise, as noise in an image increases, contrast resolution decreases. Special filters called bow-tie filters absorb weaker energy photons, which reduce the probability of scattered photons being detected by the CT detectors. An X-ray beam consists of polychromatic photons or photons having different energies. The bow-tie filters serve to absorb lower energy photons primarily to "lessen" the effects from the polychromatic nature of an X-ray beam. A soft tissue, standard or smooth algorithm is used during the reconstruction process to enhance soft tissue and contrast resolution.<sup>4</sup>

### ■ ADVANCES IN HARDWARE

The newest technology offers significant advantages, but, current CT hardware releases are far from uniform across vendors, reflecting different approaches to image acquisition in the current era. No single CT scanner offers the full range of the newest features. This underscores the importance of understanding the properties and advancements of individual components of CT scanner.

#### Advances in CT Tube

Most modern commercial scanners use a hot-cathode, high-vacuum X-ray tube which is built with a liquid-cooled, copper-backed tungsten target. Lead can be found in various parts of the CT scanner system, which reduces the amount of excess radiation.

In conventional CT, the tube and detectors moves clockwise and anti-clockwise 360° while in spiral/helical CT the

tube and detector arrays continuously move with the table. In early CT scanners, stationary anode X-ray tubes were used, since the long scan times meant that the instantaneous power level was low. Long scan times also allowed heat dissipation. Shorter scan times in later versions of CT scanners required high-power X-ray tubes and use of oil-cooled rotating anodes for efficient thermal dissipation.

Several technical advances in component design have been made to achieve these power levels and deal with the problems of target temperature, heat storage, and heat dissipation. For example, the tube envelope, cathode assembly, and anode assemblies including anode rotation and target design have been redesigned. As scan times have decreased, anode heat capacities have increased by as much as a factor of five, preventing the need for cooling delays during most clinical procedures, and tubes with capacities of 5 to 8 million heat units (MHU) are available. In addition, improvement in the heat dissipation rate (kilo-heat units per minute) has increased the heat storage capacity of modern X-ray tubes. The large heat capacities are achieved with thick graphite backing of target disks, anode diameters of 200 mm or more, improved high temperature rotor bearings, and metal housings with ceramic insulators among other factors.<sup>5</sup>

The working life of tubes used today ranges from 10,000 to 40,000 hours, with a marked improvement over the 1,000 hours typical of conventional CT tubes. Because many of the robust engineering changes increased the mass of the tube, a significant effort was also dedicated to reduce the mass to better withstand increasing gantry rotational rates required by faster scan times.

With increasing gantry rotation speed, there is also an increase in the stress on the gantry structure, since rapid movement of heavy mechanical components inside the CT gantry makes it harder to achieve a further reduction in gantry rotation time. In fact, even a small incremental gain in the gantry rotation time requires great effort in the engineering design.<sup>5</sup>

A major landmark in development of CT tubes is the advent of directly cooled X-ray tube. It allows gantry rotation time below 0.4 seconds and allows virtually unlimited volume coverage at maximum scan speed without compromise on resolution and image quality. Direct anode cooling enables extremely high cooling rates and eliminates the need for anode heat storage capacity. The very compact design is robust. The anode and inner tube assembly are significantly smaller than in the conventional tubes. In conventional X-ray tubes, the entire anode including the bearings is encapsulated in a vacuum and cannot be efficiently reached by the cooling fluid, resulting in lower cooling rates. Robust X-ray tubes with higher heat storage capacity up to 8 million heat units (MHU), allows scanning until the heat storage capacity is filled. Once overheated, even such state-of-the-art conventional X-ray tubes take five to ten minutes to cool down to normal operation temperatures.

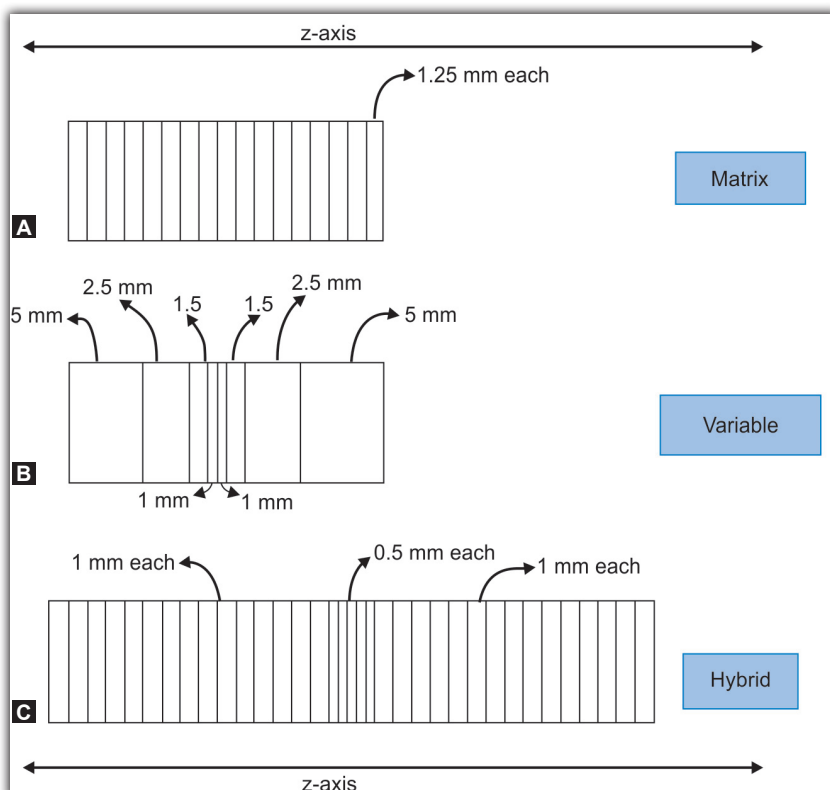
The new directly cooled X-ray tube provides direct cooling of the anode with all bearings being located outside the vacuum. Similar to a miniature electron beam CT, the electron beam in the tube is shaped and controlled by an electromagnetic field. The direct anode cooling enables unprecedented cooling rates of 4.7 MHU/min and eliminates need for large heat storage capacities. In fact, the heat storage capacity of the new anode is close to 0 MHU. Even at maximum load, these tubes cool down within only 20 seconds – much less time than needed to initiate the next scan or to position the next patient. With substantially higher tube lifetime even at much higher G-forces this revolutionary design is the key to increased gantry rotation speed and reduced life-cycle cost at the same time. A novel example of such a tube is Straton tube.<sup>6</sup>

X-ray tube with flying focus has a magnet system for deflecting and focusing the electron beam, whereby the magnet system including a carrier that is constructed as an iron yoke and that has four pole projections that are arranged around the axis of the electron beam offset from one another by 90 degree., on which two pairs of coils (z-coils and .phi.-coils) are arranged so as to be offset from one another 90 degree. The individual coils of each pair supplied with a common high-frequency alternating current that deflects the electron beam in the .phi.-and z-directions, respectively, in a pulsed manner.<sup>5</sup>

### Advances in Detectors

The detector array design in multiple-row detector CT varies with each manufacturer. The detectors are arranged in rows and columns. The number of active detector rows and the z-axis width of detectors in an array define the detector configuration. A detector design that is subdivided into equal elements, or portions, is called *uniform, matrix, or mosaic*. *Nonuniform* or Variable detectors use variable detector size in the orthogonal direction or along the z-axis (the longitudinal axis of the patient table). In combination with a physical postpatient collimator, signals from these detectors can be combined to form various values of image thickness in a manner that improves detector efficiency over that of uniform detectors. This improvement is a result of the smaller proportion of dead space due to the divisions (cell walls) between detector elements. *Hybrid detectors* has a number of narrow detector elements in the center of the detector and a different number of wider detectors (usually double the width of the narrow detectors) on both sides of the span of narrow detectors (**Figs 3A to C**). The number of narrow and wider detectors can vary among different vendors.<sup>7</sup>

Following the presentation of the first 4-slice CT scanner in 1998, all other manufacturers also offered scanners enabling acquisition of four simultaneous slices per rotation. The next step was the development of 16-slice CT scanners parallel to slimmed-down versions for the simultaneous



**Figs 3A to C** Diagram showing the basic design of matrix (A), variable (B) and the hybrid (C) detector design. The measurements indicated in the diagram are relative and not to scale

acquisition of 6, 8, or 10 slices. And as the slice counts keep going up (128, 256 and even 320) the costs and clinical capabilities go up too.

In-plane spatial resolution is determined primarily by the number of X-ray projections available for reconstruction, the scan field of view, and the image matrix. The highest in-plane spatial resolution of current MDCT scanners has been reported to be in the range of 0.23 to 0.4 mm.

During helical scanning, some overscanning in the longitudinal direction (z-overscan) is required to ensure that sufficient data are available for reconstruction. Dynamic or adaptive collimation is a hardware-based solution for collimating the X-ray beam such that extraneous radiation exposure is blocked by retractable collimator blades. Dynamic collimation has the greatest effect in reducing dose for shorter scan lengths and higher pitch values.

Z-overscanning can also occur during axial scanning. In this case, the amount of z-overscan depends on the planned scan length  $P$  and the total beam collimation. Adaptive collimation is a hardware solution offered on certain wide-detector array MDCT scanners. With this technique the detector collimation is automatically selected from a set of beam collimations in increments of 10 mm that are based on the planned scan length so as to minimize extraneous exposure. Adaptive collimation for axial scanning has the greatest effect in reducing dose with wide-detector array MDCT scanners because the portion of the total X-ray exposure in the axial scan mode attributed to z-overscanning increases with z-axis detector coverage.<sup>1</sup>

Dual energy may be principally achieved either by radiating the object with two different energy spectra from a single source through fast voltage switching or from multiple sources operating at different voltages, or by analyzing the energy spectrum on the detector side. A simple but effective solution lies in a double-layer detector design. The upper layer predominantly receives photons with lower energy and the lower layer receives photons with higher energy. Summing the signal from both detector layers returns the full signal as in a single layer detector, but separate readouts from both layers allow for simple spectral analysis of the X-ray beam.<sup>1</sup>

Most scanners use ceramic (solid-state) scintillation detectors coupled to photodiodes, which have improved spatial resolution and decreased noise compared with older xenon gas detector systems. Another milestone in CT technology lies in the development of new detector materials that exhibit higher sensitivity to radiation and allow faster sampling rates. There is a new scintillator that features a negligible afterglow in conjunction with a 100-fold faster reaction time, allowing for recording of 7000 views per second. Implementation of the new scintillator may be one of the prerequisites for single-source ultra-fast dual energy switching, promising almost simultaneous spatial and temporal registration and material decomposition

without the limitation of a reduced FOV due to the second smaller detector in dual-source CT. They have very low afterglow, extremely low radiation damage and very good chemical durability, mechanical properties, uniformity, and manufacturability. Approximately 50 percent fewer beam-hardening artifacts, metal artifact reduction, and further improvements in contrast-to-noise ratio are some of the benefits resulting from the new scintillator. The new scintillator is configured to emit fluorescence when irradiated with X-rays, and it has a primary decay time of only 30 nsec, making it 100 times faster than the conventional scintillator material. It has afterglow levels that reach only 25 percent of the levels of conventional scintillator material. The most advantageous feature of multidetector CT with garnet-based detectors is the improved spatial resolution (high-definition imaging at up to 230 mm resolution). An example of this is Gemstone, which is a newly developed transparent polycrystalline scintillator for CT from GE health care.<sup>8,9</sup>

### Advances in Reconstruction

Conventionally, Filtered back projection method has been used for image reconstruction in single section CT, which involves processing of each ray sum immediately after it is obtained while the data acquisition continues for other ray sums. It attempts to project a uniform value of attenuation over the path of the ray such that the calculated attenuation over the path is proportional to the measured attenuation. The final image obtained is rather blurred as a result of the assumption that the beam attenuation occurs uniformly over the entire path of the ray. A technique to eliminate the blurring is the 'convolution operation' or 'filtering' which involves a 'filter function' or convolution 'kernel'. The filter or kernel may be chosen by the radiologist or automatically selected for a particular procedure. The most commonly used single-section spiral interpolation schemes are the 360° and 180° linear interpolation methods.<sup>10</sup>

Spiral CT requires an interpolation of the acquired measurement data in the longitudinal (through-plane) direction to estimate a complete CT data set at the desired plane of reconstruction. The 360° and 180° linear interpolation single-section spiral reconstruction approaches can be extended to multidetector row spiral scanning in a straightforward way but the cone angle of the measurement rays is not taken into account (Fig. 4). Scanners that rely on 180° or 360° multidetector linear interpolation techniques and extensions thereof provide selected discrete pitch values to the user to provide optimized sampling schemes in the longitudinal direction and, hence, optimized image quality. Scanning at low pitch optimizes image quality and longitudinal resolution at a given collimation but at the expense of increased patient dose. To reduce patient dose, either milliamperes settings should be reduced at low pitch values or high pitch values should be chosen. A further refinement to spiral interpolation is the Z-filter approach, in

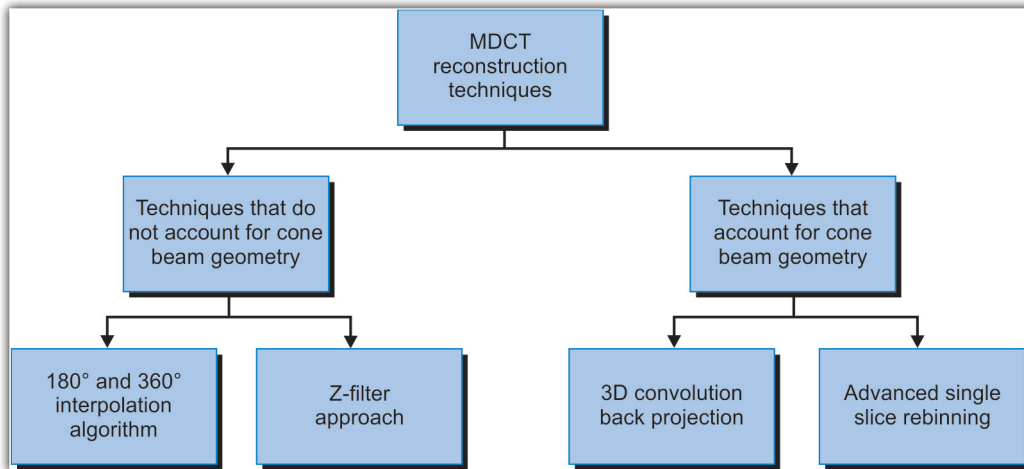


**Fig. 4** MDCT reconstruction techniques

which reconstruction is not restricted to the two rays closest to the image plane and is contributed by all rays within a selectable distance from the image plane. An example of z-filter technique is adaptive axial interpolation algorithm, which allows the system to trade off z-axis resolution with image noise. Unlike in single section spiral CT, patient dose is independent of spiral pitch.<sup>11</sup>

For CT scanners with 16 or more detector rows, modified reconstruction approaches that account for the cone-beam geometry of the measurement rays have been developed. In 3D convolution back-projection technique for multisectection spiral scanning, the reconstruction is based on sorting of raw data from individual detector channels. In the raw data space, which is typically four times as large as the image data space, the signals from the individual detector rows are computed in such a way that axial images in parallel orientation are directly obtained from the raw data.<sup>1,11</sup> Sorting of the raw data requires considerable processor power and more powerful computers. Direct 3D filtered back projection of raw data is superior to rebidding algorithms (mentioned later) in homogeneous distribution of image noise and uniform slice thickness in particular for scanners with larger cone angles. Iterative reconstruction techniques, based on back and forward projection promising significant noise reduction, have been proposed since the early times of CT technology. In single-slice spiral CT, the pitch factor did not affect image noise but higher pitch factors resulted in thicker slices and increasingly blurred anatomy. Typical pitch factors used in spiral CT ranged between 1 and 2. In multislice spiral CT, the pitch factor does not affect the slice sensitivity profile of the reconstructed section but faster table feed (higher pitch value) increases image noise because fewer photons are available for image reconstruction. This effect is compensated for on all scanners by automatically increasing the tube current (mA value) when a higher pitch factor is selected. It is thus no longer possible to reduce the radiation dose by simply choosing a higher pitch factor (which was possible on earlier spiral CT scanners). The image quality achieved with all currently available implementations of reconstruction algorithms may

vary with the pitch factor. On most current scanners, optimal image quality is obtained when using pitch values slightly less than one because computation of supplementary projections obtained by overlapping scanning generally results in higher image quality.<sup>1</sup>

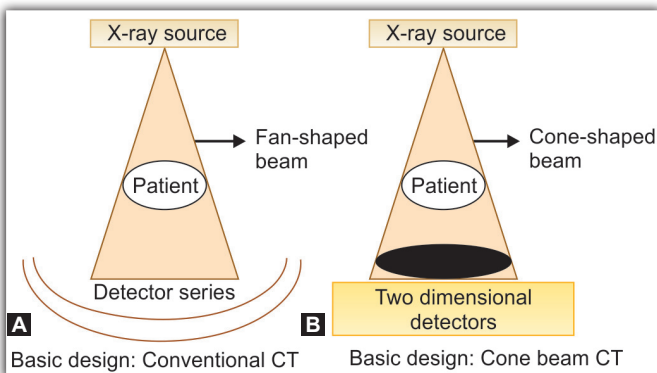
### Rebidding Algorithms

Advanced single-slice rebidding (ASSR) and its variations are algorithms optimized for small cone angles. The algorithm reduces three-dimensional (3D) cone beam data to tilted two-dimensional slices by minimizing the deviation of the reconstruction plane from the spiral. The image planes are no longer perpendicular to the patient axis; instead, they are tilted to match the spiral path of the focal spot generating pseudoaxial slices. In a final z-axis reformation step, the traditional transverse images are calculated by interpolating between the tilted original image planes. The ASSR algorithm operates efficiently and requires fairly little computing power to reconstruct images of clinically acceptable image quality. Representative examples for rebidding algorithms are the adaptive multiplanar reconstruction algorithm (AMPR) and the conjugate ray reconstruction (weighted hyperplane reconstruction).<sup>1</sup>

## SPECIAL COMPUTED TOMOGRAPHY

### Cone Beam CT (CBCT)/Volume CT

Cone beam CT is an emerging CT variant which is designed to provide a compact, low-cost, low radiation dose system that can be used to image high contrast structures as in the head and neck. CBCT uses divergent X-rays forming a “cone” between the source and detector, unlike the “fan-beam” geometry in conventional CT (**Figs 5A and B**). In CBCT multiple images are acquired during a single rotation of the gantry around the patient head producing a three-dimensional volumetric data. On the other hand, conventional CT requires both rotation as well as z-axis translation of the gantry to be able to acquire 3D data. X-ray tubes of relatively low power requirements are employed. Recent versions of the system use flat panel



**Figs 5A and B** Schematic diagram showing basic design of a conventional CT (A) and a cone beam (B) CT

detectors (FPDs) of the indirect-conversion type based on a cesium iodide (CsI) scintillator.<sup>12</sup> These digital flat panel CBCT systems can also be mounted a C-arm for applications in interventional radiology suites.

Cone beam CT thus produces an entire volumetric data set in a single gantry rotation as it utilizes a two-dimensional detector system unlike the one-dimensional detector or series used in MDCT.<sup>13,14</sup> Depending on the variants of the system devised for various applications, several terms been used in literature to describe these new volumetric imaging techniques such as cone-beam CT, C-arm CT, cone-beam volume CT, volume CT, angiographic CT, and flat-panel CT.<sup>13</sup>

### Cone Beam Geometry

Cone beam CT (CBCT) uses a high-resolution two-dimensional detector instead of a series of row of one-dimensional (1D) detector elements as in MDCT.<sup>13</sup> Images obtained by CBCT have high isotropic spatial resolution. This is due to the isotropic nature acquisition and reconstruction in CBCT systems.<sup>12</sup> The volumetric data obtained in CBCT yield a dataset with isometric voxel size as small as  $150 \times 150 \times 150 \mu\text{m}^3$  at the isocenter, thus allowing high quality multiplanar reconstructions.<sup>12,15</sup> MDCT on the other hand produces individual sections which are subsequently stacked typically yielding spatial resolution of  $500 \times 500 \mu\text{m}^2$  in-plane and 500 to 1000- $\mu\text{m}$  in the z-axis.<sup>12</sup> CBCT however suffers from poor contrast resolution due to higher scatter in cone beam acquisition, a lower DQE of CBCT systems and reduced temporal resolution and dynamic range of the FPDs.<sup>13</sup> CBCT is thus suited for imaging of high-contrast structures. Higher scatter is a major limiting factor with the cone beam vs conventional fan-beam geometry acquisition leading to image degradation. In order to counter this effect, several anti-scatter measures are employed such as grids, software correction algorithms, beam-stop scatter map ping, and alteration of object-to-detector distance (air-gap).<sup>16</sup> CBCT also suffers from limited anatomic coverage as it is based on acquisition of images during single gantry rotation.<sup>13</sup>

### Flat Panel Detector

Cone beam CT scanners use cesium iodide (CsI) scintillator detectors unlike the ceramic detectors used in MDCT. These suffer from a greater lag (afterglow) and hence scan times are much longer with CBCT relative to MDCT, thus reducing the temporal resolution of CBCT scanners. For instance, the current C-arm CBCT acquisitions take about 5 seconds.<sup>13,15</sup> In addition, CsI detectors also have a lower quantum efficiency reducing the dynamic range of the scanner.<sup>13</sup> The low dynamic range and increased also result in low contrast resolution of these systems.

### Reconstruction

Volumetric data thus acquired in CBCT as in MDCT can subsequently be manipulated and reconstructed with software to allow multiplanar as well as panoramic reconstructions.<sup>12</sup> The most commonly used reconstruction algorithm in CBCT systems is a modification of the filtered back-projection method called the Feldkamp algorithm.<sup>15</sup> Compared to MDCT, CBCT however takes longer times for acquisition as well as reconstruction of images despite the acquisition being done in a single rotation.

### Radiation Dose

The other major advantage of CBCT is reduction of radiation dose relative to MDCT. Effective dose of commercial CBCT scanner has been estimated as 0.2 mSv Vs 1–2 mSv for MDCT head.<sup>17,18</sup> However assessment of radiation dose during CBCT affords many challenges due to the altered beam geometry and underestimation of dose when using conventional methodology such as ion-chamber inserts.<sup>12,19</sup> Also, conventional dosimetry metrics such as the  $\text{CTDI}_{\text{w}}$  cannot be directly applied to CBCT imaging. It is hence suggested that the difference in absorbed dose measurements may be insignificant when FOVs and image quality parameters between CBCT and MDCT are adjusted.<sup>15,19</sup>

### Applications

Cone beam CT provides a compact system wherein the scan can be performed with the patient sitting in an upright position. It has primarily found widespread applications in maxillofacial imaging including dental imaging, sinus and temporal bone imaging. It is most popular as an office based system for dental imaging. CBCT systems for maxillofacial imaging became available in 2001.<sup>20</sup> The compact design also makes the system significantly cheaper than MDCT. It also delivers a lower radiation dose than MDCT. CBCT has high spatial resolution but low contrast resolution and limited anatomic coverage. It is not meant to be a substitute for MDCT which is distinctly superior in image quality but as a compact, inexpensive, low dose system for applications. C-arm based CBCT systems are also used in interventional radiology suites.<sup>13</sup>

### C-arm Based CBCT

The cone beam CT system is compact enough to allow it to be mounted on a C-arm. These systems allow projection radiography, fluoroscopy, digital subtraction angiography, and volumetric CT applications through a single system. This has significant utility as it eliminates the need for transporting the patient to the CT room for procedures requiring guidance of cross-sectional imaging. Currently, all commercially available C-arm mounted CBCT systems employ digital flat-panel detectors.<sup>13</sup> Also, unlike MDCT as there is no z-axis translation and all acquisition occurs in a single rotation of the tube-detectors, it allows patient to remain stationary during the procedure.

Cone beam CT has been employed for radiation therapy planning.<sup>21</sup> CBCT has also been used for surgical planning particularly in orthopedic, chest, abdominal, head and neck, and neurosurgical procedures.<sup>13,22</sup>

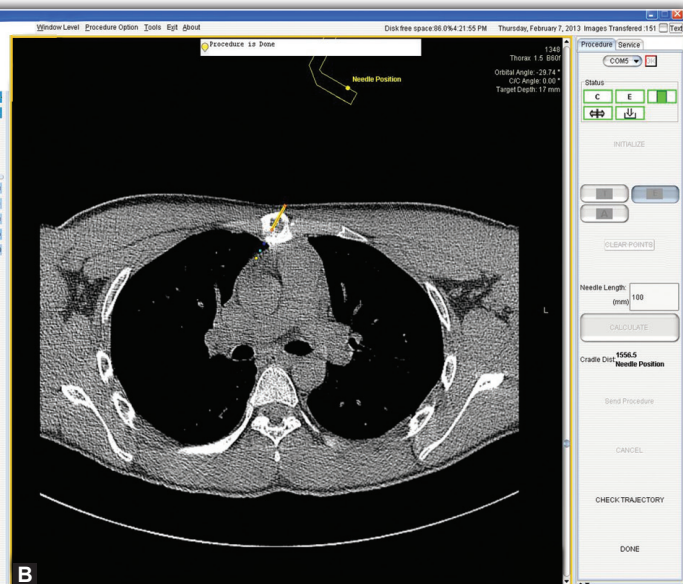
**Electron beam tomography** (EBT) is a specific form of computed tomography (CAT or CT) in which the X-ray tube is not mechanically spun in order to rotate the source of X-ray photons. In EBT, however, the X-ray tube itself is large and stationary, and partially surrounds the imaging circle. Rather than moving the tube itself, electron beam focal point (and hence the X-ray source point) is swept electronically along a tungsten anode in the tube, tracing a large circular arc on its inner surface. This motion can be very fast. The heart never stops moving, and some important structures, such as arteries, move several times their diameter during each heartbeat. Rapid imaging is, thus, important to prevent blurring of moving structures during the scan. It increasingly appears that the spiral CT designs, especially those with (b)

detector rows, (b)  $3 \times 360^\circ/\text{sec}$  rotation speeds and designed for cardiac imaging, are largely replacing the EBT design from a commercial and medical perspective.

### Navigation Systems

Several navigation systems have recently become available to aid in CT guided interventions. One of the methods used for this purpose is electromagnetic tracking. These systems involve interaction with previously acquired images to provide real time spatial navigation information. This method does not involve continuous imaging of the patient. Combining electromagnetic tracking with preacquired imaging can be beneficial in guiding interventions, for instance in allowing real time targeting of lesions using previously acquired sequences in desired phase of enhancement.<sup>23</sup> Electromagnetic tracking also allows utilization of data from other imaging modalities. Similarly this technology is also being used to guide endoscopic and surgical procedures. Previously acquired CT images are loaded into proprietary software which reconstructs 3D images as desired. These are then used to mark target locations and plan path of intervention. Real time visualization of position of the endoscope is also then available in relation to these images. Navigation devices may also be based on optical tracking systems.<sup>24</sup>

Automated guiding systems for CT-guided biopsies are also available now. These typically involve the use of a robotic, electromechanical arm (**Figs 6A and B**). A computer interface receives the CT images and calculates coordinates on DICOM images and then guides needle placement through the arm.<sup>25</sup>



**Figs 6A and B** (A) Photograph showing sternal biopsy in a patient with the help of PIGA. (B) The planner image on the console projects the expected trajectory of the needle path

## CONCLUSION

Computed tomography hardware thus is a rapidly evolving field, constantly introducing newer technologies for the user as the vendors continue to innovate.

## REFERENCES

1. Rogalla P, Kloeters C, Hein PA, et al. CT Technology Overview: 64-Slice and Beyond. *Radiol Clin N Am.* 2009;47:1-11.
2. Curry TS, Dowdye JE, Murry RC. Computed Tomography in Christensen's Physics of Diagnostic Radiology, 4th Edn. Philadelphia and London: Lea & Febiger; 1990. pp.289-322.
3. Mahesh M, Cody DD. Physics of cardiac imaging with multiple-row detector CT. *Radiographics.* 2007;27(5):1495-509.
4. Reddinger W. www.e-radiography.net, [Place unknown] Out Source, Inc., 1998[Updated 2013 January 1; cited 2013 March 08] Available from www.e-radiography.net/mrict/CT\_IQ.pdf
5. www.kau.edu.sa [cited 2013 March 08] Available from "X-Ray Tube in CT Scanner" www.kau.edu.sa/.
6. www.medical.siemens.com [cited 2013 March 08] Available from www.medical.siemens.com/.../S\_64-69\_Science\_Speed 4D.pdf
7. Cody DD, Mahesh M. Technologic Advances in Multidetector CT with a Focus on Cardiac Imaging. *Radio Graphics.* 2007; 27:1829-37.
8. www.gehealthcare.com [cited 2013 March 08]
9. Yanagawa M, Tomiyama N, Honda O, et al. Multidetector CT of the lung: image quality with garnet-based detectors. *Radiology.* 2010;255(3):944-54.
10. Miraldi F, Sims MS, Wiesen EJ. Imaging Principles in Computed Tomography in CT and MR Imaging of the Whole Body, 4th Edn. In: Haaga JR, Lanzieri CF, Gilkeson RC (Eds). United States of America: Mosby; 2003. pp.2-36.
11. Flohr TG, Schaller S, Stierstorfer K, et al. Multi detector row CT systems and image-reconstruction techniques. *Radiology.* 2005;235(3):756-73.
12. Miracle AC, Mukherji SK. Cone beam CT of the Head and Neck, Part 1: Physical Principles. *AJNR.* 2009;30:1088-95.
13. Orth RC, Wallace MJ, Kuo MD. For the Technology Assessment Committee of the Society of Interventional Radiology. C-arm cone-beam CT: general principles and technical considerations for use in interventional radiology. *J Vasc Interv Radiol.* 2008; 19:814-20.
14. Jaffray DA, Siewerdsen JH. Cone beam computed tomography with a flat-panel imager: initial performance characterization. *Medical Physics.* 2000;27:1311-23.
15. Gupta R, Grasruck M, Suess C, et al. Ultra-high resolution flat-panel volume CT: fundamental principles, design architecture, and system characterization. *Eur Radiol.* 2006;16:1191-205. Epub 2006 Mar 10
16. Endo M, Mori S, Tsunoo T, Miyazaki H. Magnitude and effects of X-ray scatter in a 256-slice CT scanner. *Medical Physics.* 2006; 33:3359-68.
17. Bauhs JA, Vrieze TJ, Primak AN, et al. CT dosimetry: comparison of measurement techniques and devices. *Radiographics.* 2008;28:245-53.
18. Alspaugh J, Christodoulou E, Goodsitt M, et al. Dose and image quality of flat-panel detector volume computed tomography for sinus imaging. *Med Phys.* 2007;34:2634.
19. Fahrig R, Dixon R, Payne T, et al. Dose and image quality for a cone-beam C-arm CT system. *Med Phys.* 2006;33:4541-50.
20. Scarfe WC, Farman AG, Sukovic P. Clinical applications of cone-beam computed tomography in dental practice. *J Can Dent Assoc.* 2006;72:75-80.
21. Moore CJ, Am A, Marchant T, et al. Developments in and experience of kilovoltage X-ray cone beam image-guided radiotherapy.
22. Daly MJ, Siewerdsen JH, Moseley DJ, Jaffray DA, Irish JC. Intraoperative cone-beam CT for guidance of head and neck surgery: Assessment of dose and image quality using a C-arm prototype. *Medical Physics.* 2006;33:3767-80.
23. Appelbaum L, Sosna J, Nissenbaum Y, Benshtain A, Goldberg SN. Electromagnetic Navigation System for CT-Guided Biopsy of Small Lesions. *AJR.* 2011;196:1194-1200.
24. Meier-Meitinger M, Nagel M, Kalender W, Bautz WA, Baum U. Computer-assisted navigation system for interventional CT-guided procedures: results of phantom and clinical studies. *Rofo.* 2008;180(4):310-7. [Article in German]
25. Chellathurai A, Kanhirat S, Chokkappan K, Swaminathan TS, Kulasekaran N. Technical note: CT-guided biopsy of lung masses using an automated guiding apparatus. *Indian J Radiol Imaging.* 2009;19(3):206-7.

# Chapter

# 5

## Dual Energy CT

Arun Kumar Gupta, Manisha Jana

### INTRODUCTION

Beginning from the single slice sequential CT scanner and advancing towards multislice spiral CT with ultrafast true isotropic volume imaging, computed tomographic imaging technology has undergone significant changes in the last few decades. Conventional CT scanners, operating at a single energy, provide morphologic imaging only, with little material-specific information in body imaging. On the other hand, dual energy CT utilizes the principle that different materials show different attenuation at varying energy levels, and this difference in attenuation can be used for tissue characterization. Since its inception, dual energy CT scanning has undergone several technical modifications. This chapter describes the development, principle and applications of dual energy CT.

### HISTORICAL PERSPECTIVE

The concept of dual energy CT existed from the very beginning of the history of computed tomographic imaging. In the early days, Sir Hounsfield proposed that "two pictures are taken of the same slice, one at 100 kV and the other at 140 kV... areas of high atomic numbers can be enhanced... Tests carried out to date have shown that iodine ( $Z = 53$ ) can be readily differentiated from calcium ( $Z = 20$ )."<sup>1</sup> Alvarez and Macovski<sup>2</sup> and Kalender et al<sup>3</sup> also described the theoretical basis of dual energy CT scanning in the late 1970s and early 1980s. The constraints in dual energy imaging in early days were poor spatial resolution, increased radiation dose, slower CT scanners leading to image misregistration, and significant noise in the lower kilovoltage image.<sup>4-8</sup> With the advent of newer multislice CT scanners having improved

temporal resolution, dual energy CT has finally become a reality in clinical applications. First commercially available dual energy CT scanner came into use in 2006<sup>8</sup> (Somatom Definition, Siemens, Erlangen, Germany). It was dual source dual energy CT scanner (DS-DECT) having two X-ray tubes and two detector systems. Over the time there have been newer modifications and advancements in the dual energy scanners. In second generation of dual source dual energy scanners, the dual energy scan FOV was increased (from 26 to 33 cm); and the addition of a selective photon shield led to increased contrast to noise ratio and better and accurate material characterization. The DS-DECT scanner was followed by the development of a single-detector, single-source DECT (SS-DECT) system with the capability for rapid alternation/fast switching between two kVp settings (Gemstone Spectral Imaging; GE Healthcare, Piscataway, NJ).<sup>9</sup> A SS-DECT scanner has a single ultrafast detector system with very short afterglow and dual energy scanning is made possible by rapid switching of the kVp settings of the tube. Currently available dual energy CT scanners employ different technologies to obtain high and low-energy datasets:

- Dual source dual energy CT (DS-DECT)
- Single source dual energy CT (SS-DECT) and
- Single source dual energy scanner with dual detector layers (under development with Philips, not commercially available).

### PRINCIPLE

In clinical imaging, compton scatter and photoelectric effect are the two predominant interactions of matter with X-ray photons. The photoelectric effect occurs when an incident

photon, having sufficient energy to overcome the K-shell binding energy of the electron in an atom, interacts with the atom to release the K-shell electron. The energy generated is released in the form of a photoelectron. The likelihood of photoelectric effect depends on the atomic number of the substance as well as the energy of the incident beam.<sup>10</sup> As the energy of the incident photon beam approaches the K-shell binding energy of an electron (which varies with the atomic number), the chances of photoelectric effect increases. K-edge refers to an increased photoelectric effect and a spike in attenuation at an incident energy level just greater than the K- shell binding energy.<sup>7</sup> The K- edge values of different materials are given in **Table 1**.

The principle of dual energy CT imaging is based on the differential absorption of energy at variable kVp settings. For example, let us consider a substance (A) with K-edge at 60 kVp and another (B) at 130 kVp. If we image multiple combinations of A and/or B at 80 and 140 kVp, there will be differential attenuation at both these energy settings depending on the relative percentage of these substances. The object containing large amount of substance A will show higher attenuation at 80 kVp and lower attenuation at 140 kVp; whereas object containing larger amount of substance B will show higher attenuation at 140 kVp. In clinical applications, the constituents of soft tissues have a different K-edge (variable from 0.01 to 0.53), away from that of iodine (33.2) or calcium (4); hence iodine or calcium can be distinguished from soft tissues at dual energy imaging (**Fig. 1**).

In diagnostic imaging, once the datasets at 80 kVp and 140 kVp are generated, the attenuation of the enhanced structures containing iodine (vessels, highly perfused organs) are more on a 80 kVp image than on a 140 kVp image. This difference in attenuation varies between different organs; for example—highly vascular organs and vessels have higher difference than muscles (**Figs 2A to H**). Post-processing softwares use this information to generate a virtual non-contrast image, or to calculate the material composition within a specific region of interest.

## DUAL ENERGY RATIO

The material characterization on DECT largely depends on their dual energy ratio. The dual-energy ratio is a material-specific parameter. It depends on the atomic number, not on the material density or concentration. For experimental derivation of dual energy ratio of a given material X, the CT attenuations at any given kVp (for example, 140 kV) at different material concentrations are assessed and arranged along a graph (A). Similar graph (B) is made for different material concentrations at another kVp (for example 80 kVp). The dual energy ratio of material X can be described as a ratio of the slope of the graph B to the slope of graph A.<sup>12</sup>

The difference between dual energy ratio of different materials depends on several factors, for example:

1. Difference in the atomic number of the materials and

**Table 1** Atomic number and k-edges of different substances and radiographic contrast agents<sup>11</sup>

Substance	Atomic number	K-edge (keV)
Hydrogen	1	0.01
Carbon	6	0.28
Nitrogen	7	0.40
Calcium	20	4
Iodine	53	33.2
Barium	56	37.45

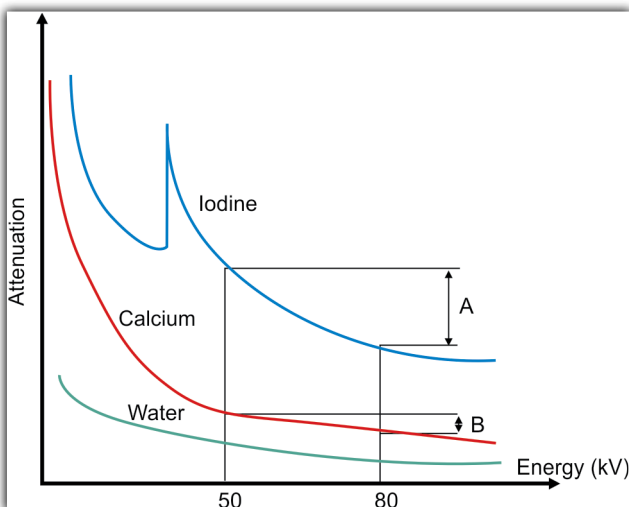
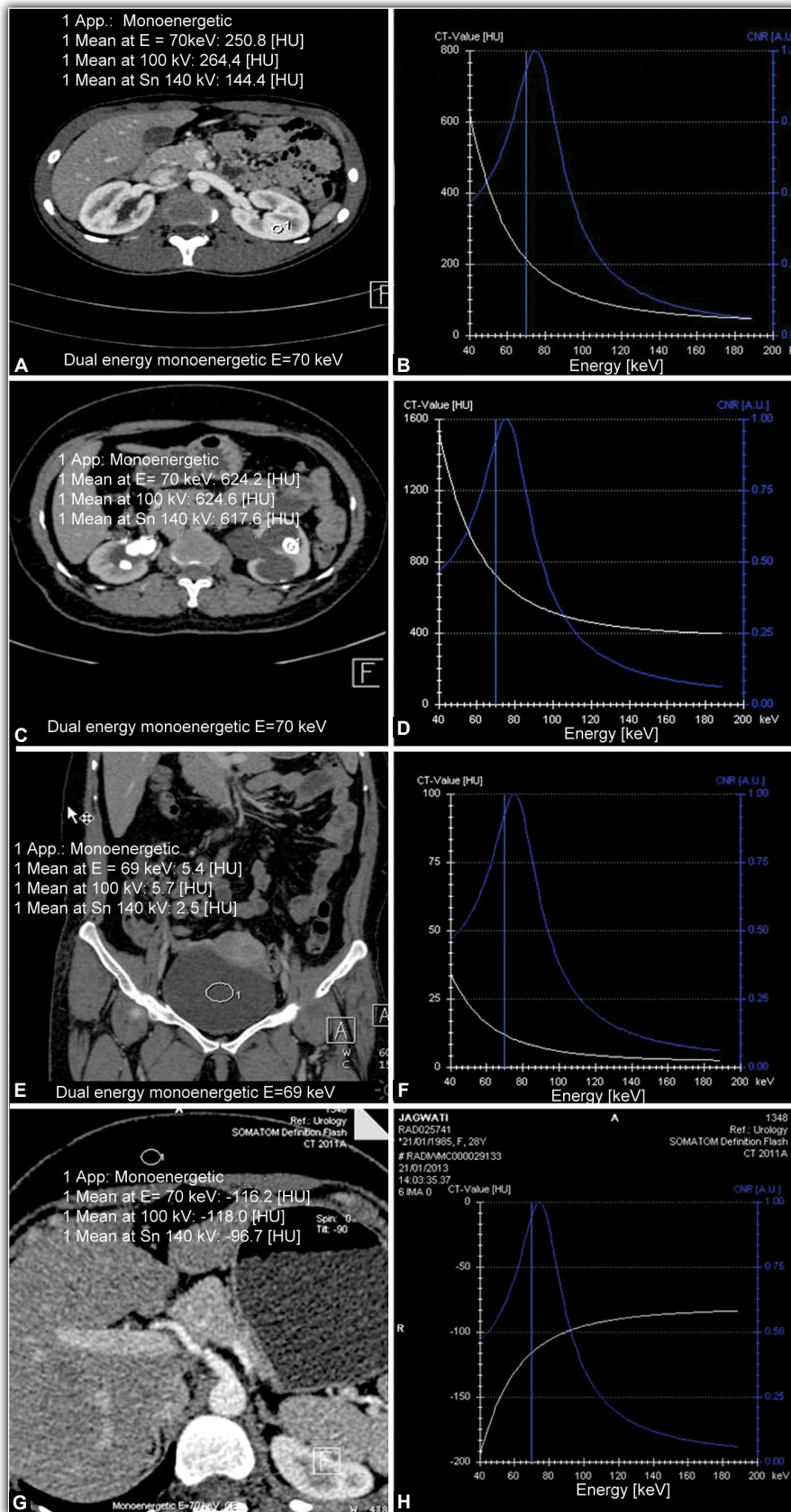


**Fig. 1** Principle of dual energy CT. Change in CT attenuation of substances at different energy levels of incident beam. Iodine (k-edge 33.2 keV), shows a peak attenuation at lower energies and a rapid decrease in attenuation at higher energies. When attenuation at 50 and 80 kVp are compared; iodine shows a greater decrease (A) in attenuation at higher energy than calcium (B). Water shows very minimal change in attenuation with changes in kV. This forms the basis of material characterization in dual energy CT

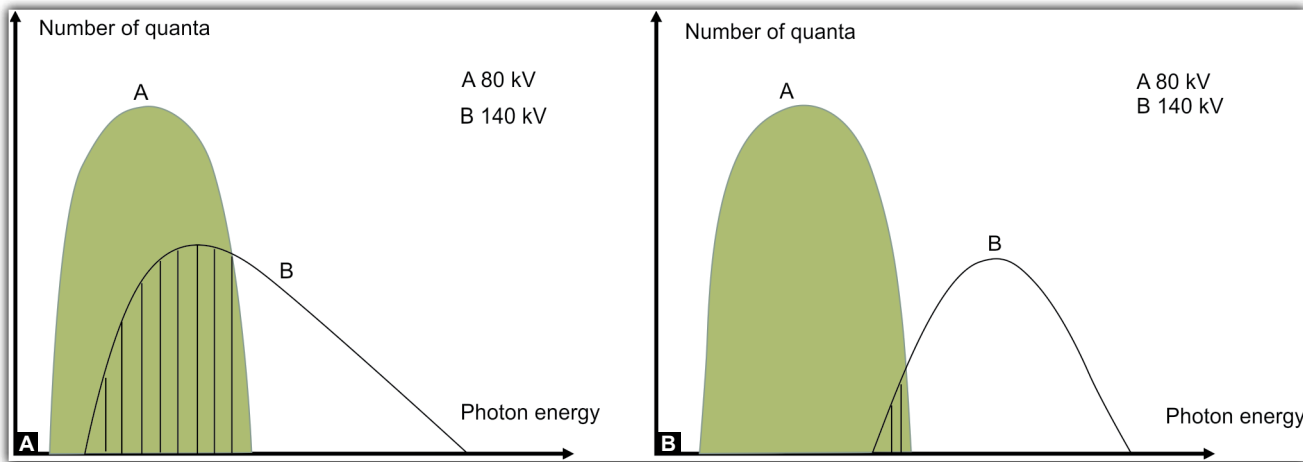
2. Spectral separation between X-ray spectra at the two energies. If the two incident X-ray beams have mean energies very close to each other, the difference in dual energy ratios among various component materials (for example, iodine and soft tissue) will be less and it will be difficult to differentiate them on imaging.

## Spectral Separation and Selective Photon Shield

As a continuation of the previous discussion, for efficient dual energy imaging the two incident X-ray beams should have sufficiently different energies. In reality, whenever X-ray is generated, it is emitted in the form of a continuous spectrum with photons having different energy levels (Bremsstrahlung) and a mean energy. The mean energy of



**Figs 2A to H** Different CT attenuation of tissues at different energy levels, based on their constituents. Highly vascular organs containing iodine on CECT shows higher attenuation at lower energy images. For example, renal parenchyma shows an attenuation of 250.8 HU at 70 kV images and 144.4 HU on 140 kV images (A and B). Calcium shows very little variation in the attenuation values over a change of energy from 70 to 140 kV (C and D). Water also shows very little change in attenuation (E and F). Fat, to the contrary, shows a minimal increase in attenuation at higher energy images (G and H); -116.2 HU at 70 kV and -96.7 HU at 140 kV



**Figs 3A and B** Spectral separation. When high (140 kV) and low energy X-rays (80 kV) are used, there is a significant energy overlap between them (shaded area A). Hence, generation of a true mono-energetic beam becomes difficult. After the use of a selective tin filter with the higher energy tube in second generation DS-DECT scanners (B), the lower energy X-rays from 140 kV tube are filtered; thereby reducing the overlap (shaded area B). This leads to better spectral separation, proper mono-energetic imaging and better material characterization

an X-ray spectrum varies with the bombarding energy (kV). When two tubes with different kV are used, two spectra are generated with significant overlap between them (spectral overlap) (**Figs 3A and B**). As described earlier, the spectral overlap makes material characterization more difficult. Spectral overlap also reduces the dose efficiency as the 140 kVp spectrum contains significant percentage of low-energy photons also, which add to the patient dose. Spectral separation indicates a situation when there is minimal overlap between the different energy spectra, i.e. less spectral overlap.

*Adequate spectral separation can be achieved by several methods*

1. Adding separate filtration to one or more tubes in DS-DECT<sup>13</sup>
2. Adding split filtration to SS-DECT<sup>14</sup>
3. Sandwich (dual) detectors
4. Energy discriminating, photon counting detectors.

In DS-DECT, either one or both the tubes can have additional filtration. However, adding filters to the low energy tube will further cut off the resultant kVp making it impossible to image a larger patient, hence it is not practiced. Adding filtration to the higher energy tube in the second generation scanners using tin filters, termed selective photon shield, has led to improved spectral separation (**Fig. 3**).<sup>12</sup> Selective photon shielding also improves the SNR efficiency and reduces dose to the patient. Tin is chosen as a filter component as it is inexpensive and easily available. The ideal thickness of filter varies between 0.5 to 0.8 mm.

### Dual Source DECT

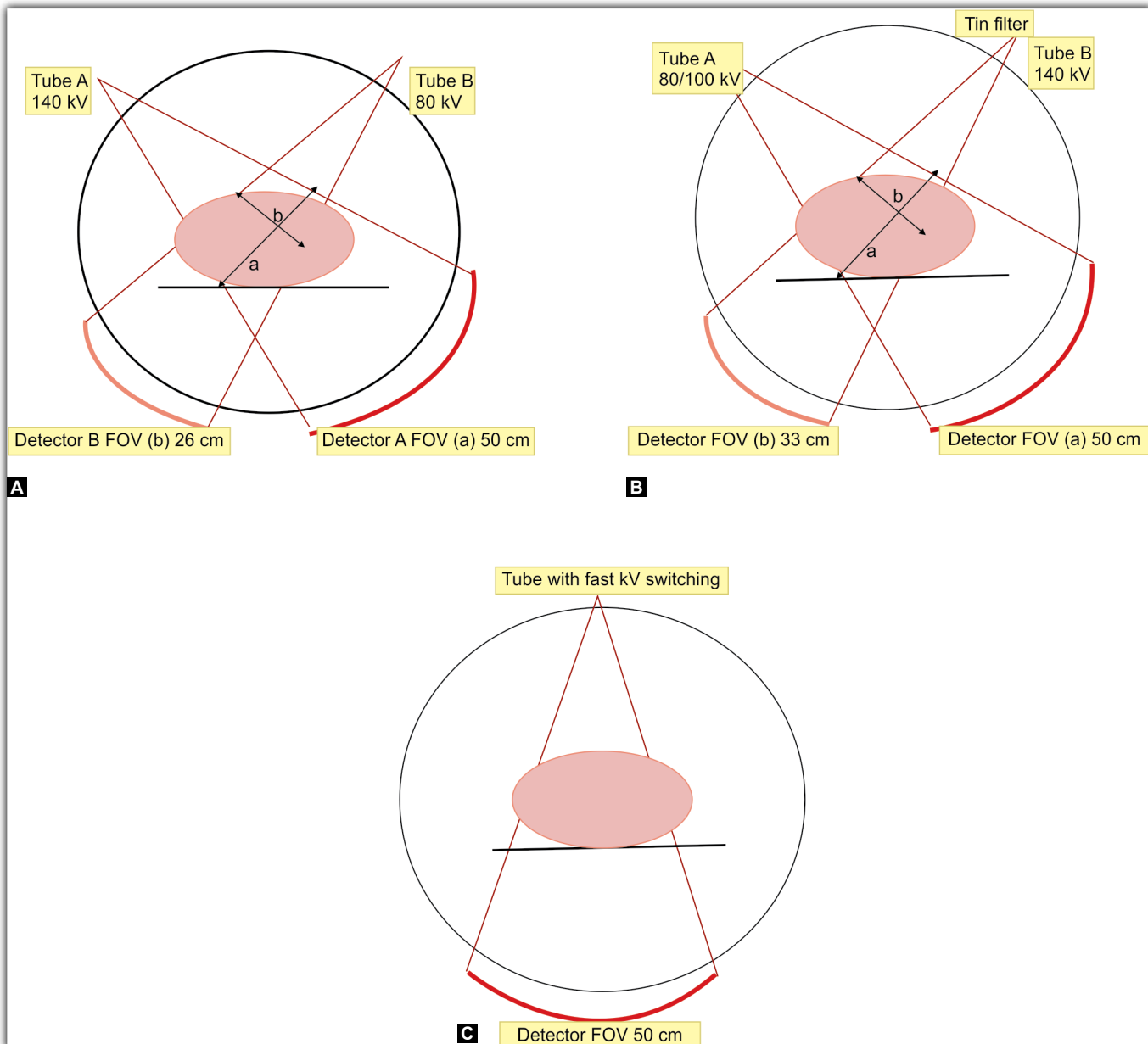
In the first generation dual source DECT scanner, X-rays are generated by two X-ray tubes, which are kept at 90 degrees

angle to each other in the same gantry and operating at different kVp (**Fig. 4A**). The average kVp of the higher energy tube is 120 to 140 and that of the lower energy tube is 80 to 100. The tube with larger kVp (tube A) has a larger detector of FOV 50 cm, and the lower energy tube (B) has a smaller FOV detector (26 cm). In the second generation DS-DECT (**Fig. 4B**) scanner, the lower energy tube (tube A) is paired with a detector with FOV of 50 cm while the higher energy tube (tube B) is paired with a smaller detector with FOV of 33 cm. Higher energy tube has a selective proton shield made of tin filter. Two separate detector arrays lead to generation of two image datasets. Since both the tube kVp can be modified independently and additional selective photon shield can be used in DS-DECT scanners, it results in better spectral separation. The temporal resolution of a DS-DECT is one-quarter of the rotation time (approximately 75 ms), as one X-ray tube acquires data during 90 degree of rotation.

However, the drawback of DS-DECT lies in term of temporal mis-registration, since the scans are not acquired simultaneously, but at a small time gap (although in ms). Another drawback is the limited dual energy FOV (33 cm), which makes it difficult to image patients with larger body habitus.

### Single Source DECT

SSDECT scanners use a single X-ray tube, which generates high and low energy X-ray spectra by rapid changing of the kVp settings (at an interval of 0.5 msec) in the same rotation (**Fig. 4C**). Since the tube current cannot be changed so rapidly, in order to maximize the contrast to noise ratio, the exposure time ratio is changed between two acquisitions. For example, 65 percent exposure time is given for the 80 kVp beam and 35 percent for the 140 kVp beam.<sup>15,16</sup> The SSDECT requires a very fast detector and data acquisition system with fast sampling capability. The detector arrays used in SS-DECT are made



**Figs 4A to C** Dual energy scanners—the first generation DS-DECT scanner (A), the second generation DS-DECT scanner (B) and SS-DECT scanner (C). In a first generation DS-DECT scanner, two tubes are placed in the gantry at an angle of 90° to each other. Tube A has a higher kVp (140) and had a larger detector array of FOV 50 cm. The smaller detector array (26 cm FOV) is paired against the lower energy tube (80 KV). In a second generation DS-DECT scanner, the smaller detector (FOV 33 cm) is paired with a higher energy tube with a selective photon shield. The SS-DECT scanner has a single tube and a detector array with 50 cm FOV. There is rapid switching of kVp in the tube

of cerium activated garnet (Gemstone Spectral Imaging; GE Healthcare, Piscataway, NJ).

*The advantage of SS-DECT over DS-DECT includes:*

1. Better temporal registration between two datasets, as the images from high and low energy acquisition are acquired almost simultaneously.

2. Larger FOV of imaging (50 cm) and easier quantification of material density.

The disadvantage of SSDECT includes a poorer spectral separation (hence less accurate material characterization compared to DS-DECT with selective photon shielding) as a selective photon shield is not commercially available in such scanners (refer to previous paragraphs).

**Table 2** Comparison between single source and dual source dual energy CT<sup>17</sup>

	<b>Single source DECT</b>	<b>Dual source DECT</b>
Tubes	Single X-ray tube with rapid switching of kVp	Two tubes operating at different kVp
Field of view (FoV)	Larger, 50 cm	FoV of dual energy acquisition 33 cm
Temporal and spatial registration	Good	Limited, as two separate image datasets are acquired
Spectral separation	Limited	Good, further improved by selective photon shield (tin filter)
Data processing	Projection space dual energy decomposition (more flexible)	Image domain decomposition (limited flexibility)
Noise on lower kVp images	Higher (as tube current can not be modulated while kVp is being altered)	Less (because of modulation of individual tube current)
Calculation of HU value on virtual NCCT image	Not possible	Possible
Prototype	Discovery CT 750 HD; GE healthcare	Somatom Definition; Siemens

### Dual Energy CT with Layered Detectors

This scanner contains a single X-ray source with hybrid detector for high and low energy imaging. The top layer captures low energy data and the bottom layer captures high energy data; which are then used to reconstruct two separate image datasets.<sup>17</sup> Such scanners are under development with Philips, not yet commercially available. **Table 2** summarizes the comparison of DS-DECT and SS-DECT scanners.<sup>18</sup>

### Processing of Data and Image Reconstruction in Dual Energy Imaging

The images generated from a DECT should have the combined morphologic data and material specific information. To obtain a material-specific image, the datasets can be processed in two ways:

1. Processing after the reconstruction of low- and high energy images; which is also called ‘image domain decomposition’. This method is used in DS-DECT scanners and dual (sandwich) layer detector DECT scanners. In DS-DECT, images are generated by linear or non-linear sigmoidal blending of both (high and low energy) datasets.<sup>19</sup> In linear blending, a specific ratio of both high and low energy data are used. In sigmoidal blending, the pixels with higher attenuation are selected from the low energy datasets and the pixels with low noise are selected from high energy datasets. Material-specific images are obtained by calculating the difference in attenuation of varying materials between the low and high energy image datasets. For abdominal DS-DECT, a three-material decomposition (soft tissue, fat and iodine) process is commonly used to generate virtual non-contrast images. A color-coded overlay image (usually iodine overlay in abdominal imaging) is generated by assigning a color to the voxels containing

the material and overlapping them on monochromatic images.<sup>20,21</sup>

2. Processing before the images are reconstructed from high and low energy sinograms; also called ‘projection-space decomposition’. It is a more robust processing which is preferred because of greater flexibility in material decomposition, and minimizing beam-hardening artifact.<sup>9</sup> In this method, after data acquisition, the 80 kVp images are not routinely reconstructed. The high and low energy datasets are calibrated and aligned in projection space to generate material density image and monochromatic images (providing energy-selective information). Material density image reconstruction is based on the theory of *basis material decomposition*; which proposes that the attenuation coefficients of any material can be computed as a weighted sum of the attenuation coefficients of two basis materials as long as the k-edge of the material is not within the evaluated energy range.<sup>2,3</sup> The two base materials should have highly different atomic number. The commonly selected dual energy basis material pairs are iodine and calcium, and iodine and water. Two separate sets of material density images are generated (iodine density and water density images, for example). The lesions containing iodine (for example, enhanced organs, vessels) will show higher attenuation on iodine density images than on water density images. Monochromatic images are generated during the processing of material density images by calculating the linear attenuation coefficient ( $\mu$ ) of an object.<sup>22</sup>

Advantage of a monochromatic image generated from a DECT over a single energy image at the same kVp includes the reduction of beam hardening artifacts and provides accurate CT numbers.

### Image Display in DECT

Images generated in DECT can have two types of display:

1. Material density display (**Figs 5A and B**). In DECT, the material density display can be iodine density display or water density display.
  - In an iodine density display, the enhanced organs containing iodine appear bright whereas unenhanced areas remain dark. In abdominal imaging, iodine density display has important role in the evaluation of a hyperdense cyst on CECT. Hemorrhagic/complicated cysts and often pose an imaging dilemma whenever incidentally detected on a CECT. On CECT images, they appear hyperdense and require an additional NCCT scan to rule out enhancement. On iodine density display, they appear dark. Also, in the renal cysts, it can help reduce the problem of misdiagnosis of a cyst as a solid lesion due to 'pseudo-enhancement' which refers to artifactual increase in CT numbers within a simple cyst on a single energy CECT.<sup>23</sup>
  - The water density display is equivalent to virtual unenhanced images. Water density display can obviate the need of an additional NCCT image acquisition when a CT urographic image detects a calculus within the pelvicalyceal system; or for detection of calcification within an enhancing mass lesion.

### 2. Monoenergetic image display (**Fig. 6**).

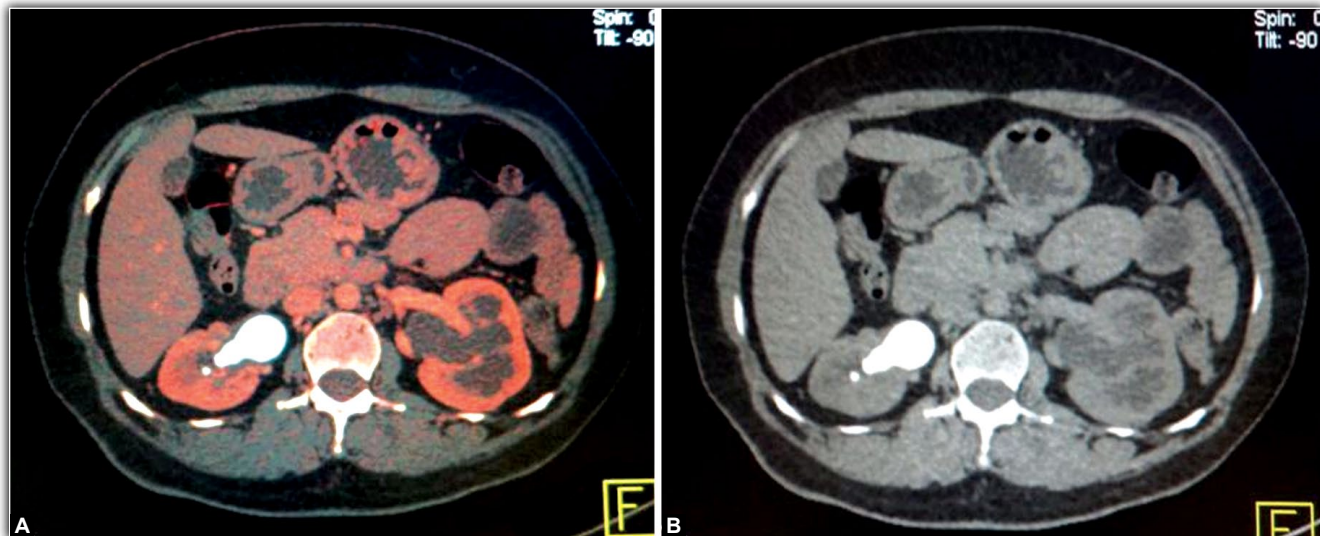
The monoenergetic or pseudomonochromatic display are energy-specific display. Images are processed at any given kVp from the dual energy datasets, which resemble images physically acquired after scanning at that given kVp. Virtual monogenetic/ pseudomonochromatic images at lower kVp show higher image contrast and make small enhancing lesions more conspicuous than routine display at 70 kVp. However, the images at lower kVp (for example 40 kV) have more noise and higher kVp images have less contrast. The optimum image contrast to noise ratio is achieved at 70 kVp.

## APPLICATIONS OF DECT

### Applications in Abdomen

#### Renal Applications

- A. **Renal calculi characterization (Figs 7A and B):** On the basis of the dominant chemical component, urinary calculi can be divided into either uric acid (UA) or nonuric acid calculi. Uric acid calculi are often associated with metabolic causes such as hyperuricemia or gout. These stones are lucent on radiograph but can be identified on CT. Nonuric acid calculi are further divided into calcium, cystine and struvite. Calcium calculi are the most common type and contains calcium oxalate monohydrate (COM), calcium oxalate dihydrate (COD), calcium phosphate and hydroxyapatite in a variable



**Figs 5A and B** Material density display. Iodine overlay map (A), created by overlapping the iodine density images over monoenergetic image, highlight the organs containing iodine (colored red). The gradient of color varies according to the degree of enhancement of the organ. The water density display (B) is equivalent to virtual unenhanced image. Note that both calcium and iodine appear dense on a routine single energy CT, but they can be differentiated on iodine map images as calcium will not be highlighted on a iodine map image (for example, the calculus in this image)

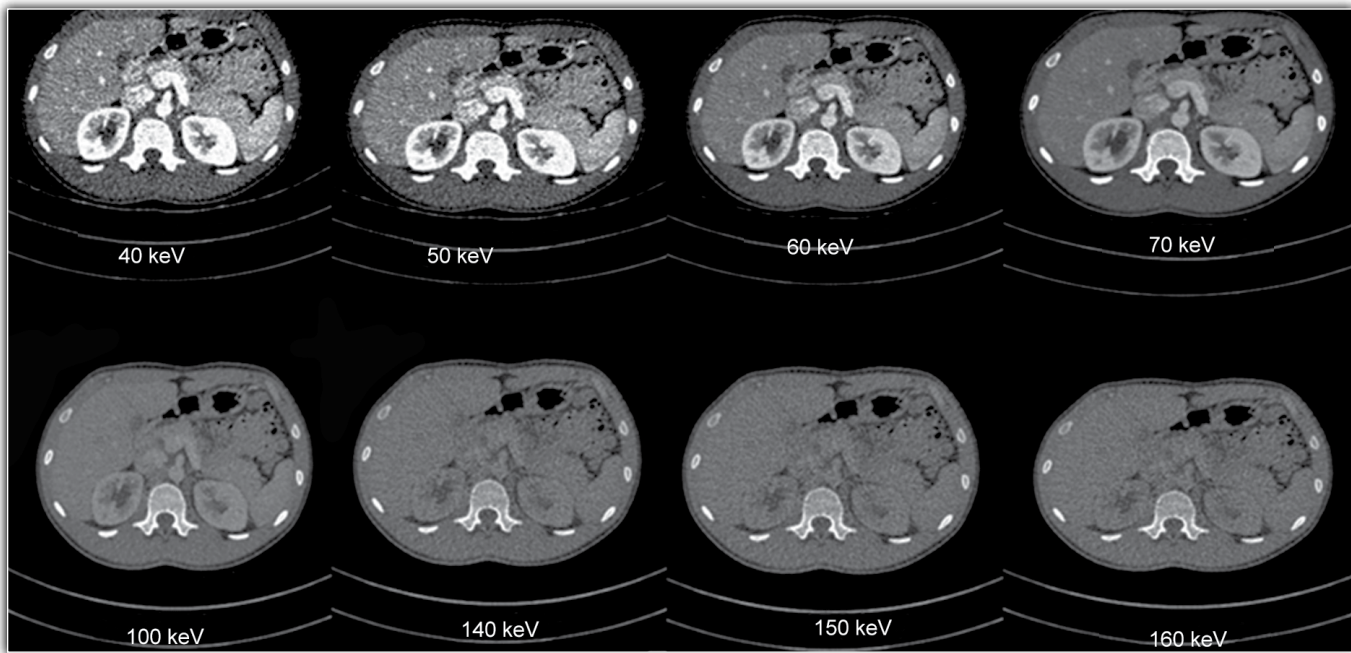


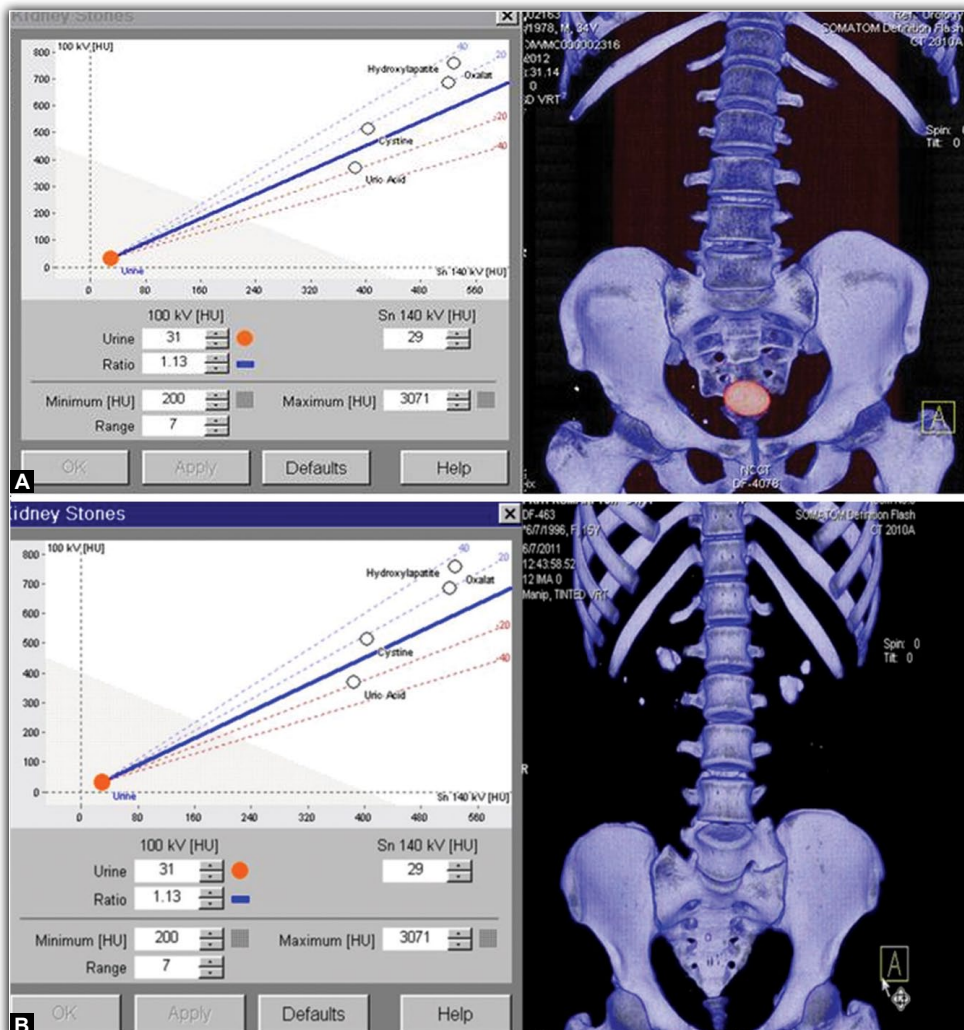
**Fig. 6** Virtual monoenergetic images generated from a DS-DECT scanner. It is evident from the images that the attenuation of iodine and the image contrast are high at lower energy images, although the images appear more noisy. As the kVp increases, the contrast difference between various tissues becomes negligible and the 160 kV image becomes identical to a noncontrast image

proportion. Struvite stones are composed of magnesium ammonium phosphate (triple phosphate) and are the major constituent of a stag horn calculus (calculus in pelvis with extension into at least two calyces). Cystine calculi are rare and associated with certain metabolic conditions such as cystinuria. A calculus containing both uric acid as well as nonuric acid component is labeled as mixed calculus. Determining the composition of calculi has direct treatment implications. Uric acid stones can be treated medically whereas cystine and COM stones are resistant to extra corporeal shock wave lithotripsy (ESWL) and percutaneous nephrolithotomy (PCNL) is preferred.<sup>24</sup>

Till now, single energy NCCT has remained the usual standard investigation for evaluating urinary tract calculi. However, single energy NCCT is unreliable for characterizing the type of calculi since calculi of different proportions of constituents can have overlapping CT attenuation values. When imaging is done on DECT scanners, the change in attenuation between high-and low-energy scans can be used to differentiate types of calculi.<sup>25</sup> UA calculi are composed of light elements whereas non-UA calculi are composed of heavy elements, hence these two groups can be differentiated on imaging. On SS-DECT, calcium and uric acid material density images are generated, uric acid calculi are depicted on uric acid material density images and calcium containing calculi on calcium density images.

DS-DECT has an added advantage of selective photon shield (tin filtration) in the 140 kVp tube for better spectral separation and more accurate composition analysis. In a DS-DECT scanner, keeping the reference dual energy ratio at 1.13, the uric acid calculi are seen to lie below the reference line and non-UA calculi above it (**Fig. 7**). Several *ex vivo* studies have demonstrated the efficacy of DECT in characterizing stones, and also the advantage of additional tin filtration.<sup>26-28</sup>

- B. **Renal cysts:** Detecting a simple cyst with water density is not an imaging challenge. Differentiating a complex/complicated renal cyst from a solid renal mass lesion is often difficult, and depends on the detection of enhancement in the lesion. Conventional single energy CT will require two acquisitions, one NCCT and another CECT. Using dual energy CT, the additional acquisition of NCCT can be avoided as it is possible to generate virtual NCCT from the datasets. On Iodine density images, the enhancing solid mass will appear bright; whereas high density cysts will be dark, since they do not have any iodine in them.<sup>29</sup> In SS-DECT, it is not possible to calculate the HU value of the lesion, which is possible with DS-DECT.<sup>30</sup> Moreover, effective beam hardening reduction in DECT helps avoid the phenomenon of 'pseudoenhancement' (vide supra).
- C. **Renal mass characterization and follow-up after ablation:** Calcification within an enhancing renal mass can be detected on a virtual NCCT image generated from



**Figs 7A and B** Renal calculi characterization by DECT. Images acquired at 100 and 140 kV in a DS-DECT scanner. A reference dual energy ratio of 1.13 is taken to differentiate uric acid from nonuric acid calculi. The uric acid calculus (A) shows a dual energy ratio less than 1.13 and are colored red (arrow). The nonuric acid calculi show a dual energy ratio above the reference line and are colored blue (B)

a dual energy dataset. After thermal ablation of solid renal masses, the imaging assessment should consist of multiphase scanning with and without contrast to detect enhancement in residual tumor tissue. While imaging on DECT scanners, one contrast enhanced acquisition can generate virtual NCCT scans, thus reducing the total dose to the patient. Iodine overlay maps help detect the enhancement in such masses.

Both DS-DECT and SS-DECT have a few technical limitations for the evaluation of renal masses. Firstly, virtual NCCT images have more image noise than real NCCT images. Second, because of the material decomposition algorithms used, calcification in renal lesions is less conspicuous on virtual unenhanced images than on real unenhanced images. Third, smaller amounts of fat in renal masses are difficult to detect on virtual NCCT images and can be measured only on conventional thin-section unenhanced CT images.

**D. CT urography:** CT urography is a routine imaging procedure in the evaluation of hematuria and multiple phase acquisitions (NCCT and delayed images) are performed for CT urography. On DECT imaging, virtual NCCT generated from the dual energy datasets can obviate the need for an additional NCCT acquisition and thus reduce the radiation dose. Takahashi and colleagues<sup>31</sup> reported that on virtual NCCT from excretory-phase CT urography performed with a DS-DECT scanner, the rate of detection of urinary tract stones was 100 percent for stones larger than 7 mm but decreased significantly (29%) for stones of 1 to 2 mm size.

Quality of the generated virtual NCCT images depends on iodine concentration within the pelvicalyceal systems, hence a highly concentrated iodinated contrast material within the PCS may lead to a 'rim artifact' at the margins and obscure small calculi. Incomplete subtraction of concentrated iodine can also be mistaken as calculi.<sup>31</sup>

## Applications in Adrenal

### Adrenal Adenoma

Adrenal adenomas are common imaging occurrences, and most of them are detected incidentally on abdominal CECT scans. Attenuation of less than 10 HU on NCCT image is virtually diagnostic of adrenal adenoma. When an incidental adrenal nodule is detected on single-energy CECT, it becomes essential to get a delayed scan or separate NCCT scan for characterization of the nodule. On a DE-CECT acquisition, virtual NCCT images generated from the dual energy datasets help eliminate the need of another NCCT scan.

The attenuation of adrenal adenoma at low and high kVp image depends on their lipid content. On several studies, there have been mixed reports related to the attenuation of adrenal adenoma on 80 and 140 kVp scans.<sup>32,33</sup>

### Hepatic Mass Characterization

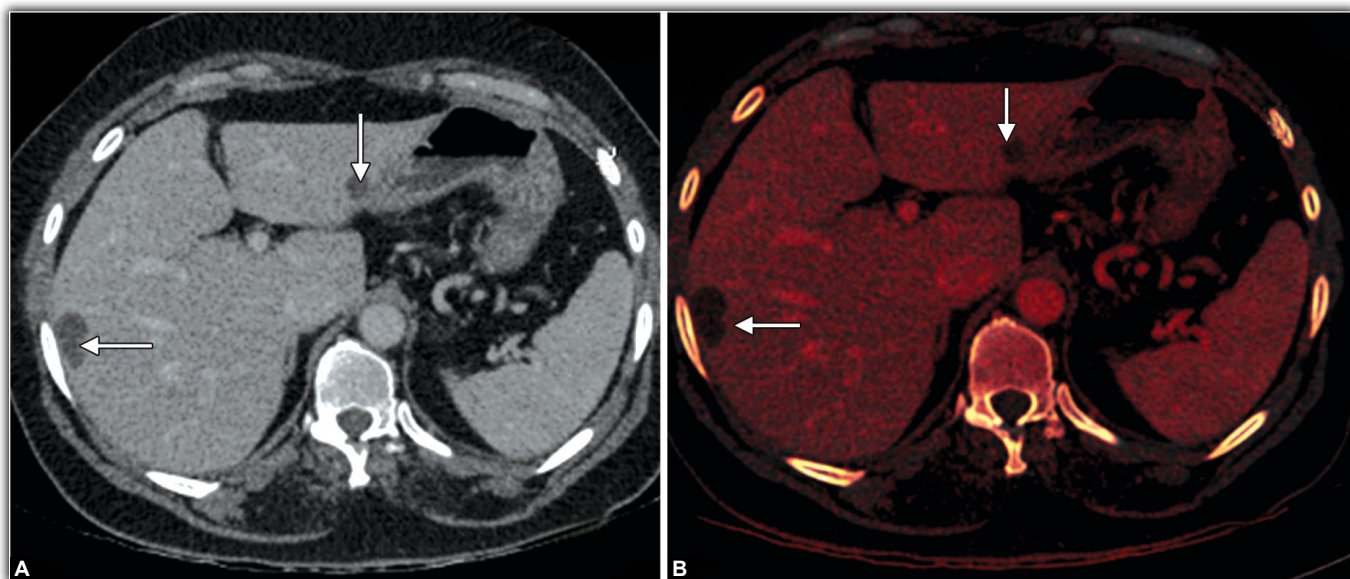
A. **Characterization of hepatic mass lesions:** Solid hepatic mass lesions are typically evaluated using a multiphase CECT. Like other organs, NCCT acquisition in liver also can be avoided by generating a virtual NCCT image from DECT acquisition in any one of the phases of multiphase CECT protocol. Secondly, hypervasculär liver lesions are most conspicuous in arterial phase of examination, however detection of a hypervasculär lesion on a delayed arterial phase becomes difficult. In such a scenario, on a DECT scan, the lesions can become more appreciable on a lower kVp image.<sup>34,35</sup> Monochromatic low kVp images and iodine density display make detection of small

hyperenhancing liver lesions easier. Non-enhancing lesions or cysts appear dark on iodine density maps (**Figs 8A and B**).

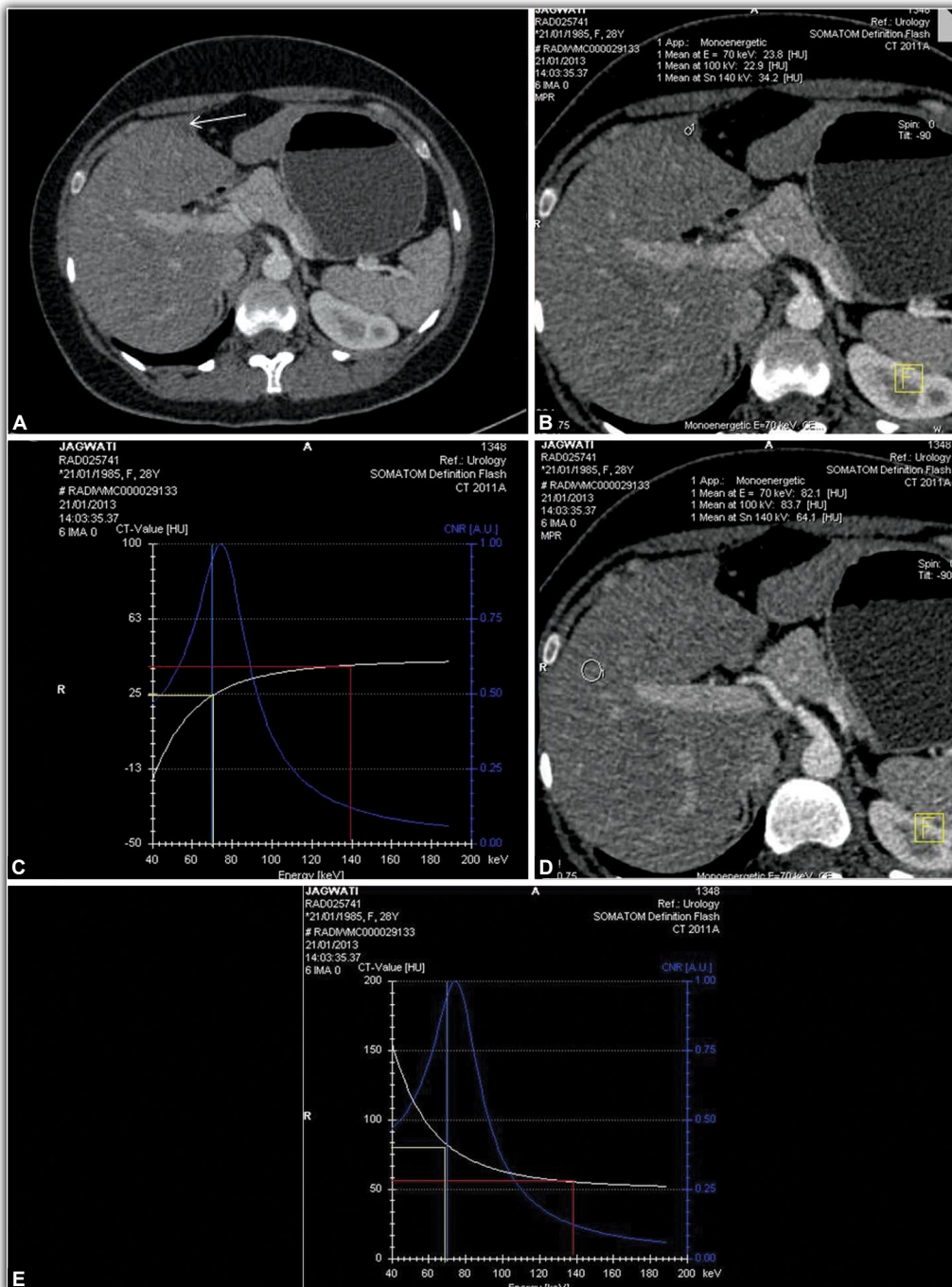
- B. **Follow-up after hepatic tumor ablation or TACE:** After tumor ablation or embolization, detection of recurrence/viable tumor depends on the demonstration of tumor mass enhancement, which in turn needs acquisition of both NCCT and a CECT scan in proper phase. With DECT, single CT acquisition can generate virtual non-contrast scans and iodine maps to detect enhancement; thereby avoiding excess radiation exposure.

A word of caution needs to be remembered while imaging hepatocellular carcinoma after chemoembolization with lipiodol. Since lipiodol contains high concentration of iodine, iodine density display images shows the lipiodol accumulation as bright spot/hyperenhancement; which should not be diagnosed as recurrent or residual tumor.<sup>36</sup>

- C. **Hepatic steatosis or iron deposition:** Hepatic focal fat deposition is often a diagnostic dilemma as it mimics solid tumor. Though there are several pointers like typical distribution and geographic nature of lesion and lack of mass effect on adjacent vasculature; sometimes the diagnosis may be difficult on a single phase single energy CT. DECT can differentiate focal fat deposition from other hepatic mass lesion in the absence of iron deposition, which is a confounding factor.<sup>11,37,38</sup> Studies have described that attenuation values that are 9 to 13 HU lower at 80 kVp than at 140 kVp are suggestive of fat infiltration<sup>37,38</sup> (**Figs 9A to E**). Iron deposition in liver



**Figs 8A and B** Simple hepatic cysts, imaging performed on a second generation DS-DECT scanner. Simulated monoenergetic image display at 70 kV generated from a dual energy dataset (A) shows hypodense focal lesions in segment III and V. Iodine overlay maps (B) show them to be dark (not taking up iodine)



**Figs 9A to E** Focal hepatic steatosis. The area of focal fat deposition is seen as a hypodensity in segment 4b adjacent to the falciform ligament (arrow in A). Monoenergetic display (B) derived from a DS-DECT scanner (Somatom Definition Flash, Siemens) with tin filtration shows the increase in attenuation in higher kV images (attenuation of 23.8 at 70 kV, shown with a yellow line and 34.2 at 140 kV, shown with a red line) (C), which is suggestive of fatty change. In comparison, normal enhancing liver parenchyma shows a decrease in attenuation (D, E) in the higher energy images (attenuation of 82.1 at 70 kV and 64.1 at 140 kV images)

parenchyma will have higher attenuation at lower energy images.<sup>11</sup>

### Application in Pancreas

Pancreatic neoplasms are usually hypovascular and their detection is based on the attenuation difference between the normally enhancing pancreatic parenchyma and hypoenhancing mass lesion. Pancreatic parenchymal enhancement is best assessed in the pancreatic phase, 40 to 70 sec after injection of contrast material. However, significant percentage of pancreatic carcinomas are difficult to detect even on pancreatic phase images.<sup>39</sup> With DECT, the normally enhancing pancreatic parenchyma shows higher attenuation on monochromatic lower energy display image and the iodine density display. It has been seen that the attenuation difference between the lesion and normal pancreatic parenchyma (hence the lesion detection) increases with 80 kVp image than a single energy routine 120 kVp scan.<sup>40</sup>

Another potential application of DECT in pancreatic imaging is the accurate identification of pancreatic necrosis; although the clinical importance is not yet established.<sup>11</sup>

### Pulmonary Applications

**A. Pulmonary thromboembolism:** Pulmonary thromboembolism (PTE) imaging has undergone significant change in the past few years. Pulmonary CT angiography (CTA) has been accepted as the imaging modality of choice in case of suspected high-risk population. Pulmonary CTA can detect intraluminal thrombus in segmental arteries and smaller vessels also, but smaller clots/partial occlusion in subsegmental arteries can be missed on CTA. When imaging is done on a DECT scanner, smaller clots can be detected on an iodine overlay map visible as a perfusion defect. Compared to CTA and scintigraphy, dual-energy CT has a high sensitivity and specificity for perfusion mapping for the assessment of pulmonary embolism.<sup>41,42</sup> The perfusion defects in cases of pulmonary embolism are usually peripheral and wedge-shaped; although they can be absent in cases of very small non-occluding thrombus in smaller vessels.

For the generation of a proper iodine perfusion map of the lungs, the maximum and minimum value for material decomposition are usually kept at -600 and -960 HU. It excludes all the enhancing mediastinal structure and all central vessels in the lung parenchyma from the iodine perfusion map. Hence the relatively less perfused area in case of thromboembolism can be easily visualized as perfusion defect (Fig. 10). For obtaining proper parenchymal enhancement, iodinated contrast agent should be injected at a proper rate (4-4.5 mL/sec), followed by 40 ml saline chase to reduce artifacts resulting from dense contrast in SVC/ brachiocephalic

vein. Imaging should be done in both pulmonary and aortic phase. A threshold value of 20 HU mean iodine attenuation can be used to differentiate areas of lung parenchyma with negligible perfusion from those with demonstrable flow.

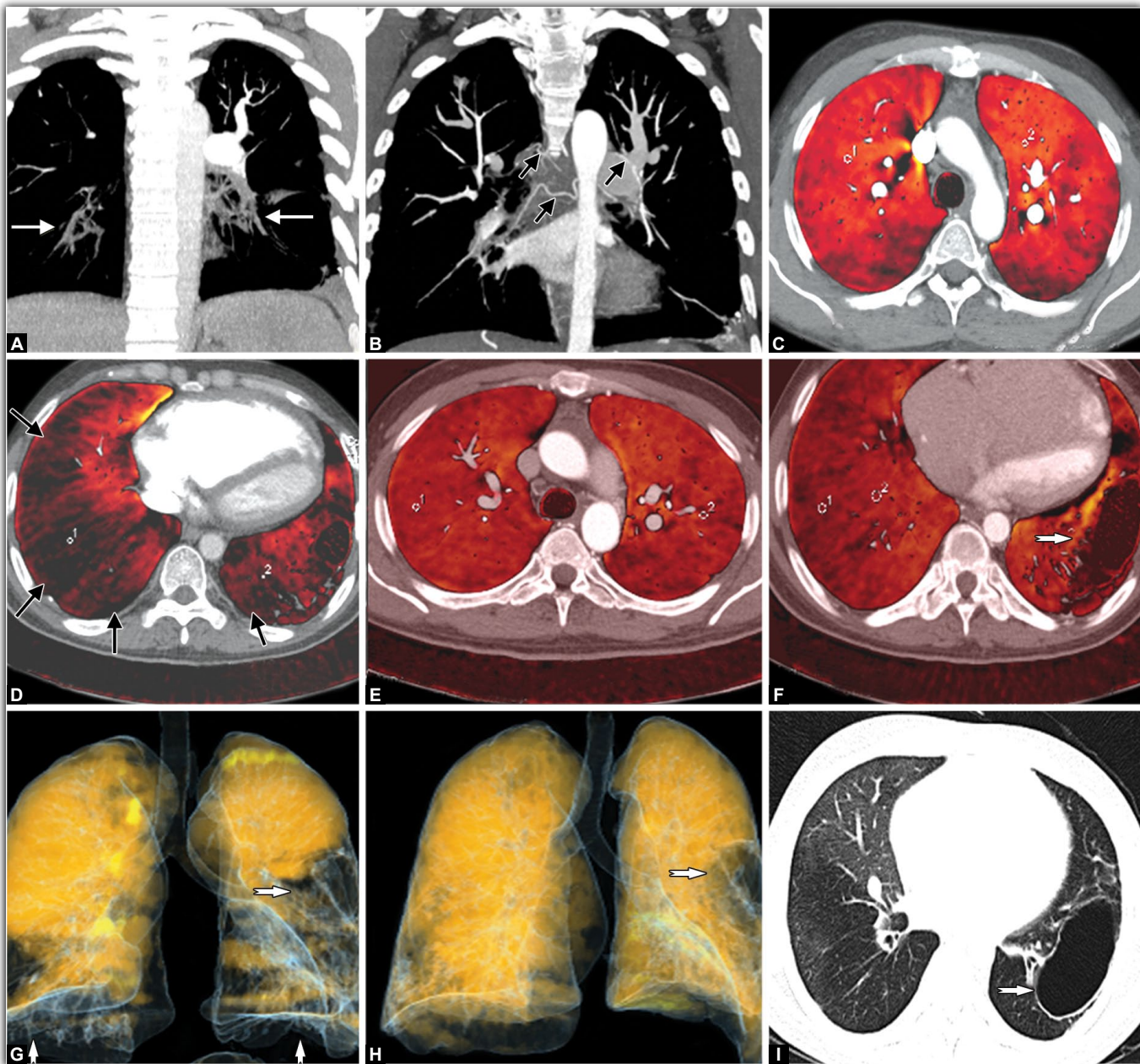
Perfusion defects can also be seen from non-PTE causes; for example in cases of aberrant pulmonary vascular supply,<sup>43</sup> or artefactual perfusion defects as in the lingual or right middle lobe (from cardiac pulsations), bilateral lower lobes near the diaphragm (from respiratory motion), in bilateral upper lobes (from streak artifacts in SVC or subclavian artery). Perfusion defects are also observed in parenchymal abnormalities such as consolidation, atelectasis or emphysema (Figs 10A to I).<sup>44,45</sup>

- B. **Xenon perfusion CT:** Xenon is a radio-opaque gas with atomic number 54 and has photoelectric absorption characteristics similar to iodine.<sup>46</sup> During xenon ventilation CT, the patient usually inhales 30 percent xenon through a xenon gas inhalation system (Zetron V; Anzai Medical, Tokyo, Japan). Overlay maps are generated similar to iodine perfusion CT. DE xenon ventilation CT can be used to generate a ventilation map with areas of bronchial obstruction or atresia showing reduced ventilation.<sup>47,48</sup>
- C. **Pulmonary nodule evaluation:** The degree of contrast enhancement on CECT is an important factor in differentiating a benign pulmonary nodule from a malignant one. DECT can generate virtual NCCT images and thereby quantify the enhancement. The differentiation of calcification from contrast enhancement is also possible on a single DE- CECT acquisition, thereby saving the additional radiation exposure of NCCT.

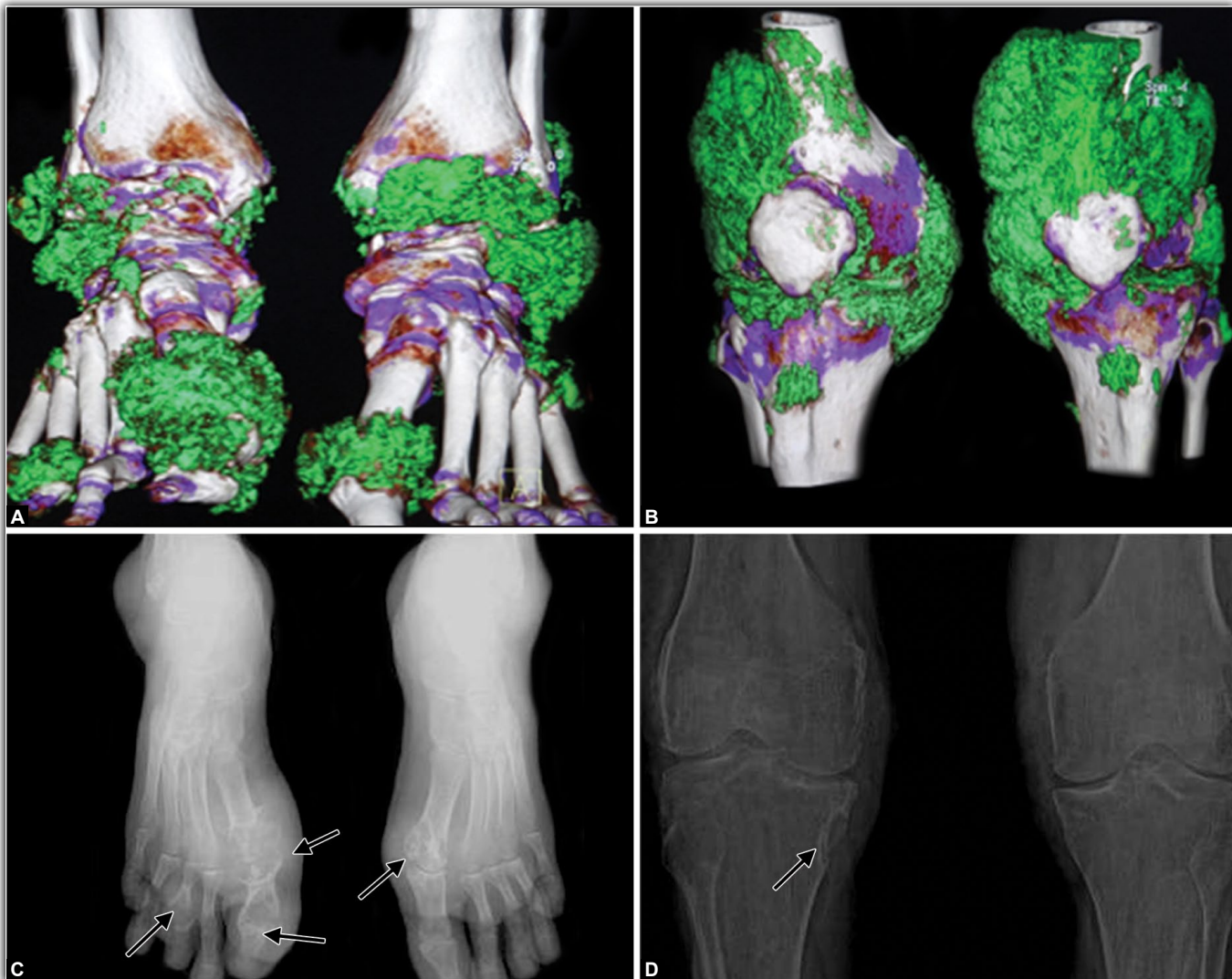
### Musculoskeletal Applications

- A. **Application in gout:** Gout is a disease resulting from intra-articular or soft tissue uric acid crystal deposition leading to severe deforming arthropathy and gouty tophi formation. The causes may be multifactorial. Most often the diagnosis can be made on clinical and biochemical basis, however, the definitive diagnosis of gout requires microscopic analysis of fluid aspirated from the joint with the finding of negatively birefringent monosodium urate (MSU) crystals.<sup>49</sup> But few studies have described a rate of negative aspiration as high as 25 percent in acute attacks.<sup>50</sup>

Plain radiography can show the arthropathy and corticated bone erosions in case of gouty soft tissue tophi. On DECT, the dual energy ratio (vide supra) of uric acid varies significantly from that of calcium, hence they can be easily differentiated. DS-DECT scans can generate material specific images and keeping the reference Dual energy ratio at 1.36, the uric acid crystals lie below the



**Figs 10A to I** Dual energy CT perfusion in chronic pulmonary thromboembolism. Coronal reformatted CTA image acquired at pulmonary phase (A) shows non-enhancement and attenuation in caliber of the lower lobe pulmonary arteries (arrows). Aortic phase image reveals hypertrophic bronchial arteries (small arrows in B). Iodine overlay maps generated from dual energy CTA during pulmonary phase (C and D) reveal patchy areas of perfusion defect in the basal segments of both lower lobes (arrows in d). Iodine maps (E and F) generated from aortic phase images shows near complete perfusion (via bronchial collaterals) in the corresponding area. Volume rendered images generated from iodine distribution maps in pulmonary phase (G) also shows the areas of perfusion defect (block arrow); whereas aortic phase image (H) shows near complete perfusion except a small area of non-perfusion (notched arrow) secondary to a large bulla. Lung window axial image (I) confirms the presence of the bulla (notched arrow)



**Figs 11A to D** DECT in gout imaging. Scanning was performed at 80 and 140 kV in a patient with chronic gouty arthritis. Keeping a reference dual energy line at 1.36, MSU crystals are color coded green. Color coded volume rendered images of the ankle (A) and knee (B) reveal extensive MSU crystal deposition around the joints. Plain radiographs of the feet and knee reveals periarticular soft tissue swellings and corticated erosions (arrows in C and D)

line and are differently color-coded (green), whereas the calcium deposits lie above the line (**Figs 11A to D**). The utility of DECT in gout diagnosis is two-fold. First, it can diagnose gout in an easy, non-invasive and reproducible manner. Secondly, using automated volume software, the tophi volume can be quantitatively measured with less inter-observer variability.<sup>51,52</sup>

- B. **Metal artifact reduction:** Imaging of patients with metallic prosthesis remains a challenge. As the X-ray beam passes through metal prosthesis, the lower energy photons are absorbed and the character of the X-ray spectrum changes (it becomes 'harder', i.e. having higher energy photons only). This gives rise to the beam hardening artifacts around metallic prostheses which

hamper the visualization of periprosthetic abnormalities. The usual modifications to reduce metal artifact in a single energy scanner include:

- Increasing the kVp,
- Increasing the mAs,
- Reducing slice collimation,
- Using a softer kernel for reconstruction and
- Thicker slice reconstruction. Using DECT, monoenergetic reconstruction at a higher kVp has been shown in several studies to be more effective than routine single energy CT images at 120 kVp.<sup>53,54</sup>

- C. **Other musculoskeletal applications:** Although evaluation of gout has remained the most widely used musculoskeletal application of DECT, there are several

other applications, for example, detection of bone marrow edema<sup>55</sup> and evaluation of ligaments and tendons.<sup>56-59</sup>

Bone marrow edema is ideally best evaluated by MRI. Pache et al<sup>55</sup> described high sensitivity and specificity of DECT imaging in the detection of post-traumatic bone marrow edema. Using a three material decomposition (water, fat and calcium), the virtual non-calcium subtracted images can be generated to detect marrow edema.

Tendons and ligaments are made up of collagen fibrils, which have a specific dual energy ratio. In DECT, for material specific image generation a three material decomposition algorithm is used (collagen, fat and soft tissue). Several studies<sup>56-59</sup> have showed conflicting efficacy of DECT in the evaluation of tendons and ligaments. Thicker ligaments like anterior and posterior cruciate ligaments and patellar ligament can be adequately visualized, however visualization of thinner anatomical structures may not be appropriate.

### Applications in Head and Neck

Like other parts of the body, DECT imaging in head and neck also has the advantage of generating a virtual NCCT image from the dual energy dataset, without the need for an additional non-contrast scanning in order to quantify enhancement in a mass lesion. Iodine overlay maps can increase lesion conspicuity of head and neck masses. Recent study by Kuno et al<sup>60</sup> has also demonstrated improved diagnostic performance and inter-observer reproducibility by DECT imaging in laryngeal cartilage invasion in head and neck squamous cell carcinoma.

### Vascular Applications

Dual energy CT angiography has been most widely used in aortic imaging. The advantages of DECT in aortic stent-graft imaging are multiple. First, virtual monoenergetic high kVp images in DECT are more effective in metal artifact reduction.<sup>54</sup> Secondly, the virtual monoenergetic low kVp images are more sensitive in detection of iodine (hence small endoleaks which are otherwise difficult to detect), though have a high image noise. An optimum monoenergetic image can be generated to balance the iodine density and the image noise. Third, the iodine overlay map can detect smaller endoleaks (differentiate between blood and contrast).<sup>61</sup> Fourth, DECT acquisition can help generate a virtual NCCT image which can detect intramural hematoma and has comparable image noise as that of a true NCCT image.<sup>62</sup> Fifth, the DE subtracted angiographic images are easier to generate and provide more complete bone removal. Finally, In endoleak detection, single delayed DECT scanning followed by reconstruction of virtual NCCT and mono energetic low-kV images has very high sensitivity, specificity and positive predictive value (96-100%) compared with a conventional multiphase single energy CTA acquisition, thereby significantly reducing the patient dose (40-64%).<sup>63,64</sup>

In peripheral or neck angiography, the drawbacks of threshold based bone subtraction is that in cases of arteries lying close to bone, a part of the artery can be subtracted and may mimic stenosis or occlusion. Since the bone subtraction in DECT is based on material differentiation, it takes less time and yields more complete bone removal (**Fig. 12**), which can reduce such artifacts.<sup>65</sup>

Unlike single energy CTA with threshold based bone subtraction, DECT CTA can remove calcified plaques also, with better visualization of vascular lumen. Compared to threshold based bone removal, DECT bone subtraction are easier, quicker and more accurate in detection of vessel stenosis.<sup>66</sup>

### Cardiac Applications

Coronary CT angiography in a multidetector row scanner has become an established imaging tool in the detection of significant coronary artery disease (CAD) in low to intermediate risk population.<sup>67,68</sup> However, the mere detection of an artery stenosis does not predict the hemodynamic significance of it, which can be predicted by myocardial perfusion imaging or wall motion abnormalities. Till now, myocardial perfusion studies have been performed using nuclear medicine studies (SPECT) and MRI. However, SPECT has poor spatial resolution and is not useful for coronary artery assessment. MRI can detect myocardial perfusion and cine-MRI can



**Fig. 12** Volume rendered CTA image of the head and neck in a 10-year-old male with proliferative hemangioma (arrow) on the right side of face. The bone removal in dual energy CTA depends on material differentiation and leads to complete and quick bone subtraction compared to threshold based bone subtraction

detect regional wall motion abnormality; but it is time-consuming and not useful for morphologic assessment of coronary artery disease.<sup>69,70</sup> With the use of DECT technology, material density (iodine) maps can be generated for the myocardium, reflecting the myocardial perfusion. Although termed 'perfusion,' the map usually reflects the myocardial blood pool and is a static acquisition. A typical DECT cardiac perfusion study consists of the following phases- an initial calcium scoring followed by arterial phase scan, injection of IV adenosine and acquisition of stress images 3 minutes after IV adenosine (140 µg/min/kg) infusion, rest scanning 2 minutes after the stress scan when the heart rate returns to the baseline level. Finally, a delayed scan (5-10 min) is acquired. Monoenergetic low kV, high kV and iodine overlay maps are generated.<sup>71</sup> Normally perfused myocardium show uniform iodine distribution (**Figs 13A and B**). Myocardial infarcts are visualized as perfusion defects both at rest and under stress, whereas reversible ischemia shows perfusion defect only in stress images. Non-viable myocardium will show hyperenhancement on delayed scans.<sup>72</sup> DECT thus can combine the benefits of superior resolution morphologic imaging in CAD coupled with detection of its hemodynamic significance in the form of ischemia/infarction, which is unique to this modality.

Material differentiation based on dual energy ratio has been tried in the characterization of plaques. Although differentiating a calcified from a non-calcified plaque is possible, but the differentiation of various types of non-calcified plaques have not been successful.<sup>73</sup>

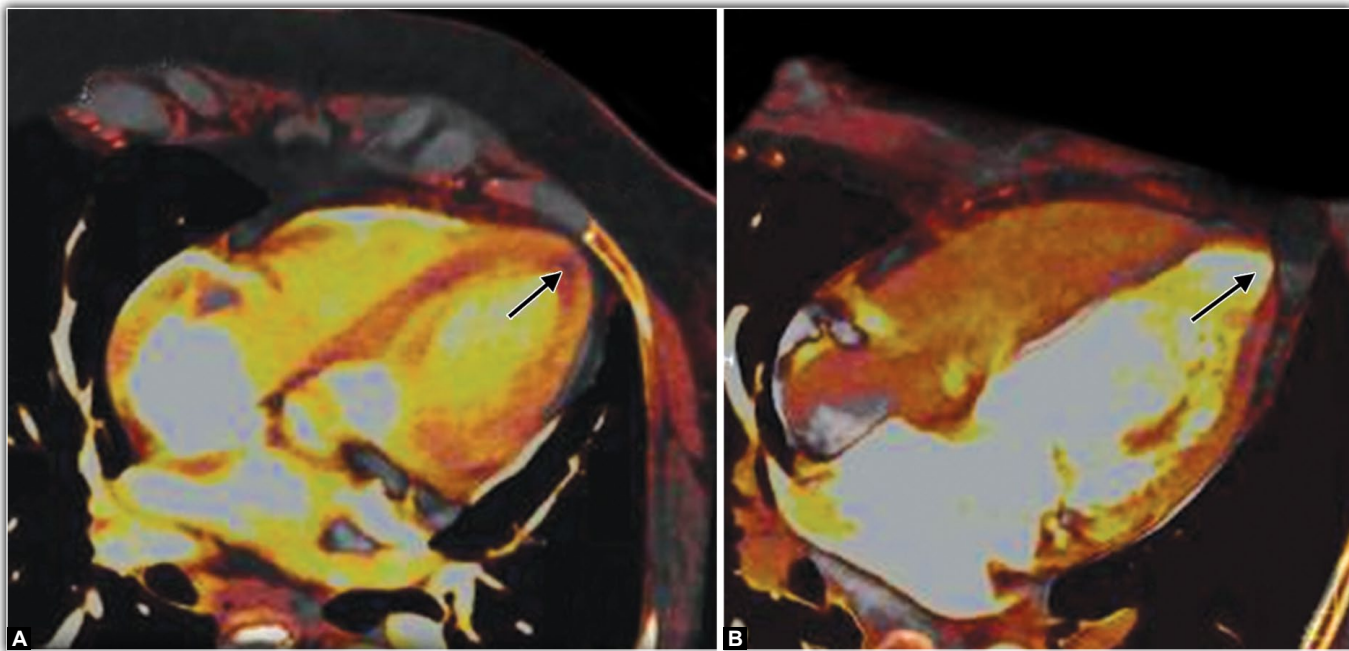
### Applications in Neuro-imaging

As discussed for CTA elsewhere in the body, dual energy CTA of intracranial vessels also has the similar advantage of easy and quick bone removal, especially with complex bony anatomy at the base of skull.<sup>74</sup> Other advantages of DECT scanning include avoidance of additional non-contrast scanning in certain circumstances. For example, In a patient with suspected subarachnoid hemorrhage, a preliminary NCCT scan can be avoided and direct dual energy CTA can be performed to look for the etiology. The virtual NCCT images generated from the dual energy dataset helps detect hemorrhage and can save crucial time.<sup>75</sup>

Studies have described dual energy CTA to be the ideal tool for evaluating an acute intracranial hemorrhage. Apart from the ease of assessment of vascular cause of hemorrhage (vide supra); iodine overlay maps can be useful in differentiating tumor bleed from a simple hematoma.<sup>76</sup> Hemorrhage within a tumor will show hyperdensity on NCCT images and detection of any enhancing mass lesion in the background of hemorrhage can be an imaging challenge. Iodine overlay maps can detect the enhancing tumor tissue in the background of hematoma with greater accuracy; and also saves the patient from an additional radiation of NCCT scan.

### DOSE CONSIDERATIONS

Although DECT scanning involves imaging with two different X-ray beams, the dose is not doubled in comparison to the single energy scan. This is because the mAs are divided in the



**Figs 13A and B** Stress myocardial perfusion imaging using DECT. A 52-year-old lady with effort intolerance. Iodine overlay maps at rest (A) shows perfusion defect (arrow) in the territory of the left anterior descending coronary artery (LAD) which is exaggerated on adenosine stress images (B); suggestive of LAD territory ischemia

two sources; the higher energy tube operates at a lower mAs and the lower energy tube utilizes a relatively higher mAs. Till date, several experimental studies have been performed regarding dose comparisons of DECT scanning and single energy scanning. Most of the experiments are based on DS-DECT scanners. Data are sparse regarding dose issues in SS-DECT. There has been various studies comparing dose of the single and dual energy scanners, but very few of them are performed with normalization of the contrast to noise ratio (CNR) or image quality.<sup>77</sup>

Schenzle et al<sup>77</sup> performed a study on anthropomorphic phantom equipped with TLDs, with scanning performed at 140 and 80 kVp, 14 × 1.2 collimation in a first generation DS-DECT scanner and in a second generation DS-DECT scanner at 140 and 100 kVp settings with selective photon shielding at 128 × 0.6 mm collimation. Dose comparison was done with a single energy scan at 120 kV and 64 × 0.6 mm collimation at an equivalent dose index of 5.4 mGy x cm. The respective doses were 2.61 mSv (first generation DS-DECT in dual energy mode), 2.69 mSv (second generation DS-DECT in dual energy mode), 2.70 mSv (second generation DS-DECT in single energy mode). The image noise were also similar in all these three imaging techniques. Hence, there was no significant dose difference between the imaging techniques.

In coronary CTA, the dose received by DECT imaging has been assessed by Kerl et al,<sup>78</sup> who compared the dose levels between DECT, first generation DS-DECT in single energy mode, and single energy single source 16 slice MDCT. The investigators reported a lower dose, higher CNR and good diagnostic image quality in DECT than single source MDCT. The increase in CNR was attributed to the low- kVp acquisition in DECT scanning by the investigators. Several other studies<sup>78,79</sup> regarding CT pulmonary angiography or CTA have shown that there is no significant increase in dose while scanning by DS-DECT scanning, compared to a single energy scanning. The added benefit of DECT scanning lies in the generation of virtual unenhanced scans, which can obviate the need of another NCCT scanning and reduce radiation dose. In renal imaging, the replacement of NCCT by virtual NCCT can result in a dose reduction of up to 35 percent in first

generation DECT and up to 50 percent in second generation DECT.<sup>80</sup> Addition of tin filter in second generation DS-DECT reduces the dose by eliminating lower energy X-ray photons from the higher energy spectrum.

Future trends in DECT imaging towards using a sandwich detector or an energy specific, photon counting detector can reduce the radiation dose further, retaining the benefits of material characterization on DECT.

### *Limitation*

In spite of having significant advantages over single energy CT in several applications, there are a few limitations of DECT (**Box 1**). First, the FOV of the smaller detector is significantly less in DS-DECT (33 cm in second generation DS-DECT) which leads to incomplete area coverage in obese patients. Second, the images generated from the lower energy tube have inherently high noise. Finally the large number of datasets generated leads to a problem in storage and archival. Pitfalls in organ-specific imaging have been discussed in their respective sections.

### **CONCLUSION**

To conclude, dual energy CT imaging adds another new dimension to conventional CT. the material- specific information gained by DECT scanning can be translated either to functional analysis of organs (for example, myocardial perfusion analysis), improvement in diagnostic confidence (non-invasive confirmation of clinical diagnosis in gout), aid in management decision- making (for example in renal calculi) or to easy image post-processing and avoidance of unnecessary scanning.

### **ACKNOWLEDGMENTS**

The authors sincerely acknowledge the contribution of Dr Gurpreet S Gulati for figure no 13 and Dr Ashu Seith Bhalla for figure no 10. The authors also sincerely acknowledge the contribution of Dr Sudeep Acharya and Dr Zohra Ahmad for figure no 7 and 11, respectively, from their MD thesis work at the Department of Radiodiagnosis, AIIMS.

**Box 1** Advantages and drawbacks of DECT

#### **Advantages of DECT**

Material specific image can be generated. Characterization of renal calculi composition made possible

Obviates the need for additional acquisition of NCCT images in many clinical indications, thereby reducing dose

Direct CT angiography- saves tedious post-processing and manual bone removal

Wider applications based on material characterization

Increased temporal resolution (helpful in cardiac CT)

#### **Disadvantages of DECT**

Increased radiation dose ( which can be reduced using SPS)

Storage needs large capacity

Lower kVp image has inherent increased noise. Scanning may not be suitable in obese patients

Second detector in DS-DECT has smaller FOV, hence may not be beneficial in obese patients

## REFERENCES

1. Computerized transverse axial scanning (tomography): Part 1. Description of system. GN Hounsfield, *BJR*. 1973;46:1016-22.
2. Alvarez RE, Macovski A. Energy-selective reconstructions in X-ray computerised tomography. *Phys Med Biol*. 1976;21:733-44.
3. Kalender WA, Perman WH, Vetter JR, Klotz E. Evaluation of a prototype dual-energy computed tomographic apparatus. I. Phantom studies. *Med Phys*. 1986;13:334-9.
4. Rutherford RA, Pullan BR, Isherwood I. Measurement of effective atomic number and electron density using an EMI scanner. *Neuroradiology*. 1976;11(1):15-21.
5. Rutherford RA, Pullan BR, Isherwood I. X-ray energies for effective atomic number determination. *Neuroradiology*. 1976; 11(1):23-8.
6. Millner MR, McDavid WD, Waggener RG, Dennis MJ, Payne WH, Sank VJ. Extraction of information from CT scans at different energies. *Med Phys*. 1979;6(1):70-1.
7. Chiro GD, Brooks RA, Kessler RM, et al. Tissue signatures with dual-energy computed tomography. *Radiology*. 1979;131(2): 521-3.
8. Flohr TG, McCollough CH, Bruder H, et al. First performance evaluation of a dual-source CT (DSCT) system. *Eur Radiol*. 2006;16(2):256-68.
9. Zou YU, Silver MD. Analysis of fast kV-switching in dual energy CT using a pre-reconstruction decomposition technique. *Proc SPIE 2008*; 6913: Bellingham, Wash: International Society for Optical Engineering, 2008.
10. Curry TS III, Dowdye JE, Murry RC. Christensen's physics of diagnostic radiology, 4th edn. Philadelphia, Pa: Lea & Febiger. 1990. pp.61-9.
11. Coursey CA, Nelson RC, Boll DT, et al. Dual-energy multidetector CT: how does it work, what can it tell us, and when can we use it in abdominopelvic imaging? *Radio Graphics*. 2010;30(4):1037-55.
12. Andrew N Primak, Juan Carlos Ramirez Giraldo, Christian D. Eusemann, Bernhard Schmidt, Birgit Kantor, Joel G. Fletcher, Cynthia H. McCollough. Dual-Source Dual-Energy CT With Additional Tin Filtration: Dose and Image Quality Evaluation in Phantoms and *In Vivo*. *AJR*. 2010;195:1164-74.
13. Kelcz F, Joseph PM, Hilal SK. Noise considerations in dual energy CT scanning. *Med Phys*. 1979;6:418-25.
14. Rutt B, Fenster A. Split-filter computed tomography: a simple technique for dual energy scanning. *J Comput Assist Tomogr*. 1980;4:501-9.
15. Chandra N, Langan DA. Gemstone detector: dual energy imaging via fast kVp switching. In: Johnson TRC, Fink C, Schönberg SO, Reiser MF, (Eds). Dual energy CT in clinical practice. Berlin, Germany: Springer-Verlag. 2011. pp.35-41.
16. Li B, Yadava G, Hsieh J, Chandra N, Kulpins MS. Head and body CTDI<sub>w</sub> of dual-energy X-ray CT with fast-kVp switching. In: Samei E, Pelc NJ, (Eds). Proceedings of SPIE: medical imaging. Bellingham, Wash: International Society for Optical Engineering, 2010. Vol 7622.
17. Vlassenbroek A. Dual layer CT. In: Johnson TRC, Fink C, Schönberg SO, Reiser MF, (Eds). Dual energy CT in clinical practice. Berlin, Germany: Springer- Verlag. 2011;21-34.
18. Kaza RK, Platt JF, Cohan RH, Caoili EM, Al-Hawary MM, Wasnik A. Dual energy CT with single and dual source scanners: current applications in evaluating the genitourinary tract. *Radiographics*. 2012;32:353-69.
19. Fletcher JG, Takahashi N, Hartman R, et al. Dual-energy and dual-source CT: is there a role in the abdomen and pelvis? *Radiol Clin North Am*. 2009;47 (1):41-57.
20. Johnson TR, Krauss B, Sedlmair M, et al. Material differentiation by dual energy CT: initial experience. *Eur Radiol*. 2007;17(6):1510-7.
21. Graser A, Johnson TR, Chandarana H, Macari M. Dual energy CT: preliminary observations and potential clinical applications in the abdomen. *Eur Radiol*. 2009;19(1):13-23.
22. Lehmann LA, Alvarez RE, Macovski A, et al. Generalized image combinations in dual kVp digital radiography. *Med Phys*. 1981;8(5):659-67.
23. Muller J, Vrtiska T, Schmidt B, et al. The impact of dual energy CT on pseudoenhancement of kidney lesions. In: Samei E, Pelc NJ, (Eds). Proceedings of SPIE: medical imaging 2010. Vol 7622. Bellingham, Wash: International Society for Optical Engineering, 2010.
24. Kambadakone AR, Eisner BH, Catalano OA, Sahani DV. New and evolving concepts in the imaging and management of urolithiasis: urologists' perspective. *Radio Graphics*. 2010; 30(3):603-23.
25. Eliahou R, Hidas G, Duvdevani M, Sosna J. Determination of renal stone composition with dual-energy computed tomography: an emerging application. *Semin Ultrasound CT MR*. 2010;31(4):315-20.
26. Joshi M, Langan DA, Sahani DS, et al. Effective atomic number accuracy for kidney stone characterization using spectral CT. In: Samei E, Pelc NJ, (Eds). Proceedings of SPIE: medical imaging 2010. Vol 7622. Bellingham, Wash: International Society for Optical Engineering, 2010.
27. Hidas G, Eliahou R, Duvdevani M, et al. Determination of renal stone composition with dual-energy CT: *in vivo* analysis and comparison with X-ray diffraction. *Radiology*. 2010;257(2): 394-401.
28. Vrtiska TJ, Takahashi N, Fletcher JG, Hartman RP, Yu L, Kawashima A. Genitourinary applications of dual-energy CT. *AJR*. 2010;194(6):1434-42.
29. Kaza RK, Caoili EM, Cohan RH, Platt JF. Distinguishing enhancing from nonenhancing renal lesions with fast kilovoltage-switching dual-energy CT. *AJR*. 2011;197(6):1375-81.
30. Mendonca PRS, Bhotika R, Maddah M, et al. Multi-material decomposition of spectral CT images. In: Samei E, Pelc NJ, (Eds). Proceedings of SPIE: medical imaging 2010. Vol 7622. Bellingham, Wash: International Society for Optical Engineering, 2010.
31. Takahashi N, Vrtiska TJ, Kawashima A, et al. Detectability of urinary stones on virtual nonenhanced images generated at pyelographic-phase dual-energy CT. *Radiology*. 2010;256(1): 184-90.
32. Boland G, Jagtiani M, Kambadakone Ramesh A, Hahn P, Sahani D, Kalra M. Characterization of lipid poor adrenal adenomas: accuracy of dual energy CT (abstr). In: Radiological Society of North America scientific assembly and annual meeting program. Oak Brook, Ill: Radiological Society of North America. 2008. pp.390.
33. Gupta RT, Ho LM, Marin D, Boll DT, Barnhart HX, Nelson RC. Dual energy CT for characterization of adrenal nodules: initial experience. *AJR*. 2010;194(6):1479-83.
34. Marin D, Nelson RC, Samei E, et al. Hypervascular liver tumors: low tube voltage, high tube current multidetector CT during late

- hepatic arterial phase for detection—initial clinical experience. *Radiology*. 2009;251(3):771-9.
35. Schindera ST, Nelson RC, Mukundan S Jr, et al. Hypervascular liver tumors: low tube voltage, high tube current multi-detector row CT for enhanced detection—phantom study. *Radiology*. 2008;246(1):125-32.
  36. Silva AC, Morse BG, Hara AK, Paden RG, Hongo N, Pavlicek W. Dual energy (Spectral) CT: applications in abdominal imaging. *Radiographics*. 2011;31:1031-46.
  37. Raptopoulos V, Karella A, Bernstein J, Reale FR, Constantinou C, Zawacki JK. Value of dual-energy CT in differentiating focal fatty infiltration of the liver from low-density masses. *AJR*. 1991;157(4):721-5.
  38. Mendler MH, Bouillet P, Le Sidaner A, et al. Dual-energy CT in the diagnosis and quantification of fatty liver: limited clinical value in comparison to ultrasound scan and single-energy CT—with special reference to iron overload. *J Hepatol*. 1998;28(5):785-94.
  39. Prokesch RW, Chow LC, Beaulieu CF, Bammer R, Jeffrey RB Jr. Isoattenuating pancreatic adenocarcinoma at multi-detector row CT: secondary signs. *Radiology*. 2002;224(3):764-8.
  40. Spieler B, Macari M, Godoy M, et al. Dual source dual energy MDCT: comparison of 80 kVp and weighted average kVp data on pancreatic lesion conspicuity (abstr). In: Radiological Society of North America scientific assembly and annual meeting program. Oak Brook, Ill: Radiological Society of North America, 2008.p.522.
  41. Fink C, Johnson TR, Michaely HJ, et al. Dual-energy CT angiography of the lung in patients with suspected pulmonary embolism: initial results. *Rofo*. 2008;180(10):879-83.
  42. Thieme SF, Becker CR, Hacker M, Nikolaou K, Reiser MF, Johnson TR. Dual energy CT for the assessment of lung perfusion: correlation to scintigraphy. *Eur J Radiol*. 2008;68(3):369-74.
  43. Boroto K, Remy-Jardin M, Flohr T, et al. Thoracic applications of dual-source CT technology. *Eur J Radiol*. 2008;68(3):375-84.
  44. Pontana F, Faivre JB, Remy-Jardin M, et al. Lung perfusion with dual-energy multidetector-row CT (MDCT): feasibility for the evaluation of acute pulmonary embolism in 117 consecutive patients. *Acad Radiol*. 2008;15(12):1494-504.
  45. Pansini V, Remy-Jardin M, Faivre JB, et al. Assessment of lobar perfusion in smokers according to the presence and severity of emphysema: preliminary experience with dual-energy CT angiography. *Eur Radiol*. 2009;19(12):2834-43.
  46. Meyer JS, Hayman LA, Yamamoto M, Sakai F, Nakajima S. Local cerebral blood flow measured by CT after stable xenon inhalation. *AJR*. 1980;135(2):239-51.
  47. Goo HW, Chae EJ, Seo JB, Hong SJ. Xenon ventilation CT using a dual-source dual-energy technique: dynamic ventilation abnormality in a child with bronchial atresia. *Pediatr Radiol*. 2008;38(10): 1113-6.
  48. Chae EJ, Seo JB, Goo HW, et al. Xenon ventilation CT with a dual-energy technique of dual-source CT: initial experience. *Radiology*. 2008;248(2):615-24.
  49. Monu JU, Pope TL Jr. Gout: a clinical and radiologic review. *Radiol Clin North Am*. 2004;42:169-84.
  50. Swan A, Amer H, Dieppe P. The value of synovial fluid assays in the diagnosis of joint disease: a literature survey. *Ann Rheum Dis*. 2002;61:493-8.
  51. Choi HK, Burns LC, Shojania K, et al. Dual energy CT in gout: a prospective validation study. *Ann Rheum Dis*. 2012;71(9):1466-71.
  52. Dalbeth N, Aati O, Gao A, et al. Assessment of tophus size: a comparison between physical measurement methods and dual-energy computed tomography scanning. *J Clin Rheumatol*. 2012;18:23-7.
  53. Bamberg F, Dierks A, Nikolaou K, Reiser MF, Becker CR, Johnson TR. Metal artifact reduction by dual energy computed tomography using monoenergetic extrapolation. *Eur Radiol*. 2011;21:1424-9.
  54. Zhou C, Zhao YE, Luo S, et al. Monoenergetic imaging of dual-energy CT reduces artifacts from implanted metal orthopedic devices in patients with fractures. *Acad Radiol*. 2011;18:1252-7.
  55. Pache G, Krauss B, Strohm P, et al. Dual-energy CT virtual noncalcium technique: detecting post-traumatic bone marrow lesions—feasibility study. *Radiology*. 2010;256:617-24.
  56. Lohan DG, Motamed K, Chow K, et al. Does dual-energy CT of lower extremity tendons incur penalties in patient radiation exposure or reduced multiplanar reconstruction image quality? *AJR*. 2008;191:1386-90.
  57. Persson A, Jackowski C, Engström E, Zachrisson H. Advances of dual source, dual-energy imaging in postmortem CT. *Eur J Radiol*. 2008;68:446-55.
  58. Deng K, Sun C, Liu C, Ma R. Initial experience with visualizing hand and foot tendons by dual energy computed tomography. *Clin Imaging*. 2009;33:384-9.
  59. Sun C, Miao F, Wang XM, et al. An initial qualitative study of dual-energy CT in the knee ligaments. *Surg Radiol Anat*. 2008;30:443-7.
  60. Hirofumi Kuno, Hiroaki Onaya, Ryoko Iwata, Tatsushi Kobayashi, Satoshi Fujii, Ryuichi Hayashi, Katharina Otani, Hiroya Ojiri, Takeharu Yamanaka, Mitsuo Satake. Evaluation of Cartilage Invasion by Laryngeal and Hypopharyngeal Squamous Cell Carcinoma with Dual-Energy CT. *Radiology*. 2012;265:488-96.
  61. Ascenti G, Mazziotti S, Lamberto S, et al. Dualenergy CT for detection of endoleaks after endovascular abdominal aneurysm repair: usefulness of colored iodine overlay. *AJR*. 2011;196:1408-14.
  62. Numburi UD, Schoenhagen P, Flamm SD, et al. Feasibility of dual-energy CT in the arterial phase: imaging after endovascular aortic repair. *AJR*. 2010;195:486-93.
  63. Stolzmann P, Frauenfelder T, Pfammatter T, et al. Endoleaks after endovascular abdominal aortic aneurysm repair: detection with dual-energy dual- source CT. *Radiology*. 2008; 249:682-91.
  64. Maturen KE, Kleaveland PA, Kaza RK, et al. Aortic endograft surveillance: use of fast-switch kVp dual-energy computed tomography with virtual noncontrast imaging. *J Comput Assist Tomogr*. 2011;35:742-6.
  65. Yamamoto S, McWilliams J, Arellano C, et al. Dual-energy CT angiography of pelvic and lower extremity arteries: dual-energy bone subtraction versus manual bone subtraction. *Clin Radiol*. 2009;64:1088-96.
  66. Brockmann C, Jochum S, Sadick M, et al. Dual energy CT angiography in peripheral arterial occlusive disease. *Cardiovasc Intervent Radiol*. 2009;32:630-7.
  67. Mowatt G, Cummins E, Waugh N, et al. Systematic review of the clinical effectiveness and cost-effectiveness of 64-slice or higher computed tomography angiography as an alternative to invasive coronary angiography in the investigation of coronary artery disease. *Health Technol Assess*. 2008;12:iii-iv,ix-143.
  68. Stolzmann P, Donati OF, Scheffel H. Low-dose CT coronary angiography for the prediction of myocardial ischaemia. *Eur Radiol*. 2010;20:56-64.

69. Gaemperli O, Schepis T, Valenta I, et al. Functionally relevant coronary artery disease: comparison of 64-section CT angiography with myocardial perfusion SPECT. *Radiology*. 2008;248:414-23.
70. Greenwood JP, Maredia N, Younger JE, et al. Cardiovascular magnetic resonance and single-photon emission computed tomography for diagnosis of coronary heart disease (CE-MARC): a prospective trial. *Lancet*. 2012;379:453-60.
71. Weininger M, Schoepf UJ, Ramachandra A, et al. Adenosine-stress dynamic real-time myocardial perfusion and adenosine-stress first-pass dual-energy myocardial perfusion CT for the assessment of acute chest pain: Initial results. *Eur J Radiol*. 2012;81(12):3703-10.
72. Arnoldi E, Lee YS, Ruzsics B, et al. CT detection of myocardial blood volume deficits: dual-energy CT compared with single-energy CT spectra. *J Cardiovasc Comput Tomogr*. 2011;5:421-9.
73. Henzler T, Porubsky S, Kayed H, et al. Attenuation-based characterization of coronary atherosclerotic plaque: comparison of dual source and dual energy CT with single-source CT and histopathology. *Eur J Radiol*. 2011;80:54-9.
74. Watanabe Y, Uotani K, Nakazawa T, et al. Dualenergy direct bone removal CT angiography for evaluation of intracranial aneurysm or stenosis: comparison with conventional digital subtraction angiography. *Eur Radiol*. 2009;19:1019-24.
75. Postma AA, Hofman PA, Stadler AA, van Oostenbrugge RJ, Tijssen MP, Wildberger JE. Dual energy CT of the brain and intracranial vessels. *AJR*. 2012;199(5 Suppl):S26-33.
76. Kim SJ, Lim HK, Lee HY, et al. Dual-energy CT in the evaluation of intracerebral hemorrhage of unknown origin: differentiation between tumor bleeding and pure hemorrhage. *AJR*. 2012; 33:865-72.
77. Schenzle JC, Sommer WH, Neumaier K, et al. Dual energy CT of the chest: how about the dose? *Invest Radiol* 2010;45:347-53, *Eur J Radiol*. 2011;80:54-9.
78. Yuan R, Shuman WP, Earls JP, et al. Reduced iodine load at CT pulmonary angiography with dual-energy monochromatic imaging: comparison with standard CT pulmonary angiography—a prospective randomized trial. *Radiology*. 2012;262: 290-7.
79. De Zordo T, von Lutterotti K, Dejaco C, et al. Comparison of image quality and radiation dose of different pulmonary CTA protocols on a 128-slice CT: high-pitch dual source CT, dual energy CT and conventional spiral CT. *Eur Radiol*. 2012;22:279-86.
80. Graser A, Johnson TR, Hecht EM, et al. Dual-energy CT in patients suspected of having renal masses: can virtual nonenhanced images replace true nonenhanced images? *Radiology*. 2009;252:433-40.

## Chapter

# 6

# CT Perfusion Imaging

*Veena Chowdhury*

Perfusion computed tomography (CT) allows functional evaluation of tissue vascularity. It measures the temporal changes in tissue density after intravenous injection of a contrast medium (CM) bolus using a series of dynamically acquired CT images. The greatest impact of perfusion CT has been on the assessment of patients who have had strokes, wherein the rapid scan timing and faster image processing have cemented its role as the modality of choice for evaluation of structural and functional status of cerebral vasculature.<sup>1</sup> In the field of oncology, perfusion CT has found applications in diagnosis, staging, prognostic evaluation and monitoring of response to therapies.<sup>2,3</sup> Although the role of ultrasound and magnetic resonance imaging have been explored for perfusion, there is a linear relationship between iodine concentration and density changes seen on CT expressed as Hounsefield units (HU), hence CT may be regarded as a preferred technique for perfusion imaging in general. Perfusion CT also has the potential to become the preferred technique for the assessment of tumor response to antiangiogenic drugs.<sup>4,5</sup>

### PERFUSION CT TECHNIQUE BASIC PRINCIPLE

The fundamental principle of perfusion CT is based on the temporal changes in tissue attenuation after intravenous administration of iodinated contrast medium. This enhancement of tissue depends on the tissue iodine concentration and is an indirect reflection of tissue vascularity and vascular physiology. After intravenous injection of the iodinated CM, the ensuing tissue enhancement can be divided into two phases based on the distribution in the intravascular or extravascular compartment. In the initial phase, the enhancement is mainly attributable to the distribution of contrast within the

intravascular space and this phase lasts for approximately 40 to 60 seconds from the time of contrast injection. In the second phase, contrast passes from the intravascular to the extravascular compartment across the capillary basement membrane and tissue enhancement results from contrast distribution between the two compartments. In the first phase, the enhancement is determined to a great extent by the tissue blood flow (BF) and blood volume (BV) whereas in the second phase, it is influenced by the vascular permeability to the contrast medium.<sup>6</sup> By obtaining a series of CT images in quick succession in the region of interest during these two phases, the temporal changes in tissue attenuation after injection of contrast medium can be recorded. By applying appropriate mathematic modeling, tissue perfusion can be quantified. The various analytical methods vary from scanner to scanner and among the commercial vendors. Two most commonly used analytical methods are:

- **Compartmental analysis:** In this kinetic modeling technique, analysis can be undertaken using the single compartment or double compartment method.<sup>4,6</sup> The single compartment method assumes that the intravascular and extravascular spaces are a single compartment and calculates tissue perfusion based on the conservation of the mass within the system. It estimates perfusion using the maximum slope of peak height of the tissue concentration curve normalized to the arterial input function.<sup>7</sup> Conversely, the double compartment method assumes that the intravascular and extravascular spaces are separate compartments and estimates capillary permeability and BV using a technique called Patlak analysis, which quantifies the passage of contrast from intravascular space into the extravascular space.

- Deconvolution analysis:** This CM kinetic modeling is based on the use of arterial and tissue time concentration curves to calculate the impulse residue function (IRF) for the tissue. The IRF is a theoretic tissue curve that is obtained from the direct arterial input, assuming that the concentration of contrast material in the tissue is linearly dependent on the input arterial concentration when the BF is constant.<sup>6,7</sup> After accounting for the flow correction, the height of this curve reflects the tissue perfusion and the area under the curve provides the relative BV estimation.<sup>7</sup> For the estimation of capillary permeability, a distributed parameter model is used, which is essentially an extended deconvolution method. Compartmental and deconvolution modeling methods have been found to be generally comparable, with differences in their theoretic assumptions and their susceptibility to noise and motion.<sup>8</sup> Compartmental analysis is based on the assumption that bolus of CM has to be retained within the organ of interest at the time of measurement, which may result in underestimation of perfusion values in organs with rapid vascular transit or with a large bolus injection.<sup>7</sup> Deconvolution analysis, however, assumes that the shape of the IRF is a plateau with a single exponential washout. Although this assumption is believed to work for most organs, it might not be suitable for assessing perfusion in such organs as the spleen and kidney, which have complex microcirculations. Hence, it is preferable to use compartmental analysis for organs with the complex circulatory pathways. Deconvolution method is appropriate for measuring lower levels of perfusion (<20 mL/min per 100 mL) because they are able to tolerate greater image noise attributable to the inclusion of the complete time series of images for calculation.<sup>7</sup> This is particularly beneficial for the accurate measurement of the lower perfusion values typically seen in tumors after treatment response. A potential drawback of including all the acquired images for the calculation is the possibility of image misregistration secondary to motion of the patient. Conversely, compartmental analysis effectively uses three images of perfusion measurement: the baseline image and the images immediately before and after the

moment the maximal rate of contrast tissue enhancement is reached.<sup>6,7</sup> Hence, patient motion has relatively less impact in compartmental analysis. The mathematic modeling technique employed also has also implications on the CT protocol used. The deconvolution method, being less sensitive to noise, allows the use of lower tube current and permits scanning with higher temporal resolution for the dynamic cine acquisition. For the compartmental model, the presence of the image noise results in miscalculation of perfusion values; hence, a higher tube current with low image frequency is preferred for the dynamic study.

## PERFUSION CT PROTOCOLS

A variety of the perfusion CT protocols have been proposed, and they typically depend upon the target organ, mathematic modeling technique, CT scan configuration and clinical objective. Nevertheless, a typical perfusion CT protocol consists of a baseline acquisition without contrast enhancement, followed by a dynamic acquisition performed sequentially after intravenous injection of CM. The dynamic acquisition study includes a first pass study, delayed study, or both depending on the pertinent physiological parameters that need to be analyzed (**Table 1**).

### Unenhanced CT Acquisition

The baseline unenhanced CT acquisition should provide wide coverage to include the organ of interest. This study basically serves as a localizer to select the appropriate tissue area to be included in the contrast enhanced dynamic imaging range. Depending upon the scanner configuration, a 2 cm coverage area (for a 4 or 16 row CT scanner) or a 4 cm coverage area (for 64 row CT scanner) can be selected for dynamic scanning. Larger coverage area (8–16 cm) is now feasible with the availability of newer scanner with 128 to 320 rows of detectors.

### Dynamic CT Acquisition

The first pass study for the perfusion measurements comprises images acquired in initial cine phase for a total of

**Table 1** Terms commonly used in computed tomography perfusion<sup>6,7</sup>

Perfusion parameters	Definition	Marker (in oncology)	Units
Blood flow (BF) or perfusion	Flow rate through vasculature in tissue region	Tumor vascularity Tumor grade	mL per 100 g/min
Blood volume (BV)	Volume of flowing blood within vasculature in tissue region	Tumor vascularity	mL per 100 g
Mean transit time (MTT)	Average time taken to travel from artery to vein	Perfusion pressure	Seconds
Permeability surface (PS) area product	Total flux from plasma to interstitial space	Immature leaky vessels	mL per 100 g/min
Time to peak (TPP)	Time from arrival of contrast in major arterial vessels to the peak enhancement	Perfusion pressure	Seconds
PEI	Maximum increase in tissue density after contrast injection	Tissue blood volume	HU

approximately 40 to 60 seconds. For the typical first pass study based on the deconvolution method, image acquisition is done every 1 second, whereas for the compartment method, image acquisition is done every 3 to 5 seconds.<sup>9</sup>

For obtaining permeability measurements, a second phase ranging from 2 to 10 minutes is supplemented after the first pass study. The second phase images are acquired every 10 seconds for 2 minutes after the first pass study for a deconvolution method-based study. For permeability measurements with compartment model, images are acquired every 10 to 20 seconds.<sup>9</sup>

### Technique of CT Perfusion

- Step I involves acquisition of unenhanced CT images to cover the entire region of interest.
- Step II involves selection of the slice for dynamic imaging. The selected slices should be chosen to cover the maximum tumor area. The total tumor coverage area is 2 cm for 16-MDCT and 4 cm for 64MDCT and up to 9 cm for 128 MDCT scanner.
- Step III involves contrast enhanced dynamic image acquisition.
- Step IV involves post-processing of CT data to generate colored perfusion maps of blood flow (BF), blood volume (BV), mean transit time (MTT) and permeability surface area product. Time attenuation curves showing the enhancement characteristics of the artery and tumor during the first pass and delayed phase of perfusion CT acquisition can be obtained.

### Contrast Medium

One of the important considerations for adequate assessment of tissue perfusion is the contrast medium (CM) bolus used for the intravenous injection. As there is a linear relation between iodine concentration and tissue enhancement, a higher concentration of CM is preferred (iodine 370 mg/mL). A contrast bolus of 40 to 70 mL and an injection rate ranging from 3.5 to 10 mL/s are normally adequate for optimal perfusion analysis. The scan delay for the cine acquisition from the start of the CM injection is determined by the CM circulation time to the region of interest. Typically, for most body applications, a scan delay of 5 to 10 seconds is considered suitable (5–8 seconds for neck/chest/abdomen studies and 10–15 seconds for studies of the pelvis and extremities).

### Acquisition Parameters

The selection of acquisition parameters for perfusion CT needs to be done judiciously in keeping with the body part scanned, modeling technique used and radiation exposure.<sup>10,11</sup> Use of lower tube voltage (kilovolt peak, kVp) and the tube current (milli-Ampere-second, mAs) is recommended to reduce the radiation exposure.

It is important to note that movement during data acquisition can lead to image misregistration and can

cause errors in the measurements of perfusion values.<sup>10</sup> Hence, efforts should be made to minimize motion by appropriate approaches, such as breath holding instructions to the patients for chest and upper abdominal applications. Likewise, anterior abdominal wall motion can be restricted by the use of abdominal straps.<sup>11</sup> Use of motility inhibiting agents, such as hyoscine butylbromide or glucagon, is recommended to curtail bowel peristalsis during the perfusion examination of bowel. In addition, luminal distention with water or saline is encouraged for study of hollow viscera to enable optimal tumor delineation. This is particularly relevant in follow-up examinations after therapy, in which tumor conspicuity is often in question after successful treatment. Metallic stents, prostheses and surgical implants cause beam hardening artifacts and can negatively influence the perfusion measurements. Finally, selecting the region of interest is crucial, and areas with excessive tumor necrosis or those located along organs with motion (in chest examinations) and areas near metallic prostheses or stents should be avoided.<sup>12</sup>

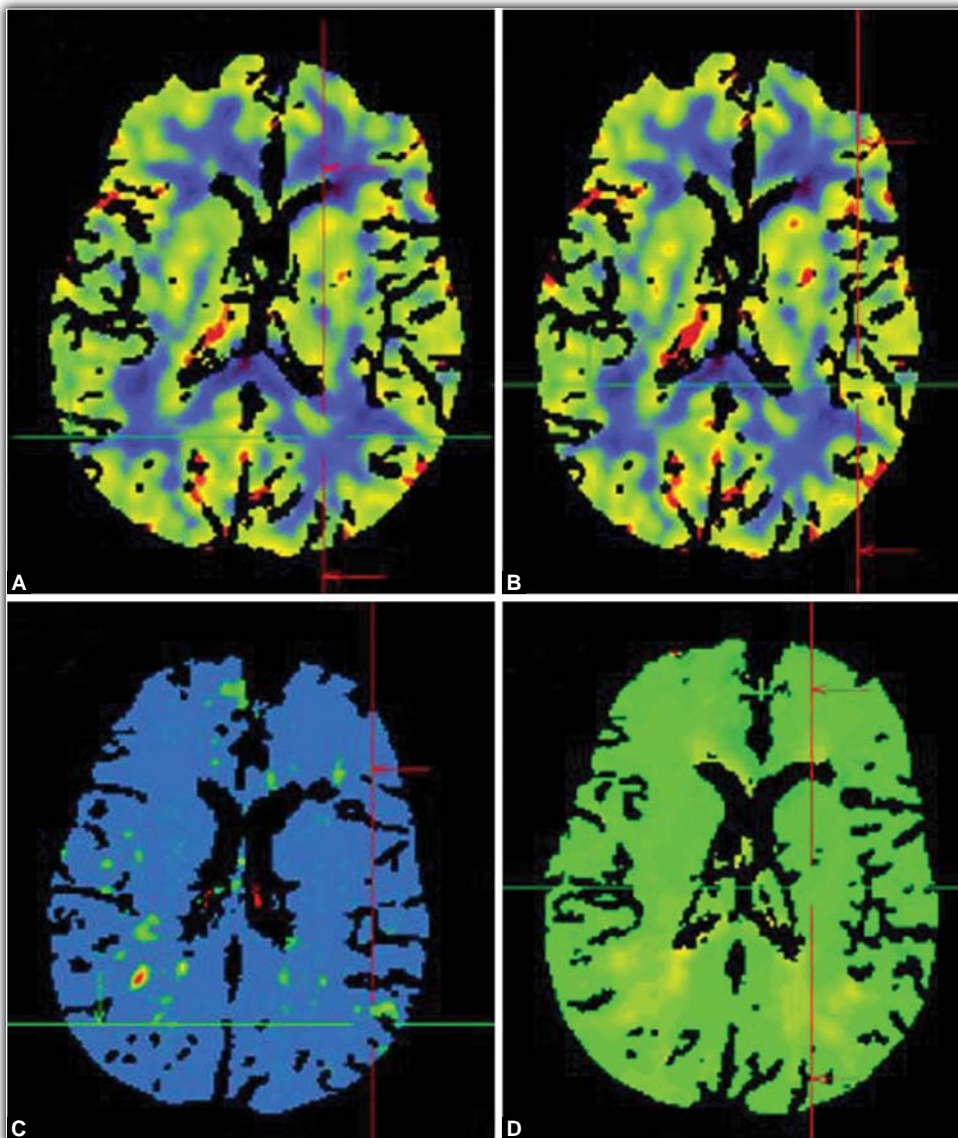
### CT PERFUSION IN ACUTE ISCHEMIC STROKE

A stroke, or cerebrovascular accident, is defined as an abrupt onset of a neurologic deficit that is attributable to a vascular cause. Stroke is one of the leading causes of mortality and disability worldwide. Atherosclerosis of the carotid arteries is by far the most common predisposing condition for stroke. Strokes are ischemic approximately 85 percent of the time with the rest being hemorrhagic.

The concept of an ischemic penumbra (tissue at risk) has been a major impetus for developing pharmacologic interventions in the treatment of acute stroke. The ischemic penumbra is defined as the part of the brain that is sandwiched between brain regions committed to die and those that receive enough blood to communicate and that the cells in the ischemic penumbra could survive if the blood flow is restored.<sup>13</sup> The penumbra phase generally begins when blood flow falls below 20 mL/100 g/min and electrical communication between neurons cease with infarction not occurring until blood flow falls below 10 or 12 mL/100 gm/min.

The identification of potentially salvageable ischemic tissue in the hyperacute period is of critical importance because the tolerance of perfusion disturbances is related to its duration, which can determine the progression of ischemia from the core into the oligemic penumbral region. This has led to the development of several functional imaging techniques such as brain perfusion imaging.

Perfusion CT imaging is a functional imaging modality to differentiate between the infarcted core and the ischemic penumbra. Perfusion CT provides absolute and relative information about brain perfusion parameters, namely cerebral blood flow (CBF), cerebral blood volume (CBV), mean transit time (MTT), and time to peak (TTP) (**Figs 1A to D**). CBF is the total volume of blood moving through a voxel



**Figs 1A to D** Normal cerebral perfusion CT maps representing CBF (A), CBV (B), MTT (C), and TTP (D) respectively

**Table 2** Perfusion abnormalities<sup>14</sup>

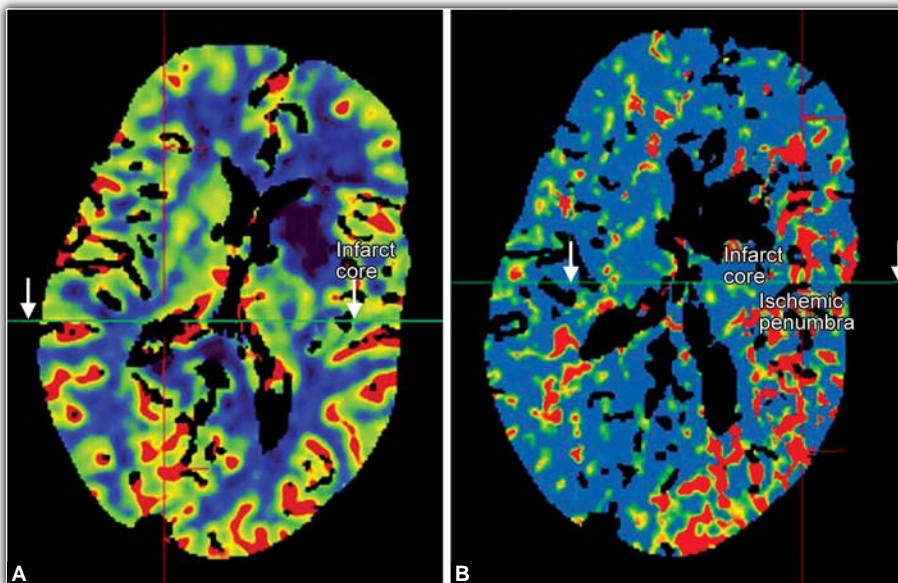
Perfusion parameter	Infarct core	Ischemic penumbra
CBF	Reduced	Reduced
CBV	Reduced	Normal or increased
MTT	Prolonged	Prolonged
TTP	Prolonged	Prolonged

in a given unit of time. CBV is a measure of the total volume of blood within a voxel which includes blood in both the tissues and blood vessels. MTT is the time elapsed between the arterial inflow and the venous outflow. TTP refers to the time elapsed from the start of the contrast material injection to the attainment of maximum attenuation within the selected

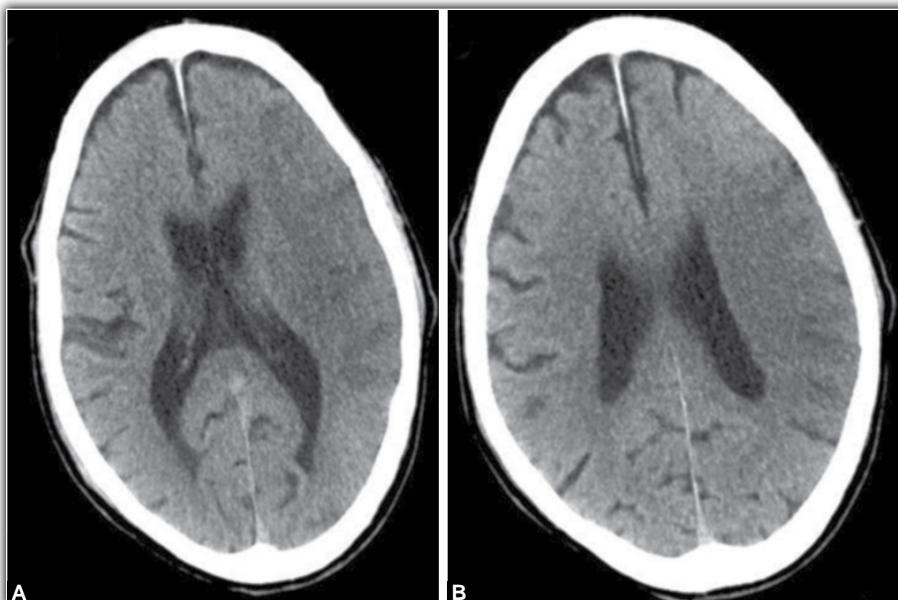
region of the brain. Normally the relationship between these aforementioned parameters is expressed by the 'central volume principle' which is expressed by the equation,  $CBF \times MTT = CBV$ .<sup>14</sup>

The diagnosis of acute ischemic stroke on perfusion CT is done commonly by visual inspection of CBF, CBV, MTT and TTP maps generated in a dedicated post-processing workstation.<sup>15,16</sup> Areas showing perfusion abnormalities in CBF, CBV and MTT maps represent the infarct core while areas having relatively preserved CBV and with prolonged MTT and reduced CBF represent the ischemic penumbra<sup>17,18</sup> (**Figs 2A and B**). The perfusion abnormalities in acute stroke are tabulated in **Table 2**.

The perfusion parameter that most accurately describes the tissue at risk of infarction in case of persistent arterial occlusion is the relative MTT >145 percent. The perfusion



**Figs 2A and B** Perfusion CT maps representing CBV (A) and MTT (B) in a patient showing a central infarct core (CBV = 1.2 mL/100 mL) in the region of the left basal ganglia with a large surrounding ischemic penumbra ( $rMTT = 210\%$ ) revealing CBV-MTT mismatch (relatively preserved CBV with increase in MTT values)—case of acute ischemic stroke



**Figs 3A and B** Noncontrast axial CT images reveal large areas of subtle loss of gray-white matter differentiation in the left frontoparietal region—case of large hemispheric infarct

parameter that most accurately describes the infarct core is the absolute CBV with an optimal threshold at 2 mL/100 g.<sup>19</sup>

Wintermark M et al have defined a widely accepted threshold of increase in the relative MTT of more than 145 percent as the most accurate parameter to define the ischemic penumbra with an absolute increase in MTT of more than 7 seconds as the next best criterion. MTT values >145 percent suggest ischemic penumbra while much higher values are seen in infarct core.

In infarct core the MTT values are prolonged and the CBV is reduced while the ischemic penumbra is the area of mismatch between the MTT and CBV maps (MTT-CBV), i.e. the MTT is prolonged while CBV is normal or increased,

which can be depicted using automated summary maps (Figs 3 and 4).<sup>20,21</sup> A significant drawback of using CBF thresholds for ischemic penumbra is that differences in gray and white matter CBF values, and their respective ischemic thresholds (with ischemic gray matter CBF values being close to normal white matter CBF values), interfere with the use of CBF thresholds to define the penumbra.<sup>22</sup> Also, CBF values to define infarct core and penumbra vary widely within the literature.

The main limitation of most of the previously available multi-detector row CT scanners in the evaluation of cerebral perfusion was the relatively narrow range of brain tissue covered primarily at the level of the basal ganglia resulting

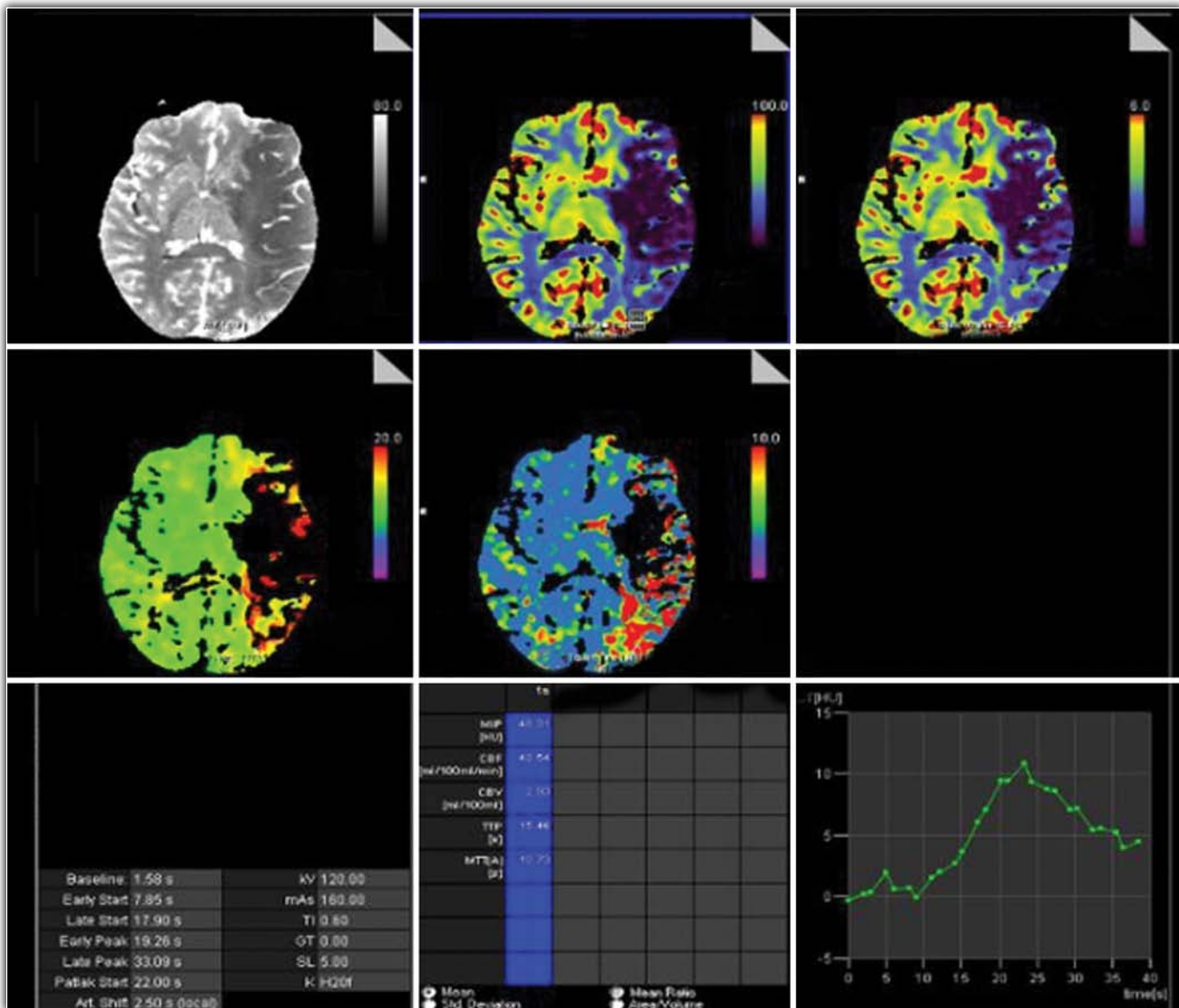


**Fig. 4** Perfusion maps (same case as in Fig. 3) show extensive area of perfusion defects involving the left cerebral hemisphere with a central infarct core revealing severely reduced CBV and CBF values and surrounding areas of ischemic penumbra demonstrating relatively preserved CBV, moderate reduction in CBF and prolongation of MTT, TTP values

in the exclusion of a large volume of brain parenchyma including the superior cerebral hemispheres, posterior fossa and brainstem. However, the advent of modern CT scanners with increased number of detector rows, whole brain perfusion CT with substantially increased vertical scanning range is feasible which allows for complete and comprehensive evaluation of the entire areas of suspected ischemia/infarction.<sup>23</sup>

There are certain inherent advantages of CT perfusion imaging over MR perfusion imaging in that CT is very fast and much more widely available as compared to MRI thus reducing the imaging time. It is relatively less expensive. In

addition, it is easily performed and MRI is much more limited by patient contraindications or intolerance.

There are multiple advantages of adding CT perfusion imaging to the routine stroke imaging protocol in an emergency setting such as:<sup>24-26</sup>

- Has been shown to increase diagnostic certainty for stroke detection.
- Permits the estimation of amount of potentially salvageable tissue, hence guiding in patient management.
- Allows the accurate prediction of the final infarct size and the evaluation of clinical prognosis for acute stroke patients at the time of emergency evaluation.

- d. Thrombolytic therapy can be extended beyond the 3 hours window if the patients are carefully selected based on perfusion mismatch.

## CT PERFUSION IN ONCOLOGY

There has been a gradual increase in the utility of perfusion CT in oncology, with a wide spectrum of clinical applications, including:

1. Lesion characterization (differentiation between benign and malignant lesion)
2. Identification of occult malignancies
3. Vascularity
4. Monitoring therapeutic response of various treatment regimens, including chemoradiation and antiangiogenic drugs.

An emerging approach of cancer care is the individualized approach, in which the treatment strategies are targeted according to the tumor biology.<sup>27</sup> One of the key elements of tumor physiology that influences the aggressiveness of cancer and its response to treatment is tumor microvasculature (neoangiogenesis), and the presence of high vascularity usually suggests aggressive behavior and is associated with a poor outcome.<sup>28,29</sup> The tumor angiogenesis is defined as a process of developing new capillary blood vessels, resulting in vascularization of the tumor. This process, which is integral part to the growth and spread of tumor, consists of several dynamic processes mediated by the host growth factors, such as vascular endothelial growth factor, fibroblast growth factor, and platelet derived endothelial cell growth factor.<sup>30,31</sup> Perfusion CT displays and permits quantification of the abnormal vasculature within tumors, thus allowing assessment of tumor aggressiveness.

Development of newer antiangiogenic drugs has necessitated the use of functional imaging techniques, such as perfusion CT or dynamic contrast enhanced MR, to monitor their therapeutic effects, because conventional methods of monitoring response are not effective for these drugs.<sup>32</sup> Moreover, given that functional changes precede morphologic changes after treatment, techniques like perfusion CT allow earlier assessment of treatment effect than conventional methods, which rely on tumor size. Perfusion CT can measure vascular physiologic changes by virtue of changes in the contrast enhancement characteristics of tissues.<sup>33</sup> Accordingly, perfusion CT can be considered as surrogate (indirect) imaging biomarker for *in vivo* evaluation of response to antiangiogenic drugs. This is in contrast to microvessel density (MVD), which represents the actual tumor blood vessels (i.e. direct biomarker) that form the target of antiangiogenic drugs, and hence is considered the "gold standard" for quantifying and monitoring angiogenesis.<sup>34</sup> MVD has also been established as a prognostic indicator for many cancers. The most direct strategy for the measurement of MVD, and hence monitoring antiangiogenic therapy, would require periodic biopsies. There are several limitations

in the routine use of microvessel density (MVD) as biomarker, including:

1. The requirement of invasive tissue sampling, such as biopsy.
2. The need for standardization.
3. The presence of random sampling errors.
4. The fact that such studies do not explore entire tumor volume, which can hamper evaluation because of heterogeneity of malignant tumors.<sup>30</sup> Indirect biomarkers like perfusion CT are hence used because of their observed benefits like noninvasiveness, they can be repeated frequently, and they dynamically reflect the microvasculatory function in a living individual. Several investigators have validated the utility of CT perfusion as a biomarker for measuring angiogenesis and monitoring response to treatment.<sup>35</sup>

## HEPATIC CT PERFUSION

The liver has a dual blood supply, the portal vein and the hepatic artery. Hepatic perfusion relies on the resolution of each component of its dual blood supply as contributions from each are altered in many diseases. Most disease processes affect blood flow regionally or globally or both. Perfusion CT can provide quantitative information about arterial and portal perfusion of liver lesions combined with a good anatomic detail (**Fig. 5**).

### Perfusion Parameters of Normal Liver

There are some disagreements in normal liver perfusion parameters from different sources due to different choices of computational model and people. However, they are all verged about 1/4 – 1/3 as the ratio of HAP/PVP, in rough approximation of the blood supply from hepatic artery and portal vein (**Table 3**).

### CT Perfusion in Hepatocellular Carcinoma

Neovascularization, production of new blood vessels within the tumors, is an essential process for sustaining tumor growth. The spatial resolution of diagnostic imaging is insufficient to visualize tumor microvessels directly, however, functional imaging has the ability to evaluate neovascularization and help in the detection of tumors even before morphologic changes.<sup>41</sup> CTA and CTAP can be used to detect blood flow of hepatic artery and portal vein for HCC evaluation. Blood in the hepatic artery is increased and decreased in the PV while the blood volume is increased.<sup>42</sup>

The enhancement imaging features of HCC lesions have been correlated with tumor microvessel density and its intratumoral distribution characteristics (**Figs 6A to C**).<sup>43</sup> HAP is increased in the periphery and decreased in the center. The hepatic blood flow and HPI are higher in primary hepatic carcinoma than the normal liver.

Changes in perfusion parameters are valuable in qualitative and differential of primary HCC. CT perfusion

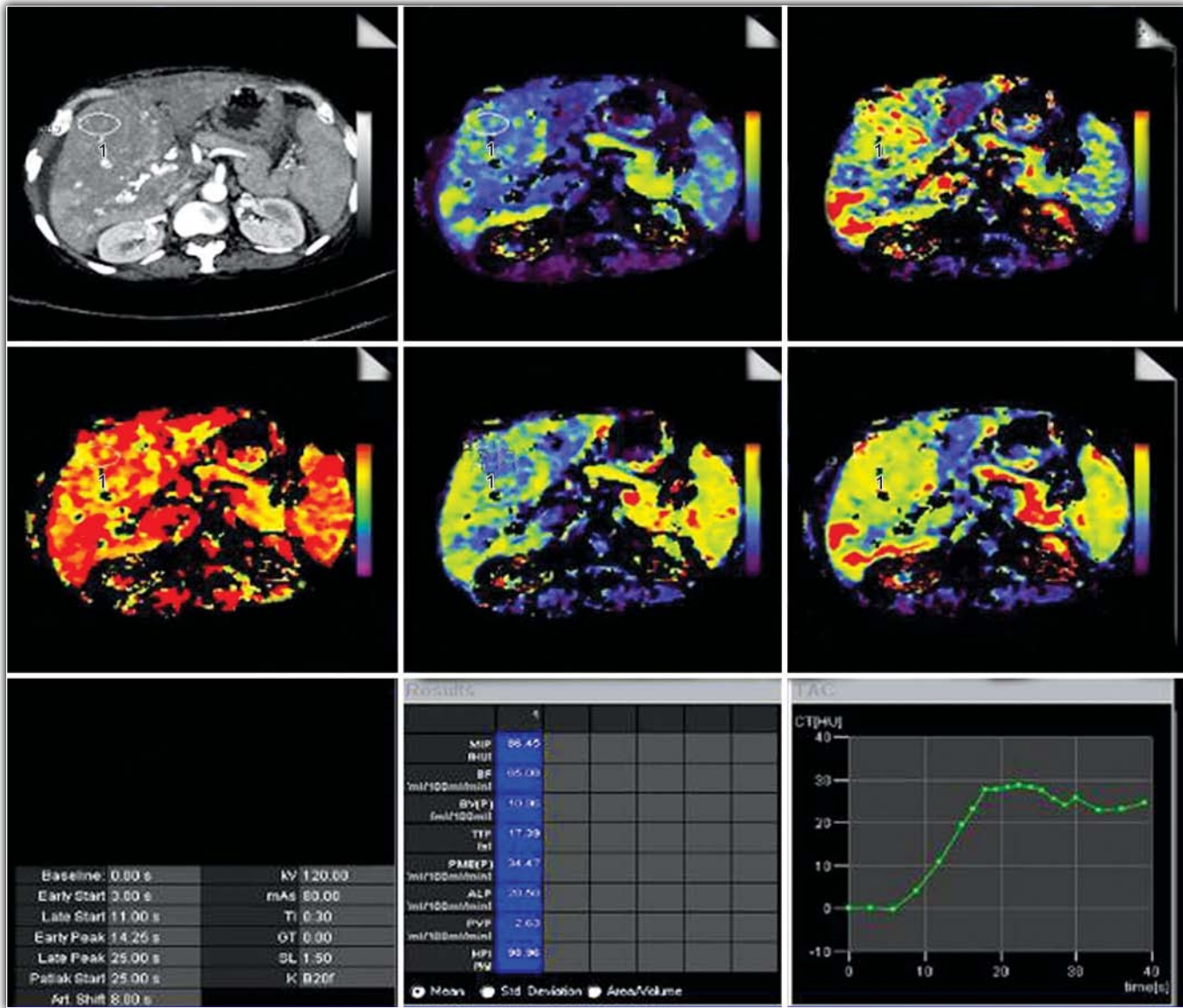


**Fig. 5** Perfusion maps in normal liver parenchyma show blood flow of 85.0 mL/100 mL/min, blood volume of 10.5 mL/100 mL and time to peak of 17s

**Table 3** Perfusion parameters of normal liver

Sources	HAP	PVP	HPI	HBF	HBV	MTT
Miles et al <sup>36</sup>	0.17	0.34	32%			
Blomley et al <sup>37</sup>	0.19	0.93				
Weidekamm et al <sup>38</sup>	0.2+/-0.08	1.02+/-0.35				
Zhou et al <sup>39</sup>	0.17+/-0.08	0.9+/-0.04	16+/-16%	106.24+/-54.53	20.24+/-8.26	15.06+/-8.94
Hashimoto et al <sup>40</sup>				18.4+/-5.6%	103.9+/-18	12.5+/-2.0
						11.1+/-1.6

[Abbreviations: HAP: Hepatic arterial perfusion (mL/min per milliliter), PVP: Portal vein perfusion (mL/min per milliliter), HPI: Hepatic perfusion index (%), HBF: Hepatic blood flow (mL/min per 100 g), HBV: Hepatic blood volume (mL/100 g), MTT: Mean transit time (S)]



**Figs 6A to C** Triphasic study reveals a large iso to hypodense lesion in right hepatic lobe on noncontrast scan (A). It shows intense enhancement in arterial phase (B), with relative washout in portal venous phase (C)—case of hepatocellular carcinoma

can detect the abnormalities in liver perfusion before morphologic changes occur.

The peak enhancement value, contrast enhancement ratio, the pattern of time density curve and the gross enhancement morphology of HCC lesions has been correlated with tumor MVD and reflects the distributive features of tumor microvessels within the HCC lesions. Correlation has been found between the likelihood of intrahepatic metastasis of the HCC lesion with densely enhanced pseudocapsules and rich pseudocapsular tumor MVD.<sup>43</sup>

In HCC, CT perfusion has a role in making the differential diagnosis, evaluating tumor aggressiveness, monitoring therapeutic effects and determining the final patient outcome. HCC demonstrates higher BF, BV and PS and lower MTT measurements compared with the background liver (**Fig. 7**).<sup>44,45</sup> There is also difference between CT perfusion values of well differentiated tumors and those of moderately and poorly differentiated tumors. Well differentiated HCCs demonstrate relatively higher BF, BV and PS and lower MTT measurements than do moderately and poorly differentiated HCCs. Tumor tissues with the highest malignant grade can be taken by biopsy under CT guidance, thus avoiding errors of grading occurring in selection of biopsy region.<sup>46</sup> The presence of cirrhosis and tumor thrombus in the portal vein does not significantly alter the perfusion values in HCC confirming that the blood supply of primary hepatic carcinoma is mainly provided by hepatic artery.<sup>47</sup>

Perfusion CT allows accurate quantification of changes in liver tumor perfusion during and after an embolization procedure thus helping to optimize therapeutic outcome. CT perfusion is also able to assess changes in liver tumor perfusion in response to antiangiogenic treatment. HCCs after bevacizumab treatment demonstrate reduction in perfusion values and the changes seen in MTT correlate with clinical outcome.<sup>47</sup> Earlier identification of tumor recurrence after various intervention procedures is also potentially possible with perfusion CT.

### CT Perfusion in Metastatic Disease

Diagnosis of liver metastatic disease is very important for its staging, prognosis and treatment. Routine CT and MRI are

insensitive to occult and early stage hepatic micrometastasis of tumors.<sup>48</sup> Although there may be no apparent abnormal morphology, CT perfusion can display changes in hemodynamics through its functional imaging. Improved detection and characterization of metastatic disease to the liver has profound implications for the prognosis and treatment of patients at risk.<sup>48,49</sup> The earlier diagnosis of the patients with micrometastatic disease may facilitate future use of targeted chemotherapeutic strategies and antiangiogenic therapies targeted against vascular endothelial growth factors. Exclusion of the presence of micrometastatic disease could obviate adjuvant chemotherapy in some patient groups.<sup>49</sup>

In a study conducted to assess changes in hepatic perfusion in patients of colorectal cancer with computed tomography, arterial and portal perfusion were calculated from temporal changes in attenuation after intravenous administration of iodinated contrast material.<sup>50</sup> Arterial perfusion greater than 0.25 mL/min/mL (0.17 mL/min/mL for normal liver) was seen in 82 percent patients with overt metastasis versus 38 percent of the patients with no overt metastasis. Portal perfusion of 0.25 mL/min/mL or less (0.34 mL/min/mL for normal liver) was found in 46 percent patients with overt metastasis versus 19 percent of patients with no overt metastasis. Follow-up imaging showed progressive metastatic disease in 11 percent patients, all of whom had decreased portal perfusion. It was concluded that increased arterial perfusion was an indication of liver metastasis whereas reduced portal perfusion could indicate progressive disease<sup>50,51</sup> (**Figs 8 and 9**).

### CT Perfusion in Focal Liver Lesions

Small liver lesions are also associated with changes in liver blood flow. Early detection of primary or metastatic hepatic focal lesions and characterization of other focal lesions may be possible on the basis of relative increase in hepatic arterial blood flow associated with these diseases. It has been suggested by some authors that differentiation between benign and malignant focal liver lesions is possible based on CT perfusion parameters.<sup>52,53</sup> Mean hepatic perfusion index (HPI) was less than 30 percent in all benign focal lesions

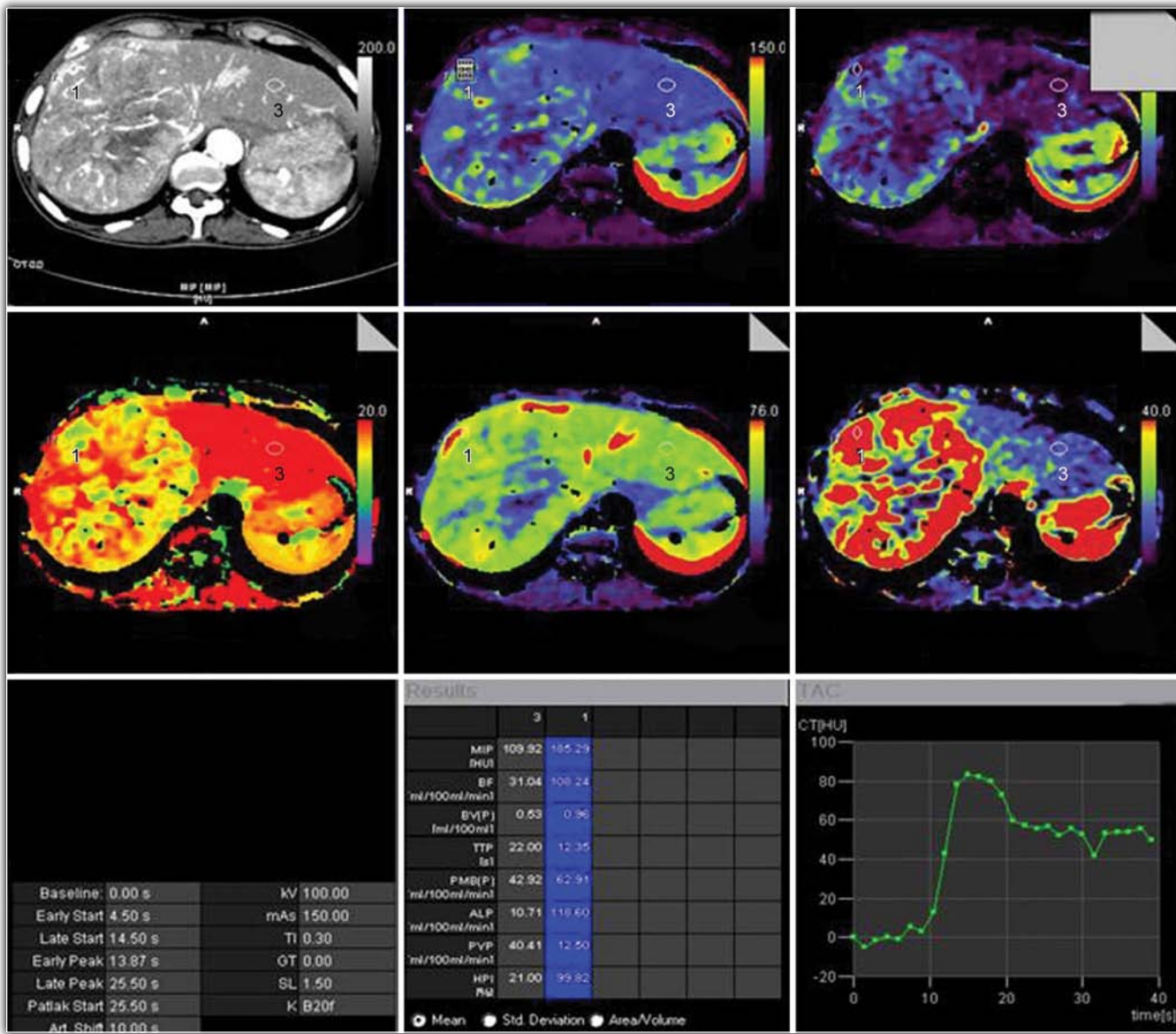


**Fig. 7** Color maps (same case as in Fig. 6) show increased ALP as indicated by red color, increased BF, BV as indicated by patchy areas of green color and decreased TTP shown by areas of yellow within the lesion in a case of hepatocellular carcinoma

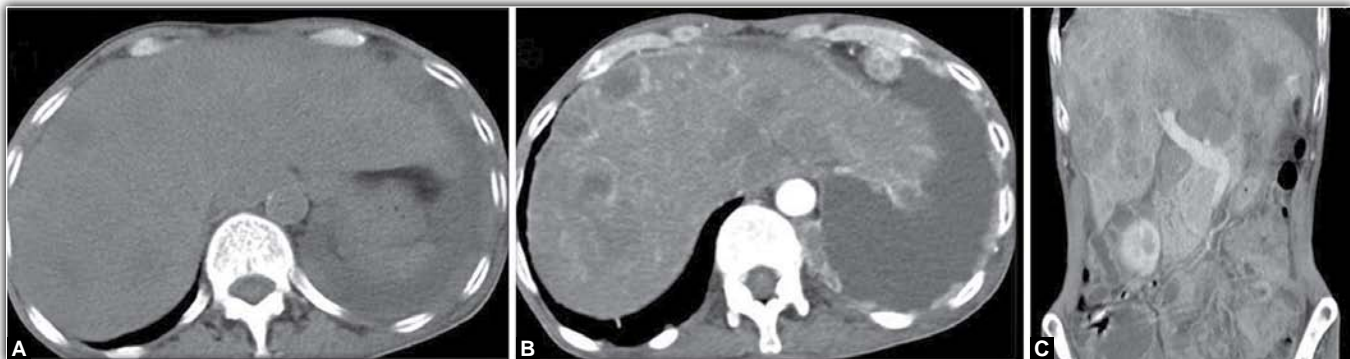
and more than 30 percent in cases of malignant focal lesions (**Figs 10 and 11**).<sup>54</sup>

### ■ CT PERFUSION IN PANCREATIC NEOPLASMS

Pancreatic cancer remains one of the most difficult neoplasms to diagnose at an early stage. Despite recent advances in imaging including multidetector CT (MDCT), only 10 to 30 percent of patients with pancreatic cancer have resectable disease at diagnosis, therefore long term survival is extremely rare. Many researchers have been making every effort to find a method for early diagnosis, accurate staging and effective treatment of pancreatic cancer (**Figs 12A to C**).<sup>55</sup>

In some clinical areas, difficulties can arise in differentiation of autoimmune pancreatitis (AIP) and chronic mass forming pancreatitis from pancreatic cancer. The differentiation between these entities is paramount in planning management for the patients. CT perfusion imaging allows noninvasive absolute quantification of pancreatic perfusion and adds to the precision of the differential diagnosis of pancreatic cancer and mass forming pancreatitis.<sup>56</sup>

All pancreatic adenocarcinomas and mass forming chronic pancreatitis exhibit a lower blood flow than controls. The low blood flow of mass forming chronic pancreatitis reflects the pancreatic fibrosis and necrosis that occurs in these cases.<sup>57</sup> The decrease of blood flow of pancreatic



**Figs 8A to C** Triphasic CT reveals hypodense lesions in noncontrast scans (A), showing complete ring enhancement in arterial phase (B). Lesions appear hypodense on portal venous phase (C)—case of metastatic adenocarcinoma

adenocarcinoma reflects that the blood perfusion in tumor areas is less than that of normal pancreas.<sup>58</sup> Decreased blood flow can be taken as the first characteristic of pancreatic adenocarcinoma and mass forming chronic pancreatitis. It has been seen in several studies that blood flow was 77 percent lower and blood volume was 65 percent lower in patients with pancreatic adenocarcinoma than in controls<sup>59</sup> (Fig. 13). There was no significant difference noted in blood flow, blood volume, permeability, peak enhancement and time to peak between pancreatic adenocarcinoma grade 1 and grade 2-3, and grade 4 and between grade 1 and grade 4. No significant difference between pancreatic adenocarcinoma stage I and stage II and III, between stage II and III and stage IV and between stage I and stage IV was found either, thereby indicating that the parameters can not predict the grade and stage of pancreatic adenocarcinoma.<sup>59</sup>

The decrease in blood volume of pancreatic adenocarcinoma and mass forming chronic pancreatitis is related to the facts that the total number of vessels in pancreatic adenocarcinoma tissue and mass forming chronic pancreatitis is relatively less than normal and the number of regional capillaries is also less and this brings about the decreases in blood volume.<sup>60</sup> Decreased blood volume is the second characteristic of pancreatic adenocarcinoma and mass forming chronic pancreatitis.

The lower peak enhancement and the longer time to peak of pancreatic adenocarcinoma and mass forming chronic pancreatitis correspond to the decrease of blood flow and blood volume and reflect the lower enhancement on contrast CT imaging. This can be taken as third characteristic which can also be visualized on time density curves by lower and later peak of enhancement of pancreatic adenocarcinoma and mass forming chronic pancreatitis as compared to controls. Permeability was 559 percent higher in pancreatic cancer and 821 percent higher in mass forming chronic pancreatitis than controls.<sup>59</sup> The increase of permeability of pancreatic adenocarcinoma and mass forming chronic pancreatitis might be associated with a decrease in the integrity of

vascular endothelium of tumorous and inflammatory vessel dilatation (Figs 14 and 15).<sup>61</sup>

Between adenocarcinoma and mass forming chronic pancreatitis, the blood flow, blood volume and peak enhancement are lower in patients with pancreatic adenocarcinoma than with mass forming chronic pancreatitis. Blood flow was 56 percent lower and blood volume was 53 percent lower in patients with pancreatic adenocarcinoma than with mass forming chronic pancreatitis.<sup>59</sup> The pancreatic adenocarcinoma is a hypovascular tumor and parenchyma of gland in patients with mass forming chronic pancreatitis appears less affected than that with pancreatic adenocarcinoma.<sup>58</sup> Malignant tumors with liver and lymph node metastasis have long MTT.

The comparison of perfusion parameters in patients with pancreatic adenocarcinoma, mass forming chronic pancreatitis and normal subjects (mean +/- SD) (Table 4).

Thus, CT perfusion provides additional quantitative information on the function of microvasculature of tumor and carries the potential to evolve as a clinically valuable tool in pancreatic cancer. It has been noted that pancreatic tumors with high pretreatment volume transfer constant ( $K_{trans}$ ) between blood plasma and extravascular space indicate regular intratumoral flow and respond better to concurrent chemotherapy and radiotherapy (CCRT).<sup>62</sup> This might aid in the development of a tailored approach to therapy in these patients.

Substantially, high blood perfusion has been observed in hypervascular tumors such as insulinomas compared with background pancreatic parenchyma (Table 5).<sup>63</sup> Whereas conventional multidetector CT can depict tumor size, vascularity and presence of liver metastasis in pancreatic endocrine tumors, perfusion CT provides additional quantitative preoperative prognostic factors that could influence therapeutic treatment of patients. For example, in patients with small pancreatic tumors located in the head, where benefit of surgery has not been proved, favorable perfusion parameters could suggest follow-up rather than an aggressive approach.<sup>64</sup> It was seen in a study that blood flow

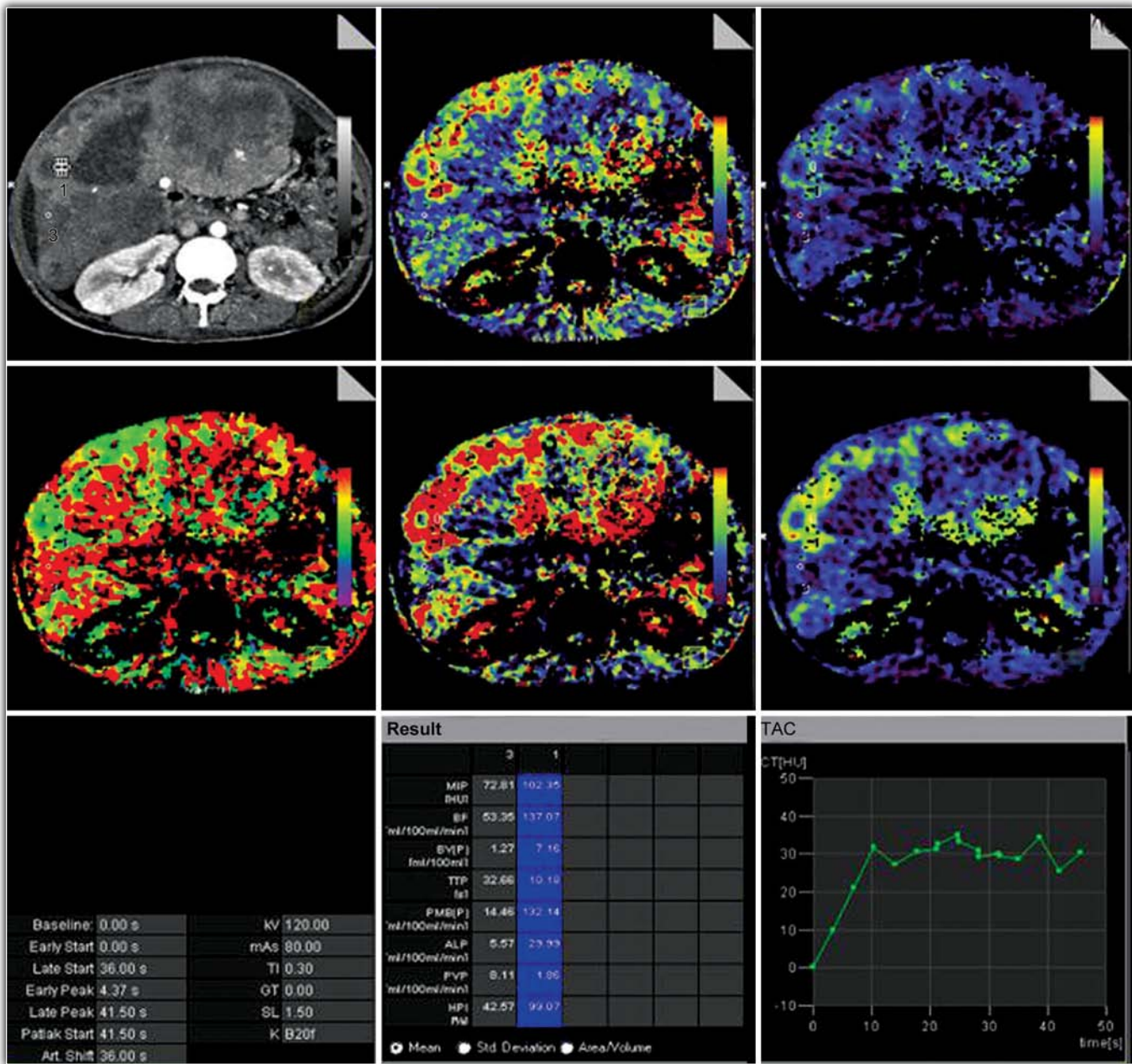


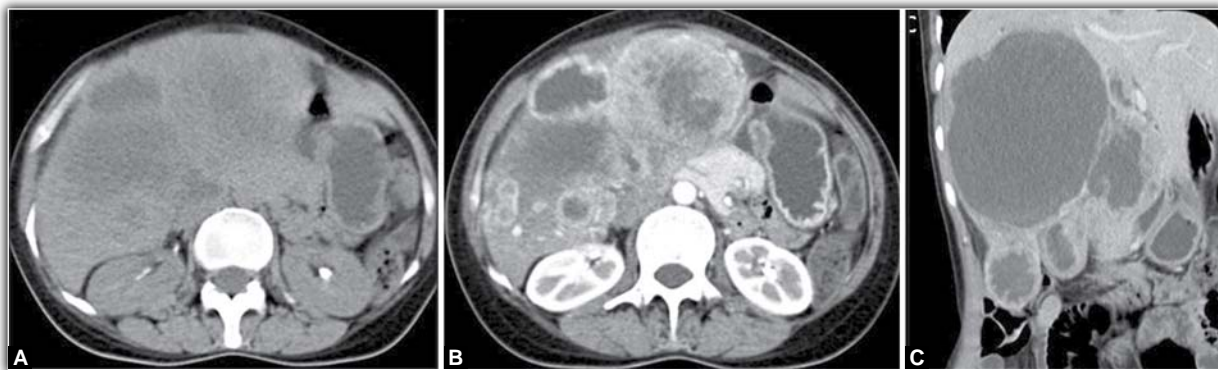
**Fig. 9** Perfusion study (same case as in Fig. 8) reveals focal areas of green and red color along anterior aspect of the largest lesion. Tumor reveals high blood flow, ALP and HPI with reduced PVP

was significantly higher in tumors measuring less than 2 cm in diameter, in those with a proliferation index of 29 percent or less and those without histological signs of microscopic vascular neoplastic involvement. A larger mean transit time was observed in tumors more than 2 cm in diameter and in those patients with lymph node or liver metastasis. Thus, in contrast to most other tumors, the greater the vascularization, the lower is the grade in endocrine tumors of the pancreas.<sup>63</sup>

The pancreatic tumor perfusion measurements performed with CT were comparable to those performed with xenon CT, which is a more validated technique of CT perfusion.<sup>65</sup>

### ■ CT PERFUSION IN COLORECTAL CARCINOMA

Perfusion CT changes in colorectal cancer reflects its proangiogenic nature, since neovascularization is considered the initial triggering event in colorectal tumor growth and



**Figs 10A to C** Triple phase study reveals multiple necrotic hypodense lesions with thick irregular walls and internal septations (A), which show enhancement during arterial phase (B) and washout in portal venous phase (C)—metastatic neuroendocrine tumor

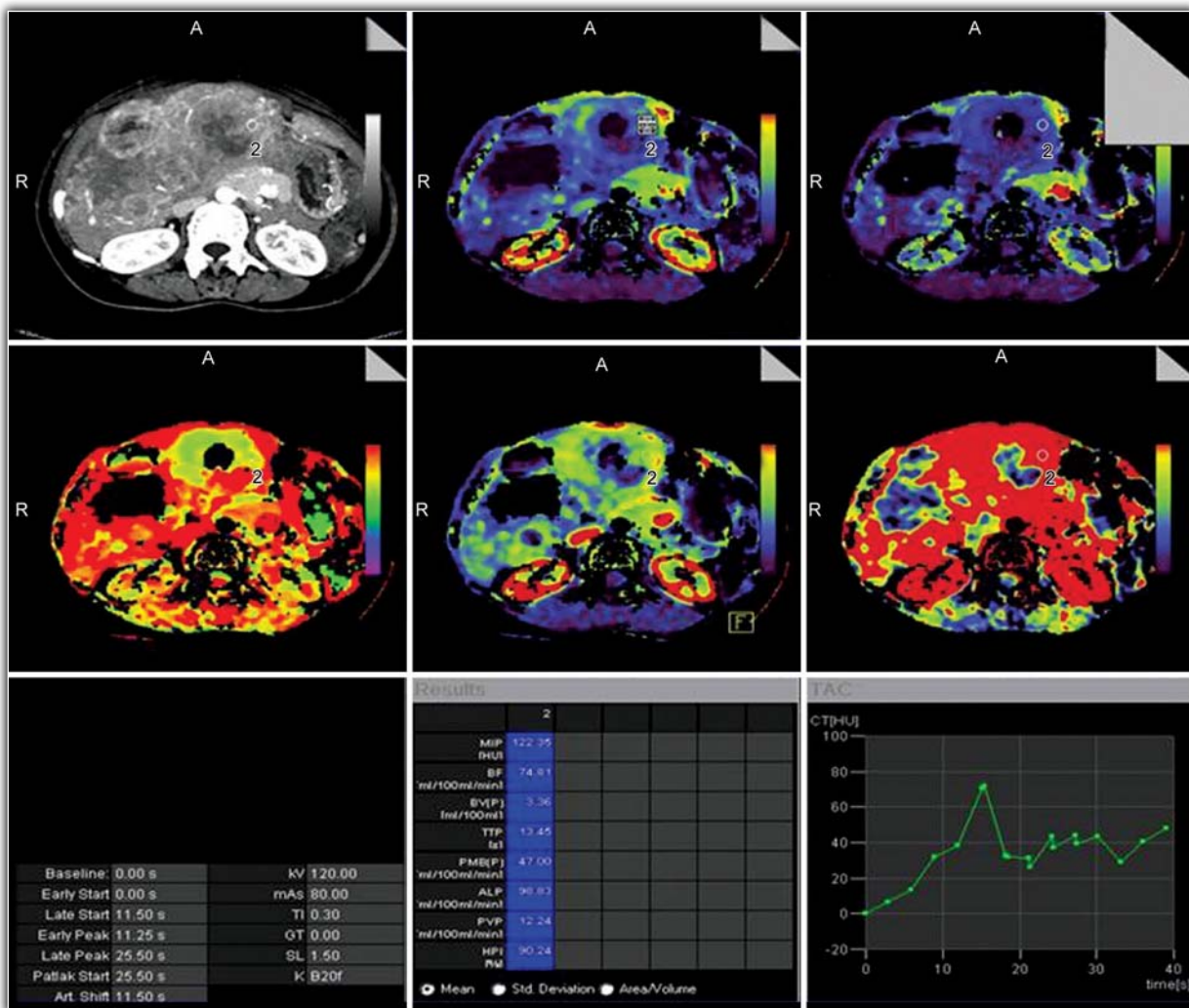
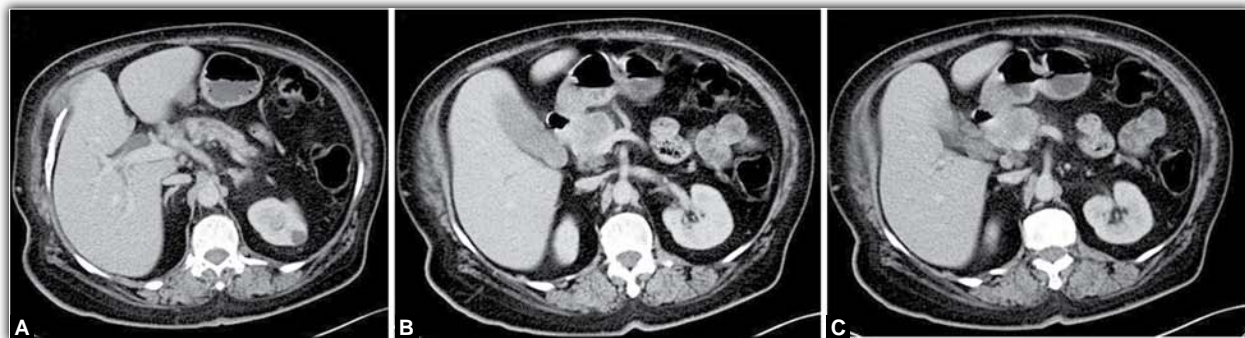


**Fig. 11** ROI placed over the edge of cavitary lesion (same case as in Fig. 10) show ALP 98 mL/100 mL/min and HPI of 90%, suggesting malignant etiology



**Figs 12A to C** Cranial to caudal: contrast enhanced CT images shows a hypodense mass lesion in the head of pancreas abutting the portal vein posteriorly and second part of duodenum medially, along with surrounding fat stranding. Upstream ductal dilatation and parenchymal atrophy is also seen—case of pancreatic adenocarcinoma

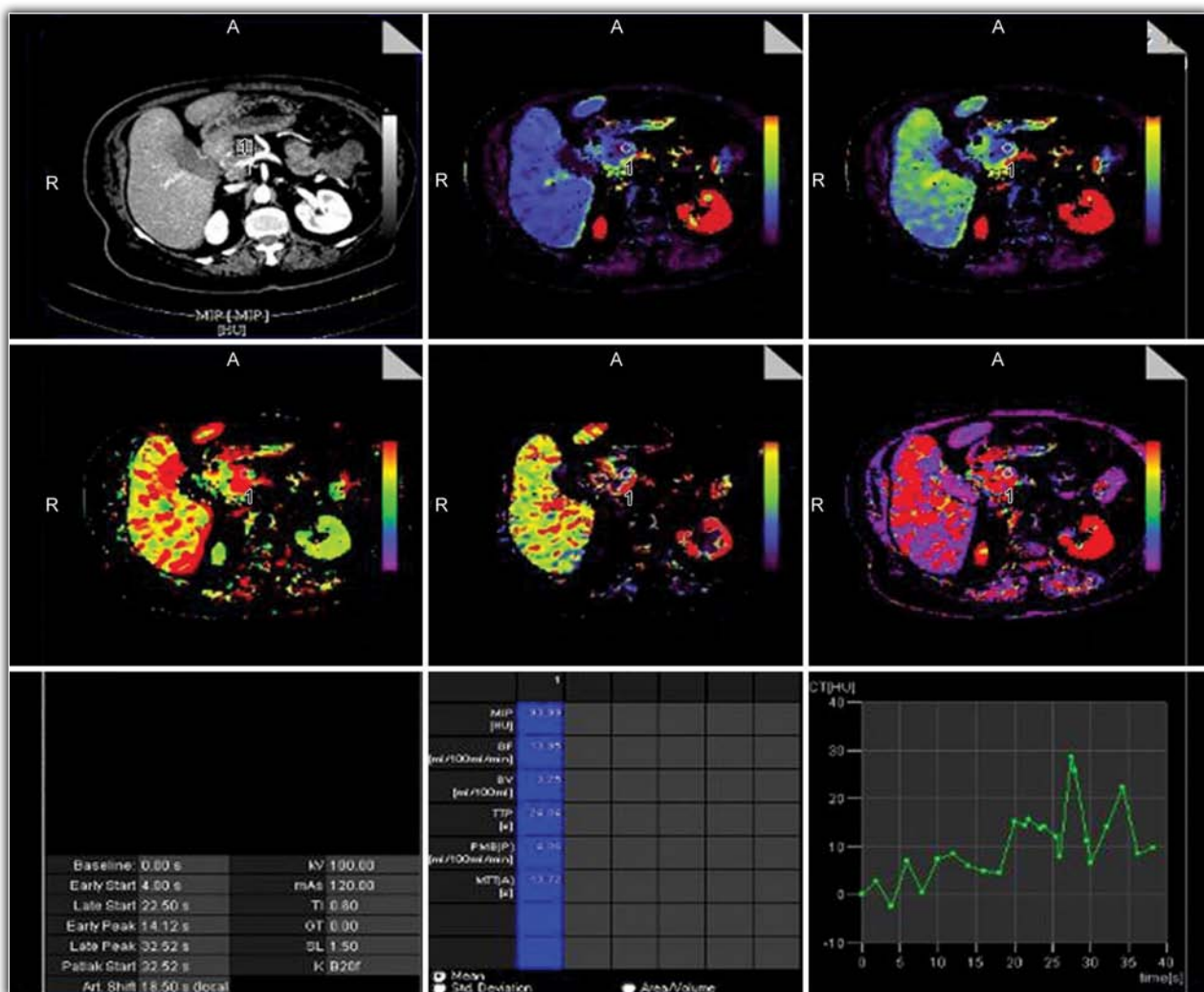


**Fig. 13** Perfusion CT image with ROI at the pancreatic mass (same case as in Fig. 12) reveals markedly reduced blood flow and blood volume within the lesion with increased permeability compared to normal controls

dissemination. Microvessel density progressively increases from normal colonic mucosa through adenoma to colorectal carcinoma.<sup>66</sup> Colorectal tumor size correlates significantly with microvessel density, and microvessel density counts from patients with lymph node metastasis, lymphatic vessel invasion, venous vessel invasion or relapse were significantly higher than those without.<sup>67</sup> Several investigators have validated the utility of CT perfusion as a biomarker for measuring angiogenesis. When compared with normal rectal mucosa, rectal cancer consistently showed higher blood flow and a shorter MTT (**Figs 16 to 19**) (**Table 6**).<sup>68</sup>

Given that functional changes precedes morphologic changes after treatment, techniques like perfusion CT allow earlier assessment of treatment effect than conventional method, which rely on tumor size. The predominant application of perfusion CT in colorectal carcinoma is in assessing the response to radiotherapy and chemotherapy.<sup>69,70</sup> It has been seen there is significant fall in perfusion after two weeks of treatment with antiangiogenic drugs (**Table 7**). After chemotherapy and radiotherapy, rectal carcinomas showed significant reduction in the blood flow and increase in mean transit time.<sup>71</sup>

Perfusion CT also has application in differential diagnosis of colonic lesions (**Figs 20 and 21**). The use of perfusion CT in characterization of colonic lesions was studied by Goh et al in 2007 in which they have found that CT perfusion measurements can be used to differentiate between diverticulitis and colorectal carcinoma better than morphologic criteria.<sup>72</sup> Perfusion CT is able to differentiate colonic wall thickening attributed to diverticulitis from colorectal cancer based on the high perfusion values in colorectal cancer. Mean BV values of  $6.0+/-1.2$  mL/100 g and mean BF values of  $80.1+/-31.5$  mL/100 g/min are seen in colorectal carcinoma; while in diverticulitis, mean BV was  $4.4+/-1.3$  mL/100 g and mean BF was  $52.0+/-27.3$  mL/100 g/min.<sup>72</sup>

The association between poor prognosis and greater intensity of angiogenesis histologically is reflected *in vivo* by perfusion CT measurements (**Figs 22A to C**). Perfusion CT assessment of primary colorectal adenocarcinoma blood flow at staging can predict subsequent metastatic disease (**Figs 23 and 24**). The patients who had tumors with high blood flow and shorter mean transit time at baseline perfusion imaging showed a poor response to chemotherapy and radiotherapy.<sup>73</sup> High perfusion values in association with a poor response to chemotherapy and radiotherapy can be explained by large numbers of intratumoral arteriovenous shunts with a high perfusion rate and low exchange of oxygen.<sup>71,74</sup>

Quantitative measurements of blood flow using perfusion CT can be used for assessing clinicopathological features and prognosis in patients with colorectal cancer.<sup>75</sup> Well differentiated tumors have higher blood flow than moderately differentiated tumors. Tumors with low blood flow show lymph

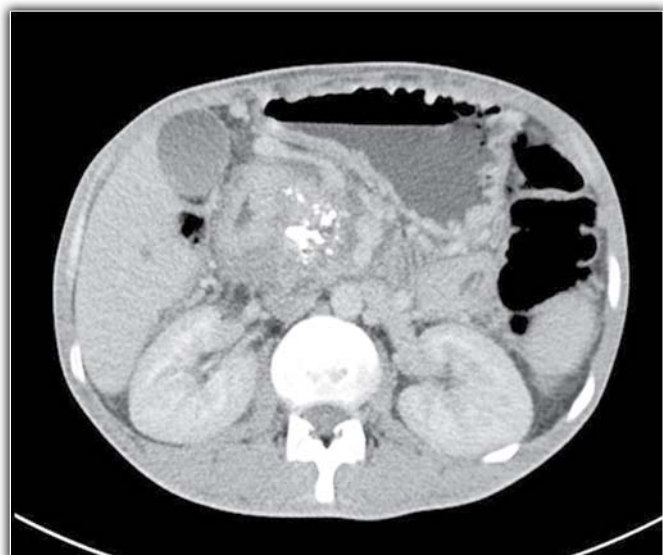


**Fig. 14** Contrast enhanced CT images shows a hypodense mass lesion with calcification in the head of pancreas abutting the portal vein posteriorly and second part of duodenum medially, along with surrounding fat stranding—case of chronic calcific pancreatitis

node metastasis, vascular invasion, lymphatic invasion and distant metastasis.

Although, histology is considered the gold standard for tumor grading, in heterogeneous tumors biopsies may be subjected to sampling error. Perfusion CT can assess tumor grade *in vivo* and can reduce the potential for sampling error by guiding biopsy to the tumor region most likely to be of the highest grade.

## CT PERFUSION IN PROSTATE CANCER

Though CT has been investigated to assess angiogenesis in malignant tumors of liver, lung, colon, rectum, pancreas, with the development of perfusion CT technique, the feasibility of the perfusion CT technique for evaluating prostate tumors has been shown only by a few studies. The reasons include:

1. Lack of contrast resolution makes identification of cancer on unenhanced CT scans impossible with the consequent inability to center the perfusion values on malignant areas;
2. Difficulty in morphologic differentiation between central and peripheral zone on CT images which do not allow identification of suspected malignant lesion.<sup>76</sup>

These problems have been overcome with the introduction of 64 and 128 MDCT scanner with larger volume coverage, enabling evaluation of the entire prostate. In a study published in 2012, substantial differences in mean values of BV, MTT and permeability surface area product parameters between prostate cancer, BPH, chronic prostatitis and healthy tissue have been found (**Figs 25 and 26**).<sup>77</sup>

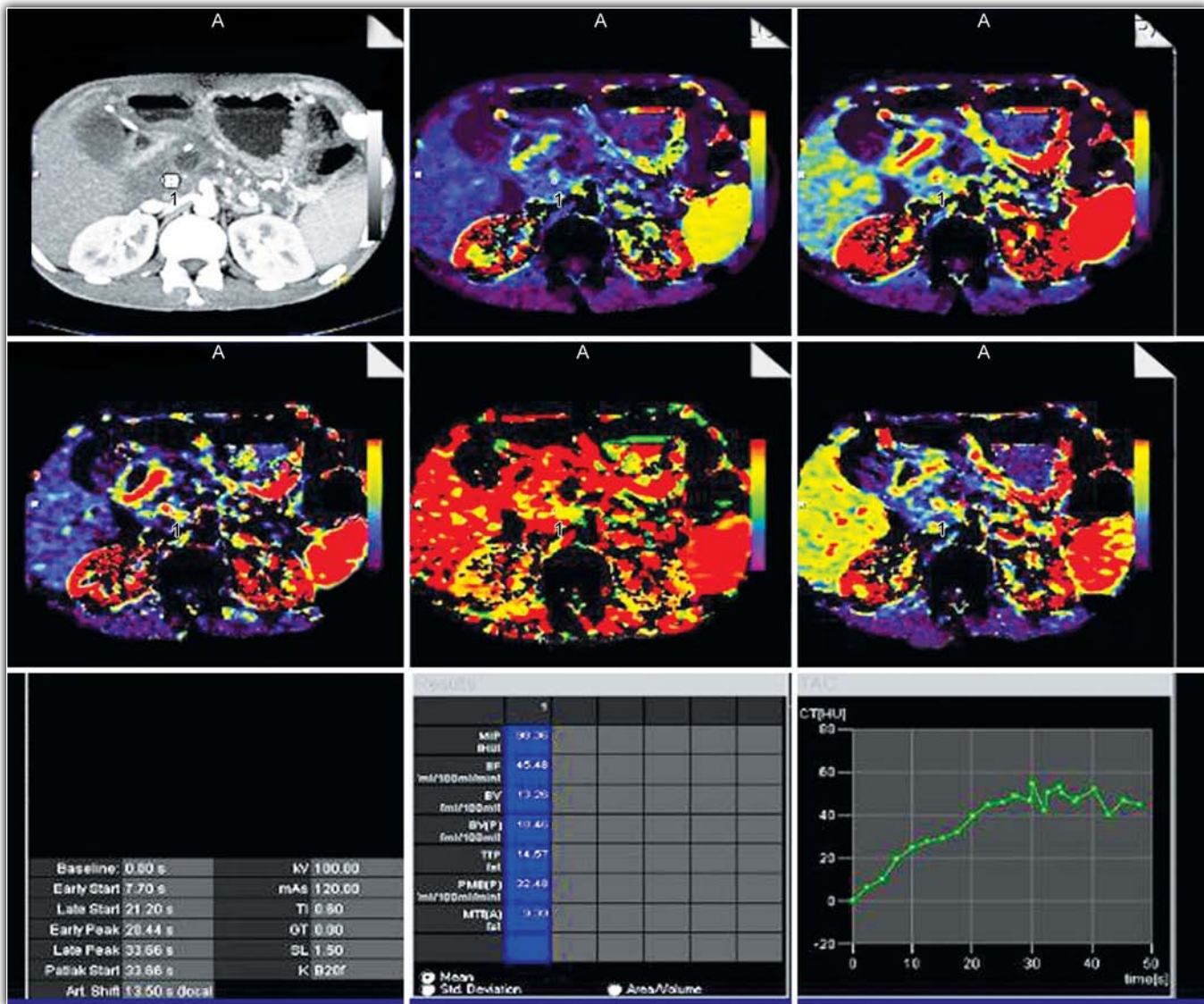


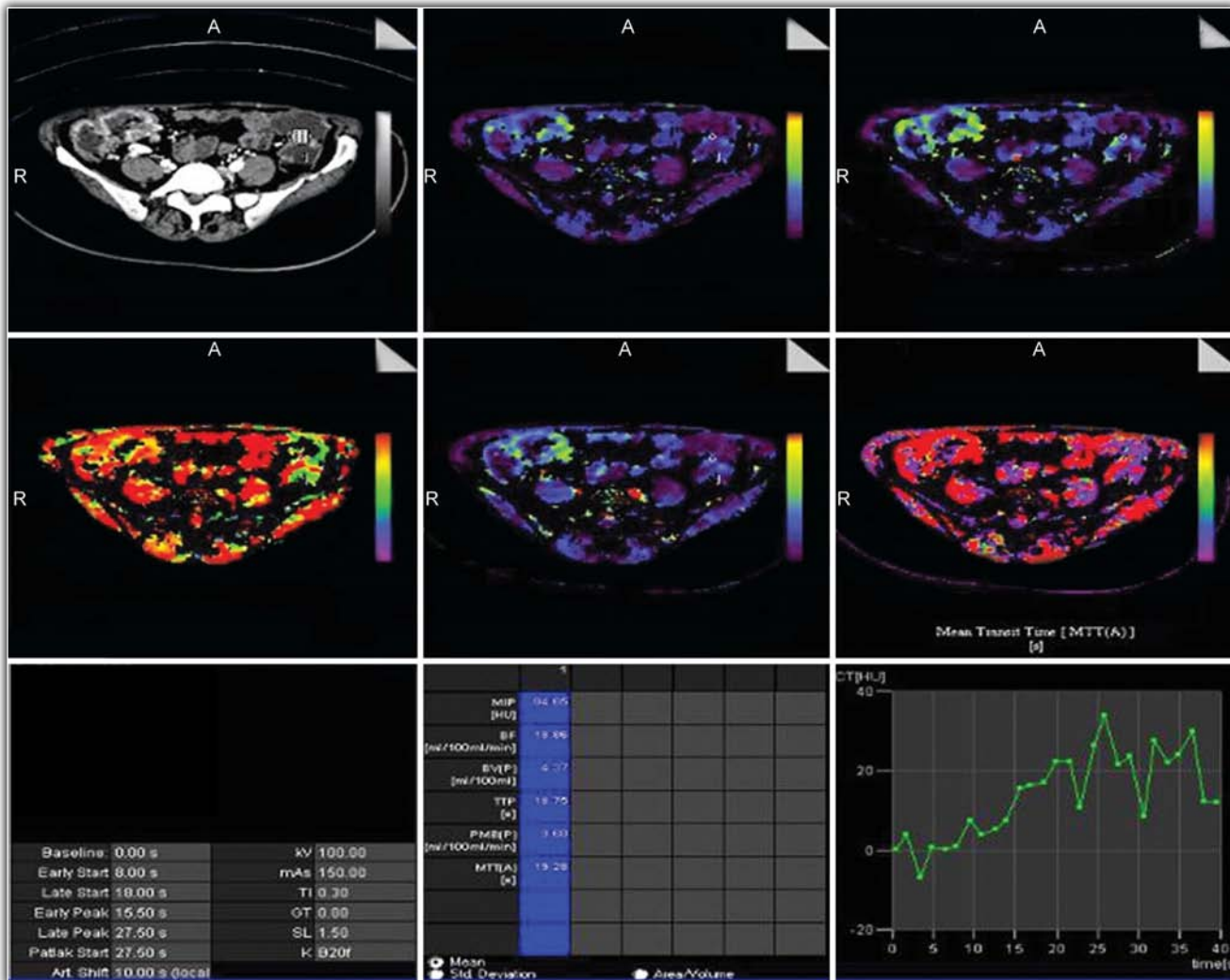
**Fig. 15** Perfusion CT image with ROI within pancreatic head (same case as in Fig. 14) reveals reduced blood flow and blood volume, and increased permeability in comparison to normal controls

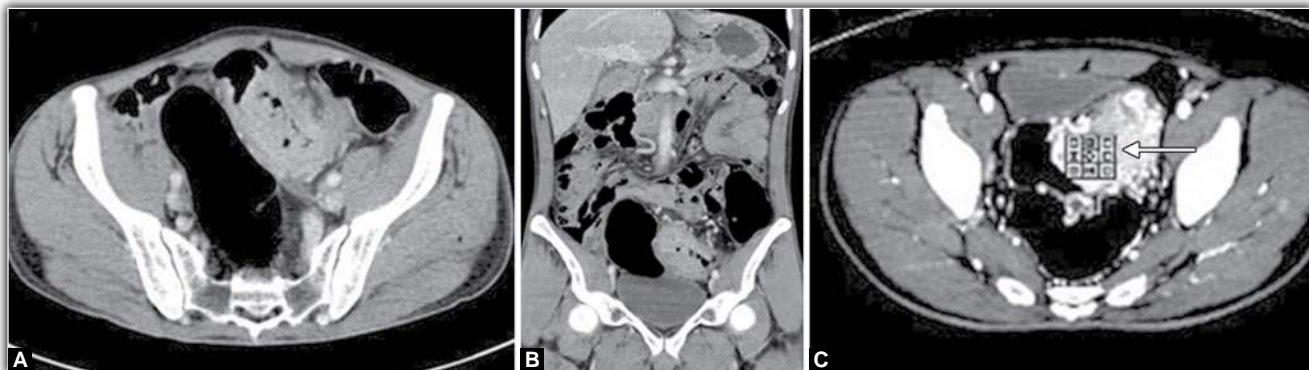
**Table 4** The comparison of perfusion parameters in patients with pancreatic adenocarcinoma, mass forming chronic pancreatitis and normal subjects (mean  $\pm$  SD)<sup>59</sup>

Parameters	Pancreatic adenocarcinoma (n = 64)	Mass forming chronic pancreatitis (n = 15)	Controls (n = 33)
Blood flow (mL/min/mL)	0.365 $\pm$ 0.204	0.820 $\pm$ 0.345	1.567 $\pm$ 0.379
Blood volume (mL/mL)	0.089 $\pm$ 0.042	0.191 $\pm$ 0.088	0.258 $\pm$ 0.041
Permeability (mL/mL/min)	0.956 $\pm$ 0.556	1.336 $\pm$ 0.582	0.145 $\pm$ 0.088
Peak enhancement (HU)	30.858 $\pm$ 15.860	42.166 $\pm$ 23.109	57.000 $\pm$ 13.382
Time to peak (seconds)	47.047 $\pm$ 6.124	36.133 $\pm$ 7.726	24.858 $\pm$ 2.881

**Table 5** CT perfusion parameters in endocrine tumors and normal pancreas mean (median)<sup>63</sup>

Parameter	Tumor	Normal pancreas	P value
Blood flow (mL/100 g/min)	239.8 (183)	130.4 (94.4)	0.06
Blood volume (mL/100 g)	23.9 (21.8)	22.4 (23.3)	0.71
Mean transit time (sec)	10.9 (9.8)	14.9 (18.2)	0.28
Permeability surface area product (mL/100 g/min)	54.9 (55.3)	32.4 (16.5)	0.14

**Fig. 16** CT perfusion maps from the normal appearing colon show blood flow of 18.8 mL/100 g/min, blood volume of 4.4 mL/100 g, permeability of 9.7 mL/100 g/min and mean transit time of 19.3 seconds



**Figs 17A to C** CECT axial (A) and coronal (B) images show asymmetric mural thickening in the sigmoid colon with heterogeneous enhancement and luminal narrowing. The maximum mural thickness was 2.7 cm. Minimal pericolonic fat stranding is noted. ROI placed over the enhancing part of the lesion is shown (arrow in C)—case of moderately differentiated adenocarcinoma

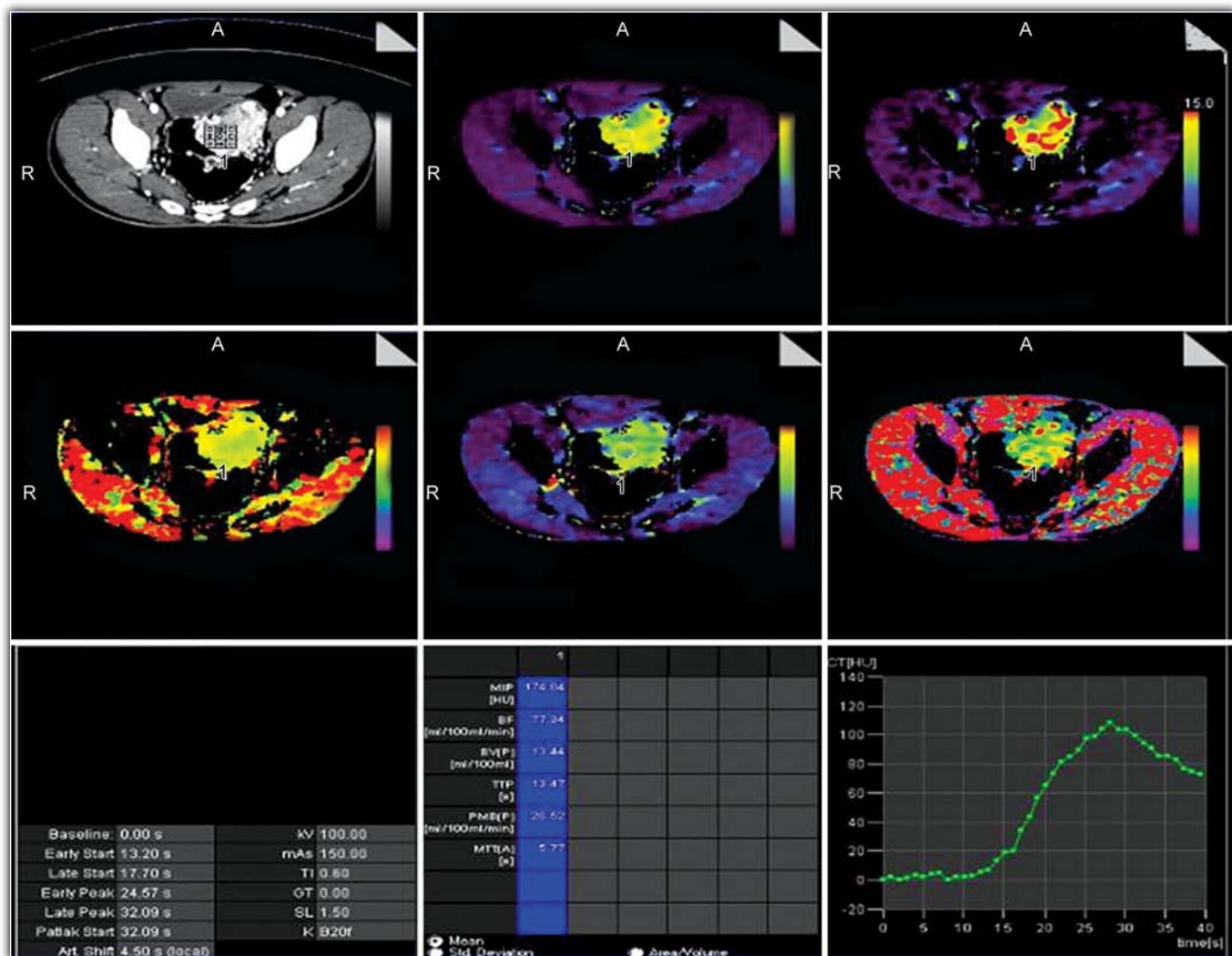


**Fig. 18** Color maps (same case as in Fig. 17) reveal very high blood flow of 77.3 mL/100 g/min, blood volume of 13.4 mL/100 g and permeability of 26.5 mL/100 g/min as coded by focal areas of green and red color (Note scale on right side with red indicating highest value and violet lowest) suggesting malignant lesion

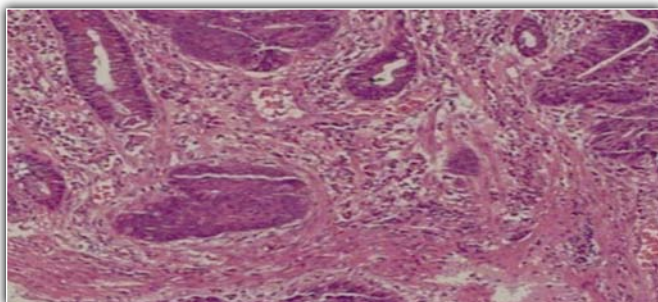


**Fig. 19** Histopathological image of the case shown in Figure 17, showing moderately differentiated adenocarcinoma infiltrating the muscularis propria

The permeability surface area product and BV, which are respectively measures of capillary leak and functional vascular density, have been found to correlate with MVD in cancer fields (**Table 8**). The blood volume (BV), permeability surface area product reflects the main features of prostate cancer tumor vascularity which includes numerous and poorly formed vessels (high BV and MVD) with high permeability to macromolecules (high permeability surface area product), intermittent or unstable flow due to transient rises in already raised interstitial pressure (low BF value) and multiple arteriovenous shunts (low MTT values).

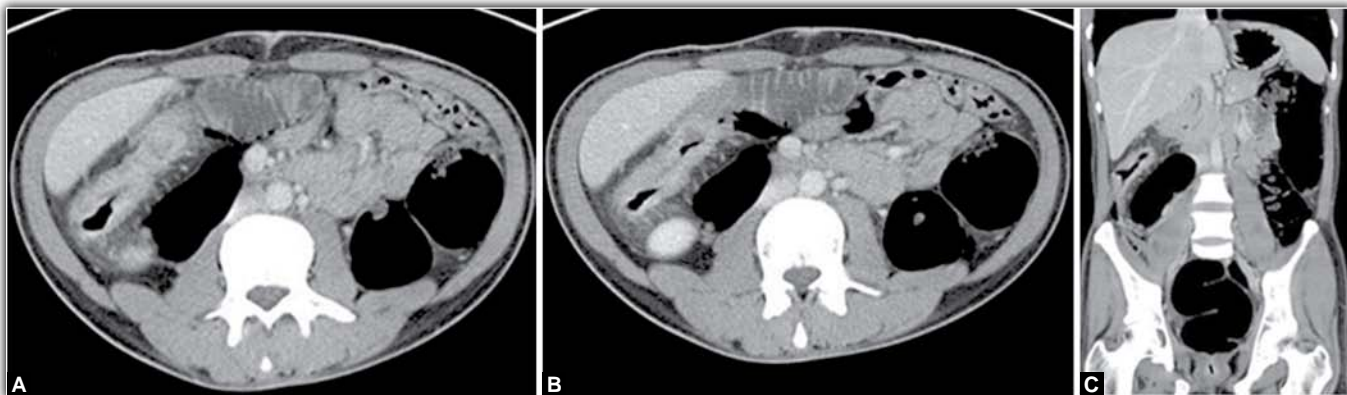
Thus quantitative assessment of microvessel density by CT perfusion may have a role in the detection of prostate cancer, metastasis, stage of disease and disease specific

**Table 6** Perfusion values in rectal tumors and in normal rectum<sup>71</sup> means+/-standard deviations

Perfusion parameter	Tumors	Normal rectum	P value
Blood flow (mL/100 g/min)	60.33+/-29.13	31.02+/-15.55	0.02
Blood volume (mL/100 g)	3.78+/-1.01	3.38+/-1.59	0.25
Mean transit time (sec)	9.51+/-4.43	16.98+/-4.27	0.002
Permeability-surface area product (mL/100 g/min)	17.36+/-4.64	17.33+/-7.45	0.49

**Table 7** Perfusion values in rectal cancer before and after therapy<sup>71</sup> mean+/-standard deviation

Perfusion parameter	Before therapy	After therapy	P value
Blood flow (mL/100 g/min)	62.57+/-26.50	23.36+/-13.18	0.001
Blood volume (mL/100 g)	3.58+/-1.18	2.83+/-1.09	0.10
Mean transit time (sec)	8.40+/-3.55	17.09+/-6.89	0.003
Permeability-surface area product (mL/100 g/min)	16.99+/-5.58	15.12+/-5.67	0.25



**Figs 20A to C** CECT axial (A and B) and coronal (C) images show circumferential mural thickening in the hepatic flexure and the ascending colon with luminal narrowing and an abrupt transition. The thickened bowel wall is homogeneously enhanced. This was misinterpreted as malignant lesion—case of tuberculous colitis

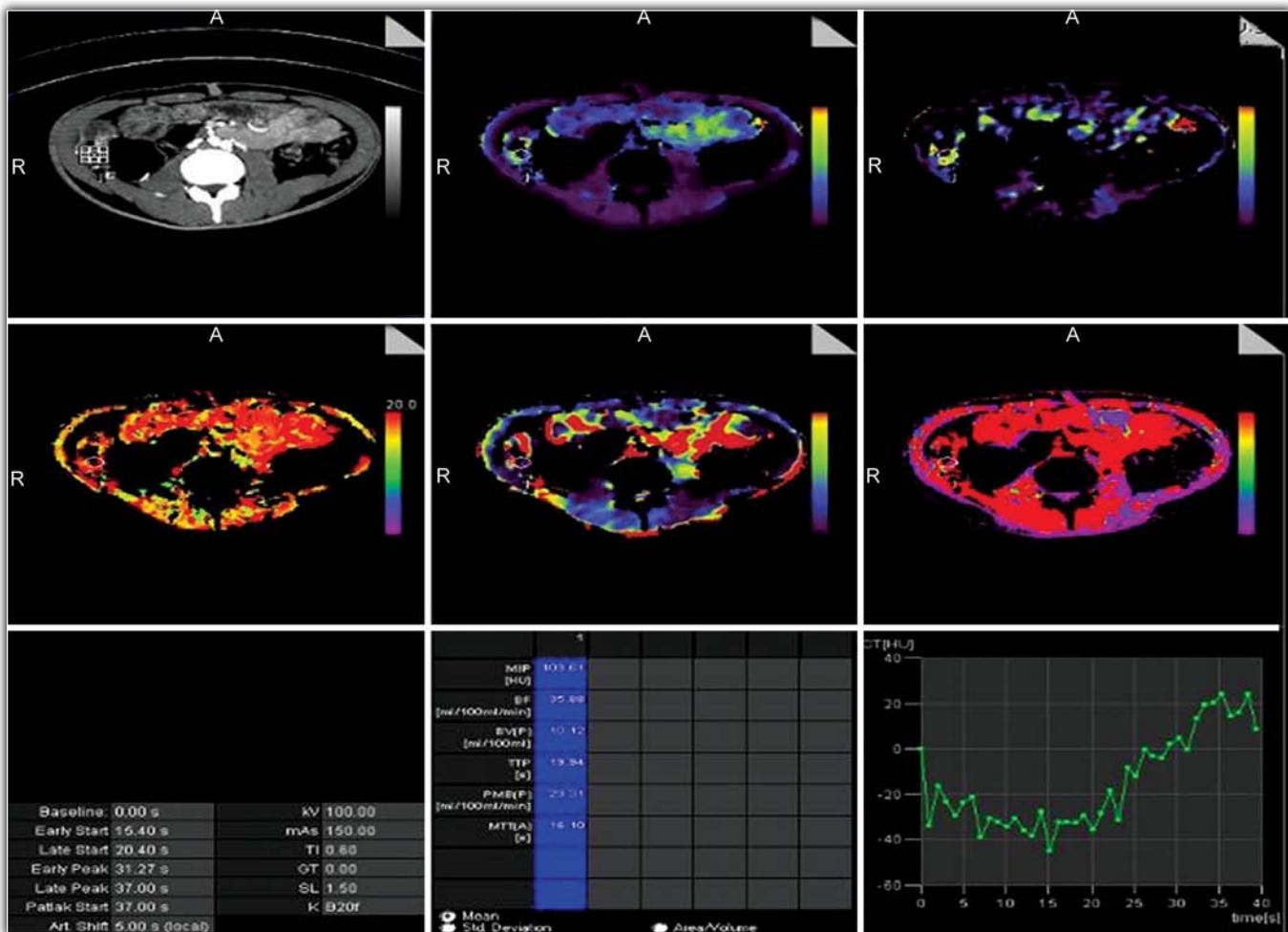
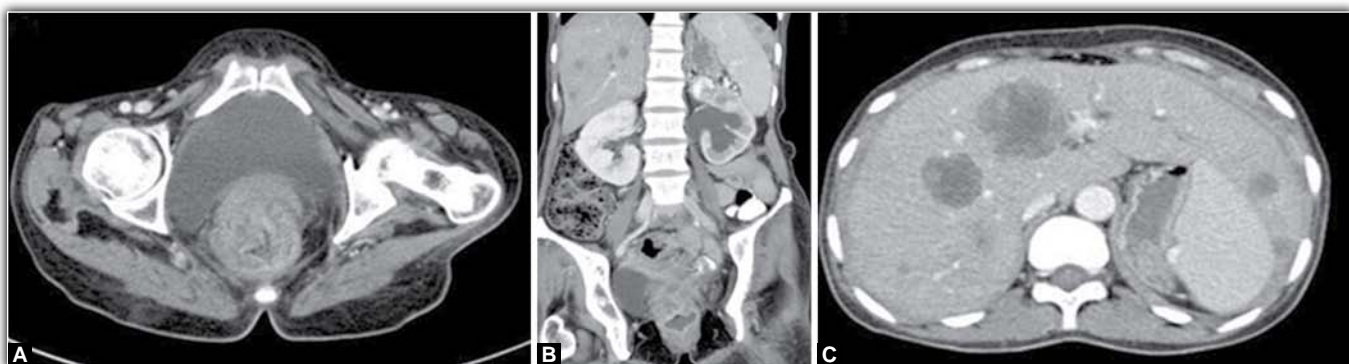


**Fig. 21** CT perfusion study shows borderline values of BF 35.8 mL/100 g/min, BV 10.1 mL/100 g, PMB 20 mL/100 g/min and MTT of 16.1 seconds from the ROI drawn over the lesion. Histopathology revealed tuberculous colitis



**Figs 22A to C** CECT axial (A) and coronal (B) images show irregular bowel wall thickening of the rectum and sigmoid colon with luminal narrowing and surrounding fat stranding. Heterogeneous enhancement is noted. Coronal MPR image (B) in addition shows left hydronephrosis. CECT axial image through the liver (C) shows multiple round heterogeneously hypodense lesions of varying sizes in the right and left lobe of liver—case of mucin secreting adenocarcinoma recto-sigmoid with hepatic metastases

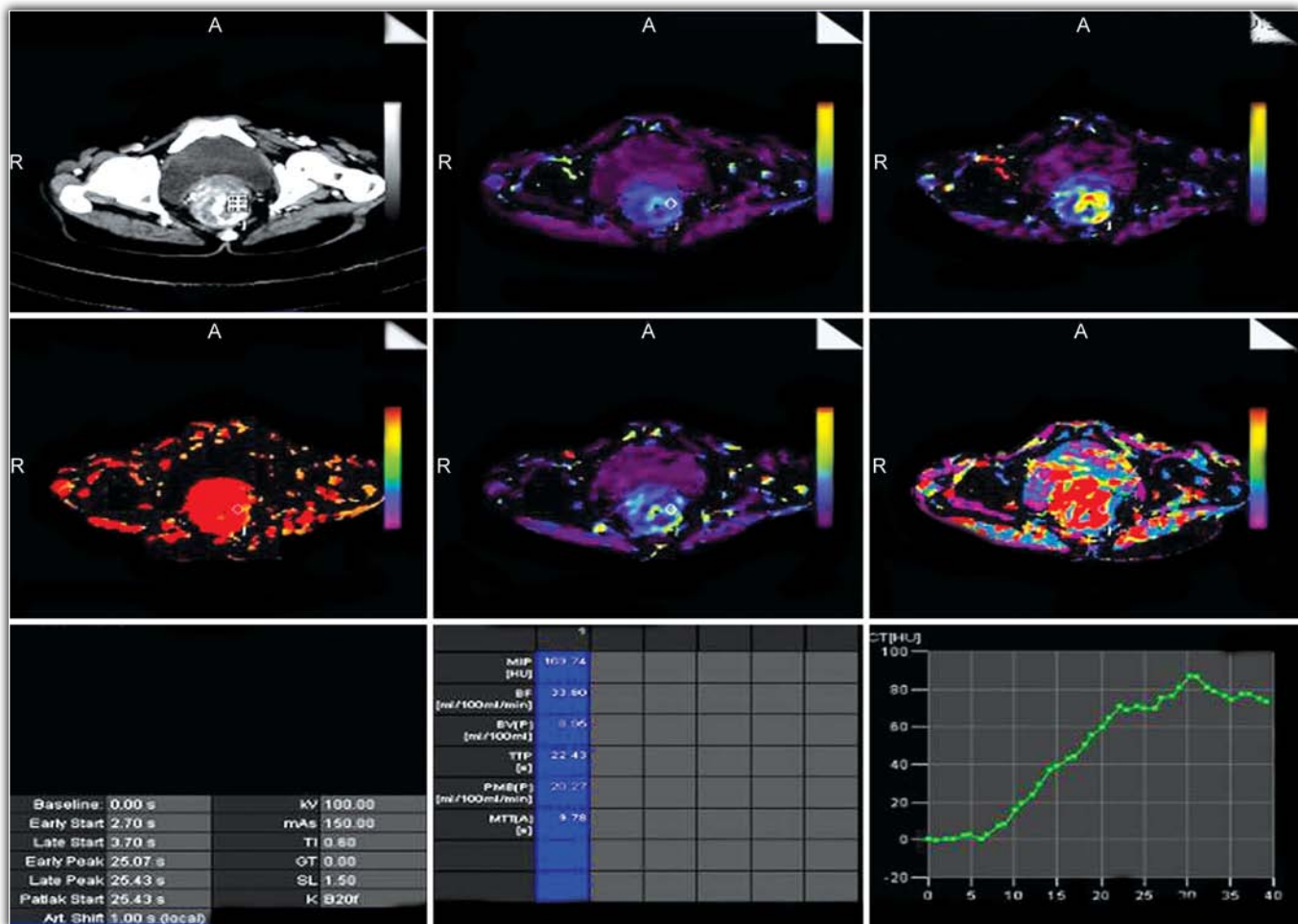


**Fig. 23** ROI placed over the lesion (same case as in Fig. 22) shows high blood flow of 33.8 mL/100 g/min, blood volume of 9 mL/100 g, permeability of 20.3 mL/100 g/min and short MTT of 9.8 seconds suggesting malignant lesion

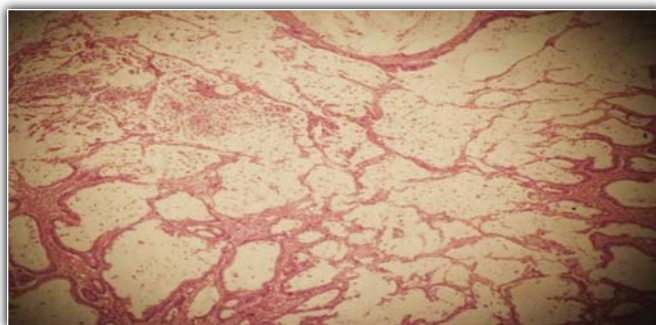


**Fig. 24** Histopathological image of the case shown in Figure 20, shows extracellular mucin pool with intermingled atypical cells s/o mucin secreting adenocarcinoma

survival. It can accurately predict and localize tumor volume preoperatively and may be useful for selecting and guiding therapy for prostate cancer. It may provide baseline values (particularly BV and permeability surface area product) that



**Fig. 25** Contrast enhanced CT image shows a diffusely enlarged prostate with homogeneous enhancement and maintained fat planes. Note is made of Foley's catheter *in situ*—case of benign prostatic hyperplasia

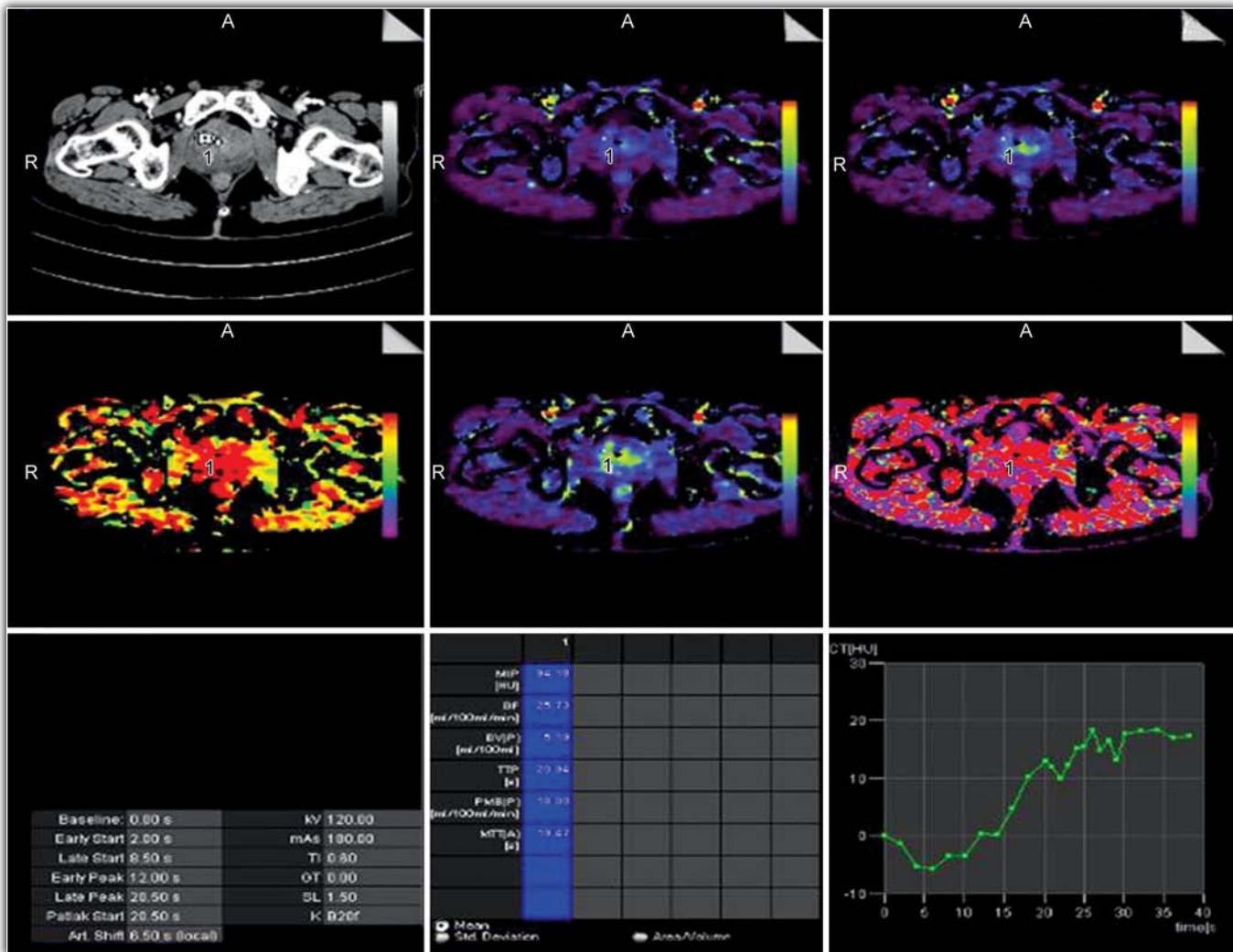


**Fig. 26** CT perfusion maps in case of benign prostatic hypertrophy reveals prostatic perfusion values within normal limits

**Table 8** Perfusion CT parameters and histologic parameters in different prostatic tissues<sup>77</sup>

Histologic diagnosis	CT perfusion					Histology	
	Blood flow	Blood volume	Mean transit time	Permeability surface area product	Mean microvascular density	Mean vascular area	
Prostate cancer (n=196)	18.36	8.45	19.19	26.34	70.78	0.0184	
Benign prostatic hyperplasia (n = 461)	19.49	6.21	18.74	18.67	64.96	0.0171	
Chronic prostatitis (n = 285)	19.67	4.94	16.24	18.08	54.91	0.0244	
Healthy fields (n = 504)	20.32	5.44	16.37	19.93	60.51	0.0159	

may be well suited for monitoring tumor response to radiation therapies or to antiangiogenic agents such as bevacizumab, docetaxel and prednisone.<sup>78</sup> Perfusion CT data may also be used for targeted radiotherapy for tumor foci with minimal radiation to the surrounding tissue. It may also be used for future delineation of intraprostate subvolumes for intensity modulated radiation therapy which is difficult to do with parametric maps of DE-MRI. It may also have a role in the development of a 3D perfusion CT computer aided diagnosis (CAD) system for the detection of prostate cancer.

### CT PERFUSION IN LYMPHOMA

Aggressive lymphomas are characterized by both a high metabolic turnover and a rather pronounced vascularity of tumor masses, whereas less aggressive lymphomas show a lower level metabolism and are generally considered to be less vascularized.<sup>79</sup> Metabolic activity is readily appreciated by <sup>18</sup>F-FDG PET imaging in these diseases, whereas vascular characteristics, such as perfusion and vessel wall permeability are detectable mainly by volume perfusion CT, dynamic contrast-enhanced (DCE) MRI, and DCE ultrasound. Contrast-enhanced volume perfusion CT measures changes in tissue density over time by using repeated CT scans of the volume being analyzed.

Subtypes of non-Hodgkin lymphomas are characterized by a differing microscopic ultrastructure and a complex and variable vascularity, sometimes even within the same tumor lesion. These differences in histopathologic microarchitecture may lead to distinctive perfusion traits that may enable a differentiation between lymphoma entities.<sup>80</sup> Mean BF, BV and K<sup>trans</sup> (transit constant) values have been found significantly higher in follicular lymphoma than in diffuse large cell lymphoma pointing towards distinct vascular properties due to differences in vascular microstructure and histopathologic lymphoma architecture. Mean BF values of 43.5+/-5.6 mL/100 mL/min and mean BV values of 9.5+/-2.3 mL/100 mL are seen in follicular lymphoma while in diffuse large B cell lymphoma the mean BF was 28.8+/-2.4 mL/100 mL/min and mean BV 4.6+/-0.5 mL/100 mL.<sup>80</sup> This is of particular relevance in patients with nonaggressive lymphomas, such as follicular lymphoma or chronic lymphocytic leukemia, which may show a transformation into high-grade lymphomas.<sup>81</sup> The use of perfusion imaging in lymphoma as a potential surrogate parameter of therapy response and early detection of transformation may allow tailoring treatment regimens accordingly.

Active lymphoma showed an increase in perfusion compared with inactive lymphoma and progression from inactive to active disease showed an increase in perfusion on serial evaluation.

### CT PERFUSION IN BRAIN TUMORS

Brain tumors are an important cause of mortality and morbidity, hence, an early diagnosis and accurate characterization is necessary (Fig. 27). Malignant brain tumors, of which gliomas are the most common primary neoplasm in adults, are very heterogeneous tumors. They are characterized by neovascularity and increased angiogenic activity resulting in higher proportion of immature and hyperpermeable vessels. High-grade gliomas can be highly invasive and extremely vascular tumors. Two of the most important factors in determining the malignancy of gliomas are their ability to infiltrate the brain parenchyma and to recruit or synthesize vascular networks for further growth (i.e. neoangiogenesis). Presently, brain tumor grading is based on the histopathological assessment of the tumor by stereotactic biopsy or cytoreductive surgery, which has inherent limitations due to sampling and its interpretation.

Histologic evaluation of tumor angiogenesis by using various markers such as microvascular density, microvascular cellular proliferation, and total vascular area is limited by this regional heterogeneity, and its confounding effect is worsened by its small size and limited number of samples obtained with surgical biopsy. These limitations can result in inaccurate classification and grading of gliomas due to sampling errors. Brain tumor angiogenesis is a continuously evolving process that can also be affected by various treatment modalities. Hence, there is a need for noninvasive *in vivo* clinical imaging tools that can study perfusion in the entire tumor which can be used to assess much larger volumes than small biopsy samples, and can probably guide biopsy and excision sites for better results.

Perfusion CT, which has also been used recently for glioma grading, provides a linear relationship between tissue attenuation and tissue concentration of a contrast agent, unlike perfusion MR imaging. Hence, it probably provides a more robust and less biased estimation of hemodynamic (tumor blood volume) and physiologic (tumor vascular leakiness) parameters. In addition, due to the wider availability, faster scanning times, and low cost compared with MR perfusion, perfusion CT is potentially well suited to study brain tumors and could potentially be useful as an easy clinical tool for quantitative estimates of perfusion parameters and their use as imaging biomarkers (Figs 28 and 29).<sup>82</sup>

In perfusion CT study for cerebral neoplasms conducted in our department, grade IV tumors show highest mean CBF as well as the highest mean CBV. Glioblastoma multiforme showed mean CBF value of 133.51, mean CBV value of 7.44 and mean permeability values of 15.15 (Figs 30 and 31). The normalized perfusion values observed in GBM were mean nCBF of 4.96, mean nCBV of 3.76 and mean nTTP of 0.85.

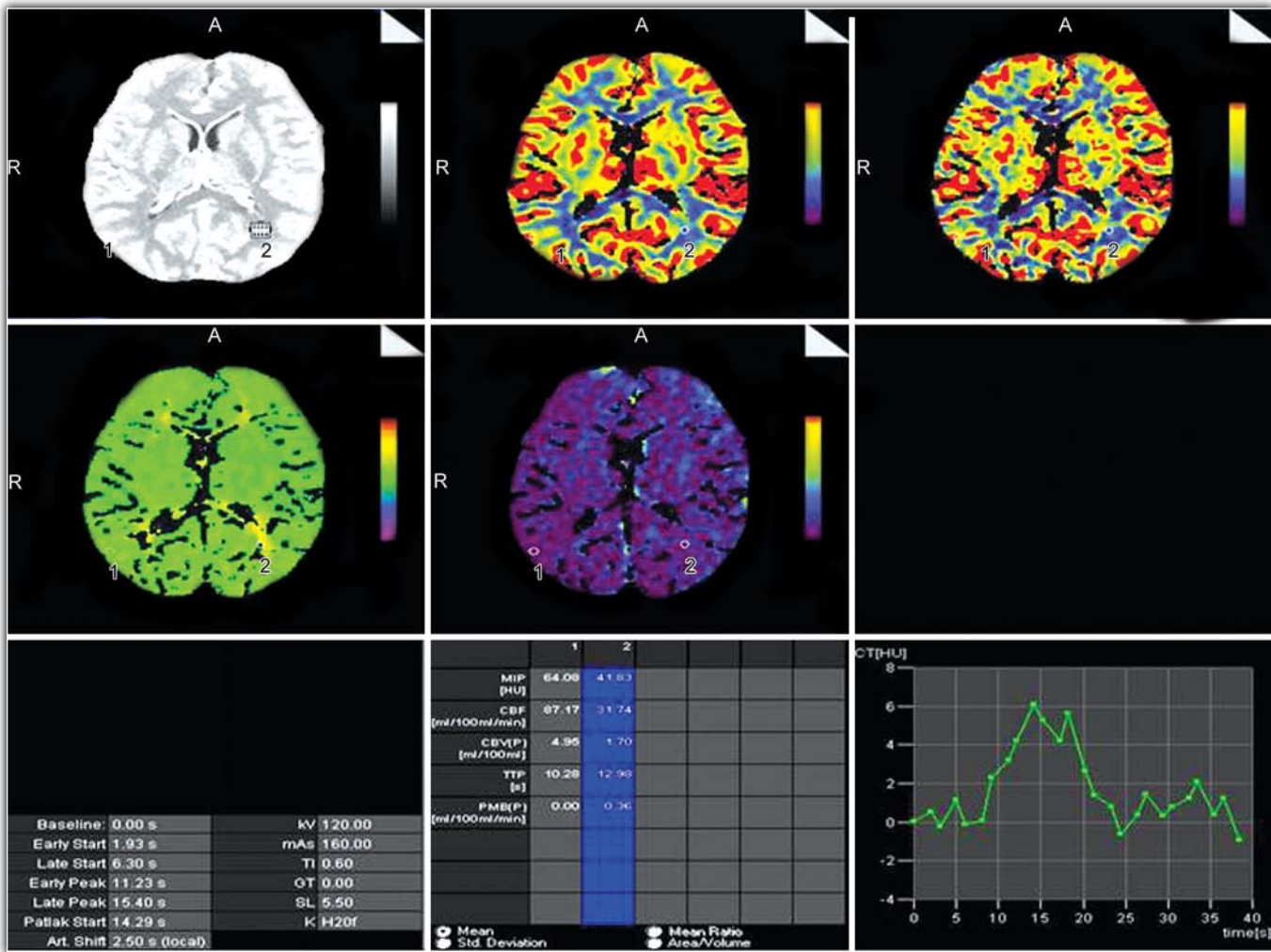


**Fig. 27** Perfusion CT maps of normal cerebral parenchyma, i.e. CBF (top middle), CBV (top right), TTP (middle left), PMB (middle). Note the scale on the right side of the maps depicting the lowest values in violet and highest values in red. The normal gray matter and basal ganglia appear yellow to red on color coded maps of CBF and CBV while normal white matter appears blue. On PMB maps normal brain appears violet indicating intact blood brain barrier. Perfusion values through the normal white matter in this case (ROI 2) are CBF of 31.74, CBV of 1.70, TTP of 12.98 and PMB of 0.36. The extreme right lower graph indicates the time attenuation curve through the ROI

Perfusion values were highest in GBM among astrocytomas. The correlation for CBF and CBV with tumor grade is better in astroglial tumors as compared to oligodendroglial tumors and is hypothesized to be due to the fine capillary network typically observed in oligodendroglomas. Mean value of PMB was seen to show progressive increment with increasing grade of tumors irrespective of histologic subtype (Figs 32 and 33).

### CT PERFUSION IN HEAD AND NECK TUMORS

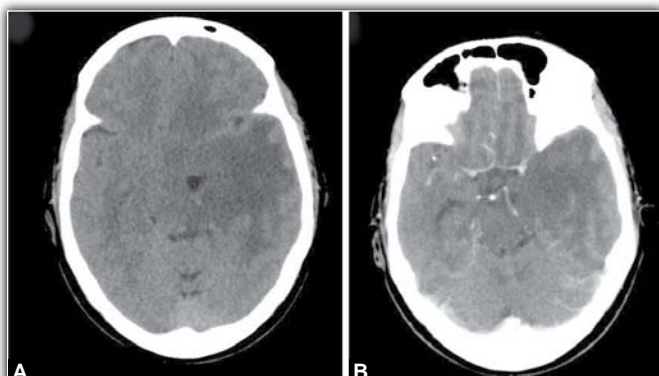
Perfusion CT is being used in the evaluation of head and neck tumors (Fig. 34). Benign tissues show lower BF and BV and longer MTT compared with malignant tissue (Figs 35 and 36).<sup>65</sup> It has been seen that squamous cell

carcinoma shows substantially increased BF, BV, PS and reduced MTT in comparison to adjacent normal tissues (Figs 37 and 38).

It has been found that tumors with lower perfusion values showed a poor response to induction chemotherapy. This is attributed to the presence of tissue hypoxia within the tumor which hinders the treatment delivery and therapeutic effect of chemoradiation.

### CT PERFUSION IN LUNG CANCER

Dynamic CT has been used for the characterization of solitary pulmonary nodules as benign or malignant based on the enhancement characteristics. Nodules with higher perfusion are more likely to be malignant. Multislice



**Figs 28A and B** Axial noncontrast CT (A) and contrast enhanced CT scans (B) show an ill defined hypodense lesion in the left temporal region showing minimal enhancement with mass effect and rotation of the brain stem—case of astrocytoma

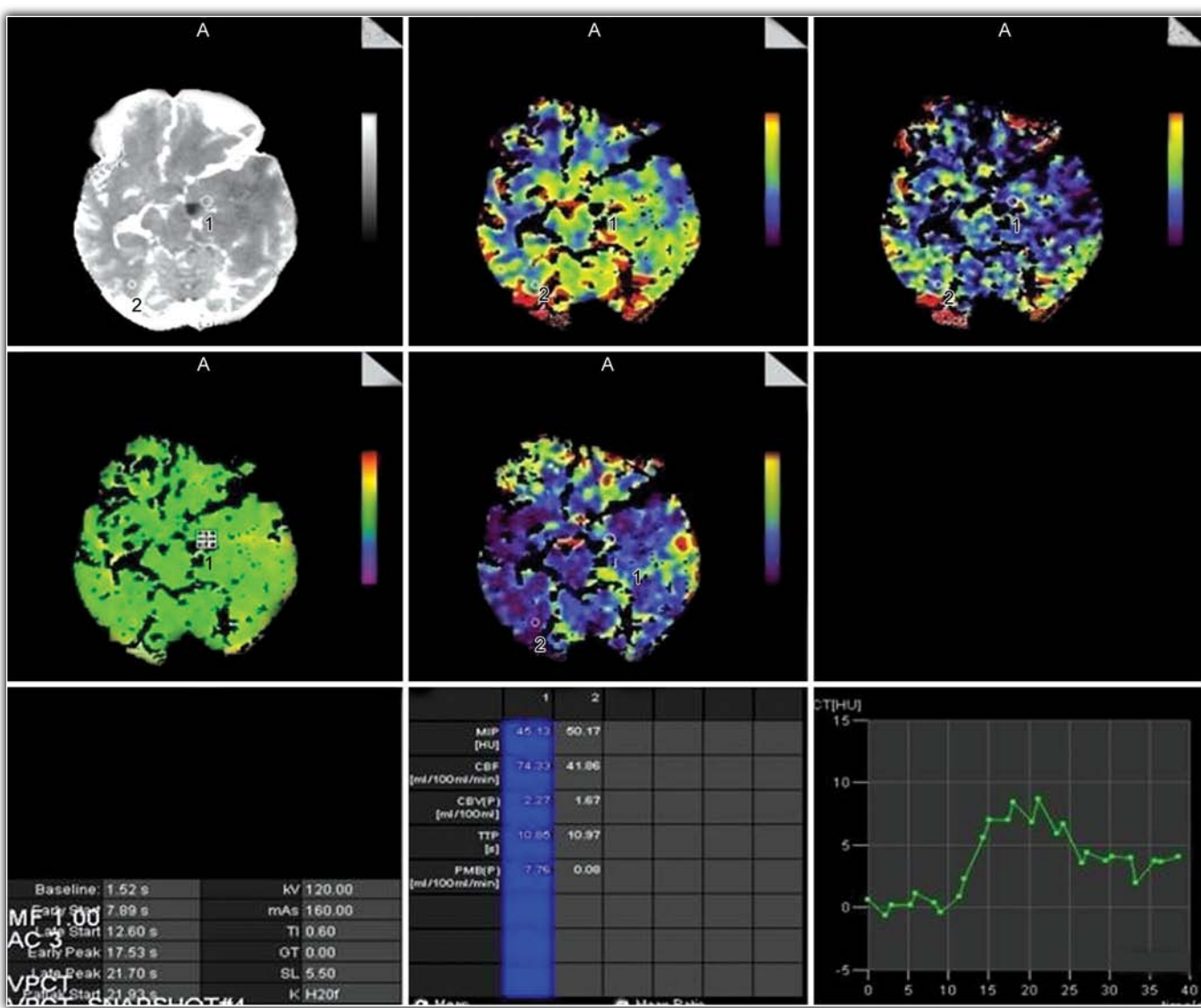
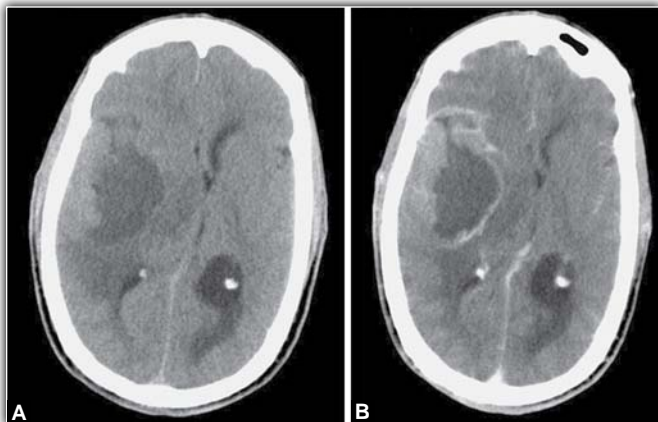


**Fig. 29** Perfusion maps show the lesion (same case as in Fig. 28) as an ill defined heterogeneous area. Perfusion values (ROI 1) from the lesion show mildly elevated perfusion parameters, i.e. CBF, CBV and permeability



**Figs 30A and B** Axial noncontrast (A) and contrast enhanced (B) CT scans showing a large heterogeneous mass lesion in the right temporoparietal region showing irregular peripheral enhancement and central nonenhancing necrotic areas with marked perilesional edema, midline shift and dilatation of contralateral ventricle—case of glioblastoma multiforme

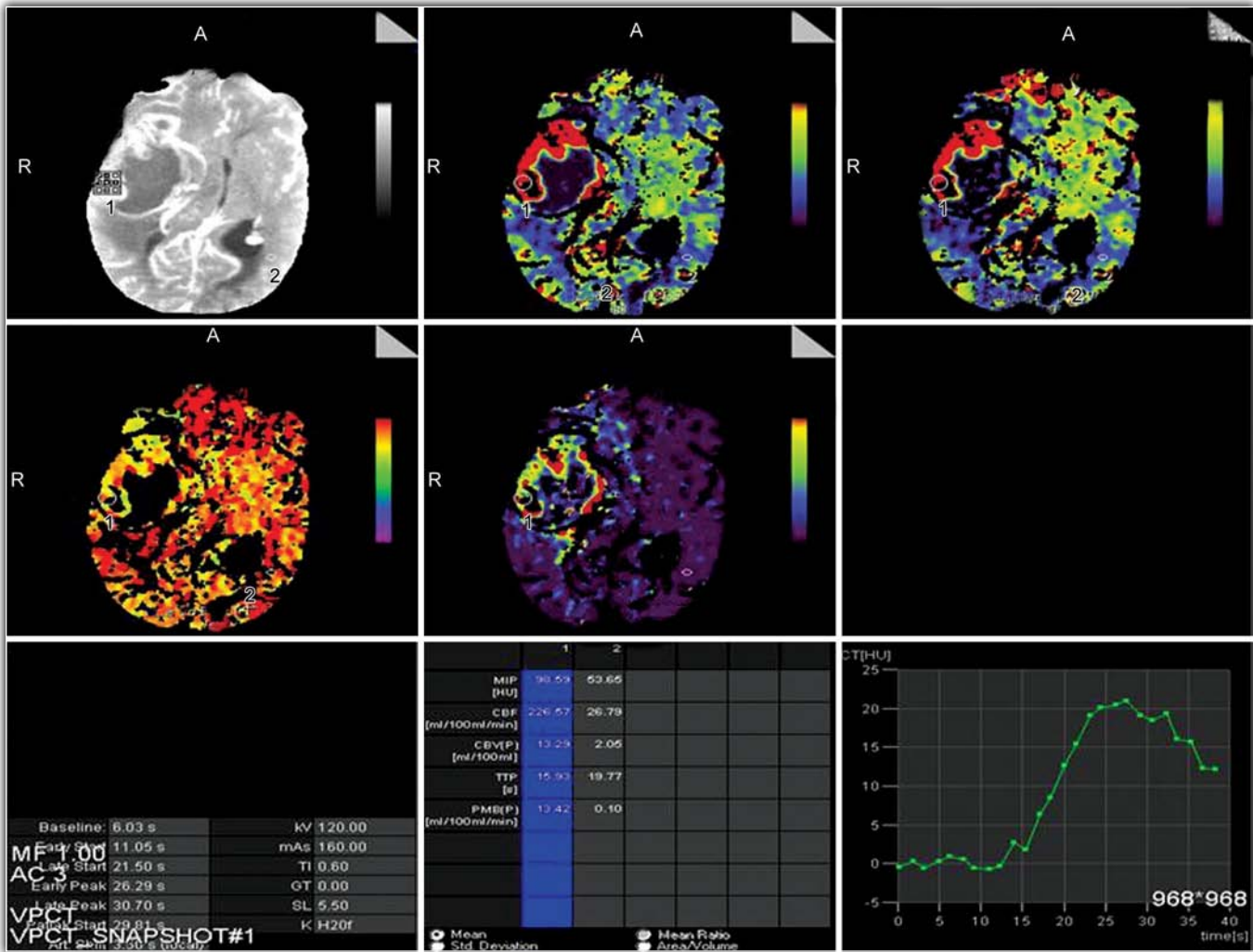


**Fig. 31** Perfusion CT maps (same case in Fig. 30) reveal markedly increased tumor blood flow of 226.57 mL/100 mL/min, blood volume of 13.29 mL/100 mL, PMB of 13.52 mL/100 mL/min, reduced TTP of 15.93s from the solid part of the lesion (ROI 1) suggesting significantly increased perfusion. The necrotic areas appear violet on perfusion maps suggesting absence of blood flow



**Figs 32A and B** In a known case of carcinoma of breast axial contrast enhanced scans shows well defined, small round lesions with moderate postcontrast enhancement in the left thalamus and left frontal region—case of cerebral metastases

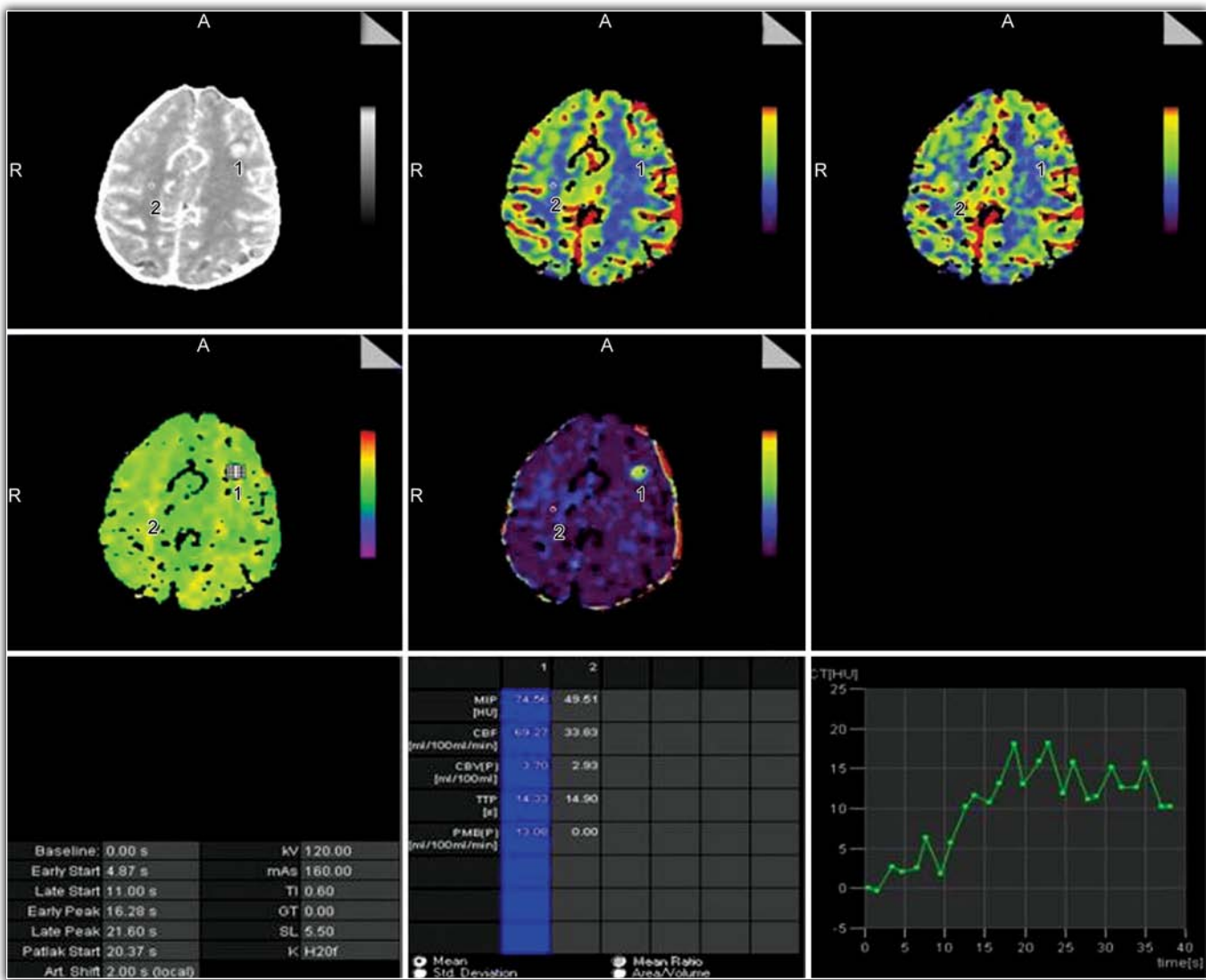


**Fig. 33** In perfusion CT image (same case as in Fig. 32) the frontal lesion is seen as a well defined area showing increased perfusion appearing green against the background of normal cerebral parenchyma which appear violet to blue

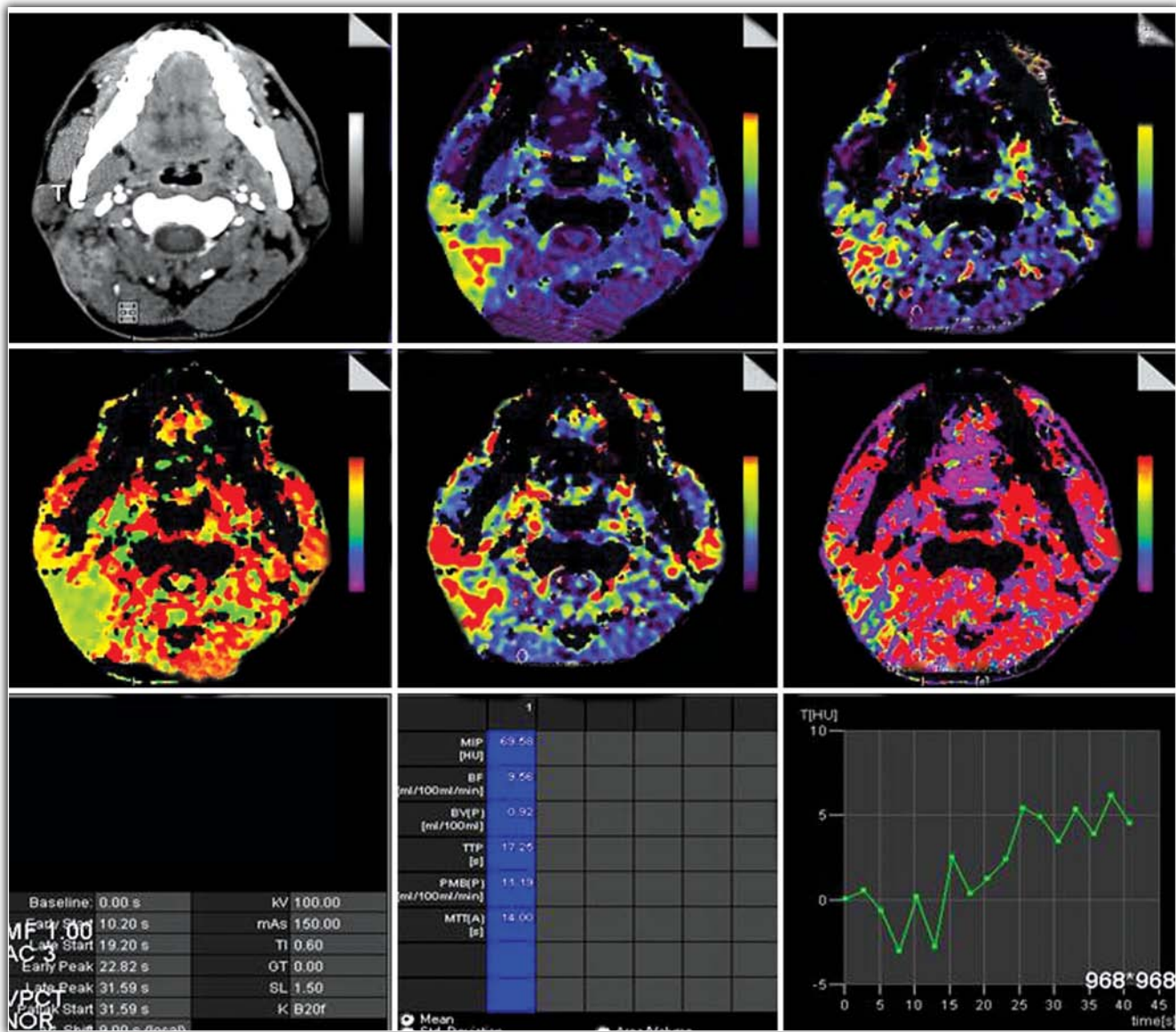
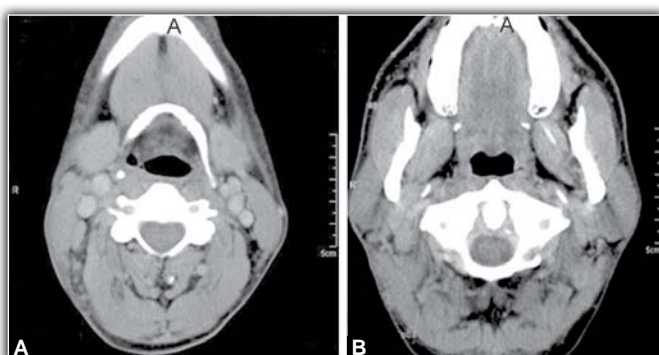
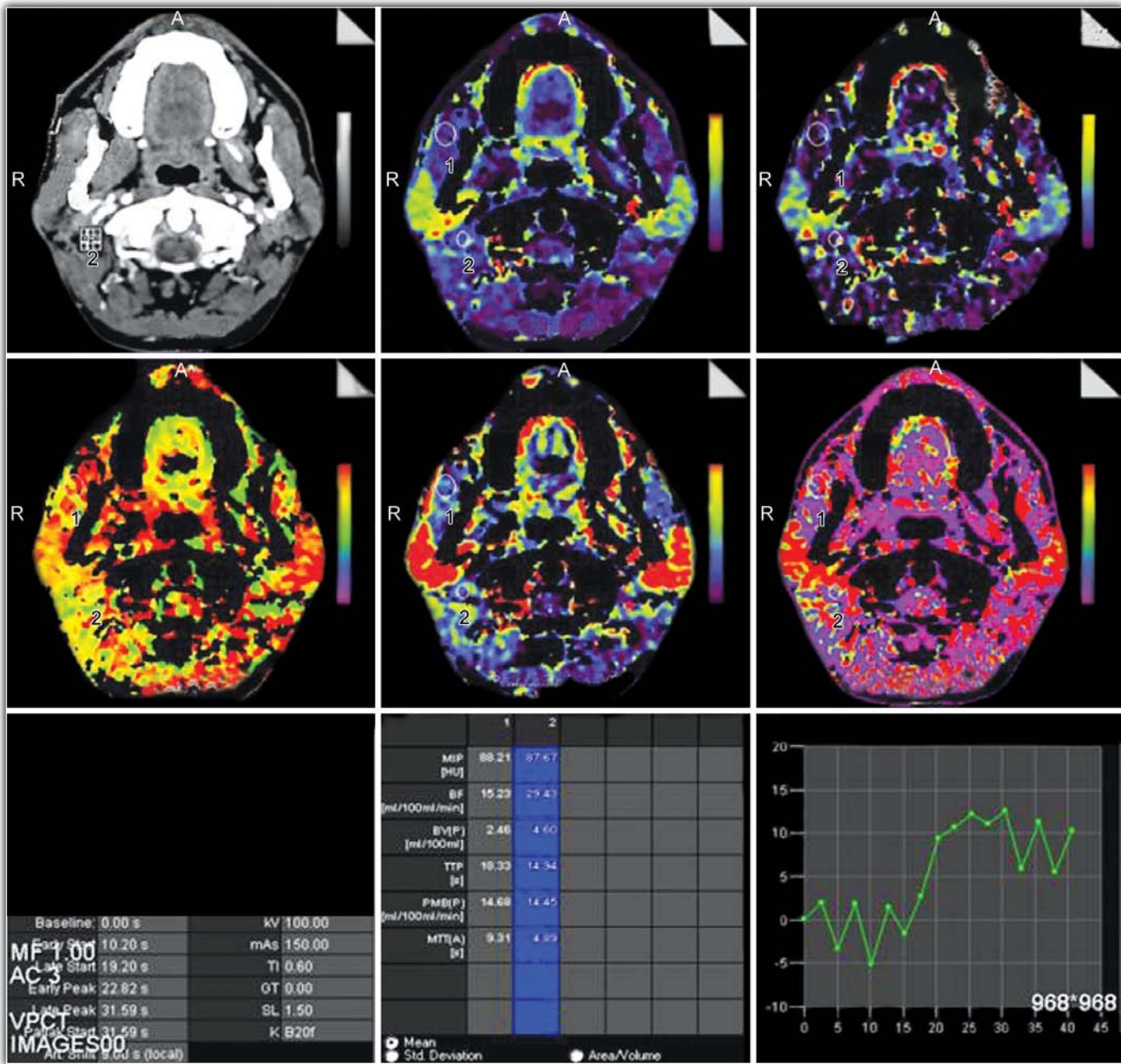


**Fig. 34** Perfusion CT map shows color maps for blood flow (BF), blood volume (BV), mean transit time (MTT) and (PMB) generated by software, in which every pixel is assigned a color that represents a numeric value for the perfusion parameter calculated for that voxel. High numeric values are represented by color shades of yellow and red, and low numeric values are represented by color shade of blue—normal perfusion CT of neck



**Figs 35A and B** Axial contrast enhanced CT scan at the level of hyoid bone (A) and at the level of atlas vertebra (B) shows multiple hypodense lymph nodes along the jugular chain—tubercular lymphadenitis



perfusion CT is also helpful to differentiate lung cancer from benign lung masses. BV, BF and PS were all found to be higher in malignant than benign masses. When BV  $\geq 5$  mL/100 mg was set as a diagnostic threshold, the sensitivity, specificity, positive predictive value and negative predictive value were 96 percent, 78 percent, 92 percent, 87 percent respectively.<sup>83</sup>

Whole tumor perfusion analysis is technically feasible with 64 or higher detector row CT. High blood volume (BV) has been observed in lung tumoral zone indicative of the presence

of numerous vessels.<sup>84</sup> Moreover, these areas also show a high capillary permeability, i.e.  $K^{trans}$ , a well known characteristic of tumoral vessels. Perfusion CT enables quantitative and qualitative assessment of lung tumor neovascularization. It is also a noninvasive tool for providing predictive and prognostic parameters in patients with lung cancer and for monitoring chemotherapy. Perfusion CT of pulmonary metastasis has potential in the assessment of early vascular changes that result from laser induced thermotherapy

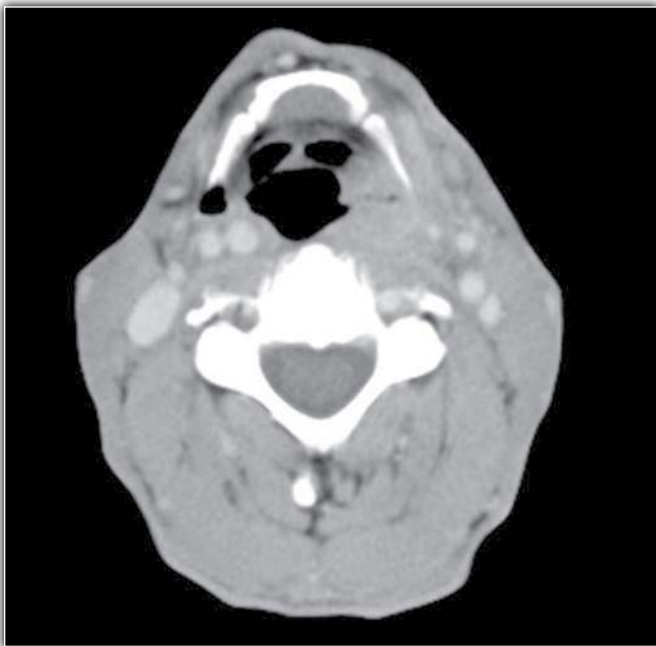


**Fig. 37** Axial contrast enhanced CT scan of the neck at the level of the hyoid bone shows an ill defined heterogeneous enhancing mass lesion involving supraglottic larynx on the left side—case of squamous cell carcinoma larynx (well-differentiated)

(LITT) and predicting technical success immediately after treatment.<sup>85</sup> Tumors with perfusion measurements that do not change after therapy indicate progressive disease.

## OTHER APPLICATIONS

### Nephrology

Dynamic CT has been used to study the relative glomerular filtration rate and to determine the relative function of each kidney. The iodinated contrast agents used for computed tomography (CT) are filtered at the glomerulus and not reabsorbed by the tubules. They can thus measure physiological indices such as contrast clearance per unit volume, which is closely related to glomerular filtration rate per unit renal volume of kidney. In normal kidneys clearance/volume averaged  $0.49+/-0.11$  mL/min/mL.<sup>86</sup> In patients with renovascular hypertension attributable to unilateral renal artery stenosis perfusion CT was capable of distinguishing renal stenosis with and without preserved perfusion. It also has a role in the differentiation of rejection as compared to other causes of dysfunction in transplant kidneys.

### Chronic Liver Diseases

Chronic liver diseases include chronic hepatitis, liver fibrosis and cirrhosis. Liver biopsy is considered the gold standard to assess the degree of liver cirrhosis. CT perfusion can show the

pathological changes in the liver before cirrhosis, even at the early stage of fibrosis and it can make noninvasive assessment of the degree of chronic liver disease.

It has been reported that total liver perfusion (TLP) is decreased in patients with cirrhosis and non-cirrhotic chronic liver disease while HPI and MTT are increased. The hepatic perfusion indices of patients without liver disease were significantly lower than that of those with child B and C liver disease. The best cutoff point to differentiate patients with cirrhosis from those without cirrhosis was considered a MTT of 22.6 second with both sensitivity and specificity of 81 percent.<sup>87</sup> It has been reported that hepatic blood flow decreases with the severity of chronic liver disease. The perfusion changes as estimated by perfusion CT correlate well with the severity of liver chronic disease and this has implications in the follow-up of patients who have chronic liver disease.

### CT Perfusion in Liver Transplantation

It is important to evaluate noninvasive liver perfusion after liver transplantation. CT perfusion can monitor the tendency of hemodynamic changes in portal vein and hepatic artery, contributing to the early diagnosis of blood vessel complications after transplantation.

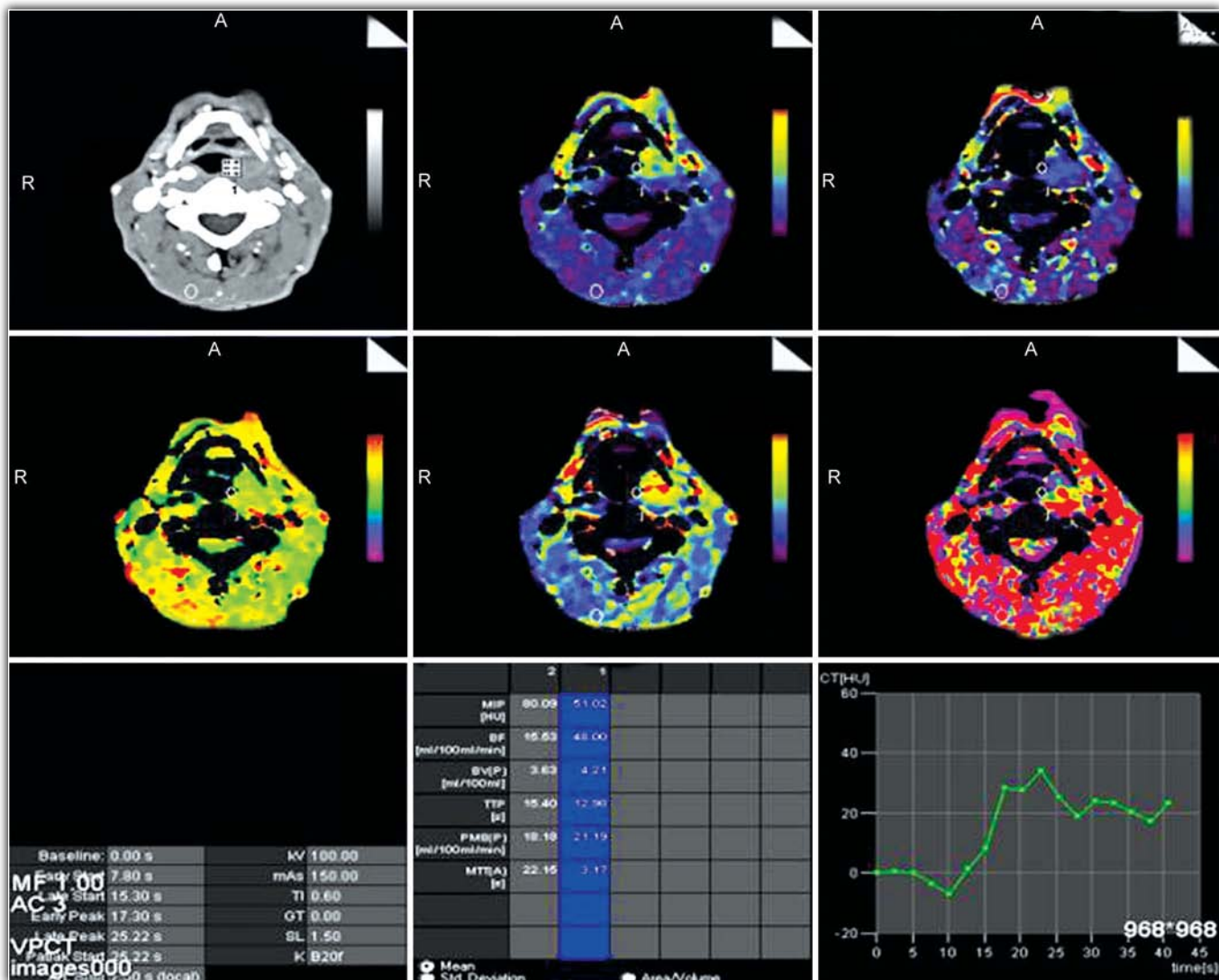
Some studies showed changes in hepatic artery perfusion (HAP), while some in portal venous perfusion (PVP) and total liver perfusion (TLP). Authors hold that it is related to the selection of patients, and examination time after the transplantation, etc. Therefore, hemodynamic change after transplantation is dynamic process, and different patients have different hemodynamic characteristics.

### Acute Pancreatitis

In acute pancreatitis perfusion CT has been found to have a sensitivity and specificity of 100 percent and 95.3 percent respectively in detection of pancreatic ischemia.<sup>88</sup> Areas with pancreatic ischemia showed a reduction in perfusion values. Compared with normal pancreas identification of these areas can help to predict the later development of pancreatic necrosis. The early detection of pancreatic necrosis allows early institution of intensive care and improves prognosis.

### RADIATION ISSUES

A major concern of perfusion CT is the risk for exposure to ionizing radiation, especially in patients who require serial perfusion studies for monitoring treatment effects. Several techniques, including reduced tube current and tube potential can be employed to reduce radiation dose. Likewise, protocol modifications involving the use of higher temporal sampling rates, such as scanning every 2 to 3 seconds instead of 1 second during the first pass and limiting



the scan duration of cine acquisition to 40 to 50 seconds, can substantially minimize the radiation exposure from each examination without compromising the data. Likewise, tailoring the perfusion CT protocol to the clinical objective or the relevant parameters can also diminish the radiation dose to the patient. For example, in clinical situations requiring tissue perfusion parameters like BF or MTT, it would be prudent to perform only the first pass study.<sup>65</sup>

## CONCLUSION

Perfusion CT has achieved great strides as a functional technique since its inception and its scope in the clinical and research settings is increasing. With the advancement in perfusion software and the development of new generation

of scanners having a wider cine acquisition, it has allowed even single or multiple organ perfusions with the advantage of decreased radiation exposure and motion artifacts. Moreover, the integration of positron emission tomography (PET) CT systems with the prospect of combining perfusion measurements with PET data represents an exciting new innovative technology that has a wide range of clinical application as a single examination. Development of new contrast agents which remain longer in intravascular compartment may also overcome the complexities of physiological modeling. Thus, perfusion CT which was primarily introduced as a research tool has emerged as a definitive functional technique not only in patients of stroke but also in oncology and other areas.

## REFERENCES

1. Mikes KA. Perfusion imaging with computed tomography: brain and beyond. *Eur Radiol.* 2006;16(suppl 7):M37-43.
2. Ma SH, Le HB, Jia BH, et al. Peripheral pulmonary nodules: relationship between multislice spiral CT perfusion imaging and tumor angiogenesis and VEGF expression. *BMC Cancer.* 2008;8:186.
3. Perini R, Choe R, Yodh AG, et al. Noninvasive assessment of tumor neovasculature: technique and clinical applications. *Cancer Metastasis Rev.* 2008;27:615-30.
4. Miles KA. Perfusion CT for the assessment of tumor vascularity: which protocol? *BJR.* 2003;76:S36-S42.
5. Harvey C, Rooho A, Morgan J, et al. Imaging of tumor therapy response by dynamic CT. *Eur J Radiol.* 1999;30:221-6.
6. Miles KA. Tumor angiogenesis and its relation to contrast enhancement on computed tomography: a review. *Eur J Radiol.* 1999;30:198-205.
7. Miles KA, Charnsagavej C, Lee FT, et al. Application of CT in the investigation of angiogenesis in oncology. *Acad Radiol.* 2000;7:840-50.
8. Cao J, Yang A, Hong XY, et al. CT hepatic volume measurement combined with CT perfusion imaging in evaluating the hepatic functional reserve. *Zhong Nan Da Xue Xue Bao Yi Xue Ban.* 2007;32(3):422-6.
9. Sahani DV, Kawa SP, Hamberg LM, et al. Assessing tumor perfusion and treatment response in rectal cancer with multislice CT: initial observations. *Radiology.* 2005;234(3):785-92.
10. Goh V, Halligan S, Gartner L, et al. Quantitative colorectal cancer perfusion measurement by multidetector row CT: does greater tumor coverage improve measurement reproducibility? *Br J Radiol.* 2006;79(943):578-83.
11. Goh V, Halligan S, Hugill JA, et al. Quantitative assessment of colorectal cancer perfusion using MDCT: inter and intraobserver agreement. *AJR.* 2005;185(1):225-31.
12. Goh V, Halligan S, Hugill JA, et al. Quantitative colorectal cancer perfusion measurement using dynamic contrast enhanced multidetector row computed tomography: effect of acquisition time and implications for protocols. *J Comput Assist Tomogr.* 2005;29(1):59-63.
13. Koenig M, Kraus M, Theek C, et al. Quantitative assessment of ischaemic brain by means of perfusion related parameters derived from perfusion CT. *Stroke.* 2001;32:431-7.
14. Hoeffner EG, Case I, Jain R, et al. Cerebral perfusion CT: technique and clinical applications. *Radiology.* 2004;231:632-44.
15. Koenig M, Klolz E, Luka B, et al. Perfusion CT of the brain: Diagnostic Approach for Early detection of Ischaemic Stroke. *Radiology.* 1998;209:85-93.
16. Mayer TE, Hamman GF, Baranczyk J, et al. Dynamic CT perfusion imaging of acute stroke. *Am J Neuroradiol.* 2009;21:1441-9.
17. Klotz E, Konig M. Perfusion measurements of the brain: using dynamic CT for the quantitative assessment of cerebral ischaemia in acute stroke. *Eur J Radiol.* 1999;30:170-84.
18. Keith C, Griffiths M, Peterson B, et al. Computed tomography perfusion imaging in acute stroke. *Australas Radiol.* 2002;46:221-30.
19. Wintermark M, Flanders AE, Velthuis B, et al. Perfusion CT assessment of infarct core and penumbra: receiver operating characteristic curve analysis in 130 patients suspected of acute hemispheric stroke. *Stroke.* 2006;37:979-85.
20. Wintermark M. Brain perfusion CT in acute stroke patients. *Eur Radiol.* 2005;15(suppl 4):D28-D31.
21. De Lucas EM, Gutierrez A, Sanchez E, et al. CT protocol for acute stroke: Tips and Tricks for general Radiologists. *Radiographics.* 2008;28:1673-87.
22. Wintermark M, Reichart M, Thiran JP, et al. Prognostic accuracy of cerebral blood flow measurement by perfusion computed tomography at the time of emergency room admission in acute stroke patients. *Ann Neurol.* 2002;51:417-32.
23. Murayama K, Katada K, Nahane M, et al. Whole brain perfusion CT performed with a prototype 256 detector row CT system: initial experience. *Radiology.* 2009;250(1):202-11.
24. Lui YW, Tang ER, Allmendinger AM. Evaluation of CT perfusion in the setting of cerebral ischaemia: Patterns and Pitfalls. *AJNR.* 2010;31:1552-63.
25. Parsons MW. Perfusion CT: Is it clinically useful? *Int J Stroke.* 2008;3:41-50.
26. Allmendinger AM, Tang ER, Lui YW, Spektor V. Imaging of stroke: part I perfusion CT- overview of imaging technique, interpretation, pearls and common pitfalls. *AJR.* 2012;198:52-62.
27. Miles KA. Functional computed tomography in oncology. *Eur J Cancer.* 2002;38(16):2079-84.
28. Brawer MK, Deering RE, Brown M, et al. Predictors of pathologic stage in prostate carcinoma. The role of neovascularity. *Cancer.* 1994;73:678-87.
29. Fontanini Q, Lucchi M, Viganti S, et al. Angiogenesis as a prognostic indicator of survival in non small cell lung carcinoma: a prospective study. *J Natl Cancer Inst.* 1997;89:881-6.
30. Cuenod CA, Fournier L, Balvay D, et al. Tumor angiogenesis: pathophysiology and implications for contrast enhanced MRI and CT assessment. *Abdom Imaging.* 2006;31(2):188-93.
31. Phongkikarun S, Kobayashi S, Kan Z, et al. Quantification of angiogenesis by functional computed tomography in a Matrigel model in rat. *Acad Radiol.* 2003;13(suppl 5):M134-8.
32. Li WW. Tumor angiogenesis: molecular pathology, therapeutic targeting and imaging. *Acad Radiol.* 2007;(10):800-11.
33. Miles KA. Tumor angiogenesis and its relation to contrast enhancement on computed tomography: a review. *Eur J Radiol.* 1999;30:198-205.
34. Provenzale JM. Imaging of angiogenesis: clinical technique and novel imaging methods. *AJR.* 2007;188(1):11-23.
35. Miles KA. Functional CT imaging in urology. *Eur J Radiol.* 2003;13(suppl 5):M134-8.
36. Miles KA, Hayball MP, Dixon AK. Functional images of hepatic perfusion obtained with dynamic CT. *Radiology.* 1993;188:405-11.
37. Blomley MJ, Coulden R, Dawson P, Kormano M, Donlan P, Bufkin C, Lipton MJ. Liver perfusion studied with ultrafast CT. *J Comput Assist Tomogr.* 1995;19:424-33.
38. Weidekamm C, Cejna M, Kramer L, Peck-Radosavljevic M, Bader TR. Effects of TIPS on liver perfusion measured by dynamic CT. *AJR Am J Roentgenol.* 2005;184:505-10.
39. Zhou ZF, Huang HL, Xu B, Lin BJ, Liu ZH, Yang JY, Qiu YC. Clinic application with MSCT perfusion in liver tumor. *Linchuang Fangshexue Zazhi.* 2006;25:233-7.
40. Hashimoto K, Murakami T, Dono K, Hori M, Kim T, Kudo M, Marubashi S, Miyamoto A, Takeda Y, Nagano H, Umeshita K, Nakamura H, Monden M. Assessment of the severity of liver disease and fibrotic change: the usefulness of hepatic CT perfusion imaging. *Oncol Rep.* 2006;16:677-83.

41. Komemushi A, Tanigauwa N, Kojima H, et al. CT perfusion of the liver during selective hepatic arteriography: pure arterial blood perfusion of liver tumor and parenchyma. *Radiat Med.* 2003;21:246-52.
42. Ippolito D, Sironi S, Pozzi M, et al. Perfusion computed tomographic assessment of early hepatocellular carcinoma in cirrhotic liver disease: initial observations. *J Comput Assis Tomog.* 2008;32(6):855-8.
43. Chen WX, Min PQ, Sony B, et al. Single level dynamic spiral CT of hepatocellular carcinoma: correlation between imaging features and density of tumor microvessels. *World J Gastroenterol.* 2004;10:67-72.
44. Sahani DV, Holakere NS, Mueller PR, Zhu AX. Advanced hepatocellular carcinoma: CT perfusion of liver and tumor tissue – initial experience. *Radiology.* 2007;243:736-43.
45. Tsushima Y, Funabasama S, et al. Quantitative perfusion map of malignant liver tumors created from dynamic computed tomography data. *Acad Radiol.* 2004;11:215-23.
46. Zhong L, Wang WJ, Xu JR. Clinical application of hepatic CT perfusion. *World J Gastroenterol.* 2009;15(8):907-11.
47. Zhu AX, Holakere NS, et al. Early antiangiogenic activity of bevacizumab evaluated by computed tomography perfusion scan in patients with advanced hepatocellular carcinoma. *The Oncologist.* 2008;2:120-5.
48. Cuenod C, Leconte I, et al. Early changes in liver perfusion caused by occult metastasis in rats: detection with quantitative CT. *Radiology.* 2001;218:556-61.
49. Shi GF, Wang SJ, et al. Effect of perfusion CT scan on hepatic hemodynamic changes in rats with liver micrometastases. *Ai Zheng.* 2006;25:849-54.
50. Legget OA, Kelley BB, et al. Colorectal Cancer: diagnostic potential of CT measurements of hepatic perfusion and implications for contrast enhancement protocols. *Radiology.* 1997;205:716-20.
51. Glover C, Douse P, Kane P, et al. Accuracy of investigations for asymptomatic colorectal liver metastasis. *Dis Colon Rectum.* 2002;215(4):476-84.
52. Wang JY, Wang SQ, Chen L, et al. Application of CT perfusion imaging in discrimination of liver carcinoma and hemangioma. *Linchuang Ganden Bing Zazhi.* 2006;22:455-7.
53. Meijerunk M, Waesberghe JV, Weide LV, et al. Total liver volume perfusion CT using 3D image fusion to improve detection and characterization of liver metastasis. *Eur Radiol.* 2008;18:2345-54.
54. Perkins AC, Whalley DR, Ballantyne KC, et al. Reliability of the hepatic perfusion indices for the detection of liver metastasis. *Nucl Med Commun.* 1987;8(12):982-9.
55. Schima W, Ba-Ssalmah A, Kolbinger C, et al. Pancreatic adenocarcinoma. *Eur Radiol.* 2007;17:638-49.
56. Kandel S, Kloeters C, Meyer H, et al. Whole organ perfusion of the pancreas using dynamic volume CT in patients with primary pancreatic carcinoma: acquisition technique, post processing and initial results. *Eur Radiol.* 2009;19:2641-6.
57. Takeda K, Mikami Y, Fukuyama S, et al. Pancreatic ischemia associated with vasospasm in the early phase of human acute necrotizing pancreatitis. *Pancreas.* 2005;30:40-9.
58. Xu J, Liang J, Hao S, et al. Pancreatic adenocarcinoma: dynamic 64 slice helical CT with perfusion imaging. *Abdom Imaging.* 2009;34:759-66.
59. Lu N, Yuan X, Hao S, et al. 64 Slice CT perfusion imaging of pancreatic adenocarcinoma and mass forming chronic pancreatitis. *Acad Radiol.* 2011;18:81-8.
60. Mirecka J, Libura J, Libura M, et al. Morphological parameters of angiogenic response in pancreatic ductal adenocarcinoma- correlation with histological grading and clinical data. *Folia Histochem Cytobiol.* 2001;39:335-40.
61. Von Dobschuetz E, Pahernik S, Hoffman T, et al. Dynamic intravital fluorescence microscopy- a novel method for assessment of microvasculature permeability in acute pancreatitis. *Microvasc Res.* 2004;67:55-63.
62. Park MS, Klotz E, Kim MJ, et al. Perfusion CT: Noninvasive surrogate marker for stratification of pancreatic cancer response to concurrent chemo and radiation therapy. *Radiology.* 2009; 250:110-7.
63. Assignies G, Couvelard A, Bahrami S, et al. Pancreatic endocrine tumors: tumor blood flow assessment with perfusion CT reflects angiogenesis and correlates with prognostic factors. *Radiology.* 2009;250(2):407-16.
64. Falconi M, Plockinger U, Kwekkeboom DJ, et al. Well differentiated pancreatic non functioning tumors/carcinomas. *Neuroendocrinology.* 2006;84:196-211.
65. Kambadakone A, Sahani DV. Body perfusion CT: technique, clinical applications and advances. *Radiol Clin N Am.* 2009; 47:161-78.
66. Li ZP, Meng QF, Sun CH, et al. Tumor angiogenesis and dynamic CT in colorectal carcinoma: radiologic pathologic correlation. *World J Gastroenterol.* 2005;11(9):1287-91.
67. Takebayashi Y, Akiyama S, Yamada K, et al. Angiogenesis as an unfavourable prognostic factor in human colorectal carcinoma. *Cancer.* 1996;78:226-31.
68. Goh V, Bartram S, Halligan S. Effect of intravenous contrast agent volume on colorectal cancer vascular parameters as measured by perfusion computed tomography. *Clin Radiol.* 2009;64:368-72.
69. Willett CG, Boucher Y, di Tomaso E, et al. Direct evidence that VEGF specific antibody bevacizumab has antivascular effects in human rectal cancer. *Nat Med.* 2004;10:145-7.
70. Bellomi M, Petralia C, Sonzogni A, et al. CT perfusion for the monitoring of neoadjuvant chemotherapy and radiation therapy in rectal carcinoma: initial experience. *Radiology.* 2007; 244:486-93.
71. Sahani DV, Kalva SP, Hamberg LM, et al. Assessing tumor perfusion and treatment response in rectal cancer with multislice CT: initial observations. *Radiology.* 2005;234:785-92.
72. Goh V, Halligan S, Taylor SA, et al. Differentiation between diverticulitis and colorectal cancer: quantitative CT perfusion measurements versus morphologic criteria- initial experience. *Radiology.* 2007;242(2):456-62.
73. Wu GY, Ghimire P. Perfusion computed tomography in colorectal cancer: protocols, clinical applications and emerging trends. *World J Gastroenterol.* 2009;15(26):3228-31.
74. Kerbel RS. Tumor angiogenesis. *N Eng J Med.* 2008;358:2039-49.
75. Goh V, Halligan S, Daley F, et al. Colorectal tumor vascularity: Quantitative assessment with multidetector CT- do tumor perfusion measurements reflect angiogenesis? *RSNA 2008.*
76. Ives EP, Burke MP, Edmonds PR, et al. Quantitative computed tomography perfusion of prostate cancer: correlation with whole mount pathology. *Clin Prostate Cancer.* 2005;4:109-12.

77. Osimani M, Bellini D, Cristofano C, et al. Perfusion MDCT of prostate cancer: correlation of perfusion CT parameters and immunohistochemical markers of histogenesis. *AJR.* 2012;199:1042-8.
78. Harvey CJ, Blomley MJ, Dawson P, et al. Functional CT imaging of the acute hyperimmune response to radiation therapy to the prostate gland: early experience. *J Comput assist Tomogr.* 2001;25:43-9.
79. Ruan J, Hajjar K, Raji S, et al. Angiogenesis and antiangiogenic therapy in non-Hodgkin's lymphoma. *Ann Oncol.* 2009;20:413-24.
80. Spira D, Adam P, Linder C, et al. Perfusion and flow extraction product as potential discriminators of untreated follicular and diffuse large B cell lymphoma using volume perfusion CT with attempt at histopathological explanation. *AJR.* 2012;198:1239-46.
81. Nogai H, Dorken M, Lenz G. Pathogenesis of non-Hodgkin's lymphoma. *J Clin Oncol.* 2011;29:1803-11.
82. Jain R. Perfusion CT imaging of brain tumors: an overview. *AJNR.* 2011;32:1570-7.
83. Jie RB, Ming-jun H, Xue H, et al. CT perfusion imaging in solitary pulmonary nodule. *Chinese Journal of Medical Imaging Technology.* 2004-06.
84. Tacelli N, Jardin MR, Copin MC, et al. Assessment of non small cell lung cancer: pathologic CT correlation in 15 patients. *Radiology.* 2010;257(3):863-71.
85. Hegenschede K, Behrendt N, Rosenberg C, et al. Assessing early vascular changes and treatment response after laser induced thermotherapy of pulmonary metastasis with perfusion CT: initial experience. *AJR.* 2010;194:1116-23.
86. Tsushima Y. Functional CT of the kidney. *Eur J Radiol.* 1999;30:191-7.
87. Beers BE, Leconte I, Materne R, et al. Hepatic perfusion parameters in chronic liver disease: dynamic CT measurements correlated with disease severity. *AJR.* 2001;176:667-73.
88. Bize PE, Platon A, Becker C, et al. Perfusion measurements in acute pancreatitis using dynamic perfusion CT. *AJR.* 2006;186:114-8.

## Section

# 3

# Advances in Magnetic Resonance Imaging

- Chapter 7** ● MR Instrumentation: An Update  
*Anjali Prakash*
- Chapter 8** ● Image Optimization in MRI  
*Jyoti Kumar*
- Chapter 9** ● Diffusion Weighted MRI  
*Devasenathipathy Kandasamy, Raju Sharma*
- Chapter 10** ● Functional MR: Perfusion and Dynamic Contrast-enhanced MRI  
*Niranjan Khandelwal, Sameer Vyas*
- Chapter 11** ● MR Angiography  
*Ajay Kumar, Sameer Vyas, Naveen Kalra*
- Chapter 12** ● MRI Pulse Sequences: An Evolution  
*Vivek Gupta, Niranjan Khandelwal*



## Chapter

# 7

# MR Instrumentation: An Update

*Anjali Prakash*

An MR image represents the relative response of specific nuclei to absorbed radiofrequency energy. The Dutch physicist CJ Gorter<sup>1</sup> first proposed the NMR concept in 1936, which was furthered by the work of Block and Purcell. They were awarded the Nobel Prize for Physics in 1952. Between 1950s and 60s, it was used primarily as an analytical tool for chemists and physicists to determine the chemical structure, configuration and reactive processes. Modern clinical use started after Paul Lauterbur's<sup>2</sup> suggestion in 1973, that operator controlled magnetic field gradients could be used to encode position dependent information in the NMR signal. MRI has been selected along with CT as example of the benefits to society of basic research in physics. In 2003, Paul Lauterbur and Sir Peter Mansfield received the Nobel Prize in medicine for their discoveries concerning magnetic resonance imaging.

The main constituents of an MRI scanner is the **magnet subsystem** which produces a spatial and temporally constant magnetic field  $B_0$ , the **gradient subsystem** to produce varying magnetic field gradients for spatial encoding, **RF subsystem** to transmit and receive radiofrequency  $B_1$  and the **computer and microprocessors** to specify and control the pulse sequence calculate, process, display, store and transfer the resultant clinical image. This includes an acquisition and control system, reconstruction system. There is viewing console for operator input of control parameters and display of imaging. In addition, magnetic and RF shielding is required. Patient table, hardware for physiological monitoring of patient (ECG and respiratory gating) and monitoring equipment is also needed<sup>3</sup> (**Figs 1 and 2**).

During imaging, patient is placed on the MRI table which brings the patient into strong magnetic field, such that the

anatomy to be imaged is in the region of maximum uniformity of the field—isocenter. The  $B_0$  field lines are aligned along the longest body axis—Z-axis. The other two short axes are X and Y-axis. A required scan is selected; the selected information is passed on to the gradient pulse generator that adjusts the amplitude and waveform of the three gradients. The gradient amplifier then increases the power required to drive the gradient coils to generate the gradient field strength required. RF transmission also starts with the host computer which sets the required  $B_1$  field frequency on the frequency synthesizer. Using an amplitude modulator, the carrier frequency is modulated into apodised fine pulses. The RF amplifier increases the power of the pulse from milliwatts to kilowatts, which is used to drive the RF transmit coil. The signal from the body is acquired with an RF receive coil which induces in it an alternating voltage of a few microvolts. After amplification by an RF amplifier (receiver), tuned to the resonant frequency, the amplitude or envelope of this signal is sampled, digitized and computer analyzed.

## THE MAGNET

The magnet is the key component of the MR scanner. It determines the appearance, cost and capacity of the device. The **strength of the magnet** is measured in tesla (T), research systems with a magnetic strength of  $9.4\text{ T}^4$  are available for use in humans. There are three types of magnets used in MRI—permanent magnets, resistive magnets and super conducting magnets.

The main magnetic field needs to be very **uniform or homogeneous** in terms of its strength and direction unaffected by ambient temperature. It defines a direction in

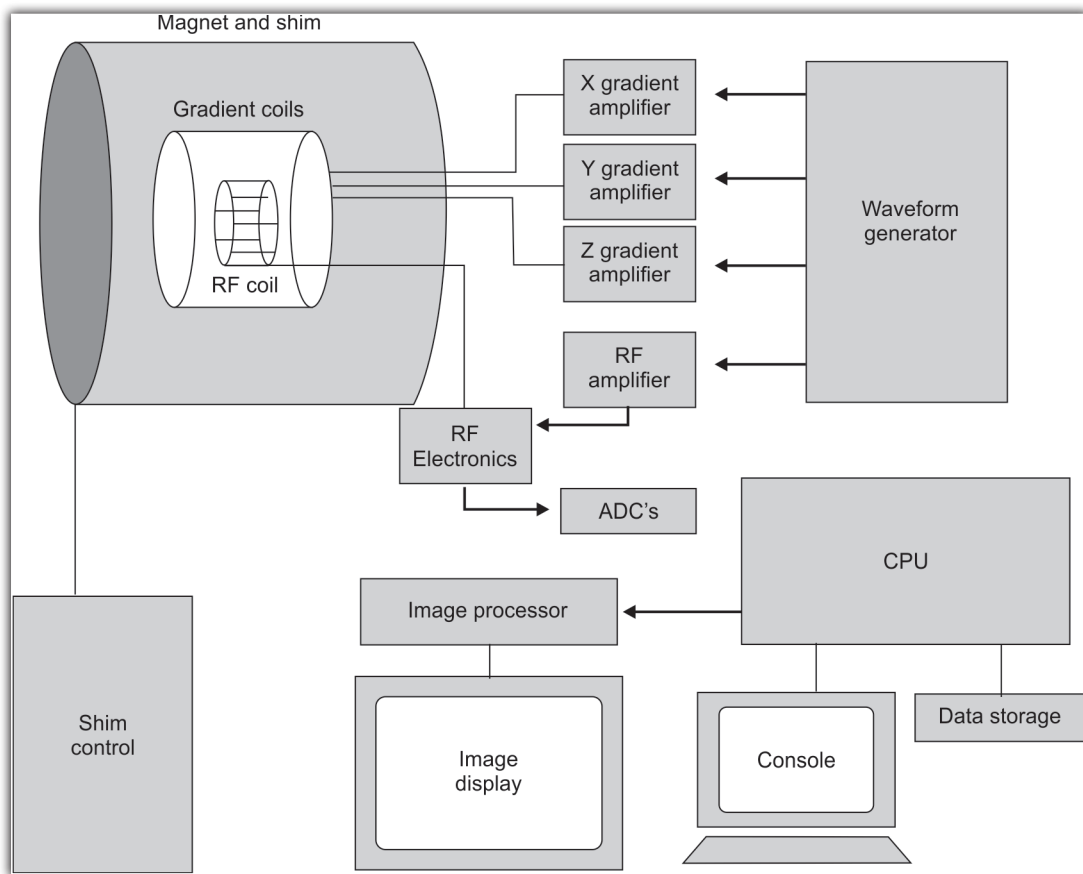


**Fig. 1** Various hardware components of MRI scanner

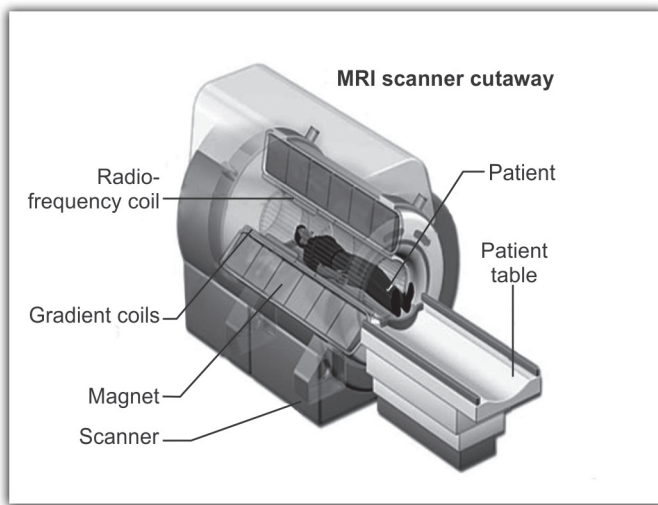


**Fig. 2** MRI scanner indicating position of various coils

space that is conventionally referred to as Z-direction. The Z-component of the main field at the center of the magnet is designated as  $B_0$ . Z-axis usually runs along the cylindrical

axis of the main magnet and in the direction from the patients head to feet (**Fig. 3**). Any variation of this longitudinal field  $B_z$  from its central value  $B_0$  has a significant effect on motions of spin system. Consequently, the design of the main field coils is chosen to minimize variations in the strength of the  $B_0$  field over the desired region of imaging. The straightness of magnetic lines within the center needs to be perfect. Within a specified region called **diameter spherical volume (DSV)** the field is uniform with a typical magnetic flux variation of 5 ppm for imaging and 1 ppm for spectroscopy. A main magnet with DSV positioned at **magnet isocenter** is called a symmetric magnet. In an asymmetric (open bore) magnet, DSV is shifted a certain distance away from the isocenter towards one end of the magnet. The magnet should have a bore size large enough to accommodate the patient. Open bore magnet allows better patient access, and helps claustrophobic patients.

The magnetic field lines form closed loops and crowd together within a solenoid but spread widely outside it as **'fringe' field**. This effect is reduced by an iron shroud weighing many tonnes or by additional shimming coils. The fringe fields are negligible in a permanent magnet, being concentrated in the iron yoke. Patients with pacemakers need to be kept away from areas where stray fields are greater

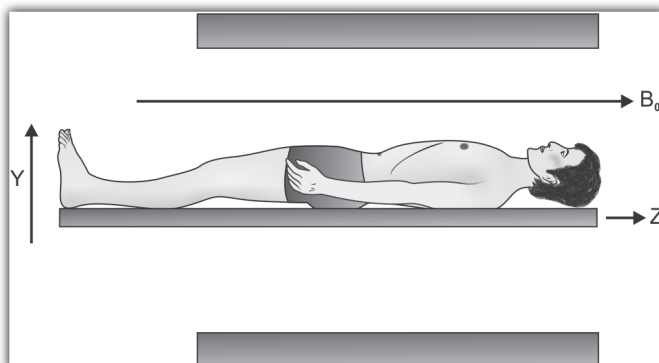


**Fig. 3** Schematic depiction of the Z-axis along the main magnetic field  $B_0$

than 0.5 mT (5 gauss line). This defines the controlled area for safety purposes around MRI installations. Siting of the machine should be done away from steel girders and reinforced concrete, which may become manifested in the fringe field (Fig. 4).

**Permanent magnet:** It consists of two opposing flat faced magnetized pole pieces fixed to an iron frame. The materials used are iron and alloys of aluminum, nickel and cobalt. Once magnetized, these maintain magnetization indefinitely without power input. Permanent magnets require no power input, and cannot be shut down. They provide low strength (0.3 T or less), vertical fields.

Permanent magnets are very heavy up to 80 to 100 tonnes. Running costs are relatively less. Permanent magnet systems are used for claustrophobic patients, children, obese adults and interventional procedures. These are constructed as open access configuration unlike solenoid magnets.

A newer magnetic alloy of iron neodymium and boron has been described which are of lower weight, with higher strength. Other materials used are metallic alloy alnico, ceramic barium ferrite and rare earth alloy samarium cobalt ( $\text{SmCO}_3$ ).<sup>5</sup>

**Resistive magnet:** This is a set of DC coils with copper or aluminum conductors, in which the magnetic field is generated by passage of electric current through a wire. It requires 50 to 100 KW of stable power supply to produce a homogenous magnetic field. The heat produced is removed by cooling water pumped rapidly through the hollow coils. The vertical or horizontal magnetic field is limited by heating to 0.5 T and has significant fringe fields. It can be switched off at the end of day or in an emergency setting. It takes 15 to 30 minutes to re-establish the magnetic field. It is cheapest and smallest, weighing only 2 tonnes. Resistive magnets have a limited role, these days.

**Hybrid magnets:** Combine feature of more than one basic type. Magnet may include both a set of permanent magnet and a set of electric coils to achieve a stronger magnetic field.

### PREPOLARIZED MRI

In 2001, a research team at Stanford University invented a new technique called prepolarized MRI/PMRI.<sup>6</sup> They demonstrated that two magnets can be used together, one strong, but not very uniform and the other very homogeneous, but not so strong. The magnet that is strong produces a strong magnetic field which varies in uniformity by as much as 40 percent. A second magnet produces a more precise magnetic field. These magnets can be ordinary copper wound magnets, lowering cost. As the magnetic field is “tuned” by the second magnet, a PMRI scan can be obtained adjacent to a metal implant.

### Superconducting Magnet

Superconductivity is a property of materials, such that they lose electrical resistance at very low temperatures. Examples of such materials are some metals (Hg) and alloys—niobium/titanium, niobium/tin and vanadium/gallium. It takes many hours for the superconducting state to be reached and the current to build up. Then the coil is short circuited and power source switched off. Once energized, the current continues in a loop as long as superconducting temperature is maintained. The current continues to flow, while using no power like permanent magnets, they require no external power source once it is energized.

A superconductive electromagnet is a DC solenoid about 1 m in diameter, commonly made of niobium-titanium alloy in a copper matrix (Fig. 5). This becomes superconducting at 10° Kelvin and the magnet is operated at temperature maintained by a cryogen-liquid helium at 4°K (-269°C/-452°F). The length of the superconducting wire in the magnet is several miles long; this length of the wire has to be constructed without interruption of its superconducting properties. The magnet is immersed in a liquid helium vessel called the cryostat—Dewar (at 4.2 K with ~1700 L of liquid helium) which is surrounded by liquid nitrogen at 77.4 K. This creates a temperature gradient from the magnet core to the surrounding room to minimize thermal energy losses and stabilizes the internal core temperature. The expensive liquid helium is replenished periodically as the cryogens boil off due to heat leaks. The coldhead is used for minimizing the helium boil-off and to recondense some helium vapor back into the liquid bath. The heat which reaches the cryo shields of the magnet is absorbed and passed via the coldhead to an external heat exchanger which is part of the refrigerator system. A rhythmical thud that is heard in the system while it is not acquiring images is due to the operation of helium refrigeration pump (Fig. 6). The coldhead must be in permanent operation.

In newer designs, the liquid nitrogen has been replaced by a cryogenic refrigerator with the cooling lines going to the cold head in the liquid helium. This eliminates the need to add liquid nitrogen and increases the hold time of liquid helium.<sup>3,7-9</sup>

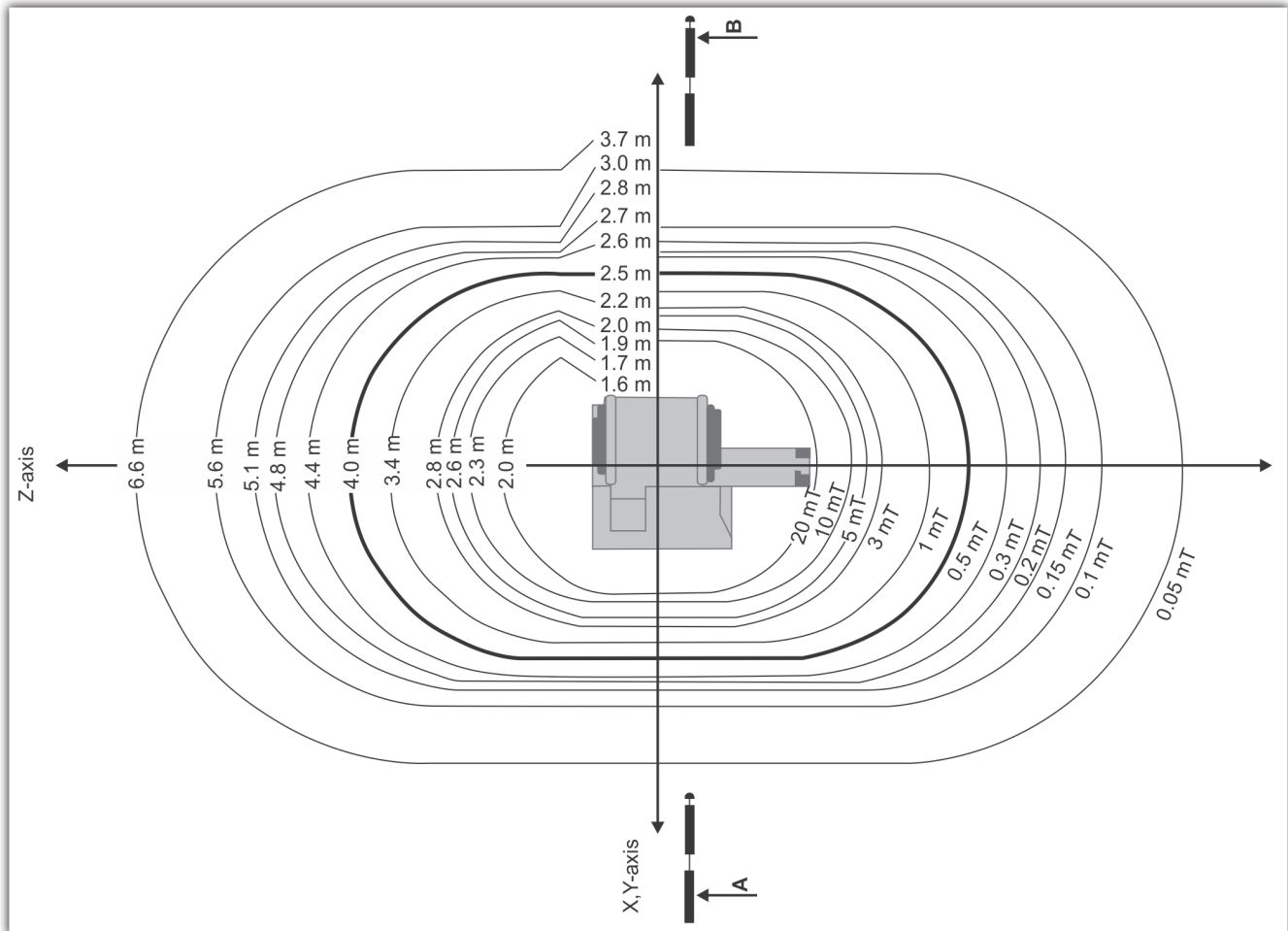


**Fig. 4** Fringe field around the MR scanner. The 0.5 mT (5 Gauss) line is marked in bold

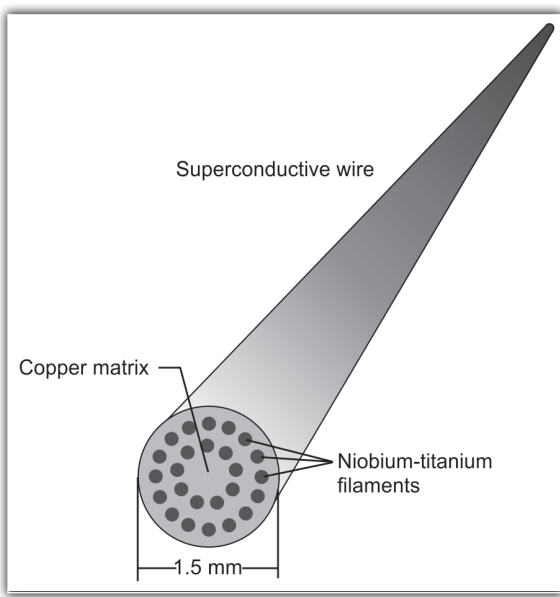


**Fig. 5** Cut section of a superconductive wire made of Niobium-titanium alloy imbedded in copper matrix

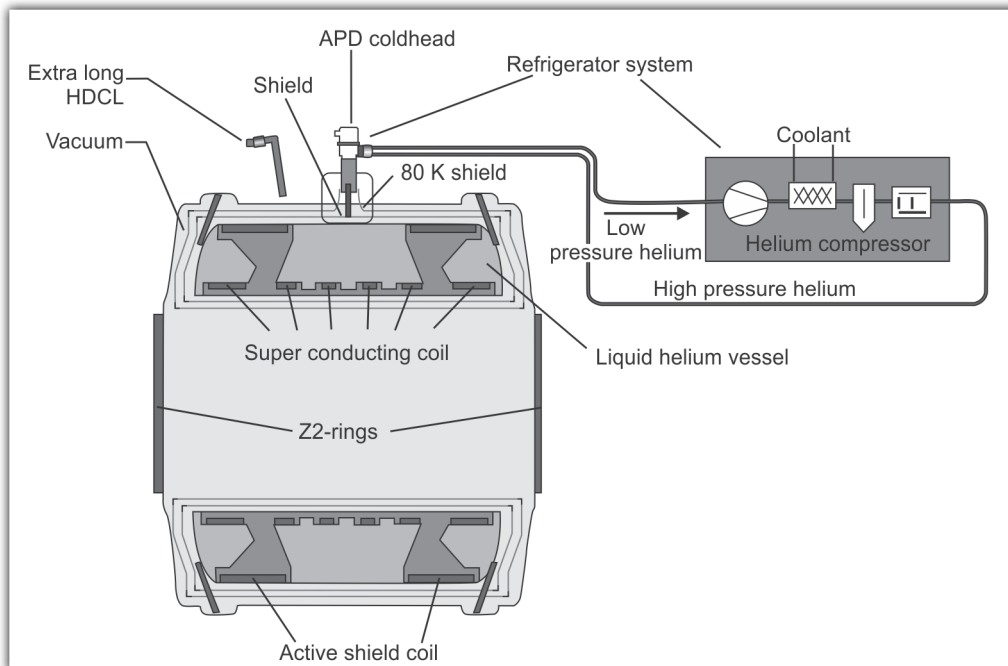


**Fig. 6** The magnet assembly in a superconducting magnet is seated into an all welded stainless steel vessel filled with liquid helium

The machine is correspondingly large and expensive. It has a tunnel configuration, which makes it claustrophobic to patients'. Typical performance specifications include a spatially uniform field, at the magnet center to be better than 10 ppm over a sphere of 40 cm and drift of the field to be less than 0.1 ppm. Ultra light magnet (magnet weight 6 tons) have been designed with nearly zero helium boil-off.

### Quench

The magnet has to be kept at a temperature below the critical/transition temperature. If a small region of wire is heated to temperature above this, it begins to dissipate heat and there is increase in temperature. This leads to a process called quench wherein the stored energy in the magnetic field is converted into heat. This raises the temperature of the liquid helium above its boiling point and magnetic field collapses. Magnets sense the onset of a quench and activate heaters that spread energy deposition throughout the coils. If this were not to happen, deposition of energy at a point could melt wire locally and destroy it.<sup>7,8</sup>

After a quench, magnet itself is rarely damaged and may be recooled and energized. To minimize possibility of quench due to frictional heating, magnet is 'trained' at the time of manufacture by cycling magnetic fields above the planned level of operation. Quenches are also possible if the cryostat vacuum fails or cryogenic fluid is not refilled in time. The coolant level is hence logged daily.

Superconducting magnets are supplied with an emergency switch system that permits a deliberate quench in case of an emergency, like a person being trapped against or inside

the magnet by a ferromagnetic object. The field decreases from initial value to nearly zero in one minute.

In a controlled quench, safety aspects need to be considered as helium gas is very cold and contact should be avoided. External venting channels should be clear. Helium may displace room oxygen and harm people.

### MAGNET GEOMETRY

**Tunnel systems:** These have a tunnel bore with horizontal magnet field, best magnetic field homogeneity and are seen only with superconducting systems.

Wide bore designs have superior homogeneity for large FOV's, while short bore magnets provide relief from claustrophobia (Fig. 7).

**Open systems** have a vertical magnetic field; can be permanent or superconducting magnet (Fig. 8).

**Specialty magnets** are specially designed for a particular type of examination usually for musculoskeletal applications. These have a superconducting/resistive magnet. 70 Mt/m of power and a slew rate of 300 T/m is the available gradient strength with one vendor.<sup>10</sup> Dedicated RF coils (80–180 mm in diameter) are available for a range of anatomies. There is a chair/recliner so that the patient is seated comfortably (Fig. 9).

### Shim Coils

The magnetic field must be stable and not affected by temperature. The homogeneity of a magnet is specified as the maximum deviation of the field in points per million (ppm)



**Fig. 7** Wide bore (70 cm) tunnel magnet



**Fig. 9** Specialty magnet system used in musculoskeletal imaging



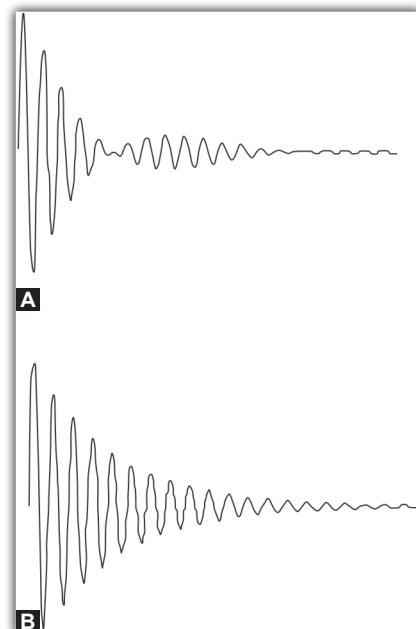
**Fig. 8** Open low field MRI with a permanent magnet

over a spherical volume of a given diameter (dsv). The uniformity should be in the range of 5 ppm.

Imperfections in manufacturing of the coils lead to harmonic error field. The process of 'shimming' is required to overcome these errors.

Two methods are available for shimming: **Passive shimming:** It is achieved by placing small permanent magnets at strategic locations at time of installation within the bore of the magnet to counteract field in homogeneities.

**Active shimming:** A set of coils is used and current is passed through these 'shim coils'. This generates small magnetic fields gradients superimposed on the main magnetic field and remove the field non-uniformities. Field homogeneity is measured by examining an FID signal in the absence of field gradients. The FID from a poorly shimmed sample shows a



**Figs 10A and B** FID signal from a poorly shimmed sample (A) Showing a complex decay envelope, while an exponentially decaying amplitude (B) indicates proper shim

complex decay envelope with many humps. Shim currents are adjusted to provide a large amplitude exponentially decaying FID indicating a homogeneous  $B_0$  field (**Figs 10A and B**). Active shimming is computer optimized for each imaging volume.

The shim coils can be superconducting and located within the cryostat and maintained at low temperature. Shim

coils can also be a set of resistive shim coils, when they are placed in the room temperature bore of the magnet.

### ■ 3 TESLA AND HIGHER MAGNET STRENGTHS

Superconducting magnets operating at 1.5 T have been the standard, though in recent years 3 T systems have gained prominence. Research systems of 7 T/9.4 T have been installed at a few sites; whereas individual prototypes of higher strength have been introduced. There are many advantages and challenges with the higher strength magnets.

The signal to noise ratio SNR is  $\propto B_1 \cdot \sqrt{N_{Ex} \cdot N_p / BW}$ , where  $B_1$  is field strength,  $N_{Ex}$  is the number of excitations,  $N_p$  is the number of phase encoding lines and BW is the receiver bandwidth. The SNR at 3 Tesla should be double that at 1.5 T, however in practice is slightly less than double.<sup>11</sup> Larger MR signal and improved SNR produce excellent images and many special applications like functional, diffusion weighted imaging and multinuclear spectroscopy are now possible.

The drawback of a higher field is increased  $T_1$ , necessitating a longer TR, and longer imaging time. Chemical shift artifacts are increased at higher field strengths. It is harder to make the static magnetic field uniform. Inhomogeneities in the magnetic field reduce  $T_2^*$ , producing focal loss of signal at air soft tissue interfaces, near metallic clips. This susceptibility artifacts increases at 3 T. The artifact can be used to increase detection of hemorrhage, free intraperitoneal air-susceptibility weighted imaging. A higher magnetic field increases the specific absorption rate SAR-energy deposited by RF field. SAR is four times higher at 1.5 T. Use of parallel imaging decrease SAR, while maintaining SNR. Another artifact that can be seen at 3 T is Dielectric shading.<sup>11,12</sup> This is non-uniform RF distribution to the body caused by the fact that waves cannot uniformly penetrate the body due to tissue conductivity and shielding effects. This is more pronounced at 3.0 T since the RF wavelength at 3 T (~25 cm) approaches the size of the body. The effects of dielectric shading are manifested in MRI images as areas with different contrast and uniformity. A common method of compensating general image non-uniformity in conventional high-field imaging systems is to use a post-processing normalization filter that derives an intensity correction function directly from the final image. These so-called "Bias Field Correction (BiFiC)" image filters<sup>13</sup> can produce a uniform image appearance.

### Gradient System

Gradient coils spatially encode the position of protons by varying the magnetic field linearly across the imaging volume. The larmor frequency will then vary as a function of position in the X,Y,Z-axis. The magnetic field gradient in the X, Y and Z directions required for an imaging study are produced by three sets of orthogonally positioned coils (Fig. 11). The slice selection gradient and RF pulse define a slice, a second magnetic field gradient applied orthogonally to the slice selection gradient serves as a readout gradient or frequency

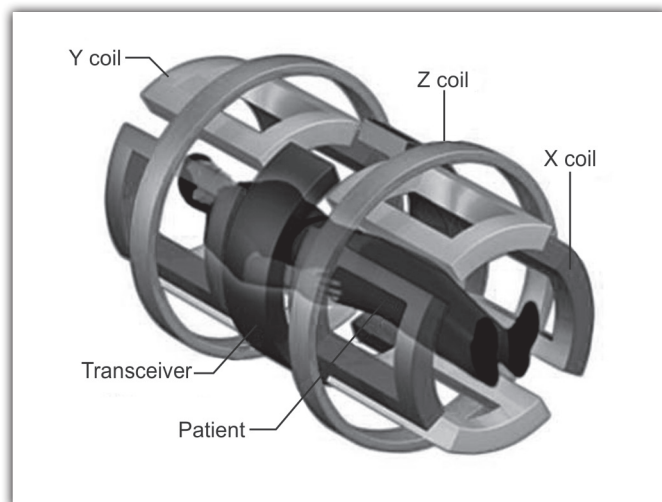


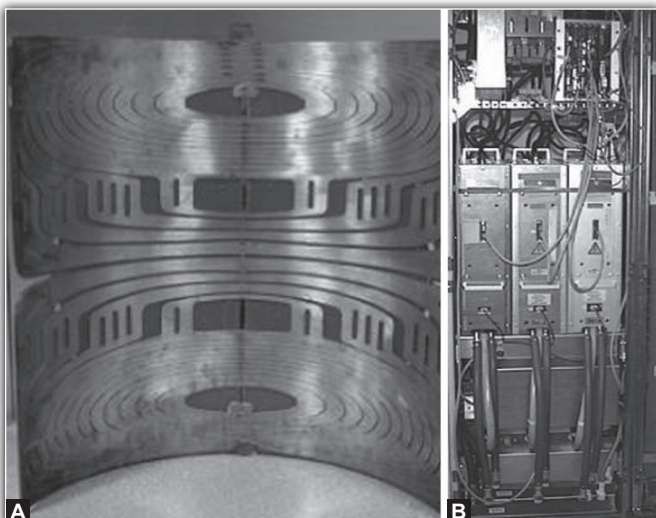
**Fig. 11** Gradient magnets in the X, Y and Z direction

encoding gradient. By repeated rotation and application of the readout gradient, spatial information in more than one direction can be obtained. A third gradient—the phase encoding gradient completes the spatial encoding of spins.

Each of the three sets of gradient coil has separate power supply, and independent computer control which alter the slope of the magnetic field. These are switched off and on frequently to allow slice selection, frequency and phase encoding. All three coils are wound on a cylinder and situated in the warm bore of the magnet. These coils are connected to **gradient amplifiers** that control the rise time and maximum value of the gradients. The direction of the current (DC) passed through the coil determines the increase or decrease in the field strength relative to the center. Each gradient individually produces a field in a specific direction; a gradient field in any chosen direction can be generated by activating two or all three of the gradient coils. This makes it possible to select imaging planes in any of the directions.

Gradients are resistive electromagnets consisting of metallic coils driven by power amplifiers. Gradient coil wires are usually made of copper and are circular or rectangular in cross-section with a diameter of ~5 mm (**Figs 12A and B**). A **Maxwell coil** produces linear variation in field along Z-axis in other axes it is done using a **saddle-golay coil**. The current necessary to generate a typical gradient field of ~40 mT/m is of the order of few hundred amperes. The peak power is an important design criterion of the gradient amplifier.

The slice select or Z-axis gradient field is switched on during the application of RF pulse. The steeper the gradient, thinner the slice. In the time of a few milliseconds, when MR signal is being received, current is passed through another set of gradient coils -XX coils. This alters the magnetic field gradient from side to side in the X direction. This is for frequency encoding, a steeper gradient is used for a smaller FOV.



**Figs 12A and B** (A) Gradient coil (B) Gradient amplifier

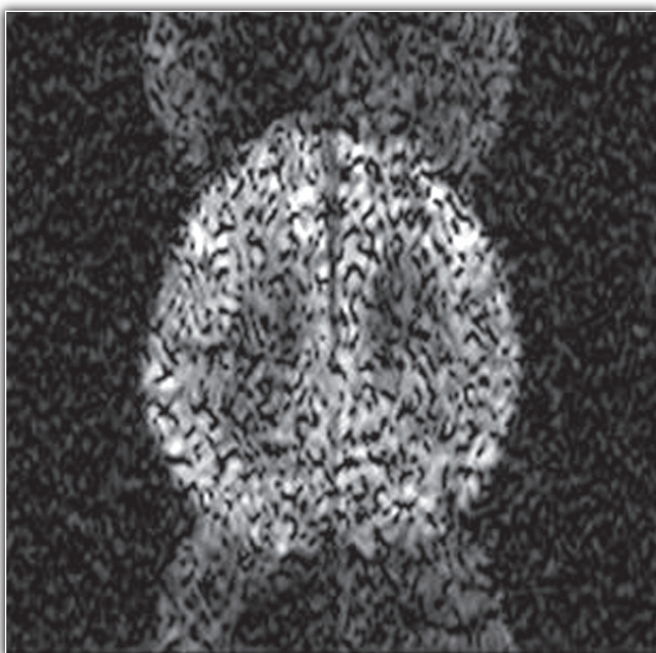


**Fig. 13** "Eddy current" artifact—in homogeneities in the gradient cause distortion in the image

The third set of coils (YY) coils for phase encoding are energized, immediately after the  $90^\circ$  pulse, but before it is inverted by the  $180^\circ$  pulse. This produces a gradient from front to back of the patient. Steeper gradients are required for finer phase matrices.

The maximum gradient amplitude that can be generated (in millitesla per meter) has a direct impact on the minimum slice thickness and FOV, and thereby of the maximum spatial resolution that is available. The current in these coils are

rapidly switched on and off (on a millisecond time scale between various levels). The time required to switch between two current levels or **slew rate** (time, rate of change of gradient length in T/m/s) is an important technical specification of the scanner capability. This sets the limit to the minimum TR and TE values that can be achieved, and consequently the minimum acquisition time. A slew rate of a gradient system (in tesla per meters per second) is defined as the ratio of gradient strength divided by rise time. Slew rate depends on both the gradient coil (it takes more time to ramp up/down a large coil than a small coil) and on the performance of the gradient amplifier (it takes a lot of voltage to overcome the inductance of the coil) with significant influence on image quality. Slew rates up to 100 to 200T/m/sec while gradient strengths upto 40 to 50 mT/m is now available.

Another factor is **linearity of the gradient**. If the gradient falls off non-linearly on either side of the magnet isocenter, then the image will be distorted at edges of FOV. Gradient performance is measured in **amplitude** (in millitesla per meter, mT/m) and **rise time** (in  $\mu$  seconds).

Scan speed is dependent on the performance of the gradient system. Stronger gradients allow faster imaging and higher resolution. Applications such as MR angiography, cardiac MR and diffusion tensor imaging require high amplitude gradients ( $>20$  mT/m) with a fast slew rate. Fast switching gradients can lead to induction of **eddy currents** due to the changing magnetic fields produced. These degrade imaging sequences by producing geometric distortion, blurred images and artifacts like ghosting (Fig. 13). To overcome this, shielding of gradient coils is done, where a second coil surrounds the primary gradient coil and carries current in the opposite direction. These cancel the eddy currents but also reduce the overall strength of the gradient fields. These actively shielded gradients are increasingly used as rapid scan imaging protocols based on gradient echoes gained prominence.

Specialized gradient coils are being developed for a variety of clinical applications. In echoplanar imaging, the requirements of gradient strengths, rise times and duty cycle have been increased as all the space is to be traversed in a single excitation. This requires each phase encoding projection to be acquired in less than 0.8 ms. Gradient coils required would have a maximum amplitude of 20 mT/m, minimum rise time of 0.1 ms (slew rate 200 T/m/s) and a duty cycle of 50 to 60 percent. This requires matching of gradient to power supplies that are capable of responding to the resonant mode at maximum amplitude and holding it at that level for a short period of time. Dual gradients' have been developed wherein there is a short, higher performance central region provided by one of the segments of the gradient tube and another mode of operation with the standard full region gradient. Specifically, in head imaging a physically smaller gradient tube can be used which combines improved gradient performance with satisfactory physical stimulation.<sup>14</sup>

At time of switching interval, the resulting force on the gradient coils is longer, producing a loud bang. **Acoustic noise**

is the signature complaint of most patients about MRI. As gradient strength is increasing, so is the noise. Improvements in mounting techniques, use of damping materials and advances in materials used, placing the gradient tube in a vacuum have all been used to decrease the acoustic noise.

One drawback of powerful gradients is **peripheral nerve stimulation**. There are standards that limit stimulation based on duration of the stimulus and the rate at which the magnetic field changes ( $db/dt$ ). The shorter the stimulus the faster the magnetic field has to change to cause the stimulus. To decrease  $db/dt$ , gradient can be made shorter.

Powerful gradient amplifiers are sited in a room with restricted access adjacent to the magnet room.

### Radiofrequency System

Radiofrequency system is required to transmit and receive signals at or near the Larmor frequency of the precessing spins. The frequency of the RF coil is defined by the Larmor equation. The Larmor frequency of protons being 63.8 MHz at 1.5 Tesla. MRI uses a Fourier transformation technique. This utilizes a brief burst of RF energy (lasting a few milliseconds) from a RF transmitter to excite the spins, followed by detection of the FID (free induction decay) signal that lasts 10 to 1000 ms. RF field  $B_1$  is two vectors rotating in opposite directions in a plane transverse to  $B_0$ . At the Larmor frequency the vector rotating in the same direction as the precessing spins will interact strongly with the spins. RF coils work efficiently when physically aligned to receive signal that originate perpendicular to the main magnetic field  $B_0$ .

The RF subsystem consists of a **transmitter**, a **receiver coils**. The RF transmission system consists of RF synthesizer; amplifier and transmitter coil (usually built into the body of the scanner). RF transmitter generates a temporally stable basic frequency for the RF, delivers an appropriate waveform to amplifier which delivers an RF pulse of shape and flip angle to the coil and time the delivery of the pulses. This can be achieved by analog or digital process. The transmitter must display linearity, i.e. the output of the power amplifier should be directly proportional to the input power. This is achieved by a process called as envelope feedback. RF amplifier converts a low level RF demand signal to a high power level. RF source is combination of independent input signal and amplifiers. **RF coil** is a combination of coil elements arranged to produce an advantageous  $B_1$  field distribution. **RF channel** denotes the number of connections to the RF coil. **Coil element** is an arrangement of electrical conductors for converting an electrical current into magnetic field.

**RF receiver subsystem:** The RF receiver consists of the coil, preamplifier and signal processing system.

The primary role of the receiver in an MRI scanner is to convert the analog coil signals into digital format. The design of a modern digital receiver is based on an analog-to-digital converter (ADC), which samples the analog MRI signal and converts it into digital format. Important characteristics of

the ADC are its conversion bandwidth and resolution. The conversion bandwidth equals half the digitization rate. State-of-the-art ADCs allow conversion bandwidth of over 50 MHz at 14 bit resolution. Since frequencies are generally well above 50 MHz, usually an alias of the MRI signal is detected.

Prior to input into the ADC, the MRI scanners signal needs to be amplified and filtered. Amplification serves to match the voltage range of the MRI signal to the input range of the ADC, in order to engage its full dynamic range. Analog filtering serves to reduce noise and interference signals that alias into the ADC conversion band from outside the target band around the MRI scanner Larmor frequency. In addition, depending on Larmor frequency, down conversion might be required to bring the signal frequency to within the input band of the ADC. The choice of ADC digitization rate is to some extent dependent on the master clock of the MRI scanner exciter. To avoid phase errors between excitation and reception, the digitization clock of the ADC needs to be synchronized to the clock of the MRI scanner exciter frequency that is a multiple of the exciter clock. In addition, it is beneficial to avoid digitization frequencies that put the Larmor alias at around 0 Hz. After digitization, digital down-sampling is performed to reduce the amount of data. The output bandwidth and center frequency can be adjusted to match those of the MRI scanner signal bandwidth and (aliased) center frequency. An added advantage of down-sampling is the increase in dynamic range, which amounts to 1 bit for every factor of 4 of down-sampling.

RF coils can be **transmit and receive** or **transmit only/receive only coils**. Receive only and transmit only coils must be electronically isolated. This means that when the transmitter is on, the receiver is open circuited to prevent the transmitting power from entering the receiving chain. During signal reception, the transmitting coil is open circuited to prevent mutual coupling. When the power amplifier is not active, its output is disconnected to avoid the output noise from interfering with the sensitive signal that is being received.

A wide range of RF coil designs are available in MRI. Ongoing developments in the RF system are one of the most profound changes in MRI system development. There are many types and geometries of the coil.

RF coils are classified into two types—**volume** and **surface coils**. Volume coils surround the imaged object, and provide homogeneous transmission and reception over a large anatomic region. These are both transmit and receive coils (transceive). Head and body coils are referred as volume coils (Fig. 14). As the noise is nonlinearly proportional to the volume of tissue being imaged; the SNR of these is lower than the surface coils. Body coils are constructed on cylindrical coils forms—diameter of 50 to 60 cm and a length of 70 to 80 cm. These are large enough to surround the patient's chest and abdomen. Head coils are smaller 40 cm long and 28 cm in diameter.

**Surface coils** are usually receiving coils with a limited area of sensitivity from which they receive signal. Surface



**Fig. 14** Circularly polarized head coil, volume coil—both transmit and receive

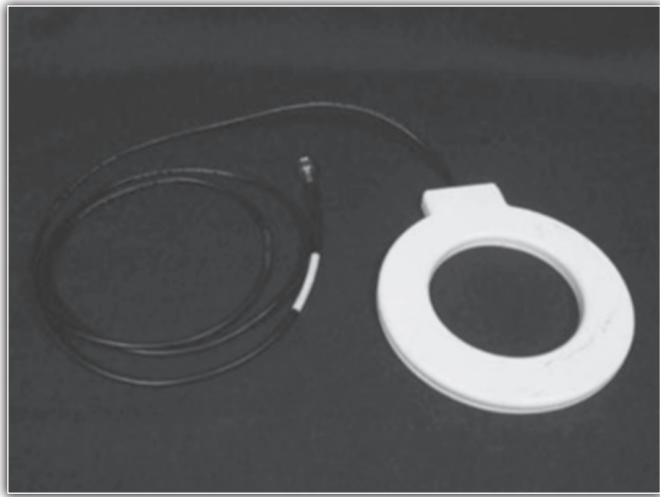


**Fig. 15** Surface loop coil—receive only

coils fit closely over specific anatomic region. The sensitivity of the coil is related to the radius of the coil. As the coil size is increased, noise will also increase. These include circular coil configuration for orbits and TM joints, rectangular coils for lumbar spine or irregular shapes for shoulder, cervical spine. Surface coils are advantageous as they increase the SNR; however the sensitivity is not uniform over its field of view. These need to be positioned carefully. Surface coils can be rigid or flexible in design. Flexible coils can be closely applied to the contour of the body, are more comfortable, and however are less durable due to higher wear and tear (**Fig. 15**).

A large coil (body coil) is used as a transmitter and a smaller surface coil as a receiver combining the advantage of uniform excitation of a large coil and increased SNR of a smaller coil. However, if two separate coils are used, they need to be tuned to the same frequency. Coil decoupling is necessary to prevent current in one coil to excite current in the other.

For a solenoidal magnet the transmitter and receiver coils are **saddle shaped** and have the volume of the greatest  $B_1$  field homogeneity along the linear portion of the coil, the ends being inhomogeneous (**Fig. 16**). An alternate design called a **bird cage coil or resonator** has improved  $B_1$  homogeneity and has higher sensitivity. These are volume coils consisting of two circular or elliptical conducting end rings joined by conducting rings or legs (**Fig. 17**). A common version uses 16 loops to span the cylinder. These coils provide a uniform RF field. **Quadrature reception** is applied with volume coils to improve SNR. Two pairs of coils (phase sensitive detectors) are used to detect signal that are out of phase. The signal of the two is combined to form a final image. A coil operating in this manner is called “**circularly polarized**” (**Fig. 18**). This increases SNR by a factor of  $\sqrt{2}$ . It requires only half the power

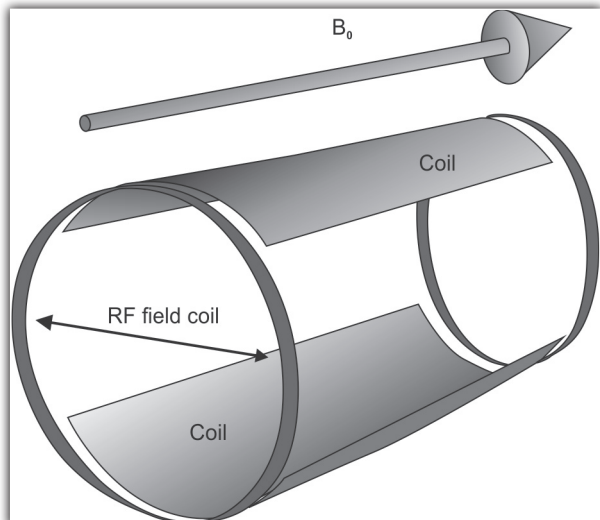


**Fig. 16** Linearly polarized body coil comprising flat conductors configured in a hollow tube

to generate; therefore less power is deposited in tissues. A circularly polarized birdcage resonator is called a quadrature coil and is the most frequently used RF coils in MRI today. Whole body sized birdcage coils are available. A related form of multimode resonator, referred to as TEM (transverse electromagnetic) resonator is also useful for head and neck imaging at higher field strengths. These are fitted just inside the gradient coil set. RF transmitting coils are also shielded to minimize power losses.<sup>15-17</sup>

**Phased array coils:** Arrays of surface coil are used to extend the effective FOV of the receiver coil while maintaining the improved SNR characteristics of a limited FOV of a single coil (**Fig. 19**). The coils in array can be activated remotely as single

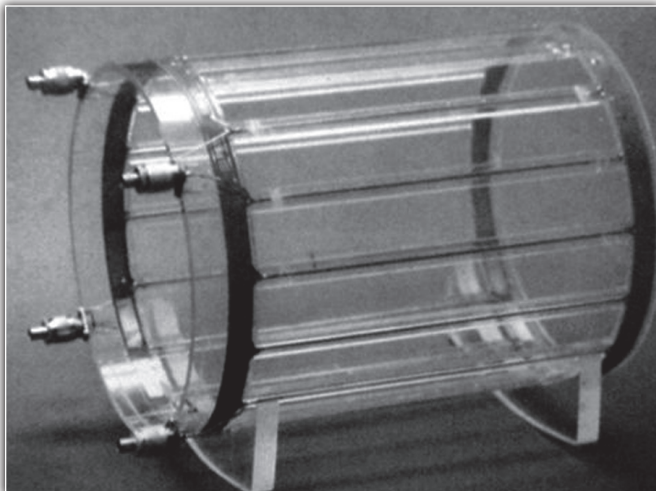


**Fig. 17** Bird cage resonator

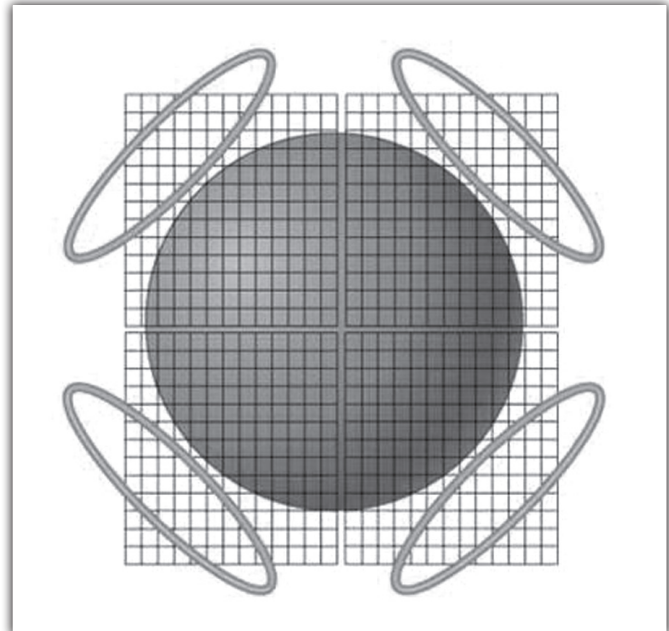


**Fig. 19** Phased array coil—multiple coil elements, increasing SNR and FOV

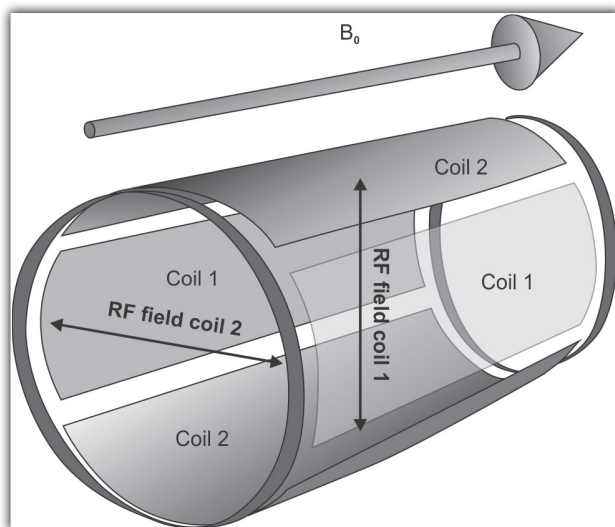


**Fig. 18** Design of a circularly polarized body coil showing 2 RF fields with a phase shift

receivers and cover a limited FOV in the region of interest. There is also another method where each coil in the phased array has a separate receiver channel. The signal is collected from all coils in the array simultaneously, data combined to give an image of a complete FOV, with a SNR equivalent to a single coil. As number of receiver channels increase, so does the cost.

The coils are electromagnetically decoupled from one another by selecting the overlap between neighboring coils, so that mutual inductances disappear. This is achieved by the use of low impedance preamplifiers on the output of each individual coil or by physically overlapping the coil receiver elements. The hexagonal arrangement of coils and extent of overlap are chosen to minimize mutual inductances between

coil elements. Noise is proportional to sensitivity volume of the coil, which is smaller for surface coil than for a volume coil.

Phased array coils have to be positioned perpendicular to the main magnetic field. Phased array coils require an individual hardware channel for each reception element demanding more computer processors. As the number of channels increase, the coil elements become smaller and penetration may be compromised. This may lead to inhomogeneous SNR, which would be maximum near the surface of the coil and less within the deeper parts. This has been overcome with the use of post processing algorithm to correct intensity variation.<sup>18</sup>

**Transmit phased array coils:** A current is produced on each element via special amplifiers. Precise control of the relative amplitude and phase of each element enables them to be mutually independent. With reduced pulse duration, higher SNR, improved field homogeneity and reduced SAR, parallel MRI can be used in the excitation phase as in transmit SENSE at higher field strengths.<sup>7</sup>

**Hybrid coil:** This is a transmit/receive coil. It consists of a localized dedicated transmitter coil whose size is just optimized for a target FOV and an independent set of receiver coils. As the transmitter coil is much smaller than the typical whole body transmitter coil, it requires less input power to generate the necessary  $B_1$  with a potentially reduced SAR. Hybrid coils are thus useful for higher static magnet fields.

Most of the RF transmit and receive subsystem component such as digital to analogue converters, analogue

to digital converters, power amplifiers, frequency mixers are sited in the electronics/cabinet room.

Careful shielding of the MR scan room is required to prevent contamination of the weak signal arising from the patient with extraneous signal at the same frequency. These can be from broadcasting stations or operation of electronic equipment. MRI rooms have a shield called as **Faraday cage**, consisting of a conductive metal lining of copper or aluminum through which RF electromagnetic radiation will not pass. It keeps external electrical noise out and the generated RF signal within the examination room. Electronic filters are used to prevent noise from entering the scan room via wiring cables. Screened rooms possess wave guides/tubes fixed into the wall of the room, through which nonconductive tubing such as fiber optical coil passes. The examination room door should be shut while acquiring data to enable the shield to work effectively. Machine should be away from lifts/elevators and power cables, which may cause RF interference, distorts the image and produce linear artifacts. A hardware and software system is provided which provides protection for the patient against the **heating effect of RF energy absorption** and RF hardware from excess transmitted RF energy or hardware failure in the RF transmit path. This takes into account various coil types, amount of transmitted power allowed for the body coil is much higher than that of a transmit receive head coil as the body coil is larger and can handle more power. Correct calibration of the MR system is essential.

### MULTICHANNEL RF COILS AND PARALLEL IMAGING

Multichannel radiofrequency and parallel imaging technologies are hardware and software implementations, respectively, aimed at improving the coverage, signal resolution and speed of MRI examinations. With multichannel RF technology, the MRI signal used to form an image is collected by an array of separate detectors, or coil elements. Each element relays signal information along a separate channel to an image reconstruction computer. Such arrays of coil elements and receivers can improve imaging coverage and the ratio of signal-to-noise in the image. The connection to the system of a coil with more elements than the number of channels requires complex logic switches in the coil number of elements in the array of detectors and receivers is an important factor in characterizing an MRI scanner. Parallel imaging technology uses complex software algorithms to reconstruct the signals from multiple channels in a way that can reduce imaging times and/or increase image resolution.

The concept of “multi-element phased arrays receive coils” started around 1990; as a result MRI systems typically had up to 4 receive channels. Towards the end of the 1990s, with the introduction of parallel imaging, the technology related to MRI receiving architecture made enormous progress: over a period of 10 years, the number of receiving channels increased from the original 2 to 32. In the last

decade, the move towards higher channel counts in coils has been at the forefront of MR development. This trend towards higher number of channels has resulted in an increased complexity of the MRI system with increased initial costs. Also upgrades to a higher number of channels are costly because a substantial expansion of the RF chain is required.

Acquisition time in MRI is proportional to the number of phase encoding steps. Increasing the distance between each phase encoding lines in k space by a factor of R, reduces the acquisition time by the same factor, while keeping the spatial resolution fixed. Acquisition time is reduced by a factor ( $R = \text{acceleration factor}$ ), equivalent to the number of independent coil elements (4–32). In practice, only a time reduction of 2 to 3 is possible as SNR is inversely proportional to  $\sqrt{R}$  and at higher R, SNR becomes unacceptably low. Decreasing the phase encoding lines decreases the FOV, resulting in aliasing or wraparound. There are two techniques to remove or prevent aliasing.

- SMASH (Simultaneous acquisition of spatial harmonics):** The missing k space lines are restored prior to fourier transformation.<sup>19</sup> GRAPPA (generalized auto-calibrating partially parallel acquisition) is a variant of SMASH in which a small number of additional lines of k space data are acquired during the acquisition, eliminating the need for a separate coil sensitivity.
- SENSE: Sensitivity encoding<sup>20</sup>**—data is first fourier transformed, resulting in an aliased image. This is then by “unwrapped” by using the spatial information from the coil sensitivity profile.

SENSE is the most commonly used parallel imaging technique available with many vendors as ASSET (GE healthcare, Waukesha, Wis), SPEEDER (Toshiba medical systems, Tokyo, Japan), SENSE (Philips medical system, Cleveland, Ohio).Siemens (Erlangen, Germany) offers both SENSE and GRAPPA as a single package under the trade name iPAT.

Parallel imaging is useful in conditions where scan speed outweighs the need for a high SNR, e.g. cardiac imaging.

**Multitransmit technology:** Imaging in conventional MR scanners, uses a single source to transmit a signal to the patient. Multitransmit uses multiple RF sources, each source individually adapted to patients anatomy. This cancels out dielectric shading seen at 3.0 T. Multitransmit also reduces local specific absorption rate SAR. Interleaved sequences and saline bags are not required. Another advantage, as claimed by the vendor, of using multiple RF sources is increase in scanning speed by 40 percent.<sup>21,22</sup>

**Total imaging matrix:** Provided by one vendor,<sup>23</sup> the system contains up to 102 matrix coil elements integrated seamlessly with up to 32 independent RF channels. These provide high SNR associated with local coils for an FOV ranging from 5 to 196 cm. There is no requirement for patient/coil repositioning. This system provides a PAT factor up to 16. Tim46 ultra high

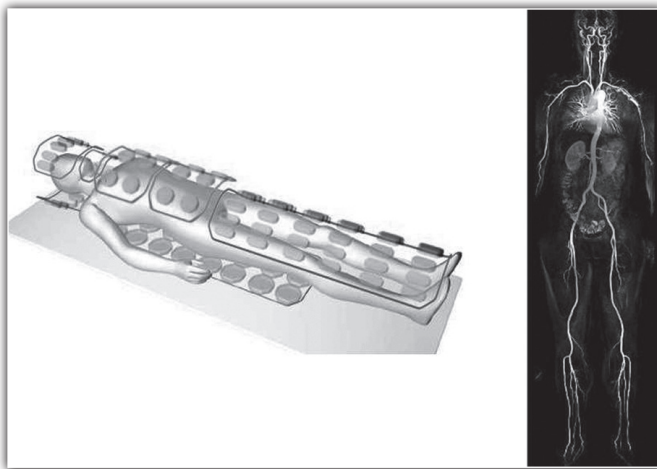


**Fig. 20** Total Imaging Matrix®—102 coil elements with 32 channels providing whole body coverage of up to 205 cm

density array up to 204 coil elements with 128 RF channels increase SNR considerably (**Fig. 20**).

### Computer

The computer is the command center of the MRI system. It shapes and times the RF pulses, turns the gradients on and off, controls the RF receiver to collect data. After data collection, it is required for manipulation, storage, retrieval. A processor is required for computation.

### Data Processing and Image Reconstruction

The two primary dedicated digital control systems are the pulse generator and the data acquisition system.

The pulse generator synchronizes the gradients and RF pulses after selection at operator console. Digital synchronization is provided for the receive channel analog to digital convertor, such that the detected signal correlate with the applied gradient and RF frequency. The **temporal positional accuracy and repeatability (TPAR)** is an important specification of the system.

Data is collected from one or more receiver channels. This may be in analog or preferable digital domain. **Digital broadband MR** is a new technology that samples the MR signal directly in the coil on the patient. The fiberoptic transmission of digital broadband data from the coil to the image reconstruction removes potential noise that is associated with analog RF. In conventional MR system, multiple analog coaxial cables are required (one per element/channel as digitization is performed away from the RF coil). In digital broadband system digitization is inside the RF receive coil, the number of RF channels is now determined by the coils, rather than the system. There is a single broadband fiberoptic cable that is independent of number of elements/channels in an RF coil. A gain of 40 percent in SNR is claimed.

System also is channel independent. In a conventional system, 8 channels can receive coils up to 8 channels; to support a 16 channel coil an upgrade would be required. Digitization in the coil makes number of channels required redundant.

Data processing from multiple channels in the digital domain allows for correction of the inhomogeneous sensitivity of the coil and produces an acceptable image with a required FOV.

The required data acquisition rate increases with the number of channels being sampled. The sampling frequency needs to be twice the receiver bandwidth to meet the Nyquist criteria and prevent aliasing. To account for phase errors that may occur, a sample frequency of four times the bandwidth is used. Analog to digital converter are used. Digital data processing speeds are critical in higher field magnets with larger matrix size.

The complex MR signal is sampled and computer analyzed into a spectrum of component frequencies using a mathematical process called Fourier analysis. The data from every signal in a selected slice are stored in k space. This space is a spatial frequency domain in the computer where the signal spatial frequencies and their origin are stored. The number of lines filled in k space matches the number of encodings in the sequence.<sup>7</sup> The central part of k space is filled with data from shallow encoding gradients, low spatial frequencies, less details, but stronger signals. The upper and lower parts are filled with data from the steeper gradients, high spatial frequencies, better detail but low signal intensity. k space has to be completely filled with the data from the imaging sequence before the signal is analyzed and processed into the image. The data once acquired, is stored in a large memory array after being filtered. The memory is very large and a cached disk system is used. Powerful reconstruction processors are used computer servers are important components of MR hardware and have many forms, rackmount servers used in many systems. Image reconstruction algorithms are implemented to distribute computational load and save time. The sample frequency and the number of simultaneously acquired channels determine the maximum data rates through the system.

After the image is reconstructed may be displaced for instantaneous viewing or stored in a database for review.

## ■ ADVANCED MR APPLICATIONS AND HARDWARE

### MR-HIFU (MRgFUS)

A noninvasive method using high density focused ultrasound and using MR for planning and temperature monitoring was first used in 2008 as an alternative to surgery for treatment of uterine fibroids. The clinical applications of this are increasing to include management of bone metastasis, prostate, etc.

A focusing transducer is used to transmit ultrasound energy into a small volume at the target locations inside the

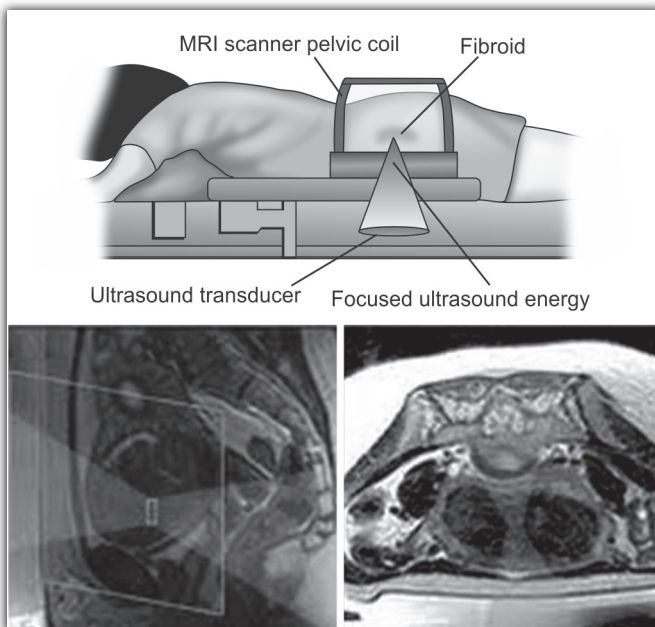


**Fig. 21** MRgFUS—depicts the position of the patient, ultrasound transducer and the focused beam

body. The ultrasound energy penetrates the intact skin and soft tissue to produce a well-defined region of coagulative necrosis by producing high temperature and only in the focused area. 3-D MR provides the anatomical reference data for planning. MR imaging based temperature map acquired in real time during ablation provides monitoring support. This is an outpatient procedure. Dedicated abdominopelvic coils designed for therapy applications are integrated within the table for positioning ease. The same system can be used for both therapy and diagnosis. This is exclusive to GE MR Systems<sup>10</sup> in collaboration with Insightec's Ex-ablate 2000 (**Fig. 21**).

### MR Elastogram

This is an acquisition hardware and reconstruction application that produces images with contrast related to stiffness of soft tissue. Sound waves (40–200 Hz) are generated in the body by using an MRI compatible acoustic driver. These are then imaged by a special phase contrast MR imaging sequence. Finally the data generated is processed to generate elastograms—color coded anatomic images that depict the relative stiffness of tissue in the cross-section of interest. The hardware component is comprised of an active sound wave generator and a passive transducer that produces vibrations in the subject to be scanned. The data is reconstructed in both magnitude and phase formats, and the latter is used to produce strain wave and relative stiffness images. This technique is used to assess liver fibrosis.

### MR Surgical Suite: Interventional MRI

Interventional MRI is the use of MR techniques for guidance of both diagnostic and minimally invasive therapeutic interventions. The magnet is of the 'open' type to allow access to the patient. There is video camera sensor array which detects the correct location and orientation of the hand held instrument. Use of new fast gradient echo pulse sequences allows continuous MR images (0.3–7 seconds per image). These are viewed through a high resolution radiofrequency shielded monitor in the operating room. This modality is especially useful in areas of complex anatomy like skull base, retropharynx, etc.

### MR-PET

Fully integrated MR-PET suite has been introduced. This has integrated cooling feature with specialized shielding to eliminate magnetic field interference in PET data processing. The detectors used in PET are MR compatible. This is dealt with in detail elsewhere in the book.

The MRI is now a widely used and well-developed modality. Intense technical development is continuing to increase its clinical applications including in the field of molecular imaging and to provide the necessary hardware for the same.

### REFERENCES

1. Gorter CJ. Negative result of an attempt to detect nuclear spins. *Physica*. 1936;3:995-8.
2. Lauterbur PC. Image formation by induced local interactions: examples employing nuclear magnetic resonance. *Nature*. 1973;242:190-1.
3. Schneck JF, Kelley DAC, Marinelli L. Instrumentation: Magnets, coils and Hardware. In: Magnetic Resonance Imaging of the Brain and Spine Atlas SW, 4th Edn. In: Wolters Kluwer (Ed.) Lippincott Williams & Wilkins. 2009. pp.2-24.
4. Vaughan T, DelaBarre L, Synder C, et al. 9.4 T human MRI: preliminary results. *Magn Med*. 2006;56:1274-82.
5. Sagawa M, Fujimura S, Togawa N, et al. New material for permanent magnets on a base of Nd and Fe. *J Appl Phys*. 1984; 55:2083-7.
6. Scott Greig, Chronik Blaine, et al. A prepolarized MRI scanner. *Proc Intl Soc Mag Med*. 2001;9:610.
7. Allisy-Roberts P, Williams J. *Farr's Physics For Medical Imaging*, 2nd edn. Saunders Elsevier. Magnetic Resonance Imaging 189.
8. McRobbie DW, Moore EA, Graves MJ, Prince MR. *MRI from picture to proton*. Cambridge:Cambridge university Press, 2003.
9. Adam A, Dixon AK, Grainger RG, Allison DJ. *Magnetic Resonance Imaging Basic Principles in Diagnostic Radiology*. 2008;87-107.
10. [www.gehealthcare](http://www.gehealthcare.com).
11. Akisk FM, Sandrasegaran K, Aisen AM, et al. Abdominal MR imaging at 3.0 T. *Radiographics*. 2007;27:1443-4.
12. Merkle EM, et al. Abdominal MRI at 3.0 T: the basics revisited. *Am J Roentgenol*. 2006;186:1524-32.

13. Jellúš V, et al. New Modification of the Homomorphic Filter for Bias Field Correction. Proc ISMRM. 2005. p. 2247.
14. Turner R. Gradient coil design: a review of methods. Magn Reson Imag. 1993;11:903-20.
15. Walker KM, Tsuruda JS, Hadley JR, et al. Radiofrequency coil selection for MR imaging of the brain and skull base. Radiology. 2001;221:11-25.
16. Fujita H. New Horizons in MR Technology: RF coil designs and trends. Magn Reson Med Sci. 2007;6(1):29-42.
17. Schenck JE. Radiofrequency coils: types and characteristics. In: Bronskill MJ, Sprawls P (eds). The Physics of MRI. Woodbury, NY: American Institute of Physics; 1993. pp.98-134.
18. Roemer PB, Edelstein WA, Hayes CE, et al. The NMR phased array. Magnetic Resonance in Medicine. 1990;16(2): 192-225.
19. Sodickson DK, Manning WJ. Simultaneous acquisition of spatial harmonics (SMASH): fast imaging with radiofrequency coil arrays. Magn Reson Med. 1997;38:591-603.
20. Pruessmann KP, Weiger M, Scheidegger MB, et al. SENSE: Sensitivity encoding for fast MRI. Magn Reson Med. 1999; 42:952-62.
21. [www.healthcare.philips.com/main/products/mri](http://www.healthcare.philips.com/main/products/mri).
22. Harvey PR, et al. SAR behavior during whole-body multitransmit RF shimming at 3.0 T, Proc. ISMRM. 2009.p. 4786.
23. [www.siemens.com/medical/solutions](http://www.siemens.com/medical/solutions).

## Chapter

# 8

# Image Optimization in MRI

*Jyoti Kumar*

Optimizing image quality means finding a balance between the different aspects of image quality and image speed. For an image to be optimal for diagnosis, the anatomic and pathologic features within the image must be distinguishable from each other.

Ideally an image should have a high signal to noise ratio, high spatial resolution, excellent contrast, minimum artifacts and an acceptable scan time. Generally, these criteria conflict with one another. Knowledge about various MR parameters within the user interface that can be modified by the radiologist helps to find the most appropriate balance between image quality and scan time.

In this chapter, we shall discuss image optimization under these major headings:

1. Signal to noise ratio
2. Contrast to noise ratio
3. Spatial resolution
4. Scan time
5. Artifacts and their remedial measures.

### SIGNAL-TO-NOISE RATIO

MR signal is the voltage received by the receiver coil from each voxel in a slice after it is stimulated by a radiofrequency pulse. This is recorded at time interval TE and at specific frequencies. Bright pixels in the image represent stronger signals, and darker pixels represent weaker signals in the image.

Noise is an unwanted occurrence in the MR image. Noise appears as a grainy random pattern superimposed on the MR image. This represents statistical fluctuations in signal intensity that is superimposed on the image and compromises image quality. It occurs at all frequencies and randomly in

time. The source of this noise is Brownian motion of charged particles throughout the body of the patient whereas signal comes from just the selected slice. The electronic noise of the receiver technology and the environment also contribute to the noise.

The signal-to-noise ratio (SNR) is defined as the ratio of the amplitude of the MR signal to the amplitude of the background noise. A high signal to noise ratio improves image quality. To increase the SNR, we need to increase the signal relative to the noise. Parameters that affect SNR are field strength, proton density, coil type and position, TR, TE, flip angle, number of signal averages, slice thickness and receiver bandwidth.

### Field Strength

With higher field strength, more protons are aligned parallel to the main field (spin up nuclei) as fewer protons have enough energy to oppose this increased field strength and lie antiparallel to the main field (spin down nuclei). The net magnetism of the patient (termed the net magnetization vector or NMV), reflects the balance between the parallel and antiparallel magnetic moments. In high field strengths, NMV increases and therefore the signal increases.

### Proton Density

The signal strength depends on the quantity of signal generating protons in the voxel (proton density). For example, pelvis contains structures with a high proton density such as fat, muscle and bone, giving a high signal. On the other hand, chest contains air filled lungs and vessels with low proton

density, and hence imaging of chest requires measures to boost SNR.

### Coil Type and Position

Imaging of small anatomical regions such as extremities (e.g. ankles, wrists), neck or the breasts require specialized surface coils to maximize both the signal-to-noise ratio and spatial resolution. Large coils such as the body coil provide much larger coverage but result in a lower SNR. A phased array coil combines the two advantages, as it uses multiple small coils that provide good SNR and the data from these are combined to produce an image with good coverage.

Positioning of coils is also important. To understand this, let us revise few basic principles of MR imaging. In an external magnetic field ( $B_0$ ), spin up and spin down nuclei are in a state of equilibrium. Excess spins generate constant magnetization in the longitudinal plane (Z-axis). Spins are also precessing like a wobbling top and they are out of phase with each other. NMV is zero in the transverse plane. When an RF pulse is applied, two things happen- energy absorption and phase coherence. Hydrogen nuclei absorb energy. If just the right amount of energy is absorbed, the number of nuclei in the spin up position equals the number in the spin down position. As a result the longitudinal magnetization reduces to zero. Secondly, on application of an RF pulse, the spins move into phase with each other. When spin up and spin down nuclei are equal in number, the net effect is one of precession so that NMV now precesses in the transverse or XY plane. As the NMV has been moved through  $90^\circ$  from the direction of the main magnetic field or the Z-axis, it is called a  $90^\circ$  RF pulse. It is the magnetization in the transverse plane that is used to produce the signal. As the NMV rotates in the transverse plane, it passes across the receiver coil to induce a voltage in it. This voltage is the MR signal. The coil is positioned so that transverse magnetization created in the XY plane is perpendicular to the coil. In a superconducting system, this means placing the coil either over, under, or to the right or left of the area being examined. A coil positioned perpendicular to the table results in zero signal generation.

### Repetition Time

Repetition time (TR) is the time between the application of two RF pulses. It is measured in milliseconds (msec). When the RF pulse is removed, longitudinal magnetization recovers (T1 recovery) and transverse magnetization begins to decay (T2 decay). The T1 time of a tissue is inherent to the tissue. It is the time it takes for 63 percent of the longitudinal magnetization to recover. The period of time in which this longitudinal recovery occurs is the time TR. The longer the TR, the greater is the recovery of longitudinal magnetization, which is now available to be flipped into the transverse plane on the application of the next excitation pulse. Hence, the SNR is improved with a long TR. A short

TR reduces the SNR. Although a short TR is required for T1 weighting, reducing this parameter too much may severely compromise the SNR.

### Echo Time

Echo time (TE) is the time between an RF excitation pulse and collection of the signal. It is also measured in milliseconds (msec). The T2 decay time of a particular tissue is also inherent to the tissue. It is the time it takes for 63 percent of the transverse magnetization to be lost. The period of time over which it occurs is the time between the excitation pulse and the MR signal or the TE. The TE determines how much T2 decay occurs in a particular tissue. At short TEs, very little transverse magnetization has dephased, so the signal amplitude and hence SNR is high. A long TE reduces the SNR. Although a long TE is required for T2 weighting, increasing this parameter too much may severely compromise the SNR.

### Flip Angle

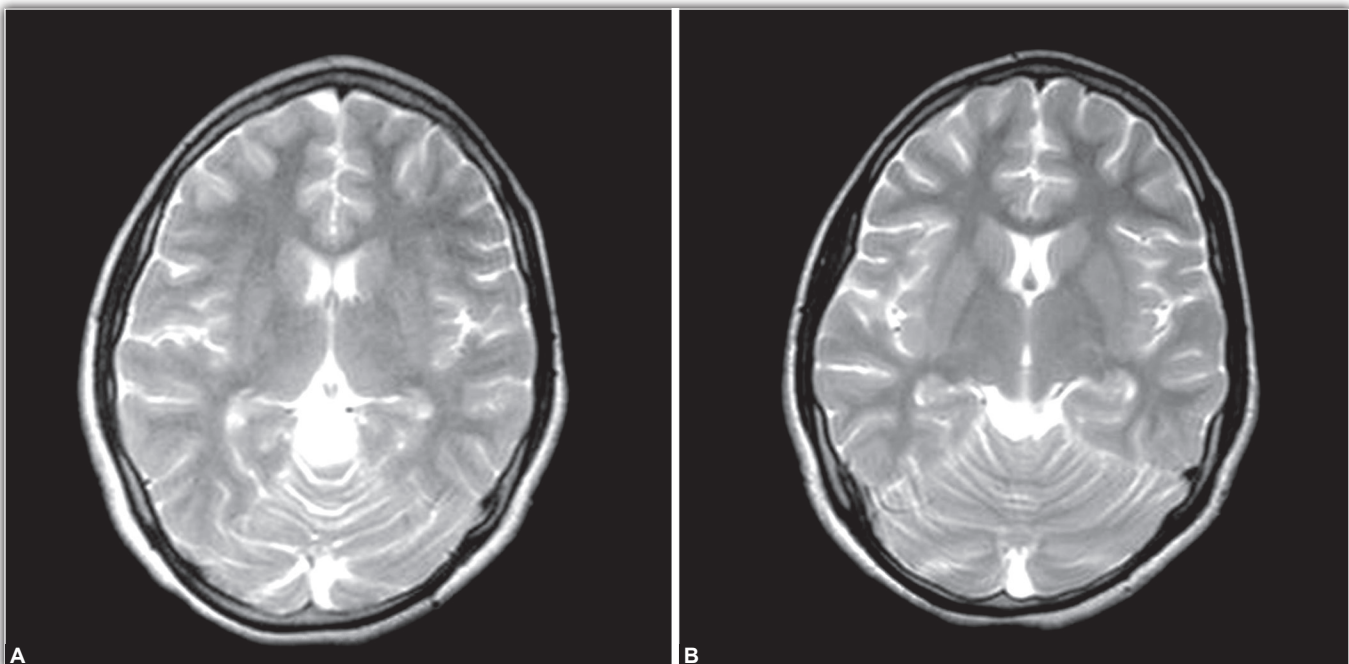
This is the angle through which NMV is moved as a result of RF excitation pulse. When a large flip angle is used, longitudinal magnetization is entirely converted into transverse magnetization resulting in maximum signal. On the other hand, small flip angles convert only a proportion of the longitudinal magnetization to transverse magnetization. A small flip angle is used in gradient echo imaging which results in a low SNR and hence measures may have to be taken to improve it.

### Number of Signal Averages

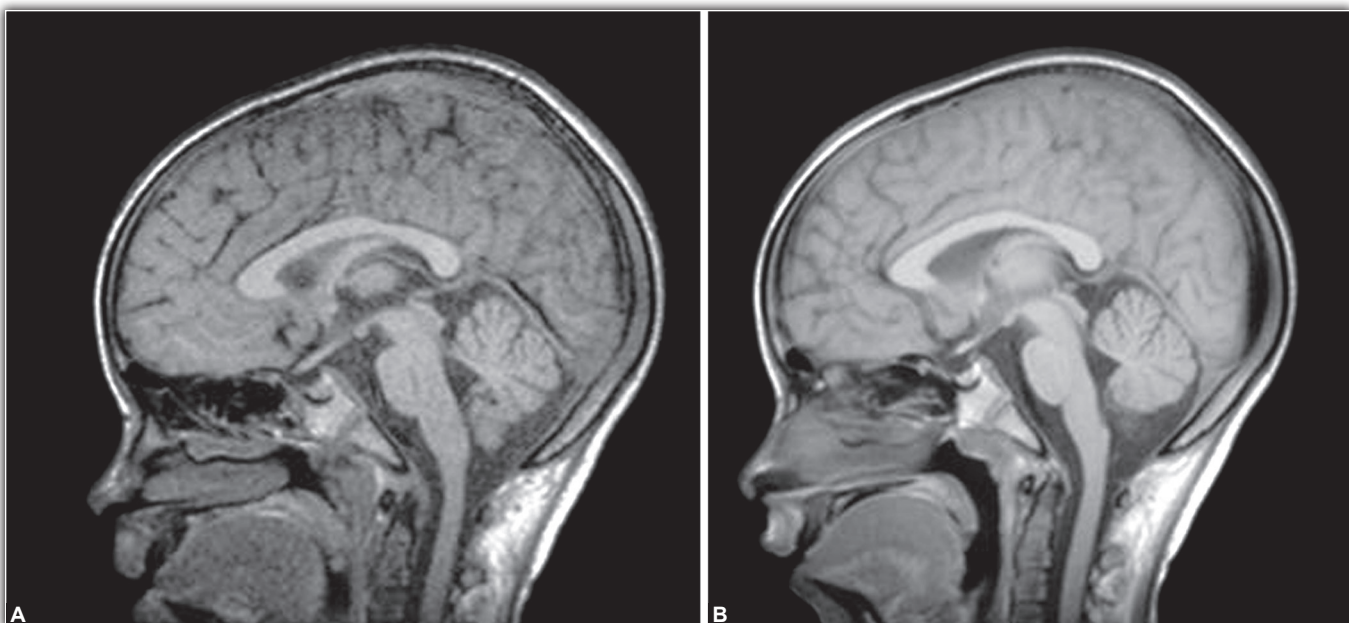
Number of signal averages (NSA) determines the number of times frequencies in the signal are sampled with the same slope of phase encoding gradient. Multiple measurements of one slice are obtained and the results are averaged in a single image. Increasing the number of excitation (NEX) increases the signal collected. We need to remember that noise is also being increasingly sampled. As noise occurs randomly and at all frequencies, doubling the number of signal averages does not double the SNR but only increases the SNR by a square root of two. Also, when NEX is doubled the time required to obtain the scan is also doubled (**Figs 1A and B**).

### Slice Thickness

When we obtain thicker slices, the voxel is enlarged and hence more proton spins contribute to the signal, thereby increasing the signal intensity. Noise remains the same because it is not just coming from the slice, but the patient's entire body and MR environment. Hence, SNR is directly proportional to the slice thickness. The drawback is that, increasing the slice thickness reduces the spatial resolution resulting in partial volume effects (**Figs 2A and B**).



**Figs 1A and B** Image comparison. T2 weighted axial images of the brain acquired with one signal average on the left (A) and four signal averages on the right (B). The SNR of the image B was double that of A. Also, the scan time of B was four times that of A



**Figs 2A and B** Image comparison. T1 weighted sagittal images of the brain. The image on the right (B) was acquired with double the slice thickness on the left (A). The SNR of the image B was double that of A. However, this occurred at the expense of spatial resolution

### Receiver Bandwidth

This is the range of frequencies sampled within the FOV during readout in the frequency encoding direction. It is measured in kilo Hertz (kHz). Reducing the receiver

bandwidth reduces the proportion of noise sampled relative to signal, hence effectively increasing the SNR.

The drawback here is that to reduce the bandwidth, the sampling time has to be increased to satisfy Nyquist

theorem. This theorem states that the sampling rate must be at least twice the frequency of the highest frequency in the echo to accurately reflect all the frequencies in the signal. If receiver bandwidth is reduced keeping all parameters unchanged, then sampling time needs to be increased to be able to sample all frequencies accurately. As the echo is centered in the middle of the sampling window, TE need to be increased. Therefore, it is not suitable for T1 or proton density weighted imaging, where a low TE is used. Also, chemical shift artifact is increased when receiver bandwidth is decreased. Reduced receive bandwidths should be used when a short TE is not required (T2 weighting) and when fat is not present (example: brain, and in any examination when fat is suppressed).

### CONTRAST TO NOISE RATIO

MR images would have no clinical value without satisfactory image contrast which is defined as the difference in signal strength between two tissues in the image. A high SNR does not guarantee easy differentiation of two structures in an image. Contrast to noise ratio (CNR) is the most important image quality factor because this allows for differentiation between anatomical tissues in the image and also in differentiation between pathological and normal tissue, hence aiding in final analysis of the image. Superior soft tissue contrast is a major advantage of MR imaging versus alternative modalities such as computed radiography.

Contrast in MR is a complex function of intrinsic characteristics of the structure, i.e. proton density, T1 and T2 relaxation times, magnetic susceptibility of the nuclei as well as programmable pulse sequence parameters, e.g. TR, TE, flip angle, slice thickness, etc. For example, longer TR allows more time for T1 relaxation and produces more signal from tissues with long T1 values. Longer TE, on the other hand, allows more time for T2 relaxation and produces more signal from tissues with long T2 values.

The factors that increase CNR are administration of a contrast agent, magnetization transfer constant, chemical suppression techniques and T2 weighting, where difference between pathology and anatomy is increased.

### Administration of a Contrast Agent

A contrast agent like gadolinium shortens the T1 time of structures, especially of pathological lesions when they have a break in blood brain barrier. Enhancing tissue appears much brighter, hence boosting the CNR.

### Magnetization Transfer Constant

In biological systems, protons can be described as existing in two pools. The 'free pool' consists of relatively mobile protons in free bulk water and some fat containing tissues. With standard MRI, this pool provides the bulk of the signal. The second pool or 'bound pool' consists of restricted protons bound in proteins, other large macromolecules, and

cellular membranes. With conventional MRI, this pool does not contribute to MR signal due to very short T2.

Under normal MR conditions magnetization is exchanged from the 'free pool' to the 'bound pool' and vice versa, resulting in an equilibrium situation characteristic for that type of tissue.

When additional RF pulses are used to suppress bound protons, it results in no net magnetization of the 'bound pool'. A difference in magnetization between the pools is thereby created. Due to cross relaxation processes, magnetization is transferred from the 'free pool' to the 'bound pool'. A new equilibrium is reached decreasing the SN ratio of a particular tissue. Hence the contrast with the surrounding tissue is accentuated. It is primarily used to suppress normal tissue.

### Chemical Suppression

Signal is suppressed either from fat or water. For example, fat suppression techniques null fat and hence CNR between lesions and surrounding normal tissues that contain fat is increased.

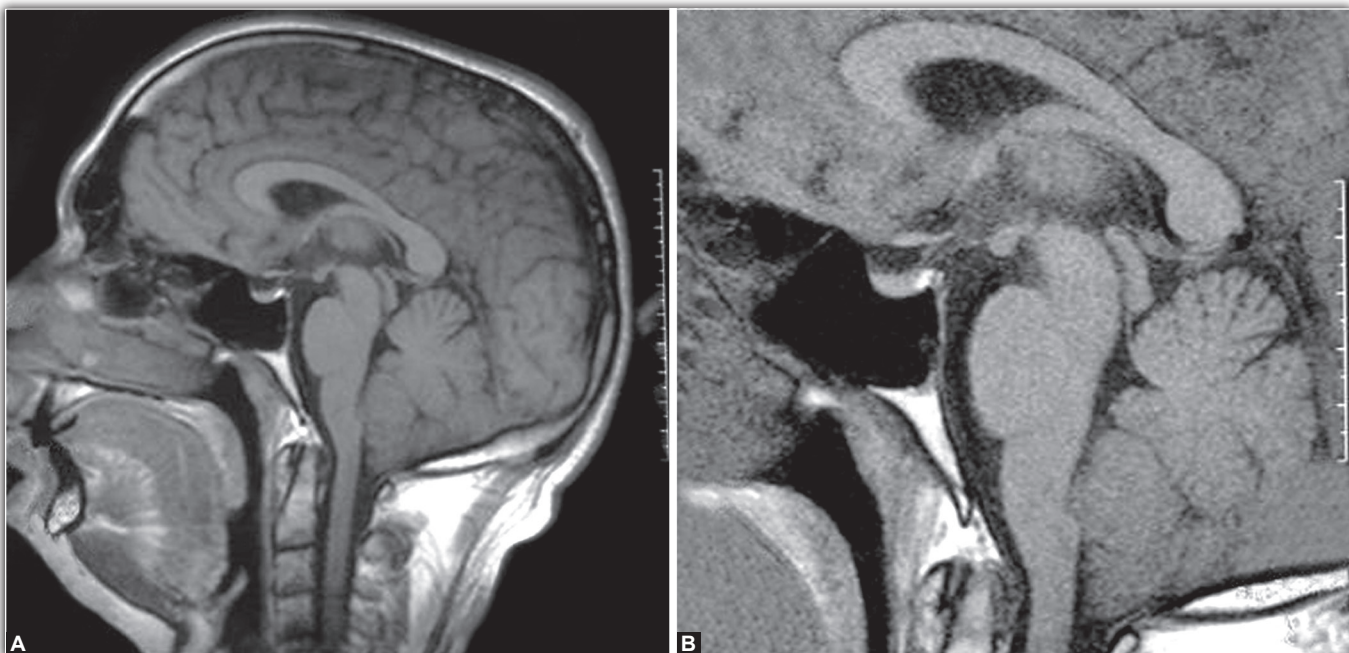
### Echo Train Length

In fast spin echo sequence (FSE), a train of 180° rephasing pulses are used. The number of these pulses and resultant echoes is called the echo train length or turbo factor. Since each echo has a different TE and data from each echo are used to produce one image, the contrast of FSE is unique. On T2 FSE, fat is hyperintense as this echo train reduces spin-spin interactions in fat, thereby increasing T2 decay time (J-coupling). Muscle appears darker because the echo train increases magnetization transfer effects that produce saturation.

### Time from Inversion

The time from inversion (TI) is the main factor that controls the contrast in Inversion recovery sequences (IR).

These are spin echo sequences that begin with a 180° pulse which flips the NMV by 180°. At time TI after the 180° inverting pulse, a 90° pulse is applied which is then followed by 180° pulse for rephasing spins that produces echo at time TE. If TI is long enough to allow NMV to pass through the transverse plane before the 90° pulse is applied, the contrast will depend on how much saturation this 90° pulse produces. Saturation is when NMV is pushed beyond the transverse plane by the 90° pulse and results in T1 weighting. TIs of 300 to 700 ms result in heavy T1 weighting. Certain specific TI values result in suppression of signal from specific tissues. For example, TI of 100 to 180 ms is used in STIR sequence. 90° pulse is here applied after this TI when NMV of fat is passing exactly through transverse plane. At this null point, there is no longitudinal magnetization of fat and hence no transverse magnetization results on application of 90° pulse, therefore resulting in no signal from fat. Similarly, TIs of 1700 to 2200 ms are used to null the signal from CSF on FLAIR imaging.



**Figs 3A and B** Image comparison. T1 weighted sagittal images of the brain. The image on the right (B) was acquired with reduced FOV and reduced pixel size compared with left (A). The spatial resolution of B was increased at the expense of reduced SNR

### ■ SPATIAL RESOLUTION

Spatial resolution is defined as the ability to distinguish between two points that are close to each other in the patient. The size of the voxel determines the spatial resolution. The imaging volume is divided into slices. Each slice displays an area of anatomy which is called the field of view (FOV). This FOV is divided into pixels. The size of the pixels is determined by the matrix. The FOV may be specified separately for the frequency encoding and phase encoding directions which may be the same in a square or isotropic FOV and different in an anisotropic or a rectangular FOV. Frequency and phase encoding gradients are applied to spatially locate the signal coming from each pixel in the FOV.

### Voxel Volume, FOV, Matrix

Voxel volume is a product of pixel size and slice thickness. Therefore, slice thickness, FOV and matrix size determine voxel volume. The greater the voxel volume, more are the number of spins that contribute to MR signal, resulting in a higher SNR per voxel. However, when the voxels are larger, spatial resolution falls as the likelihood of two points close to one another in the patient, being in separate voxels decreases.

When FOV is decreased, pixel size and hence voxel volume decreases, thereby decreasing the SNR and increasing spatial resolution (**Figs 3A and B**). When small coils are used which boost local SNR, a small FOV may be used. However, a small FOV should be used with caution with a large coil as SNR will be severely compromised unless other measures like increasing NEX is used.

When the matrix is changed, the number of pixels that must fit into the FOV also changes. As the matrix increases, the dimension of each pixel decreases. This reduces the SNR but improves spatial resolution. In addition as the phase matrix increases, the scan time also increases (**Figs 4A and B**). However, if we increase the frequency matrix only, it increases the resolution but the scan time does not increase as only the phase matrix determines scan time. A rectangular FOV where the FOV is reduced in the phase direction reduces the scan time keeping the resolution same as that of square FOV. This is especially useful when anatomy of the area examined fits into a rectangle, as in sagittal image of pelvis.

Increasing the slice thickness increases the voxel volume, hence increasing SNR at the expense of spatial resolution (**Figs 2A and B**).

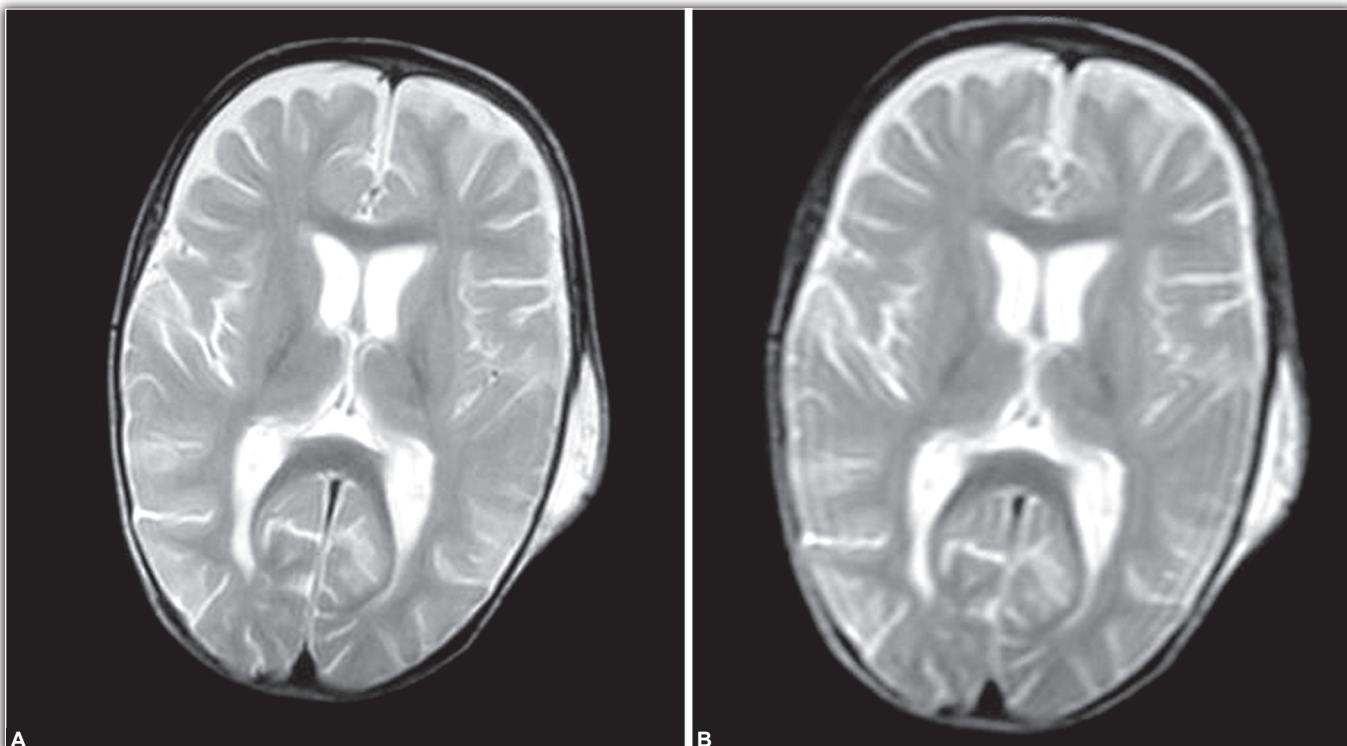
### ■ SCAN TIME

The longer the examination time, the greater the discomfort to the patient resulting in increased chances of a bad image. Good immobilization is also essential, as a few minutes spent in making the patient comfortable can save us many minutes of wasted sequences. The scan time is determined by the following factors.

$$\text{Scan time} = \text{TR} \times \text{number of excitations} \times \text{number of phase encodings}$$

### TR

The greater is the time between the application of two RF pulses, the greater is the scan time. When we reduce the TR,



**Figs 4A and B** Image comparison. T2 weighted axial images of the brain. The image on the left (A) was acquired with increased matrix and hence reduced pixel size compared with right (B). The spatial resolution of A was improved. As the phase matrix was increased, the scan time was also increased

we can reduce the scan time. However, reducing TR reduces SNR as already discussed. As less longitudinal magnetization recovers during each TR period, the next 90° pulse flips it to beyond the transverse plane. This is called saturation and increases T1 weighting. As there is less time to excite slices in this reduced TR, the number of slices that can be acquired in a single acquisition also decreases.

### Number of Excitations (NEX)

When the NEX or signal averages is increased, more and more measurements of one slice are being obtained to average the results. This increases the scan time (**Figs 1A and B**). But when we reduce the NEX to reduce scan time, SNR falls because now, the number of times data is stored in k-space is reduced. Since averaging of noise is also less, there is also an accompanying increase in motion artifact.

### Phase Matrix

Increasing the phase matrix increases scan time (**Figs 4A and B**). To understand this, we shall first discuss the basic physics behind MR gradients. Gradients are coils of wire that alter the magnetic field strength of the magnet in a controlled manner when current is passed through them. They change the precessional frequency and phase of the spins. These are

employed along three orthogonal axes, XYZ, to enable us to select a slice (slice selection gradient), and to spatially locate the signal along the two dimensions of the image within a slice (frequency encoding and phase encoding gradient).

Frequency encoding gradient is switched on to locate signal along one axis of the image (usually the long axis) and produces a frequency shift. At a frequency matrix of 256, 256 different frequencies are mapped along the long axis of the image. Fourier transformation allows us to determine signal contribution of each frequency, enabling us to allocate this signal to the location of origin along one axis of the image. Fourier transformation is like a prism (which disperses white light into its spectra) that causes physical dispersion of the frequencies collected and assigns them to a structure in the image.

Phase encoding gradient alters the phase of the nucleus, causing a phase shift. When this gradient is switched off, phase shift of spins remains. This phase shift is used to locate the signal along one dimension of the image (usually the short axis). For a phase resolution of 256, we have to generate 256 signals with different phase encodings for 256 different locations. The pulse sequence has to be repeated 256 times for a phase matrix of 256. Hence, the phase matrix is an important determinant of scan time. If we reduce the phase matrix to reduce scan time, the spatial resolution of the image falls.

### Number of Slice Encodings in 3D Sequences

In three dimensional fast scan sequences, scan time is also dependent on the number of slice locations required in the volume in addition to TR, NEX and number of phase encodings

$$\text{Scan time} = \text{TR} \times \text{number of excitations} \times \text{number of phase encodings} \times \text{slice encodings}$$

### ARTIFACTS

Artifacts are structures in the MR image that do not correspond to spatial distribution of tissue in the image plane. The cause of this signal misregistration is variable; artifacts are divided into three main types based on the cause.

1. Motion artifacts
2. Artifacts related to particular measurement technique or parameters used, e.g. chemical shift, wrap around and truncation artifacts.
3. External artifacts results from either a malfunction of the MR scanner or external interference.

### Motion Artifacts (Phase Mismapping)

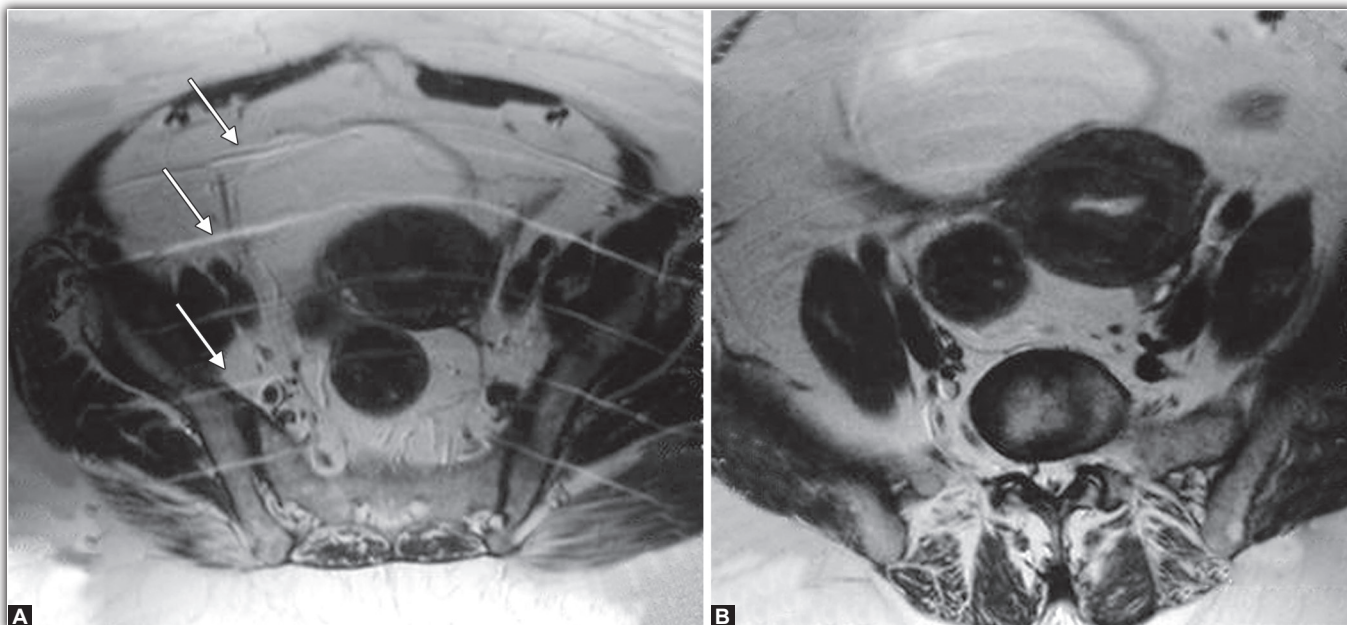
These may result from accidental patient movement, respiration, heart beat, blood flow, eye movements or swallowing motion. These signal misregistrations occur in the phase encoding direction. The tissue is excited at one location but is mapped to a different location during readout due to its motion. This occurs in the phase encoding direction

rather than the frequency encoding or readout direction because the encoding of phase by the phase encoding gradient occurs prior to signal detection, whereas frequency encoding gradient, also called the readout gradient, is applied concurrently with signal detection. For example, if the abdominal wall is at one position when the phase encoding gradient is applied, its phase shift value is allocated to it according to this position. During readout, the abdominal wall has moved to another position, the system still allocated it according to its first position resulting in ghosting artifact. Also, patient motion normally is much slower than the faster sampling process along the frequency encoding direction (in order of milliseconds). On the other hand, sampling along phase encoding direction needs all phase encoding steps and is in the order of seconds. This is another reason why motion artifacts are appreciable more along phase encoding direction.

#### *Ghosting and Smearing*

While ghosting results from periodic motion, smearing is a result of aperiodic motion.

The periodic rise and fall of thorax/abdomen during breathing produces an artifact called ghosting (**Figs 5A and B**). If the respiration rate is constant, then during inspiration, the abdomen is in several equidistant phase encoding steps during the inspiration phase and it is in the expiration phase in the intervening steps. This periodic motion is seen as locally offset double or multiple structures



**Figs 5A and B** Ghosting artifact. T2 weighted image of the pelvis (A) shows marked ghosting artifact (arrows) due to periodic respiratory motion. This was reduced in (B) by increasing the number of signal averages and placing a spatial presaturation pulse in the overlying subcutaneous fat. However, both these techniques contributed to an increase in scan time

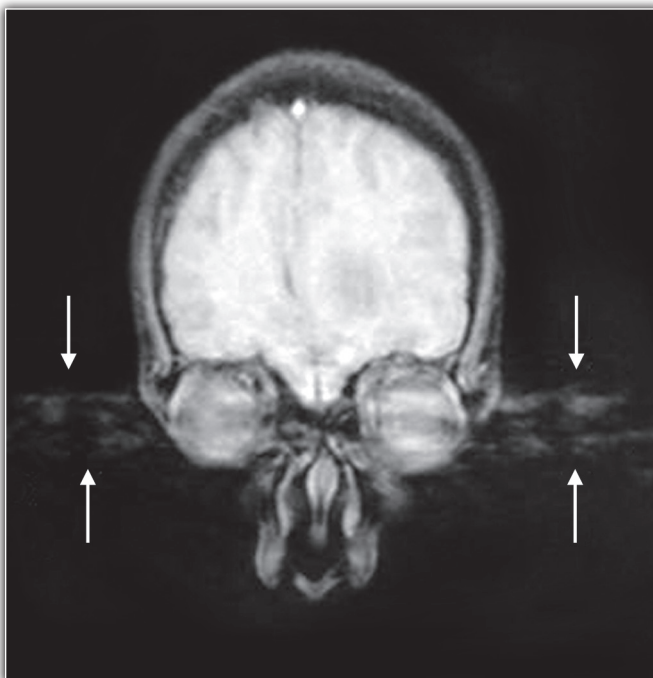


**Fig. 6** Smearing artifact. T1 weighted coronal image of the brain shows smearing artifact (arrows) due to aperiodic motion of the eyes

in the phase encoding direction. These ghosts are offset by the true image by an amount proportional to the respiration rate. Structures rich in signal, for example subcutaneous fat, further increase ghosting artifact. In a strictly periodic motion, the localization of the ghost can be predicted by a simple formula, describing the distance between the ghost image and the original structure.

$$\text{Distance} = \text{TR} \times \text{phase encoding steps} \times \text{NEX} \times \text{motion frequency}$$

The higher the frequency of the motion, e.g. higher the breathing rate, the greater the distance between the original and the ghost artifact. We can increase the distance between the ghosts by increasing TR, phase matrix or NEX so that the first ghost lies outside the image; however scan time is increased by all these methods. The brightness of the ghost depends upon the amplitude of motion; larger the pulsation, brighter the ghost.

Another type of artifact that may result from aperiodic motion like that of eyes is smearing (**Fig. 6**). Peristalsis, which is a random movement, produces motion artifacts that result in generalized blurring of the image, which appears to be superimposed by a layer of noise.

Blood flow is a very common cause of motion artifacts in the image. Fast continuous flow compared to TR produces a continuous artifact throughout the FOV, resulting in blurring, as in spin echo images. In-plane flow, parallel to the slice plane produces a diffuse artifact seen in coronal images. Flow in aorta and IVC affects the entire image acquired in coronal

plane as these great vessels extend through the entire image. CSF flow artifacts can also degrade the image of the spine on T2 weighted images. Periodic motion due to pulsatile through plane flow (flow perpendicular to the image plane) will be discussed later.

#### *Remedy*

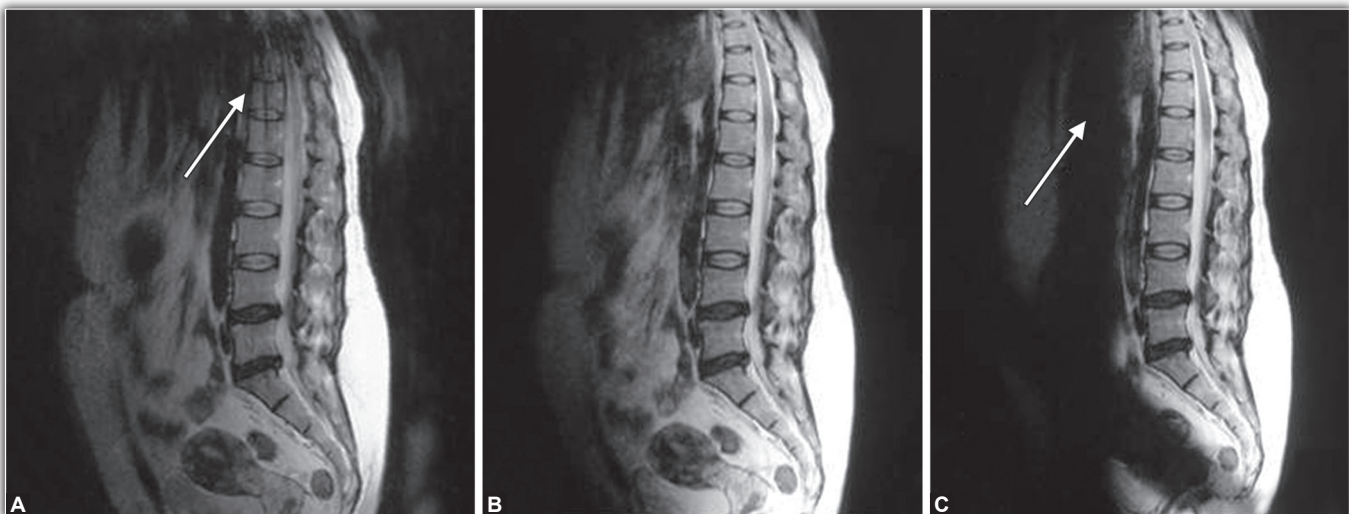
Various methods are used to reduce the severity of motion artifacts in the final image, depending upon whether signal from moving tissue is desired in the image or not. While spatial presaturation pulse may be used in the former case, other remedial measures are required when signal from moving tissue is desired in the image.

**Spatial presaturation pulse:** When signal from moving tissue is not desired, spatial presaturation pulse can be used to reduce these artifacts. These are used in spine examinations to suppress cardiac and abdominal motion artifacts (**Figs 7A to C**). These saturation pulses are applied at the beginning of the pulse sequence and hence reduce the number of imaging sections that can be obtained per TR in multislice acquisitions. They may also result in increased heat deposition when specific absorption rate (SAR) is already high.

When signal from moving tissue is desired in the image, other methods may be used. These include use of faster sequences, modification of acquisition parameters, physiological triggering and flow compensation.

**Faster imaging:** The most effective technique may be shortening of acquisition time to minimize motion artifacts. This has been potentiated by improvements in MR imaging hardware, including faster and stronger gradients, multichannel coils, and higher magnetic field strengths.

There are various techniques to obtain faster sequences. Fast spin echo sequences use multiple 180° refocusing pulses and allow multiple echoes to be obtained within a given TR. The number of additional echoes obtained is called the echo train length (ETL). However, excessive ETLs may blur the image and increase some flow artifacts. Sequences such as half Fourier single-shot turbo spin echo (HASTE) allow rapid acquisition by filling only half of k-space. Parallel imaging technique also reduces the scan time and hence motion artifacts. This technique uses multichannel, multicoil technology, with each coil possessing a distinct known sensitivity profile over the field of view. At least 2 coil elements are aligned in the phase encoding direction. The phase encoding steps are reduced by a factor of X, known as the parallel imaging factor. Only one of every X lines of k space is filled up in the phase encoding direction. The other lines are inferred from the signal amplitude and known sensitivity profile of the coils used. Several data extrapolation algorithms like GRAPPA (generalized autocalibrating partially parallel acquisition) and SENSE (sensitivity encoding) are used before and after Fourier transformation respectively. The major disadvantage is a decreased SNR. However, overall increase in SNR at 3T makes higher parallel imaging factors feasible in clinical practice.



**Figs 7A to C** Motion artifact. T2 weighted sagittal images of the spine show marked motion artifacts degrading the image in (A) (arrows) when the phase encoding direction was anterior to posterior. On changing the phase encoding direction to head to foot in (B), the motion artifacts from the heart do not degrade the image. There is further improvement in image quality when a spatial presaturation band (arrows) is used to suppress motion artifacts from the great vessels in (C)

**Radial k space filling technique:** Multi-shot radial acquisition technique (e.g syngoBLADE, Siemens healthcare, Erlangen, Germany; PROPELLOR, GE healthcare, Milwaukee, Wis) fills the k space radially instead of standard line by line rectilinear filling. With this technique, MR imaging datasets are acquired in multiple overlapping radial sections. A series of low resolution images is reconstructed from each radial section which is then combined to produce a high resolution image. Because the phase encoding direction varies with each radial section, ghosting artifact from motion is not propagated in the phase encoding direction but dispersed through the radial sections. Its main disadvantage is low spatial resolution because the periphery of k space is more sparsely filled than its central region.

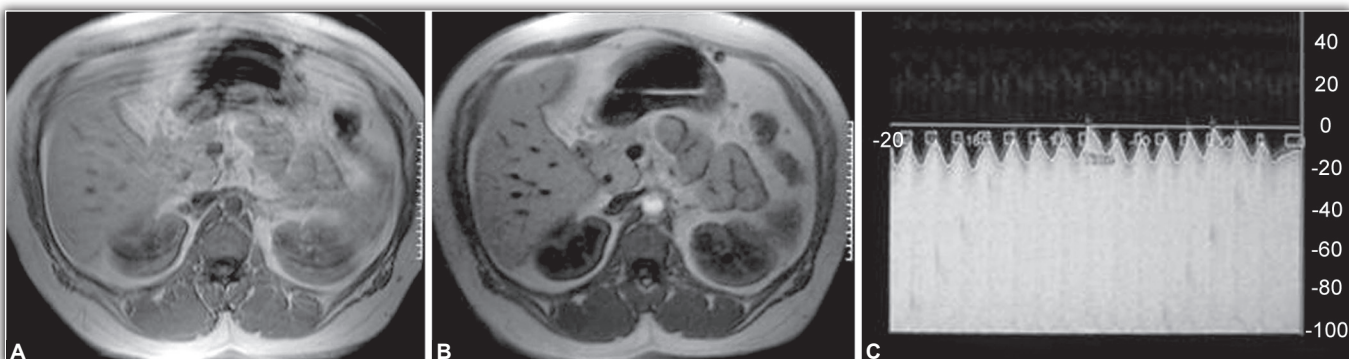
**Modification of parameters:** Parameters may be modified to alter the appearance of motion artifacts. Frequency and phase encoding direction can be swapped, which alters the position of the artifact (**Figs 7A to C**). These may now be relocated to image areas that do not affect image interpretation. For example, motion artifacts due to eye movement may obscure brain parenchyma if phase encoding direction is antero-posterior for an axial image. This may be overcome when phase encoding direction is made right to left and the artifact now lies outside the brain.

Increasing NEX is another method of reducing motion artifacts. Increasing the number of signal averages increases the signal from the tissue and the motion artifact signal is reduced relative to the tissue signal (**Figs 5A and B**).

**Physiological triggering/gating:** Physiological triggering synchronizes the data collection with a periodic signal produced by the patient, such as pulse or heartbeat allowing

normal movement of tissue. Data collection may be synchronized with ECG signal using lead wires, pulse using pulse sensor on an extremity, respiration using pressure transducer on the patient or a navigator echo indicating diaphragmatic motion. ECG gating is used in cardiac evaluation where artifacts from cardiac motion need to be minimized. This may be prospective or retrospective gating. In the prospective method, the timing signal is first detected. The echo signal is collected at the same time following the time signal. Since the moving tissue is in the same position at this time, there is minimal misregistration of signal. This is typically used in static cardiac examinations. Prospective triggering also allows the rejection of arrhythmic beats, which can degrade MR image quality. In the retrospective method, the timing signal and the echo signal are first acquired together. Data collection is not controlled by the timing signal. These are analyzed only after the scan is completed and the data collection is gated to the timing signal. This method is commonly used in cine cardiac imaging where sequential images are produced according to their time point in the cardiac cycle to allow a dynamic evaluation of cardiac function. Further artifact suppression can be achieved while imaging the heart, if the acquisition is performed during breath holding. The disadvantages of a triggered study include a longer scan time and misregistration artifacts if the trigger signal is irregular, e.g. with an irregular heart rate.

In contradistinction to cardiac gating, respiratory gating is not frequently used in clinical imaging. Breath holding is the method used to avoid respiration artifacts. In infants, children, and patients with respiratory and cognitive impairment, either short sequences are used or imaging examination is divided into multiple brief sequences if



**Figs 8A to C** Motion artifact. Axial T1 weighted gradient echo image of the abdomen shows marked respiratory motion artifact resulting in blurring of the image (A). There is marked reduction in motion artifact (B), using a navigator echo pulse (C)



**Fig. 9** Ghosting artifact from pulsatile aortic flow. Pulsatile through plane flow in the aorta is seen as ghost vessels at discrete points (arrows) on this T1 weighted axial gradient image

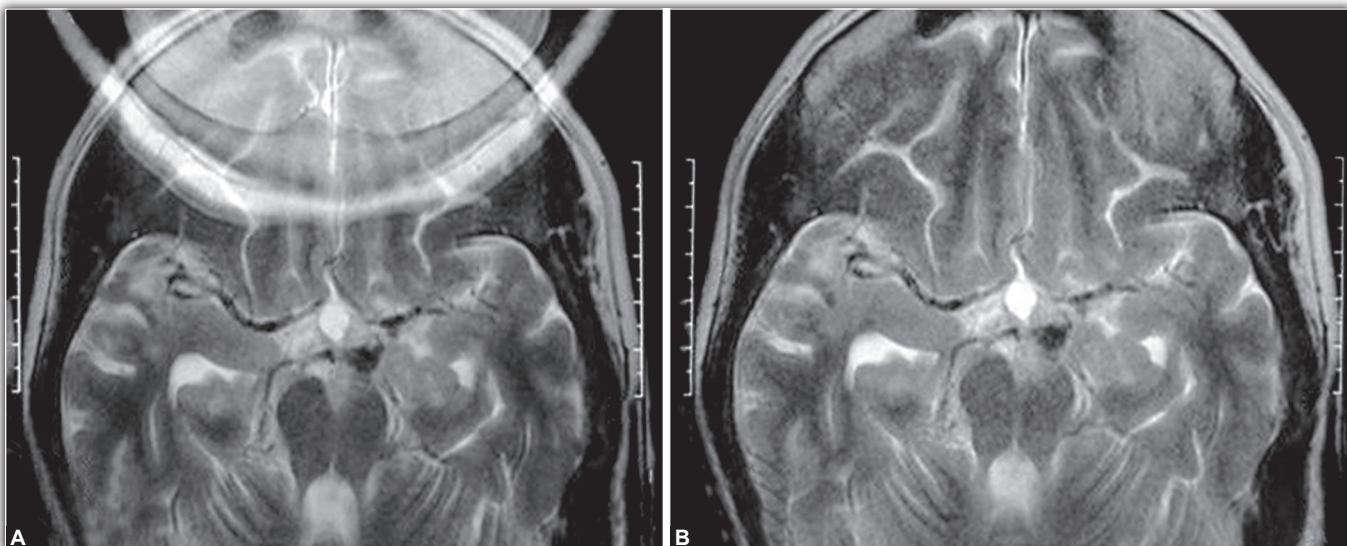
the patient can hold breath for a limited time. However, multiple breath holds require cooperation from the patient. In respiratory gating, bellows or a belt is encircled over the abdomen and the acquisition is timed to end expiration when there is minimum motion. The disadvantages include an increased acquisition time and an additional setup time. Respiratory compensation or phase reordering [respiratory ordered phase encoding (ROPE)] is another effective way to reduce respiratory artifacts. In this technique, phase encoding steps are ordered on the basis of the phase of the respiratory cycle. Kspace lines are reordered such that the adjacent samples in the final data have minimal differences in the respiratory phase. This works well only with regular respiratory rate. Navigator echo is a commonly used method to suppress periodic motion artifacts from breathing; it uses

an additional navigator pulse. This is most commonly used in abdominal imaging where a small one dimensional spatial encoding gradient is placed perpendicular to the diaphragm (**Figs 8A to C**). The imaging dataset is then corrected by the navigator echo so that only the data acquired at end expiration (when diaphragm is at peak) is used in reconstruction of final image.

**Gradient Moment Rephasing:** GRE Flow compensation uses additional gradient pulses to correct for phase shifts of the moving protons. It is also known as gradient motion rephasing (GMR) or motion artifact suppression technique (MAST). Additional gradient pulses are used to eliminate the phase shifts in moving protons, bringing them back into phase with no effect on static spins. In most instances, correction is needed only for spins flowing with constant velocity (first order motion compensation). As additional gradient pulses are used, there is a modest increase in TE. In pulse sequences in which short TEs are desired, short duration high amplitude gradient pulses need to be used. This limits the minimum FOV for the sequence. Higher order compensation can also be done for spins with constant or varying acceleration, but this increases the echo time even further.

#### Pulsatile Flow Related Artifacts

Periodic motion due to pulsatile through plane flow (flow perpendicular to the image plane) results in ghost vessels at discrete points, frequently seen in axial abdomen gradient echo images (**Fig. 9**). The distance between the ghosts depends on the difference between the heart rate and TR. GRE images are more prone to these ghost artifacts than SE sequences. In spin echo sequences, flowing blood usually appears dark. This is because after being exposed to the 90° excitation pulse in SE sequences, flowing blood moves out of the imaging section before the refocusing 180° pulse is applied, while the blood protons that move into the imaging section has not been exposed to the excitation pulse; hence resulting in dark signal. In contrast, bright blood phenomenon is seen on GRE sequences.



**Figs 10A and B** Aliasing artifact. T2 weighted axial images of the brain depict aliasing artifact when it was acquired with a reduced FOV smaller than the anatomy of the image. The tissue outside the FOV was misrepresented on the opposite side (A). This was overcome by oversampling in the phase encoding direction (B). However, there was no penalty in scan time as NEX was halved

#### Remedy

**Saturation pulse:** A common way to reduce the motion artifact due to through-plane flow is to apply a saturation band adjacent to the imaging section. The protons in this slab are saturated with the use of 90° RF pulse and then spoiled by strong gradients before image acquisition, hence resulting in no signal when spins flow into the imaging volume. When applied superior to the acquisition slab in the abdomen, it eliminates arterial pulsation artifact. When placed inferiorly, it eliminates artifacts from venous inflow in the iliac veins.

#### Advantage of pulsation artifacts

Pulsation artifacts from vascular lesions can help us reach the correct diagnosis, when in doubt. The vascular nature of the lesion is confirmed if we see associated pulsation artifacts.

### Artifacts Due to Measurement Technique/Parameters

#### Aliasing

Aliasing (wraparound artifact) occurs when the imaging FOV is smaller than the anatomy being imaged. This occurs mostly in the phase encoding direction. The tissue stimulated outside the sensitive volume of the coil contains higher or lower phase and frequency information. These are misinterpreted during Fourier transformation. This tissue is misrepresented in the image on the opposite side (**Figs 10A and B**). To explain this, let us recapitulate that the phase of the signal originating from inside the FOV has a range from 0 to 360°. Due to the circular nature of phase, a signal from outside the FOV with a phase of 400° (=360°+40°) is not distinguishable from a phase of 40° from inside the FOV and hence is misinterpreted within the FOV during Fourier

transformation. Thus, the part of the body that lies beyond the borders of the FOV is wrapped inside to the other side of the image. This can mask anatomical structures in the FOV.

Wraparound is seldom encountered along the frequency encoding axis because the frequency encoding direction is typically oversampled within the system. In the new imaging systems, the digital receiver automatically filters out unwanted high frequencies or makes use of a high bandwidth in the frequency encoding direction. Aliasing can also be seen in the section direction in volume imaging. The sidelobes of the RF pulse that excites the entire volume of tissue can also produce a signal from outside this slab and information in the first section of the slab may be aliased in the last section of the 3D acquisition (**Fig. 11**).

#### Remedy

**Increase FOV:** The wraparound can be eliminated by enlarging the phase FOV to accommodate the entire object. Increase in FOV increases the SNR but decreases the spatial resolution.

**Swapping the phase and frequency encoding direction:** The phase encoding and frequency encoding directions may also be swapped if the phase encoding is not already along the shorter axis.

**Oversampling/No phasewrap:** Oversampling may be done in the phase encoding direction. This is done by increasing the sampling points; however these are not used for image creation (**Fig. 10**). The FOV is doubled in the phase direction along with doubling of the phase matrix to avoid any decrease in spatial resolution. Oversampling increases the scan time. Hence the NEX is usually halved to compensate for doubling

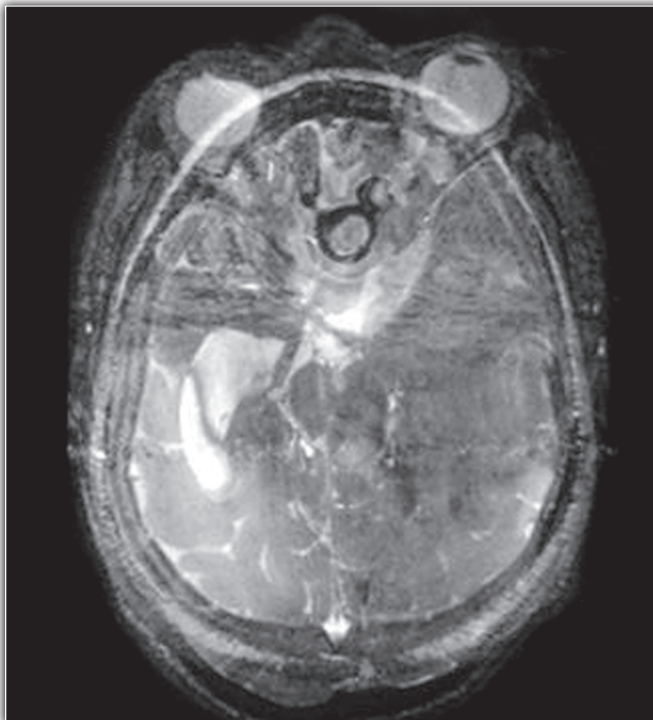


**Fig. 11** Aliasing artifact in volume imaging. 3D constructive interference in steady state (CISS) GRE sequence shows overlap of information of the first and last sections of the sequence due to aliasing



**Fig. 12** Moiré artifact. T1 gradient coronal image of the abdomen in a heavy patient using a large FOV that is still smaller than the patient depicts the moiré artifact. This is seen as stripes (arrows), and occurs as a result of a combination of aliasing and field inhomogeneities between the two edges. These are especially prominent at areas of susceptibility borders (e.g. air tissue interfaces)

of phase matrix. Usually, there is no penalty in scan time, SNR and spatial resolution. This may not be possible in fast scan techniques like those in abdominal imaging, when NEX is already minimum.

**Saturation pulse/regional coils:** Aliasing can also be minimized by suppressing signal from outside the region of interest using a presaturation pulse or with the use of regional coils to diminish the amount of signal received from outside the region of interest.

In 3D sequences, aliasing can be minimized by exciting only a limited part of the volume in the Z-direction by applying a Z-gradient pulse during the RF excitation.

#### Moiré /Fringe Artifact

In heavy patients, a special artifact may be seen in coronal imaging when a large field of view which is still smaller than the object is used. This results in aliasing superimposed on phase differences between the two edges. Over large fields of view, homogeneity of the field degrades at the edges, causing phase differences between the edges. Aliasing along with mismatched phases over the edges produces the moiré or fringe artifact (**Fig. 12**). These are seen in gradient echo images. Use of spin echo sequences eliminates these artifacts. Another measure that may be taken to reduce these artifacts is to ensure that the arms of the patient are

by the side of his/her body while positioning so that they are within the FOV while imaging chest/abdomen.

#### Chemical Shift Artifacts

The chemical shift phenomenon refers to the signal intensity alterations that result from the inherent differences in the resonant frequencies of precessing protons. Clinically, the chemical shift phenomenon is most evident between the signals of water and lipid. In water, hydrogen is linked to oxygen and in fat, it is linked to carbon. The protons hence have different chemical environments. When placed in an external magnetic field, these protons have slightly different precessional frequencies. Hydrogen in fat resonates at a lower frequency than water. Because fat and water protons have different precessional frequencies, these are allocated to different image pixels along the frequency encoding axis. Although this occurs throughout the image, this is most apparent at fat fluid interfaces, e.g. in imaging of fluid filled structures like bladder, orbits and kidneys which are surrounded by fat. When the chemical shift misregistration is greater than or equal to the size of an individual pixel, a dark or bright band of signal intensity will occur at the lipid-water interface in the frequency-encoding direction of the image.

The dark bands result from the shifting of the lipid proton signals to a lower frequency, away from the actual lipid-water interface, which causes a signal void. The bright bands result from the overlapping of water signal with "shifted" lipid signal on the high-frequency side of the interface. The bright bands, although present, may be more difficult to appreciate when the object being imaged has a curved surface.

The approximate chemical shift between lipid and water is 3.5 parts per million. At field strength of 1.5 T, protons from fat resonate at a point approximately 220 Hz downfield from water protons. This difference is directly proportional to magnetic field strength. The number of pixels involved in this shift is directly proportional to the field strength and frequency matrix but inversely related to the receiver bandwidth.

$$\text{CSA} = \Delta\omega \cdot N_{\text{freq}} / \text{BW}_{\text{rec}}$$

CSA = chemical shift artifact,  $\Delta\omega$  = frequency difference between fat and water dependent on field strength,  $N_{\text{freq}}$  = frequency matrix,  $\text{BW}_{\text{rec}}$  = receiver bandwidth

In high field strength magnets, frequency difference between fat and water increases, resulting in greater CSA. However, higher SNR at this field strength allows higher bandwidth sampling rates, which diminishes these artifacts. Use of narrow receiver bandwidths and large matrix in the frequency encoding direction can accentuate these artifacts. These artifacts were commonly seen in T2 weighted images before the invention of TSE imaging as the former used low bandwidths to increase the low SNR inherent in T2 weighted sequences.

#### *Remedy*

To reduce these artifacts, various measures may be taken. The phase and frequency encoding direction may be swapped. The frequency encoding direction may be used along the axis where there is narrow fluid fat interface or in a direction where this artifact does not hamper the primary area of interest. Suppression of fat or water signal by the use of STIR/chemical/spectral presaturation is another means of reducing this artifact.

Receiver bandwidth is another parameter that may be altered to reduce this artifact. Receiver bandwidth is the range of frequencies sampled within the FOV during readout in the frequency encoding direction. When this is increased, more frequencies are mapped across the same number of pixels. As a result, chemical shift reduces. However, when we increase the receiver bandwidth, signal to noise ratio of the image drops.

#### *Advantage*

Chemical shift along the frequency axis forms the basis of MR spectroscopic imaging.

#### *Chemical shift in echoplanar imaging*

These artifacts also occur with echoplanar imaging, but in the phase encoding direction. These are fast sequences where images are acquired in 50 ms to 80 ms. The receiver

bandwidth is normally very large in the frequency encoding direction (greater than 100 kHz), hence chemical shift is not appreciable in this direction. However, the phase encoding occurs in a continuous fashion with a low bandwidth, resulting in pronounced chemical shift artifacts in this direction. Use of fat suppression techniques is necessary to minimize the artifact (**Figs 13A and B**).

#### *Phase Cancellation Artifact*

This is the second artifact induced by chemical shift differences between fat and water protons. It can also be referred to as chemical shift artifact of the second kind. These artifacts are observed in gradient echo images and not in spin echo sequences which use a 180° refocusing pulse. This pulse redirects the fat and water proton spins back into phase with respect to one other by the time of readout (TE). The lack of a 180° refocusing radio-frequency pulse in gradient-echo sequences results in the cycling of fat and water proton signals in and out of phase with respect to each other over time. The time interval between fat and water being in phase is called the periodicity. This time, depends on the frequency shift and hence the field strength. At 1.5 T, the periodicity is 4.8 ms. This periodicity decreases at lower field strengths, hence the time at which fat and water protons are in phase with each other increases at low field strengths. At 1.5 T, fat and water signals precess in phase approximately every 4.8 msec; every 7.2 ms at 1.0 T; and every 36.7 msec at 0.2 T.

This periodicity is used to obtain in-phase and opposed-phase MR images. In in-phase images, fat and water have the same phase orientation. The signal contribution of fat and water protons therefore is additive in the final image. In opposed-phase images, the transverse magnetization of fat and water cancel each other. Hence, in voxels containing equal fat and water such as those at interfaces between fat and water based tissues, this signal cancellation results in a dark ring surrounding the tissue, also known as contour artifact (**Figs 14A and B**).

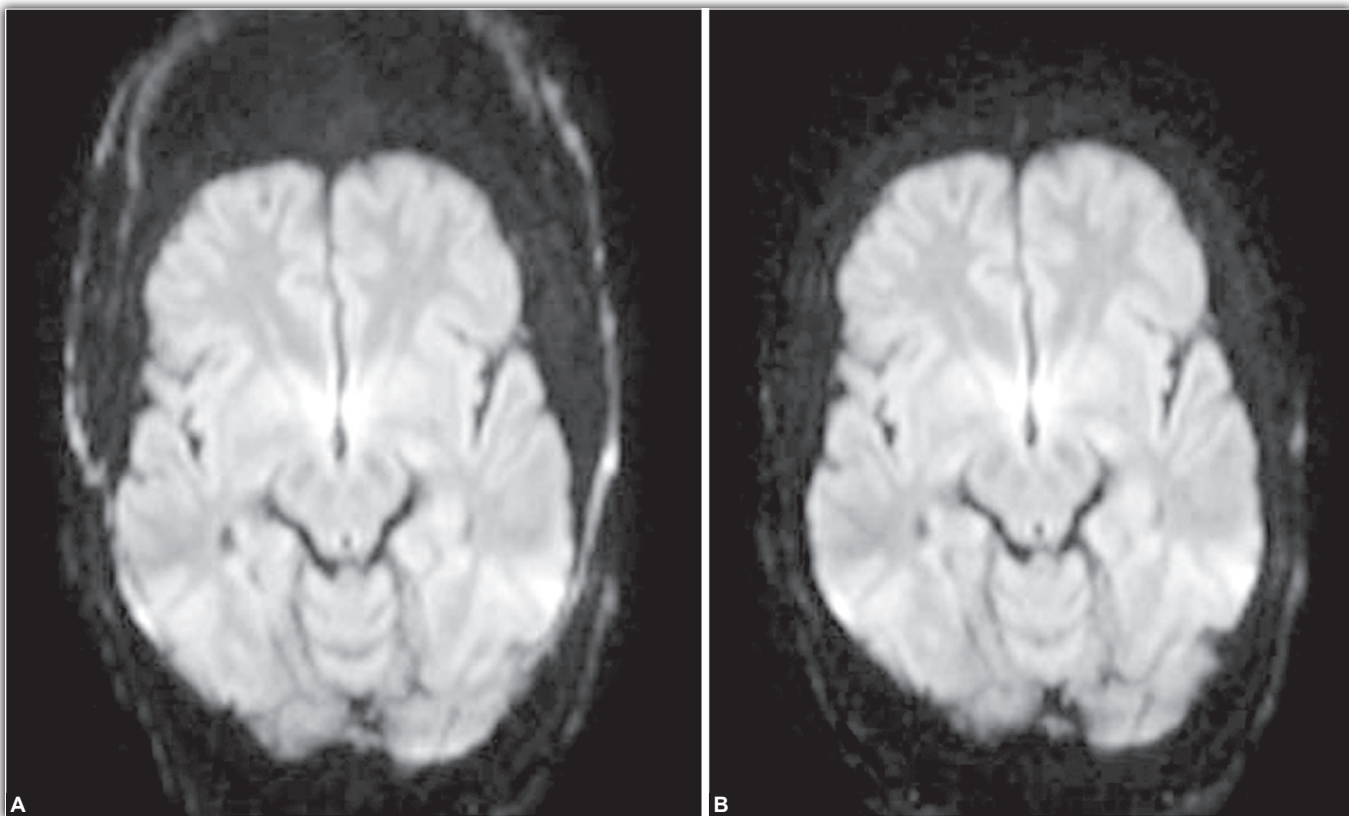
#### *Advantage*

Opposed- phase images are used to detect intracellular fat and can be used in assessment of fatty infiltration of liver, adrenal masses and in assessment of marrow infiltration.

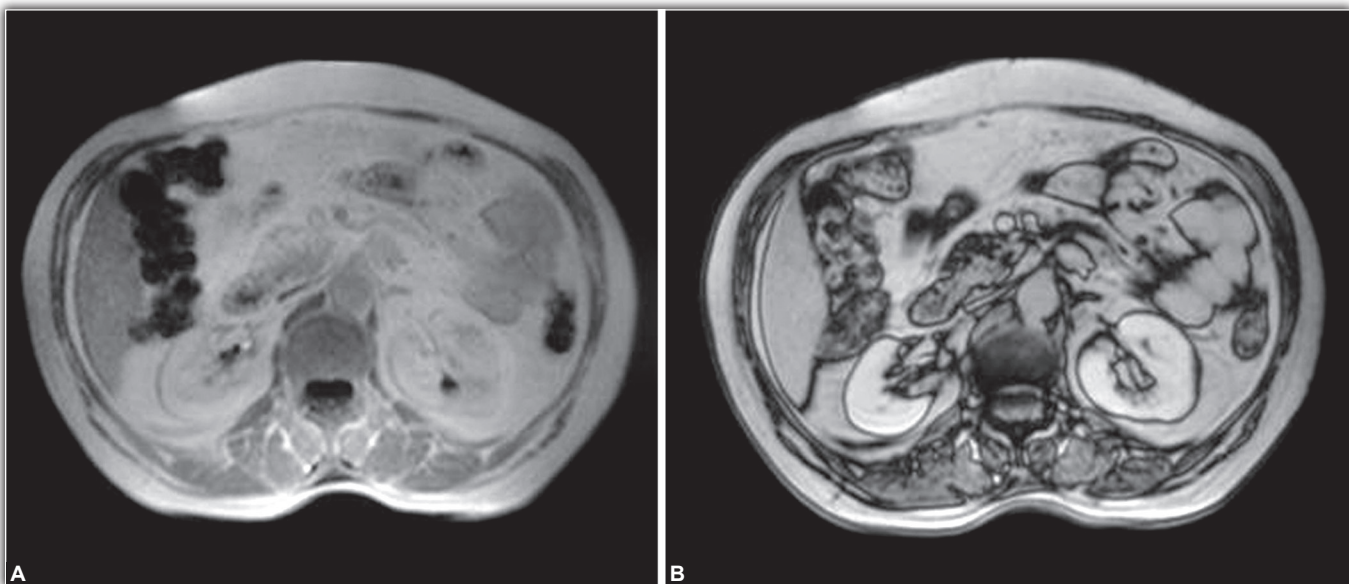
#### *Truncation Artifacts*

Truncation or Gibbs artifacts are ripple like features that appear at regions of abrupt transition between high and low signal intensity structures, e.g. in T1 weighted images when high signal from fat at the edge of the region is still present at the end of data collection or in T2 weighted MR images of the spine at the interface of low signal intensity spinal cord with high signal intensity CSF. These are seen as stripes or rings in the image with alternating high and low signal intensity. These are also known as edge oscillations.

These artifacts are a result of insufficient digital sampling of the echo. Since there is a limited window period available



**Figs 13A and B** Chemical shift artifact. Echoplanar imaging depicts chemical shift artifact in phase encoding direction which is anterior to posterior (A). Fat suppression technique can be used to minimize the artifact (B)



**Figs 14A and B** Phase cancellation artifact. In (A) and opposed phase (B) gradient echo MR images of the abdomen at TE 4.8 msec and TE 2.4 msec respectively in a 1.5 T MR system show a dark rim surrounding the structures at fat water interfaces on the opposed phase images

for measurement of signal, there is interruption of this measurement at certain locations and data is truncated or omitted in k-space. Approximation errors in Fourier transformation of these signals lead to truncation artifacts. As Fourier transformation is better used for estimating gradual transitions, abrupt transitions at high contrast interfaces results in these artifacts.

These sharp borders between areas of high contrast are represented by high spatial frequency data. The highest sampled frequency is inversely proportional to the pixel size. When we use a lower matrix, i.e. a bigger pixel size in the phase encoding direction, the higher frequencies are cut off, leading to incorrect imaging of sharp edge lines. These artifacts can be seen in both phase and frequency encoding direction. However, they are usually seen in the phase encoding direction because usually a smaller phase matrix is used as compared to frequency matrix in order to reduce the acquisition time.

#### *Remedy*

These artifacts can be diminished by decreasing the pixel size, by increasing the acquisition matrix. However, this occurs at the expense of reduced SNR and increased acquisition time. Another method of reducing these artifacts is by applying various filters. Raw data filters may be used prior to Fourier transformation (e.g. Fermi, Gaussian, Hanning filters). These filters force the signal amplitude to zero at the end of data collection period. These improve the signal to noise ratio of the image as high frequency noise is removed from the signal. However, excessive filtering may result in loss of sharpness of the image as this eliminates high frequencies responsible for edge definition, resulting in blurring. Image reconstruction of rectangular raw data matrices automatically uses a weak filter.

#### *Magnetic Susceptibility Difference Artifacts*

Magnetic susceptibility is a measure of spin polarization or magnetization induced by external magnetic field. The magnetic field contribution from the tissue may add to or subtract from the main magnetic field, depending upon whether the structure is paramagnetic or diamagnetic respectively. Differences in tissue susceptibility hence lead to magnetic field inhomogeneities. Tissues such as cortical bone or air filled organs such as lungs and bowel have small magnetic susceptibility. Soft tissues, on the other hand, have more polarisable material and greater tissue susceptibility. At the interface between these regions with high and low magnetic susceptibility, significant distortion artifacts result due to local magnetic field gradients or field inhomogeneities. These result from enhanced dephasing of protons located at the boundaries of structures with a very different magnetic susceptibility. These artifacts are seen as areas of signal void. The second effect is that of strong distortion of the main

magnetic field resulting in geometric distortion of anatomy (**Figs 15A and B**). The paranasal sinuses, the orbits, the lungs, heart, stomach and intestinal loops are the problematic areas. These are also observed in kidneys and bladder after administration of paramagnetic contrast agent which concentrates in these organs leading to significant signal loss.

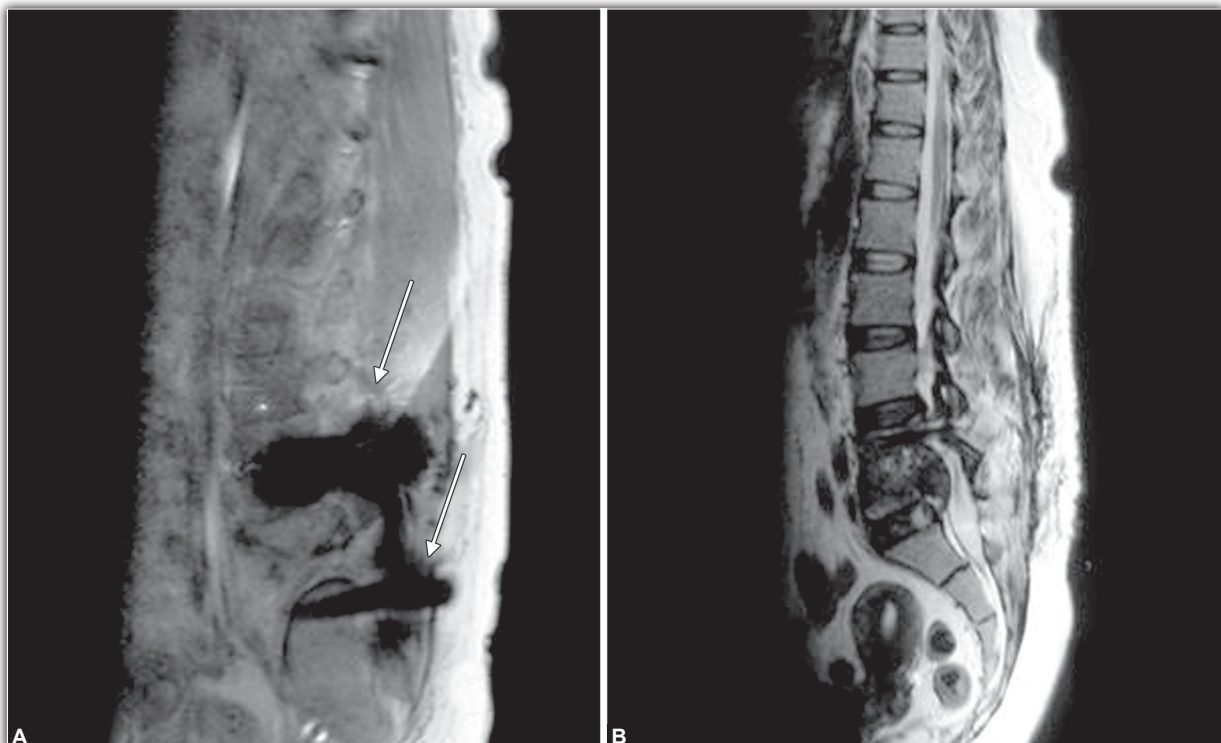
These artifacts are more pronounced with gradient echo sequences (**Fig. 15A**) and EPI imaging (**Fig. 16A**). In gradient echo imaging, signal amplitude is a function of  $T2^*$ , in which proton dephasing from magnetic field inhomogeneities is an important factor that affects image contrast. On the other hand, spin echo sequences use a refocusing  $180^\circ$  pulse which rephases the protons and hence minimizes these artifacts (**Fig. 15B**). With EPI imaging, the entirety of k-space is filled by data from one RF pulse. This single shot readout using gradient refocusing over a long period is predisposed to these artifacts. Generally, high bandwidth of this sequence in frequency encoding direction protects it from these distortions in this direction. However, low bandwidth in EPI sequence in the phase encoding direction affects distortions in this direction. Therefore, the phase encoding gradient is oriented along the axis of the susceptibility gradient (antero-posterior direction while imaging the brain) to reduce the distortion in EPI imaging (**Fig. 16B**). The higher the field strength of the main magnetic field, the stronger are these artifacts. Also, these artifacts are more pronounced when sequences with long echo times are used. The longer the TE, greater is the time available for dephasing of protons.

#### *Remedy*

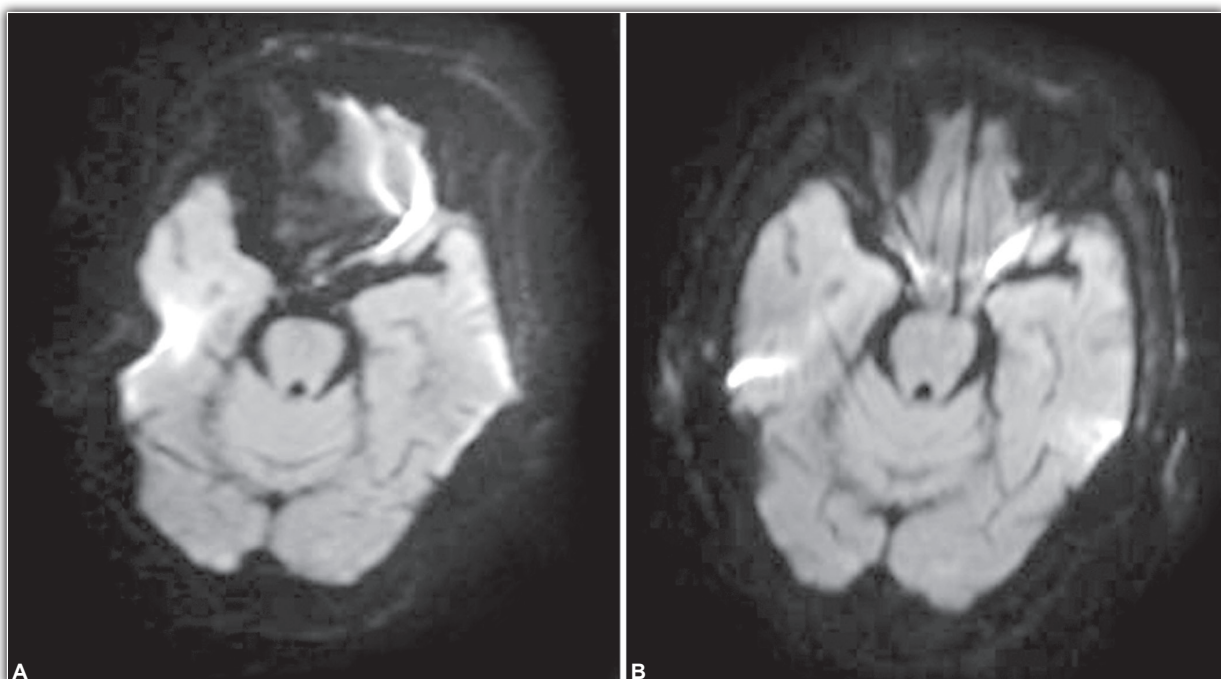
Following remedies may be done to eliminate or reduce these artifacts. Spin echo sequences may be used which use a rephasing  $180^\circ$  pulse. TE may be reduced as longer the TE, greater is the time available for dephasing of protons. The best combination of spin echo and short TE is found in fast spin echo techniques rather than conventional spin echo sequences. The voxel size may be reduced to reduce the local magnetic field inhomogeneities. Larger bandwidth sequences also reduce these artifacts. Although these susceptibility artifacts are more pronounced at higher field strengths, inherent improvement in SNR in 3T systems allows the use of higher bandwidth and parallel imaging to reduce these artifacts. These artifacts can be reduced in multishot EPI acquisitions, with parallel imaging and with radial k-space sampling technique.

#### *Advantage*

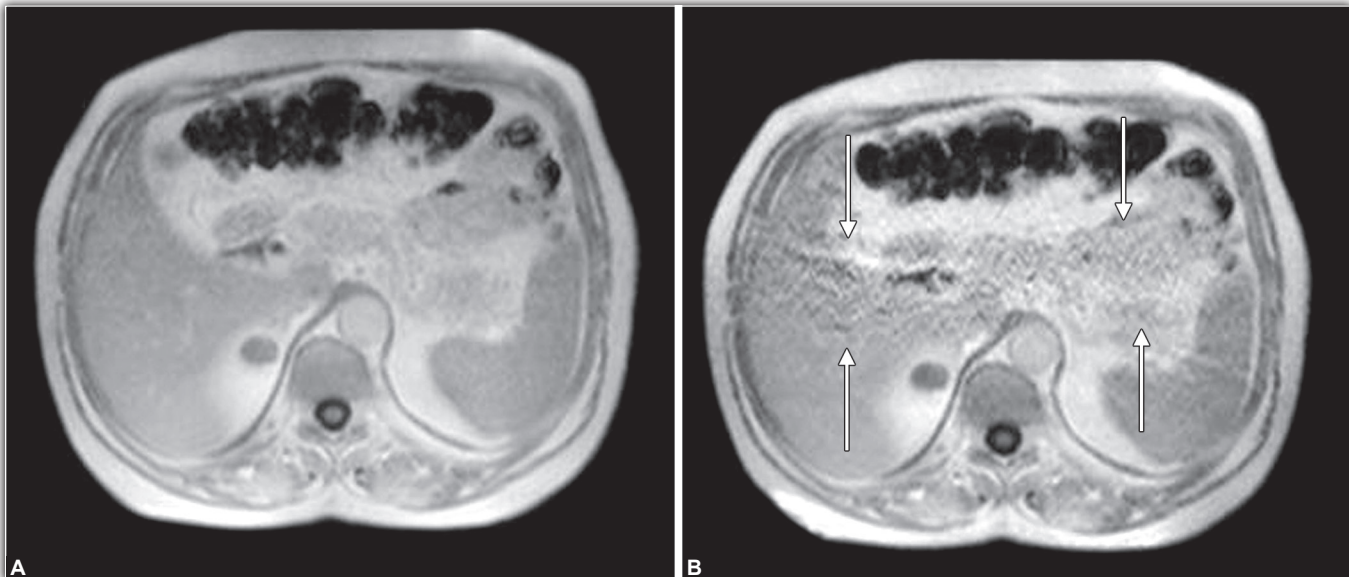
These artifacts can be used advantageously when investigating for hemorrhage, as blood products become more apparent due to magnetic susceptibility or blooming artifacts. They are also used to our advantage as they form the basis of perfusion imaging, functional imaging of the brain, quantification of liver iron content and use of reticulo-endothelial specific agents in liver imaging.



**Figs 15A and B** Magnetic susceptibility artifact. Gradient echo sagittal image of the spine shows magnetic susceptibility artifact due to a metal fixator, seen as areas of signal void and geometric distortion (arrows in A). Use of spin echo sequence (B) minimizes the artifact



**Figs 16A and B** Magnetic susceptibility artifact. Echoplanar imaging shows marked distortion when the phase encoding gradient is from right to left (A). This is minimized by keeping the direction of the phase encoding gradient from anterior to posterior, and hence along the susceptibility gradient in brain (B)



**Figs 17A and B** Parallel imaging artifact. Axial T1 weighted gradient image acquired without parallel imaging (A) and axial T1 gradient image acquired with a parallel imaging factor of 2 (B) shows noise and reconstruction artifacts in the middle of the FOV in the latter image (arrows in B) which limit the diagnostic quality of the image

### Section Cross Talk

In multisection two dimensional sequences, crosstalk artifact can result if there is no interslice gap. This is a result of imperfect shape of the RF slice profiles which should ideally be rectangular but are actually more curved shaped. Side lobes of RF pulses can excite part of adjacent sections. Hence these are excited twice by an RF pulse in the same TR, resulting in saturation and low signal intensity. This is seen in all sections except the first and last slices.

This is not seen in three dimensional sequences as the whole volume of tissue is excited together and gradients are used to obtain sections within this volume.

### Remedy

This can be overcome by using RF pulses with sharper section profiles, increased gap between sections, and/or multiple sections imaged in separate batches (interleaving).

### Parallel Imaging Artifact

Parallel imaging techniques such as GRAPPA and SENSE help us to reduce acquisition time by extrapolating data before and after Fourier transformation respectively. However, we must take care to avoid very high acceleration factors as the noise level increases and SNR falls with use of high acceleration factor. This noise can be seen in the center of the image (**Figs 17A and B**). Also, if field of view is smaller than the object being imaged, increased noise can be seen in addition to aliasing artifact. This aliasing artifact may also be projected

in the central portion of the image. This moves outwards as the parallel imaging factor is reduced.

### External Artifacts

External artifacts are generated from sources other than the patient. These could be classified into two categories—those that are hardware related and those that are not. Improper calibration of gradients, RF transmitter and receiver system can lead to various distortions and incorrect spatial localization. The gradient system and RF transmitter system can sometimes malfunction and work in an unstable manner. This can result in amplitude and phase modulations resulting in ghosting or smearing artifacts and occur throughout the image field in the phase encoding direction. These may be indistinguishable from motion artifacts. These system related artifacts could be transient effects generated within one or more of the subsystems or could be a sign of degradation of some of the electronic components in the subsystem.

### Artifacts Caused by Field Distortions

Distortions artifacts may be caused by main magnetic field inhomogeneities or non linearity of the gradient field or RF field inhomogeneities.

### Main field inhomogeneities

Despite the care taken by most manufacturers to construct MR systems with homogenous magnetic fields, some inhomogeneities occur because of field falloff toward



**Figs 18** Field distortion due to gradient field nonlinearity. Sagittal T2-weighted image of the thoracic spine shows geometric distortions resulting from gradient nonlinearity, with vertebral bodies appearing progressively smaller toward the inferior edge of the FOV (arrow in A). Distortion correction software was used to correct the distortion (arrow in B)

the magnet periphery. This is more pronounced in large bore or open MR systems. This is especially important in spectral fat suppression sequences. If the magnetic field is not homogenous, fat suppression pulse may not uniformly suppress the fat. This is mostly seen at the edges of an image with large FOV. To minimize the artifact, the anatomy should be centered within the magnet as much as possible and field homogeneity correction should be done just prior to the scan, with the patient inside the scanner.

Distortions in the main magnetic field may also result from ferromagnetic substances like zippers, metal clips on the patient's body/clothing (**Figs 15A and B**). These result in magnetic susceptibility artifacts as described above, but these are more severe as metals have much higher magnetic susceptibility than body tissues. These can be minimized by using fast SE sequences using a high bandwidth and decreased echo time. However, care should be taken in these cases as metallic objects can result in more energy absorption and heating as compared to normal body tissues.

#### Gradient field nonlinearity

Gradient field nonlinearity is related to gradient falloff due to finite size of gradient coils. Gradient coil produces a varying magnetic field that is linear through the isocenter of the magnet but tapers towards the side of the magnet. This leads to distortion and loss in spatial resolution. In a large FOV image, gradient field distortion is seen as compression

of the structures at the edge of the image (**Fig. 18A**). As this is a predictable artifact, MR imaging software can correct these distortions before the final image is reconstructed. Post processing techniques can also correct the distortions but not the accompanying loss in spatial resolution (**Fig. 18B**).

#### RF field inhomogeneities

Inhomogeneities in RF pulse do not cause geometric distortions but can lead to signal nonuniformity. These may be due to problems in RF construction or from dielectric (standing wave) effects. Dielectric effect is especially prominent at 3T systems because high frequency low wavelength RF pulse is required to excite protons at this high field strength because of increased Larmor frequency of protons. The wavelength of these RF pulses approximates the dimensions of the anatomic structure and standing waves may result. These waves manifest as bands of destructive and constructive interference, seen as dark and bright zones respectively. Use of dielectric pads to change the patient's apparent girth may be used to decrease the effect.

RF field distortions can also lead to inhomogeneous fat suppression on STIR imaging. RF shimming can help reduce the artifact. Alternatively, spectral fat saturation may be used instead of STIR sequence to suppress fat. STIR is a non specific technique of fat suppression, as signal is suppressed from all tissues with a T1 equal to that of fat. Spectral fat saturation, in contradistinction, suppresses the fat signal only because it is based upon differentiation of resonant frequency of fat from water.

#### Spike (Herringbone) Artifact

Spikes are noise bursts of short duration that can occur randomly during data collection. These are a result of loose electrical connections that produce arcs or because of breakage of interconnections in an RF coil. These are more frequently encountered when gradients are applied at high duty cycle, e.g. in echoplanar imaging. These produce bad data points or a spike of noise, in k space. Fourier transformation of this spike of noise results in a specific 'crisscross' or 'herringbone' pattern seen as dark stripes overlaid on the image (**Fig. 19**). Spike noise is usually transient but can become chronic if not attended to.

#### Advantage

This pattern of stripes produced by spiking can be used for tagging, an important technique in cardiac imaging.

#### Zipper Artifact

Zipper artifact is an artifact that is caused by external interference resulting from external RF fields, as those caused by open doors, radios, mobile telephones, electronic controls, etc. These emit interfering electromagnetic signals that hamper MR image quality. Zipper artifact appears as a



**Fig. 19.** Spike or herringbone artifact. Loss of data points in the acquisition process due to a spike of noise can lead to a "crisscross" or "herringbone" pattern of artifact

region of increased noise with a width of 1 or 2 pixels that extends perpendicular to the frequency encoding direction, throughout the image series.

#### Remedy

To prevent these artifacts, MR tomographs are installed in RF-sealed rooms, also known as Faraday cage. These sealed rooms not only protect the equipment from external RF interference but also shield the environment from RF fields generated by the tomograph. The door of the MR room should always be closed properly to prevent this interference. If any constructional changes take place after the installation

of the MR tomograph, e.g. drilling holes for cables, it may lead to interference in RF shielding. In this case, the source of interference needs to be carefully looked for. Sometimes, electrical connections from any patient monitoring device which work on alternating current can also interfere with RF shielding. The persistence of the artifact even after the equipment is removed indicates compromise of the RF shield.

#### CONCLUSION

Clinical MR imaging is becoming more and more versatile and complex, making it difficult for the radiologist to grasp the physical principles underlining the changing technology. Nevertheless, knowledge of basic MR physics plays a key role in clinical imaging as its understanding can help us modify imaging protocols to obtain optimum image quality within acceptable scan time. Good quality images enable us to reach the correct clinical diagnosis with greater confidence.

#### REFERENCES

1. Westbrook C. Image quality. In: MRI at a glance. 1st edn. Great Britain: Blackwell Science. 2002.p.64-72.
2. Westbrook C. Artifacts. In: MRI at a glance. 1st edn. Great Britain: Blackwell Science. 2002.p.73-78.
3. Brown MA, Semelka RC. Measurement parameters and image contrast. In: MRI- Basic principles and applications, 3rd edn. New Jersey: Willey Liss Inc. 2003.p.93-102.
4. Brown MA, Semelka RC. Artifacts. In: MRI- Basic principles and applications, 3rd edn. New Jersey: Willey Liss Inc. 2003.p.113-40.
5. Mitchell DG, Cohen M. In: MRI principles, 2nd edn. Philadelphia, Pa: Saunders. 2004.p.416.
6. Morelli JN, Runge VM, Ai F, Attenberger U, Vu L, Schmeets SH, Nitz WR, Kirsch JE. An image based approach to understanding the physics of MR artifacts. Radiographics. 2011;31:849-66.
7. Yang RK, Rith CG, Ward RJ, deJesus JO, Mitchell DG. Optimising abdominal MNR imaging: approaches to common problems. Radiographics. 2010;30:185-99.
8. Stadler A, Schima W, Ba-Ssalamah A, Kettenbach J, Eisenhuber E. Artifacts in body MR imaging: their appearance and how to eliminate them. Eur Radiol. 2007;17(5):1242-55.
9. Zhuo F, Gullapalli RP. MR artifacts, safety and quality control. Radiographics. 2006;26:275-97.
10. Hood MN, Ho VB, Smirniotopoulos JG, S zumowski J. Chemical shift: the artifact and clinical tool revisited. Radiographics. 1999;19:357-71.

## Chapter

# 9

# Diffusion Weighted MRI

*Devasenathipathy Kandasamy, Raju Sharma*

## INTRODUCTION

Magnetic resonance imaging (MRI) imaging has become an important imaging tool in the current clinical practice mainly because of its excellent contrast resolution without the risk of any ionizing radiation. This has become even more relevant with the growing concern for radiation issues in computed tomography (CT) and other imaging modalities which utilize ionizing radiation. Diffusion weighted imaging (DWI) is a promising technique which was originally described by Le Bihan 30 years back and because of the recent developments in MR hardware this has found a place in routine clinical MR protocols. The basic principle of DWI is based on the Brownian motion of water molecules which takes place in the body and it utilizes motion sensitizing gradients to study this motion.<sup>1,2</sup> It provides unique information at a microstructural and functional level which can be used to characterize cellular dense lesions and this has applications in oncology. Other reasons why this technique is appealing are that it can be performed rather quickly and does not require the use of exogenous contrast agents.

Diffusion can be assessed both qualitatively and quantitatively. It is quantified by the parameter called Apparent Diffusion Coefficient (ADC) which is derived from the diffusion images. The ADC is a scalar quantity which has only magnitude without any directional information.<sup>3</sup> This chapter will focus on the basic principles of DWI and optimization of the technique and briefly review its clinical applications.

## BASIC PRINCIPLE

Water molecules in the body undergo a random motion called "Brownian motion" which is as a result of body heat.<sup>2</sup>

Theoretically, these constant random motions are uniform in all directions. But the diffusion in body tissues is restricted by various organelles, membranes and tissue planes. The intracellular diffusion is more hindered than the extracellular component because of the presence of cell membrane.<sup>4</sup> In case of malignant tumors the cells are densely packed with large nuclei and scanty cytoplasm which results in restriction of diffusion (**Fig. 1**). On the other hand, benign cells are loosely packed with small nucleus and abundant cytoplasm that facilitates diffusion.<sup>5</sup> Because of the interaction of water molecule within biological tissues which can impede the actual diffusion the measured diffusion is termed as apparent diffusion coefficient (ADC) which is expressed in mm<sup>2</sup>/s. When the diffusion is not restricted in any particular direction it is called isotropic diffusion as seen in CSF space and cystic lesions. When the diffusion occurs preferentially in a particular direction it is called anisotropic diffusion which is usually seen in white matter of brain.<sup>6</sup> In white matter and peripheral nerves the water diffuses preferentially along the axon.

DWI can generate images in which the contrast between the structures is based on the diffusion characteristics. There are various types of sequences with diffusion sensitising gradients incorporated within but the basis of all of them is the technique suggested by Stejskal and Tanner in 1965 and implemented by Le Bihan in 1986.<sup>7,8</sup> Their technique essentially involves adding two diffusion sensitizing gradient, one on either side of 180° refocusing pulse. These gradient lobes have the same magnitude but are opposite in direction. The first gradient lobe is called dephasing gradient which will dephase the spins of water molecules and the second is called the rephasing gradient which will rephase the spins

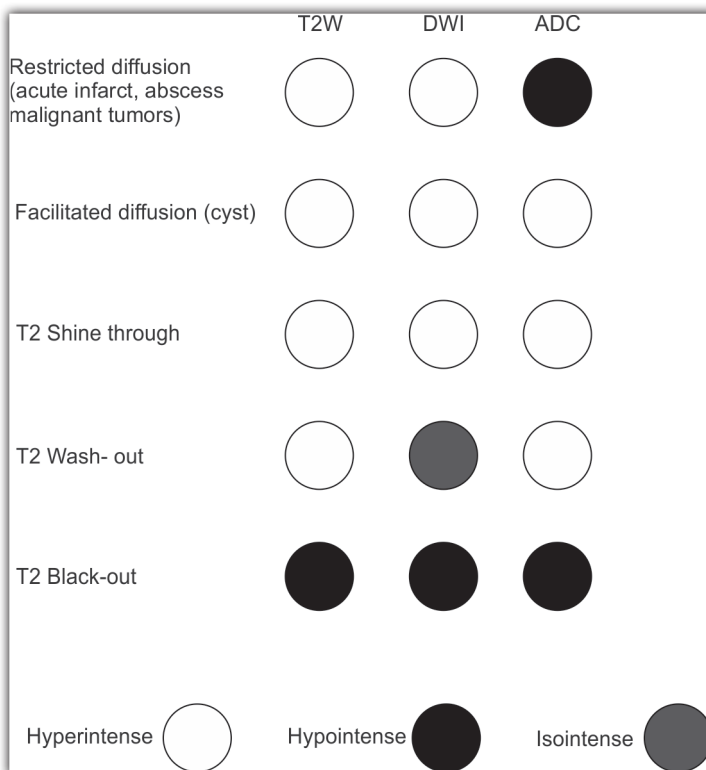


**Fig. 1** Schematic representation of signal intensities on T2W, DWI sequence and ADC map for disease entities and artifacts which are commonly encountered in day-to-day practice

to their original state. The  $180^\circ$  pulse will eliminate the dephasing due to the inhomogeneity of external magnetic field. This principle has been adopted with or without slight variation even in modern day sequences.<sup>9</sup> The idea behind this technique is that the water molecules whose diffusion is not restricted will get dephased by the first gradient lobe and during the process the molecules will move to another location in which the water molecules will be subjected to a different magnetic environment so that the rephasing pulse will not exactly rephase them to their original state. This will cause attenuation of signal from these water molecules as they are not exactly rephased to produce a strong echo. Whereas, water molecules whose diffusion is restricted will not move and they will be subjected to the same magnetic environment and the dephasing and rephasing gradients will exactly neutralize each other and their spins will be in phase to produce a strong echo. These diffusion gradients can be applied in any of the axis (x, y, z) or in any combination and it is called diffusion sensitizing direction. This diffusion gradient addition can be applied in spin echo or in steady state sequences as long as they have a long TE to accommodate them and this is the reason why the diffusion sequences are T2 weighted.

### B VALUE

The magnitude, duration of diffusion gradient applied and the duration between the dephasing and rephasing lobe determines the sensitivity of the sequence to water diffusion

which is described by a factor called diffusion weighting factor or b factor ( $\text{mm}^2$ ). All the above factors are directly proportional to the b value. Usually, the magnitude is kept maximal and the other two are altered to get a desired b value. At least 2 b values are needed for the calculation of ADC and multiple b values are used for more accurate quantification.<sup>2</sup> When multiple b values are used the TE time which is maximum for highest b value is usually kept constant for all b values for better quantification.<sup>6</sup> The choice of b value is very important and depends on the hardware, region of study, type of sequence and the quantitative or qualitative nature of the study. The usual thumb rule is that b value is about inverse of the expected ADC value.<sup>9</sup> For example if the expected ADC value of a tissue is  $1.2 \times 10^{-3}$  then the approximate b value is 800. The SNR of the sequence is grossly affected by the b value selection. When the b value is increased, the SNR of the sequence reduces and at very high values the SNR becomes very low so as to make the quantification unreliable. At the same time low b value will not generate an image whose contrast characteristics are truly based on diffusivity of water molecules. So optimal b value is a balance between the SNR required for quantification and the diffusion contrast of the image. High b values ( $>1000$ ) are used in imaging techniques like diffusion weighted whole body imaging with background body signal suppression (DWIBS) in which background signal suppression is important. Although multiple b values increase the accuracy of quantification of diffusion it also increase the acquisition time and associated artifacts. There

are several approaches developed to circumvent these issues which are discussed later in the chapter.

### ADC AND EXPONENTIAL IMAGE

ADC image is a parametric map which is derived from the DW image and it is devoid of T2 shine through (vide infra). It needs images acquired at minimum of two b values to calculate ADC and in present day scanners the calculation of ADC map is automatic. The ADC value is dependent on the b value used where it is inversely proportional to the b values used even in the same patient. It is also dependent on the field strength of the scanner, gradient hardware and the type of image processing software used.<sup>2</sup> Since ADC map is the Gray Scale representation of pixel by pixel ADC values calculated from diffusion images, the artifacts associated with the diffusion sequences will also get reflected. In addition poor SNR in high b value images also adds to the deterioration of image quality. This is the reason for ADC map having poor image quality when compared to the diffusion image and in isolation it is not very useful for diagnostic purposes. ADC values are usually inversely proportional to the degree of restriction. Area of restricted diffusion is seen as hyperintense on diffusion weighted images and hypointense on ADC and vice versa.

Another way to remove the T2 effect on the diffusion weighted image is generating an exponential image which is done by calculating the ratio of diffusion weighted image and b 0 image.<sup>10</sup> Contrary to ADC map, hyperintensity on the exponential image corresponds to hypointensity on ADC map and suggests diffusion restriction and vice versa.

### DWI SEQUENCES AND OPTIMIZATION

Many sequences are altered to introduce the diffusion gradient pair for the development of DWI sequences. Some of the most commonly used sequences are discussed here.

#### Echo Planar Imaging

Although Echo Planar Imaging (EPI) was initially proposed by Mansfield in 1978, it is the recent advancements in MR hardware and reconstruction software that made this sequence useful for clinical studies. It is an extremely fast technique which can fill the entire k space in single shot. It is robust and insensitive to motion artifacts which made it useful in DWI. After the initial excitation pulse, diffusion gradient pair, a series of fast gradient oscillations is applied for read-out and the entire k-space is filled with a long echo train (Fig. 2). This can be implemented as spin echo EPI or gradient echo EPI. Typically, separate acquisition is done for 3 orthogonal axes which are averaged into one final image. One of the disadvantages of EPI is significant phase shift gets accumulated between the water and fat protons and this leads to geometric distortion along the phase encoding direction.<sup>6</sup> As a result the fat signals can be off-set by many

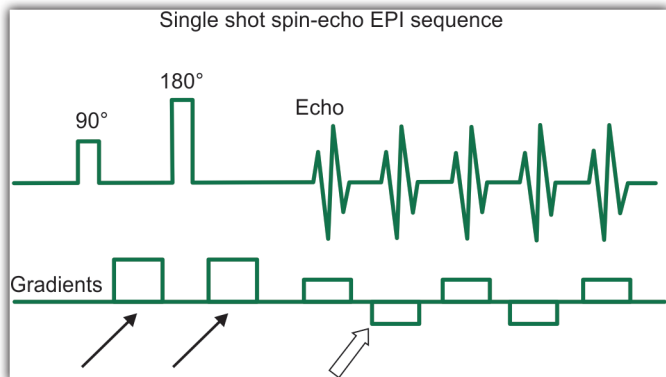


**Fig. 2** Schematic representation of DW spin echo EPI sequence showing the motion probing gradients (arrows) used to detect the diffusion of water molecules and multiple gradient oscillations (outlined arrow) to generate echoes. In this single shot sequence, the entire k space is filled in single excitation

pixels which will deteriorate the image quality, more so in higher field strengths. So, it is of paramount importance that all EPI sequences are done with fat suppression. There are various methods of fat suppression such as water only excitation, chemical fat suppression, short-tau inversion recovery (STIR) and spectral selection attenuated inversion recovery (SPAIR) of which the latter two are inversion recovery sequences. SPAIR is a very good method of fat suppression for small FOV in which the fat suppression is uniform along with good SNR. For larger FOV, STIR is the best method to provide uniform suppression but at the cost of reduced SNR. Another disadvantage of EPI is that in longer echo train the water protons tend to show phase shift especially in the air-soft tissue and bone-soft tissue interfaces resulting in geometric distortion in the phase encoding direction.<sup>9</sup> This can be reduced by using parallel imaging and high performance gradient coils which will shorten the echo train length, echo spacing and the read-out time. Another problem with single shot EPI is limited spatial resolution in the order of  $128 \times 128$  because of the rapid signal decay and limited SNR. These problems can also be reduced by splitting the acquisition into more than one excitation. This is a challenge if it has to be implemented in body imaging where motion is an important consideration. For body diffusion several approaches are followed which are discussed here. First approach is to perform a single shot acquisition with breath-hold in which the disadvantages are the poor spatial resolution, limited number of b values, less number of averages and less anatomical coverage. Poor SNR can lead to unreliable ADC values. Second approach is acquisition across multiple excitations with respiratory/cardiac trigger. This overcomes the problems with single shot breath-hold technique. However, triggers cannot totally rule-out motion artifacts and the imaging time gets prolonged. Third approach is free breathing technique with multiple averages and can use multiple b values.<sup>11</sup> Regarding the choice of b values it is a



**Fig. 3** Schematic representation of single shot fast spin echo sequence showing motion probing gradients (arrow) to detect the water diffusion. Multiple 180° refocusing pulses (outlined arrow) rather than gradient oscillations are used to generate echoes. In contrast to SE-EPI sequence, the use of refocusing pulses avoid the accumulation of phase shifts thereby reducing artifacts. This is also a fast sequence which is capable of acquiring the entire image in single excitation

balance between the accuracy of quantification and contrast resolution in the diffusion image (vide supra).

### Turbo Spin Echo Sequences or Half-Fourier-Acquisition Single-Shot Turbo-Spin-Echo

This is an alternative to DW-EPI sequence and it is also relatively insensitive to motion and can perform a single shot read-out and the entire k-space is filled in single excitation. An important difference from EPI is that 180° refocusing pulse is applied during each read-out so that the phase shift accumulation because of long echo train is avoided (Fig. 3). This reduces the geometric distortion and susceptibility artifacts. Apart from this it has other disadvantages of single shot EPI sequence. Parallel imaging can improve the spatial resolution and reduction of geometric distortions. This sequence can also be segmented into multi-shot acquisition which has similar advantages as multi-shot EPI.

### Steady-State Free-Precession

Steady-state free-precession (SSFP) is also a fast sequence so it is relatively insensitive to motion. It is an atypical diffusion sequence in comparison to the above two with regard to the usage of diffusion sensitizing gradients. Here, both the dephasing and the rephasing gradients are not applied in the same repetition time. They are applied in different repetition times (TR) and not necessarily in the immediately following (TR). Consequently, it is almost impossible to quantitate the diffusion using this sequence. However, the contrast resolution is excellent so that it can be used for qualitative assessment of images. Recently, 3D diffusion weighted sequences have also been developed.

### ARTIFACTS AND PITFALLS

There are many artifacts and pitfalls which are inherent to the technique itself, so it is very important for the radiologists

and the technicians to be aware of those. In this chapter we will discuss few of the important ones which are relevant to clinical practice.

### T2 Shine Through

This is one of the well-known phenomenon which can potentially lead to a wrong diagnosis when diffusion weighted images are interpreted in isolation. It is because DW sequence is based on a T2 weighted sequence and its effects are shown in the final image. It is very prominent in low b value images where the T2 effects predominate. For example, simple cysts in which diffusion is not restricted are seen as hyperintense structure on DW images. The ADC map or exponential images can help to overcome this pitfall since both of them eliminate the T2 effect in the image and represent diffusion characteristics only (Fig. 1). In the above example of simple cyst the ADC map will show hyperintensity because of unrestricted diffusion. At the same time when the lesion is hyperintense on T2 weighted images and hypointense on ADC, the hyperintensity in DW images will get accentuated.<sup>6</sup> When multiple b value images are available then the hyperintensity which is due to T2 effect decreases with increase in b value whereas the hyperintensity due to diffusion is retained.

### T2 Washout

This phenomenon is seen when the T2 hyperintensity is balanced by the increase in ADC in the DW image.<sup>12</sup> This is usually seen in vasogenic edema in which there is increase in ADC because of increased diffusivity and that effect is balanced by the T2 hyperintensity. Thus in the DW image the lesion appears isointense. Again this effect can be circumvented by interpreting DW images along with ADC map in which the lesion appears hyperintense (Fig. 1).

### T2 Blackout

This effect is noted when the T2 hypointensity is reflected on the DW image as hypointensity (Fig. 1). It is usually seen in hematoma which is seen as T2 hypointensity because of susceptibility effect.<sup>13,14</sup>

### Eddy Current Artifacts

Eddy current artifact is worth mentioning here because it is commonly associated with EPI sequences which is the most common sequence used for DWI. Eddy Currents are produced in the patient body and in the scanner hardware by rapidly changing magnetic gradients which are used in EPI sequence for sensing diffusion and readout. This can cause image distortion, spatial blurring and misregistration artifacts. This necessitates post processing of the data before ADC calculation to prevent quantification errors.<sup>15</sup> This artifact can also be reduced by using proper shielding in the hardware.

### Susceptibility Artifacts

This is also commonly seen in EPI sequences at the bone-soft tissue or air-soft tissue interface like close to skull base, sinuses, mastoids, bowel and lung bases. This leads to accumulation of phase shifts which are more pronounced in the phase encoding direction. This gets even worse if the matrix size is increased because of prolonged readout time. This can be reduced by using DW-HASTE sequences in which the phase shifts are periodically corrected or by using multi-shot acquisition or by using parallel imaging so that the readout time is reduced.

### Chemical Shift Artifacts

Usually in conventional spin-echo sequences the effect of difference in precession frequency of water and fat protons are seen along the frequency encoding direction. Whereas in EPI sequences the artifact is seen along the phase encoding direction and it is very prominent again because of accumulation of phase shifts during longer readouts. This can be prevented by using effective fat suppression techniques (vide supra).

### Motion Artifacts

Motion artifacts are due to gross patient movement or cardiac/respiratory/bowel motion. Although the currently available single shot techniques are fast enough to avoid motion artifacts, multi-shot techniques suffer from motion in body imaging. This can be reduced by using cardiac/respiratory triggered sequences, parallel imaging, propeller or high amplitude gradients.<sup>2</sup>

### Effect of Contrast Media

The gadolinium based contrast media used for MR imaging can have an effect on the diffusion parameters especially in kidneys where they are concentrated by causing paramagnetic effects locally. Recent evidence suggests that the ADC values of kidneys can be significantly lower in the post contrast image than the pre-contrast image. Similar effects were not found in the liver, pancreas and spleen.<sup>16</sup>

## ADVANCED DW TECHNIQUES

### Diffusion Tensor Imaging

There are newer techniques such as Diffusion Tensor Imaging (DTI) which have both magnitude and the directional information of diffusion also. The DTI is extensively studied in brain where it is used to show the white matter tracts. It uses the property of anisotropy of diffusion of water molecules. Because of the myelinated axons in the brain white matter, the diffusion is unhindered along the direction of the fiber which is called diffusion anisotropy. Diffusion information given by the DWI is a scalar quantity which lacks the directional component. To obtain the directional component gradient

lobes are used in multiple directions and the resulting data is processed. As a result each voxel has the effective direction of diffusion which is called as Eigen vector and the value of diffusion in that direction is called as Eigen value. This information is used to reconstruct fiber tract network in the brain which is called as tractography. Although this tensor model holds good in many situations, it can be limited if there are crossing fibers with different direction of diffusion in a voxel. So there are newer approaches to overcome this limitation such as high angular resolution diffusion imaging (HARDI) which can be used to study the complex diffusion process.

### Whole Body Diffusion Weighted Imaging

There is evidence that whole body diffusion weighted imaging along with anatomical images such as T1 and T2 can be very useful for the evaluation of malignant tumors.<sup>2,17</sup> The DWIBS is a whole body diffusion technique which is done typically using DW-EPI sequence and STIR for fat suppression. It is a free breathing technique in which the scans are usually taken from the skull base till the level of mid-thigh. Acquisition is done in multiple stations using multiple thin slices and a large number of signals are collected and averaged. Typically, b value in the range of 1000 is used which will provide good background suppression. But, more than one b value can be used if quantification is needed at the expense of time. These multiple slices are fused and usually displayed in inverted Gray Scale with white background similar to PET images. It can be visualized as radial projections of MIP in coronal plane. Because of the high b value, body fat muscle and most of the organs gets suppressed which highlights the abnormal areas. However, normal structures with restricted diffusion, such as spleen, lymph nodes, uterus, ovary and testis can be seen. The MIP images should always be interpreted along with the source images because improper fat suppression can lead to pseudotumor appearance. One disadvantage of this technique is long acquisition time. It has been shown to perform as well as PET/CT in the evaluation of tumors such as lymphoma and non-small cell lung cancer.<sup>18</sup> The DWIBS is a non-invasive technique without the use of radiation and has a huge potential in oncologic imaging.

### DIFFUSION KURTOSIS IMAGING

Diffusion of water molecules in a homogeneous solution follows a Gaussian distribution whereas diffusion of water molecules in biological tissues actually follows a non-Gaussian distribution.<sup>19</sup> This difference in distribution is because of cellular microstructure (cell membranes and organelles) which alter the water diffusion.<sup>14</sup> It is especially true in the brain where diffusion is restricted by the myelinated axons. Quantification of non-gaussian diffusion can be useful in characterization of intracellular structures. Kurtosis is a metric which quantifies the non-Gaussianity of any distribution. Generally, a large kurtosis signifies

higher diffusional heterogeneity and tissue complexity. This principle has been studied in the brain imaging especially in ischemia with promising results.

### Intra-Voxel Incoherent Motion

Intra-voxel incoherent motion (IVIM) was initially described by Le Bihan in 1980s.<sup>8,20</sup> They described D\* as pseudo-diffusion coefficient which is dependent on capillary perfusion. The IVIM is based on the fact that the diffusion imaging at low b values (b 0-100) will have the effect of both the tissue perfusion (pseudo-diffusion) and the true diffusion. In fact at low b values the pseudo-diffusion predominates. This effect gets reduced at high b values where the true diffusion predominates. This is one proposed reason for decrease in ADC values with increase in b value. In a normally perfused tissue at low b value the motion of water molecules because of blood perfusion in tortuous capillary network adds to the actual water diffusion. So acquiring images at increasing b values would enable us to quantify the perfusion in a tissue non-invasively. Since IVIM is very sensitive to motion and other sequence related artifacts it should be performed with single shot EPI sequence and high performance hardware. The current model available in most of the commercial scanners for the calculation of ADC is based on monoexponential function, considering that the logarithm of relative signal intensity plotted against the b value is a straight line which is not true.<sup>21</sup> So ADC calculated with the monoexponential fit would have a component of microcapillary perfusion in addition to true diffusion especially with low b values. The IVIM model suggests that the relationship between the signal intensity and b value is not monoexponential rather biexponential. Based on the IVIM model there is evidence that shows that DWI is sensitive to tissue perfusion and this potential can be applied to obtain the tissue perfusion assessment in addition to diffusion measurement.<sup>21-24</sup>

### Histogram Analysis of ADC

Usually ADC value is calculated by drawing region of interest (ROI) which will typically provide mean or median ADC value of the region. Recently attempts have been made to use histogram based analysis of ADC values. In this, the ADC values across a region can be represented as histograms, i.e. frequency of voxels having the ADC values.<sup>25</sup> This will provide better understanding of heterogeneity of the lesion. It generally, utilizes volumetric evaluation of the lesion so that all the voxels of the lesion from different slices are evaluated rather than a selected ROI. The ADC calculation by this method is reproducible because the entire lesion is analyzed and the errors in ROI placement are reduced. Histogram analysis can provide various useful metrics, such as percentiles, kurtosis and skewness of distribution of ADC values which will provide better insights into the

pattern of distribution. Comparison of these metrics based on histogram analysis between the pre- and post-treatment imaging can evaluate the response to therapy.

## CLINICAL APPLICATIONS OF DWI

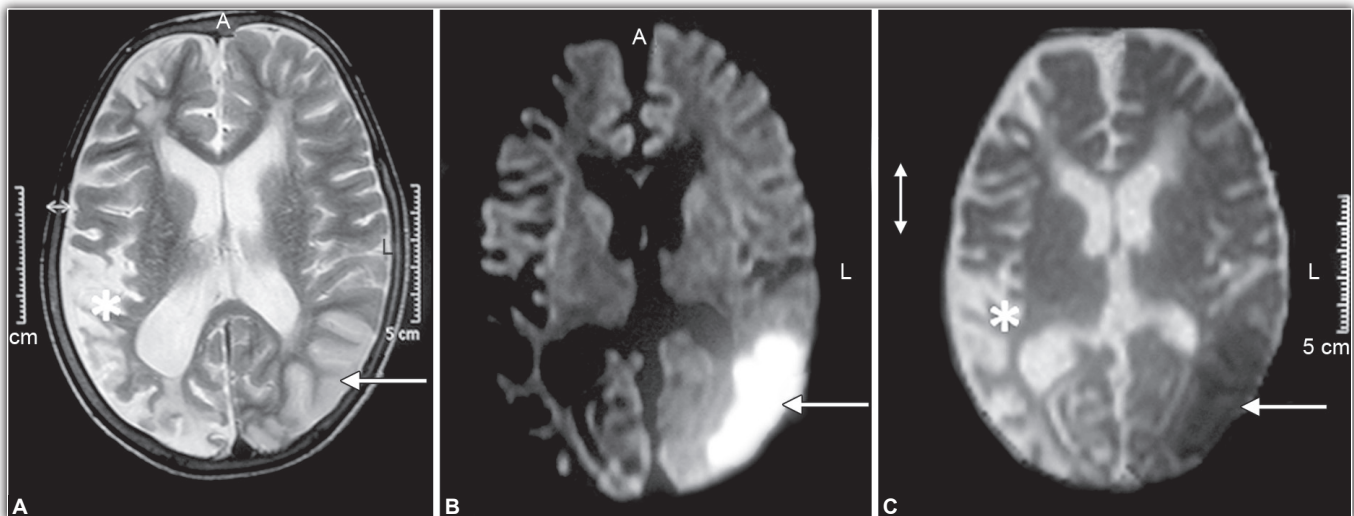
Although initially DWI was established and successfully used in neuroimaging, recent developments in the sequence protocols and their optimization, hardware enhancements and improvements in software have made this technique a robust tool for body imaging also.

### Brain

DWI has become a gold standard in imaging of stroke to identify the infarct core mainly because of its ability to detect the infarcted area within minutes after the onset of symptoms, much earlier than other MRI sequences and CT can show changes.<sup>26</sup> DWI is highly sensitive (81-100%) and specific (86-100%) in detecting the ischemic area within 12 hours of symptom onset.<sup>14</sup> It is also superior to FLAIR and T2 weighted sequences in detecting small area of infarct and has the ability to differentiate acute infarct from old lesions and non-specific white matter changes (**Figs 4A to C**). Those areas which show diffusion abnormality usually progress to infarction unless early thrombolysis therapy is started. The area of diffusion abnormality also correlates well with the final clinical outcome thereby directing appropriate management for patients. The DWI and ADC parameters are used for the prediction of hemorrhagic transformation of infarct.<sup>14</sup> The diffusion imaging in brain is further enhanced by newer sophisticated techniques such as diffusion tensor imaging (DTI) and diffusion kurtosis imaging (DKI) (vide supra). They give additional information regarding the microstructural status of the brain tissue which will help in better understanding of the disease process.<sup>27</sup> It also has an important role in brain tumor imaging as well. It helps in characterization of tumors and their response assessment to treatment. Solid gliomas which show low ADC values are associated with higher grade.<sup>28</sup> Similarly, medulloblastoma and rhabdoid tumors have been shown to have low ADC values compared to ependymoma and astrocytoma in posterior fossa.<sup>27</sup> The DTI also has a proven role in the preoperative assessment of brain tumors. Response of brain tumors after chemoradiation is assessed by DWI. Changes in ADC values in the first few weeks after the therapy are found to be noninvasive biomarkers for response to therapy and it can be used for prognostication also.<sup>29,30</sup>

### Head and Neck

DWI has potential to differentiate pleomorphic adenoma from other benign and malignant lesions of parotid gland.<sup>31</sup> Because of the presence of glandular component and fluid these tumors show significantly higher ADC value than



**Figs 4A to C** T2W axial image (A) of brain shows mild gyral hyperintensity (arrow) and swelling seen in the left parieto-occipital cortex. Multifocal areas of hyperintensities (\*) seen in right cerebral hemisphere with associated volume loss suggestive of chronic infarct. DW-EPI sequence with b value of 1000 in axial plane (B) shows a brightly hyperintense area (arrow) which on ADC map (C) shows hypointensity (arrow). The above features are suggestive of acute infarct on the left side. ADC map also shows multifocal hyperintensity in right cerebral hemisphere suggestive of facilitated diffusion. As depicted in this case, DWI along with ADC can be very useful for the chronological dating of infarcts

Warthin tumors which have hypercellular stroma.<sup>31</sup> It can differentiate sinonasal malignant lesions from benign lesions because in the former ADC is lower. The ADC values can also be used to characterize a tumor, for instance it can differentiate squamous cell carcinoma (SCC) from lymphoma. The lymphoma usually shows low ADC values compared to SCC because of the hypercellular nature.<sup>32,33</sup> The limitation of its use is that some malignant lesions like chondrosarcoma can have high ADC values.<sup>31</sup> Prediction of tumor grading can be done by ADC values as poorly differentiated solid lesions show low ADC values compared to well differentiated lesions. By differentiating necrotic area from viable tumor it can also help to identify areas from where biopsy can be performed.<sup>31,34</sup> In the assessment of tumor response to therapy one of the major limitations of PET is that it is sensitive to inflammatory changes also. The DWI has the potential to overcome this difficulty because the inflammatory lesions show high ADC values whereas tumor tissue would show low ADC values. So it can be used as a surrogate marker to assess the tumor response very early during therapy. ADC values in SCC have been shown to significantly change even after the first week of treatment and the complete responders show higher increase in ADC when compared to partial responders.<sup>35</sup> There is a recent study which evaluated the role of DWI in the orbit and suggested that it may help to differentiate pseudotumor from lymphoma and cellulitis which is again based on the fact that lymphoma shows low ADC compared to pseudotumor and cellulitis.<sup>36</sup> The DWI can reliably differentiate necrosis within a tumor from abscess formation. Abscess shows very

low ADC because of the presence of macromolecules and increased viscosity.

### Pediatric Applications

The use of ionizing radiation in children is a concern because of long term effects, so DWI can be an alternate technique in this age group. The DWI does not involve the use of contrast media so it can be used whenever contrast enhanced imaging is not possible because of deranged renal function. Experience of DWI in paediatric imaging is limited but promising. The ADC values can be used to detect malignant tumors, characterize them and assess the treatment response. Studies have been done in variety of pediatric tumors and they found that DWI performed better or similar to conventional MR imaging.<sup>37,38</sup>

### Thorax

DWI in thorax needs faster sequences with high performance gradients and parallel imaging techniques along with phased array coils. The low proton density in lung and magnetic field inhomogeneity makes quantitative DWI even more challenging. Usually, two b values are used and STIR is used for fat suppression especially if quantification is needed. It can be done in breath-holding or free breathing with respiratory and cardiac triggers. Studies have used various methods such as qualitative, semi-quantitative and quantitative to differentiate malignant lesions from benign lesions.<sup>4</sup> In qualitative method the intensity of the lesion is compared

with the intensity of spinal cord or chest wall muscle and the malignant lesions are usually hyperintense to spinal cord or chest wall muscles. In semi-quantitative analysis, the ratio of the signal intensity of the lesion and the signal intensity of the reference structure is used to characterize the lesion. The quantitative analysis depends on the ADC measurement of the lesion itself.

Most of the work has been done in lung carcinoma. Studies have shown that the ADC of the malignant lesions is usually lower than the benign lesions and small cell carcinoma which has closely packed cells shows lower ADC when compared to non-small cell carcinoma although overlap may occur. At the same time small metastatic nodules, inflammatory nodules and fibrotic nodules cannot be reliably differentiated.<sup>39</sup> In case of collapsed lung it is very difficult on routine imaging to delineate the tumor boundary. DWI has been used successfully to delineate the tumor from the collapsed lung.<sup>40</sup> DWI has also been used to characterize the mediastinal nodes in patients with carcinoma lung.<sup>41,42</sup> The ADC values of malignant nodes were significantly lower than that of benign nodes. Another potential application of DWI is in the evaluation of tumor response after therapy.

### Breast

Contrast enhanced MRI of the breast is an established technique in the diagnosis of carcinoma breast with sensitivity of 89 to 100 percent and specificity of 72 percent.<sup>18</sup> Several studies have attempted to use DWI to differentiate malignant lesions from benign. There are no uniform b values or calculation methods used by the investigators which have resulted in different ADC cut-off values. Generally, the malignant lesions showed lower ADC values when compared with benign lesions (**Figs 5A to D**). But there is significant overlap between the two groups.<sup>4</sup> Lesions with fibrotic components, such as fibroadenoma and fibrocystic disease can result in low ADC values leading to diagnostic difficulty. Many optimizations were proposed including normalization of ADC of the lesion to the ADC of ipsilateral glandular parenchyma which would eliminate the ADC variations because of scanning parameters and effects of menstrual cycle.<sup>43</sup> This approach has been shown to improve the diagnostic accuracy. Efforts have been made to use DWI in addition to dynamic contrast enhanced imaging and this has also been shown to improve diagnostic accuracy.<sup>18</sup> DWI has been used to grade the tumor, predict the histological type and to better evaluate the local extent of the tumor. Recently, many studies have been published regarding the role of DWI in the evaluation of response to treatment. Decrease in size of the lesion as response criteria is not an optimal parameter since it takes a long time to show a significant difference. Chemotherapeutic agents are toxic and they have various side effects which necessitates earlier assessment of response. Studies have shown that the increase in ADC value in comparison with the pretreatment value can be used as

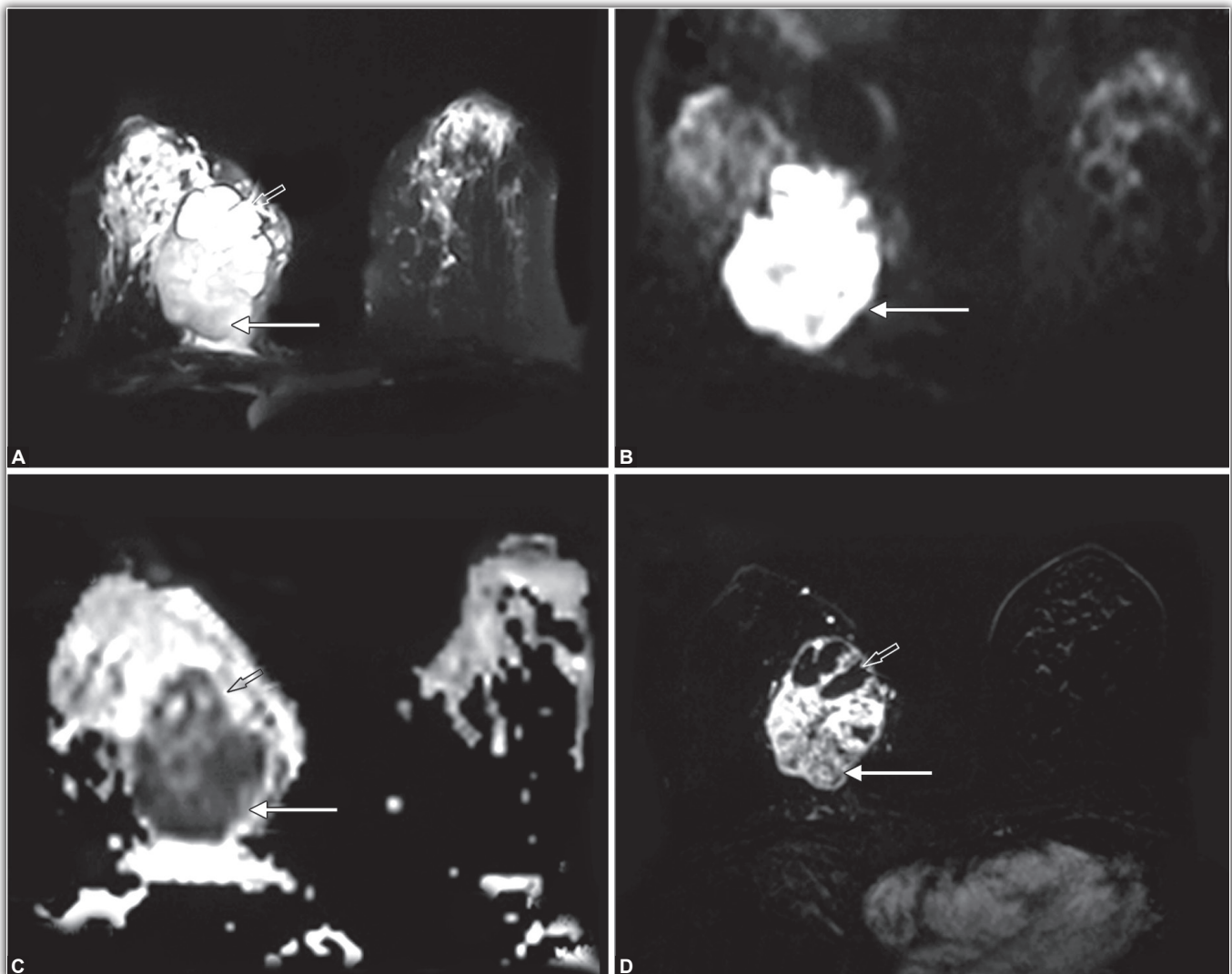
a non-invasive biomarker of disease response.<sup>44,45</sup> Using the change in ADC values, response can be evaluated as early as after the first cycle of chemotherapy and it has been found that the increase in ADC values was significantly more in responders than in non-responders.

### Liver

It is challenging to apply DWI in any abdominal organ mainly because of the respiratory motion and susceptibility. The Liver is one of the most studied organs in abdomen using DWI. The Liver parenchyma shows relatively short T2 relaxation times, so the b values and the TE of the sequence should be optimized accordingly. Too high b value might cause unacceptable signal suppression which is because of long T2 time rather than diffusion characteristics itself. Usually, the recommended b values are 0, 100 and 500.<sup>3</sup> Presence of branching vessels within the liver parenchyma poses a difficulty in the detection of small focal lesions. In black blood DWI images, the vessels are suppressed so that the lesion detection is relatively easier especially on low b values. At the same time lesion characterization is better done on high b value images. To support this studies have shown that DWI is better than fat suppressed T2 weighted sequences.<sup>46,47</sup> DWI can be applied as a useful adjunct or can be used as a reasonable alternative to contrast enhanced images for the evaluation of the liver metastasis.<sup>48,49</sup> Hemangioma and simple cysts show significantly high ADC values that they can be reliably differentiated from hepatocellular carcinoma (HCC) and metastasis which show low ADC values (**Figs 6 and 7**). However, benign solid lesions like hepatic adenoma and focal nodular hyperplasia can have overlapping values which cannot be reliably differentiated from malignant lesions.<sup>3,18</sup> Similarly, malignant lesions which are necrotic and mucinous tumors can have high ADC values and can mimic benign lesions on DWI. Diagnosis and detection of HCC and dysplastic nodules in a cirrhotic liver is very difficult based on ADC values because the diffusion is as it is restricted in cirrhotic liver as a result of fibrosis. As in other tumors, DWI has a role in the evaluation of tumor response and it has been shown to demonstrate significantly more ADC changes in responders than in non-responders. In addition, the pre-treatment high ADC values have been correlated with poorer response to therapy. It is well known that ADC values are low in cirrhotic liver and a recent study showed that ADC values correlated well with US elastography and serum markers for moderate and severe fibrosis.<sup>50</sup>

### Gallbladder and Biliary Ducts

There is emerging evidence that DWI can be helpful in differentiating malignant gallbladder lesions from benign. Malignant lesions tend to show high signal intensity on DWI and low ADC values compared to benign lesions.<sup>51</sup> It can distinguish adherent or tumefactive sludge from gallbladder malignancy. A recent study has shown that DWI



**Figs 5A to D** Axial T2W sequence of bilateral breasts (A) shows a hypointense mass lesion (arrow) in the right breast. It also shows areas of necrosis (outlined arrow) within. Diffusion weighted sequence with  $b$  value of 1000 (B) shows a markedly hyperintense lesion (arrow) with good background suppression of other structures making the lesion more conspicuous. ADC map (C) shows hypointensity (arrow) suggesting marked restriction of diffusion consistent with a highly cellular mass. Few areas show facilitated diffusion (outlined arrow) consistent with necrosis. These findings are also confirmed on subtracted post contrast T1 fat suppressed image (D). Histopathology showed infiltrating ductal carcinoma

performed better than conventional MRCP in the detection of extrahepatic cholangiocarcinoma.<sup>52</sup>

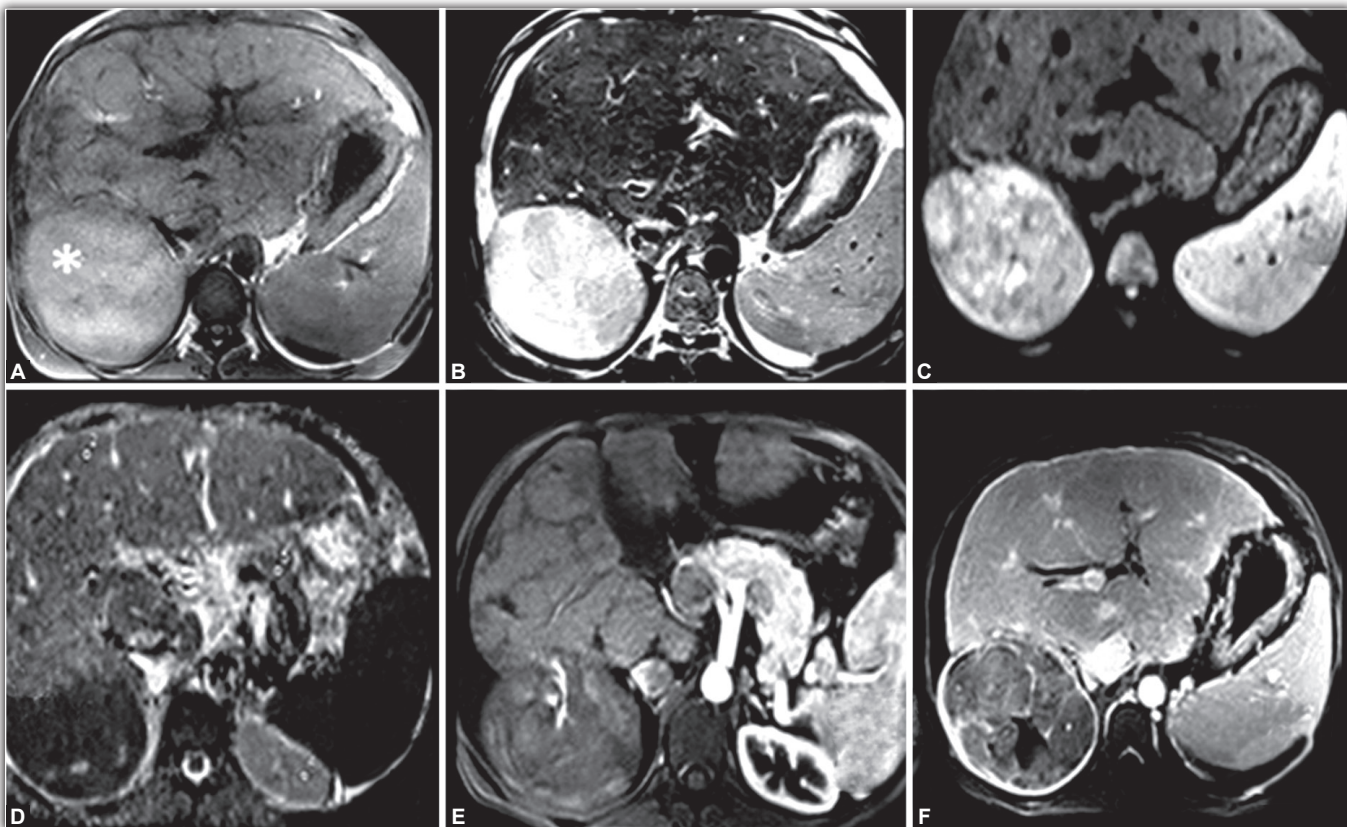
### Pancreas

ADC values of pancreas have been shown to vary with age of the patient and the location in pancreas. With increase in age pancreas undergoes atrophy, fatty replacement and fibrosis which is proposed to be a cause for change in ADC.<sup>53,54</sup> The ADC values of head and body of the pancreas is shown to be significantly more than the tail of pancreas.<sup>54</sup> Carcinoma of pancreas shows low ADC values compared to the rest of normal pancreas and the ADC values depend

on the histological characteristics as well. However, there is overlap of ADC values of carcinoma pancreas with focal pancreatitis because of which their distinction is difficult. Cystic lesions of pancreas such as pseudocysts, simple cysts show a relatively high ADC values compared to pancreatic abscesses, hydatid cysts and cystic neoplasms.<sup>55</sup>

### Kidneys and Adrenal

DWI has been successfully used in differentiating malignant renal lesions from benign lesions. Renal cysts show high ADC values than the normal parenchyma and other solid lesions (**Figs 8A to E**). Among the cysts, those with T1



**Figs 6A to F** Axial T1W GRE sequence (A) shows an exophytic mildly hyperintense lesion (\*) arising from the right lobe of liver. Rest of the liver is showing features of chronic liver disease. Lesion is markedly hyperintense on T2W sequence (B). DW image with b value of 500 (C) shows the hyperintense lesion which on ADC map (D) shows marked diffusion restriction suggestive of hypercellular tumor. With these findings along with arterial enhancement in post contrast T1W image (E) and capsule formation in delayed post contrast image (F), diagnosis of hepatocellular carcinoma was made

hyperintensity show lower ADC than those which are T1 hypointense.<sup>56</sup> This has been attributed to the presence of blood or proteinaceous content which can alter diffusion and the same can be helpful in differentiating simple cysts from necrotic neoplasms. Recent studies have shown DWI can be helpful in characterization of renal malignant masses and ADC values can be used to predict the histological subtype of renal cell carcinoma.<sup>57,58</sup> Renal Abscesses and infected cysts show low ADC values than other cystic lesions.<sup>59</sup> According to recent studies, DWI is not useful in differentiating benign adrenal lesions from malignant lesions based on ADC values although cysts and to some extent pheochromocytoma showed higher ADC values.<sup>60,61</sup>

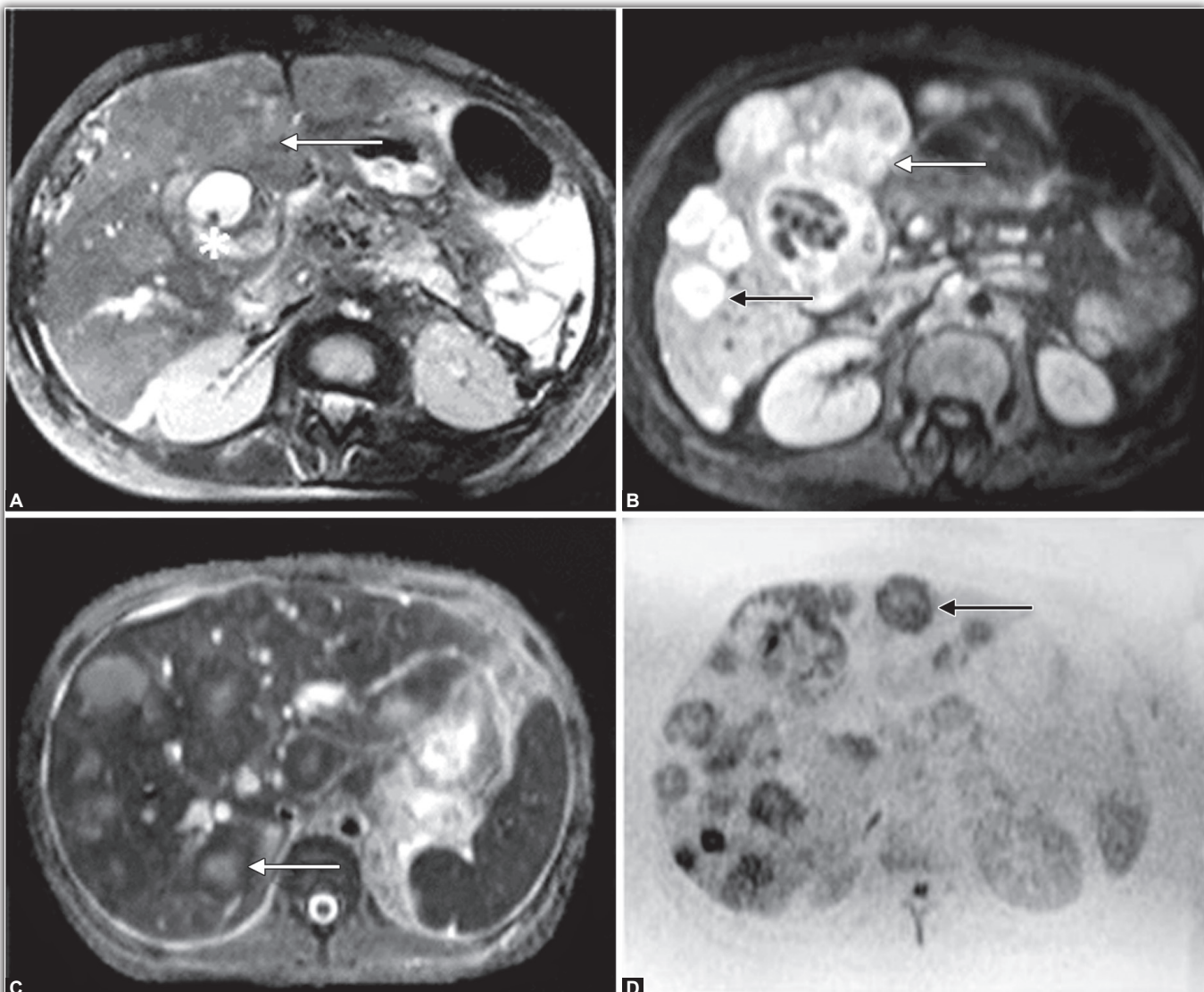
### Prostate

Prostate is rich in glandular structures which facilitates free diffusion of water. Recent usage of high field strength, advancements in hardware and sequences have made DWI possible in the prostate with good SNR. The usage of endorectal coils have been shown to improve the image

quality. Several studies have shown that prostate cancer is seen as hyperintense area in DWI and show hypointensity on corresponding ADC maps.<sup>62</sup> However, there is overlap of ADC values of prostate cancer with focal chronic prostatitis and benign prostatic hyperplasia.<sup>2</sup> There is a significant negative correlation found between the ADC values and the Gleason score which would help in management decisions. It is also found to be useful in loco-regional staging and lymph nodal detection.<sup>2</sup> It can be used as a biomarker to assess response in patients who are treated with radiation. The ADC values have been shown to increase in response to therapy.<sup>63</sup>

### Female Pelvis

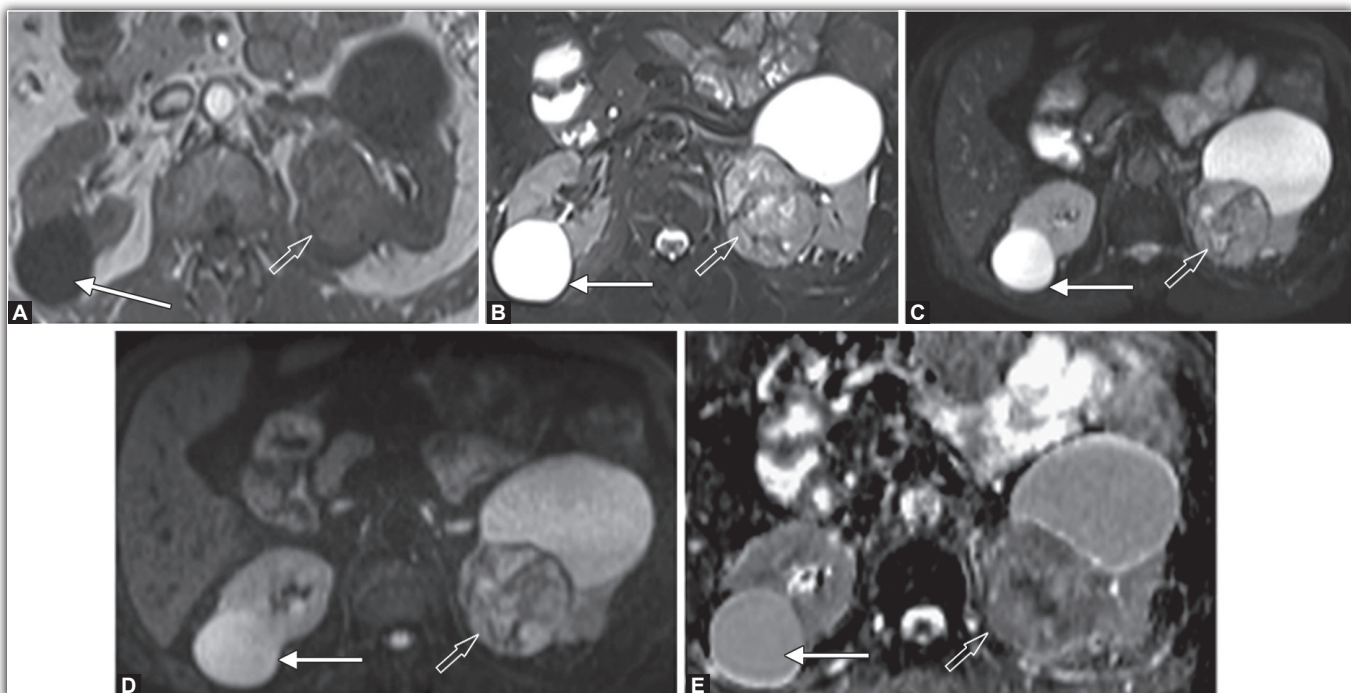
Conventional MRI has an important role in detection and staging of female pelvic malignancies. DWI can be used as an adjunct to it to increase its diagnostic accuracy. Normal endometrium shows varying diffusion characteristics and ADC values during different phases of menstrual cycle. Lowest ADC values are seen at the end of the cycle.<sup>4</sup> This variation should be taken into account while interpreting



**Figs 7A to D** Axial T2W sequence (A) shows a mass lesion involving the gallbladder (\*) with adjacent liver infiltration. Calculi were also noted in the gallbladder. Multiple subtle hyperintense lesions (arrow) in both lobes of liver seen suggestive of metastases. DW sequence with b value of 500 (B) shows these focal lesions (arrows) much better than the T2W sequence. ADC map (C) also shows multiple focal lesions (arrow) which are showing restricted diffusion in the periphery of the lesion. Most lesions on ADC map show central hyperintensity suggestive of necrosis. DW sequence with b value of 1000 displayed in inverted Gray Scale (D) shows multiple metastatic lesions (arrow) with very good background suppression which is comparable to positron emission tomography (PET) image

the DW images and ADC values. Endometrial carcinoma has been shown to have significantly low ADC value compared to the normal endometrium.<sup>4,18,64</sup> It can show the extent of myometrial invasion which is important in the management especially if contrast media cannot be used. It can differentiate endometrial carcinoma from other benign endometrial lesions such as hyperplasia and polyp. DWI can detect the malignant nodes even though they are normal according to size criteria. Cervical carcinoma is a hypercellular tumor whose ADC values are less than the normal cervical stroma. It can clearly show the depth of invasion in cervix and can

also be used for detection of involved nodes allowing to stage the disease more accurately.<sup>65</sup> Because of low ADC value of squamous cell carcinoma, it can be differentiated from adenocarcinoma of cervix. However, there is no clear-cut cut-off value for ADC available in the literature mainly because of variations in the technique and hardware used. There are contradicting reports regarding the potential of DWI to differentiate malignant ovarian lesions from benign lesions.<sup>66,67</sup> However, it improves the detection of peritoneal deposits when combined with a conventional MRI sequences than the latter alone.<sup>68</sup>



**Figs 8A to E** Axial T1W sequence of bilateral kidneys (A) shows hypointense exophytic lesions (arrow) in both the kidneys and an isointense lesion (outlined arrow) in the posterior cortex of left kidney. T2W fat suppressed and DW sequence with b value of 0 (B and C) shows markedly hyperintense lesions (arrow) in both kidneys suggestive of simple cysts whereas the posterior cortex lesion in left kidney (outlined arrow) is isointense to kidney parenchyma. On DW sequence with b value of 500 (D) the simple cysts are loosing signal compared to b 0 image whereas the posterior cortex lesion is retaining signal suggestive of solid nature of the lesion. ADC map (E) shows the cystic lesions as hyperintense to renal parenchyma which is consistent with simple cysts. The solid lesion in the left kidney (outlined arrow) is mildly hypointense to renal parenchyma which is consistent with a hypercellular solid tumor. Solid lesion in the left kidney was proven to be clear cell carcinoma

## CONCLUSION

DWI is an evolving technique that provides a new paradigm for tissue characterization. Its ability to provide both qualitative and quantitative insight into complex diffusion mechanisms and changes at a cellular level with only a small time penalty have made this technique a valuable addition to clinical MR protocols. However, DW sequences must be interpreted in conjunction with other MR sequences to avoid the pitfalls of this technique.

## REFERENCES

- Bonekamp D, Jacobs MA, El-Khouli R, Stoianovici D, Macura KJ. Advancements in MR imaging of the prostate: from diagnosis to interventions. *Radiographics*. 2011;31(3):677-703.
- Malayeri AA, El Khouli RH, Zaheer A, Jacobs MA, Corona-Villalobos CP, Kamel IR, Macura KJ. Principles and applications of diffusion-weighted imaging in cancer detection, staging, and treatment follow-up. *Radiographics*. 2011;31(6):1773-91.
- Chandarana H, Taouli B. Diffusion and perfusion imaging of the liver. *Europ Journ of Radiol*. 2010;76(3):348-58.
- Türkay B, Aras Ö, Karabulut N, Turgut AT, Akpinar E, Alibek S, Pang Y, Ertürk \cS M, El Khouli RH, Bluemke DA. Diffusion-weighted MRI for detecting and monitoring cancer: a review of current applications in body imaging. *Diagn Interv Radiol*. 2012;18:46-59.
- Herneth AM, Mayerhofer M, Schernthaner R, Ba-Ssalamah A, Czerny C, Fruehwald-Pallamar J. Diffusion weighted imaging: lymph nodes. *Eur J Radiol*. 2010;76(3):398-406.
- De Figueiredo EH, Borgonovi AFNG, Doring TM. Basic concepts of MR imaging, diffusion MR imaging, and diffusion tensor imaging. *Magnetic Resonance Imaging Clinics of North America*. 2011;19(1):1.
- Stejskal EO, Tanner JE. Spin diffusion measurements: Spin echoes in the presence of a time-dependent field gradient. *The Journal of Chemical Physics*. 1965;42:288.
- Le Bihan D, Breton E, Lallemand D, Grenier P, Cabanis E, Laval-Jeantet M. MR imaging of intravoxel incoherent motions: application to diffusion and perfusion in neurologic disorders. *Radiology*. 1986;161(2):401.
- Dietrich O, Biffar A, Baur-Melnyk A, Reiser MF. Technical aspects of MR diffusion imaging of the body. *Europ Journ Radiology*. 2010;76(3):314-22.
- Provenzale JM, Engelter ST, Petrella JR, Smith JS, MacFall JR. Use of MR exponential diffusion-weighted images to eradicate T2" shine-through" effect. *Amer Jour of Roentg*. 1999;172(2):537-9.
- Koh DM, Thoeny HC. Diffusion-weighted MR Imaging: Applications in the Body. Springer. 2010.

12. Provenzale JM, Petrella JR, Jr LCHC, Wong JC, Engelster S, Barboriak DP. Quantitative Assessment of Diffusion Abnormalities in Posterior Reversible Encephalopathy Syndrome. *AJNR*. 2001;22(8):1455-61.
13. Hiwatashi A, Kinoshita T, Moritani T, Wang HZ, Shrier DA, Numaguchi Y, Ekholm SE, Westesson PL. Hypointensity on diffusion-weighted MRI of the brain related to T2 shortening and susceptibility effects. *Amer Journ Roentg.* 2003;181(6):1705-9.
14. Fung SH, Roccatagliata L, Gonzalez RG, Schaefer PW. MR diffusion imaging in ischemic stroke. *Neuroimaging Clinics of North America*. 2011;21(2):345.
15. Haselgrave JC, Moore JR. Correction for distortion of echo-planar images used to calculate the apparent diffusion coefficient. *Magn Resonan Med.* 2005;36(6):960-4.
16. Wang CL, Chea YW, Boll DT, Samei E, Neville AM, Dale BM, Merkle EM. Effect of gadolinium chelate contrast agents on diffusion weighted MR imaging of the liver, spleen, pancreas and kidney at 3T. *Europ Journ Radiol.* 2011;80(2):e1-e7.
17. Takahara T, Imai Y, Yamashita T, Yasuda S, Nasu S, Van Cauteren M. Diffusion weighted whole body imaging with background body signal suppression (DWIBS): technical improvement using free breathing, STIR and high resolution 3D display. *Matrix*. 2004;160(160):160.
18. Bonekamp S, Corona-Villalobos CP, Kamel IR. Oncologic applications of diffusion-weighted MRI in the body. *Journ Magn Resonan Imag.* 2012;35(2):257-79.
19. Jensen JH, Helpern JA, Ramani A, Lu H, Kaczynski K. Diffusional kurtosis imaging: the quantification of non-gaussian water diffusion by means of magnetic resonance imaging. *Magn Reson Med.* 2005;53(6):1432-40.
20. Le Bihan D, Breton E, Lallemand D. Perfusion in intravoxel incoherent motion MR imaging. *Radiology*. 1988;168:497-505.
21. Koh DM, Collins DJ, Orton MR. Intravoxel incoherent motion in body diffusion-weighted MRI: reality and challenges. *Amer Journ Roentg.* 2011;196(6):1351-61.
22. Wang Z, Su MY, Najafi A, Nalcioglu O. Effect of vasodilator hydralazine on tumor microvascular random flow and blood volume as measured by intravoxel incoherent motion (IVIM) weighted MRI in conjunction with Gd-DTPA-Albumin enhanced MRI. *Magn resonan imag.* 2001;19(8):1063-72.
23. Pickens III DR, Jolgren DL, Lorenz CH, Creasy JL, Price RR. Magnetic resonance perfusion/diffusion imaging of the excised dog kidney. *Investigative radiology*. 1992;27(4):287-92.
24. Lemke A, Laun FB, Simon D, Stieltjes B, Schad LR. An *in vivo* verification of the intravoxel incoherent motion effect in diffusion-weighted imaging of the abdomen. *Magn Resonan in Med.* 2010;64(6):1580-5.
25. Downey K, Riches SF, Morgan VA, Giles SL, Attygalle AD, Ind TE, Barton DPJ, Shepherd JH, deSouza NM. Relationship Between Imaging Biomarkers of Stage I Cervical Cancer and Poor-Prognosis Histologic Features: Quantitative Histogram Analysis of Diffusion-Weighted MR Images. *AJR*. 2013;200(2):314-20.
26. Hjort N, Christensen S, Solling C, Ashkanian M, Wu O, Røhl L, Gyldensted C, Andersen G, ostergaard L. Ischemic injury detected by diffusion imaging 11 minutes after stroke. *Annals of Neurology*. 2005;58(3):462-5.
27. Heiss WD, Raab P, Lanfermann H. Multimodality assessment of brain tumors and tumor recurrence. *Journ of Nucl Med.* 2011;52(10):1585-600.
28. Arvinda HR, Kesavadas C, Sarma PS, Thomas B, Radhakrishnan VV, Gupta AK, Kapilamoorthy TR, Nair S. Glioma grading: sensitivity, specificity, positive and negative predictive values of diffusion and perfusion imaging. *Journ Neuro-oncolo.* 2009;94(1):87-96.
29. Hamstra DA, Chenevert TL, Moffat BA, Johnson TD, Meyer CR, Mukherji SK, Quint DJ, Gebarski SS, Fan X, Tsien CI. Evaluation of the functional diffusion map as an early biomarker of time-to-progression and overall survival in high-grade glioma. *Proceedings of the National Academy of Sciences of the United States of America*. 2005;102(46):16759-64.
30. Hamstra DA, Galbán CJ, Meyer CR, Johnson TD, Sundgren PC, Tsien C, Lawrence TS, Junck L, Ross DJ, Rehemtulla A. Functional diffusion map as an early imaging biomarker for high-grade glioma: correlation with conventional radiologic response and overall survival. *Journ Clini Oncol.* 2008;26(20):3387-94.
31. Razek AAKA. Diffusion-weighted magnetic resonance imaging of head and neck. *Journ Comp Assis Tomog.* 2010;34(6):808.
32. Maeda M, Kato H, Sakuma H, Maier SE, Takeda K. Usefulness of the apparent diffusion coefficient in line scan diffusion-weighted imaging for distinguishing between squamous cell carcinomas and malignant lymphomas of the head and neck. *Amer journ of Neuroradiol.* 2005;26(5):1186-92.
33. Sumi M, Ichikawa Y, Nakamura T. Diagnostic ability of apparent diffusion coefficients for lymphomas and carcinomas in the pharynx. *Europ Radiol.* 2007;17(10):2631-7.
34. Razek AAKA, Megahed AS, Denewer A, Motamed A, Tawfik A, Nada N. Role of diffusion-weighted magnetic resonance imaging in differentiation between the viable and necrotic parts of head and neck tumors. *Acta Radiologica*. 2008;49(3):364-70.
35. Kim S, Loevner L, Quon H, Sherman E, Weinstein G, Kilger A, Poptani H. Diffusion-weighted magnetic resonance imaging for predicting and detecting early response to chemoradiation therapy of squamous cell carcinomas of the head and neck. *Clinic Canc Resear.* 2009;15(3):986-94.
36. Kapur R, Sepahdari AR, Mafee MF, Puttermann AM, Aakalu V, Wendel LJA, Setabutr P. MR imaging of orbital inflammatory syndrome, orbital cellulitis, and orbital lymphoid lesions: the role of diffusion-weighted imaging. *Amer Journ Neuroradiol.* 2009;30(1):64-70.[cited 2012 Dec 23].
37. Uhl M, Altehoefer C, Kontny U, Il'yasov K, Büchert M, Langer M. MRI-diffusion imaging of neuroblastomas: first results and correlation to histology. *Eur Radiol.* 2002;12(9):2335-8.
38. Humphries PD, Sebire NJ, Siegel MJ, Olsen E. Tumors in pediatric patients at diffusion-weighted MR imaging: apparent diffusion coefficient and tumor cellularity. *Radiology*. 2007;245(3):848-54.
39. Satoh S, Kitazume Y, Ohdama S, Kimura Y, Taura S, Endo Y. Can malignant and benign pulmonary nodules be differentiated with diffusion-weighted MRI? *Amer Journ Roentgenol.* 2008;191(2):464-70.
40. Qi LP, Zhang XP, Tang L, Li J, Sun YS, Zhu GY. Using diffusion-weighted MR imaging for tumor detection in the collapsed lung: a preliminary study. *Europ radiol.* 2009;19(2):333-41.
41. Kosucu P, Tekinbas C, Erol M, Sari A, Kavgaci H, Öztuna F, Ersöz S. Mediastinal lymph nodes: Assessment with diffusion-weighted MR imaging. *Journ Magn Reson Imag.* 2009;30(2):292-7.
42. Nomori H, Mori T, Ikeda K, Kawanaka K, Shiraishi S, Katahira K, Yamashita Y. Diffusion-weighted magnetic resonance imaging can be used in place of positron emission tomography for N staging of non-small cell lung cancer with fewer false-positive results. *Journ Thorac Cardiovasc Surg.* 2008;135(4):816-22.

43. Khouri RHEI, Jacobs MA, Mezban SD, Huang P, Kamel IR, Macura KJ, Bluemke DA. Diffusion-weighted Imaging Improves the Diagnostic Accuracy of Conventional 3.0-T Breast MR Imaging. *Radiology*. 2010;256(1):64-73.
44. Sharma U, Danishad KKA, Seenu V, Jagannathan NR. Longitudinal study of the assessment by MRI and diffusion-weighted imaging of tumor response in patients with locally advanced breast cancer undergoing neoadjuvant chemotherapy. *NMR in biomed*. 2009;22(1):104-13.
45. Park SH, Moon WK, Cho N, Song IC, Chang JM, Park IA, Han W, Noh DY. Diffusion-weighted MR Imaging: Pretreatment Prediction of Response to Neoadjuvant Chemotherapy in Patients with Breast Cancer. *Radiology*. 2010;257(1):56-63.
46. Bruegel M, Gaa J, Walldt S, Woertler K, Holzapfel K, Kiefer B, Rummeny EJ. Diagnosis of hepatic metastasis: comparison of respiration-triggered diffusion-weighted echo-planar MRI and five T2-weighted turbo spin-echo sequences. *Amer Jour Roent*. 2008;191(5):1421-9.
47. Zech CJ, Herrmann KA, Dietrich O, Horger W, Reiser MF, Schoenberg SO. Black-blood diffusion-weighted EPI acquisition of the liver with parallel imaging: comparison with a standard T2-weighted sequence for detection of focal liver lesions. *Investig Radiol*. 2008;43(4):261-6.
48. Koh DM, Brown G, Riddell AM, Scurr E, Collins DJ, Allen SD, Chau I, Cunningham D, Desouza NM, Leach MO. Detection of colorectal hepatic metastases using MnDPDP MR imaging and diffusion-weighted imaging (DWI) alone and in combination. *Europ Radiol*. 2008;18(5):903-10.
49. Hardie AD, Naik M, Hecht EM, Chandarana H, Mannelli L, Babb JS, Taouli B. Diagnosis of liver metastases: value of diffusion-weighted MRI compared with gadolinium-enhanced MRI. *Europ Radiol*. 2010;20(6):1431-41.
50. Lewin M, Poujol-Robert A, Boëlle P-Y, Wendum D, Lasnier E, Viallon M, Guéchot J, Hoeffel C, Arrivé L, Tubiana J-M, Poupon R. Diffusion-weighted magnetic resonance imaging for the assessment of fibrosis in chronic hepatitis C. *Hepatology*. 2007; 46(3):658-65.
51. Sugita R, Yamazaki T, Furuta A, Itoh K, Fujita N, Takahashi S. High b-value diffusion-weighted MRI for detecting gallbladder carcinoma: preliminary study and results. *Europ Radiol*. 2009;19(7):1794-8.
52. Cui XY, Chen HW. Role of diffusion-weighted magnetic resonance imaging in the diagnosis of extrahepatic cholangiocarcinoma. *World journ gastroenterol: WJG*. 2010; 16(25):3196.
53. Ichikawa T, Haradome H, Hachiya J, Nitatori T, Araki T. Diffusion-weighted MR imaging with single-shot echo-planar imaging in the upper abdomen: preliminary clinical experience in 61 patients. *Abdomin imag*. 1999;24(5):456-61.
54. Yoshikawa T, Kawamitsu H, Mitchell DG, Ohno Y, Ku Y, Seo Y, Fujii M, Sugimura K. ADC Measurement of Abdominal Organs and Lesions Using Parallel Imaging Technique. *AJR*. 2006;187(6):1521-30.
55. Inan N, Arslan A, Akansel G, Anik Y, Demirci A. Diffusion-weighted imaging in the differential diagnosis of cystic lesions of the pancreas. *Americ Journ Roentgenol*. 2008;191(4):1115-21.
56. Zhang J, Tehrani YM, Wang L, Ishill NM, Schwartz LH, Hricak H. Renal Masses: Characterization with Diffusion-weighted MR Imaging—A Preliminary Experience. *Radiology*. 2008;247(2): 458-64.
57. Goyal A, Sharma R, Bhalla AS, Gamanagatti S, Seth A, Iyer VK, Das P. Diffusion-weighted MRI in renal cell carcinoma: a surrogate marker for predicting nuclear grade and histological subtype. *Acta Radiol*. 2012;53(3):349-58.
58. Paudyal B, Paudyal P, Tsushima Y, Oriuchi N, Amanuma M, Miyazaki M, Taketomi-Takahashi A, Nakazato Y, Endo K. The role of the ADC value in the characterisation of renal carcinoma by diffusion-weighted MRI. *British Journ Radiol*. 2010; 83(988):336-43.
59. Goyal A, Sharma R, Bhalla AS, Gamanagatti S, Seth A. Diffusion-weighted MRI in inflammatory renal lesions: all that glitters is not RCC. *Eur Radiol*. 2013;23(1):272-9.
60. Miller FH, Wang Y, McCarthy RJ, Yaghmai V, Merrick L, Larson A, Berggruen S, Casalino DD, Nikolaidis P. Utility of diffusion-weighted MRI in characterization of adrenal lesions. *Americ Journ of Roentg*. 2010;194(2):W179-W185.
61. Tsushima Y, Takahashi-Taketomi A, Endo K. Diagnostic utility of diffusion-weighted MR imaging and apparent diffusion coefficient value for the diagnosis of adrenal tumors. *Journ Magnet Reson Imag*. 2009;29(1):112-7.
62. Gibbs P, Pickles MD, Turnbull LW. Diffusion imaging of the prostate at 3.0 Tesla. *Investig Radiol*. 2006;41(2):185-8.
63. Song I, Kim CK, Park BK, Park W. Assessment of response to radiotherapy for prostate cancer: value of diffusion-weighted MRI at 3T. *Americ Journ Roentg*. 2010;194(6): W477-W482.
64. Fujii S, Matsusue E, Kigawa J, Sato S, Kanasaki Y, Nakanishi J, Sugihara S, Kaminou T, Terakawa N, Ogawa T. Diagnostic accuracy of the apparent diffusion coefficient in differentiating benign from malignant uterine endometrial cavity lesions: initial results. *Europ Radiol*. 2008;18(2):384-9.
65. Lin G, Ho KC, Wang JJ, Ng KK, Wai YY, Chen YT, Chang CJ, Ng SH, Lai CH, Yen TC. Detection of lymph node metastasis in cervical and uterine cancers by diffusion-weighted magnetic resonance imaging at 3T. *Journ Magnet Reson Imag*. 2008;28(1):128-35.
66. Moteki T, Ishizaka H. Diffusion-weighted EPI of cystic ovarian lesions: Evaluation of cystic contents using apparent diffusion coefficients. *Journ Magnet Reson Imag*. 2000;12(6):1014-9.
67. Nakayama T, Yoshimitsu K, Irie H, Aibe H, Tajima T, Nishie A, Asayama Y, Matake K, Kakihara D, Matsuura S. Diffusion-weighted echo-planar MR imaging and ADC mapping in the differential diagnosis of ovarian cystic masses: Usefulness of detecting keratinoid substances in mature cystic teratomas. *Journal of Magnetic Resonance Imaging*. 2005;22(2):271-8.
68. Low RN, Sebrechts CP, Barone RM, Muller W. Diffusion-weighted MRI of peritoneal tumors: comparison with conventional MRI and surgical and histopathologic findings—a feasibility study. *Amer Journ Roentg*. 2009;193(2):461-70.

## Chapter

# 10

# Functional MR: Perfusion and Dynamic Contrast-enhanced MRI

Niranjan Khandelwal, Sameer Vyas

## PERFUSION MAGNETIC RESONANCE IMAGING

### Introduction

Perfusion can provide valuable information for detection, characterization and monitoring therapies in various disease processes like neoplasm, inflammations and ischemia.<sup>1,2</sup> It is also referred as capillary or tissue-specific blood flow, and is an established physiologic and pathophysiologic measure of the volume of blood flowing through the microvasculature of a mass of tissue in a certain period of time. It is a quantitative measure, which can be determined with many different experimental techniques and often expressed in ml/100 gm/minute.<sup>3</sup> The values of perfusion should be comparable across measurement modalities and the theoretical equations are usually used for determining perfusion that can be translated from one measurement technique to another.

The perfusion can be noninvasive measured by the use of a tracer. Depending on the characteristics of these tracers, the blood flow measures can be divided into mainly three types viz. diffusible tracers, intravascular tracers and microsphere type tracers.<sup>4,5</sup> The diffusible tracers can easily pass through blood vessel walls and include H<sub>2</sub>O, or H<sub>2</sub>O<sup>15</sup> (used in positron emission tomography), and xenon (used in computed tomography-based perfusion measures). The intravascular tracers are those tracers which remain within the vessel walls and include iodinated contrast in CT and gadolinium and other contrast agents in magnetic resonance imaging (MRI). However, these agents are partially diffusible in most tissues of the body and separating perfusion from vessel permeability effects can be a challenge. The microsphere type tracers are slightly larger than capillaries; and hence, they get stuck within the microvasculature indefinitely. They are widely

used for invasive animal studies and are considered too risky for human studies. Clinical agents, such as the single photon emission computed tomography (SPECT) agent Tc-HMPAO mimic microspheres by remaining in the target tissue for a long time but they achieve this by diffusing into tissue and then undergoing a chemical transformation within the tissue that discourages diffusing back out.

As unusual nuclear species are readily detected in the body with MRI, perfusion imaging is possible with many different tracers including fluorinated compounds, deuterated water, O<sup>17</sup> and hyperpolarized gas Xenon.<sup>5-7</sup> The normal concentration of these tracer agents (nuclei) in tissue is almost zero and the only signal observed in clinical MRI is because of perfusion effects as the signal from these can be well separated from the water proton signal. These techniques are interesting and potentially promising, however these agents generally produce weak signals to noise ratio, have low spatial resolution, and lack the sensitivity of the proton MRI techniques, which is usually employed for clinical studies. Proton-based perfusion techniques using the strong signal from water protons in tissue have been found to be useful in the clinical setting and clinical research.

Perfusion imaging with the proton signal can be performed either by dynamic imaging following the bolus injection of an MR contrast agent or by labeling of the water in the inflowing arterial blood.<sup>8-12</sup> Contrast agent-based methods are commonly used as the effects of contrast agents in the vessels or tissue are quite strong. The bolus tracking technique is most widely used and it involves the injection of a bolus of magnetic contrast agent while repeatedly imaging.<sup>13,14</sup> It is usually performed using T2\* (or T2) contrast where the signal change is due to the magnetic susceptibility of the contrast

agent and is known as dynamic susceptibility contrast (DSC) MR perfusion or the T1 properties of the contrast agent, where the signal change is due to the T1 shortening effects of the contrast agent and is known as dynamic contrast enhancement (DCE) MR perfusion.<sup>13-17</sup> The DSC imaging is mostly employed in the brain whereas DCE MR perfusion is usually employed outside the brain. By selectively affecting the MRI signal from water in the inflowing arterial blood, imaging without contrast agent is possible and is known as arterial spin labeling (ASL) technique. It produces a smaller signal change than the contrast agent methods but the lack of an injection and the use of diffusible water as the tracer make this approach an interesting alternative option.<sup>11,15</sup>

### Magnetic Contrast Agents in Neural Tissues

MR contrast agents (paramagnetic and superparamagnetic) are intravascular within normal brain tissue as they are too large to cross the blood-brain barrier. The signal changes resulting from alterations to the intravascular signal are relatively small because the brain-blood volume is small (3-6%). However, the magnetic contrast agents within the vasculature can have effects beyond the vessels as an intravascular contrast agent and can affect tissue signal by altering the magnetic fields in the nearby tissue.<sup>18-21</sup> In addition, spins can move between small blood vessels in the microvasculature and the tissue.

### Imaging Techniques and Methods

There are three main techniques used to perform MR perfusion imaging: dynamic susceptibility contrast enhanced perfusion, dynamic contrast-enhanced perfusion and arterial spin labeling.<sup>1</sup>

All these techniques involve repetitive serial imaging during the passage of blood that has been labeled with either contrast material or with an endogenous magnetic tracer label. Dynamic susceptibility contrast enhanced (DSC) MR perfusion is simple to perform in a clinical environment and is currently the MR perfusion technique most commonly used in clinical studies.

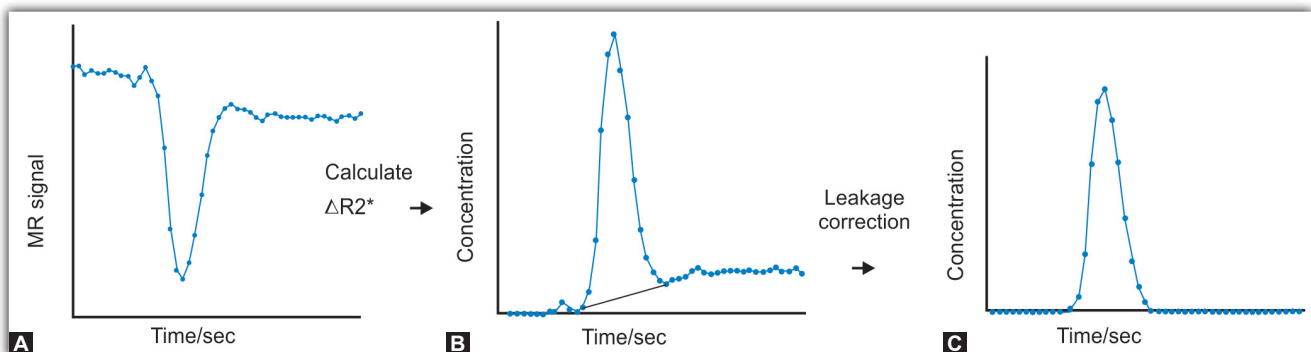
#### *Dynamic Susceptibility Contrast-enhanced MR Perfusion*

**Principle:** Dynamic susceptibility contrast-enhanced MR perfusion (DSCMRP) technique exploits the T2\* susceptibility effects of gadolinium, rather than the T1 shortening effects routinely associated with contrast enhancement on conventional imaging.<sup>22-26</sup> It uses rapid measurements of MR signal change following the injection of a bolus of a paramagnetic MRI contrast agent.<sup>1</sup> The susceptibility effect refers to the shortening of T2 and T2\* relaxation times, leading to lower signal on T2- or T2\*-weighted images. The signal loss resulting from passage of the contrast agent bolus on T2\* weighted images can be used to calculate the change in contrast concentration occurring in each pixel. Contrast

agent is treated as an intravascular marker and leakage into the interstitial space is ignored or where possible eliminated. These data can be used to produce calculated estimates of cerebral blood volume (CBV), mean transit time (MTT) and cerebral blood flow (CBF).

**Image acquisition:** The patient should be comfortably positioned with adequate cushioning to reduce movement and light restraining straps should be used in the same way as used for normal MRI. Data is acquired by using a fast imaging technique, such as single or multishot echo planar imaging (EPI) to produce a temporal resolution of approximately 2 seconds. The imaging sequence may be gradient echo which will maximize T2\* weighting or alternatively a spin echo approach can be used which will minimize the signal contribution from large vessels. A series of at least five pre-contrast images should be collected prior to the passage of the bolus and many centers will collect for up to 1 minute to provide a large number of pre-contrast images to improve the estimation of the signal intensity baseline during analysis. A standard contrast dose (0.1 mmol/kg) is adequate in most cases although double dose of gadolinium (0.2 mmol/Kg) may be used to improve signal to noise ratio. The contrast is usually injected via an 18- or 20-gauge IV catheter at a high rate (3-7 mL/sec) using a power injector, to allow for a tight bolus of contrast material. The injection should be followed by a saline flush of at least 25 mL (20-30 mL) delivered at the same rate in order to ensure that the bolus, which enters the central circulation is as coherent as possible. Alternatively, a careful manual injection technique can also be used. However, for manual techniques the injection should be given through a large cannula (at least 18 G) preferably introduced into a large antecubital vein, to reduce the resistance of the injection system. The injection should be given at an even rate and should be immediately followed by a chaser of the same amount of normal saline given at the same rate. Successive images of the region of interest (ROI) are then acquired during the first pass of contrast material.

**Data analysis:** The analysis of DSC-MRI is based on the assumption that the contrast agent remains within the vascular space throughout the examination acting as a blood pool marker.<sup>25,26</sup> This assumption is untrue except within the brain where there is no contrast leakage due to the blood-brain barrier. The drop in T2\* signal caused by the susceptibility effects of gadolinium is computed on a voxel-by-voxel basis and used to construct a time-versus intensity curve. The degree of signal drop is then assumed to be proportional to the tissue concentration of gadolinium, so that relative concentration-time curves can be obtained (delta R2 curves) (**Figs 1A to C**).<sup>26-31</sup> Relative cerebral blood volume (rCBV) can be obtained by calculating the area under the concentration-time curves, normalized to a contralateral, uninvolved region. "Relative" refers to the fact that an arterial input function is not used in the calculation of CBV, and therefore, precise quantification of cerebral blood volume is



**Figs 1A to C** Figure shows data analysis in DSC perfusion. (A) Time-versus MR signal intensity curve where signal intensity decrease during passage of contrast agent bolus and is measured from a series of MR images. (B) Tissue concentration-versus time curve where change in the relaxation rate ( $\Delta R2^*$ ) is calculated from signal intensity, and a baseline subtraction method is applied to measured data. (C) Corrected  $\Delta R2^*$  curve after leakage correction

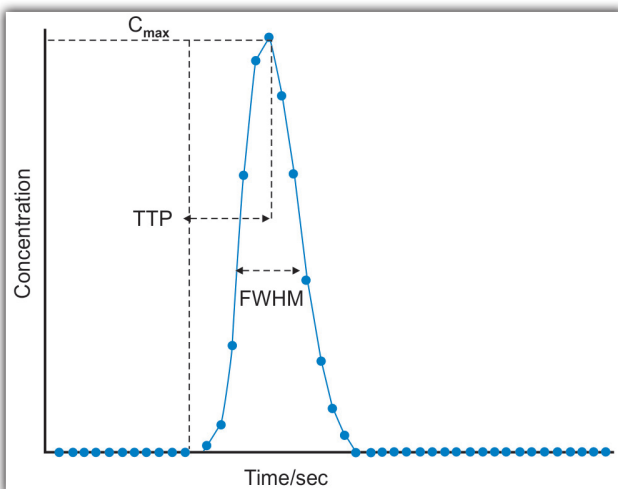


**Fig. 2** Contrast (tissue concentration) versus time curve showing the different parameters. Area under curve represents cerebral blood volume, height of curve represents cerebral blood flow and area/height of curve represents mean transit time.  $C_{\text{max}}$ , peak height and, full width half maximum (FWHM), time to peak concentration (TTP)

not performed. Repeating this process on a voxel-by-voxel basis, one can construct an rCBV map (Fig. 2). The MTT is then estimated as some form of standardized measurement of the width of the curve, such as the width at half the maximum height (full width at half maximum; FWHM). The blood flow can then be calculated using the central volume theorem  $CBF = CBV/MTT$ .

The initial calculation of local contrast concentration from the observed signal change a straightforward and contrast concentration is linearly related to the T2 rate changes ( $\Delta R2$ ), which can be calculated for using the relationship:

$$\Delta R2 = -\ln [S(t)/S(0)]/TE;$$

where,

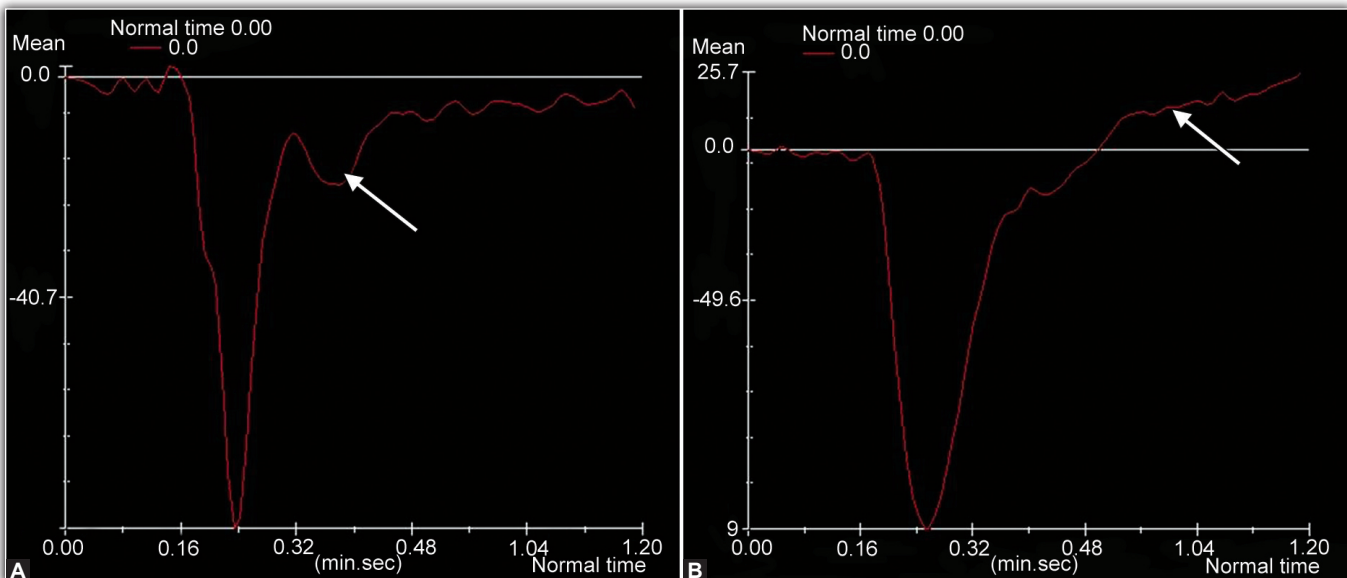
$S(0)$  is the base line signal intensity

$S(t)$  is the pixel intensity at time  $t$  and TE is the echo time.

This allows transformation of signal intensity time course data to contrast concentration time course data (Fig. 1). In addition to these flow related parameters, it is possible to produce maps based on the time the contrast takes to arrive in the voxel using the time of arrival or, more commonly the time to peak concentration (TTP).

**Problems with DSC MRI:** There are several major problems/errors with the DSC MRP, which have led to a number of major modifications of the analysis approach in an attempt to produce more accurate quantitative estimates of blood flow.<sup>26-43</sup> Three main problems with the technique include:

1. Contrast recirculation
  2. Contrast leakage
  3. Bolus dispersion.
1. **Contrast recirculation:** Analysis of the contrast bolus passage assumes that the bolus passes through the voxel and that the concentration of contrast then returns to zero. However, the contrast re-circulates through the body and a second re-circulation peak is seen following the first (Fig. 3A). As the contrast continues to circulate the bolus disperses and widens so that the second peak is lower and broader than the first and by the time of the third recirculation the intravascular contrast has mixed evenly throughout the blood volume causing a small constant baseline elevation in the contrast concentration. Errors in measurement of CBV are due to the presence of both first pass and recirculating contrast in the vessels during the later part of the bolus passage. The error can be approached is by use of curve fitting technique, which also smoothes the data, effectively reducing noise and eliminates the contamination of the first pass bolus due to contrast agent recirculation.
  2. **Contrast leakage and tissue enhancement:** Leakage of contrast into the interstitial space will cause signal changes, principally by relaxivity mechanisms. High permeability in regions of severe blood-brain barrier



**Figs 3A and B** (A) Signal intensity–time curve showing marked signal intensity decrease during arrival of the contrast agent, followed by partial recovery of the signal intensity loss. A second decrease in signal intensity (arrow) is due to recirculation. (B) Signal intensity–time curve showing contrast leakage and signal above baseline due to the T1 shortening effects of gadolinium

breakdown (e.g. high-grade neoplasm) leads to extravasation of contrast material into the interstitium, which increases signal above baseline due to the T1 shortening effects of gadolinium (i.e. enhancement) (**Fig. 3B**). Since, the algorithm for calculation of rCBV assumes a constant baseline, the area above baseline is interpreted by the algorithm as negative blood volume, and subtracted from the area below baseline caused by the drop in T2\* signal. This leads to significant underestimation of rCBV. Susceptibility based imaging methods offer the opportunity to separate these relaxivity and susceptibility based effects and to produce images in which the effect of contrast leakage is eliminated or minimized. The use of techniques with reduced T1 sensitivity, such as low flip angle gradient echo based sequences and increase the repetition time (TR), or uses a dual echo technique or use pre-enhancement [preinject an additional small dose of gadolinium (0.05 mmol/kg) to presaturate the interstitium, effectively elevating the baseline before the dynamic acquisition], which effectively removes relaxivity effects. In addition, newer contrast materials, which can act as ‘blood pool’ agents (such as gadobenate dimeglumine and monocrystalline iron oxide nanoparticles) may ameliorate this problem. The change in signal intensity resulting from T1 shortening is biexponential so that for any given sequence, there is a plateau phase during which signal intensity remains relatively constant. The effect of this response curve is that pre-enhancement of tumors will reduce the relaxivity-based signal intensity responses to subsequent contrast doses. However, each

approach offers a perfect solution and the choice of method must be based on individual analysis task to be undertaken.

3. **Bolus dispersion and the measurement of absolute CBF:** To measure the absolute CBF it is assumed that the technique can produce quantitative measurements of CBV and MTT. However, the use of the area under the curve to estimate CBV results in relative measurement that allows comparison of CBV between tissues rather than producing an absolute measurement.<sup>44-48</sup> In addition, the measurement of CBF also requires accurate estimation of MTT (calculated from the width of the contrast bolus). The width of the contrast bolus is affected by the arterial input function (AIF), changes in bolus width (due to regional alterations in flow) and physical bolus broadening (due to dispersive effects).

#### MRI sequence type

**Gradient-echo versus spin-echo:** Both gradient-echo and spin-echo acquisitions can be used, but rapid spin-echo imaging capable of dynamic perfusion measurements is only practical with echo-planar systems. Theoretically, spin-echo produces signal changes which predominantly reflect the passage of contrast through the capillary bed and reflect the tumor physiology at the capillary level; however several studies have shown that there is little effective benefit from the use of spin-echo images but compromise in terms of signal to noise ratio. Spin-echo techniques have been shown to be selectively sensitive to small vessels that are less than 20  $\mu$  in diameter, whereas gradient-echo images incorporate signals from larger tumor vessels as well as the microvasculature.

Gradient-echo techniques have shown a stronger correlation between tumor grade and blood volume.

**Spatial coverage versus time resolution:** The selection of the spatial coverage and time resolution is usually done as a compromise, according to the particular application and tissue under study. The time resolution is limited by the transit time of the bolus through the tissue as for accurate quantification of DSC MRP data, a proper characterization of the transient signal drop is required. Typically, a repetition time (TR) of 2 s or less is necessary for acquisition of the fast changes during the first pass. Therefore, the spatial coverage will be limited by the maximum number of slices that can be acquired within this TR. Echo planar imaging (EPI), segmented EPI, FLASH, etc. can be used.

**2D versus 3D sequences:** Both 2D and 3D sequences can be used. 2D sequences are usually preferable; however 3D sequence allow increased coverage, although typically at the expense of an increased TR, or a decreased spatial resolution.

**Single-echo versus dual-echo sequences:** Dual-echo sequences provide a simple way to remove the relaxivity effects and allows the quantification of changes in R2\* without assumption regarding the T1 behavior.<sup>41,42</sup> However, the sampling of two echoes increases sampling time and thus reducing the maximum number of slices that can be acquired (and therefore, coverage) in a given TR. When spatial coverage is important, single-echo sequences with a pre-dose of contrast may be used as the use of a pre-enhancement approach is proven effective.

#### *Dynamic Contrast Enhanced MR Perfusion*

Dynamic contrast enhanced MR perfusion (DCE MRP) provides insight into the nature of the tissue properties at the microvascular level by demonstrating the wash-in, plateau, and washout contrast kinetics of the tissue.<sup>43-55</sup> The DCE MRP, which is also referred as 'permeability' MRI, is an entirely different approach to MR perfusion as the main focus is on estimating tumor permeability.<sup>48-65</sup> The main advantage of T1-based techniques is that tumor leakiness (enhancement) is used for data analysis rather than considering it as an artifact as in DSC MRP. It has been established that quantification of contrast leakage can provide powerful indicators of the state of neovascular angiogenesis in pathologies, such as tumors and inflammatory tissue; and capillary leakage of contrast on MRI can provide an approach for monitoring the effects of the antiangiogenic drugs.

**Principle:** The T1-weighted technique measures the 'relaxivity effects' of the paramagnetic contrast material. The relaxivity effect of paramagnetic contrast material refers to the shortening of T1 relaxation time, leading to higher signal on T1-weighted images. The DCE MRP is based on a two-compartmental (plasma space and extravascular-extracellular space) pharmacokinetic model (**Fig. 4**).

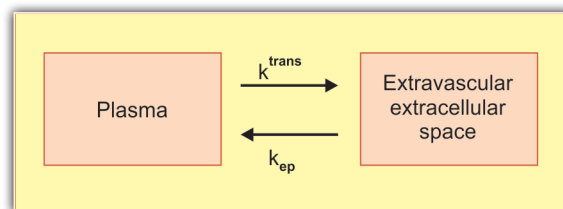


**Fig. 4** Dynamic contrast-enhanced MR perfusion: Two-compartment model demonstrates the exchange of contrast between plasma and extravascular-extracellular space

**Image acquisition:** The patient should be positioned as used for normal MRI. The general steps in acquisition of DCE MRP are: perform baseline T1 mapping, acquire DCE MRP images, convert signal intensity data to gadolinium concentration, determine the vascular input function, and perform pharmacokinetic modeling.<sup>56,57</sup> The dynamic imaging sequence must include precontrast images for a sufficient period to allow accurate estimation of the extracellular space and of the contribution of renal excretion. The data is acquired by three-dimensional (3D) gradient echo sequence. A bolus injection technique as used for DSC-MRP is used. A lower dose of gadolinium is administered (typically a single dose of 0.1 mmol/kg) at a lower rate (2 mL/sec) and repetitive acquisitions are then made through the lesion at longer intervals, typically every 15 to 26 seconds. Imaging is carried out over a much longer period of time than with T2\*-based techniques, to allow for the contrast to leak out into the extravascular space and come into equilibrium over several passes of the contrast bolus through the tumor bed.

**Data analysis:** Quantification of the contrast enhancement effect can be performed using a variety of techniques, which range from simple measures of the rate of enhancement to complex pharmacokinetic analyses.<sup>59-65</sup>

**Simple analysis techniques:** The quantification of enhancement can be done by directly comparing the signal intensity curves from ROI. There are many measurements that allow this type of analysis and are designed to minimize the variation, which will occur between patients as a result of variations in contrast dose, injection and scanning techniques and scanner type. The simplest of these is a measurement of the time taken for the tumor tissue to attain 90 percent of its subsequent maximal enhancement (T90). Another parameter measures the maximum rate of change of enhancement [maximal intensity change per time interval ratio (MITR)]. Various curve shapes can also provide insight into the quantification and calculates a standardized slope of the enhancement curve. However, the enhancement curve is poorly reproducible and most of these signal intensity based methods remain sensitive to variations between acquisition systems as there is a non-linear relationship between contrast concentration and signal intensity.

**Pharmacokinetic analysis techniques:** With pharmacokinetic modeling of DCE MRP data, several metrics are commonly derived: the transfer constant ( $k^{trans}$ ), the fractional volume of the extravascular extracellular space ( $v_e$ ), the rate constant ( $k_{ep}$ ,  $k_{ep} = k^{trans}/v_e$ ), and the fractional volume of the plasma space ( $v_p$ ). These quantitative techniques are intended to calculate the biological features, such as endothelial permeability and the endothelial surface area, which are relatively independent of imaging approach (scanner type, scanning technique or individual patient variations). The most frequently used metric in DCE MRP is  $k^{trans}$ . It can have different interpretations depending on blood flow and permeability. In situations, in which there is very high permeability, the flux of gadolinium-based contrast agent is limited only by flow, and thus  $k^{trans}$  mainly reflects blood flow; whereas if there is very low permeability, the gadolinium-based contrast agent cannot leak easily into the extravascular-extracellular space, and thus  $k^{trans}$  mainly reflects permeability. The product of the endothelial permeability and endothelial surface area represents the transfer coefficient  $k^{trans}$  which governs the leakage of contrast from the vascular to the extravascular compartment. The leakage of contrast can be calculated by:

where,  $v_e$  is the proportion of the voxel into which contrast can leak (contrast distribution space);

- $C_1$  is the concentration of contrast in the space
- $C_p$  is the concentration of contrast in the blood.
- $k^{trans}$  can be calculated if we can accurately estimate the change in concentration of contrast in the bloodstream and in the tissue over time. The calculation of contrast concentration also requires knowledge of the initial T1 value of the tissues before contrast arrival which must therefore be measured before the dynamic imaging is performed and is usually measured by the use of gradient echo images with variable flip angles.

#### Problems with quantitative measurement of DCE MRI:

The measurement of  $k^{trans}$  with pharmacokinetic analysis techniques have few disadvantages, which includes partial volume averaging effects, long acquisition time and flow dependency of  $k^{trans}$ .

**Partial volume averaging effects:** The pharmacokinetic analysis technique assumes that samples taken from voxels in blood vessels will represent blood concentration changes whereas voxels within the target tissue will represent extravascular contrast leakage. However, this assumption is incorrect and voxels within the target tissue are actually likely to represent a mixture some of which will have significant intravascular contrast content. This will result in overestimation of  $k^{trans}$  in these voxels which can be seen as areas of apparently high permeability in areas of normal brain. This problem can be approached by excluding any voxel

which produces values over a certain threshold (1.2/ min) as being vascular in origin or more complex pharmacokinetic models.

**Long acquisition time:** Another major problem with permeability imaging is long acquisition time as the measurement takes a considerable period of time (at least 5 min). There is little or no misregistration of data in brain perfusion and can be easily corrected by data co-registration. However, in other areas of the body which are affected by respiratory motion, there is significant misregistration and respiratory gating techniques markedly limit the image acquisition strategy and the temporal sampling rate which can be achieved. This can be approached by modifying the pharmacokinetic model and describing only the first passage of the contrast bolus. This technique also eliminates the problems with partial volume averaging described above and produces highly reproducible parametric maps of both  $k^{trans}$  and CBV.

**Flow dependency of  $k^{trans}$ :** The measurements of  $k^{trans}$  will be markedly affected by flow to the voxel as well as the permeability and surface area of the vascular endothelium. For measurements of  $k^{trans}$  it is assumed that for any given combination of intravascular and extravascular contrast concentrations the rate of contrast leakage will be proportional to the permeability and surface area of the vascular endothelium, however it is true only where the supply of contrast to the vascular space is sufficiently high that contrast leakage will not affect the intravascular concentration. There is limitation, in areas where there is contrast leakage and the blood flow is inadequate to replenish contrast at adequate rate; as a result plasma contrast concentration decreases and  $k^{trans}$  will reflect local blood flow.

#### Arterial Spin Labeling MR Imaging

Arterial-spin labeling (ASL) is an alternative technique of performing MR perfusion without the use of an intravenous contrast agent.<sup>66-68</sup> The ASL can be thought of as a natural extension of magnetic resonance angiography (MRA) and is also closely related to blood flow imaging with  $H_2O^{15}PET$ . Many recent studies show that ASL provides similar information to the DSC or DCE MRP, and even have more advantages as compared to these techniques including better ASL flow maps in detecting regions of disturbed vascularity and being independent of tumor permeability, so that no corrections are needed. Hitherto, limitations of ASL like long imaging times and decreased spatial resolution as compared with contrast-based techniques have excluded widespread clinical application of ASL, but with recent advancement the ASL may play an important role in the future of MR perfusion imaging.

**Principle:** ASL uses magnetically labeled blood as an endogenous contrast agent. In this technique, spatially selective excitation pulses or flow encoding gradient pulses

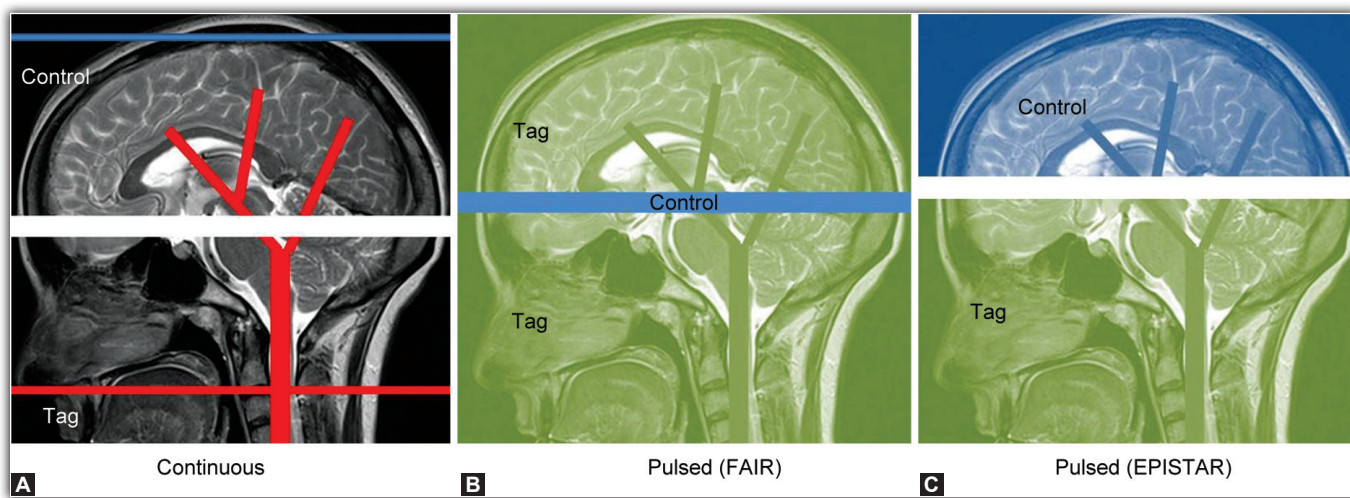
are applied to inflowing blood to differentiate between static tissue and flowing blood. Time is allowed for the blood to move out of the vessels and into the perfused tissue, and then the signal change in tissue caused by the selective labeling of the arterial blood is measured which is closely related to the blood flow into that tissue. The arterial spin labeling methods measure CBF by taking the difference of two sets of images: tag images, in which the longitudinal magnetization of arterial blood is inverted or saturated, and control images in which the magnetization of arterial blood is fully relaxed.<sup>69,70</sup> To remove the contribution of the static tissue to the tag image, a control image of the same slice is acquired in which inflowing blood is not tagged. The magnetization difference ( $\Delta M = M_{\text{contr}} - M_{\text{tag}}$ ), i.e. difference of the control and tag images yields an image that is proportional to CBF. Tag and control images are typically acquired in a temporally interleaved fashion, and the running difference of the control and tag images is used to form a perfusion time series.

**Image acquisition and labeling techniques:** Different labeling techniques of ASL, that have been described or used for *in vivo* studies, are very similar and differ only in subtle aspects of implementation. However, they are broadly divided into spatially selective ASL and velocity-selective ASL.<sup>71-79</sup> In spatially selective ASL, a spatial separation between the imaged region and inflowing arterial blood is required to cause signal change in the image whereas in velocity-selective ASL, bipolar gradients are used to label flowing blood. Velocity-selective ASL, resemble phase contrast angiography, and can be used to label blood within the slice or slab and thus may permit labeling even closer to the capillary bed than spatially selective ASL. In most of the ASL techniques, magnetization is labeled along the main magnetic field direction (Mz). The advantage of labeling Mz is that changes in Mz return back to the equilibrium on the

time scale of T1. The magnetization can also be labeled along the transverse direction (Mx or My) but since the transverse magnetization decays with T2, typically 5 to 10 times faster than T1 decay, the signal produced would be much smaller.

Spatially selective ASL is by far the well-developed technique and most studies have been performed using this technique. It is similar to time-of-flight angiography. Inflowing blood may be tagged continuously or intermittently and can be broadly divided into continuous ASL and pulsed ASL (Figs 5A to C). Different pulsed labeling strategies differ from each other in primarily two issues. First is what inversions are applied to other tissue, including the imaged region, and secondly what is done to insure that the differences between the two RF preparations do not cause direct effects on the image which are independent of perfusion.

**Pulsed ASL:** In this technique, single perturbing pulse is applied to the spins outside the slice at a single time point, and then time is given for the spins to enter the tissue (Figs 5B and C). Usually, an RF pulse is applied at a time approximately 1 second before imaging. An inversion RF pulse is usually used as it creates the largest change in the arterial magnetization and the time before imaging is referred to as TI, as in inversion recovery sequences. Two images are obtained, one with the region containing the inflowing artery inverted and one where it is not inverted. The signal change with pulsed techniques is smaller than with continuous techniques as the spins which enter the tissue later are perturbed earlier than in the continuous technique, there is additional T1 decay of the label and generally. However, this technique also have additional advantages including more traditional RF and gradient strategies, are less subject to certain types of systematic error, and can produce excellent images. Pulsed ASL methods include echo planar imaging and signal targeting with alternating radiofrequency (EPISTAR),



**Figs 5A to C** ASL techniques, schematic diagram illustrating arterial spin labeling strategies. (A) Continuous ASL (CASL) labels arterial spins as they flow through a labeling plane. (B and C) Pulsed ASL (PASL) labels arterial spins using a spatially selective labeling pulse

flow-sensitive alternating inversion recovery (FAIR), signal targeting with alternating radio frequency (STAR), transfer insensitive labeling technique (TILT) (Gobay 1999) and proximal inversion with a control for off-resonance effect (PICORE) (Wong 1997).<sup>80-84</sup>

The EPISTAR technique is the simplest pulsed inversion strategy and was first proposed by Edelman et al. In this technique, a slab-selective inversion pulse is applied inferior to the imaged brain region to label arterial spins and a superior inversion slab is applied during the control image preparation. The superior inversion insures equal magnetization transfer effects from the two preparation pulses.

The FAIR is an alternative strategy to EPISTAR where a nonselective inversion pulse is applied for the labeling and a slab selective inversion containing the entire imaged region is applied for a control image. In this technique, the effect on inflowing spins inferior to the slice is the same as in EPISTAR, but the spins in the imaged slab are inverted in both cases, rather than left unaffected.

Because any slight difference in the flip angle of the two pulses will have a big effect upon the measured signal, special RF pulses with low sensitivity to variations in RF amplitude and very sharp slice profiles must be employed. There are number of variations of these basic labeling techniques and most of them may provide small improvements to the results but variations in implementation and methods of assessment overshadow these small differences.

**Continuous ASL:** In this technique, spins are continuously inverted at a specific location before they enter the tissue. Thus spins which enter the tissue first are labeled first and spins which enter later are labeled later. One can approximate continuous saturation of spins as they flow past a certain plane by applying a series of thin saturation pulses repeatedly, but trying the same strategy with inversion pulses is problematic; some spins may remain within the saturation slab for two or more inversions and get doubly inverted. Inversion pulse is considered highly desirable to use a continuous inversion technique as it provides a stronger signal change. Continuous ASL methods include Saturation, inversion (Williams 1992) with flow-driven adiabatic inversion pulse and labeling with 2nd coil. Continuous ASL (CASL) usually employs a special RF labeling scheme known as flow-driven adiabatic inversion. Flow-driven adiabatic inversion is a simple technique because it requires only turning on a constant gradient and RF (**Fig. 5A**). While the pulsed ASL experiment is essentially a decaying bolus experiment where the labeled blood transiently enters the tissue, the continuous ASL experiment can be operated as a steady-state experiment. If the labeling is left on for a long time, a balance between the inflow of newly labeled spins and the T1 decay of the labeled spins already in the tissue is reached. This makes quantification of perfusion relatively simple. As compared with pulsed ASL, the continuous ASL can achieve a signal

approximately 2 to 3 times larger is generally more sensitive. The greatest disadvantage of the continuous labeling approach is the unusual RF requirements of the labeling. As in CASL (Flow-driven adiabatic inversion), weaker RF for an extended period of time is required, implementation may be difficult because many scanners are designed specifically for brief, widely spaced pulses of RF at high power.

**Vessel selective labeling:** A recent approach has been introduced in which arterial water is labeled selectively on the basis of the blood velocity, termed velocity-selective ASL. The main difference between velocity-selective ASL and the other ASL techniques is that the arterial water is labeled everywhere, including the volume of interest, therefore minimizing the time for the blood to reach any region of interest.

**Pseudo-continuous arterial spin labeling (psCASL):** This is also known as pulsed continuous arterial spin labeling (pCASL). This is a newly proposed technique that has eased the technical restrictions of CASL and employs a train of discrete RF pulses that mimics continuous ASL.<sup>85,86</sup> In pCASL, continuous labeling is achieved by a train of rapidly repeating low tip RF pulses and alternating sign (bipolar) magnetic field gradients which is also suitable for MR systems that do not have continuous RF capabilities. Moreover, it has been shown that pCASL can achieve better compensation of adverse MT effects than CASL.

**Data analysis (calculating blood flow from arterial spin labeling measurements):** The control and tag images ASL are acquired in an interleaved fashion and a perfusion time series is then formed from the running subtraction of the control and tag images.<sup>87-90</sup> Hence, the simple subtraction image obtained can be a good reflection of relative blood flow without any calculations. However, because differences in tissue T1 and other factors can lead to different sensitivity to blood flow across the image and quantitative measurements of blood flow can be useful for some purposes, it can be useful to convert the difference images into actual blood flow maps in physiologic units. This conversion requires some consideration of how inflow impacts tissue MR signal.

**Problems with ASL:** Despite its advantages, ASL imaging is limited by a large background signal and the motion artifacts. In addition, the small signal level of ASL reduces the signal-to-noise ratio of the ASL perfusion imaging. With recent advancement in MRI technology, good quality images can be obtained.

## DYNAMIC CONTRAST-ENHANCED MRI

Dynamic contrast enhancement techniques are well established for characterizing the benign or malignant lesions by providing functional information to the anatomically detailed morphological images as the malignant lesions usually show faster and higher levels of enhancement than

normal tissue.<sup>91</sup> This enhancement pattern of the malignant lesions reflects increased vascularity (neoangiogenesis) and higher endothelial permeability to the contrast molecules than do normal or less aggressive malignant tissues. Nowadays, dynamic contrast-enhanced MRI (DCE-MRI) is modality of choice for the diagnosis and characterization of the tumors of the brain, breast, prostate, liver, cervix and musculoskeletal system.<sup>92-95</sup>

**Principle:** The DCE-MRI relies on fast MRI sequences obtained before, during and after the rapid intravenous (IV) administration of a gadolinium-based contrast agent.<sup>64</sup> IV-injected contrast agents pass from the arteries to the tissue microvasculature and extravasate within seconds to the extravascular extracellular space. Contrast agents in vessels and in the extracellular space shorten local relaxation times, leading to increased signal on T1-weighted sequences. The ability to measure vessel leakiness is related to blood flow (i.e. it is difficult to identify leakiness if the flow is too low). Thus, the signal measured on DCE-MRI represents a combination of perfusion and permeability. The DCE-MRI is sensitive to alterations in vascular permeability, extracellular space and blood flow. The DCE-MRI enables the depiction of physiologic alterations as well as morphologic changes. It is an emerging imaging method to assess tumor angiogenesis and the clinical application of DCE-MRI for cancer is based on data showing that malignant lesions usually shows rapid, intense enhancement followed by a relatively rapid washout compared to normal healthy tissue.

**Image acquisition:** The acquisition of DCE-MRI is done by acquiring a minimum of three sections through the tumor and imaging volume that includes a region outside the tumor, such as an artery or muscle for normalization. Quantity of the injected contrast material is usually standardized according to the patient's body weight and preferentially should be injected at a constant rate with a power injector typically using 3D T1-weighted acquisition (spoiled gradient-echo sequences) to repeatedly image a volume of interest after the administration of a bolus of IV contrast agent. T1-weighted spoiled gradient-echo sequences provide high sensitivity to T1 changes, high signal-to-noise ratios, adequate anatomic coverage, and rapid data acquisition. Serial image sets are obtained sequentially every 5 seconds (ranging from 2–15 seconds) for up to 5 to 10 minutes. The rapidity with which MRI must be acquired necessitates that larger voxels (i.e. lower matrix sizes) must be obtained to maintain adequate signal-to-noise ratios.

**Data analysis:** Signal intensity (SI) enhancement patterns on T1W images can be evaluated by different analysis techniques, viz. qualitative, semiquantitative and quantitative. The complexity and standardization of analytic technique is needed to be adjusted.

**Qualitative:** The qualitative or visual analysis is most readily accessible analytic but also the least standardized method.

It is based on the general assumption that tumor vessels are leaky and more readily enhance after IV contrast material. It is expressed by a fast exchange of blood and contrast media between capillaries and tumor tissues. Thus, DCE-MRI patterns for malignant tumors are expected to show early rapid high enhancement after injection followed by a relatively rapid decline compared with a slower and continuously increasing signal for normal tissues during the first few minutes after contrast injection. The qualitative analysis shows higher accuracy and less interobserver variability but there is overlap of malignant and benign tissues, which is limiting the capabilities of this approach. Moreover, the qualitative approach is inherently subjective and therefore difficult to standardize among institutions, making multicenter trials less reliable.

**Semi-quantitative analysis:** Semi-quantitative analysis calculates various curve parameters and is also referred as curveology. It is also based on the assumption of early and intense enhancement and washout as a predictor of malignancy. Parameters are obtained to characterize the shape of the time-intensity curve, such as the time of first contrast uptake, time to peak, maximum slope, peak enhancement, and wash-in and washout curve shapes. There are three common dynamic curve types after initial uptake: type 1, persistent increase; type 2, plateau; and type 3, decline after initial upslope. Type 3 is considered to be indicator of malignancy. The semiquantitative approach is widely used and has the advantage of being simple to perform. It has limitations in terms of generalization across acquisition protocols, sequences, and all other factors contributing to the MR signal intensity, which in turn affect curve metrics, such as maximum enhancement and washout percentage.

**Quantitative analysis:** Quantitative analysis is most generalizable but most complex method. It depends on contrast concentration curves over time and use pharmacokinetic models to calculate permeability constants. Dynamic imaging data obtained with DCE-MRI can generate curves which are mathematically fit to compartment pharmacokinetic models. For functional analysis of tissue microcirculation, two-compartment model is considered for the kinetic parameters which demonstrates the exchange of contrast between plasma and extravascular space as proposed by Tofts et al. To describe tumor and tissue permeability, various kinetic parameters include,  $K^{trans}$  [transendothelial transport of contrast medium from vascular compartment to the tumor interstitium (washin)],  $k_{ep}$  [reverse transport parameter of contrast medium back into the vascular space (washout)], fpV (plasma volume fraction compared to whole tissue volume) and Ve [extravascular, extracellular volume fraction of the tumor; the fraction of tumor volume occupied by extravascular extracellular space (EES)]. Physiologically, the value of  $K^{trans}$  is tissue dependent;  $K^{trans}$  will indicate the tissue perfusion per unit volume, if the contrast uptake of the tissue is flow limited; on the other hand,  $K^{trans}$  indicates the

tissue permeability, if the uptake is permeability limited. In majority of tumors,  $k^{trans}$  indicates a combination of both flow and permeability properties of the tissue and high  $k^{trans}$  values usually reflect both high permeability and high perfusion. This is a fundamental limitation of DCE-MRI, namely the parameters it generates are inherently ambiguous with regard to their physiologic significance.

## REFERENCES

- Essig M, Shiroishi MS, Nguyen TB, Saake M, Provenzale JM, Enterline D, et al. Perfusion MRI: the five most frequently asked technical questions. *AJR Am J Roentgenol.* 2013;200:24-34.
- Hochberg AR, Young GS. Cerebral perfusion imaging. *Semin Neurol.* 2012;32:454-65.
- Lammertsma AA, Cunningham VJ, Deiber MP, et al. Combination of dynamic and integral methods for generating reproducible functional CBF images. *J Cereb Blood Flow Metab.* 1990;10:675-86.
- Axel L. Cerebral blood flow determination by rapid-sequence computed tomography. *Radiology.* 1980;137:676-86.
- Yonas H, Darby JM, Marks EC, et al. CBF measured by Xe CT: approach to analysis and normal values. *J Cereb Blood Flow Metab.* 1991;11:716-25.
- Detre JA, Eskey CJ, Koretsky AP. Measurement of cerebral blood flow in rat brain by F-19 NMR detection of trifluoromethane washout. *Magn Reson Med.* 1990;15:45-57.
- Kim SG, Ackerman JJH. Quantification of regional blood flow by monitoring of exogenous tracer via nuclear magnetic resonance spectroscopy. *Magn Reson Med.* 1990;14:266-82.
- Detre JA, Leigh JS, Williams DS, et al. Perfusion imaging. *Magn Reson Med.* 1992;23:37-45.
- McGehee BE, Pollock JM, Maldjian JA. Brain perfusion imaging: How does it work and what should I use? *J Magn Reson Imag.* 2012;36:1257-72.
- Ostergaard. Principles of cerebral perfusion imaging by bolus tracking. *J Magn Reson Imag.* 2005;22:710-7.
- Wu, Ostergaard. Technical aspects of perfusion-weighted imaging. *Neuroimaging Clin N Am.* 2005;15:623-37.
- Duyn, van Gelderen. Technological advances in MRI measurement of brain perfusion. *J Magn Reson Imaging.* 2005;22:751-3.
- Rosen BR, Belliveau JW, Buchbinder BR, et al. Contrast agents and cerebral hemodynamics. *Magn Reson Med.* 1991;19:285-92.
- Keston P, Murray AD, Jackson A. Cerebral perfusion imaging using contrast-enhanced MRI. *Clin Radiol.* 2003;58:505-13.
- Williams DS, Detre JA, Leigh JS, et al. Magnetic resonance imaging of perfusion using spin inversion of arterial water. *Proc Natl Acad Sci USA.* 1992;89:212-16.
- Calamante F, Thomas DL, Pell GS, et al. Measuring cerebral blood flow using magnetic resonance imaging techniques. *J Cereb Blood Flow Metab.* 1999;19:701-35.
- Villringer A, Rosen BR, Belliveau JW, et al. Dynamic imaging with lanthanide chelates in normal brain: contrast due to magnetic susceptibility effects. *Magn Reson Med.* 1988;6:164-74.
- Weisskoff RM, Zuo CS, Boxerman JL, et al. Microscopic susceptibility variation and transverse relaxation: theory and experiment. *Magn Reson Med.* 1994;31:601-10.
- Yablonskiy DA, Haacke EM. Theory of NMR signal behavior in magnetically inhomogeneous tissues: the static dephasing regime. *Magn Reson Med.* 1994;32:749-63.
- Kiselev VG, Posse S. Analytical model of susceptibility-induced MR signal dephasing: effect of diffusion in a microvascular network. *Magn Reson Med.* 1999;41:499-509.
- Petrella JR, Provenzale JM. MR perfusion imaging of the brain: techniques and applications. *AJR Am J Roentgenol.* 2000;175:207-19.
- Aksoy FG, Lev MH. Dynamic contrast-enhanced brain perfusion imaging: technique and clinical applications. *Semin Ultrasound CT MR.* 2000;21:462-77.
- Cha S. Perfusion MR imaging: basic principles and clinical applications. *Magn Reson Imaging Clin N Am.* 2003;11:403-13.
- Covarrubias DJ, Rosen BR, Lev MH. Dynamic magnetic resonance perfusion imaging of brain tumors. *Oncologist.* 2004;9:528-37.
- Chavhan GB, Babyn PS, Thomas B, Shroff MM, Haacke EM. Principles, techniques, and applications of T2\*-based MR imaging and its special applications. *Radiographics.* 2009;29:1433-49.
- Boxerman JL, Hamberg LM, Rosen BR, et al. MR contrast due to intravascular magnetic susceptibility perturbations. *Magn Reson Med.* 1995;34:555-66.
- Fiesel CR, Ackerman JL, Buxton RB, et al. MR contrast due to microscopically heterogeneous magnetic susceptibility: numerical simulations and applications to cerebral physiology. *Magn Reson Med.* 1991;17:336-47.
- Rempp KA, Brix G, Wenz F, et al. Quantification of regional cerebral blood flow and volume with dynamic susceptibility contrast-enhanced MR imaging. *Radiology.* 1994;193:637-41.
- Edelman RR, Mattle HP, Atkinson DJ, et al. Cerebral blood flow: assessment with dynamic contrast-enhanced T2-star-weighted MR imaging at 1.5 T. *Radiology.* 1990;176:211-20.
- Levin JM, Kaufman MJ, Ross MH. Sequential dynamic susceptibility contrast MR experiments in human brain: residual contrast agent effect, steady-state, and hemodynamic perturbation. *Magn Reson Med.* 1995;34:655-63.
- Barbier EL, Lamalle L, Decors M. Methodology of brain perfusion imaging. *J Magn Reson Imag.* 2001;13:496-520.
- Rosen BR, et al. Contrast agents and cerebral hemodynamics. *Magn Reson Med.* 1991;19:285-92.
- Kassner A, et al. Abnormalities of the contrast re-circulation phase in cerebral tumors demonstrated using dynamic susceptibility contrast-enhanced imaging: a possible marker of vascular tortuosity. *J Magn Reson Imaging.* 2000;11:103-13.
- Heiland S, Benner T, Debus J, et al. Simultaneous assessment of cerebral hemodynamics and contrast agent uptake in lesions with disrupted blood-brain barrier. *Magn Reson Imag.* 1999;17:21-7.
- Weisskoff RM, Chesler DA, Boxerman JL, et al. Pitfalls in MR measurement of tissue blood flow with intravascular tracers: which mean transit time. *Magn Reson Med.* 1993;29:553-9.
- Akbudak E, Conturo TE. Arterial input functions from MR phase imaging. *Magn Reson Med.* 1996;36:809-15.
- Duhamel G, Schlaug G, Alsop DC. Measurement of arterial input functions for dynamic susceptibility contrast magnetic resonance imaging using echoplanar images: comparison of physical simulations with *in vivo* results. *Magn Reson Med.* 2006;55:514-23.
- van Osch MJ, van der Grond J, Bakker CJ. Partial volume effects on arterial input functions: shape and amplitude distortions and their correction. *J Magn Reson Imaging.* 2005;22:704-9.

39. Perman WH, Gado MH, Larson KB, et al. Simultaneous MR acquisition of arterial and brain signal time curves. *Magn Reson Med.* 1992;28:74-83.
40. Vonken EP, van Osch MJ, Bakker CJ, et al. Simultaneous quantitative cerebral perfusion and Gd-DTPA extravasation measurement with dual-echo dynamic susceptibility contrast MRI. *Magn Reson Med.* 2000;43:820-7.
41. Vonken E, van Osch M, Bakker C, et al. Measurement of cerebral perfusion with dual-echo multi-slice quantitative dynamic susceptibility contrast MRI. *J Magn Reson Imag.* 1999;10:109-17.
42. Ostergaard L, Weisskoff RM, Chesler DA, et al. High resolution measurement of cerebral blood flow using intravascular tracer bolus passages. Mathematical approach and statistical analysis. *Magn Reson Med.* 1996;36:715-25.
43. Liu HL, Pu T, Andrews T, et al. Cerebral blood flow measurement by dynamic contrast MRI using singular value decomposition with an adaptive threshold. *Magn Reson Med.* 1999;42:167-72.
44. Calamante F, Gadian DG, Connely A. Delay and dispersion effects in dynamic susceptibility contrast MRI: simulations using singular value decomposition. *Magn Reson Med.* 2000; 44:466-73.
45. Ostergaard L, Sorensen AG, Kwong KK, et al. High resolution measurement of cerebral blood flow using intravascular tracer bolus passages. Experimental comparison and preliminary results. *Magn Reson Med.* 1996;36:726-36.
46. Calamante F, Morup M, Hansen LK. Defining a local arterial input function for perfusion MRI using independent component analysis. *Magn Reson Med.* 2004;52:789-97.
47. Mouridsen K, Christensen S, Gydensted L, et al. Automatic selection of arterial input function using cluster analysis. *Magn Reson Med.* 2006;55:524-31.
48. Lorenz C, Benner T, Lopez CJ, et al. Effect of using local arterial input functions on cerebral blood flow estimation. *J Magn Reson Imag.* 2006;24:57-65.
49. Sourbron S, Ingrisch M, Siefert A, Reiser M, Herrmann K. Quantification of cerebral blood flow, cerebral blood volume, and blood-brain-barrier leakage with DCE-MRI. *Magn Reson Med.* 2009;62:205-17.
50. Tofts PS, Brix G, Buckley DL, et al. Estimating kinetic parameters from dynamic contrast-enhanced T1-weighted MRI of a diffusible tracer: standardized quantities and symbols. *J Magn Reson Imaging.* 1999;10:223-32.
51. Dean BL, Lee C, Kirsch JE, et al. Cerebral hemodynamics and cerebral blood volume: MR assessment using gadolinium contrast agents and T1-weighted turbo-FLASH imaging. *AJR.* 1992;13:39-48.
52. Moody AR, Martel A, Kenton A, et al. Contrast-reduced imaging of tissue concentration and arterial level (CRITICAL) for assessment of cerebral hemodynamics in acute stroke by magnetic resonance. *Invest Radiol.* 2000;35:401-11.
53. Shin W, Cashen TA, Horowitz SW, et al. Quantitative CBV measurement from static T1 changes in tissue and correction for intravascular water exchange. *Magn Reson Med.* 2006;56:138-45.
54. Lu H, Law M, Johnson G, Ge Y, et al. Novel approach to the measurement of absolute cerebral blood volume using vascular-space-occupancy magnetic resonance imaging. *Magn Reson Med.* 2005;54:1403-11.
55. ME Raichle, JO Eichling, MG Straatmann, et al. Blood-brain barrier permeability of <sup>11</sup>C-labeled alcohols and <sup>15</sup>O-labeled water. *Am J Physiol.* 1976;230:543-52.
56. Edelman RR, Siewert B, Darby DG, et al. Qualitative mapping of cerebral blood flow and functional localization with echo-planar MR imaging and signal targeting with alternating radio frequency. *Radiology.* 1994;192:513-20.
57. Kwong KK, Chesler DA, Weisskoff RM, et al. MR perfusion studies with T1-weighted echo planar imaging. *Magn Reson Med.* 1995;34:878-87.
58. Paldino MJ, Barboriak DP. Fundamentals of quantitative dynamic contrast-enhanced MR imaging. *Magn Reson Imaging Clin N Am.* 2009;17:277-89.
59. Tofts PS, Brix G, Buckley DL, et al. Estimating kinetic parameters from dynamic contrast-enhanced T1-weighted MRI of a diffusible tracer: standardized quantities and symbols. *J Magn Reson Imag.* 1999;10:223-32.
60. Tofts PS, Kermode AG. Measurement of the blood-brain barrier permeability and leakage space using dynamic MR imaging. Fundamental concepts. *Magn Reson Med.* 1991;17:357-67.
61. Cron GO, Santyr G, Kelcz F. Accurate and rapid quantitative dynamic contrast-enhanced breast MR imaging using spoiled gradient-recalled echoes and bookend T(1) measurements. *Magn Reson Med.* 1999;42:746-53.
62. Cron GO, Kelcz F, Santyr GE. Improvement in breast lesion characterization with dynamic contrast-enhanced MRI using pharmacokinetic modeling and bookend T(1) measurements. *Magn Reson Med.* 2004;51:1066-70.
63. Nguyen TB, Cron GO, Mercier JF, et al. Diagnostic accuracy of dynamic contrast-enhanced MR imaging using a phase-derived vascular input function in the preoperative grading of gliomas. *Am J Neuroradiol.* 2012;33:1539-45.
64. Jackson A. Analysis of dynamic contrast enhanced MRI. *Br J Radiol.* 2004;77:S154-S166.
65. Claussen C, Laniado M, Schorner W, et al. Gadolinium-DTPA in MR imaging of glioblastomas and intracranial metastases. *AJNR.* 1985;6:669-74.
66. Talagala SL, Ye FQ, Ledden PJ, Chesnick S. Whole-brain 3D perfusion MRI at 3.0 T using CASL with a separate labeling coil. *Magn Reson Med.* 2004;52:131-40.
67. Wang Z, Wang J, Connick TJ, Wetmore GS, Detre JA. Continuous ASL (CASL) perfusion MRI with an array coil and parallel imaging at 3T. *Magn Reson Med.* 2005;54:732-7.
68. van Laar PJ, van der Grond J, Hendrikse J. Brain perfusion territory imaging: methods and clinical applications of selective arterial spin-labeling MR imaging. *Radiology.* 2008;246:354-64.
69. Buxton RB, Frank LR, Wong EC, et al. A general kinetic model for quantitative perfusion imaging with arterial spin labeling. *Magn Reson Med.* 1998;40:383-96.
70. Frank LR, Wong EC, Buxton RB. Slice profile effects in adiabatic inversion: application to multislice perfusion imaging. *Magn Reson Med.* 1997;38:558-64.
71. Golay X, Stuber M, Pruessmann KP, et al. Transfer insensitive labeling technique (TILT): application to multislice functional perfusion imaging. *J Magn Reson Imaging.* 1999;9:454-61.
72. Edelman RR, Chen G. EPISTAR MRI: multislice mapping of cerebral blood flow. *Magn Reson Med.* 1998;40:800-5.
73. Kim SG. Quantification of relative cerebral blood flow change by flow-sensitive alternating inversion-recovery (FAIR) technique: application to functional mapping. *Magn Reson Med.* 1995;34:293-301.
74. Yongbi MN, Branch CA, Helpern JA. Perfusion imaging using FOCI RF pulses. *Magn Reson Med.* 1998;40:938-43.

75. Dixon WT, Du LN, Faul DD, et al. Projection angiograms of blood labeled by adiabatic fast passage. *Magn Reson Med.* 1986;3:454-62.
76. Wong EC, Buxton RB, Frank LR. A theoretical and experimental comparison of continuous and pulsed arterial spin labeling techniques for quantitative perfusion imaging. *Magn Reson Med.* 1998;40:348-55.
77. Wong EC, Buxton RB, Frank LR. Quantitative imaging of perfusion using a single subtraction (QUIPSS and QUIPSS II). *Magn Reson Med.* 1998;39:702-8.
78. Herscovitch P, Raichle ME. What is the correct value for the brain-blood partition coefficient for water. *J Cereb Blood Flow Metab.* 1985;5:65-9.
79. Maccotta L, Detre JA, Alsop DC. The efficiency of adiabatic inversion for perfusion imaging by arterial spin labeling. *NMR Biomed.* 1997;10:216-21.
80. Siewert B, Bly BM, Schlaug G, et al. Comparison of the BOLD and EPISTAR technique for functional brain imaging by using signal detection theory. *Magn Reson Med.* 1996;36:249-55.
81. Garcia DM, Duhamel G, Alsop DC. Efficiency of inversion pulses for background suppressed arterial spin labeling. *Magn Reson Med.* 2005;54:366-72.
82. Zaharchuk G, Ledden PJ, Kwong KK, et al. Multislice perfusion and perfusion territory imaging in humans with separate label and image coils. *Magn Reson Med.* 1999;41:1093-8.
83. Alsop DC, Detre JA. Multisection cerebral blood flow MR imaging with continuous arterial spin labeling. *Radiology.* 1998;208:410-16.
84. Deibler AR, Pollock JM, Kraft RA, Tan H, Burdette JH, Maldjian JA. Arterial spin-labeling in routine clinical practice, part 1: technique and artifacts. *AJNR.* 2008;29:1228-34.
85. Järnum H, Steffensen EG, Knutsson L, et al. Perfusion MRI of brain tumours: a comparative study of pseudo-continuous arterial spin labelling and dynamic susceptibility contrast imaging. *Neuroradiology.* 2010;52:307-17.
86. Nezamzadeh M, Matson GB, Young K, Weiner MW, Schuff N. Improved pseudo-continuous arterial spin labeling for mapping brain perfusion. *J Magn Reson Imaging.* 2010;31:1419-27.
87. Golay X, Petersen ET, Hui F. Pulsed star labeling of arterial regions (PULSAR): a robust regional perfusion technique for high field imaging. *Magn Reson Med.* 2005;53:15-21.
88. Werner R, Norris DG, Alfke K, et al. Continuous artery-selective spin labeling (CASSL). *Magn Reson Med.* 2005;53:1006-12.
89. Warmuth C, Gunther M, Zimmer C. Quantification of blood flow in brain tumors: comparison of arterial spin labeling and dynamic susceptibility-weighted contrast-enhanced MR imaging. *Radiology.* 2003;228:523-32.
90. Gonzalez-At JB, Alsop DC, Detre JA. Cerebral perfusion and arterial transit time changes during task activation determined with continuous arterial spin labeling. *Magn Reson Med.* 2000; 43:739-46.
91. Hayes C, Padhani AR, Leach MO. Assessing changes in tumour vascular function using dynamic contrast-enhanced magnetic resonance imaging. *NMR Biomed.* 2002;15:154-63.
92. El Khouri RH, Macura KJ, Jacobs MA, et al. Dynamic contrast-enhanced MRI of the breast: quantitative method for kinetic curve type assessment. *AJR.* 2009;193:W295-300.
93. Overview of Dynamic Contrast- Enhanced MRI in Prostate Cancer. *AJR.* 2012;198:1277-88.
94. Jackson AS, Reinsberg SA, Sohaib SA, et al. Dynamic contrast-enhanced MRI for prostate cancer localization. *Br J Radiol.* 2009;82:148-56.
95. The role of dynamic contrast-enhanced MRI in cancer diagnosis and treatment. *Diagn Interv Radiol.* 2010;16:186-92.

## Chapter

# 11

# MR Angiography

Ajay Kumar, Sameer Vyas, Naveen Kalra

## HISTORY AND INTRODUCTION

The term angiography stands for the imaging depiction of vascular structures, and there are many ways to evaluate the vascular structures like Doppler, computed tomographic, catheter and magnetic resonance angiography (MRA). In last decade MRA has been increasing in demand because of its physiological nature on the contrary to CTA and catheter angiography which involves catheterization, radiation and nephrotoxic iodinated contrast agents. However there are many limitations such as availability, cost, time consuming and high sensitivity to motion and flow related artifacts.

The first research meeting devoted to Magnetic Resonance Angiography was hosted by Roberto Passariello in L'Aquila, Italy in 1989. Those days three-dimensional phase contrast MRA would take 19 hours from the time the patient entered the magnet until images could be seen; one hour to acquire the image and 18 hours of overnight image post-processing. Computational capabilities of modern equipment have reduced the delay to a few seconds. Post-processing now has taken a more central role in the communication of enormous amounts of data with less cumbersome two- or three-dimensional projections.

Many variations on the MRA theme have been presented over the ensuing 15 years. Dennis Parker developed the 3D multi-slab time-of-flight MRA technique which remains in routine clinical use to this day. Pulse sequence design plays a major role in the continuing advancements in the field, most notably as a consequence of more sophisticated and novel k-space filling strategies. The work of Kent Yucel and Martin Prince at the Massachusetts General Hospital in 1992 brought gadolinium-enhanced MR angiography to clinical utility. The first-pass dynamic contrast-enhanced MRA method provides

robust and reproducible imaging results that have propelled the adoption of MRA into wider clinical use. This advance reliably produced images of sufficient quality to replace invasive catheter-based X-ray contrast angiography for most diagnostic purposes.

The advent of very high field clinical scanners operating at 3.0 Tesla is now reinvigorating earlier noncontrast methods. 3.0 T MRA benefits from two key phenomena:

- The signal to noise of 3.0 T is twice that of the 1.5 T, offering the opportunity to either increase the spatial resolution or to shorten scan times by up to a factor of four
- The longer T1's of tissues at 3.0 T, ~20 to 40 percent higher than 1.5 T, provides better background suppression, additional inflow enhancement, and improved contrast-to-noise.

## FLOW PHENOMENA

Flow phenomena in blood or cerebrospinal fluid (CSF) also influence the MR image contrast; in addition to inherent tissue factors like T1, T2 and proton density. Blood flow is complex and variable inside the body, so it is important to understand the various types of flow.

- Laminar flow is flow where the particles move along in concentric sheets and laminae, i.e. different but consistent velocities across the vessel. It is seen in normal vessels.
- Plug flow is flow where all fluid particles move forward in parallel lines with the same speed and has a characteristic blunt profile. It is seen in the descending thoracic aorta.
- Turbulent flow is flow at different velocities which varies, i.e. velocities across the vessel changes and is seen at vascular bifurcations.

- Vortex flow is flow after narrowing and is seen after stricture or stenosis. In it, the high velocities are seen at the center.
- Stagnant flow is flow that nearly behaves like stationary tissue and is seen in occluded vessels and large aneurysms.

The moving spins (spins that move during acquisition of data) show different contrast characteristics from the stationary spins. The moving spins causes mismapping of the signal because of the flow phenomena and result in flow motion artifacts or phase ghosting. The flow phenomena are generally categorized into time of flight, entry slice phenomenon and intra-voxel dephasing.

### Outflow-related Signal Loss (Washout Effect, T2 Flow Void)

When images are obtained with a spin-echo (SE) pulse sequence, the blood flowing at a high velocity perpendicular to the imaging plane produces a weaker signal than the surrounding stationary tissue. This phenomenon is caused by the washout of flowing spins from the slice during the imaging process. Spin-echo techniques are characterized by a sequence of slice-selective  $90^\circ$  and  $180^\circ$  radio frequency (RF) pulses. Only those tissue components that are affected by both pulses can provide an MR signal. Moving material, such as blood in the vessels, flowing through the excited slice at a sufficiently high velocity, is affected by only one of these pulses, and therefore does not contribute to the MR signal. This is the so-called "flow void" (Figs 1A and B). The intensity of the vascular signal declines with decreasing slice thickness, increasing echo time (TE), and increasing flow velocity.

If the blood flow velocity is so high that all spins leave the slice between the  $90^\circ$  and  $180^\circ$  pulses ( $v \geq s / (TE/2)$ ), then there will be no signal and the vessel will appear dark. Spins flowing within the imaging plane are not affected by this phenomenon. The washout effect is observed only for SE sequences and is most pronounced on T2-weighted imaging because of the long echo times used. With gradient-echo (GRE) techniques, the echo is refocused without a  $180^\circ$  pulse simply by reversing the imaging gradients. Since only one RF pulse is needed to form an echo, the washout effect does not occur. With standard SE sequences the washout effect provides valuable and reliable information about blood flow. The absence of a flow void on T2-weighted imaging should be considered as indicative of very slow flow or even occlusion of the vessel. On the other hand, occlusion of the vessel can be excluded if a flow void is present.

### Inflow-related Signal Enhancement (Inflow Effect)

The signal of blood flowing rapidly out of the measured slice is reduced with SE sequences, under these circumstances the opposite effect may occur: spins flowing into the slice may generate a higher signal than the surrounding tissue. This

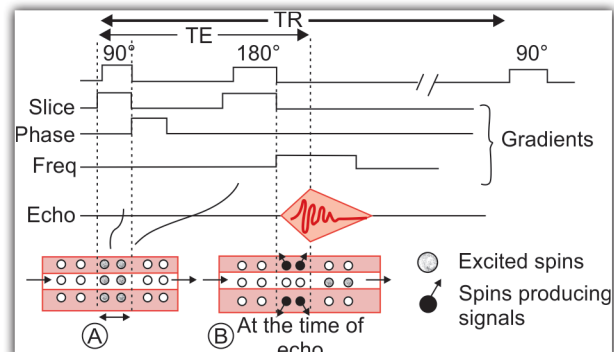


**Fig. 1A** Spin echo sequence depicting the "Flow void" phenomenon (A and B) Represents the tissue sample with shaded area as stationary tissue (spins) and central nonshaded area as vessel having moving spins. (A) At the time of  $90^\circ$  degree excitation and  $180^\circ$  degree rephasing RF pulse for that particular selected slice location. (B) Same tissue with same slice location at the time of receiving signal or TE, now only stationary spins are giving signal in the selected slice however the moving spins have migrated out of selected slice with new nonexcited spins in that place giving no signals

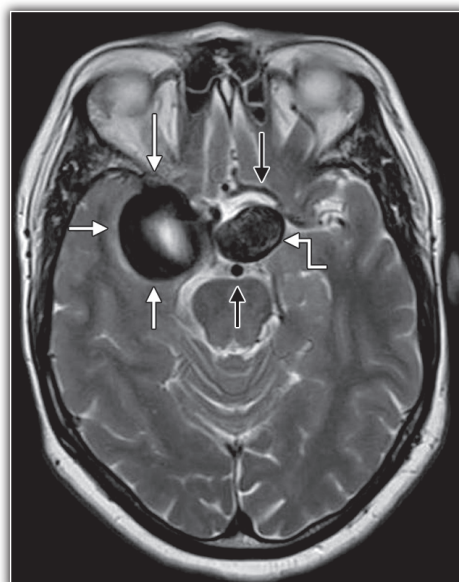


**Fig. 1B** T2W axial image of the patient with bilateral ICA aneurysms shown to explain "Flow voids"—Normal arteries, i.e. left ACA and basilar arteries (black arrows) are seen hypointense due to flow void, left aneurysm (white elbow arrow) post coiling shows heterogeneous hypointense signals due to partial thrombosis. Right patent aneurysm (white arrows) reveals flow voids at periphery due to high flow however central part giving bright signals due to relative stasis of blood

effect is referred to as "inflow enhancement". On T1-weighted imaging, contrast is generated by repeated RF pulses that are applied with a time interval (repetition time, TR) that is shorter than the T1 relaxation time of the tissue (typically  $TR < 700$  msec). As a result, the tissue components are saturated

unequally, depending on their individual T1 times. This is the basis of T1-weighted image contrast. Irrespective of flow effects, blood in the vessels would appear hypointense on a normal T1-weighted image due to its relatively long T1 time. The signal emitted by the tissue diminishes when the TR is reduced. With GRE sequences, repetition times shorter than 50 msec can be achieved. This allows the majority of non-moving spins to become saturated, thus minimizing the background signal. Spins outside the excited slice (or volume) are not influenced by the RF pulses. Consequently, blood entering into the slice being imaged is fully relaxed, experiencing not more than a few excitations on its way through the slice. As a result, flowing blood gives rise to considerably higher signal intensity relative to that of the saturated spins in the stationary tissue. This effect is called "inflow enhancement" or "flow-related enhancement". The signal intensity of flowing blood increases with decreasing slice thickness, and increasing flow velocity.

If the blood flow velocity is so high that all vessel spins are replaced by unsaturated spins in the time interval TR, flow enhancement is maximal and the vessel appears bright on a gray or black background. Although the inflow effect occurs both with SE and GRE sequences, SE sequences are not practical for the TOF method because the competing washout effect tends to overbalance the inflow effect at higher flow velocities, leading to decreased flow signal. Consequently, flow-related enhancement using GRE sequences to produce bright-blood images is the basis of time-of-flight angiography.

### Phase Effects

Phase effects concern the transverse component of the magnetization. They occur whenever spins are moving in the presence of magnetic field gradients, as are applied for spatial encoding of the MR signal. Magnetic field gradients provoke a change in the Larmor frequency depending on gradient strength and spin position. A gradient pulse of certain length and amplitude therefore induces a phase shift of the transverse magnetization, which can be compensated by a second gradient pulse with identical strength and duration but opposite sign. Thus, for stationary spins the net phase shift is zero. In contrast, the same gradients applied on a flowing spin generate a non-zero phase shift. Since the spins change their position during the bipolar gradient application, the second gradient pulse is no longer able to completely compensate for the phase shifts induced by the first gradient. The remaining phase shift  $\Phi$  is proportional to the velocity component  $v$  of the spins along the gradient direction. On standard MR imaging, this flow-induced phase shift causes a spatial mis-encoding of the signal leading to ghost artifacts that are typically found in the phase-encoding direction. Spins in a blood vessel are moving with different velocities. Often, a parabolic flow profile is found. Spins moving faster experience a larger phase shift than those moving more slowly. If there is a velocity distribution inside a voxel, phase dispersion (intra-voxel dephasing) occurs resulting

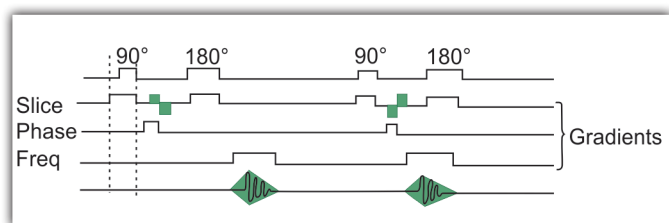


**Fig. 2** Diagrammatic representation of phase-contrast MRA pulse sequence, note the velocity encoding gradient are in slice direction

in decreased signal in the blood vessel. The extent of spin-dephasing depends on the strength and time interval of the gradient pulses, as well as the distribution of spin velocities. When complex flow patterns are encountered, for example in vessels with turbulent flow, there may be a very broad spectrum of velocities within a voxel, leading to total signal loss in the vessel.

Using additional gradient pulses of appropriate amplitude and duration, flow-induced phase shifts can be compensated, thus eliminating any signal loss. This technique is called "gradient motion rephasing (GMR)" or just "flow compensation".<sup>1</sup> However, GMR is normally restricted to first-order movements, i.e. spins that move at a constant velocity. Turbulent flow and effects of acceleration cannot be completely compensated by GMR. Optimal reduction of flow-induced phase effects can be achieved by combining GMR with as short a TE as possible, in order to reduce the time available for spin dephasing. Short echo times also diminish the impact of pulsatile blood flow and turbulence (Fig. 2).

### TIME-OF-FLIGHT ANGIOGRAPHY: TECHNIQUES

The contrast mechanism of time-of-flight (TOF) MRA is based on the inflow effect. Fully relaxed blood entering the measured volume behaves as an endogenous contrast agent, by producing a bright signal. The bright depiction of flowing blood, however, requires the use of flow rephasing techniques (GMR) in order to overcome the effects of spin dephasing due to transverse magnetization. TOF MRA using GRE sequences has several advantages: Firstly, GRE sequences are not affected by the wash-out phenomenon that diminishes the signal of fast flowing blood when using SE techniques. Secondly, GRE techniques permit the use of short repetition times ( $TR < 40$  msec), which are needed to efficiently saturate stationary tissue. Thirdly, echo times can be kept short ( $TE < 5$  msec), thus further reducing spin dephasing.

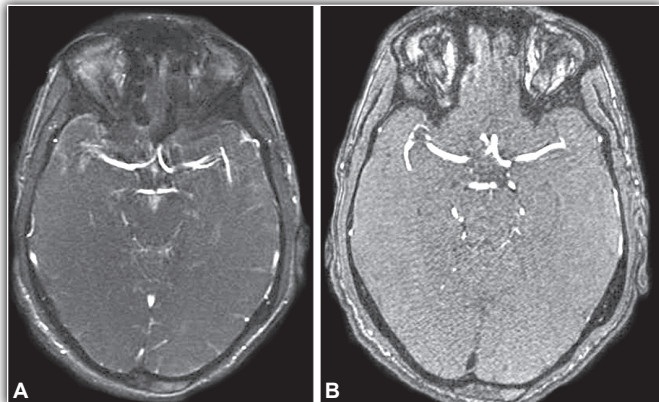
Generally, it is advisable to apply in-phase echo times in order to avoid opposed-phase effects at the vessel walls that would impair the depiction of small vessels. Finally, GRE techniques are characterized by short acquisition times which are important when acquiring volume (3D) datasets. TOF techniques can be divided into three groups:

1. Sequential 2D multislice method,

2. 3D single-slab method,
3. 3D multislab method.

With **2D techniques**, the vessel is imaged by sequentially scanning multiple thin slices. This method has two advantages in comparison to the interleaved multi-slice technique: Firstly, very short TR times can be used which boost the inflow effect, and secondly, partially saturated blood is hindered from flowing from one slice to another. The method guarantees sufficient inflow enhancement even in vessels with a very slow flow and produces constant vessel-background contrast in the covered region, because each slice is an entry slice.<sup>2</sup> Problems arise with 2D TOF MRA if the vessels to be imaged do not flow in a perpendicular direction to the imaging plane. If the vessels run partly inside the slice (in-plane) or return to the slice in a looped form, then signal loss may occur due to the partial saturation of flow (**Figs 3A and B**). In order to achieve a sufficient signal-to-noise ratio, a slice thickness of at least 2 to 3 mm is necessary. However, this results in reduced spatial resolution and increased spin dephasing due to the larger voxel size required. 2D slices do not have rectangular RF profiles and therefore exhibit signal variations at the edges that can lead to step like artifacts in maximum intensity projection (MIP) reconstructions. However, this effect can be largely overcome by overlapping the slices. In vessels exhibiting very pulsatile flow, the extent of inflow enhancement varies during the heart cycle. The periodic change of inflow enhancement generates ghost images of the vessels. Saturation of blood spins can occur due to slow flow in the diastolic phase. The use of ECG triggered 2D TOF sequences may overcome many of these problems by confining data acquisition to the phase of maximum inflow. Thus, blood signal is enhanced and ghost artifacts are eliminated. By synchronizing data acquisition with the heart cycle, the vessel is mapped in each slice with equal intensity. Unfortunately, a drawback of this approach is the prolonged acquisition time.

In **3D TOF MRA**, the entire imaging volume, usually 30 to 60 mm thick, is excited simultaneously and then partitioned into thin slices by an additional phase encoding gradient along the slice-select direction.<sup>3</sup> 3D TOF MRA has the advantage of high spatial resolution together with high signal- to-noise ratio, thereby facilitating the improved depiction of particularly small vessel structures. The technique allows slices of less than 1 mm thickness and isotropic voxels to be acquired easily. One major problem of the 3D technique, however, is the progressive saturation that occurs when blood flowing through the volume is subjected to repeated RF pulses. As a result, the signal intensity decreases continuously in the direction of flow. The extent of saturation depends on the length of time in which the blood stays inside the volume. In slow flow vessels, signal begins to diminish when only a short distance has been covered. Conversely, in faster flowing blood the signal remains visible for a greater distance. Consequently, the maximum volume thickness should be kept as small as possible, matched to the size of the



**Figs 3A and B** 2D TOF MRA (A) shows loss of flow related signal in M1 segment of left MCA due to in- plane saturation however in same patient lt MCA showing normal caliber and flow related signal on 3D TOF MRA (B)

vessel region of interest. A reduction of saturation can also be achieved by increasing the TR. Larger vessel sections can be investigated by subdividing the volume of interest into several thin 3D slabs that are acquired sequentially (**Table 1**).<sup>4</sup>

One such **multi-slab** technique, which retains the advantages of 3D TOF yet has reduced saturation effects like 2D TOF, is called multiple overlapping thin slab acquisition (MOTSA). Generally, the chosen slab thickness has to be small enough to avoid saturation within the slabs. However, adjacent slabs must overlap by about 20 to 30 percent in order to compensate for signal attenuations arising at the slab edges due to non-rectangular excitation profiles. This results in compromised time efficiency and longer overall acquisition times. Frequently, 2D TOF MRA is favored for imaging veins because of the high sensitivity to slow flow. 3D TOF MRA, on the other hand, is more appropriate for fast arterial flow and for those cases in which high spatial resolution is required (**Figs 4 and 5**).

#### *Important Points for Optimization of TOF Angiography<sup>5-7</sup>*

- Orientation of slices or volume perpendicular to flow direction.
- 2D for slow flow, 3D for fast flow.
- 3D multi-slab for larger vessel sections.
- Spatial presaturation to isolate arteries and veins.
- Use of minimum TE reduces signal loss due to spin dephasing.
- TONE pulse reduces saturation effects in 3D TOF.
- Magnetization transfer (MTC) and fat suppression improve vessel contrast.

#### **Pitfalls with TOF MRA**

- Methemoglobin in thrombosed vessels (cavernous sinus thrombosis) may mimic blood flow (i.e. vessel patency)

**Table 1** Comparison of 2D and 3D TOF

2D TOF	3D TOF
Less susceptible to saturation effect	More susceptible to saturation effect
Visualize slow as well as fast flow	Good for high flow
Low resolution and SNR	High resolution and SNR
Better for relatively larger FOVs	Smaller FOVs
Used mainly for cerebral venographies, abdominal and peripheral angiographies	Cerebral angiography

- Work around—compare MIP with pre-contrast T1 images or use phase contrast MRA
- Short T1 tissues (fat, bleeding, tissue that take up contrast) may simulate vessels
- Pulsation artifacts in CSF may simulate vessel lesions
- Signal loss occurring with turbulent or very slow flow causes overestimation of stenosis and artifacts in the depiction of aneurysms
- Signal loss due to susceptibility artifacts (coils, clips)
- Signal loss in case of in-plane flow (2D) or slow flow (3D)
- Overlap of arteries and veins after contrast administration, particularly in intracranial MRA.



**Fig. 4** 2D TOF MR venography reveals adequate visualization of cerebral venous system



**Figs 5A and B** 3D TOF MRA (A) showing very good cerebral vascular anatomy with high spatial resolution and SNR in comparison to 2D TOF MRA (B) in same patient

## PHASE CONTRAST ANGIOGRAPHY

Whereas phase effects are suppressed as fully as possible in TOF MRA, it is the flow-induced phase shift of the transverse magnetization that is employed to image blood vessels with phase contrast techniques. There are two ways of using phase effects to selectively depict blood flow:

1. Magnitude contrast (rephased-dephased) method
2. Phase contrast method

Today, magnitude contrast is only rarely used. Conversely, techniques that in a stricter sense are referred to as "phase contrast", have gained greater importance both as an imaging method and as an accurate approach to measuring blood flow velocity and direction.

### Magnitude Contrast Technique

The concept of magnitude contrast angiography is analogous to X-ray digital subtraction angiography (DSA). The basic idea is to acquire two datasets—one flow-rephased and one flow-dephased.<sup>8</sup> First a flow-compensated measurement is performed using GMR in order to image flowing blood with high signal intensity. In the second acquisition, flow-sensitizing bipolar gradient pulses are applied specifically to induce velocity-dependent phase shifts of moving spins. If the flow-sensitizing gradient is strong enough, the spins within a voxel possessing different velocities may totally dephase resulting in dark vessel signal. Since stationary tissue appears the same in both acquisitions, subtraction of one dataset from the other results in the signal of the stationary tissue being cancelled leaving only the moving blood as visible. Interleaving the acquisition of both datasets can diminish the impact of motion artifacts on the subtraction process. The signal intensity in the subtracted image depends only on the velocity component along the flow-sensitizing gradient which is normally applied in the frequency-encoding direction. Therefore, the imaging volume should be oriented in such a way that the main flow direction in the vessel of interest is parallel to the read-out direction. Information about all three orthogonal flow directions can be obtained by repeating the

flow-encoded acquisition with altered gradient orientations. As a result, a total of four acquisitions has to be performed (one rephased, three dephased), which impacts on the overall acquisition time. Although not in widespread use, magnitude contrast MRA can be considered applicable for imaging of peripheral vessels (arm, leg) since it allows larger sections of arteries to be visualized. If flow is unidirectional, a single pair of rephased and dephased acquisitions is sufficient, thereby reducing the overall acquisition time. Magnitude contrast MRA requires a spectrum of flow velocities within a voxel. Laminar flow with its parabolic flow profile is therefore readily detected. The signal acquired is a direct result of the velocity distribution in each voxel, ensuring complete background suppression. The method is well adapted for depicting slow flow with good spatial resolution, covering larger sections of vessels. One disadvantage arises from the fact that this technique does not provide any information on flow direction or flow velocity.

### Phase Contrast Technique

Similar to magnitude contrast, phase contrast angiography is based on the acquisition of two datasets that differ in the phase of moving spins.<sup>9,10</sup> At first, a flow-rephased sequence (S1) is applied which defines the phase of transverse magnetization under conditions of total flow compensation. The second measurement (S2) is flow-sensitive, utilizing special flow-encoding gradients to provoke a measurable phase shift. Contrary to the magnitude contrast technique, the chosen gradient is weak enough to avoid complete phase dispersion arising from the velocity distribution of the spins. Complex subtraction of the two datasets S1 and S2 yields the phase difference  $\Phi$  as well as the difference vector  $\Delta S$ , both of which depend on the velocity component of the spins along the flow encoding gradient. There are two different approaches to utilizing flow-induced phase shifts to generate angiographic images. In the so-called phase map images, it is the phase difference  $\Phi$  that is depicted as signal intensity. The sign of the phase shift encodes the flow direction. Non-moving tissue appears as medium shade of gray while flowing blood is either brighter or darker, according to the direction of flow. As the intensity of each pixel is linearly proportional to flow velocity, phase images are particularly well suited for flow quantification and for identifying flow direction. In the second approach magnitude images, which reveal the length of the difference vector  $\Delta S$ , are applied to anatomically image the vessels. However, while the brightness in each pixel is a measure of the local flow velocity, there is no information about the flow direction. The difference vector  $\Delta S$  increases with rising spin velocity, reaching a maximum at  $\Phi = 180^\circ$ . The corresponding critical velocity is called flow sensitivity or velocity encoding (VENC) and is determined by the strength of the bipolar flow-encoding gradients. The manufacturers of

MR scanners provide a set of sequences adapted to different velocity ranges. In clinical practice, it is important to estimate the maximum flow velocity expected to occur in the vessel in advance in order to choose the phase contrast sequence with an adequate VENC value. With phase contrast, only those velocities ranging between -VENC and +VENC, corresponding to phase shifts between  $-180^\circ$  and  $+180^\circ$ , can be uniquely detected. If the flow velocity exceeds the VENC value, there is an abrupt change of signal intensity in the phase image from bright to dark or vice versa. Blood flow that provokes a phase shift of  $190^\circ$  cannot be distinguished from oppositely directed flow that generates a phase shift of  $-170^\circ$ . This ambiguity is called aliasing. In the magnitude image, maximum intensity is reached when the flow velocity equals the VENC value. At higher velocities, the signal intensity begins to decrease again. If the flow velocity in a voxel is exactly twice the VENC value, no signal emanates from the voxel, and the vessel appears to be interrupted. As an example, for a VENC value of 40 cm/sec spins flowing at a rate of 40 cm/sec provoke a phase shift of  $180^\circ$  yielding maximum signal intensity. Spins that flow at 60 cm/sec possess a phase shift higher than  $180^\circ$ . Therefore, on the magnitude image they appear less bright than the spins flowing at 40 cm/sec, but equally as bright as spins flowing at a rate of 20 cm/sec. Likewise, if there are spins flowing at a rate of 80 cm/sec, they will provide zero signal and appear as stationary spins. The phase contrast method is sensitive only for the velocity component along the flow-encoding gradient. In order to obtain information on all flow directions, one dedicated flow-encoding gradient for each orthogonal direction of space is required. Thus, a phase contrast sequence comprises a total of four acquisitions: one flow-compensated measurement and three flow-encoded acquisitions in the X-, Y-, and Z-directions. Interleaving the four datasets can reduce artifacts caused by patient motion. Phase and magnitude images of the flow components in the three orthogonal directions are obtained by complex subtraction of flow-encoded and flow-compensated datasets. The three magnitude subtraction images can be added to obtain a sum magnitude image that depicts blood flow with bright signal regardless of flow direction (**Figs 6 and 7**).

### Optimization

- Adapting flow sensitivity (VENC) to maximum flow velocity
- Encoding different flow velocities (multivenc) or different flow directions
- Contrast agent improves flow signal
- 2D acquisition provides one single projection within a short acquisition time
- 3D acquisition permits MIP post-processing
- ECG triggering can be applied in cases of pulsatile flow
- Presaturation pulses can separate arteries and veins.

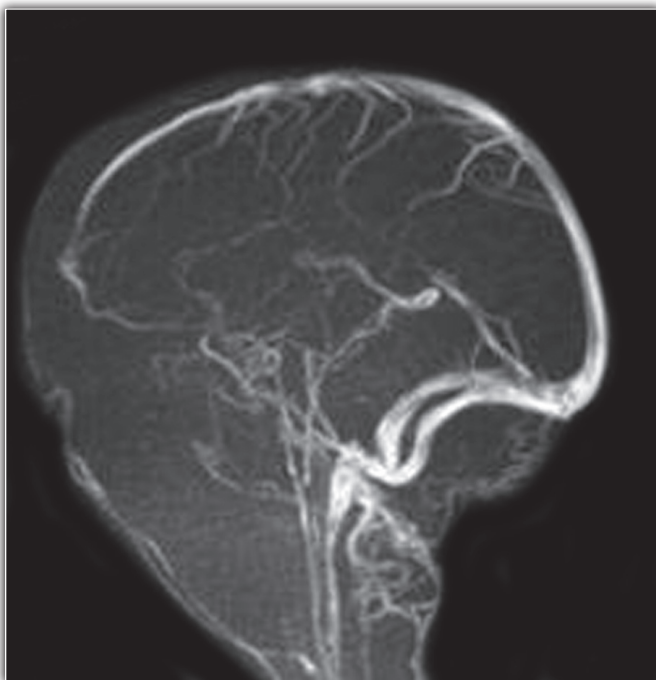


**Fig. 6** Phase contrast 3D MRV showing excellent cerebral venous system



**Fig. 7** Phase contrast 3D MRA giving adequate depiction of arterial anatomy

### CONTRAST-ENHANCED MR ANGIOGRAPHY

Contrast-enhanced MR angiography (CE-MRA) has emerged as a technique of choice for vascular images. It relies on T1 shortening effects of Gd-chelate contrast in blood. This is different from the flow based TOF and PC-MRA technique

which uses the inherent motion of blood flow to generate vascular signal.<sup>11</sup>

Unlike 3D TOF MRA, it requires a gradient system with high slew rates for ultrafast acquisition and additive tools for proper timing of scan with regard to the bolus arrival.<sup>12</sup>

The basic sequence used for CE-MRA is ultra short TR/TE 3D spoiled gradient echo sequence. The TR is made as short as possible to speed up the image acquisition and capture the first pass of contrast. The presence of Gd makes the blood immune to saturation, so the short TR tends to saturate only background tissue. In general, the highest flip angle achievable by the MRI machine is used. The TE is also made as short as possible—ideally approximately 1.0 msec, so as to limit any flow-induced dephasing effects.<sup>13</sup>

Different techniques are used to ensure optimal contrast of the arteries, e.g. bolus timing, automatic bolus detection, bolus tracking and care bolus, etc.<sup>14</sup>

The rate of injection affects the peak Gd concentration and thus the achievable arterial SNR. Generally, a faster injection rate will result in higher arterial SNR, but shorter bolus duration and earlier venous enhancement. Injection rates of 2 mL/sec are ideal for most CE MRA applications, with little benefit shown for higher rates.<sup>15</sup>

For most CE MRA examinations, a dose of 0.15 to 0.2 mmol/kg (typically 20–30 mL) is sufficient. If timing is good, lower doses (0.1 mmol/kg) have also been found to be adequate. In general, the use of a larger contrast agent dose has the benefit of prolonging the arterial phase and providing the operator with an additional buffer to compensate for errors in timing.<sup>15,16</sup>

One final consideration for contrast administration is that of saline flush. In practice, a large saline flush (at least 30 mL) should be used for all CE MRA examinations. A large flush will ensure that the entire contrast dose is administered beyond the tubing and that the bolus will travel through the peripheral veins into the right heart, thus ensuring sufficient Gd concentrations are delivered to the more distal arteries. The use of a large flush increases the slope of the enhancement curve, increases the duration of the arterial phase of the bolus (up to 50%), and delays significant venous enhancement, all of which are preferable for arterial CE MRA.<sup>15,17</sup>

The goal is to record the central region of k space during the maximum enhancement of the artery. The center of k space contains the lowest (spatial) frequency wave data, so it represents the major structures of the image and thus most of the gross image form and contrast; therefore, the center of k space should be acquired during the time of highest contrast agent concentration.<sup>18</sup>

Also, a high rate of change of the contrast agent concentration during the acquisition of central k space must be avoided to prevent ringing artifacts, arising in the Fourier transform.<sup>18</sup> So, the enhancement is maximized by timing the contrast agent injection such that the period of maximum arterial concentration corresponds to the k space acquisition.<sup>14</sup>

Special considerations with respect to timing must be undertaken with certain vascular problems such as aneurysms: since the flow can be much slower through an aneurysm, more time must be allowed between the injection of contrast agent and the image acquisition.<sup>18</sup>

A high resolution with near isotropic voxels and minimal pulsatility and misregistration artifacts should be striven for. The post-processing with the maximum intensity projection (MIP) enables different views of the 3D data set (**Figs 8 to 11**).

#### *CE-MRA Advantages<sup>14</sup>*

- The 3D MRA can be acquired in any plane, which means that greater vessel coverage can be obtained at high resolution with fewer slices (aorta, peripheral vessels)
- The possibility to perform a time resolved examination (similarly to conventional catheter angiography)
- The CE-MRA reduces or eliminates most of the artifacts of time of flight angiography or phase contrast angiography
- Minimal invasiveness with no associated risk of neurologic complications, reduced patient discomfort and inconvenience, greater cost savings
- No use of ionizing radiation; paramagnetic agents have a beneficial safety
- The CE-MRA does not prove to be better in evaluation of carotid artery atherosclerotic stenosis<sup>19</sup> however it appears to give better depiction of post coiling larger residual/recurrent aneurysms<sup>20</sup>
- Other very important use of CE-MRA is that it differentiates between active and inactive disease

in case of Takayasu arthritis by showing the intense enhancement of vessel wall.<sup>21</sup>

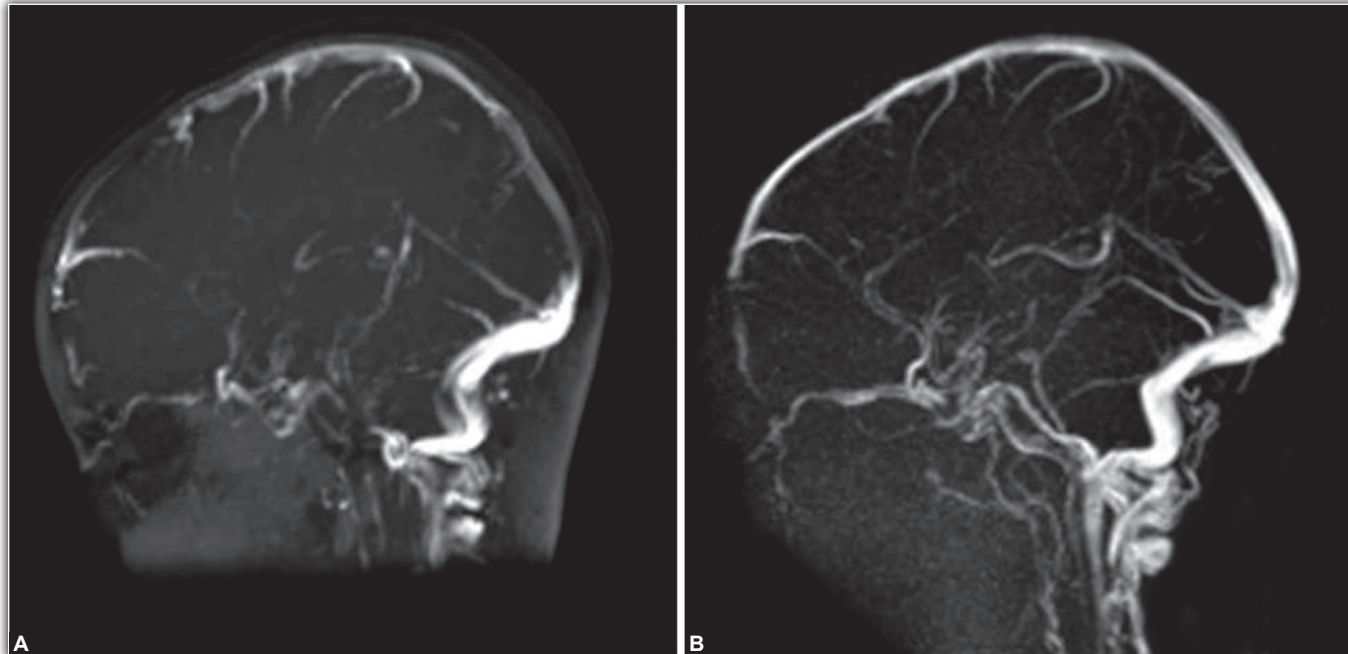
On the other hand, CE-MRA has some disadvantages. Due to the short arteriovenous transition time in the cerebral circulation, early enhancement of venous structures limits the time window for scan acquisition, and a trade-off is therefore necessary between scan time, volume coverage and spatial resolution. Another disadvantage is the possibility of a false neck remnant in post coiling patient with a intracranial aneurysm, which may be explained by the peripheral contrast enhancement of the organized thrombus or by the vasa vasorum within the aneurysm wall.<sup>12,22</sup>

#### **Parallel Imaging<sup>12</sup>**

Parallel acquisition techniques (PAT) have recently been developed and are now being increasingly used for vascular imaging. The PAT uses multichannel coil arrays to shorten the measurement time by reducing the number of phase encoding steps. The spatial information is instead extracted from the sensitivity profiles of the coil elements.

Numerous image acquisition algorithms have been described, including sensitivity encoding (SENSE), simultaneous acquisition of spatial (SMAS) harmonics, and generalized auto-calibrating partially parallel acquisitions (GRAPPA).

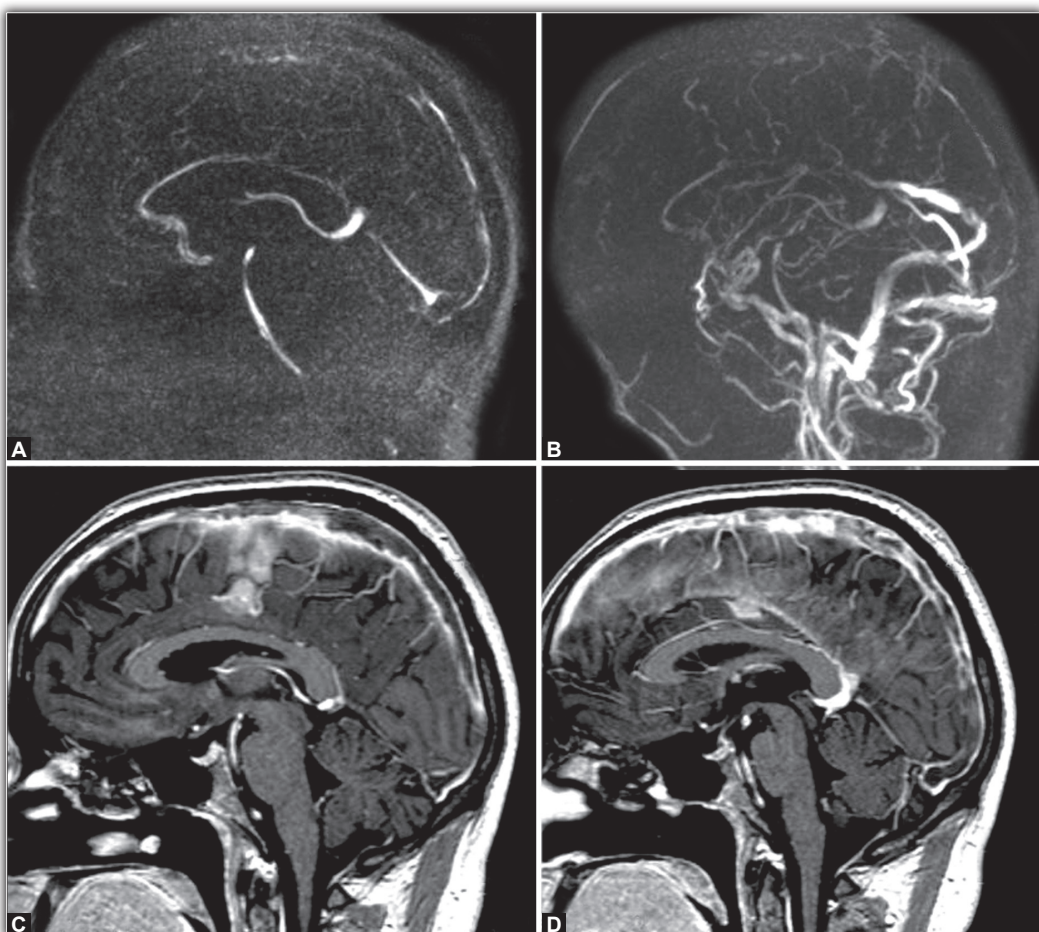
In intracranial 3D TOF imaging PAT with an eight channel phased-array head coil has been used to save 43 percent of measurement time while maintaining the same image quality. However, it must be kept in mind that using PAT reduces the signal-to-noise ratio (SNR) by approximately



**Figs 8A and B** Phase contrast 3D MRV (B) showing better cerebral venous sinuses and smaller veins than 2D TOF MRV in same patient



**Figs 9A and B** Contrast enhanced MRA showing good neck and cerebral arterial anatomy



**Figs 10A to D** Case of superior sagittal venous sinus thrombosis showing nonvisualization of sinuses on PC 3D MRV (A and B), Post-contrast T1W (C and D) confirms the filling defects in sinus

the square root of the acceleration factor. The inherently high SNR of contrast enhanced MRI makes PAT particularly suited for CEMRA.

In arterial CEMRA, PAT can be used to accelerate the acquisition (and hence avoid venous contamination), to increase spatial resolution and/or volume coverage, or to combine the two.<sup>12</sup>



**Fig. 11** CE-MRA bilateral lower limbs showing adequate visualization of lower limb arteries, early draining veins are seen on left side due to underlying vascular malformation

### Time Resolved/4D CE-MRA

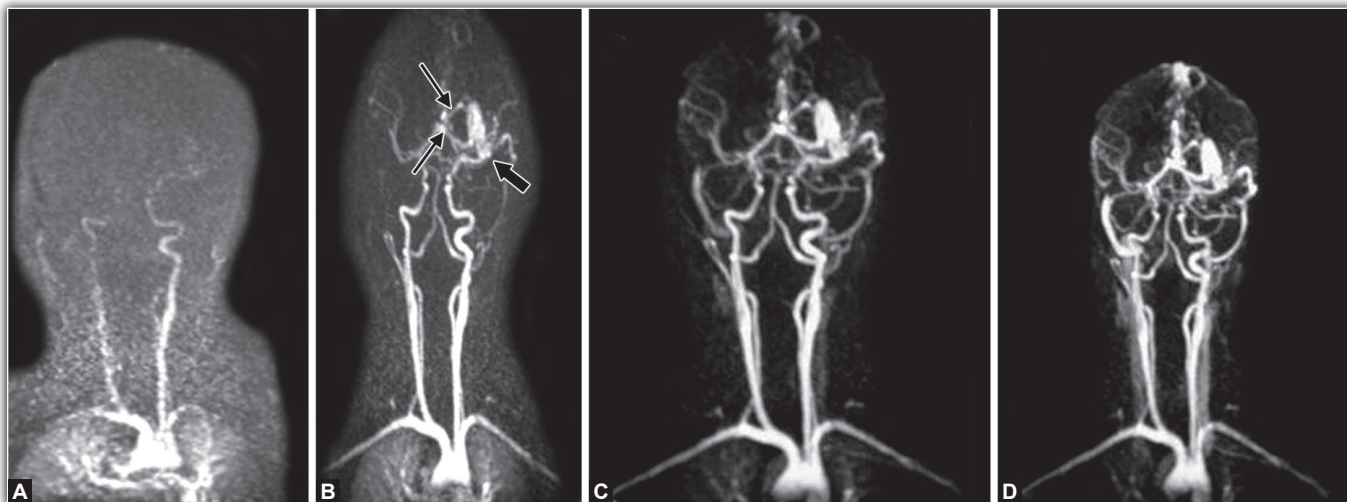
Vascular malformation imaging work up always needs a dynamic depiction of the disease. However, the conventional MRA, dynamic TOF, PC and CE-MRA lacks the ability in showing the different angiographic phases as early arterial, arterial and venous. At the same time conventional angiography suffers from motion artifacts specially in unstable patients.

The time resolved CE-MRA includes combination of *k* space segmentation into central, mid, and peripheral zones with sampling the central zones of the *k* space at a more frequent rate.

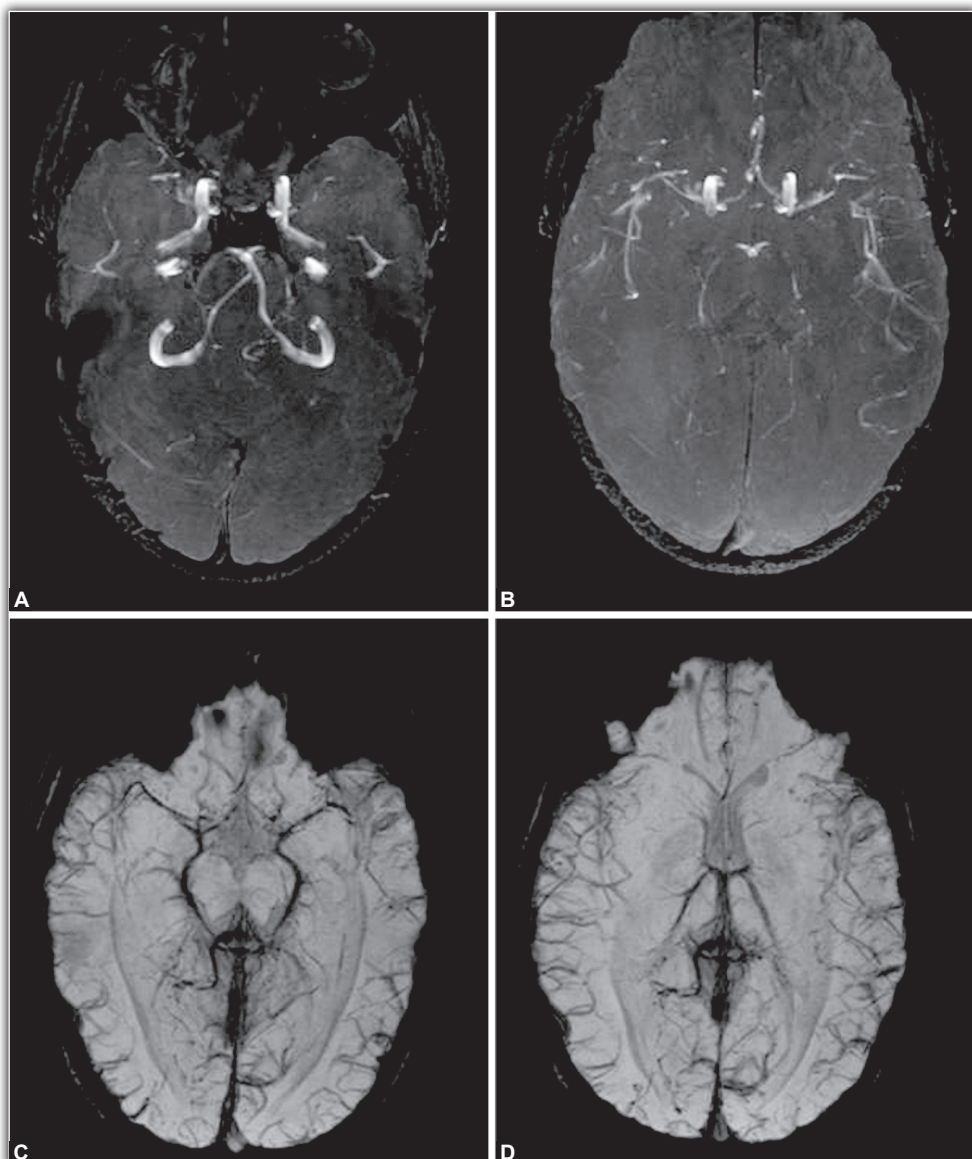
Scan parameters used for rapid acquisition short TE of 0.9 ms and a short TR of 2.2 ms, fractional echo acquisition, 2.6 mm section thickness. MR contrast is injected at a rate of 2 mL/s to a total of 15 mL, followed by 30 mL of saline. Sagittal or coronal section are obtained with a FOV of about 28 × 22.4 cm, matrix of 192 × 192, NEX of 0.75, and flip angle of 20° at every 1.8 to 2.0 seconds. About 30 to 35 section are acquired (**Figs 12A to D**).<sup>23</sup>

### Advantages of Time Resolved MRA

- Useful for unstable and moving patients<sup>24</sup>
- Better depiction of AVM feeders, nidus and venous drainages<sup>25</sup>
- Gives an idea about flow dynamics of AVM/AVF and aneurysms<sup>24</sup>
- Good for follow-up of postembolization or gamma surgery residual AVMS<sup>25</sup>



**Figs 12A to D** Time-resolved CE-MRA in a case of cerebral AVM demonstrating the AVM nidus, its feeders (thick arrow) and venous drainage (thin arrows) in a dynamic manner comparable to catheter angiography



**Figs 13A to D** PC MRA application of SW imaging, images (A and B) are showing intracranial arterial anatomy due to TOF inflow effect and images (C and D) reveals the venous structures on SWI in same patient

#### Limitation

- High dose of contrast is required
- Time taking sequences
- Nonvessel selective on the contrary to catheter angiography.

#### Future Perspectives

Presently MRA techniques are well established tool for vascular imaging however still there is need of decrease acquisition times, increase temporal and spatial resolution with more dynamic information. With advent of 3T MR scanner these problems has been addressed in clinical imaging. Use of high fields such as 7T are in developing and

research phase and the recent studies reveals that CEMRA at 7T demonstrates the feasibility and current constraints of ultrahigh field contrast enhanced MRA relative to NC MRA.<sup>26</sup>

Also there are evidences of work under research reveals that TOF MRA at 7T have increase SNR and spatial restoration, especially for the assessment of brain AVM and high grade gliomas. Other applications like arterial spin labeling are mentioned in other chapter on perfusion in this book. Newer techniques like SWI-MRA are also in developmental phase, it makes possible to image both artery as well as vein simultaneously and can be evaluated separately.<sup>27</sup> Veins are dark due to  $T_2^*$  effect with SWI processing, same time arteries are seen bright due to TOF inflow effect (**Figs 13A to D**). In addition, it can also provide the information about

hemorrhage and calcification whether parenchymal or mural in case of atherosclerotic disease.

Lastly, there is lot more in future for MRA application due to advent of ultra-high field scanners and development of advances imaging sequences.

## REFERENCES

- Lenz G, Haacke E, Masaryk T, Laub GA. Inplane vascular imaging: pulse sequence design and strategy. *Radiology*. 1988; 166:875-82.
- Keller PJ, Drayer BP, Fram EK, Williams KD, et al. MR angiography with two-dimensional acquisition and three-dimensional display. *Radiology*. 1989;173:527-32.
- Laub GA, Kaiser WA. MR angiography with gradient motion refocusing. *J Comput Assist Tomogr*. 1988;12:377-82.
- Parker GL, Yuan C, Blatter DD. MR angiography by multiple thin slab 3D acquisitions. *Magn Res Med*. 1991;17:434-51.
- Tkach J, Masaryk T, Ruggieri P, et al. Use of Tilted Optimized Nonsaturating Excitation. *SMRM*. 1992;2:3905.
- Atkinson D, Brant-Zawadzki M, Gillan G, et al. Improved MR angiography: Magnetization transfer suppression with variable flip angles excitation and increased resolution. *Radiology*. 1994; 190:890-4.
- Edelman RR, Ahn SS, Chien D, et al. Improved time-of-flight MR angiography of the brain with magnetization transfer contrast. *Radiology*. 1992;184:395-9.
- Axel L, Morton D. MR flow imaging by velocity compensated/uncompensated difference images. *J Comp Assist Tomogr*. 1987;11:31-4.
- Dumoulin CL, Hart HR. Magnetic Resonance Angiography. *Radiology*. 1986;161:717-20.
- Dumoulin CL, Souza SP, Walker MF, Wagle W. Three-dimensional phase contrast angiography. *Magn Res Med*. 1989; 9:139-49.
- Schneider G, et al. Magnetic resonance angiography: Techniques, Indications and Practical Applications. Springer-Verlag Italia. 2005.
- Papke K, Brassel F. Modern cross sectional imaging in the diagnosis of follow-up of intracranial aneurysms. *Eur Radiol*. 2006;16:2051-66.
- Lohan DJ, et al. Contrast enhanced MRA vs Non enhanced MRA: Pros and Cons. *Applied radiology, Journal of Practical medical imaging and Management*. Supplement to May 2007.
- Contrast Enhanced Magnetic resonance angiography; www.mr-tip.com
- Kopka L, Vosshenrich R, Rodenwaldt J, et al. Differences in injection rates on contrast-enhanced breath-hold three-dimensional MR angiography. *AJR Am J Roentgenol*. 1998; 170(2):345-8.
- Lee VS, Rofsky NM, Krinsky GA, et al. Single dose breath-hold gadolinium-enhanced three-dimensional MR angiography of the renal arteries. *Radiology*. 1999;211:69-78.
- Boos M, Scheffler K, Haselhorst R, et al. Arterial first pass gadolinium- CM dynamics as a function of several intravenous saline flush and Gd volumes. *J Magn Reson Imaging*. 2001; 13(4):568-76.
- Bart E Muhs, Hence JM Verhagen, Matthew G Huddle, Vinay M Pai, Elizabeth M Hecht, Alan Dardik. Theory, Technique, and Practice of Magnetic Resonance Angiography. *Vascular*. 2007;15(6):376-83.
- LS Babiarz JM, Romero EK, Murphy B Brobeck. Contrast-Enhanced MR Angiography Is Not More Accurate Than Unenhanced 2D Time-of-Flight MR Angiography for Determining >70 percent Internal Carotid Artery Stenosis. *Am J Neuroradiol*. 2009;30:761-68.
- A TJ, Kaufmann J, Huston III HJ, Cloft J Mandrekar L. A Prospective Trial of 3T and 1.5T Time-of-Flightand Contrast-Enhanced MR Angiography in the Follow-Up of Coiled Intracranial Aneurysms. *Am J Neuroradiol*. 2010;31:912-18.
- Maurizio Papa, Francesco De Cobelli, Elena Baldissera. Takayasu Arthritis: Intravascular Contrast Medium for MR Angiography in the Evaluation of Disease Activity. *AJR*. 2012; 198:W279-W284.
- Lubicz B et al. Is digital subtraction angiography still need for the follow-up of intracranial aneurysms treated by embolisation with detachable coils? *Neuroradiology*. 2008;50:841-8.
- RI Farb R, Agid RA, Willinsky DM Johnstone. Cranial Dural Arteriovenous Fistula: Diagnosis and Classification with Time-Resolved MR Angiography at 3T. *Am J Neuroradiol*. 2009; 30:1546-51.
- Kristine A. Blackham, Matthew A. Passalacqua, Gurpreet S. Sandhu. Applications of Time-Resolved MR Angiography. *AJR*. 2011;196:W613-W620.
- HK Lim, CG Choi, SM Kim. Detection of residual brain arteriovenous malformations after radio surgery: diagnostic accuracy of contrast-enhanced four-dimensional MR angiography at 3.0T. *BJR*. 2012; 85: 1064-9.
- Umutlu L, Maderwald S, Kinner S. First- pass contrast enhanced renal MRA at 7 telsa: initial result. *Eur Radiol*. 2012 Oct (Epub ahead of print).
- Samuel RS, Barnes, Mark Haacke. Susceptibility Weighted Imaging: Clinical angiographic applications. *Magn Reson Imaging Clin N Am*. 2009;17(1):47-61.

## Chapter

# 12

# MRI Pulse Sequences: An Evolution

Vivek Gupta, Niranjan Khandelwal

MR sequences are continuously evolving. From simple sequences like conventional spin echo they have increased in number as well as complexity. However, the ultimate aim of every sequence is bring about better tissue contrast in least amount of time. Therefore, different sequences are designed to account for varied tissue characteristics. Also, with the tremendous improvement in computational powers now the sequences have become less time consuming and less prone to artifacts. It is a vast and complex topic but basic understanding of the sequences is essential to interpret the MR images they produced. **Table 1** gives an overview of the present generation of pulse sequences by various vendors.

MR sequence is a series of different RF pulses, which are applied at a particular time and in a specified way to obtain an image.

A pulse sequence diagram is a schematic diagram, which depicts various pulse or gradients that are applied over a period of time.

There are minimum of four horizontal lines, which depict the excitatory RF pulse, and three representing each gradient, i.e. phase gradient, frequency gradient and slice encoding gradient (**Fig. 1**). Additional lines may be used to depict the generated echo and other pulse or gradients used.

## BASIC TERMINOLOGIES

Image contrast is generated by variation of TR (repetition time) and TE (echo time) in any given sequence. TR is the time interval between application of an RF excitation pulse and start of the next RF pulse. TE is time between the initial RF pulse and the peak of the echo, which is produced. Both are usually in milliseconds. T1- and T2-weighting are other terms, which need to be understood. T1-weighted images

would mean that though, image show all types of contrast but the T1 effect is more pronounced. T1- effect would mean that the TR and TE are both short and the difference between relaxation of longitudinal magnetization of fat and water can be detected. In T1 weighted images fat, blood products, slow moving blood and MR contrast would all be bright and tissues with fluid, mineral rich content like bone and air would be dark. T2 weighting is opposite of this. Here the TR and TE are both prolonged and thus the difference in T2 signal decay of fat and water can be detected. At short TE this difference is not apparent. This makes high free water containing tissues bright of T2 weighted images. Another type of images are proton density images where TR is long and TE is short, thus the images are neither T1 weighted and nor T2 weighted but the image contrast produced is due to difference in proton density of the tissues, those having higher density of protons giving higher signal.

## SEQUENCES TYPES

Spin echo sequences were the first sequences to be used for MR imaging. These were closely followed by gradient echo imaging. As more and more limitations of these classic sequences became apparent they were modified to bring about better tissue contrast in less time. This was followed by ultrafast sequences in both these groups. Finally sequences with features of both of these were created to generate hybrid sequences.

### Conventional Spin Echo Sequences

In a typical spin echo sequence an initial 90° RF excitation pulse is followed by a 180° rephasing pulse which is then followed by an echo (**Fig. 1**).

**Table 1** MR pulse sequences and their classification

Technique	Sequences	Weighting	Features	Application
<i>Spin Echo (SE) Sequences</i>				
1. Conventional SE	SE	T1, T2 and proton density (PD)	Robust sequences. Less susceptible to T2* effects	Now replaced by fast SE sequences
2. Fast SE (RARE)	TSE (Turbo SE) FSE (Fast SE)	T1, T2 and proton density (PD)	Faster Less susceptible to motion artifacts and T2* effects	High resolution neurological and orthopedic imaging. Single breath hold abdominal imaging.
3. HASTE	SS-FSE (single shot fast spin echo)	T2 weighting	Faster	Used in MRCP
4. Inversion recovery	IR, turbo IR, TIRM (turbo IR magnitude reconstruction), IR TSE FLAIR (fluid attenuated inversion recovery)	T1 weighting	High resolution imaging	For good contrast between white and gray matter.
	STIR (short T1 inversion recovery)	T2 weighting	Very useful in brain imaging	To suppress fluid and make adjacent lesions more prominent.
		T1 and T2 weighted	Insensitive to susceptibility artifacts	To suppress fat signal
<i>Gradient Echo (GRE) Sequences</i>				
A. <i>Cohesive Sequences</i>				
1. Postexcitation steady state sequences	FISP (fast imaging with steady state precession), GRASS (gradient recalled acquisition in the steady state), FFE (fast field echo).	T1 and T2*	High SNR and T2* weighting, suitable to 3D imaging	Application in orthopedic imaging
2. Pre-excitation steady state refocused sequences	PSIF (reversed FISP), SSFP (steady state free precession)	T2 weighted	True T2 weighting achievable, lower SNR	CSF flow studies, inner ear imaging
3. Fully refocused steady state sequences	True FISP, FIESTA (fast imaging employing steady state acquisition), Balanced FFE (fast field echo)	T1 and T2 weighting	Less sensitive to motion	Cardiac, fetal imaging Abdominal imaging
4. Combination of A3 and A4	DESS (dual echo steady state)	T1 and T2 weighting		Orthopedic imaging
5. Combination of A3 and A4	CISS (constructive interference in the steady state), FIESTA-C	T2 weighting	Less prone to banding artifacts in comparison the true FISP.	Inner ear 3D imaging
B. <i>Incoherent/Spoiled Sequences</i>				
1a. 2D-spoiled GRE	FLASH (fast low angle shot), T1-FFE (T1 fast field echo), SPGR (spoiled gradient echo)	T1 weighted imaging	Fast imaging	MR angiography, In-out phase imaging
1b. 3D-spoiled GRE	VIBE (volumetric interpolated breath hold examination), THRIVE (T1 weighted high resolution isotropic volume examination)	T1 weighting	Isotropic imaging, high resolution, fast imaging.	Body imaging
2. Ultrafast GRE	Turbo FLASH, TFE (turbo field echo)	T1 weighted	Very fast imaging	To get rapid images like to track contrast arrival
3. 3D Ultrafast GRE	MP-RAGE (magnetization prepared rapid acquisition GE), 3D-TFE	T1 weighted	High resolution 3D sequence	Cerebral T1 3D imaging.
4. Echo planner imaging	EPI	T2* weighting	Ultrafast sequence	Diffusion, perfusion and functional MRI
<i>Hybrid Sequences</i>				
1. Gradient/spin echo hybrid	Turbo GSE (gradient spin echo), GRASE (gradient echo and spin echo)	T2/T2* weighting	Fast imaging with low SAR	T2 weighting imaging of brain and orthopedic imaging

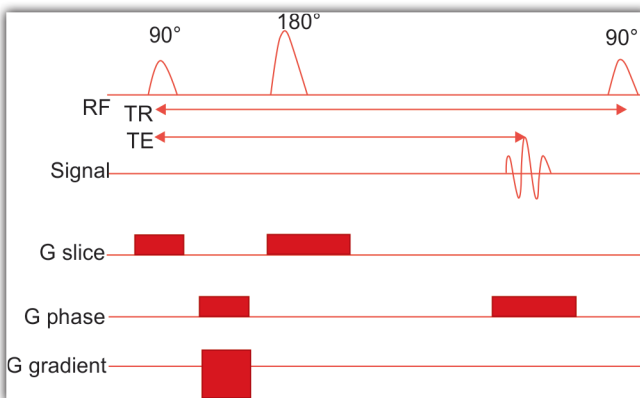


**Fig. 1** Pulse sequence diagram of conventional spin echo sequence. Here a single 180° RF pulse is applied after an initial 90° excitatory pulse. Since TR and TE are short the image is T1 weighted

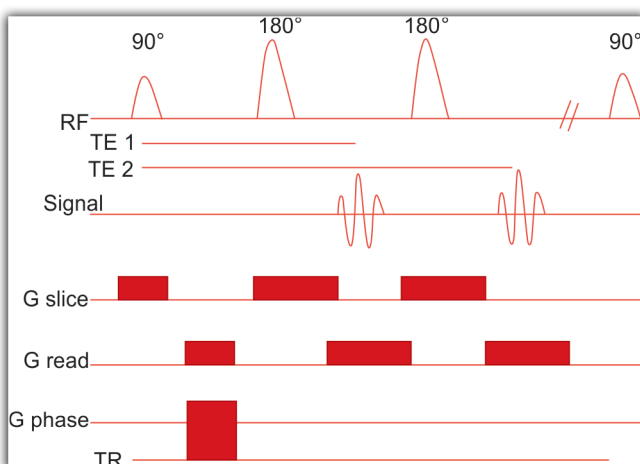


**Fig. 2** Dual echo pulse sequence. Here first echo is proton weighted as TE is short and second echo is T2 weighted as TE is prolonged. TR is prolonged

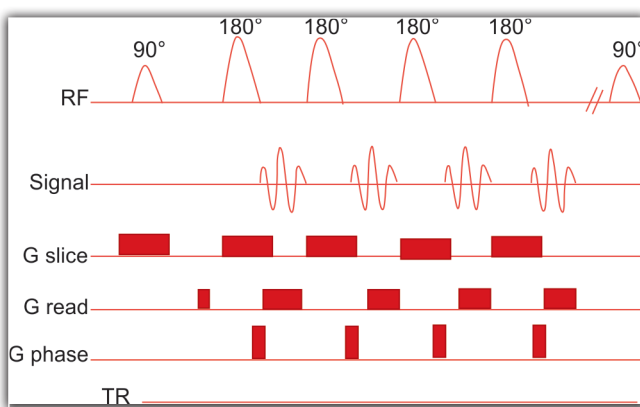


**Fig. 3** Fast spin echo sequence. Here multiple 180° pulse are applied after an initial 90° pulse. The acquisition time is reduced as for a single 90° pulse multiple phase encoding steps take place

If there is only one 180° rephasing pulse a T1 weighted image is produced since the resultant TR and TE are short. When two 180° pulse are used two images result. First image is proton density weighted since here TR is long and TE is short and the second image is T2 weighted, as TR and TE are both prolonged (**Fig. 2**).

Conventional spin echo sequences can be used in any part of the body with predictable tissue contrast characteristics. The major constrain in this sequence is the long acquisition times.

#### Parameters

Usually following parameters are applied:

##### Single echo T1-weighting:

TR-300-500 ms

TE-10-30 ms

##### Dual echo T2-weighting:

TR-2000 ms

TE1-20 ms

TE2-80 ms

#### Fast Spin Echo Sequences

This sequence was developed to overcome the limitation of conventional spin echo sequence, it involves use of multiple 180° rephasing pulses after the initial 90° RF pulse (**Fig. 3**). This sequence reduces time by reducing the phase encoding steps. (The scan time is dependent on TR, phase encoding steps and the number of signal averaging or the number of excitations).

Here each 180° rephasing pulse fills k-space by doing a phase encoding. Thus for a single excitatory RF pulse (90°) multiple 180° rephasing pulse are applied which in turn fills multiple lines in k space thereby filling the k space faster and reducing the scan time. Typically 2,4,8,16 rephasing pulse are used and the time reduction achieved is inversely proportionate to them. The number of 180° pulse and the resultant echo is called 'echo train length (ETL)'. Rapid acquisition and relaxation enhancement (RARE) sequence employ this method (e.g. Turbo SE and fast SE sequences are examples of this technique).

#### Parameters

Usually following parameters are applied:

##### Single echo T1-weighting:

TR-600 ms

TE-17 ms

ETL-4

##### Single echo T2-weighting:

TR-4000-8000 ms

TE-102 ms

ETL-16

##### Dual echo T2-weighting:

TR-2500-4500 ms

TE1 effective- 17 ms

TE2 effective-102 ms

ETL-8

### Half-fourier Acquisition Single-Shot Turbo Spin-Echo

Half-fourier acquisition single-shot turbo spin echo (HASTE) is another modification of fast spin echo where only half the lines of k space are filled in a single shot (Single shot filling of k space can also be done in RARE but filling of entire k-space will result in long acquisition time thus prone to significant T2 decay). For example, SS-FSE, FSE-ADA, FASE. Since k space is symmetrical rest half of k space can be filled with interpolation.

### Inversion Recovery Sequence

This is basically a spin echo sequence where an additional 180° inverting RF pulse is applied which inverts the net magnetizing vector (NMV) through 180°. After removal of pulse the NMV begins to recover, a 90° excitation pulse is applied at a time interval TI (inversion time) after the initial 180° inverting pulse. Following which, like in conventional spin echo sequences a 180° rephasing pulse is applied to produce an echo at a time TE (Fig. 4).

This sequence can be both T1 and T2 weighted.

If inversion time is sufficiently long to allow net magnetizing vector to pass through the transverse plane and then the 90° excitation pulse is applied then the contrast is predominantly T1 weighted. Here TE is to be kept short.

For T2 weighting the TE is prolonged so that T2 decay can occur and the resultant image is T2 weighted.

The TR, the interval between the two inverting 180° pulses should be kept long to allow for complete recovery of NMV to the longitudinal plane.

A. **Short TI inversion recovery (STIR):** This sequence is predominantly used to suppress fat to delineate the structures surrounded by fatty tissues. Here inversion time is kept low and 90° excitation pulse is applied when NMV of fat is crossing the transverse plane. At this point the longitudinal component of fat is zero so it does not contribute to any signal thus is suppressed.

B. **Fluid attenuated inversion recovery (FLAIR) sequence:** This is commonly used sequence in brain to suppress the CSF signal. Here inversion time is kept long (as opposed to in STIR) and 90° excitation pulse is applied when NMV of water is crossing the transverse plane. This selectively suppresses the CSF/free fluid signal.

### Parameters

#### STIR:

TI 100–180 ms

TE 70 ms + (for T2 weighting)

TR long

ETL-16

#### FLAIR:

TI 1500–2200 ms

TE 70 ms + (for T2 weighting)

TR long

ETL-12

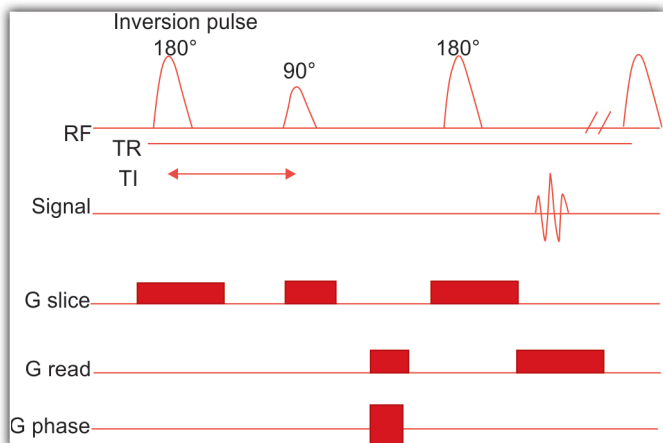


**Fig. 4** A typical inversion recovery pulse diagram. A 180° inversion pulse is applied before 90° excitatory pulse to flip NMV by 180°. Inversion time (TI) is the time interval between the inversion pulse and initial excitatory pulse

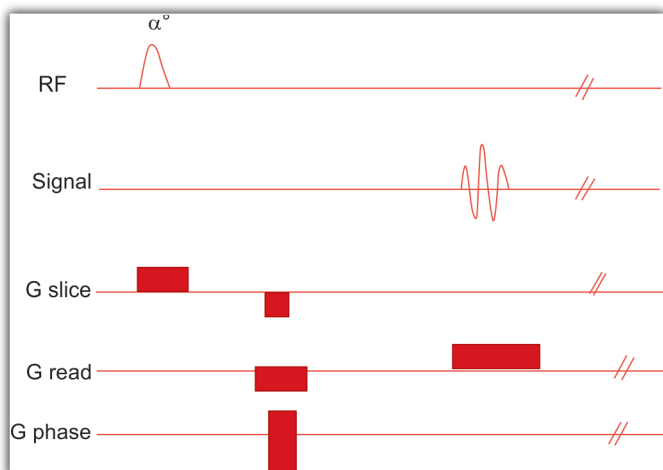


**Fig. 5** Gradient echo sequence. Here after an initial 90° pulse a gradient pulse is applied instead of 180° refocusing pulse as in spin echo sequence

### Gradient Echo Sequences

This is fundamentally different sequence when compared to spin echo sequence. In this type, an initial excitation pulse is applied with certain strength that it flips the NMV into transverse plane at an angle less than 90°. The angle to which it flips the NMV is called flip angle. After the pulse is withdrawn, the magnetic moments start to dephase due to presence of magnetic field inhomogeneities which is called as T2\* decay. A gradient pulse is then applied which dephases and then rephases the magnetic moments in the transverse component. This is followed by generation of signal called gradient echo (Fig. 5). Since the rephasing by a gradient is not as effective as the RF pulse some nuclei, which are dephased (due to t2\* effect) are not rephased and thus the resultant GRE image has some T2\* effect.

### Parameters

#### T1 weighting:

TR- <50 ms  
TE- 5-10 ms  
Flip angle- 60° -120°

#### T2\* weighting:

TR: <500 ms  
TE: 15-20 ms  
Flip angle- <30°

### Steady State Sequences

#### Concept of steady state

When a RF pulse is applied the NMV is flipped into the transverse plane and it is the sum of both longitudinal and transverse magnetization. After the pulse is switched off the transverse magnetization component begins to decrease as the magnetic moments move out of phase. If repeat excitation pulse is applied at a time shorter than T1-and T2 time of any tissue then there will be a residual transverse magnetization. This accumulates over time if repeated pulse are applied and a state is reached when NMV remains constant. This is called 'steady state.' Two types of signals are produced once the steady state is achieved. First echo (s+) is due to free induction decay after the recent RF pulse of the NMV at short TE which contains both T1 and T2\* weighting and the second signal (S-) is due to refocusing of the residual spin echo just before the next RF pulse is applied. This latter echo is predominantly T2 weighted.

### Coherent Gradient Echo Sequence

In these sequences the residual transverse magnetization is utilized by applying a rephrasing gradient, which is similar to initial phase encoding gradient but is of opposite polarity. This rephases the residual magnetic moments and bring them in phase and then they contribute to signal during second excitation.

The sequences which sample the first echo are termed as postexcitation refocused steady state sequences (**Fig. 6**) and are mainly T2\* weighted (FISP, GRASS, FFE, FAST).

The sequences which sample the second spin echo are pre-excitation steady state refocused sequences (**Fig. 7**) and are mainly T2 weighted (PSIF, SSFP, T2-FFE).

The sequences which sample both the first(S+) and second (S-) echoes are fully refocused steady state sequences (**Fig. 8**) and are both T1 and T2 weighted (true FISP, FIESTA, balanced FFE).

### CISS/FIESTA-C

#### Constructive interface in steady state/fast imaging employing steady state acquisition

These are modified fully refocused steady state sequences by different vendors. Since fully refocused steady state sequence

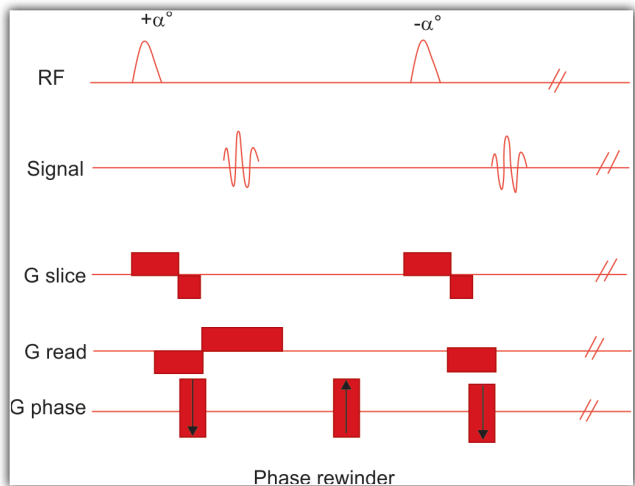


**Fig. 6** Post-excitation refocused steady state sequence. Here the first echo after the recent RF pulse is sampled which is due to free induction decay and hence is predominantly T2\* weighted (short TE)

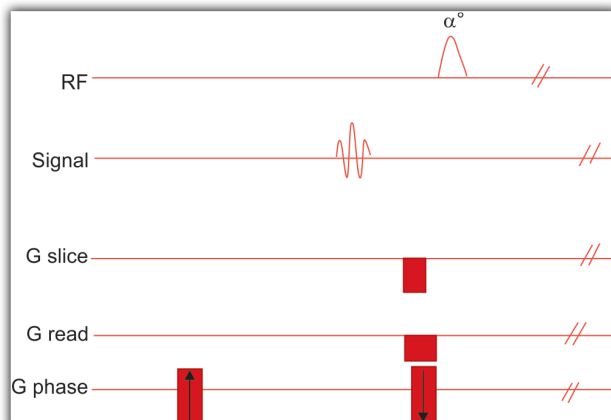


**Fig. 7** Pre-excitation steady state refocused sequence which is mainly T2 weighted as the second echo is sampled which is produced due to refocusing of the residual spin echo just before the application of next RF pulse (long TE)

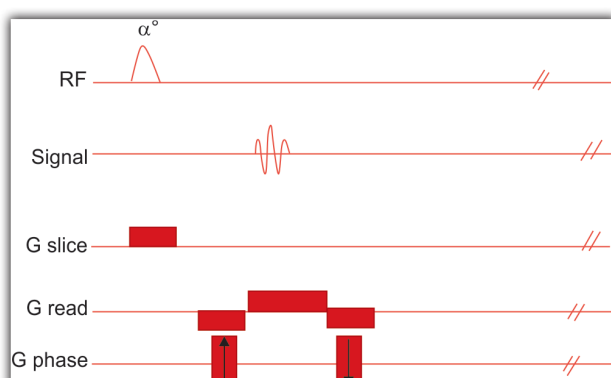


**Fig. 8** Fully refocused steady state sequence

like true-FISP is prone to 'banding artifacts', this aims to remove those. In this sequence two true-FISP sequences are acquired one with alternating phase RF pulse and second with non-alternating phase RF pulse. Combination of these two images displaces the banding artifacts. This results in high resolution 3D, T2 weighted image.

#### Dual echo steady state sequence

This is another variation of true FISP. In true FISP being a balanced sequence S+ and S- signals are combined to form the image. In DESS images are formed with FISP (S+) and reversed FISP (S-) and are then combined (Fig. 9). FISP component provides the T1 component and PSIF signal provides the T2 component of the image.

#### Incoherent/Spoiled gradient echo sequences

In these, the residual transverse magnetization is dephased by applying a gradient (Fig. 10). Thus this does not contribute to signal. Since this is also a steady state sequence TR is short and flip angle is medium. The TE is kept very short so that T2\* effect does not dominate and the resultant image is T1 weighted. (FLASH, SPGR, MPG, T1-FFE).

### Ultra-Fast Sequences

These are very fast sequences which employ multiple techniques to shorten the imaging time.

They can be discussed by the predominant weighting they employ.

#### T2\* Weighted Ultra Fast Sequences

##### Echo planner imaging

This is one of the earliest ultrafast MR sequence where the time is reduced by filling all the lines of k space in single echo train length. These echoes can be produced either by 180° rephrasing pulse or by gradients. Former is called spin echo EPI and the latter gradient EPI. Multiple echoes which are generated are phase encoded by different slope of gradient to fill separate k space lines. The phase encoding gradient and the frequency encoding gradient are very rapidly turned on and off allowing rapid filling of k space. EPI is now technique of choice for diffusion and perfusion imaging.

##### Diffusion weighted imaging

For this either echo planer or fast gradient imaging is used. Two large gradients are applied after the excitation. If the protons are not moving the first gradient dephases and the second rephrases the protons thereby giving high signal. However, if the protons are moving they are not affected by one of the gradients. They are either dephased and not rephased or opposite of this thereby attenuating the signal as compared with stationary protons.

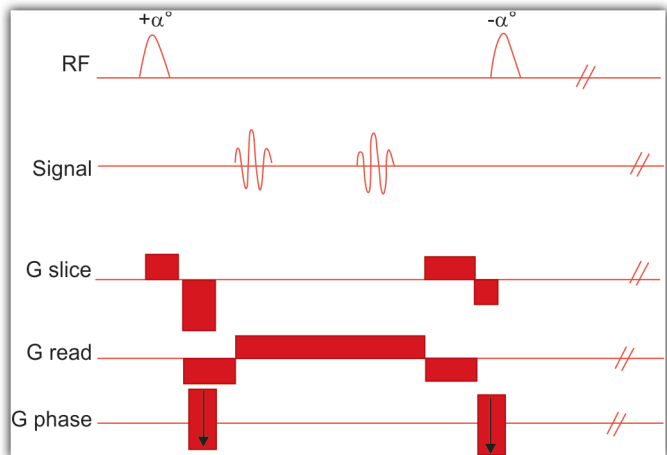


**Fig. 9** Dual echo steady state sequence

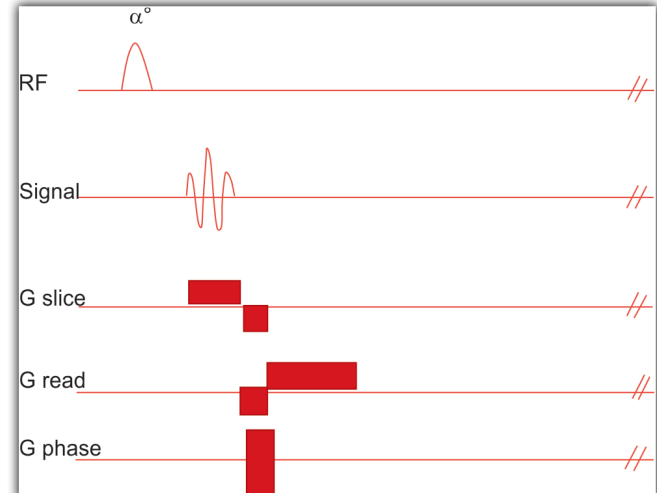


**Fig. 10** In-coherent/Spoiled Gradient Echo Sequences

##### Perfusion weighted imaging

It employs ultrafast T2 or T2\* sequences. It employs use of intravenous gadolinium contrast bolus which decrease the T2 or T2\* signal in and around the microvessels that perfuse the tissue. This attenuation is plotted against time to generate cerebral blood volume, flow and mean transit time.

Perfusion imaging can also be carried out without contrast injection by tagging the spins with an inversion pulse before they enter the imaging volume. Single shot EPI sequence is commonly used for this imaging technique.

##### Ultrafast Gradient Echo Sequence

GE sequences, which acquire the images in less than one second are called ultrafast. This is achieved by first applying

a magnetization preparation pulse before a GE sequence is applied. Typically it is a 180° RF pulse. This increases the T1 weighting in the image and all lines of kspace are acquired after this. Images in this can be acquired in less than a second which is advantageous in tracking the arrival of contrast in a given area, typically used in bolus tracking MR angiography. For example, Turbo FLASH, TFE, Fast SPGR.

### *3D-Ultrafast Gradient Echo Sequence*

This is the 3D variant of above mentioned sequence. The difference in these two sequences is that it is a 3D sequence the acquisition time is long. Thus a single preparatory magnetization pulse is not sufficient and instead multiple preparatory pulse are applied before filling a set of k space lines. This sequence is applied to acquire very high resolution 3d t1-weighted images of the brain. For example, MP-RAGE, 3D TFE, 3D fast SPGR.

## **Hybrid Sequences**

### *Gradient/Spin Echo Hybrid*

This sequence employ combination of spin echo (RARE) and gradient echo (gradient EPI) for faster image generation. Like in RARE sequence multiple 180° rephocusing pulses are applied after an initial 90° pulse to generate multiple echos.

But in addition multiple gradient echoes are generated by switching gradient after each 180° pulse. This sequence is generally employed to get high-resolution T2 weighted images.

## **SUGGESTED READINGS**

1. Chavhan GB, Babyn PS, Thomas B, Shroff MM, Haacke EM. Principles, techniques, and applications of T2\*-based MR imaging and its special applications. Radiographics. 2009;29(5):1433-49.
2. Chavhan GB, Babyn PS, Jankharia BG, Cheng HL, Shroff MM. Steady-state MR imaging sequences: physics, classification, and clinical applications. Radiographics. 2008;28(4):1147-60.
3. Pooley RA. AAPM/RSNA physics tutorial for residents: fundamental physics of MR imaging. Radiographics. 2005;25(4):1087-99.
4. Boyle GE, Ahern M, Cooke J, Sheehy NP, Meaney JF. An interactive taxonomy of MR imaging sequences. Radiographics. 2006;26(6):e24.
5. Eugene Lin. Body MRI sequences: A conceptual framework. Applied radiology. 41(1), January 2012.
6. Bitar R, Leung G, Perng R, et al. MR pulse sequences: what every radiologist wants to know but is afraid to ask. Radiographics. 2006;26(2):513-37.
7. MRI at a Glance. Catherine Westbrook Hoboken, 2nd Edn. NJ: Wiley-Blackwell; 2010.

## Section

# 4

# Advances in Radiography and Interventional Radiology

**Chapter 13** • Digital Radiography: An Update  
*Alpana Manchanda*

**Chapter 14** • Digital Mammography  
*Smriti Hari, Chandrashekara SH, Surabhi Vyas*

**Chapter 15** • Fluoroscopy and Digital Subtraction Angiography  
*Deep Narayan Srivastava, Madhusudhan KS*

**Chapter 16** • Tools in Interventional Radiology  
*Atin Kumar, Chandan Jyoti Das*



## Chapter

# 13

# Digital Radiography: An Update

*Alpana Manchanda*

Radiography is an art and science of recording images produced by X-rays on X-ray film. Till the past decade, the conventional film screen system was the most widely used and accepted method of recording images, wherein the film acts as an image receptor, display medium and a source of permanent record. Though these films are relatively inexpensive and provide high image quality, they have many limitations.<sup>1</sup>

### LIMITATIONS OF FILM SCREEN RADIOGRAPHY

- Radiographic film has a defined latitude (range of densities) that can be recorded simultaneously. This problem is particularly highlighted in chest radiography where 40 percent of lung area is obscured by heart, mediastinum and diaphragm. Mediastinum and retro cardiac portion of lung remain under penetrated when exposure is given for optimal lung details.
- Film – screen systems are intolerant to exposure errors, with under/over exposure leading to loss of radiographic contrast.
- Films cannot be transmitted or duplicated without some loss of quality and this involve significant cost.
- Acquisition, display and storage of image are non-separable.
- Another limitation of radiographic film is the noise inherent in these images. Both radiography and fluoroscopy use area beams, i.e. large rectangular beam of X-rays. The Compton scattered portion of the remnant X-ray beam increases with increasing field size. This increases the noise of the image.
- Storage of conventional radiographs also poses a problem.

- Film quality can deteriorate with time, especially if chemical processing is suboptimal.
- Another important limitation of film screen imaging system is that the image cannot be manipulated before it is displayed and image quality is therefore not necessarily the same in all the images.

Image optimization is therefore essential to achieve good diagnostic images at the lowest possible dose.

Significant advancement in electronics and computer technology have resulted in film screen radiography (FSR) systems being replaced by digital radiography (DR) systems which have become the standard technology in most departments. The process wherein digital detectors are used to capture information of an object is termed as digital radiography. There are many advantages of producing images in a digital format -in a format that can be stored and processed in a computer and displayed on a monitor.

### ADVANTAGES OF DIGITAL RADIOGRAPHY<sup>2,3</sup>

- Digital images do not deteriorate physically or degrade chemically over time
- They allow a true reproduction of quality from copy to copy and from generation to generation
- Digital images are flexible, allowing a variety of manipulation such as magnification, cropping, edge enhancement, compression, etc.
- Digital detectors allow implementation of a fully digital picture archiving and communication system (PACS) in which images are stored digitally and available anytime.
- The images can be distributed electronically by web-based technology with no risk of losing clarity.

- A higher patient throughput is possible as compared to FSR system
- Increased dose efficiency and wide dynamic range of digital detectors with possible reduction of radiation exposure to the patient.

### ■ EVOLUTION OF DIGITAL RADIOGRAPHY

Digital imaging system was installed in the 1970s until the microprocessor and semi-conductor memory systems were developed in the 1980s and were designed to process the large amount of data generated from this system.<sup>3</sup> **Table 1** highlights the developments in digital radiography.

### ■ THE PHYSICS BEHIND DIGITAL RADIOGRAPHY

Digital imaging uses binary system in which information is interpreted as bits. A binary (base 2) digit can assume only one of two values, rather than one of ten as for decimal (base 10) system. The decimal representation of a binary number is calculated such that the digits are multiplied by power of 2 rather than power of 10.

Most digital systems handle individual pixels with eight-bit accuracy for displayed brightness. An individual pixel can therefore have any brightness value from 0 through 255 decibel, a total of  $2^8$  (256) possible brightness values. Most of the information in radiology is displayed as shades of black and white. The analog imaging system displays a smooth variation in brightness from completely dark to maximum brightness. In digital system the display would be more step like.

Thus, digital information is any information that is represented in discrete units, while analog information is one that is represented in continuous rather than discrete fashion (**Fig. 1**).<sup>4</sup>

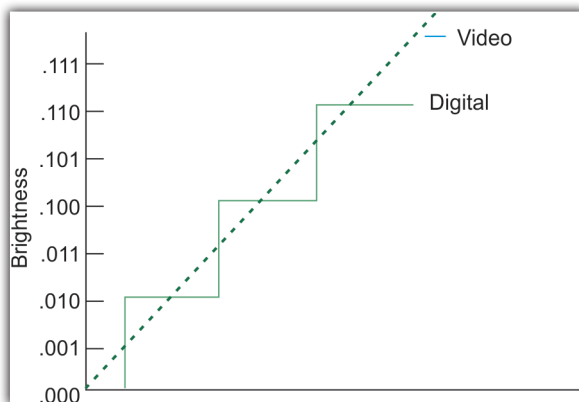


**Fig. 1** Comparison of analog video voltage and digitized values

In contrast to film screen radiography (FSR) in which the film serves as both detector and storage medium, digital detectors are used only to generate the digital image, which is then stored on a digital medium.

Digital imaging consists of four separate steps:

1. Image generation
2. Image processing
3. Image archiving
4. Presentation of the image

### ■ PRINCIPLE OF DIGITAL RADIOGRAPHY

The digital detector is exposed to X-rays generated by a standard tube. The energy absorbed by the detector is transformed into electrical charges, which are then recorded, digitized and quantified into a gray scale. After sampling, post-processing software is required for organizing the raw data into a clinically meaningful image.<sup>3</sup>

### ■ DIGITAL RADIOGRAPHY SYSTEMS

Digital radiography systems have evolved in recent years as advancements in FSR technology had almost reached the limit of further improvement.

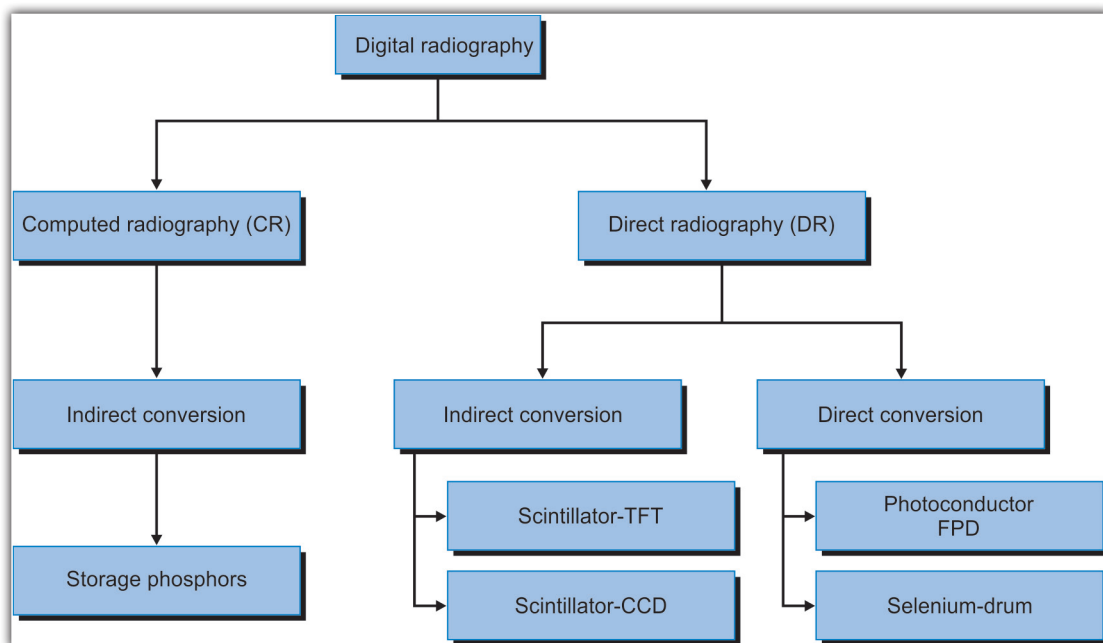
In digital radiography, a digital detector replaces films and intensifying screens. There are two basic types of digital radiography systems depending upon the types of detectors used to capture the radiographic information.<sup>3,5</sup>

1. **Computed radiography (CR) system** use a storage Phosphor image plate (photostimulable phosphor plate) enclosed in a light tight cassette. CR utilizes a two stage process with image capture and image readout done separately.
2. **Direct digital radiography (DR)** uses detectors that have a combined image capture and image read out process. DR systems can be further divided to direct and indirect conversion groups, depending on the type of X-ray conversion used (**Flow chart 1**).

**Table 1** Evolution of digital radiography<sup>3</sup>

Year	Technique
1977	Introduction of digital subtraction angiography (DSA)
1980	DSA first put into clinical use
1980	Use of storage phosphor image plates
1987	Amorphous selenium based image plates
1990	Charge couple device (CCD) was introduced for direct capture of X-rays for digital image
1994	Selenium drum DR
1995	Amorphous silicon-cesium iodide (scintillator) flat-panel detector
1997	Gadolinium-based (scintillator) flat-panel detector
2001	Gadolinium-based (scintillator) portable flat-panel detector
2001	Dynamic flat-panel detector fluoroscopy digital subtraction angiography
2007	Portable CR system

**Flow chart 1** Various types of digital detectors



## Computed Radiography

Computed radiography (CR) systems use storage phosphor image plates with a separate image read out process. In CR systems, photostimulable crystals, i.e. photostimulable phosphor plates (PSP) is the detective layer in place of films and screens. These plates are coated with europium activated barium fluorohalide ( $\text{Ba FX: Eu}^{2+}$ ), the halide being bromide, iodide or a combination of both. CR cassettes are used on conventional X-ray machines like normal cassettes and are available in similar sizes. Image generation in CR is a two step process.

When the storage phosphor image plates (IP) are exposed to X-rays, the X-ray energy is absorbed and temporarily stored by the crystals (detective layer of the plate) by bringing electrons to higher energy levels. X-ray energy can be stored for several hours depending on the specific physical properties of the phosphor crystals used. However, the readout process should start immediately after exposure because the amount of stored energy decreases over time.

In the readout process, the image plate/detective layer after exposure to X-rays is taken to a CR reader where it is scanned by a high energy laser beam of a specific wavelength. The stored energy is set free as higher energy blue light having a wavelength different from that of the red laser light. This light is collected by photodiodes/photomultipliers and signal converted digitally into electrical signal by an analog-to-digital converter (ADC) then amplified, digitized and used to form an image (Figs 2 and 3).<sup>5</sup>

The imaging plate is ready for use again after exposure to white light.<sup>5</sup>

In a CR system, the patient information and cassette ID needs to be linked as there is no direct electrical connection between the CR reader and the cassette. A bar code reader or

a chip embedded on the CR cassette is used for this purpose. The PSP imaging plates may be flexible or rigid, with the base in these plates being opaque or translucent. Different types of CR cassette designs and image readers are available, so all cassettes from the same vendor may not be compatible with all readers. Some of the CR plate readers can process one plate while holding multiple cassettes in a queue. This is known as “drop and go” which helps improve workflow.<sup>5</sup>

Some CR systems using PSP plates with translucent bases have a dual side readout. These systems use laser scanning from one side but capture light from both sides of the plate, increasing the DQE by 50 to 100 percent (DQE or detective quantum efficiency refers to the efficiency of a detector in converting incident X-ray energy into an image signal).

The spatial resolution of the CR images depends on:

- The laser spot size
- Photostimulable phosphor plate characteristics (packing density, thickness of the phosphor layer)
- Sampling rate of the emitted light.

Diffusion of the scanning laser light and emitted light leads to some loss of spatial resolution.

The time taken for scanning a PSP plate varies from 40 to 90 seconds and depends on the plate size, resolution desired and dual/single side readout. Some newly introduced CR systems use line scanning techniques thereby reducing the image readout time to 20 to 30 seconds or even less.

Phosphor plates have a more linear, optical density versus radiation exposure response curve than the classic sigmoid - shaped curve of the conventional film-screen combination (Fig. 4).

The CR technology thus gives a greater latitude of exposure which is useful under challenging radiographic circumstances such as the intensive care unit. It allows

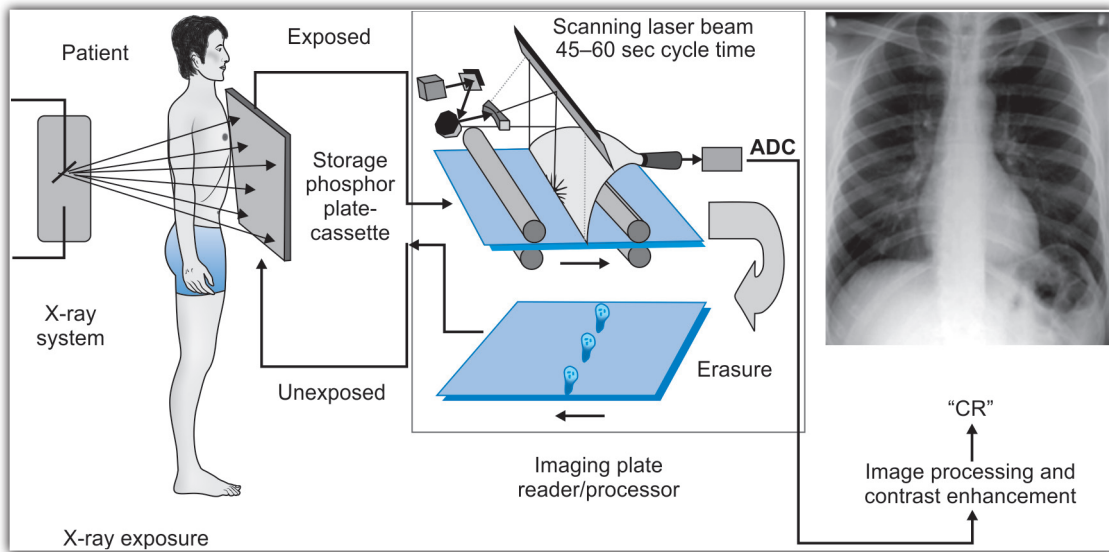


**Fig. 2** Schematic representation of a CR imaging system, screen and scanner

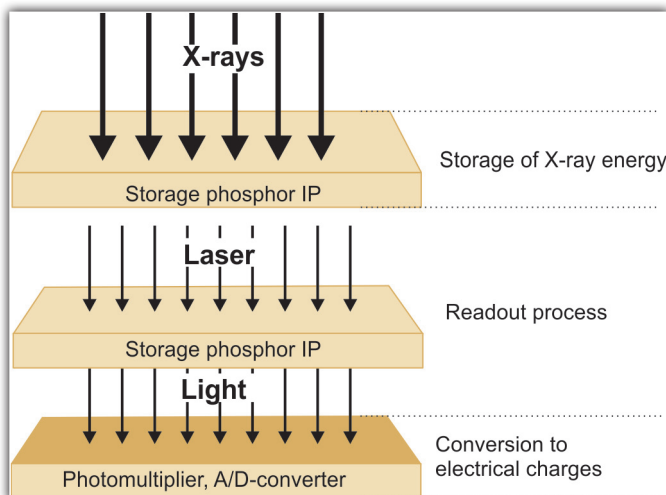


**Fig. 3** Illustrates a CR system based on storage – phosphor image plates

structures of widely differing radiographic density to be well visualized on the same image, such as the area behind the cardiac silhouette and the lung vessels or the soft tissue of the neck or cervico thoracic junctions. This feature allows a reduction compared with FSR in the number of repeat images taken due to errors in selecting the correct exposure. The spatial resolution of CR is lower (i.e. 2½ line-pairs per mm) than that of conventional FSR which is approximately 5 line pairs per mm. But its superior contrast resolution more than compensates for its limited spatial resolution. Phosphor plates can be reused repeatedly for a thousand or more exposures. CR equipment is cheaper than direct DR equipment, especially for mobile radiographic units.<sup>6</sup>

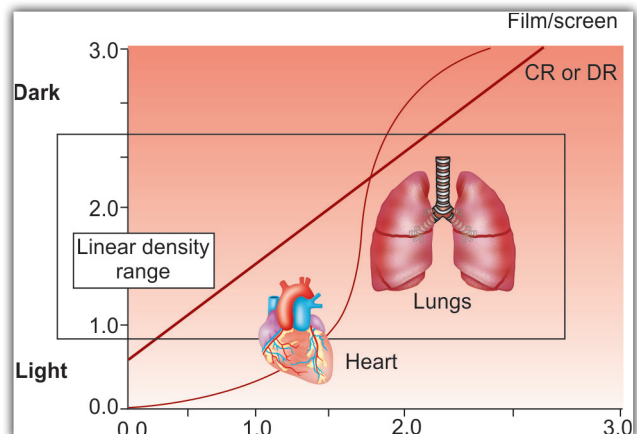


**Fig. 4** Optical density vs. radiation exposure response curves

#### Advantages of Storage Phosphor Systems

- Being cassette based, CR systems can easily be integrated into existing radiographic equipment.
- Single CR systems can convert multiple radiography rooms to digital technology.
- They have a wide dynamic range leading to reduced rates of failed X-ray exposure.
- They are easy to use for bed side examinations and immobile patients.
- CR cassettes can be placed in any position thereby enabling flexibility for positioning for difficult views.
- Multiple cassette sizes are available.
- In case of defect in the image plate, it can easily be replaced by the radiographer with no need for specialized equipment or service personnel.

### Drawbacks of CR/Storage Phosphor Systems

- It is a time consuming technique.
- Image reader takes time before the image can be displayed, with time taken being comparable to that required for film processing.
- Spatial resolution is lower than that of film screen radiography.
- Radiation dose required is same or more than film screen radiography.

### Direct Digital Radiography

Digital radiography (DR) or direct digital radiography is a way of converting X-ray into electrical charges by means of a combined image capture and image readout process. DR systems are also called DDR or ddR systems by some vendors. DR systems can be further divided into direct and indirect conversion groups depending on the type of X-ray conversion used.<sup>7</sup>

- **Direct conversion detectors** have an X-ray photoconductor such as amorphous selenium that directly converts X-rays photons into an electric charge.
- **Indirect conversion detectors** have a two-step process for X-ray detection
  - A scintillator is the primary material for X-ray interaction. When X-rays strike the scintillator the X-ray energy is converted to visible light.
  - The visible light is then converted into an electric charge by means of photodetectors such as amorphous silicon photodiode arrays or CCDs (charged couple device).

In both direct and indirect conversion detectors, the electric charge pattern that remains after X-ray exposure is sensed by an electric readout mechanism, and analog-to-digital conversion is performed to produce the digital image.

### Direct Conversion

Direct conversion type of detectors uses amorphous selenium as photoconductor that converts X-rays photons into electrical charges by setting electrons free. The photoconductor materials include amorphous selenium, lead iodide, thallium

bromide and gadolinium compounds. The more commonly used element is selenium. All these elements have a high intrinsic spatial resolution. As a result, the pixel size, matrix and spatial resolution of direct conversion detectors are not limited by the detector material itself, but only by the recording and readout devices used.<sup>3</sup>

Selenium-based direct conversion DR systems are equipped with either (a) a selenium drum or (b) a flat panel detector.

#### Selenium Drum-based System of Direct Conversion

A rotating selenium drum with a positive electric surface charge is exposed to X-rays. During exposure, a charged pattern proportional to that of incident X-rays is generated on the drum surface and is recorded during rotation by an analog-to-digital converter (**Fig. 5A**).

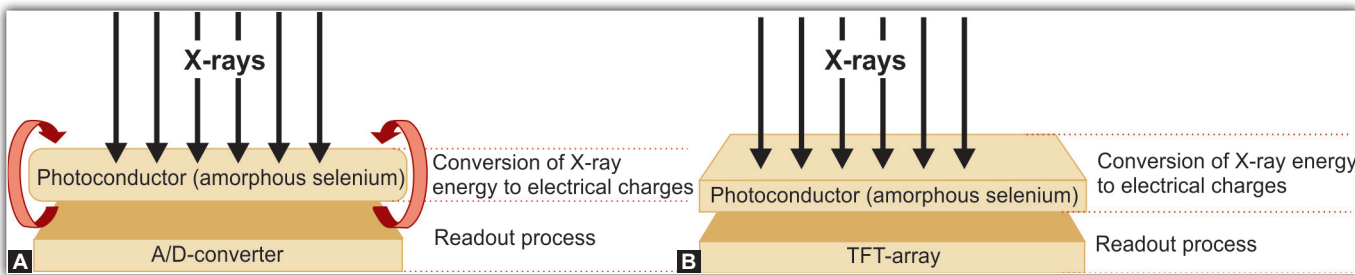
Several clinical studies have proved that selenium drum detectors provide good image quality that is superior to that provided by film-screen or CR system.<sup>8</sup> However, a limitation of selenium drum detectors is that they are dedicated thorax stand systems with no mobility at all.<sup>3</sup>

#### Large area, thin film transistor arrays

Thin-film transistor arrays (TFTs) are used as active electronic elements in both direct and indirect conversion, flat-panel detectors. Thin film transistor arrays are typically deposited onto a glass substrate in multiple layers, beginning with readout electronics at the lowest level and followed by charge collector arrays at higher levels. Then, depending on the type of detector being constructed, X-ray elements, light sensitive elements, or both, are deposited to form the top layer of TFT array. The whole assembly is encased in a protective enclosure with external casing for computer connection.<sup>7</sup>

#### Thin Film Transistor—Direct Conversion

Direct conversion system based on thin-film transistor arrays are constructed by adding an X-ray photoconductor as the top layer of the electronic thin-film transistor sandwich. Amorphous selenium is used as the photoconductor material because of its excellent X-ray detection properties and extremely high intrinsic spatial resolution.



**Figs 5A and B** Direct conversion DR system: (A) Selenium drum-based system; (B) Thin film transistor

It is sandwiched between two electrodes to which high voltage is applied. When this layer is exposed to X-rays, electrons and holes are produced, proportional to the amount of X-rays absorbed. The applied voltage separates the electrons and holes, so that the signal does not spread. The electronic charge is stored in capacitors and is read out sequentially. Thus, the X-rays are directly converted to electrical signal (Fig. 5B). These detectors have very high spatial resolution, moderate X-ray absorption efficiency (DQE) and an excellent fill factor. The area of the detector that is sensitive to X-ray in relation to the total detector area is known as the "fill factor". Detectors with higher fill factors use absorbed radiation more efficiently.<sup>5</sup>

An advantage of amorphous selenium TFT array over selenium drum is that these detectors can be mounted on thorax stands and bucky tables. As selenium is used in its amorphous form, selenium plates can be made by means of evaporation relatively easily and inexpensively.<sup>7</sup>

Direct conversion of DR technology has mainly been derived from the use of selenium drums in photocopier machines and xeroradiography. Selenium has relatively low atomic number resulting in less X-ray absorption in general radiography KV range. The K-edge of selenium is more suited for the diagnostic KV range required in mammography. As a result, direct conversion FPDs are more popular in mammography than in routine radiography.<sup>5</sup>

#### *Thin Film Transistor—Indirect Conversion*

Indirect conversion based on thin-film transistor (TFT) arrays are constructed by adding amorphous silicon photodiode circuitry and a scintillator as the top layers of the thin-film transistor sandwich. These layers replace the X-ray photoconductor layer that is used in direct conversion devices.

#### *Mechanism*

When X-rays strike the scintillator, visible light is emitted proportional to the incident X-ray energy. Visible light photons are then converted into an electric charge by the photodiode array, and the charge collected at each photodiode is converted into a digital value by using the underlying readout electronics (Fig. 6).

### **TYPES OF SCINTILLATORS**

The scintillators used in indirect conversion detectors can be either structured or unstructured (Fig. 7).

**Unstructured scintillator:** With use of unstructured scintillator, the visible light emitted by the material can spread to adjacent pixels, thereby reducing spatial resolution.

**Structured scintillators:** To reduce the problem of scatter, some manufacturers now use a structured scintillator that consists of cesium iodide crystals that are grown on the detector. The crystalline structure consists of discrete and parallel 'needles' (5–10  $\mu$  wide) which channel most of the signal directly to the photodiode layer. As light spreading

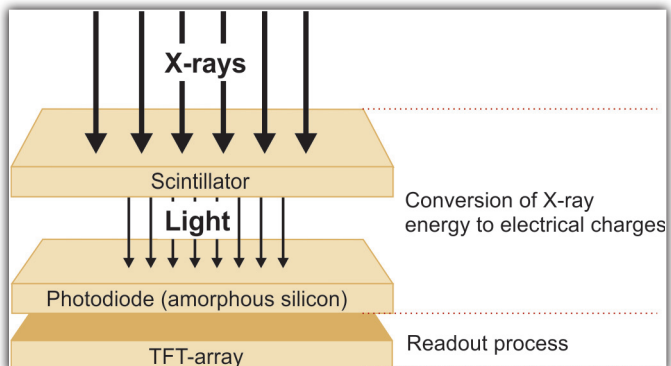


**Fig. 6.** Drawing illustrates an amorphous silicon based indirect conversion DR system

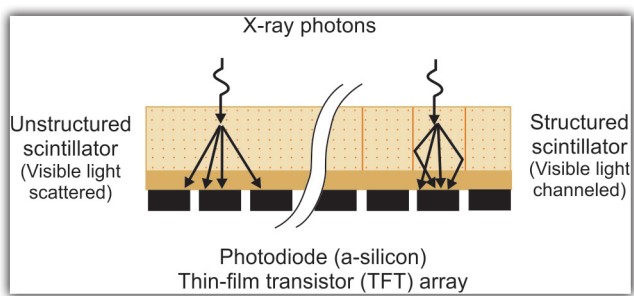


**Fig. 7** Diagrammatic representation of indirect conversion detectors—the X-ray scintillator can be structured or unstructured

is greatly reduced in a structured scintillator, it maintains a good spatial resolution. Thicker layer of the material can be used in the detector. This increases the number of X-ray photon interactions and thus the available visible light.

Thallium-doped cesium iodide (CsI) is the most commonly used phosphor material. Another material that is used is gadolinium oxysulphide or Gadox ( $Gd_2O_2S$ ). It has an amorphous structure that permits spread of light produced by X-ray absorption, resulting in poorer, spatial resolution. CsI-based detectors are more efficient in X-ray absorption than gadox detectors and have better DQE.<sup>5</sup>

The small size of the flat panel detectors is of advantage as it allows integration into existing bucky table or thorax stands. But as CsI-based flat-panel detectors are highly vulnerable to mechanical load because of their fragile nature, these detectors are to be handled with the utmost care. These systems cannot be used outside fixed installations and hence lack mobility. Portable flat panel detector systems make use of  $Gd_2O_2S$ -based scintillators as they are resistant to mechanical stress.<sup>3</sup>

Most flat panel detectors are available in large sizes of  $43 \times 43$  cm,  $41 \times 41$  cm,  $43 \times 35$  cm, etc. Image generation with flat panel detectors is almost instant, with a time lapse less than 10 seconds. Also more number of patients can be imaged in the same amount of time than with other radiographic devices.<sup>3</sup>

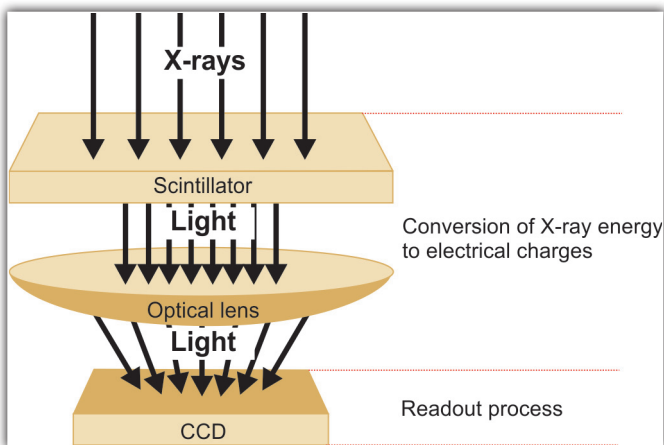


**Fig. 8** Lens coupled CCD based indirect conversion DR system

### Charge Coupled Devices

Charged coupled devices (CCDs) is a light sensitive sensor for recording images that consists of an integrated circuit containing an array of linked or coupled capacitors. X-ray energy is converted into light by a scintillator such as thallium doped cesium iodide. The amount of light emitted is then recorded by the CCD, and the light is converted into electrical charges. As the detector area cannot be larger than the CCD chip, it is necessary to combine several chips to create larger detector areas.<sup>3</sup>

Charged coupled devices can be used for radiography as part of either (a) a lens coupled CCD system, or (b) a slot-scan CCD system.

The *lens system* is an array consisting of several CCD chips which form a detector area similar to that of a flat panel detector. Optical lenses are needed to reduce the area of the projected light to fit the CCD array (**Fig. 8**). A drawback of

the lens system is that it substantially reduces the number of photons that reach the CCD. This increases the image noise (quantum mottle) and degrades image quality. In addition, optical coupling with lenses can introduce geometric distortion, optical scatter, and reduce spatial resolution.

*Slot-scan CCD system*—makes use of a special X-ray tube with a tungsten mode. The patient is scanned with a collimated fan-shaped beam, which is linked to a simultaneously moving CCD detector array having a matching detector. The combination of a small collimated beam and a concordant detector reduces the impact of scattered radiation in the images. The exposure time to the patient is about 20 m sec, and the readout time takes about 1.3 seconds.<sup>3</sup> Slot-scan CCD systems are dedicated to chest radiography, mammography or dental radiography.

The performance of lens-coupled CCD system has been found to be inferior to that of slot-scan system because of their technical principle, substantially lower quantum efficiency, and lower signal-to-noise ratio.

### Photon Counting Type DR System

Photon counting type of DR system has construction similar to the slot scanning type, but uses a different type of detector. These systems use a multislit detector made of crystalline silicon (Si) as a scintillator. The principle is similar to the one used in direct type of flat panel detector. A voltage of about 100 volts is applied across the array of thin Si crystals (50 µm). The absorbed X-ray produce electrons and holes which is counted in a meter. The photon counting type of DR system produces images with a high SNR as the electrical pulse generated is much higher than the electronic noise. The images are of high contrast and detail resolution with no ghost image due to previous exposure residue. Presently, this technology is used for mammography.<sup>9</sup> In **Table 2**, differentiating features of direct and indirect types of flat panel digital detectors are enumerated.

**Table 2** Main differentiating features of direct and indirect type of flat panel digital detectors<sup>9</sup>

S. No.	Direct digital conversion	Indirect digital conversion
1.	Direct conversion of X-rays to electrical signal  X-rays → electrical signal	Indirect conversion of X-rays to electric signal  X-rays → light → electrical signal
2.	Uses a photoconductor that directly converts the absorbed X-rays to electrical signal without any intermediate light production	Phosphor converts X-rays to light and photodiode array converts emitted light into electrical signals
3.	Detector material used – amorphous selenium (a-Se)	Phosphor used commonly – thallium doped cesium iodide (CsI) or gadolinium oxysulphide (Gd <sub>2</sub> O <sub>2</sub> S)
4.	The signal does not spread as the applied high voltage separates the electrons and holes produced by absorbed X-rays	Light scatter reduces spatial resolution more with Gd <sub>2</sub> O <sub>2</sub> S as phosphor than CsI
5.	Resolution of the images is maintained as the thickness of the photoconductor is increased	With increasing phosphor thickness, poorer resolution images are obtained
6.	Fill factor ~ 100%	Moderate fill factor depending on pixel size
7.	Moderate DQE for KV used for conventional radiography, but high DQE for mammography KV range	High DQE for KV range used in conventional radiography

## IMAGE PROCESSING

After exposure and readout, the raw imaging data needs to be processed for display on the computer. Image processing is one of the important features of digital radiography and greatly influences the way the image appears to the radiologist. Even though software products from several manufacturers use similar algorithm such as edge enhancement, noise reduction and contrast enhancement to alter the appearance of the image, the resulting image may differ considerably.<sup>3</sup>

Image processing is used to improve image quality by reducing noise, remove technical artifacts and optimize contrast for viewing. Spatial resolution cannot be influenced by the processing software as it is dependent on the technical variables of the detector (pixel size).

Noise limits the ability to see low contrast detail. In real time acquisition system such as fluoroscopy, noise can be reduced by adding the signal from successive frames to give a time averaged image. This is equivalent to increasing exposure time in radiography. Frame averaging is a useful technique provided that there is no movement between frames, otherwise the image will be blurred.

Noise may also be reduced by low-pass spatial filtering. In this technique, to the gray scale value stored in each pixel, a proportion of the value of the neighboring pixels and resultant value is averaged. The effect is to smooth the final image, but it blurs small details or edges.

Direct radiography systems convert X-ray image information into electronic charges held by the TFT array. As indirect-conversion systems rely on light, substantial scatter occurs before the energy is converted to charge which reduces signal-to-noise ratio.

Edge enhancement or high pass filtering has the opposite effect. Rather than display a weighted average value of neighboring pixels, a high pass filter adds in a proportion of the difference between the grayscale value of the pixel and that of its neighbor. The effect is to exaggerate the contrast at the boundary between structures, thus making the structures more visible.<sup>10</sup>

Image processing software is usually bundled with the detector and cannot be replaced by other software.

## ASPECTS OF IMAGE QUALITY

Although the image in digital technique may appear as a conventional video or radiographic image, it is not. It is formed from individual image elements—pixels. With conventional imaging, X-rays form an image directly on the receptor. Efficient detection of the spatially dependent, attenuated transmitted beam is the first and most important task of an X-ray detector. With digital technique, X-rays form an electronic image on a radiation detector and are manipulated by a computer, temporarily stored in memory and displayed as a matrix of intensities, each having a dynamic range of values.

The major factors effecting digital image quality are mentioned below:

### Pixels

The pixel is the foundation block of digital imaging. It is the smallest complete sample of an image. The two dimensional collection of pixels in the images is called the matrix, which is usually expressed in length (in pixels) by width (in pixels). Maximum achievable spatial resolution is defined by pixel size and spacing. Pixel size is a measure of resolution, wherein, smaller the pixel size (or larger the matrix), better the resolution.

### Detector Size

The physical dimensions of the X-ray detector have an influence on the radiographic examinations performed. The detector should be sufficiently large to capture the desired anatomic views and sufficiently compact for all clinical applications.<sup>7</sup> Larger detector areas are needed for chest imaging than for imaging of the extremities.

### Gray Scale

Gray scale refers to shades of gray available for reproducing faithfully subtle differences in densities in an accurate manner. Gray scale images are different from black and white images. Unlike the latter, which have two colors (black, white), gray scale images have a number of shades of gray in between. More the number of shades available, superior is the display. The shades of gray that compose an image range from pure black at the weakest intensity to pure white at the strongest.

For routine visual display,  $2^8$  or 256 intensities (shades of gray) are recorded on a nonlinear scale. However, in medical imaging more shades of gray are required which allows  $2^{16}$  or 65536 gray levels.

### Spatial Resolution

It describes the ability to distinguish fine spatial detail and to differentiate objects in an image. In digital acquisition systems, resolution is governed by a term called spatial frequency. Resolution implies how frequently an object is sampled. As a rule of thumb:

- Increasing the sampling frequency helps to increase resolution
- Images composed with a greater number of pixels have a higher spatial resolution. However, images with higher resolution require large file sizes.<sup>2</sup>

Increasing the radiation applied to the detector will not improve the maximum spatial resolution. In fact, scattering of X-ray and light photons with the detector influences the spatial resolution. Hence, spatial resolution for selenium-

based direct conversion detectors is higher than for indirect conversion detectors. Structured scintillators are advantageous over unstructured scintillators.<sup>3</sup>

The image resolution in capturing devices is not synonymous with the image resolution of output devices such as computer monitors or printers. In general, for capturing devices, the imaging resolution is expressed as ppi (pixel per inch) and for output devices as dpi (dots per inch).<sup>3</sup>

Spatial resolution in digital acquisition systems is expressed as pixel size, pixels/mm, or line pairs per millimeter (lp/mm). Line pairs per millimeter are a measure of resolution wherein pairs of lines are closely approximated. The unaided human is capable of distinguishing about 10 to 14 lp/mm. More the lines placed within a millimeter implies higher the resolution.

The spatial resolution of newer digital acquisition systems such as CR and DR are comparable to each other, but less than film-screen radiography.<sup>2</sup> It is possible to achieve a resolution of 5 to 10 pixel/mm in general purpose CR cassettes while a resolution of 20 pixel/mm is available in most CR systems approved for mammography.<sup>5</sup>

- Detection of signal in a noisy background and noise reduction methods are:
  - Flat fielding
  - Signal averaging
  - Anti-scatter grids
- Dose reduction methods
  - High peak voltage
  - Added tube filtration
  - Detector technology
- Image processing, consistency and reproducibility are achievable by DR.

### Contrast Resolution and Dynamic Range

Contrast resolution refers to the amount of gray scale differentiation that exists in an image. For digital image acquisition equipment, it means the number of shades of gray that a detector can capture. Digital detectors have high contrast resolution thus enabling thousands of shades of gray to be displayed. The superior contrast resolution of digital detectors more than compensates for the reduced spatial resolution.<sup>2</sup>

Dynamic image is the measure of the signal response of a detector that is exposed to X-rays. In a conventional film-scan combination, the dynamic range is S-shaped with a narrow exposure range for optimal film blackening, i.e. the film has a low tolerance for exposure at higher or lower than required, resulting in failed exposures or insufficient image quality (**Fig. 9**).

In digital detectors, dynamic range is the range of X-ray exposure over which a meaningful image can be obtained. Digital detectors have a wide and linear dynamic range. In contrast to film screen system, the curve for digital detectors

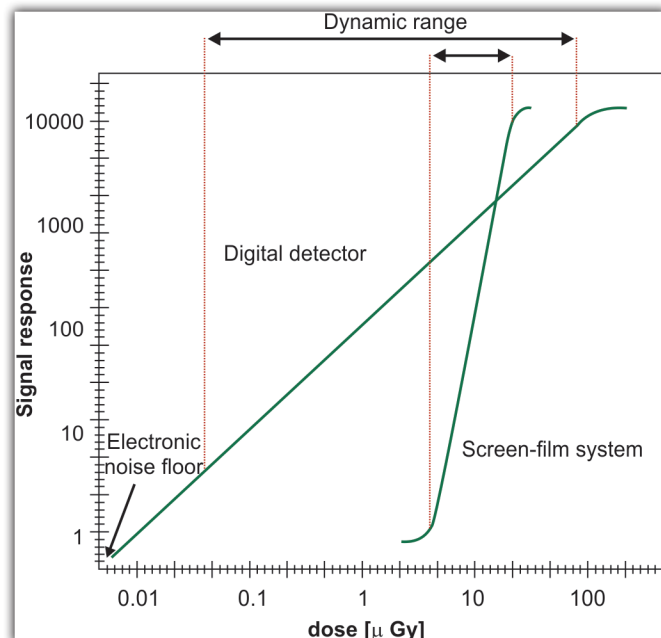


**Fig. 9** Graph illustrates the dynamic range of screen—film combinations and digital detectors

is less steep and covers a wider range. As a result an optimal signal response will occur over a wider exposure range with digital detectors than with film screen combinations. Another advantage of a wide dynamic range is that differences between specific tissue absorption (e.g. bone vs soft tissue) can be displayed in one image without the need for additional images.<sup>3</sup>

### Modular Transfer Function

Objective methods can be used to determine detectors and X-ray system performance (image quality) and efficiency (dose). Measurement include frequency dependent signal transfer via the MTF(f), noise power spectrum NPS(f) and signal transfer efficiency (input to output) via the DQE metric [DQE(f)]. Different detectors have different modulation transfer characteristics.

Modular transfer function (MTF) is the capacity of the detector to transfer the modulation of the input signal at a given spatial frequency to its output. At radiography, objects having different sizes and opacity are displayed with different gray scale values in an image. MTF has to do with the display of contrast and object size. It is responsible for converting contrast values of different sized objects (object contrast) into contrast intensity levels in the image (image contrast).<sup>10</sup>

The ratio of the output and input modulation is known as the modulation transfer function. MTF varies with spatial frequency. Generally reduces progressively from 100 percent at low spatial frequencies towards zero at higher frequencies.<sup>10</sup>

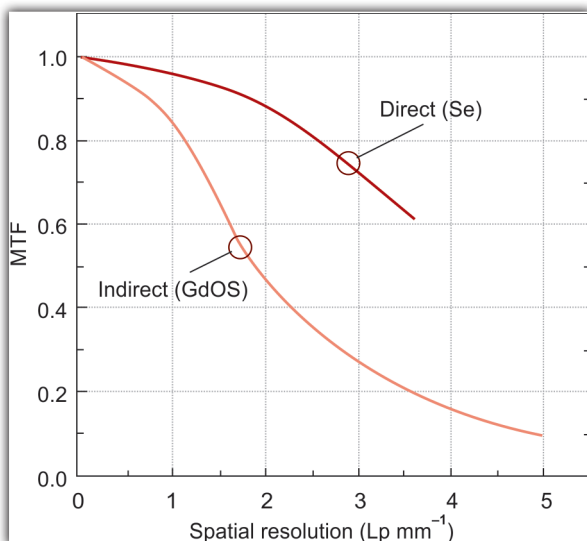


**Fig. 10** MTF of direct and indirect digital systems

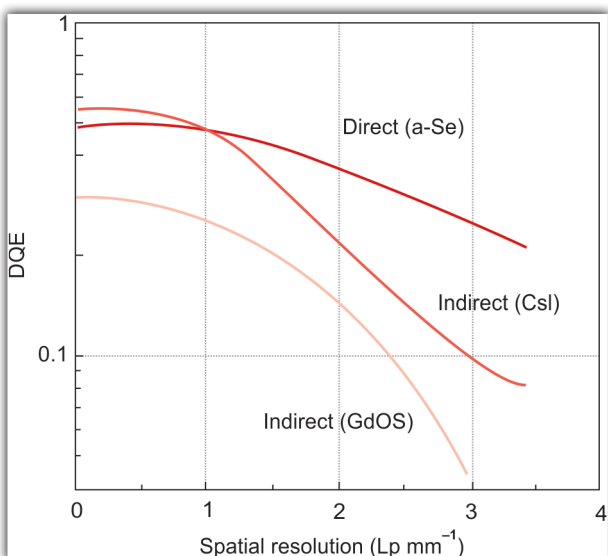


**Fig. 11** DQE as a function of spatial frequency for 3 detector systems at 70 kVp

### Detective Quantum Efficiency

Detective quantum efficiency (DQE) is one of the important physical variables related to image quality in radiography and refers to the efficiency of a detector in converting incident X-ray energy into an image signal. It is calculated by comparing the signal to noise ratio at the detector output with that at the detector input as a function of spatial frequency. DQE depends on radiation exposure, spatial frequency, modulation transfer function, detector material and quality (voltage and current) of the radiation applied.<sup>3</sup>

An ideal situation is 100 percent quantum detection and conversion efficiency. Three types of materials are used and they are classified into three categories:

1. Unstructured scintillators (e.g. gadolinium oxysulphide and barium fluorobromide)
2. Structured phosphors (e.g. Cesium iodide, cesium bromide)
3. Semiconductor direct detectors (e.g. Amorphous selenium).

Digital systems with structured phosphors or semiconductors can achieve good spatial resolution. However indirect TFT technology based systems are more dose efficient.

Detectors with higher DQE will require less radiation dose than the detectors with lower DQE for similar image quality or signal-to-noise ratio. Both MTF and DQE are depicted in the form of a graph as a function of frequency or spatial resolution in line pairs/mm<sup>3</sup> (lp/mm) (Fig. 10). Both are higher at low resolution and decrease with increasing spatial resolution.<sup>5</sup>

An ideal detector should have a DQE of 1 which means that all the radiation energy is absorbed and converted into image formation. However, in practice, the DQE of digital detectors is limited to about 0.45 at spatial frequency of 0.5 cycles/mm<sup>3</sup>. While the maximum reported DQE for film-screen and computed radiography are typically 0.15 to 0.25 under similar conditions (Fig. 11).<sup>11</sup>

Over the years, various methods for measuring DQE have been established. In 1999 the IEC62220-1 standard was established to improve the comparability of DQE measurements of digital X-ray imaging devices. The exposure level is measured at the detector surface with calibrated radiation meters after removing all protective parts including anti-scatter grid, the AEC chamber and other cover plates out of the beam. The IEC62220-1 standard will enable manufacturers to specify DQE values on the basis of an internationally accepted methodology. This helps users to compare detectors and imaging systems and to make optimal use of the detectors.<sup>12</sup>

### Radiation Exposure

Digital detectors besides providing better image quality have the potential for substantially lowering the patient exposure. Efforts have been made to optimize both image quality and exposure in digital radiography. The most obvious way of minimizing patient exposure is to greatly reduce the number of failed exposures and requisite additional images.

In contrast to storage phosphor systems in which the possibility of exposure reduction is limited, DR systems offer a significantly higher potential for general exposure reduction because of their far superior quantum efficiency. Various studies have concluded that flat-panel detectors achieve the best results in high image quality at lower doses, followed by other DR systems such as selenium drum and CCD-based systems.<sup>3,13</sup>

Use of CR for chest imaging leads to an increased in radiation dose, as storage phosphor plates are not suited for high KVP techniques. Moreover, storage phosphor plates are more sensitive to scatter, which makes the use of high ratio grids mandatory and so radiation exposure is increased.<sup>13</sup>

Studies show that digital system optimization is an important parameter in reducing patient dose. Hence technical requirements for digital systems should be set for achieving the same.<sup>13</sup>

### Newer Applications in CR

Newer technological advances in CR have been introduced to overcome some of the limitations of CR system such as cassette handling, long readout time of PSP plates, low DQE and poor resolution.

- Automated CR systems:** Efficiency of CR systems has been recently improved by reducing the readout time and by removing the step of cassette handling. The readout time of PSP plate is reduced to less than 10 sec by line scan lasers and photodiode detectors in automated CR systems. In these systems, the image data acquisition is totally automatic as there is no cassette handling.
- Newer structured phosphor for PSP plates:** Newer phosphors like cesium bromide having a structured needle-shaped configuration of crystals have been recently introduced which reduce light diffusion. They are also more efficient with an increased DQE.
- Mobile CR systems:** To save labor, time and improve workflow of critically ill patients requiring bedside X-rays, portable, compact CR systems have been introduced in 2007. These systems have a mobile X-ray unit with an integrated CR reader which does away with the physical transport of the cassette to the CR reader, hence image is available in less than 25 seconds.<sup>9</sup>

### Newer Applications in DR

A number of technological advancements have taken place in digital radiography in hardware as well as software applications (**Table 3**).

- Tomosynthesis:** In this technique multiple low dose exposures are given from various angles while the X-ray tube moves in an arc and the detector remains stationary. Multiple images with different focal zones can be created by addition of these low dose images after pixel shift. The images can be viewed singly or in a wire loop. An additional advantage of digital tomosynthesis compared to conventional tomography is that computer processing methods can be used to minimize the contribution of the blurred out of plane structures to the images deducted at each plane of interest.<sup>14</sup> It is considered useful in chest, IVU studies and mammography.<sup>9</sup>
- Dual energy imaging:** Dual energy radiography methods are used to generate separate images of bone and soft tissue structures from two exposures made using different radiographic techniques, i.e. using high and low kilo voltage technique.<sup>14</sup> It is particularly useful in chest radiography where the interference of ribs is removed from lung tissue. Dual energy techniques are most effective when both images are acquired simultaneously. Similar results are obtained with two exposures within a very short period of time. Though flat panel dual energy systems produce images with less noise, they are prone to artifacts from tissue motion occurring between the two exposures. Dual energy imaging is useful in chest radiography particularly in the evaluation of partially calcified nodules and pleural plaques.<sup>9</sup>
- Computer aided diagnosis (CAD):** They are important in early detection of cancer of the lung and breast. The suspicious areas are marked by the software for review by the radiologist. The main advantage of CAD is that it alerts the radiologist to avoid overlooking diagnostically significant findings.<sup>9</sup>
- Automatic image stitching:** This feature is useful when precise measurements in lengthy anatomical regions

**Table 3** List of select manufacturers of DR systems with details of their exposure indicator (EI)

Manufacturer	EI name	EI symbol	Units
Agfa	Log of median of histogram	1gM	Bels
Alara CR	Exposure indicator value	EIV	Mbels
Canon	Reached exposure value	REX	Unitless
Canon	EXP	EXP	Unitless
Carestream (formerly Kodak)	Exposure index	EI	Mbels
Fujifilm	S value	S	Unitless
GE	Uncompensated detector exposure	UD Exp	$\mu\text{Gy}$ air kerma
GE	Compensated detector exposure	CD Exp	$\mu\text{Gy}$ air kerma
GE	Detector exposure index	DEI	Unitless
Konica	Sensitivity number	S	Unitless
Philips	Exposure index	EI	Unitless
Siemens	Exposure index	EI	$\mu\text{Gy}$ air kerma

like the spine or lower limb are required. With use of the largest flat panel DR plates, i.e.  $43 \times 43$  cm, only a limited portion of the body can be imaged at a time. To overcome this problem of inability of studying the whole spine or entire lower limb, multiple sequential exposures at different patient positions are acquired in a patient who is absolutely still. Automatic stitching is then performed to reconstruct a larger composite image.

5. **Mobile DR:** It consists of a  $17 \times 14$  inch flat panel detector connected by a cable to a mobile X-ray system having a monitor. The high cost and fragility of the FPDs hampers the use of mobile DR system. On comparison with FSR system, a mobile DR system is not affected by the availability, storage, transportation and disposal of films and chemicals.
6. **Wireless FPDs:** A wireless portable DR system can transfer image data wirelessly to the DR system. It does not have any cables and does not interfere with surrounding machines. A  $17 \times 14$  inch image is ready within 3 seconds and allows radiography of difficult regions of the body like the axilla or the TM joint. Also, with wireless FPDs, radiography of a limb with limited mobility (flexed/having contractures) is possible.
7. **Fluoroscopy and radiography:** Real time digital imaging facilitates high quality radiography and fluoroscopy with up to 30 images/sec. The fluoroscopy feature is used in gastroenterology, urology and vascular applications.

### Exposure Indicator for Digital Radiography

In contrast to FSR, where visual features such as under/overexposure help in recognizing exposure errors, digital system lack in recognizing the same. As a result, the radiographer needs to monitor the exposure indicator (EI) associated with digital imaging system. Exposure indicators have been developed by most equipment manufacturers. The purpose of the EI is to allow the radiographer to know the level of exposure the receptor has received and thereby determine if the correct exposure technique for the image was used. It is important to note that EIs are not measures of radiation dose to the patient but records the level of exposure to the image receptor.

The exposure indicator varies among different manufactures, even having different names, symbols and units. Table 3 shows a list of select manufactures and details regarding their EI as of 2011.<sup>15</sup>

### ACR Practice Guideline for Digital Radiography

Radiographic examinations represent more than two-thirds of all radiologic examinations performed in both adults and children.<sup>16</sup> The Society for Pediatric Radiology in 2004 emphasized the need for ALARA Principle in digital imaging. The ACR developed a practice guideline of digital radiography in 2007 in "order to deliver optimal image quality at appropriate radiation doses so as to provide excellent

safety and care for patients undergoing digital radiography examination".<sup>15</sup>

### CONCLUSION

The future of radiography is digital and it is imperative that radiologists be familiar with the technical principles, criteria for image quality and radiation exposure issues with the various digital radiography systems that are currently available along with the technological advancements that are taking place.

### REFERENCES

1. Selman J. The fundamentals of X-ray and radium physics, 8th Edn. Charles C Thomas, 1994.
2. Indrajit IK, Verma BS. Digital imaging in radiology practice: An introduction to few fundamental concepts. IJRI. 2007;17(4): 230-6.
3. Körner M, Weber CH, Wirth S, Pfeifer KJ, Reiser MF, Treitl M. Advances in digital radiography: physical principles and system overview. Radiographics. 2007;27(3):675-86.
4. Cury TS, Dowdye JE, Murry RC. Digital radiography in Christensen's Physics of Diagnostic Radiology, 4th Edn. Lea and Febiger. 1990. pp.392-431.
5. Verma BS, Indrajit IK. Advent of digital radiography: Part I. IJRI. 2008;18(2):113-6.
6. Strickland NH. Picture archiving and communication system and digital radiology. In Grainger & Allison Diagnostic Radiology. A textbook of Medical Imaging, 5th Edn, Vol I: 3-30, 2008, Edited by Adam A, Dixon AK, Chruchill Livingstone.
7. Chotas HG, Dobbins JT 3rd, Ravin CE. Principles of digital radiography with large-area, electronically readable detectors: a review of the basics. Radiology. 1999;210(3):595-9.
8. Fischbach F, Freund T, Pech M, Werk M, Bassir C, Stoever B, et al. Comparison of indirect CsI/a:Si and direct a:Se digital radiography. An assessment of contrast and detail visualization. Acta Radiol. 2003;44(6):616-21.
9. Verma BS, Indrajit IK. Impact of computers in radiography: the advent of digital radiography, Part-2. IJRI. 2008;18(3):204-9.
10. Roberts PA, Williams J. Digital radiography in Farr's Physics for Medical Imaging (2<sup>nd</sup> edn), Saunders Elsevier. 2008;79:90.
11. Dowsett DJ, Kenny PA, Johnston RE. The digital image in The Physics of Diagnostic Imaging (2nd edn), International Thomson Publishing. 2006. pp.313-63.
12. Illers H, Buhr E, Hoeschen C. Measurement of the detective quantum efficiency (DQE) of digital X-ray detectors according to the novel standard IEC 62220-1. Radiat Prot Dosimetry. 2005;114(1-3):39-44.
13. Neofotistou V, Tsapaki V, Kottou S, Schreiner-Karoussou A, Vano E. Does digital imaging decrease patient dose? A pilot study and review of the literature. Radiat Prot Dosimetry. 2005;117 (1-3):204-10.
14. Flynn M. Technical advances in CR and DR part 2. Available from: [http://www.imagingeconomics.com/issues/articles/2004-04\\_16.asp](http://www.imagingeconomics.com/issues/articles/2004-04_16.asp) (Last accessed on 2008 April 25<sup>th</sup>)
15. Herrmann TL, Fauber TL, Gill J, Hoffman C, et al. Best practices in Digital Radiography. White Paper (American Society of Radiologic Technologists). 2012. pp.1-26.
16. Harmon R. Realizing the full benefit of digital radiography. Imaging Economics 2001. Available from: [http://www.imaging-economics.com/issues/articles/2001\\_12.20.asp](http://www.imaging-economics.com/issues/articles/2001_12.20.asp).

## Chapter

# 14

# Digital Mammography

*Smriti Hari, Chandrashekha SH, Surabhi Vyas*

## INTRODUCTION

Mammography is one of the most technically challenging areas of radiography, requiring high spatial resolution, excellent soft tissue contrast, and low radiation dose. In thicker and denser breasts, wide image latitude is also needed. Reported sensitivities of screening mammography range from 45 percent to 85 percent with performance suffering as parenchymal density increases.<sup>1</sup> Several studies have shown improved detection of cancer with digital mammography in younger women who have dense breasts.<sup>2,3</sup>

Although the digital technique has many similarities to screen film and many of the requirements for an optimal image are the same, such as correct compression and positioning, the digital mammogram is constructed in a different way from screen film images. Having an understanding of how the images are created and how different variables influence image quality is important to the radiologist for both diagnostic reasons and quality assurance purposes. New applications of digital mammography such as digital breast tomosynthesis (DBT), stereo mammography and contrast enhanced mammography are expected to further improve the diagnostic accuracy of mammography.

## DIGITAL MAMMOGRAPHY

Although screen-film mammography (SFM) produces images of extremely high spatial resolution, the analog system can only function within a narrow dynamic range; markedly reducing the degree of object contrast that can be depicted in the image.

For this reason digital platforms capable of mammographic imaging were developed. These digital systems have

allowed the functions of image acquisition, display, and archiving to be decoupled, thus allowing their individual optimization. The practical result of this implementation has been a significant increase in the dynamic range of contrast that can be captured in the mammographic image, potentially offsetting the effect of increasing breast density on the sensitivity of the examination. In digital mammography, the image is obtained in the same manner as in SFM, using a compression plate and an X-ray tube, with the screen-film cassette replaced by a digital detector.

## BASIC PHYSICS OF DIGITAL MAMMOGRAPHY

### Detectors

The first part of the digital imaging chain is the acquisition unit. From a technical point of view, the efficient use of the X-ray beam and the resultant quality of the image is dictated by the materials of the system and the method by which the X-ray beam information is recorded. There are several types of technology deployed in digital detectors.<sup>4</sup> Detectors are classified as either direct or indirect capture. In indirect capture, the energy from the X-ray beam is converted by an X-ray scintillator first into light and then into a digital signal. This is similar to how the image is produced with SFM. Charge couple devices (CCDs), photostimulable phosphors, and amorphous silicon are types of indirect digital detectors currently in use. Direct capture units do not have this light conversion step; instead the substrate used is a photoconductive material that is able to directly convert the X-ray photons into an electrical charge. Amorphous selenium detectors are direct capture as are crystal silicon detectors that use photon counting technology. Selenium is

an ideal material for a mammography detector, because of its high X-ray absorption efficiency, extremely high intrinsic resolution, low noise and a well-established manufacturing process.<sup>5</sup> With every alteration of the X-ray beam, noise is introduced into the images and information is lost; in theory then, direct capture units have the advantage of potentially using more of the primary beam than indirect systems.

Another approach to digital mammography is the computed radiography (CR) approach, which uses a photo-stimulable phosphor plate. The plate is used to absorb X-rays just as a screen-film cassette. However, rather than emitting light immediately after exposure through fluorescence, X-ray absorption causes electrons within the phosphor material to be promoted to higher energy levels within the crystal. The image is then read out by placing the screen in a separate reader and scanned with a laser beam, electrons are released, and higher-energy (blue) light is emitted in proportion to the X-ray exposure. The amount of blue light emitted and measured by an optical collecting system (photomultiplier tube). Currently, new detectors have size of 50 µm and read out from both sides. The major advantages of this technology are small detector-element size, ease of having multiple plate sizes, and relative lower cost. Problems with this system include inefficient light collection and scatter of laser light in the phosphor material resulting in loss of spatial resolution and increased noise.

### Spatial Resolution

All systems capture the exposure onto a digital matrix that is comprised of a grid of detector elements, or dels. The spatial resolution of a system is determined in large part by the size and spacing of the dels (dels are also called pixels and the distance between the center of 2 adjacent dels is called pixel pitch). The smallest structure that can be resolved by the detector turns out to be one that is twice the size of a del. This is called the Nyquist frequency of the detector.<sup>6</sup> So for a detector with a 70 µm pixel pitch, the smallest resolvable structure is 140 µm. In SFM, spatial resolution is defined by how many line pairs could be resolved per millimeter of film. Now, we must translate our understanding of spatial resolution to pixel pitch and dels. It so happens that half of the pixel pitch in millimeters is equal to the line pair resolution. So, for the same 70 µm detector, the line pair resolution would be  $0.5 \times 7 \text{ mm} = 3.5 \text{ line pairs/mm}$ . For comparison, screen-film systems have a requirement to have a minimum of 11 or 13 line pairs/mm depending on the orientation of the X-ray tube.

Pixel pitch is only part of the determination of spatial resolution as it is also dependent on the focal spot size, the spread of the signal in the detector, and motion. Each of these variables is evaluated by its modulation transfer function (MTF). The MTF is the percentage of the signal strength entering the system relative to the signal coming out

of the system, at varying frequencies and is a good measure of spatial resolution. In essence, the MTF simply describes how precisely any shape is transmitted through the system. Another way to think of MTF is that it describes how much of the original contrast is lost in the system for each exposure. Most systems have a nearly perfect MTF (of 1) for large shapes and a lower MTF as shapes become more fine. The MTF gives some but not all of the indication of system efficiency. The other important parameter is the detective quantum efficiency (DQE), which takes into account not only the spatial resolution (and thus considers pixel pitch and MTF) of a system but also the signal to noise ratio (SNR).<sup>7</sup> The DQE basically describes what percentage of the beam (or signal) produces an image versus how much is lost as noise in the system. Digital systems have higher DQEs than screen-film units and so direct-conversion systems offer the possibility of similar image quality at lower doses or improved image quality at the same dose as screen-film.

### Analog to Digital Units

Once the energy from the beam is captured in the detector, the signal is converted into an image. All detectors have a matrix into which the signal from the acquisition is stored. The matrix is divided into rows and columns of pixels (dels). As the X-ray energy is collected in the pixels, the information is stored as analog to digital units (ADUs). Essentially, each time an electron reaches a pixel, it is counted as an ADU. Therefore, the denser the patient tissue overlying anyone pixel, the lower the ADU count of that pixel. For each exposure, an ADU map is created on the matrix. This ADU map is converted into a gray scale image. The size of each pixel and the size of the matrix vary between equipment. As mentioned earlier, pixel pitch describes the distance from the center of one pixel to the center of the adjacent pixels. Currently available systems have pixel pitches of 50, 70 or 100 µm. Although there are detectable differences in the clinical images from these different pixel pitches, no study to date has definitively shown anyone of all the available units to be better for cancer detection than another.

Most systems have an automatic exposure control (AEC) that determines the optimal imaging parameters, such as kilovolt peak (kVp), and milliamps (mA). Unlike screen film mammography where the AEC is used primarily to control image brightness, the AEC in digital mammography is used mainly to ensure that the radiation exposure is optimized for appropriate SNR.<sup>8</sup> This feature works by having a very low-dose fast test exposure given to the patient before the diagnostic exposure which generates a test ADU map that allows the system to evaluate one or more areas for determination of the correct exposure. The AEC uses this information along with the compressed breast thickness to determine the correct exposure parameters.

## Processing Algorithms

To convert the digital signals captured during an exposure into a readable mammographic view, multiple types of processing algorithms are applied. The first category of processing is detector correction algorithms designed to remove any inhomogeneity's in the detector that may be perceived on the final image. Two examples are masking of dead pixels and flat-field calibration.

The second type of processing is used to generate a diagnostic image. These include thickness equalization (also called peripheral equalization) and contrast enhancement algorithms. Thickness equalization refers to a process whereby the areas of breast tissue containing high ADU counts, such as the subcutaneous fat and retroglandular fatty areas, are enhanced so that they can be easily seen at display. Contrast enhancement algorithms bring out the differences in ADU counts between adjacent pixels or groups of pixels by making those differences larger. This processing enhances calcifications and fine details like the spicules of a cancer and are meant to aid visibility because of the lower MTF of the systems for these high-frequency structures.

## Dynamic Range

The bit depth of a system describes how many shades of gray are available for viewing. Most digital systems collect 12 to 14 bits of data, but through processing and transfer some of this information is lost and so at display, only 8 to 10 bits of data are available to the radiologist. This is the dynamic range of the image.

## Comparison between Digital Mammograms and Film/Screen Mammograms

Screen-film cassettes used for mammography have a line-pair resolution of 18 to 21 lp/mm. Full-field digital mammography (FFDM) systems have spatial resolutions ranging from 5 to 10 lp/mm. In digital mammography systems, it is the size of the pixels that determines the spatial resolution. The pixel size for FFDM systems range from about 50 to 100 microns. As the pixel size of any digital imaging system is made smaller, the amount of data contained in the image rapidly increases, which increases system costs in terms of data storage, network bandwidth and display capabilities.<sup>9</sup>

The lower spatial resolution of FFDM systems compared to SFM is offset by the increased contrast resolution of FFDM systems. The contrast resolution of a system is described in terms of dynamic range. Screen-film has a limited dynamic range, which prevents visualization with equal clarity of all breast tissue regions from the chest wall to the skin line. As the digital system has greater dynamic range, it can record and differentiate subtle variations in contrast, that are not differentiated by screen film.

Unlike SFM, in which the image can not be manipulated after exposure and processing, FFDM images can be optimized after image capture by image postprocessing and adjustment of image display. The window width and window level for all digital images viewed with soft copy display on review workstations can be adjusted, changing the contrast and brightness of the images, respectively, as well as digitally magnifying images.

Another important difference between SFM and FFDM is that screen-film images have a linear relationship between the logarithm of X-ray exposure and film optical density only in the central portion of the characteristic curve. In FFDM systems, there is a linear relationship between X-ray exposure and signal over the entire dynamic range of the detector. Thus, digital images do not suffer contrast loss in underexposed or overexposed areas of the mammogram, and instead show similar contrast over the full dynamic range of the detector (**Fig. 1**). Digital mammography also eliminates the variability and noise added by film processing.

In terms of breast dose, FFDM has a mean glandular dose lower than, or comparable to, the radiation dose of SFM. The average single-view mean glandular dose for FFDM is 1.86 mGy, 22 percent lower than the average SFM mean glandular dose of 2.37 mGy.<sup>10</sup>

A number of studies have evaluated the performance of digital mammography compared to screen-film mammography for screening asymptomatic women for breast cancer. Early studies showed comparable or slightly worse results for FFDM compared to SFM.<sup>11,12</sup> Larger studies

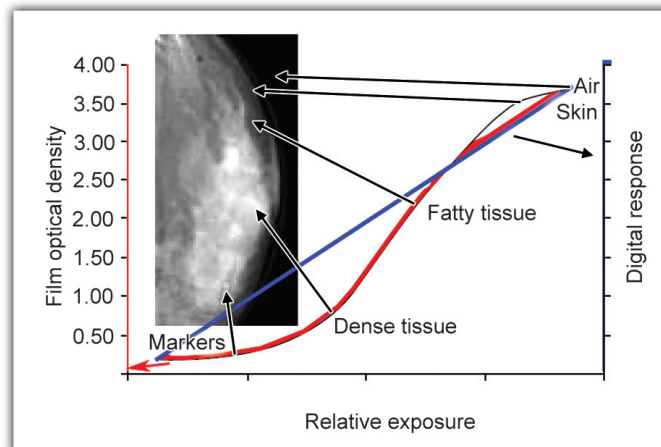


**Fig. 1** Typical response curves for screen-film mammography (SFM) and digital mammography. Screen-film images have a linear relationship between the logarithm of X-ray exposure and film optical density only in the central portion of the characteristic curve. In FFDM systems, there is a linear relationship between X-ray exposure and signal over the entire dynamic range of the detector leading to visualization with equal clarity of all breast tissue regions from the chest wall to the skin line

however showed some benefits of FFDM compared to SFM. The American College of Radiology (ACR) Imaging Network Digital Mammographic Imaging Screening Trial (ACRINDMIST), which included nearly 50,000 women, showed no difference overall but found that FFDM was a better screening tool than SFM for women under age 50, for premenopausal and perimenopausal women, and for women with denser breast tissue (BIRADS density categories 3 and 4).<sup>13</sup>

### Storage of Digital Images

The FFDM systems present specific technical challenges regarding the image size and the storage and archiving of digital images by computer systems. A digital image is a two-dimensional grid of picture elements (pixels), which is defined by its size and bit depth. The size of an image is its length in pixels multiplied by its width in pixels, and the bit depth is the number of shades of gray that can be displayed. The demand for high spatial resolution in mammography requires smaller pixel size and higher digitization. Therefore, FFDM image size depends on the digital detector size, the number of pixels per image, and the type of digitization. If the detected digital signals are digitized to 12 bits, it implies 212 or 4,096 signal values stored per pixel, and 14-bit digitization yields 214 or 16,384 signal values stored per pixel. Whether the system provides 12- or 14-bit digitization, a digital detector of  $N$  pixels requires  $2N$  bytes of storage. In general, a typical

screening mammography examination (two craniocaudal and two mediolateral oblique images) requires anywhere from 33 to more than 200 MB of computer storage space.

### Display of Digital Images

Various approaches are currently taken in displaying digital images. In the absence of soft-copy reading, digital images were printed on dry laser printers and read on high-luminance view boxes, similarly to SFM images. This approach does not allow the user to benefit from the full range of advantages available on digital displays. Soft-copy display on high-resolution (5-megapixel) computer monitors allows easy manipulations of resolution, contrast, and gray scale (**Fig. 2**). Workstations need to be fast as mammography screening and diagnosis requires efficiency (i.e. ability to review old studies, magnification of areas of concern and comparison of both breasts and different views).

The workstation should be entirely compatible with PACS. Integrated multimodality workstation should be linked to the general archival system, so that different imaging modalities can be correlated to arrive at final diagnosis.

### Artifacts

Artifacts in digital mammography can arise from a detector failure, a processing failure, corrupted calibration files, extraneous objects in between the X-ray target and detector,



**Fig. 2** Soft-copy display on high-resolution (5-megapixel) computer monitors allows easy manipulations of resolution, contrast, and gray scale

or a failure of the components such as the grid or the plate transporter in a CR unit. Aside from dust and debris on the surface of the detector or paddles, detector artifacts are the most commonly seen artifacts and include ghosting, dead pixels, and flat-field inhomogeneities. Ghosting is the result of latent charge remaining in the detector from previous exposures and is specific to and one of the weaknesses of using amorphous selenium direct detectors and photostimulable phosphor plates in CR imaging. Both substrates retain charge and need to be cleared. For the phosphor plates, the charge can generally be cleared by putting the plate through the cassette reader, which uses laser technology to clear it. For amorphous selenium, a flat field can be done and the detector recalibrated to overcome the ghosting or, in some instances, the detector must be replaced.

All digital detectors can have dead pixels. A few are of no clinical concern and they appear as bright white dots on the image. A row of dead pixels is seen as a straight thin white line. Many detectors are constructed as groups of arrays with associated amplifiers that are smaller than the matrix. These arrays are placed in the detector housing to create the matrix. Occasionally, 1 array may appear different than the adjacent ones and this background inhomogeneity can be visible to the radiologist.<sup>14</sup> If an exposure is done at high dose or a display has little dynamic range, these arrays are visible in the background of the image. A flat-field image using an acrylic slab will identify these and a flat-field recalibration will generally correct it.

Processing algorithms occasionally fail and this can create artifacts. Typically, these are seen as dark straight lines in the images. Occasionally, when the quality control technologist performs the unit calibration, the collimator is not properly aligned and this will produce either a dark or white vertical band at the chest wall side of the image. To eliminate this artifact, the system must have a flat-field recalibration after the collimator position is corrected.

Because mammography evaluates calcifications of 300  $\mu\text{m}$  on average, detectors are built to have a maximal spatial resolution higher than that and the resultant mammographic images are large. For example, if a detector has a pixel pitch of 50  $\mu\text{m}$ , the matrix can contain more than 20 million pixels. Mammography display monitors typically have only 5 million pixels, and so the mammogram at full resolution will not fit in the field of view for display in most cases. As a result, the workstation has the requirement of intelligently displaying the mammograms with different sampling of the data so that the radiologist can perform the tasks of comparison to prior images and close inspection of the current study. Most workstations have the ability to create hanging or display protocols to accomplish this. There are only a few display modes used for all protocols, and they are called fit to viewport, same size, true size, view actual pixels, and magnification. The radiologist chooses the order of these modes when building a protocol.

Fit to viewport is the mode whereby adjacent pixels' ADUs are averaged together and displayed as 1 ADU to fit the image onto a portion of the monitor. Same size is a variation of fit to viewport whereby the workstation takes into account the different matrices from different manufacturers or different paddles (i.e. 100  $\mu\text{m}$  vs 70  $\mu\text{m}$  or small detector vs large detector from the same vendor) and scales all the images to look the same size to the radiologist. This allows for much more efficient evaluation of change over time. These modes are used for comparison of current and prior studies and comparison of right and left images. The workstation should readily display the functional pixel pitch of display and what percentage that resolution is compared with both true size and view actual pixels. True size is the mode that displays the true physical size of the breast and is useful when planning for surgery or stereotactic biopsy or when printing hard copy for comparison with screen-film mammography. The mode view actual pixels displays each acquired pixel on one display pixel. This is the mode that gives full-resolution images and is best for evaluation of calcifications and subtle mass margins. The mammogram is almost always bigger than the monitor in this mode so either manual panning of the image or some predetermined stepwise display of the image is needed to see the entire breast. Zooming the image with optical magnification at the workstation can be done but this is a mathematical up interpolation of data and does not provide more information to the image; it is just making the image larger for ease of viewing and at the same time introduces some noise to the image. Air gap magnification (using a magnification stand exactly like the technique used for SFM) allows a small portion of the breast to be sampled by the detector increasing spatial resolution, because more pixels in the detector are used to sample a smaller area of the breast. For this reason magnification has been shown to be beneficial for evaluating calcifications with digital mammography and should still be used.<sup>15</sup>

## ■ APPLICATIONS OF DIGITAL MAMMOGRAPHY

The development of digital breast imaging does not constitute an end point but rather represents the beginning of a new era for mammography: an era in which the digital platform serves as the basis for development of innovative radiographic methods of imaging the breast, innovations that were not possible on the analog platform.

### Computer-aided Detection and Computer-aided Diagnosis

Computer-aided detection (CADe) and computer-aided diagnosis (CADx) are computer software systems that are designed to review mammograms for bright clustered specks and converging lines, which represent microcalcifications and spiculated masses, respectively. These programs were developed to help radiologists search for signs of cancer against the complex background of dense breast tissue.

The CAD marks potential abnormalities directly on the image displayed on the workstation (**Fig. 3**). The radiologist interprets and analyzes the marked findings, and each finding is dismissed as insignificant or further worked up. It thus decreases the chances of overlooking these abnormalities.<sup>16</sup> It acts as second opinion to the experienced radiologists and may help inexperienced radiologists.<sup>17</sup> The CADe refers to those algorithms that simply mark areas to be reviewed without providing any information regarding likelihood of malignancy. The CADx algorithms go a bit further and actually convey some additional information through variable sizing of marks and lesion metrics, such as likelihood of malignancy of similar lesions that were used to train the system. These marking methods are meant to be adjunctive to the radiologist's interpretation and not intended to cause the radiologist to dismiss any lesion that was seen without the aid of the CAD marks.

### Dual-energy Subtraction Mammography

Dual-energy subtraction mammography is based on the principle that if exposures are taken with both high and low operating potentials, using the same radiographic projection, some breast structures will exhibit greater absorption of low-energy compared with high-energy photons. Thus, assuming that there is no patient motion between exposures, one digital image can be electronically subtracted from the other causing most structures (those that do not exhibit differential absorption) to cancel out completely.<sup>18</sup> It takes advantage of the fact that the change in attenuation is greater for calcifications than for soft tissues when the kVp is altered from high energies to low energies. Dual energy mammography requires a modified mammographic machine that is capable of producing normal mammographic images and images obtained at higher energy (45–50 kV).

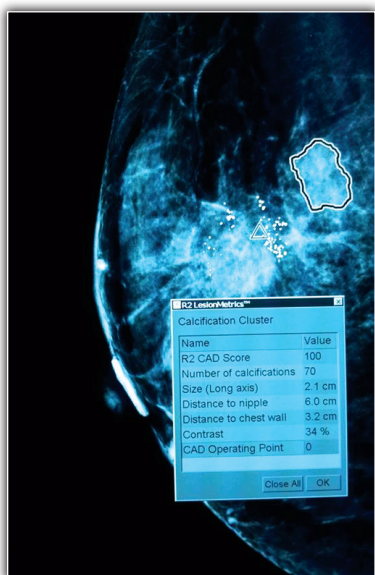


**Fig. 3** CAD marks potential abnormalities directly on the image displayed on the workstation

### Contrast-enhanced Digital Mammography

The advantage of contrast enhanced digital mammography is to obtain the functional contrast information attributed to the malignant neovascularity directly linked to high-quality anatomic information.<sup>19</sup> A precontrast image is obtained, and then images are obtained following the intravenous administration of the contrast agent. By subtracting the two, only the contrast image remains, making the cancer more evident because of its nest of neovascularity.<sup>19</sup> There are two main methods described for contrast enhanced digital mammography; serial examinations over time and dual energy imaging. Use of iodinated contrast material and modified digital mammography units are required for the technique. Before contrast injection, a noncontrast image is obtained. Next, series of images are taken after injecting the contrast. The enhanced images are subtracted from the baseline image leaving areas of enhancement visible with simultaneous construction of enhancement curves. The major problem with this study is the ability to image the breast in a single projection at a time. For this reason, dual energy methods have been developed to allow imaging of both breasts with a single contrast administration. After injecting the contrast, the patient is subjected to two pair of exposures, one at low kilovolts and other at high kilovolts. A subtraction image is produced that highlights areas of iodine concentration or enhancement. The mammographic image at low energy can be used as a routine gray scale mammographic interpretation. This technique does not allow for kinetic assessment of enhancement curves.

### Digital Breast Tomosynthesis

Digital breast tomosynthesis (DBT) has been developed to improve detection and characterization of breast lesions especially in women with dense breasts. In this technique, multiple projection images are reconstructed allowing visual review of thin breast sections offering the potential to unmask cancers obscured by normal tissue located above and below the lesion.

#### Technique

In conventional digital mammography, a compressed breast is exposed to ionizing radiation. The X-ray tube is stationary, the breast is stationary, and the detector is stationary. The image that is produced is a two-dimensional representation of three dimensional space. In DBT, the X-ray tube is moved through a limited arc angle while the breast is compressed and a series of exposures are obtained (**Fig. 4**). If there is a 45° arc of movement and an exposure is taken every 3°, there are 15 individual exposures. These projection image datasets are reconstructed using specific algorithms. The radiologist is presented with a series of slices (typically 1mm thickness) through the entire breast that are read at a workstation similar to review of a computed tomography or magnetic resonance imaging study.

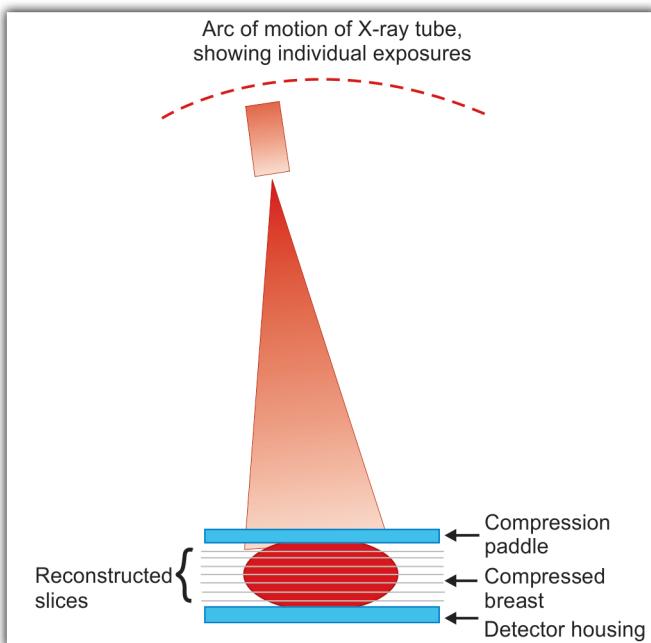
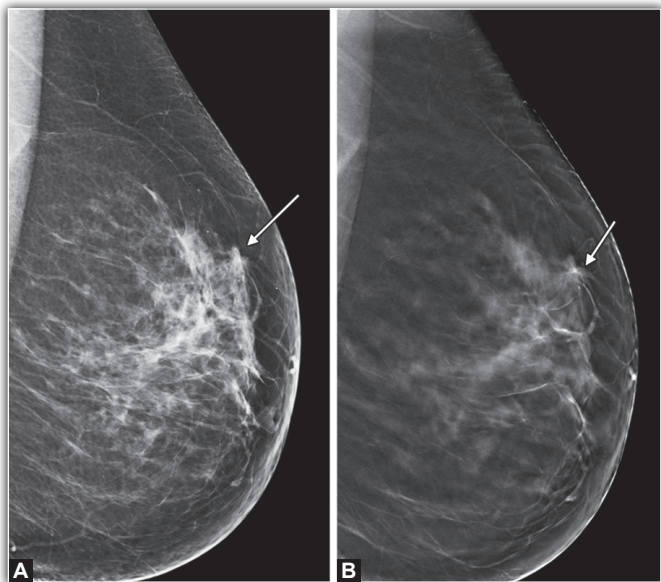


**Fig. 4** Digital breast tomosynthesis: The X-ray tube moves through a narrow arch while the breast is in compression. A series of exposures results in multiple projection image datasets. Each exposure is a fraction of the dose of a conventional mammographic view. Projection image datasets are reconstructed into multiple thin-slice images (e.g. 1 mm thickness) for interpretation by the radiologist



**Figs 5A and B** Conventional film screen MLO mammography view (A) of a patient with invasive ductal cancer. The cancer, although vaguely apparent on the conventional mammogram (arrow), is much better visualized on the 1-mm thick tomosynthesis image (B) (arrow). Note the clarity of the spicules and the separation from surrounding tissue

Several manufacturers have applied different methods to develop and perform tomosynthesis. Engineering constraints include total radiation dose, image time, patient motion, detector performance, detector motion, and ability to image the entire breast. Manufacturers vary the arc of movement (typically 11–60°), the number of individual exposures, use of continuous or pulsed exposure, stability or movement of the detector, exposure parameters, total dose, effective size of pixels, X-ray source/filter source, single or binned pixels, and patient position. The dataset can be reconstructed for the radiologist to read by displaying different thicknesses. For example, if a 60 cm compressed breast is reconstructed at 1-mm thickness, there will be 60 slices for the physician to review. If the images are reconstructed at 0.5 mm thicknesses, there will be 120 images to be reviewed. If the images are reconstructed at 10 mm thick slabs using maximum intensity projection (MIP) thick slices, there will be 6 images to review.

#### Radiation Dose

A major consideration for DBT manufacturers and regulators is the balance between dose and image quality. Because image quality tends to be directly related to dose, compromises are necessary. All manufacturers have produced equipment with dosing parameters less than the current FDA limit of 300 mrad

per exposure. The common conventional mammographic dose per view is 150 to 250 mrad.

#### Potential Benefits of Clinical Breast Imaging with Tomosynthesis

The potential benefits of DBT include improvement in screening sensitivity, improvement in lesion size at detection, improvement in characterization, and decrease in recall rates. The DBT may be useful in both the screening and diagnostic evaluation. Neither has been proved in randomized controlled trials. In theory DBT, with thin section display, should allow superior detection of lesions that historically have been masked by overlying tissue (**Figs 5A and B**). The primary benefit of DBT is expected to be for noncalcified mammographic findings such as masses, asymmetries, and distortion.

Although many regard tomosynthesis as a technique for dense breast tissue, it may also have significant applications for those patients with nondense breasts by allowing detection of smaller lesions. The DBT also offers the possibility that characterization or specificity may be increased by better assessment of detected lesions and reduction in false-positive recalls. This is because the margin of a mass or character of an asymmetry may be better visualized. Malignant lesions may appear more malignant and benign lesions more benign. If these concepts are borne out, DBT may allow for improved

sensitivity coupled with improved specificity. Diagnostic evaluation of potential masses and asymmetries found by screening mammography could also be a DBT function.

### Clinical Tomosynthesis Evaluations

Several early experimental clinical DBT studies for masses have generally shown good patient acceptance, physician preference for DBT images, improvement in sensitivity, improvement in characterization, and often longer physician reading times<sup>20-22</sup>.

There is limited literature regarding clinical microcalcification assessment by DBT for detection and characterization. Although the in-plane resolution of DBT is good, out-of-plane resolution is poor. Because calcifications may be dispersed in three-dimensional space, viewing thin DBT images may make perception of calcification clusters difficult as only 1 or 2 may be seen on a slice. To overcome this issue, manufacturers have developed MIP images consisting of thick slices such as 1 to 2 cm for reviewing calcifications.

### Teleradiology Applications

Telemammography can become very effective with digital mammography, since it allows underserved and geographically remote populations to access the latest in breast care. Electronic transfer of digital images to remote viewing sites can be accomplished almost as rapidly as between the display workstation and computer storage. Radiologists who work in several different hospitals can monitor and interpret examinations that are carried out in nearby, or distant locations. Mammography screening in mobile units can be made more efficient, not only by eliminating the need to transport films from the site of examination to the site of interpretation, but also by permitting interpretation while patients are still available for repeat or additional examination. In addition, teleradiology can be used to facilitate second opinion interpretation by providing rapid transfer of images to the second reader's display monitors.

### Stereotactic Breast Biopsy

A full-field digital mammography detector can also be used for diagnostic and stereotactic-breast-biopsy imaging. This enables a multi-purpose system ideal for both screening and follow-up imaging tasks.

### Stereo Mammography

Acquisition of binary images, separated by a few degrees, allows the display of mammograms in a stereo fashion, to facilitate the visualization of the three-dimensional characteristics of mammographic features.<sup>23</sup> Computer display of stereo images requires either glass synchronized to

display frame updates, or polarizing glasses. This technique has shown promise in improving three-dimensional depth discrimination in mammograms.

### CONCLUSION

Full-field digital mammography offers the potential for significant advances in breast cancer diagnosis, including lower radiation dose with improved cancer detection rates. Transition from conventional film screen mammogram to digital mammogram is quite expensive but is compensated by numerous benefits. Radiologists face unique challenges when transitioning to digital mammography. The advanced applications and future developments available with digital mammography hold great promise for the improved early diagnosis and screening of breast cancer.

### REFERENCES

1. Mandelson MT, Oestreicher N, Porter P. Breast density as a predictor of mammographic detection: comparison of interval- and screen-detected cancers. *J Natl Cancer Inst.* 2000;92:1081-7.
2. ED Pisano, C Gatsonis, E Hendrik. Diagnostic performance of digital versus film mammography for breast-cancer screening. *N Engl J Med.* 2005;353:1773-83.
3. S Vinnicombe, S Pinto Pereira, VA McCormack, et al. Full-field digital versus screen-film mammography: comparison within the UK breast screening program and systematic review of published data. *Radiology.* 2009;251:347-58.
4. CJ D'Orsi, MS Newell. Digital mammography: clinical implementation and clinical trials. *Semin Roentgenol.* 2007;42:236-42.
5. Pisano ED, Yaffe YJ. Digital Mammography. *Radiology.* 2005; 234:353-62.
6. A Noel, F Thibault. Digital detectors for mammography: the technical challenges. *Eur Radiol.* 2004;14:1990-8.
7. E Samei, NT Ranger, A Mackenzie, et al. Detector of system? Extending the concept of detective quantum efficiency to characterize the performance of digital radiographic imaging systems. *Radiology.* 2008;249:926-37.
8. ED Pisano, MJ Yaffe. Digital mammography. *Radiology.* 2005;234:353-62.
9. Rowlands JA, Zhao W, Blevis IM, et al. Flat-panel digital radiology with amorphous selenium and active-matrix readout. *Radiographics.* 1997;17:753-60.
10. Hendrick RE, Pisano ED, Averbukh A, Moran C, Berns EA, Yaffe MJ, Herman B, Acharyya S, Gatsonis C. Comparison of acquisition parameters and breast dose in digital mammography and screen-film mammography in the American College of Radiology Imaging Network Digital Mammographic Imaging Screening Trial. *AJR Am J Roentgenol.* 2010;194(2):362-9.
11. Lewin JM, Hendrick RE, D'Orsi CJ, et al. Comparison of full-field digital mammography with screen-film mammography for cancer detection: results of 4,945 paired examinations. *Radiology.* 2001;218:873-80.
12. Skaane P, Young K, Skjennald A. Population-based mammography screening: comparison of screen-film and full-field digital mammography with soft-copy reading- Oslo I study. *Radiology.* 2003;229:877-84.

13. Pisano ED, Gatsonis C, Hendrick E, Yaffe M, Baum JK, Acharyya S, Conant EF, Fajardo LL, Bassett L, D'Orsi C, Jong R, Rebner M. Digital Mammographic Imaging Screening Trial (DMIST) Investigators Group. Diagnostic performance of digital versus film mammography for breast-cancer screening. *N Engl J Med.* 2005;353(17):1773-83.
14. RS Ayyala, MA Chorlton, RH Behrman, et al. Digital mammographic artifacts on full-field system: what are they and how do I fix them? *Radio Graphics.* 2008;28:1999-2008.
15. MJ Kim, EK Kim, JY Kwak. Characterization of microcalcification: can digital monitor zooming replace magnification mammography in full-field digital mammography? *Eur Radiol.* 2009;19:310-7.
16. Birdwell RL, Ikeda DM, O'Shaughnessy KF, et al. Mammographic characteristics of 115 missed cancers later detected with screening mammography and the potential utility of computer-aided detection. *Radiology.* 2001;219:192-202.
17. Karssemeijer N, Otten JD, Verbeek AL, et al. Computer-aided detection versus independent double reading of masses on mammograms. *Radiology.* 2003;227:192-200.
18. Lewin JM, Isaacs PK, Vance V, Larke FJ. Dual-energy contrast-enhanced digital subtraction mammography: feasibility. *Radiology.* 2003;229(1):261-8.
19. Jong RA, Yaffe MJ, Skarpathiotakis M, et al. Contrast-enhanced digital mammography: initial clinical experience. *Radiology.* 2003;228:842-50.
20. Poplack SP, Tosteson TD, Kogel CA, et al. Digital breast tomosynthesis: initial experience in 98 women with abnormal digital screening mammography. *Am J Roentgenol.* 2007;189: 616-23.
21. Andersson I, Ikeda D, Zackrisson S, et al. Breast tomosynthesis and digital mammography: a comparison of breast cancer visibility and BIRADS classification in a population of cancers with subtle mammographic findings. *Eur Radiol.* 2008;18:2817-25.
22. Gur D, Abrams GS, Chough DM, et al. Digital breast tomosynthesis: observer performance study. *AJR Am J Roentgenol.* 2009;193:586-91.
23. Goodsitt MM, Chan HP, Hadjiiski L. Stereomammography: evaluation of depth perception using a virtual 3D cursor. *Med Phys.* 2000;27(6):1305-10.

# Fluoroscopy and Digital Subtraction Angiography

Deep Narayan Srivastava, Madhusudhan KS

## OVERVIEW

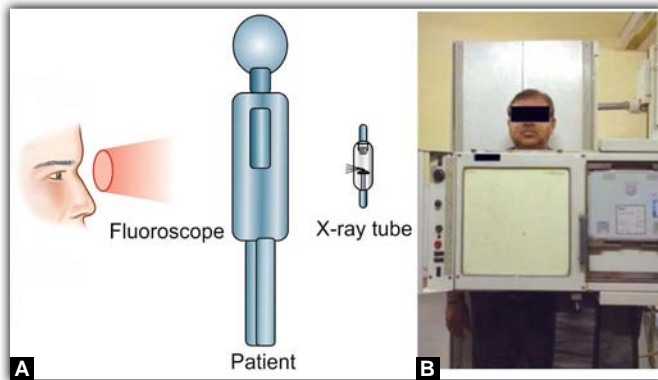
Fluoroscopy is an imaging technique which uses X-rays for real-time visualization of internal organs or structures of the body. A fluoroscope is used for the same which in its basic form consists of an X-ray source and a fluorescent screen between which patient is positioned. From its initial use in the early 20<sup>th</sup> century, the fluoroscope has undergone significant technological improvements with current fluoroscopic machines using larger sized flat panel detector with digital processing.<sup>1</sup> Digital subtraction angiography (DSA) is a fluoroscopic technique in which real-time subtraction of precontrast images is done for better visualization of contrast filled structures.<sup>2</sup> Fluoroscopy is used in various diagnostic and therapeutic procedures, including assessment of dynamic processes such as swallowing and cardiac function, provision of road map for positioning vascular or nonvascular catheters, evaluation of vessels using contrast in DSA and detection of gastrointestinal abnormalities in barium studies. For safe and efficient use of fluoroscopy it is essential to have adequate knowledge of these equipments and newer developments. The chapter describes principles of fluoroscopy, early fluoroscopic equipments and newer advances in fluoroscopic imaging along with safety issues.

## FLUOROSCOPY

The term fluorescence means emission of light by a substance when it is exposed to electromagnetic radiation. Fluoroscope consists of this substance in the fluorescent screen which is stimulated by X-rays. The fluorescent substance used in the initial days of fluoroscopy was barium platinocyanide which produced very dim images. Also, the substance was unstable.

This substance was later replaced by cadmium tungstate and subsequently by zinc cadmium sulfide which though increased image brightness but still needed dark room.<sup>1</sup> Fluorography means serial acquisition of higher quality images for diagnosis and documentation.

In its early days, fluoroscopy was performed in a dark room (dark room fluoroscopy) as the light emitted by the fluorescent screen was dim. The radiologist had to adapt his/her eyes in the room for some time to enhance visualization. The image emitted by the screen was directly viewed by the examiner (**Figs 1A and B**). The performance of the technique was mainly affected by the limitations of human eye at low light levels which reduced spatial and contrast resolution of the image viewed. This shortcoming was removed by image



**Figs 1A and B** Dark room fluoroscopy. (A) Shows early hand held fluoroscope used in dark room for direct visualization. (B) Is an improvised dark room fluoroscope fixed to the table, but movable in all four directions. Here, X-ray tube is under the table

intensifier (II) which was introduced in 1953.<sup>3</sup> The II amplified the brightness of the light image for improved visualization. The major problem with the initial II was small viewing angle which needed the radiologist to move his/her position frequently as and when the II moved (**Fig. 2**). This limitation was overcome with the development of video camera for image viewing and displaying it on monitor (**Fig. 3**). Today, the II has larger size (40 cm) compared to the older ones (15 cm). With the development of digital technique, there is improvement in the performance of the imaging chain. The latest addition is the introduction of flat panel detector which has replaced the II and video camera.

The main advantage of fluoroscopy over radiography is the use of low tube currents, in the range of 1 mA to 6 mA compared to 500 to 800 mA for routine radiography. Typical exposure rate of fluoroscopy for an average adult is in the range of 10 to 30 mGy/min (compared to a chest radiograph -0.3 mGy/30 msec or 600 mGy/min). But longer times may increase the risk of radiation injury. Hence, highly sensitive imaging receptors are needed to detect such low photon flux.

### Components of Fluoroscopic System

The typical fluoroscopic imaging chain consists of a generator, X-ray tube, collimators and filters, grid, image intensifier and video camera system (**Fig. 4**). The generator, X-ray tube, collimator and grid are similar to radiography system with few differences which are described here.

The generator used for fluoroscopy is similar to that used for radiography with an additional circuit for fluoroscopic procedure.<sup>4</sup> High frequency generator with faster switching is preferred due to its best exposure reproducibility (beneficial for DSA).

The X-ray tube has two focal spots: small (0.3 to 0.6 mm) and large (1.0 to 1.2 mm). Small focal spot is used for fluoroscopy as it provides sharp images. For radiographic exposure, either of them can be used. The main additional feature in the tube used for fluoroscopy is high heat capacity (about 700 kHU) which is needed for prolonged X-ray exposure.<sup>5</sup> This is achieved by high speed anode rotation (above 10000 rpm), oil heat exchanger and cooling fans in the housing assembly and grid controlled exposures. Further, in the modern imaging system, the tube heat loading is constantly monitored which regulates exposure if there is tube overheating. Mobile C-arm systems incorporated with X-ray tubes having fixed anode contain single or dual focal spots (0.5 mm for fluoroscopy and 1.8 mm for radiography) and lower heat capacity (30 to 50 kHU). Modern C-arms have rotating anode for longer fluoroscopy procedures.

Collimators and filters are used to reduce unwanted radiation. One of the filters which needs special mention here is 'equalization filter'. It is used to reduce glare near the edges of the patient. They are partially radiolucent and made of lead-rubber or lead-acrylic material (**Figs 5A and B**). To

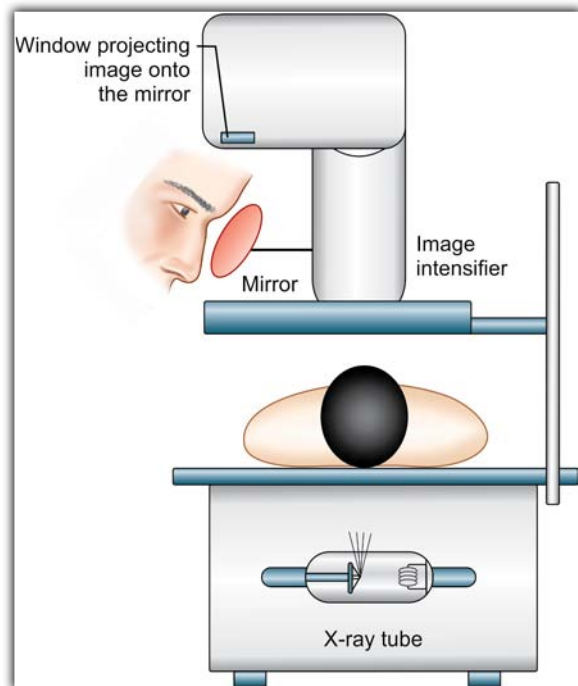


**Fig. 2** First fluoroscopy machine with image intensifier. The image formed is intensified and reflected on to the mirror for visualization by the operator

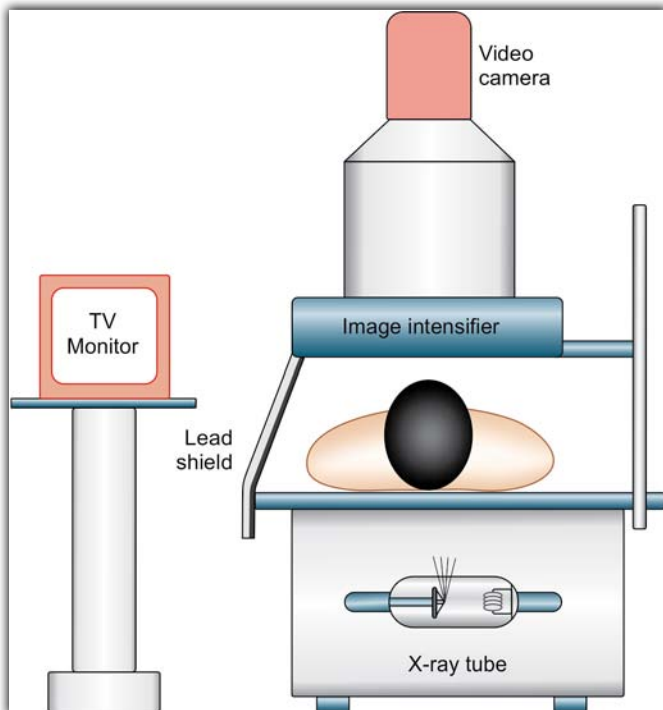


**Fig. 3** Image intensifier fluoroscopy system with optical coupling system, video camera and television monitor display

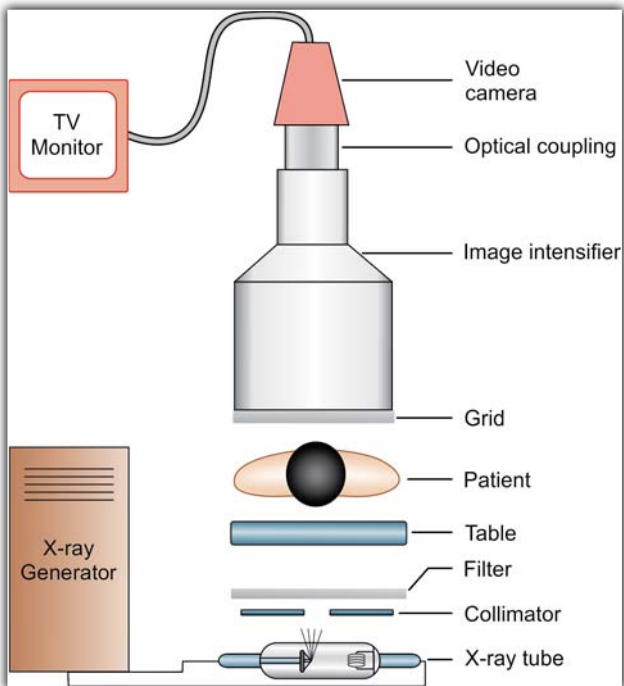
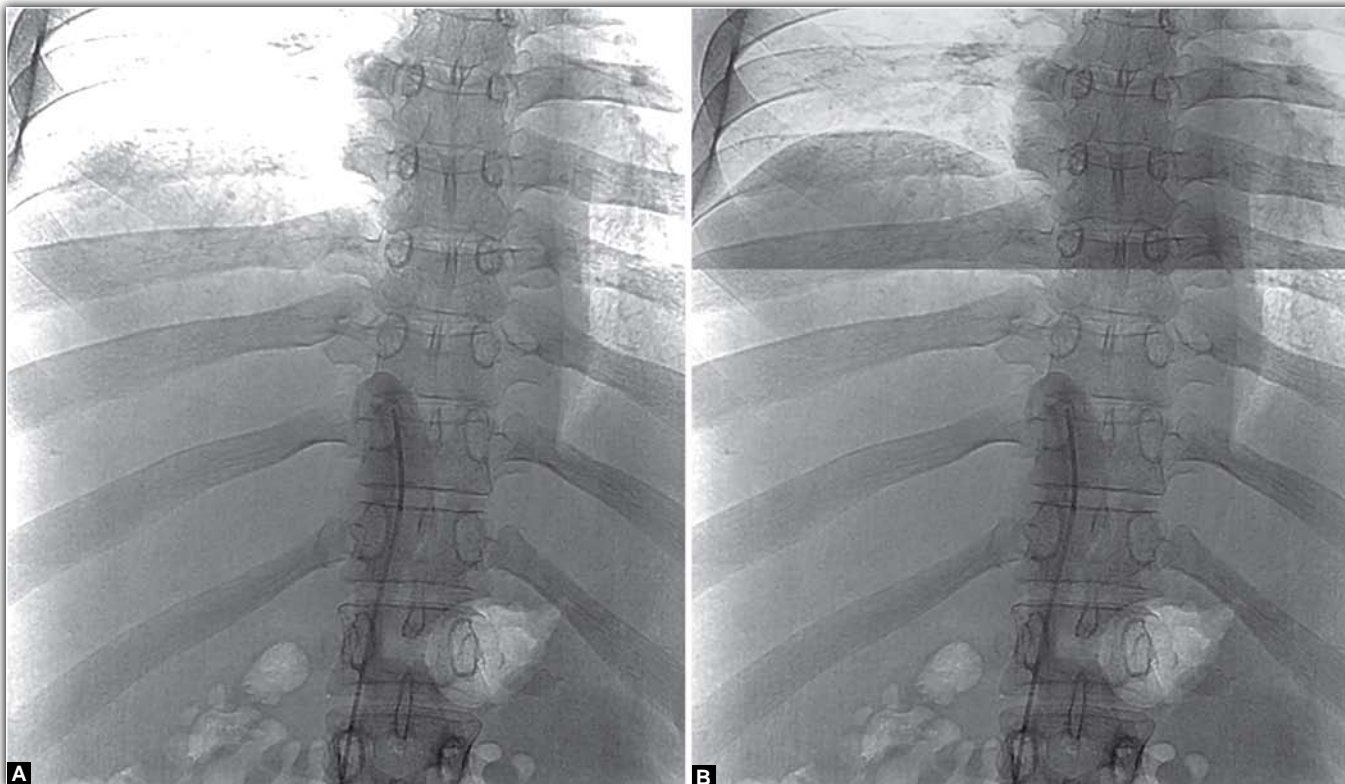


**Fig. 4** Components of image intensifier fluoroscopy system

attenuate low energy X-rays (beam hardening), copper filters are preferred over aluminium as they are more effective in filtering low energy X-rays. The grids used in fluoroscopy are of lower ratios (6:1 to 10:1) compared to that used for radiography (8:1 to 16:1) to limit increase in radiation dose. Some systems provide grids which can be removed when small part of the body is examined or small FOV is used and when II is positioned at a distance from the patient (for access for intervention or difficult anatomical part) which results in air gap. These modes produce less scatter and grid can be avoided to reduce patient radiation dose.

Conventional continuous fluoroscopy involves continuous production of X-rays at low mA and images are acquired at 30 frames per second (fps). Pulsed fluoroscopy (PF) is a mode of operation in which X-rays are generated in pulses (2.5 to 30 fps) by two methods – generator controlled and tube controlled (**Fig. 6**). In conventional generator controlled PF the current is supplied to the X-ray tube in short pulses lasting 3 to 10 milliseconds. However, due to the presence of long high resistance cables between the generator and the tube the pulse has a bell shaped curve (slow rise to peak and fall to zero; **Fig. 7**). This increases the low energy X-rays which results in reduced image quality and no significant decrease in radiation dose, a limitation overcome by grid controlled PF. In grid controlled PF, a negative charge is applied between



**Figs 5A and B** In a patient with inferior venacavogram, veiling glare is seen in the regions of lower lungs affecting the visualization of diaphragm and subdiaphragmatic regions (A). After placement of equilibration filter, the glare is significantly reduced with better visualization of diaphragmatic outline (B)

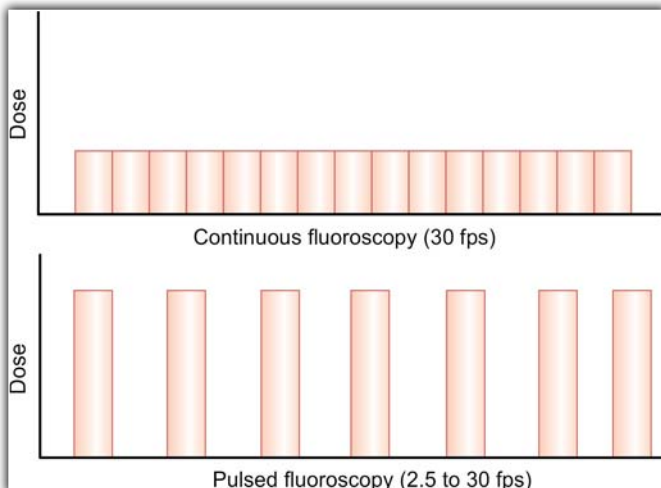


**Fig. 6** Schematic diagram comparing continuous and pulsed fluoroscopy. Although there is increase in dose per pulse in the latter to maintain same image details, overall radiation dose is reduced

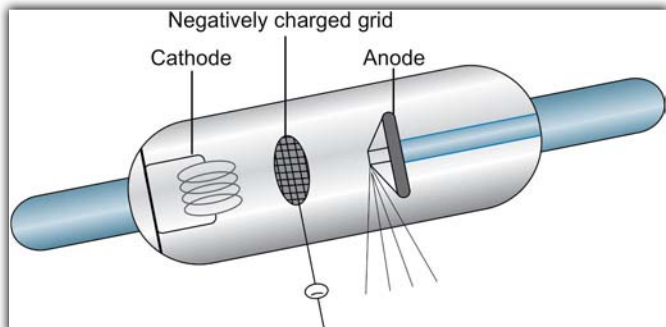


**Fig. 8** Grid controlled X-ray tube shows negatively charged grid between cathode and anode which can be switched on and off to control incidence of electrons on anode

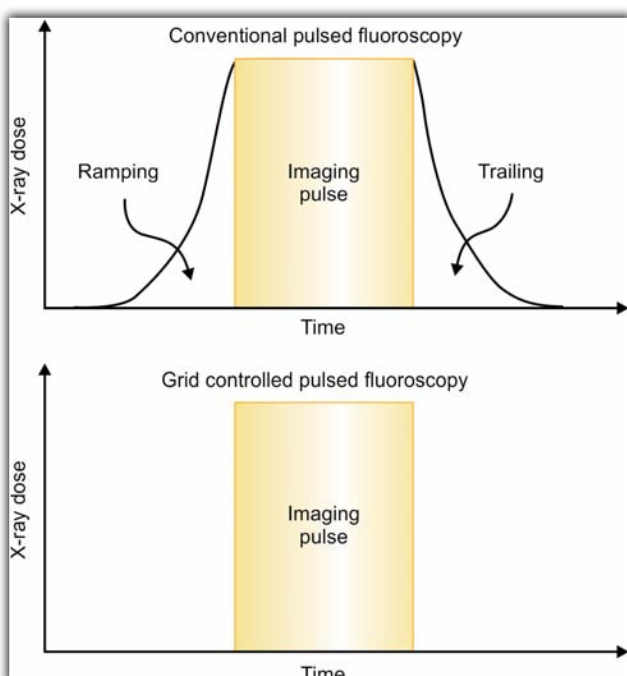


**Fig. 7** The pulsing in conventional PF shows initial ramping and terminal trailing leading to generation of low energy X-rays which increases radiation dose. Grid controlled PF shows no such effect

cathode and anode of X-ray tube in a pulsatile manner which regulates incidence of electrons on anode (**Fig. 8**). It produces uniform pulses without any low energy photons (**Fig. 7**). The advantages of pulsed fluoroscopy are improved temporal resolution (which reduces motion blur) and reduced radiation dose. The disadvantages include increase in noise perception, flicker effect and reduced visibility of fine catheters/guide wires. The flicker effect may be reduced

by interleaved image display where gap between two frames are filled by previous images from memory. The reduced radiation dose with pulsed fluoroscopy happens only when mAs remains constant. But often, vendors try to increase the mAs to compensate for increase in noise that occurs with reduced pulse rate. This may result in only modest decrease in radiation dose.

### Image Intensifier

The main purpose of image intensifier is to amplify the brightness of the fluoroscopic image, thus obviating the need of dark adaptation by the radiologist. Two important functions of II are fluorescence (conversion of X-ray photons into visible light) and light signal amplification.<sup>6</sup> The basic elements that make an image intensifier are contained in a vacuum case and include input phosphor, photocathode, focussing lenses, anode and output phosphor (**Fig. 9**). The vacuum case itself is covered by a protective metallic housing which is made of lead to absorb scatter radiation, mu-metal to protect electrostatic lenses from external magnetic forces and an outer aluminium shell. This aluminium shell also covers and protects the input window of the II.

### Input Screen

This consists of input window, supporting layer (of aluminium), input phosphor and photocathode. Input window is a part of the vacuum case of II. It is convex in shape and is made of 1 mm thick aluminium. The convex shape reduces II to patient distance and increases field of view. The support layer for input phosphor and photocathode is thin enough to allow all the X-rays to pass through.

The main function of input phosphor is to convert X-ray photons into light photons. In modern equipments, input phosphor is made of cesium iodide-sodium (CsI:Na) (**Fig. 10**). The advantages of CsI:Na over the previously used zinc cadmium sulphide (ZnCdS) are:

- a. CsI:Na has a mass attenuation coefficient which better matches with the radiation emitted from the patient than ZnCdS

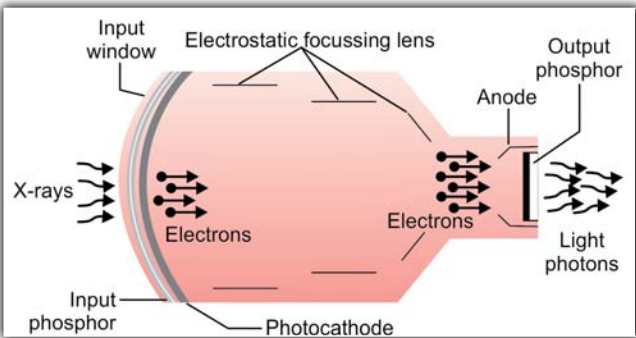


**Fig. 9** Schematic diagram of image intensifier

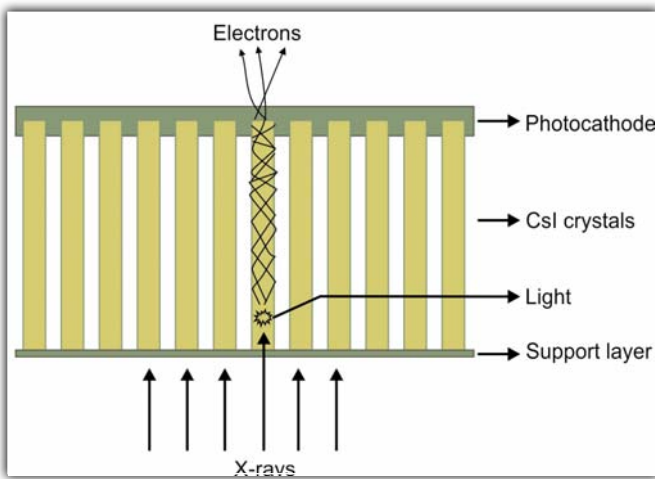


**Fig. 10** Schematic diagram of input phosphor of image intensifier showing cesium iodide (CsI) crystals in needle form. This significantly reduces lateral scatter of light photons

- b. It has higher atomic number resulting in higher X-ray absorption
- c. It can be crystallized in needle form which reduces lateral scatter and improves spatial resolution
- d. Light emitted by CsI:Na has a range which matches with the sensitivity spectrum of the photocathode.

The thickness of the input phosphor is a trade-off between X-ray absorption efficiency (which increases with thickness) and spatial resolution (which decreases with increased thickness due to increased lateral scatter). The thickness in the presently used II is usually between 300  $\mu$  and 500  $\mu$  with efficiency of 60 to 70 percent.

The photocathode is adjacent to the input phosphor and is made of antimony cesium ( $SbCs_3$ ) measuring about 20 mm in thickness. Its production efficiency is about 10 to 15 percent. A single X-ray photon of 60 keV incident on the screen is converted into about 2600 light photons of which 1600 reach photocathode, which converts these into approximately 200 to 300 photoelectrons.

### Electrostatic Lens

It consists of 3 sets of focussing electrodes which accelerate the photoelectrons to the anode. The voltage between input and output phosphor is about 25 to 35 keV. The electrodes increase the velocity and kinetic energy of the photoelectrons incident on output phosphor which increases the number of light photons generated per electron. The electrodes are sensitive to external electric and magnetic fields and are protected by efficient housing assembly.

### Output Phosphor and Anode

The output phosphor is a fluorescent compound made of silver activated ZnCdS (ZnCdS:Ag, also called P20). It is in the form of a thin layer (4  $\mu$  to 8  $\mu$ ) on the inner aspect of output window of vacuum chamber. About 2000 photons are produced by the output phosphor for every 25 keV photoelectron. The anode is a thin layer of aluminium on the vacuum side of output phosphor surface.

### Properties of Image Intensifier

The performance of an II is determined by various characteristics including input size, spatial resolution, brightness gain, conversion factor, contrast ratio and magnification mode.<sup>6</sup> Larger input size provides larger viewing field but increases the cost. Larger sized II are useful in gastrointestinal and genitourinary investigations. The spatial resolution of II is about 4 to 6 line pairs/mm which increases with magnification.

*Brightness gain* is defined as the ratio of output luminance of II to that of a fluorescent screen when both are exposed to same level of radiation. This measurement is not reproducible. Hence, actual measurement is a function of two factors: minification gain and flux gain. Minification gain is the ratio of input area to output area of II. Flux gain is defined as number of photons generated by the output phosphor for every photon generated by input phosphor. Brightness gain is the product of minification gain and flux gain. It is usually in the range of 5,000 to 20,000.

*Conversion factor* is currently used by many manufacturers for evaluating the efficiency of II. It is defined as the ratio of output luminance level ( $Cd/m^2$ ) of an II to its entrance exposure rate ( $\mu Gy/sec$ ). The typical values range from 25 to 30  $Cd-sec/\mu Gy-m^2$ . The output of an II reduces over time.

*Contrast ratio* is the ratio of brightness of the periphery to the center of the output window when the center of the II input window is completely blocked by appropriately thick lead disc. It is the measure of veiling glare. The typical values for modern II range from 10:1 to 30:1.

*Magnification* is performed by collimating to the region of interest thus reducing the field of view at input screen. This however reduces minification gain. To compensate for this,

there is increase in exposure at the input screen. Thus when magnification is increased, radiation dose to the patient is also increased.

### Limitations of Image Intensifier System

Various drawbacks and artifacts of older II have led to the development of better systems. However, knowledge of these is important to identify them and take adequate measures to their correction wherever possible.

The II system is bulky which results in some difficulty in positioning patients. The system includes a vacuum tube which is associated with risk of air leak. Air leak affects transmission of electrons and thus image quality. The dynamic range of II is lower compared to flat panel detector (FPD). Magnification reduces FOV and thus increases radiation dose to maintain brightness.

*Dofocusing* is an effect which occurs when electrons do not pass through in proper plane leading to image blurring. It results from alterations in voltage of electrostatic plates which occurs in older systems or by external magnetic field. This drawback also leads to *S distortion*, where effect of the external magnetic field is more on the outer beam of electrons than the central beam. Mu metal protects the plates from external effects, although not completely.

*Lag* is the delay that occurs after formation of an image by II before it is ready to transmit next image. This reduces the temporal resolution of the system. Older systems had a lag of 30 to 40 ms, but modern systems have a lag of about 1 ms.

As the input phosphor is convex and the output phosphor is flat, the outer electrons travel a longer path compared to the central ones. This results in two artifacts: vignetting and pin cushion distortion. *Vignetting* refers to increased brightness of the centre of an image compared to its periphery due to higher concentration of electrons in the center than periphery. *Pin cushion* distortion refers to magnification and stretching of the periphery of an image.

*Veiling glare* or flare occurs due to scattering of light and defocusing of electrons within the II (Fig. 5A). Here, areas of low density like lungs or external air partially occupying the FOV result in high electron flux leading to saturation of the phosphor. This results in difficult visualization of adjacent structures. Glare also occurs for a short time period when image intensifier is moved from a dense area to less dense area till automatic exposure control adjusts the exposure. This can however be significantly reduced by use of pulsed fluoroscopy.

Quality control should be done at regular basis to evaluate spatial and contrast resolution and radiation exposure. The resolution and brightness gain of II decrease over time and these need regular monitoring. Further details regarding quality control are described in a different chapter.

### Optical Coupling and Video System

The II is optically coupled to a camera which converts light photons from II to voltage signal.<sup>7</sup> This signal is then

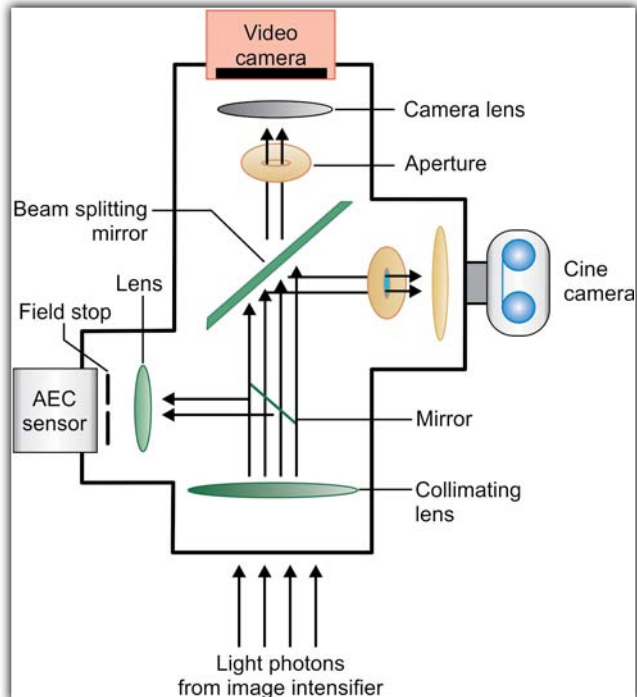


**Fig. 11** Optical distributor system with its components

transmitted to film camera or video camera for viewing. The system consists of an optical distributor and a video system.

### Optical Distributor System

The main functions of optical distributor are:

- Transmission of clear focussed image from the output phosphor to all the cameras in the system
- Transmission of images of sufficient intensity/brightness to each camera, and
- Transmission of brightness information to the automatic exposure control (AEC) circuit of the X-ray generator. The system consists of a series of mirrors, lenses and camera apertures (Fig. 11).

Beam splitting mirror is partially silvered and splits the light beam exiting the output phosphor through collimating lens into two, one reaching the film camera for recording and the other to video camera for viewing. There is an additional small mirror or prism between the collimating lens and beam splitting mirror which transmits part of the light beam to AEC sensor. The AEC sensor uses a field stop between it and its lens to prevent the periphery of the light beam, which is not usually the area of interest, reaching the sensor to determine exposure.

Two types of lenses are present in the optical coupling system. The collimator lens is located at a distance from the output phosphor equal to the focal length of the lens. The light beam exiting the lens is collimated and parallel. Camera lens is present in each of the camera used in the system and is

located at a distance equal to its focal length from the camera target.

The light beam reaching the camera lens is controlled by camera aperture or iris. The aperture determines the speed of the system which is a measure of total X-ray exposure needed to produce a proper image on camera. It is designated by f-number. Faster the speed, lesser is the X-ray exposure required. The apertures used can either be fixed or adjustable. Fixed apertures are usually used where detected X-ray exposure level is same across patients as in film cameras. But in video cameras, the X-ray exposure varies from low levels in fluoroscopy to high levels in angiography and thus need an adjustable aperture (motor driven iris). Sometimes, additional neutral filter may be needed to prevent overexposure at high doses.

Every region in the light beam from the collimating lens contains information from all points of output phosphor. Hence, mirrors and apertures placed between two lenses are not visualized on the image.

### Video System

This plays role in image display and recording and also provides input to the digital processor. It includes a camera head which converts light image into voltage signal and a camera control unit which process the voltage signal for display and digitization (**Fig. 12**).

Two types of devices are used for signal generation, older vacuum tube sensor (pickup tube) and the modern CCD sensor. The pickup tube contains a photoconductor which absorbs the light photons to generate electron-hole pairs within it. The electric field placed across the target causes the holes to move towards the inner surface of the target. The hole density, which is proportional to the light image intensity, is measured by focussed electron beam and converted into voltage signal constituting the video output of the pickup tube. The photoconductor used include antimony trisulfide ( $Sb_2S_3$ ; Vidicon), lead oxide (Plumbicon) or a composite of amorphous selenium, arsenic and tellurium (Saticon). Plumbicon has very low lag time with good temporal resolution and hence used in cardiac angiography. Saticon has the advantage of linear response to light intensity. In CCD system, the target (Thallium doped Cesium Iodide) generates electron-hole pairs but the electrons accumulate in potential wells depending on the intensity of the light photons incident on it. The charge is then transferred to adjacent storage region where it is readout to generate an image. CCD is better than the pickup tube as it results in better dynamic range (12-bit depth), higher SNR and contrast resolution thus reduced patient dose. Its linear response is very useful in subtraction imaging. Further it is compact, robust, consumes less electricity, lacks maintenance and is not associated with lag phenomenon and geometric distortion. Currently, CCD cameras are available for both fluoroscopy and angiography systems.

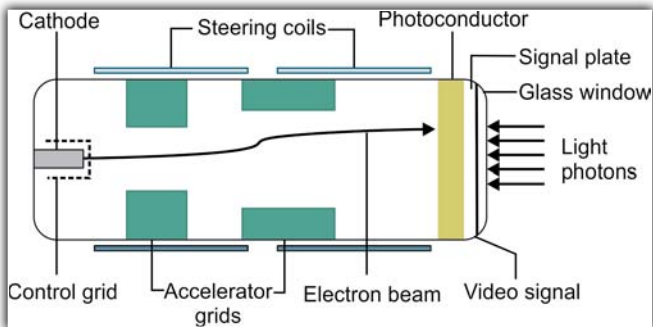


**Fig. 12** Video camera pick-up tube and its components

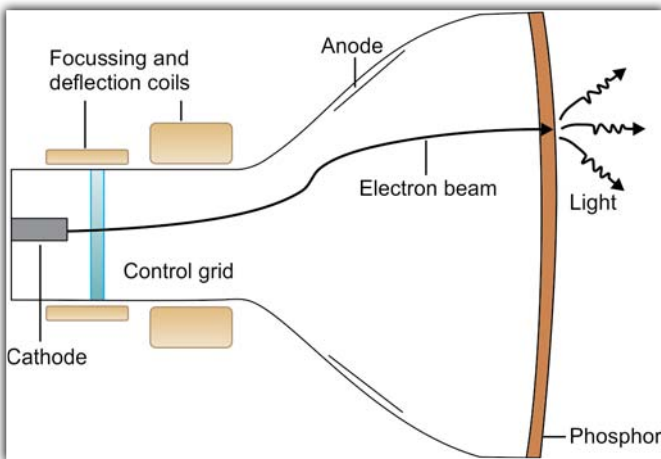


**Fig. 13** Television picture tube and its operation

Two operating properties of video system are lag and linearity. *Lag* refers to the time delay in the output of the video system in response to the changes in the input sensor of the video camera. CCD cameras have no lag. In pickup tubes, lag varies with high values seen in those using  $Sb_2S_3$  as target material. Lag is also higher in dark parts of the image than bright parts. Lag results in blurring of moving objects. One advantage of higher lag is significant reduction in image noise, which is high in CCD cameras. *Linearity* indicates relationship between light input and video signal output. A non-linear response is desirable as smaller signals are better amplified.

The video output signal from the target (pickup tube or CCD) is converted into one-dimensional voltage signal which is displayed on the monitor by raster scanning (**Fig. 13**). Here, the voltage signal is scanned in a horizontal line from one end to the other, which is terminated by H-sync signal moving the scanning to next line. Once the whole screen is filled by horizontal lines, the V-sync signal shifts the scanning to the top of the image to restart scanning. H-sync and V-sync pulses produce dead time, equal to about 15 percent of the total horizontal period for the former and 7 percent of the

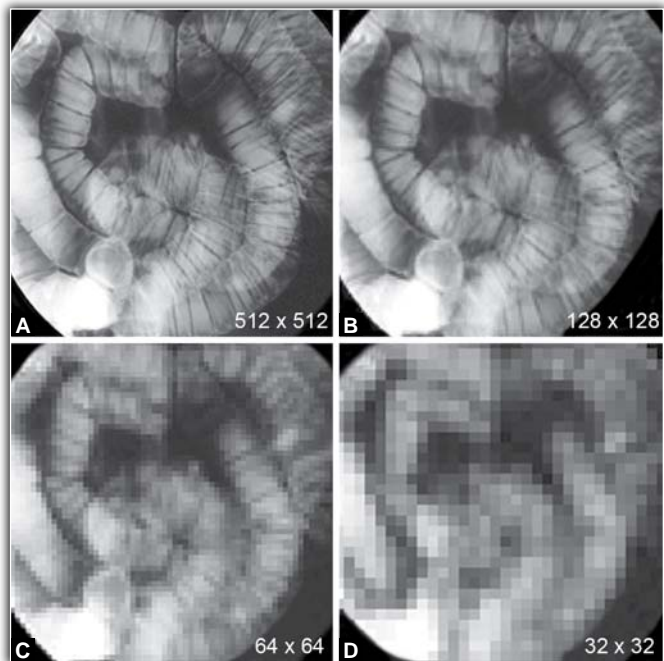
total vertical period for the latter. The video scanning may be done in continuous manner (line 1, line 2, line 3 etc. in order) or interlaced manner (odd lines first followed by even lines). The standard scanning mode of a conventional video is 30 fps, 525 lines per frame and 2:1 interlaced video. Modern systems employ 60 fps and above and scan conversion for improved visualization. One has to note that this frame rate is different from the frame rate of X-ray generator.

The spatial resolution of fluoroscopic equipment is determined by the size of focal spot, the II, the digital system and the video system. The resolution of video system has two components: vertical resolution and horizontal resolution. Vertical resolution is determined by the number of horizontal lines on the screen and measured in terms of line pairs per mm. It is calculated by taking into account the size of II, magnification and number of lines of horizontal scanning. Older systems employed 525 lines per scan height but modern angiography system use 1049 lines. Horizontal resolution of video system is decided by the bandwidth of the system. A low-pass filter limits the bandwidth preventing too low or too high values thus ensuring that horizontal resolution matches vertical resolution. The bandwidth ranges from 4.5 MHz for 525 line system to 18 MHz for 1049 line system at 30 fps. Currently, many equipments use 1023-line raster line video system with liquid crystal display (LCD) monitor.

### Digital Fluoroscopy

The initial fluoroscopic systems used cassettes for documentation of images. This resulted in high film usage, lag time between cassette changes and delay in viewing the spot films. Further, conventional fluoroscopic systems are associated with longer examination times, higher radiation doses, need for repetition of acquisitions due to nonavailability of post processing, need for multitasking (turning on fluoroscopy, cassette changes, patient positioning) by radiologist and more staff. These problems are surmounted by the development of digital fluoroscopy which is easy to use, provides better image quality by post processing, reduced examination time and radiation dose.

The main principle behind digital fluoroscopy is conversion of analog video signal into digital data using an analog-to-digital convertor (ADC).<sup>2</sup> Other methods of digitization are use of CCD cameras and flat panel detectors. The fundamental theory of digital imaging included binary numbers, pixels and gray levels. Binary system uses two digits i.e., 0 and 1 the values of which are determined by the number of digits (bits). A 2-bit number has  $2^2$  or 4 values (00, 01, 10, 11). A 3-bit number (000 to 111) can have  $2^3$  or 8 values, 4-bit number (0000 to 1111)  $2^4$  or 16 values, 8-bit number  $2^8$  or 256 values and so on. Each pixel in an image has a position, size and value. Pixel size is determined by field of view (FOV) and matrix size. Smaller the pixel size better is the resolution and sharper are the images. This can be done by increasing the matrix and / or reducing the FOV (**Figs 14A to D**). Pixel value is the gray level of the image. The range of gray scale in an



**Figs 14A to D** Spatial resolution of fluoroscopic image at various matrix sizes. Note the decrease in spatial resolution as matrix size is reduced

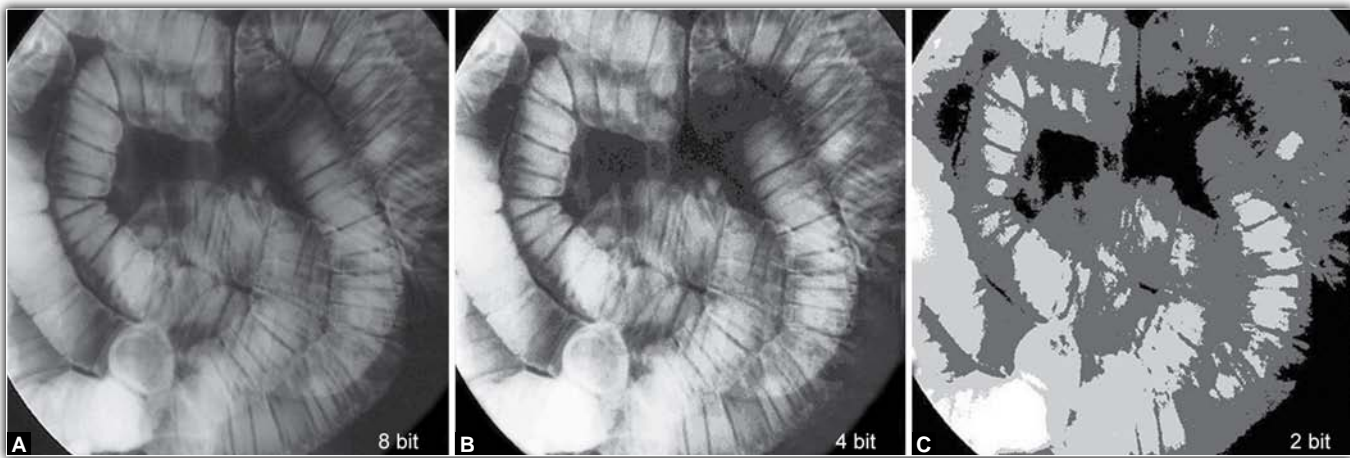
image depends on the bit depth of the system. Higher the bit depth, better is the contrast resolution (**Figs 15A to C**).

The ADC system collects the output signal of the video camera at regular intervals and converts it into binary values (0 and 1) for storage. The range of values depends on the bit depth of the ADC (e.g. an 8-bit ADC displays  $2^8$  or 256 values) and are expressed as varying gray scale intensity. The resolution of ADC system is determined by the resolution of the video camera which is about 1 to 2 lp/mm. The digital image thus formed can be stored for subsequent printing on film. Further the images can be processed to improve visualization.

CCD cameras have substantially reduced the size of the bulky video system. As mentioned in previous section, the CCDs convert light signal from the scintillator into electrical charges which is readout and transmitted to the monitor. The CCDs have a resolution of 1.7 lp/mm. Flat panel detectors (described later) used in some of the modern fluoroscopy systems do not need a video system.<sup>8</sup> They directly or indirectly convert X-ray photons incident on them into electronic signals which are displayed on the monitor. The electronic signal generated varies with the intensity of incident X-ray photons. With both these systems, ADC digitizes the signal for display and storage.

### Post Processing Techniques

*Last image hold (LIH)* is an important feature of digital fluoroscopy. The last image/frame of cine fluoroscopy at



**Figs 15A to C** Contrast resolution of fluoroscopic image at various bit depths. Note the drastic fall in contrast resolution with reduction in bit depth (range of gray scale)

which imaging stops, is captured and continuously displayed on the monitor even after switching-off the fluoroscopy. This image can be transferred to reference monitor and is used for guidance without additional radiation to the patient and medical staff. This is applicable for static objects. For areas which are in motion (e.g. cardiac imaging) *fluoroscopy loop* can be captured and made available for review when needed. Here, the last 150 to 300 frames or about 10 seconds of fluoroscopy can be saved.

*Gray scale processing* involves adjustment of brightness and contrast of the image. This is done by adjusting two values: window level and window width. Window level is the central value of the gray scale range of the image and window width is the range displayed on either sides of window level. For example, window level of 80 and window width of 50 means the central value of gray scale is 80 and 25 gray scale values can be visualized on either side of 80 (55 to 105) beyond which the image is either black or white. The level and width are adjusted depending on the region of interest with darker objects needing lower window level, brighter objects higher window level and soft tissues needing higher window width values.

*Temporal frame averaging* is a feature to reduce image noise. Here two or more images are averaged to form single image with less noise. The drawback of this property is image lag in dynamic fluoroscopic imaging, but may be useful for static images. *Edge enhancement* increases the sharpness of the image and may be used to make lesion more conspicuous.

*Measurement* of distance of objects can be done on digital image. This usually needs calibration by measuring known dimension of a reference object (e.g. catheter) in the field of view. The machine calculates this in terms of number of pixels and uses it as reference for distance measurements on the image. Other techniques which are available

include black-white reversal, image flip (horizontal/vertical), electronic shutter and annotation.

### DIGITAL SUBTRACTION ANGIOGRAPHY

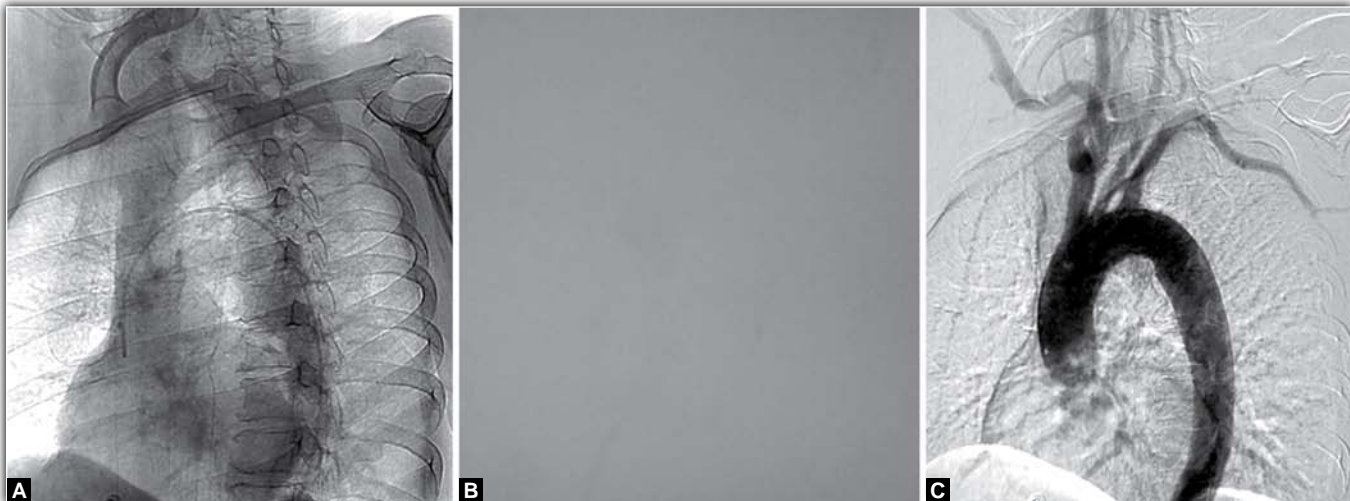
Digital subtraction angiography (DSA) refers to a digital imaging technique for better visualization of contrast filled vessels.<sup>9</sup> This technique permits use of lower amount of contrast medium. Here, the precontrast image is digitally subtracted from post-contrast image to provide background suppression. This allows better visualization of low contrast vessels, but at a cost of increase in noise. Usually the effect of noise is overcome by averaging two or more frames. Thus, this technique (subtraction) increases the noise which is countered by increased mA (compared to unsubtracted image).

#### Types of Subtraction

The types of subtraction techniques include mask mode, time interval, dual energy and hybrid subtractions.

*Mask-mode subtraction* is the most widely used process of DSA in which temporal subtraction is done (**Figs 16A to C**). It involves initial acquisition of a frame of region of interest which is used to stabilize the exposure factors. Then a second image is taken and stored as mask image. This mask image is subtracted from subsequently acquired images on pixel-by-pixel basis and show only contrast filled structures. If any movement occurs after acquisition of mask image, misregistration occurs in the subtracted images. This can be overcome to some extent by pixel shifting.

*Time interval difference subtraction* is another mode of temporal subtraction where a consecutive previous frame is subtracted from current frame (e.g. frame 1 from frame 2, frame 2 from frame 3 and so on). This technique is very useful in cardiac imaging where there is rapid motion. The



**Figs 16A to C** Mask mode subtraction. (A) Is the initial image stored as mask. (B) Shows the first subtracted image without any bones or vessels. (C) Shows subtracted aortogram depicting only vessels

images obtained can then be stacked to provide a composite image without motion.

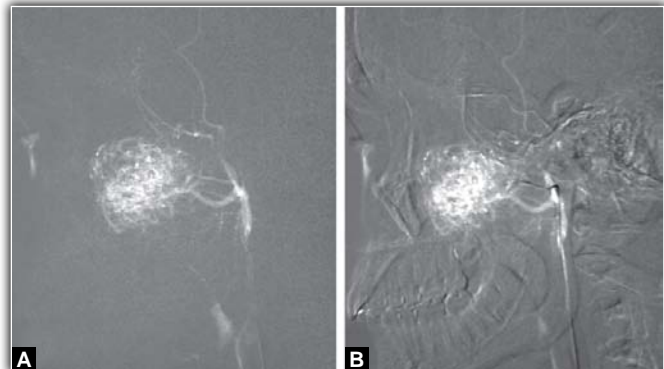
**Dual energy subtraction** is another technique in which the region of interest is exposed to higher kV (120 to 130 kV) and lower kV (70 kV) at very short interval (about 50 ms). Then, the higher kV image is subtracted from the lower kV image to produce an iodine and bone image (the soft tissue and gas shadows are eliminated). This technique has the advantage of elimination of motion artifacts. The limitations of this mode of subtraction include increased radiation dose, reduced opacity of contrast opacified structures, reduced SNR and increased complexity of the equipment.

**Hybrid subtraction** is a combination of dual energy and temporal subtraction.

#### Techniques used in DSA

**Road map** is a technique in which static fluoroscopic image is subtracted from densely opacified vessel. Here, a short contrast run of the vessel is done under fluoroscopy to select the frame with maximum opacification of the vessel as the road map mask, which is stored in memory. Then subsequent live fluoroscopic image is subtracted from the road map mask for visualization of the vessel and the catheter/guide wire (**Figs 17A and B**). This technique is very useful in placement of catheters and guide wires in complex and small vessels. Motion after road map acquisition may affect subsequent intervention. Another similar technique is *fluoroscopy fade* in which a reference DSA image is overlaid on the real time fluoroscopic image. Dynamic 3D road mapping which is new development allows projection of 3D reconstructed vessel on live 2D fluoroscopic image.

Peripheral DSA can be performed with single contrast injection using *stepping technique*. This is of two types. In stepping table technique, the table moves into three stations



**Figs 17A and B** Road map in a case of pre-operative embolization of nasopharyngeal angiofibroma. Subtracted fluoroscopic image with maximum contrast opacification is stored as mask image (A) and subsequent images are subtracted from mask image to visualize the guide wire/catheter within the opacified vessel (B)

with X-ray tube and detector remaining fixed. In stepping gantry method, the tube-detector/II moves keeping the table fixed. In both methods, precontrast images are acquired at different stations and stored as mask image. Subsequently, matching postcontrast injection images are taken at same positions while chasing the bolus of contrast and subtracted from the corresponding mask image to produce clear image of peripheral arteries. The benefits of this technique are significantly reduced use of contrast and reduced examination time. The main disadvantage is increased chances of movement between precontrast and postcontrast images.

An important advancement in digital fluoroscopy is *rotational angiography* where the X-ray tube - detector system rotates through usually 90° to 180° while acquiring

continuous images.<sup>10</sup> Rotational angiography was available with II systems too. But with improvements in mechanical aspects of systems (rotation) and availability of faster detectors today they produce good quality images (**Figs 18A and B**). Mask images are initially acquired at 0.8° to 2° gaps followed by postcontrast rotation and acquisition at same positions. Then DSA images are produced at each angle and reconstructed to produce 3D angiograms. The same technique without subtraction is used in some systems to provide axial images (volume or cone beam CT; **Fig. 18C**). The volume data acquired is reconstructed in different planes at a predetermined thickness. This helps in accurate planning of complicated interventions, but at the cost of higher radiation dose. Also, the images have very low contrast resolution due to higher proportion of scatter radiation (due to divergent beam or cone beam).

#### *Post-processing in DSA*

*Mask pixel shift* is a software modification feature used when smaller patient motion occurs after the mask image is acquired. By shifting the pixels of the mask image, reregistering of the mask with post contrast image is possible thus obviating motion artifacts (**Figs 19A and B**). This technique may be manual or automatic. *Remask* is a similar feature where another mask image is selected, which is temporally closer to the contrast image. This is useful when

patient motion occurs prior to contrast image, but after initiation of the acquisition.

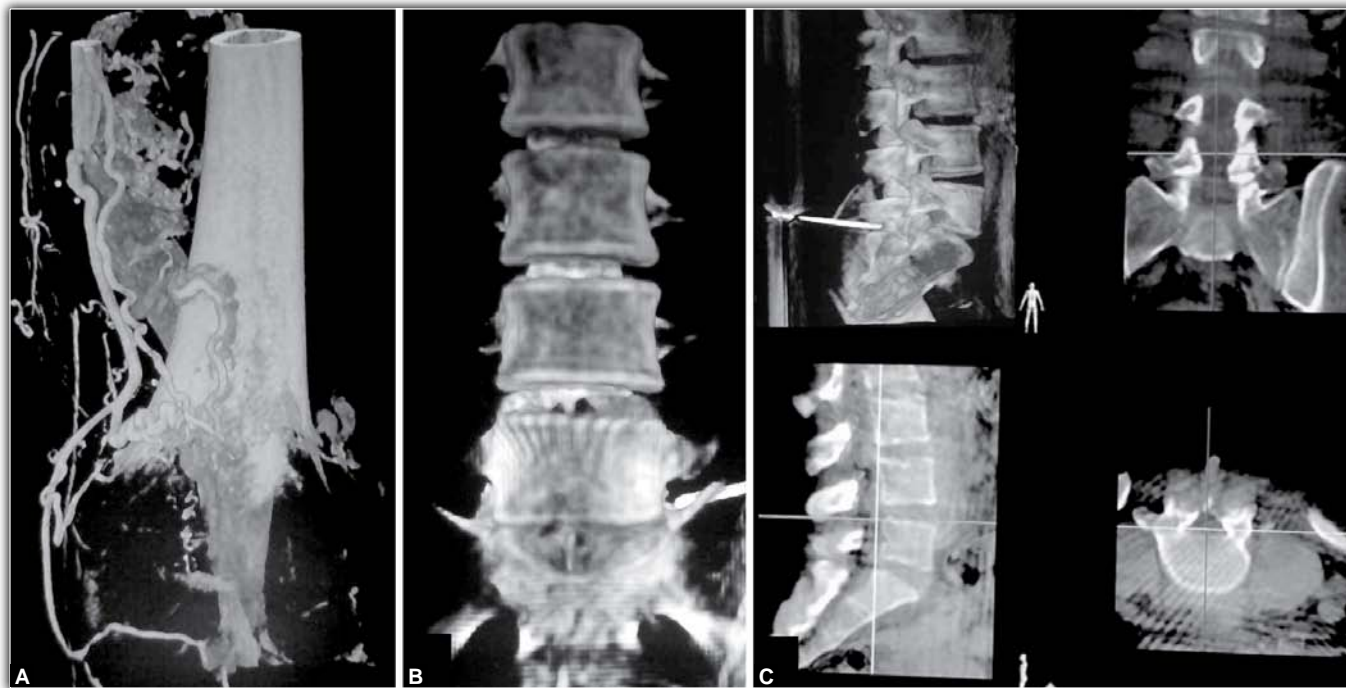
*Image summation* is a property in which two or more frames of a DSA acquisition are summed into a single image (**Figs 20A to C**). This is beneficial when rapid acquisition opacifies part of a vessel in each frame and summation adds up the frames to produce a single image showing the entire vessel. Stacking is a similar technique used in carbon dioxide angiography where the fragmented boluses of the gas are added to produce a complete picture of the opacified structure.

*Land marking* is a feature in which lesser intensity (10–20%, but is manually adjustable) of original image is added to the subtracted image (**Figs 21A to C**). This provides anatomical landmarks in subtracted images, useful in subsequent intervention.

#### **Flat Panel Detector**

Even after their availability in early 90s, the use of flat panel detectors (FPD) in fluoroscopy was delayed due to the requirement of rapid recording and read out process. The first commercial unit was made available in 2001 intended for cardiac imaging.<sup>11</sup>

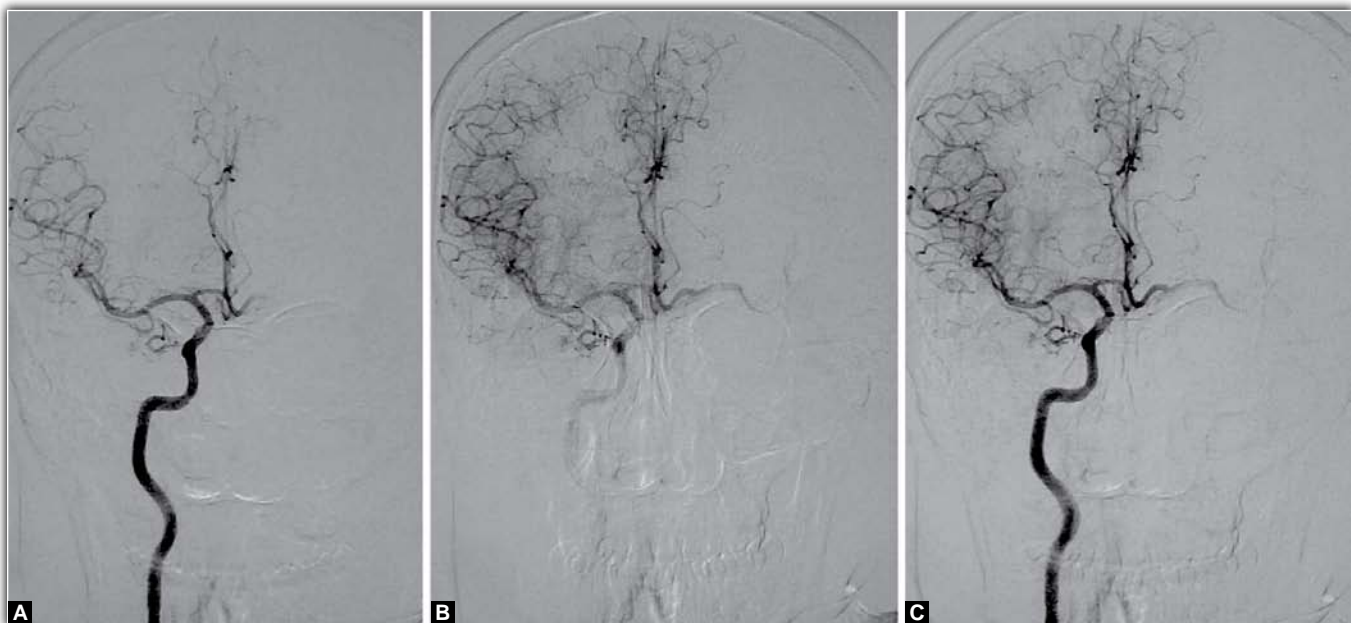
Flat panel detector is the modern solid-state detector array which is used as image receptor.<sup>8</sup> The detector



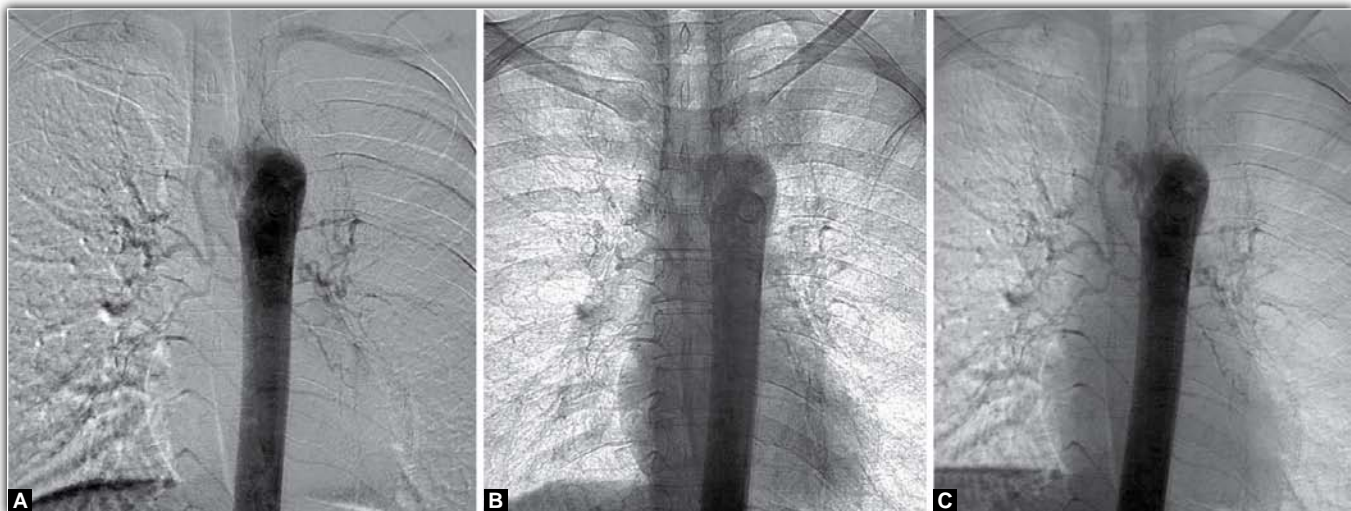
**Figs 18A to C** 3D rotational angiography image (A) acquired during contrast injection with rotation of the tube and detector in a case of arterio-venous fistula of lower limb. (B) shows lumbar spine during disc intervention. Note the images are of high contrast without soft tissue visualization. Cone beam CT (C) is similar with the ability of multiplanar reconstructions



**Figs 19A and B** Motion after acquiring mask image results in misregistration and degradation of image quality (A). This can be partially overcome by pixel shift technique (B)



**Figs 20A to C** A and B shows partial opacification of right internal carotid artery and its branches which can be overcome by summation technique (C) which adds the images to provide a composite image

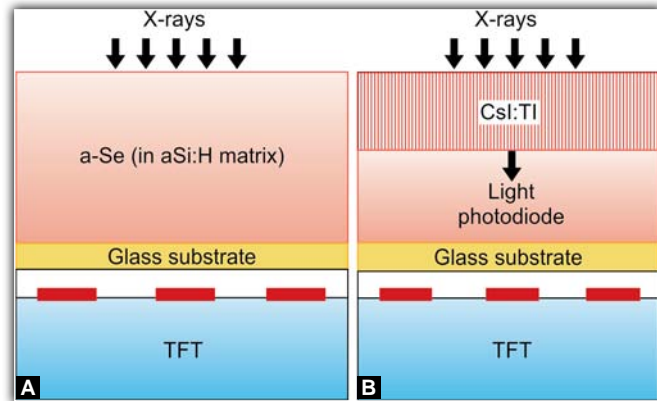


**Figs 21A to C** (A) Subtracted aortogram with bronchial and intercostal arteries without bony landmarks. Conventional image (B) although shows bones well, the arteries are not well seen. Land marking (C) shows both the arteries and bones

consists of an array of detector elements (DELs), the size of which range from  $140\text{ }\mu\text{m}$  to  $200\text{ }\mu\text{m}$ . Each DEL consists of photodiodes or capacitors and thin film transistors (made of hydrogenated amorphous silicon) depending on the type of conversion. The total size of the detector varies from  $25 \times 25\text{ cm}$  to  $43 \times 43\text{ cm}$  and thus each FPD may house 1.5 to 5 million individual DELs. This feature is responsible for the high cost of FPD. Thus they are mainly used in interventional angiography suites and rarely for diagnostic fluoroscopy. The X-rays passing through the patient are directly incident on the FPD and its DELs. This process generates an electronic signal either indirectly or directly (**Figs 22A and B**).

*Indirect system* FPDs consist of DELs which contain a scintillation layer made of thallium-activated cesium iodide (CsI:Tl). The CsI is arranged in the form of crystals which convert incident X-rays into light signal, intensity of which depends on the amount of incident X-ray flux. Cesium ( $Z = 55$ ) and Iodine ( $Z = 53$ ) have high atomic numbers and thus good X-ray absorption property. The arrangement of CsI is in the form of closely packed needle shaped crystals which reduces scatter and thus improves spatial resolution. Hence, thicker layers ( $550\text{ }\mu\text{m}$  to  $650\text{ }\mu\text{m}$ ) can be used which reduced patient dose. The DQE of CsI is in the range of 60 to 70 percent. The light signal from scintillator is then transmitted to the adjacent photodiode-transistor layer (contained in thin layer of hydrogenated amorphous silicon-aSi:H) which generates electronic signal depending on the light intensity. Majority of current systems (Siemens, Philips, GE) use this type of detector in combination with grid controlled pulsed fluoroscopy.

*Direct system* FPDs directly convert incident X-rays into electric signal. These detectors are made of amorphous



**Figs 22A and B** Basic structure of flat panel detector, with direct conversion (A) and indirect conversion (B)

selenium (a-Se) in aSi:H matrix. Selenium has lower atomic number ( $Z = 34$ ) and hence lower X-ray absorption efficiency. Thus thicker layers (up to  $1000\text{ }\mu\text{m}$ ) are needed to avoid increase in radiation dose. Higher thickness results in partial loss of charge as it travels to the storage material. Also, increased noise aliasing is encountered with direct conversion. Higher voltages ( $\sim 10\text{ kV}$ ) which need to be applied across the detector may damage the TFT. Shimadzu and Toshiba manufacture direct conversion fluoroscopic systems.

The process of image formation by FPDs is different from other methods. Here, each DEL is connected to a capacitor which is fully charged initially. During X-ray exposure, the capacitor discharges its stored charge, the amount of which depends on the intensity of the incident X-ray flux. Once exposure is over, the read out electronics measure the change

in the charge of all the capacitors in the FPD to produce an image. Subsequently, a light is flashed to discharge the capacitors before fully charging them again. This process is repeated many times per second.

### *Advantages and Limitations of FPD Systems*

The FPD is small, compact and reliable. Most of the artifacts associated with image intensifier systems are not seen with FPD. As DELs are arranged in rows and columns S-distortions pin cushion artifacts are not encountered. The digital detector system ensures excellent uniformity which obviates vignetting. The fixed positions of DELs prevent defocusing effects. The detector directly produces an electronic signal and a television camera is not needed. The digital system reduces image noise. The FPD has larger dynamic range than II (14-bit vs 4 to 6-bit) and hence flare or veiling glare is usually not seen. The DQE (ratio of number of detected photons to number of incident photons) of FPD is better than II.

The limitations include increased cost of the detector and difficulty in manufacturing FPD not containing defective DELs. The data from such DELs are interpolated by software which results in some artifacts. The FPDs are temperature and mechanical shock sensitive, changes in which may damage the detector elements.

The spatial resolution of FPD is about 2.5 to 3.4 lp/mm which is lower than that of II (4 to 6 lp/min; although the effective displayed resolution is 1 to 1.2 lp/mm). The resolution is limited by size of DELs (pitch) and by binning. Although reducing the size of DELs may improve spatial resolution, this happens at a cost of increase in radiation, as the effective readable surface area (which actually forms image or fill factor) is reduced. This increases image noise which is overcome by increasing radiation. Further with larger FOV, large numbers of elements are activated which substantially increases data transfer rates difficult to be handled by the system. To surmount this limitation, manufacturers carry out a process called *binning* for large FOVs where data from four DELs are grouped to form a single data (similar to single DEL). This reduces spatial resolution but also reduces noise. Further, magnification with FPD system also increases radiation dose to reduce noise, but to a lesser extent than that of II.

Another limitation of FPD system (and also II system) is 'ghosting'. This occurs because of persistence of previous image in the scintillation crystal as a ghost and thus affects image quality. Another reason for ghosting is recursive software filtration which adds previous frames of fluoroscopy to current frame. This results in image blurring/ghosting while scanning moving structures. However, this may be beneficial for static imaging as it reduces noise and improves signal to noise ratio.

Features	Image intensifier system	Flat panel detector system
Size	Large and bulky	Small and compact
Construction	In vacuum tube (risk of air leak)	Solid state
Cost	Cheaper	Expensive
Defocussing effect	Present	Absent
Pin cushion effect	Present	Absent
S distortion	Present	Absent
Vignetting	Present	Absent
Veiling glare	Present	Absent
Resolution of II	About 5 lp/mm	2.5–3 lp/mm
Dynamic range	Lower (30:1)	Higher (14-bit)
Television system	Needed; Low resolution (1-1.2 lp/mm)	Not needed
Image noise	High	Low

### **Automatic Exposure Control**

Regulation of radiation exposure to image detector is needed in fluoroscopy and image documentation.<sup>12</sup> Automatic exposure control (AEC) frees the operator from adjusting kVp and mA to obtain optimal penetrated and bright image. A feedback signal is provided by an ionization chamber in case of spot films or photodiode in case of cameras. The signal is then stored in a capacitor until a predefined value is reached when the exposure is terminated. This principle is followed during recording of images. For fluoroscopy, the exposure is not terminated but continuously compared with a reference value and regulated accordingly. This technique is usually referred as automatic brightness control (ABC). Another method is to use the TV video output signal as feedback to X-ray generator. The exposure rate is adjusted by varying kVp, mAs and X-ray pulse width. ABC has a response time of 1 to 1.5 sec. This can be overcome by the use of automatic gain control (AGC). In AGC, TV camera electronically increases the brightness of the image on the monitor when it is dim and noisy. This only maintains brightness and does not change radiation exposure. The lag time for AGC is in terms of milliseconds. Dynamic density optimization (DDO) is a real time pre-processing algorithm which results in uniform Gray Scale distribution across the image in both fluoroscopy and DSA.

### **Recording Fluoroscopic Images**

A number of techniques are available for recording and storing fluoroscopic images.<sup>12</sup> They are broadly classified

into three types. They include direct film recording, indirect recording and recording of motion.

### *Direct Film Recording*

Here, as the name suggests, the images are directly exposed on photographic films located in front of II. Two types of devices do this type of image recording.

*Spot film devices* use conventional screen-film cassettes for documenting images. The cassette is parked out of the way during routine fluoroscopy and during acquisition moves into the field. The images can be documented in different formats (from 1 to 6 images) on a single film, which has a resolution of about 7 lp/mm and speed of 400. The limitations include inability to use larger sized cassettes ( $14'' \times 17''$ ) and delay that occurs during acquisition for the cassette to move into the field.

*Automatic film changers* are mounted on II and include a supply magazine containing unexposed films (up to 30 films), pair of high speed screens, a receiving magazine which receives exposed films and a motor system for moving films (usually at a maximum rate of 4 films/second). The films have a resolution of 5 lp/mm and speed of 800 which reduces radiation dose. The disadvantages include use of only single film size, delay in documentation, motion blurring, film fogging and jamming and missed exposures.

### *Indirect Recording*

These devices are placed behind the II and hence called indirect recording. This can be done by photofluorography and digital fluorography.

*Photofluorography* allows rapid filming up to an extent of 12 films per second. The photospot camera is side mounted and obtains image transmitted from beam splitting mirror. The films used are roll films which are typically 105 mm wide. Thus the images here are minified. Although, the roll films have resolution of about 200 lp/mm, this is limited by the resolution of II (4 to 5 lp/mm). The advantages include reduced dose, cheaper films, less storage space and less delay in exposure. The limitations include poorer resolution and smaller sized images.

*Digital fluorography* uses CCD cameras or FPD where the images are digitally stored. The matrix may vary from 1 to 9 megapixels with resolution varying from 2.4 lp/mm to 3.4 lp/mm. This limitation in resolution is surmounted by the ability of postprocessing of the images. Other benefits include option of film less system, immediate viewing of images without delay and linear response which obviates over or under exposure.

### *Recording Motion*

Motion recording is useful in visualization and reviewing of dynamic processes of the body. Cine camera and videotapes are used for this purpose.

*Cine fluorography* is regularly used for recording of movement of contrast in the vessels. It uses smaller (35 mm wide) and longer (120 m) film with acquisition capacity of 90 images/second. The frame rate of exposure can be adjusted as needed. Grid controlled tubes are often used to turn X-ray exposure on and off quickly in synchrony with the camera shutter. Since II produces a circular image, exact framing is needed to fit this image on rectangular film. The effective resolution of the system is 16 lp/mm.

*Videotape recording* uses super VHS (S-video) technology with its electronic bandwidth matching with that of the TV. They however produce half the resolution of cine fluorography.

### **Types of Fluoroscopic Equipment**

Various configurations of fluoroscopic systems are available depending on the individual needs. Each system has its own advantages and disadvantages. The types of machines available are as follows.

#### *Radiography – Fluoroscopy Unit with Under-Couch Tube*

This system has an under the table X-ray tube and collimator with image intensifier or detector above the table (**Figs 23A and B**). The II or detector with the tube can be adjusted by the operator to the field of interest. The advantage of this machine is reduced scatter radiation and thus reduced dose to the operator and patient. The disadvantages include need for an additional X-ray tube for radiography which adds to the cost and need for the presence of operator within the examination room for positioning and fluoroscopy (which exposes the operator to radiation) as remote control switches are not available with such systems. The II/ detector is fixed with a handle grip which allows effortless and smooth movement of the detector in all four directions; further it is integrated with fluoroscopic/acquisition button on it.

#### *Radiography – Fluoroscopy Unit with Over-Couch Tube*

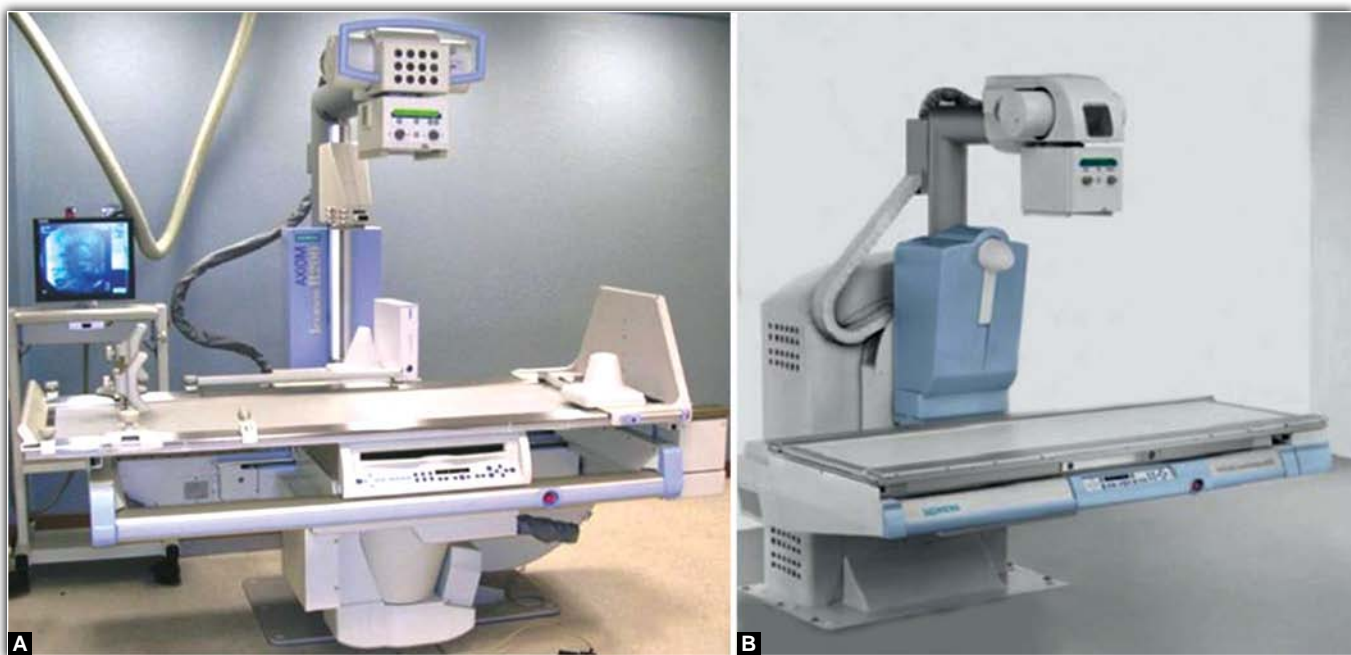
Here, the tube is located above the table at a distance, which is either fixed or adjustable to some extent depending on the vendor (**Figs 24A and B**). The detector is under the table. The benefits include available space for patient access, option for tube angulation, remote control operation (with some units) and ability to use the same tube for radiography. The remote control operation prevents primary beam irradiating the operator. The disadvantages are increased scatter radiation, need of additional lead protection devices (additional cost) and operator away from the patient.

#### *Fixed C-Arm Fluoroscopic System*

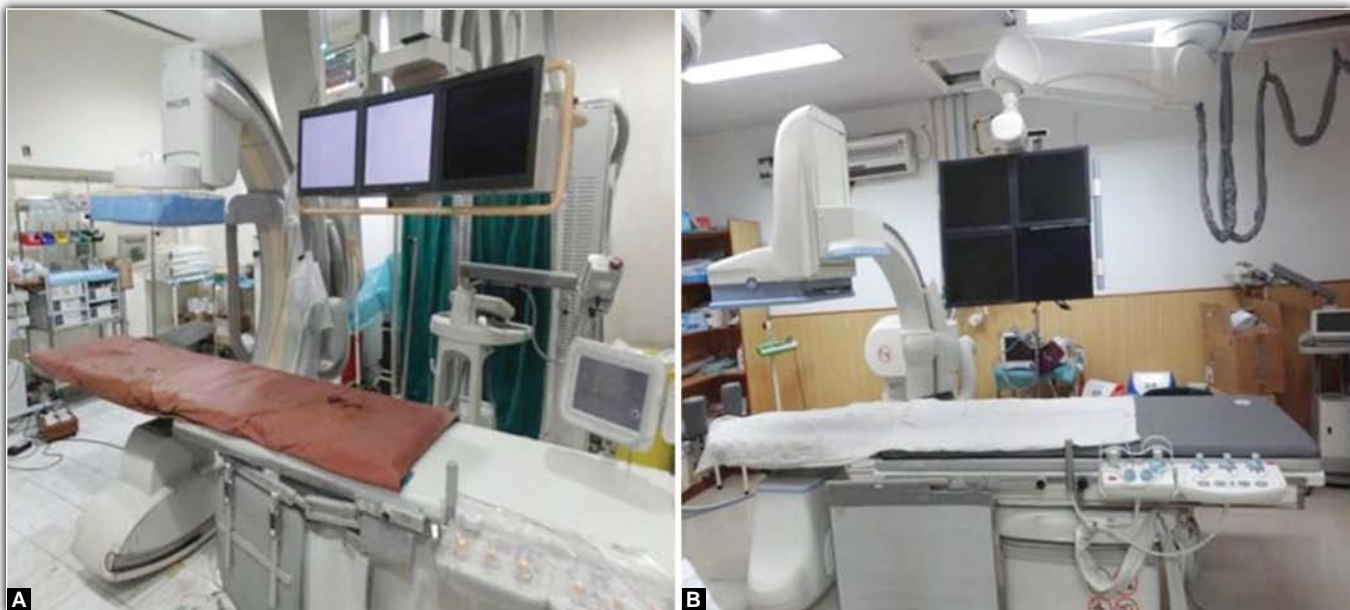
This type of system is mainly used in angiography. This consists of a C-shaped apparatus with X-ray tube assemble at one end and II or detector at other end (**Figs 25A and B**). The shape allows for increased mobility of tube-detector



**Figs 23A and B** Radiography – fluoroscopy unit with under the couch X-ray tube (A). The second ceiling mounted X-ray tube is used for radiography. Close up view of the image intensifier is seen with handle grip (B). (*Courtesy: Siemens Medical Systems*)



**Figs 24A and B** Radiography – fluoroscopy unit with over-couch X-ray tube and under the table image intensifier (A) and flat panel detector (B; *Courtesy: Siemens Medical Systems*)



**Figs 25A and B** Fixed C-arm flat panel detector fluoroscopy system used for angiography with the C-arm being ceiling mounted (A; Courtesy: Philips Medical Systems) or floor mounted (B; Courtesy: GE Medical System)

assembly. The C-arm is either ceiling mounted or floor mounted. In addition, it includes a mobile floating table which is fixed to the floor at one end. Biplane C-arm system includes two C-arms, one ceiling mounted and the other floor mounted (Fig. 26). This unit allows acquisition in two projections (e.g. AP and lateral) with single contrast injection.

#### Mobile C-Arm System

This system is mainly used in operation theaters and wards to check the position of orthopaedic implants, pacemakers or vascular implants (Fig. 27). This system is cheaper and mostly uses image intensifiers, usually with CCD cameras. Due to the cost involved and need of proper care, FPD C-arm systems are slowly increasing in availability.

#### Factors Affecting Image Quality

The quality of fluoroscopic images is determined by a number of factors. The image quality is most importantly defined by spatial resolution and contrast resolution.

Spatial resolution of an image is determined by FOV, matrix, size and number of DELs, binning, video capability, focal spot size and mode of fluoroscopy (continuous vs pulsed). Contrast resolution is affected by scatter, glare, kVp, filtration, collimation, mA (which determines noise/SNR) and image processing techniques. Other factors include source—image receptor distance, patient-image receptor distance, ABC, aperture of optical—video system and conversion gain.

Evaluation of image quality is the most important part of quality control in fluoroscopy. Contrast resolution is

evaluated using an aluminium step wedge with holes of different diameter, spatial resolution by line pair phantom, focal spot size by star phantom and temporal resolution by motor driven rotating disc. These quality control tests should be carried out at regular intervals, typically annually, for optimal performance.

#### Radiation Safety in Fluoroscopy

From the initial days when fluoroscopy was introduced in medicine, there has been an increase in its utilization. In the past two to three decades, tremendous increase in its utilization in various diagnostic and interventional procedures has occurred which has increased the total fluoroscopy times greatly, sometimes even over one hour. Availability of newer intravascular devices has further added to its growth. All these together have increased radiation exposure to patients and to medical staff working with fluoroscopy. Most important of various radiation induced effects is skin burns caused by radiation. It has an insidious onset and takes weeks to manifest in its full extent. The radiation induced skin injury is a deterministic (nonstochastic) effect with severity increasing with increase in exposure dose. The importance of skin injury in fluoroscopy is due to the fact that radiation dose is highest at skin entrance point and that skin in the region of interest suffers as the fluoroscopy time increases. The measurements which are typically used to measure radiation dose of a fluoroscopy system are receptor entrance exposure and skin entrance exposure rates.<sup>13</sup>

Receptor entrance exposure (REE) is defined as exposure at the entrance of image receptor required to produce a single



**Fig. 26** Biplanar fixed C-arm system, with one arm ceiling mounted and the other floor mounted. (Courtesy: Philips Medical System)



**Fig. 27** Mobile C-arm fluoroscopy unit. (Courtesy: Siemens Medical Systems)

image with grid removed. Skin entrance exposure (SEE) is the dose at entrance surface of a patient and usually measured under simulated conditions. The SEE limit for normal fluoroscopy is 100 mGy/min and high dose fluoroscopy is 200 mGy/min. The values depend on kVp, patient thickness, grid, SID etc. The typical fluoroscopic SEE rate for an average adult is about 10 to 30 mGy/min, but higher for acquisition modes. Usually, diagnostic procedures are associated with lower fluoroscopic times and exposure rates compared to interventional procedures.

#### Patient Dose Monitoring Methods

These methods are described in detail elsewhere. In short, they are of two types.

*Direct methods* use thermoluminescent dosimeters (TLD), photographic films and diodes or metal-oxide semiconductor field effect transistor (MOSFET) detectors. The TLD is the most accurate but due to smaller size cannot cover the entire field and may not correctly measure the peak dose field. Photographic films are inexpensive and useful in determining high dose region and the dose. But the sizes available are limited. Both these methods are associated with time delay in reading out the measured doses. The MOSFET detectors provide dynamic measurement of skin dose and are accurate.<sup>14</sup> They have good linear response, low detection threshold and low error percentage (10%), but are detectable in the imaging field.

*Indirect method* most widely used is dose area product (DAP) meter. Since it is a product of dose and area, same values can be obtained with low dose exposed to larger area and higher dose exposed to smaller area. But the skin effect of these two modes is not the same as the latter results in more skin damage. The SEE can be computed from DAP reading if dose rate and field size data is available. But this is often difficult as both, dose rate and field size change dynamically during fluoroscopy. Still, DAP meters are widely used in modern systems for dose measurement. One new system is available which dynamically measures and displays an estimate of SEE and is called PEMNET (Patient Exposure Management Network). This records patient dose from all radiation related procedures (CT, cardiac, angiography, interventions) and is available for review from any workstation in the network. Currently however there is no perfect dose monitoring system for fluoroscopy and interventional procedures.

#### Dose Reduction Techniques

Various dose reduction techniques include reduction of exposure time, improving collimation, reducing tube current, reducing spot exposures, using better detectors and reducing II/ detector-patient distance.

Intermittent fluoroscopy is the most important due to the fact that the radiologist can control fluoroscopy time and can judiciously use it intermittently to reduce total patient and personnel dose. Last image hold (LIH) has been described above. Use of reference image, especially in DSA is helpful in significantly reducing radiation dose and contrast medium. Modern systems are available with electronic collimation which can be done on LIH without additional fluoroscopy.

Pulsed fluoroscopy provides substantial reduction in patient radiation exposure. Reducing the number of pulses increases image noise and this is overcome in many models by increasing mA which increases dose. Thus instead, there is only modest reduction in dose. The radiation dose of continuous fluoroscopy and pulsed fluoroscopy at 30 fps are similar. When the pulse rate is reduced from 30 to 15, 10, and 7.5 per second, the dose is approximately reduced by 22, 38 and 49 percent respectively.<sup>15</sup> No significant change in image

quality is seen between continuous fluoroscopy and PF at 15 fps, 7.5 fps and 3.75 fps.<sup>16</sup> Further, at lower frame rates and magnified fields, instead of increasing exposure, the video camera aperture can be increased to maintain brightness. Automatic dose rate and image quality (ADRIQ) control modulates kVp, mAs, pulse width and filtration as per patient characteristics to produce lowest radiation with good image quality.<sup>17</sup>

The use of cumulative exposure timer, typically set at 5 minutes, alerts the operator of fluoroscopy time. Further, real time display of total exposure time, kVp, mAs and total dose also helps the radiologist to regulate patient radiation exposure.

Dose spreading is a method to reduce skin dose when lengthy interventional procedures are performed. Here, the tube-detector system is rotated about the region of interest as center to spread the skin dose to different area, so that single area is not overexposed. The quality of X-ray beam can be adjusted to remove low energy X-rays (beam hardening). This can be done by increasing kVp (which reduces SEE) and use of metal filters like aluminium or copper (especially the latter as 0.1-0.3 mm of Cu reduces SEE by 30 to 50 percent).<sup>18</sup>

Magnification, either geometric or electronic results in increase in skin dose. Higher magnification may result in reduced spatial resolution due to focal spot blur if smaller focal spot is not used. High dose fluoroscopy mode, available in few systems, is uncommonly used for very obese patients or thick body regions and results in high skin dose.

## SUMMARY

Fluoroscopy is one of the basic X-ray techniques and is widely used for various diagnostic and interventional procedures. From the initial dark room fluoroscopy considerable advancements have led to the development of image intensifiers, digital processing techniques and the present day flat panel detectors. Solid state FPD systems produce better image with less artifacts and results in less radiation dose. Radiologists, as end users, should be aware of the basic structure and function of these equipments so that judicious adjustments are made on case to case basis. A constant note has to be made of the fluoroscopic time and radiation dose to the patient during each procedure. Adequate knowledge of methods of dose reduction during fluoroscopy and DSA is important to prevent radiation effects, especially on skin. Some recent technological developments like new detector technology based on crystalline silicon, emitter technology of X-ray tube, functional imaging protocols that provide physiological information of the lesion and patient and intravascular ultrasound with angiography are in the initial stages of research and may have potential to get established in the field of interventional radiology.

## REFERENCES

1. Schueler BA. The AAPM/RSNA physics tutorial for residents: General overview of fluoroscopic imaging. *Radiographics*. 2000;20:1115-26.
2. Pooley RA, McKinney JM, Miller DA. The AAPM/RSNA physics tutorial for residents: Digital fluoroscopy. *Radiographics*. 2001; 21:521-34.
3. Krohmer JS. Radiography and fluoroscopy, 1920 to the present. *Radiographics*. 1989;9:1129-53.
4. Seibert JA. The AAPM/RSNA physics tutorial for residents: X-ray generators. *Radiographics*. 1997;17:1533-57.
5. Zink FE. The AAPM/RSNA physics tutorial for residents: X-ray tubes. *Radiographics*. 1997;17:1259-68.
6. Wang J, Blackburn TJ. The AAPM/RSNA physics tutorial for residents: X-ray image intensifiers for fluoroscopy. *Radiographics*. 2000;20:1471-7.
7. Van Lysel MS. The AAPM/RSNA physics tutorial for residents: Fluoroscopy: optical coupling and the video system. *Radiographics*. 2000;20:1769-86.
8. Nickoloff EL. The AAPM/RSNA physics tutorial for residents: Survey of modern fluoroscopy imaging: flat panel detectors versus image intensifiers and more. *Radiographics*. 2011; 31:591-602.
9. Curry TS III, Dowdye JE, Murry RC Jr. Christensen's physics of diagnostic radiology, 4th Edn. Philadelphia, Pa: Lea & Febiger, 1990.
10. Orth RC, Wallace MJ, Kuo MD. Technology Assessment Committee of the Society of Interventional Radiology. C-arm cone-beam CT: general principles and technical considerations for use in interventional radiology. *J Vasc Interv Radiol*. 2008; 19:814-20.
11. Cowen AR, Davies AG, Sivananthan MU. The design and imaging characteristics of dynamic, solid-state, flat-panel X-ray image detectors for digital fluoroscopy and fluorography. *Clin Radiol*. 2008;63:1073-85.
12. Geise RA. The AAPM/RSNA physics tutorial for residents: Fluoroscopy: recording of fluoroscopic images and automatic exposure control. *Radiographics*. 2001;21:227-36.
13. Mahesh M. The AAPM/RSNA physics tutorial for residents: Fluoroscopy: patient radiation exposure issues. *Radiographics*. 2001;21:1033-45.
14. Miksys N, Gordon CL, Thomas K, Connolly B. Estimating effective dose to pediatric patients undergoing interventional radiology procedures using anthropomorphic phantoms and MOSFET dosimeters. *AJR Am J Roentgenol*. 2010;194:1315-22.
15. Aufrecht R, Xue P, Thomas CW, Gilmore GC, Wilson DL. Perceptual comparison of pulsed and continuous fluoroscopy. *Med Phys*. 1994;21:245-56.
16. Boland GWL, Murphy B, Arellano R, Niklason L, Mueller PR. Dose reduction in gastrointestinal and genitourinary fluoroscopy: use of grid-controlled pulsed fluoroscopy. *AJR Am J Roentgenol*. 2000;175:1453-7.
17. Lin PJ. The operation logic of automatic dose control of fluoroscopy system in conjunction with spectral shaping filters. *Med Phys*. 2007;34:3169-72.
18. Nicholson R, Tuffee F, Uthappa MC. Skin sparing in interventional radiology: the effect of copper filtration. *Br J Radiol*. 2000;73:36-42.

## Chapter

# 16

# Tools in Interventional Radiology

*Atin Kumar, Chandan Jyoti Das*

The common procedures performed in an interventional radiology set-up could be vascular as well as nonvascular. The need of hardware starts from the giving of local anesthesia or intravenous access till the suturing or plastering of the wound of the procedure in interventional radiology. Both the procedures have some common as well as specific needs. The common needs are like local anesthetic agent, blades, puncture needles and suturing agent. Some of the tools used to perform the interventional procedures are common for both vascular and nonvascular procedures while some are specific to each type.

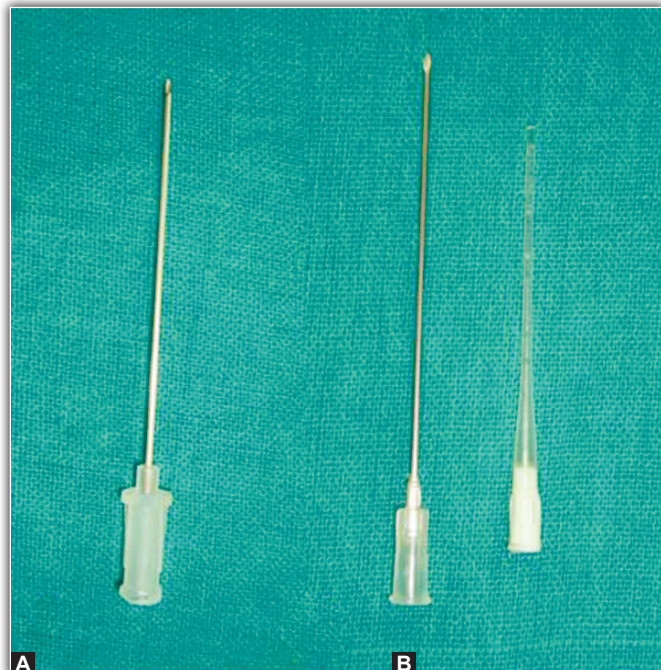
The various tools which constitute the armamentarium of an interventional radiologist are discussed below.

### PUNCTURE NEEDLES

These are small sized needles which are used to gain access to the vessel and are therefore also called as access needles. They are also used for nonvascular indications like gaining access to bile duct, pelvicalyceal system, abscess, etc. The typical access needle has a sharp, beveled distal edge for puncturing the artery (**Fig. 1A**). The guidewire is introduced through its lumen into the vessel once blood comes out from the proximal end. Some access needles have an inner stylet which protrudes slightly out of the outer lumen needle. The tip of the inner stylet is sharp to puncture the artery but the tip of the outer needle is round and blunted to prevent vessel injury. Once the vessel is punctured, the stylet is removed to allow entry of guidewire.

The size of the access needle is measured in gauges. Higher gauge number indicates smaller lumen diameter. The typical access needles are of size 18 G or 19 G.

The seldinger needle (Medicut 18G) is a double lumen type of access needle commonly used in vascular puncture in which the outer lumen is soft, pliable and nontraumatic cannula with a stylet with sharp and beveled edge within its lumen (**Fig. 1B**). Once the vessel is entered, the inner



**Figs 1A and B** Puncture needles: Single piece needle (A) and Seldinger needle (Medicut) (B)

stylet is removed and the soft cannula remains within the vessel through which the guidewire can be introduced. The commonly used intravenous cannula is almost similar and can be used for the same purpose. It is important to check the compatibility of the guidewire through the lumen of the access needle before the vessel is punctured. A 19 G needle accepts a 0.035 inch guidewire.

The vessel puncture can be single or double wall puncture. In the single wall technique, only the anterior wall of the artery is punctured by the advancing needle and when the tip is in the lumen (as evidenced by pulsatile backflow of blood), the guidewire is advanced within the lumen. The nonstylet access needles are preferred for this type of puncture whereas the needles with stylet are used for the double wall technique. In the double wall technique, the puncture needle is advanced through the vessel till it punctures the posterior wall also. Then the stylet is removed and the needle slowly withdrawn till the tip is within the lumen of the vessel. The double wall technique is comparatively easier. The single wall technique is preferred in cases of coagulopathy or when thrombolysis is planned to prevent excessive bleeding.

Another technique of vessel puncture is by micropuncture access set (Fig. 2). In this the needle is a sharp beveled tip needle of very small diameter (usually 21G) which is initially used to puncture the vessel. A compatible 0.018 inch guidewire is then introduced through the needle followed by removal of the needle. A co-axial dilator system with a 3F inner dilator within a 4F or 5F outer dilator is then advanced over the guidewire. It is then followed by removal of the guidewire and the inner dilator to provide a large bore access within the lumen through which the normal 0.035 inch guidewire can be introduced. This technique is commonly used in situations where the access is difficult, e.g. antegrade femoral puncture, brachial artery punctures, pediatric patients, anatomically sensitive regions like jugular venous access and in conditions where thrombolysis is planned.

Seldinger technique is the systematic procedure of gaining access into the vessel. The vessel is first punctured with a needle which is followed by guidewire insertion through it. The needle is then removed over the wire and exchanged with a tapered catheter of appropriate size. This technique is also used in nonvascular procedures to gain access into biliary channels, pelvicalyceal system or into an abscess cavity.

### DILATORS (FIG. 3)

Dilators are short stiff tapered plastic catheters which are used to spread the soft tissues/fascia and the wall of the vessel so as to facilitate the subsequent passage of a catheter. Sequential use of increasing size dilators over a guidewire (preferably stiff guidewire) leads to an increase in the size of the initial percutaneous puncture. The dilators are also frequently used in nonvascular percutaneous procedures to dilate the



**Fig. 2** Micropuncture access set. Consists of bevelled tip needle, co-axial dilators and a 0.018 guidewire

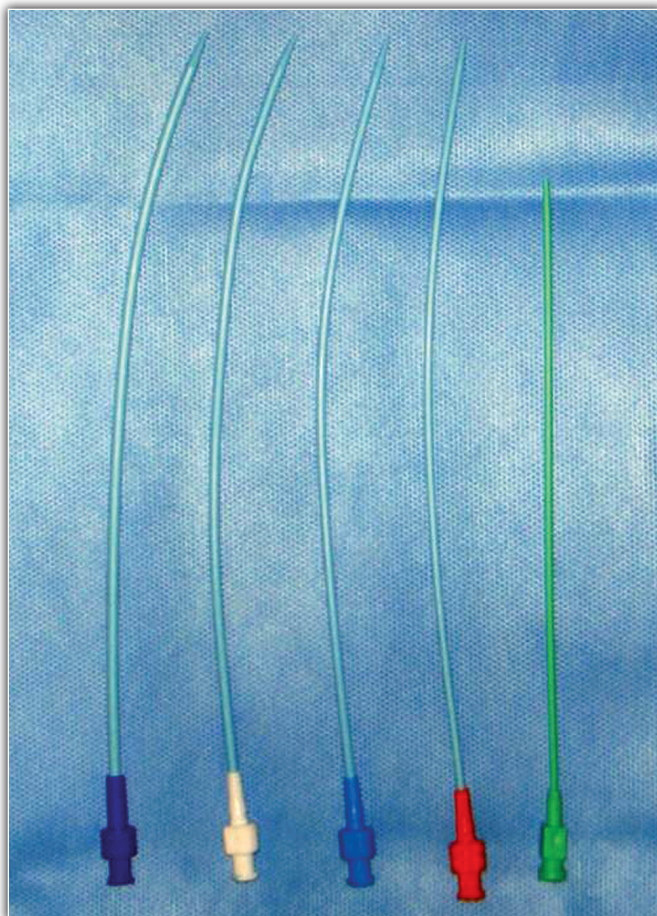


**Fig. 3** Dilators of varying sizes (increasing from right to left). Each size is universally color coded

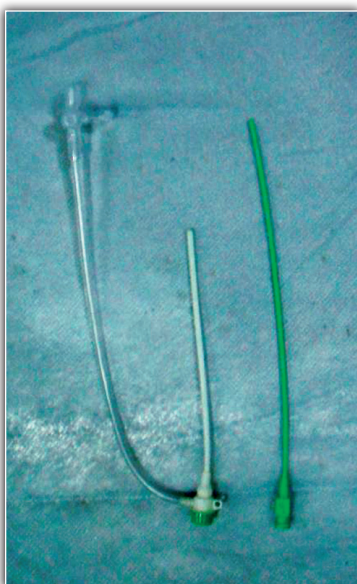


**Fig. 4** Sheath: Size 6F (green color)

track like in abscess drainage, percutaneous nephrostomy, percutaneous transhepatic biliary drainage, etc.

The sizes of the dilators (and access needles) are measured in Gauges. The size in inches equals 1/gauge. Hence, a 20 G needle measures 0.05 inches whereas a 25 G needle measures 0.04 inches. Smaller gauges indicate larger diameters.

### SHEATHS (FIG. 4)

Introducer sheaths are small thin walled catheters which are open at one end and are capped with a hemostatic valve or diaphragm at the other end. There is a short clear side arm which is used for flushing or injection of contrast. The distal end of the sheath is generally nontapered in contrast from normal catheters. The purpose of the sheath is to provide a continuous secured access within vessel lumen for multiple exchanges of various catheters and guidewires through a single puncture and access site. It is introduced as a coaxial system with a dilator within it to ensure smooth access. The introducer sheaths are also widely used for access in nonvascular interventions and drainage of fluid collections.

The sheaths, being slightly stiffer, are also used to improve the pushability of a diagnostic catheter through them into tortuous vessels. Long length sheaths are also available which are mainly used for interventional procedures including nonvascular procedures. The use of crossover sheaths (across the aortic bifurcation) significantly enhances the selective catheterizations of contralateral iliac/femoral vessels and use of long sheaths can enable easy and direct advancement of catheters into selective distal main vessels.

The sheath sizes are described in French (F) and represents the maximum actual size in French of the catheter which can be introduced through its lumen. Hence, a 5F sheath size means that a 5F catheter can be introduced through

it. Note that for sheaths the size represents the inner lumen diameter whereas for catheters and dilators it represents the outer diameter. The sheaths are available in diameters 4-14F with lengths ranging from 10 to 90 cm. There is a universal color coding system for the sizes of the sheaths. 4F sheaths are of red color, 5F gray, 6F green and 7F orange colored.

### CATHETERS

The word catheter is derived from a latin word 'katheter' which means to push down. It is a hollow flexible tube that can be inserted into a body cavity, duct or vessel thereby allowing drainage or injection of fluids, distending a passageway or providing access to surgical instruments. The process of inserting a catheter is catheterization.

Catheters are the backbone of an interventional radiological procedure. They come in various shapes, sizes and material types with each serving a specific function.

### Parts of Catheter (Fig. 5)

A typical catheter consists of following parts:

1. Tip—the distal tapered part.
2. Shaft—the long tubing.
3. Hub—the proximal part with a plastic funnel for ease of guidewire insertions and attachment of syringes for contrasts injections.

### Materials

The catheters can be made of various materials including Teflon (polytetrafluoroethylene or PTFE), polyethylene, polyurethane or nylon. The choice of the material decides the



**Fig. 5** Catheter parts: Hub (H), shaft (S) and tip (T)

torque, stiffness, flexibility, thrombogenicity, burst pressure and the friction. Stiffness allows the pushing of the catheter while flexibility allows bending of the catheter to follow the curve of the vessel. High burst pressure measures the strength of the material and its ability to withstand the high injection rate without bursting. The ability of the catheter tip to rotate based on rotation of the catheter hub measures its torque ability. Mechanical braiding of the catheter wall by materials such as nylon or stainless steel enhances the torque ability of the catheter and facilitates selective catheterization of vessels. Decreased friction of the catheter material on the luminal surface allows higher flow rates and on the outer surface enables easier advancement of the catheter with minimal buckling and wedging. Catheters can be coated by hydrophilic polymers to allow easier trackability, e.g. slip catheter (Cook). Impregnation of the catheter wall with barium sulfate, tungsten or lead salts is often done to increase the fluoroscopic visibility as the catheters are generally faintly radiopaque.

In general PTFE or nylon catheters are stiffer with high tensile strength and burst pressure and hence are used for purpose of flush injections requiring high flow rates and pressures. In contrast polyethylene catheters are less stiff and more flexible and hence are used for purpose of selective catheterizations.

## Sizes

The catheters can be of varying diameter and lengths.

The diameter of the catheter is conventionally measured in French size (F).  $3F = 1 \text{ mm} = 0.038 \text{ inches}$ . The catheter size in French refers to the outer diameter of the catheter. It is a factor in deciding the size of the catheter to be used based upon the size of the vessel to be catheterized. The general use intravascular catheters are commonly of size 4F to 6F. Catheters smaller than 4F are not used for flush purpose but are required for pediatric use and for selective catheterization of tortuous or smaller vessels like intracerebral vessels. They are known as microcatheters and are usually of 2F or 3F size. Larger catheters of size 7F to 9F are used as guiding catheters and are mainly used to guide smaller catheters or devices within them to be used as a co-axial system. The guiding catheters are usually stiffer and firmer to allow passage of balloon catheters, PTCA wires and stent delivery system through them. Mild stiffness comes due to the wire braided design. It should be noted that for guiding catheters the size in French refers to the inner diameter of the catheter (like the introducer sheaths) in contrast to standard use catheters and hence is determinant of the size of the standard catheter which can be co-axially passed through it. For example, a 6F guiding catheter would be able to accommodate a 6F standard catheter.

The length of the catheter is the distance between the hub and the tip. It is conventionally measured in centimeters and usually varies between 60 to 110 cm for standard catheters. Smaller catheter lengths are required when the target vessel

is close to the site of puncture (usually the femoral artery) such as contralateral iliac, renal or visceral arteries and in pediatric patients. Longer lengths measuring up to 260 cm are required for upper limb, calf, intracranial vessels selective catheterization. The microcatheters are usually of long length as they are to be used co-axially within another catheter and their tips must come out a reasonable distance out of the outer catheter.

## Shapes and Holes

The shape of the catheter tip is the most essential element determining the type of use of the catheter. Depending upon the shape, the catheters are categorized as:

1. **Simple straight/angled tip catheters:** These have a single curve or angle (Fig. 6). The curve ranges from slightly curved (multipurpose), to more angled (hockeystick or picard) to completely circular (pigtail). These are either used as flush catheters (pigtail) or to catheterize arteries with angled origins to the direction of catheter like aortic arch branches (picard).
2. **Complex curve catheters:** These have more than one curve and are usually used for selective catheterization of branches of the descending aorta. The curve closest to the tip is known as the primary curve while the farther curves are known as secondary curves or the tertiary curves. The primary curve helps to hook a target vessel at an angle while the secondary curve hits the back wall of the main vessel (the wall opposite to the origin of target vessel) and helps to push the catheter further into the target vessel. These catheters may be of two types:
  - a. The primary and secondary curves are in the same direction, e.g. Cobra, renal double curve, head hunter, etc (Figs 7A to C). They are best used for

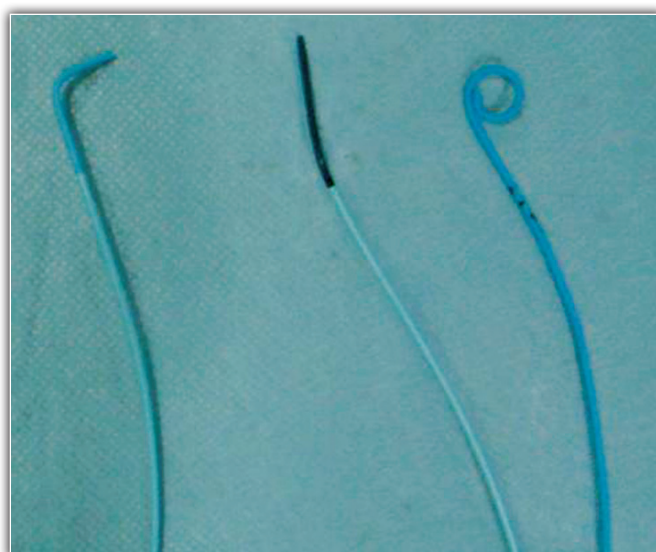
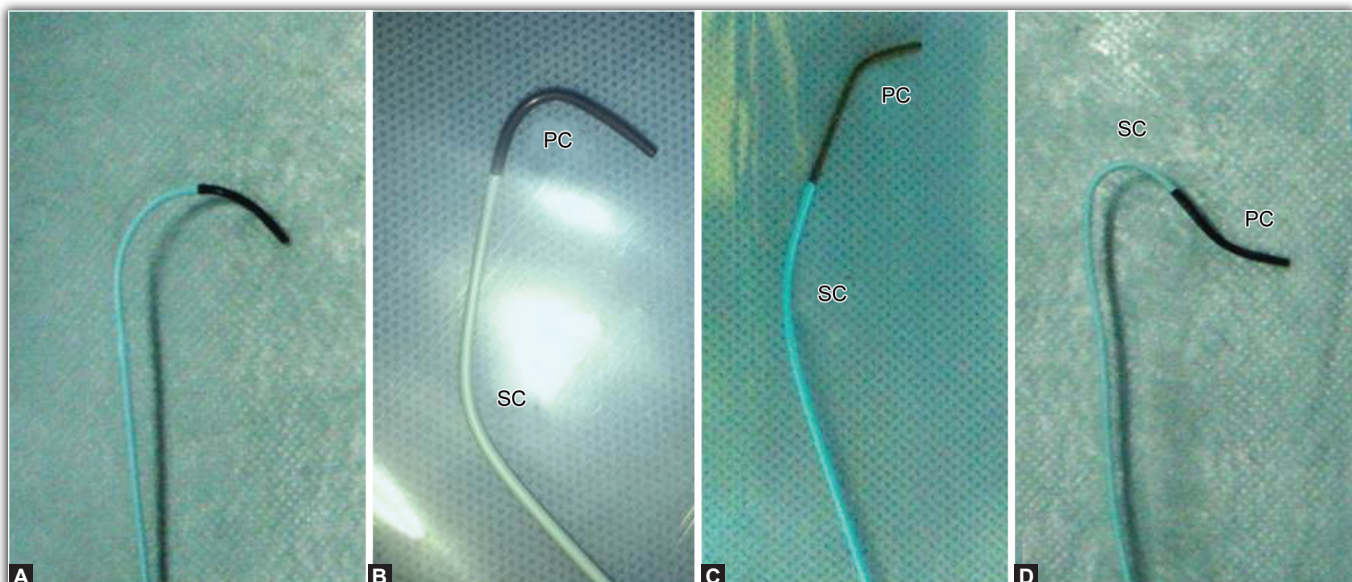


**Fig. 6** Simple curve catheters: From left to right—picard, multipurpose and pigtail



**Figs 7A to D** Complex curve catheters: The primary and secondary curves are in same direction in Cobra (A), renal double curve (B) and head hunter (C) catheters while in reverse curve catheters they are in opposite direction as in Simmons catheter (D)

- selective catheterization of vessels which have origins angled caudally like the visceral arteries.
- b. The primary and secondary curves in opposite direction—Reverse curve catheters, e.g. Simmons (1,2 and 3) catheters (**Fig. 7D**). These are best used for selective catheterization of vessels which have steep obtuse angle like the left gastric artery or steep acute angled vessels (sometimes visceral arteries, left common carotid in atherosclerotic aortic arch). These catheters are straightened over a guidewire before advancing and their curves need to be reformed within the aorta after removal of guidewire. Several techniques have been described for the formation of these curves either in the arch or at aortic bifurcation. After hooking the target vessel by the tip of the catheter over a guidewire, these catheters are advanced into the vessel till the level of apex of secondary curve by partial withdrawal of the catheter at the groin (instead of pushing as done in all standard forward curve catheters). Only after this point the catheters can be further pushed into the vessel by advancing over a stiff guidewire. Due to their shape they have increased chances of vessel wall injury while pulling out. Hence, these catheters should always be withdrawn after straightening over a guidewire under fluoroscopic monitoring.

Depending upon the position and number of holes, the catheters are divided into two types:

1. **End hole catheter:** These are the standard diagnostic catheters which have a single hole at the tip of the catheter. The size of the hole is tapered to allow the

maximum allowable sized guidewire to just pass through it snugly. These are used for selective catheterization. Pressure injector is not used with these catheters as it may cause plaque dislodgement and dissection.

2. **Side hole catheters:** The side holes are usually multiple with an end hole. These catheters are used as flush catheters to obtain angiograms of large vessels. The side holes vary in number with typical pigtail flush catheter having 8 to 12 side holes. Though the size of an individual side hole is smaller than the size of the end hole (to prevent exiting of guidewire through this hole), the combined size of the side holes is larger than the end hole allowing much larger volume of contrast dispersal through these holes than the end hole. The multiple side hole catheters are preferred for flush injections as they cause uniform dispersal of contrast in the vessel. The side hole catheters are also used for thrombolysis as they result in uniform distribution of the thrombolytic agent within the thrombus. However, these catheters are not used for embolization as the embolising agents may either diffuse out through these holes resulting in nontarget embolization or may occlude the end hole at the tip due to lesser pressure delivered at the tip. The embolising coils may also get struck within the side holes.

The commonly used catheters in clinical practice are:

1. **Multipurpose (Fig. 6):** It has straight tip. It can have end hole which is used for selective catheterization of small vessels or in pediatric patients. The side holes multipurpose catheter is used for flush injections in smaller vessels which cannot accommodate the loop of pigtail catheter, e.g. iliac vessels.

2. **Pigtail (Fig. 6):** It is a multiple side hole and end hole catheter with a circular shape and is used for flush injections in large lumen vessels like aorta. The pigtail shape prevents direct intimal injury and ensures much less recoil of catheter after forceful injection of contrast through a pressure injector. It is also commonly used for drainage of collections as it gets secured within the cavity.
3. **Picard (Fig. 6):** It is an end hole catheter with tip angled at obtuse shape (100 degree). It is commonly used to selectively catheterize forward facing angled origin vessels like the arch vessels and bronchial arteries.
4. **Cobra (Fig. 7A):** It is an end hole catheter with a double curve shape and is commonly used for selective catheterization of visceral vessels. It is available in three different curve shapes C1, C2 and C3 with C2 being the most commonly used.
5. **Renal double curve (RDC) (Fig. 7B):** As the name suggests it has two curves and is used for catheterization of renal vessels. The secondary curve rests against the aortic wall whereas the primary curve enters the vessel.
6. **Head hunter (Fig. 7C):** It has three curves. It is used for selective catheterization of the head and neck vessels.
7. **Simmons (Fig. 7D):** These are reverse curved catheters which are available in three curve shapes S1, S2 and S3 with increasing length of the curved segment. They are used to catheterize vessels with very acute or obtuse angled origin.
8. **Slip catheter:** These are catheters with a special hydrophilic coating to increase their pushability within the vessel. They can be of various tip shapes from straight to curved.

### Balloon Catheters

These are catheters with a balloon mounted on them close to their distal end. These are used for dilatation of a stenosed vessel, i.e. angioplasty. The balloons can be compliant, i.e. get stretched and increase their diameter on inflation beyond a certain pressure or noncompliant, i.e. do not get stretched beyond a maximum diameter. A noncompliant balloon provides greater dilating force than a similar compliant balloon.

The balloons are most commonly made of polyethylene terephthalate (PET) which is a relatively noncompliant polyester derivative. It appears like a very thin plastic. These balloons should not be used on calcified plaques or metal stents because of high chances of rupture.

Balloons are also made of nylon derivatives which are relatively more compliant than PET. These are softer but more scratch resistant than a PET balloon. They are commonly used for mounting balloon expandable stents.

The balloons used in interventional radiological practice are of two types:

1. **Noncompliant, high pressure balloons:** Mainly used for angioplasty. They are most often made of PET. These are used mainly in lower limb, renal, visceral and internal carotid arteries. The larger sized balloons are used in aorta, veins or in valves. They may also be used for nonvascular applications like dilatation of esophagus, duodenum or colon.
2. **Compliant, low pressure balloons:** Made of latex, silicone or polyurethane. They are used for temporary vascular occlusion, embolectomy or molding of stent grafts. The vascular occlusion by balloon may be required for the purpose of preventing reflux of embolic material proximally during embolization, or to minimize antegrade blood flow during embolization when alcohol is used as embolizing material as in alcohol embolization of renal cell carcinomas or arteriovenous malformations. The embolectomy balloon catheters used for removing acute thrombi and clots from vessels are also compliant. The most commonly used is the Fogarty balloon catheter.

### GUIDEWIRE

Medical guidewire is used to access the vascular, biliary and pelvicalyceal system for a variety of diagnostic and therapeutic medical procedures. The purpose of the guidewire is safe introduction and selective positioning of the catheter which is subsequently placed. An initial guidewire, or access wire, is first inserted through body passageways to a location where a medical procedure or treatment is to take place. In the next step, a catheter is advanced over the inserted guidewire, which enables the catheter to follow its predefined pathway to the point of treatment. Thereafter, other devices or fluids may be inserted via the catheter tubing, as needed. A guidewire is typically advanced beyond a stenosed area to allow balloon catheters and stents to treat the area.

The typical guidewires used in interventional radiology are constructed of a tightly wound fine outer wire of steel and a stiff inner "Mendrel" core wire. Addition of nitinol may be done to prevent kinking. Platinum and gold are added for better radio-opacity. These wires are made in a variety of sizes and lengths but usually range from 0.010 to 0.038 inch in diameter and 50 to 300 cm in length. The outside of guidewire is frequently has hydrophilic coating or Teflon coating to reduce friction and may be impregnated with heparin to reduce thrombogenicity. The hydrophilic coating works best when the wire is wet. The inner core provides the rigidity of the wire. The inner core wire is tapered towards the introduction end of the guide wire and ends at a variable distance from the tip. Varying the taper and the distance that the core extends towards the ends of guidewire allows one to vary tip flexibility and the transition zone length. Some wires have movable cores so that the flexibility of the tip can be changed at will. Most guidewires have a fine safety wire along the full length to prevent the outer wire coil from uncoiling and breaking off.

Flexible tip standard wires are generally used for routine percutaneous introduction of catheters. Tip flexibility allows the wires to buckle and avoid damaging the vessel. However, one must be aware that even a flexible guidewire may act as a sharp object when it first exits the tip of catheter. Exchange wires are long and allow enough length of the wire between the target site and external site so that a new catheter may be introduced without losing wire purchase internally.

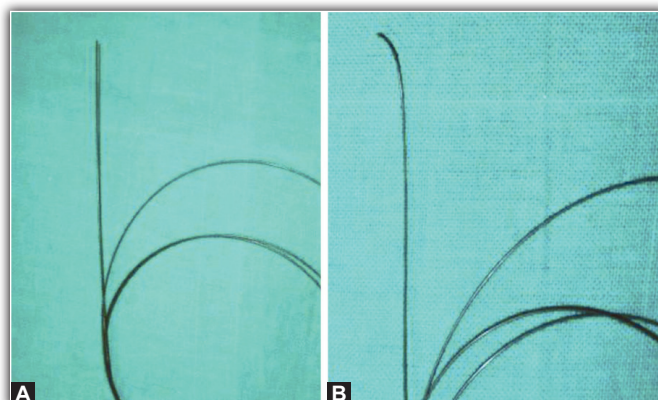
Based on the stiffness of the guidewire, they may be classified as floppy, of normal stiffness (e.g. Terumo hydrophilic guidewire) or stiff/extrastiff (e.g. amplatz). The guidewires may also be classified as (1) Steerable—which have shaped tips with good torque control and hydrophilic coating and are used for negotiating stenosis, and (2) Nonsteerable, which are stiffer wires allowing the positioning of the catheter but not used for crossing the stenosis.

Most guidewires are fragile and can be very expensive. Care should be taken to preserve their useful life as long as possible. Guidewires should be wiped with a saline soaked gauze or lint free pad after each introduction into the body. The build-up of blood clot, fibrin, or dried contrast can render the wire useless. It may also cause it to stick inside the catheters or cause emboli. The guidewires should be stored loosely coiled in a bowl of saline. The saline can be heparinised (5000 U/L) to help prevent thrombus formation.

### Selection of Guidewires

Guidewires are a tactile-based surgical tool, which means that physicians take several factors into consideration when choosing their guidewire. Some wires have tapered cores at each ends allowing both ends to be used for introduction. Some guidewires are specially made to enhance their torquability which is the ability to translate rotational movement of the wire on the outset to the tip inside the patient. These wires can be steered into the desired location in the body.

Based on the shape of the tip, the wires are of two types—J-tip or straight tip (**Figs 8A and B**). The J-tip wires are



**Figs 8A and B** Guidewire: Straight tip (A) and J-tip (B)

frequently used for hooking the ostium of various arteries. Straight tip guidewire is used to negotiate biliary obstruction during percutaneous biliary drainage (PTBD). The hard end of the guidewire may be used to push the coil inside the catheters from the cartage where it is lodged. The extra or superstiff guidewire are commonly used for inserting percutaneous drainage catheters or insertion of stents into biliary system.

### FNAC AND BIOPSY NEEDLE

Biopsy or Fine Needle Aspiration Cytology (FNAC) are procedures to obtain a sample of tissue from a tumor for pathological examination. The FNAC is a simple and fast procedure for cytological diagnosis. The core needle biopsy is more reliable than FNAC but requires thicker needle, longer processing time and is a little more invasive than FNAC. Needle biopsy may be used to take tissue or fluid samples from muscles, bones and organs, such as the liver or lungs.

The various types of needles that are commonly used for radiologic procedures are as follows:

1. **Needle size:** Fine needles (20 to 25 Gauge) are ideal for cytology and can be safely introduced even through the bowel (except colon) with less chance of hemorrhage. Larger needles (14 to 19 Gauges) have a better yield of tissue which can help in further subtyping. But it is more traumatic.
2. Cutting edge of the needle could be end cutting (acute bevel/ninety degree bevel) or side cutting (cannula gap/stylet gap).
3. Spring loaded/automated side cutting needles are also available.

The selection of the size of needles usually depends on the procedure, size and location of the target. Small lesions at deeper location may require 20 G needle as it stiffer than 22 G which can bend during insertion. However, 22 G needles will be optimum for FNAC of superficial lesions like thyroid or lesions located in the surface of liver. Whenever there is a need to transgress bowel (as in FNAC of pancreatic mass or mesenteric nodes) or a potential space (as in FNAC of lung mass through pleura) or in very hypervascular mass (as in kidney, thyroid), fine needles of 20 to 25 G need to be used for less complication. Thicker needles (14 to 19 G) should be used in suspected case of lymphoma as well as in equivocal fine needle aspirate in case of unknown primary. Longer needles like Chiba (20–25 G, Cook catheter, Bloomington, IN) are used whenever samples to be taken from a deeper location.

When a single needle technique is used, multiple punctures are required to obtain multiple samples. This can be more traumatic at times. Alternatively, a co-axial needle system can be used to obtain multiple samples using a single puncture. In this system, a thinner inner needle is inserted through a larger outer needle called an introducer. True-cut-type cutting needles powered by spring-activated handles can be used to obtain a bigger core of tissue, which is of particular importance in the diagnosis of benign lesions (as

in benign lung nodules- granulomas/hamartomas) and in lymphoma.

### STENT

A stent is a fine tubular structure open at both end that is usually placed into a tubular structure to keep its lumen open.

The procedure of placing a stent is called stenting. Commonly placement of stents is done in vascular, biliary and urinary system. Other reasons to use stents include keeping open a blockage in the airways. The general categories of stents are self-expanding (SE), balloon-expandable (BE), and stent-grafts (SGs).

SE stents (**Fig. 9A**) are composed of nitinol or elgiloy that are compressed into a delivery catheter that is unjacketed at the point of delivery. They are flexible but are prone for foreshortening. The example of SE stents are wallstent (Boston Scientific), SMART (Cordis Endovascular) and Zilver (Cook).

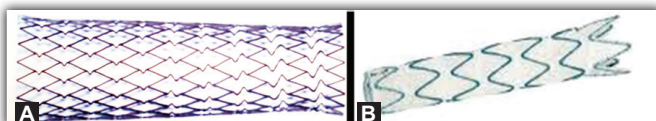
The BE stents are manufactured premounted on a balloon and deployed by dilating with a balloon with an inflator. The BE stents possess stronger radial force but have the potential for dislodgement from the balloon. The Palmaz (Cordis Endovascular) and Express (Boston Scientific) are examples of BE stents.

The stent-grafts (SGs) may SE or BE which are covered with synthetic material such as Dacron or PTFE (**Fig. 9B**). Potentially they can prevent the restenosis by their barrier effect but they are costly. Wall graft (Boston Scientific) is a self-expanding stent graft whereas iCast (Atrium Medical,Hudson) is a balloon-expandable stent graft used for aorto-iliac occlusion. These are used when the walls of the vessel need to be covered as in pseudoaneurysms and arterio-venous fistulas. The disadvantage of these stent grafts in vascular use is that if there are any branches arising from the segment of parent vessel in which graft is placed, they get blocked.

Commonly placement of stents is used in vascular, biliary and excretory system. Other reasons to use stents include keeping open a blockage in the airways.

### Vascular Stent

The commonly performed vascular stenting is used for coronary, carotid, aorta and lower limb arteries. Vascular stenting is used after angioplasty to treat conditions that involve a narrowing or blockage of arteries or veins throughout the body, including:



**Figs 9A and B** Stents: Self expanding stent (A) and covered stent graft (B)

- Narrowing of large arteries (aorta and its branches) due to atherosclerosis, or hardening of the arteries, a gradual process in which cholesterol and other fatty deposits, called plaques, build-up on the artery walls.
- Peripheral artery disease (PAD), a narrowing of the arteries in the legs or arms. In patients with PAD, angioplasty alone or angioplasty with stenting may be used to open up a blocked artery in the pelvis, leg or arm.
- Renal vascular hypertension, high blood pressure caused by a narrowing of the kidney arteries. Angioplasty with stenting is a commonly used method to open one or both of the arteries that supply blood to the kidneys. Treating renal arterial narrowing is also performed in some patients to protect or improve the kidney function.
- Carotid artery stenosis, a narrowing of the neck arteries supplying blood to the brain.
- Coronary artery disease, a narrowing of the coronary arteries that carry blood and oxygen to the heart muscle. An intraluminal coronary artery stent is a small, self-expanding, metal mesh tube that is placed inside a coronary artery after balloon angioplasty to prevent the artery from reclosure.
- Venous narrowings involving the central veins (in the chest, abdomen or pelvis). In some cases, stenting of the narrowed vein is also needed.
- Keeping artificial communication between hepatic vein and portal vein in TIPS.
- Narrowing in dialysis fistula or grafts. When there is decreased flow in the graft or fistula so that is not adequate for dialysis, angioplasty is generally the first line of treatment. Stenting or stent grafting may also be needed in some cases.

A drug-eluting stent is coated with a medicine that stops the growth of fibroblast further prevent the arteries from re-closing. It is like any other coronary artery or peripheral artery stents which is left permanently in the artery.

### Biliary Stent

Biliary stents are usually placed to relieve a benign or malignant obstruction of the biliary tree. It may be plastic or metallic and the two most common methods that are used to place a biliary stent are endoscopic retrograde cholangiopancreatography (ERCP) and percutaneous transhepatic cholangiography. Biliary stenting is used to treat obstructions that occur in the bile ducts. There are a number of conditions, malignant or benign, that can cause strictures of the bile duct. Pancreatic cancer is the most common malignant cause, followed by cancers of the gallbladder, bile duct, liver, and large intestine. Noncancerous causes of bile duct stricture include injury to the bile ducts during cholecystectomy, gallstones, pancreatitis and primary sclerosing cholangitis.

An internal stent prevents the problems related to external drainage like, pericatheter leakage of bile. The disadvantage is the procedure of insertion which is invasive.

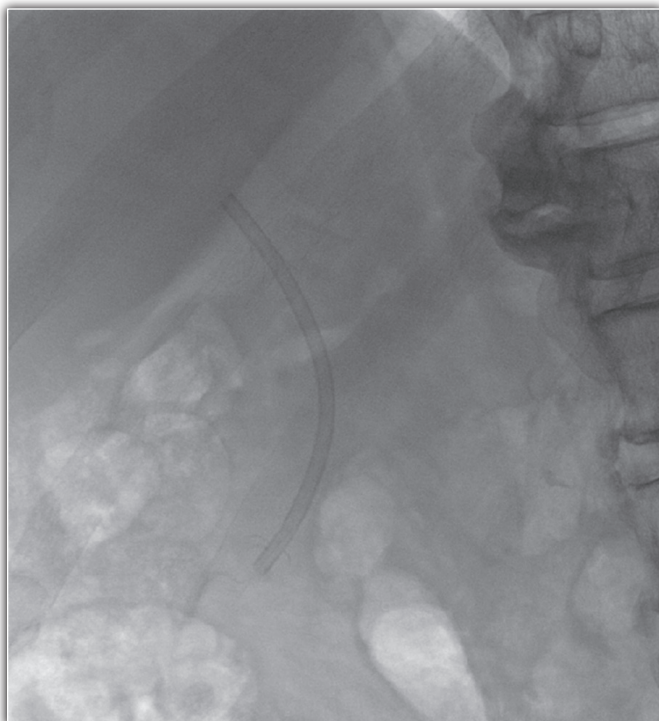


**Fig. 10** Plastic stent seen within the common bile duct

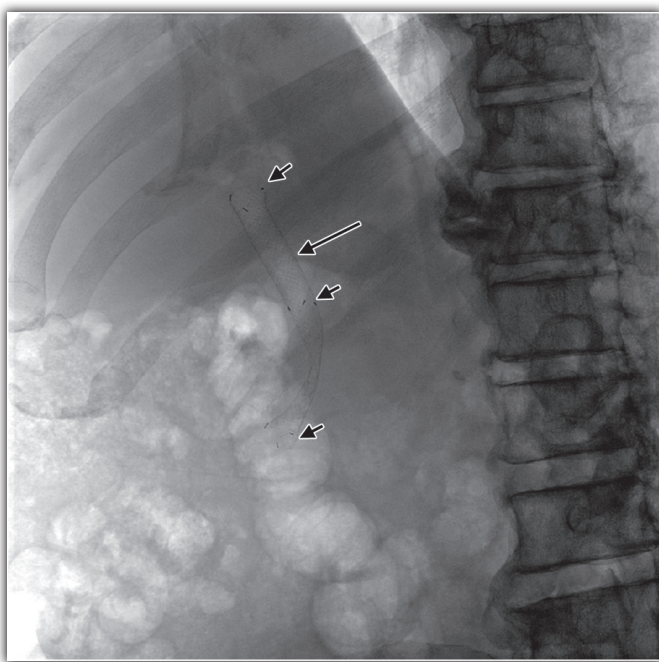


**Fig. 11** Metallic stent inside the CBD—note the radiopaque markers (short arrows) in the upper, mid and lower part of the stent

Better patency rates are reported with metallic than with plastic stents in cases of malignant obstruction, though no effect on survival is noted. Plastic internal stents (**Fig. 10**) are cheapest but reportedly prone to migration. Various types of plastic stents in use include the Carey-Coons stent (Percuflex; Meditech/Boston Scientific) and silicone stents (Malecot; Cook, Inc).

Metallic stents (**Fig. 11**) are generally not used in the treatment of benign disease because studies have shown poor long-term patency rates. The Gianturco-Rosch Z stent (Cook, Inc), a metallic stent, has been used in benign strictures, but it should not be used for primary treatment. Limited applications may include the treatment of patients who are poor surgical candidates or of those in whom surgical treatment fails. Most postoperative strictures are treated surgically, though endoscopic and (less commonly) percutaneous placement of nonmetallic stents has increasingly been used in the past few years.

In cases of malignant obstruction, stents are placed as a palliative measure only if the tumor is unresectable. Various stents are approved for use in the biliary system, including self-expanding and balloon-mounted stents. Various self-expanding stents include the Wallstent (Boston Scientific; Natick, Mass), Luminex stent (Bard; Tempe, Ariz), and Smartstent (Cordis Endovascular; Miami, Fla).

### Ureteral Stents (Fig. 12)

Ureteral stents are used to ensure the patency of a ureter. Ureteral stents are used to relieve ureteral obstruction, promote ureteral healing following surgery, and to assist with ureteral identification during pelvic surgery. This method is sometimes used as a temporary measure to prevent damage to a blocked kidney until a procedure to remove the stone can be performed. Indwelling times of 12 months or longer are indicated to hold open ureters which have been compressed by tumors in the neighborhood of the ureter or by tumors of the ureter itself. In many cases these tumors are inoperable and the stents are used to ensure drainage of urine through the ureter. If drainage is compromised for longer periods,



**Fig. 12** Plastic double J ureteric stent with the pusher

the kidney can be damaged. The main complications with ureteral stents are dislocation, infection, and blockage by encrustation. Recently, stents with coatings (e.g. heparin) have been approved to reduce infection, encrustation and, therefore, the frequency of stent replacement.

### EMBOLISING AGENTS

Embolising agents are materials used to acutely stop blood flow in a vessel by mechanical occlusion. The clinical uses are to stop hemoptysis, hematuria, hematochezia, internal bleed or a pseudoaneurysm. Embolization may also be done as an adjunct to surgery or for palliation of malignant tumors. The embolising agents can be temporary or permanent. The embolization can be done in proximal vessel or in distal bed. Further, the embolization may or may not lead to organ/cellular death. Based on these requirements, the embolising agents are divided into four main categories:

#### Permanent Proximal Occluders

- a. **Coils:** These are made of steel or platinum. They commonly have constituent thrombogenic polyester fibers. They are introduced within the vessel in straightened condition but form a spring shape when ejected out of the distal end of delivery catheter. They form a scaffolding upon which thrombus forms leading to permanent occlusion of the vessel. The coils come in various sizes depending upon the size of the wire used, the length of the coil and the diameter of the unconstrained coil. A typical example is 35-3-4. The 35 represents the diameter of the wire used to make the coil in inches which in turn determines the catheter lumen through which it will pass through. The 3 represents the length of straightened coil in cm which is chosen based on length of vessel available for deployment of coil and the 4 represents the diameter of the unconstrained coil loop in mm which is chosen based on diameter of the vessel in which the coil is to be deployed. Coils measuring .018 inches or less are termed microcoils and require microcatheters for their deployment. Nester coils are special fibred coils on a platinum strut which are soft and pliable. They conform to the target vessel anatomy when deployed and mainly used for filling-up space in large vessels or aneurysms as they bunch up within the lumen. The coils are of two types based on method of deployment: (i) pushable-can be pushed out of the catheter by a guidewire or coil pushers, and (ii) detachable-are detached from the catheter tip *in vivo* by either mechanical pressure or electrolytically.
- b. **Amplatzer vascular plug** is a nitinol mesh device which is self-expandable occlusive agent. It is deployed by mechanical detachment and is used to occlude vessels ranging from 4 to 16 mm diameter.

The other less commonly used materials in this category are detachable balloons made of latex or silicon (used for treatment of carotico-cavernous fistulas), small intestinal submucosa, suture material and bare angiographic wires.

#### Permanent Distal Occluders

- a. **Polyvinyl alcohol (PVA) particles (Fig. 13A):** This is an inert plastic particle which comes in varying sizes from 100 to 1100  $\mu\text{m}$ . It is available in small vials with each vial having particles of a range of sizes, e.g. 300 to 500  $\mu\text{m}$ , 500 to 700  $\mu\text{m}$  etc. It is in fine dry coarse powder form which needs to be suspended in saline or contrast before it is injected through the catheter. The size of the particles to be injected is chosen based on the size of the distal vessel bed to be embolized. The particles go and form clumps within the vessels to permanently occlude it. If larger size particles are chosen they may cause clumping within the catheter or proximal vessel itself to lead to their occlusion. These are most commonly used in tumor bed embolizations (often preoperatively to decrease the vascularity), bronchial artery embolizations, uterine fibroid embolizations, etc. The end point is distal occlusion of the small arterioles without proximal vessel occlusion thereby keeping the option of future repeat embolization of the same vascular territory. One vial of PVA particles costs approximately ₹ 5000. PVA is also available in the form of spherical PVA which makes it more compressible and therefore facilitates the delivery. The typical examples are bead block made of hydrogel PVA or embospheres constituted from triacryl gelatin spherical hydrophilic spheres.
- b. **Sclerosants:** These are liquid agents which produce vascular occlusion by causing inflammation and thrombosis. Absolute alcohol and sodium tetradecyl sulfate (STS) are the two most commonly used sclerosants. Absolute alcohol, besides causing permanent vessel occlusion, also leads to cell death and tissue ablation. It is therefore reserved for use where the end organ cell death is acceptable, e.g. in renal cell carcinomas. It is a very painful procedure and thus is best performed under general anesthesia or liberal analgesia atleast. The use of protective devices like proximal balloons is often required with the use of alcohol to prevent nontarget embolization. Sodium tetradecyl sulfate (STS) (Fig. 13B) is a relatively milder sclerosant which does not lead to cell death. A 3 percent concentration solution is used. It is mainly used for spermatic vein ablations, pelvic congestion syndrome and for venous vascular malformations.
- c. **Cyanoacrylates:** These are tissue adhesives. The most common used product is N-butyl cyanoacrylate (NBCA) or glue (Fig. 13C). These are in the form of clear liquids at room temperature which get instantly



**Figs 13A to D** Embolising agents: PVA particles of various sizes (A), sodium tetradecyl sulfate (B), N-butyl cyanoacrylate (C) and Gelfoam (D)

polymerized when they come in contact with an ionic environment. Thus even a small amount of saline or blood leads to initiation of polymerization reaction of cyanoacrylates. For this reason when they are to be injected via the delivery catheter, the catheter should be flushed completely with a nonionic solution (most commonly used 20% dextrose) before and after each injection to prevent polymerization of the agent within the catheter. As soon as the agent ejects out of the distal catheter tip within the vessel, it comes in contact of blood (ionic) and gets polymerized to form a cast. Also since the cyanoacrylates are radiolucent, they are delivered by mixing them with a radiopaque substance to make them visible under fluoroscopy. Ethiodol (brand name Lipiodol by Guerbet) is the most commonly used nonionic substance for the same. It is usually mixed in ratio of 1:1 to 5:1 to make 50 to 20 percent concentration of glue respectively. Higher the concentration of glue (lesser the amount of ethiodol added), the more proximal and earlier is the cast formation of glue when it comes in contact with blood at the distal end of catheter within the body. A lesser concentration leads to farther delivery of the embolic agent with a slightly delayed cast formation. The embolus which ultimately forms is larger than anticipated with the amount of cyanoacrylate as the substance draws blood elements within it. One vial of glue costs approximately ₹ 500.

- d. **Onyx:** It is a liquid embolic agent formed by combination of ethylene-vinyl alcohol copolymer, dimethyl sulfoxide and tantalum powder. It comes in the form of two vials, one containing the copolymer mixed with tantalum

powder and the other containing dimethyl sulfoxide. These need to be mixed and shaken in a shaker for 20 minutes immediately prior to injection for the agent to become ready for use. The onyx forms a cast as soon as it gets in contact with ionic material (like glue). The cast formation starts from outer surface to inner region. The major advantage of using onyx is much better control over the injection than glue but the deterrent is the significantly higher cost with one vial costing approximately ₹ 40,000.

- e. **Thrombin:** It is an enzyme which participates in the coagulation pathway and converts fibrinogen to fibrin. It is mainly used for hemostasis on surgically cut surfaces in the operation theater. Intravascularly it has been used to induce thrombosis of pseudoaneurysms. Care is required to prevent its propagation into main vessel so as to prevent its occlusion.
- f. **Ethiodol:** It is manufactured under the brand name lipiodol. It is an inert oil-based contrast agent which is also used as embolising agent. The radiopaque properties of lipiodol help to make it visible during embolization procedure. Once injected into the vessel, the fat droplets get released and travel distally into smaller vessels till they cannot cross due to their size and then occlude the vessel. This level of distal embolization is at the level of small arterioles. It is commonly used mixed with glue for embolization. The radiopacity of lipiodol adds contrast to glue while the oil-based structure does not allow glue to solidify within the syringe/catheter till it comes in contact with ionic blood. Lipiodol is also used for embolization of hepatocellular carcinoma

in combination with chemotherapeutic agents. It has affinity for the lesion and gets deposited in it even when injected nonselectively besides providing radiopacity to the mixture.

### Temporary Proximal Occluders

- a. **Gelatin sponge:** It is most commonly used in the form of gelfoam (**Fig. 13D**). It is available as a block which is cut into small pledges and is made as a slurry mixed with contrast agent for intravascular injection. It leads to temporary mechanical occlusion of proximal vessels for a period of one week to few months. It is used in situations where preservation of blood flow is required in the long term, e.g. to control bleeding from liver, spleen and in immediate preoperative embolization of tumors. Being inexpensive and easy to use, it is often used as a scaffold for combined embolization with coils.
- b. Autologous clot used for very short term temporary embolization as it gets lysed within few hours. May be used in coagulopathic patients to control bleeding.
- c. Nondetachable occlusion balloon used in specific situations like before surgery to reduce intraoperative blood loss, for precise placement of embolic material or to reduce reflux of embolizing material into parent vessel.

### Temporary Distal Occluders

- a. **Starch microspheres:** These are produced from vegetable sources like corn and potato. They are used for very short duration (few minutes) occlusion of

distal small vessels, e.g. in procedures like intra-arterial chemotherapy.

- b. **Gelatin sponge powder:** It is also available in powder form. When delivered it reaches distal circulation to block it temporarily.

### BIBLIOGRAPHY

1. Bakal CW. In Image-guided interventions, Mauro MA, Murphy K, Thomson K, Venbrux AC, Morgan R and Zollikofer CL (Eds). Philadelphia: Elseviers, 2008.
2. Gabelmann A, Hamid H, Brambs HJ, Rieber A. Metallic stents in benign biliary strictures: long-term effectiveness and interventional management of stent occlusion. AJR Am J Roentgenol. 2001;177(4):813-7.
3. Kaufman JA. In Image-guided interventions, Mauro MA, Murphy K, Thomson K, Venbrux AC, Morgan R and Zollikofer CL (Eds). Philadelphia: Elseviers, 2008.
4. Klein JS, Solomon G, Stewart EA. Transthoracic needle biopsy with a coaxially placed 20-gauge automated cutting needle: results in 122 patients. Radiology. 1996;198:715-20.
5. Lopez RR Jr, Cosenza CA, Lois J, et al. Long-term results of metallic stents for benign biliary strictures. Arch Surg. 2001; 136(6):664-9.
6. Seldinger SI. Catheter placement of needles in percutaneous arteriography: a new technique. Acta Radiol. 1953;39:328-76.
7. Stavropoulos SW, Rajan D, Cope C. In Abram's angiography: vascular and interventional radiology, Baum S and Pentecost MJ (Eds), 2nd edition. Philadelphia: Lipincott Williams & Wilkins, 2006.
8. Strauss KJ, Damiano MM and Kandarpa K. In Handbook of interventional radiological procedures, Kandarpa K and Aruny JE (Eds), 3rd edition. Philadelphia: Lipincott Williams & Wilkins, 2002.

## Section

# 5

# Update in Contrast Media

- Chapter 17** ● MR Contrast Media  
*Anju Garg*
- Chapter 18** ● Ultrasound Contrast Agents  
*Shashi Bala Paul, Manisha Jana*
- Chapter 19** ● Iodinated Contrast Media: An Update  
*Chandrashekhar SH, Thulkar S*
- Chapter 20** ● Contrast Reactions and Its Management  
*Gaurav Pradhan, Rajat Jain*



## Chapter

# 17

# MR Contrast Media

*Anju Garg*

### INTRODUCTION

In the early days of magnetic resonance imaging it was thought that the excellent soft tissue contrast would obviate the need for any type of contrast agent, making the procedure completely noninvasive. Contrast in MRI arises mainly from the heterogeneous distribution of tissue relaxation times, and the lack of need for contrast materials is one of the major advantages of MR over other imaging techniques. However, it was noted that many important pathological conditions did not display specific enough changes in relaxation times to differentiate them from surrounding healthy tissue. Exogenous MR contrast agents were therefore developed shortly after the first commercial MR system became available in the 1980s. Presently exogenous contrast agents are frequently used in a significant proportion of MR examinations:

- To differentiate structures that are similar in appearance
- To provide additional specificity in describing regions of abnormal signal
- To specify or highlight spaces
- To depict tissue vascularity and perfusion.

### BASIC PRINCIPLES OF MR CONTRAST AGENTS

Contrast agents for X-ray and CT show contrasting effects according to the electron-density difference, and they produce direct contrast effects on their positions. However, the contrast mechanism is more complicated for MRI, where the contrast enhancement occurs as a result of the interaction between the contrast agents and neighboring water protons, which can be affected by many intrinsic and extrinsic factors such as proton density and MRI pulse sequences.

The basic principle of MRI is based on nuclear magnetic resonance (NMR) together with the relaxation of proton spins in a magnetic field. When the nuclei of protons, i.e. the body's hydrogen atoms, are exposed to a strong magnetic field, their spins align either parallel or antiparallel to the magnetic field. During their alignment, the spins precess under a specified frequency, known as the Larmor frequency which is dependant on the strength of the magnetic field applied. When a 'resonance' frequency in the radiofrequency (RF) range is applied, the protons absorb energy and realign from a longitudinal to a perpendicular (or transverse) axis. After the disappearance of the RF pulse, the excited nuclei relax to their initial, lower-energy state. There are two different relaxation pathways. The first, called longitudinal or T1 relaxation, involves the decreased net magnetization recovering to the initial state. The second, called transverse or T2 relaxation, involves the induced magnetization on the perpendicular plane disappearing by the dephasing of spins.

MR contrast agents act by altering these relaxation times and this is measured as relaxivity. The relaxivity of an agent is proportional to the magnitude of its moment, its tumbling frequency in solution and its spin relaxation time. Based on their relaxation processes, the contrast agents are classified as T1 and T2 contrast agents.

Molecules or ions with one or more unpaired electrons when placed in a magnetic field, generate a magnetic moment which aligns with the applied field. These ions or molecules are referred to as paramagnetic, superparamagnetic or ferromagnetic ions depending on their specific electronic configuration. The most commonly used MR contrast agents are a group of exogenous paramagnetic compounds of gadolinium, manganese and iron.

## CLASSIFICATION OF MR CONTRAST AGENTS

MR contrast agents can be classified according to:

1. The magnetic property of the agent
2. The dominant effect of the agent on the signal intensity
3. The bio-distribution of the agent.

### Magnetic Properties

This is the most common method used to classify the contrast agents into 2 main groups, namely paramagnetic and superparamagnetic.

#### Paramagnetic Contrast Agents

Paramagnetic materials have their own magnetic field and the local magnetic field of a paramagnetic agent reduces the T1 and T2 relaxation times of surrounding hydrogen nuclei, thus increasing signal on T1 weighted images. There are many paramagnetic metal ions that could potentially be used as MR contrast agents but the transition metal gadolinium ( $Gd^{3+}$ ) is by far the most commonly used. This is due to a favorable combination of many (seven) unpaired electrons combined with a long electron spin relaxation time which makes this metal a very efficient relaxation enhancing agent. Manganese, which has relaxation properties similar to gadolinium has also been used. All paramagnetic contrast agents are chelated with an appropriate ligand to minimize *in vivo* toxicity of free metallic ion.

#### Superparamagnetic Contrast Agents

Superparamagnetic agents behave in a manner similar to a paramagnetic substance. In clinical MRI, small or ultrasmall particles of superparamagnetic iron oxide are used as contrast agents. If the iron ions are magnetically ordered within the crystal, the net magnetic moment is so large that it greatly exceeds that of typical paramagnetic ions. This effect is referred to as superparamagnetism and is characterized by a large magnetic moment in the presence of an external magnetic field but no remnant magnetic moment when the field is zero. Superparamagnetic agents can also induce strong enhancement of the T1 relaxation rate of water (depending on size and composition of the particles), but their dominant effect is on T2/T2\* relaxation due to the large magnetic moment of the nanoparticles.

### Image Enhancement

The effect of the contrast agent on the signal intensity can either be positive (increase in signal or T1-enhancement) or negative (signal reduction or T2-enhancement). Almost all MR contrast agents will affect both T1- and T2-relaxation times and the distinction depends on many MR-specific parameters as well as contrast agent dose, e.g. gadolinium generally act as a positive enhancers on T1 weighted images but also have a weak T2 negative enhancing effect whereas

iron oxide based contrast agents have a predominant T2 and T2\* shortening effect and are negative agents.

### Biodistribution

The biodistribution of a contrast agent describes how the agent is distributed *in vivo* after intravenous administration.

#### Extracellular Fluid Agents

Small molecular weight (MW) paramagnetic agents are small enough to diffuse from the plasma into the interstitium and are thus distributed to the extracellular fluid. These agents are referred to as extracellular fluid (ECF) agents. They are not taken up by cells and are therefore eliminated by renal excretion with a half-life determined by the glomerular filtration rate, e.g. gadolinium based contrast agents.

#### Intravascular Agents

Intravascular agents are contrast agents with a MW large enough to prevent leakage from the vascular to the extravascular space. All iron oxide nanoparticles are intravascular agents, with a half-life in blood ranging from a few minutes to several hours. In blood, iron oxide agents with the appropriate composition can produce significant T1 shortening and several studies have investigated the use of nanoparticles for MR angiography. Other types of intravascular agents are based on macromolecular gadolinium compounds. Such agents are designed either by linking  $Gd^{3+}$  ions to a macromolecular polymer during synthesis or by making the  $Gd^{3+}$  complex bind to plasma proteins after injection and thus forming macromolecules in blood.

#### Tissue Specific Agents

Tissue specific agents are agents which have been specifically designed to accumulate in a given organ or tissue type. Intravascular iron oxides are taken up by the Kupffer cells of the liver, spleen and lymphatic system. Once taken up by the liver the nanoparticles will be accumulated into larger particulate clusters in the Kupffer cells and relaxation will be completely dominated by T2/T2\* effects. Iron oxides can thus be said to be both intravascular agents as well as tissue specific agents. Mangafodipir trisodium and few gadolinium chelates also act as liver specific agents as they are taken up by hepatocytes.

Contrast agents have also been developed, and are in clinical testing, for targeting of atherosclerotic plaques as well as different types of tumor antibodies.

## GADOLINIUM BASED CONTRAST AGENTS

In the early 1980's, Copper ( $Cu^{2+}$ ), Manganese ( $Mn^{2+}$ ) and Gadolinium ( $Gd^{3+}$ ) were recognized as paramagnetic ions capable of shortening the  $T_1$  of water. After extensive testing

of many paramagnetic chelates, the gadolinium diethylenetriamine penta acetic acid salt (Gd-DPTA) was singled out because of its high tolerability in animals and preserved good relaxation properties. Gadolinium-DTPA was first tested in humans in 1983 and in early 1988, the pharmaceutical product gadopentetate dimeglumine was launched as the first MR contrast medium.<sup>1</sup>

Gadolinium has an atomic number 64 and is one of a series of 17 chemically inert metals, the lanthanides. Gadolinium is named after the Finnish chemist Johan Gadolin.<sup>2</sup> It is a paramagnetic agent because of its seven unpaired electrons. This strong paramagnetic effect disturbs the relaxivity of nearby water protons resulting in a decrease of both T1 and T2 relaxation times. The reduction in the T1 relaxation time is greater at low gadolinium concentrations and this is seen as increased signal intensity on T1 weighted spin-echo or gradient-echo images.

Free Gd<sup>3+</sup> ion is highly toxic *in vivo* because it competes with calcium. As gadolinium has a higher binding affinity for calcium-binding enzymes, it can displace calcium and thus alter all biological processes catalyzed by these enzymes. Free gadolinium also interferes with calcium channels to block physiological pathways that rely on Ca<sup>2+</sup> influx, i.e. neural transmission and coagulation.<sup>3</sup> However, when it is bound (or chelated) to an organic ligand, gadolinium is generally regarded as safe for use as an MR contrast agent.

Currently there are nine GBCAs approved for use in the United States and/or the European Union. Most available GBCAs are low molecular weight polyamino-carboxylate compounds (**Table 1**).

They can broadly be classified into two categories based on their binding to serum proteins: (1) The nonspecific extracellular gadolinium chelates or agents

which do not bind to serum proteins and (2) The high relaxivity agents, which bind to serum proteins. The **nonspecific extracellular GBCAs** include—gadopentetate, gadoterate, gadodiamide, gadoteridol, gadobutrol, and gadoversatamide. They do not bind to any protein and their biodistribution and pharmacokinetics are essentially similar to iodinated water-soluble contrast media. After intravenous injection, they rapidly diffuse into the interstitial extra-vascular space. Reverse diffusion into the intravascular compartment also occurs and a state of equilibrium between diffusion in and out is usually reached within 2 hours. They are eliminated unchanged from the intravascular compartment by passive glomerular filtration and by 24 hours greater than 95 percent of the injected dose is excreted in urine with normal renal function. A very small amount (less than 0.1%) is eliminated via feces. Biological half-life is approximately 1.5 hours in patients with normal renal function.

Three basic phases of vascular and tissue enhancement occur following administration of GBCAs: arterial, blood pool and extracellular phases. Routine post contrast images are acquired when the contrast has reached the extracellular interstitial space i.e. approximately 2 minutes after injection. As the extracellular enhancement changes little over several minutes, fast scanning techniques are not essential for imaging. Interstitial enhancement is particularly conspicuous with suppression of the lipid signal intensity and TIW, fat suppressed images give the best contrast. However, if fat is nulled via inversion recovery with a short inversion time (STIR), enhancing tissue is also nulled because of its short T1 relaxation time. Therefore, the STIR technique is not recommended after administration of T1-shortening contrast agents.

**Table 1** Gadolinium based contrast agents approved for clinical use<sup>6</sup>

Generic Name	Trade Name/ Manufacturer	T1 relaxivity (L/mmol/s at 1.5 T)	Molecular weight	Excretion	Protein binding
Gadopentetate dimeglumine Gd-DTPA	Magnevist/Bayer	4.1	939.0	Renal	None
Gadoterate meglumine Gd-DOTA	Dotarem/Guerbert	3.6	558.6	Renal	None
Gadodiamide Gd-DTPA-BMA	Omniscan/GE	4.3	573.6	Renal	None
Gadoteridol Gd-HP-DO3A	ProHance/Bracco	4.1	558.7	Renal	None
Gadobutrol Gd-DO3A-butrol	Gadovist/Bayer	4.7	604.7	Renal	None
Gadoversatamide Gd-DTPA-BMEA	Optimark/Mallinckrodt	4.7	661.8	Renal	None
Gadobenate disodium Gd-BOPTA	MultiHance/Bracco	8.3	1058.2	96% Renal, 4% Hepatic	<5%
Gadoxetate disodium Gd-EOB-DTPA	Primovist, Eovist/Bayer	6.9	682.0	50% Renal, 50% Hepatic	<10%
Gadofosveset trisodium	Vasovist, Ablavar/Bayer	19	958.0	91% Renal, 9% Hepatic	>85%

Interstitial contrast agent is particularly prominent in tissues such as neoplasms and areas of inflammation. Fibrous tissue typically has a large interstitial space, therefore is much enhanced on extracellular phase images even though it is usually hypovascular. Many metastases also have large interstitial spaces and are hyperintense on extracellular phase images. Brain and testicular capillaries are not permeable to these contrast agents, unlike capillaries throughout the rest of the body. So the enhancement of the brain is minimal, owing entirely to enhancement of the blood pool. Tumors and injured brain parenchyma enhance much more because of the enhancement of their interstitial space and so the depiction of brain lesions in post contrast images is very high. In addition to diffusing across tissue capillary walls, GBCAs diffuse across glomerular walls into the renal tubules, within which they are concentrated as water is reabsorbed. This makes them highly effective for enhancing the kidneys and the urinary tract.

Arterial phase images are best acquired during the first pass of contrast agent through the arterial system i. e. within 20 seconds of contrast administration. Early arterial images are best for depicting arteries, and later arterial phase images are better for depicting hypervascular tissues. Blood pool or the portal venous phase occurs at 60-90 seconds after contrast administration during which contrast is typically distributed throughout the body's vessels. Maximum liver parenchymal enhancement is also achieved during this phase. Dynamic imaging for detection and characterization of lesions in the liver and other organs can be performed, similar to CT, using nonspecific extracellular GBCAs.

The **high relaxivity agents** include gadobenate, gadoxetate and gadofosveset. These agents bind to proteins and have a higher T1 relaxivity than the above mentioned gadolinium chelates (**Table 1**). **Gadobenate and gadoxetate** act as nonspecific extracellular gadolinium chelates immediately after the bolus injection but later they are taken up by liver cells and so act as liver specific agents in the delayed phase. They are excreted through both, renal and hepatobiliary pathways. *Gadobenate dimeglumine* has a capacity for weak and transient protein bonding. Only 2 to 4 percent of the injected dose is taken up by liver cells and its delayed imaging time is 90 to 120 minutes. *Gadoxetate disodium* has the maximum biliary excretion (almost equal biliary and renal excretion) and has a convenient delayed imaging time of 10 to 20 minutes. It also results in a much more intense liver parenchymal enhancement than gadobenate. These two agents behave similarly to other gadolinium chelates during the initial phase and thus are helpful in assessing tumor enhancement and characterization. During the later phases, they selectively increase the signal intensity of the liver (via hepatocyte uptake), thus aiding in the detection of small tumors. This is dependent on the degree of differentiation of the tumor, as well-differentiated hepatocellular carcinoma may take up the contrast and become less conspicuous. However, these agents are best

utilized for detection of metastases. In addition, because of biliary excretion during the delayed phase, the biliary ducts can be mapped well using T1 weighted images.

**Gadofosveset** has 80 to 90 percent binding to serum albumin. This high protein binding has 2 effects: firstly it markedly increases the relaxivity (hence requiring lower doses and concentration) and secondly, it results in the agent being effectively confined to the vascular space. Due to its prolonged intravascular retention, it has been successfully used as a blood pool agent for MR angiography. The protein binding is reversible and gadofosveset is ultimately excreted unchanged by the kidneys through glomerular filtration.

As mentioned earlier, gadolinium must be chelated to reduce its toxicity. There are differences in the chemical structure of chelates used to bind the gadolinium ion—macrocyclic or linear. The chemical structure of a typical linear and a typical macrocyclic GBCA are depicted in **Figures 1A and B**. Gadolinium chelates can also be categorized into 4 classes based on their biochemical structure—macrocyclic or linear, and ionicity—ionic or nonionic as given below:

Linear, ionic—gadopentetate, gadobenate, gadoxetate and gadofosveset.

Linear, nonionic—gadodiamide and gadoversetamide.

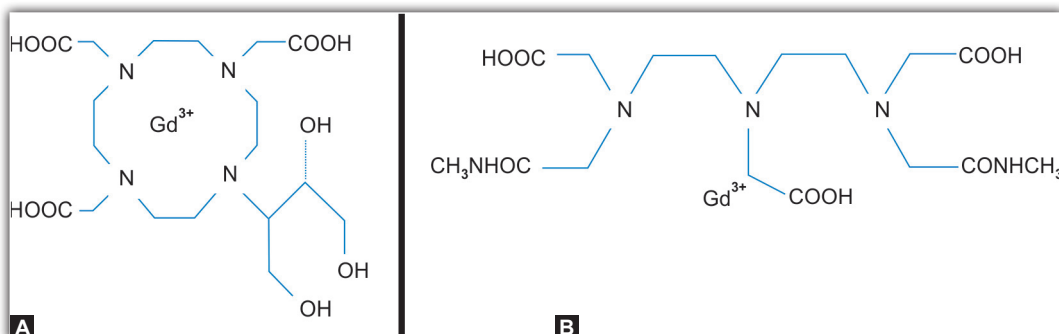
Macrocyclic, ionic—gadoterate.

Macrocyclic nonionic—gadoteridol and gadobutrol.

The GBCAs vary with respect to osmolality and viscosity. Their osmolality ranges between 0.63 osmol/kg to 1.97 osmol/kg (**Table 2**). *In vivo*, the the osmotic load of all the GBCAs is very low, compared to iodinated contrast media, because only a small amount of the contrast agent is required to produce a diagnostic MR examination. The nonionic agents tend to have lower osmolarity and are less viscous. Nonionic low osmolar GBCAs also have fewer negative isotropic effects, which is an important consideration for cardiac patients. Low viscosity GBCAs require less pressure to inject and can be administered using smaller gauge needles or catheters.

The stability of an agent describes the affinity of the gadolinium atom for its compound and depends on its thermodynamic and conditional stability. The dissociation constants (**Table 2**) can be used to describe the stability of the linear GBCAs. The higher the dissociation constants, the greater the stability of the agent. Unlike the linear agents, the macrocyclic agents require a significant amount of energy to dissociate the gadolinium complexes. With these agents the kinetics of dissociation are described by the dissociation rate and the dissociation half-life. In general, the ionic agents are more stable than the nonionic ones.<sup>4</sup> When considering agents by class, the stability increases from nonionic linear to ionic linear to macrocyclic agents.<sup>5,6</sup>

Given the toxicity of the free metal ion, many agents are bound to excess chelate (**Table 2**). The excess chelate is considered necessary because of the possibility for transmetallation with trace amounts of zinc in the blood



**Figs 1A and B** Chemical structure of gadolinium based contrast agents. (A) Typical macrocyclic agent—gadobutrol and (B) Typical linear agent—gadodiamide

**Table 2** Physicochemical properties of gadolinium based contrast agents<sup>7</sup>

Generic name/ Trade name	Osmolality (37°C, osmol/kg H <sub>2</sub> O)	Viscosity (mPa at 37°C)	Thermodynamic stability constant	Conditional stability constant at pH 7.4	Metal chelates (mg/mL)	Excess chelates (mg/mL)
Gadopentetate/Magnevist	1.96	2.9	22.1	18.1	469	0.4
Gadoterate meglumine/ Dotarem	1.35	2.0	25.8	18.8	278.3	0
Gadodiamide/Omniscan	0.79	1.4	16.9	14.9	287	12
Gadoteridol/Prohance	0.63	1.3	23.8	17.1	279.3	0.23
Gadobutrol/Gadovist	1.6	4.96	21.8	14.7	605	0.5
Gadoversetamide/Optimark	1.11	2.0	16.6	15.0	330.9	28.4
Gadobenate/Multihance	1.97	5.3	22.6	18.4	334	0
Gadoxetate/Primovist/Eovist	0.688	1.19	23.5	18.7	181.4	1
Gadofosveset/Vasovist	0.825	1.8	22.1	18.9	244	0.27

and a resulting release of free gadolinium ion. Accordingly, the least stable agents, gadodiamide and gadoversetamide, the two agents with the weakest thermodynamic stability constants, each have considerably larger amounts of excess chelate (12 mg/mL and 28.4 mg/mL respectively) than the most stable agents, gadoterate and gadoteridol (0 and 0.23 mg/mL of excess chelate respectively). The presence and quantity of excess chelate can be taken as an indirect marker of the instability of the contrast agent.<sup>6,7</sup>

#### *Interaction between Extracellular MRI Contrast Agents with Clinical Tests*

Extracellular MRI contrast agents may cause spurious hypocalcaemia as they can interfere with the assay method of calcium measurement. Awareness of this effect on calcium measurements by some MRI contrast agents is important in order to avoid incorrect and potentially hazardous treatment. Caution should be exercised when using colorimetric assays for angiotensin-converting enzyme, calcium, iron, magnesium, total iron binding capacity and zinc in serum samples of patients who have recently received gadolinium

based contrast media. Therefore, biochemical assays are better performed before contrast media injection, or delayed for at least 24 hours afterwards or longer in patients with renal impairment.

**Dose:** Generally the recommended dose for clinical use is 0.1 mmol/kg body weight, but up to 0.3 mmol/kg body weight may be used, particularly for MRA. Smaller doses can be used for the high relaxivity agents.

#### **Adverse Effects of GBCAs**

Extracellular MRI contrast agents are well tolerated and have a low incidence of adverse effects. Mild adverse reactions such as nausea, vomiting and urticaria occasionally occur after GBCA administration. Other uncommon adverse events include headache, taste disturbance, dizziness, and paraesthesia. While adverse reactions are rare in the general patient population, they are more common in patients with a history of asthma or allergy, and in patients injected at a faster rate.<sup>3</sup>

These types of adverse events are similar with all GBCAs, with no significant differences between agents. The incidence

of mild adverse effects is less than 5 percent. Anaphylactoid reactions have been reported, but they are very infrequent. Life threatening reactions are very rare with an incidence around 1:100000. Fatal reactions may occur, however, are extremely rare.<sup>8,9</sup>

### *Contrast-Induced Nephropathy*

Extracellular MRI agents are more nephrotoxic than iodinated contrast media in equimolar doses. However, as the dose of gadolinium based contrast medium required for a diagnostic MRI examination is very small in comparison to doses of iodinated contrast media for CT and other radiographic examinations, nephrotoxicity due to these agents is uncommon even in patients with renal disease. In patients with marked reduction in renal function (particularly due to diabetes mellitus), contrast-induced nephropathy (CIN) may occur even at the standard doses of gadolinium based MR contrast agents.<sup>10</sup>

Gadolinium attenuates X-rays and hence its use for radiographic examinations instead of iodinated contrast media has been advocated in patients with history of serious adverse reactions to iodinated contrast media and in patients who are to undergo imminent thyroid treatment with radioactive iodine, providing the renal function of these patients was normal. In patients with renal impairment, GBCAs should not be used in place of iodinated contrast media as they can induce nephrotoxicity at the doses required to produce adequate radiographic enhancement.<sup>3</sup>

### *Extravasation*

Monitoring a patient for extravasation can be a challenge in MRI, especially when the patient is deep in the bore of the MR unit. An extravasation can occur at a distance from the injection site. Extravasation of GBCAs into the surrounding tissues can cause edema, inflammation and necrosis.<sup>3</sup> However, in most cases the effect is minimal with no long-term sequelae. Certain patient categories like infants, young children, unconscious and debilitated patients, patients with arterial insufficiency or compromised venous/lymphatic drainage are less able to tolerate extravasation. Low-osmolar, nonionic GBCAs reduce the risk of an extravasation because they tend to be lower viscosity, and because they are better tolerated, the severity is less following extravasation.<sup>11</sup>

### *Nephrogenic Systemic Fibrosis*

Gadolinium enhanced MRI was considered one of the safest imaging procedures. However, the concern of associated nephrogenic systemic fibrosis (NSF) have forced the radiology community to rethink its imaging practices. The first case of NSF was described in 1997 as a skin disorder resembling scleromyxedema and termed as nephrogenic fibrosing dermopathy.<sup>12</sup> Later, when systemic manifestations were identified, the nomenclature was changed to

nephrogenic systemic fibrosis. NSF is characterized by scleroderma-like skin changes (swelling, skin induration, skin colored erythematous papules, woody skin) that mainly affect the limbs—lower limbs more than upper limbs and trunk. Fibrotic changes may also affect other organs such as muscles, heart, lungs, liver, kidneys and testes. The disease can be aggressive in some patients leading to severe physical deformity or even death.

The association of gadolinium with development of NSF was first described in 2006 by Grobner.<sup>13</sup> Since then, several studies have documented the presence of gadolinium in the tissues of patients with NSF and have supported the causative role of the contrast agent in the development of this condition.<sup>14-16</sup> The time between injection of GBCA and the onset of NSF symptoms occurs within days to months in the vast majority of patients; however, in rare cases, symptoms have appeared years after the last reported exposure.<sup>6</sup>

Although, the exact mechanism of NSF is not yet established, it is known to occur exclusively in patients with decreased renal function (glomerular filtration rate < 30 mL/min/1.73 m<sup>2</sup>). The most widely held hypothesis is that because of the prolonged clearance time of GBCAs in renally impaired patients, gadolinium chelates have a propensity to undergo transmetallation, in which other cations in the body displace gadolinium from its chelate, releasing free gadolinium. This free gadolinium then binds with an anion such as phosphate, and the resulting insoluble precipitate is deposited in various tissues. A fibrotic reaction ensues involving the activation of circulating fibrocytes. This theory is supported by the presence of gadolinium in affected tissues of NSF patients relative to unaffected states.<sup>15</sup>

Currently, there is no effective treatment for NSF. Trials with corticosteroid, photopheresis, plasmapheresis, thalidomide, methotrexate, etc. have not had much success. There is also no evidence that immediate hemodialysis protects against the development of NSF. Improving renal function seems to slow or arrest progression of this condition.

### *Risk factors for NSF*

**Patient factors:** The patients at highest risk for development of NSF are those on dialysis or with acute or chronic renal failure. It is estimated that patients with end-stage chronic kidney disease (CKD5, eGFR <15 mL/min/1.73 m<sup>2</sup>) and severe CKD (CKD4, eGFR 15 to 29 mL/min/1.73 m<sup>2</sup>) have a 1 to 7 percent chance of developing NSF after one or more exposures to at least some GBCAs. There has been only one published case report of a patient with eGFR values above 30 mL/min/1.73 m<sup>2</sup>.<sup>17</sup>

It is not understood why some patients with severe CKD or acute kidney injury (AKI) develop NSF following exposure to GBCAs and others do not. One study described 30 patients who had an eGFR of under 30 mL/min/1.73 m<sup>2</sup> and who were exposed to high doses of gadodiamide (median dose of 90 mL and range of 40 to 200 mL). One of the 30 patients

subsequently developed NSF, an observed incidence of about 3 percent.<sup>18</sup> So it is postulated that gadolinium is necessary but not sufficient to trigger NSF. A number of possible cofactors have been postulated to play a role. These include metabolic acidosis or medications that predispose patients to acidosis, elevated iron, calcium, and/or phosphate levels, high-dose erythropoietin therapy, immunosuppression, vasculopathy, and infection, or other acute pro-inflammatory events.<sup>19</sup> However, none of these have been consistently confirmed as true cofactors. As a result, routine screening for them prior to GBCA administration is not recommended, although such screening may be performed on an optional basis. Hepatic disease in and of itself, in the absence of AKI or severe CKD, is not considered a risk factor for NSF.<sup>20</sup>

**Contrast medium factors:** NSF cases have been reported for almost all GBCAs. Although the majority of NSF cases involve the linear GBCAs—the most commonly reported agent being gadodiamide followed by gadopentetate and gadoversatamide—NSF has also been reported for gadoteridol, the macrocyclic formulation.<sup>21</sup> The stability of the binding of the gadolinium within the chelate has been found to be an important factor in pathogenesis of NSF (as discussed above), with macrocyclic chelates offering better protection and binding to gadolinium ion in comparison to the linear molecules. However, the American College of Radiology (ACR) Manual on Contrast Media states, “It must be emphasized that the frequency with which NSF has been associated with different GBCAs may reflect a combination of differences in toxicity, market share, number of years that the agent has been in use, and possible reporting bias. In addition reported frequency is also further confounded by the fact that some agents, particularly gadodiamide, may have been used disproportionately more frequently in patients receiving high doses of GBCAs for magnetic resonance angiography”<sup>20</sup>.

The ACR has classified the GBCAs into three groups based on the reported prevalence of NSF with the various agents (**Table 3**). There is limited data for Group III agents, although, to date, few, if any, unconfounded cases of NSF have been reported.<sup>20</sup>

Besides the chelate stability, high doses of GBCAs, either as a single administration or cumulatively in multiple administrations over months to years, are also associated with higher incidence of NSF.

In spite of differences in the incidence of NSF, there is no evidence that any of the approved GBCAs are safe in the at-risk patient population. Conversely, in patients without renal disease, all gadolinium based contrast agents seem to be safe.

### Guidelines on GBCA Usage

The American College of Radiology (ACR), the Food and Drug Administration in the United States (FDA) and European Commission/European Medicines Agency (EC/EMA) have all given their recommendations on the use of GBCAs. The three groups use different words, however, there are only minor

**Table 3** ACR classification of GBCAs based on reported prevalence of NSF<sup>20</sup>

Group I: Agents associated with the greatest number of NSF cases
Gadodiamide (Omniscan®)
Gadopentetate dimeglumine (Magnevist)
Gadoversetamide (OptiMARK)
Group II: Agents associated with few, if any, unconfounded cases of NSF
Gadobenate dimeglumine (MultiHance)
Gadoteridol (ProHance)
Gadoteric acid (Dotarem)
Gadobutrol (Gadovist)
Group III: Agents which have only recently appeared on the market in the US
Gadofosveset (Ablavar)
Gadoxetate disodium (Eovist)

differences between their recommendations.<sup>22</sup> The ACR guidelines are given below:

The ACR recommends that, prior to an MRI using a GBCA, physicians should identify patients who have severe renal failure ( $\text{GFR} < 30 \text{ mL/min}/1.73 \text{ m}^2$ ) by questioning patients for a history of renal disease and should obtain an eGFR measurement within six weeks of the procedure in patients with (1) renal disease (including patients with a solitary kidney, renal transplant, or renal neoplasm), (2) over the age of 60 years and (3) with hypertension, diabetes mellitus, or a history of severe liver disease. When a high-risk patient is identified, the ACR recommends considering alternative studies and informing these patients about the potential risks of GBCA-enhanced studies and should such studies be deemed necessary, using the lowest possible dose of GBCA to obtain the necessary clinical information, and avoiding double or triple dose studies, if possible, and avoiding using those GBCAs that have been most frequently associated with NSF.

*The ACR has specific recommendations for specific groups of patients:*

**Patients with end-stage renal disease on chronic dialysis:** If a contrast-enhanced cross-sectional imaging study is essential it would be reasonable to consider administering iodinated contrast media and performing a CT rather than an MRI. However, if a contrast-enhanced MR examination must be performed in a patient with end-stage renal disease on chronic dialysis, injection of group I agents (see **Table 3**) is contraindicated. Also, use of the lowest possible dose needed to obtain a diagnostic study is recommended and is appropriate. The ACR also recommends that GBCA-enhanced MRI examinations be performed as closely before hemodialysis as is possible, as prompt post-procedural hemodialysis, although unproven to date, may reduce the likelihood that NSF will develop.

**Chronic kidney disease stage IV or V (eGFR <30 mL/min/1.73 m<sup>2</sup>) not on dialysis:** The correct course of action in this patient group is problematic, as administration of iodinated contrast media for CT may lead to further deterioration of renal function, while administration of GBCA for MRI could result in NSF. It is recommended that any GBCA be avoided in this patient group. However, if GBCA enhanced MRI is deemed essential, use of the lowest possible dose needed to obtain a diagnostic study is recommended. Although there is no absolute proof that any GBCA is completely safe in this patient group, group I agents (see Table 3) have been contraindicated. Further, it may be prudent to avoid readministration of GBCA for several days to a week.

**Chronic kidney disease stage III with eGFR between 30 and 59 mL/min/1.73 m<sup>2</sup>:** NSF developing after GBCA administration to patients with eGFR >30 mL/min/1.73 m<sup>2</sup> is exceedingly rare. However, eGFR determinations may fluctuate from one day to the next (with an eGFR level just above 30 on one day changing to an eGFR below 30 on another day). It is for this reason that the precautions described above for CKD4 and CKD5 patients are also recommended for inpatients with an eGFR <40 mL min/1.73 m<sup>2</sup>. In comparison, no special precautions are required in patients with an eGFR of 40 to 59 mL/min/1.73m<sup>2</sup>.

**Chronic kidney disease stage I or stage II with eGFR >60 mL/min/1.73 m<sup>2</sup>:** There is no evidence of increased risk of NSF and all GBCAs can be safely administered using a dose of less than or equal to 0.1 mmol/kg.

**Patients with acute kidney injury (AKI):** Due to the temporal lag between eGFR (which is calculated using serum creatinine values) and actual glomerular filtration rates, it is not possible to determine whether a given patient has AKI based on a single eGFR determination. Accordingly, caution should be exercised in use of GBCA in patients with known or suspected AKI regardless of measured serum creatinine or calculated eGFR values. The GBCA should only be administered to these patients if absolutely necessary. When GBCA administration is required, agents associated with the greatest apparent NSF-associated risk (Group I agents) should be avoided and lowest possible dose used.

**Patients on hemodialysis:** There is no evidence supporting the use of hemodialysis in preventing or treating NSF in patients not already undergoing hemodialysis, but it may be useful to remove GBCAs in patients already on hemodialysis according to the EMA. The ACR recommends that enhanced MRI be done shortly before hemodialysis and if the patient is totally anuric, CT (using iodine based contrast material) should be considered.

#### GBCA Administration in Children<sup>20</sup>

To date, few pediatric cases of NSF have been reported, and no cases have been reported in children under the age of 6

years. Nevertheless, there is not enough data to demonstrate that NSF is less likely to occur in children than in adults with similarly significant renal disease. Therefore, it is prudent to follow the same guidelines for adult and pediatric patients as described above. It should be noted, however, that eGFR values in certain premature infants and neonates may be <30 mL/min/1.73 m<sup>2</sup> simply due to immature renal function (and not due to pathologic renal impairment). In these individuals, the ACR Committee believes that caution should still be used when administering GBCAs, although an eGFR value <30 mL/min/1.73 m<sup>2</sup> should not be considered an absolute contraindication to GBCA administration.

#### GBCAs During Pregnancy and Lactation<sup>20</sup>

It is known that GBCAs cross the human placenta and into the fetus when given in clinical dose ranges. No adequate and well-controlled teratogenic studies of the effects of these agents in pregnant women have been performed. A single cohort study of 26 women exposed to gadolinium chelates during the first trimester of pregnancy showed no evidence of teratogenesis or mutagenesis in their progeny.<sup>23</sup> Because it is unclear how gadolinium-based contrast agents will affect the fetus, these agents should be administered only with extreme caution. Each case should be reviewed carefully and gadolinium-based contrast agent administered only when there is a potential overwhelming benefit to the patient or fetus that outweighs the possible risk of exposure of the fetus to free gadolinium ions. The radiologist should confer with the referring physician and document the following in the radiology report or the patient's medical record:

1. That information requested from the MR study cannot be acquired without the use of contrast or by using other imaging modalities.
2. That the information needed affects the care of the patient and fetus during the pregnancy.
3. That the referring physician is of the opinion that it is not prudent to wait to obtain this information until after the patient is no longer pregnant. It is recommended that the pregnant patient undergoing an MR examination provide informed consent to document that she understands the risk and benefits of the MR procedure to be performed, and the alternative diagnostic options available to her (if any), and that she wishes to proceed.<sup>20</sup>

Only tiny amounts of GBCAs given to a **lactating mother** reach the milk and only a minute proportion is absorbed from the baby's gut,<sup>24</sup> therefore the ACR recommends that they can be safely administered to a lactating mother. However, the EMA recommends discontinuation of breast feeding for at least 24 hours for all patients receiving high NSF risk GBCAs.

As healthcare providers have been restricting their use of GBCAs in patients at risk for NSF, the incidence of NSF has been dropping. This reduction reflects the changes that have been implemented in MR practice since the risks of NSF have widely publicized.<sup>25</sup>

## MANGANESE BASED CONTRAST AGENTS

Manganese ( $Mn^{2+}$ ) like gadolinium ( $Gd^{3+}$ ) is also a strongly paramagnetic substance due to the presence of five unpaired electrons in its structure. Its compound, Mangafodipir trisodium (MnDPDP, Teslascan) has a chemical similarity to vitamin  $B_6$ , and because of this, it is specifically taken up by hepatocytes. It increases the signal intensity of normal hepatic parenchyma thus giving a high lesion-to-liver contrast and providing improved detection, characterization and evaluation of liver lesions.<sup>26</sup> During the later phases, MnDPDP is excreted into bile and provides excellent biliary ductal detail aiding in the diagnosis of various biliary pathologies.<sup>27</sup> MnDPDP was also found to accumulate in the pancreatic parenchyma and has been clinically useful for the evaluation of pancreatic lesions.

Unlike the gadolinium agents, MnDPDP readily dissociates after injection to yield free manganese ions. The instability of the chelate *in vivo* raised concerns in the scientific literature about potential toxicity. Free manganese, in chronic exposure, accumulates in the brain and causes a parkinsonism-like syndrome. It can also have a depressive action on heart function. Moreover, evidence suggests that significant neurological risk is associated with manganese intoxication in subjects with chronic liver failure whose ability to eliminate manganese is reduced. Hence, MnDPDP has effectively been withdrawn from the market.<sup>7</sup>

Mn-based nanoparticles are currently under research for use as high performance contrast agents with reduced toxicity.

## IRON OXIDE BASED CONTRAST AGENTS

Superparamagnetic iron oxide particles were suggested as a potential liver specific MR contrast agents as early as 1980s. These agents contain a crystalline core of water insoluble iron oxide crystals, usually magnetite ( $Fe_3O_4$ ) or maghemite ( $\gamma-Fe_2O_3$ ) with a core diameter in the range of 4 to 10nm. To prevent particle aggregation, these iron oxide crystals are coated by dextran or some other biodegradable polysachharide which makes the total size of the iron oxide particle substantially larger and also modifies their biological behavior.<sup>28</sup>

Each iron oxide crystal contains several thousand paramagnetic Fe ions ( $Fe^{2+}$  and  $Fe^{3+}$ ). When these particles are subjected to an external magnetic field, they exhibit strong magnetization which can cause microscopic field inhomogeneity and activate the dephasing of protons. Thus, iron oxide nanoparticles shorten T2 and T2\* relaxation times of the neighboring regions, and produce a decreased signal intensity in T2- and T2\* weighted MR images.

Unlike low-molecular weight water soluble GBCAs, iron oxide agents do not leak into the interstitium and therefore, act as intravascular contrast agents or blood pool agents as long as the vessel endothelium is not altered by any pathological process. They are eliminated from blood by uptake into the

reticuloendothelial system (RES) cells in liver, spleen, bone marrow and lymph nodes.<sup>28</sup>

The blood half-life and biological distribution of the nanoparticles are directly dependant on their size. They have been subdivided into two groups according to their mean total diameter and the distribution of particle sizes of the iron oxide agent (1) Superparamagnetic iron oxide particles (SPIOs) (2) Ultrasmall superparamagnetic iron oxide particles (USPIOs).

### 1. Superparamagnetic iron oxide particles (SPIOs):

These are particles with aggregated iron oxide cores and a mean particle diameter greater than 50 nm. Two SPIOs have been developed clinically and approved for MR imaging:

a. *Fexumoxide* (also known as Feridex or AMI-25) with a particle size of 50 to 180 nm. It has a thin, incomplete dextran coating that causes individual particles to form polycrystalline aggregates. These aggregates behave in solutions or within cells as large particles. They are phagocytosed rapidly by reticuloendothelial cells and are cleared from the blood in an hour or less. It is administered as a slow I/V infusion over 30-60 minutes. Imaging is typically performed 1 to 4 hours after infusion. The liver appears darkest on T2\* weighted and T2 weighted images in the first 24 hours after the infusion. Complete metabolism requires 14 to 28 days but the signal intensity of the liver typically returns to normal within 7 to 14 days. The most common complication of Feridex is acute severe low back pain, which may lead to discontinuation of the infusion in patients. This complication can be minimized with a slow infusion.<sup>29</sup>

b. *Ferucarbotran* (also known as Resovist or SH U 555 A) has a particle size of about 60 nm. The SPIO particles are coated with low molecular weight carboxydextrans. Resovist is provided as a ready to use formulation and is administered as a rapid bolus and so is used with both dynamic and delayed imaging. The reported overall incidence of adverse events with Resovit was 7.1 percent, with vasodilation and parasthesias the common event reported.<sup>7</sup>

As mentioned before, these iron oxide contrast agents are phagocytosed by macrophages throughout the body. The SPIO agents are preferentially entrapped by the Kupffer cells in the liver and spleen and reduce the T2 relaxation time of these organs, thus the normal liver appears dark on T2 weighted images. Most liver tumors, whether benign or malignant, primary or metastatic - are deficient in Kupffer cells and do not exhibit SPIO particle uptake and appear relatively hyperintense after SPIO administration. However, well differentiated tumors which have not lost all their Kupffer cells, will take up SPIO agents and exhibit reduced signal intensity.<sup>27,29</sup>

Some, not all, focal nodular hyperplasias show SPIO uptake. Use of SPIO agents may help improve detection of HCC in cirrhotic patients. SPIO agents may also be used in combination with GBCAs to increase overall lesion detection.<sup>29</sup>

2. ***Ultrasmall superparamagnetic iron oxide particles (USPIOS):*** These are particles with non-aggregated (monodisperse) iron oxide cores with mean diameter less than 50 nm. As USPIOS are very small, they are extravasated from the blood vessels into interstitial spaces and transported to lymph nodes via the lymphatic channels. MR imaging is done 24 to 36 hours after contrast administration. The accumulation of the contrast within the normal nodes causes them to appear dark in T2 or T2\* weighted while diseased nodes (e.g. metastatic nodes) do not show any change in signal intensity and appear uniformly or focally bright. When the hyperintense focus accounts for more than 30 percent of the nodal area, the node is considered metastatic. Harisinghani et al reported the successful detection of lymph-node metastases in patients with prostate cancer using USPIOS.<sup>30</sup> Sinerem and Combidex are two commercially available USPIO agents. USPIOS have also been tested as blood pool agents as they remain in the intravascular space for a long time.<sup>31</sup>

## ORAL CONTRAST AGENTS

Oral contrast agents are required to delineate bowel pathology and distinguish bowel from other organs or mass lesions. The properties of an ideal oral contrast agent should be—little or no absorption by the stomach or intestines, complete excretion, no motion or susceptibility artifacts, uniform marking of the GI tract, good patient acceptance in terms of taste, volume to be ingested and timing of oral administration, be safe, and be of low cost.<sup>32</sup> A variety of oral contrast agents have been developed for improved delineation of the bowel in MR imaging studies. They can broadly be divided as:

- a. Low signal intensity on all pulse sequences – low-low intensity (proton displacement or T2 shortening)
- b. High signal intensity on all pulse sequences – high-high intensity (T1 shortening)
- c. Low signal intensity on T1 weighted images and high signal intensity on T2 weighted images – low-high intensity (water based)
- d. High signal intensity on T1 weighted images and low signal intensity on T2 weighted images – high-low intensity (T1 and T2 shortening)

The last two categories are also known as biphasic agents.

### Low-Low Intensity (Dark Lumen)

The signal intensity in bowel can be reduced by displacing the bowel contents with a material that contains no protons, such as air. Air can be administered by intubating the small bowel or rectum. However, due to patient discomfort and

degradation of T<sub>2</sub>\* weighted gradient echo images and echoplanar images by susceptibility artefacts, air is not featured as an oral contrast agent.

**Perfluorocarbons** are agents which do not contain protons, but they have the same susceptibility as water and thus, do not cause artefacts. Perflubron, a perfluorocarbon formulation was the first oral MR contrast agent approved for clinical use. However, as it was very expensive, it was withdrawn from the market.<sup>33</sup>

**SPIOS** in high concentration can shorten T2 and T2\* enough to eliminate signal from bowel even on so-called T1 weighted images. Their major disadvantage is the resulting distortion of the local magnetic field, which can exacerbate artefacts making fat-suppression particularly vulnerable. Currently, ferumoxsil – a silicon-coated SPIO is commercially available as GastroMARK (Mallinckrodt) or Lumirem (Guerbert) for use as an oral contrast agent. Side effects such as nausea and vomiting, flatulence and feeling of fullness have been reported in 15 percent of patients.<sup>32</sup>

**Clays** such as kaolin, attapulgite and helonite restrict the motion of water, thus shortening the T1 and T2 relaxation times. However, T1 weighted gradient echo images with a T<sub>E</sub> of less than 3 msec have little T2 contrast and therefore depict clay in bowel contents as high signal intensity owing to their short T1.<sup>33</sup>

### High-High or Bright Lumen

Positive contrast agents cause a reduction of T1 relaxation time; consequently they act on T1 weighted images by increasing the signal intensity of the bowel lumen (bright lumen). Positive contrast agents are represented by paramagnetic materials, mainly gadolinium chelate solutions but also ferrous and manganese ions. Gadolinium chelate solution was among the first contrast agents proposed as an oral contrast for MRI. Gadolinium chelate dissolved in water at a concentration of approximately 1 mmol/L provides sufficient reduction of the T1 relaxation time of water to generate an increase in signal intensity on T1 weighted images. As the concentration is low it has no T2 effect, so it does not shorten the T2 relaxation time; consequently the signal intensity is also high on T2 weighted images. One of the first commercially available positive oral contrasts was gadopentetate dimeglumine solution (Magnevist Enteral – Schering AG).

Blueberry juice can be used as a positive agent due to its high content of manganese, a paramagnetic ion, which shortens the T1 relaxation time. Fat containing food materials like milk, vegetable oil and ice-cream have an intrinsically short T1, thus providing high signal on T1 weighted MRI.<sup>32</sup>

### High-Low Intensity

Materials which shorten both T<sub>1</sub> and T<sub>2</sub> relaxation times enough that bowel contents have high signal intensity on T<sub>1</sub> weighted images and low signal intensity on T<sub>2</sub> weighted

images. The major advantage is that the resulting signal intensity of bowel on all the pulse sequences is different from those of tumors and simple fluid collections, which tend to have low signal intensity on T<sub>1</sub> weighted and high signal intensity on T<sub>2</sub> weighted images. However, some T<sub>2</sub> weighted pulse segments (e.g. fast spin echo) may depict bowel more clearly if its contents have high signal intensity, so this form of contrast is not necessarily desirable for every application.

Examples of this type of contrast agent include clay, gadolinium chelates in high concentration and compounds of manganese. Manganese is present in high concentrations in some foods such as bananas and blueberries.

### Low-High Intensity

The least expensive, most widely available, and best understood oral contrast agent used for MRI is water which makes bowel as low signal intensity on T1 weighted and high signal intensity on T2 weighted images. It provides good small bowel distension, but its major limitation is intestinal absorption, which does not allow good distention of distal small bowel. For this reason, water is used in conjunction with different additives that reduce intestinal absorption, e.g. mannitol, sorbitrate, etc.

Dilute suspensions of BaSO<sub>4</sub> or dilute solutions of iodinated contrast material such as those used in opacification of bowel for CT are very useful as low-high MR oral contrast agents.

Polyethylene glycol (PEG) is a strong hydrophilic molecule, which simulates the properties of water with regard to signal intensity with the added advantage of nonabsorbability. Using 600 mL of PEG, a good distension of bowel loops can be obtained with no significant side effects.<sup>32</sup> Low-high agents are also useful for delineating the pancreas, however, bowel may be difficult to distinguish from simple fluid collections and tumors; high bowel signal intensity can intensify motion artefacts.

The choice of a single agent presents advantages and disadvantages; thus the radiologist should choose the appropriate contrast agent according to clinical setting, MR experience, availability of agent and patient tolerance.

### Ongoing Research and Future Trends

Currently most available MR contrast agents are useful in improving visibility and definition of pathology, but are not suitable for extended intravascular (blood pool) or tissue/organ specific imaging and do not allow molecular imaging. The iron oxide agents, although organ specific, are negative contrast agents and give a signal decreasing effect, which renders images of lower contrast than T1 contrasted agents. To overcome these limitations, there have been continuing efforts in searching for more specific contrast agents that can offer diagnosis with the accuracy approaching that otherwise only achievable with biopsy or histopathology.

T1 nanoparticulate agents, target specific agents tumor specific, thrombus specific etc, smart agents like enzyme activated agents, chemical exchange saturation transfer (CEST And PARACEST) agents, fluorinated agents are some of the agents under research. The majority of these agents are in preclinical levels of research; however, successful *in vivo* imaging has been reported with many preclinical studies.<sup>31,34-36</sup>

### CONCLUSION

At present gadolinium chelates are the most widely used contrast agents in MR imaging and the only MR contrast agents available in India. They are easily available, have good tolerability and provide excellent lesion detection and characterization. The main concern with GBCAs is NSF, which is seen to occur only in patients with severe renal disease. The tissue-specific agents can be used for specific indications, depending on their availability.

### REFERENCES

1. De Haen. Conception of the first magnetic resonance imaging contrast agents; a brief history. Top Mag Reson Imaging. 2001; 12:221-30.
2. Wastie ML, Latief KH. Gadolinium: named after Finland's most famous chemist. Br J Radiol. 2004;77:146-7.
3. Ersoy H, Rybicki FJ. Biochemical safety profiles of gadolinium-based extracellular contrast agents and nephrogenic systemic fibrosis. J Magn Reson Imaging. 2007;26:1190-7.
4. Kei PL, Chan LP. Gadolinium chelate-associated nephrogenic systemic fibrosis. Singapore Med J. 2008;49:181-5.
5. Schmitt-Willich H. Stability of linear and macrocyclic gadolinium based contrast agents. Br J Radiol. 2007;80(955): 581-2.
6. Juluru K, Vogel-Claussen J, Macura KJ. MR Imaging in Patients at risk for developing nephrogenic systemic fibrosis: protocols, practices, and imaging techniques to maximize patient safety. Radiographics. 2009;29:9-22.
7. Runge VM. Contrast Agents: Safety profile at <http://cds.ismrm.org/ismrm-2008/files/Syllabus-069.pdf>.
8. Muroff LR. MRI contrast: current agents issues. Appl Radiol. 2001;30(suppl):5-7.
9. Thomsen HS. Contrast media, safety issues and ESUR guidelines. Berlin Heidelberg New York, Springer, 2006.
10. Thomsen HS, Almen T, Morcos SK. The members of the contrast media safety committee of the European Society of Urogenital Radiology (ESUR): gadolinium-containing contrast media for radiographic examinations: A position paper. Eur Radiol. 2002; 12:2600-5.
11. Bellin MF, Jakobsen JA, Tomassin I, et al. Contrast medium extravasation injury: guidelines for prevention and management. 2002;12:2807-12.
12. Cowper SE. Gadolinium - is it to blame? J Cutan Pathol. 2008;35: 520-2.
13. Grobner T. Gadolinium—a specific trigger for the development of nephrogenic fibrosing dermopathy and nephrogenic systemic fibrosis? Nephrol Dial Transplant. 2006;21:1104-8.
14. Broome DR, Girguis MS, Baron PW, et al. Gadodiamide-associated nephrogenic systemic fibrosis: why radiologists should be concerned. AJR. 2007;188(2):586-92.

15. High WA, Ayers RA, Chandler J, et al. Gadolinium is detectable within the tissue of patients with nephrogenic systemic fibrosis. *J Am Acad Dermatol.* 2007;56(1):21-6.
16. Mackermann P, Skov L, Rossen K, et al. Nephrogenic systemic fibrosis: suspected causative role of gadodiamide used for contrast-enhanced MRI. *J Am Soc Nephrol.* 2006;17(9):2359-62.
17. Shibusi K, Kataoka H, Sato N, Watanabe Y, Kohara M, Mochizuki T. A case of NSF attributable to contrast MRI repeated in a patient with stage 3 CKD at a renal function of eGFR > 30 mL/min/1.73 m<sup>2</sup>. *Japanese Journal of Nephrology.* 2009;51:676.
18. Bridges MD, St Amant BS, McNeil RB, Cerniglia JG, Dwyer JP, Fitzpatrick PM. High-dose gadodiamide for catheter angiography and CT in patients with varying degrees of renal insufficiency: Prevalence of subsequent nephrogenic systemic fibrosis and decline in renal function. *AJR Am J Roentgenol.* 2009;192:1538-43.
19. Swaminathan S, Shah MV. New insights into nephrogenic systemic fibrosis. *J Am Soc Nephrol.* 2007;18:2636-43.
20. American College of Radiology. Manual on Contrast Media. Version 8 2012. Available at : <http://www.acr.org/~media/ACR/Documents/PDF/QualitySafety/Resources/Contrast%20Manual/FullManual.pdf>.
21. Elmholt TR, Jorgensen B, Ramsingh M, et al. Two cases of nephrogenic systemic fibrosis after exposure to the macrocyclic compound gadobutrol. *NDT Plus Advance Access.* Published online On March 19, 2010. Available at : <http://ndtplus.oxfordjournals.org/cgi/content/abstract/sfq028>.
22. Thomsen HS. Contrast-enhanced MRI in patients with impaired renal function: Recent recommendations to minimize the risk of nephrogenic systemic fibrosis. *Solutions in contrast imaging.* 2010;1(2):1-8.
23. Webb JA, Thomsen HS, Morcos SK. The use of iodinated and gadolinium contrast media during pregnancy and lactation. *Eur Radiol.* 2005;15:1234-40.
24. Hylton NM. Suspension of breast-feeding following gadopentetate dimeglumine administration. *Radiology.* 2000; 216:325-6.
25. Singer RM. A review of gadolinium-based contrast agents in magnetic resonance imaging. <http://www.cewebsource.com/coursePDFs/ReviewGBCAsMRI.pdf>.
26. Rofsky NM, Earls JP. Mangafodipir trisodium injection (MnDPDP): a contrast agent for abdominal MR imaging. *Magn Reson Imaging Clin N Am.* 1996;4:73-85.
27. Kalva SP, Blake MA, Sahani DV. MR Contrast agents. *Appl Radiol.* 2006;35:18-27.
28. Wang YXJ, Hussain SM, Krestin GP. Superparamagnetic iron oxide agents: physicochemical characteristics and applications in NMR imaging. *Eur Radiol.* 2001;11:2319-31.
29. Gandhi SN, Brown MA, Wong JG, et al. MR contrast agents for liver imaging: What, When, How. *Radiographics.* 2006;26: 1621-36.
30. Harsinghani MG, Barentsz J, Hahn PF, et al. Noninvasive detection of clinically occult lymph-node metastases in prostate cancer. *N Engl J Med.* 2003;348:2491-9.
31. Na HB, Song C, Hyeon T. Inorganic Nanoparticles for MRI Contrast Agents. *Advanced Materials.* 2009;21:2133-48.
32. Laghi A, Paolantonio P, Iafrate F, et al Oral contrast agents for magnetic resonance imaging of the bowel. *Topics in Magnetic Reson Imaging.* 2002;13:389-96.
33. Mitchell DG, Cohen MS. "Particulate and oral contrast agents" in MRI principles 2nd edn. Elsevier. 2004.pp.295-304.
34. Laurent S, Elst LV, Muller RN. *Contrast Agents for MRI: recent Advances.* eMagRes. Online John Wiley & Sons, Ltd, 2009.
35. Knight JC, Edwards PG, Paisley SJ. Fluorinated contrast agents for magnetic resonance imaging: a review of recent developments. *RSC Advances.* 2011;1:1415-25.
36. Vithanarachchi SM, Allen MJ. Strategies for target-specific contrast agents for magnetic resonance imaging. *Current Molecular Imagin.* 2012;1:12-25.

## Chapter

# 18

# Ultrasound Contrast Agents

*Shashi Bala Paul, Manisha Jana*

## INTRODUCTION

Ultrasound imaging technology has evolved incessantly and come a long way since the time. It was first used in medical practice in 1942 by Dr Karl Theodore Dussik in Austria.<sup>1</sup> Ultrasound is the most widely used imaging modality owing to its characteristics of wide availability, simple to perform, lack of radiation, real time scanning ability and above all the cost-effectiveness. With the development of the digital technologies, the last sixty years have witnessed the multifaceted evolution of diagnostic ultrasound with the emergence of innovative techniques like tissue harmonic imaging, color Doppler, power Doppler and the use of contrast agents (UCAs) for ultrasound imaging called contrast enhanced ultrasound (CEUS).

CEUS has twin components, the ultrasound contrast agent (UCA) and the contrast specific imaging modes. CEUS can detect the hemodynamics of the targeted organ and provide detailed information of the microvascularity and microperfusion observed by real time scanning. Thus, CEUS has exhibited the potential of overcoming the limitations of conventional B mode ultrasound (US) and color (CD) or power Doppler (PD) ultrasound.<sup>2</sup>

UCAs are microbubbles of gas with a protein, lipid or polymer shell. They are blood pool agents and remain confined to the intravascular space after intravenous injection as they are unable to pass through the vascular endothelium. Small microbubbles (1-10 um) can pass through the lung capillaries and remain in circulation for a short time and eventually get dissolved. The gas gets exhaled while the shell gets metabolized in the liver.<sup>3-4</sup> The UCAs, while in circulation, strongly increase the ultrasound

backscatter and produce enhancement of echogenicity for the assessment of blood flow.<sup>2</sup> Contrast enhanced Doppler imaging is possible because the low mechanical index (MI) amplifies the Doppler signals for better characterization of tumor vascularity. Low MI of 0.07 to 0.2 is needed for real time evaluation of different phases of enhancement (arterial, venous and delayed ) of the target organ subsequent to the intravenous administration of UCAs.<sup>5</sup> Detection of this flow requires the contrast specific imaging modes like the pulse inversion or amplitude modulation technology which are now available in the ultrasound machines. These sequences take advantage of the nonlinear behavior of the microbubbles within the ultrasound field, bringing real-time perfusion imaging of the target organs into reach.

CEUS based parametric imaging (pCEUS)) is used for quantitative assessment of the perfusion of the tumors. A dedicated software (Qontrast 4.00. Bracco, Milan, Italy) is used for generating perfusion maps of the tumor vascularity using the acquired data of tumoral enhancement obtained by continuous recording after the UCA injection. The time to peak (TTP), estimated perfusion (EP), peak intensity (PI) and area under the time-intensity curve (AUC) can be generated providing quantitative information on the tumor vascularity.<sup>6</sup>

## EVOLUTION OF UCAs

The first generation UCAs came into existence in the late 1960s.<sup>2</sup> (**Table 1**). These comprised of soluble gas and thus had a short life. Moreover, their large size prevented them from passing through the pulmonary circulation.<sup>7</sup> Thus; they were used primarily for right heart imaging. Evaluation of the heart and great vessels by injecting agitated liquid via

**Table 1** First generation ultrasound contrast agents

UCAs	Gas	Stabilization
Agitated saline	Air	None
Echovist	Air	None
Levovist	Air	Palmitic acid*
Albunex	Air	Sonicated albumin*

\*Have transpulmonary stability

a catheter was first undertaken by Gramiak et al.<sup>8</sup> The air bubbles within the solution greatly increased the returning echoes, but had a tendency to dissolve into the solution very quickly, resulting in short imaging window. Apart from the agitated saline, hydrogen peroxide, iodocyanine green dye, and iodinated contrast agents were also tried as ultrasound contrast media. In 1991, Echovist (Bayer Schering Pharma AG, Berlin, Germany), the first commercially available UCA, was introduced.<sup>9</sup> It was made of air bubbles coated with galactose and too had a very short life in the blood with minimal transpulmonary circulation limiting its clinical utility. Echovist was predominantly used for the evaluation of the cardiac shunt and the female genital tract.

Albunex (molecular biosystems Inc, San Diego, CA, 1994) was the first FDA approved contrast agent used clinically. It was composed of air filled albumin microspheres suspended in 5 percent w/v human albumin solution.<sup>10</sup> *In vitro*, the linear relationship of Albunex concentration with scattered power was demonstrated by De Jong.<sup>11</sup> It had a mean size of approximately 3.5 µm. Although it was stable in albumin solution *in vitro*, it did not have significant recirculation (half life < 5 minutes) *in vivo*. It was used predominantly for the evaluation of cardiac shunts and valvular regurgitation with limited extra-cardiac applications. It is no longer manufactured.

In 1996, a relatively longer lasting UCA called Levovist came up. It contained air bubbles with a galactose/ palmitic acid surfactant coating (Schering). Main indications for use were cardiac, intracranial and abdominal. However, the Levovist bubbles easily collapsed under ultrasound emission owing to its fragile properties, therefore real time images could not be obtained for a longer period.

By now, the need to develop more stable UCAs for prolonged window period for imaging, was very evident. This formed the basis for the development of the second generation UCAs.

*Second generation UCAs* (**Table 2**) contain insoluble gases like sulphur hexafluoride (SF6) or perfluorocarbons and have a surface shell made of different substances like phospholipids, albumin or polymers providing better stabilization. Their smaller size enables a successful transpulmonary passage to reach the various target organs. After intravenous injection, due to their low solubility in water, better stabilization and strong harmonic response,

**Table 2** Second generation ultrasound contrast agents

UCAs	Gas	Stabilizing shell
Optison	Octafluoropropane (approved in US and Europe)	Sonicated albumin
Lumivity	Octafluoropropane perflutren	Lipids
Sonovue*	Sulfur hexafluoride (SF6)	Phospholipids
Sonazoid#	Perfluorobutane	Sonicated albumin

\* The only available contrast in India, # Approved only in Japan

prolonged visualization of dynamic enhancement of the organ can be observed on real-time ultrasound scanning.<sup>7</sup>

In 1998 and 2006, Optison (GE Healthcare) and Lumivity (Bristol-Myers Squibb) made of octafluoropropane coated with albumin and lipid shell respectively, were introduced. The octafluoropropane gas has low water solubility and is more stable providing longer imaging period. However, their sole indication for use has been cardiac.

In 2001, SonoVue (Sonovue, Bracco Milan, Italy) was introduced which contains sulphur hexafluoride stabilized by phospholipid shell. The second generation UCAs are pure blood pool agents as they are unable to destroy the vascular endothelium and thus remain exclusively intravascular resulting in prolonged enhancement of the vascular system. No extravasation into the interstitial fluid occurs. These pharmacokinetics are different from the contrast used in computed tomography (CT) and magnetic resonance imaging (MRI) which is rapidly cleared from the blood into the extracellular space.<sup>2</sup> These features make SonoVue an ideal ultrasound contrast agent for vascular phase imaging of different target organs and is being used widely with promising results.<sup>2,12</sup> SonoVue is the only contrast agent available in India.

The most recent second generation UCA is Sonazoid (Daiichi-Sankyo, Tokyo, Japan), which contains perflubutane and has a hard shell. Sonazoid differs from other agents in exhibiting the longest window period for imaging, the extended late phase. It has been successfully used in the evaluation of liver tumors. This UCA can depict the hemodynamics of the liver in the vascular and the post vascular phase also called the 'Kupffer phase'. This is because, the Kupffer cells of the liver phagocytose Sonazoid microbubbles and thus persist in the liver for long.<sup>13</sup> The experience with Sonazoid is limited to Japan only since it is available exclusively in that country.

CEUS is a promising modality and has many advantages over CT/MRI. It is a simple procedure which is easily available and requires few minutes to perform. It is free from ionizing radiation and can be safely used for repeated follow-up. No laboratory investigations for assessment of renal function are required prior to the study unlike that for CT/MRI as the UCAs are not nephrotoxic. Portability is another advantage. The CEUS machine with the contrast specific modes can be carried anywhere in the hospital for performing bedside procedures on immobile patients.

## TECHNIQUE OF CEUS

A good US machine equipped with low MI contrast imaging mode is required. For intravenous use, the usual recommended dose of SonoVue is 2.4 ml. A higher dose is used for endoscopic contrast enhanced ultrasound (CE-EUS) and when using high frequency transducers. For renal and pancreatic evaluation a low dose of 1.0 ml is used. For extravascular use, a few drops of SonoVue in 10 to 100 ml of saline may be sufficient.<sup>14</sup>

For intravenous use of UCAs, an access in the antecubital fossa using 20 gauge venflon with a three way connector is obtained. The contrast material in the vial, e.g. (SonoVue) is prepared in the soluble form 5 minutes prior and shaken well to be properly dissolved for use. The target organ is visualized on the B mode US and then keeping the lesion in focus the contrast-specific imaging mode is turned on. A simultaneous display of the tissue and contrast signals can be seen on the monitor as a dual window (option in some machines) which ensures the target lesion remains in the field of view throughout the study. The freshly prepared Sonovue is administered as an intravenous bolus followed by flushing with 10 ml of 0.9 percent normal saline. The enhancement characteristics of the target organ is observed on real time by continuously scanning till the three vascular phases post injection. The observation is recorded on the cine mode. Post procedure, the patient is observed for about an hour for any adverse reaction if any due to the UCA.

## SAFETY OF UCAs

UCAs are well tolerated and are safe with few non-specific side effects. The clearance of UCA is very fast and 80 to 90 percent of it gets eliminated through the lungs in 11 minutes.<sup>15</sup> Life threatening anaphylactoid complications are very rare (0.001%).<sup>16</sup> With its use in echocardiography, some fatal incidents have been reported in very ill patients. The use of UCAs mandate precautionary measures to be ready despite low incidence of side-effects. Unlike other contrast agents used for CT or MRI, the UCAs are not nephrotoxic as they have no renal excretion. Hence, CEUS can be safely done in patients with compromised renal function.<sup>17</sup> Contraindications to the use of UCAs are cardio-pulmonary disease, use prior to extra-corporeal shock wave therapy, pregnancy, breast-feeding and severe coronary artery disease. Cautious use is recommended in neonates.

## DIAGNOSTIC APPLICATIONS OF UCAs

A set of guidelines and recommendations for the use of CEUS were developed in early 2004 by the European Federation of Societies for Ultrasound in Medicine and Biology (EFSUMB).<sup>18</sup> These advocated its use for hepatic imaging and since then, CEUS has fully established itself for its use in a whole lot of applications in liver conditions.<sup>14</sup> Over period of time, various non-hepatic applications have also been developed with early encouraging results.<sup>12</sup>

## Applications in Hepatic Imaging

CEUS is ideally suited for the evaluation of liver lesions. It is because of the fact that liver has a dual blood supply comprising of the hepatic artery and the portal vein which allows evaluation of the liver by real time scanning in three vascular phases after the intravenous administration of the UCA. The continuous change in the intra-lesional hemodynamics depicted as the enhancement pattern of the liver nodule is observed in the arterial phase (AP) upto 30 secs, portal venous phase (PP) from 31 to 120 secs and the delayed phase (DP) from 120 to 180 secs. Intermittent scanning is done in individual cases where the contrast is seen persisting in the late phase upto 5 minutes or so. If another mass needs to be studied in the same patient, then the same procedure is repeated with a fresh bolus of UCA after 10 minutes.

### *Detection of Focal Liver Lesions by CEUS*

Traditionally, US has been the first imaging modality for the detection of focal liver lesion (FLL). However, its diagnostic accuracy for the detection and characterization of FLL is much lower than CT and MRI.<sup>19,20</sup> The sensitivity of US is low for early detection of HCC in patients of chronic liver disease. US is unable to detect small nodules less than a cm, isoechoic nodules in a cirrhotic liver and lesions located in the subdiaphragmatic regions. Therefore evaluation of vascularity of the suspicious liver nodules by CD and PD also have limitations like- inability to detect slow flow, evaluate deep seated vessels and frequently associated artifacts.<sup>21,22</sup>

With the use of CEUS, the diagnostic accuracy of FLL has improved from 27 to 42 percent of conventional US to 87 to 89 percent by CEUS.<sup>23,24</sup> Studies have also reported superiority of CEUS over CT in detection of FLL and a comparable accuracy of the two for the overall performance.<sup>25,26</sup>

Small malignant lesions are invariably seen as hypoenhancing nodules in the PP or LP of the multiphasic imaging of CT/MRI. CEUS, by virtue of the use of the UCA, acquires similar ability to study the hemodynamics of the nodule in different vascular phases. Due to this fact, CEUS has led to improved detection of small lesions compared to conventional US and even in comparison to CT.<sup>26,27</sup>

Further improved results have been shown with the use of a newly launched UCA called Sonazoid (only available in Japan). It has the additional advantage of Kupffer imaging which allows prolonged scanning upto 60 minutes resulting in better detection of malignant lesions in the post vascular phase.<sup>27</sup> CEUS with Sonazoid has shown a high sensitivity of 95 percent and specificity of 93 percent for detection of malignant lesions.

### *Characterization of FLL*

Characterization of FLL should be done with the prior knowledge of the clinical history and any previous imaging. It is important to know whether the FLL is present in an underlying normal liver or a cirrhotic liver because the

tumor types vary in the cirrhotic and non-cirrhotic livers. CEUS is a useful modality for the characterization of FLL and can safely be considered as the first imaging modality for this purpose.<sup>28,29</sup> It has a high sensitivity of 98 percent and an accuracy of 93 percent in differentiating benign from malignant nodules.<sup>30</sup>

The enhancement pattern of the liver nodule is termed in relation to the adjacent liver parenchyma. The nodule is hyperenhancing if it enhances more, isoenhancing if it is similar to the liver parenchyma and hypoenhancing if it is less enhancing than the surrounding liver parenchyma. No enhancement refers to no change in enhancement subsequent to the contrast administration.

Confident and accurate characterization of the nodules requires eliciting their enhancement patterns in the different phases of CEUS. Late phase of CEUS is a vital part of the study helping in the characterization of the liver nodules. Benign liver lesions are iso to hyperenhancing in the PP and LP, while the malignant lesions characteristically are

hypoenhancing (show wash out).<sup>31</sup> This occurs because, in the benign lesion the UCA is retained in the healthy liver due to slow flow through the sinusoids whereas, in the malignant lesions the UCA fail to retain due to lack of sinusoids resulting in hypoenhancement of the nodules (seen as dark defects).<sup>32</sup> This pattern occurs in 86 to 93 percent of benign and 78 to 98 percent of malignant liver nodules.<sup>30,33,34</sup>

#### *CEUS patterns of benign focal liver lesions (Table 3)*

**Hemangioma** is the most common benign liver tumor with a prevalence of 1 to 20 percent.<sup>35</sup> CEUS has a sensitivity of 95 percent and specificity of 98 percent in diagnosing hemangioma.<sup>36</sup> The most common pattern of enhancement is the early peripheral nodular arterial enhancement with delayed centripetal fill in which is similar to that seen on CT or MRI (**Figs 1A to C**). It is encountered in 52 to 88 percent of the cases. Sustained enhancement during the late phase has been reported in as high as 83 to 100 percent of cases.<sup>33,34,37-39</sup>

**Table 3** Enhancement patterns of benign focal liver lesions

Focal liver lesion	Arterial phase	Portal venous phase	Late phase
<i>Noncirrhotic liver</i>			
<b>Hemangioma</b>			
Typical features	Peripheral nodular enhancement	Partial/complete centripetal fill in	Complete enhancement
Additional features (small lesion)	Complete, rapid centripetal enhancement		Nonenhancing regions
<b>Focal nodular hyperplasia</b>			
Typical features	Hyperenhancing from the center, complete, early	Hyperenhancing	Iso/hyperenhancing
Additional features	Spoke wheel arteries, feeding artery	Unenhanced central scar	Unenhanced central scar
<b>Hepatocellular adenoma</b>			
Typical features	Hyperenhancing, complete	Isoenhancing	Isoenhancing
Additional features	Nonenhancing regions	Hyperenhancing	Slightly hypoenhancing
<b>Focal fatty infiltration/sparing</b>	Isoenhancing	Isoenhancing	Isoenhancing
<b>Abscess</b>			
Typical features	Peripheral enhancement, no central enhancement	Hyper-/isoenhancing rim, no central enhancement	hypoenhancing rim, no central enhancement
Additional features	Enhanced septa hyperenhanced liver segment	Hypoenhancing rim Enhanced septa hyperenhanced liver segment	
<b>Simple cyst</b>	Nonenhancing	Nonenhancing	Nonenhancing
<i>Cirrhotic liver</i>			
Regenerative nodule ( $\pm$ dysplastic)			
Typical features	Isoenhancing	Isoenhancing	Isoenhancing
Additional features	Hypoenhancing		
In cirrhotic liver simple cysts, hemangiomas and abscesses may also be found and show the same enhancement pattern as in noncirrhotic livers. All other entities are rare findings in cirrhotic livers.			

Source: <https://www.thieme-connect.com/ejournals/pdf/10.1055/s-0032-1325499.pdf>. Guidelines and good clinical practice recommendations for CEUS in liver-update 2012. Accessed on Dec 25, 2012



**Figs 1A to C** Hemangioma – Typical pattern. CEUS images of the FLL in segment VII showing peripheral nodular enhancement (arrow heads) in the AP at 23 secs post-contrast injection (A) with progressive centripetal enhancement (B) becoming isoenhancing (arrow) in the LP at 240 secs (C)

The high diagnostic accuracy of hemangioma on CEUS is comparable to that of MRI, which includes even small hemangiomas. If the typical features of enhancement are seen, further confirmation of the diagnosis by any other imaging is not required.<sup>40</sup> Atypical features occur in very small shunts (<15 mm), very large (more than 4 cm) hemangiomas which have arterio-porto-venous shunts called high flow hemangiomas or shunt hemangiomas which are rapidly filling and the ones that have features of calcification, thrombosis or venoliths.<sup>41</sup> The chance of missing out on any rapidly enhancing hemangiomas (flash-filling) on CEUS is remote because of the advantage of continuous real time scanning.

**Focal nodular hyperplasia (FNH)** is the second most common benign liver tumor with a prevalence of 0.9 to 3 percent.<sup>42</sup> It results from the proliferation of abnormally arranged non-neoplastic hepatocytes as a response to an area of vascular malformation or venous thrombosis. It is commonly associated with a central fibrous scar and anomalous arteries. It is important to differentiate FNH from other entities like hepatic adenoma or carcinoma (fibrolamellar type), because FNH is managed conservatively.

Being a hypervascular tumor, FNH shows homogenous hyper-enhancement in the arterial phase in nearly all the cases. In the portal and late phase, it is isoenhancing or slightly hyperenhancing, seen in about 87 to 100 percent of the cases.<sup>38,43,44</sup>

The central scar occurs in 23 to 31 percent of cases and shows two types of enhancement - the stellate vascularity and centrifugal filling. An anomalous artery courses in the scar in a linear and stellate fashion depicting a spoke wheel pattern, seen in 45 to 89 percent of the cases.<sup>39,45,46</sup>

**Hepatocellular adenoma (HA)** is a rare, benign liver tumor. It has a relatively non-specific pattern of enhancement on CEUS. Being hypervascular, the usual pattern

is of hyper-enhancement in the AP. Small HA show homogenous hyperenhancement while the larger ones are heterogeneously hyperenhancing due to the presence of intratumoral hemorrhage or necrosis. Very rarely, it may show iso or hypoenhancement on the portal and late phases of enhancement and may thus mimic HCC posing a diagnostic dilemma. Even on histopathology, differentiation of HA from well differentiated HCC is often challenging. Similar pattern may be depicted by hypervascular metastasis as well.<sup>46</sup>

**Liver abscess:** Pyogenic abscess is most frequently encountered abscess in the liver. The CEUS findings like the conventional US, vary with the stage of the abscess. The abscess usually shows areas of hyperenhancement.<sup>47</sup> Early abscess is generally solid and shows diffuse heterogeneous enhancement in the AP persisting in the PP and LP. A transient peri-lesional enhancement also occurs in the AP which in very few cases may show hypoenhancement in the PP.<sup>47</sup> If this rare finding is seen, this needs to be differentiated from a necrotic metastasis which appears as a punched out enhancement defect in the LP, while the abscess depicts an ill-defined area of hypoenhancement. As the abscess matures, it develops fluid within which shows as an enhancing rim post contrast injection. The internal septations enhance on CEUS leading to a honeycomb appearance.

**Liver cysts** always need to be diagnosed on conventional US where they are seen as thin walled, anechoic well defined areas with posterior enhancement. Cysts lack enhancement on any phase of CEUS.

**Focal fatty change (Fatty infiltration of fatty sparing)** may mimic masses on US. However, their location is typical - adjacent to the falciform ligament, portal veins and gall bladder. They have geographical margins with no mass effect and vessels are seen traversing through the lesion.<sup>48</sup> If they are nodular or atypical in location, they may pose a diagnostic dilemma. After contrast enhancement, areas of focal fatty

**Table 4** Enhancement patterns of malignant focal liver lesions

FLL	Arterial phase	Portal venous phase	Late Phase
<i>Noncirrhotic liver</i>			
<b>Metastasis</b>			
Typical features	Rim-enhancement	Hypoenhancing	Hypo/nonenhancing
Additional features	Complete-enhancement Hyperenhancement nonenhancing regions	Nonenhancing regions	Nonenhancing regions
<b>HCC</b>			
Typical features	Hyperenhancing	Isoenhancing	Hypo/nonenhancing
Additional features	Nonenhancing regions	Nonenhancing regions	Nonenhancing regions
<b>Cholangiocarcinoma</b>			
Typical	Rim-like hyperenhancement, central hypoenhancement	Hypoenhancing	Nonenhancing
Additional features	Nonenhancing regions Inhomogenous/hyperenhancement	Nonenhancing regions	Nonenhancing regions
<i>Cirrhotic liver</i>			
<b>HCC</b>			
Typical features	Hyperenhancing, complete nonenhancing areas (if large)	Isoenhancing	Hypoenhancing (slightly or moderately)
Additional features	Basket pattern, chaotic vessels Enhancing tumor thrombus Hypo/nonenhancing	Nonenhancing regions Nonenhancing	Isoenhancing Nonenhancing

*Explanation:* Other malignancies in cirrhosis have the same patterns as in noncirrhotic livers.

*Sources:* Sources: <https://www.thieme-connect.com/ejournals/pdf/10.1055/s-0032-1325499.pdf>. Guidelines and good clinical practice recommendations for CEUS in liver-update 2012. Accessed on Dec 25, 2012

change show similar enhancement as the adjoining hepatic parenchyma in all the vascular phases.

#### *CEUS patterns of Malignant focal liver lesions (Table 4)*

CEUS has a sensitivity of 90 percent and specificity of 99 percent and an accuracy of 89 percent in diagnosing malignant lesions.<sup>49</sup> It is useful for detection of metastases, HCC in high risk patients of cirrhosis, evaluate multistep carcinogenesis of HCC, serve as a guidance procedure for the biopsy or percutaneous ablative therapy and for assessment of therapeutic response to loco-regional treatment for HCC.

**Metastases** is the most frequent indication for performing US of the liver. The diagnosis can be simple when the patient has a known primary but very challenging if no such history is available.

Conventional US has limitations in detection of metastases and its accuracy is significantly lower than CT/MRI.<sup>50</sup> Improved accuracy has been noted with the use of CEUS.<sup>51</sup> Metastases show variable patterns of enhancement depending upon the vascularity of the primary tumor in the AP, while, they are typically rapidly hypo-enhancing (within 20 secs) during the PP.<sup>33,43</sup>

More than 85 percent of the metastases show very short lasting peripheral rim enhancement, diffuse or mosaic enhancement followed by rapid washout.<sup>33,38,43</sup>

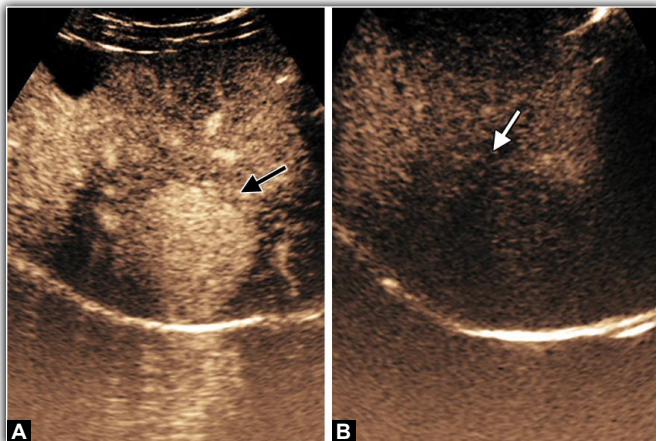
Rim enhancement with early wash out is the hallmark of metastases. Hypervasculat metastasis showing complete

enhancement may be mistaken for HCC in which case other findings like clinical history, serum alpha-fetoprotein levels may come to rescue.

**Hepatocellular carcinoma (HCC):** HCC is the most common primary hepatic malignancy. More than 80 percent of HCC occur in patients with chronic liver disease of viral etiology.<sup>52</sup> The curative therapeutic options of HCC can be applicable only if the disease is diagnosed early. Hence, early detection and characterization of the nodule is imperative.

CEUS plays a pivotal role in evaluating the multi-step carcinogenesis of HCC in cirrhosis . HCC is exclusively supplied by the abnormal arteries while the regenerative nodule (RN) and the dysplastic nodule (DN) contain normal hepatic arteries and portal veins. In the process of progression of DN towards malignancy, the abnormal arterial supply increases while the normal arterial and portal supply decreases.<sup>5</sup>

RN are small and seen on Conventional US as either coarse and heterogenous liver or as multiple, tiny, hypo or hyperechoic nodules. On CEUS, most RN and DN do not show any enhancement (iso-enhancing) in any phase. At times they may show transient hypo enhancement in the AP. DN may have variable and inconsistent arterial and portal supplies or significant overlaps of vascular supply leading to problems in diagnosis on all modalities (CEUS, CT, MRI). Since CEUS has the advantage of continuous real time scanning, it may



**Figs 2A and B** HCC-Typical pattern. AP image of CEUS at 26 secs showing hyperenhancement (arrow) of the FLL (A) with hypoenhancement (arrow) in the VP at 45 secs

pick up subtle transient patterns of enhancement in order to differentiate between HCC and DN.<sup>5</sup>

**CEUS patterns of HCC:** Typical HCC is supplied exclusively by the abnormal arteries. More than 90 percent of the HCCs are hyperenhancing in the AP, also termed arterialization. About one third of the cases show a basket pattern (peripheral vascularity and penetrating the lesion)<sup>38</sup> On the late phase, 83 percent to 97 percent of HCCs show hypoenhancement, classically called washout (**Figs 2A and B**). This wash out is generally slower and milder than that seen in metastases.

A good co-relation of the enhancement pattern is seen with the histological differentiation of HCC. The more the differentiation of the lesion, more slowly is the wash out of the nodule in the late phase. Moderately differentiated HCC shows typical pattern of arterial hyperenhancement and LP hypoenhancement. Atypical patterns are common with well differentiated and poorly differentiated HCC.<sup>53</sup> Well differentiated HCC may or may not show hypoenhancement in the LP as they take long to wash out (**Figs 3A to C**). In such cases, the observation on real time scanning should be done for a longer duration. In a patient of cirrhosis, any nodule that is isoenhancing in the PP and LP should not be considered benign as about half of the well differentiated HCCs do not show washout.<sup>53,54</sup>

CEUS can reliably differentiate between benign and malignant thrombus of the portal vein. Benign thrombus is generally avascular while the malignant one shows heterogeneous enhancement or irregular linear vessels following contrast injection.<sup>55</sup>

**Intrahepatic cholangiocarcinoma (ICC):** ICC typically depicts peripheral rim enhancement in the AP.<sup>56,57</sup> Hypoenhancement is seen in the PP and LP. This feature is in contrast to the findings of ICC seen on CT/MRI where, centripetal enhancement of the tumour occurs. This

difference in pattern again is probably largely due to the fact that contrast agents of CT and MRI diffuse into the extracellular space leading to the enhancement of the tumor in the LP.

#### *Guidance for Interventional Procedures*

Ultrasound is the most commonly used modality for guiding procedures for tumor biopsy or percutaneous ablation. Conventional ultrasound fails to detect nodules that are isoechoic to liver parenchyma, with indistinct margins or infiltrative in nature. In some cases, the liver nodule may not be seen at all and management of such nodules becomes problematic.

Since 2004, CEUS guidance has been used successfully for ablating the tumor that was not seen on conventional US.<sup>58</sup> CEUS plays a key role in the intervention of such cases. It improves the detectability of the nodules and aids in accurate guidance of the needle placement resulting in decreased number of treatment sessions for complete ablation.<sup>59</sup> Better local tumor outcome in terms of local tumor progression rate following CEUS guided RFA has been reported in the range of 0 to 12 percent in the follow-up of 4.3 months to 11 months.<sup>60-62</sup>

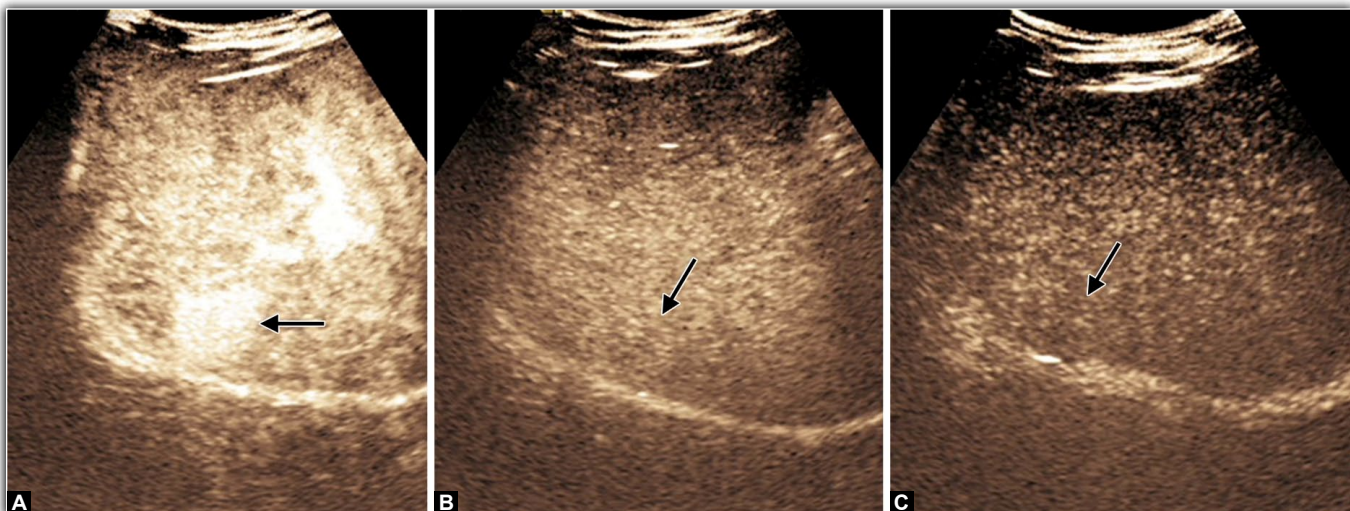
Many a times, the tumors with indistinct margins are seen larger in size on CEUS because the margins get well delineated and the extent of malignant infiltration can be reliably depicted following contrast injection.

#### *Assessment of Treatment Response of Malignant Tumors and Plan Additional Treatment*

Monitoring of response to loco-regional therapy for HCC can be done with the use of CEUS. Loco-regional therapy is the most commonly used treatment for HCC which comprises of trans-arterial chemoembolization (TACE) and percutaneous ablative therapies like radiofrequency ablation (RFA), ethanol (PEI) or acetic acid ablation (PAI) and microwave/laser ablation.

Percutaneous ablative therapies aim at producing coagulation necrosis of the tumor rendering it non-viable. The response to therapy is assessed by estimating the presence of the residual viable tumor tissue depicted by residual vascularity of the remaining tumor. Multiphasic CT/MRI have been the gold standard imaging modalities for assessment of treatment response of HCC.<sup>36</sup> However, these cross sectional imaging modalities have their own limitations. Easy availability, cost effectiveness is a big issue. With CT, because of the association of ionizing radiation, and errors in contrast bolus timing, repeat scanning has its own risks which undermines its utility for follow up use.

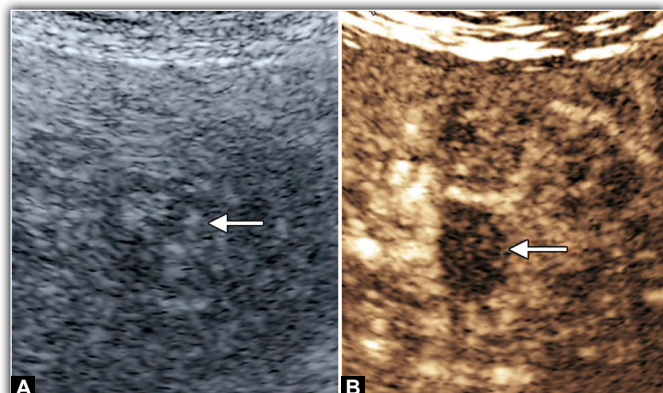
CEUS has the potential to overcome these shortcomings and can reliably differentiate between viable and non-viable tumor tissue following all types of percutaneous ablative therapy. This ability of CEUS is comparable with that of CT or MRI.<sup>63</sup> Post ablation, the completely ablated tumor is seen as



**Figs 3A to C** HCC- Atypical pattern. AP CEUS image of a known patient of cirrhosis with FLL showing homogeneous hyperenhancement (arrow) of the lesion at 30 secs (A) with retained contrast appearing isoenhancing (arrows) in the VP and LP at 110 and 240 secs respectively (B and C). Histopathology suggested well differentiated HCC

a hypoenhancing, well defined area with margin of uniform thickness all around and no area of hyperenhancement within or in the periphery of the hypoenhancing defect (**Figs 4A and B**). Residual disease following ablation is often seen as an area of hyperenhancement in the AP at the margin or within the ablated tumor site , showing washout in PP and LP (**Figs 5 and 6**). CEUS can accurately detect the residual tissue post ablation. The assessment post RFA can be done as early as immediately post ablation and the results are comparable to CT performed at 24 hours.<sup>63,64</sup> CEUS can be safely used for repeated follow-up post therapy as it is free from ionizing radiation and has a low risk of allergic and hypersensitivity reactions.

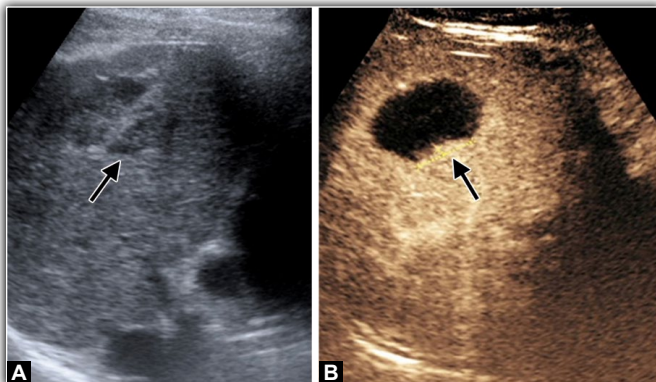
TACE involves delivery of mixture of chemotherapeutic drugs with iodised oil (lipiodol) through the hepatic artery feeding the malignant liver tumor and subsequently embolizing the feeding artery temporarily. This results in devascularising the hypervascular HCC. Post TACE assessment of response involves the depiction of residual viable, enhancing tumor. Multiphasic CT (MPCT) often has limitations in detecting the residual disease following TACE because the lipiodol used in TACE gets deposited in the viable as well as in the nonviable areas of the hepatic parenchyma and thus MPCT has to be undertaken after a minimum period of 4 weeks for proper assessment of response.<sup>32</sup> Moreover, the presence of deposited lipiodol in the tumor masks the status of viability of the tumor tissue in the adjoining hepatic parenchyma. MRI is considered the modality of choice in these cases. Diagnostic accuracy of CEUS in picking up residual disease in the lipiodol covered tumor is high as the UCAs particularly Sonazoid can demonstrate intranodular blood flow and produces prolonged sustained enhancement of the tumor tissue which can well depict the viable tumor



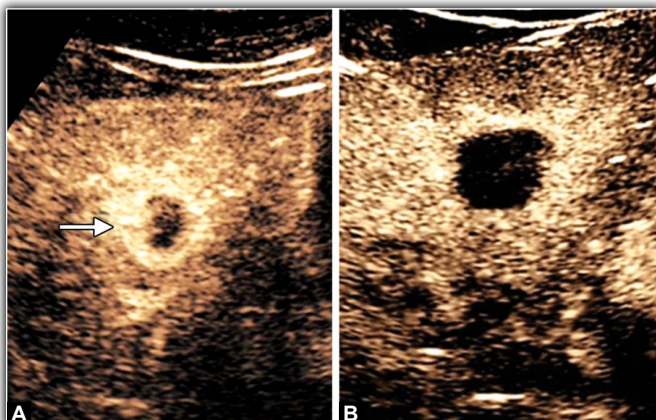
**Figs 4A and B** Post RFA complete response of segment IV A HCC. Simultaneous US display images of tissue and contrast signal, showing a heteroechoic , ill defined focal liver lesion [arrow (A)] which on CEUS shows a well defined hypoenhancing ablative defect (arrow) with no hyperenhancing viable tissue within or at the margin on AP image of CEUS (B) suggesting complete response to ablation

despite the presence of lipiodol. CEUS has been found to be useful in detecting response as early as one week following TACE.<sup>65</sup> The viable disease would show up as areas of hyperenhancement in AP with washout in the PP and LP, while the non-viable tissue doesnot show any enhancement (**Figs 7 and 8**).

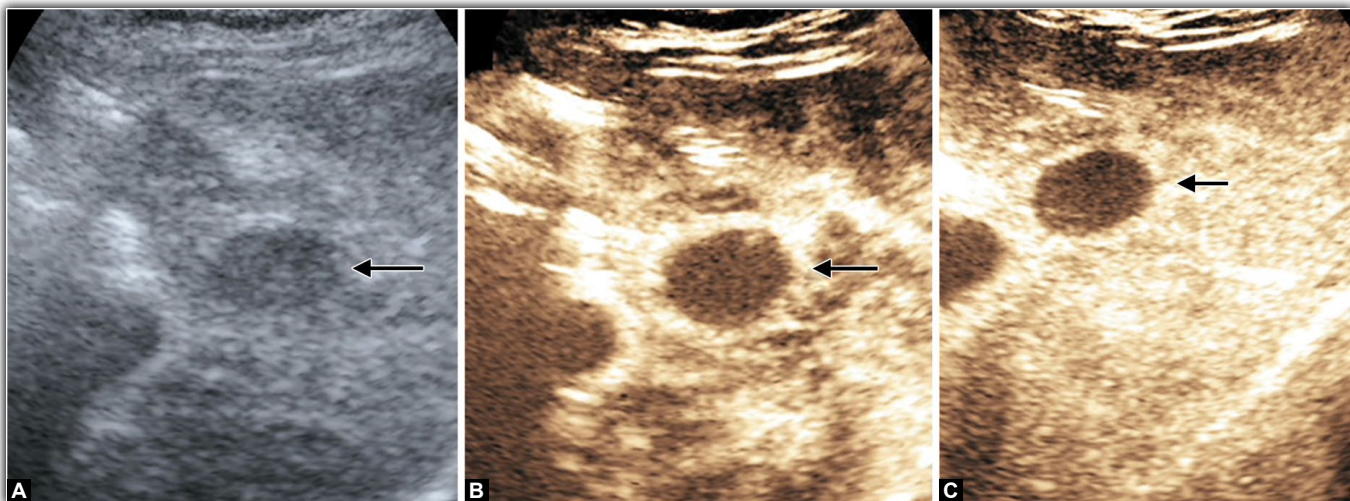
Parametric CEUS can additionally provide information by quantitative assessment of the perfusion of the residual tumor. The evaluation of the tumor vascularity can be done and perfusion maps illustrating contrast kinetics like TTP, PI and the AUC can be generated.<sup>66</sup> The PI in CEUS could reflect the microvessel density (MVD) in HCC. Therefore,



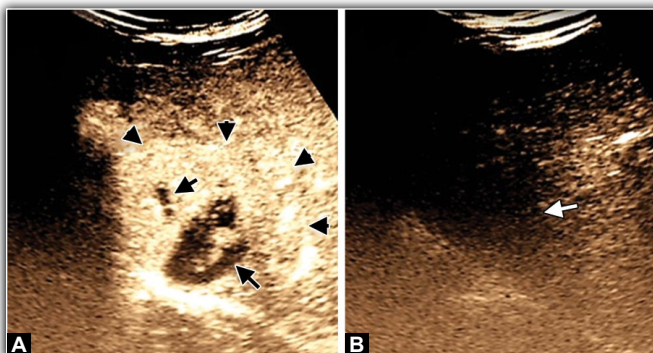
**Figs 5A and B** Residual disease Post RFA in a patient of cirrhosis with solitary HCC. On response assessment at one week post RFA, the US image showing a heterogeneous mass lesion in the liver with no clue of the viable or nonviable tumor tissue (A). On CEUS , the mass shows a focal area of hyperenhancement along the posteroinferior margin of the RFA defect (arrow) suggesting residual disease (B). A repeat RFA was planned subsequently



**Figs 6A and B** Post PAL Residual disease: AP image of CEUS done at 4 weeks following PAL, depicting hyperenhancing area all along the margin and predominantly in the superolateral aspect (arrow) of the segment II/III HCC suggestive of residual disease (A) A repeat PAL was done and CEUS performed subsequently showing smooth margins of the ablative lesion with no enhancing tissue suggesting complete response (B)



**Figs 7A to C** Post TACE complete response—Segment II HCC post TACE, seen as a well defined hypoechoic lesion (arrow) with slightly hyperechoic margins on US (A). On CEUS, the mass is seen as a hypoenhancing lesion with uniform hyperenhancing margins (arrows) in the AP at 22 secs and DP at 62 secs suggesting complete response post TACE (B and C respectively)



**Figs 8A and B** Residual disease Post TACE. CEUS performed for a large segment VII HCC treated with TACE, showing , a large hyperenhancing tissue (arrow heads) with hypoenhancing necrotic areas (small arrows) within, in the AP (A) and showing uniform hypoenhancement (arrow) in the LP (B). Findings are suggestive of significant residual disease post TACE. A repeat session of TACE was planned

quantification of CEUS seems to be helpful for assessment of tumor vascularity in HCC and provide quantitative assessment of the residual disease in the tumor post therapy.

Monitoring response to anti-angiogenic therapy for advanced HCC can also be done with CEUS and pCEUS. The antiangiogenic drugs induce necrosis of the tumor without eradicating the tumor. CEUS can reliably depict reduced or absent tumor vascularity following therapy indicating response to treatment.<sup>67,68</sup>

#### Hepatic Vein Transit Time Estimation

The arrival time of the UCA bolus in the hepatic artery and portal/hepatic vein can be measured and the calculation of the transit times can be done. Shortening of the transit time is encountered in pathologies like liver cancer, cirrhosis and chronic hepatitis and this finding is quite nonspecific.<sup>69,70</sup>

CEUS has a number of limitations as well despite having established itself as an important imaging tool for the evaluation of liver. Lesions located in the subdiaphragmatic areas are difficult to evaluate. Moreover, since CEUS has limited penetration, in patients of chronic liver disease, the deep seated lesions may not be visualized due to steatosis and fibrosis of the liver. Small sized metastases less than 5 to 10 mm can often be missed as they may be too small to be detected. CEUS is not useful for staging of malignancy because of the difficulty in examining the entire liver in the arterial phase. Moreover, one injection of UCA per nodule is required if the nodules are present in different segments of liver. This defeats its purpose of cost-effectiveness. CT/MRI needs to be resorted to in such a situation.

#### Liver Transplant

CEUS has also been tried in patients of liver transplant for evaluation of hepatic artery flow. Hepatic artery thrombosis is the most common vascular complication following transplant even though portal vein, hepatic vein and caval thrombosis can also occur but these conditions are relatively less common. Though Doppler is very useful in majority of the patients, however at times due to postoperative edema, inaccessible hepatic arteries, it may fail to provide an answer. In such patients, CEUS has been tried with successful results.<sup>31</sup>

#### Applications in Pancreatic Imaging

The main utility of CEUS in pancreatic diseases lies in the characterization of pancreatic mass lesions and in the imaging of acute pancreatitis. After administration of UCAs, the pancreatic parenchyma shows early enhancement, immediately after aortic enhancement (10-30 sec). Maximal enhancement is reached at 60 seconds. After the arterial phase, a venous phase imaging should also be performed (30-100 seconds).<sup>12,71,72</sup> Once the pancreatic study is completed, delayed imaging of the liver should also be performed to rule out metastases, utilizing the same contrast agent.<sup>73</sup>

#### Detection of Focal Pancreatic Lesions

For pancreatic adenocarcinomas, the usual investigation modality is CECT. They are schirrrous tumors and commonly hypovascular compared to the normal pancreatic parenchyma. The detectability of small pancreatic mass lesions on CEUS is superior to US alone, comparable efficacy with that of EUS and more diagnostic accuracy than CT in the detection of tumors less than 2 cms.<sup>71</sup> Four patterns of enhancement of focal pancreatic lesions are seen- no enhancement (type I), vascularity less than adjacent pancreatic parenchyma (type II), vascularity equal to (type III) and more than the (type IV) adjacent pancreatic parenchyma. Pancreatic adenocarcinoma usually demonstrate type I and II patterns.<sup>71</sup>

Pancreatic neuroendocrine tumors can depict significant enhancement in the arterial phase of CEUS even when it may not show significant increased vascularity on Doppler imaging.<sup>74,75</sup>

#### Differentiation of Cystic Pancreatic Tumors from Pancreatic Pseudocyst

Common pancreatic cystic neoplasms include mucinous and serous cystic tumors, intraductal papillary mucinous tumors (IPMT). Mucinous cystic tumors are potentially malignant lesions. Imaging features include unilocular cystic lesions with internal septations and echogenic content. On CEUS, they show avid enhancement of the wall, internal septations and nodules.<sup>76</sup> Serous cystadenomas are usually microcystic lobulated masses, hypervascular and show enhancement

of the internal septations. CEUS can differentiate a cystic pancreatic neoplasm from a pseudocyst by demonstrating the enhancement of septae, nodules and solid components in a tumor.<sup>73</sup> On the contrary; pancreatic pseudocysts are devoid of any contrast enhancement, even though the internal contents may appear echogenic on US.<sup>76</sup>

IPMT can be of the main duct type or branch duct type. In the main duct type, the main pancreatic duct is dilated and may show intraductal debris/clot. Branch duct type IPMT usually presents as a multiseptated cystic mass lesion in the head of pancreas. In IPMT, CEUS can differentiate a clot (which is avascular) from an enhancing nodule.

#### *Detection of Pancreatic Necrosis in Acute Pancreatitis*

The detection of necrosis at an early stage of development is of significant clinical importance as early treatment of necrosis (either percutaneous drainage or surgical debridement) can be planned to reduce morbidity and mortality. The routine diagnostic imaging modality in acute pancreatitis is CECT. CEUS can also be used as an alternative to CECT in the follow-up of acute pancreatitis.<sup>77</sup> After administration of UCAs, the necrotic pancreatic parenchyma remains unenhanced.<sup>77</sup>

#### *Contrast Enhanced Endoscopic Ultrasound (CE-EUS)*

CE-EUS is a newer imaging modality which combines the benefit of superior resolution of EUS and assessment of enhancement characteristics (as in CEUS) in a single investigation.<sup>78-82</sup>

CE-EUS is useful for the differentiation of pancreatic ductal adenocarcinoma from focal pancreatitis and other focal lesions; and to differentiate cystic pancreatic tumor from pancreatic pseudocyst.<sup>12</sup> Since pancreatic adenocarcinomas tend to be fibrous in nature and have a tough capsule, they show less or no venous signals, owing to increased intratumoral pressure. On the contrary, focal pancreatitis shows both arterial and venous signals. CE-EUS increases the sensitivity of EUS (from 73.2% to 91.1%) in differentiation of pancreatic adenocarcinoma from focal pancreatitis.<sup>83</sup>

#### **Applications in Renal Imaging**

The main role of CEUS in renal lesions include the evaluation of a focal renal lesion,<sup>84-87</sup> differentiating a renal tumor from a pseudotumor,<sup>88</sup> and also in the evaluation of renal vascular lesions.<sup>86,89</sup> Other applications include guidance to radiofrequency ablation of renal tumors<sup>90-93</sup> and monitoring of renal abscesses in proven cases of urinary tract infection.<sup>94</sup> Kidneys are highly perfused organs and the microbubble contrast enhancement pattern of the kidneys follow a pattern similar to that seen on CECT. After administration of UCAs, the vascular pedicle of kidney enhances first, followed by the cortex and the medulla at the last. The tip of the renal medullary pyramid is the last to enhance. UCAs do not show excretion into the pelvicalyceal system.

CEUS is recommended for the following renal indications.<sup>12</sup>

#### *Characterization of Renal Masses*

CECT is the usual investigation for characterization and staging of renal mass lesions. However, on a single phase CECT, it becomes difficult to differentiate complicated hyperdense cyst and a solid enhancing mass lesion. Similarly, a hypodense non-enhancing solid mass lesion may be difficult to differentiate from a cystic lesion on CECT. Since CEUS is more sensitive to detection of blood flow than CECT, it can differentiate a solid mass lesion from a cystic one with greater accuracy. It also scores over CECT in characterization of complex cystic renal masses as it can detect the septa and solid components in Bosniak grade 2 to 4 cysts with better sensitivity than CECT.<sup>84-87</sup>

#### *Differentiation of Renal Tumors from Pseudotumors*

Renal pseudotumors are proliferation of normal renal tissue which mimic tumor. US may fail to differentiate the two. After administration of UCAs, the enhancement of pseudotumors is similar to the normal renal parenchyma on all phases of enhancement.<sup>88</sup> On the contrary, the enhancement pattern of solid renal tumors differs from that of the normal renal parenchyma in at least one phase of enhancement. Although the differentiation of a benign from a malignant renal tumor cannot be done on the basis of enhancement characteristics, it is helpful in differentiating a 'true' renal tumor from a pseudotumor.

#### *Renal Vascular Lesions*

Renal infarcts are better differentiated from ischemic areas on CEUS compared to unenhanced Doppler US/ US as the infarcted area shows no enhancement whereas hypoperfused area retains its blood flow, although reduced.<sup>86,89</sup> CEUS also differentiates renal infarct from cortical necrosis, which shows preserved hilar vascularity.

#### *Renal Tumor Ablation Under CEUS Guidance*

Like the use of CEUS guidance for liver tumors, renal tumors too can be ablated. CEUS can be used before the ablation procedure to increase tumor visibility. After the ablation procedure, CEUS performed 5 to 10 minutes later (once the gas and related artifacts disappear) can detect residual viable tumor seen as areas of enhancement whereas ablated regions appear non-enhancing.<sup>90,91</sup> Studies have demonstrated CEUS to be as accurate as CT and MRI in assessing adequacy of ablation treatment.<sup>92,93</sup>

#### **Application in Abdominal Trauma**

CECT is the gold standard imaging modality in blunt abdominal trauma. The present role of CEUS in the

abdominal trauma lies in the evaluation of intra-abdominal solid organ injuries and triaging critically ill trauma patients without hampering with the resuscitation procedure in the emergency ward. Although bedside US has proven an effective modality to detect free intraperitoneal fluid, its utility is limited in detecting parenchymal injuries in solid abdominal organs.<sup>95-96</sup> Studies have shown that CEUS can detect intra-abdominal solid organ injuries (including liver, splenic, renal lesions) with higher sensitivity and specificity than US.<sup>97-98</sup>

The solid abdominal organs can be evaluated in a staged manner in two-part examination (once for the right hypochondrium, evaluating liver and right kidney) and another examination for the left hypochondrium for spleen and left kidney. Normal organs usually show homogeneous increased echogenicity in the parenchymal phase of the examination. A contusion is seen as a hypoechoic area within the enhancing parenchyma with ill defined borders; a laceration is a more well defined linear non-enhancing area. In hypovolemic shock all the abdominal solid organs show reduced enhancement. Since UCAs are not excreted in the urine, they can not be used to detect renal collecting system injury.

### Applications in Breast Imaging

The main role of CEUS in breast is in the characterization of indeterminate breast masses. Mammography is the established screening modality in breast cancer, and US is widely employed for evaluation of palpable and imaging detected masses.<sup>99</sup> The utility of US can be limited in characterization of BI-RADS category 3 and 4 lesions, and role of different modalities like Doppler sonography and elastography has been evaluated in this group of patients.<sup>100-102</sup> Doppler sonography has shown limited utility in the characterization of breast lesions prior to the use of CEUS.

The advent of breast MRI led to an increase in sensitivity in cancer detection, although it had a low specificity.<sup>103</sup> The cancer detection on breast MRI was based upon both morphologic as well as contrast enhancement kinetics. The principle of use of CEUS in the detection of breast cancers depends on similar rationale of gaining superior resolution grey scale image, coupled with contrast imaging to assess neo-vascularity. Although one of the earliest applications of CEUS was in the evaluation of breast masses, unfortunately, till now it does not have any recommended role<sup>12</sup> as no specific pattern of enhancement or CEUS characteristics could be consistently detected as a marker of malignant mass lesion. The potential roles of CEUS in breast are as follows:

### Characterization of Breast Masses

Several studies have described difference in tumor vascularity between benign and malignant masses. The benign lesions

(fibroadenoma for example) show smooth vessels at the periphery and less avid enhancement (**Figs 9A and B**); whereas the malignant masses appear spiculated (**Figs 10A and B**), have more tortuous vessels with irregular course, and have inter-vascular shunts.<sup>104,105</sup> Although several studies have shown malignant lesions to enhance earlier than benign lesions,<sup>104</sup> there is significant overlap between the two in other studies.<sup>105</sup>

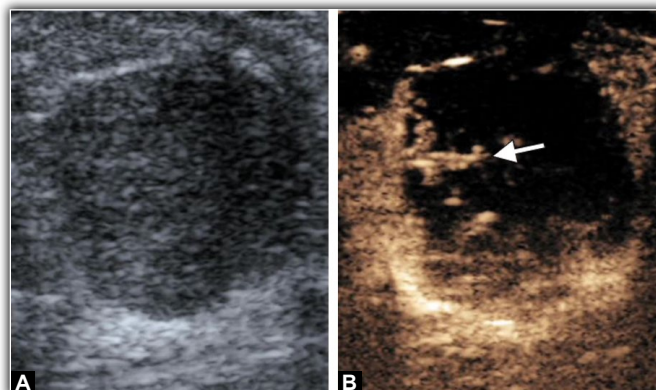
### Assessment of Tumor Response after Chemotherapy in Breast Cancer

Breast cancers which are not amenable for upfront surgery usually undergo neoadjuvant treatment and the response to neoadjuvant chemotherapy can predict prognosis of the patient. Malignant tumors exhibit neo-vascularization, and the characterization and detection of tumor vessels can be useful for prediction of biologic activity of the tumor. After chemotherapy or hormone therapy, tumors tend to show reduced neo-angiogenesis. Studies have shown CEUS to be more effective than Doppler US in the detection of tumor vascularity before and after treatment.<sup>106</sup>

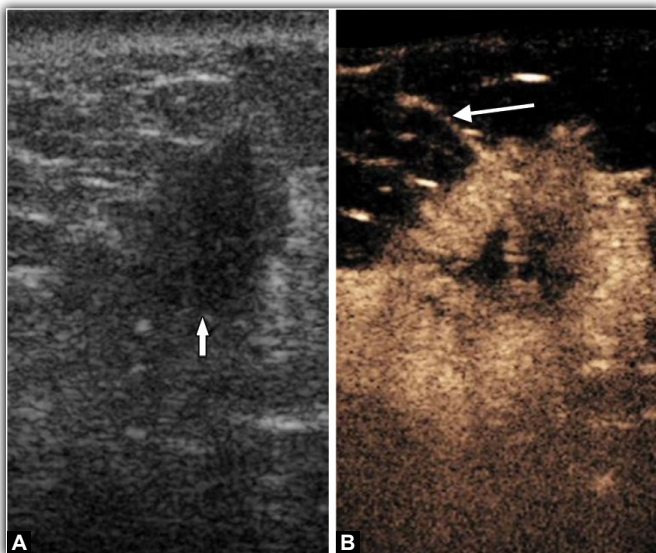
### Application in Prostatic Imaging

Till date, the evidence towards CEUS as a diagnostic modality in prostatic imaging is limited and described as a research tool.<sup>12</sup>

Prostatic adenocarcinoma is associated with neovascularity, but the detection of these micro-vessels is beyond the resolution of Doppler US. UCAs can increase the sensitivity of Doppler sonography. Prostatic adenocarcinoma tends to show early enhancement after administration of UCAs (**Figs 11A and B**). Several studies have compared the efficacy of CEUS guided targeted biopsy with systematic biopsy. It has been demonstrated that CEUS increased the



**Figs 9A and B** Benign breast mass (Fibroadenoma). Simultaneous US display image shows a well defined smoothly marginated mass lesion without posterior acoustic shadowing (A). CEUS image reveals minimal enhancement and peripheral branching vessels (arrow) (B)



**Figs 10A and B** Invasive ductal carcinoma of breast. Simultaneous US display image (A) reveals an illdefined hypoechoic mass lesion (block arrow) which is taller than wide. CEUS (B) demonstrates the spiculated margins of the mass and avid peripheral enhancement with central nonenhancing area. The ductal extension of tumor also shows avid enhancement (arrow)

detection rate of malignancy in the peripheral zone, but was not helpful in the central zone.<sup>107,108</sup> Some studies compared the yield of CEUS guided targeted biopsy with systematic biopsy and found a significantly increased detection rate on targeted biopsy,<sup>109,110</sup> although the detection of enhanced lesions lacked specificity or specific pattern of enhancement in adenocarcinomas.<sup>111-113</sup>

### Miscellaneous Intravascular Applications

In the gastrointestinal tract, UCAs have been used in the disease activity evaluation in inflammatory bowel diseases<sup>114-118</sup> and clinical monitoring of Crohn's disease activity.<sup>119</sup> UCAs have also been used to differentiate between inflammatory and fibrotic strictures.<sup>120</sup> In spleen, UCAs can be used for lesion characterization<sup>121</sup>, to characterize suspected accessory spleen<sup>122</sup> and to confirm splenic infarction.<sup>123</sup> Tumor response assessment can be done in metastatic GIST using UCAs.<sup>124-125</sup>

While performing testicular sonography, use of UCAs have been recommended in the evaluation of a suspected segmental infarction (for better delineation of the infarct)<sup>126</sup>, testicular trauma (for better detection of fracture line),<sup>127</sup>, detecting areas of abscess formation in epididymo-orchitis,<sup>128</sup> and differentiating a neoplastic from a non-neoplastic focal lesion.<sup>129</sup>

Endometrial carcinoma is another frontier where the utility of CEUS has been explored where transvaginal CEUS can assess the depth of myometrial invasion; especially when the endometrial lining is thin after biopsy.<sup>130</sup>

Application of CEUS in lung and pleural diseases is limited. In peripheral consolidations, CEUS can be used to differentiate embolic consolidation from an inflammatory etiology and to detect an area of abscess within a peripheral area of lung consolidation.<sup>131-133</sup> Vascular applications include carotid plaque characterization, differentiating a complete carotid occlusion from a tight stenosis, detection of dissection of carotid vessels and aorta,<sup>134-137</sup> characterization of suspected inflammatory abdominal aortic aneurysm, and detection, characterization and follow-up of endoleaks after abdominal aortic aneurysm repair.<sup>138-140</sup> For lymph node evaluation, it has been used for sentinel lymph node sampling in cancer patients, although not recommended in recent guidelines.<sup>141</sup>

### Intracavitary Applications

CEUS has non-vascular applications as well. Assessment of the physiological cavities include voiding sono-cystourethrogram or the evaluation of vesicoureteric reflux,<sup>142</sup> sono-hysterosalpingo-contrast sonography for tubal patency assessment<sup>143</sup>, CEUS guided percutaneous cholangiography,<sup>144</sup> T-tube cholangiogram<sup>145</sup>, CEUS sialography for obstructive lesions of the salivary ducts<sup>146</sup>, CEUS guided nephrostogram. Non-physiologic cavities too can be evaluated by CEUS. Delineation of fistulae, abscesses and intraperitoneal collections and gastro-esophageal reflux can be done successfully by different approaches.<sup>147-149</sup>

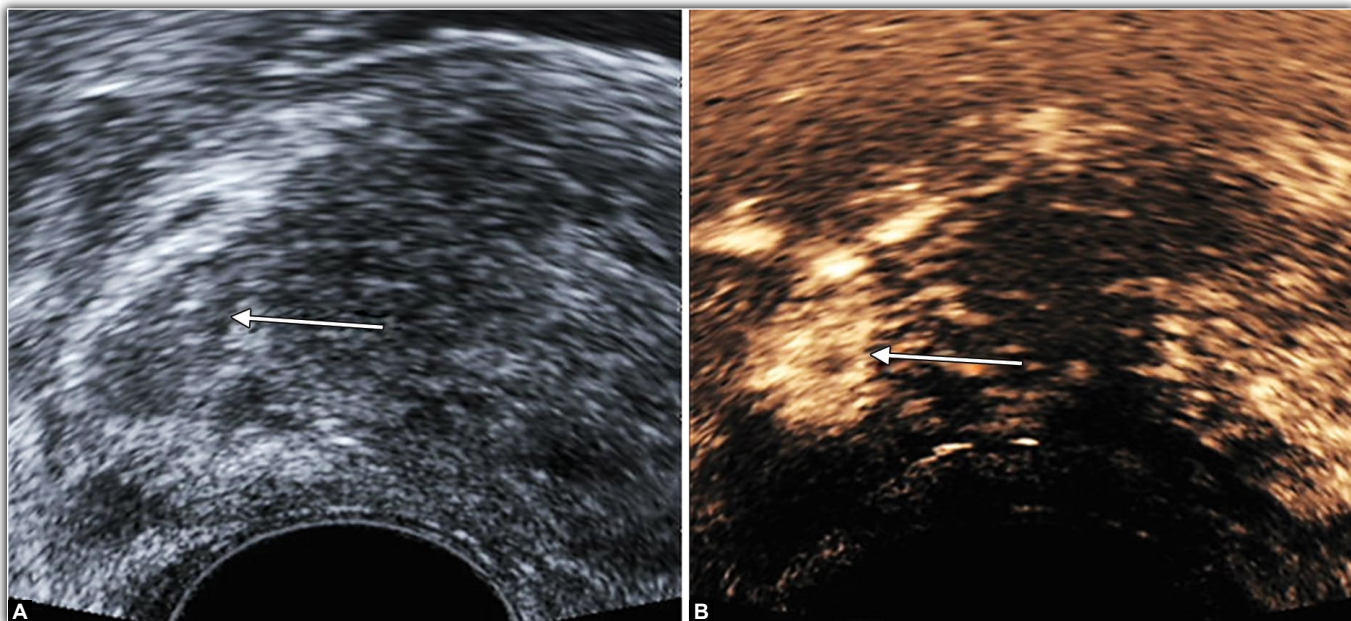
### Upcoming Applications

CEUS is being tried in a big way for various novel applications. Some of the newer applications are worth mentioning in this chapter such as assessment of transplanted kidneys<sup>150</sup>, perforator vessels in vascularized myocutaneous flaps, post-operative assessment of vascularity in myocutaneous flaps,<sup>151-154</sup> differentiation of an adherent GB sludge from a mass and detection of GB perforation in the setting of acute cholecystitis and for assessment of vascularity in uterine artery embolization for uterine fibroids.<sup>155</sup>

To conclude, the advent of UCAs have revolutionized the role of US in clinical practice. CEUS has emerged as a major player in hepatic imaging. It combines the advantage of superior spatial resolution of US with the real time contrast kinetics assessment of focal liver lesions. While several non-hepatic applications are still in the experimental stage, but, the combination of new generations of UCAs and new ultrasound image sequences appears to be very promising. CEUS has the potential to become the most widely used imaging modality.

### ACKNOWLEDGEMENTS

The authors acknowledge the contribution of Dr Sanjay Sharma and Dr Vishal T for Figure no 11 (A,B), from the MD thesis work performed in the Department of Radiology, AIIMS ( November 2009- November 2011).



**Figs 11A and B** Transrectal sonography of adenocarcinoma of prostate. Simultaneous display US figure (A) shows hypoechoic mass lesion in the right half of the prostate (arrow); which shows increased enhancement compared to the rest of the gland after administration of UCAs (arrow in figure B)

## REFERENCES

- Shampo MA, Kyle RA. Karl Theodore Dussik- pioneer in ultrasound. Mayo Clinic Proceedings. 1995;70:1136.
- Claudon M, Cosgrove D, Albrecht T, Bolondi L, Bosio M, Calliada F, et al. Guidelines and good clinical practice recommendations for contrast enhanced ultrasound (CEUS) - update 2008. Ultraschall Med. 2008;29:28-44.
- Brannigan M, Burns PN, Wilson SR. Bloodflow patterns in focal liver lesions at microbubble-enhanced US. Radiographics. 2004;24:921-35.
- Cosgrove D, Blomley M. Liver tumors: evaluation with contrast-enhanced ultrasound. Abdom Imaging. 2004;29:446-54.
- Kim TK, Lee KH, Khalili K, Jang HJ. Hepatocellular nodules in liver cirrhosis: contrast-enhanced ultrasound. Abdom Imaging. 2011;36:244-63.
- Moschouris H, Malagari K, Marinis A, Kornezos I, Stamatou K, Nikas G, et al. Hepatocellular carcinoma treated with transarterial chemoembolization: Evaluation with parametric contrast-enhanced ultrasonography. World J Radiol. 2012;4: 379-86.
- Hui-Xiong Xu. Contrast-enhanced ultrasound: The evolving applications. World J Radiol. 2009;1:15-24.
- Gramiak R, Shah PM. Echocardiography of the aortic root. Invest Radiol. 1968;3:356-66.
- Nico de Jong, Marcia Emmer, Annemarie van Wamel, and Michel Versluis. Ultrasonic characterization of ultrasound contrast agents. Med Biol Eng Comput. 2009;47:861-73.
- Christiansen C, Kryvi H, Sontum PC, Skotland T. Physical and biochemical characterization of Albunex, a new ultrasound contrast agent consisting of air-filled albumin microspheres suspended in a solution of human albumin. Biotechnol Appl Biochem. 1994;19(Pt 3):307-20.
- N de Jong, L Hoff. "Ultrasound scattering properties of Albunex microspheres". Ultrasonics. 1993;31:175-181.
- Piscaglia F, Nolsoe C, Dietrich CF, et al. The EFSUMB guidelines and recommendations on the clinical practice of contrast enhanced ultrasound (CEUS): Update 2011 on non-hepatic applications. Ultraschall in Med. 2012;33:33-59
- Yanagisawa K, Moriyasu F, Miyahara T, Yuki M, Iijima H. Phagocytosis of ultrasound contrast agent microbubbles by Kupffer cells. Ultrasound Med Bio. 2007;33:318-25.
- Dietrich CF, Cui XW, Schreiber-Dietrich DG, Ignee A. EFSUMB guidelines 2011: comments and illustrations. Ultraschall Med. 2012;33:S11-21.
- Dietrich CF, Cui XW, Boozari B, Hocke M, Ignee A. Contrast enhanced ultrasound (ceus) in the diagnostic algorithm of Hepatocellular and Cholangiocellular carcinoma, comments on the AASLD Guidelines. Ultrasound in Med. 2012;33:557-66.
- Piscaglia F, Bolondi L. The safety of SonoVue in abdominal applications: retrospective analysis of 23188 investigations. Ultrasound Med Biol. 2006;32:1369-75.
- Lencioni R, Piscaglia F, Bolondi L. Contrast-enhanced ultrasound in the diagnosis of hepatocellular carcinoma. Journal of Hepatology. 2008;48:848-57.
- Albrecht T, Blomley M, Bolondi L, et al. Guidelines for the use of contrast agents in ultrasound. Ultraschall in Med. 2004;25:249-56.
- Noone TC, Semelka RC, Chaney DM, Reinhold C. Abdominal imaging studies comparison of diagnostic accuracies resulting from ultrasound, computed tomography, and magnetic resonance imaging in the same individual. Magn Reson Imaging. 2004; 2219-24.
- Werneck K, Rummeny E, Bongartz G, Vassallo P, Kivelitz D, Wiesmann W, et al. Detection of hepatic masses in patients with carcinoma comparative sensitivities of sonography, CT, and MR imaging. AJR Am J Roentgenol. 1991;157:731-9.

21. Dietrich CF, Ignee A, Hocke M, Schreiber-Dietrich D, Greis C. Pitfalls and artifacts using contrast enhanced ultrasound. *Z Gastroenterol.* 2011;49:350-6.
22. Mitchell DG. Color Doppler imaging principles, limitations, and artifacts. *Radiology.* 1990;177:1-10.
23. Dai Y, Chen MH, Yin SS, Yan K, Fan ZH, Wu W, Wang YB, Yang W. Focal liver lesions: can SonoVue-enhanced ultrasound be used to differentiate malignant from benign lesions? *Invest Radiol.* 2007;42:596-603.
24. Bartolotta TV, Taibbi A, Galia M, Runza G, Matranga D, Midiri M, Lagalla R. Characterization of hypoechoic focal hepatic lesions in patients with fatty liver: diagnostic performance and confidence of contrast-enhanced ultrasound. *Eur Radiol.* 2007;17:650-61.
25. Hohmann J, Albrecht T, Hoffmann CW, Wolf KJ. Ultrasonographic detection of focal liver lesions: increased sensitivity and specificity with microbubble contrast agents. *Eur J Radiol.* 2003;46:147-59.
26. Solbiati L, Tonolini M, Cova L, Goldberg SN. The role of contrast-enhanced ultrasound in the detection of focal liver lesions. *Eur Radiol.* 2001;11:E15-E26.
27. Hatanaka K, Kudo M, Minami Y, Maekawa K. Sonazoid-enhanced ultrasonography for diagnosis of hepatic malignancies comparison with contrast-enhanced CT. *Oncology.* 2008;75 (Suppl) 1:42-7.
28. Xu HX, Liu GJ, Lu MD, Xie XY, Xu ZF, Zheng YL, Liang JY. Characterization of small focal liver lesions using real-time contrast-enhanced sonography diagnostic performance analysis in 20patients. *J Ultrasound Med.* 2006;25:349-61.
29. Sporea I, Badea R, Martie A, Dumitru E, Ioanitescu S, Sirli R, et al. Contrast enhanced ultrasound for the evaluation of Focal liver lesions in daily practice: A multicentric study. *Medical Ultrasonography.* 2012;14:95-100.
30. Nicolau C, Vilana R, Catalá V, Bianchi L, Gilabert R, García A, Brú C. Importance of evaluating all vascular phases on contrast-enhanced sonography in the differentiation of benign from malignant focal liver lesions. *AJR Am J Roentgenol.* 2006;186:158-67.
31. Claudon M, Dietrich CF, Choi BI, Cosgrove DO, Kudo M, Nolsøe CP, et al. Guidelines and Good Clinical Practice Recommendations for Contrast Enhanced Ultrasound (CEUS) in the Liver - Update 2012. *Ultraschall Med.* 2012 - PMID: 23129518
32. Kono Y, Steinbach GC, Peterson T, Schmid-Schönbein GW, Mattrey RF. Mechanism of parenchymal enhancement of the liver with a microbubble-based US contrast medium; an intravital microscopy study in rats. *Radiology.* 2002;224:253-7.
33. Von Herbay A, Vogt C, Willers R, Haussinger D. Real-time imaging with the sonographic contrast agent SonoVue differentiation between benign and malignant hepatic lesions. *J Ultrasound Med.* 2004;23:1557-68.
34. Wilson SR, Burns PN. An algorithm for the diagnosis of focal liver masses using microbubble contrast-enhanced pulse-inversion sonography. *AJR Am J Roentgenol.* 2006;186:1401-12.
35. Mergo PI, Ros PR. Benign lesions of the liver. *Radiol Clin North Am.* 1998;36:319-31.
36. Xu HX. Contrast-enhanced ultrasound: The evolving applications. *World J Radiol.* 2009;1:15-24.
37. Ding H, Wang WP, Huang BJ, Wei RX, He NA, Qi Q, Li CL. Imaging of focal liver lesions low-mechanical-index real-time ultrasonography with SonoVue. *J Ultrasound Med.* 2005;24:285-97.
38. Leen E, Ceccotti P, Kalogeropoulou C, Angerson WJ, Moug SJ, Horgan PG. Prospective multicenter trial evaluating a novel method of characterizing focal liver lesions using contrast-enhanced sonography. *AJR Am J Roentgenol.* 2006;186:1551-9.
39. Morin SHX, Lim AKP, Cobbold JFL and Taylo-Robinson SD. Use of second generation contrast-enhanced ultrasound in the assessment of focal liver lesions. *WJG.* 2007;13:5963-70.
40. Burns PN, Wilson SR. Focal liver masses enhancement patterns on contrast-enhanced images--concordance of US scans with CT scans and MR images. *Radiology.* 2007;242:162-74.
41. Dietrich CF, Mertens JC, Braden B, Schuessler G, Ott M, Ignee A. Contrast-enhanced ultrasound of histologically proven liver hemangiomas. *Hepatology.* 2007;45:1139-45.
42. Nguyen BN, Flejou JF, Terris B, Belghiti J, Degott C. Focal nodular hyperplasia of the liver a comprehensive pathologic study of 305 lesions and recognition of new histologic forms. *Am J Surg Pathol.* 1999;23:1441-54.
43. Quaia E, Calliada F, Bertolotto M, Rossi S, Garioni L, Rosa L, Pozzi-Mucelli R. Characterization of focal liver lesions with contrast-specific US modes and a sulfur hexafluoride-filled microbubble contrast agent diagnostic performance and confidence. *Radiology.* 2004;232:420-30.
44. Shortell CK, Schwartz SI. Hepatic adenoma and focal nodular hyperplasia. *Surg Gynecol Obstet.* 1991;173:426-31.
45. Kim TK, Jang HJ, Burns PN, Murphy-Lavallee J, Wilson SR. Focal nodular hyperplasia and hepatic adenoma differentiation with low-mechanical-index contrast-enhanced sonography. *AJR Am J Roentgenol.* 2008;190:58-66.
46. Dietrich CF, Schuessler G, Trojan J, Fellbaum C, Ignee A. Differentiation of focal nodular hyperplasia and hepatocellular adenoma by contrast-enhanced ultrasound. *Br J Radiol.* 2005; 78:704-7.
47. Catalano O, Sandomenico F, Raso MM, Siani A. Low mechanical index contrast-enhanced sonographic findings of pyogenic hepatic abscesses. *AJR Am J Roentgenol.* 2004;182:447-50.
48. Kim TK, Jang HJ, Wilson SR. Benign liver masses: imaging with microbubble contrast agents. *Ultrasound Q.* 2006;22: 31-9.
49. Von Herbay A, Westendorff J, Gregor M. Contrast-enhanced ultrasound with SonoVue differentiation between benign and malignant focal liver lesions in 317 patients. *J Clin Ultrasound.* 2010;38:1-9.
50. Hagspiel KD, Neidl KE, Eichenberger AC, Weder W, Marincek B. Detection of liver metastasescomparison of superparamagnetic iron oxide-enhanced and unenhanced MR imaging at 1.5 T with dynamic CT, intraoperative US, and percutaneous US. *Radiology.* 1995;196:471-8.
51. Dietrich CF, Kratzer W, Strobel D, Danse E, Fessl R, Bunk A, et al. Assessment of metastatic liver disease in patients with primary extrahepatic tumors by contrast-enhanced sonography versus CT and MRI. *World J Gastroenterol.* 2006;12:1699-705.
52. Pisani P, Parkin DM, Ferlay J: Estimates of the world wide mortality from eighteen major cancers in 1985: implications for prevention and projections of future burden. *Int J Cancer.* 1993; 55: 891-3.
53. Jang HJ, Kim TK, Burns PN, Wilson SR. Enhancement patterns of hepatocellular carcinoma at contrast-enhanced US: comparison with histologic differentiation. *Radiology.* 2007;244:898-906.
54. Jang HJ, Yu H, Kim TK. Imaging of focal liver lesions. *Semin Roentgenol.* 2009;44:266-82.

55. Rossi S, Ghittoni G, Ravetta V, Torello Viera F, Rosa L, Serassi M, et al. Contrast-enhanced ultrasonography and spiral computed tomography in the detection and characterization of portal vein thrombosis complicating hepatocellular carcinoma. *Eur Radiol.* 2008;18:1749-56.
56. Chen LD, Xu HX, Xie XY, Xie XH, Xu ZF, Liu GJ, Wang Z, Lin MX, Lu MD. Intrahepatic cholangiocarcinoma and hepatocellular carcinoma: differential diagnosis with contrast-enhanced ultrasound. *Eur Radiol.* 2010;20:743-53.
57. Vilana R, Forner A, Bianchi L, García-Criado A, Rimola J, de Lope CR, Reig M, Ayuso C, Brú C, Bruix J. Intrahepatic peripheral cholangiocarcinoma in cirrhosis patients may display a vascular pattern similar to hepatocellular carcinoma on contrast-enhanced ultrasound. *Hepatology.* 2010;51:2020-9.
58. Numata K, Isozaki T, Ozawa Y, Sakaguchi T, Kiba T, Kubota T, Ito A, Sugimori K, Shirato K, Morimoto M, Tanaka K. Percutaneous ablation therapy guided by contrast-enhanced sonography for patients with hepatocellular carcinoma. *AJR Am J Roentgenol.* 2003;180:143-9.
59. Masuzaki R, Shiina S, Tateishi R, Yoshida H, Goto E, Sugioka Y, Kondo Y, Goto T, Ikeda H, Omata M, Koike K. Utility of contrast-enhanced ultrasonography with Sonazoid in radiofrequency ablation for hepatocellular carcinoma. *J Gastroenterol Hepatol.* 2011;26:759-64.
60. Maruyama H, Takahashi M, Ishibashi H, Okugawa H, Okabe S, Yoshikawa M, Yokosuka O. Ultrasound-guided treatments under low acoustic power contrast harmonic imaging for hepatocellular carcinomas undetected by B-mode ultrasonography. *Liver Int.* 2009;29:708-14.
61. Minami Y, Kudo M, Hatanaka K, Kitai S, Inoue T, Hagiwara S, Chung H, Ueshima K. Radiofrequency ablation guided by contrast harmonic sonography using perfluorocarbon microbubbles (Sonazoid) for hepatic malignancies: an initial experience. *Liver Int.* 2010;30:759-64.
62. Miyamoto N, Hiramatsu K, Tsuchiya K, Sato Y. Contrast-enhanced sonography-guided radiofrequency ablation for the local recurrence of previously treated hepatocellular carcinoma undetected by B-mode sonography. *J Clin Ultrasound.* 2010;38: 339-45.
63. Lu MD, Yu XL, Li AH, Jiang TA, Chen MH, Zhao BZ, et al. Comparison of contrast enhanced ultrasound and contrast enhanced CT or MRI in monitoring percutaneous thermal ablation procedure in patients with hepatocellular carcinoma: a multi-center study in China. *Ultrasound Med Biol.* 2007;33:1736-49.
64. Meloni MF, Andreano A, Franzia E, Passamonti M and Lazzaroni S. Contrast enhanced ultrasound: Should it play a role in immediate evaluation of liver tumors following thermal ablation. *European Journal of Radiology.* 2012;81:e897-e902.
65. Xia YU, Kudo M, Minami Y, Hatanaka K, Ueshima K, Chung H et al. Response evaluation of Transarterial chemoembolization in Hepatocellular carcinomas :The usefulness of Sonazoid-enhanced harmonic sonography. *Oncology.* 2008;65:99-105.
66. Wang Z, Tang J, An L, Wang W, Luo Y, Li J, Xu J. Contrast-enhanced ultrasonography for assessment of tumor vascularity in hepatocellular carcinoma. *J Ultrasound Med.* 2007;26:757-62.
67. Lassau N, Chami L, Chebil M et al. Dynamic contrast enhanced ultrasonography (DCE-US) and antiangiogenic treatments. *Discov Med.* 2011;11:18-24.
68. Lassau N, Koscielny S, Chami L et al. Advanced hepatocellular carcinoma: Early evaluation of response to Bevacizumab therapy at Dynamic contrastenhanced US with Quantification-Preliminary results. *Radiology.* 2010;b258:291-300.
69. Li N, Ding H, Fan P, Lin X, Xu C, Wang W, Xu Z, Wang J. Intra-hepatic transit time predicts liver fibrosis in patients with chronic hepatitis B: quantitative assessment with contrast-enhanced ultrasonography. *Ultrasound Med Biol.* 2010;36:1066-75.
70. Lim AK, Taylor-Robinson SD, Patel N, Eckersley RJ, Goldin RD, Hamilton G, Foster GR, Thomas HC, Cosgrove DO, Blomley MJ. Hepatic vein transit times using a microbubble agent can predict disease severity non-invasively in patients with hepatitis C. *Gut.* 2005;54:128-33.
71. Kitano M, Kudo M, Maekawa K, et al. Dynamic imaging of pancreatic diseases by contrast enhanced coded phase inversion harmonic ultrasonography. *Gut.* 2004;53:854-9.
72. Badea R, Seicean A, Diaconu B, Stan-Iuga R, Sparchez Z, Tantau M, Socaciu M. Contrast-Enhanced Ultrasound of the Pancreas -a Method Beyond its Potential or a New Diagnostic Standard? *CLINICAL IMAGING J Gastrointestin Liver Dis* June. 2009; 18(2):237-42.
73. D'Onofrio M, Megibow AJ, Faccioli N, et al. Comparison of contrast-enhanced sonography and MRI in displaying anatomic features of cystic pancreatic masses. *Am J Roentgenol.* 2007; 189:1435-42.
74. D'Onofrio M, Mansueti G, Falconi M, et al. Neuroendocrine pancreatic tumor: value of contrast enhanced ultrasound. *Abdom Imaging.* 2004;29:246-58.
75. Dietrich CF, Braden B, Hocke M, et al. improved characterisation of solitary solid pancreatic tumours using contrast enhanced transabdominal ultrasound. *J Cancer Res Clin Oncol.* 2008;134: 635-43.
76. Rickes S, Wermke W. Differentiation of cystic pancreatic neoplasms and pseudocysts by conventional and echo-enhanced ultrasound. *J Gastroenterol Hepatol.* 2004;19:761-6.
77. Ripolles T, Martinez MJ, Lopez E, et al. Contrast-enhanced ultrasound in the staging of acute pancreatitis. *Eur Radiol.* 2010; 20:2518-23.
78. Becker D, Strobel D, Bernatik T, et al. Echo-enhanced color-and power- Doppler EUS for the discrimination between focal pancreatitis and pancreatic carcinoma. *Gastrointest Endosc.* 2001;53:784-9.
79. Bhutani MS, Hoffman BJ, van Velse A, et al. Contrast-enhanced endoscopic ultrasonography with galactose microparticles: SHU508 A (Levovist). *Endoscopy.* 1997;29:635-9.
80. Dietrich CF, Ignee A, Frey H. Contrast-enhanced endoscopic ultrasound with low mechanical index: a new technique. *Z Gastroenterol.* 2005;43:1219-23.
81. Dietrich CF. Contrast-enhanced low mechanical index endoscopic ultrasound (CELMI-EUS). *Endoscopy;* 2009;41 (Suppl 2):E43-E44.
82. Kitano M, Sakamoto H, Matsui U, et al. A novel perfusion imaging technique of the pancreas: contrast-enhanced harmonic EUS (with video). *Gastrointest Endosc.* 2008;67:141-50.
83. Hocke M, Schulze E, Gottschalk P, Topalidis T, Dietrich C F. Contrast-enhanced endoscopic ultrasound in discrimination between focal pancreatitis and pancreatic cancer. *World J Gastroenterol.* 2006;12(2):246-50.
84. Quaia E, Bertolotto M, Cioffi V, et al. Comparison of contrast-enhanced sonography with unenhanced sonography and contrast-enhanced CT in the diagnosis of malignancy in complex cystic renal masses. *Am J Roentgenol.* 2008;191:1239-49.

85. Clevert DA, Minaifar N, Weckbach S, et al. Multislice computed tomography versus contrast-enhanced ultrasound in evaluation of complex cystic renal masses using the Bosniak classification system. *Clin Hemorheol Microcirc.* 2008;39:171-8.
86. Park BK, Kim B, Kim SH, et al. Assessment of cystic renal masses based on Bosniak classification: comparison of CT and contrast-enhanced US. *Eur J Radiol.* 2007;61:310-4.
87. Ascenti G, Mazziotti S, Zimbaro G, et al. Complex cystic renal masses: characterization with contrast-enhanced US. *Radiology.* 2007;243:158-65.
88. Mazziotti S, Zimbaro F, Pandolfo A, et al. Usefulness of contrast-enhanced ultrasonography in the diagnosis of renal pseudotumors. *Abdom Imaging.* 2010;35:241-5.
89. Bertolotto M, Martegani A, Aiani L, et al. Value of contrast-enhanced ultrasonography for detecting renal infarcts proven by contrast enhanced CT. A feasibility study. *Eur Radiol.* 2008; 18:376-83.
90. Wink MH, Lagerveld BW, Laguna MP, et al. Cryotherapy for renal-cell cancer: diagnosis, treatment, and contrast-enhanced ultrasonography for follow-up. *J Endourol.* 2006;20:456-8, discussion 458-9.
91. Johnson DB, Duchene DA, Taylor GD, et al. Contrast-enhanced ultrasound evaluation of radiofrequency ablation of the kidney: reliable imaging of the thermolesion. *J Endourol.* 2005;19:248-52.
92. Hoeffel C, Poussset M, Timsit MO, et al. Radiofrequency ablation of renal tumours: diagnostic accuracy of contrast-enhanced ultrasound for early detection of residual tumour. *Eur Radiol.* 2010;20:1812-21.
93. Meloni MF, Bertolotto M, Alberzoni C, et al. Follow-up after percutaneous radiofrequency ablation of renal cell carcinoma: contrast-enhanced sonography versus contrast-enhanced CT or MRI. *Am J Roentgenol.* 2008;191:1233-8.
94. Correas JM, Claudon M, Tranquart F, et al. The kidney: imaging with microbubble contrast agents. *Ultrasound Q.* 2006;22:53-66.
95. Paajanen H, Lahti P, Nordback I. Sensitivity of transabdominal ultrasonography in detection of intraperitoneal fluid in humans. *Eur Radiol.* 1999;9:1423-5.
96. Poletti PA, Kinkel K, Vermeulen B, et al. Blunt abdominal trauma: should US be used to detect both free fluid and organ injuries? *Radiology.* 2003;227:95-103.
97. Valentino M, Serra C, Zironi G, De Luca C, Pavlica P, Barozzi L. Blunt Abdominal Trauma: Emergency Contrast-Enhanced Sonography for Detection of Solid Organ Injuries. *AJR.* 2006; 186:1361-136.
98. Catalano O, Aiani L, Barozzi L, et al. CEUS in abdominal trauma: multicenter study. *Abdom Imaging.* 2009;34:225-34.
99. Del Cura JL, Elizagaray E, Zabala R, Legorburu A, Grande D. The use of unenhanced Doppler sonography in the evaluation of solid breast lesions. *AJR Am J Roentgenol.* 2005;184:1788-94.
100. Ozdemir A, Ozdemir H, Maral I, Konuş O, Yücel S, İşık S. Differential diagnosis of solid breast lesions: contribution of Doppler studies to mammography and gray scale imaging. *J Ultrasound Med.* 2001;20(10):1091-101.
101. Italian Society of Medical Radiology. Charta senologica. Diagnostic approach to breast diseases. *Radiol Med.* 2004;108:569-87
102. Chapellier C, Balu-Maestro C, Bleuse A, Ettore F, Bruneton JN. Ultrasonography of invasive lobular carcinoma of the breast: sonographic patterns and diagnostic value: report of 102 cases. *Clin Imaging.* 2000;24:333-6.
103. Baum F, Fischer U, Vosshenrich, Grabbe E. Classification of hypervasculatized lesions in CE MR imaging of the breast. *Eur Radiol.* 2002;12:1087-92.
104. Kedar RP, Cosgrove D, McCready VR, Bamber JC, Carter ER. Microbubble contrast agent for color Doppler US: effect on breast masses—work in progress. *Radiology.* 1996;198:679-86.
105. Stuhrmann M, Aronius R, Schietzel M. Tumor vascularity of breast lesions: potentials and limits of contrast-enhanced Doppler sonography. *AJR Am J Roentgenol.* 2000;175:1585-9.
106. Vallone P, D'Angelo R, Filice S, Petrosino T, Rinaldo M, De Chiara A, Gallipoli A. Color-doppler using contrast medium in evaluating the response to neoadjuvant treatment in patients with locally advanced breast carcinoma. *Anticancer Res.* 2005;25:595-9.
107. Halpern EJ, McCue PA, Aksnes AK, et al. Contrast-enhanced sonography of the prostate with Sonazoid: comparison with prostatectomy specimens in twelve patients. *Radiology.* 2002;222:361-6.
108. Halpern EJ, Ramey JR, Strup SE, et al. Detection of prostate cancer with contrast enhanced sonography using intermittent harmonic imaging. *Cancer.* 2005;104:2372-83.
109. Mitterberger MJ, Aigner F, Horninger W, et al. Comparative efficiency of contrast-enhanced colour Doppler ultrasound targeted versus systematic biopsy for prostate cancer detection. *Eur Radiol.* 2010;20:2791-6.
110. Wink M, Frauscher F, Cosgrove D, et al. Contrast-enhanced ultrasound and prostate cancer, a multicentre European research coordination project. *Eur Urol.* 2008;54:982-92.
111. Aigner F, Pallwein L, Mitterberger M, et al. Contrast-enhanced ultrasonography using cadence-contrast pulse sequencing technology for targeted biopsy of the prostate. *BJU Int.* 2009;103:458-63.
112. Sano F, Terao H, Kawahara T, et al. Contrast-enhanced ultrasonography of the prostate: various imaging findings that indicate prostate cancer. *BJU Int.* 2010;107:1404-10.
113. Strazdina A, Krumina G, Sperga M. The value and limitations of contrast-enhanced ultrasound in detection of prostate cancer. *Anticancer Res.* 2011;31:1421-6.
114. Robotti D, Cammarota T, Debani P, et al. Activity of Crohn disease: value of Color-Power-Doppler and contrast-enhanced ultrasonography. *Abdom Imaging.* 2004;29:648-52.
115. De Pascale A, Garofalo G, Perna M, et al. Contrast-enhanced ultrasonography in Crohn's disease. *Radiol Med.* 2006;111:539-50.
116. Serra C, Menozzi G, Labate AM, et al. Ultrasound assessment of vascularization of the thickened terminal ileum wall in Crohn's disease patients using a low-mechanical index real-time scanning technique with a second generation ultrasound contrast agent. *Eur J Radiol.* 2007;62:114-21.
117. Migaleddu V, Scanu AM, Quaia E, et al. Contrast-enhanced ultrasonographic evaluation of inflammatory activity in Crohn's disease. *Gastroenterology.* 2009;137:43-52.
118. Girlich C, Schacherer D, Jung EM, et al. Comparison between a clinical activity index (Harvey-Bradshaw-Index), laboratory inflammation markers and quantitative assessment of bowel wall vascularization by contrast-enhanced ultrasound in Crohn's disease. *Eur J Radiol.* 2011; epub DOI: 10.1016/j.ejrad.2011.02.054.
119. Guidi L, De Franco A, De Vitis I, et al. Contrast-enhanced ultrasonography with SonoVue after infliximab therapy in Crohn's disease. *Eur Rev Med Pharmacol Sci.* 2006;10:23-6.
120. Wilson SR, Burns PN. Microbubble-enhanced US in body imaging: what role? *Radiology.* 2010;257:24-39.

121. Yu X, Yu J, Liang P, et al. Real-time contrast-enhanced ultrasound in diagnosing of focal spleen lesions. *Eur J Radiol*. 2011; epub DOI: 10.1016/j.ejrad.2010.12.052.
122. Gorg C, Bert T. Second-generation sonographic contrast agent for differential diagnosis of perisplenic lesions. *Am J Roentgenol*. 2006;186:621-6.
123. Gorg C, Graef C, Bert T. Contrast-enhanced sonography for differential diagnosis of an inhomogeneous spleen of unknown cause in patients with pain in the left upper quadrant. *J Ultrasound Med*. 2006;25:729-34.
124. Lassau N, Lamuraglia M, Chami L, et al. Gastrointestinal stromal tumors treated with imatinib: monitoring response with contrast-enhanced sonography. *Am J Roentgenol*. 2006;187:1267-73.
125. Giorgi U, Aliberti C, Benea G, et al. Effect of angiosonography to monitor response during imatinib treatment in patients with metastatic gastrointestinal stromal tumors. *Clin Cancer Res*. 2005;11:6171-6.
126. Bertolotto M, Derchi LE, Sidhu PS, et al. Acute segmental testicular infarction at contrast-enhanced ultrasound: early features and changes during follow-up. *Am J Roentgenol*. 2011;196:834-41.
127. Valentino M, Bertolotto M, Derchi L, et al. Role of contrast enhanced ultrasound in acute scrotal diseases. *Eur Radiol*. 2011; epub DOI: 10.1007/s00330-010-2039-5.
128. Moschouris H, Stamatiou K, Lampropoulou E, et al. Imaging of the acute scrotum: is there a place for contrast-enhanced ultrasonography? *Int Braz J Urol*. 2009;35:692-702, discussion 702-695.
129. Lock G, Schmidt C, Helmich F, Stolle E, Dieckmann KP. Early experience with contrast-enhanced ultrasound in the diagnosis of testicular masses: a feasibility study. *Urology*. 2011;77:1049-53.
130. Liu ZZ, Jiang YX, Dai Q, Yang M, Zhu QL, Zhao DC, Gao P. Imaging of endometrial carcinoma using contrast-enhanced sonography. *J Ultrasound Med*. 2011;30:1519-27.
131. Gorg C. Transcutaneous contrast-enhanced sonography of pleuralbased pulmonary lesions. *Eur J Radiol*. 2007;64:213-21.
132. Bertolini FA, Goerg C, Mathis G. Echo contrast ultrasound in subpleural consolidations. 2008; 18 (Suppl S395): Abstract
133. Gorg C, Bert T, Gorg K. Contrast-enhanced sonography for differential diagnosis of pleurisy and focal pleural lesions of unknown cause. *Chest*. 2005;128:3894-9.
134. Coli S, Magnoni M, Sangiorgi G, et al. Contrast-enhanced ultrasound imaging of intraplaque neovascularization in carotid arteries: correlation with histology and plaque echogenicity. *J Am Coll Cardiol*. 2008;52:223-30.
135. Giannoni MF, Vicenzini E, Citone M, et al. Contrast carotid ultrasound for the detection of unstable plaques with neoangiogenesis: a pilot study. *Eur J Vasc Endovasc Surg*. 2009;37:722-7.
136. Clevert DA, Horng A, Jung EM, et al. Contrast-enhanced ultrasound versus conventional ultrasound and MS-CT in the diagnosis of abdominal aortic dissection. *Clin Hemorheol Microcirc*. 2009;43:129-39.
137. Clevert DA, Sommer WH, Zengel P, et al. Imaging of carotid arterial diseases with contrast-enhanced ultrasound (CEUS). *Eur J Radiol*. 2011; epub DOI: 10.1016/j.ejrad.2010.12.103.
138. Clevert DA, Schick K, Chen MH, et al. Role of contrast enhanced ultrasound in detection of abdominal aortic abnormalities in comparison with multislice computed tomography. *Chin Med J (Engl)*. 2009;122:858-64.
139. Clevert DA, Minaifar N, Weckbach S, et al. Color duplex ultrasound and contrast-enhanced ultrasound in comparison to MS-CT in the detection of endoleak following endovascular aneurysm repair. *Clin Hemorheol Microcirc*. 2008;39:121-32.
140. Ten Bosch JA, Rouwet EV, Peters CT, et al. Contrast-enhanced ultrasound versus computed tomographic angiography for surveillance of endovascular abdominal aortic aneurysm repair. *J Vasc Interv Radiol*. 2010;21:638-43.
141. Sever AR, Mills P, Jones SE, et al. Preoperative sentinel node identification with ultrasound using microbubbles in patients with breast cancer. *Am J Roentgenol*. 2010;196:251-6.
142. Lebowitz RL, Olbing H, Parkkulainen KV, et al. International system of radiographic grading of vesicoureteric reflux. International Reflux Study in Children. *Pediatr Radiol* 1985; 15:105-9.
143. Lanzani C, Savasi V, Leone FP, et al. Two-dimensional HyCoSy with contrast tuned imaging technology and a second-generation contrast media for the assessment of tubal patency in an infertility program. *Fertil Steril*. 2009;92:1158-61.
144. Ignee A, Baum U, Schuessler G, et al. Contrast-enhanced ultrasound-guided percutaneous cholangiography and cholangiodrainage (CEUSPTCD). *Endoscopy*. 2009;41:725-6.
145. Mao R, Xu EJ, Li K, et al. Usefulness of contrast-enhanced ultrasound in the diagnosis of biliary leakage following T-tube removal. *J Clin Ultrasound*. 2009;38:38-40.
146. Zengel P, Berghaus A, Weiler C, et al. Intraductally applied contrast-enhanced ultrasound (IA-CEUS) for evaluating obstructive disease and secretory dysfunction of the salivary glands. *Eur Radiol*. 2011;21:1339-48.
147. Henrich W, Meckies J, Friedmann W. Demonstration of a recto-vaginal fistula with the ultrasound contrast medium Echovist. *Ultrasound Obstet Gynecol*. 2000;15:148-9.
148. Volkmer BG, Nesslauer T, Kufer R, et al. [Diagnosis of vesico-intestinal fistulas by contrast medium enhanced 3-D ultrasound]. *Ultraschall in Med*. 2001;22:81-6.
149. Chew SS, Yang JL, Newstead GL, et al. Anal fistula: Levovist-enhanced endoanal ultrasound: a pilot study. *Dis Colon Rectum*. 2003;46:377-84.
150. Lefevre F, Correas JM, Briancon S, et al. Contrast-enhanced sonography of the renal transplant using triggered pulse-inversion imaging: preliminary results. *Ultrasound Med Biol*. 2002;28:303-14.
151. Gardiner MD, Nanchahal J. Strategies to ensure success of microvascular free tissue transfer. *J Plast Reconstr Aesthet Surg*. 2010;63:e665-73.
152. Prantl L, Pfister K, Kubale R, et al. Value of high resolution ultrasound and contrast enhanced US pulse inversion imaging for the evaluation of the vascular integrity of free-flap grafts. *Clin Hemorheol Microcirc*. 2007;36:203-16.
153. Prantl L, Schmitt S, Geis S, et al. Contrast harmonic ultrasound and indocyanine- green fluorescence video angiography for evaluation of dermal and subdermal microcirculation in free parascapular flaps. *Clin Hemorheol Microcirc*. 2008;38:105-18.
154. Prantl L, Schreml S, Walter M, et al. Evaluation of microcirculation of free flaps of the lower leg by contrast harmonic imaging (CHI) with time intensity curve (TIC) analysis. *Clin Hemorheol Microcirc*. 2008;39:343-50.
155. Marret H, Sauget S, Giraudeau B, et al. Contrast-enhanced sonography helps in discrimination of benign from malignant adnexal masses. *J Ultrasound Med*. 2004;23:1629-39, quiz 1641-42.

## Chapter

# 19

# Iodinated Contrast Media: An Update

*Chandrashekara SH, Thulkar S*

### INTRODUCTION

Iodinated contrast media (ICM) are widely used pharmaceutical agents in radiology and have become an integral part of many diagnostic imaging studies. Most commonly they are used intravenously, but for many diagnostic studies, they can also be used intra-arterially, intrathecally, orally and intra-abdominally. Although ICM are safe to use, adverse events do occur, which vary from mild physiological disturbances to life-threatening complications. The radiologists must recognize early and manage these adverse reactions, which are inherent in the use of contrast media.<sup>1</sup>

The ideal qualities of intravascular contrast agents are:

- Water solubility
- Chemical and heat stability
- Biological inertness (non-antigenic)
- Low viscosity
- Lower or same osmolality as human serum
- Selective excretion (i.e. kidney)
- Safety
- Low cost
- Their formulations should be free of substances interfering with physiological homeostasis.<sup>2-4</sup>

### HISTORY OF DEVELOPMENT OF ICM

All the researches in the development of contrast media have proceeded with basic objectives (i.e. increased efficacy and reduced toxicity) which characterize all pharmaceutical research.

- In 1920s, the first radiographic contrast medium introduced for clinical practice was sodium iodide, which

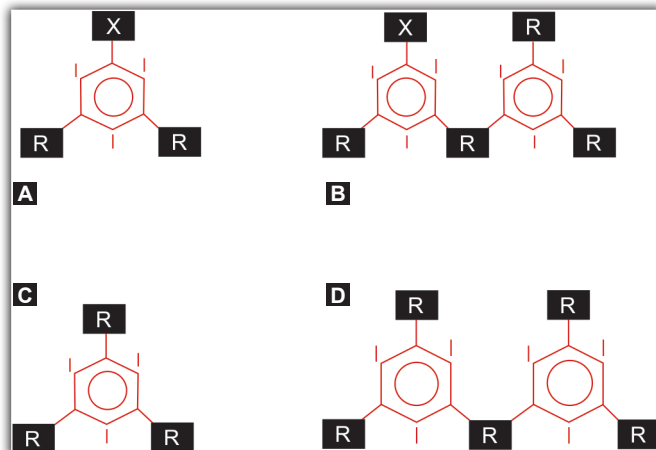
had limitations of high toxicity and poor radiographic contrast.<sup>5</sup>

- The first major breakthrough in the development of safer contrast media came, when iodine was bound to organic molecules, enabling significant reduction of iodine toxicity compared with sodium iodide (an inorganic salt). First organic salt, uroselectan (Iopax) was developed by Moses Swick, was readily excreted by kidneys and was surprisingly of relatively low toxicity. However, the major disadvantage of uroselecton was lesser efficacy in terms of contrast enhancement, as each molecule bound to only one iodine atom. Uroselectan-B (Neoiopax) [which is a bisodium salt with two iodine atoms, and two particles in solution] quickly replaced uroselectan, providing slightly more iodine per molecule, lower toxicity, and improved solubility.
- Diodrast (Iodopyracet), a di-iodinated N-pyridone compound was the dominant agent for excretory urography from early 1930s until acetrizoate was developed.
- In the 1950s, sodium and meglumine salts of tri-iodinated benzoic acid (acetrizoic acid), were introduced, which were of much lower toxicity but hyperosmolar (having osmolality five to eight times that of the blood). Acetrizoate (Urokon) provided adequate urograms at that time. In order to improve efficacy and safety, various modifications of this tri-iodinated contrast medium, i.e. acetrizoic acid were done. It was postulated that the presence of a hydrogen atom on the tri-iodinated benzene ring gives a higher degree of protein binding than when the hydrogen atom has been substituted. It was also hypothesized that an increase in protein binding factor incited anaphylactic reactions.<sup>6</sup>

- Diatrizoate (Hypaque, Renografin) replaced acetrizoate (Urokon) in 1955 to 1956 as sodium and meglumine salts of diatrizoic acid proved safer and more diagnostically efficacious than earlier drugs. In diatrizoate, the unsubstituted hydrogen of acetrizoate has been exchanged for another acetamido unit, which caused increased biologic tolerance.<sup>7</sup>
- In the 1960s, majority of water soluble contrast media used were salts of iodinated fully substituted benzoic acid derivatives. These organic acids have 3 hydrogen atoms replaced by iodinated atoms and 3 hydrogen atoms replaced by simple side chains; for every 3 iodine atoms in solution, 2 particles are produced (one anion and one cation) in the ratio of 3:2. Subsequently, iothalamate (Conray) joined the market place in 1962, and the meglumine salt was first designed for urography.
- The next major development came in the 1970s with the introduction of low osmolar contrast media (LOCM), which was achieved by converting tri-iodinated benzoic acid into a nonionic molecule by replacing the ionizing carboxylic acid ( $\text{COOH}$ ) radical with hydrophilic structures that could be covalently bound to the benzene ring, i.e. an amide ( $\text{CONH}_2$ ). This molecule does not dissociate in solution providing three atoms of iodine with only one active particle [ratio of 3:1] compared to a ratio of 1.5 [3 iodine atoms: 2 particles] seen with high osmolar contrast medium. Dr Torsten was the first one to propose that nonionic molecules could reduce osmolality. Subsequently, Almen introduced the first ratio-three nonionic monomer, metrizamide in 1977.<sup>8-10</sup> Low osmolar contrast media of this generation, which are now in widespread clinical use includes iohexol, ioversol, iopamidol and iobitridol.<sup>11</sup> Iohexol (Omnipaque) is the first nonionic contrast agent introduced, has the longest track record worldwide and is used for intravascular and intrathecal imaging studies. Iopamidol (Isovue) is used for intravascular and intrathecal imaging studies and ioversol (Optiray) used in intra-arterial and IV applications.
- In the 1980s nonionic dimeric contrast media were introduced; two nonionic tri-iodinated benzoic rings were attached, giving iodine: particle ratio of 6:1, since there are 6 iodine atoms and only one active particle in each molecule.
- In the 1980s and 1990s, there has been an ongoing development of nonionic isotonic dimers. These agents are consequence of further applications of principles, such as eliminating ionicity, increasing hydrophilicity, lowering osmototoxicity and increasing the iodine atoms per molecule.

### BASIC CHEMISTRY OF ICM

Tri-iodinated benzene ring is the basic constituent of all ICM (**Figs 1A to D**). Benzene ring has 6 carbons numbered 1 to 6 clockwise. Carbon 1 attachment differentiates ionic



**Figs 1A to D** Types of iodinated contrast media. All ICM are based on tri-iodinated benzene ring. (A) Ionic monomer, (B) Ionic dimer, (C) Nonionic monomer (D) Nonionic dimer (R-Hydrophilic, nonionizing side chains; X-Ionic moiety,  $-\text{COO}^-$  and a either sodium or meglumine cation)

from nonionic contrast media. At C1 in ionic contrast media, acidic group with sodium or meglumine is attached. At C1 in nonionic contrast media, amide group is attached.<sup>12,13</sup> Iodine atoms are attached at position 2, 4, 6 carbons. C3 and C5 have amide attachments to increase solubility and also to reduce protein binding. Iodine (atomic weight 127) provides excellent radio-opacity because of higher atomic number and K-shell electron binding energy of 34 keV, which is lower than but closed to mean energy used in diagnostic X-rays and thus maximizing the photoelectric effect.

### Types of ICM

Iodinated contrast media are divided based on their osmolality and ionicity. **High-osmolar contrast media (HOCM)** have more than 1400 mOsm/kg  $\text{H}_2\text{O}$  osmolality (5-8 times the osmolarity of plasma) and most of them are ionic. **Low-osmolar contrast media** have 600 to 800 mOsm/kg  $\text{H}_2\text{O}$  (2-3 times the osmolarity of plasma) and consists of both ionic and nonionic contrast media. **Iso-osmolar contrasts** have osmolality of 290 mOsm/kg  $\text{H}_2\text{O}$  (same osmolarity as blood, plasma and cerebrospinal fluid) and only one product, which is nonionic is currently available.

Broadly, ICM are characterized as ionic or nonionic types. Ionic contrast medium breakdown into cations (positively charged particles) and anions (negatively charged particles) when enter solutions such as blood.<sup>11</sup> This results in more molecules per kilogram of water with increase in osmolality. For every 3 iodine molecules present in an ionic contrast media, one cation and one anion are produced on entering a solution and thus described as 3:2 compounds. In contrast, nonionic contrast media do not dissolve into charged particles on entering a solution. For every 3 iodine

molecules in a nonionic contrast media, one neutral molecule is produced and thus referred as 3:1 compounds.

Ionic and nonionic contrast media can be monomeric or dimeric types. Usually each benzene ring of ICM produces 3 iodine atoms. Monomer contains only one benzene ring. To deliver more iodine with each molecule of contrast, 2 benzene rings may be combined to produce a dimer, which would deliver 6 iodine atoms with each molecule.

The iodinated benzene ring contains ionizing carboxyl groups with a cation, usually sodium or meglumine.<sup>2</sup> Meglumine is an organic cation chosen because of its lower pharmacological activity than that of the sodium ion (and therefore better tolerance), but being a much larger ion, it increases viscosity. The carboxyl groups ionize in solution, making the agents water soluble. Since these compounds dissociate into ions in solution and contain only one iodinated benzene ring, these are described as **ionic monomeric agents**. Commonly used contrast material anions are diatrizoate and iothalamate. In a solution, ionic monomers break up into their anion and cation components, delivering 3 iodine atoms (3:2 ratio of iodine to osmolar particles). Thus, these have a relatively high osmolality (>1400 mOsm/kg at 50 to 76 percent by weight concentrations). Ionic monomer preparations, commonly available in India are meglumine iothalamate, sodium iothalamate, meglumine and sodium diatrizoate.

Nonionic monomers are the most widely used among lower-osmolality contrast agents. In nonionic monomers, the tri-iodinated benzene ring is made water soluble by the addition of five or six hydrophilic hydroxyl groups to organic side chains placed at 1, 3 and 5 positions. As there is no carboxyl group, these do not ionize in solution and a single molecule delivers 3 iodine atoms (3:1 ratio of iodine to osmolar particles). These have relatively low osmolality (600 to 800

mOsm/kg) at comparable iodine concentrations. Nonionic monomer preparations currently available in India are iohexol, ipromide, ioversol, iopamidol and iomeprol.

Ionic dimers are formed by joining two ionic monomers together and eliminating one of the carboxyl groups. These would deliver 2 ionic components per 6 iodine atoms (6:2 ratio of iodine to osmolar particles). These agents have concentration of 59 percent (320 mg iodine/mL) and a relatively low osmolality of 600 mOsm/kg at comparable iodine concentrations. Ioxaglate (Hexabrix) is the only ionic dimer currently available and is used widely for peripheral arteriography than for intravenous studies.

Nonionic dimers consist of two joined nonionic monomers. Single nonionic dimer delivers 6 iodine atoms (6:1 ratio of iodine to osmolar particles) and thus, are the most ideal contrast medium as they deliver the most iodine with the least effect on osmolality (approximately 290 mOsm/kg). At approximately 60 percent by weight concentration, these are iso-osmolar with plasma.<sup>3</sup> However, it results in higher viscosity and greater resistance to catheter injection.<sup>14</sup> Nonionic dimer iodixanol (Visipaque) is currently available in India and has an osmolality of 290 mOsm/kg H<sub>2</sub>O, same as blood.

In brief, there are four classes of ICM, i.e. high osmolar ionic monomers, low osmolar nonionic monomers, low osmolar ionic dimers and iso-osmolar nonionic dimers (**Table 1**). These are available in various iodine concentrations and have different physicochemical properties (osmolality, viscosity, hydrophilicity, ions content and pH). All ICM are distributed in the extracellular compartment and do not cross an intact blood-brain barrier, and all are excreted via glomerular filtration.<sup>3</sup>

The iodine concentration of an individual contrast agent determines radio-opacity of the contrast agent. The higher the

**Table 1** Most commonly available iodinated contrast media

Name of the contrast media	Iodine/particle ratio	Iodine concentration (mg/kg)	Osmolality (mOsm/kg)	Viscosity (cPs at 37°C)
• <i>Ionic monomer</i>				
– Diatrizoate (Hypaque 50; GE Healthcare)	3/2(1.5)	300	1,550(high)	5.2
– Metrizoate Isopaque (Coronar 370; Nycomed A/S)		370	2,100(high)	2.34
• <i>Ionic dimer</i>	6/2(3.0)	320	580(low)	7.5
• <i>Non-ionic monomer</i>				
– Iopamidol (Isovue-370; Bracco Diagnostics Inc.)	3/1(3.0)	370	796(low) 884(low)	3.0-9.4 1.5-10.4
– Iohexol (Omnipaque 350; GE Healthcare)		350	618(low)	7.5
– Iomeprol (Iomeron-350,400; Bracco Intl.)		350 400	726(low)	12.6
• <i>Nonionic dimer</i>	6/1(6.0)	320	290(iso)	6.3-11.8
– Iodixanol (Visipaque 320; GE Healthcare)				

iodine concentration, more the X-ray photons will be absorbed and thus particular contrast agent may be more radio-opaque than comparative low iodine concentrated agent. The iodine concentration has an effect on the severity of an adverse reaction. Higher the iodine concentration, more the risk of an adverse reaction. Thus, more iodine ratio represents better opacification and fewer particles of contrast medium mean lower osmotoxic effect.<sup>15</sup>

### ■ ICM PHARMACOKINETICS

The salient pharmacokinetic properties of ICM are high water solubility, low lipid solubility, low plasma protein binding and molecular weight ranging from 600 to 1650. They are distributed only in the extracellular fluid and not metabolized. They are excreted mainly by glomerular filtration. Due to affinity for proteins and membrane bound receptors, ICM have minimal pharmacological action. Small size of the contrast molecules and high water solubility permits free distribution of contrast across the vascular endothelium, and thus between the intravascular extracellular space (blood pool) and extravascular extracellular compartment (interstitium).

There is no evidence of any substantial penetration of these contrast media molecules through the intact cell membrane or into the interior of the viable cells, except for the proximal tubular cells of the kidney. Theoretically, the differences in the molecular weight and size between the monomeric and dimeric contrast agents could lead to slightly slower distribution rates into extracellular space for the larger dimers. This effect, however, appears to be quite small and is probably clinically insignificant. The effects of isotonic dimers on increased renal intratubular viscosity are yet to be fully assessed.<sup>16-17</sup>

When the contrast media molecules enter the systemic circulation, the molecules quickly equilibrate across capillary membranes (except an intact blood-brain barrier) and are distributed throughout the intra- and extravascular extracellular space.<sup>18</sup> In the first phase of distribution, increase in the intravascular osmolality for the hypertonic agents, including the LOCM, causes a rapid fluid shift across capillary membranes toward the hypertonic (intravascular) compartment. As the contrast medium molecules pass through the capillary bed, rapid movement occurs through the capillary pores into the interstitial, extracellular space, as well as glomerular filtration into the renal tubules. Early vascular enhancement depends on the rate of iodine administration and blood flow; whereas parenchymal enhancement depends on the total iodine dose and volume of distribution. The main factors which influence the contrast enhancement include cardiac output, and central blood volume, which are both correlated with the body weight.

All the current commercially available ICM are excreted in the kidney by glomerular filtration with no significant tubular excretion or resorption. Few older contrast media, such as iodopyracet (Diodrast) were excreted by means of both glomerular filtration and tubular secretion. Around

99 percent of the intravenous dose of contrast medium is eliminated through the kidney, and instantaneous rate of removal is equal to the glomerular filtration rate times the plasma iodine concentration. Less than one percent is excreted through extrarenal routes that include hepatobiliary system, small and large intestines, sweat, tears and saliva. Vicarious excretion of contrast material occurs through extrarenal routes, in cases of renal insult or renal failure.

The half-life of iodinated contrast media in patients with normal glomerular filtration rate is approximately 2 hours whereas in patients with severe renal dysfunction it can be prolonged to over 30 hours depending on the extent of renal impairment.<sup>10</sup> Therefore, in patients with end-stage renal failure the plasma contrast medium concentration remains high for a long period of time. In these patients, the extracellular concentration of iodine will reach the value given by the total iodine injected divided by the extracellular volume, which is approximately 200 mL per kilogram of body weight. The requirement of emergent dialysis after contrast administration has been debated in renal failure patients. The ICM are readily dialyzable as they are not protein bound and possess relatively low molecular weights. It is believed that approximately one third of either HOCM or LOCM would have already been naturally eliminated through extrarenal routes before dialysis can be set up and begun.<sup>11</sup> The HOCM produces larger osmotic diuresis and so have lower urinary concentration than LOCM.

### Basic Properties

The biocompatibility of iodine and its physical properties (k-edge at photon energy of 34 KeV) allow safe intravascular injection of large volumes at high concentration. All the other chemical elements in the molecules serve only to carry, or protect the iodine on the benzene ring. It is the iodine in the radiographic beam and the volume distribution of the contrast material that provide optional contrast enhancement for imaging.<sup>19</sup> The basic properties of ICM include osmolality, viscosity and ionicity.

**Osmolality** of intravascular contrast media refers to the number of particles in solution, per unit liquid, as compared to blood. Most of ICM have a greater osmolality than blood plasma. High osmolality contrast media have osmolality approximately in the range 1400 to 1515 mOsm/kg, or about 5 to 8 times that of human blood. Low osmolality contrast media have much lower osmolality ranging approximately 600 to 800 mOsm/kg, or roughly 2 to 3 times the osmolality of human blood.<sup>18</sup> Hyperosmolar contrast cause tissue damage and responsible for the sudden drawing of water from the cellular and interstitial spaces towards plasma, thereby producing local effects, such as heat and pain. Increased osmolality can cause systemic effects such as vasodilatation, alteration to the permeability of vessel endothelium, hyperemia and osmotic diuresis. The HOCM cause strong osmotic diuretic effect. The lower osmotic effect of the LOCM, however is not significant disadvantage because a higher iodine concentration

achieved in the urine. For urography and to some extent for CT scanning, some degree of osmotic diuresis is required. Nonionic dimer contrast agent (Visipaque, GE Healthcare) has the osmolality 290 mOsm/kg or equal to that of blood and is referred to as an iso-osmolar contrast media. It has been suggested that iso-osmolar contrast media may offer some advantages, particularly in patients at risk of renal complications.

**Viscosity** is a physical property which is the thickness or friction of the fluid as it flows. The viscosity is related to the concentration, the size of the molecules in a specific contrast agent, and the temperature of the contrast agent. This property will influence the injectability of intravascular agents through small bore needles and intravenous catheters. Contrast media with higher viscosity values have to be injected at a slower rate. The other factors which influence contrast media flow are iodine concentration, temperature of the contrast media, catheter inner diameter, catheter length, and the number of catheter holes. The viscosity of the contrast material can be significantly decreased by heating the liquid to body temperature for injection. The concentration of iodine in the ICM affect its viscosity; the higher the concentration of iodine, the more viscous the solution. The viscosity is largely controlled by the compositions of the side chains on the molecules. Meglumine side chain in the ICM helps to achieve water solubility and biologic tolerance but also increases the viscosity. Ionic ICM have reduced viscosity and high hyperosmolality; Nonionic ICM have reduced viscosity and limited hyperosmolality; nonionic dimers have high viscosity and iso-osmolarity. Viscosity also plays a role at the level of the nervous system, as a direct correlation has been observed between viscosity of the solution and magnitude of damage to the blood-brain barrier.<sup>20</sup> If associated with high viscosity, isotonicity of radiopaque solutions also produces unwanted effects at renal level.

**Ionicity** is the characteristic of a molecule to break up into a positively charged cation and a negatively charged anion, resulting in more molecules per kilogram of water and thus increasing osmolality. Nonionic agents do not have this property and hence are less osmolar. Ionic contrast agents are composed of molecules that will disassociate into ions when in solution. The molecules contained in nonionic contrast media do not disassociate. Although most nonionic contrast agents also have low osmolality, the two terms are not synonymous.

### Pulmonary Effects of ICM

Pulmonary adverse effects of ICM include bronchospasm, increased pulmonary vascular resistance and pulmonary edema. Patients with history of asthma, pulmonary hypertension and incipient cardiac failure are at increased risk. It is recommended to use iso-osmolar contrast media and avoid large doses of contrast media to reduce the risk of pulmonary adverse effects.

### Effects of ICM on Blood and Endothelium

It is recognized that all contrast media have anticoagulant properties, especially ionic agents. The HOCM may induce thrombosis due to endothelial damage, particularly in phlebographic procedures. Low or iso-osmolar contrast media should be used for diagnostic and interventional angiographic procedures. Meticulous angiographic techniques with advanced interventional devices reduce the thromboembolic complications.

### General Policies for ICM Administration

There are certain policies, which everybody should follow in administering ICM. Only authorized persons, i.e. technologists and registered nurses should inject ICM under the supervision of radiologist. The dose and technique of ICM injection is decided under the guidance of radiologist. The ICM should be stored at less than 37°C for maximum period of one month. Multidose bottles of iodinated contrast media should be discarded if not used within 8 hours after being opened. All multidose contrast containers/vials should be properly labelled along with the time they were opened. All ICM stock should be monitored by designated nursing and CT staff. All radiologists/ technologists/nurses should personally inspect contrast containers/vials for integrity, signs of contamination and also check expiry date. All the expired contrast containers/vials should be timely disposed. Most of the adverse contrast reactions tend to occur immediately or within 20 minutes after contrast injection and hence, all the patients should be observed for sometime in the radiology department after ICM administration. All areas where contrast is given must be equipped with an emergency box containing supplies required for the treatment of contrast reactions.

### Guidelines for Intravenous Administration of ICM

Intravenous injection via stable intravenous (IV) access is the most common parenteral route of contrast administration. Contrast is injected directly into the vein with a butterfly needle, an angiocatheter or through an established IV line. When the power injector is utilized, 22 G or large needle or cannula 1.25" to 1.5" length is preferred for IV contrast injection. It is advisable to obtain a good backflow of blood to test adequate positioning of the needle in the vein. Adequate position of the cannula in the vein is checked again by saline flush into the vein before injecting the contrast.

Care has to be taken when injecting ICM through existing access routes. Only power-injection rated peripherally inserted central catheters (PICC) or central lines are approved for power injection. Pre-existing IV lines will be flushed with 10 mL of saline flush, to ensure patency, prior to contrast injection. The maximum flow rate and psi set for adult and pediatric injections are 5 mL/sec at <300 psi and 2 mL/sec at <300 psi respectively. The injection rate will be dependent

on the specific catheter type, size, and specific examination protocol.

Special care is to be taken whenever injecting contrast media via any central line catheters. If not power rated, the contrast injection must be hand injection. Hand injection of contrast is acceptable if the examination does not require arterial phase of injection. The 5 rights for medication administration (i.e. right patient, right contrast/medication, right dose, right route, and right time) should be strictly followed.

It is essential to know the serum creatinine levels and glomerular filtration rate (GFR) before injecting the contrast. Ideally, recent serum creatinine reports (done within 6 weeks) should be obtained. If there has been significant interval change in the patient's condition, a more recent serum creatinine report can be considered. If the serum creatinine level is  $> 1.5$  mg/dL in a diabetic patient,  $> 2.0$  mg/dL in a nondiabetic patient, or the GFR is  $< 30$  mL/min, the injection of ICM ideally should be avoided and alternate diagnostic test should be considered. The contrast may be given after discussion with the referring clinician/nephrologist considering risk benefit ratio. This conversation must be properly documented. For patients with end-stage renal disease who are on chronic peritoneal dialysis, noncontrast study should be considered and contrast should only be given after discussion with the patient's nephrologist. Immediate dialysis is advised after the contrast study in the patients of significant renal compromise.

### Dosage of Iodinated Contrast Media Administration

Dose of ICM is considered as potential risk factor for adverse contrast reactions and nephropathy. In practice, dose is only a concern in certain situations, such as patients undergoing catheter angiography and CT on the same day. In such circumstances, due regard should be given to the clinical need for an optimal study, rather than rigid adherence to a relatively empiric maximum recommended dose. Regardless of the type of iodinated contrast agent, the lowest dose necessary to obtain adequate visualization should be used. It is advisable to discuss the relative risks and benefits with the patient and referring clinician. Standard dose of iodinated contrast administration is 1-2 mL/kg at concentration of 300 mg/mL. The maximum limit of contrast administration is typically 200 mL of an agent with a concentration of 320 mg/mL (a total of 64 gram of iodine). In general volumes of over 250 to 300 cc in a 24-hour period should be avoided. The maximum safe dose may also depend on the individual factor, such as a patient's level of hydration. It should be noted that specific circumstances may necessitate exceeding this 200 mL guideline. A radiologist is responsible for determining in what instances, and to what extent, standard guidelines can be safely exceeded.

### Adverse Reactions

Iodinated contrast agents are one of the safe and widely used medications. However, these agents are not completely devoid of risks, and adverse side effects can occur. The LCOM generally cause less discomfort to the patient and lesser adverse reactions than do HOCM. Reactions are usually infrequent and range from 5 to 12 percent for HOCM and from 1 to 3 percent for LOCM.<sup>21,22</sup> The mild and moderate contrast reactions occur more frequently with HOCM (6-8%) than for LOCM (0.2%), but the incidence of severe reactions remains similar. Anaphylactic reactions are more common with HOCM, whereas cardiovascular decompensation is more common with LOCM. It is impossible to accurately predict which patients will have an adverse reaction. The drugs and equipment needed to treat acute contrast reactions must be readily available and all the radiology staff must be trained to treat quickly. Adverse reactions and their relationship to pre-existing conditions and treatment are discussed in detail in the separate chapter. Since 1996, the Contrast Media Safety Committee has reviewed all the safety aspects of ICM and formulated the guidelines for the use and management of contrast reactions. European Society of Urogenital Radiology (ESUR) guidelines have been well received by the Radiology Community all over the world and are now standards for good practice at many institutions.<sup>23</sup>

In spite of taking all the precautions of the risk factors and selecting appropriate contrast media, it is not possible to opine confidently how the patient will ultimately react to contrast media. Hence, considering the medicolegal aspects, it is advisable that a proforma outlining the availability of various contrast media, their possible reactions, and the cost should be made available to the patient. One must discuss directly with the patient /his relatives on these issues before planning a study and an informed consent signed by the patient and relative is mandatory.

### ICM Interaction with Other Drugs and Clinical Tests

The ICM may interact with other drugs and interfere with biochemical assays. It is essential to be aware of the patient's drug history and keep proper records of the ICM injection (time, dose, name and batch number). Drugs which require special attention include metformin, cyclosporine, cisplatin, aminoglycosides, nonsteroidal anti-inflammatory drugs, beta blockers, interleukin-2 and hydralazine. Beta blockers may impair the response to treatment of bronchospasm induced by contrast medium. The ICM should never be mixed with other drugs in the tubes or syringes. Biochemical analysis of blood or urine, collected within 24 hours of ICM injection should be avoided. One of the pharmacodynamic effects of the ICM is the reduction of renal function, particularly in patients with pre-existing renal dysfunction. This leads to the retention of drugs, which are excreted exclusively through the

kidneys. The ICM injection may interfere with some isotope studies, and should be avoided for at least 24 hours before isotope bone scanning and before labeling red blood cells for isotope studies. Patients undergoing the radioactive iodine therapy should not have received ICM for at least 2 months before treatment. Isotope imaging of the thyroid should be avoided for 2 months after ICM injection.<sup>24</sup>

### Guidelines for Selective use of LOCM

Few of the studies have suggested that the cost-effectiveness of low-osmolality agents is poor if they are used indiscriminately for the general population. The agents should be used selectively for patients at the highest risk for a reaction to a high-osmolality agent.<sup>25</sup> Various organizations, such as American College of Radiology or the American College of Cardiology have recommended the guidelines, which can serve as starting points for the establishment of institution's policies and procedures for the use of contrast media.

American College of Radiology (ACR) developed guidelines for the selective use of LOCM.<sup>1</sup> It recommends that LOCM be administered to:

- Patients having history of a previous adverse reaction to contrast material, except for a sensation of heat or flushing or a single episode of nausea or vomiting;
- Patients having history of asthma or allergy;
- Patients with history of cardiac dysfunction, including recent or potentially imminent cardiac decompensation, severe arrhythmias, unstable angina pectoris, recent myocardial infarction, and pulmonary hypertension;
- Patients with generalized severe debilitation;
- Any other circumstances, such as patients having sickle-cell disease, increased risk for aspiration, anxious patients, patients with whom communication cannot be established to know about the risks, and patients who request for the use of LOCM.

Many institutions use low-osmolality iodinated contrast media agents in patients with pre-existing renal insufficiency alone or accompanying diabetes.<sup>26</sup> Nowadays, most of the institutes use the LOCM in all or most of the patients, whenever contrast need to be given.

It is not always possible to limit the use of LOCM to a selected group of patients. This is because some of the above mentioned guidelines can be interpreted differently by different individuals. Also, there is tendency for referring clinicians and radiologists to use the better tolerated nonionic agents increasingly to reduce patient discomfort or the likelihood of a reaction. There is also tendency for low risk patients to choose nonionic agents when they are allowed specifically to select the type of contrast material that they are to receive.

It is also difficult to identify the patients, who are at risk for the administration of any contrast media. Estimations of patient risk are derived from a variety of sources and previous history. However, not all at risk patients are always readily identified. In emergency situations or when adequate assessment with steroid is not possible, all patients should be

injected by LOCM. It is also essential to use minimum dose of contrast media for the given study and decrease waste of contrast material. The final decision on choice of contrast usage depend on public policy makers, organized medicine, individual physician and the patient.

### Iso-osmolar Dimeric Contrast Media

Iso-osmolar dimeric nonionic contrast medium currently available is iodixanol, which is sold under the trade name Visipaque (GE Healthcare) in two main concentrations 270 mgI/mL, 320 mg/mL and hence the name Visipaque 270 or 320. It has osmolality of 290 mOsm/kg H<sub>2</sub>O, similar to blood. Contrast-induced renal vasoconstriction and renal ischemia (major factor in the pathogenesis of contrast induced nephropathy) increases with increasing osmolality of the contrast agent. Isotonicity and lack of osmototoxicity of these contrast media result in better renal tolerance. Because of its physical properties, iodixanol would be expected to produce a lower incidence of adverse events than other nondimeric contrast media. Indeed, pharmacodynamic studies indicate that iodixanol has fewer cardiovascular effects, causes less renal damage and is associated with similar or smaller changes to the blood-brain barrier and neurological function when compared with nondimeric nonionic contrast media. Iodixanol generally causes less frequent and less intense discomfort on injection. However, it is relatively expensive. It was believed that the use of low-osmolar contrast media is associated with a significantly lower incidence of contrast-induced nephropathy (CIN) compared with high-osmolar contrast media in patients with renal failure. Recently, the opinion regarding use of iso-osmolar dimeric contrast media in CIN has been divided among experts. Recent studies and clinical trials found no significant reduction in the risk of CIN with the use of iodixanol, as compared with LOCM.<sup>27</sup>

### FUTURE OF ICM

The current nonionic dimers are highly viscous. High viscosity has been real problem in injection through thin catheters and occurrence of nephrotoxicity. In future, a low viscous nonionic iso-osmolar dimer may find place in the market. New contrast media including organ specific agents are expected in near future.

### CONCLUSION

Iodinated contrast media are most widely used and are quite safe to use. Reactions, when they occur, are usually mild but may occasionally progress to life-threatening proportions. A thorough knowledge of contrast media, their adverse reactions, causes, predisposing factors, clinical features, management strategies, choice of agents and premedication regimens for high risk patients, is essential to minimize the threats posed by these factors.

**REFERENCES**

1. American College of Radiology Manual on Contrast Media, 4th Edn. Reston, VA: American College of Radiology; 1998.
2. Katzberg RW. Acute reactions to urographic contrast medium: incidence, clinical characteristics, and relationship to history of hypersensitivity states—a commentary. *AJR*. 2008;190(6):1431-2.
3. Cohan RH, Ellis JH. Iodinated contrast material in uroradiology—choice of agent and management of complications. *Rad Clin North Am*. 1997;24(3):471-91.
4. Henrik S Thomsen, Judith AW Webb. Contrast Media: Safety Issues and ESUR Guidelines, 2nd revised Edition. Springer publications; 2009.
5. McClellan BL, Preston M. Hickey memorial lecture. Ionic and nonionic iodinated contrast media: evolution and strategies for use. *AJR*. 1990;155(2):225-33.
6. Contrast media—a multifactorial approach. In: Carlo Del Favero-Intramed communications; 1997.
7. Lesser E, Farr RS, Fusjimagari T, et al. The significance of protein binding of contrast media in roentgen diagnosis. *AJR*. 1962;87:338-60.
8. Almen T. Contrast agent design: some aspects on the synthesis of water soluble contrast agents of low osmolality. *J Theor Biol*. 1969;24:216-26.
9. Almen T. Development of nonionic contrast media. *Invest Radiol*. 1985;20:52-9.
10. Almén T, Boijesen E, Lindell SE. Metrizamide in angiography I. Femoral angiography. *Acta Radiol Diagn (Stockh)*. 1977;18(1):33-8.
11. Katzberg RW. Urography into the 21st century: new contrast media, renal handling, imaging characteristics, and nephrotoxicity. *Radiology*. 1997;204(2):297-312.
12. Costa N. Understanding contrast media. *J Infus Nurs*. 2004; 27:302-12.
13. Bettmann MA, Morris TW. Recent advances in contrast agents. *Radiol Clin North Am*. 1986;24:347-57.
14. Peter Dawson. Adverse reactions to intravascular contrast agents. *BMJ*. 2006;333(7570):663-4.
15. Almen T. Visipaque- a step forward. A historical review. *Acta Radiol Suppl*. 1995;399:2-18.
16. Dobrato M, Powell CJ, Holtz E. Biochemical and morphological effects of contrast media on the kidney. *Acta Radiol*. 1995; 36:196-203.
17. Jokobson JA. Renal effects of iodixanol in healthy volunteers and patients with severe renal failure. *Acta Radiol*. 1995;36:196-203.
18. Rapport SI, Levitan H. Neurotoxicity of X-ray contrast media: relation to lipid solubility and blood-brain barrier permeability. *Am J Roentgenol*. 1974;122:186-94.
19. McClellan BL, Stolberry HO. Intravascular contrast media. Ionic versus nonionic: current status. *Radiol Clin North Am*. 1991;29(3):437-54.
20. Segal AJ. Optimizing urography. *World J Urolol*. 1998;16(1):3-8.
21. Jagdish Singh, Aditya Daftary. Iodinated contrast media and their adverse reactions. *J Nucl Med Technol*. 2008;36:69-74.
22. Cochran ST, Bomyea K, Sayre JW. Trends in adverse events after IV administration of contrast media. *AJR*. 2001;176:1385-8.
23. Thomsen HS. European Society of Urogenital Radiology (ESUR) guidelines on the safe use of iodinated contrast media. *Eur J Radiol*. 2006;60:307-13.
24. Morcos SK, Thomsen HS, Exley CM. Members of contrast media safety committee of European society of urogenital radiology (ESUR). Contrast media: interaction with other drugs and clinical tests. *Eur Radiology*. 2005;15:1463-8.
25. Ratko T. Technology assessment: low-osmolality contrast media. Oak Brook. UHC Technology Advancement Center, University Hospital Consortium;1993.
26. Cohan RH, Ellis JH, Dunnick NR. Use of low-osmolar agents and premedication to reduce the frequency of adverse reactions to radiographic contrast media: a survey to the society of uroradiology. *Radiology*. 1995;194:357-64.
27. Heinrich MC, Häberle L, Müller V, Bautz W, Uder M. Nephrotoxicity of iso-osmolar iodixanol compared with nonionic low-osmolar contrast media: meta-analysis of randomized controlled trials. *Radiology*. 2009;250(1):68-86.

## Chapter

# 20

# Contrast Reactions and Its Management

Gaurav Pradhan, Rajat Jain

## INTRODUCTION

Iodinated contrast media are among the most commonly used contrast agent in the modern radiology practice. These contrast agents can be used almost anywhere in the body by whatever route, i.e. oral, intravenous, rectal, intra-arterial and intrathecal. It is important to remember that ionic contrast media should not be used intrathecally, as it can be life-threatening. Only non-ionic contrast should be used for intrathecal administration and also for children with tracheoesophageal fistula.

The iodinated contrast agents are usually safe and adverse reactions are generally mild and self-limiting. Nonetheless, as any drug can cause side effects, contrast agents are no exception and severe or life-threatening reactions can occur.

Radiologists and other medical personnel involved in the use of contrast agents must be aware of risk factors for reaction to contrast media. They should be aware of and use strategies to minimize adverse events and be prepared to promptly identify and manage them.

For immediate reactors, the intradermal tests are the most sensitive, whereas delayed intradermal tests in combination with patch tests are needed for optimal sensitivity in non-immediate reactors. Contrast medium cross-reactivity is more common in the non-immediate than in the immediate group. The data suggests that at least 50 percent of hypersensitivity reactions to contrast media are caused by an immunologic mechanism. Skin testing appears to be a useful tool for diagnosis of contrast medium allergy and may play an important role in selection of a safe product in previous reactors.<sup>1,2</sup>

## TYPES OF ADVERSE REACTION

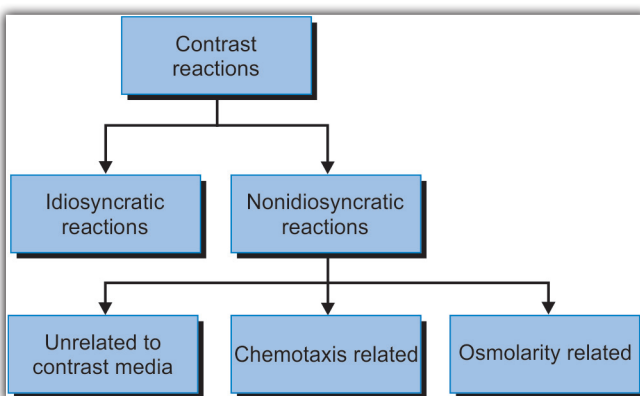
Adverse reactions to contrast media are broadly divided into two main groups (**Flow chart 1**):

1. Idiosyncratic anaphylactoid reactions
2. Nonidiosyncratic reactions.

### Idiosyncratic Anaphylactoid Reactions

Idiosyncratic anaphylactoid reactions (also described as allergy-like or anaphylactoid) are defined as unpredictable reactions which occur within 1 hour of contrast medium administration, and which are unrelated to the amount of contrast medium above a certain level. They are the most dreaded and most serious complications as they occur

**Flow chart 1** Adverse reactions



without warning, cannot be reliably predicted and are not preventable in the present state of our knowledge.

#### *Mechanism of Idiosyncratic Anaphylactoid Reactions<sup>1,3-7</sup>*

Idiosyncratic reactions vary greatly in severity and clinically may closely mimic true anaphylactic and allergic reactions, although there is no confirmatory evidence of a true antigen IGE antibody immunological reaction to contrast media. The mechanisms by which idiosyncratic reactions occur are not fully understood. However, they do appear to involve the release of active mediators, such as histamine, bradykinin, leukotrienes, prostaglandins and complement factors. Available evidence suggests that there are a variety of complex interactions between the complement, contact, coagulation and immune systems.<sup>1,3-6</sup>

1. **Inhibition of enzymes:** Cholinesterase resulting in increased concentration of acetylcholine; may lead to vagal overstimulation, e.g. cardiovascular collapse, bradycardia, bronchospasm.
2. **Release of vasoactive substances:** Histamine, serotonin or bradykinin may result in vasomotor collapse.
3. **Activation of physiological cascade systems:** Complement activation system, the kinin system with bradykinin release, the coagulation system inducing intravascular coagulation and the fibrinolytic system causing lysis of fibrin and blood clots.
4. The immune system disturbances.
5. **Anxiety, apprehension and fear:** Activating a hypothalamic reaction resulting in cardiovascular and respiratory collapse and even death.

It is probable that many of these mechanisms are inter-related and that a self-perpetuating vicious circle is established, resulting in severe and perhaps fatal cardiovascular collapse.

#### *Risk Factors for Acute Idiosyncratic Drug Reactions<sup>8</sup>*

##### **Risk factors for acute reactions**

- Type of contrast agent
- Previous adverse reaction to contrast medium
- Asthmatics
- Allergic and atopic patients
- Patients on certain drugs like beta-adrenergic blockers
- Patients with impaired cardiovascular and renal systems
- Diabetics
- Patients with various metabolic and hematological disorders
- Thyrotoxic: goitrous patients
- Feeble infants and aged patients
- Patients with a severe general debility
- Very nervous, anxious patients

1. **Type of contrast agent:** More with high osmolality contrast agent than with low/iso-osmolar contrast agent.

##### **2. Previous adverse reaction to contrast medium:**

- Most important patient factor predisposing to an acute idiosyncratic reaction
- With ionic agents, the risk of a reaction in a patient who reacted previously has been stated to be 16 to 35 percent
- When a patient who previously reacted to an ionic agent is given a nonionic agent, the risk of a repeat reaction is reduced to approximately 5 percent.

3. **Asthmatics:** Katayama et al described an 8.5 times increased risk with ionic agents and a 5.8 times increased risk with nonionic.<sup>8</sup>

##### **4. Allergic and atopic patients:**

- A history of allergy to foods, drugs or other substances is associated with an increased risk of contrast medium reaction, usually by a lesser amount than with a history of asthma.
- Other conditions, such as hay fever, eczema, etc. are associated with an increased risk of reaction, but by a lesser amount than asthma.

##### **5. Patients on certain drugs like beta-adrenergic blockers:**

- Whether or not beta-blockers affect the incidence of idiosyncratic contrast medium reactions is controversial. It is however agreed that the use of beta-blockers can impair the response to treatment if a reaction does occur.
- Patients who are receiving or have received interleukin-2 are at increased risk of adverse events following iodinated contrast media.

##### **6. Patients with impaired cardiovascular and renal systems:** A high sodium load caused by a large volume of HOCM containing sodium salts may exacerbate cardiac decompensation due to hypervolemia and myocardial depression

7. Diabetics
8. Patients with various metabolic and hematological disorders
9. Thyrotoxic: goitrous patients
10. Feeble infants and aged patients
11. Patients with a severe general debility
12. Very nervous, anxious patients.

#### *Prevention of Acute Idiosyncratic Reactions<sup>9-11</sup>*

If a patient has previous history of reaction to contrast media than, the possibility of obtaining the necessary diagnostic information from another test, not using iodinated contrast medium (e.g. ultrasonography, magnetic resonance imaging), must be considered. If iodinated contrast medium is still considered necessary, the risk can be reduced by an appropriate choice of contrast medium and premedication. Patient should remain in the radiology department for at least 30 minutes as most severe reactions occur within the first 30 minutes after contrast medium injection. In high-risk subjects, monitoring for the first hour is recommended.<sup>9,10</sup>

1. **Choice of contrast media:** The single most important method of reducing the risk of idiosyncratic contrast medium reactions is to use nonionic, low-osmolality agents, which are associated with a 4 to 5 times lower risk of reaction.<sup>8,12-14</sup> If there is prior documentation of contrast reaction from one contrast agent, then change to different low-osmolality contrast agent may be helpful.<sup>15,16</sup>
2. **Premedication:**<sup>1,17-19</sup> Most frequently, steroids with or without additional H<sub>1</sub> antihistamines have been recommended.
  - a. **Elective premedication:** Prednisone—50 mg by mouth at 13 hours, 7 hours, and 1 hour before contrast media injection and diphenhydramine—50 mg intravenously, intramuscularly, or by mouth 1 hour before contrast medium.
  - If the patient is unable to take oral medication, 200 mg of hydrocortisone intravenously may be substituted for oral prednisone.
  - b. **Emergency premedication:** Hydrocortisone sodium 200 mg intravenously every 4 hours until contrast study required and diphenhydramine 50 mg IV, 1 hour prior to contrast injection
    - No use of steroids if given less than 4 to 6 hrs before contrast administration.
    - Diphenhydramine 50 mg IV (with no steroids) in very urgent scans.

### *Types and Management of Acute Idiosyncratic Reactions<sup>1</sup>*

*Guidelines from ACR Manual on Contrast Media Version 8; 2012<sup>1</sup>*

Acute idiosyncratic reactions are usually characterized as mild, moderate or severe. Mild or minor reactions include nausea, mild vomiting, urticaria and itching. They usually do not require medical treatment other than reassurance and restoration of the patient's confidence. Vital signs should be obtained to detect hypotension that may be clinically silent while the patient is supine. Any patient with a mild allergic-like reaction should be observed at least for 20 to 30 minutes to ensure clinical stability or recovery. Treatment with an antihistamine may be given however, is not required most of the times.

Moderate reactions include more severe vomiting, marked urticaria, bronchospasm, facial or laryngeal edema, and vasovagal reactions. Moderate reactions require close patient monitoring until they resolve completely. Moderate adverse events are not immediately life-threatening, but often require medical treatment. The treatment depends on the type of reaction encountered.

1. **Urticaria:**
  - a. Discontinue injection if not completed
  - b. No treatment needed in most cases
  - c. Give H<sub>1</sub>-receptor blocker: diphenhydramine PO/IM/IV 25 to 50 mg.

- If severe or widely disseminated: give alpha-agonist adrenaline S/C (1:1,000) 0.1 to 0.3 mL (if no cardiac contraindications).
2. **Facial or laryngeal edema:**
  - a. Give O<sub>2</sub> 6 to 10 liters/min (via mask).
  - b. Give alpha-agonist adrenaline SC or IM (1:1,000) 0.1-0.3 mL or, especially if hypotension evident, adrenaline (1:10,000) slowly IV 3 mL preferably under ECG control.
  - c. Repeat as needed up to a maximum of 1 mg.
  - d. If not responsive to therapy or if there is obvious acute laryngeal edema, seek appropriate assistance (e.g. cardiopulmonary arrest response team).
3. **Bronchospasm:**
  - a. Give O<sub>2</sub> 6 to 10 liters/min (via mask). Monitor: electrocardiogram, O<sub>2</sub> saturation (pulse oximeter), and blood pressure.
  - b. Give beta-agonist inhalers (bronchiolar dilators, such as metaproterenol, terbutaline, or albuterol) 2 to 3 puffs; repeat as necessary. If unresponsive to inhalers, use SC, IM, or IV adrenaline.
  - c. Give adrenaline SC or IM (1:1,000) 0.1 to 0.3 ml or, especially if hypotension evident, adrenaline (1:10,000) slowly IV 1-3 mL preferably under ECG control.

Repeat as needed up to a maximum of 1 mg.

Call for assistance (e.g. cardiopulmonary arrest response team) for severe bronchospasm or if O<sub>2</sub> saturation <88 percent persists.

Severe reactions include severe hypotension, hypertension, cardiac arrhythmias, cardiac arrest, convulsion and pulmonary edema.
1. **Hypotension with tachycardia:**
  - a. Legs elevated (preferred) or Trendelenburg position.
  - b. Monitor: Electrocardiogram, pulse oximeter, blood pressure.
  - c. Give O<sub>2</sub> 6 to 10 liters/min (via mask).
  - d. Rapid intravenous administration of large volumes of Ringer's lactate or normal saline.

If poorly responsive: Adrenaline (1:10,000) slowly IV 1 mL.

Repeat as needed up to a maximum of 1 mg.

If still poorly responsive seek appropriate assistance (e.g. cardiopulmonary arrest response team).
2. **Hypotension with bradycardia (Vagal reaction):**
  - a. Secure airway: Give O<sub>2</sub> 6 to 10 liters/min (via mask)
  - b. Monitor vital signs.
  - c. Legs elevated 60° or more (preferred) or Trendelenburg position.
  - d. Secure IV access: Rapid administration of Ringer's lactate or normal saline.
  - e. Give atropine 0.6 to 1 mg IV slowly, if patient does not respond quickly to steps 2 to 4.
  - f. Repeat atropine up to a total dose of 0.04 mg/kg (2-3 mg) in adult.

- g. Ensure complete resolution of hypotension and bradycardia prior to discharge.
3. **Hypertension, severe:**
- a. Give O<sub>2</sub>, 6 to 10 liters/min (via mask).
  - b. Monitor: Electrocardiogram, pulse oximeter, blood pressure.
  - c. Give nitroglycerine 0.4 mg tablet, sublingual (may repeat × 3); or, topical 2 percent ointment, apply 1-inch strip.
  - d. If no response, consider labetalol 20 mg IV, then 20 to 80 mg IV every 10 minutes up to 300 mg.
  - e. Transfer to intensive care unit or emergency department.
  - f. For pheochromocytoma: Phentolamine 5 mg IV (may use labetalol if phentolamine is not available).
- Seizures or convulsions*
- a. Give O<sub>2</sub>, 6 to 10 liters/min (via mask).
  - b. Consider diazepam 5 mg IV (or more, as appropriate) or midazolam 0.5 to 1 mg IV.
  - c. If longer effect needed, obtain consultation; consider phenytoin infusion — 15 to 18 mg/kg at 50 mg/min.
  - d. Careful monitoring of vital signs required, particularly of pO<sub>2</sub> because of risk to respiratory depression with benzodiazepine administration.
  - e. Consider using cardiopulmonary arrest response team for intubation if needed.
4. **Pulmonary edema:**
- a. Give O<sub>2</sub>, 6 to 10 liters/min (via mask).
  - b. Elevate torso.
  - c. Give diuretics: Furosemide 20 to 40 mg IV, slow push.
  - d. Consider giving morphine (1-3 mg IV).
  - e. Transfer to intensive care unit or emergency department.

### Nonidiosyncratic Reactions<sup>22-25</sup>

These are dose-related reactions and dependent on the physico-chemical properties of the contrast medium, i.e. chemical composition, osmolality and concentration of contrast medium and also on the volume, speed and multiplicity of the injection.

1. **Reactions unrelated to contrast media:** Pyrogenic (unsterile injection), vasovagal especially in anxious or psychosomatic patients, hypertensive attacks in patients with pheochromocytoma, excessive dehydration, and hypoglycemia.
2. **Chemotoxic reactions:** As iodine is very firmly bound to the benzene rings, these side effects are probably due to toxicity to the contrast medium ion rather than to its iodine content. These include cardiac, neurological and renal toxicity as well as vascular manifestations.

3. **Hyperosmolar reactions:** Due to very high osmolality of these compounds predominantly HOCM, adverse reactions may occur when large volumes are injected into the circulation predominantly because of erythrocyte damage, endothelial damage, blood brain barrier damage, vasodilatation, hypervolemia and cardiac decompression. As these reactions are predominantly related to the hyperosmolality of the contrast media and depend on the dose, concentration and volume of contrast used, they can be significantly reduced by substituting LOCM for the very hypertonic HOCM.

### Extravasation of Contrast<sup>26-30</sup>

It refers to the escape of contrast material from the vessel into which it is introduced, into the surrounding tissue or body cavity. It occurs with a frequency of about 0.1 to 0.9 percent of patients getting contrast injections, more commonly seen in patients having atherosclerotic peripheral vascular disease, diabetic vascular disease, Raynaud's disease, venous thrombosis, prior radiation therapy or extensive surgery, severely ill or debilitated patients, injection through indwelling peripheral intravenous lines (> than 24 hours) and multiple punctures into the same vein.

### Clinical Features

- **Mild:** Tissue edema, erythema, stinging, tenderness
- **Severe:** Compartment syndromes, skin ulceration and tissue necrosis.

Prevention is better than cure and a good secured intravenous access reduces the incidence, along with extravasation detectors as present in some of the modern automatic pressure injectors prevents excess of contrast extravasation.

### Contrast Extravasation Treatment

<20 mL extravasation	> 20 mL extravasation	> 100 mL extravasation
<ul style="list-style-type: none"> <li>• Elevate the arm and observe</li> </ul>	<ul style="list-style-type: none"> <li>• Aspirate</li> <li>• Intermittent ice</li> <li>• Hyaluronidase (50-250 U) at local extravasation site</li> </ul>	<ul style="list-style-type: none"> <li>• Aspirate</li> <li>• Intermittent ice</li> <li>• Hyaluronidase (50-250 U) at local extravasation site</li> <li>• Immediate plastic consult if: <ul style="list-style-type: none"> <li>– Blistering,</li> <li>– Altered perfusion,</li> <li>– Pain worsens after 2-4 hr</li> <li>– Change in sensation distally</li> </ul> </li> </ul>

### Contrast Induced Nephropathy

Contrast-induced nephrotoxicity (CIN) is a sudden deterioration in renal function following the recent intravascular administration of iodinated contrast medium in the absence of another nephrotoxic event.

### Diagnosis

There are no standard criteria for the diagnosis of CIN; criteria used in the past have included percent change in the baseline serum creatinine (an increase of variously 25% to 50%) and absolute elevation from baseline serum creatinine (e.g. an increase of variously 0.5 to 2.0 mg/dL). One of the most commonly used criteria has been an absolute increase of 0.5 mg/dL.

### Acute Kidney Injury Network: Definition of Acute Kidney Injury<sup>28</sup>

The diagnosis of acute kidney injury is made according to the AKIN criteria if one of the following occurs within 48 hours after a nephrotoxic event (e.g. intravascular iodinated contrast medium exposure):

1. Absolute serum creatinine increase of  $\geq 0.3$  mg/dL ( $\geq 26.4$   $\mu\text{mol/L}$ ).
2. A percentage increase in serum creatinine of  $\geq 50$  percent (1.5-fold above baseline).
3. Urine output reduced to  $\leq 0.5$  mL/kg/hour for at least 6 hours.

### Pathogenesis

The exact pathophysiology of CIN is not understood. Nephrotoxicity of contrast media is likely to be due to:

- Decreased renal perfusion due to renal vasoconstriction (low BP, peripheral vasodilatation)
- Glomerular injury manifests as proteinuria.
- Tubular injury due to osmolarity, chemotoxicity, ischemia.
- Contrast media precipitation of Tamm Horsfall protein that blocks tubules.
- Swelling of renal tubular cells causing obstruction.
- Both osmotic and chemotoxic mechanisms may be involved, and some investigations suggest agent-specific chemotoxicity.

**Symptoms:** Usually asymptomatic. Creatinine peaks in 3 to 5 days. In severe oliguric patients: peaks in 5 to 7 days.

**Incidence:**<sup>32-38</sup> The incidence of CIN in patients with normal renal function is <1 percent with intravenous and 2 to 7 percent with intra-arterial administration of contrast media. The incidence is higher (16%) in nonazotemic diabetic patients. The incidence may be as high as 33 percent in patients with pre-

existent azotemia. Incidence of 3 to 16 percent has been reported in patients undergoing percutaneous coronary interventions. Patients undergoing percutaneous coronary interventions (PCI) often have associated risk factors for developing contrast-induced nephropathy, such as diabetes mellitus, congestive heart failure and pre-existing renal impairment.

### Risk Factors for CIN

- Pre-existing renal impairment (Serum creat > 1.3 mg/dL, GFR < 60 mL/min)
- Dehydration
- CHF
- Use of nephrotoxic drugs (NSAID, aminoglycosides)
- Hypersensitivity disease (Multiple myeloma)
- Hypertension
- Hyperuricemia (as in active gout)
- Proteinuria ( $> 0.5$  gm/dL)
- DM
- Age  $> 70$  years.

### Prevention of contrast induced nephropathy in high risk patients<sup>11,39-46</sup>

1. **Avoidance of iodinated contrast medium:** In high risk patient it is best to avoid use of iodinated contrast media and the possibility of obtaining the necessary diagnostic information from another test, not using iodinated contrast medium (e.g. ultrasonography, magnetic resonance imaging), must be considered. In some clinical situations where the use of intravascular iodinated contrast medium may be necessary the lowest possible dose of contrast medium to obtain the necessary diagnostic information should be used.<sup>9-11</sup>
2. **Contrast media selection:** Increased osmotic overload on the diseased kidney is considered to be the major etiology of CIN. This can be significantly reduced by substituting LOCM for the very hypertonic HOCM.<sup>39</sup>
3. **Hydration:** Adequate hydration is considered to be the single most effective way to prevent CIN. The ideal infusion rate and volume is unknown, but isotonic fluids are preferred (Lactated Ringer's or 0.9% normal saline). One possible protocol would be 0.9 percent saline at 100 mL/hr, beginning 6 to 12 hours before and continuing 4 to 12 hours after intravascular iodinated contrast medium administration. Oral hydration has also been utilized, but with less demonstrated effectiveness. Pediatric infusion rates are variable and should be based on patient weight.<sup>40,41</sup>
4. **Sodium bicarbonate:** It has been found to be useful in prevention from CIN according to some studies.<sup>42,43</sup>
5. **N-acetylcysteine:** The role is controversial. There is evidence that it reduces serum creatinine in normal

volunteers without changing cystatin-C (cystatin-C is reported to be a better marker of GFR than serum creatinine). This raises the possibility that *N*-acetylcysteine might be simply lowering serum creatinine without actually preventing renal injury. *N*-acetylcysteine should not be considered a substitute for appropriate preprocedural patient screening and adequate hydration.<sup>44,45</sup>

6. **Diuretics (Mannitol and furosemide):** There is no reported benefit and neither mannitol nor furosemide is recommended for CIN risk reduction.<sup>46</sup>
7. **Other agents:** The evidence for other theoretically renal-protective medications, such as theophylline, endothelin-1, and fenoldopam is even less convincing. Use of these agents to reduce the risk of CIN is not recommended.

#### *Renal Dialysis Patients and the Use of Iodinated Contrast Medium<sup>1</sup>*

Contrast agents are not protein-bound, have relatively low molecular weights, and are readily cleared by dialysis. Unless an unusually large volume of contrast medium is administered or there is substantial underlying cardiac dysfunction, there is no need for urgent dialysis after intravascular iodinated contrast medium administration.

Patients with anuric end-stage chronic kidney disease can receive intravascular iodinated contrast medium without risk of further renal damage because their kidneys are no longer functioning.

Patients receiving dialysis are also at theoretical risk from the osmotic load imposed by intravascular iodinated contrast medium because they cannot clear the excess intravascular volume. This osmotic load can theoretically result in pulmonary edema and anasarca. Hence, contrast medium dosing should be as low as necessary to achieve a diagnostic result (as in all patients).

#### *Recommendation of Contrast Agents Based on Serum Creatinine Level*

Serum creatinine	Recommendations
< 1.5 mg/dL	Can use either ionic or nonionic contrast
1.5–2 mg/dL	Use nonionic contrast
2–2.5 mg/dL	Use of nonionic only in extreme indications, but contraindicated in diabetics
> 2.5 mg/dL	No contrast to be given

#### *Contrast Administration and Pregnancy<sup>1</sup>*

Diagnostic iodinated contrast media have been shown to cross the human placenta and enter the fetus when given in usual clinical doses.

While it is not possible to conclude that iodinated contrast media present a definite risk to the fetus, there is insufficient evidence to conclude that they pose no risk. Consequently, the Committee on Drugs and Contrast Media recommends the following:

- A. The radiologist should confer with the referring physician and document in the radiology report or the patient's medical record the following:
  1. That the information requested cannot be acquired without contrast administration or via another image modality (e.g. ultrasonography).
  2. That the information needed affects the care of the patient and fetus during the pregnancy.
  3. That the referring physician is of the opinion that it is not prudent to wait to obtain this information until after the patient is no longer pregnant.
- B. It is recommended that pregnant patients undergoing a diagnostic imaging examination with ionizing radiation and iodinated contrast media provide informed consent to document that they understand the risk and benefits of the procedure to be performed and the alternative diagnostic options available to them (if any), and that they wish to proceed.

#### *Contrast Administration and Lactation<sup>1</sup>*

Less than 1 percent of contrast media are secreted in human milk and < 1 percent of ingested contrast is absorbed by gut, thus it appears safe to continue breast-feeding after receiving such an agent. If the mother remains concerned about any potential ill effects to the infant, she may abstain from breast-feeding for 24 hours with active expression and discarding of breast milk from both breasts during that period. Expressed breast milk prior to contrast study may be used during this period.

#### *Contrast Administration in Patients on Metformin<sup>1</sup>*

Metformin, an oral biguanide hyperglycemic therapy for diabetes mellitus Type 2, is primarily excreted unchanged by the kidneys, probably by both glomerular filtration and tubular excretion. The renal route eliminates approximately 90 percent of the absorbed drug within the first 24 hours. Metformin seems to cause increased lactic acid production by the intestines. Any factors that decrease metformin excretion or increase blood lactate levels are important risk factors for lactic acidosis. Renal insufficiency, then, is a major

consideration. In patients with severe renal impairment, intravascular accumulation of the biguanide may occur after contrast media, and this may precipitate biguanide lactic acidosis (vomiting, diarrhea, somnolence)—a potentially fatal complication.

Limiting the amount of contrast medium administered and hydrating the patient lessen the risk of contrast media-induced dysfunction; both of these measures should be considered in patients with known or incipient renal dysfunction.

#### *Recommendations<sup>1</sup>*

Category 1	Category 2	Category 3
Normal renal function with no known comorbidities No reason to discontinue metformin	Normal renal function with known co-morbidities +, then suspend metformin for 48 hrs  If the patient had normal renal function at baseline, was clinically stable, and had no intercurrent risk factors for renal damage (e.g. treatment with aminoglycosides, major surgery, heart failure, sepsis, repeat administration of large amounts of contrast media), metformin can be restarted	Renal dysfunction then suspend metformin for 48 hrs and restart only if repeat KFT is normal

#### *Comorbidities for Lactic Acidosis with Use of Metformin*

- Decreased metabolism of lactate
- Liver dysfunction
- Alcohol abuse
- Increased anaerobic metabolism
- Cardiac failure
- Myocardial or peripheral muscle ischemia
- Sepsis or severe infection.

**Remember:** Metformin + Chronic renal insufficiency + IV contrast = Lactic acidosis.

#### *Contrast Administration and Interleukin-2 Therapy<sup>47,11</sup>*

- Always ask the oncologist of possible IL-2 therapy
- Inform patient of possible risk involved
- Generally mild symptoms (12% patients), e.g. rash, flu-like symptoms, pruritis, hypotension, tachycardia, joint pain, but few may require hospitalization

- Steroids cannot be given (steroids counteracts intended IL-2 action)
- If previous history of reaction to contrast present, then do not give contrast until extremely necessary
- Monitor patient for 2 hours, if uneventful send patient home.

#### *Contrast Administration and Thyroid Dysfunction<sup>11</sup>*

- Manifest active hyperthyroidism is an absolute contraindication to radiographic contrast media administration.
- Patients at risk: Graves' disease and multinodular goiter with thyroid autonomy (especially in elderly/patients living on iodine deficient diet)
- Contrast may cause thyrotoxicosis (though rare)
- Patient becomes unfit for diagnostic thyroid scintigraphy, radio-iodine treatment of thyroid malignancy for 2 months.

#### *Prophylaxis of Contrast Induced Thyrotoxicosis*

##### *Elective contrast-enhanced studies*

Sodium perchlorate 300 mg 3 times daily (Start the day before and continue for 8 to 14 days).

##### *Emergency contrast-enhanced studies*

Sodium perchlorate 800 mg once daily (Directly prior to examination, continue with 3 × 300 mg for 8 to 14 days).

#### *Contrast Administration in Pheochromocytoma and Paraganglioma<sup>11</sup>*

There is a theoretical risk of hypertensive crisis in patients of paragangliomas due to release of catecholamine however, studies have shown no elevation of catecholamine levels after the IV injection of nonionic contrast media. Direct injection of either type of contrast medium into the adrenal or renal artery is to be avoided, however, as this may cause a hypertensive crisis.

#### *Contrast and Drug Interaction<sup>47</sup>*

- Drugs which enhance renal effect of contrast: NSAIDS, Gentamycin, Cisplatin, Cyclosporine
- Drugs which enhance diuretic effect of contrast: Acetazolamide, Furosemide, Spironolactone
- Drugs which enhance allergic reactions: β-blockers, IL-2, Interferons, and Hydralazine (should be avoided until extremely necessary as it can provoke SLE like syndrome)
- Drugs which enhance negative inotropic effect of contrast: CCB, digoxin.

### *Delayed Adverse Events to Iodinated Contrast Media*

These are uncommon reactions occurring from 30 to 60 minutes to up to one week following contrast material exposure, with the majority occurring between three hours and two days. The most frequent delayed adverse events following contrast media administration are allergic-like and cutaneous in nature.<sup>49,50</sup> They are more frequent in patients with previous history of reaction to contrast and in patients with asthma or other allergic disorders. Delayed cutaneous reactions commonly manifest as urticaria and/or a persistent rash which, may occasionally present with a maculopapular exanthem or generalized exanthematous pustulosis. Few cases resembling Stevens-Johnson syndrome, toxic epidermal necrolysis, and cutaneous vasculitis have also been described.

A variety of non-cutaneous sign and symptoms like nausea, vomiting, fever, drowsiness, and headache have also been reported. Each of these is usually self-limited and does not require therapy.

Iodide "mumps" (iodine-related sialoadenopathy or salivary gland swelling) and a syndrome of acute polyarthropathy are two additional delayed contrast reactions that have been reported rarely after contrast media administration. These reactions appear to be more frequent in patients with renal dysfunction.<sup>51,52</sup>

Low molecular nonionic contrast has been reported to cause fewer delayed skin reactions as compared to iso-osmolar contrast. Prophylaxis is not recommended for delayed adverse reactions.

#### *Treatment*

Most of these reactions are self-limiting and do not require any treatment, treatment is usually supportive, with antihistamines and/or corticosteroids used for cutaneous symptoms, antipyretics for fever, antiemetics for nausea, and fluid resuscitation for hypotension. If manifestations are progressive or widespread, or if there are noteworthy associated symptoms, consultation with an allergist and/or dermatologist is an appropriate next step.<sup>53</sup>

### **Recommendations for the Departments Performing Contrast Related Investigations<sup>54,55</sup>**

- The radiologist must always weigh the risk-benefit ratio for the possible advantages from the diagnostic procedure against the very small but ever-present risk of a severe adverse reaction (and even death) to the contrast medium.
- In high-risk patient it is best to avoid use of iodinated contrast media and the possibility of obtaining the necessary diagnostic information from another test, not using iodinated contrast medium (e.g. ultrasonography, magnetic resonance imaging), must be considered.
- In the presence of risk factors, the referring clinician should be consulted and advised. The patient should also be informed, consulted and reassured. The discussion and result should be recorded in the patient's notes.

- Although a routine test dose is generally not necessary, it is advisable to perform a small 1 ml test dose, either by IV or dermal testing in patients considered to be at increased risk of contrast reactions.
- In high-risk patients premedication is strongly advised, especially in asthmatic and allergic patients according to the protocols.
- Before administering the injection, the emergency trolley, alarm system and availability of experienced assistance must be confirmed.
- An individual trained in recognizing and treating severe contrast reactions, including anaphylaxis, should be immediately available in the department
- Adequate hydration must be ensured in all patients receiving contrast media particularly if there is previous renal impairment and those patients receiving large quantities of contrast media, in order to excrete the contrast media as completely and quickly as possible.
- Nonionic, low or iso-osmolar agents are five to ten times safer than the high osmolar ionic agents.
- The smallest dose of contrast media that will give reliable, comprehensive diagnostic results should be used.
- A patient should not be left alone or unsupervised in the first five minutes after an injection of the contrast agent.
- Patient should remain in the premises for 15 to 30 minutes after the contrast administration as most of the contrast reactions occur during this period only.
- All contrast reactions, with details of their nature, severity and the agent used, should be included in the radiological report and updated in the patient's hospital notes.
- Radiographic contrast media like any drug are useful for the patient but not free from side effects and minor to severe life-threatening side effects can occur with their use and hence radiologists and other medical personal involved in the use of contrast agents should be aware of and use strategies to minimize adverse events and be prepared to promptly identify and manage them.
- Reactions related to MR contrast media are covered in Chapter "MR contrast media".

### **REFERENCES**

1. ACR Committee on Drugs and Contrast Media; ACR Manual on Contrast Media. 2012;Version 8.
2. Brockow K, Romano A, Aberer W, Bircher AJ, Barbaud A, et al. Skin testing in patients with hypersensitivity reactions to iodinated contrast media—a European multicenter study. *Allergy*. 2009;64(2):234-41.
3. Nelson RC, Anderson Jr FA, Birnbawm BA, et al. Contrast medium extravasation detection accessory. *Radiology*. 1988; 209:837-43.
4. Dawson P, Cosgrove DO, Grainger RG. *Textbook of Contrast Media*, Oxford, Isis Medical Media, 1999.
5. American College of Radiology: *Manual on Contrast Media*, 4th edition. Reston, Virginia, USA, American College of Radiology, 1999.

6. Thomsen HS, Muller RN, Mattrey RF. Trends in Contrast Media. Germany: Springer-Verlag; 1999.
7. European Society of Urogenital Radiology. 2003; Version 3.0.
8. Katayama H, Yamaguchi K, Kozuka T, Takashima T, Seez P, Matsuura K. Adverse reactions to ionic and non-ionic contrast media. A report from the Japanese committee on the safety of contrast media. *Radiology*. 1990;175:621-8.
9. Hartman GW, Hattery RR, Witten DM, Williamson B. Mortality during excretory urography: Mayo Clinic experience. *Am J Roentgenol*. 1982;139:919-22.
10. Shehadı WH. Death following intravascular administration of contrast media. *Acta Radiol Diagn*. 1985;26:457-46.
11. Thompson HS, Webb JAW. Contrast media; Safety issues and ESUR Guidelines. 2nd revised edition. 2009.p. 40-9.
12. Palmer FJ. The RACR survey of intravenous contrast media reactions: final report. *Austr Radiol*. 1988;32:426-8.
13. Wolf GL, Miskin MM, Roux SG, et al. Comparison of the rates of adverse drug reactions: ionic contrast agents, ionic agents combined with steroids and nonionic agents. *Invest Radiol*. 1991;26:404-10.
14. Bettman MA, Heeren T, Greenfield A, Gondev C. Adverse events with radiographic contrast agents: results of the SCVIR Contrast Agent Registry. *Radiology*. 1997;203:611-20.
15. Thomsen HS, Bush WH. Adverse effects of contrast media: incidence, prevention and management. *Drug Safety*. 1998; 19:313-24.
16. Dewachter P, Laroche D, Mouton-Fqaivre C, Clement O. Immediate and late adverse reactions to iodinated contrast media: a pharmacological point of view. *Anti-Inflammatory Anti-Allergy Agents Med Chem*. 2006;5:105-17.
17. Lasser EC, Berry CC, Talner LB, et al. Pretreatment with corticosteroids to alleviate reactions to intravenous contrast material. *N Engl J Med*. 1987;317:845-9.
18. Greenberger PA, Patterson R. The prevention of immediate generalized reactions to radiocontrast media in high-risk patients. *J Allergy Clin Immunol*. 1991;87:867-72.
19. Greenberger PA, Halwig JM, Patterson R, Wallemark CB. Emergency administration of radiocontrast media in high-risk patients. *J Allergy Clin Immunol*. 1986;77:630-4.
20. Grainger RG. Intravascular contrast media. The past, the present and the future. *Br J Radiol*. 1982; 55:1-18.
21. Morris TW. X-ray contrast media. Where are we now and where are we going?. *Radiology*. 1993;188:11-6.
22. Aspelin P, Aubrey SG, Fransson SG, et al. Nephrotoxic effects in high-risk patients undergoing angiography. *N Engl J Med*. 2003;348:491-9.
23. Heinrich MC, Kuhlmann MK, Grgic A, et al. Cytotoxic effects of ionic high-osmolar, nonionic monomeric and non-ionic iso-osmolar dimeric iodinated contrast media on renal tubular cells *in vitro*. *Radiology*. 2005;235:843-9.
24. Yoshikawa H. Late reactions to nonionic contrast media. *Radiology*. 1992;183:737-40.
25. Spring DB, Bettman MA, Barkan HE. Deaths related to iodinated contrast media reported spontaneously to US Food and Drug Administration 1978-1994: Effect of availability of low osmolality contrast media. *Radiology*. 1997;204:333-7.
26. IV extravasation management guidelines at children hospital; Westmead) practice guideline No: 0/C/12:8007-01:00.
27. <http://radres.ucsd.edu/documents/CALL/Extravasation.pdf>. ucsmc policy/procedure-radiology Intravenous Contrast Media Guidelines-Adult.
28. Bellin MF, Jakobsen JA, Tomassin I, et al. Contrast medium extravasation injury: guidelines for prevention and management. *Eur Radiol*. 2002;12:2807-12.
29. Cohan RH, Ellis JH, Garner WL. Extravasation of radiographic contrast material: recognition, prevention, and treatment. *Radiology*. 1996;200:593-604.
30. Wang CL, Cohan RH, Ellis JH, Adusumilli S, Dunnick NR. Frequency, management, and outcome of extravasation of nonionic iodinated contrast medium in 69,657 intravenous injections. *Radiology*. 2007;243:80-7.
31. Mehta RL, Kellum JA, Shah SV, et al. Acute Kidney Injury Network: report of an initiative to improve outcomes in acute kidney injury. *Crit Care*. 2007;11:R31.
32. D'Elia JA, Gleason RE, Alday M, Malarick C, Godley K, Waram J, et al. Nephrotoxicity from angiographic contrast material: a prospective study. *Am J Med*. 1982;72:719-25.
33. Porter GA. Radiocontrast-induced nephropathy. *Nephrol Dial Transplant*. 1994;9(Suppl 4):146-56.
34. Barrett BJ, Parfrey PS, Vavasour HM, McDonald J, Kent G, Hefferton D, et al. Contrast nephropathy in patients with impaired renal function; high versus low osmolar media. *Kidney Int*. 1992;41:1274-9.
35. Lautin EM, Freeman NJ, Schoenfeld AH, Bakal EW, Haramati N, Friedman AC, et al. Radiocontrast associated renal dysfunction: Incidence and risk factors. *Am J Roentgenol*. 1991;157: 49-58.
36. Rihal CS, Textor SC, Grill DE, Berger PB, Ting HH, Best PJ, et al. Incidence and prognostic importance of acute renal failure after percutaneous coronary intervention. *Circulation*. 2002; 105:2259-64.
37. McCullough PA, Wolyn R, Rocher LL, Levin RN, O'Neill WW. Acute renal failure after coronary intervention: Incidence, risk factors, and relationship to mortality. *Am J Med*. 1997;103:368-75.
38. Gruberg L, Mehran R, Dangas G, Mintz GS, Waksman R, Kent KM, et al. Acute renal failure requiring dialysis after percutaneous coronary interventions. *Catheter Cardiovasc Interv*. 2001;52:409-16.
39. Barrett BJ, Carlisle EJ. Meta-analysis of the relative nephrotoxicity of high- and low-osmolality iodinated contrast media. *Radiology*. 1993;188:171-8.
40. Weisbord SD, Palevsky PM. Prevention of contrast-induced nephropathy with volume expansion. *Clin J Am Soc Nephrol*. 2008;3:273-80.
41. Taylor AJ, Hotchkiss D, Morse RW, McCabe J. Preparation for Angiography in Renal Dysfunction: a randomized trial of inpatient vs outpatient hydration protocols for cardiac catheterization in mild-to-moderate renal dysfunction. *Chest*. 1998;114:1570-4.
42. Merten GJ, Burgess WP, Gray LV, et al. Prevention of contrast-induced nephropathy with sodium bicarbonate: a randomized controlled trial. *JAMA*. 2004;291:2328-34.
43. Navaneethan SD, Singh S, Appasamy S, Wing RE, Sehgal AR. Sodium bicarbonate therapy for prevention of contrast-induced nephropathy: a systematic review and meta-analysis. *Am J Kidney Dis*. 2009;53:617-27.
44. Stenstrom DA, Muldoon LL, Armijo-Medina H, et al. N-acetylcysteine use to prevent contrast medium-induced nephropathy: premature phase III trials. *J Vasc Interv Radiol*. 2008;19:309-18.
45. Vaitkus PT, Brar C. N-acetylcysteine in the prevention of contrast-induced nephropathy: publication bias perpetuated by meta-analyses. *Am Heart J*. 2007;153:275-80.

46. Solomon R, Werner C, Mann D, D'Elia J, Silva P. Effects of saline, mannitol, and furosemide to prevent acute decrease in renal function induced by radiocontrast agents. *N Engl J Med.* 1994; 331:1416-20.
47. Sameh K Morcos, Henrik S. Thomsen, CM Exley. Contrast media: interactions with other drugs and clinical tests *Eur Radiol.* 2005;15:1463-8.
48. Katayama H, Yamaguchi K, Kozuka T, et al. Adverse reactions to ionic and nonionic contrast media. *Radiology.* 1990;175:621-8.
49. Meth MJ, Maibach HI. Current understanding of contrast media reactions and implications for clinical management. *Drug Saf.* 2006;29:133-41.
50. Christiansen C, Pichler WJ, Skotland T. Delayed allergy-like reactions to X-ray contrast media: mechanistic considerations. *Eur Radiol.* 2000;10:1965-75.
51. Berman HL, Delaney V. Iodide mumps due to low-osmolality contrast material. *Am J Roentgenol.* 1992;159:1099-1100.
52. Gilgen-Anner Y, Heim M, Ledermann HP, Bircher AJ. Iodide mumps after contrast media imaging: a rare adverse effect to iodine. *Ann Allergy Asthma Immunol.* 2007;99:93-8.
53. Webb JA, Stacul F, Thomsen HS, Morcos SK. Late adverse reactions to intravascular iodinated contrast media. *Eur Radiol.* 2003;13:181-4.
54. Ronald G Grainger, Henrik S Thomsen, Sameh K. Morcos. Intravascular Contrast Media for Radiology, CT and MRI. In Adam: Grainger & Allison's Diagnostic Radiology, 5th Edn.
55. Royal College of Radiologist. Standard for intravascular contrast agent administration to adult patients. Approved guidelines by board of faculty of clinical radiology July 2011.

## Section

# 6

# Miscellaneous

- Chapter 21** ● Picture Archiving and Communication System and Radiology Information System  
*Shivanand Gamanagatti, Devasenathipathy Kandasamy, Arun Kumar Gupta*
- Chapter 22** ● Evidence Based Radiology  
*Sanjay Sharma, Manisha Jana*
- Chapter 23** ● Radiation Hazards and Radiation Units  
*Pratik Kumar, Anil K Pandey*
- Chapter 24** ● Radiation Protection  
*Sapna Singh*
- Chapter 25** ● Planning a Modern Imaging Department  
*SC Bansal, Niranjan Khandelwal, Ajay Gulati*
- Chapter 26** ● Recent Advances in PET/CT and PET/MR  
*Rakesh Kumar, Anil Chauhan*
- Chapter 27** ● Common Drugs Used in an Imaging Department  
*Anupam Lal, Vivek Gupta, Manphool Singhal*
- Chapter 28** ● Molecular Imaging  
*Anish Bhattacharya, BR Mittal*
- Chapter 29** ● Ethical and Legal Issues in Radiology  
*Mandeep Kang, Manavjit Singh Sandhu*



## Chapter

# 21

# Picture Archiving and Communication System and Radiology Information System

*Shivanand Gamanagatti, Devasenathipathy Kandasamy, Arun Kumar Gupta*

## INTRODUCTION

Imaging informatics is a well-recognized subspecialty of radiology which deals with the flow of information from person to other or one place to other.<sup>1,2</sup> It covers every aspect of radiologists and technicians day-to-day work in any digital radiology department. Modality, radiology information system(RIS)andpicturearchivingandcommunicationsystem(PACS)form the important component for reliable running of the radiology service. The concept of PACS was envisioned in 1980s by the members of radiology community and since then it has grown into a robust entity. In the last decade there have been numerous PACS installations worldwide. It greatly reduces the turn-around time which is the time interval between the acquisition and preparation of report. After the acquisition images are available instantaneously for the radiologists to report and the previous imaging studies can be prefetched for comparison. This increases the efficiency of the workflow in a department and deceases the manual filing and entries. Security issues are paramount regarding the patient data which is transferred across networks for various purposes. Security implementations are easier and robust in a digital environment than in analog environment because they provide application level security and tiered access to data. With digital environment, clinicians can place an order, it can be tracked and once the reports are ready they have access to both the image and report. This makes PACS and RIS more clinician friendly and helps them to efficiently use their time also. RIS and PACS are considered to the heart of a digital radiology department and because of numerous advantages and improvements in computer technology it is set to become more popular and the standard of care in near

future. Current industry standards and important aspects of PACS and RIS will be discussed in this chapter.

## PICTURE ARCHIVING AND COMMUNICATION SYSTEM

PACS is an acronym for picture archiving and communication system:

**Picture:** Referring to radiographic images and radiology reports.

**Archiving:** Referring to the film file or film jacket component of storing images.

**Communications:** Referencing multiple viewers of images and reports at virtually unlimited viewing sites called workstations.

**System:** Adopting the concept that a complex coordinated network makes it all possible.

The PACS is hardware and software that stores and manipulates digital information in the form of images and text data. It provides a modern radiology department with optimal storage of images and patient data files. It is also a digital centralized electronic storage system that provides easy access to images transmittable to any workstation on its network.<sup>3</sup>

There are several advantages claimed for PACS.

These include:

1. The increased efficiency of acquisition, viewing and reporting of images
2. Efficient data management, including fewer lost films
3. Cost savings
4. Space savings
5. Environmental benefits
6. Increased efficiency of retrieval of historical images

Potential disadvantages include:

1. High capital investment, and on-going costs (training, specialist staff and equipment, and so on)
2. The necessary infrastructure may not be available—PACS can place high demands on computer networks, and so it may be necessary to install a new network
3. The technical skills required for the support of a PACS may be in short supply.

The PACS is an important aspect in the digital radiology department which handles the images generated by various digital modalities and it is generally interfaced with RIS. PACS comprises of various components such as acquisition modalities, workstations, network and storage. The size of the storage, network bandwidth and number of workstations vary among institutions with around 50 GB of data are generated in larger institutions. Apart from the components of PACS, well trained information technology team with in-depth knowledge is also a requirement for the smooth running. But there are some basic aspects of PACS which the radiologists should know will be discussed here.

### Components and Architecture of PACS

Hurlen et al (2008) defined the properties of a PACS, as a system that typically acquire, store, transmit, display, and process digital images.<sup>4</sup>

On the basis of this definition the basic components can be separated into:

1. For acquiring and pre-processing of the images an image acquisition component is needed.

2. An archive server is composed of a database server or image manager, short-term and long-term storage, and a computer that controls the PACS workflow, known as a workflow manager.
3. Finally, to display the digital images, a viewing component is required, referred to as workstation.

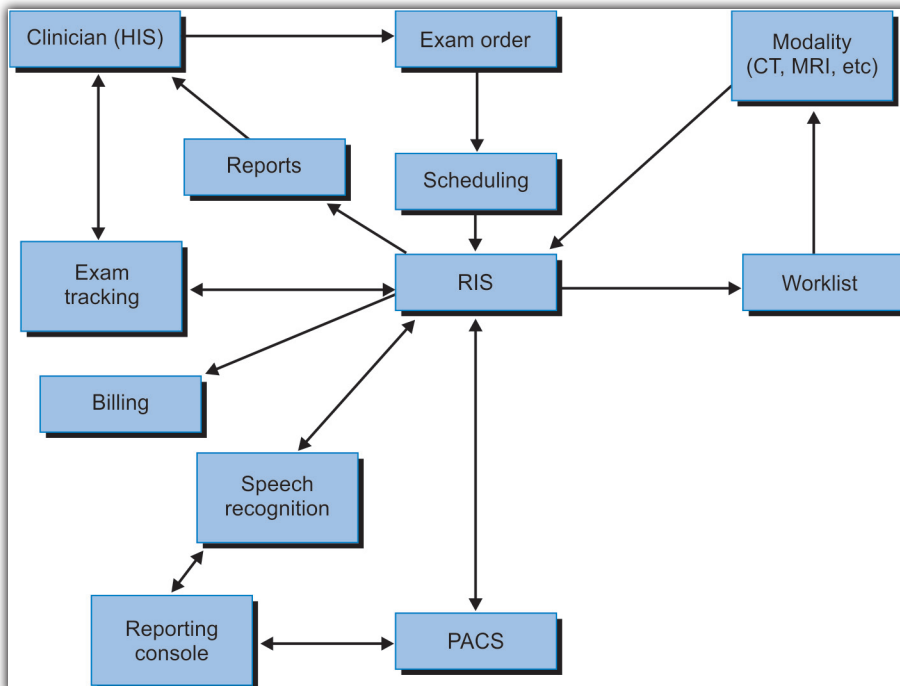
### Workflow

Workflow is a term simply means how a process is done, step by step. In radiology, the term *workflow* is used to describe how we complete an examination from order entry to transcribed report (**Flow chart 1**).

### Mini-PACS

A mini-PACS generally refers to a small-scale PACS, usually limited to one imaging modality or department. In a typical mini-PACS installation, one or more image acquisition devices of the same modality are connected to a local digital storage device, and one or two workstations are attached to the storage device, allowing retrieval and display of stored images.

A mini-PACS has some advantages and disadvantages over a full PACS. Advantages include the relatively low initial investment compared to a full PACS implementation, the possibility of a mini-PACS growing into a full PACS, and the chance for hospital staff to gain familiarity with PACS concepts. Disadvantages are centered on the fact that the benefits of a PACS are not fully realized—for example, if



**Flow chart 1** Workflow in a typical radiology department

images need to be viewed outside the area covered by the mini-PACS, film still needs to be printed.

### Teleradiology

Teleradiology can be defined as the ability to acquire a diagnostic image at one location and review it at a remote location, that remote location not being attached to the same local area network as the original image acquisition device. The basic components of a teleradiology system are the image acquisition and sending device, the network used to transfer the image data, and the receiving and viewing station.

Although there are many parallels between PACS and teleradiology, and in the equipment used to create PACS and teleradiology systems, there is a fundamental difference in the ultimate aim of the two systems: a PACS is designed to store image data and to transmit that data for display within an institution; a teleradiology system transmits image data to a remote location for diagnosis, but may or may not include an element of archive storage.

### Acquisition

Image acquisition forms the entry point for PACS data, so any error at this point will affect the entire process. Digital modalities like CT, MRI and digital radiography (DR) can directly send the images to PACS. Even in fully digital radiology departments there is a requirement for digitization of films coming from outside hospitals for comparison. This is done by digitizers which scan the films using visible light or laser and they are converted into digital format. Usually the output of these digitizers is in DICOM format which can be transmitted to PACS using DICOM interface. In computed radiography (CR) the existing conventional X-ray machine can be used along with photostimulable phosphor plates to generate digital images.

### Image Compression

Average radiology exam is (e.g: CT Head) = 20MB

#### *Types of image compression*

- Lossless compression - JPEG : 2:1 = 10 MB/Exam
- Lossy compression - Wavelet : 20:1 = 1 MB/Exam
- JPEG 2000:
  - Combines lossless techniques and lossy wavelet
  - Standards based on wavelet compression
  - DICOM approval of advanced compression by 2000

There are two types of compression (A) Lossy and (B) Lossless.

In lossy compression, the decompression of the image will not result in the original image. There will be an irreversible loss of image information during this process.

Using the lossless compression technique, which is a completely reversible process the original image can be obtained after decompression. This is the most preferred compression algorithm used in PACS.

### *Bits and Bytes*

Single bits are rarely seen alone in computers. They are almost always bundled together into 8-bit collections, and these collections are called bytes. In medical imaging devices (CT, MR, US, CR, etc.), typically references 8-bit, 10-bit or 12-bit Gray Scale images are encountered. This means each digital element of the image called a pixel, will be represented by 8-bit, 10-bit or 12-bit values.

- 1 bit = a light switch, ON or OFF, 0 or 1 (2 values)
- 1 byte = 8 bits '0000'0000' to '1111'1111' (256 values)
- 1 kilobyte (KB) = 1,000 bytes
- 1 megabyte (MB) = 1,000 KB
- 1 gigabyte (GB) = 1,000 MB
- 1 terabyte (TB) = 1,000 GB
- 1 petabyte (PB) = 1,000 TB

The word pixel stands for "picture element", and represents the smallest element in a digital image. A digital image is a 2-dimensional array of pixels that represent an image. For example, if we talk about a  $640 \times 480$  pixel image, it means that the image consists of 640 rows of pixels, with 480 pixels in each row. This would equate to a total of 307,200 total pixels ( $640 \times 480 = 307,200$ ), each having a separate grayscale or color intensity value (**Table 1**). As we decrease grayscale resolution from 12-bits (2 Bytes) to 8-bits (1 Byte), we are decreasing the level of subtle details that we will capture from the film, but the file size that has to be transferred is half the size due to the storage of 1 byte of data per pixel instead of the 2 bytes required for the 12-bit image (**Fig. 1**).<sup>5</sup>

### **Database Server**

The main PACS server holds a database of all patient examination information. This database includes details of patient demographics, and the examinations the patient has had since the PACS was installed (and possibly earlier examinations, if digitized). It also contains the information necessary for the PACS to be able to find the images for those examinations, and to direct copies of the images to local storage as required (depending on the architecture of the system). The server also performs routine scheduled tasks required for system maintenance, and allows the system administrator to carry out manual tasks and system tuning as required. The regularly scheduled tasks can include daily and/or weekly backups, pre-fetching of historical images for review purposes, "flushing" of the online storage. Manual tasks can include management of user accounts, reconciling discrepancies within the database, and managing interfaces with external information systems.<sup>5</sup>

**Table 1** Relationship between pixel size; bit depth and storage size

Array size	Total pixels	Storage size (Bytes)			
		8-bit image (1 byte/pixel)	10, 12 and 16-bit images (2 bytes/pixel)	24-bit image (3 bytes/pixel)	32-bit image (4 bytes/pixel)
256x256	= 65536	65536	131072	196608	262144
512x512	= 262144	262144	524288	786432	1048576
1024x1024	= 1048576	1048576	2097152	3145728	4191304
2048x2048	= 4194304	4194304	8388608	12582912	16777216
2048x2560	= 5242880	5242880	10485760	15728640	20971520
4096x5120	= 20971520	20971520	41943040	62914560	83886080

Note: Shaded cells represent the most common resolution/bit depth configurations

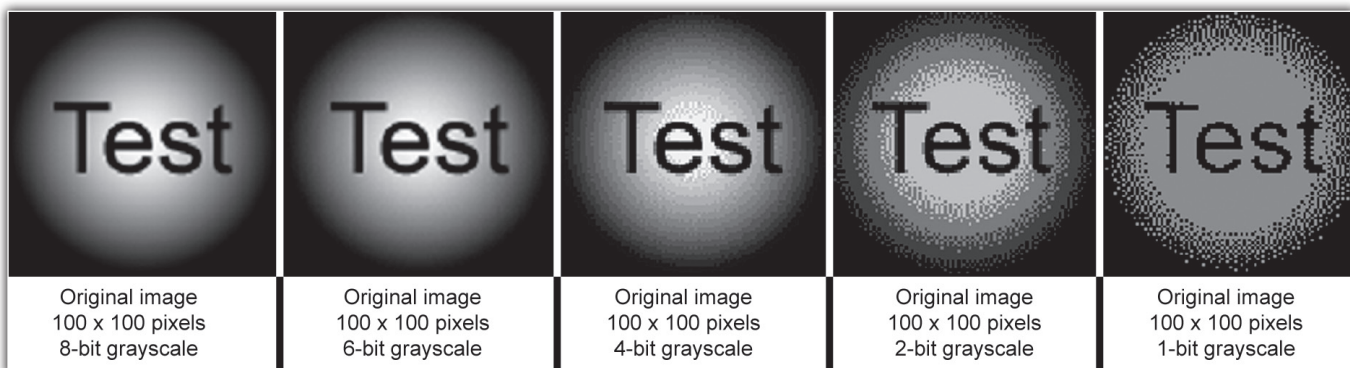


**Fig. 1** Diagrammatic representation on showing relationship between bit size and resolution of image

## Storage

### Data archive

Following acquisition, image data is likely to be stored on online, hard disk-based storage. The data may subsequently be saved on near-line or offline archive storage, which may be tape or disk based.

Archiving can be online, near-line or offline depending on the availability of data. Usually hard drive is used for online storage and data in online storage is readily available and it can be accessed almost immediately. Tapes and optical media which are loaded automatically by juke-box are called as near-line storage.<sup>6</sup> In near-line storage, data is available in less than a minute. In offline storage data is loaded manually and the loading time may vary. Some authors discourage the use of the term near-line.<sup>2</sup> This multi-tier system is used because the cost factor involved in online storage. But the cost of hard drives have been decreasing day by day so the use of offline storage should be reduced as far as possible mainly because of the manual intervention and the errors associated with it.

Another method is to store the data in a long-term archive in addition to PACS. In this case the data is stored permanently and available in long term archive even when the study is not

available online. Availability of imaging data used in health care is very critical so it is also sometimes recommended to store a copy of data in a different geographical location which is called as disaster recovery.

The amount of storage needed for a department should be calculated based on the number and types of imaging studies done and also the time duration for which they are kept in archive. Another consideration in choosing an appropriate storage is that it should be a robust and viable technology and should be upgradable in future. Any storage technology can fail so it is very important to have a failover mechanism especially in health care services. This is typically done by creating redundant copies so that even if a storage medium fails data can be recovered from another medium.

In order to calculate the archive storage requirements for a PACS, the data on the typical image sizes for each modality can be used. For each modality, multiply the typical image size by the average number of images per exam, and multiply this figure by the number of examinations performed in a year. This will give the annual storage requirements. This figure can be modified according to the amount of compression to be used on the data.

- 280,000 exams = ~ 5.6 Terabytes/year

### Storage Hardware

The most common types of hardware used to provide storage solutions are those using magnetic and optical technologies. This can be further broken down into disk and tape technologies.

#### Disk-based storage

**Redundant array of inexpensive disks:** The redundant array of inexpensive disks (RAID) was devised at the University of California in the late 1980s as a solution to the cost of large hard disks.

The RAID is a popular technology employed in PACS and is exclusively used for online storage. Instead of using a single large hard disk to provide the required storage capacity, the RAID uses a number of smaller, cheaper disks to provide, in total, the same storage capacity. The RAID is a disk system that allows online access to the data and can provide fault tolerance and redundancy through the use of data striping and data mirroring. The functioning of this array of hard drives as a unit is controlled by the RAID controller. Since data is stored in multiple hard drives recovery of data possible when there is a failure.

**Data striping:** This technique spreads the blocks of each file across multiple disks but provides no redundancy of the data. Each file is separated into fixed sized blocks, or stripe units, and striped across multiple disks in a "Round Robin" manner. However, the use of this striping provides no redundancy of the data. Round Robin is a scheduling algorithm in which processes are activated in a fixed cyclic order.

**Data mirroring:** A technique in which data is written to two duplicate disks simultaneously hence providing redundancy in the system. If one of the disk drives fails, the system can instantly switch to the other disk without any loss of data or service. The disadvantage of data mirroring is that there is no increase in speed of access with a higher cost and double the capacity being required. Disk mirroring is used commonly in online database systems, where it is critical that the data be accessible at all times.

**RAID levels:** There are number of different RAID "levels," each providing differing amounts of speed of access and fault tolerance. The most common are level 0, level 3, and level 5.

The various levels are defined as:

- **Level 0:** Provides data stripping. This improves data transfer performance but does not deliver fault tolerance or redundancy.
- **Level 1:** Provides disk mirroring. This data transfer is similar to a single disk and provides redundancy in the system.
- **Level 2:** Bits (rather than bytes or groups of bytes) are interleaved across multiple disks. Although this has high transfer rates, it is rarely used.
- **Level 3:** Same as Level 0, but also reserves one dedicated disk for error correction data. It provides good performance and some level of fault tolerance.

- **Level 4:** Similar to Level 3, but manages disks independently rather than in unison. Not often used.
- **Level 5:** Provides data striping at the byte level and also stripe error correction information. This results in excellent performance and good fault tolerance.
- **Level 6:** Highest reliability, but not widely used. Similar to RAID 5, but does two different parity computations or the same computation on overlapping subsets of the data.

The access capability should be able to withstand disk failure and can have the facility to reconstruct the data from a failed disk.

**Digital versatile disk (DVD):** This is a form of storage media which uses a similar technology to CD-ROM. However it has a more efficient recording algorithm. Digital versatile disks (DVDs) come in several formats: they can be dual sided, and they can have multiple layers, which in turn allows for an increase in storage capacity. DVD has the ability to store large amounts of data, up to 4.7 GB per side for single sided, single layer disks.

**Magneto optical disk (MOD):** A type of disk that combines magnetic disk technologies with CD-ROM technologies. The Magneto optical disk (MOD) uses a laser to read the disk and a laser and magnet to write to the disk using the magneto-optical effect. A double-sided disk can store up to 9.1 GB of data.

#### Tape storage

There are many tape formats used for near-line and offline storage.

**Advanced intelligent tape:** Advanced intelligent tape (AIT) comes in two formats, AIT-2 and AIT-3, which can store 50 and 100 GB respectively, with a data transfer rate of 12 MB/sec for the AIT-3. The advantage of this technology over other tapes is the in-built chip in the tape housing, which holds indexing information of the data stored on the tape. This facilitates fast retrieval of data, since it is not necessary to read indexing information from the tape in order to locate the required data. This also allows for less wear and tear on the tape as limited searching through the tape is required to retrieve the data.

**Jukebox:** The media used in archive storage are housed in a device known as a jukebox. A jukebox can contain one of many types of media (CD-ROM, tape or disks). The jukebox moves the media from its storage location, by means of a robot or carousel, to a reading/writing area; the time for this movement of disk to read is usually in the order of 10 to 30 seconds.

#### SAN vs NAS

Although the names sound similar, each storage technology is different.

NAS stands for **Network Attached Storage**

SAN stands for **Storage Area Network**.

### NAS unit

A NAS is a unit that typically has multiple hard drives. The drives are then arranged in a RAID configuration to prevent against data loss due to hardware failure. Then, an operating system is embedded in the NAS unit to perform all of the file operations, sharing, network communication, etc. Most NAS units are connected to your network via IP and can be managed through a web interface. The embedded operating system allows the unit to create users, shares, permissions, and sometimes even act as an FTP (file transfer protocol) server to allow the access of files via the internet.

NAS units offer better sharing capabilities between different operating systems such as Windows and MAC due to the different file access methods in the embedded NAS operating system. NAS units also offer many additional features, such as automated backup., bit torrent downloading, file quotas, and print sharing.

### SAN unit

SAN units are also comprised of multiple disks configured in RAID to protect against data loss due to hardware failure. SAN units typically use higher end hard disks that spin between 10,000 RPM and 15,000 RPM for increased performance. SAN units do not have any type of embedded operating system, SANs deal with data on the block level. This means that in order to utilize a SAN in your environment, it has to be attached to a host or multiple host machines. SANs connect to their host machine via a Fibre Channel. The host machine controls the file operations, sharing, permissions, etc. Typically, SANs are used in enterprise environments or in environments where fast input-output operations are required.

SAN units usually offer larger storage capacities due to the amount of physical hard drives they support. Also, data read and write speeds are faster in part due to the Fibre Channel link between the host server and the unit as well as the high end hard drive speeds.

### Which is best NAS or SAN?

Choosing the right storage unit can be tricky. A NAS is a good choice if your organization is looking to create a centralized file storage system or your organization just needs some extra file storage. If you are a larger enterprise and larger storage requirements as well as read write performance are necessary, then it may be wise to invest in a SAN over a NAS.

## Workstation

It is the interactive component of PACS where the radiologists interpret and generate a report. It is the responsibility of the radiologist to ensure the image quality which necessitates the radiologists to understand the basics of hardware. A typical workstation comprises display monitors, computer, local storage which is connected by network cables. The computer should have enough computing power in the order of 3 MHz or above, more and faster random access memory

(RAM) to do 3D rendering of large CT and MRI data sets.<sup>1</sup> In advanced workstation used for cardiac and vascular studies dedicated video graphics card is usually present to improve the performance.

### Display Monitors

For radiologists basic knowledge of display monitors is very important. Cathode ray tube (CRT) monitors utilize older technology which has been used in televisions for decades and they are relatively cheaper. Liquid crystal display (LCD) is a newer technology which is relatively expensive. However, the LCD technology has been improved to match the quality of best CRT monitors and they are becoming cheaper. It is expected that in near future LCD monitors will replace CRT monitors. Compared to CRT the advantages of LCD monitors are:

- a. Thin and light weight
- b. Less power consumption
- c. Brightness of display
- d. Flat surface
- e. Aspect ratio is maintained.

One disadvantage of LCD monitor which is worth mentioning is that it has narrow viewing angle than CRT monitors.

### Resolution

Spatial resolution of monitors is expressed in megapixels which is the number of million pixels. Very high resolution monitors are expensive and they are slow to respond. So it is important to choose the resolution of monitors for the type of usage and workstation requirements.<sup>2</sup> For modalities like US, CT and MRI which have fixed matrix size can be viewed optimally in 2 megapixel monitors. Radiographs pose a problem because they have very high resolution which is usually more than the resolution of display monitors. One approach is to down sample the original image and it is displayed at a lower resolution in the monitor. Although finer details are lost in the process of down sampling it has been shown that resolution of more than 2 to 3 megapixels has no significant improvement in diagnostic accuracy.<sup>7</sup> Another approach is with lower resolution monitors the image can be zoomed and panned so that the finer details are visualized. Visualization of microcalcification is very critical in mammography and it demands for higher resolution monitors. Monitors with 5 megapixel resolution are recommended for mammography interpretation.<sup>2</sup>

### Color and Gray-Scale display

Most of the radiological images are in gray scale although Doppler, PET, nuclear medicine images used colors. Color LCD monitors are very good in displaying color images. The quality of display of gray scale monitor is superior to the corresponding color monitors because the images are blurred and less bright in color monitor. Color monitor is also

expensive than the gray scale monitor which is also a reason for increasing usage of gray scale monitors in many radiology departments. Lower resolution color monitors are used for viewing colored images whereas gray scale monitors are used to view high resolution images. Typically, one low resolution color monitor and two high resolution gray scale monitors are used in workstations.

### *Radiologist Reading Stations*

The radiologist reading station is used by a radiologist when making a primary diagnosis. The reading station has the highest quality hardware, including the best monitor. The computer hardware meet the needs of the PACS vendor, but it will usually be very robust, requiring little downtime. The keyboard and mouse can be customized. There are many different styles of mice available that can increase the efficiency of the software being used.

There is generally access to a nearby RIS, with a dictation system near or even connected to the PACS station. Many PACS have software that integrates the RIS and dictation system.

### *Physician Review Stations*

The physician review workstations is a step-down model of the radiologist reading station. Many vendors use the same level of software but may eliminate some of the more advanced functions. One of the most important features on a physician review station is the ability to view current and previous reports along with images.

### *Network*

Network is another important component which transmits data from one place to other. Four important factors to be considered while setting up a PACS network are (a) performance or the speed of the network, (b) reliability, (c) upgradability and (d) the cost involved. The workstations or computers used by radiologists to report are usually clients which are connected to a server. Clients get data from the server based on various queries. Typically there are many clients connected to a server by means of network cables. There are various equipment in a network such as router, switch which are used to manage the network and use the bandwidth efficiently. This kind of connections between computers with in a hospital is called as local area network (LAN). This can be a wired network using cables or a wireless network. Usually wired network is preferred because of its performance, reliability and security reasons. When multiple LANs are connected it is called as wide area network (WAN). Performance of the network and the reliability depends on how it is managed which necessitates the requirement of trained personnel in the department. Network and error logs need to be checked on daily basis to ensure smooth running of network. Another technology which is virtual private network

(VPN) is commonly used nowadays to view the images from anywhere in the world using the internet infrastructure. One of the problems in transmitting the images outside the hospital is lack of control and security over the transmitted data. Using this VPN protocol the internet infrastructure is tunnelled and used to reach the hospital LAN. This protocol ensures security of the transmitted data though the data is transmitted across various public networks. This also enables the radiologists to use all the facilities in the hospital LAN as if there are within the LAN. Users are given username and passwords and their privileges are set-up so that the data is secured in the network and it is not misused. Also, numerous network and PACS configurations are possible such as certain information will be accessed by certain people.

It is very important to have a dedicated network for PACS and it should not be shared with other non-PACS network. This will ensure proper functioning and reduce congestion in the network. When many users are using the network simultaneously it will cause congestion and network will be slow to respond which can occur even in high bandwidth networks. To avoid this problem to some extent, there are techniques to compress the image which will reduce the network load.

### *System Architecture*

System architecture can be defined as the hardware and software infrastructure of a computer system. In a PACS, the system architecture normally consists of acquisition devices, storage, display workstations, and an image management system. The following discussion outlines three common PACS architectures and takes a look at the flow of images after acquisition.

### *Client/Server-based Systems*

In a client/server-based system, images are sent directly to the archive server after acquisition and are centrally located. The display workstation functions as a client of the archive server and accesses images based on a centralized worklist that is generated at the archive server. The health care worker at the display workstation chooses a name from the central list, and the archive server sends the image data to display station. Once the "client's session" is finished, the image data is flushed from its memory. Most systems allow basic image manipulation at the display workstation or "client," and the changes are saved on the archive server.

### *Advantages*

Any examination sent to the PACS is available anywhere without other interventions. Only one person can open the study with the intent to read it. Others that open the study will receive a message that the study is open and being read. There is no need to pull or send historic images to a particular workstation because the old studies are available along with the new studies on the archive.

### *Disadvantages*

The archive server is seen as a single point of failure. If the archive goes down, the entire system is down, and no image movement can take place. All newly acquired images must remain at the modality until the archive is up and can again receive the images.

The system is heavily network dependent. The images are flying back and forth between the archive and the workstations, and the network can become bogged down because of the large volume of data being moved. The archive server is handling many requests at once and can become bottlenecked because of the high volume of requests.

### *Distributed Systems*

In a distributed or stand-alone system, the acquisition modalities send the images to a designated reading station and possibly to review stations, depending on where the order originated (i.e. ICU or ER). In some systems, the images are sent from the modality to the archive server, and the archive server distributes the images to the designated workstation. The reading station designations may be designed based on radiologist reading preferences. For example, MRI may be sent to one station and CT to another, or all cross-sectional neurological images may be sent to one station but all body imaging are sent to another. The designation is decided after extensive workflow observation. Moreover, in a distributed model, the workstations can query and retrieve images from the archive. All images are then stored locally and then are sent to the archive server after they have been read. These images remain on the local hard drive of the workstation until they are deleted either by a user or by system rules.

### *Advantages*

If the archive server goes down, local reading at the workstations is not interrupted, other than not being able to get historic images. After the archive comes backup, the images that have been changed and signed off by the radiologist will be forwarded automatically to the archive to be saved. Because the images can be distributed to many locations at once, copies of an examination exist at various locations. Therefore it is less likely that PACS data will be lost. The system is less dependent on the network for its speed. The user can be working on one examination while the workstation is pulling and getting the next examination ready to be read. The workstation can fetch historic images according to rules the user sets up.

### *Disadvantages*

There is heavy reliance on the assumption that the distribution of images is being done correctly. If the distribution is wrong, the prefetching of historic examinations will not be correct either. Each workstation has a different worklist, and therefore only one person can be working on that list at a time. It can be inconvenient to read additional studies; the

radiologist would have to move to another workstation to read the images designated for that workstation. The users must depend on the query-and-retrieve function when nonscheduled examinations arrive at the workstation to be read.

It is also possible for two radiologists to be reading the same examination and not knowing until they try to start dictation. The paper requisition is very important with this type of PACS.

### *Web-based Systems*

A web-based system is very similar to a client/server system in how data flow. The significant difference is that both the images and the application software for the client display are held centrally. In a client/server system, the client still has application software locally loaded to the client, and only the images are held at the archive.

### *Advantages*

The hardware at the client can be anything that will support an appropriate web browser. This allows for greater flexibility with hardware but can also be a disadvantage because image displays (monitors) may not be able to support diagnostic quality. The same application can be used on site and at home in teleradiology situations. Teleradiology is a term used to describe the reading of images outside the hospitals walls. It can be down the road at the radiologist's home or on the other side of the world during night-time hours.

### *Disadvantages*

The system's functionality may be limited because the software is not installed locally. The bandwidth of the network connection limits the amount of data that can be transmitted for download, and some programs are too large to be transmitted over the network that is installed. As with client/server systems, the network is the biggest obstacle to performance.

### *Related Applications*

Apart from RIS and PACS, radiologists also commonly use various applications and software which can make the interpretation of images easier, to do advanced postprocessing and generating reports in quicker and easier way. Some of the commonly used applications are discussed here.

### *Three dimensional and advanced viewing*

In the modern era of imaging thin high resolution images are routinely acquired and they are utilized in three dimensional (3D) reconstructions. Many currently available commercial applications can provide a range of 3D reconstructions such as maximum intensity projection (MIP), surface shaded display (SSD) and volume rendering technique (VRT), etc. These techniques help the radiologists to make use of the fullest potential of the modality. Curved reconstructions

and VRT used to be a time consuming exercise but now these processes are automated by a click of a button. Other postprocessing techniques such as virtual bronchoscopy and colonoscopy can provide virtual endoluminal view. Modern workstations are also equipped with advanced postprocessing applications such as dual energy applications and computer aided detection (CAD).

With the emerging technology of dual energy CT, various postprocessing applications are available to decompose the image based on the material density. In this way it is possible to generate iodine only image and virtual noncontrast scans. Spectral imaging is also possible in which the keV can be changed by the user and image is processed by the workstation according to the selected keV. This processing can be useful in studying the material characteristics over a range of photon energies. The clinical application of this technique is in differentiating hyperdensity because of bleed from contrast enhancement in postcontrast scans.

Computer aided detection is a technique in which the computer will analyze the image to show the region of interest based on predefined rules. Those areas will be again analyzed by the radiologist to come to a conclusion. This method has been applied in mammography, lung nodule detection and polyp detection. Advanced segmentation algorithms are available nowadays which can be useful in determining the volume of tumor or any solid organ. This can be very useful in determining the response evaluation of tumors.

#### *Speech recognition*

Report generation is a time consuming process if it involves typing of the report. Speech recognition software is aimed at reducing the time delay involved in typing a report. Various attempts were made since 1980s to device a robust speech recognition software.<sup>6</sup> But the earlier applications suffered many setbacks because of poor accuracy and inability to adapt to the accent of the radiologists. Various improvements have been made since then and the currently available speech recognition applications are robust enough to adapt itself to the accent of user and it has in-built spelling check which includes words used in radiology. In addition, it has seamless integration with the PACS software.

#### **Industry Standards**

Earlier, transmission of textual or image data across network used to be very difficult because the differences in the vendor, operating system and the application environment. To facilitate free flow of information across modalities and networks in health care industry standards have been developed. By this way, images and data from various vendors can be handled in an organized manner. Currently, Health Level 7 (HL7) is the industry standard for the transmission of textual information and digital imaging and communications in medicine (DICOM) is the industry standard for the image data and communication protocols. Vendors have quickly

adopted these standards and because of their conformance to these standards it is possible to seamlessly transmit data across hospital information system (HIS), RIS and PACS and even between hospitals.

#### *HL7 (Health Level Seven International)*

HL7 is an international community of healthcare subject matter experts and information technology scientists collaborating to create standards for the exchange, management and integration of electronic health care information. HL7 standard was established in 1984 by a committee formed by the vendors and the users. It established the standard of exchange of electronic information in health care. It uses the highest level which is the application layer in open systems interconnection (OSI) model and it is independent of other lower layers. The information is exchanged as messages in HL7 format. Whenever there is an event such as admission, discharge or transfer, HIS sends a message containing key details RIS parses the message and updates its database. RIS can also send messages in HL7 format to PACS carrying key information. HL7 has been improved and updated thereafter in versions 2 and 3.

**Digital imaging and communications in medicine (DICOM):** It is a standard for handling, storing, printing, and transmitting information in medical imaging. It was also necessary to standardize the format of images and communication protocols used in imaging so as to facilitate flow of information across the hospital regardless of the vendors involved. A standard was developed together by American College of Radiology (ACR) and National Electrical Manufacturers Association (NEMA) to promote exchange of information among equipment from various vendors. This was aimed to integrate various equipment used in radiology such as radiography machines, CT scanners, MRI, printers, digitizers, etc. with PACS. The first version was released in 1985 and it was called as ACR-NEMA version 1. Later in 1988, the second version namely ACR-NEMA 2.0 was also released with enhancements. In 1992, a newer version was released with major improvements and it was named as DICOM 3.0.<sup>6</sup>

#### **RADIOLOGY INFORMATION SYSTEM**

In the modern digital radiology department radiology information system (RIS) forms the backbone which controls almost all aspects of radiology workflow. The RIS drives the workflow and transfer of information across the department. It deals with nonimage text based computing functions such as scheduling of an appointment, generation of worklist, order tracking, billing and reporting.<sup>5</sup> Scheduling can be done from RIS or the orders can come from HIS. RIS is responsible for collecting the patient demographic data and it will send it to the modality where it is needed in the form of worklist. The modality can use the worklist and proceed with the acquisition. In this way manual entry of patient data in the modality is avoided since manual data entry

is the common cause of error. The accuracy of the patient data is very important so that the older imaging studies can be automatically prefetched from the archive and to enable correctness in the billing procedure. Pre-fetching of images can be done from the long term storage (LTS) or list of patients can be generated which is to be taken out manually from the record room. The scheduling can be done automatically by the software based on the set of rules or manually. Once the scheduling is done the status of the exam can be tracked till the generation of the report.

After the scheduling, RIS will prepare the worklist and provide necessary data to the radiologist and technician who will perform the exam in the modality. This worklist can be either in paper format or electronic format. Besides the patient data and the clinical information it will also provide information regarding the patients ambulatory condition, sensitivity to drugs and contrast, etc. which is important in proper completion of the exam. Since the patient data is fetched electronically by the modality there is no scope for manual entry errors. Once the study is completed the images are sent to PACS and then RIS and PACS will interact to validate the available image information by matching with the order placed. Then RIS will generate a list of studies and will send

it to appropriate specialty or radiologist in the department. The reports are then sent to the destined department and that is available for viewing and it will also update the billing department of the hospital. RIS archives the order, exam data and report. Thus, RIS controls the workflow in the radiology department.

## REFERENCES

1. Branstetter BF 4th. Basics of imaging informatics. Part 1. Radiology. 2007;243(3):656-67.
2. Hersh WR. Medical informatics. JAMA: the journal of the American Medical Association. 2002;288(16):1955-8.
3. Keith J Dreyer, Amit Mehta, James H Thrall (Eds). PACS – A Guide to the Digital Revolution, (New York: Springer-Verlag, 2002) ISBN 0-387-95291-8.
4. Hurlen P, Stbye T, Borthne A, Gulbrandsen P. 2008. Introducing PACS to the Late Majority. A Longitudinal Study. Journal of Digital Imaging Online.
5. Huang HK (Ed). PACS: Basic Principles and Applications (Wiley-Liss, New York, 1999), ISBN 0471-25393-6.
6. Mildnerger P, Eichelberg M, Martin E. Introduction to the DICOM standard. European Radiology. 2002;12(4):920-7.
7. Simborg DW. The case for the HL7 standard. Comput Health. 1988;9(1):39-40.

## Chapter

# 22

# Evidence Based Radiology

*Sanjay Sharma, Manisha Jana*

## INTRODUCTION

Evidence-based medicine (EBM) is defined as the integration of best research evidence with clinical expertise and patients' values and expectations.<sup>1-3</sup> Dr Guyatt and Dr Sackett, from the Evidence-based Medicine Working Group at McMaster University, Ontario, Canada, are the pioneers of EBM in modern clinical practice and first coined this term.<sup>4</sup> For proper understanding of EBM, all three of its basic constituents must be imbibed. Best research evidence implies clinically relevant research (which has been properly validated), in the field of diagnostic or therapeutic practice. Clinical expertise depends on the decision making ability and expertise in treatment, based on one's clinical knowledge, experience and skill.

This chapter includes the overview of evolution, types, components, strength and caveats of Evidence-based Practice (EBP) in our daily lives.

## BACKGROUND

The practice of medicine has hitherto remained 'eminence based' that is, based on individual experience and expertise.<sup>3</sup> According to Fieldland,<sup>5</sup> the basic assumptions of this traditional medical practice are as follows:

1. The measure of authority is proportional to the weight of individual experience.
2. Understanding patho-physiology forms the foundation for clinical practice.
3. Conventional medical training and common sense are enough to enable a physician to evaluate new tests and treatments.
4. Clinical experience and expertise in a given subject area are enough for the physician to develop clinical practice guidelines.

Traditional 'eminence based practice' is more didactic, based on individual expertise and does not always take into consideration the existing best research evidence. This is where the proponents of EBP differ from traditional practice. The foundation of EBP rests upon the proper use of validated research evidence (e.g. meta analysis, randomized controlled trials) to support one's clinical decision in diagnostic procedures, interventions and therapy. In no way it undermines the importance of individual knowledge or patho-physiology of disease.<sup>6</sup>

## Why Evidence-based Practice?

The growing awareness and practice of EBP worldwide can be explained by a few basic needs in healthcare services. Firstly, with the ever-increasing number of newer disease entities, the physician needs to be constantly updating himself about the diagnosis, prognosis and treatment of the disease.<sup>7</sup> In this respect the conventional text books as a resource often prove inadequate.<sup>8</sup> Also searching for the desired data from the deluge of available medical journals is practically impossible for a busy medical practitioner, owing to the lack of time.<sup>9,10</sup> Secondly, the improved clinical skills in an experienced professional very often coexists with a declining up-to-date knowledge.<sup>11</sup> This forms an increasing 'knowledge gap' among the practitioners. In clinical practice, the knowledge of healthcare workers forms the backbone of the clinical decision making. The 'knowledge gaps' appear when the healthcare provider's knowledge is insufficient to meet the need of the patient.<sup>3,12</sup> The gap can be in 'background knowledge' i.e. general information regarding a disease or treatment; or 'foreground knowledge' which pertains to the latest information regarding the disease condition, any new

diagnostic test or intervention.<sup>3</sup> The 'background knowledge' is usually obtained from books and well established texts, e.g. radiological anatomy and procedures for radiologists. 'Background knowledge' gaps can be encountered in rare diseases or an uncommonly performed procedure.<sup>3</sup> 'Foreground knowledge' gaps are more common. Sources of this type of knowledge lie in latest published literature. It becomes important for a practicing physician to identify the knowledge gap and be aware about where to search for the required evidence.<sup>13</sup>

The rising costs of healthcare make it imperative to justify the decision for any specific diagnostic test or treatment. Moreover, the freely available internet, effective search engines (MEDLINE, Pubmed, Google scholar, etc) and development of systematic reviews of the existing evidences in healthcare such as the 'Cochrane Collaboration' have made tracking any evidence easier,<sup>14</sup> further supporting the evidence based approach towards medical decisions. Archie Cochrane, a British epidemiologist, highlighted in 1972 that most treatment decisions were not based on systematic review of clinical research but on random selection of existing evidence or 'expert opinion'.<sup>15</sup> Cochrane collaboration is a non-profit organization consisting of volunteers all over the world who analyse the existing evidence and make the up-to-date evidence based information available.<sup>14</sup> Another reason for growing popularity of EBP is the development of evidence-based journals (e.g. *Evidence-based Medicine*) which contain systematic reviews, meta-analyses and evidence-based guidelines.<sup>16</sup>

### *Forms of Evidence-based Practice*

There are two forms of EBP, the 'top-down' and the 'bottom-up'.<sup>3,17</sup> The 'top-down' practice is usually carried out by experts working for a government, large centralized resource like Cochrane Collaboration or a professional body like American College of Radiology. However, what practitioners (clinician or radiologist) are more concerned in daily life is with the 'bottom-up' approach. 'Bottom-up' EBP starts from the practitioner who encounters a problem, asks an answerable question regarding the problem, searches for the best available evidence and applies it in his practice after critical appraisal. These two forms of EBP are not mutually exclusive, but complimentary.<sup>18</sup> In the following sections of this chapter, we have elaborated the steps of 'bottom-up' EBP.

### *'Bottom-Up' Evidence-based Practice*

As described earlier, bottom-up EBP is the more relevant to daily practice of a busy clinician or radiologist. The concept was started by David Sackett in 1996. These steps are listed in **Table 1**.

#### *Step 1: Ask*

The first step of 'bottom-up EBP' is asking a question, arising from either the background or foreground knowledge gap.

**Table 1** Steps of bottom-up EBP<sup>2,3</sup>

Step	Summary	Explanation
1.	Ask	Asking an answerable question
2.	Search	Searching for the best available research evidence
3.	Appraise	Critical appraisal of the evidences for validity and impact assessment
4.	Apply	Application of the evidence in practice
5.	Evaluate	Evaluation of efficacy and effectiveness of first 4 steps

It is the foreground question that is usually needed to be answered to address the clinical problem. The foreground questions usually have four components, patient, intervention, comparator and outcome (PICO)<sup>1,19</sup> (**Table 2**).

The questions in clinical practice can relate either to the etiology, risk factors, diagnosis or management of a certain entity. The radiologists in practice are more concerned with the diagnosis or management of a disease entity. While searching for the answers to a question, the practitioner should be aware of the kind of study to be looked for. For example, if a question relates to an etiology or risk factor, the ideal study design would be a randomized control trial (RCT), prospective cohort study or case control study. The questions related to disease frequency can be best answered by a prospective cohort study or a cross-sectional study. For questions related to diagnostic procedures, a cross-sectional study with consecutive or random sampling may be ideal. A cohort/survival study will be ideal to answer a question related to the disease prognosis; and therapy/intervention related questions can be better answered by a RCT or cohort study.<sup>3</sup>

While searching for evidence, one should be aware about the hierarchy of evidence.<sup>20,21</sup> The study designs are graded by the levels of evidence. On top of the hierarchy, are the systematic reviews of RCTs and cohort studies (Level 1a) which are considered the least biased evidences. Level 1b includes RCTs and cohort studies with good validation and follow-up. Hitherto considered a superior evidence, an 'expert opinion' is downgraded at level 5. The levels of evidence are tabulated below (**Table 3**).

In evidence-based radiology (EBR), when one searches for evidence, it must be valid and relevant. Since diagnostic imaging is not directly related to patient outcome and in view of the increasing cost of medical imaging, the technology assessment of an imaging tool has to be performed with assessment of some additional parameters.<sup>22</sup> The need for separate technology assessment also stems from the concern regarding risk of increased radiation exposure in the imaging modalities.<sup>22</sup> A conceptual framework of the technologic assessment was described by Thornbury,<sup>23</sup> McNeil et al<sup>24</sup> and later Fryback.<sup>22,25</sup> In short, the hierarchy of technical assessment deals with the following level:

**Table 2** Components of a question (PICO), illustrated by an example<sup>19</sup>

*Example:* How effective is CT pulmonary angiography in the detection of pulmonary embolism compared to ventilation-perfusion scan, in patients with suspected pulmonary embolism?

Component	Explanation	Example
Patient population/clinical problem (P)	Patient's clinical situation or the problem of interest	Patients with suspected pulmonary embolism
Intervention (I)	Main intervention, which can be an exposure, diagnostic procedure or a treatment in question	CT pulmonary angiography
Comparator (C)	Exposure, diagnostic test or treatment to which the main intervention is compared	Ventilation-perfusion scan
Outcome (O)	Result/outcome of interest	The accuracy in the diagnosis of pulmonary embolism

**Table 3** Levels/Hierarchy of evidence<sup>20,21</sup>

Level of evidence	Description
1a	Systematic review (with homogeneity) of level 1 diagnostic studies or a clinical decision rule with 1b studies from different clinical centers
1b	Independent blind comparison of an appropriate spectrum of consecutive patients, all of whom have undergone both the diagnostic test and the reference standard
1c	Diagnostic finding for which specificity is so high that positive result rules in the diagnosis or for which sensitivity is so high that negative result rules out the diagnosis
2a	Systematic review (with homogeneity) of level 2 diagnostic studies
2b	Independent blind comparison but either in nonconsecutive patients or confined to a narrow spectrum of study patients (or both), all of whom have undergone both the diagnostic test and the reference standard; or a clinical decision rule not validated by means of a test set
3a	Systematic review (with homogeneity) of studies with a level of 3b and better
3b	Nonconsecutive study or independent blind comparison of an appropriate spectrum, but reference standard not applied to all study patients
4	Reference standard not applied independently or not applied blindly
5	Expert opinion without explicit critical appraisal or based on physiology, bench research, or "first principles"

1. The technical efficacy.
2. Diagnostic accuracy (described by sensitivity, specificity, PPV, NPV).
3. Diagnostic thinking efficacy (the pre and post-test probability and likelihood ratios).
4. Therapeutic efficacy (whether the imaging modality can change the treatment decision).
5. Patient outcome efficacy (impact of the test on the patient).
6. Societal efficacy (the cost-effectiveness).

The statistical terms used are explained later in this chapter.<sup>22,25</sup>

#### Step 2. Search

Once the question is formulated, the next step in EBP is searching for the best evidence. For this, the practitioner needs to be aware of how and where to look for. As already described, the textbooks are a good source of background knowledge, but the foreground knowledge gap need latest

evidences, which can not usually be found in textbooks, as they may be already outdated by the time they are published. The most up-to date resources for the best evidences are the electronic resources (journals, search engines, information systems).<sup>3</sup> The common electronic resources are listed in **Table 4**.

**Radiologic electronic resources:** Unfortunately, there are limited available electronic resources providing information regarding diagnostic imaging modalities. Evidence based radiology website (<http://www.evidencebasedradiology.net>) was developed by the St Vincent's University hospital in Ireland and provides proper 5-step process of EBM. Critical appraisal worksheets and excel spread sheets can be downloaded to create graph of conditional probabilities.<sup>26,27</sup>

#### Step 3. Critically appraise

Once the proper evidences are available, one needs to assess them for validity and impact assessment. In routine practice, we

**Table 4** Electronic resources for EBM<sup>13</sup>

Name	Web Link
McMaster University Health Information Research Unit: Evidence Based Health Informatics	<a href="http://hiru.mcmaster.ca/hiru">http://hiru.mcmaster.ca/hiru</a>
Pubmed: US National Library of Medicine and National Institutes of Health	<a href="http://www.ncbi.nlm.nih.gov/sites/entrez">http://www.ncbi.nlm.nih.gov/sites/entrez</a>
Google Scholar	<a href="http://scholar.google.com">http://scholar.google.com</a>
MD Consult	<a href="http://www.mdconsult.com">http://www.mdconsult.com</a>
Cochrane Collaboration	<a href="http://www.cochrane.org">http://www.cochrane.org</a>
SUM Search	<a href="http://sumsearch.uthscsa.edu">http://sumsearch.uthscsa.edu</a>
American College of Physicians Journal Club	<a href="http://www.acpjc.org">http://www.acpjc.org</a>
British Medical Journal Evidence Based Medicine	<a href="http://ebm.bmj.com">http://ebm.bmj.com</a>
BMJ Clinical Evidence	<a href="http://clinicalevidence.bmj.com/ceweb">http://clinicalevidence.bmj.com/ceweb</a>
National Library of Medicine	<a href="http://www.nlm.nih.gov">http://www.nlm.nih.gov</a>
Center for Evidence-based Medicine at Oxford	<a href="http://www.cebm.net">http://www.cebm.net</a>
Center for Evidence-based Radiology at the Brigham and Women's hospital	<a href="http://www.brighamandwomens.org/cebi/default.aspx">http://www.brighamandwomens.org/cebi/default.aspx</a>

**Table 5** Assessment of validity of study in PICO format<sup>29</sup>

Questions PICO	Assessment RAMMbo	Possible error/bias	Ways to circumvent
Patient (P)- population in the study	Assessing for fair recruitment (R)	R Selection bias (the subjects are not representative of the population of interest), or Small study sample leading to imprecise results	Randomization or Consecutive recruitment  Increase the size of study population
Intervention (I)	How fairly were the subjects allocated (A) into groups? Whether equal management and follow-up were done (fair Maintenance) in both (except for the index test/ intervention)?	A Allocation bias (Lack of proper matching of subjects in the two groups, e.g. age, sex, etc.) Treatment bias  M	Randomization  Equal management in both the groups apart from the index test or intervention
Comparator (C)	Same as above	Same as above	
Outcome (O)	Assessing for fair Measurement – valid and unbiased outcome measurement	M b o Measurement bias	Double-blinding

tend to read an article without its proper critical appraisal. First step of critical appraisal of a primary research article (first-hand studies, such as RCT, experiments and survey) is the assessment of its validity, that is, whether the study is close to the truth and without bias.<sup>28</sup> The next step comprises of the impact assessment and applicability in one's own clinical practice.

1. **Validity assessment:** The simple steps for validity assessment of a study are searching for answers to the following questions:<sup>29</sup>
  - What is the PICO of this study and whether they are relevant in one's own clinical scenario?
  - How well was the study performed?
  - Can the results be due to chance (bias)?

Assessment of validity of a study by asking the PICO questions is done by following the steps described by an acronym **RAMMbo** (**Table 5**). It also describes the processes to eliminate bias at each step. While critically appraising any study, the practitioner must try to get answers to all these questions, in order to decide if the results of the study are trustworthy.

Additionally, while appraising the internal validity of a study describing any new diagnostic test, the following questions are to be answered.<sup>29</sup>

- Whether the test was evaluated on a group of patients similar to those on whom it is to be used in practice?

- Whether there was an independent reference standard for proper blinded comparison?
- Was the reference standard applied on all patients, independent of the test result?
- Was the test validated on a separate, independent group of patients?

In an ideal study, answers to all of the above questions should be 'yes'. After the internal validity and methodology assessment, if study comes out to be a proper blinded randomized study without bias, the results are to be assessed for their relevance. A statistically significant result is known by its p value. It is a measure of the probability that the result is purely by chance.<sup>28,30</sup> A p value of less than 0.05 is considered statistically significant. Confidence intervals (CI) are an estimate of the range of values that are likely to include the real value. Usually they are described with 95 percent CI values.<sup>28</sup> Studies with larger samples tend to have narrower CI and are therefore more reliable.<sup>31-33</sup>

## 2. Impact assessment:

- *Impact Assessment of Diagnostic Literature:* After assessment for validity, the study should be evaluated for its impact or strength, usually found in the 'result section'. The important statistical parameters to be considered are sensitivity, specificity (with 95% CI), positive predictive value, negative predictive value, positive likelihood ratio, negative likelihood ratio and how these affect the pre- and post-test probability.<sup>34</sup> For understanding these parameters, let us start with a contingency table (**Table 6**).

True positive indicates the persons who are having the disease and are correctly detected positive by the test and true negative indicates persons who do not have the disease and are correctly identified with the test. Sensitivity is a measure of how well a test can correctly identify the persons having a disease. Specificity is a measure of how well a test can detect the persons not having a disease. Sensitivity is closely related to a type II error/β (accepting a null hypothesis when it should have been rejected) and specificity is closely related to the type I error/α (rejecting a null hypothesis when it should have been accepted). Sensitivity and specificity, ideally, should be expressed with a 95 percent CI, which

gives a better estimate of precision. For example, if a study states a range of sensitivity and specificity with 95 percent CI, it means that if the study is repeated 100 times, the values of sensitivity and specificity will lie within the given range 95 percent of the times.<sup>31-33</sup>

**Likelihood ratios** (LR, positive and negative) reflect the discriminative power of a test.<sup>35</sup> Positive likelihood ratio (PLR) is the ratio of probability of a positive test result in a patient with disease to the probability of a positive test in a person without disease. Similarly, negative likelihood ratio (NLR) is the ratio of probability of a negative test in a person with disease to the probability of a negative test in a person without disease. A PLR >10 and NLR <0.1 is considered significant. A PLR of >10 is considered strongly positive, 2 to 5 moderately positive and 0.5 to 2 weakly positive. Similarly, NLR of <0.1 is considered strongly negative and 0.2 to 0.5 moderately or weakly negative.

**Pretest probability** is the likelihood that the person will have the disease in question even before the test is performed. It is usually decided by the prevalence of the disease and assessed by clinician without any mathematical analysis being involved (**Table 7**). The pretest probability is important for interpreting the results of a diagnostic test, comparing more than one test or deciding whether it is worth doing the test at all.<sup>34,36</sup> Once the pretest probability and likely ratios are known, the post-test probability can be calculated. If LR >1, the post-test probability will be higher than the pretest probability. It is the post-test probability that the practitioner is more concerned about while treating a patient. The concern is whether the test has altered the disease probability so that it now lies above the treatment threshold or below an exclusion threshold.<sup>37</sup> To calculate the post-test probability, one can multiply the pretest odds by the LR, or refer to the graph of conditional probability or Fagan's nomogram (**Fig. 1**).<sup>38-40</sup> Further details of these tools are beyond the scope of this chapter.

For better understanding, let us consider a situation relevant to a practicing radiologist. When a clinician questions whether it is prudent to perform a CT pulmonary angiography (CTPA) in a patient with suspected pulmonary thromboembolism (PTE), the radiologist needs to know the pretest probability of PTE, i.e. what according to the clinician is the risk of PTE in the given patient. The pretest probability of 50 percent means that the clinician thinks there is a 50 percent chance that the patient may have PTE. Now after proper literature search, he finds that the PLR of CTPA is 10 and NLR is 0.02. Consulting the Fagan's nomogram, he finds that the positive post-test probability is around 90 percent and negative

**Table 6** A 2 × 2 Contingency table describing outcome of a diagnostic test<sup>27</sup>

Test outcome	Disease	
	Present	Absent
Positive	True positive (TP)	False positive (FP)
Negative	False negative (FN)	True negative (TN)

**Table 7** Statistical jargon explained

Term	Mathematical expression/relationship	What does it imply for a diagnostic test
Sensitivity	$TP/TP+FN$	How well a test can identify patients with the disease
Specificity	$TN/ TN+FP$	How well a test can identify the persons without the disease
Positive predictive value	$TP/TP+FP$	
Negative predictive value	$TN/TN+FN$	
True positive rate	$TP/TP+FN$	Equivalent to sensitivity
True negative rate	$TN/TN+FP$	Equivalent to specificity
False positive rate	$FP/FP+TN$ or $1-\text{specificity}$	
False negative rate	$FN/FN+TP$ or $1-\text{sensitivity}$	
Power	$1-\text{false negative rate}$ or $= \text{sensitivity}$	Probability that the test will reject a false null hypothesis (i.e. it will not make a type II error) or The true positive detection rate
Accuracy	$TP+TN/TP+TN+FP+FN$ or True results/total population or $\text{Sensitivity} \times \text{prevalence} + (\text{Specificity}) / (1 - \text{prevalence})$ , provided the prevalence is known.	100 % accuracy implies that the test will rightly detect all patients with or without the disease in a given population
Prevalence	$TP+FN/ TP+FN+TN +FP$	
Positive likelihood ratio (PLR)	$\text{Sensitivity}/ (1-\text{specificity})$	High PLR implies that if the test result is positive there is a high chance that the disease will be present
Negative likelihood ratio (NLR)	$(1-\text{sensitivity})/ \text{specificity}$	Low NLR implies that if the test result is negative there is a high chance that the disease will be absent
Pretest odds	$\text{Prevalence} / (1-\text{prevalence})$	
Pretest probability	$\text{Patients with a disease}/ (\text{patients with a disease} + \text{patients without the disease})$	Represents the likelihood of a disease in subject, prior to investigation. Usually determined by clinicians based on the likelihood of the patient having a disease. Zero % pretest probability indicates that the patient in all probability will not have disease
Post-test odds	Pretest odds x likelihood ratio	Represents how confident a radiologist/ physician is that the patient will have the suspected disease, after performing the test in question. It increases if the pretest probability is high
Post-test probability	$\text{Post-test odds}/(\text{post-test odds}+1)$	
p value	Measurement of the probability that a result is purely by chance	Lower the p value, higher the probability that the observed result is statistically significant and not by chance

post-test probability of around 0.3 percent. This means the test can effectively rule in or rule out PTE, and, therefore, can be used.

- *Impact Assessment for Therapeutic Literature:* Critical appraisal for a therapeutic literature for

internal validity should be performed in similar ways as described before. For impact assessment of a therapeutic literature, the important statistical parameters are relative risk (RR), absolute risk reduction (ARR), relative risk reduction (RRR),

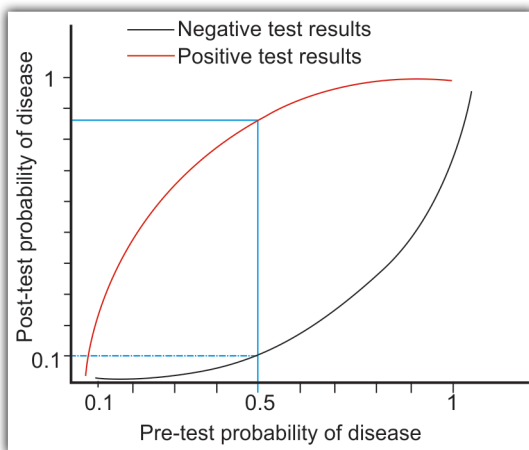


**Fig. 1** Graph of conditional probability of a test showing high sensitivity and high specificity. Here, for a pretest probability of 0.5, the post-test probability of a negative diagnostic test outcome is 0.1 and post-test probability of a positive test result is 0.85 (85%), which means the test can successfully 'rule out' the diagnosis as well as 'rules in' (confirm) the diagnosis

**Table 8** A  $2 \times 2$  Contingency table describing a therapeutic test outcome<sup>41</sup>

Exposure	Outcome of events		
	Yes	No	Total
Yes	Events in experimental group (a) EE	b	(a+b) Subjects in experimental group ES
No	Events in control group (c) CE	d	(c+d) Subjects in control group CS

absolute risk increase (ARI) or relative risk increase (RRI), number needed to treat (NNT) or number needed to harm (NNH) and odds ratio.<sup>41</sup>

For calculation of the above mentioned parameters, let us consider another contingency **Table 8**.

Relative risk means the risk of an event or developing a disease relative to exposure.<sup>41</sup> Mathematically, RR can be expressed as the ratio of risk in the treated/exposed group to the risk in the control group  $[(a/(a+b))/(c/(c+d))]$ . A relative risk  $>1$  implies increased risk in the exposed group. Absolute risk reduction is the difference in the event rate between treatment and control groups  $[(a/(a+b)) - (c/(c+d))]$ . Relative risk reduction is the difference in event rate between treatment and control groups, expressed as percentage ( $1-RR$ ). Another important parameter is the number needed to treat (NNT) which is the inverse of ARR. A lower NNT means that only a small number of patients are needed to be treated to get a desirable benefit in at least some of them.<sup>41-43</sup>

### Diagnostic Systematic Review and Meta-analysis:

Meta-analyses are statistical methods used to combine results from a number of different studies. A systematic review is a systematic assembly, critical appraisal, and synthesis of all relevant studies on a specific topic.<sup>44</sup> Over the last few decades, as the number of available diagnostic and screening tests have increased significantly, the need of systematic analysis of all the available literature has also increased. Some of these studies may have inherent biases in their design whereas others may be well conducted. Since there is a plethora of evidence, a summary of all the available evidences should be deducted from them. Meta-analysis model aims at estimating: (a) the summary sensitivity and specificity and/or summary ROC curves, and (b) common threats to the validity of the summary estimates.<sup>45-48</sup>

The steps involved in conducting a systematic review of a diagnostic test includes:

1. Finding the evidence
2. Assessing the study quality and applicability
3. Summarizing the evidence qualitatively and quantitatively (meta-analysis), and
4. Clinical interpretation and application in developing a recommendation.<sup>45</sup> Steps 1 and 2 have been discussed earlier. Discussion on the meta-analytical integration of evidence and the analysis is beyond the scope of this chapter. In the integration of diagnostic data, two or more paired statistics are taken into consideration viz. sensitivity and specificity, PPV and NPV, etc. Summary estimate of sensitivity and specificity of various studies can be derived from various methods, summary ROC curves, Forrest Plot, etc.

While pooling data for meta-analysis, 'publication bias' should be kept in mind. It refers to the association of the publication probability of a study to its statistical significance. A study showing positive or good statistical significance is more likely to get published. There are several methods to estimate publication bias in a meta-analysis, e.g. Funnel plot. For the detailed understanding of Funnel plot the readers are requested to refer to more detailed treatise.<sup>44</sup>

In the clinical interpretation of evidence related to a diagnostic test, the important step is to determine the post-test probability, using the Fagan's nomogram or a graph of conditional probability, as described above.

### Step 4. Apply

After proper critical appraisal of the available evidences, one should assess its applicability in the prevailing clinical context. This step can also be called 'external validation'.<sup>49</sup> Before applying the results in the individual patient, the following points should be considered.

1. Whether the diagnostic test/treatment are feasible in your existing set-up?
2. Are there any other feasible alternatives?
3. Are the patients in existing clinical scenario sufficiently similar to the subjects of the study?
4. Whether the diagnostic test is changing the pre-test probability?

(Here one needs to calculate the LR of a study, which can be calculated from sensitivity and specificity, vide supra. If the PLR of a study is >10 or NLR < 0.1, the test can significantly alter the pretest probability).

5. Consider the pros and cons of the diagnostic/or therapeutic test.

(It is particularly important when the test or treatment under consideration has side effect or a risk, e.g. radiation exposure in diagnostic CT. In such cases, the risks associated with the test/treatment can be outweighed by the risk of the disease).<sup>50</sup>

6. Must take into consideration the patient's opinion.

#### *Step 5. Evaluate*

The last step is to evaluate your results in clinical practice, after going through all the four previous steps. This can be performed by evaluating the efficiency in executing all the four steps, and taking initiative to improve them.

#### *How does Evidence-based Radiology differ from Evidence-based Medicine?*

Since Radiology is a technology based subject, the practice of EBR differs from that of EBM in a few additional points under the step 'critical appraisal'. The additional five questions to be asked when assessing any imaging modality are as follows:<sup>51</sup>

1. Has the imaging methodology been described in sufficient detail to allow to reproduce the study in your own department?
2. Has the reference (gold standard) and the imaging test under evaluation been performed to the same standards of excellence?
3. Have technology development within the same modality been adequately considered in the study design and discussion?
4. Has the issue of radiation exposure been considered?
5. How were the MRI/CT images reviewed, on hard copy images or on a monitor?

#### *Limitations of Evidence-based Practice*

While the proposers of EBP see it as a tool of paradigm shift in the clinical decision-making, the critics suggest that it should be considered as an additional tool in the existing practice, giving importance to the other alternate forms of clinical practice also. They criticize the 'bottom-up EBP' for being time-consuming and not practically feasible in daily clinical practice. While EBP necessitates the convergence of various modalities and enhances multimodality practice, it is

often seen as unhelpful. Some also believe that it is unproven, threatens professional autonomy and narrows the research agenda.<sup>52,17</sup>

#### *How can a Radiologist Practice EBR in his or her daily life?*

1. **In justifying a new diagnostic test:** When confronted to a question about performing a new diagnostic test in a patient, follow the previously stated five steps of EBP. It can help the radiologist in deciding whether the test is going to change the pretest probability so as to establish or exclude the diagnosis.
2. **While studying an article, critically appraising it** (as described above) before applying its recommendations in your practice. Most radiology articles lack in proper statistical analysis and the information needed to assess validity is inadequate. Consolidated standards of reporting trials (CONSORT)<sup>53</sup> and the standards for reporting of diagnostic accuracy (STARD)<sup>54</sup> are two initiatives to improve the reporting of clinical trials and studies of diagnostic accuracy. While studying any article, the radiologist should test them using the STARD or CONSORT criteria. One can use the proper format for critical appraisal of a diagnostic literature (available at <http://www.srs-mcmaster.ca>). In this manner, knowing the strength and weakness of the existing literature can help the radiologist to plan a proper study in a specific field.
3. **Applying principles of EBR in academic activities:** While presenting an article in a departmental Journal Club, a radiology resident could critically appraise it in the proper format, check for adequacy of the STARD criteria and summarize the strength and caveats of the article. This will help to spread the practice of EBR among the fellow colleagues.

## CONCLUSION

To conclude, evidence based practice in radiology is a relatively new concept with its own advantages and limitations. Every radiologist should be aware of its concept and be able to apply it in their daily practice. In practice, clinical decision making remains a combination of 'expert opinion,' critical appraisal of the existing evidence and the judgment of the practitioner. A perfect balance between them can bring out the best patient care.

## REFERENCES

1. Strauss SE, Rosenberg W, Glasziou P, et al. Introduction, in Evidence Based Medicine: How to Practice and Teach EBM 3rd edn. Churchill Livingstone, Edinburgh, Elsevier. 2005. pp.1-12.
2. Sackett DL, Rosenberg WM, Gray JA, et al. Evidence based medicine: what it is and what it isn't. BMJ. 1996;312:71-2.
3. Guyatt Kelly Am. Evidence based practice: an introduction and overview. Semin in Roentgenol. 2009;43:131-9.

4. Guyatt G, Cairns J, Churchill D, et al. Evidence-based medicine, a new approach to teaching the practice of medicine. *J Am Med Assoc.* 1992;268:2420-5.
5. Friedland D. Introduction, In evidence based medicine: a framework for clinical practice. Stamford, Conn, Appleton and Lange. 1998.pp.2-3.
6. Woods BP. What's the evidence? *Radiology.* 1999;213:635-7.
7. Currie LM, Graham M, Allen M, et al. Clinical information needs in context: an observational study of clinicians while using a clinical information system. *AMIA Annu Symo Proc.* 2003.pp.190-4.
8. Antman EM, Lau J, Kupelnick B, et al. A comparison of results of meta-analyses of randomized control trials and recommendations of clinical experts. Treatments for myocardial infarction. *JAMA.* 1992;268:240-8.
9. Haynes RB. Loose connections between peer-reviewed clinical journals and clinical practice. *Ann Intern Med.* 1990;113:724-8.
10. Sackett DL, Strauss SE. Finding and applying evidence during clinical rounds: the evidence cart. *JAMA.* 1998;280:1336-8.
11. Shuval K, Berkovits E, Netzer D, et al. Evaluating the impact of an evidence-based medicine educational intervention on primary care doctors' attitudes, knowledge and clinical behavior: a controlled trial and before and after study. *J Eval Clin Pract.* 2007;13:581-98.
12. Strauss SE, Richardson WS, Haynes RB. Our reactions to knowing and not knowing, in *Evidence Based Medicine: How to Practice and Teach EBM* 3rd edn. Churchill Livingstone, Edinburgh, Elsevier. 2005.pp.18-9.
13. Kelly AM. Evidence based radiology: step 2- searching the literature (search). *Semin Roentgenol.* 2009;43:147-52.
14. Cochrane Collaboration Website: available at <http://www.cochrane.org>.
15. Cochrane AL. Critical review, with particular reference to the medical profession, in *Medicines for the year 2000*. London, Office of Health Economics. 1979.pp.1-11.
16. Evidence based medicine journal website. Available at <http://ebm.bmjjournals.org>.
17. Malone DE, Staunton M. Evidence-based practice in Radiology: step 5 (evaluate) - caveats and common questions. *Radiology.* 2007;243: 319-28.
18. Van Beek EJ, Malone DE. Evidence-based practice in radiology education: why and how should we teach it? *Radiology.* 2007;243:633-40.
19. Glasziou P, Del Mar C, Salisbury J, et al. Formulate an answerable question, in: *Evidence based practice workbook* 2nd edn. Boston, Blackwell Publishing. 2007.pp.21-34.
20. Levels of evidence. Oxford Centre for Evidence-Based Medicine Website. [http://www.cebm.net/levels\\_of\\_evidence.asp](http://www.cebm.net/levels_of_evidence.asp).
21. Dodd JD. Evidence-based practice in Radiology: steps 3 and 4- Appraise and apply diagnostic radiology literature. *Am J Radiol.* 2007;242:342-54.
22. Fryback DG, Thornbury JR. The efficacy of diagnostic imaging. *Med Decis Mak.* 1991;11:88-94.
23. Thornbury JR, Fryback DG. Technology assessment- an American view. *Eur J Radiol.* 1992;14:147-56.
24. McNeil BJ, Adelstein SJ. Determining the value of diagnostic and screening tests. *J Nucl Med.* 1976;17:439-48.
25. Finberg HV. Evaluation of computed tomography: achievement and challenge. *Am J Roentgenol.* 1978;131:1-4.
26. Center for evidence based radiology in Ireland. Available at <http://www.evidencebasedradiology.net/index.html>.
27. Maceneaney PM, Malone DE. The meaning of diagnostic test results: a spreadsheet for swift data analysis. *Clin Radiol.* 2005;55:227-35.
28. Cronin P. Evidence-based Radiology: step 3- primary literature validity (critical appraisal). *Semin Roentgenol.* 2009;43:153-7.
29. Sackett DL, Strauss SE, Richardson WS, et al. *Evidence Based Medicine: How to Practice and Teach EBM* 2nd edn. Churchill Livingstone, Edinburgh, Elsevier, 2000.
30. Guyatt G, Jaeschke R, Heddle N, et al. Basic Statistics for clinicians:1. Hypothesis testing. *CMAJ.* 1995;152:27-32.
31. Gardner MJ, Altman DG. Confidence intervals rather than p values: estimation rather than hypothesis testing. *BMJ (Clin Res Ed).* 1986;292:746-50.
32. Guyatt G, Jaeschke R, Heddle N, et al. Basic Statistics for clinicians: 2. Interpreting study results: confidence intervals. *CMAJ.* 1995;152:169-73.
33. Montori VM, Kleinbart J, Newman TB, et al. Tips for learners of evidence based medicine: 2. Measures of precision (Confidence intervals). *CMAJ.* 2004;171:611-5.
34. Cronin P. Evidence-based Radiology: step 3- critical appraisal of diagnostic literature. *Semin Roentgenol.* 2009;43:158-65.
35. Cronin P, Dwamena BA, Kelly AM, et al. Solitary pulmonary nodules and masses: A meta-analysis of the diagnostic utility of alternative diagnostic tests. *Eur Radiol.* 2008;18:1840-56.
36. McGinn T, Jervis R, Wisnivesky J, et al. Tips for teachers of evidence-based medicine. Clinical prediction rules (CPRs) and estimating pretest probability. *J Gen Intern Med.* 2008;23:1261-8.
37. Chang PJ. Bayesian analysis revisited: A radiologist's survival guide. *AJR Am J Roentgenol.* 1988;152:721-7.
38. Sackett DL, Haynes RB, Guyatt GH, et al. The interpretation of diagnostic data, in *Clinical Epidemiology: A basic Science for clinical medicine* edn 2. Boston/Toronto/London, Little, Brown. 1991.pp.92-3.
39. Fagan TJ. Nomogram for Bayes theorem. *N Eng J Med.* 1975;293:257.
40. Sackett DL, Richardson WS, Rosenberg W, et al. Is this evidence about a diagnostic test important? In *Evidence based medicine, how to practice and teach EBM* edn 1, vol 127. Edinburgh, Churchill Livingstone, 1998.
41. Cronin P. Evidence-based Radiology: step 3- critical appraisal of therapeutic literature. *Semin Roentgenol.* 2009;43:166-9.
42. Jaeschke R, Guyatt G, Shannon H, et al. Basic statistics for clinicians. III. Assessing the effects of treatment: measures of association. *Can Med Assoc J.* 1995;152:351-7.
43. Barratt A, Wyer PC, Hatala R, et al. Tips for learners of evidence based medicine. I. relative risk reduction, absolute risk reduction and number needed to treat. *Can Med Assoc J.* 2004;171:353-8.
44. Jonathan AC Sterne and Roger M. Harbord. Funnel plots in meta-analysis. *The Stata Journal (2004)* 4, Number 2, pp. 127-141.
45. Dwamena BA. Evidence-based radiology: step 3- diagnostic systematic review and meta-analysis (critical appraisal). *Semin Roentgenol.* 2009;43:170-9.
46. Whiting P, Rutjes AWS, Reitsma JB, et al. The development of QUADAS: a tool for the quality assessment of studies of diagnostic accuracy included in systematic reviews. *BMC Med Res Methodol.* 2003;3:25.

47. Lijmer JG, Bossuyt PM, Heisterkamp SH. Exploring sources of heterogeneity in systematic reviews of diagnostic tests. *Stat Med.* 2002;21:1525-37.
48. Deeks JJ, Macaskill P, Irwig L. The performance of tests of publication bias and other size effects in systematic reviews of diagnostic test accuracy was assessed. *J Clin Epidemiol.* 2005; 58:882-93.
49. Cronin P. Evidence-based Radiology: step 4- Apply. *Semin Roentgenol.* 2009;43:180-1.
50. Del Mar C, Doust J, Glasziou P. Clinical Thinking: evidence, communication and decision making. London, BMJ Books. Blackwell Publishing Ltd. 2006.
51. Dodd JD, MacEnenaey PM, Malone DE. Evidence based radiology: how to quickly assess the validity and strength of publication in the diagnostic radiology literature. *Eur Radiol.* 2004;14:915-22.
52. Trinder L. A critical appraisal of evidence based practice. In: Trinder L, Reynolds S, (Eds). Evidence-based practice: a critical appraisal. Oxford, England: Blackwell Science. 2000. pp.212-41.
53. Moher D, Schulz KF, Altman D. The CONSORT statement: revised recommendations for improving the reports of parallel group randomized trials. *JAMA.* 2001;285:1987-91.
54. Bossuyt PM, Teitsma JB, Bruns DE, et al. Towards complete and accurate reporting of studies of diagnostic accuracy: the STARD initiative. *BMJ.* 2003;326:41-4.

## Chapter

# 23

# Radiation Hazards and Radiation Units

*Pratik Kumar, Anil K Pandey*

Radiation can be defined as a packet of energy. The amount of energy the radiations can deposit in a given space varies with each type. It also differs in the power to penetrate. It may be ionizing and nonionizing. Nonionizing radiations do not affect at molecular levels. They may cause electrical shocks and burns. For example, prolonged exposure to microwaves radiation, which is nonionizing, may cause cataracts.

Ionizing radiations such as X-rays have power to penetrate inside the body; therefore, they interact as well as provide information at the atomic level. X-rays are directed towards the patient body and transmitted X-rays are used to form the image. Since X-rays are very small in size (in the unit of Angstrom), some of them can cross the body without interaction, some will interact with atoms and lose its energy completely, others will get scattered and come out from the body. Thus, the transmitted X-rays have energy from zero to a maximum value and when they fall on a two dimensional image receptor and deposit its energy, they create an image of the organ exposed.

X-ray (radiation) is extremely useful and becoming integral part of diagnosis and disease management. On the other hand, it ionizes the atoms and molecules when they pass through the body and creates biological damage.

In this chapter we are going to discuss the harmful effect of radiation on human body (radiation hazards), how to protect the patient, staff, and public from radiation generated during the diagnostic and interventional procedures performed in radiology, and units associated with measurement of radiation in these modalities.

## RADIATION HAZARDS

Harmful effect of radiation on human body is called Radiation Hazards which can be created by direct and indirect mechanism of interaction of X-rays with human body.

Interaction of radiation with living things (human body cells) and nonliving things is different. All human beings are made of tiny structures called cells. The bigger a person is, the more number of cells he or she has. Children do not have as many cells as adults, but they have greater proportion of dividing cells. Chemical contents, physical shape and size of a living cell are continuously changing. A new cell is made when an existing cell grows and divides into two. The new cell is an exact copy of the old one. This change may be rapid or slow. In natural growth cycle of a cell, one step is linked with other as it is a continuous process, but for convenience these steps are named as different phase of growth cycle of the cell such as M phase, G<sub>1</sub> phase, S phase and G<sub>2</sub> phase. The cells are most sensitive to radiation during Mitosis (i.e. M phase) and G<sub>2</sub> phase (i.e. Premitosis or RNA synthesis) and least sensitive during S phase (DNA synthesis).

First step of cell development is necessary to move on to the second step. In case of rapid development, the gap between the first step and second step is less, so the minimum time required to repair the damage created by the radiation, may not be available in case of rapid developing cells. In slow developing cell the time period to repair the break is available; therefore, slow developing cells are less sensitive to radiation in comparison to the fast/rapid developing cells. Similarly, any damage inflicted by radiation on the cell is expressed

soon in case of rapidly developing cells as they progress fast through their cell-cycles.

### DAMAGE TO DNA BY THE RADIATION

The X-ray energy used in the diagnostic radiology varies from 25 to 125 kVp. They deposit their energy in a very small volume and are sufficient to produce ionization inside the human body. Radiation creates damage to the DNA by direct and indirect mechanism. In the direct mechanism, the X-ray hits the DNA molecules directly. DNA molecule gets ionized resulting in damage. In indirect mechanism, water molecules absorb the X-ray energy and dissociates into  $H^+$  and  $OH^-$ . OH free radical contains an unpaired electron in the outer shell and is highly reactive. It reacts with DNA and creates the damage. It is estimated that 60 to 70 percent of radiation-caused DNA damage is due to OH free radical.

### THE EFFECT OF RADIATION

Chemical bonds hold DNA together. Loss of electrons causes chemical bond to change. Thymine one of the four bases of DNA, is supposed to bind with adenine on its opposing strand. However, loss of electrons caused by radiation makes thymine bind with another thymine on the same strand. When DNA is replicated to make new cells, coding errors occur and mutations result. Mutations result in damaged chromosomes. Cells then reproduce abnormally, causing both defects and cancer.

The types of damage that can occur to DNA molecules are:

- DNA single strand breaks
- DNA double strand breaks
- Sugar damage
- Base damage
- Local denaturation (separation of the two strands)
- DNA-DNA cross links
- DNA-Protein cross links.

These damages can lead to:

- Slow down in the cell synthesis (copies of its own DNA) so that there is a delay in cell dividing into two cells
- Delay in repair mechanism that will delay the cell cycle progression (as the cell progresses towards next cell division)
- Delays in cell proliferation (increase in cell number) of a population of cells
- Death of the cell
- Mutation of the cell
- Cell transformation (changes in the cell which will make them to behave as a cancer cell).

Cell death have been given special names also as cell necrosis (death of a contiguous fields of cell, the content of the cell leaks out into the surrounding tissue and blood supply), cell lysis (the cell simply bursts open and releases its

contents into the surrounding), apoptosis (or programmed cell death) which is under genetic control (specific gene must be present active or inactive) and it requires energy and when the cells die, DNA fragments of specific sizes, and the content of the cells, are encapsulated in membranes as small vesicles.

The damages incurred by different kinds of tissue vary with the type of radiation to which the person is exposed and the means of exposure. Direct exposure to radiation can affect the whole body. The body attempts to repair the damage caused by the radiation. However, at times the damage is so severe and widespread that repair is impossible. For example, thyroid gland is one of the most radiation-sensitive parts of the body, especially in babies and children. Absorption of too much radioactive iodine can cause thyroid cancer to develop several years after the exposure.

Different types of cell aberration can occur depending on the position of the cell cycles at the time of exposure to ionizing radiation. Most common is formation of dicentric and ring which can be visualized under microscope after the exposure above 10 to 25 cGy. Visualization of the ring or dicentric aberration means cell death has occurred. Certain types of aberration and/or mutation in gene can cause cancer.

Mutation may occur even at low dose. There is no threshold of dose below which an ionizing radiation cannot induce mutation. However, at low doses and dose rates, the risk of mutation is very low, and it is lower for low dose rates at all doses. The relationship may be either linear or linear quadratic depending on type of radiation. X-rays follow linear-quadratic model, at low doses the relationship is linear with increase in dose, while at higher dose the relationship is square of the dose.

### Stochastic and Nonstochastic (Deterministic) Effects

The effect of radiation can be broadly classified as stochastic and deterministic effect. Stochastic effects are observed at low doses and these effects have no threshold. At low radiation dose the probability of occurrences of stochastic effect is low. As the dose increases the probability of occurrence of stochastic effect also increases. There is a linear relationship between absorbed dose and probability of effect. Examples of stochastic effects include hereditary effects and cancers. Cancer (which includes leukemia) and genetic effects follow linear nonthreshold dose response relationship.

Deterministic effects start after the absorption of certain amount of dose. It has a threshold, once the absorbed dose crosses the threshold these effects appear in all exposed subjects, and as the absorbed dose increases, the severity of the effect also increases. Examples of deterministic (also called nonstochastic) effects are various somatic effects including skin erythema, epilation, cataracts, impaired fertility etc. The threshold for skin effect is above 2 Gy.

## Radiation Doses and Expected Effect

The radiation dose to human body and its effect can be summarized in a table as follows:

Radiation dose	Observable effects
0–50 mSv	None (irrespective of acute or protracted exposure)
50–100 mSv	None, might not be existing or too small to detect (irrespective of acute or protracted exposure)
100–500 mSv	Slightly increased cancer risk. Decrease in blood counts at around 500 mSv
500–1 Sv	Some observable effect may be visible in acute exposure Increased cancer risk over longer duration Above 500 mSv some changes in blood cells occur but recovers quickly
1–2 Sv	Nausea and fatigue in acute exposure Increased cancer risks over longer duration
2–3 Sv	Nausea and vomiting within 24–48 hours, medical attention is required
3–5 Sv	Nausea, vomiting, and diarrhea within hours, Loss of hair and appetite occurs within a week, medical attention is must, half of the population exposed will die if no medication attention is given
5 Sv–12 Sv	Death within a few days
Greater than 100 Sv	Death within few hours

## Radiation Effect on Embryo

All human beings start life as a single cell that divides over and over again and grows into babies inside their mothers' bodies.

Embryo is composed of relatively few cells and has high rates of cell division and cell differentiation. Rapidly developing cells have found to be more sensitive to the radiation. Since Embryo/fetus has rapid developing cells, they are more sensitive to radiation than the adult.

Radiation produces no unique abnormalities. The effects vary with the amount of radiation dose, dose rate with which exposure has occurred and stage of development of the embryo/fetus. Many researchers follow the limit of 10 rad (100 mGy) to fetus in case of accidental exposure. Even in case of radiation dose to fetus in excess of 10 rad the risk incurred remains low for lower doses.

The effects of radiation on embryo/fetus are loss of pregnancy (embryonic, fetal or neonatal death), malformations and mental retardation. However, these occur at high doses generally not encountered in diagnostic radiology during normal investigations. Any decision for termination of pregnancy due to fetal exposure during

radiological examination must be weighed against the information that the rate of spontaneous abnormality is quite high at 4 to 6 percent with respect to risk incurred due to fetal radiation exposure.

## Ten Day Rule

It must be emphasized that both the ICRP and NCRP recommended application of the 10-day rule only to those studies that do not contribute to management of current disease. It, therefore, follows that studies which do contribute to diagnosis or treatment of current disease should be performed in fertile women without regard to stage of the menstrual cycle. It is suggested that all potential female patients due to radiological investigations should be inquired about her probable pregnancy. Missing menstrual period should be taken as pregnancy. If the patient does not think that she is pregnant (there is no missing period) the radiological investigation may be carried out. If it turns out that the patient is pregnant the radiologist/referring physician should weigh benefit and risk associated with the X-ray investigation and should obtain informed consent from the patients and her attendants for the further necessary action.

## Protection of Patient, Staff, and Public from Radiation

### Radiation Risk

Radiation risk calculation are based on the type of radiation, amount of energy absorbed, and which part of the body these energies is deposited. For example, certain amount of radiation energy deposited to the wrist has really no effect, however similar amount of energy deposited to blood forming organ may have an effect. One of worth-notable effect of low dose radiation which we come across in diagnostic and therapeutic radiological investigations is probability of cancer induction. The probability of cancer induction is low at low dose but never zero theoretically and therefore calls for the optimisation of radiation doses for all radiological investigations. One should keep in mind that it is not possible to differentiate or detect the cancer caused by diagnostic X-rays from cancer caused by other factors such as environmental, chemical or biological. The latency period of cancer induction may be in years or even in decade. This may be true for all carcinogens including radiation. This is especially true for low dose and low dose rate radiation. If the low level of radiation exposure has occurred today, its effect as a cancer may be expressed after few years of exposure.

### Radiation Protection Guidelines and LNT Model

In 1950s, the scientific group created the radiation protection guidelines. At that time no one really knew the effect of low dose of radiation. It was decided to assume that the relation between the radiation dose and its effects are linear and proportional. It was also decided that any dose, no matter

how small, could bring an effect. This is called a linear no threshold (LNT) model. Still this LNT model is in use to set radiation protection guidelines. Since this concept was easy to use and explain, most people presented this as a fact rather than saying that we do not know the effects of low doses of radiation or whether the low doses of radiation is safe. Effect of radiation at low doses is a controversial topic since it is difficult to get ideal epidemiological data. Cancer induction may be the only effect at low dose of radiation but there are also spontaneous incidences of cancer without radiation exposure (due to various other environmental carcinogens and biological factors). Such comparison demands similar control and study group in terms of life style, socioeconomic status, environment, age, sex, etc. except in radiation exposure history. Obviously it is hard to meet this ideal situation. Ubiquitous background radiation is another confounding factor which exposes all people living on this planet all the time with an average 2 to 3 mSv (milli Sievert) annual dose.

On the other hand there are researchers and their preliminary experimental results which may indicate about the existence of beneficial effect of low level radiation (called radiation hormesis) (Fig. 1). At present it is thought prudent to consider low level radiation having linear relationship with risk (without having any threshold of a minimum dose) which signifies that even low level radiation entails some risk.

Every country has a regulatory authority to set the guidelines regarding radiation protection, make laws and to enforce them. These guidelines are based on LNT model and made in such a way that if followed properly, patient, staff and public all are protected. We must obey them. Atomic Energy Regulatory Board (AERB), Mumbai is the competent authority to enforce radiation safety in practice in India.

The first principle of radiation protection for the patient is justification.

### *Justification*

X-ray examination should be undertaken only when there is medical question which need to be answered, the amount of benefit which patient is going to receive in comparison to the risk associated with this X-ray examination is high, and the information needed cannot be answered by any other investigation involving nonionizing radiation. In such condition, we say that X-ray examination is justified.

### *Some facts that can help in protecting staff/patients and public from radiation*

- X-rays are produced, emitted in isotropic direction; X-ray tube is shielded to protect patient and staff operating the machine.
- X-rays produced from the X-ray machine have a mixture of continuous spectrum starting from zero to maximum energy (equal to the kVp applied) and characteristic spectrum. If the spectrum is not filtered, the low energy X-rays (also called soft X-rays) will be absorbed

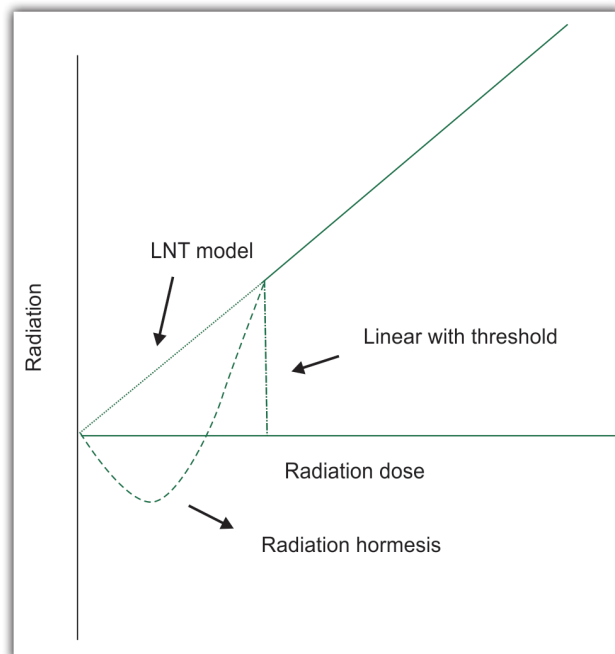


**Fig. 1** Various hypotheses of low level radiation dose and its effect

completely on superficial organs of the patient body and contribute the patient dose; however these X-rays will not contribute in the image formation. X-rays are passed through the filter to remove these soft X-rays. Application of additional filter reduces the patient dose significantly.

- The X-rays emitted from the X-ray tube and directed towards the patient body are called primary X-rays. When these primary X-rays interact with the patient body, as a result of interaction scattered radiation are emitted in all direction.
- The energy of scattered radiation is almost equal to the primary radiation (a few keV less than the primary radiation). So it is most likely that the person standing in the room while X-rays are being energized will receive radiation exposure from the secondary radiation emitted from the patient body as a result of scattering.
- In case of over couch X-ray tube, the radiologist will receive maximum exposure to the face, because scattered X-rays from the patients are directed towards the face. In under couch X-ray tube, the scattered radiations are directed towards the legs. Therefore, lead rubber flaps can be used to protect legs. Goggles must be used to protect the eyes.
- The lead apron of 0.25 to 0.50 mm Pb equivalent is worn by the radiologist to protect them from the secondary scattered radiation. In the interventional procedures they have to wear it for a longer duration. Due to prolonged time period of wearing the lead apron, some orthopedic problems of spinal injury have been reported in the literature for the interventional radiologist. Therefore,

it is important (for both the radiologist and patient's viewpoint) that interventional radiological procedures or radiation related procedures will only be adopted when there is no other option available. Now-a-days, vest-skirt type lead aprons are available which shifts weight of the skirt apron at the waist.

- Lead free aprons incorporating Tungsten, Antimony and Bismuth or Barium, Aluminum, Tin, Titanium, Bismuth are available in the market. These aprons are environment friendly and recyclable as well. Lead is toxic and therefore, disposal of lead aprons needs proper care. It is desirable to check the protection/attenuation efficiency offered by these new lead-free protection aprons before it is put to use. Lead free aprons may offer the weight which is 20 to 40 percent lesser than that of conventional lead apron.
- Radiation burns (Radiation hazards) are different than the burn by the fire and hence requires specific expertise and experience to treat such cases. Radiation burns have been reported in the literature during the interventional fluoroscopic examinations. This needs to be prevented.

Since X-rays have high penetrating power, X-ray machines are needed to be installed in room having sufficient wall thickness such that outside the room the radiation penetrating through the wall must not exceed the limit set for public exposure. The entry of public or attendants is not allowed in the X-ray room while X-rays are being energized. There must be some warning signal displayed outside the X-ray room so that public must know that X-rays are being produced here. Public must know that X-rays beam is ON. The wooden door of the X-ray room must have sufficient lead shielding.

**Cardinal principle of radiation protection** is distance, time and shielding. The dose from the X-ray beam diminishes with the square of its distance from the source. This law is known as inverse square law. If the distance from the source is doubled, the dose reduces by  $\frac{1}{4}$ . So, one should maintain the maximum distance from the source to reduce dose. Radiation dose is directly proportional to the time duration spent with the source. It indicates to complete the job quickly (i.e. efficiency in job). By interposing shielding between the source and detector, the radiation dose decreases. One HVL (Half Value Layer) of a shielding material like lead, concrete or brick is the thickness of the material which when interspersed will attenuate the radiation to half.

*General dose reduction measures that can be adopted to reduce patient doses are:*

- Increasing the distance between X-ray tube and patient helps to reduce dose. Doubling the distance will make the dose one-fourth.
- Collimation at the target/patient's body reduces dose and improves image quality also due to lesser scattering.
- Compression of the body reduces the thickness of the body and hence volume of irradiation. Amount

of scattering is directly proportional to the volume of irradiated tissue. Therefore, compression of body reduces the amount of scattering and improves image contrast. With reduced thickness lower radiation dose is absorbed inside the body. That is why breast is compressed during mammography.

- Antiscatter grids are located between the patient and the image intensifier, or cassette or digital detector. Grids absorb most of the scatter radiation. Higher the grid ratio, better is the image quality but higher is the radiation dose to the patient. So, an optimum value of grid ratio needs to be selected. 8:1 for radiography and 5:1 for mammography is optimum. In radiography of children one may remove the grid since there is less scatter anyway due to smaller body volume of the children. Removing grid will enable the radiographer to reduce the radiographic parameters and hence reduce the dose to the pediatric cases.
- With increase in kVp, penetrating power of X-ray beam increases. It will deposit less amount of energy inside the patient body during radiography and hence the patient dose will reduce. However, this will reduce the contrast in the image. In CT, higher kVp increases the patients' dose.
- X-ray beam contains both soft and hard X-rays. When X-ray beam is allowed to pass through the filter made of copper and aluminum the filter will attenuate the soft X-rays and allow the hard X-rays to pass through. Soft X-rays get absorbed on superficial organs and contribute to absorbed radiation dose and do not take part in the image formation. There is regulatory limit of minimum 2.5 mm aluminum total equivalent filtration to be present in X-ray beam in all radiography machines having 100 kVp or more.
- X-ray machines are available with automatic exposure timing control facility called automatic exposure control (AEC). These sensors monitors the transmitted X-ray from the patients, when amount of X-ray beam required for an optimum image quality is reached, it automatically turns off the X-ray beam falling on the patient body. In this way, it ensures the smallest amount of radiation have been administered to patient.
- Table top material should not absorb much radiation as the X-ray passes through it before reaching to patient/detector. However, it should be strong enough to carry the bulky patients. Carbon fiber has been proven to be the best material for X-ray system table top.
- Pulsed fluoroscopy reduces the dose to patients and staff significantly in interventional fluoroscopy. In pulse fluoroscopy the X-ray is emitted in pulses instead of continuous exposure. This effectively reduces the total time of emission of X-rays. Fifteen frames per second reduces radiation dose by about 25 percent while 7.5 frames per second may reduce the radiation dose to half. However, very low frame rate may lead to choppy image

especially during imaging of a moving organ. Modern technology uses digital refresh memory to digitize the last image and showing it in the gap time of two consecutive X-ray pulses unless next pulse refreshes the image. This reduces the flickering of the image on monitor when very low frame rate pulse fluoroscopy is operated.

We need to quantify the damage created by the ionizing radiation. Following radiation units are used in radiology.

### Radiation Units

When X-rays used in medical imaging interacts with any medium (human body or material like cassette, imaging plate, film, etc.), it transfers energy to the medium. This energy transfer is influenced by many factors. It is important to understand its nitty-gritty since risk to radiation has to be defined on the basis of the energy transfer pattern between interacting radiation and the medium it traverses through.

### Fluence

X-ray may be thought of consisting of stream of energy packets (particles like) called X-ray photons. The stream of X-ray photons is called "X-ray Fluence" which is defined as number of X-ray photons passing through per unit area when the area is perpendicular to the direction of photon stream.

$$\text{Hence, X-ray fluence} = \frac{\text{Number of photons}}{\text{Area of cross-section}}$$

Unit for fluence is  $\text{cm}^{-2}$ .

### Flux

X-ray flux is defined as the X-ray fluence per unit time. In other words, number of X-ray photons passing through per unit area per unit time is called Flux. It may be seen that flux is nothing but fluence rate which is fluence per unit time.

$$\text{X-ray flux} = \frac{\text{Number of photons}}{\text{Area}} \times \frac{1}{\text{Time}}$$

In fluoroscopy the concept of flux is important since radiation is "on" for longer time.

### Energy Fluence

It is defined as amount of energy passing through unit area. If we know the energy of each X-ray photon the energy fluence may be defined as:

$$\text{Energy fluence} = \text{Fluence} \times \text{Energy of each X-ray photon}$$

Since X-ray photons from x-ray tube are polyenergetic, therefore mean energy of X-ray photons have to be considered while calculating energy fluence.

$$\text{Mean energy of X-ray photons} = \frac{\text{Total energy of photons}}{\text{Number of photons}}$$

$$\begin{aligned}\text{Energy fluence} &= \frac{\text{Number of photons}}{\text{Area}} \times \frac{\text{Total energy of photons}}{\text{Number of photons}} \\ &= \frac{\text{Energy}}{\text{Area}}\end{aligned}$$

The energy of X-ray photon is in terms of keV.

(The maximum energy of X-rays photons is the maximum potential applied across cathode-anode in X-ray tube by selecting tube voltage at control console in terms of kVp).

Energy fluence has unit keV per  $\text{Cm}^2$  which may be written as  $\text{keVCm}^{-2}$ .

### Exposure

Exposure is defined as electrical charge produced by ionization created by the incident X-rays (radiation) in unit mass of air.

$$\begin{aligned}\text{Exposure} &= \frac{\text{Amount of charge produced}}{\text{Irradiated mass of air}} \\ &= \frac{\text{Charge}}{\text{Mass}} \\ &= \frac{\text{Coloumb}}{\text{Kg}} \text{ (SI unit)}\end{aligned}$$

Traditional unit is Roentgen (R) which is defined as  
 $1 \text{ R} = 2.58 \times 10^{-4} \text{ Coulomb/kg of air}$

Or,  $3876 \text{ R} = 1 \text{ Coulomb/kg of air}$

The exposure rate is expressed in R/hr or mR/min.

R is valid for X-rays and gamma rays with energy up to 3 MeV. It is to note that the exposure and its unit R take care of the interaction of X-rays and gamma rays with air only.

Exposure is not applicable to electrons, beta or any charged particle. Exposure may be measured using ionization chamber. Since, there is not much difference between effective atomic number of air and soft tissue for the diagnostic range of energy, the absorbed dose to air or soft tissue may be regarded same. The concept of absorbed dose is for material.

### Absorbed Dose

Absorbed dose indicates the amount of energy deposited by interacting ionization radiation (X-rays, gamma rays, electrons, beta, neutrons, alpha, protons, all radiation) with unit mass of matter.

$$\text{Absorbed dose} = \frac{\text{Amount of energy deposited}}{\text{Mass of matter}}$$

The unit of absorbed dose is Joule per Kilogram ( $\text{J kg}^{-1}$ ) and a special name has been given to this in SI unit is Gray.

$$1 \text{ Gray (Gy)} = 1 \text{ Joule/kg}$$

The traditional unit of absorbed dose is rad (Radiation absorbed dose)

$$1 \text{ Gy} = 100 \text{ rad}$$

$$1 \text{ rad} = 0.01 \text{ Gy} = 0.01 \text{ Joule/kg}$$

The conversion factor between "Exposure" and "Absorbed Dose" is called Roentgen to rad Conversion Factor (or F factor)

$$F = \frac{\text{Absorbed dose (rad)}}{\text{Roentgen (R)}}$$

F is defined as the absorbed dose in rad for a matter per Roentgen exposure for a given energy. For diagnostic energy range the F factor is about 1 for soft tissue and it signifies that

for keV range R and rad is approximately same. However, value of 'F' for bone in keV range of X-rays is about 4 and this shows that bone absorbs about 4 times more dose than soft tissue due to predominant photoelectric effect at lower energy which increases with substance of high atomic number (like bone with respect to soft tissue).

The relation between absorbed dose to air and exposure is:

$$\text{Dose to air (mGy)} = 8.76 \times \text{Exposure (R)}$$

1 R deposits 0.877 rad to dry air. This dose to air or air dose may also be equated with air kerma. The unit for air kerma is gray (Gy). Air kerma in air is the sum of kinetic energy of all charged particles generated when X-rays and gamma rays pass through unit mass of air.

### Kerma

The ionizing radiation may be of two types, directly ionizing and indirectly ionizing. Directly ionizing radiations are those which carry charge with it (like alpha, electrons and beta). Directly ionizing radiation interacts with the electron of the atom of the medium through columbic forces. Indirectly ionizing radiation does not carry any charge and includes neutron, X-rays and gamma rays. The indirectly ionizing radiation deposits energy in the medium through two steps. In the first step, the interacting X-rays (or gamma and neutron) deliver/provides kinetic energy to the electrons of the medium through photoelectric, compton or pair production processes depending upon the energy of the incident X-rays. The electrons so produced are directly ionizing and in step two, they deposit their energy in the medium through the process of ionization and excitation. In some cases, where the range of such electrons is sufficiently high, some electrons may escape the medium.

The kerma stands for the kinetic energy released in the medium and is defined as total initial kinetic energy of all charge particles (electrons) released in the medium by the interacting X-ray (indirectly ionizing radiation) in a given mass. Kerma defines the above step one.

$$\text{Kerma (K)} = \frac{E_{tr}}{m}$$

$E_{tr}$  = Sum of kinetic energy of electrons produced

m = Mass of the medium

Unit of kerma is joule/kg which is the unit for dose as well. SI unit for kerma is Gray (Gy) and traditional unit is rad. Kerma is defined for X-ray, Gamma ray and neutrons only.

The kerma may be considered made of two parts, collision part and radiative part. When the electrons are liberated by the incident X-ray on the medium of low atomic number (air, water, soft tissue) the majority of these electrons expend their energy during interaction with the orbital electrons of the atoms of the medium. A very small part of liberated electrons may interact with the nuclei of the atoms of the medium giving off Bremsstrahlung X-rays (radiative

part). If the energy transferred by the incident X-rays to the liberated electrons in the medium is deposited locally and Bremsstrahlung loses (radiative loss) is negligible, the absorbed dose equals to kerma. For diagnostic energy range absorbed dose equals to kerma. At higher energy of incident X-rays and gamma rays radiative loss is not negligible.

The quantity "Exposure" indicates the amount of ionization in air due to radiation interaction while radiation dose (or called radiation absorbed dose) refers the amount of radiation energy deposited to the medium (may be patient's body) with which the radiation (X-ray) has interacted. The term "Radiation Exposure" and "Radiation Dose" are many times used interchangeably especially in case of medical imaging where energy of X-rays used is in kilo-voltage range. Generally "Exposure" is measured using ionization chamber or any suitable measuring device while "Dose" is calculated from exposure and energy absorbed by X-rays per unit mass of the body.

### Equivalent Dose

Equivalent dose may also be called radiation protection unit as it takes into account the potential of the radiation to cause biological damage. The ability to cause biological damage (effectiveness) varies with the type of radiation and is closely related with its ionizing capability. Various types of radiation has been assigned a "quality factor" which, though arbitrary chosen, may be linked with its relative biological effectiveness (RBE) related to linear energy transfer (LET) of radiation. The quality factor is called radiation weighing factor ( $W_R$ ).  $W_R$  for X-rays, gamma rays, beta and electrons are 1, protons (>2 meV) has 5, neutrons (depending upon energy) has 5 to 20 and alpha particles  $W_R$  are 20.

$$\text{Equivalent dose} = \text{Absorbed dose} \times W_R$$

The traditional unit for equivalent dose is Rem and the SI unit is Sievert (Sv). For X-rays  $W_R = 1$  and hence, 1 mGy = 1 mSv.

### Effective Dose

Radiosensitivity of various tissues is different. Therefore, radiation induced effect in different tissues are likely to be different even for similar equivalent dose for these tissues. Tissue have been assigned a tissue weighting factor ( $W_T$ ) which represents the detriment (risk) of the radiation exposure to that tissue with respect to the uniform whole body radiation exposure. Bone marrow, colon, lung, breast, stomach each have been given  $W_T$  at 0.12, gonads at 0.08, bladder, liver esophagus and thyroid at 0.04, skin bone surface, brain and salivary glands have been given 0.01.

$$\text{Effective dose} = \sum \text{Equivalent dose} \times W_T$$

Effective dose may be defined as sum of weighted radiation equivalent dose to various tissues/organs.

Effective dose has similar units as that of equivalent dose, i.e. traditional unit is Rem and SI unit is Sievert (Sv).

### Radiation Dose Measurement in CT

The radiography is a projection imaging while CT scanner is a cross-sectional imaging. In the former, the radiation enters single body surface and maximum dose was delivered to the skin at the entrance. This measurement in case of radiography was called entrance skin dose (ESD). The ESD depends upon kV and mAs set on the control panel of the radiography machine. In contrast, radiation enters the body from all direction as X-ray tube revolves around the patient during exposure in CT scan. It makes the measurement of dose complex due to presence of significant amount of scatter dose and transmitted radiation when the X-ray tube is not directly over the point of measurement. Due to narrow collimation and requirement of good image, the mAs used in CT scanner are much higher than that in radiography. CT doses are measured in cylindrical phantom made of acrylic (or PMMA) with holes at center and periphery for placing ionization chambers (**Fig. 2**). The body phantom has a diameter of 32 cm and head phantom has a diameter of 16 cm. Both phantoms have a length of 15 cm in Z-axis. The holes with diameter of 1 cm are made at 12, 3, 6, and 9'o clock positions and are provided with well-fitted acrylic plug to fill the gap (hole) when not in use (by ionization chamber).

### Computed Tomography Dose Index

Computed tomography dose index (CTDI) was originally planned as an index of dose and not a real patient dose. However, later CT dosimetry method for patient dosimetry was based upon CTDI. The CTDI<sub>100</sub> is a dose measured in a 100 mm long cylindrical ionization chamber when the chamber is placed in CT scanner at its isocenter. The ionization chamber is aligned (its long axis) with the axis of the patient couch (i.e. Z-axis). One single axial scan is performed at the center of the ionization chamber without movement of the table.

$$\text{CTDI}_{100} = \frac{1}{\text{Beam width}} \times \int_{1=-50 \text{ mm}}^{1=+50 \text{ mm}} D(z) dz$$

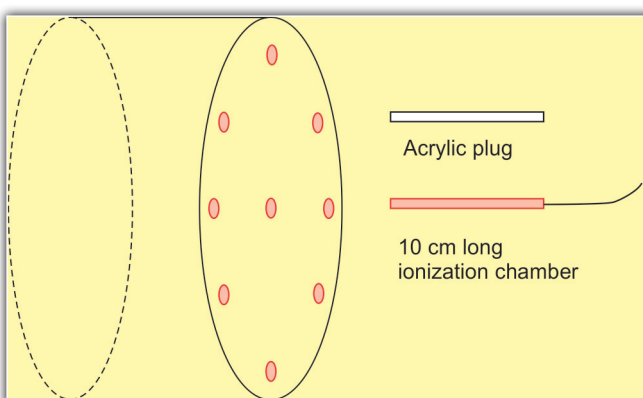


**Fig. 2** CTDI phantom with chamber

D(z) = radiation dose profile along Z-axis

The single axial scan at the center of the chamber with its beam width (i.e. in MDCT it is the product of number of channels and the size of the detector in channel) opened causes collection of charges created in ionization chamber, 50 mm on either side of its center due to scatter radiation along the Z-axis as well. Beam width may be denoted as NT where N is number of tomographic sections imaged or number of data channel used and T is the width of tomographic section along the Z-axis imaged by single data channel. For CTDI<sub>w</sub>, the measurement of CTDI<sub>100</sub> is done at central and peripheral holes of the cylindrical acrylic (or PMMA) phantom.

CTDI<sub>w</sub> is a weighted measurement of CTDI<sub>100</sub>

CTDI depends upon the field of view (FOV). Doses at the periphery and center of the phantom (i.e. CTDI<sub>100, center</sub> and CTDI<sub>100, periphery</sub>) are not equal. CTDI at surface may be double of that at center. The average CTDI<sub>100</sub> which represents average dose to phantom has been termed as CTDI<sub>weighted</sub> or CTDI<sub>w</sub>.

$$\text{CTDI}_w = \frac{1}{3} \text{CTDI}_{100, \text{center}} + \frac{2}{3} \text{CTDI}_{100, \text{periphery}}$$

In real work, we use CT scanner for series of slices or scans. These slices may be at gap, contiguous or overlapped. CTDI<sub>volume</sub> describes the dose to phantom in CT scan with series of slices and abbreviated as CTDI<sub>vol</sub>.

$$\text{CTDI}_{\text{vol}} = \frac{1}{\text{Pitch}} \times \text{CTDI}_{100}$$

Pitch is defined in helical or spiral CT scanning as distance travelled by patient table in gantry (mm) during a full rotation of X-ray tube around the patient or phantom for unit beam width (NT) in mm.

$$\text{Pitch} = \frac{\text{Table movement per axial scan (mm)}}{\text{Nominal beam width (NT) (mm)}}$$

CTDI<sub>vol</sub> represents the average radiation dose to phantom during scan and is reported on CT console for specific scan protocol. These values have been fed by the manufacturer after carrying out the measurement in phantom using specific scan protocol.

DLP is dose length product which is the product of CTDI<sub>vol</sub> and length of the CT scan.

$$\text{DLP} = \text{CTDI}_{\text{vol}} \times \text{scan length}$$

The unit for CTDI<sub>vol</sub> is mGy. It should be noted that CTDI<sub>vol</sub> though represents average radiation dose to phantom but may be substantially different for a phantom which has different size from the phantom used in measurement. CTDI<sub>vol</sub> is independent of the length of the scan, i.e. coverage of scan. However, DLP takes length of scan into account. AAPM report 204 provides conversion factor for CTDI<sub>vol</sub> for different sizes of phantom which is called size specific dose estimates (SSDE). These factors may help us in arriving near the real doses involves in CT scan.

### Radiation Dose Measurement in Fluoroscopy

In fluoroscopy the users may use direct or indirect method of assessment of radiation dose to patient and staff.

Direct method utilizes some measurement devices to be put at the point of measurement (patient's skin, at some reference point etc.) The measurement devices may be TLD, radiochromic film, MOSFET (Metal Oxide Semi Conductor Field Effect Transistor) dosimeter etc. Indirect method provides an estimate of radiation dose to patient by the direct measurement of some radiation-linked quantities (like, fluoroscopy time or dose area product i.e., DAP).

All fluoroscopy machines come equipped to measure the fluoroscopy X-ray "on" time. Fluoroscopy X-ray active time is also called "fluoroscopy time". This parameter is not good enough to provide the estimate of patient skin dose or staff dose.

Another indirect method to measure radiation dose to patient is dose area product (or kerma area product). DAP or KAP meter is a large area, flat, transparent, ionization chamber that is fitted into the collimator of X-ray tube. The X-ray passes through it and KAP meter intercepts the whole beam (X-ray field). It gives the measurement as the product of kerma and the area of the radiation beam in the unit Gy.cm<sup>2</sup> or any of its derivative like mGy.cm<sup>2</sup>, Gy.m<sup>2</sup>, cGy.cm<sup>2</sup> etc. This quantity is independent of distance and can be measured anywhere in the beam. This is true since as we go away from X-ray source the X-ray dose decreases with square of the distance from source (inverse square law) but area of the beam increases due to divergence, again, with square of the distance. This results in the product of radiation dose (kerma) and the X-ray field (area of the beam) to remain constant throughout the X-ray beam and hence KAP can be measured anywhere in the X-ray beam (**Fig. 3**). KAP represents the total energy incident on the patient and hence is considered a good indicator of stochastic risk of the radiation exposure. KAP values may be used to arrive at effective dose as the conversion factor is available in literature.

The KAP takes nonuniformity of the dose within the X-ray field into account like due to heel effect or due to utilization of any semi-transparent shutter in any area of the field. It is easy to measure and all new fluoroscopy machines provide this data in real time. In some fluoroscopy machine, KAP may be calculated (rather measured) using generator and collimator settings. One should bear in mind that cumulative KAP reading does not indicate the risk of skin-exposure (skin burn) directly in the patient. Nonetheless, the scatter dose around the patient is largely proportional to KAP reading

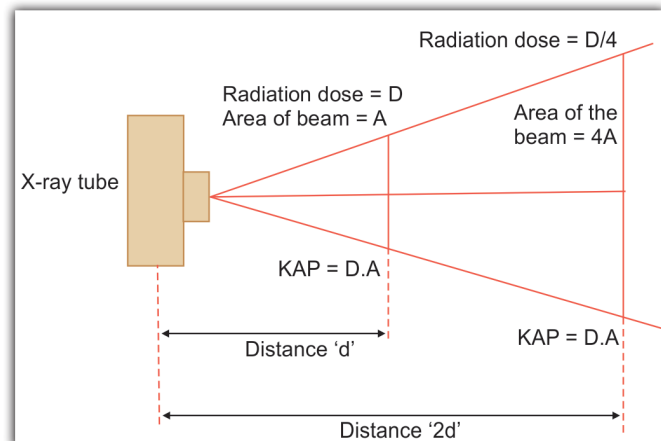


**Fig. 3** Dose area product is independent of distance

and hence may be a relative indicator of the radiation field around.

Nowadays, the fluoroscopic machines give cumulative doses at some reference point in terms of mGy which was designed to be an indicator of skin dose in the patient. The point of measurement of air kerma (calibrated free in air) has been defined at 15 cm from the isocenter of the isocentric machine (like c arm) towards the X-ray source. This point is intended to refer to the skin of the patient where radiation beam enters the patient. This reference point is called interventional reference point (IRP) and has been defined by International Electrotechnical Commission (IEC) standard 60601-2-43. However, one should keep in mind that cumulative dose at IEC reference point does not take into account back-scatter, table attenuation or in-field nonuniformity of dose. Also, actual skin may not be at IRP since the skin's position depends upon the position of the patient with respect to isocenter, patient thickness, angulations of beam etc.

## BIBLIOGRAPHY

1. JT Bushberg, JA Seibert, Leidholt EM Jr, JM Boone. The essential Physics of Medical Imaging. Lippincott Williams & Wilkins, 2002.
2. IAEA. Radiation Protection of Patients. <https://rpop.iaea.org/RPoP/RPoP/Content/index.htm>.
3. Faiz M Khan. The Physics of Radiation Therapy, Lippincott Williams & Wilkins, 2009.

## Chapter

# 24

# Radiation Protection

*Sapna Singh*

In November 1895 Wilhelm Roentgen discovered X-rays. Roentgen was diligent in his investigation of the behavior of these new-found rays and he established their physical characteristics almost fully within a short period. It was, however, the tragedy of the radiation pioneers that drew attention to the fact that these X-rays were not only wonderful and useful in medicine, but harmful too. However, it took several years before radiation protection measures and the concept of a limit to the exposure dose for radiation workers was established.<sup>1</sup>

### HISTORICAL PERSPECTIVE

Within few months of Roentgen's discovery, eye complaints and severe progressive dermatitis were reported. In 1896, one of Edison's assistants Clarence E Dally, involved in the production of X-ray tubes, who had been using his own hand to test their output, developed ulcerating carcinoma of his repeatedly exposed left hand. Delayed effects of radiation began to be documented only 20 years after their initial discovery, through individual case reports. The death of Professor Benjamin Brown in 1911 was also attributed to X-ray exposure causing visceral degeneration, as a result of his earlier experiments, of fluoroscoping his own abdomen continuously for a 2 hours period during 1896. Germ line mutation as a delayed effect of ionizing radiation was documented by Muller in 1927 and won him the Nobel Prize. In 1928, Murphy reported 14 cases of microcephaly and mental retardation in children of mothers who had received pelvic radiotherapy early in pregnancy. In 1929, Murphy and

Goldstein documented 16 more patients with similar defects of microcephaly and mental retardation among children whose mothers had received pelvic radiotherapy early in pregnancy. In 1936, Percy Brown, a Radiologist historian, recorded case histories of adverse effects of radiation which occurred in people exposed from 1911 onwards. In 1940s and 1950s it was a common practice to treat ankylosing spondylitis patients with radiation. It was a permanent cure and remained the treatment of choice for approximately 20 years, until it was discovered that some who had been cured by radiation are dying from leukemia. In 1942, Dunlap reported radiation induced leukemia in radiologists and other radiation workers.<sup>2</sup>

In 1947, the Atom Bomb Casualty Commission (ABCC) was established to undertake scientifically designed studies in Hiroshima and Nagasaki, to establish the radiation effects following the atomic bomb blasts in these two cities. This commission reported the incidence of genetic effects, mutations, cataracts, leukemias and other malignancies in the population exposed in these blasts. These studies also documented effects on unborn fetuses, including microcephaly and mental retardation. In 1956, Stewart et al reported increased frequency of leukemia in children with history of radiation exposure during fetal life. In 1975, the ABCC was reorganized and renamed the RERF (Radiation effects and research foundation), funded equally by the United State of America and Japan. The RERF continues its work on genetics, cancer induction and other delayed effects of ionizing radiation.<sup>2</sup>

## RADIATION UNITS

### Conventional Units

These are such units as the “three Rs”, the roentgen, rad (radiation absorbed dose), rem and curie. All of these are very practical units. However, they did not fit into the SI unit system that is being promoted for the sake of having one unified system of units for all physical quantities.

### SI Units

The SI radiation units have been adopted by most organizations and publications. These are Gray (Gy), Sievert (Sv), Coulomb/kilogram (C/kg) and Becquerel.

	Exposure	Absorbed dose	Dose equivalent	Radioactivity
Common units	Roentgen (R)	Rad	Rem	Curie (Ci)
SI units	Coulomb/kilogram(C/kg)	Gray (Gy)	Sievert (Sv)	Becquerel (Bq)

## SPECIFIC QUANTITIES AND THEIR ASSOCIATED UNITS

### Exposure

The unit of radiation exposure is the Roentgen (R). Roentgen is defined as an amount of X-rays or gamma rays that produces a specific amount of ionization in a unit of air under standard temperature and pressure. This quantity can be measured directly in the air chamber, it is  $2.58 \times 10^{-4}$  C/kg of air.<sup>3</sup>

Exposure is quantified by the unit of kerma. Kerma is an acronym for kinetic energy released in material. Kerma quantifies the amount of energy transferred to charged particles from ionizing photon radiation. The unit of kerma was the rad and now gray (Gy).

### Absorbed Dose

Absorbed dose is defined as the quantity of radiation energy absorbed per unit mass of tissue.<sup>4</sup>

### Units

The conventional unit for absorbed dose is the rad, which is equivalent to 100 ergs of absorbed energy per g of tissue.

The SI unit is the gray (Gy), which is equivalent to the absorption of 1 J of radiation energy per kg of tissue.<sup>4</sup> The relationship between the two units is:

$$1 \text{ gray (Gy)} = 100 \text{ rads}^3$$

$$10 \text{ mGy} = 1 \text{ rad}$$

For a specific type of tissue and photon energy spectrum, the absorbed dose is proportional to the exposure (R) delivered to the tissue.

## BIOLOGICAL IMPACT

It is sometimes desirable to express the actual or relative biological impact of radiation. It is necessary to develop a distinction between the biological impact and the physical quantity of radiation because all types of radiation do not have the same potential for producing biological change. For example, one rad of one type of radiation might produce significantly more radiation damage than one rad of another type. In other words, the biological impact is determined by both the quantity of radiation and its ability to produce biological effects. The following two radiation quantities are associated with biological impact.

### Dose Equivalent

Dose equivalent (H) is the quantity commonly used to express the biological impact of radiation on persons receiving occupational or environmental exposures. Personnel exposure in a clinical facility is often determined and recorded as a dose equivalent.

Dose equivalent is proportional to the absorbed dose (D) and the quality factor or weighting factor ( $W_R$ ) for the radiation.<sup>5</sup> That is,

$$\text{Dose equivalent (Sv)} = \text{Absorbed dose (Gy)} \times W_R^5$$

The conventional unit for dose equivalent is the rem (roentgen equivalent man), and the SI unit is the sievert (Sv).

Sievert is defined as the dose in gray multiplied by quality factor. When the quality factor is 1, the different relationships between dose equivalent (H) and absorbed dose (D) are

Dose equivalent values can be converted from one system of units to the other by:

$$1 \text{ Sv} = 100 \text{ rem}$$

Most radiations encountered in diagnostic procedures (X-ray, gamma, and beta) have quality factor values of 1. Therefore, the dose equivalent is numerically equal to the absorbed dose. Some radiation types consisting of large (relative to electrons) particles have weighting or quality factor values greater than 1. For example, alpha particles have a quality factor value of approximately 20.<sup>6</sup>

S. No.	Type of radiation	Weighting/Quality factor
1.	X, gamma or beta radiation	1
2.	Alpha particles and multiple charged particles	20
3.	Neutrons	
	< 10 keV	5
	10 keV to 100 keV	10
	> 100 keV to 2 MeV	20
	> 2 MeV to 20 MeV	10
	> 20 MeV	5
4.	Protons	2

Three quantities: exposure, absorbed dose, and dose equivalent, although each expresses a different aspect of radiation, they all express radiation concentration. For the types of radiation used in diagnostic procedures, the factors that relate the three quantities have values of approximately 1 in soft tissue. Therefore, an exposure of 1 R produces an absorbed dose of approximately 1 rad, which, in turn, produces a dose equivalent of 1 rem.

### Effective Dose Equivalent (Effective Dose)

Irradiation from external environment affects the entire body, whereas medical diagnostic procedures generally affect only selected areas. To compare the risk assessment for all types of exposures the concept of effective dose equivalent has been developed. It takes into account the specific organs and areas of the body that are exposed. The point is that all parts of the body and organs are not equally sensitive to the possible adverse effects of radiation, such as cancer induction and mutations.

For the purpose of determining effective dose, the different areas and organs have been assigned tissue weighting factor ( $w_T$ ) values. For a specific organ or body area the effective dose is: Effective Dose Equivalent (Sv) = Dose Equivalent (Sv)  $\times w_T$ .

If more than one area has been exposed, then the total body effective dose is just the sum of the effective doses for each exposed area. Also, by using effective dose it is possible to put the radiation received from diagnostic procedures into perspective with other exposures, especially natural background radiation.

The weighting factors for various tissues are:<sup>5,7</sup>

Tissue	Weighting factor
Gonads	0.2
Active bone marrow, colon, lungs, stomach	0.12
Bladder, breast, esophagus, liver, thyroid	0.05
Bone surfaces, skin	0.01

There is often a need to compare the amount of radiation received by patients for different types of X-ray procedures, for example, a chest radiograph and a CT scan. The effective dose is the most appropriate quantity for doing this.

Effective dose equivalent from a chest radiographic examination is 0.02 mSv; it means that the risk involved from a CXR is the same as the risk involved in exposing the entire body to an X-ray exposure of 0.02 mSv.

### Typical Effective Doses from Exposure to Medical Radiation<sup>8</sup>

Diagnostic procedure	Typical effective dose (mSv)	Number of chest X-rays leading to comparable exposure
Chest (PA)	0.02	1
Extremities	0.01	0.5
Skull	0.07	3.5
Thoracic vertebrae	0.7	35
Lumbar vertebrae	1.3	65
Hip	0.3	15
Pelvis	0.7	35
Abdomen	1.0	50
Mammography (bilateral in 2 planes)	0.5	25
Intravenous pyelography	2.5	125
Head CT	2.3	115
Chest CT	8	400
Abdomen or pelvis CT	10	500
Positron emission tomography	7.2	360

This leads to the conclusion that a chest CT leads to 400 folds greater radiation exposure for the patient than conventional chest projection radiography.<sup>9</sup>

## INTERACTION OF RADIATION WITH MATTER

### Radiation Types and Sources

Radiation can take several different forms and is simply a mechanism whereby energy is transmitted through space. Medical imaging modalities that involve ionizing radiation make use of electromagnetic waves located near one end of the electromagnetic spectrum. This spectrum consists of differing electromagnetic waves that are defined by their electromagnetic wavelength. At one end of the spectrum are the long-wavelength and relatively innocuous radio- and microwaves. As the electromagnetic wavelength decreases, radiation passes through the spectrum of visible light, after which the short-wavelength, high-energy X-rays, gamma rays, and cosmic rays are encountered. This energy has the capacity to be harmful to biologic tissue because it carries the potential

to displace electrons from its energy level or shell around the nucleus. This can lead to ionization of the affected atom and explains why these forms of electromagnetic waves are termed “ionizing radiation.” The effects of ionizing radiation on biologic tissues at the atomic and molecular level are concerning for several reasons. First, a displaced electron can cause damage to other cell components as it is ejected rapidly from its orbit. Second, the resulting highly chemically reactive ionized atom, or “free radical,” can have deleterious effects on the cell of which it is a part. Third, the altered structure of the atom that occurs once an electron is lost may affect the function of the tissue involved; this result may be particularly grievous if the involved tissue is a chromosome within a radiosensitive cell such as those found in the breast or ovary.

Humans are exposed to unavoidable forms of ionizing radiation each day. This type of radiation is classified as background radiation and is an unavoidable consequence of living. Background radiation originates from radon gas seeping out of the earth, natural radioactivity being emitted from rocks and other organic compounds in the ground, and cosmic rays that constantly rain down from space, among other sources. Although man-made radiation sources include airport security scanners, smoke detectors, television sets, and fluorescent lamp starters, medical imaging accounts for 95 percent of all exposure from man-made radiation sources. The reason for this rapid alteration in the proportions of exposure from man-made radiation sources over the past few years has been the phenomenal increase in the use of ionizing radiation in medical imaging.<sup>10</sup>

There are three major ways in which radiation, especially X-rays is absorbed and results in ionization: The photoelectric effect, the Compton effect and Pair production.

- At low energies (30 to 100 keV), as in diagnostic radiology, the photoelectric effect is important. In this process, the incident photon interacts with an electron in one of the inner shells of an atom (typically K, L, or M). If the energy of the photon is greater than the binding energy of the electron, then the electron is expelled from the orbit with a kinetic energy that is equal to the energy of the incident photon minus the binding energy of the electron<sup>11</sup>. The photoelectric effect varies as a function of the cube of the atomic number of the material exposed ( $Z$ ); this fact explains why bone is visualized much better than soft tissue on radiographs (Fig. 1).
- At intermediate energies, as used in therapeutic radiology, the Compton effect dominates. In this process, the incident photon interacts with an electron in an orbital shell. Part of the incident photon energy appears as kinetic energy of electrons and the residual energy continues as a less energetic deflected photon (Fig. 2).<sup>11</sup>
- At energy levels above 1.02 MeV, the photons may be absorbed through pair production. In this process, both a positron and an electron are produced in the absorbing material. A positron has the same mass as an electron but has a positive instead of a negative charge. The positron travels a very short distance in the absorbing medium

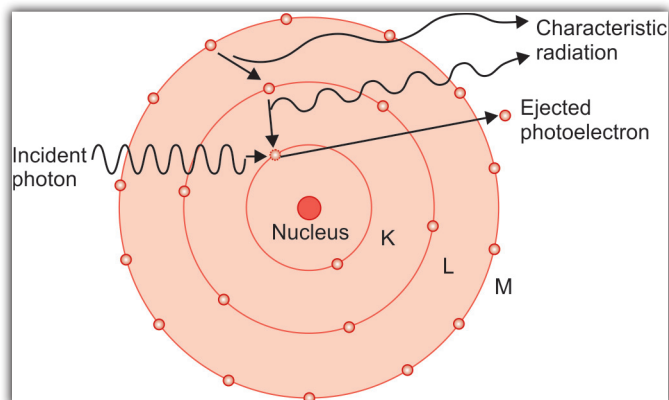


**Fig. 1** Photoelectric effect

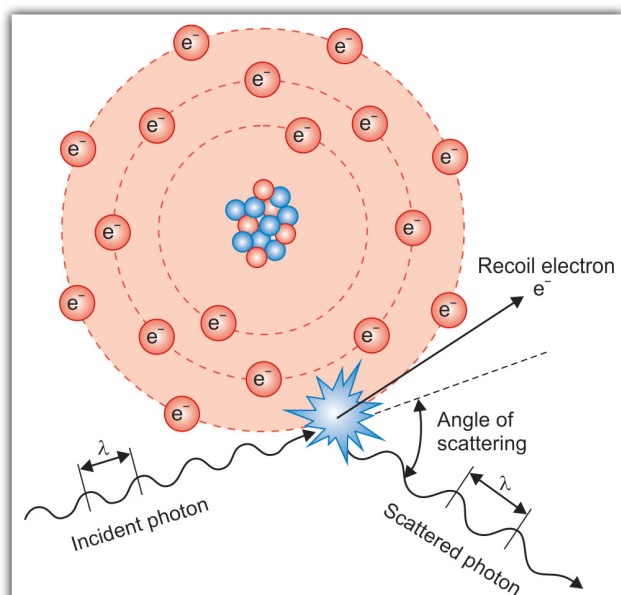


**Fig. 2** Compton scattering

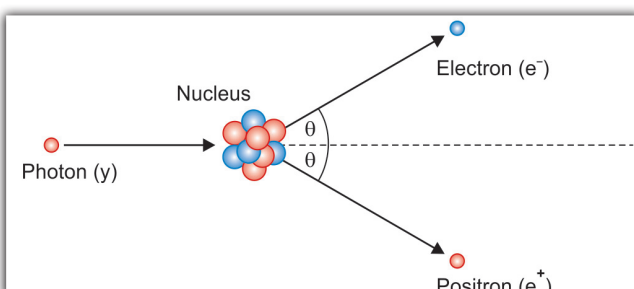


**Fig. 3** Pair production

before it interacts with another electron. When that happens, the entire mass of both particles is converted to energy, with the emission of two photons in exactly opposite directions (Fig. 3).

## BIOLOGICAL EFFECT OF RADIATION

- Critical target in cell-DNA
- Result from damage to DNA
- Radiation may be directly or indirectly acting (**Fig. 4**).  
**Direct action:** (DNA) directly gets ionized or excited-leading to biological damage.

**Indirect action:** Radiation interacts with other atom/molecules (water) to produce free radicals which than damage DNA. 2/3rds of X-ray damage to DNA caused by hydroxyl radical.<sup>12</sup>

Absorption of radiation may result either in killing of cell or its modification by genetic change.

## CLASSIFICATION OF RADIATION INJURY

Since the majority of radiation exposure is from man-made sources and that the majority of this exposure originates from medical imaging, it is important to understand the possible effects and risks of this radiation exposure for the human body. Radiation effects can be divided into two general types: deterministic effects and stochastic effects.

### Types of radiation effects

Type	Effects
Deterministic	Erythema, epilation, skin necrosis, cataract formation
Stochastic	Carcinogenesis, hereditary effects

- Deterministic effects are the result of the excessive cell death that can occur following ionizing radiation exposures. These effects include skin erythema, epilation, necrosis, and lens cataract formation. Because these effects occur only after a critical mass of cells have died, they have a known radiation exposure threshold below which their occurrence can be avoided. Thus deterministic effects or certainty effects are directly related to a known dose of radiation and have a dose threshold and their severity is also dose related.
- Stochastic radiation effects are random events which are not dose related but their probability increases with an increase in radiation dose. Stochastic effects include carcinogenesis and hereditary effects. The possibility of a stochastic effect taking place supports the practice of exposures being kept as low as reasonably achievable (ALARA).

To summarize,

### Deterministic effects      Stochastic effects

1. Cell killing	Cell modification
2. Threshold described	No threshold for occurrence
3. Severity is dose dependent	Severity is independent of dose
4. Erythema, epilation, skin necrosis, cataract formation	Carcinogenesis, hereditary effects

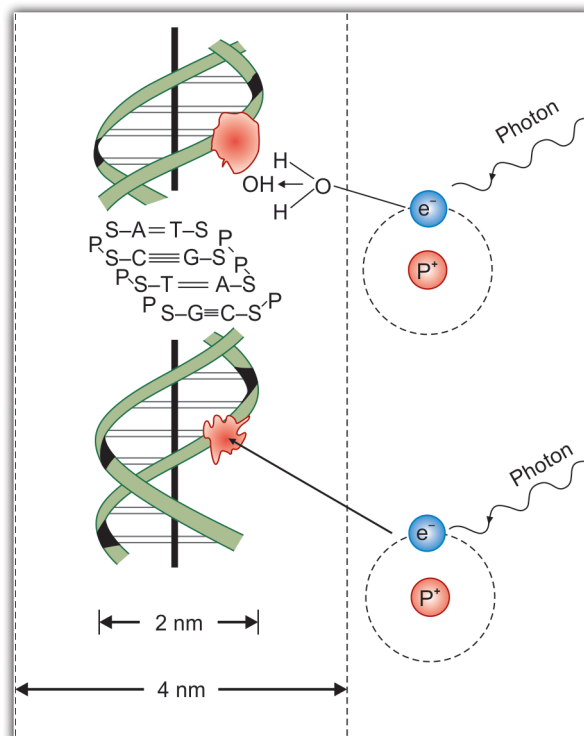


**Fig. 4** Radiation may be directly/indirectly acting on the DNA of the cell

## Malignancies Associated with Radiation Exposure

Carcinogenesis is stochastic in nature.

**Leukemia:** Two types of adult leukemias are associated with radiation exposure. These are acute and chronic myeloid leukemias. Radiation exposure during childhood results in an increased incidence of acute lymphatic leukemia. The latency period of leukemia is a minimum of 2 years, peaks at 7 to 12 years and returns to zero at about 30 years.<sup>13</sup>

**Other radiation induced cancers:** Malignancies of skin, lung, bone, blood dyscrasias and meningiomas have been described.. Other malignancies known to be associated with radiation are osteosarcomas, breast carcinoma and thyroid carcinoma.<sup>14</sup>

## Genetic Effects of Radiation

Genetic effects are stochastic by their nature.

- Radiation can either damage the DNA or affect the chromosome itself. Genetic effects on humans manifest as mutations leading to congenital defects in the offspring or causing malignancies.
- The genetic effects of radiation are evaluated on the basis of their mutational effects which is expressed as the “genetic doubling dose”. Genetic doubling dose is an estimate of the amount of acute radiation which will double the spontaneous mutation rate or will cause an increase in the mutation rate which is equal to the

number of spontaneous mutations which normally occur.

- The most common genetic effects such as autosomal and X linked changes and chromosomal alterations in an exposed population have been estimated to be occurring at  $1 \times 10^{-2}$  per Sv (0.01 mutations per Sv).<sup>12,13</sup>
- Genetically significant dose (GSD):** GSD is a genetic dose index. It is the gonad dose, that if received by every member of the population would be expected to produce the same total effect on the population as the sum of the individual dose as actually received. The GSD is therefore a genetic dose index of the presumed genetic impact of radiation exposure on the total population due to radiation induced mutations on the reproduction cells of this generation that can be translated as risk to the descendants.<sup>15</sup> The GSD is merely an attempt at estimating the dose received by the population gene pool<sup>1</sup> and an analysis of the GSD from diagnostic radiology can be used to estimate possible detriment from a specific practice.<sup>15</sup>

## DETERMINISTIC EFFECTS AS DOCUMENTED FROM RADIATION ACCIDENTS

### Acute Total-Body Irradiation

The data regarding the acute effects of total-body irradiation on humans comes primarily from Japanese survivors of the atomic bomb, Marshall Islanders exposed to fall out radiation and victims of a few nuclear installation accidents, such as Chernobyl (in Ukraine).<sup>16</sup> Clinical manifestations depend on the total-body dose.

- At doses in excess of 100 Gy to the total body, death usually occurs within 24 to 48 hours from neurologic and cardiovascular failure. This is known as the cerebrovascular syndrome. Because cerebrovascular damage causes death very quickly, the failure of other systems do not have time to develop.
- At doses between 5 and 12 Gy, death may occur in a matter of days, as a result of the gastrointestinal syndrome. The symptoms during this period may include nausea, vomiting and prolonged diarrhea for several days, leading to dehydration, sepsis and death.
- At total-body doses between 2 and 8 Gy, death may occur several weeks after exposure and is due to effects on the bone marrow, which results in the hematopoietic syndrome. The full effect of radiation is not apparent until the mature hematopoietic cells are depleted. Death from the hematologic damage occurs at about 20 to 30 days after exposure and the risk of death continues over the next 30 days. Clinical symptoms during this period may include chills, fatigue and petechial hemorrhage. The threshold for this syndrome is 1 Gy.<sup>16</sup>
- Mean lethal dose or LD 50:** The lethal dose 50 or LD 50 is a term borrowed from pharmacology and is defined as

the dose of an agent that causes mortality in 50 percent of given population in a given time. For radiation, LD 50 has been estimated from the atomic bomb explosion at Hiroshima and Nagasaki and from accidental exposures. Based on these data and the observation that with medical support humans can survive a total body dose of 4 Gy, estimates of LD 50 for humans is 3 to 4 Gy.<sup>12</sup>

### Chronic Radiation Effects

These effects result from prolonged exposure of lower intensity or may appear as late effects in survivors of more acute exposures. These may be due to whole body or partial body irradiation.

**CNS:** Mild encephalopathy, focal neurological changes and transverse myelitis are known side effects of CNS irradiation. A unique late effect of cranial radiation combined with chemotherapy known as leukoencephalopathy, has been described as a necrotizing reaction and is usually noted 4 to 12 months.<sup>16</sup> Radiation necrosis occurs in 1 to 5 percent of patients after 55 to 60 gray doses fractionated over 6 weeks, 75 percent of the cases occur within 3 years.<sup>17</sup>

- Skin:** The changes include erythema, desquamation, thinning of epidermis, pigmentation and hair loss.
- Heart and blood vessels:** Asymptomatic pericardial effusion, chronic constrictive pericarditis and pancarditis.
- Lung:** Radiation pneumonitis develops in 3 to 6 weeks following exposures of >25 Gy. This can lead to permanent scarring.<sup>17</sup>
- GIT:** Chronic phase of radiation enteropathy usually presents between 6 months and 5 years of exposure. The terminal ileum is the most commonly affected part. The changes include fibrosis, perforation, fistula formation, stenosis, etc.
- Hematopoietic system:** Fatty replacement of marrow occurs above a threshold of 50 Gy.<sup>17</sup>
- Eye:** Cataract has been recorded at 2 to 8 Gy of single exposure.<sup>17</sup>
- Bladder:** Interstitial fibrosis, telangiectasia, ulceration and reduced capacity.

### THE REGULATORY BODIES

There are several regulatory bodies at the International and National level.

The regulatory bodies lay down norms for protection against radiation and also recommend the dose limits for radiation workers and the general public. The ICRP or the International Commission for radiation protection is the international regulatory body. Each country has its national counterpart of the ICRP. In America the counterpart is the NCRP or The National Commission for Radiological Protection and in India it is the AERB or the Atomic Energy Regulatory Board.

- The International Commission of Radiation Protection (ICRP) was formed in 1928, on the recommendation of the first International Congress of Radiology in 1925. The commission consists of a chairman, a secretary and 12 members who are chosen from across the world based on their expertise. ICRU is the International Commission on Radiation Units and measurements.<sup>18</sup>
- The Indian regulatory board is the AERB, Atomic Energy Regulatory Board. It was constituted on November 15, 1983 by the President of India by exercising the powers conferred by Section 27 of the Atomic Energy Act, 1962 (33 of 1962) to carry out certain regulatory and safety functions under the Act. The Board consists of a full time chairman, an exofficio member, three part time members and a secretary.<sup>19</sup>
- Radiation safety act in India:** Radiation safety in handling of radiation generating equipment is governed by section 17 of the Atomic Energy Act, 1962, and the Radiation Protection Rules (RPR), GSR- 1601, 1971 issued under the Act. The "Radiation Surveillance Procedures of Medical Applications of Radiation, GSR - 388, 1989", issued under rule 15 specify general requirements for ensuring radiation protection in installation and handling of X-ray equipment.<sup>19</sup>

### Role of AERB

According to AERB safety code for medical diagnostic X-ray equipment and installations document, regulatory controls of AERB are as follows:<sup>19</sup>

- Design Certification:** Every medical diagnostic X-ray equipment shall meet the design safety specifications stipulated in the AERB Code. The manufacturer/vendor shall obtain design certification from the competent authority prior to manufacturing the X-ray equipment.
- Type Approval/No Objection Certificate:** Prior to marketing the X-ray equipment the manufacturer shall obtain a Type Approval Certificate from the competent authority for indigenously made equipment. Only type-approved and NOC validated equipment shall be marketed and used in the country.
- Approval of layout:** No X-ray unit shall be commissioned unless the layout of the proposed X-ray installation is approved by the competent authority.
- Registration of X-ray equipment:** Acquisition of X-ray equipment, by purchase, transfer, gift, leasing or loan, shall be registered with the competent authority by the person acquiring the equipment. Registration shall be done only after the installation is approved from radiation safety viewpoint.
- Commissioning of X-ray equipment:** No X-ray equipment shall be commissioned unless it is registered with the competent authority.
- Inspection of X-ray installations:** The diagnostic X-ray installations shall be made available by the employer/

owner for inspection, at all reasonable times, to the competent authority or its representative, to ensure compliance with the code.

- Decommissioning of X-ray installations:** Decommissioning of X-ray equipment shall be registered with the competent authority immediately by the employer/ owner of the equipment/ installation.
- Certification of RSO:** Any person accepting consultancy assignment to discharge the duties and functions of RSO in diagnostic X-ray installations shall do so only after obtaining certification from the competent authority for the purpose. Such certification shall be granted on the basis of adequacy of the person's qualifications, experience and testing/survey/dosimetry equipment available.
- Certification of service engineers:** Only persons holding a valid certificate from the competent authority shall undertake servicing of X-ray equipment. Certification shall be granted on the basis of qualifications, training, experience, and safety record of such person and availability of servicing facilities.
- Penalties:** Any person who contravenes the provisions of the Radiation Protection Rules, 1971, elaborated in this Code, or any other terms or conditions of the license/ registration/certification granted to him/her by the competent authority, is punishable under sections 24, 25 and 26 of the Atomic Energy Act, 1962. The punishment may include fine, imprisonment or both, depending on the severity of the offence.

### Radiation Protection Survey and Program

The responsibility for establishing a radiation protection program rests with the hospital administration/owners of the X-ray facility. The administration is expected to appoint a Radiation Safety Committee (RSC), and a Radiation Safety Officer (RSO). Every department should have an RSO. This Officer should be an individual with extensive training and education in areas such as radiation protection, radiation physics, radiation biology, instrumentation, dosimetry and shielding design. In India AERB has specified duties of the RSO which include assisting the employer in meeting the relevant regulatory requirements applicable to his/her X-ray installation.<sup>19</sup> He/she shall implement all radiation surveillance measures, conduct periodic radiation protection surveys, maintain proper records of periodic quality assurance tests, and personnel doses, instruct all workers on relevant safety measures, educate and train new entrants, and take local measures, including issuance of clear administrative instructions in writing, to deal with radiation emergencies. The RSO should also ensure that all radiation measuring and monitoring instruments in his/her custody are properly calibrated and maintained in good condition.<sup>19</sup> The duties also include maintaining a record of all radiation surveys performed, deficiencies observed and remedial actions taken.

It is recommended that the RSC (Radiation Safety Committee) should comprise of a radiologist, a medical physicist, a nuclear medicine personnel, a senior nurse and an internist. It is the duty of RSC to perform a regular radiation protection survey. This survey has 5 phases which are:<sup>18</sup>

1. **Investigation:** To obtain information regarding layout of the department, workload, personnel monitoring and records.
2. **Inspection:** Each diagnostic installation in the department is examined for its protection status with respect to its operating factors, control booth and availability of protection devices.
3. **Measurement:** Measurements are conducted on exposure factors. In addition scattered radiation and patient dose measurements in radiography and fluoroscopy are performed.
4. **Evaluation:** The radiation protection status of the department is evaluated by examination of records, equipment working, status of protective clothing and the radiation doses obtained from phase-3.
5. **Recommendations:** A report is prepared on the protection status of the department and the problem areas if any identified, for which recommendations are made regarding corrective measures.<sup>18</sup>

## PROTECTION AGAINST RADIATION HAZARD

### Principles of Radiation Protection

The current radiation protection standards are based on three general principles, which are recommendations of the International Commission on Radiological Protection (ICRP) and include:<sup>20</sup>

- **Justification:** No practice shall be adopted unless its introduction produces a net positive benefit.
- **Optimization:** All exposures shall be kept as low as reasonably achievable, economic and social factors being taken into account.
- **Dose limitation:** The dose equivalent to individuals shall not exceed the limits recommended for the appropriate circumstances.

- **Justifiable use:** A practice that entails exposure to radiation should only be adopted if it yields sufficient benefit to the exposed individuals or to society to outweigh the radiation detriment it causes or could cause (i.e. the practice must be justified).<sup>21</sup> Internationally, in countries with regulatory bodies, it is recommended that all diagnostic practices should be justified. This involves the correct assessment of the clinical indications for the requested examination, knowledge of the expected yield from the examination and the way in which the results are expected to influence the diagnosis and subsequent medical management of the patient. The expected clinical benefit must be such that it will offset the radiation detriment. For example, benefit to risk ratio is high for CT brain in cerebrovascular hemorrhage and low in screening mammography in women below 35 years. However, since CT examinations are known to contribute a large dose of diagnostic radiation, it is recommended that CT referrals should be reviewed meticulously.<sup>22</sup>

It has been reported that in a well justified series of barium enema examinations, justification being determined by the degree of symptoms suffered, only 30 percent of the examinations will be positive. This may seem a low return and indicate that too many people are subjected to the procedure. However, the conclusion drawn was that the examination is well justified and that a negative finding is a positive result.<sup>23</sup>

- **Optimization and alara:** Radiation sources and installations should be provided with the best available protection and safety measures under the prevailing circumstances, so that the magnitudes and likelihood of exposures and the numbers of individuals exposed be kept As Low As Reasonably Achievable (ALARA), economic and social factors being taken into account.<sup>24</sup> In the United Kingdom (UK), this has for reasons of legal precedent been amended to read ALARP-As Low As Reasonably Practicable (ALARP).<sup>25</sup> Following

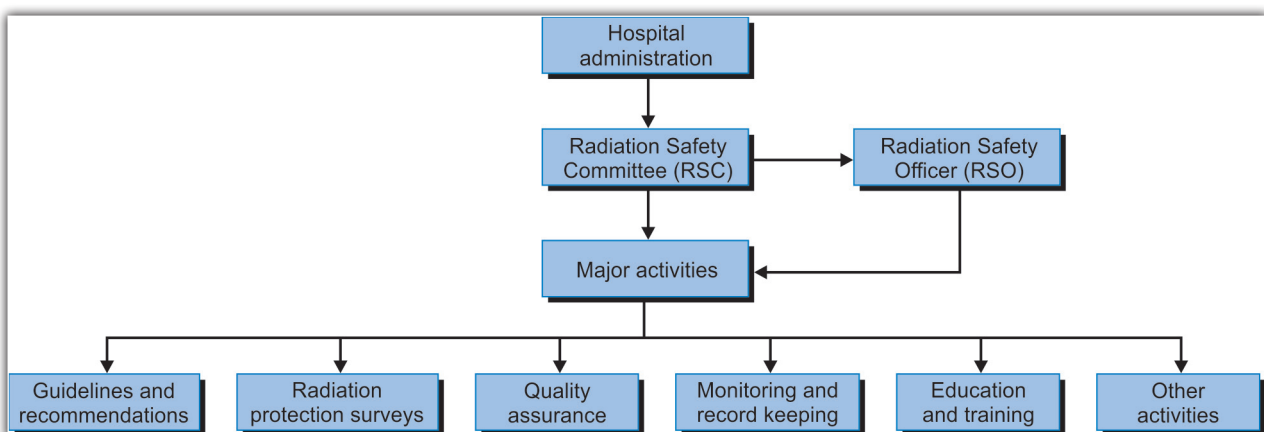


**Table 1** Recommended dose limits for radiation workers and general public<sup>18,19</sup>

Occupational workers		Public	
	Limit	Annual Equivalents	Limit
ICRP	20 mSv/yr over 5 years	20 mSv	1 mSv/yr over 5 years
NCRP	Cumulative dose = Age in yrs × 10 mSv	50 mSv	5 mSv for 5 years period
AERB	100 mSv for 5 years period	30 mSv	1 mSv/yr for 5 years

the principle of ALARA or ALARP, the radiation protection worker is generally more structured and controlled than in the case of the patient where rules and regulations are more difficult to standardize.

- **Dose limitation:** There is no absolute evidence of a threshold below which no damage occurs. Even the lowest doses may cause damage to the cells which might, later lead to malignancy or hereditary effects if the cells irradiated are germ cells in the gonads. Therefore, we have to assume that the probability of radiation induced cancer or serious hereditary defects are proportional to the radiation dose right down to the lowest levels.<sup>26</sup> This suggests that no radiation dose, however low, can be considered absolutely safe. Although this may be an overestimation of the true radiation effects at low dose levels, it is preferable to hold the model and it is the basis for radiation protection standards today. Individual doses due to the combination of exposures from all relevant practices should not exceed specified dose limits for occupational and public exposure. Different dose limits are specified for the radiation workers as the expected benefit from the work they do while handling radiation will outweigh the small increase in risk (**Tables 1 and 2**).
- **Maximum permissible dose equivalent (MPD):** It may be defined as the maximum dose of ionizing radiation which an individual may accumulate over a long period of time with a negligible risk of significant body or genetic damage.
  - $MPD = 5(N-1)R$ , where N is age in years >18 years and R is the exposure in Roentgens. The unit of MPD is rem.
  - The newer recommendation is  $MPD = \text{Age in years} \times 1 \text{ rem}$ , i.e. the individual effective dose for a lifetime should not exceed the value of his/her age.

## CARDINAL PRINCIPLE OF RADIATION PROTECTION

The triad of radiation protection measures is “time-distance-shielding”, that is:

1. Keep the time of exposure to radiation as short as possible.
2. Maintain as large a distance as possible between the radiation and the exposed person.

**Table 2** Recommendations for dose limits to eye and skin for occupational workers<sup>18,19</sup>

Dose limits to skin, hands, Feet (mSv/yr.)	Dose limits to lens of eye (mSv/yr.)
ICRP 500	150
NCRP 500	150
AERB 500	150

3. Insert shielding material between the radiation source and the exposed person.

**Time:** The exposure time is related to radiation exposure and exposure rate (exposure per unit time) as follows:

$$\text{Exposure} = \text{Exposure rate} \times \text{Time}$$

The algebraic expressions simply imply that if the exposure time is kept short, then the resulting dose to the individual is small.<sup>18</sup>

**Distance:** The second radiation protection action relates to the distance between the source of radiation and the exposed individual. The exposure to the individual decreases inversely as the square of the distance. This is known as the inverse square law, which is stated mathematically as:

$$I \sim \frac{1}{d^2}$$

Where I is the intensity of radiation and d is the distance between the radiation source and the exposed individual. For example, when the distance is doubled the exposure is reduced by a factor of four.<sup>4</sup>

## Shielding

The third radiation protection action relates to shielding. Shielding implies that certain materials (concrete, lead) will attenuate radiation (reduce its intensity) when they are placed between the source of radiation and the exposed individual.

1. X-ray tube shielding
2. Room shielding
  - a. X-ray equipment room shielding
  - b. Patient waiting room shielding.
  - c. Control room shielding
3. Personnel shielding
4. Patient shielding

Three types of radiations have to be considered in radiation protection:

1. Useful beam is the radiation passing through the tube aperture, previously called the primary beam.
2. Leakage radiation—includes all the radiation passing through the tube housing, other than the useful radiation.
3. Scattered radiation—which has undergone a change in direction during passage through matter.

### X-ray Tube Shielding (Source Shielding)

The X-ray tube housing is lined with thin sheets of lead because X-rays produced in the tube are scattered in all directions. This shielding is intended to protect both patients and personnel from leakage radiation. Manufacturers of X-ray devices are required to shield the tube housing so as to limit the leakage radiation exposure rate to  $< 0.1 \text{ R hr}^{-1}$  at 1 meter from the tube anode.<sup>27</sup> AERB recommends a maximum allowable leakage radiation from tube housing not greater than 1 mGy/hour/100 cm.<sup>19</sup>

### Room Shielding (Structural Shielding)

- The lead lined walls of radiology department are referred to as protective barriers because they are designed to protect individuals located outside the X-ray rooms from unwanted radiation.
- 2 mm lead is equivalent to 25 mm layer of high quality barium plaster, 225 mm of solid brick, 150 mm of concrete or  $\frac{1}{2}$  brick thickness and  $\frac{1}{2}$  inch plaster.<sup>11</sup>
- A basic principle of permanent barriers is that joints and holes must be covered by the same or equivalent protective barrier as the wall.

There are two types of protective barriers

- a. *Primary barrier:* It is one which is directly struck by the primary or the useful beam and whose atomic number and thickness is sufficient to reduce the exposure rate of the useful beam to the MPD.
  - b. *Secondary barrier:* It is one which is exposed to stray radiation either by leakage from X-ray tube or by scattered radiation from the patient.
- The shielding of X-ray room is influenced by the nature of occupancy of the adjoining area. In this respect two types of areas have been identified.
    - a. *Control area:* It is defined as the area routinely occupied by radiation workers who are exposed to an occupational dose. For control area, the shielding should be such that it reduces exposure in that area to  $< 26 \text{ mC/kg/week}$ .
    - b. *Uncontrolled areas:* They are those areas which are not occupied by occupational workers. For these areas, the shielding should reduce the exposure rate to  $< 2.6 \text{ mC/kg/week}$ .

### Exposure calculations

Five factors must be considered for exposure calculations at any point:<sup>28</sup>

1. **Workload (W):** It is the quantity of X-rays generated per week.  

$$\text{Workload} = \text{mAs/patient} \times \text{patients/hour} \times \text{hours/week} = \text{mAs/week.}$$
2. **Exposure (E):** Roentgen per mA.min at 1 meter. This is to convert the workload into Roentgens.
3. **Use factor (U):** It is the fraction of time that the beam is directed at a particular barrier.
4. **Occupancy factor (T):** Amount of time that the area will be occupied. T = 1 means that the area will be occupied by the same individuals throughout the full workday.
5. Distance (d).

Weekly exposure at a point in question (E) can be calculated as

$$E = E' WUT/d^2.$$

The value thus calculated can be used to determine the thickness of the primary barrier.

- **Half value layer (HVL):** It is the thickness of a specific substance that when introduced into the path of a beam of radiation, reduces the exposure rate by 50 percent.<sup>28</sup>

Tube potential (kVp)	HVL <sup>28</sup>	
	Lead (mm)	Concrete (inches)
40	0.03	0.13
80	0.19	0.42
100	0.24	0.6
125	0.27	0.76
150	0.28	0.86

- For example, if the exposure at a point is 3.2 R/week and the permissible exposure is 0.1 R/week, the required number of HVLs calculated, which will reduce 3.2 R/week to 0.1 R/week, is 5. If the HVL of the beam is 0.25 mm of lead, the barrier thickness would be 1.25 mm ( $0.25 \times 5 = 1.25 \text{ mm}$ ).
- In general, the primary protective barrier should consist of 1/16 inch lead extending 7 feet from the floor, when the X-ray tube is 5 to 7 feet from the wall. This barrier also takes care of the leakage radiation.
- A secondary protective barrier under the same operating conditions should consist of 1/32 inch of lead. This secondary barrier extends from the top of the primary barrier to the ceiling and should overlap the primary barrier at least 0.5 inches at the seam.<sup>28</sup>
- Patient waiting areas are provided outside the X-ray room. A suitable warning signal such as red light and a warning placard at a conspicuous place should be

provided and kept 'ON' when the unit is in use to warn persons not connected with the particular examination from entering the room.<sup>19</sup>

#### *Shielding of the X-ray control room*

The control room of X-ray equipment is a secondary protective barrier which has two important aspects:

- The walls and viewing window of the control booth, which should have lead equivalents of 1.5 mm.
- The location of control booth, which should not be located where the primary beam falls directly, and the radiation should be scattered twice before entering the booth.

The AERB recommends the following shielding for the X-ray control room:<sup>19</sup> The control panel of diagnostic X-ray equipment operating at **125 kVp or above** (as in CT) is installed in a separate room located outside but contiguous to the X-ray room and provided with appropriate shielding, direct viewing and oral communication facilities between the operator and the patient. In case of X-ray equipment operating up to 125 kVp, the control panel can be located in the X-ray room. AERB recommends that the distance between control panel and X-ray unit/chest stand should not be less than 3 m for general purpose fixed X-ray equipment. In mobile radiography, where there is no fixed protective control booth, the technologist should remain at least 2 m from the patient, the X-ray tube and the primary beam during exposure. In this respect, the ICRP as well as the NCRP recommends that the length of the exposure cord on mobile radiographic units should be at least 2 m long. The size of the CT room housing the gantry of the CT unit as recommended by AERB should not be less than 25 m<sup>2</sup>.<sup>19</sup>

#### *Personnel Shielding*

Shielding of occupational workers can be achieved by following methods:

- Personnel should remain in the radiation environment only when necessary (step behind the control booth, or leave the room when practical)
- The distance between the personnel and the patient should be maximized when practical as the intensity of radiation decreases as the square of distance (inverse square law).
- Shielding apparel should be used as and when necessary which comprise of lead aprons, eye glasses with side shields, hand gloves and thyroid shields.

Lead aprons are shielding apparel recommended for use by radiation workers. These are classified as a secondary barrier to the effects of ionizing radiation. These aprons protect an individual only from secondary (scattered) radiation, not the primary beam.<sup>29</sup>

- The thickness of lead in the protective apparel determines the protection it provides. It is known that 0.25 mm lead thickness attenuates 66 percent of the beam at 75 kVp and 1 mm attenuates 99 percent of the beam at same kVp. It is

recommended that for general purpose radiography the minimum thickness of lead equivalent in the protective apparel should be 0.5 mm.<sup>29</sup> It is recommended that women radiation workers should wear a customized lead apron that reaches below midthigh level and wraps completely around the pelvis. This would eliminate an accidental exposure to a conceptus.<sup>30</sup>

- **Care of the lead apparel:** It is imperative that lead aprons are not abused, such as by dropping them on the floor, piling them in a heap or improperly draping them over the back of a chair.<sup>31</sup> Because all of these actions can cause internal fracturing of the lead, they may compromise the apron's protective ability. When not in use, all protective apparel should be hung on properly designed racks. Protective apparel also should be radiographed for defects such as internal cracks and tears at least once a year.
- **Gonad shield:** Gonad shields shall have a minimum lead equivalence of 0.5 mm.
- Other protective apparel includes eye glasses with side shields, thyroid shields and hand gloves. The minimum protective lead equivalents in hand gloves, gonadal shields and thyroid shields should be 0.5 mm.

#### *Patient Shielding*

Radiation protection of the patient involves both technical and medical decisions. The technical decisions relate to the choices of the appropriate equipment and to the technique. It is noted that the reduction in radiation dose by changes in the equipment will result in a more consistent reduction while reduction due to radiological technique need constant effort to maintain the benefit.<sup>32</sup>

#### *Equipment*

There are many radiation protection features and accessories on modern X-ray equipment. These include:

- **Beam filtration** causes lower energy photons to be absorbed by the filters and thus increase the mean energy of the beam and its penetration power and hence decrease the patient dose. Absorption primarily takes places with X-rays of less than 40 keV of energy and virtually all X-rays below 10 keV are absorbed.<sup>33</sup> These low energy X-rays contribute to patient dose without contributing to the image.

According to the AERB safety code for medical diagnostic X-ray equipment and installations.<sup>19</sup>

#### Minimum total filtration for X-ray tubes

Maximum rated tube potential (kVp)	Minimum total filtration (mm Al)
Less than 70	1.5
70 to and including 100	2.0
Above 100	2.5

Total filtration should be indicated on the tube housing. The total permanent filtration in the tube should be not less than 1.5 mm Al.

For mammography, the AERB guideline states that the total filtration in the useful beam shall be not less than 0.03 mm of molybdenum for screen-film mammography for Mo-W alloy target type and 0.5 mm of aluminium for xeromammography for W-target X-ray tubes.<sup>19</sup>

- **Beam collimation:** During any radiographic procedure, the area of the patient exposed to the X-ray beam should be limited to the area of clinical interest. Tissues inside the primary beam receive doses that are orders of magnitude higher than doses received by tissue outside the primary beam. By using collimation to expose only the area of clinical interest, one can substantially reduce unnecessary patient exposure.<sup>34</sup> Use of collimation has another important effect: By reducing the area of the X-ray beam, the amount of scattered radiation that reaches the image receptor is also decreased. The resulting images have better contrast.
- The table top should be one which allows a high beam transmission which increases the quantity of diagnostically important photons reaching the film. A carbon fiber material is generally used for a high transmission table top.
- **Image receptors:** The intensifying screen was designed to optimize absorption of the radiation by converting absorbed X-ray energy into visible light, which would be more readily absorbed by the film than the more energetic X-ray photons. The advent of fluorescent intensifying screens, which act as an image amplifier and their use with X-ray film, which is highly sensitive to the visible light photons, significantly reduce the absorbed dose to the patient while still maintaining the image quality. The intensification factor is the radiation exposure required without screens divided by the exposure required with screens to provide the same film blackening effect. This factor is dependent on the screen, the film and the exposure factors. One method of classifying screens is to put them into categories according to their relative light output or speed. In radiography the speed of an image receptor is inversely related to the radiation exposure required to produce a certain amount of film blackening. Therefore, a fast screen (high speed) requires less X-ray exposure than a slow screen (low speed) to provide a given image density. Rare-earth screen film combinations, in use today, reduce the patient dose considerably without loss of diagnostic quality.<sup>35</sup> The image intensifier tubes, in use today, also have efficient input phosphors that play a role in reducing the dose to the patient.
- **Source to image receptor distance (SID):** The dose to the patient is reduced when the source-to-skin-distance (SSD) is increased and the SSD is related to the source-to-image-receptor distance (SID). Therefore, equipment with a larger SID will result in a lower dose to the patient.

This is of importance both for standard radiography and for fluoroscopy. The recommended source-to-skin distance for an under couch fluoroscopic tube is a minimum of 30 cm and more when possible as the patient dose is very much higher when the tube is close to the table top.<sup>32</sup>

- **Antiscatter grids** reduce scattered radiation reaching the film thus improving the quality of the resulting radiograph and reducing chances of repeat exposures.<sup>18,31</sup>

**Fluoroscopy X-ray equipment:** According to the AERB safety code, the following have been recommended for fluoroscopy X-ray equipment.<sup>19</sup>

- **Fluoroscopy tube housing and filtration:** Every housing for medical diagnostic X-ray equipment shall be so constructed that leakage radiation through the protective tube housing in any direction, averaged over an area not larger than 100 cm<sup>2</sup> with no linear dimension greater than 20 cm, shall not exceed an air kerma of 1 mGy in one hour at a distance of 1.0 m from the X-ray target when the tube is operating at the maximum rated kVp and for the maximum rated current at that kVp. There shall be a distinctly visible mark on the tube housing to indicate the plane of focus.
- **Protective lead glass:** Protective lead glass covering of the fluorescent screen shall have a lead equivalent thickness of 2.0 mm for units operating up to 100 kVp. For units operating at higher kilovoltages the lead equivalence shall be increased at the rate of 0.01 mm per kVp.
- **Lead rubber flaps:** X-ray table and fluoroscopy screen shall be provided with means of adequate protection for the radiologist and other staff against scattered X-rays. Protective flaps having lead equivalence of not less than 0.5 mm and sufficient dimensions to protect the radiologist shall be so provided that they are suspended (a) from the bottom of the screen such that the flaps overlap the fluoroscopic chair in vertical fluoroscopy, and (b) from the edge of the screen, nearest to the radiologist, such that the flaps extend down to the table top in case of horizontal fluoroscopy. The 'bucky-slot' shall be provided with a cover of 0.5 mm lead equivalence on the radiologist's side.
- **Tube-screen alignment:** X-ray tube and fluoroscopic screen shall be rigidly coupled and aligned so that both move together synchronously and the X-ray beam axis passes through the center of the screen in all positions of the tube and screen.
- **Field limiting diaphragm:** Tube housing should be provided with a field-limiting diaphragm. Its control mechanism should be so mechanically restricted that even when the diaphragm is fully opened and the screen is at the maximum distance from the table, there is still an unilluminated margin of at least 1 cm all along the edges of the screen. The diaphragm control knobs shall be located on the frame of the fluorescent screen and provided with local shielding of at least 0.25 mm lead equivalence.

- **Focus-to-table top distance:** The focus-to-table top distance should be not less than 30 cm for fluoroscopy units.
- **Fluoroscopy timer:** The unit shall have a cumulative timer and its maximum range shall not exceed 5 minutes. There shall also be provision for an audible signal at the end of the preset time. Fluoroscopy units should have a built-in cumulative timer device and an audible warning system which rings after a preset fluoroscopy time has elapsed. This can be reset without canceling the recording of the total screening time and radiologists must be aware of the serious patient dose implications if the alarm is reset during the examination such that the screening time exceeds the preset time. The elapsed timer does not ensure safe operation but is of value as a training device for physicians learning the techniques of fluoroscopy and for all users as a means for monitoring the passage of exposure time.
- **Foot-switch and visual indicator:** A foot-operated pressure switch should be provided for conducting fluoroscopy examinations. There should be a visual indication on the control panel when the beam is "ON".
- **Table-top exposure:** The air kerma rate measured at table top for the minimum focus-to-table top distance shall be as low as possible, and in any case shall not exceed 5 cGy per min.
- **Control panel:** Control panel should be provided with means to indicate control and exposure parameters including tube potential, exposure time and tube current/integral exposure in mAs. A clearly marked and identifiable indicator shall be provided at the control panel to show whether the X-ray beam is "ON" or "OFF".

**Technique:** The use of good radiographic technique and optimum film processing is important for the quality of the image but is also a critical factor in patient dose as repeat exposures to the patient give an additional radiation dose. It must be stressed that repeat images taken due to technical error must be kept to a minimum in order to reduce the patient dose from this unnecessary exposure.

- **Optimum film processing** helps to avoid repeat examinations.
- **Tube voltage and tube current:** The radiographer can alter the beam quality, that is the penetrating power of the beam, by adjusting the kVp and the beam quantity, which is the number of photons in the primary beam, by adjusting the mA. A higher kVp means that the electrons move faster in the tube current, which results in an increase in the quality of X-rays produced that in turn leads to a more penetrating primary beam. Doses will generally be lower at high kV because of the better penetration of the beam that leads to reduced scatter within the body. A compromise must be sought in order

to use the highest kVp possible, so that the dose to the patient is at the lowest possible level, without reducing the image contrast to an unacceptable level. The NCRP recommends that the kVp and mA should be visible to the person doing the fluoroscopy at all times.<sup>32</sup>

- **Screening time and exposure factors:** Significant reduction in radiation dose to the patient can be made by conscious efforts of the practitioner to keep the screening time to a minimum. Intermittent fluoroscopy rather than continuous fluoroscopy is often adequate and should be followed. The screening mA and kV should be kept as low as gives an adequate image. During fluoroscopy, the beam should be collimated the smallest that still shows. The magnification mode should be avoided as this increases the dose.

## SAFETY OF RADIOGRAPHIC IMAGING DURING PREGNANCY

**10 day rule:** The greatest risk to the fetus of chromosomal abnormalities and subsequent mental retardation is between 8 and 15 weeks of pregnancy and examinations involving radiation to the fetus should be avoided during this period. For examinations in a female of reproductive age group, the radiograph should be carried out during the first 10 days of the menstrual cycle to avoid irradiating any possible pregnancy.

When a patient undergoes diagnostic procedures and subsequently finds she is pregnant, the immediate concern is about abnormalities in the developing fetus. Effects on the fetus may be both deterministic and stochastic. Deterministic effects result from the killing of the cells and there is a threshold dose. Examples are fetal death, gross malformations, mental retardation and growth retardation. Fetal malformations reported in the CNS are exencephaly, microcephaly, mental retardation, skull malformations and hydrocephalus. The ocular malformations reported with radiation are absence of eyes, microphthalmia, absence of lens and cataract. Skeletal malformations are stunting, cleft palate, club feet, deformed arms and spina bifida. Other malformations are genital malformations.<sup>36</sup> Animal data suggest that doses of 5 to 10 rad (50–100 mGy) received before embryonic implantation may result in prenatal death. Small head size (microcephaly) has been the primary anomaly reported, in children of the survivors of Hiroshima and Nagasaki, who sustained in utero radiation exposure. The most sensitive period for this defect is 2 to 15 weeks after conception. In fetuses who received *in utero* exposure during the later half of this period, i.e. 8 to 15 weeks, severe mental retardation and intellectual deficits are also of concern at low doses as low as 10 rad (100 mGy).

The following table presents the effects of prenatal exposure as a function of gestational age.<sup>4</sup>

Gestational stage	Days after conception	Fetal dose Rad	Fetal dose mGy	Observed effect
Perimplantation	0–14	5–10	50–100	Prenatal death
Major organo-genesis	8–56	20–25	200–250	Most sensitive stage for growth retardation
	14–105			Small head size; most sensitive time for induction of childhood cancer
Rapid neuron development and migration	56–105	>10	>100	Small head size, seizures, decline in IQ points: 25 points/100 rad (1 Gy)
				Increased risk of childhood cancer
After organo-genesis and rapid neuron development	105–term	>10	>100	
		>50	>500	Severe mental retardation observe at 16–25 wk

Radiation induced childhood malignancy caused by *in utero* radiation exposure is also a concern. Data suggest that a fetus exposed *in utero* to 1 rad (10 mGy) during the first trimester would be 3.5 times more likely to develop childhood malignancy. In the unexposed population, the frequency of childhood cancer is one in 1500 or 0.07 percent. Because natural frequency is so low, 3.5 times that value is still quite low ( $3.5 \times 0.07 = 0.25\%$ ), which leaves a high probability of 99.75 percent that the child exposed *in utero* will not develop childhood cancer.<sup>37</sup>

The following table gives the recommendation for continuing pregnancy after radiation exposure as a function of gestational age and dose.<sup>37</sup>

Fetal absorbed dose			
Gestational age	<5 rad (<50 mGy)	5–15 rad (50–150 mGy)	>15 rad (>150 mGy)
< 2 wks	Recommended	Recommended	Recommended
2–8 wks	Recommended	May consider termination (in presence of other risk factors)	May consider termination (in presence of other risk factors)
8–15 wks	Recommended	May consider termination (in presence of other risk factors)	Higher risk conditions, but termination is not necessarily recommended
15 wks to term	Recommended	Recommended	Recommended

## RECOMMENDED DOSE LIMITS TO PREGNANT WOMEN<sup>18,19</sup>

The recommendations of various authorities are as follows:

1. **ICRP:** In pregnant females, a supplementary equivalent dose limit of 2 mSv applied to the surface of her lower abdomen for the remainder of her pregnancy once pregnancy is established.
2. **NCRP:** Recommends dose limit 0.5 mSv per month for the embryo/fetus for occupational pregnant workers.
3. **AERB:** Recommends that once pregnancy is established the equivalent to surface of pregnant woman's abdomen should not exceed 2 mSv for the remainder of the pregnancy.

## RADIATION DETECTION AND MEASUREMENT

The instruments used to detect radiation are referred to as radiation detection devices. Instruments used to measure radiation are called radiation dosimeters.

### Methods of Detection

There are several methods of detecting radiation, and they are based on physical and chemical effects produced by radiation exposure. These methods are:<sup>31</sup>

1. Ionization
2. Photographic effect
3. Luminescence
4. Scintillation.

### Ionization

The ability of radiation to produce ionization in air is the basis for radiation detection by the ionization chamber. It consists of an electrode positioned in the middle of a cylinder that contains gas. When X-rays enter the chamber, they ionize the gas to form negative ions (electrons) and positive ions (positrons). The electrons are collected by the positively charged rod, while the positive ions are attracted to the negatively charged wall of the cylinder. The resulting small current from the chamber is subsequently amplified and measured. The strength of the current is proportional to the radiation intensity.

### Photographic Effect

The photographic effect, which refers to the ability of radiation to blacken photographic films, is the basis of detectors that use film (e.g. film badge).

### Luminescence

Luminescence describes the property by which certain materials emit light when stimulated by a physiological process, a chemical or electrical action, or by heat. When radiation strikes these materials, the electrons are raised to higher orbital levels. When they fall back to their original

orbital level, light is emitted. The amount of light emitted is proportional to the radiation intensity. Lithium fluoride, for example, will emit light when stimulated by heat. This is the fundamental basis of thermo luminescence dosimeter (TLD), a method used to measure exposure to patients and personnel.

### Scintillation

Scintillation refers to a flash of light. It is a property of certain crystals such as sodium iodide and cesium iodide to absorb radiation and convert it to light. This light is then directed to a photomultiplier tube, which then converts the light into an electrical pulse. The size of the pulse is proportional to the light intensity, which is in turn proportional to the energy of the radiation.<sup>18</sup>

### PERSONNEL DOSIMETRY

Personnel dosimetry refers to the monitoring of individuals who are exposed to radiation during the course of their work. Personnel dosimetry policies need to be in place for all occupationally exposed individuals. The data from the dosimeter are reliable only when the dosimeters are properly worn, receive proper care, and are returned on time. Proper care includes not irradiating the dosimeter except during occupational exposure and ensuring proper environmental conditions. Monitoring is accomplished through the use of personnel dosimeters such as the pocket dosimeter, the film badge or the thermoluminescent dosimeter. The radiation measurement is a time-integrated dose, i.e. the dose summed over a period of time, usually about 3 months. The dose is subsequently stated as an estimate of the effective dose equivalent to the whole body in mSv for the reporting period. Dosimeters used for personnel monitoring have dose measurement limit of 0.1 to 0.2 mSv (10–20 mrem).<sup>18</sup>

### Pocket Dosimeter

The pocket dosimeter monitors dose to personnel. It consists of an ionization chamber with an eyepiece and a transparent scale, as well as a hollow charging rod and a fixed and a movable fiber. When X-rays enter the dosimeter, ionization causes the fibers to lose their charges and, as a result, the movable fiber moves closer to the fixed fiber. The movable fiber provides an estimate of gamma or X-ray dose rate.

### Film Badge Monitoring

- These badges use small double coated X-ray films sandwiched between several filters to help detect radiation.
- Emulsion on one side is slow and that on the other side is fast.
- The film dosimeter is energy dependant, because silver and bromine have much higher atomic numbers than the tissue or air.

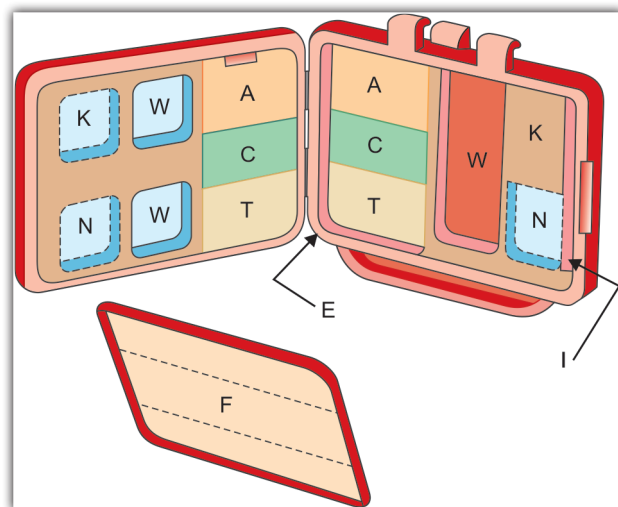


**Fig. 5** A film badge

- To identify various components of incident radiation, film badge sandwiches the film between at least 6 pairs of filters (**Fig. 5**).
- *Six type of windows:*
  1. *Open window:* Alpha rays
  2. *Plastic:* Gray- beta rays
  3. *Cadmium:* Yellow-slow neutrons
  4. *Thin copper:* Green-diagnostic X-rays
  5. *Thick copper:* Pink-gamma and therapeutic rays
  6. *Lead:* Black-fast neutrons and gamma rays
- Radiation of a given energy is attenuated to a different extent by various type of absorbers. Therefore, the same quantity of radiation incident on the badge will produce a different degree of darkening under each filter.
- In India, film badges have been replaced by TLD badges.<sup>31</sup>

### Thermoluminescent Dosimetry (TLD) Monitoring

The limitations of the film badge are overcome by the thermoluminescent dosimeter (TLD). Thermoluminescence is the property of certain materials to emit light when they are stimulated by heat. Materials such as lithium fluoride ( $\text{LiF}$ ), lithium borate ( $\text{Li}_2\text{B}_4\text{O}_7$ ), calcium fluoride ( $\text{CaF}_2$ ), and calcium sulfate ( $\text{CaSO}_4$ ) have been used to make TLDs.

- When a  $\text{LiF}$  crystal is exposed to radiation, a few electrons become trapped in higher energy levels. For these electrons to return to their normal energy levels, the  $\text{LiF}$  crystal must be heated. As the electrons return to their stable state, light is emitted because of the energy difference between two orbital levels. The amount of light emitted is measured (by a photomultiplier tube) and it is proportional to the radiation dose.<sup>28</sup>
- The measurement of radiation from a TLD is a two-step procedure.

- In step 1, the TLD is exposed to the radiation.
- In step 2, the LiF crystal is placed in a TLD analyzer, where it is exposed to heat. As the crystal is exposed to increasing temperatures, light is emitted. When the intensity of light is plotted as a function of the temperature, a glow curve results. The glow curve can be used to find out how much radiation energy is received by the crystal because the highest peak and the area under the curve are proportional to the energy of the radiation. These parameters can be measured and converted to dose.

Whereas the TLD can measure exposure to individuals as low as  $1.3 \mu\text{C/kg}$  (5 mR) the pocket dosimeter can measure up to  $50 \mu\text{C/kg}$  (200 mR). The film badge, however, cannot measure exposures  $< 2.6 \mu\text{C/kg}$  (10 mR). TLDs can withstand a certain degree of heat, humidity, and pressure; their crystals are reusable; and instantaneous readings are possible if the department has a TLD analyzer. The greatest disadvantage of a TLD is its cost.

### Electronic Dosimeters

- Direct reading electronic dosimeters based on Geiger-Muller tubes or single silicon diodes.
- Can provide immediate dose readings and effective alarms when dose limit is exceeded.
- The sensitivity is 50 to 200 times that of TLD badges.
- The advantages and disadvantages can be tabulated as follows:<sup>11,28</sup>

Advantages	Disadvantages
<i>Film badges</i>	
Relatively cheap	Requires dark room and wet processing
Permanent record of exposure	Lower threshold for hard gamma radiation is 0.15 mSv
Wide dose ranges (0.2–2000 mSv)	Is affected by heat, humidity and chemicals
Identifies type and energy of exposure	
Easy to identify individual dosimeters	
<i>TLD badges</i>	
Chips can be reused	Requires high capital initially
Wide dose range (0.1–2000 mSv)	No permanent record (other than glow curves)
Direct reading of personal dose	Cannot distinguish radioactive contamination
Energy independent within $\pm 10\%$	
Compact: suitable for finger dosimetry	
<i>Electronic personal dosimeter</i>	
Direct reading and cumulative record storage (up to 16 Sv)	Requires a filtered badge to provide energy discrimination
Flat response (20 keV to 10 MeV)	High cost
Can be 'zeroed' by user without deleting cumulative record	Linear response to dose is quite heavy
Measures personal dose at depth and at the skin directly to 1 micro Sv	Battery should be renewed every year
Audible warning at high dose rates	

### Wearing the Dosimeter

#### During Radiography

During radiography (when no protective lead apron is worn), the personnel dosimeter is worn at one of two regions:

1. On the trunk of the body at the level of the waist.
2. On the upper chest region at the level of the collar area outside the lead apron.

At these positions, the dosimeter readings represent an estimate of exposure at two different levels, i.e. the whole body exposure is estimated by the trunk level badge and exposures dose to internal organs like thyroid is measured by the collar level badge.

#### During Fluoroscopy

During fluoroscopy a protective apron should always be worn. It is further recommended that ideally two dosimeters should be worn by radiation personnel, one at the collar level outside the lead apron and the other at the level of trunk underneath the lead apron.

The one at the collar level gives an accurate estimate of the radiation dose to the unprotected regions of head and neck. The dosimeter worn underneath the lead apron at the trunk level provides an accurate estimate of the radiation to the protected organs. If only one dosimeter is worn it must be worn at the collar outside the lead apron, because, the neck receives 10 to 20 times more radiation than the trunk which is protected by lead.

## COMPUTED TOMOGRAPHY (RADIATION EXPOSURE AND DOSE MODULATIONS)

### Radiation Dose Measures: CT Specific

Because of its geometry and usage, CT is a unique modality and therefore has its own set of specific parameters for radiation dose. This modality is unique because the exposure is essentially continuous around the patient, rather than a projectional modality in which the exposure is taken from one or two source locations.<sup>37</sup>

Projectional radiographic exposures are taken from one source position and the entrance skin dose is much larger than the exit skin dose, creating a large radiation dose gradient across the patient (Fig. 6).

### Conventional Radiographic Projections

In contrast the tomographic exposure of CT scans with a full  $360^\circ$  rotation results in a radially symmetric radiation dose gradient within the patient.

### CT Radiation Projections

However there is a radial dose gradient which exists in computed tomography scanning (Fig. 7).

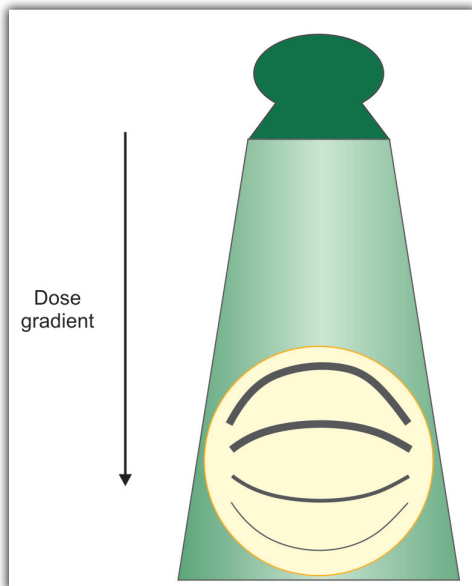


**Fig. 6** Dose gradient resulting from a projectional radiographic exposure in which the source is stationary at one position. The thicker lines represent the entrance skin dose, which is much larger than the exit skin dose, represented by the thinner lines. This difference creates a linear difference through the patient<sup>37</sup>

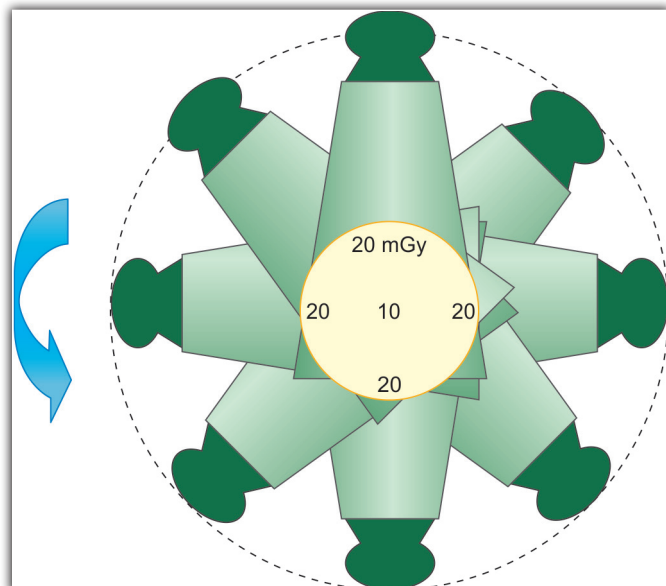


**Fig. 8** Typical dose measurements in a 32 cm diameter (body) phantom from a single detector CT scan<sup>37</sup>

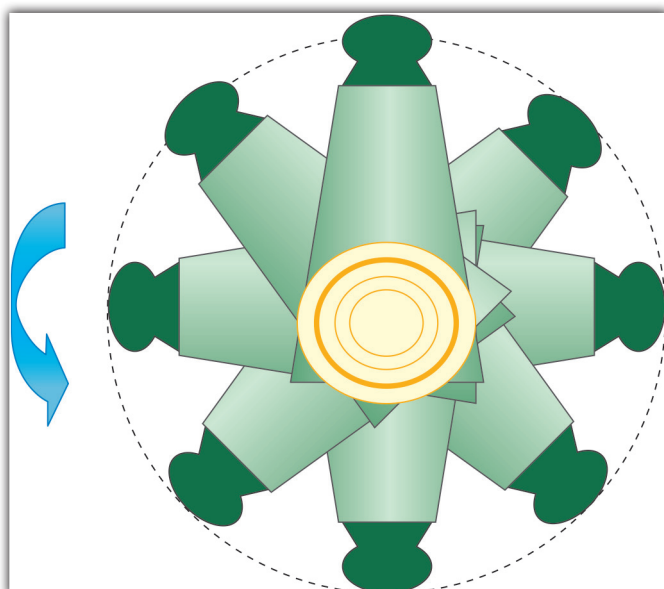


**Fig. 7** Dose gradient resulting from a full 360° exposure from a CT scan. The thicker lines represent the entrance skin dose, which is much larger than the dose at the inner radius, represented by the thinner lines. This difference results in a radially symmetric radiation dose gradient within the patient<sup>37</sup>

## TYPICAL DOSE MEASUREMENTS

The radial dose gradient (the size of the difference from center to periphery) will be affected by several factors, including the size of the object, the X-ray beam spectrum, and the attenuation of the material or tissue (Fig. 8).<sup>37</sup>

In addition to the variations within the scan plane, there are variations along the length of the patient or phantom. These can be characterized by the z-axis dose distribution or radiation profile (Fig. 9). The radiation profile is not limited to the primary area being imaged, and there are tails to this distribution from the nonideal collimation of the X-ray source and from scatter of photons within the object being exposed. These contributions can add up, creating additional absorbed dose in the primary area being imaged.

To account for the effects from multiple scans, several dose descriptors were developed.<sup>37</sup>

1. Multiple scan average dose (MSAD)
2. Computed tomography dose index (CTDI)
3.  $\text{CTDI}_{100}$
4.  $\text{CTDI}_W$
5.  $\text{CTDI}_{\text{vol}}$
6. Dose length product

### Multiple Scan Average Dose

This is defined as the average dose resulting from a series of scans over an interval  $I$  in length.<sup>38</sup>

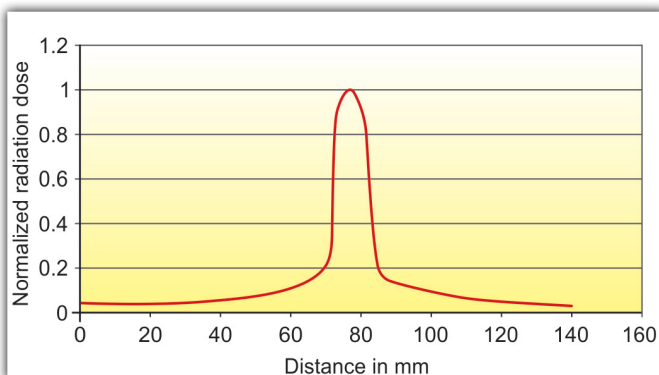


**Fig. 9** Radiation profile of a full-rotation CT scan measured at isocenter. This profile is the distribution of radiation dose along the axis of the patient (the z-axis) and is known as  $D(z)$

$$\text{MSAD} = (1/I) \int_{-\pi^2}^{\pi^2} D \text{ series}(z) dz$$

where ' $I$ ' is the interval of the scan length and ' $D$  series( $z$ )' is the dose at position  $z$  parallel to the  $z$  (rotational) axis resulting from the series of CT scans.

### Computed Tomography Dose Index (CTDI)

It is defined as the radiation dose normalized to beam width measured from 14 contiguous sections.<sup>39</sup>

$$\text{CTDI} = (1/nT) \int_{-\pi}^{\pi} D \text{ single}(z) dz$$

where  $n$  is the number of sections per scan,  $T$  is the width of the interval equal to the selected section thickness, and  $D$  single( $z$ ) is the dose at point  $z$  on any line parallel to the  $z$  (rotational) axis for a single axial scan.

However, to be measured according to the definition, only 14 sections could be measured and one had to measure the radiation dose profile—typically done with thermoluminescent dosimeters (TLDs) or film, neither of which was very convenient. Measurement of exposure could be done with pencil ionization chamber but its fixed length of 100 mm meant that only 14 sections of 7 mm thickness could be measured with that chamber alone.

To overcome the limitations of CTDI with 14 sections, another radiation dose index— $\text{CTDI}_{100}$ —was developed.

### $\text{CTDI}_{100}$

This index relaxed the constraint on 14 sections and allowed calculation of the index for 100 mm along the length of an entire pencil ionization chamber.<sup>38</sup> This index can be measured and calculated for the center location as well as at least one of the peripheral positions.<sup>40</sup>

$$\text{CTDI}_{100} = (1/NT) \int_{-5\text{cm}}^{5\text{cm}} D \text{ series}(z) dz$$

where ' $N$ ' is the number of acquired sections per scan (also referred to as the *number of data channels used during*

*acquisition*) and ' $T$ ' is the nominal width of each acquired section.

### $\text{CTDI}_w$

$\text{CTDI}_w$  was created to represent a dose index that provides a weighted average of the center and peripheral contributions to dose within the scan plane. This index is used to overcome the limitations of  $\text{CTDI}_{100}$  and its dependency on position within the scan plane.

$$\text{CTDI}_w = (1/3)(\text{CTDI}_{100})_{\text{center}} + (2/3)(\text{CTDI}_{100})_{\text{periphery}}$$

### $\text{CTDI}_{\text{vol}}$

One final CTDI descriptor takes into account the parameters that are related to a specific imaging protocol, the helical pitch or axial scan spacing, and is defined as  $\text{CTDI}_{\text{vol}}$ .

$$\text{CTDI}_{\text{vol}} = \text{CTDI}_w \times NT/I$$

where  $N$  is the number of acquired sections per scan and  $T$  is the nominal width of each acquired section. The product of  $N \times T$  is meant to reflect

The total nominal width of the X-ray beam during acquisition and  $I$  is the table travel per rotation for a helical scan. Hence  $NT/I = 1/\text{pitch}$

$$\text{And } \text{CTDI}_{\text{vol}} = \text{CTDI}_w / \text{pitch}.$$

### Dose-Length Product (DLP)

This value is simply the  $\text{CTDI}_{\text{vol}}$  multiplied by the length of the scan (in centimeters) and is given in units of milligray-centimeters:

$$\text{DLP} = \text{CTDI}_{\text{vol}} \times \text{scan length}^{41}$$

This descriptor is used to obtain an estimate of effective dose.

DLP values are easily converted to millisieverts by using conversion factors specific to the anatomic region imaged: The conversion factors listed by the American Association of Physicists in Medicine for the chest, abdomen, and pelvis are 0.014, 0.015, and 0.015.<sup>42</sup> These conversion factors are periodically updated, so care should be taken to apply the most recent ones.

*Effective radiation doses calculated from DLP values in a routine oncologic CT examination of the abdomen and pelvis.<sup>43</sup>*

Region scanned	DLP (mGy·cm)	Conversion factor	Effective dose (mSv)
Abdomen and pelvis (portal venous phase)	681	0.015	10.2
Kidneys (delayed phase)	230	0.015	3.5
Bladder (delayed phase)	214	0.015	3.2

### Techniques for Controlling Radiation Dose at CT

Multidetector CT protocols can be directly modified in a variety of ways. These include using an automated

exposure control system or modifying individual acquisition parameters such as the number of phases, section thickness, peak voltage (kVp setting), tube current-time product, and pitch.

### ■ USING AUTOMATED EXPOSURE CONTROL

Automated exposure control (AEC) systems are designed to reduce the radiation dose by dynamically altering the tube current as the X-ray tube rotates around the patient during multidetector CT scanning. The tube current is automatically modulated according to the attenuation level (i.e. the size) of the patient.<sup>44</sup> For smaller patients, i.e. the pediatric patients, the tube current is automatically decreased to adapt to the lower attenuation level. Conversely, the tube current is appropriately increased for larger patients. Use of AEC is an efficient way to tailor radiation dose to achieve a target image quality.

### ■ MODIFYING THE ACQUISITION PARAMETERS

Acquisition parameters such as the number of scanning phases and the section thickness may be modified to achieve deeper dose reductions even when an automated exposure control system is used.

If CT angiography-venography protocol initially includes four scanning phases (precontrast, postcontrast arterial phase, postcontrast portal venous phase, and postcontrast delayed scanning), by decreasing the number of scanning phases to two (postcontrast arterial phase and slightly later portal venous phase), the radiation dose can be reduced by 50 percent.

The acquisition section thickness also has an important effect on image noise and, consequently, on the amount of radiation needed to meet the preset noise value. With regard to section thickness at 64-row multidetector CT, if the section thickness of 5 mm were decreased to 2.5 mm, Kanal and colleagues found, the noise index of 15.3 would have to be increased to 23.4 to keep the dose constant. Conversely, if the noise index were kept constant at 15.3, the relative dose with 2.5 mm thick sections would be approximately 2.3 times that with 5 mm thick sections.<sup>45</sup>

### Reducing the Milliamperes-Seconds Value

The radiation dose is linear with milliamperes seconds value, when all other factors are held constant, so the milliamperes-seconds value is reduced by 50 percent, the radiation dose will be reduced by the same amount. However, this reduction will increase image noise by  $1/\sqrt{mAs}$ , which means that a 50 percent reduction in the milliamperes-seconds value results in a noise increase of 41 percent.

For example, detection of high-contrast objects in the lung may not require a low-noise imaging protocol and the reduction in milliamperes-seconds may be well tolerated. On the other hand, imaging low-contrast lesions in the liver

does require a low-noise imaging protocol and the reduction in milliamperes-seconds may limit the ability to detect these lesions.

### Increasing Pitch

The radiation dose is inversely proportional to pitch. Increasing the pitch decreases the dose, increases the image noise, increases the effective section thickness, and reduces the scanning time.<sup>46</sup> The trade-off in increasing pitch is an increase in effective section thickness, which results in increased volume averaging, which in turn may reduce the image signal. The ability to use this type of dose reduction again depends on the clinical applications.

### Varying the Milliamperes-Seconds Value by Patient Size

Computed tomography is an example of a digital modality in which the image quality continues to improve as the exposure increases. This is contrasted with analog projectional film, in which too high of an exposure results in an overexposed (too dark). However, the radiation dose to the smaller patient is potentially higher than is necessary to obtain a diagnostic image. Therefore, significant effort has recently been put into developing size- and weight-based imaging protocols. This has typically been in the form of a reduced milliamperes-seconds value for reduced patient size and has led to the development of suggested technique charts for pediatric patients.

### Optimum Tube Potential<sup>47</sup>

Use of an optimum tube potential may help improve image quality or reduce radiation dose particularly in pediatric CT examination. The main benefit of a lower tube potential is that it provides improved contrast enhancement, a characteristic that may compensate for the increase in noise that often occurs at lower tube potential and may allow radiation dose to be substantially reduced. The use of a lower tube potential should be carefully evaluated for each type of examination to achieve an optimum trade off among contrast, noise, artifacts and scanning time.<sup>47</sup>

### ITERATIVE RECONSTRUCTION

Computed tomography scanner vendors have been working to develop various image reconstruction techniques as alternatives to traditional filtered back projection for reducing image noise.

One such technique is iterative reconstruction, which is also known by the trade names iDose (Philips), Iterative Reconstruction in Image Space (IRIS; Siemens), Adaptive Iterative Dose Reduction (AIDR; Toshiba, Tochigi, Japan), and Adaptive Statistical Iterative Reconstructions (ASIR GE health care).<sup>48</sup> For example, the selection of "ASIR 30 percent" results in a combination of 70 percent filtered back projection data and 30 percent adaptive statistical iterative reconstruction data.

Ongoing development of iterative reconstruction techniques holds promise for achieving even lower levels of image noise, which will allow further reductions in radiation dose.

## CONCLUSION

When used under properly controlled conditions, radiation is a safe and indispensable tool for medical diagnosis. Proper radiation safety management should ensure that radiologists and clinicians are knowledgeable about typical patient doses that are important in each type of radiologic examination and about the factors that affect these doses. This should ensure a judicious requisition for a radiological examination as well as help keep doses as low as possible while still creating optimum diagnostic quality images.

## REFERENCES

- Engel Hells P. Radiation protection in medical imaging. Radiography. 2006;12:153-60.
- Millew RW. Delayed effects of external radiation exposure: a brief history. Radiation research. 1995;144:160-9.
- Brateman L. Radiation safety considerations for diagnostic radiology personnel. Radiographics. 1999;19:1037-55.
- Parry RA, Glaze SA, Archer BR. Typical patient radiation doses in Diagnostic Radiology. Radiographics. 1999;19:1289-302.
- International Commission on Radiological Protection. Recommendations of the ICRP. ICRP publication no. 26 Ann ICRP 1(3) Oxford, England Peragamon, 1977.
- International Commission on Radiological Protection. Recommendations of the ICRP. ICRP publication no. 60 Ann ICRP 21(1-3) Oxford, England Peragamon, 1990.
- National Council on Radiation Protection and Measurements. Limitation of exposure to ionizing radiation. NCRP report no 116, Bethesda Md:NCRP, 1993.
- Strahlenschutzkommision: Orientierungshilfe fur radiologische und nuklearmedizinische. Untersuchungen Heft 30, Berlin H Hoffman 2006.
- Shannoun F, Blettner M, et al. Radiation protection in Diagnostic Radiology. Dtsch Arztsbl Int. 2008;105(3):41-6.
- Hricak H, Brenner DJ, Adelstein SJ, et al. Managing radiation dose in medical imaging: a multifaceted challenge. Radiology. 2011;258(3):889-905.
- Selman Joseph. The fundamentals of X-ray and radium physics. 7th Edn. Charles Thomas Publisher. 1985.pp.184-94.
- Travis E. Bioeffects of radiation. In: Seeram E (ed). Radiation protection. Philadelphia, New York: Lippincott. 1997;73-81.
- Sinclair WK. Radiation protection recommendations on dose limits: the role of the NCRP and the ICRP and future developments. Int J Radiation Oncology Biol Phys. 1995;31(2): 387-92.
- Schwenn MR, Brill AB. Childhood cancers 10 years after the Chernobyl accident. Curr Opin Pediatr. 1997;9(1):51-4.
- Hall EJ. Radiobiology for the radiologist. 4th (Ed). Philadelphia: JB Lippincott Company;1994.pp.419-52.
- Cho LC, Glatstein E. Radiation injury. In: Fauci AS, Braunwald E, Isselbacher KJ et al (Eds). Harrison's principles of internal medicine, 14th (Edn). Hill: New York;1998.pp.2259-504.
- Rubin P, Constine LS, Williams JP. Late effects of cancer treatment: radiation and drug toxicity In: Perez CA, Brady LW (Eds). Principles and practice of radiation oncology 3rd Edn. Philadelphia, New York:Lippincott Raven;1998.pp.155-211.
- Seeram E, Travis EC. Radiation protection. Philadelphia, New York: Lippincott;1997.
- AERB safty Code (Code no AERB/SE/MED-2), Mumbai:2001; 1-20.
- International Commission on Radiological Protection. Recommendations of the International Commission on Radiological Protection. ICRP publication. Oxford: Peragamon Press;1991:60.
- Shrimpton PC, Wall BF, Croft JR, Webb GAM. Medical exposure guidance on the 1990 recommendations of ICRP. Documents of NRPB. 1999;4(2):43-80.
- Goldstone K, Yates SJ. Radiation issues governing radiation protection and patient doses in diagnostic imaging. Grainger and Allison's Diagnostic Radiology: a textbook of medical imaging 5th Edn. Adam A, Dixon AK, Grainger RG, Allison DJ, (Eds). New York Churchill Hill Livingstone;2008.pp.159-71.
- Burniston B. The barium enema - a worthwhile examination? Radiography Today. 1993;59(675):4-12.
- National Council on Radiation Protection and Measurements. Implementation of the principle of As Low As Reasonably Achievable (ALARA) for medical and dental personnel. NCRP report no 107,Bethesda, Md: NCRP, 1990.
- Webb GAM. The requirement to keep radiation exposures as low as reasonably practicable (ALARP). London HMSO, National Radiological Protection Board (NRPB/P/B)1984.
- Wall BF, Fisher S, Shrimpton PC, Rae S. Current levels of gonadal irradiation from a selection of routine X-ray examination in Great Britain Harwell: National Radiological Protection Board (NRPB - R 105)1980.
- Simpkin DJ, Dixon RL. Secondary shielding barriers for diagnostic X-ray facilities: scatter and leakage revisited. Health Phys. 1998;74(3):350-65.
- Christensen Radiation Protection. In Christensen's Physics of Diagnostic Radiology, 4th Edn. Curry TS, Dowdley JE, Murry RC (Eds). Philadelphia, London;1990.
- Shymko MJ. Minimizing occupational exposure. Radiologic Technology. 1998;70(1):89-90.
- Wagner LK, Hayman LA. Pregnancy and women radiologists. Radiology. 1982;145:559-62.
- Grover SB, Kumar J, Gupta A, Khanna L. Protection against radiation hazards: regulatory bodies, safety norms, dose limits and protection devices. Indian J Radiol Imaging. 2002;12:157-67.
- National Council on Radiation Protection and Measurements. Medical X-ray, electron beam and gamma X-ray protection for energies upto 50 meV (equipment design, performance and use). Bethesda: NCRP publications (NCRP report no 102);1989.
- Sprawl P Jr. Physical principles of medical imaging 2nd Edn. Gaithersburg Md: Aspen;1993.pp.165-7.
- Graham DT, Cloke P. Principles of radiological physics 4th Edn. Edinburgh:Churchill Livingstone;2003.pp.325-38.
- Bushong SC. Radiological science for technologists, physics biology and protection 6th Edn. St Louis year book; 1997. pp.442-7.
- Steenvoorde P, Pauwels EKJ, Harding LK, et al. Diagnostic nuclear medicine and risk for the fetus. Eur J Nucl Med. 1998; 25:193-9.

37. McNitt Gray. Radiation dose in CT. *Radiographics*. 2002;22: 1541-53.
38. Jucius RA, Kambic GX. Radiation dosimetry in computed tomography. *Appl Opt Instrum Eng Med*. 1977;127:286-95.
39. Shope TB, Gange RM, Johnson GC. A method for describing the doses delivered by transmission. *X-ray Computed Tomography Med Phys*. 1991;8:488-95.
40. McCollough CM, Schueler BA. Calculation of effective dose. *Med Phys*. 2000;27:838-44.
41. Shrimpton PC, Edyvean S. CT scanner dosimetry. *Br J Radiol*. 1998;71:1-3.
42. American Association of Physicists in Medicine. The measurement, reporting and management of radiation dose in CT. Report no 96, College park Md: American Association of Physicists in Medicine, 2008.
43. Tamm EP, Rong XJ, Coly D, et al. CT radiation dose reduction: how to implement change without sacrificing diagnostic quality. *Radiographics*. 2011;31:1823-32.
44. Lee CH, Goo JM, Lee HJ, et al. Radiation dose modulation technique in multidetector CT era: from basics to practice. *Radiographics*. 2008;28:1451-9.
45. Kanal KM, Stewart BK, Kolokythas O, et al. Impact of operator selected image noise index and reconstruction slice thickness on patient radiation dose in 64 MDCT. *AJR*. 2007;189(1):219-25.
46. Primak AN, McCollough CH, Bruesewitz MR, et al. Relationship between noise, dose and pitch in cardiac multidetector row CT. *Radiographics*. 2006;26(6):1785-94.
47. Yu L, Bruesewitz M, Thomas KB, et al. Optimal tube potential for radiation dose reduction in Pediatric CT: principles, clinical implementations and pitfalls. *Radiographics*. 2011;31: 835-48.

## Chapter

# 25

# Planning a Modern Imaging Department

*SC Bansal, Niranjan Khandelwal, Ajay Gulati*

During recent years, there has been increasing recognition that diagnostic imaging is an integral part of modern healthcare. Perhaps more than any other clinical service diagnostic imaging has been transformed by developments in information technology fueled by digital information technologies over the last thirty years. This has enabled earlier, more accurate diagnosis and more appropriate interventions for almost all major health conditions.

It is important to recognize that diagnostic imaging is not a technical service, but a clinical service that interprets information and requires the clinical expertise of imaging clinicians, who are increasingly making decisions about the management of patient care. There is increasing recognition of the need to place imaging early in care pathways to reduce the time to diagnosis and treatment and to improve efficiency and effectiveness.<sup>1</sup>

Most diagnostic imaging is carried out in clinical radiology departments, which deliver a range of services either within a hospital or as a stand-alone center. Apart from providing routine and specialized diagnostic services with various imaging techniques for indoor, out-patients and walk-in patients, the modern departments also provides therapeutic services like interventional radiology (minimally invasive treatments performed with imaging guidance). This acts as a big source of revenue generation for a hospital or a stand-alone center with high profitability.<sup>2</sup>

## ■ PLANNING AND ORGANIZATION

With rapid advancements in investigative technology, there is a continuous changing demand in the field of radiodiagnosis and imaging service resulting in an advanced and detailed

systematic planning and organization for launching a modern imaging department. An understanding of what has changed – and what has not – is essential to developing safe, productive and comfortable imaging departments.

Launching a new diagnostic and therapeutic imaging center involves very specific requirements and roadmaps that have a direct impact on planning. The essential first step is to do a critical project analysis. Doing a cost-benefit analysis and determining if the return on the investment will be positive are important for a project's success. Good planning and communication with key staff members of the healthcare institution and the members of the design and construction team will help ensure successful implementation of any project. Analyzing the requirements for imaging equipment, space and personnel are other necessary steps. These are followed by scheduling and designing various aspects of the project.<sup>3</sup>

There are three horizontal levels of workflow (strategic, managerial and operational) in any organization, whether it is a government hospital or multi-national corporate running a hospital. Planning must focus on the strategic level of decision making. The second level is the managerial or administrative level which focuses on daily issues such as employee attendance and productivity, patient backlogs, staff scheduling and reassignments. The operational level is where the work actually gets done in any organization<sup>4</sup> (**Fig. 1**).

*The major objectives of a radiology department include:*

- a. To provide comprehensive high quality imaging service
- b. Establishment and confirmation of clinical diagnosis
- c. Providing high quality therapeutic/interventional radiology
- d. Commitment to training and research.

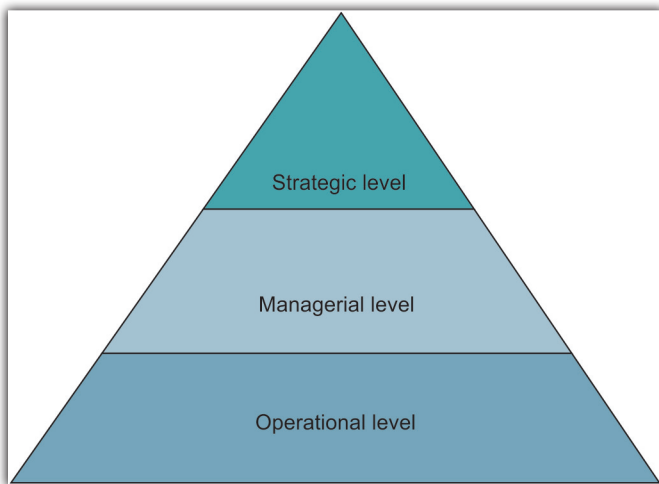


**Fig. 1** Levels of radiological workflow

## Divisions of the Radiology Department

Radiology department generally has diagnostic as well as therapeutic sections.

The major components of Radiology/Imaging services are:

- Radiography (X-ray machines/CR and DR System)
- Mammography
- Dual-energy X-ray absorptiometry (DEXA)
- Computed Tomography (CT scan)
- Ultrasound and color Doppler
- Magnetic Resonance Imaging (MRI)
- Digital Subtraction angiography (DSA)
- Nuclear Imaging Systems.

To manage such large number of sophisticated machines whose rays/emissions are hazardous to healthcare calls for critical planning taking in to consideration the safety aspect of patient , public and the department staff.<sup>5</sup>

## LOCATION

The location of the department and the relative positions of the examination rooms have a considerable bearing upon the protection requirements. Aspects for planning are accessibility, convenience, privacy and traffic flow considerations, etc. i.e. that should be well connected. Accessibility towards OPD and emergency is a major point of consideration for this department. Central location on the ground floor with some space for future expansion is essential to allow up-gradation and augmentation of services.<sup>2</sup> The location should be 10 meters away from the elevators due to their effect on the functioning of equipment in the department.<sup>5</sup>

The correct design of medical imaging facilities will reduce radiation and non-radiation hazards and contribute to the care and well-being of patients and staff. It is the general responsibility of the medical imaging service to ensure the optimum design of their facility and to ensure that there is

no radiation risk to anyone working or waiting in any room adjoining the radiation zone. Therefore, strategic planning must be done to have a clear understanding of the operations in the department (staff movement, patient flow, material flow, technical procedures). Special attention to minor details related to operations can have significant impact on staff effectiveness and morale. Study of traffic patterns is the key to the efficiency of an imaging department. This study should be based on interactive discussions with the staff of the department and should consider the various activities like:<sup>6</sup>

- Movement of patients in and out of procedure rooms
- Activity sequence within procedure rooms
- Film processing and handling
- Image interpretation and reporting
- Filing.

## LAYOUT

The layout of the department depends on the great extent the way the processes in the department are aligned and take place. Layout shall be prepared as per the AERB guidelines for layout and shielding of X-ray equipment. Planning should be done to create a safe, pleasant and efficient staff work environment. For a safe radiation environment, there are certain principles and considerations like “separation” of different functional areas helps control access:

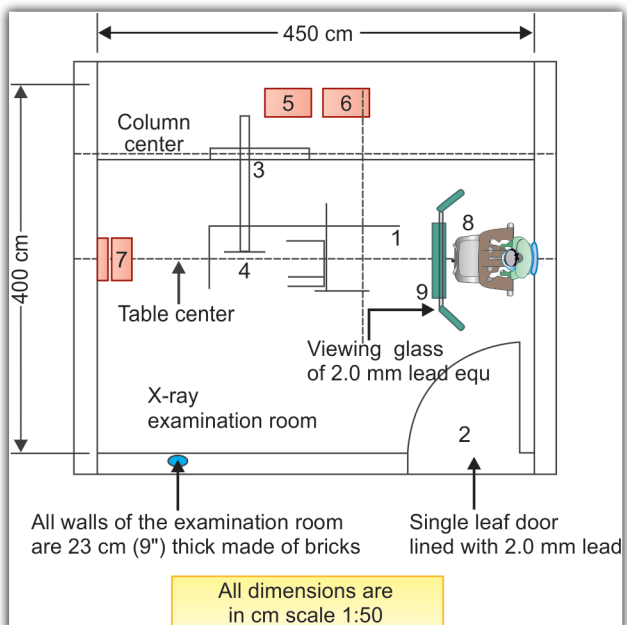
- Public areas (waiting room, changing rooms, etc.)
  - Staff areas (offices, reporting rooms, etc.)
  - Work areas (radiation rooms, console rooms, labs etc.)<sup>2</sup>
- Corridors and doors leading to all patient areas and examination rooms should allow easy and safe movement of all patients, including handicapped or injured. Availability of toilet facilities is essential, particularly those suitable for handicapped patients. Also, the provision of safe storage facilities for patients' clothing and valuables during imaging is necessary.<sup>6</sup>

## EQUIPMENT

The equipment used in this department are highly sophisticated and expensive. Major equipment are described below:

### Conventional Radiography

The most important and easily performed imaging service in the front line of medical care is plain radiography. The X-ray unit must be able to perform all essential general radiographic examinations like chest, abdomen and extremities. Information is represented in the analog or continuous form rather than a discrete fashion. In conventional radiography, majority of the radiographic examinations have been carried out by projecting the beam through the patient allowing the transmitted beam to strike X-ray film or Intensifying screen to produce the latent image. The latent image can be made visible and permanent by processing the film with suitable chemicals (**Fig. 2**).



1. Examination table; 2. Spot film device; 3. Column stand; 4. X-ray tube head; 5,6. Unit electronics; 7. Chest stand; 8. Control unit; 9. MPB with lead glass viewing window of 1.7 mm lead equivalence

**Fig. 2** Model Layout—X-ray installation

### Dark Room

When designing a dark room, beside the operational considerations concerning the film development, the primary concern is the shielding of unexposed film from exposure to radiation (X-rays and daylight). The common location for a main darkroom is central in the imaging department. All construction provisions must be made to ensure that all potential openings to the outside are light tight (doors, ventilation, pass through, windows). Dry and wet areas should be separate from each other and chemicals must be stored safely.<sup>6</sup>

### Digital Radiography

Digital radiography is a form of X-ray imaging where digital X-ray sensors are used instead of radiography film. Digital radiography systems are replacing films in the modern departments. It is a representation of continuous analog information into digital form by the use of computer which processes the digital data to form an image. It not only has revolutionized communication between radiologists and clinicians, but also has improved image quality and allowed for further reduction of patient exposure. However, digital radiography also poses risks, such as unnoticed increase in patient dose and suboptimum image processing that may lead to suppression of diagnostic information. Advanced processing techniques such as temporal subtraction, dual energy subtraction and computer aided detection (CAD) will

play an increasing role in the future and are all targeted to decrease the influence of distracting anatomic background structures and to ease the detection of focal and subtle lesions.<sup>7</sup>

The two most important objective performance measures to describe digital radiography systems with respect to dose requirements and detail resolution are the modulation transfer function (MTF) and the detector quantum efficiency (DQE).<sup>8</sup> DQE describes the efficiency of a detector to generate signal from X-ray quanta. MTF is a measure of image quality of an imaging system with respect to structural contrast and spatial resolution. Optimizing MTF and DQE simultaneously is a challenge: thicker detector material, for example, will improve absorption (thus, DQE), but generally also will induce more blur (deteriorate MTF).

The following sections discuss recent developments for the three main digital detector technologies: storage phosphors (computed radiography; CR), flat-panel detectors (digital radiography; DR) and CCD detectors.

### Storage Phosphor Radiography (Computed Radiography)

Computed radiography (CR) systems use storage-phosphor image plates having a detective layer of photostimulable crystals and separate image readout process.<sup>9</sup> A major advantage of CR systems is that they are cost effective way to getting digital images since they allow reutilization of existing X-ray equipment. CR cassettes utilize storage phosphors where electrons are trapped during exposure and subsequently extracted through a laser scanner.<sup>10</sup> Standard CR systems use a single laser beam and a detector screen covered with an amorphous (powder-based) detector material.

### Dual-reading CR systems

Dual-reading CR systems are based on transparent detector material and employ light collection optics in the front and the back side of the detector. It improves quantum detection (DQE) and has only a minimum deteriorating effect on spatial resolution (MTF).<sup>11</sup>

### Parallel Reading (Line Scanning)

Traditional CR scanners use principle of flying spot scanning for readout where a tightly focused laser beam stimulates the latent image in a moving storage phosphor plate one point at a time over the entire screen surface. Parallel reading employs a linear array of laser diodes (linear-line laser diode) that reads out all pixels in one line simultaneously, therefore speeding up the process tremendously. The dual side the reading and line scanning reading with columnar phosphors provide remarkable improvement compared to conventional CR systems and yield results comparable to most digital detectors for radiography.<sup>10</sup>

### *Needle-crystalline CR Detectors*

A new crystalline detector material ( $\text{CsBr}:\text{Eu}^{2+}$ ) for storage phosphor systems allows for creating a thicker detector layer (better DQE) without deteriorating spatial resolution (MTF). The principle is similar to that of indirect flat panel systems ( $\text{CsI}$ -photodiode/TFT detectors).

### *Flat-panel Direct Detector Systems*

Two different DR technologies are available, both of which are based on TFT matrix arrays. Indirect conversion systems or opto-direct systems use a scintillator (e.g. cesium iodide,  $\text{CsI}$  or gadolinium oxysulphide, GOS or Gadox) layered on top of an array with light-sensitive photodiodes with thin-film transistors (TFTs). The scintillator converts radiation into light that is detected by the photodiode/TFT array.  $\text{CsI}$ -photodiode/TFT systems are widely used for chest radiography and provide better DQE than standard CR or Gadox-TFT systems<sup>12,13</sup> (**Figs 3 and 4**).

Direct conversion systems or electro-direct systems use a photo conducting layer (amorphous selenium, a-Se), in which the absorbed X-ray energy is directly converted into charge on top of a TFT array. These systems are excellent for the high spatial frequencies required for mammography, but because they absorb less X-ray energy, they suffer from a lower dose efficiency (DQE), which makes them less suited for chest radiography.<sup>12,14</sup>

### *CCD Detector Technology*

The light emitted by a scintillator screen has to be collimated to the CCD by optical coupling (demagnification), which can reduce dose efficiency and degrade image quality.<sup>15</sup> Recent improvements in coupling mechanism and use of larger CCD sensors have made these systems more attractive for chest radiography.<sup>16</sup>

### *Slot-scanning CCD Technology*

No demagnification is required for slot-scanning CCD technology: a  $\text{CsI}$  scintillator is coupled to a linear array of CCDs that covers the whole slot that is used to scan the chest. The increased signal to noise yielded by scatter reduction effectively compensates for the 2.5 times lower intrinsic DQE of CCD technology.<sup>17</sup> The increased SNR can be used to improve image quality or to reduce patient dose.

The most advanced processing algorithms aim at analyzing images (CAD), selectively enhancing bones and soft tissues (dual-energy subtraction), and at visualizing change at follow-up (temporal subtraction).

### *Computer-aided Diagnosis*

Computer-aided diagnosis (CAD) programs have the goal to aid the radiologist in detecting or differentiating various disease entities in the chest. Usually the system suggests a



**Fig. 3** DR flat panel X-ray unit

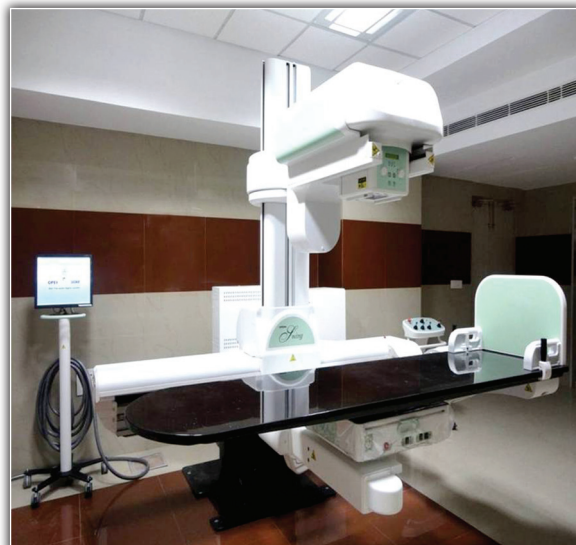


**Fig. 4** DR and fluoroscopy unit (flat panel)

lesion or abnormal region that then has to be verified by the radiologist.

### *Dual-energy Subtraction*

Dual-energy subtraction radiography involves taking a chest exposure at two different X-ray energies. By exploiting the difference in energy dependence of attenuation between bone and soft tissue, either bone or soft tissues can be eliminated by locally weighted subtraction of the two images.. Dual-energy subtraction allows for differentiation of calcified and non-calcified lesions, improved detection of nodules and masses, especially in critical areas, and improved detection of rib lesions.<sup>18,19</sup>

### Temporal Subtraction

Temporal subtraction is a processing technique based on the matching and subsequent subtraction of a follow-up radiograph and a baseline image.

### Digital Tomosynthesis

Digital tomosynthesis is a medical imaging technique using a flat panel detector and tube rotation producing a series of slices at different depths. These projection images are subsequently shifted and added to bring objects in a given plane into focus, while other structures are spread across the image and are rendered with varying amounts of blur.<sup>20</sup> Most developments in tomosynthesis have been in breast imaging, but orthopedic, chest and urinary applications have also been used.<sup>21</sup>

*X-ray equipment fall broadly into two groups portable/mobile and fixed*

**Portable radiography** equipment means the X-ray unit is capable of being taken to the destination to be used. It is very simple to use and can be packed into carrying cases and so transported. Portable sets relatively have low mA setting, can be dismantled for transfer. The word “mobile” means that X-ray equipment is capable of being moved. It is mounted on the wheels and can be pushed by human power. It is larger and heavier than portable sets and need to be motorized or pushed between locations. It cannot be separated into smaller components and cannot be taken outside the hospital. Mobile sets have high MA value.

The digital mobile units are the ultimate solution to mobile X-ray imaging for digitalization in emergency rooms (ER), traumatology, intensive care units (ICU), in patient wards and pediatrics. These systems represents an evolutionary move in mobile diagnostic imaging equipment and include unique features in terms of operability, mobility and image quality.<sup>22,23</sup>

**Wireless FPDs:** Wireless portable DR system is now a reality. After exposure, it wirelessly transfer image data to the DR system. Alternatively the image data can be transferred to DR console via an Ethernet cable. It has no cables and does not interfere with surrounding machines, so it is easy to handle as a CR cassettes.<sup>24</sup> Typically a 17" × 14" image size is made available within 3 seconds (Fig. 5).

### Mobile Image Intensifiers Units

Mobile unit for fluoroscopy with an image intensifier is generally used in operating theater. This reduces the number of radiographs taken and saves the time during surgery.

### MAMMOGRAPHY

Mammography is a specific type of imaging using high precision X-ray machine which gives a reliable radiographic examination of the breast. The low dose X-ray study using



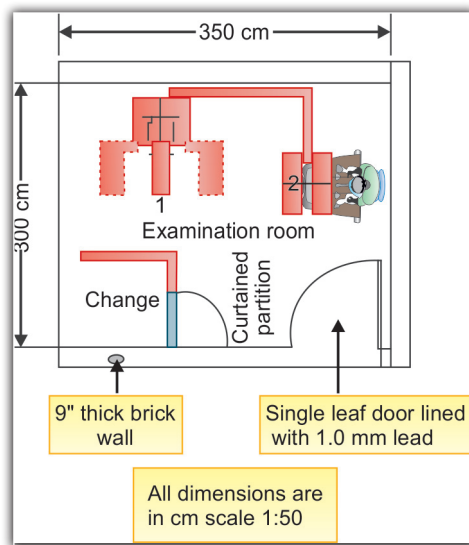
**Fig. 5** Mobile digital radiography unit

mammography machine can aid in the early detection and diagnosis of breast diseases in women.<sup>5</sup> The use of mammography in breast cancer screening and treatment has represented a critical advance in the management of this disease. Current guide lines in India and by the American College of Radiology (ACR) recommended annual screening in women above the age of 40 years.

Screen film mammography (SFM) was traditionally considered the gold standard in mammography until recently, however full field digital mammography (FFDM) is now increasingly being recognized as an attractive alternative to SFM (Fig. 6). The recent advances in mammography include digital mammography, computer-aided detection, breast tomosynthesis and performing stereotactic biopsy from indeterminate lesions.

Digital mammography, also called full-field digital mammography (FFDM), is a mammography system in which the X-ray film is replaced by solid-state detectors that convert X-rays into electrical signals. The electrical signals are used to produce images of the breast that can be seen on a computer screen or printed on special film similar to conventional mammograms.<sup>25</sup> FFDM has improved contrast resolution and greater ability to image dense breast tissue thereby increasing the diagnostic accuracy.<sup>51</sup>

**Computer-aided detection (CAD) systems** use a digitized mammographic image and computer software then searches for abnormal areas of density, mass, or calcification that may indicate the presence of cancer. The CAD system highlights these areas on the images, alerting the radiologist to the need for further analysis and therefore improve the diagnostic capabilities.



1. Mammography equipment, 2. Control unit with protective barrier of 1.5 mm lead equivalence

**Fig. 6** Model layout—mammography installation

**Breast tomosynthesis**, also called three-dimensional (3-D) breast imaging, is a mammography system where the X-ray tube and imaging plate move in an arc during the exposure. It creates a series of thin slices through the breast that allow for improved detection of cancer and reduces the recall rates for additional imaging.<sup>26</sup>

**Dual Energy Subtraction Mammography and Contrast-enhanced digital mammography** are also newer advanced techniques which help in improved lesion detection in difficult and indeterminate lesions.

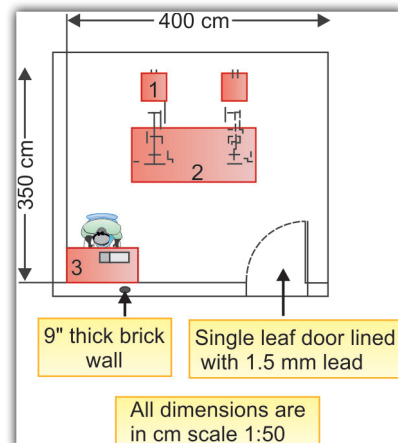
#### Dual-energy X-ray Absorptiometry

Dual-energy X-ray absorptiometry (DEXA) is an imaging technology that uses a very low amount of X-ray energy to measure bone mineral density (BMD).

The technique relies on transmission measurements made at two photon energies to allow calcium and thereby bone mineral, be assessed. When soft tissue absorption is subtracted out, the BMD can be determined from the absorption of each beam by bone. The first-generation of modern DEXA scanners used a pencil X-ray beam; later designs employ fan beams, cone beams and c-arm technology and thereby, allow more rapid and convenient scanning<sup>27,28</sup> (**Fig. 7**).

Dual-energy X-ray absorptiometry is the most widely used and most thoroughly studied bone density measurement technology.

The DEXA scan is the most accurate and reliable way to diagnose and follow osteoporosis and predicts the future risk of fracture. It contrasts to the nuclear bone scan, which is sensitive to certain metabolic diseases of bones in which



1. BMD equipment; 2. Examination table; 3. Evaluation unit

**Fig. 7** Model layout—BMD installation

bones are attempting to heal from infections, fractures, or tumors. DEXA scans can also be used to measure total body composition and fat content with a high degree of accuracy comparable to hydrostatic weighing with a few important caveats.<sup>29</sup> However, it has been suggested that, while very accurately measuring minerals and lean soft tissue (LST), DEXA may provide skewed results as a result of its method of indirectly calculating fat mass by subtracting it from the LST and/or body cell mass (BCM) that DEXA actually measures.

Sites central—Lumbar spine, hip, whole body

Peripheral—forearm, calcaneous.

Whole body DEXA includes assessment of total Body Bone Mineral Content (calibrated against hydroxyapatite and consisting of about 80% cortical bone), total body lean mass (calibrated against saline and consisting of lean soft tissue), total body fat mass (calibrated against stearic acid and consisting of fatty soft tissue).<sup>29</sup>

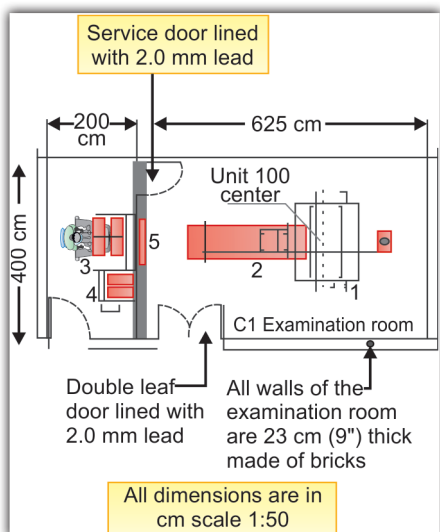
#### COMPUTED TOMOGRAPHY

CT scan is a medical imaging modality which has become one of the most powerful tool for various diagnostic and therapeutic purposes in virtually all medical disciplines. The modern day CT systems generate volume of data that can be acquired by various techniques and protocols based on the clinical concern. CT is the workhorse imaging tool for the evaluation of chest, abdomen and pelvis. In a time sensitive situation particularly trauma, CT is generally the initial approach.

Innovations in image acquisition and reconstruction technologies have greatly expanded the range of CT applications available in the routine clinical setting. The modern day CT scanner (64 and 128 slice) can acquire sub-millimeter resolution images of entire body regions in a few seconds, allowing depiction of fine anatomical detail uncompromised by motion artifact (**Figs 8A and B**). With sophisticated



**Figs 8A and B** 128 slice Dual source CT scanner



1. CT gantry; 2. Examination table; 3. Control unit; 4. Electronics;
5. Viewing glass 100 cm × 80 cm of 2.0 mm lead equivalence

**Fig. 9** Model layout CT-scan installation

visualization software, image data can be processed into multi-planar, volume-rendered, cine and other formats to better display anatomical abnormalities and facilitate newer applications such as dynamic CT, CT angiography, enterography, urography, tracheobronchography and cardiac CT. Newer applications including dual-energy material decomposition CT are furthering the transition of CT from a purely morphological to a combined anatomical, functional and metabolic imaging technique.<sup>31</sup>

CT angiography (CTA) enables the display of entire vascular system aided by injections of contrast medium. Several imaging post processing techniques are available

enabling good display of the entire vascular system. The most widely used techniques are multi-planar reformation (MPR), thin-slab maximum intensity projection (MIP), shaded surface display (SSD) and volume rendering technique (VRT). Sophisticated segmentation algorithms, bone removal with thresh holding or subtraction algorithms and vessel analysis tools are also newer techniques which provide quality of vessel analysis comparable to DSA (Conventional angiography). The clinical applications for these various image post processing methods include steno occlusive disease, aneurysms, vascular malformations.<sup>55</sup>

Virtual endoscopy (VE) is a recent development in post-processing technique which is used to generate virtual endoscopic views. This technique is used to obtain a perspective view of the display region mainly for anatomical cavities. These include, for example, the bronchial tree, large vessels, the colon and paranasal sinuses. VE is also used for areas not directly accessible for conventional endoscopy. The perspective volume rendering technique allows real-time fly through at high resolution mimicking the true endoscopy.

Installation of X-ray and CT scanner unit requires approval of AERB and need to conform to radiation protections measures (**Fig. 9**). However CT examination involves radiation exposure with potential risks and should be performed judiciously particularly in children who are more radio sensitive than adults.

## ■ ULTRASOUND

It is a non invasive diagnostic medical modality that uses high frequency sound waves to visualize the internal structures of the body in real time. It has the important advantages of being widely available, low cost and does not use ionizing radiation. This modality has become one of the most preferred imaging for diagnostic, interventional, monitoring and follow-up of

patients. It has a vital role in obstetrical imaging and is used both for assessing the fetal development and early diagnosis of many fetal anomalies.

Ultrasound is also useful for various guided interventions and can be performed on bed side in the triage of trauma patients. The quality of examination is however highly dependent on the experience of the sonographer in addition to the patient body habitus. The advanced ultrasound system includes capable of harmonic imaging, color and power Doppler and 3D and 4D reconstructions (Fig. 10). Technical advances like elastography and computer aided diagnosis have expanded the clinical applications especially in breast sonography.<sup>33</sup> Recently therapeutic applications with high intensity focused ultrasound (HIFU) and micro-bubble assisted delivery of drugs and genes has shown great promise.<sup>34</sup>

### Magnetic Resonance Imaging

MRI is a medical imaging technique used in radiology which makes use of the property of nuclear magnetic resonance (NMR) to image nuclei of atoms inside the body. Unlike CT scans or traditional X-rays, MRI does not use ionizing radiation. MRI uses strong magnetic field to align atomic nuclei (usually hydrogen protons or any other nuclei with odd number of protons) within body tissues and various radio frequency pulses are put on and off repeatedly. The signal from human tissues are received by coils placed near the area of interest and fed to computer, which converts these signals into an image.

MRI provides excellent contrast between the different soft tissues of the body and can be used to image any part of the body. It is especially useful in musculoskeletal radiology and neuroradiology. It can detect or sometimes help in characterizing vital 'lesions' that might be missed or indeterminate on other imaging modalities.<sup>35</sup> The MRI provides excellent white and gray matter differentiation of nervous tissues. An advantage of MRI is its ability to produce images in axial, coronal, sagittal and multiple oblique planes with equal ease. MRI scans give the best soft tissue contrast of all the imaging modalities. The advanced MR imaging techniques like perfusion imaging, diffusion-weighted imaging, and MR spectroscopy can improve the accuracy in diagnosis especially in the field of neuro imaging. With advances in scanning speed and spatial resolution and improvements in computer 3D algorithms and hardware, MRI has become an indispensable medical imaging technique in the current medical practice.

One disadvantage is the patient has to hold still for long periods of time in a noisy, cramped space while the imaging is performed. Claustrophobia severe enough to terminate the MRI exam is reported in up to 5 percent of patients. Recent improvements in magnet design including stronger magnetic fields (3 Tesla), shortening exam times, wider, shorter magnet bores and more open magnet designs, have brought some relief for claustrophobic patients (Fig. 11).



**Fig. 10** Advanced ultrasound system



**Fig. 11** 3Tesla MRI system with coils

The modality is however contraindicated for patients with pacemakers, cochlear implants, some indwelling medication pumps, certain types of cerebral aneurysm clips and metallic prostheses.<sup>36</sup>

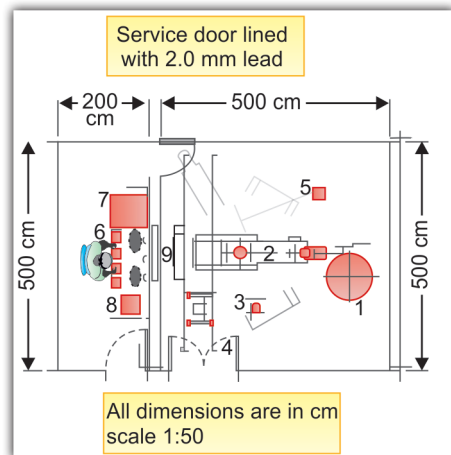
### Digital Subtraction Angiography

Digital subtraction angiography (DSA) is a type of fluoroscopy technique used in interventional radiology to clearly visualize blood vessels in a bony or dense soft tissue environment. Images are produced using contrast medium by subtracting a 'pre-contrast image' or the mask from later images, once the contrast medium has been injected.

Most cerebral angiography can be done with 3–5 frames per second (fps). Higher rates (e.g. 8–20 fps) are useful for imaging arteriovenous malformations and other high-flow lesions.<sup>37</sup> Not only anatomy but also function of blood flow can be studied using DSA, as X-ray images can be produced at a frame rate of up to 50 frames per second.<sup>38</sup> DSA is very successful in displaying the vascular system of the entire body and can be used both for diagnostic and therapeutic purposes.

While offering excellent spatial and temporal resolution as well as good contrast, single plane DSA suffers from its incapability of representing and displaying three-dimensional relationships. Such information can be introduced, if biplane angiography is applied (**Figs 12 and 13**). In biplane angiography, two X-ray devices generate images, which rotate around a common centre (called *isocenter*).

Planning and executing neuroradiological intervention is guided by biplane angiography because it provides fast information on the vascular system with high quality with 3-D reconstructions. There has also been considerable



1. C-arm; 2. Examination table; 3. Monitor trolley; 4. Over head rails; 5. Fixed radiation shield; 6. Control unit; 7. Electronics; 8. Additional electronics; 9. Lead glass viewing window 120 cm × 100 cm with 2.0 mm lead equivalence

**Fig. 12** Model layout—interventional radiology installation

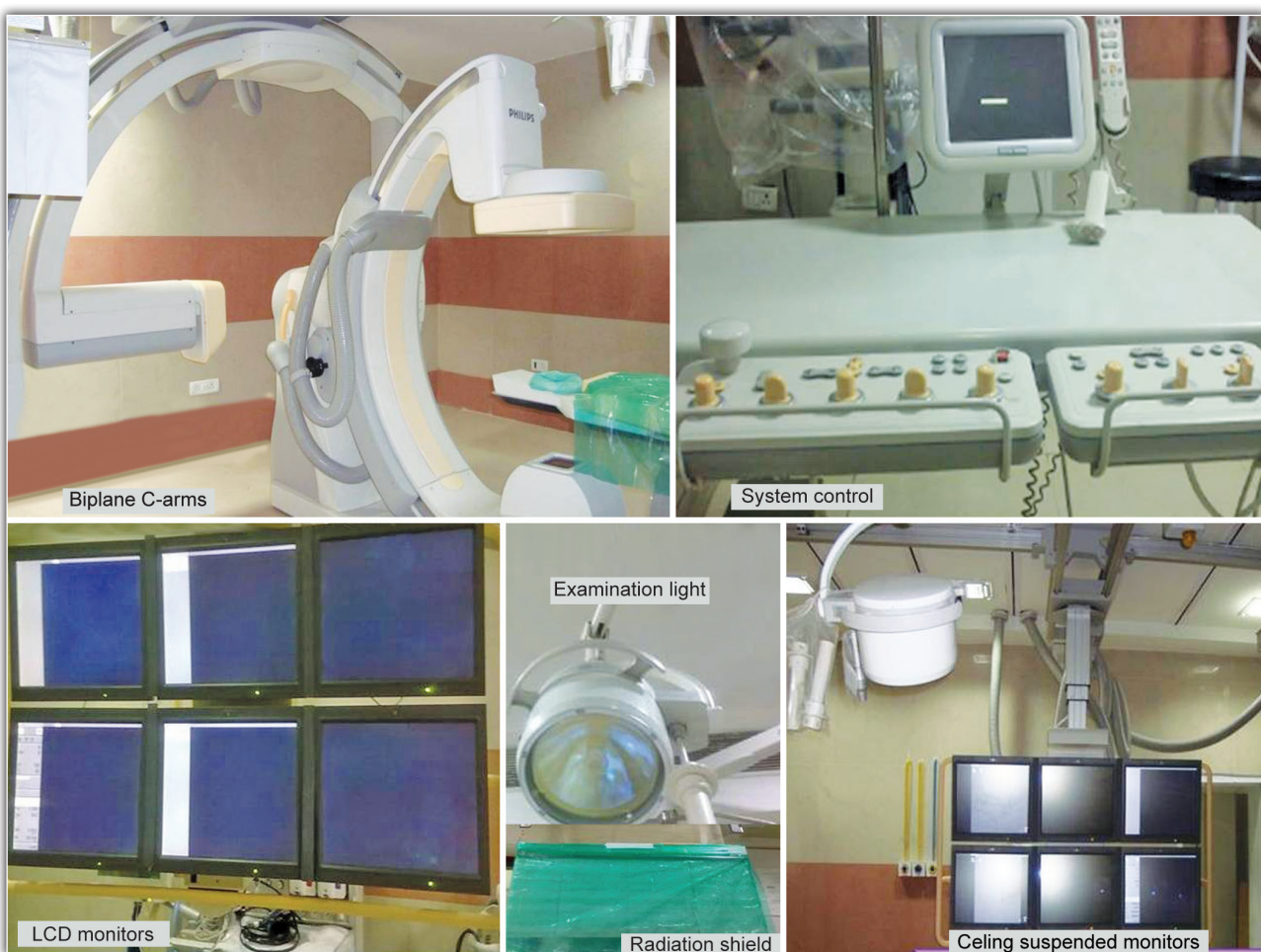


**Fig. 13** Biplane DSA Lab

progress in the development of catheters and embolization material. Using special micro-catheters, the interventional neuroradiologist is able to reach almost every point in the brain by endovascular approach.

Three-dimensional (3D) reconstruction of the dataset acquired during rotational DSA represents the latest development in the neurovascular imaging armamentarium. This technique combines the anatomic resolution of DSA with the 3D visualization abilities previously offered only by CT or MR angiography, and hence provides more detailed information than does DSA alone. The adequate evaluation of 3D-DSA requires post processing by 3D reconstruction algorithms at an external workstation. 3D DSA has taken a prominent role in treatment planning by enabling exquisite detailed anatomic information of complex vascular lesions and also helps in choosing the most appropriate working projection for subsequent endovascular therapy. It provides precise vascular information in sophisticated tasks such as aneurysm volume measurement. Three-dimensional DSA is therefore essential for optimal diagnosis and endovascular management of cerebral aneurysms/arteriovenous malformations and can reduce the number of exposures.<sup>39</sup>

**Digital flat-panel detector cone-beam computed tomography (CBCT)** has recently been adapted for use with C-arm systems. This configuration provides projection radiography, fluoroscopy, digital subtraction angiography, and volumetric computed tomography (CT) capabilities in a single patient setup, within the interventional suite. Such capabilities allow the intervention list to perform intra procedural volumetric imaging without the need for patient transportation.<sup>40</sup>

## Nuclear Imaging Systems

Nuclear medicine imaging non-invasively provides functional information at the molecular and cellular level by measuring the uptake and turnover of target-specific radiotracers in tissue. These functional processes include tissue blood flow and metabolism and by providing information on these processes, nuclear medicine imaging offers a broad array of tools for probing normal and disease-related states of tissue.

The principal imaging device is the gamma camera which detects the radiation emitted by the tracer in the body and displays it as an image. With computer processing, the information can be displayed as axial, coronal and sagittal images (SPECT images, single-photon emission computed tomography). SPECT has enabled the evaluation of disease processes based on functional and metabolic information. Positron emission tomography (PET) is also a nuclear medical imaging technique that produces a three-dimensional image or picture of functional processes in the body. The system detects pairs of gamma rays emitted indirectly by a positron-emitting radionuclide (tracer), which is introduced into the body on a biologically active molecule. If the biologically active molecule chosen for PET is FDG (fluorodeoxy glucose), the concentrations of tracer imaged then give tissue

metabolic activity, in terms of regional glucose uptake. Use of this tracer to explore the possibility of cancer metastasis (i.e. spreading to other sites) is the most common type of PET scan in standard medical care (90% of current scans). However, on a minority basis, many other radiotracers are used in PET to image the tissue concentration of many other types of molecules of interest.

The addition of anatomic imaging provided by Integration of computed tomography (CT) to functional imaging of positron emission tomography (PET) and single photon emission computed tomography (SPECT) has further expanded the utility and accuracy of nuclear medicine imaging. By using combined-modality PET/CT and SPECT/CT hybrid imaging, functional processes can be localized at anatomic sites or, in some instances, as yet unidentifiable structural alteration. These modalities have enhanced the accuracy of detection, determination of the extent and severity, and improved the ability to monitor patient's response to therapy in oncology patients.<sup>41</sup>

## PICTURE ARCHIVING AND COMMUNICATION SYSTEMS (PACS)

The development of electronic (filmless) department depends on the technological advances pertain to imaging and those arising from generally available computer technology. PACS are computer systems dedicated to the storage, retrieval, distribution and communication of medical images from multiple modalities. Electronic images and reports are transmitted digitally via PACS; this eliminates the need to manually file, retrieve, or transport film jackets. The universal format for PACS image storage and transfer is DICOM (Digital Imaging and Communications in Medicine). Development of PACS has replaced the conventional analogue film, paper clinical request forms and reports with a format that has completely computerized electronic display. PACS offers several advantages to radiologists and radiology departments as they work to trim costs, improve patient care, increase throughput and efficiency and have a major added value is efficiency of data management. Access to electronic images helps foster collaboration and support seamless care for patients across the primary and secondary care sectors.

A modern PACS has (or should have) excellent capabilities for displaying new examinations in a user-friendly manner, perfecting and displaying pertinent prior examinations for comparison and providing access to prior reports. One would consider these features to represent baseline or core functionality for any modern PACS.<sup>42</sup>

*The PACS architecture comprises of:*

Centralized PACS-(hub and spoke, star topology)—single short term storage unit to which every modality and every workstation is connected on a point to point basis.

Distributed PACS—composed of number of linked clusters, each with its own short-term storage unit and one

or more image acquisition modalities and several diagnostic/review workstations. Short-term storage is provided by one or more RAIDs (Random Array of Inexpensive Disks). RAID is composed of magnetic hard disks which is linked to a server which is connected directly to the PACS workstations. Connection can be made at various bandwidths, the highest generally being gigabit ethernet (**Figs 14A and B**).

The major benefits of PACS result from digitization of data which allows easy comparison, simultaneous multi location viewing, faster image retrieval, automatic chronological ordering and rapid database search.

Some of the disadvantages include the inherent costs and technological complexity which requires adequately trained hospital staff. A dedicated maintenance programme and a carefully devised plan to provide essential clinical services in case of PACS failure.<sup>43,44</sup>

There should be tight integration of the digital dictation stations to the PACS workstations. This eliminates keying errors on the part of the radiologists when logging in to read a particular case.

**Digital Reporting Rooms:** Incorporating image interpretation, PACS and radiology information systems are carefully

designed for physical space demands, lighting and ergonomics. Lighting must be placed to avoid glare on the monitor. Individual work spaces must be designed to allow privacy and collaboration at the same time.

**Hospital Information System (HIS)** Stores demographic data of all the patients, e.g. patient name, identification number, date of birth and also records admission and discharge dates, outpatient appointments, clinicians responsible for patient care and so forth.

**Radiology information system (RIS)** can be a stand-alone computer platform, or may be a module of the HIS. It stores information specific to the radiology department including radiological reports. Modern RIS will incorporate some DICOM features such as modality work list, modality performed procedure step, interpretation work list, and structured reporting.

Health level 7 is an internationally accepted standard for HIS and RIS systems. HIS-RIS-PACS integration should preferably be bidirectional. Input of demographic data is only once thereby minimizing human error. Any update to a patient's demographic data or any scheduling is propagated to all systems HIS, RIS, or PACS automatically, hence providing advanced notice of events and allowing them to prepare.<sup>45</sup>

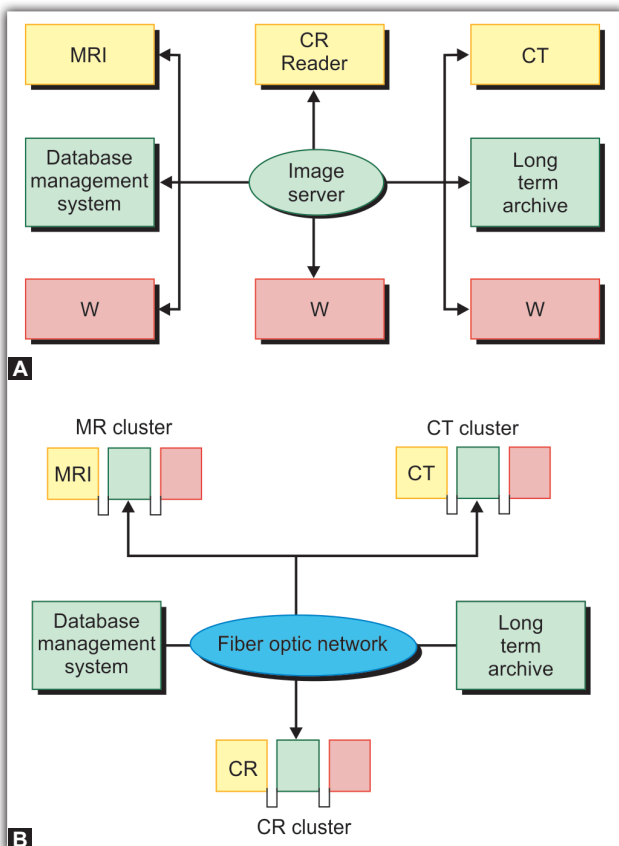
## Safety Standards and Quality Assurance

Safety standards and guidelines are an important aspect in early planning stages of a project. It is essential from the radiological safety viewpoint, to exercise strict regulatory control over the safe use of ionizing radiation used in various diagnostic equipment. Statutory requirements for the safe operation of medical diagnostic equipment by hospitals, clinics and other medical institutions in India are given by atomic energy regulatory board, government of India.

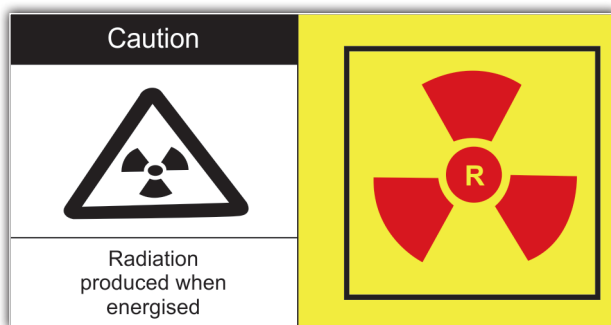
Adopted safety guidelines should be referenced in planning standards or regulations. For ionizing radiation, shielding characteristics are based on the National Council on Radiation Protection and Measurements (NCRP) Report 147: Structural shielding design for medical X-ray imaging facilities. The information has been updated, including guidelines on new modalities.

Further, radiation protection devices (**Fig. 15A**) like lead flaps, radiation shield, thyroid shield, lead apron, lead goggles and lead gloves, etc. should have appropriate lead equivalent as per AERB guidelines. Further radiation warning signs (**Fig. 15B**) should be prominently displayed in front of the doors of all the radiation rooms in the radiology department.

Although the clinical use of X-rays is governed by optimization, justification and the as-low-as-reasonably-achievable (ALARA) principle, these are to be supplemented by sound quality control (QC) practices. Imaging professionals should develop clearly defined guidelines that promote quality assurance in accordance with the latest technical knowledge of the equipment concerned. This professional



**Figs 14A and B** PACS architecture (A) with workstation (B) with networking

**Fig. 15A** Radiation protection devices**Fig. 15B** Radiation warning signs

approach will promote the due process of developing technical specifications, standards, and quality management.<sup>46</sup>

Digital images are created and processed with different parameters that must be continually assessed, different artifacts are possible from the digital processes, and complex computer systems can fail in subtle ways. Acceptance testing, regular calibration and proactive and consistent QC can prevent systematic errors that occur in digital acquisition or processing equipment and can contribute to overall department quality.<sup>47</sup>

## ■ TELERADIOLOGY

Teleradiology is the transmission of radiographic images from one location to another for interpretation by a radiologist. It is most often used to allow rapid interpretation of emergency room, ICU and other emergent examinations after hours of usual operation, at night and on weekends. The major

advantage of teleradiology is the ability to utilize different time zones to provide real-time emergency radiology services around-the-clock. The disadvantages include higher costs, limited contact between the ordering physician and the radiologist, and the inability to cover for procedures requiring an onsite radiologist.

Successful planning of a modern imaging department depends on many things, and one of the most important factors relates to the amount of time and the quality of effort spent on strategic planning at the outset. Neglecting or skimping at this stage may lead to unforeseen problems that could ultimately derail the project. Fortunately, there are lessons that can be learned and applied from other healthcare organizations and even from the corporate world. Effectively utilizing planning as described in this article may help to steer a team in the right direction and ensure that underlying issues and the concerns of all facilities have been adequately addressed. Putting a high priority on strategic planning will relieve many of the headaches that can occur before, during and after the planning of a modern imaging department.

## ■ REFERENCES

1. Edwina H. The Future Delivery of Diagnostic Imaging Services in Wales. 2009.
2. Aggarwal R. Planning an Imaging Department—Express Healthcare. (<http://www.expresshealthcare.in>).
3. Woodford DA. Project planning in the diagnostic imaging department. Radiol Manage. 1997;19(3):35-9.
4. Evan Leepson. Strategic Planning for Radiology: Opening an Out-patient Diagnostic Imaging Center. Radiology management. 2003.
5. Singh H, Gayatri S. Radiology and Imaging Department. (<http://www.drharisingh.com>)

6. Salem D. Standard Specifications for Basic Diagnostic Radiology Departments. 2011. ([moh-gr.org/pdf/Standard%20Specifications.pdf](http://moh-gr.org/pdf/Standard%20Specifications.pdf))
7. Cornelia schaefer- Prokop, Uirich Neitzal, Henk W. Venema, et al. Pigtail chest radiography: on and control of image quality update on modern technology dose containments. *Eur Radio*. 2008;18:1818-30.
8. Samei E. Performance of digital radiographic detectors: Quantification and assessment methods. Advances in digital radiography: RSNA: Categorical course in diagnostic Radiology Physics. 2003;pp.37-47.
9. Körner M, Weber C H, Wirth S, Pfeifer K, Reiser M F, Treitl M. Advances in Digital Radiography: Physical Principles and System Overview. *Radio Graphics*. 2007;27:675-86.
10. Rivetti S, Lanconelli N, Bertolini M, Nitrosi A, Burani A, Acchiappati D. Comparison of different computed radiography systems: physical characterization and contrast detail analysis. *Med Phys*. 2010;37(2):440.
11. Arakawa S, Itoh W, Kohda K, et al. Novel computed radiography system with improved image quality by detection of emissions from both sides of an imaging plate. SPIE Medical Imaging, poster presentation. 1999.
12. Samei E, Flynn MJ. An experimental comparison of detector performance for direct and indirect digital radiography systems. *Med Phys*. 2003;30(4):608-22.
13. Metz S, Damoser P, Hollweck R, et al. Chest radiography with a digital flat-panel detector: experimental receiver operating characteristic analysis. *Radiology*. 2005;234(3):776-84.
14. Bacher K, Smeets P, Vereecken L, et al. Image quality and radiation dose in digital chest imaging: Comparison of an amorphous silicon and an amorphous selenium flat-panel system. *AJR*. 2006;187(3):630-7.
15. Bath M, Sund P, Mansson LG. Evaluation of the imaging properties of two generations of a CCD based system for digital chest radiography. *Med Phys*. 2002;29:2286-97.
16. Lawinski C, Mackenzie A, Cole H, et al. Digital detectors for general radiography: A comparative technical report. National Health Service report 05078. 2005. K-CARE website. <http://www.kcare.co.uk/publications/abstracts/report05078.htm>
17. Samei E, Saunders RS, Lo JY, et al. Fundamental imaging characteristics of a slot scan digital chest radiographic system. *Med Phys*. 2004;31(9):2687-98.
18. MacMahon H. Improvement in detection of pulmonary nodules: digital image processing and computer-aided diagnosis. *Radiographics*. 2000;20(4):1169-77.
19. Gilkeson RC, Sachs PB. Dual energy subtraction digital radiography: technical considerations, clinical applications, and imaging pitfalls (review). *J Thorac Imag*. 2006;21(4):303-13.
20. Dobbins JT, Godfrey DJ, McAdams HP. Chest tomosynthesis. Syllabus RSNA, Advances in digital radiography: RSNA categorical course in diagnostic radiology physics. 2003;pp.211-7.
21. Brice J. Will new DR technologies offer alternative to CT? Part 2. <http://www.auntminnie.com/index.aspx?Sec=sup&Sub=xr&Pag=dis&ItemId=90041>. Updated March 25, 2010. Accessed October 28, 2010.
22. Heber MacMahon, Nicholas J. Yasillo, Michael Carlin Laser Alignment System for High Quality Portable Radiography *Radio Graphics*. 1992;12:111-20.
23. [www.e-radiography.com](http://www.e-radiography.com)
24. Lehnert T, Naguib NN, Ackermann H, Schomerus C, Jacobi V, Balzer JO, Vogl TJ. Novel, portable, cassette-sized, and wireless flat-panel digital radiography system: initial workflow results versus computed radiography. *AJR Am J Roentgenol*. 2011; 196(6):1368-71.
25. <http://www.radiologyinfo.org/en/info.cfm?pg=mammo>
26. Katherine A. Leslie. Digital Mammography: Planning, Implementation, and Integration (Available at <http://www.eradimaging.com>)
27. Larkin A, et al. Commissioning and Quality Assurance of Dual Energy X-ray Absorptiometry (DEXA) systems, *Rad. Prot. Dosim*. 2008 (in press).
28. Sheahan NF, Dowling A, O'reilly G, Malone JF. Commissioning and quality assurance protocol for dual energy X-ray absorptiometry systems, *Rad. Prot. Dosim*. 2005;117:288-90.
29. Lohman TG, Harris M, Teixeira PJ, Weiss L. Assessing body composition and changes in body composition. Another look at dual-energy X-ray absorptiometry. *Ann N Y Acad Sci*. 2000; 904:45-54.
30. Lorente Ramos, RM, Azpeitia Armán J, Arévalo Galeano N, Muñoz Hernández A, García Gómez JM, Gredilla Molinero J. Dual energy X-ray absorptiometry: Fundamentals, methodology, and clinical applications *Radiología*. 2012;54 :410-23.
31. Guillerman RP. Newer CT applications and their alternatives: what is appropriate in children? *Pediatr Radiol*. 2011;41(Suppl 2):534-48.
32. Lell MM, et al. New Techniques in CT Angiography. *Radio Graphics*. 2006;26:S45-S62.
33. Weinstein SP, Conant EF, Sehgal C. Technical advances in breast ultrasound imaging. *Semin Ultrasound CT MR*. 2006;27(4):273-83.
34. Harvey CJ, Pilcher JM, Eckersley RJ, Blomley MJ, Cosgrove DO. Advances in ultrasound. *Clin Radiol*. 2002;57(3):157-77.
35. Elsayes KM, et al. MRI characterization of 124 CT-indeterminate focal hepatic lesions: evaluation of clinical utility. *HPB (Oxford)*. 2007;9(3):208-15.
36. <http://www.frankshospitalworkshop.com/equipment/documents/X-ray/wikipedia/Radiology.pdf>
37. Biplanar DSA Diagnóstico Cerebral Angiography - Springer ([www.springer.com/cda/content/document/cda.html?contentID=9781588297556-c1.pdf](http://www.springer.com/cda/content/document/cda.html?contentID=9781588297556-c1.pdf))
38. Toennies KD, Oishi S, Koster D, Schroth G. Accuracy of distance measurements in biplane angiography.
39. J V Byrne, C Colominas, J Hipwell, et al. Assessment of a technique for 2D-3D registration of cerebral intra-arterial angiography. *The British Journal of Radiology*. 2004;77:123-8.
40. Orth R C, Wallace M J, Michael D. Kuo M D C-arm Cone-beam CT: General Principles and Technical Considerations for Use in Interventional Radiology *Vasc Interv Radiol*. 2008;19:814-21.
41. Nuclear Medicine Imaging in Diagnosis and Treatment. National Research Council (US) and Institute of Medicine (US) Committee on State of the Science of Nuclear Medicine. Advancing Nuclear Medicine through Innovation. Washington (DC): National Academies Press (US). 2007.
42. Ralston, Coleman R M, Beaulieu D M, Scrutfield K, Perkins T. Progress toward Paperless Radiology in the Digital Environment: Planning, Implementation, and Benefits. *J Digit Imaging*. 2004 Jun; 17(2):134-43. Epub 2004 Apr 19.
43. Ehsan Samei, J Anthony Seibert, Katherine Andriole, Aldo Badano, Jay Crawford, Bruce Reiner, Michael J. Flynn, Paul Chang. AAPM/RSNA Tutorial on Equipment Selection: PACS Equipment Overview General Guidelines for Purchasing and Acceptance Testing of PACS Equipment. *Radio Graphics*. 2004; 24:313-34.

44. Bryan S, Weatherburn GC, Watkins JR, Buxton MJ. "The benefits of hospital-wide picture archiving and communication systems: a survey of clinical users of radiology services". *Br J Radiol.* 1999; 72(857):469-78.
45. Dundas DD. Installation of a PACS system. *The British Journal of Radiology.* 2005;78:480-2.
46. Korir G K, Wambani J S, Korir I K. Establishing a quality assurance baseline for radiological protection of patients undergoing diagnostic radiology. *SA Journal of Radiology.* 2011.
47. Herrmann T L, et al. Best Practices in Digital Radiography. White paper Published by the American Society of Radiologic Technologists.
48. Model layout figures for various equipment and installations are courtesy (Amendment to AERB safety code on medical X-ray equipment and installations (AFRB/SC/MED-2(Rev.1),2001)

## Chapter

# 26

# Recent Advances in PET/CT and PET/MR

*Rakesh Kumar, Anil Chauhan*

## INTRODUCTION

The last decade has witnessed a rapid advancement in the field of nuclear medicine. In this ever-expanding field, the onus goes to the advancement in instrumentation and radiotracers for clinical use, which is particularly evident in positron emission tomography/computed tomography (PET/CT) imaging. In this era of evidence-based medicine, the clinical indications for PET-CT has been increasing and expanding beyond oncology. Positron emission tomography/magnetic resonance (PET/MR) imaging has been used in experimental setups for last 2 decades and recently has been introduced for clinical imaging in many centers.

The authors would discuss major recent advances in the clinical nuclear medicine related to PET/CT and PET/MR and their clinical applications. It is beyond the scope of this chapter to include the recent advances of the instrumentation and radiotracers.

## PET/CT

The PET is a functional diagnostic imaging technique, which can provide metabolic information for the underlying process that can either be normal physiological activity in the body or a pathological entity. There are many radiotracers that can be used for PET imaging, to provide information on glucose, amino acid and fatty acid metabolism, or target a particular receptor.

The PET alone is now universally replaced by PET/CT in routine clinical practice, as it had poor anatomical localization and early PET-only scanners had limited resolution of abnormal radiotracer accumulation in the body tissues. To overcome these two important limitations, combined PET/

CT scanners were introduced in routine clinical practice after 2000. This widespread use of PET/CT was evidence based as PET/CT demonstrated higher specificity and sensitivity than either PET or CT alone for the management of various diseases especially in the field of oncology. PET/CT can provide the functional and morphological details of various pathological conditions in one procedure. Although many radiotracers are being used for PET-CT, <sup>18</sup>F-fluoro-2-deoxy-D-glucose (FDG) is the most commonly used radiotracer in PET/CT imaging. FDG is an analog of glucose and the uptake is proportional to the metabolism of glucose by the pathological conditions. Most of these pathological conditions usually demonstrate high glucose metabolism and show preferential uptake of FDG as compared to surrounding normal cells. After transport into tumor cell, FDG is phosphorylated by hexokinase into FDG-6-phosphate, which cannot continue through glycolysis because it is not a substrate for enzyme glucose-6-phosphate isomerase.<sup>1,2</sup> As a result, <sup>18</sup>F-FDG-6-phosphate is biochemically trapped within the cell. <sup>18</sup>F-FDG-PET is now an established standard in the initial staging, monitoring the response to the therapy, and restaging after treatment of patients with various cancers as well as some non-oncological conditions. In addition to qualitative image display, it is possible to quantify the FDG uptake value normalized to the injected dose and body weight/surface area, which is known as "standardized uptake value" (SUV). The SUV provides an approximate indicator that correlates with FDG metabolism in the tissue. A lesion with an SUV greater than 2.5 is considered to have a high probability of malignancy. However, that is not always true. Recently, a new quantitative parameter has been introduced which is described as tumor burden. This is a product of

tumor volume and SUV. It has been reported to have higher accuracy than SUV alone in evaluating treatment response of solid tumors to chemotherapy.<sup>3</sup>

### Clinical Applications of PET/CT

The PET/CT plays an important role in the management of cancer patients. It is primarily indicated for characterization of lesion equivocal on anatomical imaging, initial staging, treatment response evaluation, evaluation for recurrence, in detecting primary cancer in metastatic disease from unknown primary, and to provide prognostic information for various cancers.

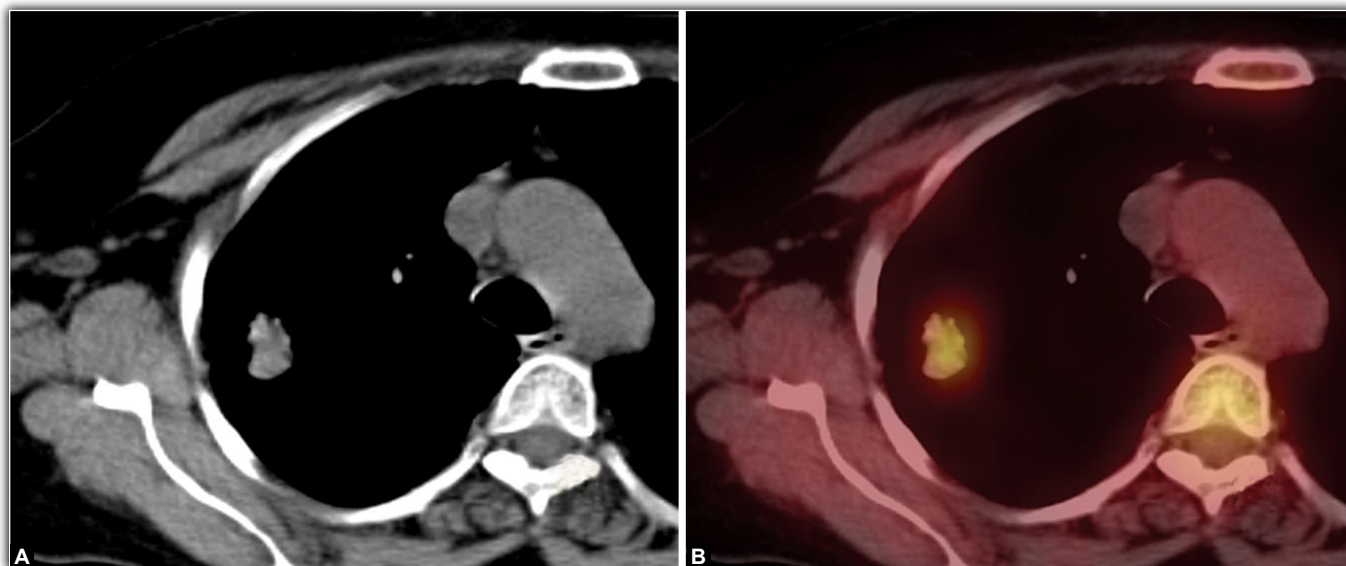
#### Diagnosis

The CT is the imaging modality of choice for detection and follow-up of lung nodules but has limited specificity especially in nodules less than 10 mm in size. PET/CT is increasing being used to characterize small solitary pulmonary nodule (SPN), which are difficult to evaluate on CT. PET/CT provides additional functional information and is useful in differentiating benign lesions from malignant ones (**Figs 1A and B**). Two systematic reviews of the literature with meta-analysis reported sensitivity ranging from 96 to 97 percent and specificity of 78 to 86 percent using PET for detection of malignant SP.<sup>4,5</sup> It is important to note the limitations of PET-CT. FDG PET/CT has low sensitivity in detecting low grade tumors like bronchoalveolar carcinoma and bronchial carcinoid. Sarcoidosis and active granulomatous infection like tuberculosis, and fungal infections (histoplasmosis or coccidioidomycosis) can be metabolically active and lead to false positive results.

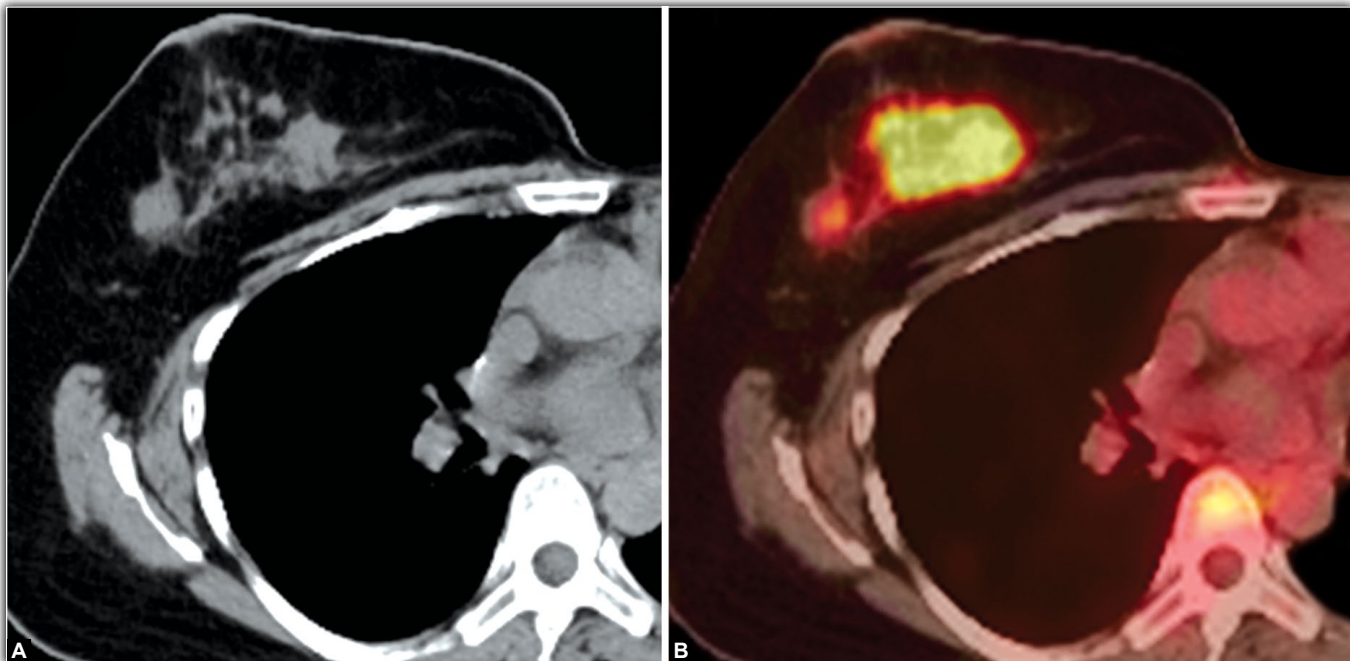
Patients with cervical lymph node metastasis from an unknown primary tumor present a big diagnostic dilemma from management perspective. FDG-PET can be a valuable tool in this subset of patients with an occult primary tumor in the head and neck region.<sup>6</sup> PET-CT is a valuable tool in these patients and can identify the primary tumor in approximately 30 percent patients.

Mammography is the widely used screening imaging technique for the detection of primary breast cancer but found to have lower sensitivity in women with radiographically dense breasts and in women with breast implants. PET/CT is useful in patients with dense breasts and patients with breast implants. PET/CT has also been found to be useful in detecting additional primary in contralateral breast in known breast cancer patients (**Figs 2A and B**). However, MRI remains the gold standard for this purpose in selected cases. Recently positron emission mammography (PEM) has been introduced for characterization of breast lesions and has shown encouraging results.<sup>7</sup> Patients with carcinoma-*in situ*, low-grade tumors, well-differentiated ductal and lobular breast cancer usually have significantly lower SUVs and can be misinterpreted as benign lesions.

Till recently, the role of FDG-PET in bladder cancer was very limited due to urinary excretion of FDG. The detection of primary tumor and local visceral tumor recurrence is limited due to the presence of excreted FDG in the urinary tract, which often masks the pelvic lesion. An intervention, thus, to reduce the urinary radioactivity without altering the tumor uptake seems needed. In a recent study, we used diuretics administration as an intervention, and demonstrated a sensitivity of 92 percent and specificity of 96 percent in patients with bladder carcinoma.<sup>8</sup> Diuretic administration



**Figs 1A and B** Chest CT of PET/CT shows solitary pulmonary nodule in right lung (A). PET/CT chest showing FDG uptake in the nodule suggestive of malignancy (B). FNAC of nodule confirmed the diagnosis of malignancy (adenocarcinoma)



**Figs 2A and B** CT of PET/CT shows multiple nodules in right breast of patient who was treated for left breast cancer previously (A). PET/CT shows increased FDG uptake in all nodules suggestive of malignant nature of nodules (B) (additional primary in contralateral breast in known breast cancer patient)

significantly improved the detection of the primary tumor involving the bladder wall (**Figs 3A to D**).

Thymic tumors represent a broad spectrum of neoplastic pathologies with variable overlap in clinical and imaging presentation. PET/CT is useful in differentiating thymic hyperplasia from neoplasms, especially thymoma, carcinoma and lymphoma.<sup>9</sup> We have demonstrated that the difference between SUV max for thymic hyperplasia, thymoma and thymic carcinoma was statistically significant (**Figs 4A and B**).<sup>10</sup>

The FDG PET/CT has lower sensitivity and specificity for neuroendocrine tumors (NET). In addition to FDG, other positron-emitting radionuclides such as somatostatin analog DOTA-D-Phe<sup>1</sup>-Tyr<sup>3</sup>-octreotide (DOTA-TOC), <sup>11</sup>C-Hydroxyephedrine, <sup>11</sup>C-Epinephrine, <sup>11</sup>C-5-hydroxytryptophan and <sup>18</sup>F-DOPA, etc. are also used. Functional imaging with <sup>68</sup>Ga-DOTA-TOC is a valuable diagnostic tool in NETs as it targets the somatostatin receptors, which are molecular characteristics of most of these tumors. Our group demonstrated advantages of <sup>68</sup>Ga-DOTA-TOC over conventional FDG PET/CT in various NETs (**Figs 5A to C**).<sup>11</sup> <sup>68</sup>Ga-DOTATOC PET/CT emerged as the superior imaging technique with 100 percent sensitivity and PPV for detecting primary tumor, as compared to CECT that had a sensitivity of 83 percent in patients with NET. <sup>68</sup>Ga-DOTA-NOC PET-CT has been reported to be highly sensitive and specific for the detection of pheochromocytoma and paragangliomas as reported by Naswa et al in 35 patients.<sup>12</sup> It seems better than <sup>131</sup>I MIBG Scintigraphy for this purpose. Contrast-enhanced CT (CECT) is a standard investigative

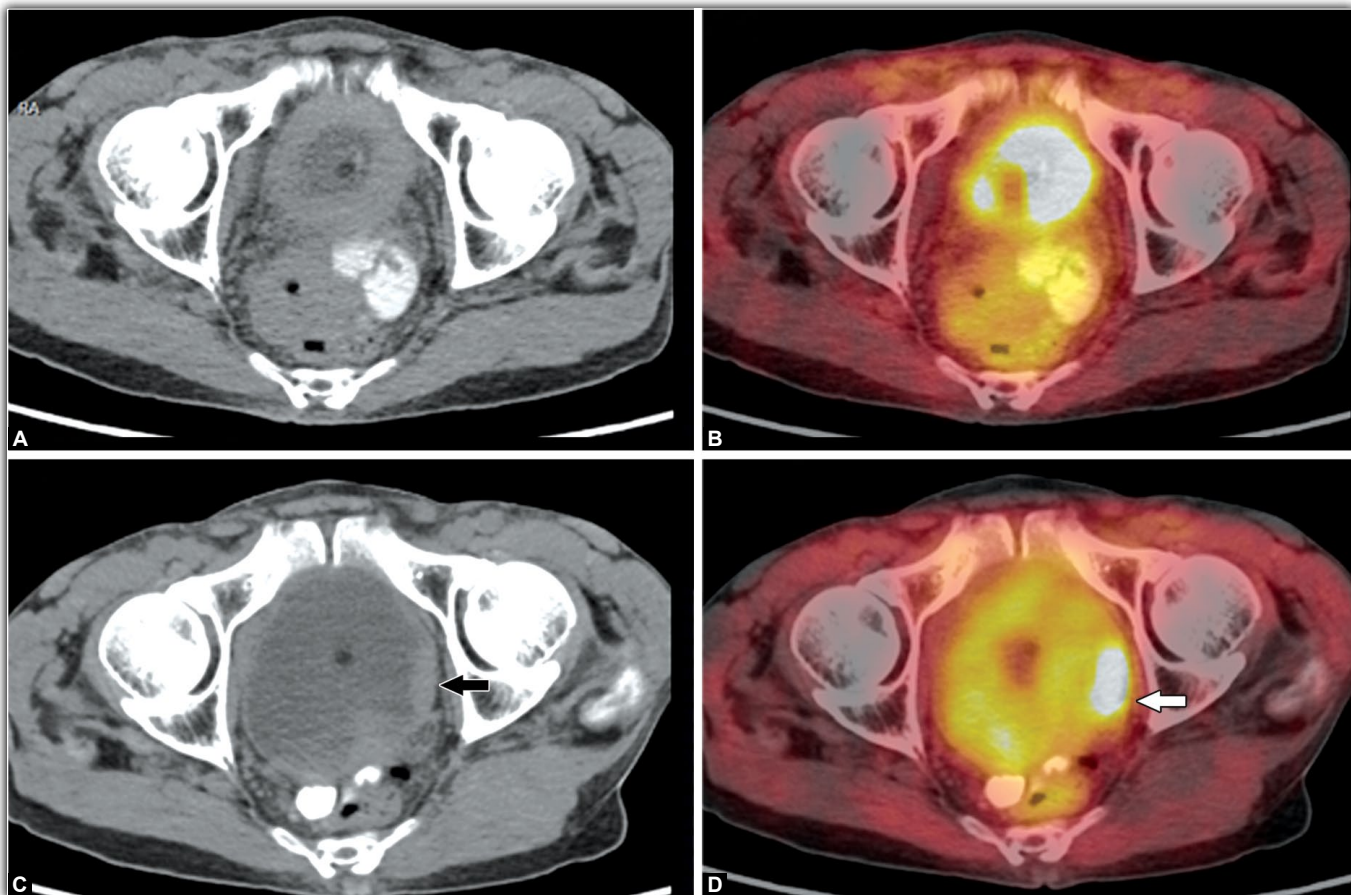
procedure in the localization of gastrinomas. Small tumors are often missed and metastatic lesions may remain occult on CT. Naswa et al demonstrated usefulness of <sup>68</sup>Ga-DOTANOC PET/CT in patients with gastrinoma with negative or equivocal results on CECT.<sup>13</sup>

In brain tumors, FDG PET/CT has limited application due to inherent high glucose metabolism by brain parenchyma. FDG-PET CT may detect high-grade gliomas. FDG PET/CT has some role to play in patients with brain tumors treated by radiation therapy, where anatomical imaging modalities like CT and MRI can be limited in differentiating radiation necrosis from residual/recurrent tumor. New radiotracers like <sup>11</sup>C-methionine (<sup>11</sup>C-MET), <sup>11</sup>C-tyrosine, <sup>18</sup>F-fluorotyrosine, <sup>18</sup>F-fluoroethyltyrosine (<sup>18</sup>F-FET), 8-cyclopentyl-3-(3-<sup>18</sup>F-fluoropropyl)-1-propylxanthine (<sup>18</sup>F-CPFPX) and <sup>18</sup>F-fluorothymidine (<sup>18</sup>F-FLT) have been studied as FDG has not much role due to its high normal uptake in brain. These nonFDG radiotracers however are still experimental and not used in routine clinical practice.

#### Initial Staging

The PET/CT has been found to play an important role in the initial staging of various tumors, which refers to assessing the extent of malignant neoplasms, and in differentiating localized from disseminated disease.

For lung cancers, the FDG PET/CT has been primarily studied for nonsmall cell lung cancer (NSCLC) patients.



**Figs 3A to D** A 63-year-old man with carcinoma of the urinary bladder underwent staging PET/CT. Unenhanced axial CT image shows an diffuse thickening of urinary bladder wall with a catheter *in situ* (A). Corresponding axial PET/CT image shows a relative photon-deficient area in the region of the catheter bulb with urinary radioactivity occupying the remaining bladder cavity (B). Spot views of the urinary bladder were taken after diuretic administration which reveals the left lateral bladder wall thickening in a distended bladder on CT (C, bold arrow), which shows intense uptake on axial PET/CT (D arrow) with a high target to background ratio after the residual bladder activity has been cleared

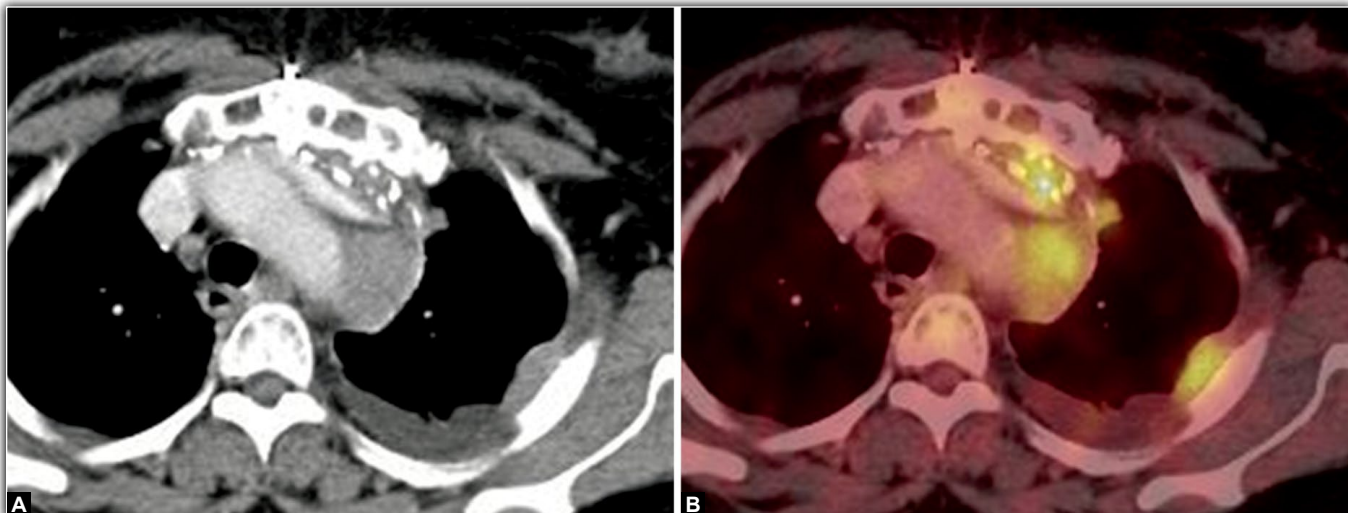
In these patients regional and distant spread of the disease will change staging and guide the therapeutic approach (**Figs 6A to E**). PET/CT more accurately determines the T staging compared with either CT or PET alone. In one meta-analysis, PET/CT accurately predicted the T stage in patients with NSCLC in 82 percent of cases compared with 55 percent and 68 percent with PET alone and CT alone, respectively.<sup>14</sup> The additional advantages of PET/CT over CT are in differentiating central tumors from post obstructive atelectasis and detection of subtle areas of invasion.

In patients with Hodgkin's disease (HD) and Non-hodgkin's lymphoma (NHL), PET/CT detects more lesions, which change the stage of the disease in almost 15 percent of patients when compared to conventional imaging like CT.<sup>15</sup> For histopathological examination of the lesion in HD and NHL, PET-CT can guide the biopsy from suitable and easily accessible site.

In colorectal cancer (CRC) patients, regional nodal or distant metastasis is present in majority of them at initial

presentation. CT is used as initial investigation for staging but PET/CT is superior in detecting unexpected hepatic and extrahepatic metastases (**Figs 7A to D**). In a recent meta-analysis on the value of FDG PET/CT in preoperative staging of colorectal cancer demonstrated a pooled sensitivity of 91 percent, and pooled specificity of 91 percent.<sup>16</sup> Mucinous adenocarcinoma is a subtype of CRC, which is less FDG avid and can produce false negative results in many cases.

PET/CT can be useful in initial staging evaluation of breast cancer as it can detect axillary node involvement, however it is inferior in detecting lymph node metastasis when compared to sentinel lymph node biopsy. In selected patients who have high risk of nodal metastases, a clearly positive PET/CT carries a high positive predictive value for nodal metastases. The advantage of PET/CT in initial staging in breast cancer is detection of internal mammary lymph node and distant metastasis (**Figs 8A and B**). FDG PET/CT was found to be significantly more accurate for detecting axillary lymph node and distant metastases in 106 women in a



**Figs 4A and B** A 54-year-old man with thymic carcinoma underwent PET/CT. CECT axial image shows anterior mediastinal mass abutting arch of aorta with calcification. In addition there is left pleural thickening (A). Corresponding axial PET/CT image shows a intense uptake in the anterior medistinal mass seen on CT (B)

recently published study.<sup>17</sup> Management of 15 patients (14%) was altered based on the FDG PET/CT findings, including 3 patients with axillary lymph node metastases, 5 patients with extra-axillary lymph node metastases, 4 patients with distant metastases and 3 patients with synchronous malignancies.

PET/CT differentiates resectable and unresectable disease in esophageal and gastric cancers and helps in avoiding futile surgeries; however, the detection of regional nodal metastases is limited due to the small volume of disease in some lymph nodes and small size of the metastatic lymph nodes (**Figs 9A to G**). In a recent study authors from Australia have shown that PET/CT changed the stage group in 56 (40%) patients and changed management in 47 (34%) of 139 patients.<sup>18</sup> The authors concluded that PET/CT provides incremental staging information compared with conventional imaging, changes management in one third of patients, and has powerful prognostic stratification in the primary staging of esophageal cancer. In a systematic review, Mazola et al concluded that it appears reasonable to include FDG PET/CT in the diagnostic algorithm of patients with esophageal cancer in order to better define the optimal therapeutic approach.<sup>19</sup>

The FDG PET/CT has a limited role in detecting soft-tissue metastasis to pelvic lymph nodes in patients with prostate cancer, owing to urinary excretion of FDG and low glucose uptake by tumor cells (usually a well-differentiated neoplasm) in these patients. <sup>11</sup>C-choline PET/CT is more accurate than FDG PET/CT in patients with prostate cancer. In a systemic review and meta-analysis of <sup>18</sup>F-choline and <sup>11</sup>C-choline PET/CT in the lymph node staging of prostate cancer prior to surgery involving 10 studies and 441 patients, Evangelista et al demonstrated pooled sensitivity 49.2 percent and pooled specificity 95 percent.<sup>20</sup> Another radiotracer <sup>18</sup>F-fluoro-5α-

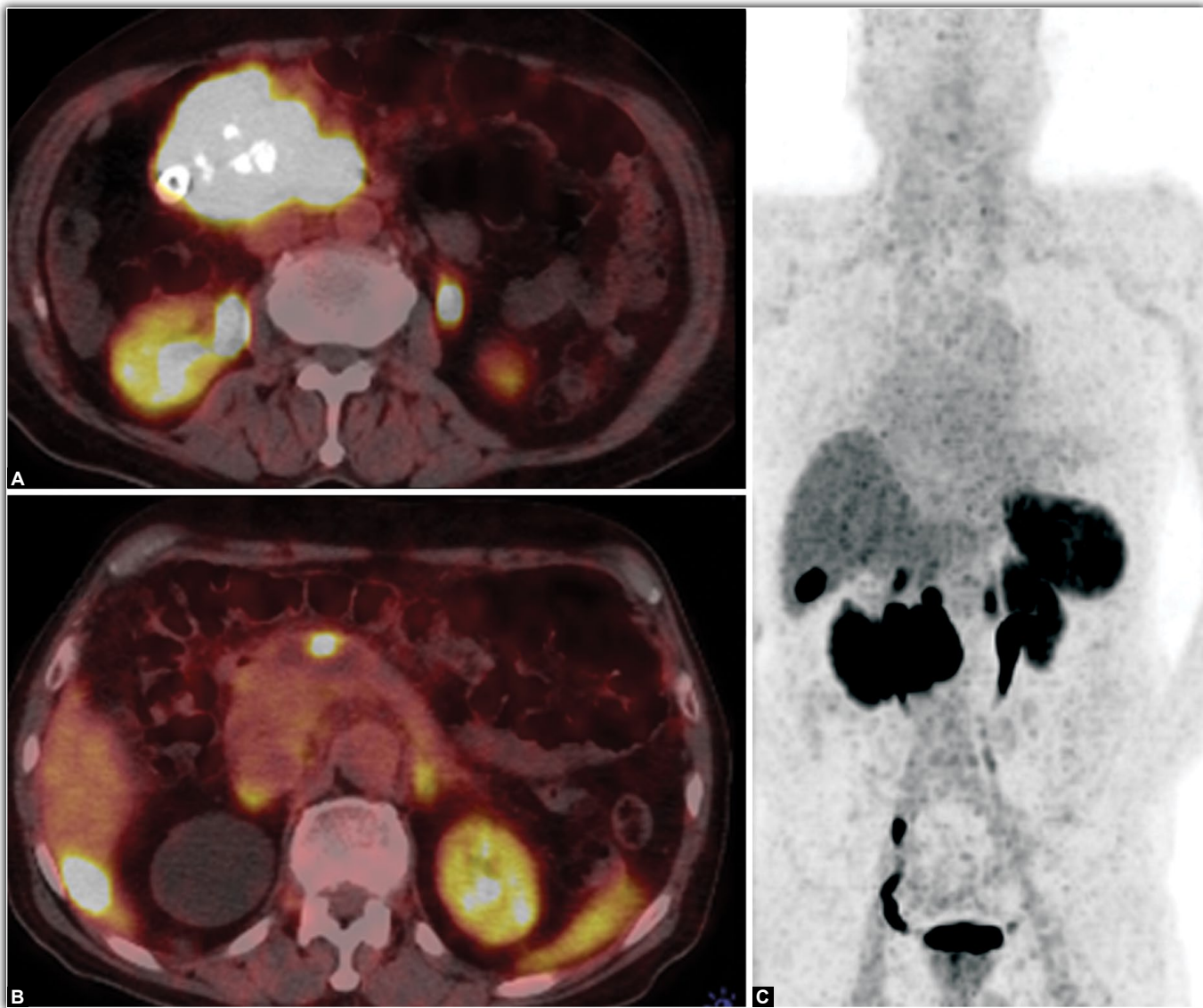
dihydrotestosterone (<sup>18</sup>F-FDHT), a labeled analog of the major ligand for androgen receptor di-hydro-testosterone; has been used by some authors in limited number of patients. F18-Na-Fluoride PET/CT has high sensitivity for detecting bone metastases as compared to conventional bone scan due to high resolution of PET/CT scan.

The detection and staging of primary urothelial tumor and local visceral tumor recurrence is limited due to the presence of excreted FDG in the urinary tract, which often masks the pelvic lesion and probably the adjacent lymph nodes. Diuretic administration significantly improved the detection of the primary tumor involving the bladder wall and regional lymph nodes metastasis.<sup>8</sup> In a recent study, Divgi et al studied the utility of iodine-124 <sup>124</sup>I-girentuximab PET/CT in 195 patients with renal masses and demonstrated higher sensitivity and specificity as compared to CECT.<sup>21</sup>

In NET, <sup>68</sup>Ga-DOTA-TOC PET/CT is superior to conventional imaging and FDG PET/CT for detecting occult metastasis. In our experience, we have found that <sup>68</sup>Ga-DOTA-TOC PET/CT is most sensitive and specific technique for initial staging of NET. CECT found to have higher accuracy as compared to FDG PET/CT but lower accuracy than <sup>68</sup>Ga-DOTA-TOC PET/CT.<sup>11,12</sup>

#### Treatment Response Evaluation

The PET/CT has emerged as a useful imaging modality that can evaluate the therapy response and differentiate responders from nonresponders during and after completion of treatment. Since many of the chemotherapeutic drugs used for targeted therapy are cytostatic and not citocidal, conventional imaging like CT and MRI has limited value in evaluating the treatment response. The PET/CT being a



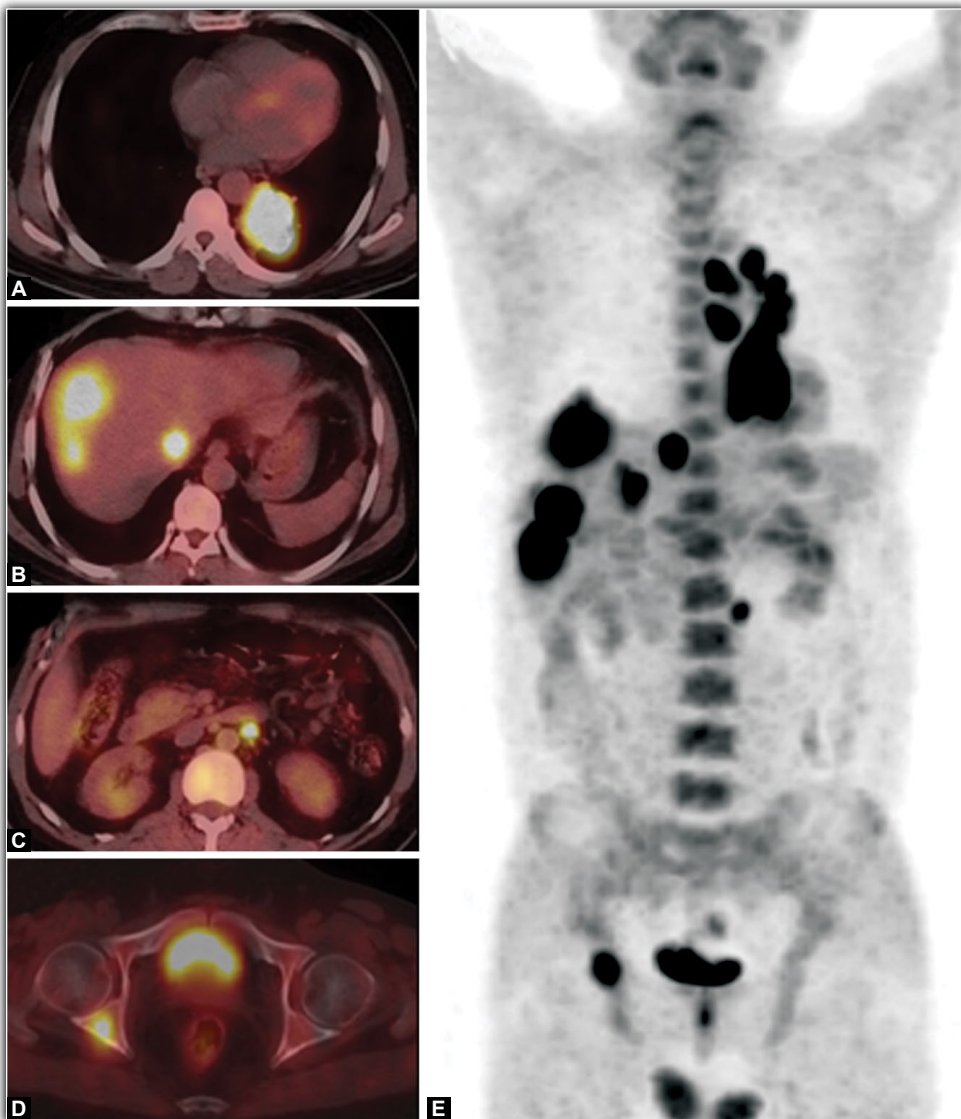
**Figs 5A to C** Transaxial  $^{68}\text{Ga}$ -DOTATOC PET/CT images of abdomen (A) of a 42-year-old male patient presenting with pain abdomen showing intense tracer uptake in the pancreatic mass suggesting SSTR receptor expressing tumor. Also note a lesion in the liver showing increased  $^{68}\text{Ga}$ -DOTATOC uptake suggesting metastasis (B). Projection image of whole body PET showing above described findings (C). A diagnosis of pancreatic NET was made. On histopathology the mass turned out to be a well differentiated NET

metabolic imaging modality, can demonstrate the treatment response earlier by determining the glucose uptake by tumor, which decreases earlier than the size in solid tumors. The PET/CT performed after 1 to 2 cycles of chemotherapy can differentiate non-responsive disease from adequate response better than conventional imaging modalities in various malignancies and can guide the treatment plan accordingly.

The PET-CT plays an important role in evaluation of treatment response soon after 1 to 2 cycles of chemotherapy in patients with lymphoma. It has been shown to have higher sensitivity, specificity and prognostic value when compared

with CECT for mid-term therapy response (**Figs 10A to J**). PET-CT does not show any significant advantages over CECT when therapy evaluation is done after completion of treatment. In a recent study published by our group concluded though PET/CT depicts additional sites compared with contrast-enhanced CT and results in upstaging of disease. However, either PET/CT or contrast-enhanced CT may be used for response assessment and prognostication in stage III or IV nonlymphoblastic pediatric NHL.<sup>22</sup>

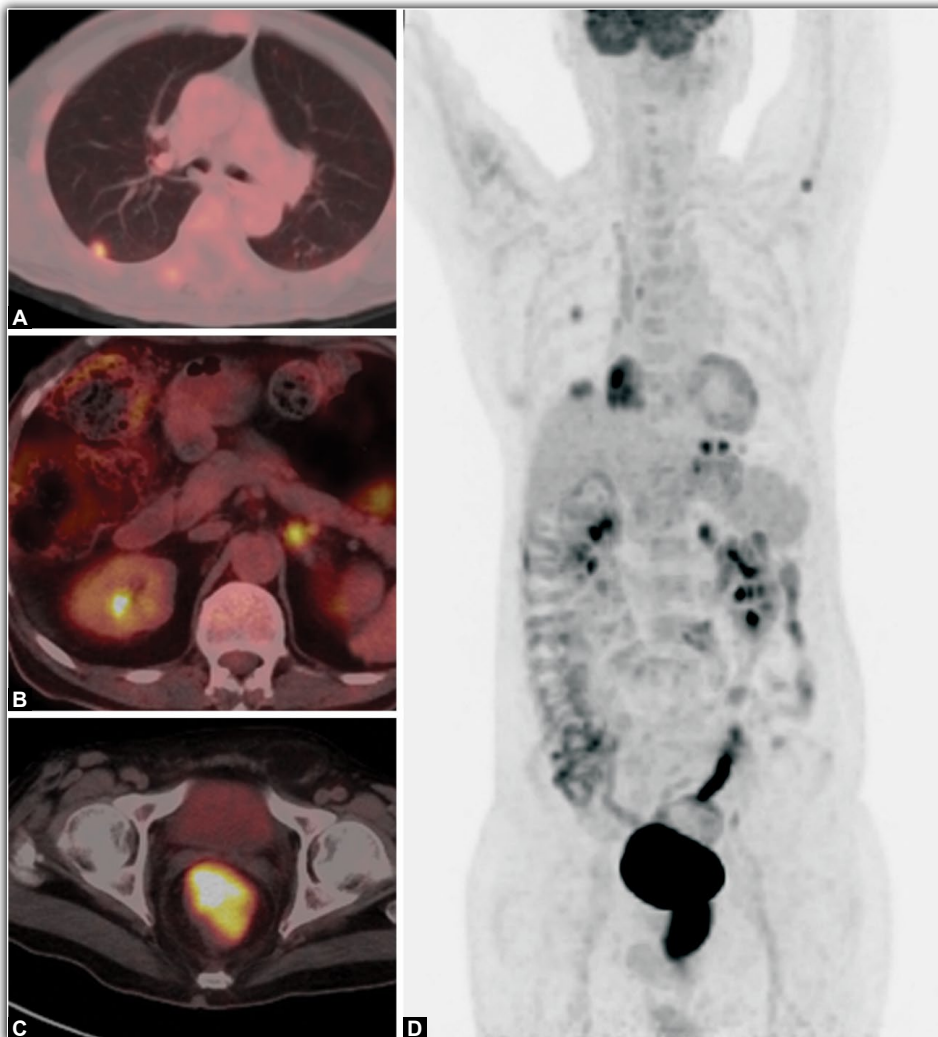
In breast cancer patients, PET/CT detects treatment-related metabolic changes much earlier than conventional



**Figs 6A to E** Transaxial  $^{18}\text{FDG}$ - PET/CT images of chest, abdomen and pelvis (A to D) of a 62-year-old male patient presenting with chest pain and hemoptysis, showing intense tracer uptake in the left lower lung mass suggestive of malignant tumor (A). Also note multiple focal areas of increased FDG uptake in liver (B), left adrenal (C) and right acetabulum marrow (D) suggestive of metastatic disease. Projection image of whole body PET showing above described findings (E)

imaging and clinical examination, once the chemotherapy has been initiated. There is strong correlation between the quantitative changes in SUV and overall clinical assessment of response of skeletal metastases to therapy and changes in tumor markers in breast cancer patients. We evaluated the role of FDG PET/CT for the assessment of response after two cycles of neo-adjuvant chemotherapy (NACT) for breast cancer and concluded that FDG PET/CT can differentiate responders from non-responders with high accuracy after two cycles of NACT in patients with locally advanced breast cancer (LABC).<sup>23</sup>  $^{90}\text{Y}$  radioembolization (selective internal radiation therapy [SIRT]) has emerged as a valuable therapeutic option in unresectable, chemotherapy-refractory hepatic metastases from breast cancer. FDG PET/CT appears to be useful for predicting survival in these patients.<sup>24</sup>

Neoadjuvant chemoradiation therapy may result in significant tumor regression in patients with gastro-intestinal malignancies. Delta SUVmax (Absolute SUVmax change) and response index (RI, percent SUVmax change) are best predictive parameters in response evaluation of neoadjuvant chemotherapy. Hendlisz et al assessed the predictive value of FDG PET/CT metabolic response after a single course of chemotherapy in patients with metastatic colorectal cancer and concluded that metabolic response measured by FDG-PET/CT after a single course of chemotherapy in metastatic CRC is able to identify patients who will not benefit from the treatment.<sup>25</sup> In patients with esophageal carcinoma, PET/CT is more specific than CT and endoscopic USG for loco-regional lymph node metastasis and response evaluation to neoadjuvant chemotherapy.



**Figs 7A to D** Transaxial  $^{18}\text{FDG}$ - PET/CT images of chest, abdomen and pelvis (A to C) of a 78-year-old male patient presenting with rectal mass, showing intense tracer uptake in the rectal mass suggestive of malignant primary tumor (C). Also note multiple focal areas of increased FDG uptake in the right lung (A) and left adrenal (B) suggestive of metastatic disease. Projection image of whole body PET showing above described findings (D)

In bone tumors, PET/CT shows markedly reduced uptake early after the chemotherapy, while CT does not show definite change in tumor size. We studied 31 treatment naive osteosarcoma patients prospectively for treatment response by PET/CT scan after 3 cycles of neo adjuvant treatment and demonstrated that response can be predicted reliably by PET/CT scan early in disease course and PET/CT parameters correlate well with histologic necrosis.<sup>26</sup>

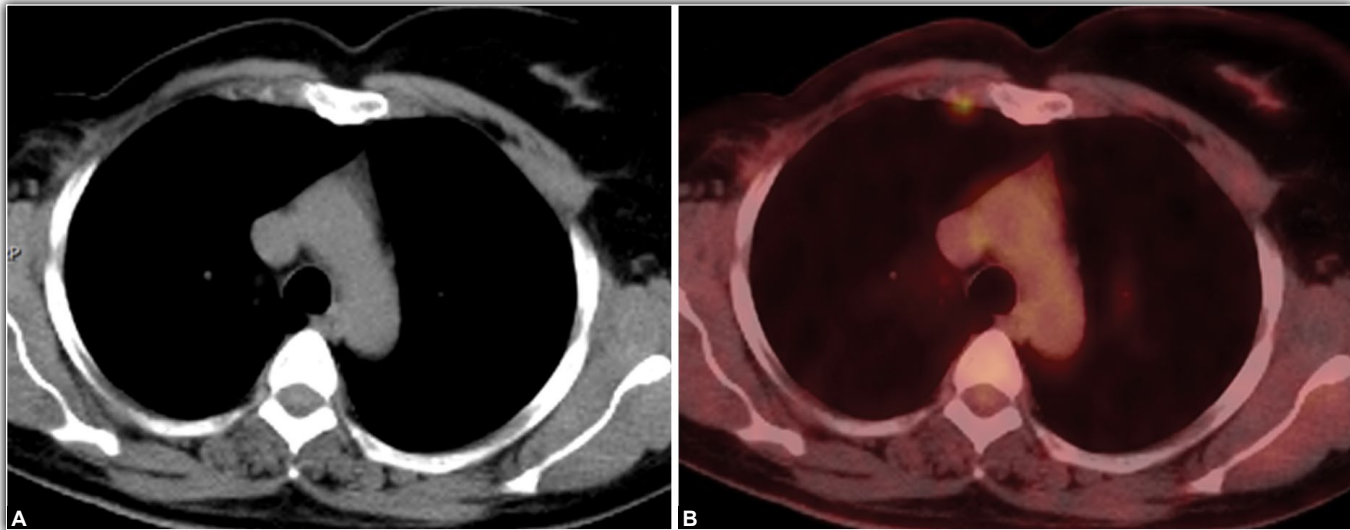
The CT scanning is the imaging modality of choice in gastrointestinal stromal tumors (GIST), which can locate a mass lesion, contiguous organ invasion and distant metastases. Since the introduction of Imatinib mesylate, PET/CT is being used widely in GIST. The PET/CT may show significant decrease in FDG uptake early after Imatinib therapy, while on conventional morphological imaging, tumor size may remain constant for a significant time and thereby, PET/CT accurately separates responders from non-responders in an early stage.

The PET-CT has shown promising results for assessment of treatment response from newer anti-angiogenic agents (sunitinib and sorafenib) in patients with metastatic renal cell carcinoma, which might not show anatomical response such as decreasing size on conventional imaging.

#### *Restaging/Recurrence/Prognosis*

Many of the cancers recur even after the successful initial therapy. The PET/CT is becoming standard of care in detecting the recurrence of various cancers and in determining the prognosis. This is one of the most acceptable clinical indications of PET/CT in oncology. PET/CT has proven role in assessing the prognosis of colorectal cancer, NSCLC, pancreatic cancer, lymphoma (**Figs 11A to D**), cervical cancer, melanoma, and other cancers.

In colorectal cancer, CT is frequently used to localize the site of possible recurrence, which has lower sensitivity and specificity. In a meta analysis, comparing the diagnostic



**Figs 8A and B** Chest CT of PET/CT shows no abnormality in a patient of right breast cancer (A). PET/CT chest showing FDG uptake in the sub centimeter right internal mammary suggestive of metastasis (B) Resolution of lymph node in post chemotherapy PET/CT confirmed the diagnosis of metastasis

performance of PET, PET/CT, CT and MRI as whole-body imaging modalities for the detection of local and/or distant recurrent disease in CRC patients who have a (high) suspicion of recurrent disease, based on clinical findings or rise in carcinoembryonic antigen (CEA) level, demonstrated that whole-body PET and PET/CT are very accurate for the detection of local and/or distant recurrent disease in these patients (**Figs 12A to F**).<sup>27</sup> In another meta analysis on colorectal liver metastases, FDG PET/CT had significantly higher sensitivity on a per-patient basis, compared with that of the CT, but not on a per-lesion basis. Sensitivity estimates for MR imaging with contrast were significantly superior to those for helical CT.<sup>28</sup>

The PET/CT has higher sensitivity and specificity compared to PET alone and diagnostic CECT for lesion detection in suspected recurrence in patients of gall bladder cancer. We have demonstrated a sensitivity of 97.6 percent and specificity of 90 percent in detecting gall bladder cancer recurrence using PET/CT in 62 PET-CT studies of 49 patients.<sup>29</sup>

In ovarian cancer, PET-CT has very important role in patients with rising tumor marker (CA-125) (**Figs 13A to E**). In a review by Son et al, PET/CT scan was found to be superior to CECT and MRI for detection of recurrent or residual ovarian cancer.<sup>30</sup> However, PET/CT may yield false-negative results in patients with small, necrotic, mucinous, cystic, or low-grade tumors. The PET/CT may be false positive in the post-therapy setting, inflammatory and infectious processes. Despite these drawbacks, PET/CT is superior to CT and MR imaging for depiction of recurrent disease.

In NET, FDG PET/CT has no definite role except in evaluation of prognosis. A positive FDG PET/CT in patients

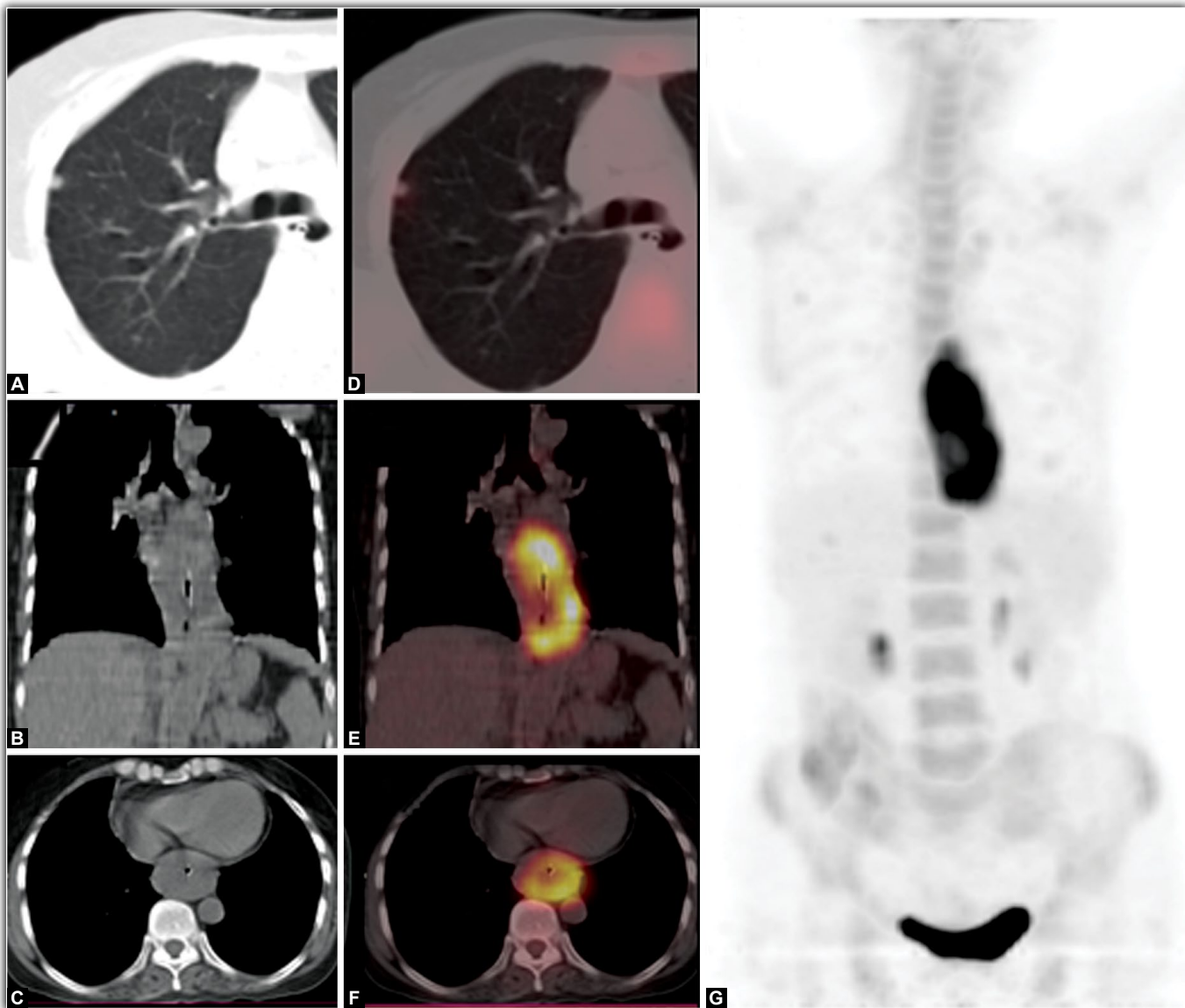
with NET is suggestive of undifferentiated NET (WHO grade III) and poor prognosis.

Total lesion glycolysis (TLG), which combines volumetric and metabolic information from FDG PET/CT can provide a better evaluation of the prognosis. In 105 consecutive patients with NSCLC who underwent staging FDG PET/CT before any therapy, the 1-year PFS was 0.0 percent for patients with high whole-body TLG ( $>655$ ) and 50.0 percent for those with low whole-body TLG ( $\leq 655$ ).<sup>31</sup> This paragraph needs to be higher in hierarchy and another sentence about NSCLC needs to be included to talk in general and switch to more specific detail on TLG?

There are enough data in the literature on PET/CT regarding non-oncology indications; however, there are no significant recent advances. Therefore, in this section, we have not discussed these as in non-oncology indications of PET/CT.

### PET/MR

The PET/CT has certain notable shortcomings, including the inability to perform simultaneous data acquisition leading to imaging artifacts and the significant radiation dose to the patient contributed by CT.<sup>32,33</sup> In addition, PET/CT has poor contrast among soft tissues and areas of complex anatomy, i.e. head and neck and pelvis. After 20 years of research work, an integrated PET/MR scanner (Siemens) which enables simultaneous acquisition of PET and MR imaging was launched in 2010 Munich, Germany.<sup>34</sup> There were many technical and practical hurdles before PET/MR was available for clinical imaging. Firstly, the photomultiplier (PMT)-based PET scanners do not work within or near the



**Figs 9A to G** Chest CT of PET/CT shows diffuse thickening of lower half of esophagus and right pulmonary nodule (A to C) Corresponding  $^{18}\text{FDG}$ -PET/CT images (D to F) show intense tracer uptake in the primary esophageal mass suggestive of malignant tumor and lung metastasis. Projection image of whole body PET showing above described findings (G)

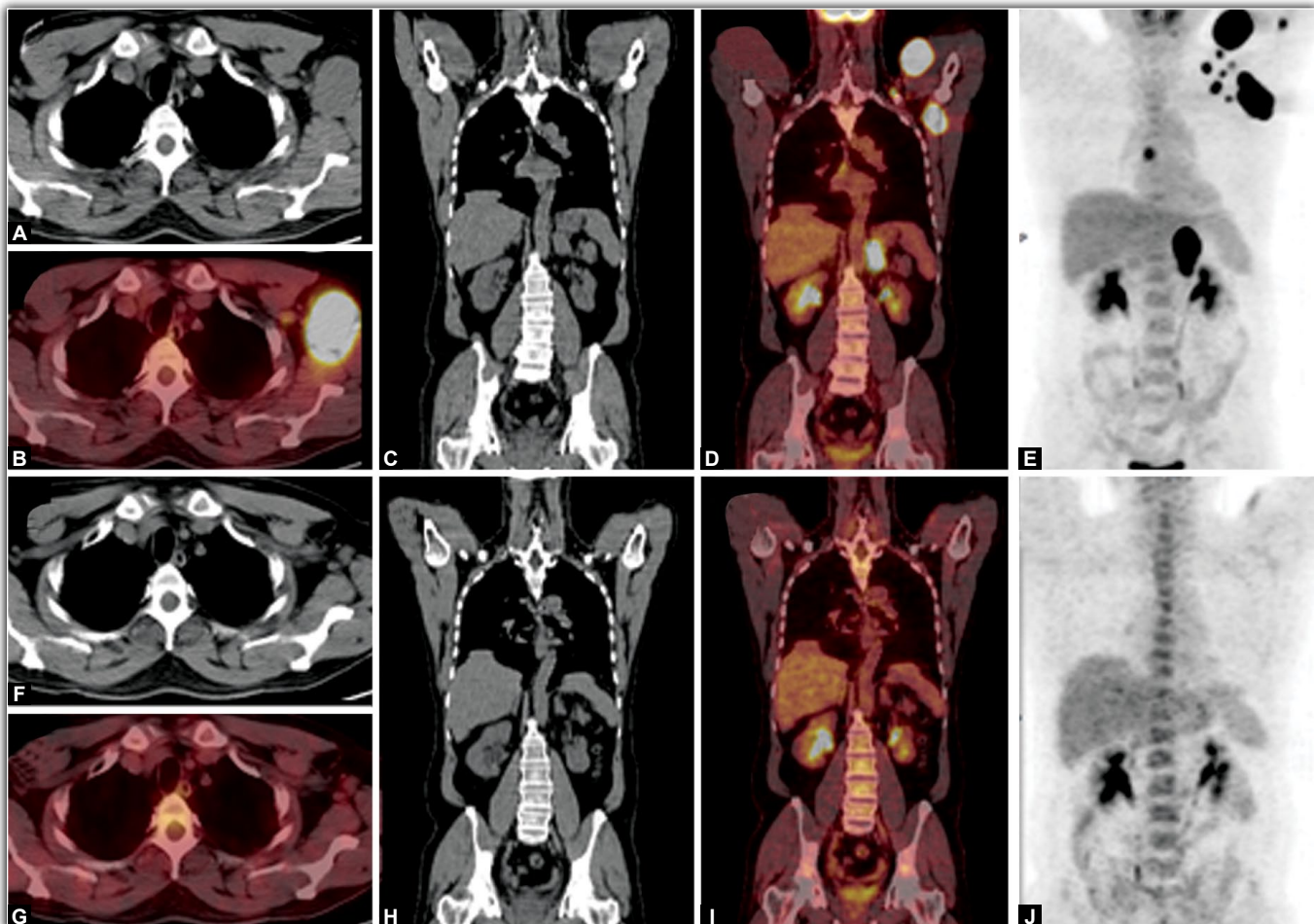
magnetic environment of an MR scanner. To overcome this, the developers used avalanche photo diode or silicon PMT-based PET detector systems.<sup>35</sup> Secondly, metallic objects such as surface coils used to get best MR image quality interfere with the gamma rays from PET, causing unwanted attenuation. This can be achieved by modification of surface coils to reduce their metal content. Thirdly, MR data are not readily usable for attenuation correction like PET/CT.<sup>36</sup> Therefore, quantification of PET data was not possible. Various approaches to overcome this problem are currently under investigation.<sup>37</sup>

## Clinical Applications of PET/MR

### Oncology

#### Staging

Correct staging is very important for management of various cancers. Combined PET/MR imaging obtains concerted information about anatomy, cellularity and biological activity of the tumor. The sensitivity and specificity in oncology staging can be significantly improved using PET/MR. There is relatively high physiological FDG-activity in liver in PET/

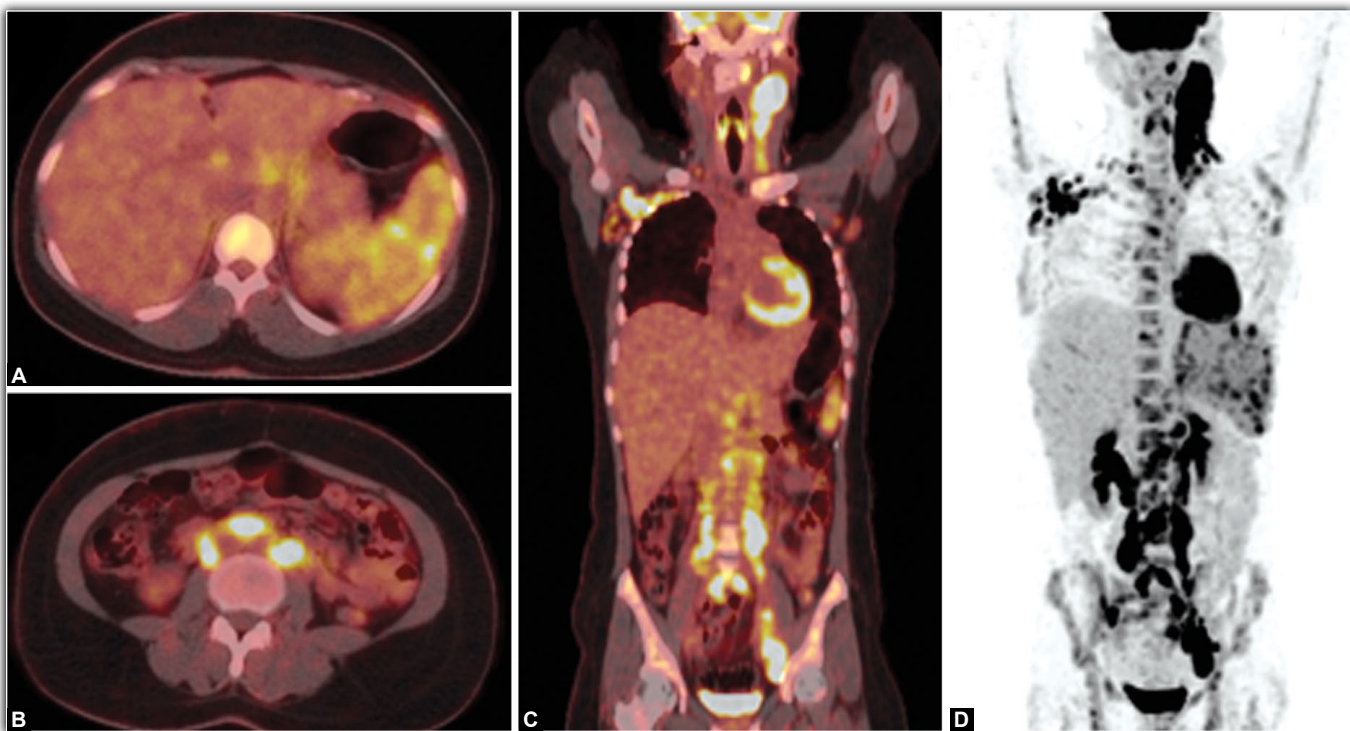


**Figs 10A to J** A 44-year-old man with NHL underwent baseline and post chemotherapy PET/CT for treatment response evaluation. In the baseline study (upper row), non-contrast CT of PET/CT shows enlarged left axillary lymph nodes, left deltoid muscle deposit and left adrenal lesions (A and C) Corresponding  $^{18}\text{FDG}$ - PET/CT images (B and D) show intense tracer uptake in all lesion noted on CT. Projection image of whole body PET showing above described findings (E) PET/CT done after 2 cycles of chemotherapy (lower row) demonstrated resolution of all lesions, suggestion of complete remission (F to J)

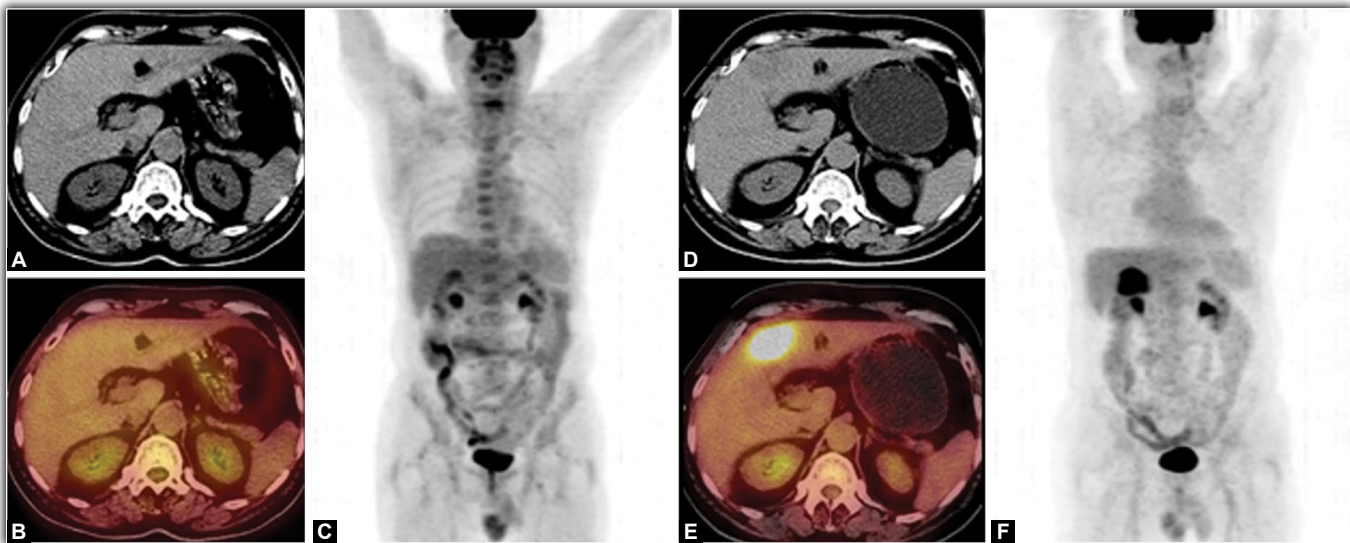
CT leading to masking of focal liver lesions with only slightly elevated FDG activity. CT also has intrinsically lower soft-tissue contrast compared with MRI in the liver. Lesion conspicuity was significantly better on the MRI component when compared with the CECT component.<sup>38</sup> That is why the most common indication of PET/MR is the detection and characterization of liver lesions (primary and metastatic) (**Figs 14A to E**). PET/MR is likely to be advantageous over PET/CT in the assessment of tumor invasion into adjacent structures in rectal, bladder, prostate and gynecological cancers.<sup>39,40</sup> Another indication requiring only regional extent imaging and expected advantages of PET/MRI is head and neck cancer due to its higher soft-tissue contrast. In these tumors, surrounding soft-tissue infiltration is important for local staging as well as surgical and radiotherapy planning.<sup>39,40</sup>

In addition, PET/MR will demonstrate improved accuracy in the assessment of spread to regional lymph nodes, especially in the pelvic, mediastinum and head-and-neck region (**Fig. 15**).<sup>41</sup> It appears that combined PET/MR will enable a more thorough biological characterization of primary tumor and eventually metastases. Recently, Hirsch et al, reported PET/MR hybrid imaging in 15 children with multifocal malignant diseases and concluded that PET/MR is stable and reliable hybrid imaging modality, which generates a complementary diagnostic study of great additional value in pediatric cancer (**Figs 16A to C**).<sup>42</sup>

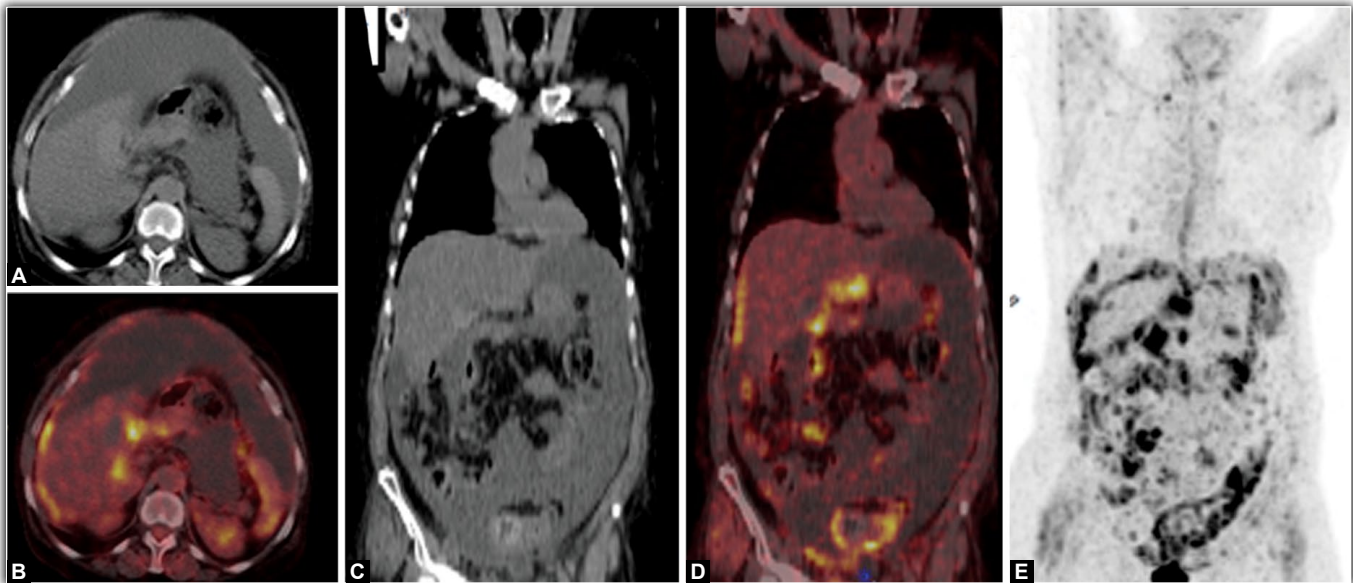
Overall, PET/MRI imaging has several advantages over PET/CT in many oncologic indications. Currently, the PET/CT-MRI approach offers the highest flexibility to provide complete staging concepts.



**Figs 11A to D** A 32-year-old man with NHL with complete remission after 6-cycles of chemotherapy presented with left cervical swelling and underwent PET/CT for restaging. Axial and coronal section of PET/CT shows splenic deposit, retroperitoneal, left pelvic, right axillary and left cervical lymph nodes (A to C) Projection image of whole body PET showing above described findings (D) These findings were suggestive of recurrent disease



**Figs 12A to F** A 65-year-old man with a diagnosis of colorectal cancer who had normal PET/CT scan (right panel of images A to C) and CEA, 1-year back presented with recent rise in CEA levels, underwent PET/CT for restaging. CT of PET/CT shows hypodense liver lesion in segment IV (D) PET/CT shows increased FDG uptake in liver lesion suggestive of metastasis (E) Projection image of whole body PET showing above described findings (F) These findings were suggestive of recurrent disease



**Figs 13A to E** A 67-year-old woman with a diagnosis of ovarian cancer presented with recent rise in CA-125 levels and ascites, underwent PET/CT for restaging. CT of PET/CT shows ascites and ? peritoneal deposit (A and C) PET/CT shows increased FDG uptake in peritoneal deposit and ascites suggestive of metastasis (B and D) Projection image of whole body PET showing above described findings (E). These findings were suggestive of recurrent disease

#### Response evaluation

Accurate assessment of tumor response is essential in the management as well as in prognostication of cancer patients. Currently response is mainly evaluated by anatomical measures, known as the response evaluation criteria in solid tumors (RECIST) criteria. There are many limitations using these criteria in evaluating treatment response especially when patients are being treated with conventional cytotoxic therapy or molecularly targeted agents, which can provide therapeutic benefit without significantly reducing the tumor size. The use of PET/CT, combining metabolic and anatomical information for therapy evaluation, has a huge potential impact on the quality of patient treatment as well as on the evaluation of new therapy regimes. Standardized criteria for response evaluation in solid tumors by PET/CT - PERCIST - was suggested in 2009,<sup>43</sup> and the impact of PET in response evaluation in, e.g. lymphoma, is well established.<sup>44</sup> Similarly, diffusion-weighted MRI (DW-MRI) suggested that early changes in tumor diffusion values correlate with response to therapy. Additionally, dynamic contrast enhanced MRI can provide kinetics of tumor perfusion in pre and post-treatment setting to assess the response to therapy. Therefore, the PET/MR may provide unique advantages of both PET and MRI in exploring more specific changes in the tissue, making early therapy evaluation a safer endeavor.

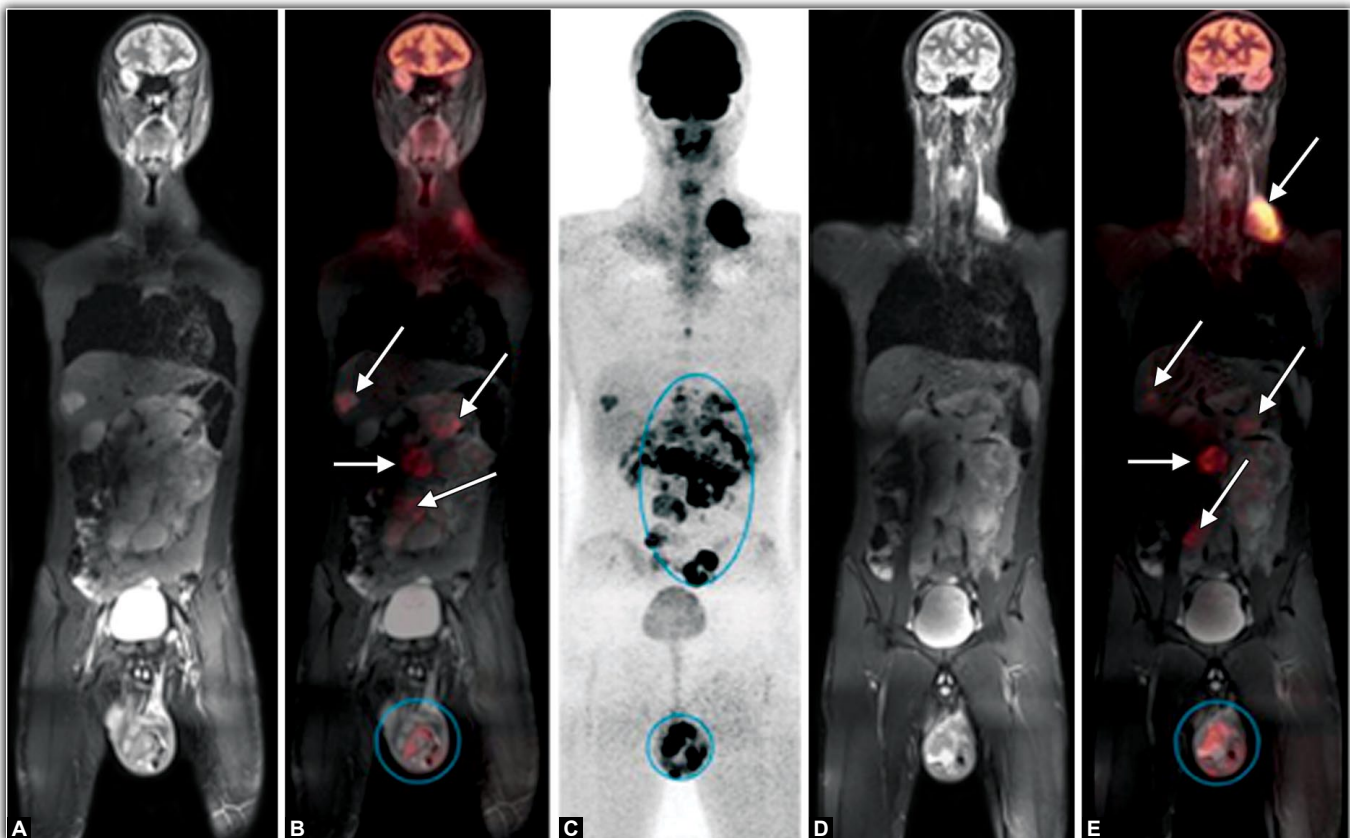
#### Restaging

The FDG-PET/CT can contribute in significant ways to the clinical management of patients particularly which have been

previously treated by surgery or radiation and there is question of discrimination between post-treatment scar and recurrent tumor. However, in patients with brain tumors, metastatic liver disease and head neck cancer, PET/CT has limitations due to increased physiological FDG uptake and poor soft tissue contrast. In these patients PET/MR will demonstrate improved accuracy in detecting recurrence. It has been demonstrated that CECT has high sensitivity for liver lesions, but generally MRI is still considered superior. However, there are only few studies evaluating CE PET/CT compared with MRI. A large meta-analysis did not find statistically significant differences in lesion detection.<sup>45</sup> Initial comparison of data acquired PET/CT-MRI system shows no difference in lesion detection when comparing CE PET/CT and non-CE MRI.<sup>46</sup>

#### Radiotherapy Treatment Planning

The best results of radiotherapy are obtained by the maximum radiation dose delivery to target tissue and reducing dose to minimum to surrounding normal tissue. This can be obtained by the dose painting principle. Since PET/MR has advantages of better tumor delineation because of high resolution of MR and metabolic status of tumor by PET, it can be used for better defining targeted radiotherapy of tumor and avoiding normal tissues. Another issue in radiotherapy is tumor hypoxia, which is a key mechanism leading to radiotherapy resistance. Therefore, imaging technique for hypoxia mapping which can be integrated with radiotherapy planning systems is always warranted.<sup>47</sup> Thorwarth et al demonstrated feasibility of dose painting using a dynamic 18F-MISO-PET scan.<sup>48</sup>



**Figs 14A to E** A 15-year-old boy with left testicular tumor with left retroperitoneal, supraclavicular and hepatic metastases (arrows). The primary tumor in the left testicle and the retroperitoneal metastasis exhibit a very inhomogeneous enhancement of the glucose metabolism with larger metabolically inactive areas showing no enhancement. This can only be explained in part by tumor necrosis. The liver metastasis shows significantly enhanced glucose uptake (*Reproduced: With permission from Franz Wolfgang Hirsch, Department of Pediatric Radiology, University of Leipzig, Liebigstr. 20a, 04103, Leipzig, Germany, hirw@medizin.uni-leipzig.de*)<sup>42</sup>

PET based techniques using  $^{64}\text{Cu}$ -ATSM,  $^{18}\text{F}$ -MISO or  $^{18}\text{F}$ -FAZA can image hypoxia by binding to intracellular macromolecules when  $\text{pO}_2 < 10 \text{ mmHg}$ .<sup>49</sup> Accumulation of most of PET tracers is flow-dependent while, MRI is thought to be most sensitive to perfusion related hypoxia. By simultaneous PET/MR it will be possible to describe tissue hypoxia by PET hypoxia tracer together with blood oxygen level dependent (BOLD) sequences, DW-MRI and/or DCE-MRI to distinguish between perfusion and diffusion as the most dominant cause of tumor hypoxia.<sup>50,51</sup>

## Neurology

Anatomical imaging data is usually a prerequisite for processing and analysis of functional data in patients with neurological disorder. Till now this was achieved by software image fusion of structural and functional data. However, software image fusion has certain limitations, such as misregistration. Therefore an integrated PET/MR will be helpful in patients with where visualized functional processes are time dependent in PET and MR. In functional

neuropsychiatric examinations measuring task-induced changes of blood flow and oxygen consumption rate or the measurement of the arterial input function by MRI for its use in compartment modeling in quantitative PET studies.

In patients with Alzheimer's disease, PET/MR can be used for the early diagnosis, evaluation of disease progression and therapy response. In addition, morphologic images are essential to exclude other causes of dementia like multi-infarct dementia or normal-pressure hydrocephalus.<sup>52,53</sup>

Patients with refractory epilepsy despite medical treatment require surgery to resect the epileptogenic focus.<sup>54</sup> For success of surgical procedure structural and functional imaging data is of outmost importance. Therefore, these patients needs to undergo a battery of imaging and non-imaging tests like morphologic MRI, functional MRI, PET, and EEG for correct localization of epileptic focus. The PET/MR will be useful in such patients and data can be obtained using single imaging test in one day rather than multiple imaging tests on different days causing immense loss of time and money.

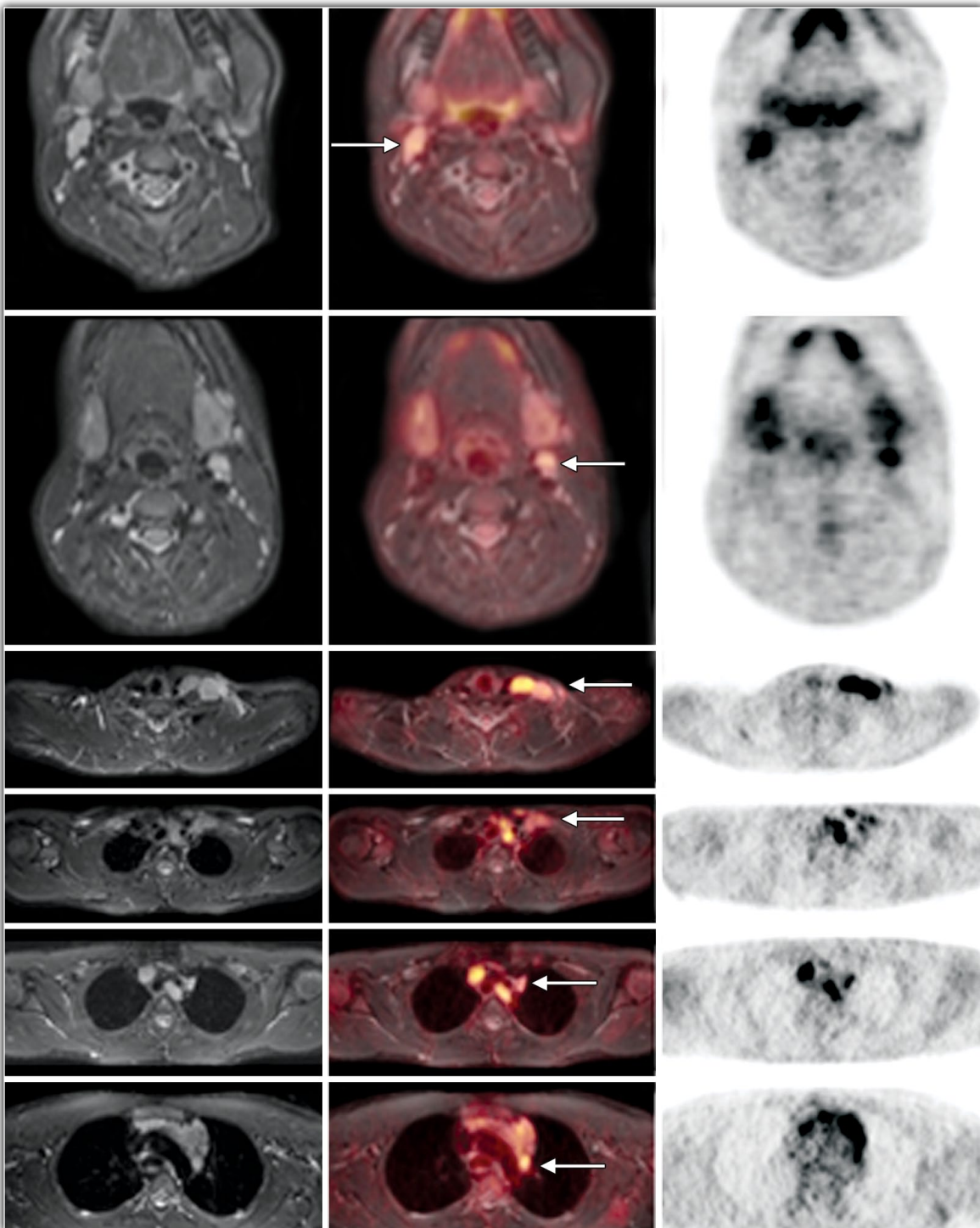
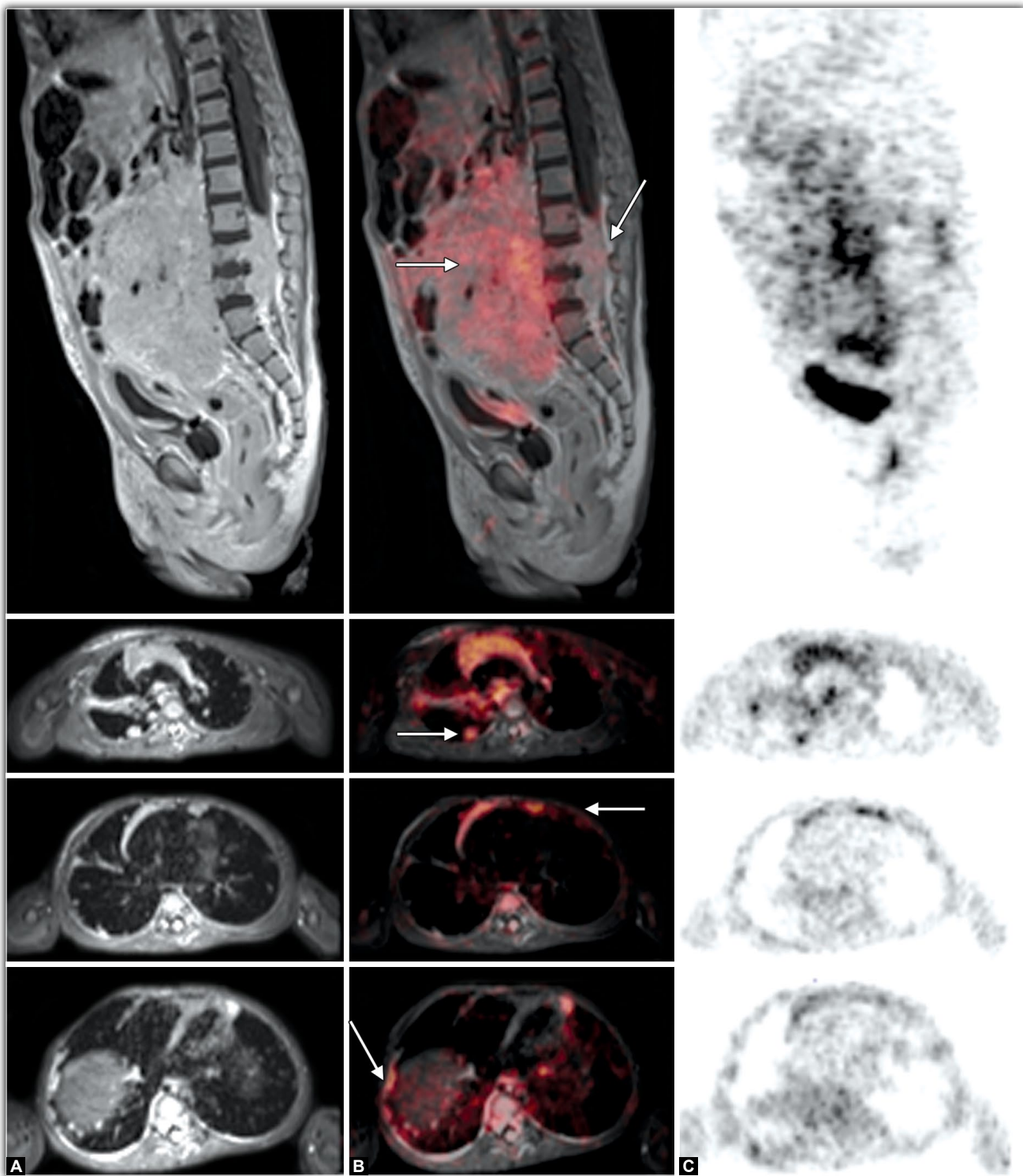


**Fig. 15** A 13-year-old boy with Hodgkin disease stage II show involvement of both sides of the submandibular, cervical, and upper and middle mediastinum (arrows). Involvement of the submandibular lymph nodes (arrows) was not positively identified on MR criteria (size), but the PET image shows significantly enhanced FDG uptake. Arrows indicate positive PET/MR findings (*Reproduced: With permission from Franz Wolfgang Hirsch, Department of Pediatric Radiology, University of Leipzig, Liebigstr. 20a, 04103, Leipzig, Germany, hirw@medizin.uni-leipzig.de.*)<sup>42</sup>



**Figs 16A to C** A 2-year-old boy with a large abdominal neuroblastoma that emanates from the sympathetic chain. Top row: the tumor (arrows) is growing into the spinal canal and involves the fourth and fifth lumbar vertebrae. The highly differentiated tumor shows only slightly intense inhomogeneous FDG uptake. Lower row: transaxial slices show multiple (arrows) lung metastases and pleural metastases. The metastases are seen on the concordant respiratory-triggered T2-weighted TIRM images (A) and on the PET images (B and C); smaller metastases of 3–5 mm are clearly shown on the MR images. Arrows indicate positive PET/MR findings (Reproduced: With permission from Franz Wolfgang Hirsch, Department of Pediatric Radiology, University of Leipzig, Liebigstr. 20a, 04103, Leipzig, Germany, hirw@medizin.uni-leipzig.de.)<sup>42</sup>

## Cardiology

Myocardial perfusion imaging (MPI) using SPECT and SPECT/CT is well established technique for the management of coronary artery disease (CAD). PET still plays a limited role in daily clinical routine for MPI as there is lack of solid data to support a superior accuracy of PET over SPECT. The PET is the most reliable noninvasive tool for identification of myocardial viability in ischemic dysfunctional left ventricles and the only method validated in a prognostic interventional outcome study. However it has not been used as there are competing radiation-free methods in the hands of cardiologists, such as echocardiography and MRI, which allow identification of viability. The PET/MR may be useful in evaluation of the vascular wall and the identification of plaques prone to rupture. It may help to explore evolving and investigational fields of cardiovascular imaging, such as vulnerable plaque characterization, *in vivo* stem cell tracking, and assessment of angiogenesis.

## ACKNOWLEDGMENTS

We are highly thankful to Franz Wolfgang Hirsch for providing PET/MR **Figures 14 to 16**. These images were reproduced with permission from Franz Wolfgang Hirsch, Department of Pediatric Radiology, University of Leipzig, Liebigstr. 20a, 04103, Leipzig, Germany, hirw@medizin.uni-leipzig.de. Ref 42]

We thank Dr Suhas Singla and Dr Abhishek Kumar, Senior Resident, Nuclear Medicine, AIIMS for their help in selecting and getting other figures.

## REFERENCES

- Mochizuki T, Tsukamoto E, Kuge Y, et al. FDG uptake and glucose transporter subtype expressions in experimental tumor and inflammation models. *J Nucl Med*. 2001;42:1551-5.
- McGowan KM, Long SD, Pekala PH. Glucose transporter gene expression: regulation of transcription and mRNA stability. *Pharmacol Ther*. 1995;66:465-505.
- Sharma P, Gupta A, Patel C, Bakhshi S, Malhotra A, Kumar R. Pediatric lymphoma: Metabolic tumor burden as a quantitative index for treatment response evaluation. *Ann Nucl Med*. 2012;26:58-66.
- Gould MK, Maclean CC, Kuschner WG, Rydzak CE, Owens DK. Accuracy of positron emission tomography for diagnosis of pulmonary nodules and mass lesions: a meta-analysis. *JAMA*. 2001;285:914-24.
- Fischer BM, Mortensen J, Hojgaard L. Positron emission tomography in the diagnosis and staging of lung cancer: a systematic, quantitative review. *Lancet Oncol*. 2001;2:659-66.
- Miller FR, Hussey D, Beeram M, Eng T, McGuff HS, Otto RA. Positron emission tomography in the management of unknown primary head and neck carcinoma. *Arch Otolaryngol Head Neck Surg*. 2005;131:626-9.
- Berg WA, Madsen KS, Schilling K, Tartar M, Pisano ED, Larsen LH, Narayanan D, Kalinyak JE. Comparative effectiveness of positron emission mammography and MRI in the contralateral breast of women with newly diagnosed breast cancer. *AJR Am J Roentgenol*. 2012;198:219-32.
- Nayak B, Dogra PN, Naswa N, Kumar R. Diuretic (18)F-FDG PET/CT imaging for detection and locoregional staging of urinary bladder cancer: prospective evaluation of a novel technique. *Eur J Nucl Med Mol Imaging*. 2012. [Epub ahead of print]
- Gawande RS, Khurana A, Messing S, et al. Differentiation of normal thymus from anterior mediastinal lymphoma and lymphoma recurrence at pediatric PET/CT. *Radiology*. 2012;262:613-22.
- Kumar A, Regmi SK, Dutta R, et al. Characterization of thymic masses using 18F-FDG PET-CT. *Ann Nucl Med*. 2009;23:569-77.
- Kumar R, Sharma P, Garg P, Karunanthi S, Naswa N, Sharma R, Thulkar S, Lata S, Malhotra A. Role of (68)Ga-DOTATOC PET-CT in the diagnosis and staging of pancreatic neuroendocrine tumors. *Eur Radiol*. 2011;21:2408-16.
- Naswa N, Sharma P, Nazar AH, Agarwal KK, Kumar R, Ammini AC, Malhotra A, Bal C. Prospective evaluation of <sup>68</sup>Ga-DOTANOC PET-CT in pheochromocytoma and paraganglioma: preliminary results from a single centre study. *Eur Radiol*. 2012;22:710-9.
- Naswa N, Sharma P, Soundararajan R, Karunanthi S, Nazar AH, Kumar R, Malhotra A, Bal C. Diagnostic performance of somatostatin receptor PET/CT using (68) Ga-DOTANOC in gastrinoma patients with negative or equivocal CT findings. *Abdom Imaging*. 2012. [Epub ahead of print]
- De Wever W, Stroobants S, Coolen J, Verschakelen JA. Integrated PET/CT in the staging of non-small cell lung cancer: technical aspects and clinical integration. *Eur Respir J*. 2009;33:201-12.
- El-Galaly TC, d'Amore F, Mylam KJ, de Nully Brown P, Bøgsted M, Bukh A, Specht L, Loft A, Iyer V, Hjorthaug K, Nielsen AL, Christiansen I, Madsen C, Johnsen HE, Hutchings M. Routine bone marrow biopsy has little or no therapeutic consequence for positron emission tomography/computed tomography-staged treatment-naïve patients with Hodgkin lymphoma. *J Clin Oncol*. 2012;30:4508-14.
- Brush J, Boyd K, Chappell F, Crawford F, Dozier M, Fenwick E, Glanville J, McIntosh H, Renehan A, Weller D, Dunlop M. The value of FDG positron emission tomography/computerised tomography (PET/CT) in pre-operative staging of colorectal cancer: a systematic review and economic evaluation. *Health Technol Assess*. 2011;15:1-192.
- Riegger C, Herrmann J, Nagarajah J, Hecktor J, Kuemmel S, Otterbach F, Hahn S, Bockisch A, Lauenstein T, Antoch G, Heusner TA. Whole-body FDG PET/CT is more accurate than conventional imaging for staging primary breast cancer patients. *Eur J Nucl Med Mol Imaging*. 2012;39:852-63.
- Barber TW, Duong CP, Leong T, Bressel M, Drummond EG, Hicks RJ. 18F-FDG PET/CT has a high impact on patient management and provides powerful prognostic stratification in the primary staging of esophageal cancer: a prospective study with mature survival data. *J Nucl Med*. 2012;53:864-71.
- Marzola MC, De Manzoni G, Grassetto G, Cordiano C, Al-Nahhas A, Alavi A, Rubello D. Extended staging of oesophageal cancer using FDG-PET - a critical appraisal. *Eur J Radiol*. 2012;81:21-30.
- Evangelista L, Guttilla A, Zattoni F, Muzzio PC, Zattoni F. Utility of Choline Positron Emission Tomography/Computed Tomography for Lymph Node Involvement Identification

- in Intermediate- to High-risk Prostate Cancer: A Systematic Literature Review and Meta-analysis. *Eur Urol.* 2012; doi:pii: S0302-2838(12)01107-4.
21. Divgi CR, Uzzo RG, Gatsonis C, Bartz R, Treutner S, Yu JQ, Chen D, Carrasquillo JA, Larson S, Bevan P, Russo P. Positron Emission Tomography/Computed Tomography Identification of Clear Cell Renal Cell Carcinoma: Results From the REDECT Trial. *J Clin Oncol.* 2013;31:187-94.
  22. Bakhshi S, Radhakrishnan V, Sharma P, Kumar R, Thulkar S, Vishnubhatla S, Dhawan D, Malhotra A. Pediatric non-lymphoblastic non-Hodgkin lymphoma: baseline, interim, and posttreatment PET/CT versus contrast-enhanced CT for evaluation—a prospective study. *Radiology.* 2012;262:956-68.
  23. Kumar A, Kumar R, Seenu V, Gupta SD, Chawla M, Malhotra A, Mehta SN. The role of 18F-FDG PET/CT in evaluation of early response to neoadjuvant chemotherapy in patients with locally advanced breast cancer. *Eur Radiol.* 2009;19:1347-57.
  24. Haug AR, Tiega Donfack BP, Trumm C, Zech CJ, Michl M, Laubender RP, Uebelis C, Bartenstein P, Heinemann V, Hacker M. 18F-FDG PET/CT predicts survival after radioembolization of hepatic metastases from breast cancer. *J Nucl Med.* 2012; 53:371-7.
  25. Hendlisz A, Golfinopoulos V, Garcia C, Covas A, Emonts P, Ameye L, Paesmans M, Deleporte A, Machiels G, Toussaint E, Vanderlinden B, Awada A, Piccart M, Flamen P. Serial FDG-PET/CT for early outcome prediction in patients with metastatic colorectal cancer undergoing chemotherapy. *Ann Oncol.* 2012; 23:1687-93.
  26. Bajpai J, Kumar R, Sreenivas V, Sharma MC, Khan SA, Rastogi S, Malhotra A, Gamnagatti S, Kumar R, Safaya R, Bakhshi S. Prediction of chemotherapy response by PET-CT in osteosarcoma: correlation with histologic necrosis. *J Pediatr Hematol Oncol.* 2011;33:e271-8.
  27. Maas M, Rutten IJ, Nelemans PJ, Lambregts DM, Cappendijk VC, Beets GL, Beets-Tan RG. What is the most accurate whole-body imaging modality for assessment of local and distant recurrent disease in colorectal cancer? A meta-analysis: Imaging for recurrent colorectal cancer. *Eur J Nucl Med Mol Imaging.* 2011;38:1560-71.
  28. Bipat S, van Leeuwen MS, Comans EF, Pijl ME, Bossuyt PM, Zwinderman AH, Stoker J. Colorectal liver metastases: CT, MR imaging, and PET for diagnosis—meta-analysis. *Radiology.* 2005;237:123-31.
  29. Kumar R, Sharma P, Kumari A, Halanaik D, Malhotra A. Role of 18F-FDG PET/CT in detecting recurrent gallbladder carcinoma. *Clin Nucl Med.* 2012;37:431-5.
  30. Son H, Khan SM, Rahaman J, Cameron KL, Prasad-Hayes M, Chuang L, Machac J, Heiba S, Kostakoglu L. Role of FDG PET/CT in staging of recurrent ovarian cancer. *Radiographics.* 2011;31:569-83.
  31. Chen HH, Chiu NT, Su WC, Guo HR, Lee BF. Prognostic value of whole-body total lesion glycolysis at pretreatment FDG PET/CT in non-small cell lung cancer. *Radiology.* 2012;264:559-66.
  32. Chawla SC, Federman N, Zhang D, Nagata K, Nuthakki S, McNitt-Gray M, et al. Estimated cumulative radiation dose from PET/CT in children with malignancies: a 5-year retrospective review. *Pediatr Radiol.* 2010;40:681-6.
  33. Mattsson S, Söderberg M. Radiation dose management in CT, SPECT/CT and PET/CT techniques. *Radiat Prot Dosimetry.* 2011;147(1-2):13-21.
  34. Delso G, Fürst S, Jakoby B, Ladebeck R, Ganter C, Nekolla SG, et al. Performance measurements of the Siemens mMR integrated whole-body PET/MR scanner. *J Nucl Med.* 2011; 52:1914-22.
  35. Pichler BJ, Judenhofer MS, Catana C, Walton JH, Kneilling M, Nutt RE, et al. Performance test of an LSO-APD detector in a 7-T MRI scanner for simultaneous PET/MRI. *J Nucl Med.* 2006;47:639-47.
  36. Hofmann M, Pichler B, Schölkopf B, Beyer T. Towards quantitative PET/MRI: a review of MR-based attenuation correction techniques. *Eur J Nucl Med Mol Imaging.* 2009;36(Suppl 1): S93-104.
  37. Zaidi H, Ojha N, Morich M, Griesmer J, Hu Z, Maniawski P, et al. Design and performance evaluation of a whole-body Ingenuity TF PET-MRI system. *Phys Med Biol.* 2011;56:3091-106.
  38. Assiri Y, Schmid D, Pietsch C, et al. Contrast-enhanced PET/CT vs. non-contrast enhanced PET/MRI in abdominal oncological lesions—Initial results. Annual Congress of the European Association of Nuclear Medicine, Milan, Italy, 2012.
  39. Punwani S. Diffusion weighted imaging of female pelvis cancers: Concepts and clinical applications. *Eur J Radiol.* 2011; 78:21-9.
  40. Giannarini G, Petralia G, Thoeney HC. Potential and limitations of diffusion-weighted magnetic resonance imaging in kidney, prostate, and bladder cancer including pelvic lymph node staging: A critical analysis of the literature. *Eur Urol.* 2012; 61:326-40.
  41. Jansen JFA, Schöder H, Lee NY, Stambuk HE, Wang Y, Fury MG, Patel SG, Pfister DG, Shah JP, Koutcher JA, Shukla-Dave A. Tumor metabolism and perfusion in head and neck squamous cell carcinoma: pretreatment multimodality imaging with 1H magnetic resonance spectroscopy, dynamic contrast-enhanced MRI and [18F] FDG-PET. *Int J Radiat Oncol Biol Phys.* 2012;82: 299-307.
  42. Hirsch FW, Sattler B, Sorge I, Kurch L, Viehweger A, Ritter L, Werner P, Jochimsen T, Barthel H, Bierbach U, Till H, Sabri O, Kluge R. PET/MR in children. Initial clinical experience in paediatric oncology using an integrated PET/MR scanner. *Pediatr Radiol.* 2013 Jan 11. [Epub ahead of print]
  43. Wahl RL, Jacene H, Kasamon Y, Lodge MA. From RECIST to PERCIST: Evolving Considerations for PET Response Criteria in Solid Tumors. *J Nucl Med.* 2009;50:122S-150.
  44. Hutchings M, Loft A, Hansen M, Pedersen LM, Buhl T, Jurlander J, Buus S, Keiding S, D'Amore F, Boesen AM, Berthelsen AK, Specht L. FDG-PET after two cycles of chemotherapy predicts treatment failure and progression-free survival in Hodgkin Lymphoma. *Blood.* 2006;107:52-9.
  45. Niekel MC, Bipat S, Stoker J. Diagnostic imaging of colorectal liver metastases with CT, MR imaging, FDG PET, and/or FDG PET/CT: A meta-analysis of prospective studies including patients who have not previously undergone treatment. *Radiology.* 2010;257:674-84.
  46. Crook DW, Mader C, Kuhn FP, et al. Diagnostic performance of PET/MR versus PET/CT in the abdomen. Presented at: European Congress of Radiology, Vienna, 2012.
  47. Bentzen SM, Gregoire V. Molecular imaging-based dose-painting: a novel paradigm for radiation therapy prescription. *Semin Radiat Oncol.* 2011;21:101-10.
  48. Thorwarth D, Eschmann SM, Paulsen F, Alber M. Hypoxia dose painting by numbers: a planning study. *Int J Radiat Oncol Biol Phys.* 2007;68:291-300.

49. Nehmeh SA, Lee NY, Schröder H, Squire OD, Zanzonizo PB, Erdi YE, Greco C, Mageras G, Pham HS, Larson SM, Ling CC, Humm JL. Reproducibility of intratumor distribution of <sup>18</sup>F-fluoromisonidazole in head and neck cancer. *Int J Radiat Oncol Biol Phys.* 2008;70:235-42.
50. Padhani AR, Krohn KA, Lewis JS, Alber M. Imaging oxygenation of human tumors. *Eur Radiol.* 2007;17: 861-72.
51. Dirix P, Vandecaveye V, De Keyzer F, Stroobants S, Hermans R, Nuyts S. Dose painting in radiotherapy for head and neck squamous cell carcinoma: value of repeated functional imaging with <sup>18</sup>F-FDG PET, <sup>18</sup>F-Fluoromisonidazole PET, diffusion-weighted MRI, and dynam contrast-enhanced MRI. *J Nucl Med.* 2009;50:1020-27.
52. Ossenkoppele R, Tolboom N, Foster-Dingley JC, et al. Longitudinal imaging of Alzheimer pathology using [<sup>11</sup>C]PIB, [<sup>18</sup>F]FDDNP and [<sup>18</sup>F]FDG PET. *Eur J Nucl Med Mol Imaging.* 2012;39:990-1000.
53. Kenny ER, Blamire AM, Firbank MJ, et al. Functional connectivity in cortical regions in dementia with Lewy bodies and Alzheimer's disease. *Brain.* 2012;135:569-81.
54. Duncan J. The current status of neuroimaging for epilepsy. *Curr Opin Neurol.* 2009;22:179-84.

## Chapter

# 27

# Common Drugs Used in an Imaging Department

*Anupam Lal, Vivek Gupta, Manphool Singhal*

The beneficial or toxic effects of many plant and animal materials were known to us since the prehistoric times. Advances in chemistry and the further development of physiology in present time laid the foundation needed for understanding how drugs work at the organ and tissue levels. The last few decades have seen an exponential growth of information and understanding of the molecular basis for drug action. Better understanding of drug receptors and pharmacokinetics have led to modifying existing drugs for selective action or synthesizing newer drugs previously unknown to mankind.

The recent era has also witnessed a dramatic growth in the field of electronics and computerization, leading to development of faster and more precise medical imaging equipment that have made possible the minimally invasive image guided interventional procedures. The interventional procedures continue to evolve and the list is ever increasing, that includes central venous catheter placements, tumor treatments (uterine fibroid therapy, radio- and chemoembolization of tumor, percutaneous radiofrequency and cryoablation), and procedures such as angioplasty, abdominal aortic aneurysm stent-graft repair, vertebroplasty, kyphoplasty, and varicose vein therapies. There have also been advancements in standard biliary and urinary drainage procedures, percutaneous gastrointestinal feeding tube placement, and transjugular intrahepatic portosystemic shunts. These complicated procedures mandates use of drugs required for patient preparation, therapeutic applications and for preventing complications of the radiological interventions. The radiologists are no longer supervising only contrast administration and managing contrast reactions but also providing therapies for many diseases. The present imaging

departments thus are equipped with modern anesthetic and life support machines and a large number of drugs that will be required in various interventional procedures. A thorough knowledge and understanding of these drugs is of paramount importance to the interventional radiologist for their judicious use and for preventing untoward reactions. A brief description of common drugs used in modern radiology department follows. The readers are encouraged to refer to standard textbooks of pharmacology for dosing and drug interactions in specific clinical scenario. Medications commonly used in radiology department can be divided into the following broad categories:

- Drugs used for patient preparation
- Drugs used for optimizing imaging evaluation
- Drugs affecting coagulation and antiplatelets
- Sclerosants and embolizing agents
- Drugs for transarterial chemoembolization (TACE).

## DRUGS FOR PATIENT PREPARATION

### Sedatives

**Midazolam** is the most commonly used short-acting benzodiazepine that possesses potent anxiolytic, amnestic, hypnotic, anticonvulsant, skeletal muscle relaxant, and sedative properties. Like all benzodiazepines it bind to specific GABA<sub>A</sub> receptor subunits at central nervous system (CNS) neuronal synapses facilitating GABA-mediated chloride ion channel opening and enhance membrane hyperpolarization. Midazolam is roughly 3 to 4 times more powerful and has twice the affinity for benzodiazepine receptors than diazepam and has more potent amnesic effects and also has a fast recovery time. Typical adult dose

is 1 to 2.5 mg IV, and can be repeated every 5 to 10 minutes to a maximum dose of 10 mg. Midazolam has more potential than other benzodiazepines to cause respiratory depression and arrest hence should be administered slowly and extreme caution to be exercised in pediatric patients.

Intravenous midazolam is indicated for procedural sedation (often in combination with an opioid, such as fentanyl), for pre-procedural sedation and for the induction of general anesthesia. Flumazenil, a benzodiazepine antagonist drug, can be used to treat an overdose of midazolam, as well as to reverse sedation. However, flumazenil can trigger seizures in mixed overdoses and in benzodiazepine-dependent individuals, so is not used in most cases.

Among the antihistaminics used for sedation, promethazine (Phenergan) 12.5 to 25 mg every 4 hourly or diphenhydramine (Benadryl) 25 to 50 mg are the most commonly employed.

### Local Anesthetics

Local anesthetics (LA) effectively and reversibly block impulse conduction along nerve axons and other excitable membranes that use sodium channels as the primary means of action potential generation. Clinically, local anesthetics are used to block pain sensation from or sympathetic vasoconstrictor impulses to specific areas of the body. Newer local anesthetics were introduced with the goal of reducing local tissue irritation, minimizing systemic cardiac and CNS toxicity, and achieving a faster onset and longer duration of action.

They are broadly classified as follows:

- Aminoamides, e.g. Lignocaine, Bupivacaine, Rapivacaine, etc.
- Aminoesters, e.g. Procaine, Benzocaine, cocaine, etc.

Lidocaine, is still a widely used local anesthetic, was synthesized in 1943 by Löfgren.

### Methods of Administration

The choice of local anesthetic for infiltration, peripheral nerve blocks, and central neuraxis (spinal/epidural) blockade is usually based on the duration of action required. Procaine and chloroprocaine are short-acting; lidocaine, mepivacaine, and prilocaine have an intermediate duration of action; and tetracaine, bupivacaine, levobupivacaine, and ropivacaine are long-acting local anesthetics. The anesthetic effect of the agents with short and intermediate durations of action can be prolonged by increasing the dose or adding a vasoconstrictor agent (e.g. epinephrine or phenylephrine). The vasoconstrictor slows the removal of the local anesthetic from the injection site. In addition, it decreases the blood level and the probability of cardiovascular and CNS toxicity. The onset of local anesthesia can be accelerated by the addition of sodium bicarbonate (1–2 mL) to the local anesthetic solution. This maximizes the amount of drug in the more lipid-soluble

(unionized) form. Repeated injections of local anesthetics can result in loss of effectiveness (i.e. tachyphylaxis) due to extracellular acidosis.

#### *Infiltration Anesthesia*

It is injecting the agent directly into the tissue without taking into consideration of course of cutaneous nerves. It is so superficial as to include only the skin. However deeper structures can also be included.

#### *Others*

- Surface anesthesia
- Nerve block
- Spinal anesthesia
- Epidural anesthesia
- Intravenous regional anesthesia.

#### *Adverse effects*

**CNS:** Causes stimulation of CNS, producing restlessness and tremors that may proceed to clonic convulsions.

**CVS:** Usually due to inadvertent intravascular injection. Hypotension, due to arteriolar dilatation and cardiovascular collapse probably due to action on pacemaker or sudden onset ventricular fibrillation may occur.

**Hypersensitivity:** It is very rare and slightly more common with aminoesters. It can manifest either as allergic dermatitis or a typical asthmatic attack.

#### *Sting free LA*

Addition of sodium bicarbonate reduced the stinging sensation related to the acidic nature of adrenaline containing LA.

- Two percent lignocaine, 19 mL
- Adrenaline 1: 1000, 0.1 mL
- Normal saline, 20 mL
- Sodium bicarbonate (8.3%), 4 mL.

## DRUGS USED FOR OPTIMIZING IMAGING EVALUATION

### Diuretics

Loop diuretics selectively inhibit NaCl reabsorption in the thick ascending limb of loop of Henle. Because of the large NaCl absorptive capacity of this segment and the fact that the diuretic action of these drugs is not limited by development of acidosis, as is the case with the carbonic anhydrase inhibitors, loop diuretics are the most efficacious diuretic agents currently available. Furosemide is the prototype of this group and is often used for optimizing urologic diagnostic procedures. The duration of effect for furosemide is usually 2 to 3 hours. Half-life depends on renal function. Reduction in the secretion of loop diuretics may result from simultaneous administration of agents such as NSAIDs or probenecid, which compete for weak acid secretion in the proximal tubule.

## Uses

- MRU:** Intravenous injection of low-dose furosemide (5–10 mg) and gadolinium (Gd) chelate is used for achieving a uniform distribution of the contrast material inside the entire urinary tract.
- CTU:** Supplemental intravenous furosemide (10 mg) may be used to optimize urinary collecting system opacification and distention.
- IVU:** 10 to 20 mg lasix (1 mg/kg pediatric dose) is used to differentiate between complete or partial PUJO, PUJO and extra-renal pelvis at 4 hours of IVU study.

## Contraindications

Furosemide, bumetanide, and torsemide may exhibit allergic cross-reactivity in patients who are sensitive to other sulfonamides, but this appears to be very rare. Overzealous use of any diuretic is dangerous in hepatic cirrhosis, borderline renal failure, or heart failure.

## Vasodilators

They are used to treat angiographic and clinical vasospasm either alone or in combination with transluminal balloon angioplasty (TBA). Commonly used agents include Papavarine, Calcium channel blocker (Nimodipine, Verapamil, Nicardipine) and Milrinone.

## Papavarine

Papaverine has been the most commonly used vasodilator for intra-arterial infusion therapy, a benzylisoquinoline alkaloid and a potent smooth muscle relaxant, is believed to act by the inhibition of phosphodiesterase activity in smooth muscle cells.. It has been associated with seizures and elevations in intracranial pressure.

**Dosage:** 300 mg of papavarine diluted in 100 ml of normal saline forming a concentration of 0.3 percent. Approximately 2 to 4 ml of 0.3 percent papavarine solution injected as pulse spray. Papaverine should not be mixed with contrast agents or heparin because it may cause precipitation of crystals. Infusion of highly concentrated papaverine may have fewer vasodilatory effects and a higher risk of temporary deterioration, possibly because of emboli formed from papaverine precipitates.

## Nimodipine

It is a dihydropyridine type of calcium channel blocker and specifically block L- type voltage gated calcium channels. Dosage (intra-arterial) - Nimodipine diluted in a solution of NaCl 0.9 percent to obtain a 25 percent concentration. Typical dose administered is 1 to 4 mg (5–20 ml) per vessel with the maximum rate of 2 ml/min. Intensive blood pressure monitoring is required during therapy as it can lead to hypotension.

## Milrinone

Milrinone is a bypyridine methyl carbonitrile analog of amrinone. Its mechanism of action is similar to that of papaverine, which is a nonselective inhibitor of phosphodiesterase. Milrinone works as an inotropic drug and a vasodilator (an “inodilator”) by selective inhibition of cAMP-specific phosphodiesterase III in both cardiac and vascular smooth muscle. Parenteral milrinone delivered in large doses can cause systemic hypotension. Unlike Papavarine no significant elevation in intracranial pressure is seen.

**Dosage:** (Intra-arterial) Milrinone diluted in a solution of NaCl 0.9 percent to obtain a 25 percent concentration. Typical dose is infusion at a rate of 0.25 mg/min, with a total dose of 10 to 15 mg.

Recurrence of cerebral vasospasm, however, is common after vasodilator infusion, as these drugs have relatively short half-lives, therefore requiring additional infusion or TBA. At authors institute, Intra-arterial Nimodipine is used and is reserved for patients with symptomatic vasospasm who have vessel diameter reduction between 25 and 50 percent of the initial diameter angiographically and in patients with distal vessel vasospasm not amenable to balloon angioplasty.

## Patient Preparation in Suspected Pheochromocytoma

Older literature suggested premedication with oral alpha and beta-adrenergic blockade (phentolamine 5 mg and metoprolol 10 mg) for IV contrast medium usage in patients with pheochromocytoma, for preventing adrenergic crisis. It is to be remembered that beta blockade should never be used without alpha blockade in patients with pheochromocytoma. However recent studies indicate no need for routine prophylaxis when nonionic contrast media are employed.

## Drugs for Cardiac Imaging

### Cardiac CT

Cardiac CT (coronary angiography) is unique in that, the image quality is inversely proportional to motion artifacts and the best image quality is achieved at low heart rates <65 beats per minute. Thus, aggressive reduction of a patient's heart rate is advised before a scan for all patients with heart rates of more than 70 beats per minute especially when study is planned on 64-slice scanners, however with the availability of higher slice and dual-source CT scanners regulation of heart rate is not a concern but preferable. For regulation of heart rate to less than 65 beats per minute and make the rhythm regular the use of cardio selective ( $\beta$ 1)  $\beta$ -blockers and newer drug ivadrabine is advocated.<sup>1,2</sup>

### $\beta$ -blockers

$\beta$ -blockers reduce the heart rate by decreasing the frequency of the sinus node, slowing conduction in the atria and atrioventricular node, and by increasing the functional

refractory period of the atrioventricular node. Various  $\beta$ -blockers in use are metoprolol, atenolol and esmolol, however metoprolol is the most preferred drug. Metoprolol can be given either oral or intravenous and protocols for its administration may vary from center to center. Intravenous yields higher (95%) bioavailability than oral (40%) administration due to high first-pass metabolism, hence for faster reduction of heart rate intravenous administration is preferred. Its half-life is 3 to 4 hours. 50 to 100 mg oral metoprolol 1 hour before or intravenous metoprolol 5 to 20 mg immediately before the procedure can be employed. Intravenous administration should be slow over 1 to 2 minutes to be given in doses of 2.5 to 5 mg which can be repeated if required. In some centers oral metoprolol followed by intravenous metoprolol or esmolol is given. Esmolol being short acting (half-life- 9 minutes) can be given as bolus doses for effective control of heart rate.<sup>1,2</sup>

**Contraindications:** Asthma and COPD patients, aortic stenosis, carotid stenosis, pulmonary embolism, atrioventricular block.

$\beta$ -blockers causes significant reduction in ejection fraction, stroke volume and cardiac output therefore these agents should be avoided prior to imaging for evaluation of left ventricular functional analysis.<sup>1</sup>

#### Ivabradine

Ivabradine is a new drug which is pure heart rate lowering agent that acts by inhibiting ionic current in the pacemaker activity of sinoatrial node.<sup>1</sup> Results are better with higher heart rates. At present it is available in oral form with dosage of 5 to 7.5 mg twice a day. It can be given as an alternative or adjunct to  $\beta$ -blockers.

#### Cardiac Stress MRI

The stress cardiac MRI is increasing being evaluated and now is clinical practice for the evaluation of inducible ischemia in patient with coronary artery disease and detection of myocardial viability. To invoke the cardiac stress during the MRI examination pharmacologic agents either positive inotrope (dobutamine or arbutamine) or vasodilator (dipyridamole or adenosine) are used.

#### Dobutamine

Dobutamine increases myocardial contractility and heart rate.<sup>3</sup> During the MRI (pre- and post-dobutamine) the myocardial functions, contractility, perfusion and viability is assessed typically after injection of MRI contrast. It is given intravenously in the doses of 2.5 to 4.0 mg/kg/min. The side effects are chest discomfort and arrhythmias. Its use should be terminated immediately once the signs of myocardial ischemia are detected by use of intravenous atropine in the doses of 0.3 mg increments every minute up to total dose of 1.5 mg.

#### Adenosine

Adenosine is a short acting (half-life less than 10 seconds) systemic arterial vasodilator. The intravenous dose is 140  $\mu$ g/kg/min over 4 to 6 minutes (for a total dose of 0.84 mg/kg). The common side effects include flushing, chest discomfort, anxiety, dyspnea and headache.<sup>4</sup>

### DRUGS AFFECTING COAGULATION

#### Procoagulants

##### Thrombin

Thrombin is the product of the hemostatic response that converts fibrinogen to fibrin. It is also responsible for the aggregation of blood platelets in the formation of the "platelet plug" as well as the activation of factor VIII, factor V, factor XI, factor XIII and protein C. Percutaneous ultrasound-guided thrombin injection into the lumen of the pseudoaneurysm is a quick and valuable therapeutic alternative to endovascular management.<sup>5,6</sup> The technique has proven quick, safe, and comfortable for the patient, even in patients who have received anticoagulation and antiplatelet therapy. The most serious complication is distal arterial embolization, with a frequency of about 2 percent.

The initial thrombin was bovine in origin, and its use had been complicated by the formation of antibodies that cross react with human coagulation factors. This has been associated with life threatening bleeding and in some circumstances anaphylaxis and death. Human thrombin, isolated from pooled plasma of donors, has been developed in an effort to minimize these risks, but its downside is the potential of transmitting blood-borne pathogens and limited availability. Recombinant thrombin has the advantage of being minimally antigenic and devoid of the risk of viral transmission. Human thrombin is more effective than bovine thrombin and thus the required dose for treating pseudoaneurysm is less. An injection of thrombin into the pseudoaneurysm is made through a thin 22 or 23 gauge needle and small boluses (0.1-0.3 mL) of the thrombin solution is given under ultrasound guidance till complete thrombosis of the aneurysm sac is achieved.<sup>6</sup> Thrombin is often used in conjunction with other hemostatic aids, including absorbable agents (like gelfoam, collagen, and cellulose), and with fibrinogen in fibrin glues. Fibrin glues contain thrombin and fibrinogen. When combined, the fibrinogen is activated by thrombin and converted into fibrin monomers. This forms an adhesive glue at the tissues applied. The fibrin monomers go on to interact with the patient's own factor XIII and calcium to convert the final product into a fibrin polymer that allows for platelet activation and aggregation with subsequent hemostasis. Fibrin glues come packaged with a dual chamber syringe that allows for the combination of the thrombin and fibrinogen after the plunger is depressed. The human thrombin is part of a commercial package sold as a fibrin sealant kit (500 U/mL or 1000U/mL). Each packet

contains a solution of human thrombin in calcium chloride and a fibrinogen concentrate with factor XIII and other proteins.

### *Anticoagulants*

Intravascular procedures using indwelling catheters and sheaths would be impossible without inhibition of the coagulation cascade. These can be classified as

#### *Parenteral*

- Heparin
  - Unfractionated Heparin (UFH)
  - Low molecular weight Heparin eg- Enoxiparin, Deltaparin, Tenzaparin
  - Heparinoids
  - Pentsaccharides- Fondoparinix
- Direct Thrombin Inhibitors (DTI)- Hirudin, Bivalirudin.

#### *Oral*

- Warfarin
- Acenocumarole
- Phenindiones
- Factor Xa inhibitors- Rivaroxaban
- Thrombin inhibitors Eg- Xemilgatron.

### *Heparin*

Heparins in medical use are a heterogeneous population of linear polysaccharides belonging to the glycosaminoglycan family with molecular weight of 10,000 to 20,000. Heparin acts indirectly by activation of antithrombin (AT), leading primarily to the inactivation of clotting cascade factors Xa and thrombin (factor IIa). Thrombin is most sensitive to inhibition, and is 10 times more sensitive than factor Xa. Low dose of heparin prolong aPTT without significantly prolonging PT. High concentration of heparin prolong both aPTT and PT.

Injected IV, it acts instantaneously but after SC injection, anticoagulant effect develops after ~60 min. Heparin does not cross blood brain barrier or placenta (the anticoagulant of choice during pregnancy). It is metabolized in liver and excreted in urine, so its half-life is longer in cirrhotics and renal failure patients. After IV injection of doses <100U/kg, the average half life is 1hr. Monitoring of heparin dosage during intervention procedures is guided by measuring activated clotting time (ACT) taken with 2cc of whole blood. Normal range of ACT is 91 to 151s and it is to be taken every 1/2 hr.

#### *Dosage of UFH for Optimal ACT values in endovascular procedures<sup>7-10</sup>*

- IV bolus of 3000 U, 5000 U, and 10,000 U, or ranging from 50 U/kg to 100 U/kg. A typical dose used in intervention procedures is 80U/kg bolus followed by 18 U/Kg/Hr.
- Target ACT from 150–200 seconds to 350–400 seconds.
- For low-risk procedures ACT - 250–300 seconds

- For high-risk procedures such as angioplasty and stent placement, ACT range of 300–350 seconds is recommended
- Goal of 400 sec for stent with filter device.

Bleeding due to overdose is the most serious complication of heparin therapy. Heparin induced thrombocytopenia and osteoporosis (on long term use) are the other adverse effects of heparin.

### *Heparin antagonist*

Protamine sulphate is a strongly basic low molecular weight protein obtained from the sperm of salmon fish. It is used during hemorrhage in intervention procedure (AVM, aneurysm, vessel rupture). Given IV slowly it neutralizes heparin weight for weight i.e. 1mg is needed for every 100 U of heparin. In absence of heparin it itself has weak anticoagulant action. Being basic in nature it can release histamine in the body and can lead to hypersensitivity reactions.

### *Low molecular weight (LMW) heparins*

Low molecular weight heparins (MW 3000-7000) have different anticoagulant profile; selectively inhibit factor Xa with little effect on factor IIa. Thrombocytopenia is less frequent. The major advantages are better subcutaneous availability with once daily s.c. administration. Dose is calculated on body weight basis. Since aPTT is not prolonged laboratory monitoring is not needed. They are mainly used in prevention and treatment of deep venous thrombosis.

### *Thrombolytics*

Thrombolytic agents are used for the treatment of myocardial infarction, thromboembolic strokes, deep vein thrombosis and pulmonary embolism. They may also be used to clear blocked catheters that are used in long-term medical therapy.

#### *Classification of thrombolytics*

1. **1<sup>st</sup> generation (Non fibrin specific):**
  - Streptokinase
  - Urokinase
2. **2<sup>nd</sup> generation (Fibrin Specific):**
  - Prourokinase
  - Recombinant tissue plasminogen activator: Alteplase (Rt.-PA)

**Table 1** Half-life of thrombolytic agents

Agent	Half-life (min)
Streptokinase	30-80
Urokinase	14-20
Prourokinase	20
Alteplase	3-5
Reteplase	15-18

3. **3<sup>rd</sup> generation (Fibrin Specific):**

- Reteplase (r- PA)
- Tenecteplase (TNK-tPA)
- Desmopletase.

Streptokinase is obtained from  $\beta$  haemolytic Streptococci group C. It is inactive as such: combines with circulating plasminogen to form an activator complex which then cause limited proteolysis of other plasminogen molecules to plasmin. It has limited usefulness because many patients have preformed antistreptococcal antibodies and have potential for anaphylactic reaction. It is the least expensive of all the fibrinolytics.

**Dosage:** Bolus: 50,000U, Infusion: 5000U/hr for 12 hours.

Urokinase is an enzyme isolated from human urine and now prepared from cultured human kidney cells. It is non antigenic.

**Dosage:** Bolus: 30,000 – 60,000U, Infusion: 4000U/hr for 2 hours, 2000U/hr for next 2 hours and 1000U/hr for next 8 hours.

Alteplase is produced by recombinant DNA technology. It is fibrin specific with little effect on circulating plasminogen. It has the drawback of lowering the levels of fibrinogen and plasminogen, leading to an increased risk of hemorrhagic complications. Presently, Rt.-PA is the only agent approved by the FDA specifically for IV thrombolysis for ischemic stroke.

**Dosage:** It is available as 20 - 50 mg Lyophilized powder, to be reconstituted.

- **Intravenous:** 0.9 mg/kg, 15 percent - Bolus, 85 percent - Infusion over a period of 30 minutes.
- **Bridging therapy:** 0.6 mg/kg IV (60 mg maximum over 30 minutes) followed by intra-arterially administration at the site of clot up to a total dose of 22 mg over two hours of infusion or until lysis of thrombus was obtained.

3rd generation agents offer the theoretical advantage of longer half life and greater penetration into the thrombus matrix when compared to 2nd generation agents. Retapase is a genetically engineered, smaller derivative of recombinant r t-PA that has increased potency and is faster acting than r tPA. Dosage: Intraarterial: 0.5U/hr, Intravenous: 1U/ hr, maximum dose of 24U in 24 hour.

Reversal of all thrombolytics can be done by administering fresh frozen plasma in the event of hemorrhagic complication.

### Contraindications

#### Absolute

1. Intra cranial bleed
2. Drug allergy

#### Relative

1. Surgery within 10 days
2. Serious GI bleed within 3 months
3. Hypertension with diastolic BP  $\geq$  110 mm Hg

4. Active bleeding or hemorrhagic disorder
5. Aortic dissection

#### Adverse effects

- Bleeding complications at catheterization site, gastrointestinal and cerebral hemorrhages may occur.
- Re-thrombosis can occur following thrombolysis and therefore anticoagulants such as heparin are usually co-administered, and continued after thrombolytic therapy.

### Antiplatelets

These drugs decrease platelet aggregation and thrombus formation. They are effective in arterial circulation where anti-coagulants have little effect. Antiplatelets can be classified as:

- Cyclooxygenase-1 (COX-1) inhibitor: Aspirin
- P2Y12 inhibitors (Thienopyridines): Ticlopidine, clopidogrel prasugrel
- Phosphodiesterase inhibitors: Dipyridamole, cilostazol
- GPIIb/IIIa blockers: Abciximab, eptifibatide, tirofiban.

#### Cyclooxygenase-1 inhibitor

**Aspirin** induces a permanent functional defect in platelets, which can be detected clinically as a prolonged bleeding time. It primarily, acts by irreversible acetylation of COX-1, responsible for the formation of prostaglandin (PG) H2, the precursor of thromboxane (TX) A2.

The non-linear relationship between inactivation of platelet COX-1 and inhibition of TXA2-dependent platelet function by low-dose aspirin has important implications: (i) a substantial reduction in platelet inhibition is associated with less than maximal inactivation of COX-1; (ii) recovery of platelet function is disproportionately rapid, occurring within 3 to 4 days upon drug withdrawal.

Moreover, inhibition of TXA2-dependent platelet function by aspirin leaves other platelet pathways [adenosine diphosphate (ADP)-P2Y12, thrombin-protease-activated receptor (PAR)-1] largely unaffected, thus providing a rationale for dual or triple antiplatelet therapy in high-risk settings.

**Dosage:** 50 to 325 mg oral.

#### Thienopyridines

Thienopyridines inhibit ADP dependent platelet function by irreversible modification of the platelet P2Y12 receptor through short-lived active metabolites, generated by liver cytochrome P-450 (CYP) isozymes. Recovery of platelet function after drug withdrawal occurs linearly over 7 to 8 days as a function of platelet turnover.

Genetic variation of the liver enzymes responsible for the metabolism of clopidogrel as well as drug-drug interactions [e.g. with proton pump inhibitors (PPIs)] are important determinants of the variable circulating levels of its active

metabolite. These, in turn, are associated with variable inhibition of ADP-induced platelet aggregation and variable clinical response to clopidogrel treatment. It is used at a dosage of 75 mg for 3 to 5 days prior to the procedure followed by 75 mg maintains dose, post procedure for 3 months. In case of emergency scenario it can be used at the dosage of 450 to 600 mg 2 to 6 hours prior to the procedure. It is typically used in combination with aspirin.

**Prasugrel** is also a pro drug. It has more profound and less variable inhibition of platelet function observed when compared with clopidogrel. In contrast to clopidogrel, the lack of drug interaction potential and the apparent independence of CYP2C19 genetic variance result in a predictable antiplatelet response to prasugrel.

Antiplatelet agents such as aspirin and clopidogrel are cornerstones that have allowed and increased the use of minimally invasive treatment of cerebro vascular diseases and have reduced thromboembolic events.

#### *Antiplatelet resistance*

Drug resistance to antiplatelet agents has been a long-term problem, especially in known diabetic and hypercholesterolemia patient. These patients usually require a higher dose of these drugs for desired effect.

#### *GPIIb/IIIa blockers*

GPIIb/IIIa is an adhesive receptor (integrin) for fibrinogen and von Willebrand factor through which agonists like collagen, thrombin, TXA<sub>2</sub>, ADP, etc. induce platelet aggregation. Thus antagonists prevent fibrinogen binding to activated GPIIb/IIIa receptors and, thus, formation of fibrinogen bridges between platelets.

Abciximab, a non-competitive inhibitor of GPIIb/IIIa, is the humanized chimeric Fab-fragment of the monoclonal mouse antibody 7E3. Their effect on platelet aggregation is closely linked to plasma concentrations. Owing to their short plasma half-lives, continuous infusion is needed for sustained platelet inhibition.

Abciximab is used as a rescue agent in the management of thrombotic complications of intracranial and carotid angioplasty, intracranial Aneurysm coiling. It has also been used in combination with fibrinolytic agents to enhance thrombolysis.

**Dosage:** Abciximab - 0.25 mg/kg IV bolus followed by 0.125 micro gram/kg/min continuous IV infusion for 12 hour.

**For thrombosis associated with Aneurysmal coiling:** Abciximab diluted with saline at concentration of 0.2 mg/ml. Injected intra arterially as bolus of 4 to 10 mg over a period of 10 to 20 minutes.

#### *Phosphodiesterase inhibitors*

Cilostazol is a reversible type III phosphodiesterase inhibitor, with vasodilator and antiplatelet effects. It increases intra platelet CAMP, reduces cellular adenosine uptake, and

inhibits vascular smooth muscle cell proliferation. Added to a standard combination of aspirin plus clopidogrel, cilostazol 100 mg bid has been found to potentiate inhibition of ADP-induced platelet aggregation when compared with aspirin and clopidogrel.

### SCLEROSANTS AND EMBOLIC AGENTS

Historically, the first agent used for embolotherapy was autologous blood clot. This was easily and quickly obtained and was inherently biocompatible. The drawback of autologous blood clot is that as the body's natural clot lysis dramatically limits the durability of occlusion; recanalization can recur within hours to days. The next agents developed were fascial strips harvested from dura and tensor fascia lata. Silk threads were also historically used as embolic agents, notably for intracranial vascular malformations. Today with the advent of modern liquid and particulates, silk, clot, and fascia are not used. Modern embolic agents are either temporary or permanent. Permanent agents are more common, and there are many applicable subsets including liquid agents, particulates, coils, and detachable plugs and balloons.

### GELATIN FOAM

Gelatin foam (Gelfoam, Upjohn, Kalamazoo, MI) has been used as an intravascular embolization agent for more than 30 years, with the first intravascular use in 1964 for cavernous carotid fistulas. Use of Gelfoam is off-label for embolization, but its use is within the standard of care. Gelatin foam is a biologic substance made from purified skin gelatin. It is available in sterile sheets and as a powder comprised of 40 to 60 mm particles. Sheets can be cut into a variety of shapes. Gelfoam cut into small 1 to 2-mm pieces can be mixed with dilute contrast and injected as pledges, or be prepared as slurry.

Gelatin foam causes mechanical obstruction, slowing blood flow and hastening thrombus formation. In addition, it provides a scaffold for clot formation. Gelfoam embolization provides temporary vessel occlusion, allowing recanalization in a few weeks. The temporary nature of gelatin foam occlusion can be either an advantage or disadvantage depending on the clinical situation (e.g. temporary nature is advantageous in case of hemoptysis or trauma). Other advantages of Gelfoam include low cost, versatility of use, and extensive clinical experience. However, it has been postulated that Gelfoam can be associated with infection due to trapped air bubbles. Further, gelatin foam powder can potentially cause ischemia due to the small size (especially at sizes < 70 mm) of the particles, allowing distal embolization.

### POLYVINYL ALCOHOL

First introduced as an intravascular embolization agent in 1974 in the form of a sponge, current intravascular use of polyvinyl alcohol (PVA) is primarily in the form of particles.

The particles are made from a PVA foam sheet that is vacuum dried and rasped into particles. The particles are filtered with sieves and are available in sizes ranging from 100 mm to 1100 mm. Because of the method of preparation, PVA particles are slightly irregular in size. Particles are sorted by their ability to pass through a larger sieve, but not through a smaller sieve. Thus, oblong particles may have a long axis that is much longer than the stated size. One study evaluating actual size of PVA particles found that the majority were larger than the stated minimum size, with a few very small particles observed once the PVA particles were suspended in solution. Polyvinyl alcohol particles are irregular in shape, which promotes aggregation. They can be oblong, oval, irregular, sharp and angulated with small fragments after suspension.

Polyvinyl alcohol particles provide permanent occlusion by adherence to the vessel wall, causing stagnation of flow, in addition to lodging in the smallest vessel into which they will fit. The results are an inflammatory reaction and focal angio necrosis, with vessel fibrosis developing over time. Polyvinyl alcohol particles are biocompatible, and there is vast cumulative clinical experience with PVA particle embolization. The major disadvantage of PVA particles is their tendency to aggregate, occluding vessels more proximally than might be expected based on stated size. Particle clumping can also cause catheter occlusion, which is preventable by dilution of particles, proper suspension, and slow infusion. In addition, PVA particles can accumulate in the catheter hub and theoretically cause subsequent non target embolization when the catheter is flushed.

### ■ TRIS-ACRYL GELATIN MICROSPHERES

Use of tris-acryl gelatin microspheres was approved by the US Food and Drug Administration (FDA) in 2000 and gained specific approval for uterine fibroid embolization in December 2002. Embospheres are available in six size ranges: 40 to 120 mm, 100 to 300 mm, 300 to 500 mm, 500 to 700 mm, 700 to 900 mm, and 900 to 1200 mm. Embospheres are packaged in 20-mL prefilled syringes containing 2 mL of spheres in saline. Embosphere gold particles are colored for visibility. Tris-acryl gelatin microspheres are made from an acrylic polymer matrix impregnated and embedded with porcine gelatin. They are nonresorbable hydrophilic particles that are precisely calibrated by size. In addition, TAGM can be temporarily compressed by 20 to 30 percent of their initial diameter. Unlike PVA particles, TAGM are smooth and spherical in shape and fragmentation is not observed. Particle accumulation in the catheter hub, particle aggregation fragmentation, and catheter occlusion are uncommon with TAGM. In fact, larger TAGM may deform allowing delivery through a micro catheter with a lumen smaller than the maximum diameter of the sphere. By avoiding particle aggregation, Embospheres may penetrate into smaller vessels compared with PVA particles of the same size. Embospheres cause vascular occlusion by lodging in vessels and inciting a

histological reaction similar to PVA particles when studied at 48 hour and 4 weeks. Embospheres are still identifiable in the tissue at 4 weeks, both intra- and extra vascularly, and degeneration of the spheres has not been observed.

Disadvantages of Embospheres include the need for intermittent agitation to prevent sedimentation and maintain suspension. In addition, Embospheres are partly composed of porcine gelatin, which has allergic potential. Careful attention to sizing is necessary. The same size of Embosphere will penetrate more deeply compared with PVA and could cause unintended ischemia in some vascular beds such as the colon. The difference in effective particle size when using PVA particles versus Embospheres can be significant.

### ■ N-BUTYL-2 CYANOACRYLATE

N-butyl-2 cyanoacrylate (NBCA) is synthetic glue that was approved by the FDA in 2000 for cerebral AVM embolization. It is supplied as one or two 1-g tubes of NBCA, 10 mL of ethiodized oil, and 1 g of tantalum powder, which are mixed together immediately before use. It has been reported in the treatment of extra cerebral and spinal tumors and spinal AVMs and AVFs. It has also been used for embolization of brain and spinal cord tumors, cerebral AVMS, and brain and spinal cord dural AVFs. N-butyl-2 cyanoacrylate is supplied as a free monomer, which is clear and free flowing. When exposed to an anionic environment such as blood or water, polymerization occurs. Ethiodol is used as a vehicle and acts as a polymerization retardant. Tantalum powder is included to provide radiographic opacification, but also slows initiation of polymerization. Before use, adequate visualization should be confirmed with fluoroscopy. Polymerization of NBCA starts immediately on contact with anions, at a rate dependent on the concentration of the NBCA. Polymerization rate can be altered by varying the NBCA concentration with Ethiodol (Savage Laboratories, Melville, NY, USA) or glacial acetic acid. To avoid unintended polymerization by premature contact with anions, catheter flushes should be performed with dextrose 5 percent (D5W) in water. In addition, cyanoacrylate can destroy polycarbonate, so polypropylene syringes should be used. N-butyl-2 cyanoacrylate embolization requires a special setup that includes attaching a syringe of NBCA and a syringe of D5W to the catheter via a three-way stopcock. Initial contrast injection is performed to determine the volume of glue injection required. Immediately after glue injection, the catheter tip is retracted to avoid catheter adherence to the vessel lumen. The catheter often occludes after one to two glue injections.

N-butyl-2 cyanoacrylate makes a permanent cast of the vessel, independent of inherent coagulation. It incites an acute inflammatory reaction in the vessel wall, which progresses to chronic inflammation and fibrosis. Recanalization can occur if only partial embolization is achieved. Advantages of NBCA are that it works instantly, completely occludes vessels, and is permanent. Disadvantages are that use of NBCA

requires expertise. The catheter can become entrapped in the occluded vessel. Polymerization can spread distally or reflux proximally to the intended location. Finally, as part of embolization, catheter position must be abandoned.

### **ETHYLENE VINYL ALCOHOL COPOLYMER**

Ethylene vinyl alcohol copolymer (EVOH) (Onyx, Micro Therapeutics, Inc. Irvine, CA) was first used as an embolic agent by Dr Taki in 1990 and was granted FDA approval in July 2005 as an embolic agent for cerebral AVM. It is a copolymer of ethylene vinyl alcohol prepared with dimethyl sulfoxide (DMSO) as solvent. Tantalum powder is added for opacity. On contact with blood, the DMSO diffuses away allowing polymerization of the EVOH, which forms a cast of blood vessels. In the United States, EVOH is available under the trade name Onyx, and comes prepared as Onyx 18 and Onyx 34, which differ in viscosity. Onyx 500 is available outside the United States and is indicated for the treatment of cerebral aneurysms. Lower concentration of Onyx results in a lower viscosity solution that can be injected into smaller vessels. Onyx comes packaged with a separate vial of DMSO, and special DMSO-compatible catheters must be used for the procedure. Once the catheter is placed in desired position, a small amount of DMSO is injected to fill the catheter dead space and to inhibit in-catheter Onyx polymerization. Once the catheter is in position, Onyx is delivered through the catheter under fluoroscopy. Histologic analysis of AVMs on a few patients embolized with Onyx demonstrated filling of the vessel lumen either partially or completely. Specimens resected 1 day post embolization showed with mild inflammation or angio necrosis. No specimen demonstrated extravasated Onyx. Others have reported successfully using Onyx alone or in combination with coils to treat peripheral vascular malformations.

Advantages of EVOH include that it is non-adhesive. This allows for longer injection times and the ability to temporarily suspend embolization and proceed with further angiography mid procedure if necessary. Although, there is a risk of embedding the catheter in Onyx if it refluxes around the catheter tip, the material is not adhesive and will not adhere to the catheter as does NBCA glue. Disadvantages of EVOH include the need for DMSO-compatible catheters and syringes. DMSO is toxic, and rapid injection of DMSO can cause vasospasm and necrosis. The safe injection rate is < 0.3 mL injected longer than 40 seconds. The lowest toxic dose of Onyx in humans (that is, the maximum safe allowable dose) is 600 mg/kg.

### **ABSOLUTE ALCOHOL**

Ethanol causes tissue infarction by inciting denaturation of proteins with resultant acute thrombosis and subsequent fibrosis. Use of absolute ethanol is generally limited to cases in which non target embolization is unlikely, such as in the

kidney. It is generally used with flow control using balloons either in the arterial or venous portions or in some cases by using coils to slow the flow to acceptable levels. Venous outflow occlusion may be required if there is rapid systemic drainage of the lesion. Disadvantages of absolute alcohol embolization include difficulty to control placement, lack of opacity, and rapid dilution by vascular inflow. There are additional risks of damaging normal adjacent tissues including skin, mucosa, and nerves.

### **SODIUM TETRADECYL SULPHATE**

It is synthetic surface acting substance composed of sodium isobutyl ethyl octyl sulfate and 2 percent benzyl alcohol. It causes endothelial damage and intimal fibrosis. It is administered as a 3 percent solution, dose should not exceed 2 ml (usually used 0.1- 1ml).

### **Transarterial Chemoembolization**

Chemoembolization is a palliative administration of anticancer drug directly into a tumor through its feeding blood supply, with concurrent or subsequent blockage of the feeding vessel by occlusive agents that are injected through the delivery catheter. This permits a higher concentration of drug to be in contact with the tumor for a longer period of time. Chemoembolization is most beneficial to patients whose disease is predominately limited to the liver. Cancers that may be treated by chemoembolization include hepatocellular carcinoma and hepatic metastasis from colon, breast, carcinoid or other neuro endocrine tumors, islet cell tumors of the pancreas, ocular melanoma, sarcoma and other vascular primary tumors in the body. Chemoembolization with drug-eluting beads represents a new and clinically proven delivery device that can deposit a chemotherapeutic agent in the liver with minimal release into adjacent tissues.<sup>11</sup>

Lipiodol (iodized oil), an iodinated ethyl ester of poppy seed oil, was introduced as a drug carrier and an embolic agent in the early 1980s. When injected into the hepatic artery, Lipiodol selectively remains more in tumor nodules for several weeks to over a year due to a siphoning effect from hyper vascularization of the tumor vessels and an absence of Kupffer cells inside tumor tissues resulting in the embolic effects on smaller vessels. Lipiodol functions as a micro vessel embolic agent, as a carrier of chemotherapeutic agents and as an augmenter of antitumor effects of TACE by efflux into the portal veins. The anticancer drugs are vigorously mixed with the Lipiodol to prepare an emulsion, and when the emulsified Lipiodol and drug mixture is injected into a tumor supplying vessels, the anticancer drug is slowly released from Lipiodol and remains in high concentrations within the tumor for a prolonged period. The stability of the emulsion could be more enhanced by adjusting the specific gravity of the contrast medium by adding a small amount of distilled water so it is close to the specific gravity of Lipiodol.

Anticancer drugs used in conjunction with Lipiodol include doxorubicin, epirubicin, aclarubicin, 5-fluorouracil, mitomycin, cisplatin and SMANCS (styrene maleic acid neocarzinostatin). Several chemotherapeutic agents have been used with doxorubicin and cisplatin being the most common.

**Doxorubicin (Adriamycin)** is an anthracycline antibiotic, closely related to the natural product daunomycin, and like all anthracyclines, it works by intercalating DNA, with the most serious adverse effect being life-threatening heart damage. It is commonly used in the treatment of a wide range of cancers, including hematological malignancies, many types of carcinoma, and soft tissue sarcomas. Doxorubicin is photosensitive, and containers are often covered by an aluminum bag and/or brown wax paper to prevent light from affecting it. Doxorubicin is also available in liposome-encapsulated forms that forms a better emulsion with lipiodol.

**Cisplatin** was the first member of a class of platinum containing anti cancer drug, which now also includes carboplatin and oxaliplatin. These platinum complexes react *in vivo*, binding to and causing cross linking of DNA which ultimately triggers apoptosis. It is used to treat various types of cancers, including sarcomas, carcinomas (small cell lung cancer, ovarian cancer), lymphoma and germ cell tumors. Usual dose for doxorubicin and cisplatin per session is 10 to 70 mg and 10 to 120 mg respectively. The criteria to determine the dosages of chemotherapeutic agents are variable and not standardized. Studies have failed to show significant differences in survival between the use of doxorubicin and other drugs such as cisplatin or epirubicin, and to date, there is no evidence of the superiority of any single chemotherapeutic agent over other drugs or for mono-drug chemotherapy versus combination chemotherapy.

## REFERENCES

- Pannu HK, Alvarez W Jr, Fishman EK. Beta-blockers for cardiac CT: A primer for the radiologist. AJR. 2006;186:S341-5.
- Mahabadi AA, Achenbach S, Burgstahler C. Safety, efficacy, and indications of beta-adrenergic receptor blockade to reduce heart rate prior to coronary CT angiography. Radiology. 2010; 257:614-23.
- Hundley WG, Hamilton CA, Thomas MS, et al. Utility of fast cine magnetic resonance imaging and display for the detection of myocardial ischemia in patients not well suited for second harmonic stress echocardiography. Circulation. 1999;100:1697- 702.
- Ranholzky A, Kempthorne-Rawson J. The safety of intravenous dipyridamole thallium myocardial perfusion imaging. Intravenous dipyridamole thallium imaging study group. Circulation. 1990;81:1205-9.
- Lew WK, Weaver FA. Clinical use of topical thrombin as a surgical hemostat. Biologics. 2008;2(4):593-9.
- Victoria V, Reus M, Piñero A, Abellán D, Canteras M, de Rueda ME, Morales D, Parrilla P. Human Thrombin for Treatment of Pseudoaneurysms: Comparison of Bovine and Human Thrombin Sonogram-Guided Injection. AJR. 2005;184(5):1665-71.
- Schumacher HC, Meyers PM, Higashida RT, et al. Reporting standards for angioplasty and stent-assisted angioplasty for intracranial atherosclerosis. Stroke. 2009;40:e348-65.
- Jiang WJ, Wang YJ, Du B, et al. Stenting of symptomatic M1 stenosis of middle cerebral artery: an initial experience of 40 patients. Stroke. 2004;35:1375-80.
- Castellan L, Causin F, Danieli D, et al. Carotid stenting with filter protection: correlation of ACT values with angiographic and histopathologic findings. J Neuroradiol. 2003;30:103-8.
- Qureshi AI, Luft AR, Sharma M, et al. Prevention and treatment of thromboembolic and ischemic complications associated with endovascular procedures. Part II. Clinical aspects and recommendations. Neurosurgery. 2000;46:1360-75, discussion 75-76.
- Takayasu K. Transarterial chemoembolization for hepatocellular carcinoma over three decades: current progress and perspective. Jpn J Clin Oncol. 2012;42(4):247-55.

## Chapter

# 28

# Molecular Imaging

Anish Bhattacharya, BR Mittal

## INTRODUCTION

Molecular imaging is the characterization and measurement of the key biomolecules and molecularly based events using noninvasive medical imaging techniques. It helps in early detection, exact localization and determination of the extent of disease. In the era of personalized medicine, it helps physicians to personalize patient care by evaluating the response to specific therapy and selecting the most effective therapy based on the unique biological characteristics of the patient.

Molecular imaging has several advantages above anatomical imaging, because disease specific abnormal cellular activity occurs well before structural changes. Molecular imaging incorporates several modalities like optical imaging, nuclear imaging, ultrasound, magnetic resonance imaging, etc. (**Table 1**). Nuclear medicine is a branch of molecular imaging, where the imaging agent is a radiotracer, a compound labeled with a radioisotope. The nonradioactive part of the tracer may be a pharmaceutical agent, an antibody, a protein fragment or even living cells. After introduction into the body, the radiotracer accumulates in a specific target

organ or attaches to specific cells. The imaging device (gamma camera/positron emission tomography (PET) scanner) detects the signal from the radioactive part of the tracer to show its distribution within the body.

The following pages provide a brief overview of molecular imaging techniques used in nuclear medicine and their clinical applications.

## MOLECULAR IMAGING PROBES IN NUCLEAR MEDICINE

Molecular imaging probes can be divided into four categories:<sup>1</sup>

1. *Phenotypic probes* are used to assess general physiological features, such as metabolic changes secondary to pathology (F-18 FDG), cell proliferation (F-18 FLT), hypoxia (F-18 FMISO), angiogenesis, apoptosis and receptor study (Ga-68 DOTATATE).
2. *Targeted probes* are used to image specific biomolecules (e.g. signal transduction proteins or tumor-associated antigens) that are characteristic of a cell type.

**Table 1** Molecular imaging modalities

Modality	Mechanism	Sensitivity range	Spatial resolution	Quantitative
Ultrasound	High frequency sound waves	~ 10 μM	~50 μm	+
MRI	Radiowaves	μM	~20 μm	++
SPECT	Gamma rays	nM	<1 mm (mSPECT)	+++
PET	Annihilation photons	nM	1 mm (mPET)	+++
Optical imaging	Visible NIR	pM	Several mm	No

3. *Cell-tracking probes* are used to localize and follow the movement of cells that may be of importance for tumor survival (e.g. cancer cells, vascular endothelium, stromal cells).
4. *Reporter gene probes* are used to monitor the actions of genes in biologic systems *in vivo*.

## CLINICAL APPLICATIONS OF NUCLEAR MOLECULAR IMAGING

### Oncology

#### *Diagnosis and Staging*

In the present time, the molecule that is most commonly used in PET is fluorine-18 fluorodeoxyglucose (F-18 FDG), a glucose analogue, developed to image glucose metabolism in the body. FDG is taken up in cells by glucose transporters. However, unlike glucose, subsequent conversion of FDG to FDG-6-monophosphate by the intracellular enzyme hexokinase leads to trapping of the metabolite within the cells.<sup>2</sup>

Cancer cells usually have a higher rate of glucose utilization than normal cells (the Warburg effect) due to over-expression of glucose transporters and the transcription factor hypoxia inducible factor-1, which regulates genes involved in glycolysis.<sup>3</sup> The measurement of glucose metabolism as a surrogate marker of tumor activity has been utilized for a number of applications in cancer management, including cancer staging, recurrence detection, response assessment, prognostic evaluation and radiotherapy treatment planning. FDG is not specific for tumor cells, as any cells with increased metabolism will show increased FDG uptake. Furthermore, the low or variable glycolytic activity of some tumor types has limited the utility of F-18 FDG PET in tumors, such as renal cell carcinoma, primary prostatic cancer and hepatocellular cancer. In addition, physiological uptake in the brain, nonspecific bowel uptake and urinary excretion of FDG also limit tumor detection.

Therefore, other PET tracers are emerging. FLT is a promising PET tracer for proliferation. It is taken up by proliferating cancer cells by thymidine kinase (TK-1) and trapped intracellularly.<sup>4</sup> Initial clinical studies have also demonstrated that FLT is more sensitive than FDG to image recurrent high-grade brain tumors, correlated better with Ki-67 values, and is a more powerful predictor of tumor progression and survival. There are studies emerging in support of F-18 FLT being useful in staging of nonsmall cell lung cancer, high grade brain tumors, etc.

F-18 fluoride bone scan is useful for detection of bony metastases in many cancers, such as breast cancer, prostate cancer, urinary bladder cancer. It has an advantage over conventional gamma camera bone scintigraphy due to better image resolution and the ability to provide 3-dimensional images. <sup>18</sup>F-fluoro-dihydrotestosterone (FDHT), an antiandrogen receptor tracer, has shown promise in the

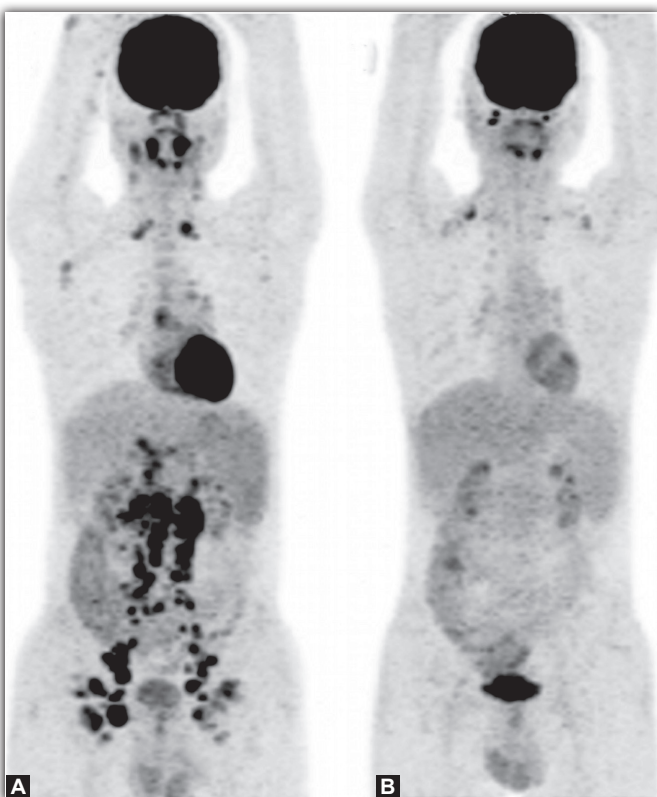
detection of bone metastases in prostate cancer. Studies have shown that in many cases, bone metastases as well as lymph node involvement detected with FDHT PET/CT were not detected with either FDG-PET/CT or bone scan. This helps in accurate staging of prostate cancer. F-18 fluorocholine (FCH) has demonstrated promise in prostate cancer by detecting additional bony lesions and lymph nodes compared to FDG PET. C-11 choline PET/CT has high sensitivity and specificity for staging and restaging of prostate cancer.

Ga-68 DOTATATE and DOTANOC, being specific for somatostatin receptor expressing cells, are new tracers for imaging of neuroendocrine tumors. F-18 fluorodihydroxyphenylalanine (F-DOPA) is another tracer useful in diagnosis and staging of neuroendocrine tumors and low grade brain tumors. Several other investigational tracers, like C-11 methionine for brain tumors and C-11 acetate for gliomas and prostate cancer, have been studied. All tumors do not behave in the same biological pattern in every individual. Thus, these new tracers help in understanding the heterogeneity of tumor biology.

#### *Assessment of Response to Treatment*

In routine clinical practice, treatment response is usually evaluated with anatomical imaging modalities, with reduction in tumor size as a response guide. However, anatomical changes after treatment become evident much later than functional changes. Early identification of non-responders may lead to alteration to more suitable therapy; thereby reducing the costs and side effects of ineffective therapy. Furthermore, with the introduction of cytostatic agents, which may not necessarily lead to tumor shrinkage, response evaluation is challenging with structural imaging. Thus, molecular imaging has a great role in early response assessment to treatment. Recently, FDG PET/CT has shown promising results in early response evaluation to treatment in many cancers like, lymphomas,<sup>5</sup> lung cancer,<sup>6</sup> esophageal cancer<sup>7</sup>, etc. In malignant lymphomas, where anatomical imaging after completion of therapy often reveals residual masses that could represent either persistent disease or fibrotic tissue, FDG PET/CT has been accepted as the modality of choice for response evaluation (**Figs 1A and B**). Also, F-18 FLT PET/CT has shown acceptable results in evaluation of response to cytostatic drugs in nonsmall cell lung carcinoma.

Several studies have evaluated the prognostic value of FDG-PET/CT. These studies in a variety of cancers such, as lymphomas,<sup>8</sup> lung cancer,<sup>6</sup> esophageal cancer<sup>7</sup>, etc. have demonstrated that early metabolic responders have a longer survival than non-responders. Such a prognostic estimation by metabolic imaging could serve as a guide for modification of therapy. Several studies have demonstrated that persistent or increased focal FDG uptake in initially involved tumor sites in patients with Hodgkin's disease or non-Hodgkin's lymphoma is highly predictive for residual or recurrent



**Figs 1A and B** F-18 FDG PET maximum intensity projection (MIP) images in a patient with non-Hodgkin's lymphoma. (A) Pre-treatment study showing involvement of lymph nodes both above and below the diaphragm; (B) Scan after 4 cycles of chemotherapy showing complete metabolic response in the involved lymph nodes

disease and associated with a poor outcome.<sup>9,10</sup> In addition, residual FDG uptake after completion of treatment has been associated with poor prognosis in other tumors such as sarcomas,<sup>11</sup> esophageal,<sup>12</sup> lung,<sup>13</sup> head and neck<sup>14</sup> and cervical carcinomas.<sup>15</sup> Hypoxia imaging markers like F-MISO may be used in solid tumor for detection of radio-sensitivity of tumor cells to radiotherapy.

#### Role in Drug Development

Metabolic imaging also serves as a pharmacodynamic endpoint in drug development, especially in studies with newer target-directed agents, where higher doses may not necessarily be better and an optimal therapeutic dose may exist. This will prevent an erroneous rejection of certain cytostatic agents, where a functional response may be observed in the absence of decrease in tumors size.

In addition, PET can provide information on *in vivo* normal tissue and tumor pharmacology, which has, so far, relied on surrogate information obtained from body fluids. Understanding of both the drug's pharmacokinetics and pharmacodynamics has the potential of rational

modifications to drug development processes and hence save time. A number of PET tracers such as  $[^{15}\text{O}]H_2\text{O}$  and  $[^{18}\text{F}]FDG$  have already been adopted as PET pharmacodynamic markers and used in the evaluation of anti-neoplastic agents. PET may be used to evaluate a number of pharmacodynamic endpoints, which may either be a true endpoint or a validated surrogate endpoint. PET studies have confirmed a pharmacodynamic relationship between dose and efficacy. For example, in patients with metastases from colorectal cancer, labelled 5-FU PET has shown that higher 5-FU-tumor uptake (SUV), was associated with longer survival.<sup>16</sup>

## CENTRAL NERVOUS SYSTEM DISORDERS

#### Epilepsy

SPECT and PET imaging are useful to detect brain disorders like stroke, Moya-Moya disease (Fig. 2), dementia, epilepsy and movement disorders. Epilepsy is one of the common central nervous system disorders. Epilepsy is controlled by medication in around 70 percent of patients. In the rest of the patients who remain intractable to medical treatment, resection of the epileptogenic cortex may be considered. Nuclear medicine plays a crucial role in the presurgical assessment of patients with refractory epilepsy.

Ictal perfusion imaging with  $^{99\text{m}}\text{Tc}$ -ethyl cysteinate dimer (ECD) or  $^{99\text{m}}\text{Tc}$ -hexamethylpropyleneamine oxime (HMPAO) is commonly used to detect the seizure onset zone in a majority of cases. However, ictal SPECT of the brain is only possible in some tertiary care centers. Interictal SPECT imaging is more widely available, but is unreliable to determine the ictal onset

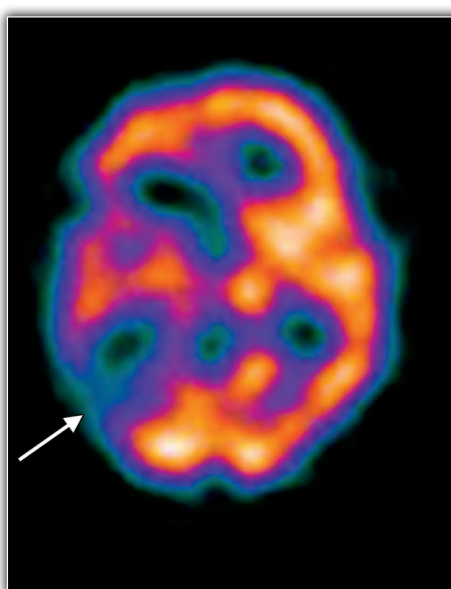


**Fig. 2** Tc-99m ECD SPECT scan of the brain in a patient with Moya-Moya disease showing a focal perfusion defect in the right posterior parietal cortex

zone. Interictal FDG PET is more commonly used to detect a hypometabolic area in the brain, which usually encompasses but tends to be larger than the seizure onset zone. It has been shown that FDG PET is quite sensitive in detecting such sites, with 85 to 90 percent accuracy using modern techniques.<sup>17</sup>

In recent years, novel PET tracers have been developed to visualize specific receptor systems. In patients with epilepsy, changes in the  $\gamma$ -amino-butyric acid receptor (with <sup>11</sup>C- or <sup>18</sup>F-labeled flumazenil), opioid receptors (with <sup>11</sup>C-carfentanil for  $\mu$ -opioid peptide receptors; <sup>11</sup>C-methylnaltrindole selective for  $\delta$ -opioid peptide receptors), <sup>5</sup>HT<sub>1A</sub> serotonin receptors (with <sup>18</sup>F-FCWAY a selective <sup>5</sup>HT<sub>1A</sub> receptor antagonist), nicotinic acetylcholine receptors and others may be detected with the newer PET tracers. However, their use in clinical practice is limited at the moment.

## Dementia

FDG PET measurements of cerebral glucose metabolism are well validated in early diagnosis, differential diagnosis, and the evaluation of drug treatment for patients with dementia. Moreover, newer PET tracers (**Table 2**) have been developed to study the neuropathology and alterations of neurotransmitter systems underlying dementia, to advance our understanding of the pathophysiology of dementia, and to improve diagnostic accuracy. C-11 Pittsburgh compound B (PiB) appears most promising among all these new tracers, which has high sensitivity in detecting amyloid pathology *in vivo*. It binds with high affinity to neuritic A $\beta$  plaques but not to diffuse plaques and neuro-fibrillary tangles.<sup>18</sup>

## Movement Disorders

PET imaging with F-18 FDG has been extensively used to assess local synaptic activity in the resting state in various movement disorders. Additionally, the discovery of several tracers (**Table 3**) useful for assessment of movement disorders has helped enormously in the clinical management of patients. Among the compounds that have been explored, tracers that visualize the dopaminergic system have the highest potential for the assessment of movement disorders, for example F-18-6-fluoro-L-dopa (F-DOPA).<sup>19</sup> Presynaptic dopamine transporters (DAT) SPECT tracers show high sensitivity for detecting atypical Parkinsonian syndromes, for example, <sup>123</sup>I- N-3-fluoropropyl-2b-carbomethoxy-3b-(4-iodophenyl) tropane (<sup>123</sup>I-FP-CIT).

## CARDIOVASCULAR DISORDERS

### Myocardial Viability

The hibernating myocardium in known coronary artery disease (CAD) patients represents a state of persistent left ventricular dysfunction in chronically decreased blood flow but preserved viability. Approximately 55 to 60 percent of

**Table 2** PET tracers useful in evaluation of dementia

Radionuclide tracer	Molecular targets
F-18 FDG	Glucose metabolism
C-11 Pittsburgh compound B (PiB)	Amyloid plaques
F-18 FDDNP	Tau-protein
C-11 PK11195	Microglial activation
F-18 DOPA	Dopaminergic neurons, dopa decarboxylation, and vesicular storage
F-18/C-11 altanserin	5HT <sub>2A</sub> receptors

**Table 3** Potential PET radiotracer that can be used in investigations of movement disorders

Radiotracers	Molecular target
F-18 DOPA	Dopaminergic neurons, dopa decarboxylation, and vesicular storage
F-18 FDG	Glucose metabolism
C-11 DTBZ	Type 2 vesicular monoamine transporters
F-18 CFT	Presynaptic dopamine transporters
C-11 raclopride	Postsynaptic dopamine D2 receptors

the hibernating myocardium is expected to demonstrate functional improvement after intervention. In ischemic myocardium, normal free fatty acid metabolism switches to glucose as the main energy source. Increased F-18 FDG uptake is therefore considered a marker of viability (**Fig. 3**). F-18 FDG PET is considered the 'gold standard' for the detection of viable myocardium, with positive predictive value 74 percent and negative predictive value 87 percent.

### Coronary Flow Reserve

The PET is the best noninvasive method for absolute quantification of myocardial blood flow (MBF) and quantification of coronary flow reserve (CFR). It is based on tracer kinetic models. O-15 water, N-13 ammonia and rubidium-82 are commonly used tracers. Clinical applications of absolute MBF quantification include preclinical diagnosis of CAD, accurate noninvasive diagnosis of multi vessel disease, distinguishing the presence of collaterals and early hibernating myocardium is known as CAD and assessing response to therapy or intervention for CAD.

### Atherosclerosis

Many tracers have been tried for imaging of atheroma, such as I-125 autologous human LDL, Tc-99m LDL, Tc-99m annexin V, FDG, etc. It has been seen that FDG is taken up in the atherosclerotic vessels. There is evidence that the uptake

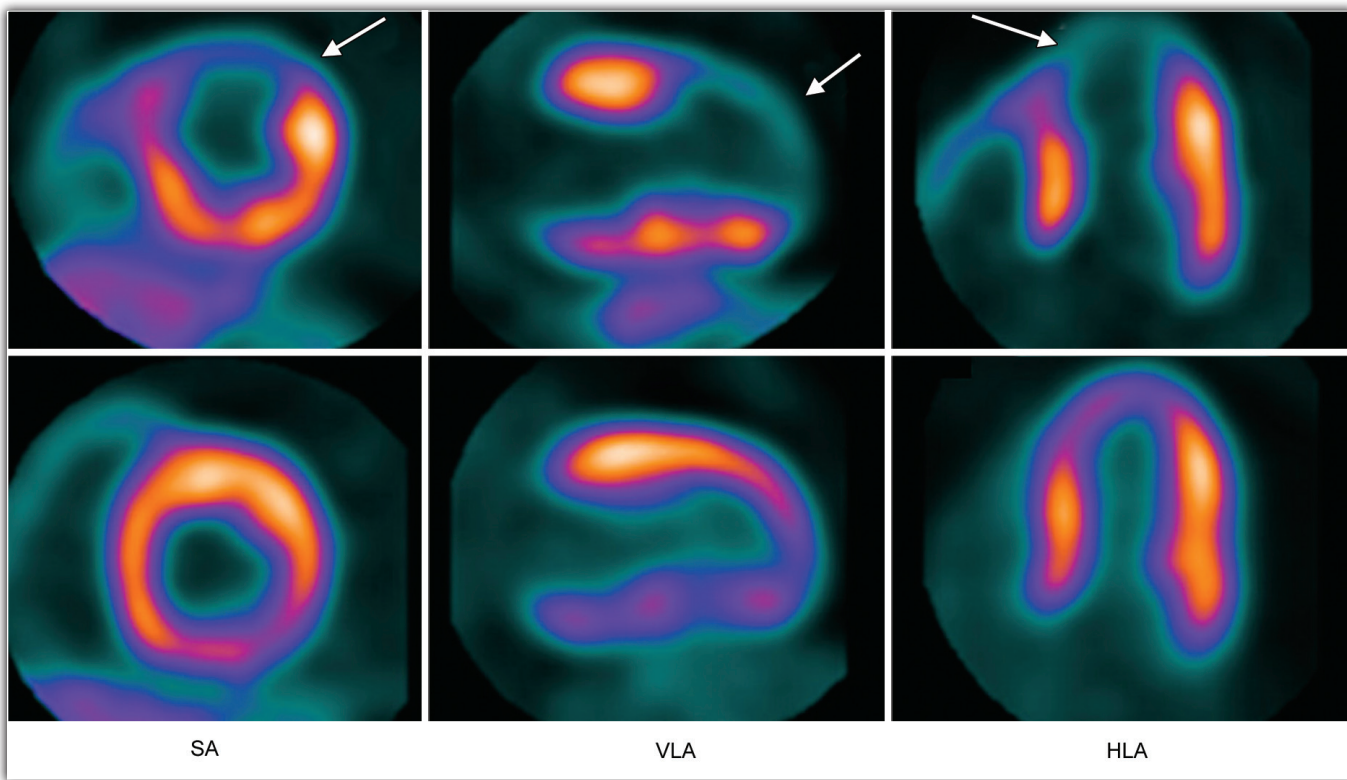


**Fig. 3** PET images using N-13 Ammonia (top row) and F-18 FDG (bottom row) showing perfusion-metabolic mismatch. The perfusion defects in the antero-apical segment and apex (arrows) show good metabolic activity, indicating viable myocardium in these segments. (Abbreviations: SA: Short axis; VLA: Vertical long axis; HLA: Horizontal long axis)

is mainly located in the intima and likely represents high metabolic activity in macrophages, which are in abundance in the atherosclerotic plaques. It is also likely that the smooth muscles in the arterial wall are visualized due to high glucose use by this tissue.

### ■ INFECTION AND INFLAMMATORY PROCESSES

Of the radiopharmaceuticals currently approved for imaging of infection/inflammation none is specific for inflammation, and none offers the possibility of directly distinguishing sterile from septic inflammation. The accumulation of these agents in inflamed tissue is based on different mechanisms. Most radiolabeled agents would accumulate at sites of infection if the local blood flow and the vascular permeability were increased. While scintigraphy with labeled activated leukocytes specifically depends on cellular migration to the site of inflammation, glucose uptake into inflamed tissue (as a result of increased metabolism) is another reliable mechanism to detect inflammation. Finally, Ga-67 binds to transferrin, with the complex being extravasated at sites of inflammation because of increased vascular permeability and then being transferred to locally present lactoferrin.<sup>20</sup>

Ga-67 citrate is not used these days due to poor imaging characteristics, relatively high radiation exposure

and prolonged imaging time (up to 72 hours). White blood cell scintigraphy comprises the isolation of autologous leukocytes, the *ex-vivo* labeling of these cells with either Tc-99m hexamethylpropylene amine oxime (HMPAO) or In-111 oxine and re-injection of the labeled cells into the patient. Radiolabeled autologous leukocytes are regarded as the most specific tracer for imaging of acute infection. However, the procedure requires handling of the patient's blood and meticulous attention to asepsis, in addition to imaging time of 24 hours.

### Newer Agents for Imaging Infection/Inflammation

Several investigational radiopharmaceuticals, including radiolabeled nonspecific IgG, antigranulocyte antibodies, chemotactic peptides, interleukins (e.g. interleukin [IL]-1, IL-2, and IL-8), chemokines, and liposomes have been proposed as potential agents for imaging infection and inflammation. Four monoclonal antibodies, CEA-47, BW 250/183, IMMUNN3, and MCA-480 have been examined for abscess/infection detection in humans. These agents have been investigated as potential replacements for radiolabeled leukocytes. Some of these have shown great promise in animal experiments. However, problems of cost, availability, immunological reactions and unforeseen adverse event reports, including

2 deaths and 15 life-threatening cardiopulmonary complications, have resulted in the suspension of their routine use.<sup>21</sup>

The broad-spectrum antibiotic ciprofloxacin is a fluoroquinolone analog with specific binding to bacterial DNA gyrase that is present in all viable bacteria. Because of its specific binding to bacteria, it was hypothesized that Tc-99m labeled ciprofloxacin, a tracer designed to image microorganisms, may identify only the sites of infection and thus distinguish between sterile inflammation and infection. Localization, however, appears to be based primarily on extravasation and stasis at the sites of increased vascular permeability. It is rapidly cleared from circulation by the kidneys and shows no uptake in bone marrow, and minimal localization in liver and abdominal area. In clinical studies, Tc-99m labeled ciprofloxacin showed acceptable sensitivity and specificity in identifying a wide variety of infectious foci, but it does not appear to distinguish between infection and sterile inflammation.<sup>22</sup>

During recent years, increasing evidence for the application of 18F-fluorodeoxyglucose positron emission tomography (FDG-PET) in the evaluation of several infectious and aseptic inflammatory disorders has been published.<sup>23,24</sup> Although FDG-PET cannot reliably distinguish infection from non-infectious inflammation, it offers several practical advantages over conventional nuclear medicine techniques (white blood cell/bone marrow/bone imaging) including:

1. Completion of the examination within a short period of time (1.5–2 hours)
2. High-resolution tomographic images
3. High target-to-background contrast ratios
4. High sensitivity for chronic infections
5. Minimal labor intensity
6. High interobserver agreement
7. Low radiation dose (2–3 times lower than that of most conventional nuclear medicine techniques)
8. Detection of infection in the axial skeleton; white blood cell (WBC) scanning in particular is of limited value in this setting.

The potential applications of FDG-PET imaging include evaluation of the complicated diabetic foot, painful joint prosthesis, fever of unknown origin (FUO), acquired immunodeficiency syndrome (AIDS)-related disorders, vascular graft infection and fistula, inflammatory bowel disease (IBD) and a variety of noninfectious inflammatory diseases.<sup>21,25</sup>

Recently, PET-CT imaging with F-18 FDG labeled leukocytes has been shown to combine the superior imaging characteristics of PET with the fine anatomical detail of CT and the specificity of leukocytes localizing to sites of acute inflammation.<sup>26</sup> In view of the negligible physiological uptake of F-18 FDG labeled cells in the intestine or urinary system, this tracer may be optimal to detect inflammatory foci within the gastrointestinal tract, with minimum confounding background physiological tracer activity.<sup>27</sup> The scanning procedure is completed within 2 to 3 hours after

tracer injection, compared to more than 24 hour required for imaging with both In-111-oxine and Tc-99m HMPAO leukocytes.

The clinical applications of molecular imaging continue to grow, with the advent of newer radiotracers. While many new agents have shown great promise in laboratory or animal studies, the cost, availability and safety of these tracers remain limitations in their routine use. With increasing applications of these techniques worldwide, it is hoped that these noninvasive investigative methods will provide viable solutions to many clinical dilemmas in future.

## REFERENCES

1. Weissleder R, Pittet MJ. Imaging in the era of molecular oncology. *Nature*. 2008;452:580-9.
2. Buck AK, Herrmann K, Stangardt T, Dechow T, Krause BJ, Schreyogg J. Economic evaluation of PET and PET/CT in oncology: evidence and methodologic approaches. *J Nucl Med*. 2010;51:401-12.
3. Lu H, Forbes RA, Verma A. Hypoxia-inducible factor 1 activation by aerobic glycolysis implicates the Warburg effect in carcinogenesis. *J Biol Chem*. 2002;277:111-5.
4. Barthel H, Perumal M, Latigo J, et al. The uptake of 3'-deoxy-3'-[<sup>18</sup>F] fluorothymidine into L5178Y tumours *in vivo* is dependent on thymidine kinase 1 protein levels. *Eur J Nucl Med Mol Imaging*. 2005;32:257-63.
5. Juweid ME, Wiseman GA, Vose JM, et al. Response assessment of aggressive non-Hodgkin's lymphoma by integrated International Workshop Criteria and fluorine-18-fluorodeoxyglucose positron emission tomography. *J Clin Oncol*. 2005;23:4652-61.
6. Hoekstra CJ, Stroobants SG, Smit EF, et al. Prognostic relevance of response evaluation using [<sup>18</sup>F]-2-fluoro-2-deoxy-D-glucose positron emission tomography in patients with locally advanced non-small-cell lung cancer. *J Clin Oncol*. 2005;23:8362-70.
7. Weber WA, Ott K, Becker K, et al. Prediction of response to preoperative chemotherapy in adenocarcinomas of the esophagogastric junction by metabolic imaging. *J Clin Oncol*. 2001;19:3058-65.
8. Mikhaeel NG, Hutchings M, Fields PA, O'Doherty MJ, Timothy AR. FDG-PET after two to three cycles of chemotherapy predicts progression-free and overall survival in high-grade non-Hodgkin lymphoma. *Ann Oncol*. 2005;16:1514-23.
9. Cremerius U, Fabry U, Neuerburg J, et al. Prognostic significance of positron emission tomography using fluorine-18-fluorodeoxyglucose in patients treated for malignant lymphoma. *Nuklearmedizin*. 2001;40:23-30.
10. Spaepen K, Stroobants S, Dupont P, et al. Prognostic value of positron emission tomography (PET) with fluorine-18 fluorodeoxyglucose ([<sup>18</sup>F]FDG) after first-line chemotherapy in non-Hodgkin's lymphoma: is [<sup>18</sup>F]FDG-PET a valid alternative to conventional diagnostic methods? *J Clin Oncol*. 2001;19:414-9.
11. Schuetze SM, Rubin BP, Vernon C, et al. Use of positron emission tomography in localized extremity soft tissue sarcoma treated with neoadjuvant chemotherapy. *Cancer*. 2005;103:339-48.

12. Swisher SG, Erasmus J, Maish M, et al. 2-Fluoro-2-deoxyglucose positron emission tomography imaging is predictive of pathologic response and survival after preoperative chemoradiation in patients with esophageal carcinoma. *Cancer.* 2004;101:1776-85.
13. MacManus MP, Hicks RJ, Matthews JP, et al. Positron emission tomography is superior to computed tomography scanning for response-assessment after radical radiotherapy or chemoradiotherapy in patients with non-small-cell lung cancer. *J Clin Oncol.* 2003;21:1285-92.
14. Kunkel M, Forster GJ, Reichert TE, et al. Radiation response non-invasively imaged by [18F]FDG-PET predicts local tumor control and survival in advanced oral squamous cell carcinoma. *Oral Oncol.* 2003;39:170-7.
15. Grigsby PW, Siegel BA, Dehdashti F, et al. Post-therapy [18F] fluorodeoxyglucose positron emission tomography in carcinoma of the cervix: response and outcome. *J Clin Oncol.* 2004;22:2167-71.
16. Moehler M, Dimitrakopoulou-Strauss A, Gutzler F, et al. 18F-labeled fluorouracil positron emission tomography and the prognoses of colorectal carcinoma patients with metastases to the liver treated with 5-fluorouracil. *Cancer.* 1998;83:245-53.
17. Newberg A, Alavi A, Reivich M. Determination of regional cerebral function with FDG-PET imaging in neuropsychiatric disorders. *Semin Nucl Med.* 2002;32:13-34.
18. Leinonen V, Alafuzoff I, Aalto S, et al. Assessment of beta-amyloid in a frontal cortical brainbiopsy specimen and by positron emission tomography with carbon 11-labeled Pittsburgh compound B. *Arch Neurol.* 2008;65:1304-9.
19. Brooks DJ, Ibanez V, Sawle GV, et al. Differing patterns of striatal 18F-dopa uptake in Parkinson's disease, multiple system atrophy, and progressive supranuclear palsy. *Ann Neurol.* 1990;28:547-55.
20. Gotthardt M, Bleeker-Rovers CP, Boerman OC, et al. Imaging of inflammation by PET, conventional scintigraphy, and other imaging techniques. *J Nucl Med.* 2010;51:1937-49.
21. Basu S, Zhuang H, Torigian DA, et al. Functional imaging of inflammatory diseases using nuclear medicine techniques. *Semin Nucl Med.* 2009;39:124-45.
22. Goldsmith SJ, Vallabhajosula S. Clinically proven radiopharmaceuticals for infection imaging: mechanisms and applications. *Semin Nucl Med.* 2009;39:2-10.
23. Zhuang H, Yu JQ, Alavi A. Applications of fluorodeoxyglucose-PET imaging in the detection of infection and inflammation and other benign disorders. *Radiol Clin North Am.* 2005;43:121-34.
24. Zhuang H, Alavi A. 18-fluorodeoxyglucose positron emission tomographic imaging in the detection and monitoring of infection and inflammation. *Semin Nucl Med.* 2002;32:47-59.
25. Basu S, Chryssikos T, Moghadam-Kia S, et al. Positron emission tomography as a diagnostic tool in infection: present role and future possibilities. *Semin Nucl Med.* 2009;39:36-51.
26. Dumarey N, Egrise D, Blocklet D, et al. Imaging Infection with 18F-FDG-Labeled Leukocyte PET/CT: Initial Experience in 21 Patients. *J Nucl Med.* 2006;47:625-32.
27. Bhattacharya A, Kochhar R, Sharma S, et al. Infection of pancreatic pseudocyst demonstrated on PET/CT using [18F] fluorodeoxyglucose-labeled autologous leukocytes. *Clin Nucl Med.* 2012;37:618-9.

## Chapter

# 29

# Ethical and Legal Issues in Radiology

*Mandeep Kang, Manavjit Singh Sandhu*

With great power and the ability to handle human lives comes great responsibility. The Hippocratic Oath makes us realize our duties and reiterates human expectations desired from us as medical professionals. We as true 'workers' try to achieve and maintain the greatest standards in treating 'OUR' patients. But being human, we falter at times, sometimes unknowingly and sometimes, though very rarely, knowingly. We have to realize the indubitable fact that in spite of doing the best we can as professionals, we are bound to be answerable for our actions even for the ones done for the betterment of patients. We cannot rest in the shade of the 'noble' medical profession. We have to be better equipped to prove at every step that the decisions we take are for the treatment of patient's infirmity. They say charity begins at home and the sooner we realize this, the better.

The two most significant changes in medicine in the past century were scientific development and the belief that no mistake, inadequacy and failure should be accepted as a normal part of life.

As we all live in a world governed by rules, laws and regulations which affect all citizens including doctors, we as radiologists, like all other doctors may be challenged legally on various grounds. Right from being accused by the police of committing a crime, facing claims of malpractice in a civil court to being charged with unprofessional conduct by medical boards and colleges, our community may be the subject of complaints registered by citizens through government agencies. In modern society the dictum 'If you provide a service, you may be sued' is very true. The increasing accountability of service providers including doctors has lead to cessation of many specialized examinations by them because of high rates of such examinations landing up in court. An example is that many radiologists have given up

interpreting mammograms especially in the West, where stricter laws hold them responsible for even minutest of shortcomings, e.g. delay in personal communication of results to the referring physicians.

The radiologists, as other medical professionals, have to be equipped to safeguard their privileges and be vigilant towards their duties and responsibilities. They should have knowledge of the ethical and legal issues that are bound to crop up during their day-to-day practice and be able to handle them with courage and self-belief. The following chapter highlights the various aspects, apart from the clinical/patient-oriented work, which one has to experience as a doctor with some suggestions regarding how to handle them.

## ETHICAL ISSUES

The Hippocratic Oath teaches us to be ethically reasonable in our duties.<sup>1</sup> The moral principles or ethics as they are called are usually ingrained within us as individuals, however, there are circumstances when we may falter in the path to our duties and may inadvertently choose an unethical road which may bring our profession to disrepute. More often than not, this occurs as a result of our lack of awareness to certain regulations to be followed during practice. The various ethical issues are briefly discussed below.

## DOCTOR-PATIENT RELATIONSHIP

Since time immemorial the doctor-patient relationship is one of sacred trust. A patient usually approaches a doctor with complete trust and faith to seek a solution to his/her pain and ailment. He assumes that the doctor has the requisite knowledge, skills and competence to treat the illness and thus

confides in him. It thus becomes an unwritten agreement once the doctor begins on his job. The doctor cannot promise or guarantee a cure but should be empathetic and truthful towards the patient and his own-self, be it in diagnosis or treatment. If the doctor feels that a certain case requires special attention in which he is not competent enough, he should rightfully transfer the patient to the appropriate specialist.

The medical community must realize that the patient confides in them and thus confidentiality of the patient's information regarding the illness and disease should not be disclosed to anyone unless absolutely necessary. The radiologist should hand over the report to either the patient or the referring physician. All the investigations and procedures that are advised should be in the patient's interest and not be guided by other gains. The patient should be allowed to make informed decisions.

The doctor and all staff working under him/her should display utmost respect for the privacy and dignity of the patient. Their conduct and etiquette should be dignified and delicate. At the same time, the doctor must protect his own interests e.g. performing a trans-vaginal ultrasound in the presence of a female attendant, to avoid embarrassing situations in case of any misunderstandings.

The doctor may be approached by patient's attendants at times who may try to influence him/her for any act of commission or omission that may not be in compliance with professional ethics or legal provisions, e.g. sex determination in a pregnant lady. In these cases, the doctor should remain vigilant, lest he/she may land in legal trouble. One should not easily succumb to any pressures or emotional blackmail and must not cross the ethical and legal boundaries.

## RADIATION ISSUES

A radiologist must comply with legislation and appropriate measures to protect the health of patients and staff as he is the one who heads the gamut of various radiation-associated imaging procedures. He should ensure regular maintenance check of machines, adhere to badge monitoring requirements for staff and avoid excessive radiation exposure to patients in X-ray/CT examinations.<sup>2</sup> In all studies, he should adhere to the as low as reasonably achievable (ALARA) principle, especially in young patients who are most prone to the development of radiation-induced cancers in later life.

The radiologist heading a facility should ensure a detailed and documented procedure for protection of the patients and staff.

## Patient Protection

The various measures that should be adopted are avoidance of unnecessary investigations, use of radiation protection devices and minimizing the radiation exposure times. In case of contrast-induced reactions in patients undergoing any radiological investigation, quick action must be taken

by a concerned specialist. More practically, the radiologist himself/herself should be trained in the same.

## Staff Protection

Radiation protection measures in the form of lead aprons, protective gloves, use of screens, personalized radiation dose monitoring equipment should be adhered to. The pregnant staff should be relocated in the radiation free zones for work.

The radiation records of the department personnel should be preserved during the working life of an individual until one attains the age of seventy-five years or at least 30 years after terminating work involving radiation exposure. The radiation records should be transferred to the next employer in case a worker changes jobs.

## Public Protection

Appropriate signage should be displayed at appropriate places in the department which are under high radiation exposure. The attendants should not be asked to accompany the patients for radiological investigations unless required and if so, with full protection. Periodic surveillance of radiation levels should be carried out in and around rooms housing the radiation equipment. A radiation safety officer having necessary qualifications should be appointed for the overview of radiation zones.

Pregnancy, whether in staff or public, requires special consideration as all such personnel should not be allowed to enter the radiation fields. It becomes the responsibility of the radiologist to perform radiation free imaging in such patients. Inadvertent use of radiation may be harmful to the developing fetus and may lead to litigations at a later date. Thus, all the investigations requiring ionizing radiation should be withheld unless there is definite beneficial effect on the patient's condition.

## Protection During Interventions

Interventional radiology has emerged as a therapeutic subspecialty of radiology and has picked up momentum over the last couple of decades as a minimally invasive treatment option. The risks involved in interventional procedures are more closely related to surgery than to diagnostic radiology. Thus, the duties of the radiologist performing interventions become stricter beginning right from when the patient comes for or is referred for some intervention till the time his/her condition improves for which he/she had been referred for initially. Just like any surgical procedure, the nature of the disease process and treatment options needs to be explained to the patient after which he can make an informed decision regarding the option chosen by him. A written informed consent should subsequently be taken before embarking on the procedure. It is an interventional radiologist's duty to perform the procedure to the best of his/her capability in keeping with international guidelines.<sup>3,4</sup> Moreover, he should regularly follow-up the patient on OPD basis.

## ■ **LEGAL ISSUES**

The physician community falls under constant surveillance due to the consumer-provider relationship that it shares with the patients. A thorough awareness of our expected responsibilities and understanding of the legalities associated with our profession will help us to provide our best to the patients without undergoing the stress of any repercussions. The specific aspects, where radiologists should be strategic are:

### **Image Interpretation and Reporting**

A radiologist is responsible for all aspects of a diagnostic examination. But it is his interpretation of the information obtained, embodied in the radiological report, that is the essential end product resulting from the contract between him and the patient. But the human eye and brain cannot match the extensive progress that radiology has seen in the recent past. In the words of Robinson:

*The performance of the human eye and brain has failed to keep pace with the enormous technical progress in the first full century of radiology. Errors and variations in interpretation now represent the weakest aspect of clinical imaging.*

Alleged misdiagnoses account for majority of malpractice lawsuits (60-70%) against radiologists. Thus interpreting the obtained images forms the major component of a radiologist's job. A uniform approach may prevent inadvertent error in studying the images of the necessary examination.

### **First Study the Images**

The clinical information should be withheld until after the images have been read because it can generate a *framing bias* and alter a radiologist's independent opinion. Also try not to refer to previous reports until you have formulated your own opinion.

### **Know How the Examination was Performed**

With such a wide range of imaging modalities available, the technical knowledge required has increased manifold. A radiologist should be well aware of the various technical aspects in various modalities like positioning, centering, etc in radiography, pulse sequences in MRI, pitch in helical CT, Doppler effects in ultrasound, the physiology of contrast media, digital image evaluation and various artifacts involved in different imaging modalities.

### **How to Look (Detect the Abnormalities)**

It is the most important task requiring skills and practice. One should be adept at detecting the normal range of appearances. Patient data should be checked along with the dates of examinations before interpreting any examination. A pattern approach should be followed so that no region of the image is missed. Tuddenham studied the eye movements of experienced radiologists during film reporting and found an

organized pattern of scanning, contrasting with the random scanning pattern of a beginner. Also try to think three-dimensionally!

### **When an Abnormality is Found**

It is the knowledge and experience that determine the probabilities that come to mind on viewing abnormal images. A detailed description of the abnormality is desirable for which following things should be kept in mind:

1. Determine the anatomy of each abnormality
2. Assess the radiopathology of each abnormality
3. Check any previous imaging investigations.

### **Reach a Conclusion**

In reaching a conclusion to complete the interpretation, it is important to realize that 'common diseases occur commonly' and it is reasonable to favor the most likely diagnosis. A radiologist should be in a sound position to suggest the most appropriate further investigation, if further diagnostic specificity is required. In formulating the report, it is helpful to clearly separate the objective findings from the subjective conclusion.

Interpretation of the imaging findings is followed by a written radiology report which has come to be regarded as factual, rather than the radiologist's subjective opinion in legal circles. The essence of report writing is the ability to describe things and express opinions concisely and precisely. An ideal radiology report is 'most often right, though sometimes wrong, easy to read and not too long' as defined by a leading author.

### **When to Make the Report**

The report should not be recorded until after the processes of interpretation and conclusion have been thought through as a thorough understanding of the case is essential for an accurate and precise report.

### **Giving the Report a Title**

The title of the imaging should precisely include the region covered in the examination, e.g. a frontal view of the chest radiograph should be specified lest the examination is assumed to include both the frontal and lateral projections and may have a bearing on the future medicolegal consequence. It is also important to indicate the techniques used, especially in specialized CT and MR examinations where a particular technique or sequence can miss a particular finding, e.g. subarachnoid hemorrhage may be missed on a routine T1 and T2 image while it can be exquisitely demonstrated on a FLAIR or DWI sequence.

### **Proofread the Report**

Before issue, the report should be checked by the reporting radiologist thoroughly, especially for typographical errors.

If an error is realized after dispatch of the report, a second report should be issued, replicating the first one with an addendum instead of an amended report.

### *General Format*

The report can fall into two categories: those having a definite diagnosis and those in which a range of differential diagnoses are considered.

**Definite Diagnosis:** Clearly mentioned in the final impression with utmost precision when in no doubt.

**Indefinite Diagnosis:** When the diagnosis remains speculative, the format of the report should be divided into 'Findings' and 'Conclusion.' The findings section should record the objective data obtained from the images. Never try to give your subjective opinion in the findings. Conclude by giving what you think is the possible diagnosis. However, when in doubt, give the differentials along with an advice of appropriate further investigations.

### *Length of the Report*

In general, brevity is a virtue. Lengthy reports are not recommended because they tax the patience of referring physicians. It has been suggested that clinicians judge the confidence of the radiologist to be inversely proportional to the length of the report.

### *Negative Reporting*

It is conventionally accepted that radiology reports record abnormalities and things not mentioned can be taken to be normal. In cases where the clinical information suggests an abnormal finding but the images appear normal, the report should report normality. There are cases where the borderline between normal and abnormal is uncertain. In such cases, it is reasonable to state 'No definite abnormality seen...'

### *Internal Architecture*

Sentence construction, use of descriptive phrases and the order in which things are set out are all part of the report architecture. Such skills accumulate with experience though some guidelines may be helpful. A good report should have 'brevity, relevance and clarity.' The main objectives of the report should be to

1. Focus the reader's attention early.
2. Report the abnormalities as they are.
3. Use phrases and adjectives to qualify nouns.
4. Use familiar words.
5. Get the anatomical terms right.
6. Immediately communicate the findings to the referring physician when a life-threatening abnormality is detected.
7. Recommend further diagnostic investigations, if diagnosis is inconclusive.

Appropriate image interpretation and report writing form the major roles of a radiologist and thus should be as precise and accurate as possible. In spite of that there are occasions when the radiologist's report is put under scanner by the patient<sup>5</sup> and his/her physician. Most of these pertain to specific investigations and body systems like mammography for breast cancer, chest radiograph for lung cancer, etc.

## **LAWS/LEGAL ACTS APPLICABLE TO MEDICINE**

### **PCPNDT Act**

**The Pre-Natal Diagnostic Techniques (Regulation and Prevention of Misuse) Act (1994) and Pre-Conception and Pre-natal Diagnostic Techniques (Prohibition of Sex Selection) Rules, 1996**

The PNDT [(Pre-natal Diagnostic Techniques (Regulation and Prevention of Misuse)] Act came into existence in 1994<sup>6</sup> after the government realized that the cause of skewed sex ratio especially in parts of Northern India was the prenatal termination of female fetus. The advent and easy availability of ultrasound was being wrongly used for determining the sex of the fetus inside the mother's womb. As the girl child is unwelcome in many homes due to the traditional thinking, there was a high prevalence of 'killing' the female child even before 'she' was born. The census 2011<sup>7</sup> further reveals that the situation is far worse in respect of girl child population, particularly in the affluent areas of Punjab (893 girls to 1000 boys), Haryana (877), Chandigarh (817) and Delhi (866). To check and curb this malpractice, strict rules were formulated which banned the communication regarding the gender of the fetus by the sonologist to the patient/attendants.

In spite of the implementation of the PCPNDT Act, the situation did not improve significantly as expected even after the amendment in the year 2002. An All India Conference of State Secretaries was thus called in 2005 in New Delhi where certain guidelines were revised and few new ones added. The ones pertaining to the radiologist community is that records of all diagnosis done by the ultrasound machines or other machines, as well as charts, forms, reports, consent letters, etc. used for the purpose of prenatal diagnosis should be maintained for at least two years. All new machines should have the facility of blocking any deletion from the memory unless authorized. A detailed overview of the guidelines can be had directly from the PCPNDT Act or from a recent issue of the Indian Journal of Radiology and Imaging (IJRI 2012 Vol 22 Issue 2).

The Act has been a blessing as there has been a constant though gradual increase in the female sex ratio. However, many doctors including the radiologists and gynecologists believed that the paperwork involved was too much which was eating into their occupation time. The laws were so strict that not completing the required data would invite strict action against them even if they had followed all the legal rules.

A study on Doctors' Perspective on PNDT Act was conducted by Dhaduk et al.<sup>8</sup> A total of 26 obstetricians and

8 radiologists participated in the study. All the participants were given pretested and structured proforma to give their opinion on various aspects related to the PNDT Act, viz difficulties faced, penalties for violation, punishment for violation, genuineness of information (Forms F and G), repercussions of the PNDT Act, demand for gender determination, and suitable amendments in the PNDT Act. Only 5.91 percent of the doctors felt that the PNDT Act is the only tool for improving the gender ratio. As many as 79.41 percent of the doctors were of the opinion that the PNDT Act is not the only tool to improve the gender ratio while 14.7 percent had no opinion. About a quarter (26.55%) of the doctors were of the view that penalties for violating the PNDT Act are very heavy while three-quarters (73.45%) did not feel so. A total of 67.6 percent of the doctors were of the view that publicity through the media of court cases related to breaches of the PNDT Act by doctors is beneficial for improving the gender ratio as it will act as a deterrent against flouting the provision of the PNDT Act by doctors. A total of 32.41 percent of the doctors did not feel the same way.

On inquiring regarding completing forms F and G genuinely and completing it with true information, about half (55.9%) of the doctors stated that they completed these forms genuinely and with correct information; 2.9 percent stated that the information completed was absolutely false and 41.2 percent were not sure. With regard to the impact of the PNDT Act on the future progress of the invention related to use of ultrasound technique in Medical Sciences; as many as 41.2 percent of doctors felt that the PNDT Act can hamper the future course of medical invention, 44.1 percent of the doctors did not think so, and 14.7 percent of the doctors did not know. When asked about the demand from doctors for gender determination by patients in the Outpatient Department, 97.1 percent confirmed that there is such a demand from patients or her family. Other difficulties faced by the doctors are given in **Table 1**.

The various State Governments have implemented the PNDT Act in letter and spirit with all sincere efforts in order to check the declining sex ratio. An example of the actions taken is being quoted with respect to the state of Haryana. Haryana had been the first state where the first 3 court cases under this Act were launched. It was also here that the first conviction took place under the PNDT Act. 14 doctors/persons have been convicted in the State so far, under PNDT Act with 2 convictions under MTP Act. 1036 Ultrasound Clinics/Genetic Clinics and 67 Genetic Counseling centers have been registered. 42 ultrasound machines have been registered in Govt. sector while 115 ultrasound machines have been seized and sealed on account of being unregistered/other violations. 9296 inspections of various ultrasound clinics have been conducted. Registration of 245-ultrasound centers has been suspended/cancelled. Four prosecutions were launched in the district courts by Faridabad in the month of Feb-March 2009. This is just an example of how the states across India are carrying on this work with zeal and the results have started

**Table 1** Different kinds of difficulties faced by doctors because of the PNDT Act

Difficulties	No. of respondents	Percent
Excessive clerical work	29	85.29
Social difficulties	3	8.8
Hospital administrative difficulties	15	44.1
Police interference more than expected	10	29.4
No difficulties	6	17.6

showing up in the form of increase in the female ratios as observed in interim census across states.

The Indian Radiological and Imaging Association (IRIA) has also given support to this cause with active propagation of the theme of *Save the Girl Child* in form of sensitization of various individuals associated with it. It has started campaigns and is arranging various seminars to sensitize the member doctors to help in the government strategy of achieving the required goals of women empowerment and improving sex ratios.

A recent article<sup>9</sup> has shown that selective abortions of girls have increased tremendously in India, especially at homes where the first born child is a girl. The increasing sex selection among the Asian communities in US and UK has forced the respective governments to introduce new legislation for curbing this Act. The Prenatal Nondiscrimination Act (PRENDA) has recently been introduced in US which bans sex selective abortions.

### The Consumer Protection Act (1986)

This Act was formulated by the government of India in the year 1986 as an Act to provide for better protection of the interests of consumers and for that purpose to make provision for the establishment of consumer councils and other authorities for the settlement of consumers' disputes and for matters connected therewith. Of the various service providers included in the Act, doctor-patient relationship is also established as a consumer provider one. The doctor community is responsible for its actions and can be taken to task if an ill will can be proved against them. This may be harsh on us doctors as most of the times we try to alleviate the sufferings of 'our' patients with utmost care. We should not be delegated to the same level as other service providers like shopkeepers, etc., because our jobs are vastly different. Yet malpractice by certain unscrupulous elements in our community has made our whole profession answerable. Medical negligence constitutes a wide portal in the present judiciary which has seen many doctors being tried for their negligent acts. Many a times doctors have been punished who have been bringing the medical profession to disrepute. Apart from the state judiciary which imposes sanctions on

these individuals, the Medical Council of India also acts in coherence with the law agencies by debarring the practicing medical professionals from the state/national registers. These individuals can thereafter not practice medicine until and unless their names have been cleared of misdeeds.

The radiologists may become a part of various law suits due to a number of reasons. The following discussion enumerates the various aspects of duty required of us and how to be careful in the provision of these duties for the betterment of the patient without being held up by the consumer laws. A radiologist's role may primarily be as a defendant or as a witness.

## Radiologist as a Defendant

### *In a Malpractice Claim*

On receiving a court notice regarding a malpractice claim, the radiologist should act calmly and not be intimidated by the notice. One should:

1. Read the statement carefully to determine the exact nature of alleged malpractice.
2. Assemble all of the available documents you have including radiology reports, request forms and diagnostic images, if in your possession. Make copies and form a separate file.
3. Contact your insurer or medical defence lawyer without delay.

### *Duty of Care*

A duty of care is intangible but generally accepted to be an obligation recognized by law to exercise diligence, care, knowledge, skill and caution in management. The duty may be different at different times for different patients. To further objectify the same, the Bolam principle is followed in many regions of the world and is most popular in Britain. It states that 'a doctor is not negligent if he acts in accordance with a practice accepted at the time as proper by a responsible body of medical opinion.' In spite of all linguistic endeavors regarding defining 'duty of care', it is ultimately, for the judge to determine the breach of care which varies from case to case. Radiologists are required to provide the duty of care right from patient care to the interpretation of imaging findings.

### *Consent*

The key elements of consent are that:

1. It must be voluntary
2. It must be informed
3. It must be given in writing by a person who has capacity to give it and should be witnessed preferably by a person unrelated to both the parties.

We as radiologists should personally obtain consent before carrying out an investigation even if it has been previously taken by the referring physician as he may not know precisely the risks involved in a particular investigation.

It is of more importance in case of invasive procedures like angiographies and radiological guided therapeutic procedures.<sup>10</sup> Any invasive procedure without informed consent is legally an assault—that is, the unlawful direct application of force to another individual. This is applicable in many countries across the world. No invasive procedure should be carried out without taking a written informed consent from the patient or nearest attendant.

### *Archiving and Ownership of Diagnostic Imaging Data*

There are laws in many jurisdictions regarding retention of films in the public arena for a certain duration which may range from a minimum of 3 years till up to 25 years of patient's age after which they may be destroyed without seeking patient consent. Till this time, it is the responsibility of the concerned radiologist to preserve the imaging on which his/her reports are based. However, most patients and referring physicians opt to keep the films with them. The concept that the radiologist owns the images as 'tools of trade' is most important as the digital revolution portends a future of filmless radiology.<sup>11</sup> Until that is achieved, radiologists must record relevant hardcopy images on film, tape or disc. It is important that the images provided substantiate the dictated report.

### *Patient Referral*

Although not a legal requirement, the importance of retaining referral information on each patient cannot be overstated from a medicolegal risk management point of view. Many a times the referral form by the physician is incomplete with respect to the clinical findings and provisional diagnosis. The information on the request form, often scanty, may be a telling factor in a radiologist's defence.

The second issue is whether a patient can self refer himself/herself to a radiologist or has to be referred by a treating physician.<sup>12</sup> The patient can do a self-referral till the time it is not seen to transgress into the ethical and legal responsibilities of the radiologist.

## Radiologist as a Witness

### *As Expert Witness*

Radiologists are the expert witnesses allowed to give an opinion, and the basis for it, within their recognized field of specialized knowledge and experience. A radiologist may be required to give evidence-testimony-in court for various reasons; as a defendant, or when the radiologist's report is relevant in other court actions. A summons is issued when a radiologist is required to provide evidence involving parties other than the radiologist. Refusal to attend court is not an option and failure to comply is a criminal offence.

### *Writing a Radiological Opinion*

The document must show name, qualifications and address. The opinion should be honest, objective and based on the

radiologist's experience and knowledge. Opinion should not be given on matters beyond one's limit of expertise.

#### *Comments on Other Radiological Reports*

As an expert, a radiologist may be required to be judgmental about reports by other professional colleagues. Without any bias, one should make his own opinion without belittling his fellow colleagues.

#### *Appearing in Court*

A good expert witness should understand his role and be well prepared, objective, independent, and credible. One should be able to use simple, non-technical language, explain technical terms to lay people, answer questions directly and clearly, use consistent body language and should dress like a professional.

#### *Personal Communication by the Radiologists*

Malpractice lawsuits alleging failure of communication of radiologic results are prevalent and becoming more so in the western world. One analysis of court transcripts disclosed that communication problems were present in more than 70 percent of depositions while another claims it to be a causative factor in as many as 80 percent of malpractice lawsuits. A survey categorizing causes of malpractice litigation involving radiologists released in 1997 by the Physician Insurers Association of America and the American College of Radiology (ACR) found that the number of medical malpractice claims alleging communication failure had grown to become the fourth most frequent primary allegation against radiologists. This survey also disclosed that in nearly 60 percent of malpractice lawsuits involving radiologists, the referring physician had not been directly contacted regarding urgent or significant unexpected findings, even though in 75 percent of these cases, the medical record had shown that a radiology report was issued in a timely manner. Thus, approximately 75 percent of claims against radiologists stems from various sorts of errors in communication.<sup>13</sup>

Malpractice litigation involving radiologic communication is moving to center stage in the legal arena. Traditionally, radiologists have considered themselves to be consultants or "doctors' doctors," in the sense that they initiated radiologic examination only on the request of a referring physician and then rendered a radiographic interpretation and transmitted it to the same physician. Most radiologists believed that their duty to communicate interpretations was fulfilled with the sending of the radiology report from the radiology department, destined to be received by the referring physician without being concerned that the report might not be received or noticed by that physician. Nowadays due to easy and wide availability of radiologic techniques, we are receiving referrals for 'screening' for various disorders with no apparent symptoms. In the traditional referral,

the referring physician suspected an abnormality, actively awaited the radiologic results, and was likely to follow-up with the radiologist if a written report was not forthcoming in a timely fashion. In the case of screening investigation, however, the patient would have no clinical sign or symptom; it was likely that both the physician and patient expected the radiology report to reveal normal findings, and, therefore, they might not actively seek the report—thus setting the stage for radiology reports to go astray without being noticed.

In the 1980s, the ACR issued its first Standard for Communication: Diagnostic Radiology. It stated: Some circumstances... may require direct communication of unusual, unexpected, or urgent findings to the referring physician in advance of a formal written report.... The timeliness of direct communication should be based upon the immediacy of the clinical situation.

#### *Issue of Self Referral*

The medicolegal responsibility of the radiologist when reporting X-ray films is the same whether they were ordered by a registered medical practitioner, a physician or the patient himself. He has a duty of care to interpret the films correctly, accurately and having taken account of all the information available. As radiological assessment nowadays involves complex imaging techniques, many of them being invasive involving considerable risks to the patient, the radiologist has to decide whether to agree to the request, having taken into consideration the source of the request, and whether the request is in the patient's best interest.<sup>14</sup> The radiologist would also have a duty to perform the test to the required standard, and without harm to the patient. If he agrees, he has a duty to ensure that the interpretation is correctly applied, having considered the individual patient and his clinical circumstances, even if the imaging has been done elsewhere.<sup>15</sup>

### **■ TELERADIOLOGY: WHO IS RESPONSIBLE?**

Telemedicine has been defined by the World Medical Association as 'The practice of medicine over a distance, in which interventions, diagnostic and treatment decisions and recommendations are based on data, documents and other information transmitted through telecommunication systems.'

The teleradiology system has evolved in a huge way over the last couple of decades. Safeguards aimed at limiting access to only those authorized to have access, and to prevent breach of patient confidentiality need to be in place. It is arguable whether there is a doctor-patient relationship in teleradiology between the remote radiologist, who acts more like a consultant, and the patient. However, it may be argued that a duty of care exists once the radiologist accepts a request to provide medical services.<sup>16</sup> The radiologist responsible for the report may be in breach if it can be shown that he has not taken sufficient care when interpreting the

films or in producing his report. Case law and legislation have yet to catch up with this rapidly developing area of healthcare. Recent reviews by Pattynama et al<sup>17</sup> and Ross et al<sup>18</sup> with relevance to the European system have generated apt questions and answers in this field of responsibility sharing. They have addressed some of these issues in their articles in the European Journal of Radiology.

The day we take the Hippocratic Oath on the completion of our medical graduation, we promise ourselves the care, hard work, truth and just treatment that we would provide to all our patients. Although most of us strive to attain this at all cost, there may be times when we may falter either due to the governing circumstances or our inappropriate decisions. It is during this time that we are expected to stand for ourselves as practicing medical professionals and prove to the world our integrity. An awareness and knowledge of the medicolegal aspect of our practice is thus warranted. The brief review provided above may thus help in avoiding the legal hassles involved in providing appropriate care towards our patients. This review touches a few fronts where one can be challenged by patients, the duty that is often expected from us as professionals and some practical ways by which one can project one's work to the outer world without falling into legal conundrum in spite of giving our best for the community. Though a lot remains to be done in the Indian scenario with respect to the legal aspect of medicine, a thorough knowledge of medicine and laws is still essential for saving ourselves when the situation demands and to provide the best we can to our community and nation.

## REFERENCES

1. Jhala CI, Jhala KN. The Hippocratic Oath: A comparative analysis of the ancient text's relevance to American and Indian modern medicine. *Indian J Pathol Microbiol.* 2012;55:279-82.
2. Lau LS, Pérez MR, Applegate KE, Rehani MM, Ringertz HG, George R. Global quality imaging: Emerging issues. *J Am Coll Radio.* 2011;8:508-12.
3. Zibners H. Legal Issues in Interventional Radiology: A Private Practitioner's Perspective. *Semin Intervent Radiol.* 2001;18: 389-94.
4. Potchen EJ, JD, Hollstein BR. Information Management and the Legal Aspects of Interventional Radiology. *Semin Intervent Radiol.* 2001;18: 367-74.
5. Capaccio E, Podestà A, Morcaldi D, Sormani MP, Derchi LE. How often do patients ask for the results of their radiological studies? *Insights Imaging.* 2010;1:83-5.
6. The Pre-Natal Diagnostic Techniques (Prohibition of Sex-Selection) Act, 1994. Act No. 57 of 1994 [20th September, 1994].
7. C Chandramouli (23 August 2011). Census of India 2011: A Story of Innovations. Press Information Bureau, Government of India.
8. Dhaduk KM, Parmar DV, Yadav BS, Yadav S. A Study on Doctors' Perspective on PNDT Act. *Indian J Community Med.* 2009; 34:160-61.
9. Jha P, Kesler MA, Kumar R, Ram F, Ram U, Aleksandrowicz L, et al. Trends in selective abortions of girls in India: Analysis of nationally representative birth histories from 1990 to 2005 and census data from 1991 to 2011. *Lancet.* 2011;377:1921-8.
10. Teoh MK. Medico-Legal Issues in Radiology. *SMA News.* 2005;37:7-9.
11. Berlin R. Storing Unread Radiologic Images in a PACS. *Am J Roentgenol.* 2011;196:W100.
12. Kilani RK, Paxton BE, Stinnett SS, Barnhart HX, Bindal V, Lungren MP. Self-referral in medical imaging: A meta-analysis of the literature. *J Am Coll Radiol.* 2011;8:469-76.
13. Berlin L. Communicating Findings of Radiologic Examinations: Whither Goest the Radiologist's Duty? *Am J Roentgenol.* 2002;178:809-15.
14. Hutchinson M, Rowe E. Yet another flawed study of self-referral? *Am J Roentgenol.* 2012;199:W414.
15. Berlin L. Malpractice and Ethical Issues in Radiology: Limiting Requests for Outside Radiographic Interpretations. *Am J Roentgenol.* 2013;200:W92.
16. Ross P, Sepper R, Pohjonen H. Cross-border teleradiology-experience from two international teleradiology projects. *Eur J Radiol.* 2010;73:20-5.
17. Pattynama PMT. Legal aspects of cross-border teleradiology. *Eur J Radiol.* 2012;73: 26-30.
18. Ross P, Pohjonen H. Images crossing borders: Image and workflow sharing on multiple levels. *Insights Imaging.* 2011;2: 141-8.

# Index

Page numbers followed by *f* refer to figure and *t* refer to table

## A

- Achilles tendons 49
- Acoustic
  - noise 130
  - radiation force
    - imaging 46
    - impulse 39
  - shadowing 25
  - shadows 25*f*
- Acquisition parameters 88
- Acute
  - hepatitis 43
  - ischemic stroke 88
  - kidney injury 266, 301
    - network 301
  - pancreatitis 115
  - total body irradiation 343
- Adenocarcinoma 103*f*, 374
- Adenomyosis 49
  - of anterior wall of gallbladder 23*f*
- Adenosine 395
- Adequate spectral separation 69
- Adrenal adenoma 75
- Adriamycin 401
- Advanced
  - DW techniques 161
  - MR applications and hardware 135
  - ultrasound system 366*f*
- Advantages of
  - digital radiography 205
  - pulsation artifacts 148
  - storage phosphor systems 208
- Air tissue interfaces 149*f*
- Alzheimer's disease 386
- Amorphous selenium 214
- Amplatzer vascular plug 254
- Angle correction 29
- Angled tip catheters 248

## Anterior

- abdominal wall 23*f*
- descending coronary artery 81*f*

### Antiplatelet resistance 398

### Appearance of normal tendons 49

- Applications in
  - abdomen 72
  - abdominal trauma 281
  - breast imaging 282
  - gout 77
  - head and neck 80
  - hepatic imaging 273
  - neuro-imaging 81
  - pancreas 77
  - pancreatic imaging 280
  - prostatic imaging 282
  - renal imaging 281

### Applications of digital mammography 221

### Arterial

- input function 174
- spin labeling 172, 176

### Arteriovenous fistula of lower limb 236*f*

### Aspirin 397

### Assessment of

- liver transplant 46
- portal hypertension/varices 46

### Astrocytoma 110

### Atherosclerosis 405

### Autoimmune pancreatitis 95

### Automated CR systems 215

### Automatic

- film changers 240
- image stitching 215

### Axial shear strain imaging 40

## B

### Balloon catheters 250

### Barium fluorobromide 214

## Basic

- physics of digital mammography 217
- principles of MR contrast agents 259

### Baum's bumps 24

### Beam

- collimation 349
- width artifact 21

### Benign

- breast mass 282*f*
- focal liver lesions 274*f*
- prostatic hyperplasia 48

### Biliary stent 252

### Bird cage resonator 133*f*

### BMD installation 364*f*

### B-mode flow imaging 35

### Brain 162

- tumors 108

### Breast 41, 164

- cancer 282

### Bridging therapy 397

## C

### Calcium oxalate

- dihydrate 72
- monohydrate 72

### Carcinoma of

- breast 112*f*
- urinary bladder 376*f*

### Cardiac

- applications 80

### CT 394

- stress MRI 395

### Cardinal principle of radiation protection 333, 346

### Cardiovascular disorders 405

### Catheter parts 247*f*

### CCD detector technology 362

### Central nervous system 392

- disorders 404

- Cerebral
    - arterial anatomy 191*f*
    - blood
      - flow 88, 172
      - volume 88, 172
    - metastases 112*f*
    - venous system 187*f*
  - Cerebrospinal fluid 183
  - Certification of
    - RSO 344
    - service engineers 344
  - Cervical
    - cancer 48
    - elastography 48
  - Cesium
    - bromide 214
    - iodide 214
  - Characterization of
    - breast masses 282
    - FLL 273
    - C hepatic mass lesions 75
    - renal masses 281
  - Charge couple device 206, 211, 217
  - Chemical
    - shift artifacts 149, 161
    - suppression 141
  - Chinese hat artifacts 22
  - Cholangiocarcinoma 47, 276
  - Chronic
    - calcific pancreatitis 100*f*
    - gouty arthritis 79*f*
    - kidney disease 266
    - liver diseases 115
    - pancreatitis 101
    - pulmonary thromboembolism 78*f*
  - Cirrhosis 43, 44
  - Cirrhotic liver 276
  - Cisplatin 401
  - Classification of
    - MR contrast agents 260
    - radiation injury 342
    - thrombolytics 396
  - Clear cell carcinoma 168*f*
  - Coded pulse excitation 34
  - Coherent gradient echo sequence 199
  - Color
    - and gray-scale display 314
    - Doppler scan of
      - common carotid artery 6*f*
  - Colorectal
    - cancer 376
    - carcinoma 97
  - Comet tail artifact 23
  - Communication system 205
  - Complex
    - curve catheters 248, 249*f*
    - cyst 42
  - Components of
    - fluoroscopic system 227
    - MRI scanner 124*f*
  - typical Doppler
    - ultrasound transducer 6*f*
  - Compression
    - elastography 38, 49
    - ultrasonography 47
  - Compton scattering 341*f*
  - Computed
    - radiography 206, 207, 361
    - tomography 57, 353, 360, 364, 373
      - dose index 336, 355
      - perfusion 87*t*
  - Computer aided detection 215, 221, 317, 363
  - Concept of steady state 199
  - Cone beam geometry 63
  - Consumer protection Act 413
  - Contrast
    - enhanced
      - digital mammography 222, 364
      - endoscopic ultrasound 281
      - MR angiography 189
      - ultrasound 271
    - induced nephropathy 264, 301
    - medium 88, 265
    - recirculation 173
    - resolution 58, 59
  - Conventional
    - radiographic projections 353
    - spin echo sequence 195, 197*f*
  - Coronary artery disease 80, 389
  - Curvilinear array transducer 5
  - Cyanoacrylates 254
  - Cystic pancreatic tumors 280
- D**
- Dark room fluoroscopy 226*f*
  - Dementia 405, 405*t*
  - Depiction of elastogram 38
  - Depth setting 19
  - Detection of
    - focal
      - liver lesions 273
      - pancreatic lesions 280
      - pancreatic necrosis in acute pancreatitis 281
  - Determinants of optimal image 58
  - Diameter spherical volume 124
  - Different elastography
    - techniques 38
  - Diffuse liver diseases 43
  - Digital
    - breast tomosynthesis 217, 222, 223
    - broadband MR 135
    - flat-panel detector cone-beam
    - computed tomography 368
    - fluoroscopy 233
    - mammography 217
    - radiography 205, 206, 216, 361
    - reporting rooms 369
  - subtraction angiography 226, 234, 360, 366
  - tomosynthesis 363
  - versatile disk 313
  - Direct
    - conversion detectors 209
    - digital
      - conversion 211
      - radiography 206, 209
    - film recording 240
  - Display
    - monitors 314
    - of digital images 220
  - Distance gain compensation 19
  - Distributed systems 316
  - Diuretics 393
  - Divisions of radiology department 360
  - Dobutamine 395
  - Dose
    - length product 355
    - reduction techniques 243
  - Doxorubicin 401
  - Dual
    - echo
      - pulse sequence 197*f*
      - steady state sequence 200, 200*f*
    - energy CT 66, 71
    - scanners 70*f*
    - subtraction 362
    - subtraction mammography 222, 364
    - X-ray absorptiometry 360, 364
  - Ductal extension of tumor 283*f*
  - Dynamic
    - contrast enhancement 172, 178
    - CT acquisition 87
    - susceptibility contrast-enhanced
      - MR perfusion 172

**E**

    - Edges of fibroadenoma breast 26*f*
    - Elastographic appearances of
      - breast masses 42
    - Elastography 9, 41
      - techniques for liver diseases 46*t*
    - Elastosonographic score 41
    - Electron beam tomography 64
    - Electronic dosimeters 353
    - Electrostatic lens 230
    - Emergency contrast-enhanced studies 303
    - Endoscopic
      - retrograde
        - cholangiopancreatography 252
        - ultrasonography 51
    - Epidural anesthesia 393
    - Epilepsy 404
    - Esophageal varices 46
    - Ethiodol 255
    - Ethylene vinyl alcohol copolymer 400

## Index

Evolution of  
  digital radiography 206, 206t  
  UCAS 271

External artifacts 154

Extracellular fluid 260

Extracorporeal shock wave lithotripsy 73

Extravascular extracellular space 175f

**F**

Faraday cage 134

Fast spin echo sequence 197, 197f

Fatty  
  infiltration of fatty sparing 275  
   villous proliferations 50

Feldkamp algorithm 63

Female pelvis 166

Ferucarbotran 267

Fexumoxide 267

FFDM systems 219f

Fibroadenoma 42  
  of breast 34f

Fibroids 49

Fibroscan 46

Fibrosis 43

Film  
  badge monitoring 352  
  screen radiography 205, 206

First study images 411

Fixed C-arm fluoroscopic system 240

Flash artifact 32

Flat panel  
  detector 63, 231, 236, 239  
  direct detector systems 362

## Flip angle 139

Flow  
  phenomena 183  
  sensitive alternating  
    inversion recovery 178

Fluid attenuated inversion recovery  
  sequence 198

Fluoroscopy 226  
  and digital subtraction angiography 226  
  and radiography 216

loop 234  
timer 350  
tube housing and filtration 349  
X-ray equipment 349

FNAC and biopsy needle 251

## Focal

fatty change 275  
hepatic steatosis 76f  
liver lesion 47, 94, 274  
nodular hyperplasia 47, 274, 275

Foot-switch and visual indicator 350

**G**

Gadobenate dimeglumine 262

Gadolinium oxysulphide 214

Gadoxetate 262  
  disodium 262

Gallbladder  
  and biliary ducts 164  
  calculi 13f

Gastrointestinal stromal tumors 380

Gelatin  
  foam 398  
  sponge 256  
  powder 256

Generalized auto-calibrating partially  
  parallel acquisitions 190

Ghosting artefact 144f, 147f

Glioblastoma multiforme 111f

Gradient  
  amplifiers 129  
  echo 174  
    sequences 196, 198, 198f  
  moment rephasing 147  
  motion rephasing 185  
  subsystem 123  
  system 129

Gray scale 38, 212

  elastograms 38  
  gain 31  
  imaging 18  
  processing 234  
  settings 26  
  sonography 51

Guidewire 250, 251f

**H**

Half-life of thrombolytic agents 396t

Harmonic motion imaging 41

Head hunter 250

Heart and blood vessels 343

Hemangioma 47, 274, 275

Hematopoietic system 343

Heparin antagonist 396

Hepatic  
  artery perfusion 115

  blood  
    flow 93

    volume 93

  mass characterization 75

  perfusion index 93

  steatosis 75

  vein transit time estimation 280

  venous pressure gradient 46

Hepatocellular

  adenoma 274, 275

  carcinoma 47, 92, 94f, 95f, 276

High

  frequency transducer 3

  intensity focused ultrasound therapy 41

  low intensity 268

Hodgkin disease 387f

Homogeneous hyperenhancement 278f

Hospital information system 317, 369

Hyaline cartilage 50

Hybrid

  coil 133

  detectors 60

  magnets 125

  sequences 196, 201

Hydronephrotic kidney 13f

Hydroureronephrosis 105f

Hyoid bone 113f

Hypercellular tumor 166f

Hypertrophic bronchial arteries 78f

Hypoechoic nodule 42f

**I**

Idiosyncratic anaphylactoid  
  reactions 297

Image

  intensifier system 239

  optimization in

    MRI 138

    ultrasound 17

Indirect

  conversion detectors 209

  digital conversion 211

Infectious synovitis 50f

Inferior venacavogram 228f

Inflammatory synovitis 50

Inflow-related signal enhancement 184

Intensifier fluoroscopy system 228f

Intracavitary applications 283

Intraductal papillary

  mucinous tumors 280

Intrahepatic cholangiocarcinoma 277

Intravenous regional anesthesia 393

Intra-voxel incoherent motion 162

Introduction of digital subtraction

  angiography 206

Invasive

  ductal carcinoma 43

    of breast 283f

    tumor of breast 43

Inversion recovery sequence 198

Ionic monomer 291

Ionizing carboxylic acid 290

Ischemic penumbra 89

Iso-osmolar

  contrasts 290

  dimeric contrast media 295

Ivabradine 395

**L**

Large

  abdominal cystic lesion 13f

  hemispheric infarct 90f

Lead rubber flaps 349

Lens system 211

Leukemia 342

Lidocaine 393

Limitations of  
 EUS elastography 51  
 film screen radiography 205  
 image intensifier system 231  
 Linear array transducer 5  
 Linearity of gradient 130  
 Lipoma abrorescens 50  
 Liquid crystal display monitor 233  
 Liver  
 abscess 275  
 cysts 275  
 stiffness measurement 44, 46  
 transplantation 115  
 Low  
 frequency transducer 3  
 high intensity 268, 269  
 molecular weight heparins 396  
 pressure balloons 250  
 Lower lobe pulmonary arteries 78/  
 Low-osmolar contrast media 290  
 Lung cancer 109  
 Lymph nodes 48  
 Lymphoma 108

## M

Magnet  
 geometry 127  
 isocenter 124  
 Magnetic resonance  
 angiography 183  
 imaging 171, 360, 366  
 susceptibility  
 artefact 153/  
 difference artifacts 152  
 Magnetization transfer constant 141  
 Magneto-optical disk 313  
 Magnitude contrast technique 187  
 Malignant focal liver lesions 276/  
 Mammography 360, 363  
 installation 364/  
 Management of  
 acute idiosyncratic reactions 299  
 Mask-mode subtraction 234  
 Mass forming chronic pancreatitis 101  
 Mathematical expression/relationship 324  
 Maximum  
 intensity projection 316, 404/  
 rated tube potential 348  
 MDCT reconstruction techniques 62/  
 Mean transit time 88, 172  
 Mechanism of idiosyncratic  
 anaphylactoid reactions 298  
 Medium frequency transducer 3  
 Metal artifact reduction 79  
 Metastatic  
 adenocarcinoma 96/  
 disease 94  
 neuroendocrine tumor 98/  
 Metformin 303

Methods of  
 administration 393  
 detection 351  
 Micropuncture access set 246  
 Microvessel density 92  
 Million heat units 59  
 Minimum total filtration 348  
 Mirror image artifacts 14, 23, 30  
 Mobile  
 digital radiography unit 363/  
 image intensifiers units 363  
 Modifying acquisition parameters 356  
 Modular transfer function 213  
 Modulation transfer function 218, 361  
 Moiré artefact 149/  
 Molecular  
 imaging 402  
 modalities 402/  
 target 405  
 weight 261  
 Motion artifacts 144, 161  
 Movement disorders 405  
 MRI pulse sequences 195  
 Multi-planar reformation 365/  
 Multiple hypodense lymph nodes 113/  
 Multi-shot radial acquisition  
 technique 146  
 Multitransmit technology 134  
 Musculoskeletal  
 applications 77, 79  
 system 33  
 Myocardial perfusion imaging 389  
 Myofascial pain 50

## N

Navigation systems 64  
 Needle-crystalline CR detectors 362  
 Nephrocalcinosis 8/  
 Nephrogenic systemic fibrosis 264  
 Nerve block 393  
 Nimodipine 394  
 Nodular regenerative hyperplasia 47/  
 Non-alcoholic fatty liver disease 43, 46  
 Non-Hodgkin's lymphoma 376, 404/  
 Normal  
 cerebral parenchyma 109/  
 Doppler signals in kidney 6/  
 muscle 49  
 pancreas 102  
 rectum 104  
 Nuclear imaging systems 360, 368  
 Number of excitations 143

## O

Optical  
 density 208/  
 distributor system 231, 231/  
 Ovarian cancer 385/  
 Overall gain 18

## P

Pancreatic  
 adenocarcinoma 99/*f*, 101, 101/*f*  
 neoplasms 95  
 pseudocyst 280  
 Parallel  
 acquisition techniques 190  
 imaging artefact 154, 154/*f*  
 Parts of catheter 247  
 Percutaneous nephrolithotomy 73  
 Perfluorocarbons 268  
 Perfusion  
 magnetic resonance imaging 171  
 parameters of normal liver 92, 93/*t*  
 weighted imaging 200  
 Peripheral nerve stimulation 131  
 Permanent  
 distal occluders 254  
 proximal occluders 254  
 Pharmacokinetic analysis techniques 176  
 Pheochromocytoma 303  
 Phosphodiesterase inhibitors 398  
 Photon counting type DR system 211  
 Photostimulable phosphor plates 207  
 Picture archiving and  
 communication system 205, 309, 368  
 Pigmented villonodular synovitis 50  
 Planning modern imaging department 359  
 Poisson's ratio 38  
 Polyethylene terephthalate 250  
 Polyvinyl alcohol 254, 398  
 Portable radiography 363  
 Portal  
 fibrosis 44  
 hypertension 46  
 vein perfusion 93  
 Positron emission  
 mammography 374  
 tomography 116, 368, 373, 402  
 Posterior acoustic enhancement 42/*f*  
 Post-processing techniques 233  
 Prevention of acute idiosyncratic  
 reactions 298  
 Principle of  
 digital radiography 206  
 dual energy CT 67/*f*  
 radiation protection 345  
 Propagation velocity artifact 24  
 Prophylaxis of contrast induced  
 thyrotoxicosis 303  
 Prostate 47, 166  
 cancer 100  
 Protein binding 261  
 Proton density 138  
 Pseudo-flow 30  
 Pseudo-continuous arterial spin labeling 178  
 Pseudo-tumors 281  
 Pulmonary  
 nodule evaluation 77  
 thromboembolism 77

Index

Truncation artifacts 150

Tube

  current 350

  voltage 350

Tubercular lymphadenitis 113*f*

Tuberculosis 50

Tuberculous colitis 104*f*

Tube-screen alignment 349

Tumor 102, 104

  necrosis 386*f*

Tunnel systems 127

Twinkling artifact 30

Types of

  digital detectors 207

  fluoroscopic equipment 240

  ICM 290

  image compression 311

  iodinated contrast media 290*f*

  radiation 339

  scintillators 210

  subtraction 234

  transducers 5

## ■ U

Ultrafast

  gradient echo sequence 200

Ultrasmall superparamagnetic

  iron oxide particles 268

Ultrasound

  contrast agents 271

  elastography 37, 44

  instrumentation 3

Unfractionated heparin 396

Unstructured scintillator 210

Ureteral stents 253

Urinary bladder wall 376*f*

## ■ V

Vascular

  applications 80

  stent 252

Venous thrombosis 51

Vessel selective labeling 178

Video system 232

Viscosity 37, 291, 293

## ■ W

Wall filters 29

Wearing dosimeter 353

Web link 322

Writing radiological opinion 414

## ■ X

Xenon perfusion CT 77

X-ray tube shielding 347

Young's modulus of

  elasticity 38

## ■ Z

Z-component 124

Z-direction 124

Zipper artifact 155